Number 1 Volume 22 1958

p1

BULLETIN
# of the
Academy of Sciences of the USSR
- Physical Series -

(Izvestiia Akademii Nauk SSSR)
(Seriia fizicheskaia)

Reproduction rights reserved

by

Columbia Technical Translations
5 Vermont Avenue
White Plains, New York

Single Issues
$20

Annual Subscription
$215

Transactions
# of the
First All-Union Conference on the Synthesis and Investigation of Scintillators for the Detection of Nuclear Radiation

TECHNIQUE OF GROWING ALKALI HALIDE PHOSPHORS FOR SCINTILLATION COUNTERS

- L.M.Shamovskii, L.M.Rodionova & A.S.Glushkova

Alkali halide single crystals used for optical purposes are usually grown from melts of the appropriate high-purity salts. The presence in the melt of even minor amounts of impurities often seriously complicates the crystallization process. Mixed crystals are readily synthesized if the composition of the melt and the solid phase in equilibrium with it are identical (minimum in the phase equilibrium diagram). Even minor deviations from this composition may have an adverse influence on the quality of the resultant single crystals. A particularly deleterious effect is produced by impurities which upon cooling of the melt fall out in the form of a eutectic mixture and also by polyvalent ions having surface active properties with respect to the synthesized salt.

When the fused salt interacts with water vapor from the atmosphere there appear hydroxyl ions in the melt, which in the process of growth of the single crystal only partially enter into its lattice in the form of substitutional impurities.[1] As they accumulate, there begins to crystallize out a eutectic mixture which at first produces a slight opalescence in the crystal and then separates out in the form of an opaque porcelaneous mass. Hydrolysis tends to be particularly intense in melts of lithium and sodium iodide. Hence in growing large single crystals one must carefully dehydrate the initial salts and take all necessary measures for protecting the melt from contact with atmospheric moisture.

In growing alkali halide phosphors, however, impurities (serving as activators) are introduced on purpose. As all other impurities, they complicate the conditions of growth and render the procedure more difficult.

Commonly alkali metal iodide crystals activated with thallium halides are used for scintillation counters. Thallium salts are very volatile at high temperatures, consequently in growing crystals in open crucibles (by the Kyropoulos method) in a vacuum furnace or in hermetically sealed heaters with an inert atmosphere, it is difficult to regulate the activator dosage and obtain scintillator crystals with standard, uniform characteristics.

In order to obtain good scintillators it is essential that the activator be uniformly distributed through the volume of the single crystal. In crystal growth by the Kyropoulos procedure evaporation of the activator is usually neither regulated nor monitored. Hence large single crystals formed by this procedure are generally characterized by sharp variations in the thallium concentration.

The fact that the activator impurity is introduced on purpose in synthesizing crystal phosphors does not mean that the exacting requirements as regards purity of the initial materials can be relaxed. The initial materials must be thoroughly purified to remove all traces of heavy metals, which produce absorption bands overlapping the emission bands of the given crystal, as well as of all impurities that further formation of a polyhedral substructure in the crystal.

Procedure for growing phosphor single crystals

The procedure for growing single crystals developed by us is based on a modification of the Stockbarger technique. The crystallization is carried out from a melt in sealed cylindrical tubes of quartz glass. With this procedure the difficulties associated with activator dosage are eliminated. At the same time there is realized complete isolation of the salt from atmospheric moisture, thus precluding any possibility of chemical decomposition.

Digitized by the Internet Archive
in 2024

https://archive.org/details/russian-academy-of-sciences-physics-bulletin_1958_22

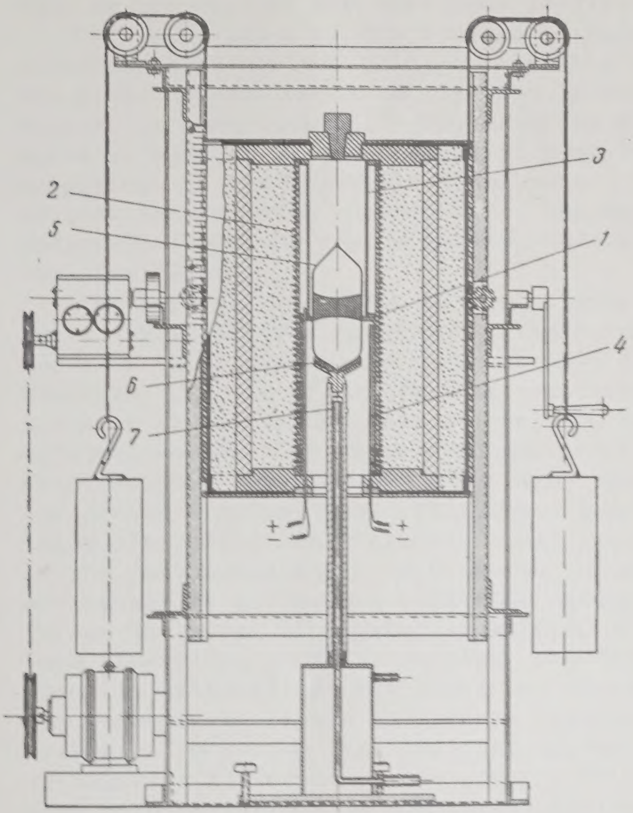

Fig.1. Two-section furnace for growing crystal phosphors.

The synthesis is carried out in the tubular two-section furnace shown schematically in Fig.1. It is separated into two sections by a septum 1. Each section has an independent nichrome wire heating element. For successful single crystal growth it is essential that there be virtually no temperature gradient vertically or horizontally within each section or chamber. This condition is realized by nonuniform distribution of the nichrome winding over the tube 2 and by the installation in both chambers of the temperature equalizing metal plates 3 and 4. In contrast, in the crystallization zone, located at the level of the septum, there must be an appreciable temperature gradient both vertically and from the center to the periphery. The sealed tube 5 containing the reagents may either be suspended or supported on the water-cooled stand 6. Removal of heat through the cooling device 7 increases the temperature gradient in the crystallization zone; this not only increases the rate of growth but also makes it feasible to obtain virtually perfect single crystals.

The rate of crystal growth is controlled by the rate of displacement of the sealed ampoule in the furnace. At the beginning of the process a seed crystal forms in the apex of the tube cone. This determines the subsequent orientation of the entire single crystal. It is essential that in the crystallization zone at the level of the septum (or somewhat above), the temperature distribution over the cross section be characterized by a paraboloid with its apex at the center of the septum. Under these conditions crystallization always begins from a single center at the point of the quartz tube and all the impurities that do not enter into the crystal are forced upward into the melt and towards the walls of the tube. An external indication characterizing the correctness of the growth conditions is convex shape of the growth isotherm. If the crystallization occurs below the septum or if in the upper section of the furnace above the crystallization zone there appears an appreciable temperature gradient, the growth isotherm acquires a concave surface* and then the

---

*Simple calculations show that in a furnace with a temperature gradient of 50° per cm in the crystallization zone, a 5° decrease in temperature over a period of 5 minutes results in an increase of 12 mm/hour in the rate of crystallization during this interval.

crystallization proceeds from the periphery to the center and polycrystals are likely to form. In this case, impurities accumulate in the central portion of the crystal and sometimes cavities may appear.

The temperature of the furnace is maintained constant by means of a EPD-12 potentiometric control that periodically cuts in a ballast resistor and varies the power dissipated in the furnace by up to 10-15%. The heat inertia in the furnace is made minimal.* The metallic plates in the furnace (3 & 4 in Fig.1) serve as buffers in the process of heat transfer and enhance the thermostating conditions in the crystallization zone. The sensing element of the EPD-12 control is a Pt-PtRh thermocouple, the hot junction of which is located immediately above the septum between the tube carrying the nichrome winding and the steel plate.

The crystal growth isotherm must remain constant over the entire growth cycle. Particularly dangerous in this respect are periodic and sharp displacements of the isotherm due to inadequate thermostating: with a decrease in temperature the rate of crystallization increases and, accordingly, the growth isotherm rises; in the case of increase in temperature, on the contrary, the crystallization zone is lowered and the rate of growth slows down. Where such fluctuations, even though short-term, result in an appreciable acceleration of the growth process, they involve the danger of the crystal engulfing the impurities (including the activator) that are normally concentrated in a thin layer of the melt immediately adjacent to the growing single crystal. Segregation of impurities and excess activator seriously impairs the optical and scintillation qualities of crystal phosphors: in the case of single crystals the long wave absorption limit is shifted, the efficiency is reduced, the phosphorescence is intensified, the light scattering is increased, the crystal acquires the tendency to become colored in daylight. Inhomogeneities in activator distribution connected with periodic segregation of impurities often have a stronger negative influence on the quality of phosphors than inhomogeneities associated with variations in phase equilibrium between the crystal and the melt.

Periodic segregation of impurities can be eliminated by precise thermostatic control of the furnace. In our case this was realized by redistribution of the resistances in the EPD-12 unit with a resultant increase in its sensitivity by a factor of 8-10. Close thermostatic control in the case of our furnace is also facilitated by the heat-resistant steel interliners and an air space between the inside chamber of the furnace and the tube carrying the nichrome windings. The degree of accuracy of thermostatic control is closely connected with the selected rate of crystal growth, the mean concentration of the introduced activator and extraneous impurities (as well as their diffusion coefficient in the melt) and by the temperature gradients that are established in the furnace at the level of the septum and in its vicinity.

Activator distribution in the crystal phosphor

The impurity concentration in different parts of the single crystal does not remain constant whenever, in the process of its growth from the melt, the equilibrium concentrations of the solid and liquid phases are not equal. Usually the factor characterizing the distribution of chance or deliberately

---

*In the case of a furnace with a large thermal inertia, equilibrium between the heated volume and surrounding medium is established only after many hours of heating. Consequently, the simpler procedure of heating by means of a stabilized steady current with no special thermal regulators does not give the requisite thermostatic accuracy.

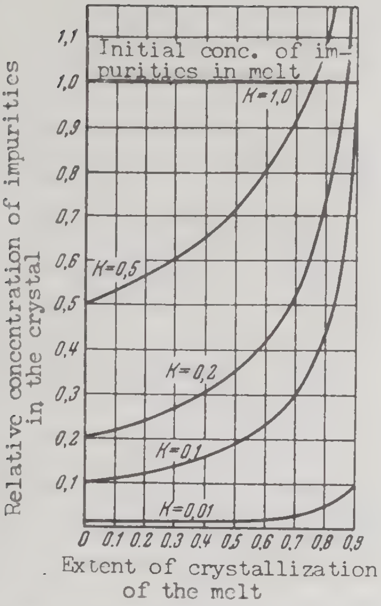

Fig.2. Variation of the relative concentration of impurities in a crystal with the degree of crystallization of the melt in height. $K = C_{cr}/C_{melt}$.

introduced impurities between the two phases is less than unity. Then with growth of the single crystal, the concentration of impurities in it increases both in height and from the center out to the sides. Data characterizing the concentration distribution in height are shown in Fig.2; these data are for the case when impurities virtually do not diffuse in the crystal, there is ideal mixing in the melt, there is no appreciable volatilization of the components and there is no zonal segregation. Inhomogeneity in the composition of a mixed crystal decreases with increasing dimensions both in height and in diameter; hence for scintillation and other applications where small phosphor crystals are desired it is expedient to prepare them by cutting up large specimens.

In the case of crystal growth by the Stockbarger technique, mechanical mixing is not employed and convection currents are generally negligible. Hence the character of the equilibrium distribution of impurities is influenced by a number of additional factors, dependent on the rate of crystallization and the coefficient of diffusion of the impurities in the melt. Usually there is a certain degree of condensation or concentration of the impurities on the faces of the growing crystal. Consequently, the growing crystal tends to contain a greater concentration of impurities than their average content in the remaining liquid phase. With high rates of growth or low temperature gradients in the crystallization zone one can, in principle, realize an almost homogeneous impurity distribution.[2] Nevertheless, there inevitably occur periodic segregations of the activator and the extraneous impurities which result in even greater inhomogeneity in composition on a microscopic scale. Such zonal separations of the activator may be hardly noticeable to the naked eye or in some cases may appear in the form of semi-opaque belts. In both cases this involves a marked impairment of the quality of the crystal phosphor.

The scintillation pulse amplitude produced by a given monochromatic γ-radiation varies with the activator concentration in the crystal phosphor. At first, at low concentrations, the pulse height increases linearly with the activator content, then attains a maximum (usually a more or less extended plateau) and finally begins to decrease. According to the data of Harshaw et al[2], in NaI activated with TlI the scintillation pulse height for the Cs^{137} photopeak remains constant with variation of the TlI concentration in the range from 0.1 to 0.4%. Hence in growing such crystals the activator is introduced in the amount of 0.5%. Then in the initial stage of growth of the single crystal, i.e., at the apex of the crystal cone, approximately 0.1% TlI (or 20% of the introduced amount) enters into the composition of the phosphor. In the center of the crystal the TlI concentration increases to 0.25%. The upper third of the fully formed crystal already contains an excessively high activator and is discarded in cutting the scintillation crystal.

Selection and proportioning of the activator

We established, through our investigation[3] of the structure of alkali halide phosphors and the mechanism of luminescence excitation therein, that the activator as a surface-active substance in consequence of the dual character of its distribution in the crystal produces a polyhedral substructure which is not eliminated by annealing. Part of the introduced impurity enters into the composition of the substitutional solid solution, while the other part is distributed over the contact surfaces. Here there are formed deep electron traps. The additional absorption bands of the phosphor are associated only with this part of the activator. The electrons and holes appearing upon excitation of the luminescent crystal are localized on the contact surfaces, where their thermodynamic potential is lower than in the crystal lattice or on any of the "sticking" levels. Recombination of the electrons with holes on these contact surfaces is accompanied by emission of light with the frequency corresponding to the energy difference between their local states. The same electron-hole recombination inside the crystal lattice (i.e., not on the contact surfaces) is realized by the nonradiative mechanism and the recombination energy is dissipated in the form of thermal agitation of the ions. If there are present in the crystal internal surfaces not associated with the activator they too act as electron and hole traps. In this case, however, the luminescence is observed only at low temperatures and has a different spectral composition. Hence at ordinary temperatures pure crystals exhibit virtually no luminescence.

In the light of these concepts regarding formation of luminophors, it became logical to seek activator compounds which, like the thallium halides, would give rise to a polyhedral structure in the crystal but at the same time would not form a substitutional solid solution with the host material. We found that such activators as thallium and indium when introduced into the crystal in the form of pure metal, the oxide or the sulfide, form phosphors with the same properties as when the Tl or In are introduced in the form of one of their halides.[4] In all cases, the same absorption and emission bands appear. As may be seen from Fig.3, however, the less soluble activator compounds at equal molar concentrations of them in the crystal are appreciably more effective than the more soluble ones. In other words at equal molar concentrations in the phosphor, the less soluble compounds produce far higher concentrations of centers of additional absorption and emission in the crystal.

As may be seen from Fig.2, when fully soluble compounds are used, a far more uniform distribution of the impurity in the crystal is obtained throughout most of the volume of the crystal, while the excess impurity is concentrated in the remaining (last) parts of the melt.* Consequently, one can utilize an appreciably greater

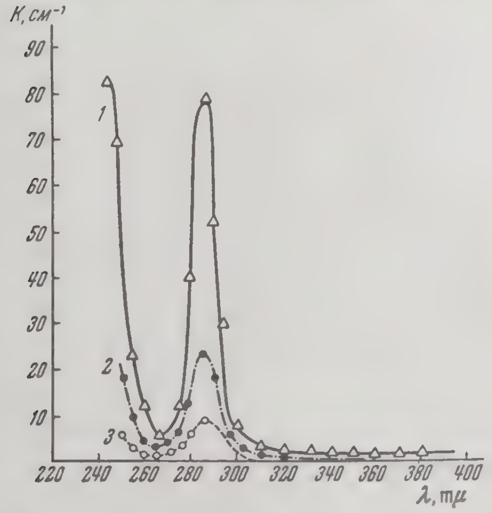

Fig.3. Dependence of the spectrum of long wavelength activator absorption in KI(Tl) phosphor with the same thallium concentration ($1.5\cdot10^{-3}$ molar %) on the form in which the thallium is introduced: 1) metallic thallium, 2) Tl_2O and 3) TlI.

---

*The areas under the curves in Fig.2 should be equal regardless of the value of K inasmuch as the concentrations are given in relative units.

portion of the crystal for scintillation counters in this case.

The curves of Fig.2 characterized the equilibrium distribution of impurities between the crystal, i.e., the substitutional solid solution, and the melt. In the case of highly soluble impurities the amount of activator lodging on the contact surfaces amounts to only a small fraction of its total concentration in the crystal and hence proportion-wise is negligible. In the case of relatively insoluble impurities, in contrast, the amount distributed over the contact surfaces may account for the major fraction of the impurities in the crystal. Nevertheless, all the relationships established for the impurity distribution in the solid solutions remain valid in this case also since the dual distribution of the activator reflects an equilibrium process.

In growing NaI(Tl) phosphors the optimal dosage of the activator in the form of Tl_2O is 0.04-0.05%. This is approximately one tenth the amount of activator introduced in the form of the iodide. Actual concentration of activator in the crystal is also appreciably reduced in this case. The thallium distribution in NaI(Tl) phosphor when 0.05% Tl_2O is added to the melt is shown in Fig.4. Thus we come to the conclusion that only part of the introduced thallium acts as an activator in the synthesized phosphor.[4] If a sufficiently pure salt is employed there are obtained with Tl_2O completely transparent single crystals and the process of growth is appreciably simplified.

Theoretically, in the case of metallic thallium the activator dosage should be even smaller, but unfortunately, the use of metallic thallium is limited in view of the fact that its solubility in the molten salt is too low (10^{-3} molar %).

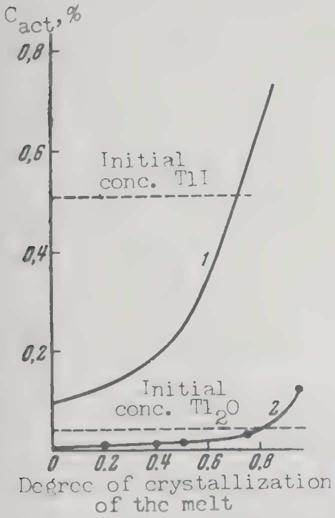

Fig.4. Distribution of activator in NaI(Tl) phosphor grown with 1) 0.5% TlI and 2) 0.05% Tl_2O.

Heat treatment of the crystals

After completion of the growth process the crystals are extracted from the tube by the surface fusing technique. They are then quickly transferred to the annealing furnace preheated to almost the melting point of the given phosphor.

The crystals grown from a melt are obtained with substantial structural distortions formed under the influence of plastic deformations due to mechanical stresses and temperature changes. When large single crystals are grown by the Kyropoulos method they are deformed in the process of crystallization under the influence of their own weight. In crystallization by the Stockbarger procedure deformations are produced due to the difference between the coefficients of thermal expansion of the salt and the material of the container, particularly in those cases when the crystal adheres to the walls of the tube or crucible. In addition deformations are caused by the stresses incident to uneven cooling of the crystals. Alkali halide crystals are characterized by a low heat conductivity; hence rapid cooling gives rise to steep temperature gradients and, consequently, appreciable deforming forces. As a result a dislocation network develops in the single crystals, the far-range order is disturbed and mosaicity appears. The presence of polyhedral structure in such crystals can be determined from light scattering[3] and Laue diffraction patterns.[6] Such crystals do not readily split along cleavages and

their newly exposed internal surfaces generally exhibit coarse structural dislocations.

Annealing of the single crystals eliminates the mosaic structure if this is due to plastic deformations. After holding at the appropriate high temperature the crystals must be cooled slowly. The optimal annealing temperature is that at which intense recrystallization occurs. Each reheating temperature is characterized by a corresponding degree of recrystallization and mean grain size. Ordering of the crystal structure occurs by the process of plastic flow which, with increasing temperature, encompasses an increasingly greater volume in from the surface of each block. The recrystallization process is closely associated with the coefficient of self-diffusion which, in turn, depends on the equilibrium concentration of the structural defects of the lattice. The activation energy for self-diffusion processes in alkali halide crystals is rather high (~ 2 ev). hence annealing can only be effective at temperatures close to the melting point of the material.

To obviate repeat deformation, the crystal after annealing must be cooled very slowly. This is particularly important in the range of medium and low temperatures when the crystallized salt acquires a rigid structure and its heat conductivity is sharply reduced. In the case of pure crystals all mosaic (which can be detected from x-ray diffraction patterns) is wholly eliminated by proper heat treatment; at the same time light scattering losses are sharply reduced. If, on the other hand, the crystal contains an activator or other surface-active impurities only improvement of the structure occurs in the process of annealing: the mosaicity due to plastic deformation is largely eliminated, but the polyhedral substructure resulting from the dual distribution of the activator persists. This is illustrated by the Laue diffraction patterns of an NaCl(Ag) phosphor obtained before and after annealing.

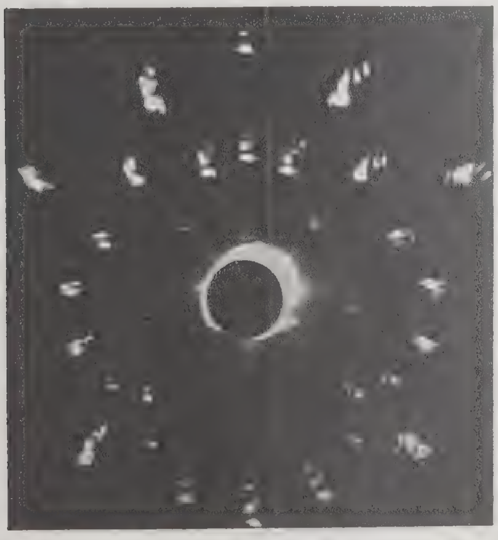
Fig.5. Laue diffraction pattern of NaCl(Ag) phosphor before annealing.

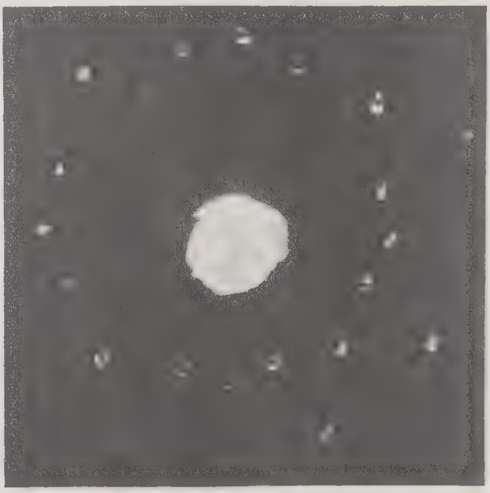
Fig.6. Laue diffraction pattern of the same phosphor as in Fig.5 after annealing.

In our laboratory the crystal phosphors are annealed inside a massive steel cup in a shaft furnace. They are kept for 2-3 hours at a temperature 5-10° below the melting point of the given phosphor. The temperature of the furnace is maintained constant by means of an EPD-12 potentiometric control. After the

2-3 hour heating period, the temperature is gradually reduced automatically by decreasing the input voltage; the temperature decrease over a period of 15-20 is usually 400-450°. The subsequent cooling of the crystals to room temperature is realized by cooling with the furnace, the time for this cooling stage being 10-15 hours.

In the case of NaI(Tl) crystals annealing at a temperature close to the melting point results in an appreciable increase of the light yield and improved resolution of the photopeaks as may be seen from the curves of Figs. 7 & 8. The resolution of the photopeaks from Cs^{137} varies between 8.4 and 12%. The measurements were carried out on a multiple channel analyzer with a standard FEU-S photomultiplier.* Annealing at lower temperatures (some 50° below the melting point) for the same period results in only a minor improvement of the resolution (from ~20 to 15-17%).

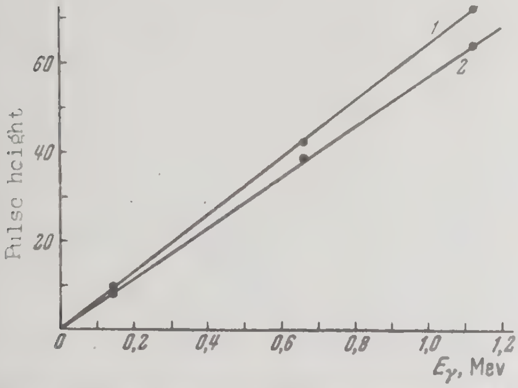

Fig.7. Variation of the scintillation pulse height in NaI(Tl) phosphor with the γ-radiation energy: 1) annealed crystal and 2) non-annealed crystal.

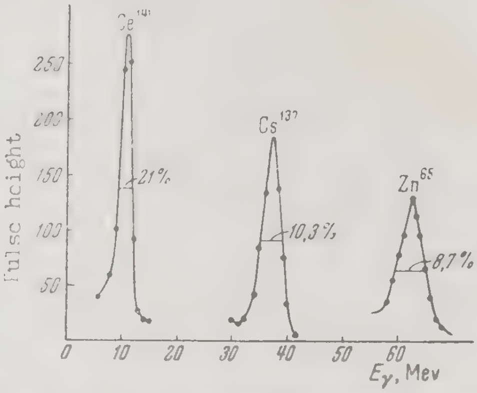

Fig.8. Variation of the scintillation pulse height in NaI(Tl) phosphor with the energy of monochromatic γ-radiation.

In the light of the data cited above, we can draw certain preliminary conclusions regarding the character of the changes occurring in crystal phosphors in the process of annealing.

Although the coefficient of diffusion of impurities through the crystal lattice does increase at high temperatures, tests show that the heat treatment does not lead to complete homogenization of the phosphor composition. There occurs only a certain redistribution of the impurities over the intercrystalline surfaces. Where improvement of the quality of the crystal is concerned this factor apparently plays only a secondary role, inasmuch as annealing also increases the luminescence efficiency of crystals with a low activator concentration where redistribution of the impurity during annealing must be negligible. Ordering of the crystal structure during annealing reduces the internal light scattering and, consequently, enhances the transparency of the crystal. This factor, however, also cannot be the principal reason for improvement of the spectrometric properties of the phosphor inasmuch as virtually the same improvement is observed for large and for small crystals.

In the opinion of the writers there is a more important reason for the depressed luminescence yield of crystals with a polyhedral substructure. As we have noted above, the emission of crystal phosphors is a result of recombina-

---

*The authors take this occasion to thank B.V.Efimov for his assistance in determining the spectrometric characteristics of the crystals.

tion of electrons with holes on the contact surfaces formed by the activator. Obviously, the luminescence yield depends on the fraction of electrons and holes that reach these surfaces in their migration from the points where they appear under the influence of the ionizing particles or radiation. At ordinary temperatures recombination at locations other than the contact surfaces is nonradiative. It is known, however, that other internal surfaces not associated with the activator may exist in crystals. These, too, serve as effective traps for electrons and holes and hence decrease the scintillation yield. Proper annealing of the crystals improves their structure as is clearly evident from Laue diffraction patterns: in the patterns of annealed crystal phosphors there persists only some splitting of the spots due to the polyhedral substructure formed by virtue of the dual distribution of the activator and not wholly eliminated by the annealing.

All-Union Institute of Mineral Raw Materials

References

1. Scarpa, Atti R. Accad. Lincl, 5, 24, I 955 (1915); 5, 24, II, 410 (1915).
2. J.A.Harshaw, H.S.Kremers, E.C.Stewart, E.K.Warburton & J.O.Hay, Atomic Energy Commission Report, NYO - 1577 (1952).
3. L.M.Shamovskii, Opt.i spektr., 1, 407 (1956).
4. L.M.Shamovskii & Iu.N.Zhvanko, Doklady AN SSSR, 111, 140 (1956).
5. Owen Hymphreys, Proc.Phys.Soc., B65, 350 (1956).
6. L.M.Shamovskii, L.M.Rodionova, G.A.Sidorenko & Iu.N.Zhvanko, Doklady AN SSSR, 99, 235 (1954).

INVESTIGATION OF SCINTILLATORS CONTAINING BORON-ORGANIC COMPOUNDS

- A.N.Nikitina, M.D.Galanin, P.M.Aranovich, T.A.Shchegoleva & B.M.Mikhailov

It is now a familiar fact that certain boron-organic compounds can be used for detecting slow neutrons. As yet, however, only a small number of boron-organic compounds have been investigated for their usefullness in this regard. The studied compounds include four boric acid esters: trimethyl, ethyl, propyl and butyl borates[1], and trinaphthyl borine[2]. It is reported[1] that the best results were obtained with trimethyl borate and this is now extensively used in mixture with a liquid scintillator for detecting thermal neutrons.

In the present investigation we tested a number of boron-organic compounds (some of them prepared for the first time[3]) for the purpose of determining their suitability for detecting thermal neutrons. From this standpoint it was of interest to establish whether the scintillation intensity of the main scintillator (the fluorescent medium) is reduced upon the addition of the boron-organic compound to it. Inasmuch as many of the synthesized compounds contain aryl substitution groups and can themselves scintillate, we deemed it desirable to determine their scintillation intensity. In addition, it was necessary to clarify the influence of the aryl radicals in the substitution compound on the scintillation intensity of the main scintillator. In all, we investigated 16 boron-organic compounds of which 13 were boric acid esters and mono- and disubstitution products of boron-organic acids. The main scintillator was a standard fluorescent solution of p-terphenyl (or 2,5 diphenyl-oxazole) in toluene. The tested compounds were added in equal volume to the standard solution. The fluorescence was excited by Co^{60} γ-rays. The scintillation intensity was determined by measuring the relative pulse heights. The accuracy of measurement was about 10%. The total volume of the liquid scintillator was ~8 cm^3.

The results of our measurements are summarized in the accompanying table. The percentages listed in the "Relative scintillation intensity" column refer to the scintillation intensity of the standard solution containing p-terphenyl alone. As will be seen from the table, 9 of the tested compounds (Nos.1 thru 9) did not contain aryl substitution groups. Most of these compounds have had little or no effect on the scintillation intensity, while trimethyl borate weakens it by approximately 50%. In contrast, aryl substituted compounds (Nos. 10 - 14) appreciably reduce the scintillation intensity. As will be evident from the table, the amount of decrease in intensity is directly connected with the boron content in the given compound.

We also measured the scintillation intensity of aryl substituted boron-organic compounds without the main scintillator, i.e., without p-terphenyl in the solution. We investigated the compounds listed under Nos.10 through 14 in the table as well as the n-butyl ester of di-parachlorphenyl boric acid $(ClC_6H_4)_2BOC_4H_9$ and tri-α-naphthyl boronbenzene $(\alpha\text{-}C_{10}H_7)_3BC_6H_6$. Their scintillation intensity proved low: 10-30% relative to that of the standard p-terphenyl solution.

We also carried out tests for the purpose of determining the effect of the listed boron-organic compounds on the intensity of γ-excited scintillation of p-terphenyl and 2,5 diphenyl-oxazole. It was found that in the presence of the isobutyl ester of diphenyl boric acid the scintillation intensity of 2,5 diphenyl-oxazole solution amounts to 40% relative to the intensity of the 2,5 diphenyl-oxazole itself and that the scintillation intensity of p-terphenyl solution with the same compound falls to 20% of the intensity of p-terphenyl alone. In the presence of butyl boric acid and butyl ester the respective percentages are 70% for 2,5 diphenyl-oxazole and 90-100% for p-terphenyl.

Scintillation intensity of solutions of p-terphenyl with various boron-organic compounds (1 to 1 mixtures)

No.	Boron-organic compound		Relative scintillation intensity,%	Boron concentration,%
	Formula	Name		
1	$n\text{-}C_4H_9B(O\text{-}n\text{-}C_4H_9)_2$	n-Dibutyl ester of n-butyl boric acid	90-100	5.4
2	$B(O\text{-}iso\text{-}C_4H_9)_3$	Triisobutyl borate	85-90	4.7
3	$B(O\text{-}iso\text{-}C_5H_{11})_3$	Triisoamyl borate	90-100	4.0
4	$B(O\text{-}n\text{-}C_6H_{13})_3$	Tri-n-hexyl borate	90-100	3.5
5	$n\text{-}(C_4H_9)_2BO\text{-}iso\text{-}C_4H_9$	Isobutyl ester of n-butyl boric acid	90	5.4
6	$C_2H_5(C_4H_9)BO\text{-}n\text{-}C_4H_9$	n-Butyl ester of ethylbutyl boric acid	90	7.0
7	$n\text{-}C_3H_7(n\text{-}C_4H_9)BO\text{-}n\text{-}C_4H_9$	n-Butyl ester of n-propylbutyl boric acid	80	6.0
8	$n\text{-}C_4H_9BO$	n-Butyl boric anhydride	50	13.0
9	$B(OCH_3)_3$	Trimethyl borate	50	10.0
10	$C_6H_5B(O\text{-}n\text{-}C_4H_9)_2$	n-Butyl ester of phenyl boric acid	50	3.9
11	$(C_6H_5)_2BO\text{-}n\text{-}C_4H_9$	n-Butyl ester of diphenyl boric acid	30	4.6
12	$(\alpha\text{-}C_{10}H_7)_2BO\text{-}iso\text{-}C_4H_9$	Isobutyl ester of di-α-naphthyl boric acid	20	2.6
13	$(C_6H_5)_2BO\text{-}iso\text{-}C_4H_9$	Isobutyl ester of diphenyl boric acid	20	4.2
14	$(\alpha\text{-}C_{10}H_7)_2BOH$	Di-α-naphthyl boric acid	10	3.3

Conclusions

1. Upon introduction into the liquid scintillator (p-terphenyl solution) the investigated alkyl and dialkyl boric acid esters virtually do not reduce the γ-scintillation intensity of the p-terphenyl solution.
2. Trimethyl borate, which is now extensively used in experimental nuclear physics, weakens the γ-luminescence of p-terphenyl solution by 50%.

3. The addition of aryl and diaryl substituted boric acid esters to the standard p-terphenyl solution reduces the scintillation intensity of the solution by 50-90%. Aryl substituted boron-organic compounds themselves exhibit a weak γ-luminescence.

"N.D.Zelinskii" Institute of Organic Chemistry and
"P.N.Lebedev" Physical Institute,
Academy of Sciences of the USSR

References

1. C.O.Muehlhause & G.E.Thomas, Phys.Rev., 85, 926 (1952); Nucleonics, 11, 44 (1953).
2. J.J.Zolingen & J.J.Went, Physica, 18, 976 (1952).
3. B.M.Mikhailov & V.A.Vaver, Doklady AN SSSR, 102, 531 (1955); B.M.Mikhailov & V.A.Vaver, Izv. AN SSSR, Otd.Khim.nauk., 4, 451 (1956).

SCREENS FOR DETECTING SLOW NEUTRONS

- T.V.Timofeeva & S.P.Khormushko

The purpose of our work was to develop scintillators with the highest possible counting efficiency for thermal neutrons in the presence of a strong γ-background. We utilized the familiar $B(n,\alpha)$ reaction. For recording the resultant α-particles we used zinc sulfide phosphors which are characterized by a high α-radioluminescence efficiency as compared with other types of luminophors and a relatively lower sensitivity to γ-rays as compared with organic crystals in solutions.

The neutron counting efficiency is determined by the magnitude and number of scintillations produced in the detector. The scintillation intensity depends on the composition and mode of preparation of the scintillator. The number of scintillations can be increased within certain limits by the introduction of larger amounts of boron and by increasing the thickness of the fluorescent layer. Increase in the thickness of the layer is accompanied by two competing effects: on the one hand, the number of nuclear reactions and, consequently, the number of scintillations increases with increasing thickness, while on the other hand, the transparency of the layer decreases since the scattering of the fluorescence light increases.

The total number of scintillations emitted from the screen can also be increased by using scintillators with a larger surface, for example, by replacing the conventional flat screen with a screen in the shape of a hollow body (cone, cylinder or sphere) coated on the inside with the activated phosphor.

Accordingly, our work consisted of 1) finding the best procedure for preparation of the scintillation phosphor, 2) investigating the variation of the detecting efficiency for neutrons as a function of the thickness of the phosphor layer, the phosphor grain size and the nature of the suspending or binding medium and 3) determining the best shape of the screen and the most suitable method of preparing it.

We investigated the emission and reflection spectra, the relative counting efficiency for neutrons and the relative brightness of the α-luminescence.

The spectral distribution of the photoluminescence was investigated by the method of photographic spectrometry with the phosphor excited by the 313-366 $m\mu$ group of mercury lines from the observation side. The spectral reflection curves of the phosphor powders were measured on an automatic spectrophotometer. The absorption curves given below were obtained from the reflection curves by subtraction of the reflection values from the total light flux. The set-up for measuring the relative counting efficiency η_n for slow neutrons consisted of an FEU-19 photomultiplier viewing the sample and connected to standard "B" type equipment [a rectifier, amplifier and indicating assembly designed for use with GM counters]. The samples were tested in the form of a layer of the phosphor powder compressed between two 4 x 4 cm glass plates (the superficial density of the layer, ≥ 70 mg/cm^2, was determined by weighing).

For investigating the variation of the detecting efficiency with the layer thickness and grain size samples were prepared both by seiving and by settling from alcohol. In the latter case, to allow for the grain size gradient over the thickness of the layer, the measurements were made from both sides of the sample. The samples were mounted directly on the window of the photomultiplier (without optical contact or bonding) so that interchange of the samples presented no difficulty. The RaBe source, having a continuous neutron spectrum, was located 1.5 cm above the sample. The metallic housing encasing the phosphor sample, photomultiplier and source was surrounded with a 5 cm thick layer of paraffin for slowing down the neutrons. This arrangement insured the

highest detecting efficiency, yet with a continuous neutron spectrum with thermal neutrons predominating passing through the phosphor. Inasmuch as the "B" unit has a constant gate (fixed cut-off), separation of the pulses due to other causes (α-background, dark current, etc.) from the pulses due to the $B(n,\alpha)$ reaction was realized by varying the voltage on the photomultiplier. In a series of separate experiments on a "D" unit (linear amplifier with a scaling circuit), we established that variation of the photomultiplier voltage with a constant bias was equivalent to variation of the grid bias with a constant voltage on the photomultiplier. The neutron source used in this case did not emit γ-rays. The sensitivity to γ-rays was determined by means of a radium source located at a distance corresponding to the given (in μr/sec) background (as calculated). Tests to take into account the pulses due to fast neutrons were carried out on the same set-up without paraffin. The relative brightness of α-radioluminescence (B_r) with excitation by polonium α-particles was measured by means of a photocell with a dc amplifier. The superficial density of the layer used ($\geqslant$15 mg/cm^2) insured complete absorption of all α-particles.

Two procedures for preparing boron-loaded zinc sulfide phosphors for detection of neutrons are described in the literature.[2-8] These are the mechanical mixing procedure[2-6] and the sintering technique[7,8].

We used three different procedures in preparing the scintillation phosphors: 1) the method of joint heating of the phosphor and the boron compound, 2) the method of adding the appropriate boron compound to the previously prepared phosphor and 3) the sintering procedure in which the previously prepared phosphor is introduced into the melt of the boron compound by heating a mechanical mixture of the components to the fusion temperature.

In the first procedure, the boron compound was added to the initial phosphor batch and went through all the usual synthesis stages: drying, heating and removal of the incrustation. Then the resultant phosphor was ground and separated into coarseness fractions by sifting through No.28, 38 and 58 silk screens and elutriation.

The joint heating technique was used to prepare ZnS:Zn, Zns:Ag and ZnS:Cu phosphors with Li, Na, K, Mg, Ca, Sr and Ba chlorides and fluorides as fluxes and different concentrations of boric acid. According to our tests, borax and boron oxide yield the best results. Curves characterizing the variation of η_n and B_r with the boric acid content for ZnS:Ag[Na] phosphor are shown in Fig.1. These curves are typical of all similar phosphors regardless of the method of preparation. B_r decreases in all cases with increasing boric acid content since this increase is accompanied by an increase in the inactive absorption of the α-particle energy in the acid and by greater light scattering with subsequent reabsorption. The curve characterizing η_n has a more or less smeared out maximum in view of the fact that increase in the number of scintillations is accompanied by a decrease in their intensity.

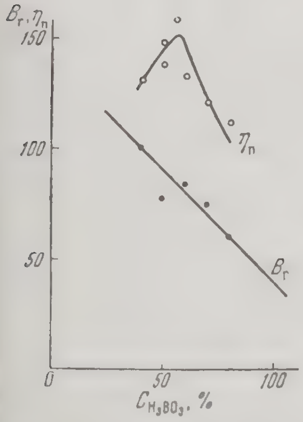

Fig.1. Variation of the neutron detecting efficiency η_n and the α-luminescence brightness B_r with the boric acid content (expressed in percent of the ZnS content).

The neutron counting efficiency for phosphors prepared by the method of joint heating depends significantly on the structure of the boric acid crystals as determined by the preliminary heat treatment of the acid. This will be evident from Fig.2 which shows the dependence of η_n on the temperature of drying of the phosphor batch before heating for dif-

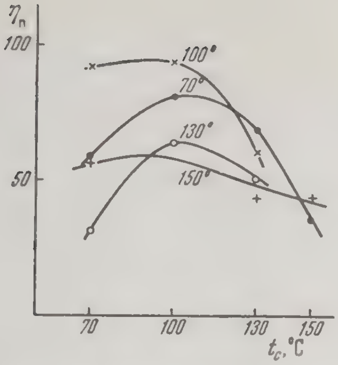

Fig.2. Variation of the neutron detecting efficiency η_n with the temperature t_c of drying of the initial phosphor batch for different temperatures of the preliminary drying of the boric acid.

ferent temperatures for preliminary dessication of the boric acid after its crystallization. The maximum of the curve in each case occurs at about 100°; at higher temperatures the boric acid transforms into metaboric. Below this temperature, as crystal-optical analysis on a polarization microscope showed, orthoboric acid exists in two crystal modifications: at a drying temperature $\leqslant 70^o$ the crystals have the appearance of hexagonal anisotropic lamellae of the monoclinic system with $n_1 = 1.471$ and $n_2 < 1.471$. As the drying temperature is increased to ~105° the lamellae gradually become colored by a very fine-grain superficial formation. At $t > 110^o$ (metaboric acid) there begin to form individual prismatic crystals with $n_1 = 1.471$ and $n_2 \gg 1.471$.

The highest efficiency for detection of slow neutrons was obtained for a ZnS:Ag phosphor containing 55% H_3BO_3 prepared by the joint heating procedure with the initial batch heated at 100°. This efficiency was taken as unity for further reference purposes. With a γ-background equal to 300 μr/sec produced by a radium source, the efficiency fell off by a factor of 4. Fast neutrons are virtually not detected by our phosphor (the detecting efficiency is $\leqslant 1\%$ for fast neutrons).

The position of the phosphor spectrum in the wavelength scale is virtually independent of the flux used and is determined primarily by the activator. The maximum lies at about 440 mμ for ZnS:Ag (curve 1 in Fig.3) and at 460 mμ for ZnS:Zn (curves 2,3 & 4 in Fig.3). With increasing boric acid content the spectrum is shifted to the red side and the intensity peak broadens as evident from the character of curves 2,3 & 4 in Fig.3, which pertain to ZnS:Zn phosphors prepared by the sintering technique without boric acid and with 40 and 80% H_3BO_3, respectively.

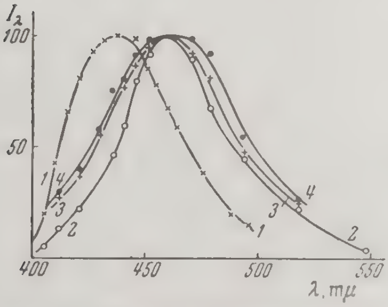

Fig.3. Photoluminescence intensities: 1) ZnS:Ag phosphor - 60% H_3BO_3, 2) ZnS:Zn phosphor, no boric acid, 3) ZnS:Zn phosphor - 40% H_3BO_3, 4) ZnS:Zn phosphor - 80% H_3BO_3.

We tested mechanical mixtures of ZnS:Zn and ZnS:Ag with borax, boron oxide and boric acid with boron concentrations varying in the range from 2 to 7.5%. The grain size of the phosphor and boron containing compound in the mixtures varied from $\leqslant 7$ to 300 μ. The neutron detecting efficiency with a 70 mg/cm^2 thick layer amounted to 1/5 the maximum value attained in preparing the scintillation phosphor by the joint heating technique (the value referred to as unity above).

We also tested detectors prepared by sintering ZnS:Zn and ZnS:Ag with boric acid at a temperature close to its melting point (600-630°). Sintering with ZnS:Ag gives inferior results as compared with ZnS:Zn. With ZnS:Zn and H_3BO_3 taken in the proportion of 2:1, the neutron detecting efficiency is 4 times higher than in the case of corresponding mechanical mixture and equals 0.8 of the maximum (unity) value obtained by the joint heating procedure.

The neutron detecting efficiency is strongly dependent on the surface density d of the layer and the phosphor grain size: η_n increases up to a certain optimum value d_{opt}, depending on the grain size, and then remains virtually

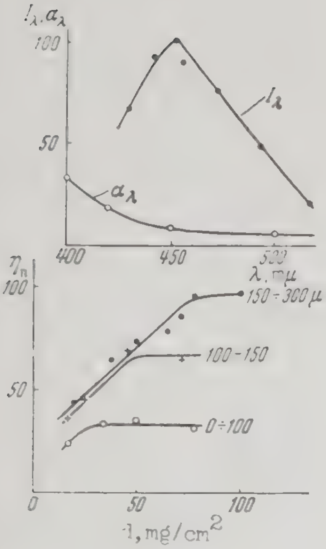

Fig.4

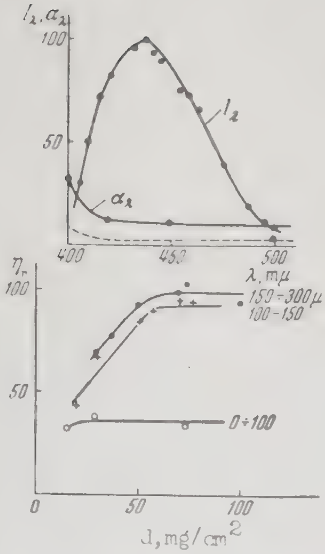

Fig.5

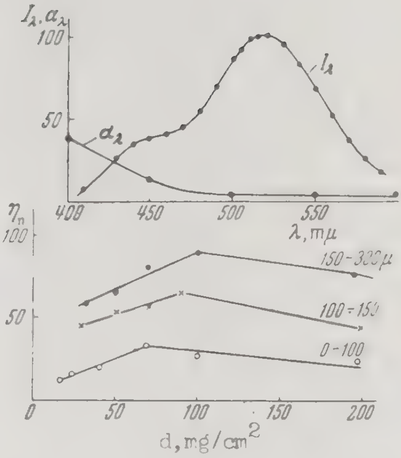

Fig.6

Above - Photoluminescence I_λ and absorption α_λ spectra of phosphors. Below - Variation of the neutron detecting efficiency η_n with the superficial density of the layer for different phosphor grain sizes. Fig.4 - ZnS:Zn; Fig.5 - ZnS:Ag; Fig.6 - ZnS:Cu.

constant or decreases slowly. This will be evident from the η_n vs d curves for ZnS:Zn, ZnS:Ag and ZnS:Cu phosphors reproduced in Figs. 4,5 & 6. The optimum surface density increases with grain size and generally equals 2-3 times the grain diameter for all grain sizes. Apparently, all the light from scintillations in such 2-3 grain thick layers reaches the photomultiplier and is recorded.

As may be seen from the curves in the upper parts of Figs.4,5 & 6, the absorption and emission spectra of our phosphors overlap. The greater the overlapping of the spectra, the greater the opacity of the phosphor layer and hence the smaller the added gain obtained by increasing the grain size if the size is $\geqslant d_{opt}$, so that increasing the grain size above 300 μ proved to be inexpedient. The noticeable decrease in efficiency observed in the case of the ZnS:Cu phosphor with increasing layer thickness above the peak η_n value is connected with decrease in the density of the neutron flux traversing the full thickness of the layer.

As the immersion medium in the suspension tests we used colorless transparent vinylite lacquer with an index of refraction of only 1.47, for it is impossible to find a good medium matching the high index of refraction of zinc sulfide (2.35). Instead of increasing the efficiency, suspending the scintillation phosphor in the lacquer reduces it by a factor of 2-3, the reduction being the greater, the larger the grain size. Apparently, although it enhances the overall optical transparency, the lacquer inactively absorbs the energy of the α-particles moving between the grains and thereby reduces the number and intensity of the scintillations. Use of metallic aluminum and magnesium oxide on the glass as backing for lacquer suspension coatings and for layers of dry powder had little influence (less than 10%) with surface densities $\geqslant$80 mg/cm^2. For thinner layers, aluminum backing proved to be 10-20% better than MgO backing probably due to its more direct reflection.

By way of hollow bodies we tried a hemisphere, a sphere, a cone and a cylinder. Their use increases the absolute neutron count for a given size of the photomultiplier cathode by virtue of collection of scintillations from a larger surface. The increase in the number of counts is not equal to the ratio of the areas of the flat disc and hollow body with an opening equal to the area of the disc, but is smaller since the intensity of scintillation is reduced in the hollow body due to multiple scattering, reabsorption and reflection. The greatest increase in the number of neutron counts is obtained with a sphere or a cylinder; less improvement is obtained with a cone and hemisphere. The efficiency of utilization of the scintillation light is higher for a cylinder than for a sphere; thus our tests showed that a sphere 7 cm in diameter with a 3 cm opening to receive the photocathode increases the count by a factor of 10, whereas the disc-to-interior of the sphere areas are related as 1 to 22, while a cylinder 9.5 cm high and 4.0 cm in diameter, i.e., with a 1 to 10 ratio of the areas, increases the count by a factor of 8. In view of this and considerations of practical convenience, the cylindrical form is to be preferred to the spherical.

We found that our phosphors were somewhat hygroscopic and that the efficiency fell off by 30 to 70% (depending on the flux used in preparation of the phosphor) after exposure for 5 days to an atmosphere of saturated water vapor at room temperature. The decrease in η_n is connected with increased absorption as is evident from Fig.5 where the solid α_λ curve shows the absorption of the ZnS:Ag phosphor after it had absorbed moisture and the dash line shows the absorption of a freshly prepared phosphor. We protected a number of screens against moisture with a coating of lacquer; after which they operated for 2 years without noticeable decrease in efficiency.

In practice we found it convenient to prepare screens of the two types shown in Fig.7. The flat screen consists of a coarse-grained (100-300 μ) phosphor layer with a thickness of 80 mg/cm^2 compressed between a 4 cm diameter glass window and an aluminum backing plate. The cylindrical screen consists of an aluminum cylinder 9.5 cm high and 4.0 cm in diameter coated on the inside with a similar phosphor layer applied as a suspension in a vinylite lacquer and covered with a glass window. Both detectors are designed to be mounted directly over the cathode window of the photomultiplier tube.

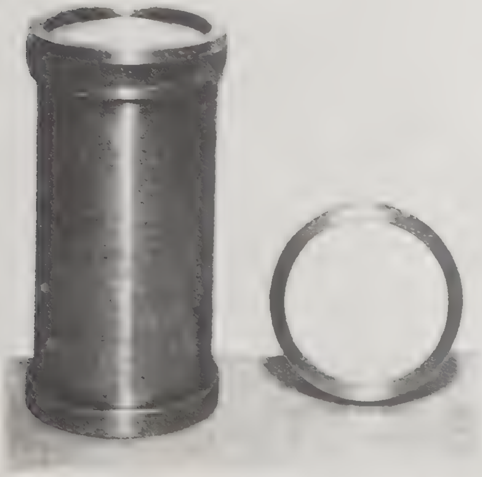

Fig.7. Scintillation screens for detecting slow neutrons: at left - cylindrical screen (inside surface coated with the scintillation phosphor); at right - flat screen.

The neutron counting efficiency of the flat screen was evaluated to be ~5%, while the efficiency of the cylindrical screen was found to be 3 times greater. The neutron counting efficiencies cited by other authors[2,4 & 6] vary between 1 and 6%. The reproducibility of efficiency measurements is ±4% for phosphors, ±2% for flat screens and ±6% for cylindrical screens.

Finally, let us consider the question of the maximum possible counting efficiency of a flat screen. It is known that the boric acid does not enter into the zinc sulfide lattice since it can be washed out with water. Thus a scintillation phosphor consists of a conglomeration of zinc sulfide grains transparent to visible light, coated with a layer of boron oxide; under a microscope the

grains appear completely white, i.e., strongly scattering (the absorption changes very little with introduction of boric acid). The fact that the efficiency varies with the grain size indicates, however, that inside the grains are transparent (if they consisted of a finely dispersive medium like opal glass, the observed size dependence of the efficiency would not obtain). Of the α-particles produced in the boron oxide only those whose energy is absorbed in the zinc sulfide give rise to scintillations. At the optimum proportion of components of 1 molecule of ZnS to 1 molecule of B_2O_3, the probability of excitation of fluorescence is 0.5, inasmuch as an α-particle has an equal chance of being absorbed in a ZnS molecule or in a B_2O_3 molecule. In practice the probability may be assumed equal to 0.4 in view of the observed 2.5 fold decrease in the luminescence brightness as a result of addition of boric acid to a phosphor. Analysis shows that the boron content in the final scintillation phosphor is 7.2%. The theoretical yield of the $B^{10}(n,\alpha)$ reaction, i.e., fraction of incident neutrons absorbed with formation of an α-particle in a layer having a superficial density of 80 mg/cm^2 containing 7.2% boron, is 21.5%. Hence the overall detecting efficiency is 21.5 x 0.4 = 8.6%, i.e., about 9%.

In using phosphor grains 100 to 300 μ in diameter, we reduce the maximum attainable efficiency by about 20%. In addition, we block out a certain number of light pulses. Hence we believe that the counting efficiency of ~5% attained by us is actually the maximum possible efficiency for scintillation phosphors of the given type.

Conclusions

1. We tested three procedures for preparing zinc sulfide base boron-loaded scintillator phosphors for detecting slow neutrons: the joint heating procedure, the mechanical mixture procedure and the sintering procedure. The best results were obtained with the first procedure.

2. The neutron counting efficiency increases with increasing thickness of the phosphor layer and increasing grain size to an optimal value corresponding to a layer equal to 2-3 times the grain diameter.

3. Suspending the scintillation phosphor in a lacquer reduces the detecting efficiency by a factor of 2-3.

4. The neutron count obtained with screens prepared in the form of a hollow body (sphere or cylinder) coated on the inside with a layer of the scintillation phosphor is 8 to 10 times higher than the count obtained with a flat screen.

5. Zinc sulfide scintillation phosphors are hygroscopic and consequently must be protected against moisture.

6. On the basis of our tests we recommend two types of screens: a) a flat screen consisting of a layer of phosphor powder compressed between a glass plate and an aluminum backing and b) a cylindrical screen coated with a layer of phosphor bound in lacquer. The neutron counting efficiency of a cylindrical screen is three times higher than that of the flat screen. The neutron counting efficiency for a flat screen has been evaluated to be ~5%, which according to our estimate is close to the maximum theoretical value.

References

1. A.N.Sevchenko, Izv. AN SSSR, Ser.fiz., 9, 535 (1945).
2. E.Gatti, E.Germagnoli, A.Persano & E.Zimmer, Nuovo Cimento, 9, 1012 (1952); 10, 3, Suppl., 322 (1953).
3. T.Kahan, J.Debiesse, R.Champeix, Bizot,K.Sun & W.Shoupp, J.Phys.et Rad., 9, 25 (1948).
4. P.Koontz, G.Keepin & J.Ashley, Rev.Sci.Inst., 26, 352 (1955).
5. K.Sun & W.Shoupp, Rev.Sci.Inst., 21, 395 (1950).
6. D.Alburger, Rev.Sci.Inst., 23, 769 (1952).
7. C.Palevsky, H.Muether & A.Stolovy, Phys.Rev., 93, 920 (1954).
8. J.Schenck, Nucleonics, 10, 54 (1952).

GROWTH OF SCINTILLATION CRYSTALS BY THE KYROPOULOS PROCEDURE

- L.M.Beliaev, V.P.Panova, V.A.Perl'shtein, V.V.Chadaeva & I.N.Tsigler

In view of the activator-concentration dependence of the luminescence efficiency of alkali halide phosphors (this is particularly strong in the region of low concentrations), any inhomogeneity as regards activator distribution through the crystal seriously impairs its usefulness as a scintillator in nuclear spectrometry. The causes for inhomogeneity of activator distribution are to be sought both in the physical-chemical characteristics of the components from which the crystal is grown and in the distinctive features of the growth process. When the crystals are grown by the Kyropoulos technique, an appreciable portion of the activator is lost by evaporation due to its higher vapor pressure and lower melting point as compared with the other phosphor components. In growing crystals by the Obreimov-Shubnikov procedure there occurs a process akin to zone refining during growth and the activator is forced into the upper part of the crystal. Consequently, neither method allows of obtaining crystals with a truly uniform activator distribution.

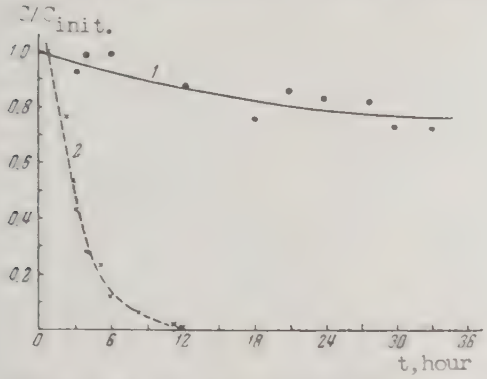

Variation of the activator concentration in a phosphor melt with the time in the furnace: 1) in the hermetically sealed furnace, 2) in an open furnace.

If, however, one increases the activator concentration to say $4\text{-}5\cdot10^{-4}$ TlI per mole NaI in preparing NaI(Tl) phosphor, the variation of fluorescence efficiency with activator concentration becomes virtually unnoticeable. In order to obtain such an activator concentration in a crystal grown by the conventional Kyropoulos technique one must introduce as much as 3% activator into the initial batch which greatly hampers the crystal growth particularly at the initial stages. An obvious remedial measure is to take steps to reduce the activator loss due to evaporation.

To this end we designed a hermetically sealed furnace. The cover of the furnace is equipped with a window through which one can observe the crystal growth without disturbing the seal. We measured the activator loss in such a furnace using radioactive thallium. The activator loss from such a furnace is compared with the loss from a conventional open furnace in the accompanying figure. It will be seen from the curves that almost all the activator initially present is volatilized from an open crucible within 12-15 hours, whereas the activator concentration fell off by only 2% after a period of 32 hours in the case of our sealed furnace. Taking this into account, we proportioned the initial batch so that the amount of activator present would be great enough for any inhomogeneity of its distribution not to have a noticeable effect on the efficiency of the crystal.

Sealing off the furnace volume also has the advantage of preventing contact of the melt with atmospheric moisture, thereby obviating the formation of alkali compounds which frequently give rise to opaque regions in the crystal. Reducing the activator loss makes it possible to grow sodium iodide crystals of large size. We have prepared and tested scintillators made from crystals grown in our furnace by this modified Kyropoulos technique.

Crystals 55 to 80 mm in diameter and 35 to 45 mm in length excited by the radiation from Cs^{137} and viewed by an FEU-24 photomultiplier yielded an amplitude resolution of 8.5 to 11%.

Institute of Crystallography,
Academy of Sciences of the USSR

ON THE USE OF DOMESTIC PHOSPHORS FOR SCINTILLATION COUNTING (Abstract)

- A.N.Prisarevskii & E.D.Teterin

We investigated NaI(Tl) crystals of domestic manufacture (Institute of Crystallography, VIMS, Kharkov Chemical Reagents Plant) and found that they have satisfactory spectrometric properties and yield a resolution not inferior to 12% (as low as 8% for the best samples) for the 660 kev γ-line of Cs^{137}. With CsI(Tl) crystals we obtained a resolution of 10-11%. The decay time of the CsI(Tl) phosphor is 1.2-1.5 microsec. When stored for a prolonged period or exposed to radioactive radiations the crystals become colored red and the luminescence decay time is increased to 2.5 microsec.

We carried out preliminary studies with a view to finding efficient crystals for detecting neutrons (both slow and fast). At our request N.I.Bispen grew LiF crystals with different activators (Tl, Ti, Sn, Eu, Mn, etc.). Unfortunately, impurities are not readily incorporated into LiF. Of the different activators tried, it proved possible to introduce only Ti and Sn in any appreciable quantity. With titanium in LiF the intensity of the scintillations was only about 1/30th the intensity in NaI(Tl) with irradiation by γ-rays of the same energy. In the case of introduction of Sn the flashes were 2-2.5 times stronger than with Ti. In both cases the decay times were less than 2 microsec. Obviously, in both these cases the amount of activator introduced were far below the optimal. This research is being continued.

I.V.Stepanov presented us with BaF_2 crystals (without activator) grown by him. These crystals are of interest from the standpoint of detection of fast neutrons. According to preliminary measurements, the intensity of the scintillations in BaF_2 equals 12-15% of the intensity in NaI(Tl). This result is rather hopeful and work in this direction will be continued. We also tested CaF_2(Eu), CaF_2(Ce) and CaF_2(Gd) crystals. The first two gave scintillation having some 8-10% the intensity of the scintillations in NaI(Tl), while the CaF_2(Gd) yielded appreciably weaker scintillations. The decay constants of both the BaF_2 and the activated CaF_2 crystals were less than 1 microsec. We hope that further work with these phosphors will lead to the development of effective neutron detectors.

IMPURITY QUENCHING OF THE PHOTOLUMINESCENCE OF STILBENE

- A.P.Kilimov & N.P.Shimanskaia

Trans-stilbene (I), which has recently acquired a certain importance as a luminescent material, may contain a number of impurities forming in the process of synthesis. Among such associated or secondary materials are benzoin (II), desoxybenzoin (III), hydrobenzoin (IV), phenylbenzylcarbinol (V), 1,2 dibenzylpinacol (VI), 1,2 diphenylethane (VII) and phenanthrene (VIII):

I
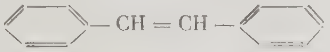

V
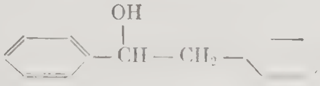

II
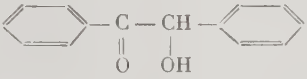

VI
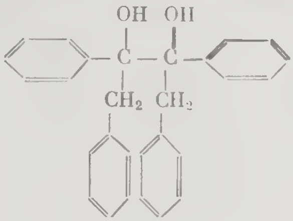

III
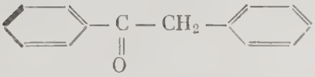

VII
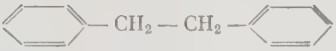

IV
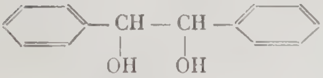

VIII
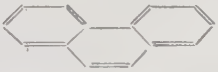

The influence of the listed substances on the luminescence of stilbene in solid state has not been studied although it is of obvious interest to know their effect, if only to specify the requisite degree of purity of the stilbene.

We investigated the relative photoluminescence efficiency of stilbene powder as a function of the impurity concentration where the above listed substances, except V, are concerned.

The influence of phenylbenzylcarbinol (V) on the luminescence of stilbene was not investigated since this compound is relatively unstable and upon heatint readily transforms into stilbene. All the materials were purified by 3-4 fold crystallization, the criterion for sufficient purification being no increase in the melting point upon repeat recrystallization. The stilbene used for preparing the samples was purified by the chromatographic procedure.

The experimental procedure was the following. A weighed amount of stilbene together with a certain amount of the investigated impurity was melted in a test tube, the melt thoroughly shaken and then rapidly cooled. The resultant sample was then ground and the powder sieved to obtain the desired grain size. Preliminary tests showed that the optimal grain size is 0.1 mm. Use of fine grains of this size reduces the distortion of the luminescence measurements due to reabsorption.[1-2]

The luminescence was excited by the 3650 Å line of mercury from a UO-1 ultraviolet source.

The luminescence intensity of the stilbene samples containing known amounts of the various impurities were compared on a universal UF-1 photometer with the intensity of a sample obtained by melting, grinding and screening pure stilbene. Since we compared the luminescence intensities in the region of the luminescence peak of stilbene, the experimental intensity ratio was equal

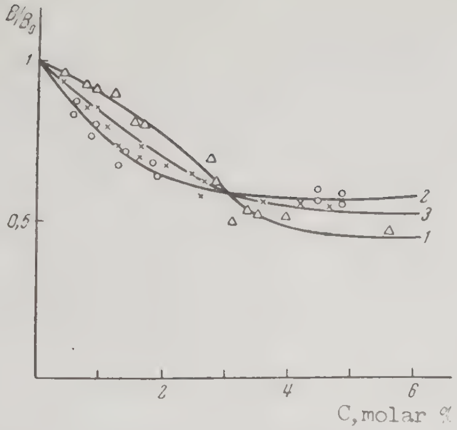

Fig.1. Variation of the relative quantum efficiency of photoluminescence of stilbene with the impurity concentrationL 1) benzoin, 2) hydrobenzoin and 3) desoxybenzoin.

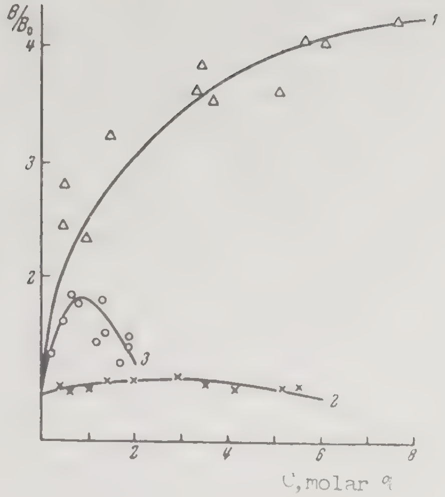

Fig.2. Same as Fig.1, but for 1) phenanthrene, 2) 1,2 diphenylethane, 3) 1,2 dibenzylpinacol.

to the ratio of the quantum efficiencies of the pure stilbene and impurity containing samples (B/B_0).

The variation of the ratio B/B_0 for samples of stilbene with different impurities as a function of the impurity concentration (C) is shown in Figs.1 & 2. As will be evident from an examination of the curves that benzoin, hydrobenzoin and desoxybenzoin even at low concentrations exhibit an appreciable quenching influence on the luminescence of stilbene. Up to a concentration of 3 molar percent of the impurity the quenching is strongly dependent on the impurity concentration; at higher concentrations there is little further increase in quenching.

The influence of the other three impurities proved to be far different. It will be evident from the curves of Fig.2 that 1,2 diphenylethane, 1,2 dibenzylpinacol and phenanthrene enhance the luminescence significantly. In the case of phenanthrene there is observed a continuous increase (true, at a gradually slower rate) of the luminescence up to a concentration of 9-10 molar percent.

At first, 1,2 diphenylethane and 1,2 dibenzylpinacol yield a sharp increase in the luminance with increasing concentration. With increasing concentration, however, appreciable quenching develops. This effect is apparently connected with concentration self-quenching of the impurity dissolved in the stilbene.

With a view to determining the nature of the influence of these impurities on the photoluminescence of stilbene we recorded the luminescence spectra of pure stilbene, phenanthrene and 1,2 diphenylethane and the emission spectra of samples of stilbene containing certain amounts of substances II, III, IV, VI and VII and VIII. The set-up used for recording the spectra consisted of a source (a PRK-4 mercury tube), a sample holder and a Zeiss glass optics spectrograph. The components were arranged in the conventional order.[3] The comparison source was a calibrated incandescent bulb. The spectrograms were processed on an MF-4 microphotometer.

The photometric curves are shown in Figs.3 through 7. As will be evident from Fig.3 the shape of the spectral curves for stilbene with benzoin and with hydrobenzoin differs little from that for pure stilbene: the long wavelength

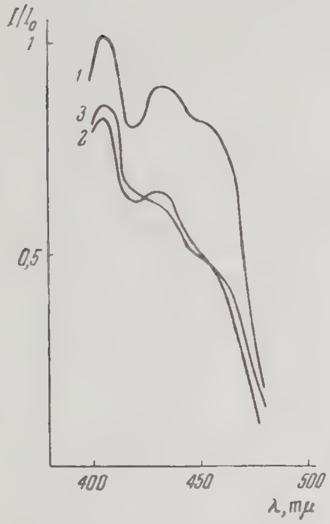

Fig.3. Luminescence spectra of 1) pure stilbene, 2) stilbene + + 0.009% hydrobenzoin, 3) stilbene + 0.007% benzoin.

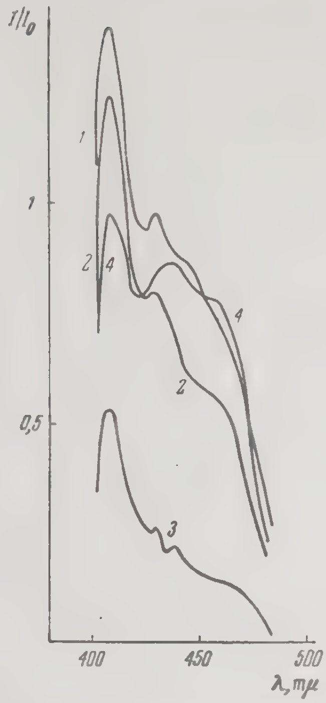

Fig.4. Luminescence spectra of 1) pure stilbene, 2) 1,2 diphenylethane, 3) stilbene + + 0.005% 1,2 diphenylethane, 4) stilbene + + 0.015% 1,2 diphenylethane.

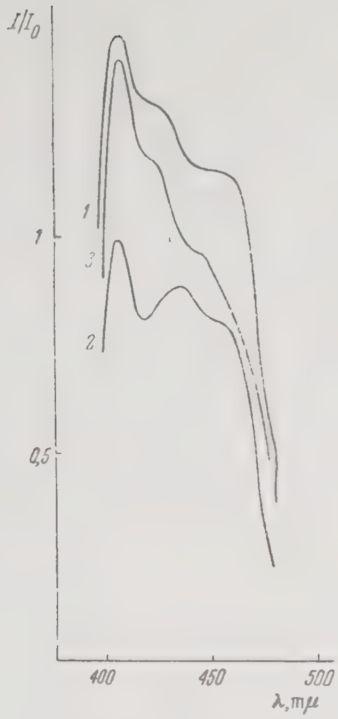

Fig.5. Luminescence spectra of 1) pure stilbene, 2) stilbene + + 0.002% 1,2 dibenzylpinacol, 3) stilbene + + 0.006% 1,2 dibenzylpinacol.

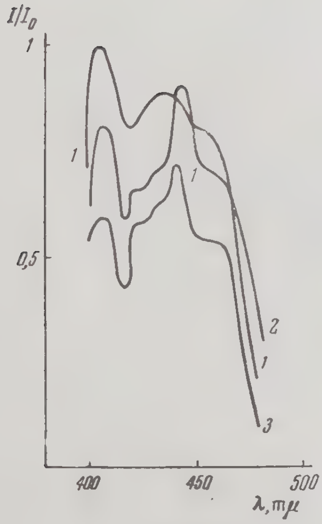

Fig.6.

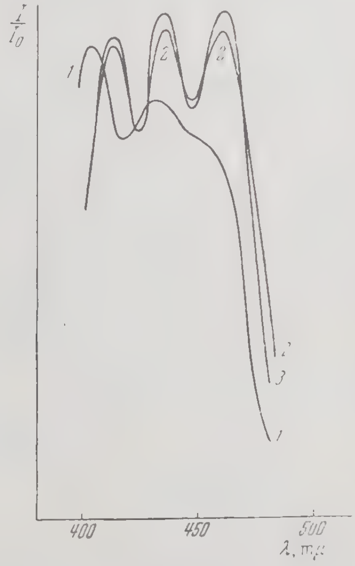

Fig.7.

Fig. 6. Luminescence spectra of 1) pure stilbene, 2) stilbene + 0.011% desoxybenzoin, 3) stilbene + 0.032 % desoxybenzoin.

Fig.7. Luminescence spectra of 1) pure stilbene, 2) phenanthrene, 3) stilbene + 0.005% phenanthrene. All percentages in captions of Figs.3 through 7 are molar.

peak remains in the same position. Consequently, in this case we have the usual luminescence of stilbene weakened by the quenching influence of the impurities.

In the case of 1,2 diphenylethane (Fig.4) and 1,2 dibenzylpinacol (Fig.5) the position of the principal maximum at 405 mμ also coincides with its position for pure stilbene. One cannot draw any unambiguous deductions from the experimental results regarding the character of the enhanced luminescence produced by the addition of these substances to stilbene, particularly since there is no basis for assuming any appreciable excitation energy transfer to the impurities.

The luminescence spectra of stilbene with desoxybenzoin (Fig.6) have a clearly pronounced peak at 442 mμ which does not appear in the spectrum of stilbene. In this case it may be deduced from the shape of the spectral curve that there may be transfer of excitation energy from the stilbene molecules to the desoxybenzoin molecules. The energy transfer at the investigated impurity concentrations is not complete, however, as is evident by the persistence of the principal maximum of stilbene at 405 mμ and the weaker stilbene peaks at 435 and 460 mμ.

It may be assumed that the excitation energy is emitted partly in the form of luminescence by the stilbene particles and is partly transferred to the desozybenzoin molecules. Apparently, the quantum efficiency of desoxybenzoin is rather low so that the energy emitted by the desoxybenzoin molecules in the form of luminescence amounts to only a fraction of the energy transferred to them from the stilbene molecules. Consequently, there is observed a general reduction of the luminescence intensity of stilbene upon the addition of desoxybenzoin.

Highly characteristic results were obtained for the mixture of stilbene with phenanthrene. The luminescence spectrum of phenanthrene, shown in Fig. 7, has three clearly pronounced peaks at 412, 435 and 460 mμ. As a whole, this spectrum is displaced to the long wavelength side relative to the luminescence spectrum of stilbene and the long wavelength peaks have an appreciably greater intensity than the corresponding sections of the stilbene spectrum.

The luminescence spectrum of the mixture of stilbene with phenanthrene faithfully repeats the luminescence spectrum of phenanthrene. This clearly indicates that at low phenanthrene concentrations there is virtually complete transfer of the excitation energy from the stilbene to the phenanthrene. The marked increase in emission in such systems is due to sensitized luminescence.

A significant factor here is the closer coincidence of the luminescence spectrum of phenanthrene with the spectral sensitivity curve of the human eye, as a result of which in measurements by means of the universal (visual comparison) photometer there are obtained higher values than as are yielded by objective spectrographic measurements.

As for the mechanism of excitation energy transfer in the given compounds, it may be assumed that the principal role here is played by nonradiative transfer just as in the case of mixed anthracene-naphthacene, naphthalene-anthracene and similar crystals.[4,5]

Conclusions

1. We investigated the influence of benzoin, desoxybenzoin, hydrobenzoin, 1,2 dibenzypinacol, 1,2 diphenylethane and phenanthrene on the luminescence of stilbene. Benzoin, desoxybenzoin and hydrobenzoin, i.e., compounds containing carbonyl or hydroxyl radicals, were found to exert a quenching effect.

2. 1,2 Diphenylethane, 1,2 diphenypinacol and phenanthrene- substances capable of luminescing themselves - strengthen the luminescence of stilbene.

3. At high concentrations of 1,2 dibenzylpinacol and 1,2 diphenylethane quenching sets in; this is appreciably stronger in the case of oxygen-containing 1,2 dibenzylpinacol.

4. From a comparison of the luminescence spectra of pure stilbene and stilbene doped with phenanthrene and desoxybenzoin, it may be concluded that in the case of these impurities there occurs significant energy transfer from the stilbene molecules to the impurity molecules.

5. No significant changes in the luminescence spectra were observed incident to the addition of benzoin and hydrobenzoin to stilbene.

6. The changes occurring in the spectrum of stilbene upon the addition of 1,2 dibenzylpinacol and 1,2 diphenylethane are not sufficiently clear-cut to allow of any deductions regarding the processes responsible for the enhanced luminescence produced by the addition of these compounds.

Kharkov Branch of the
All-Union Scientific Research Institute of Chemical Reagents

References

1. J.B.Birks & T.Wright, Proc.Phys.Soc., B 67, 657 (1954).
2. A.P.Ivanov, Zhur.eksp.i teor.fiz., 26, 275 (1954).
3. V.L.Levshin, Fotoliuminestsentsiia zhidkikh i trerdykh veshchestv (Photoluminescence of liquids and solids) M.-L., 1951.
4. I.Ia.Faidish & A.N.Kucherov, Dopoviki (Reports) AN Ukrainian SSR, 1, 57 (1956).
5. G.C.Wolf, ZS.,f.Physid, 145, 116 (1956).

MIGRATION AND TRANSFER OF ELECTRON EXCITATION ENERGY IN ANTHRACENE AND NAPHTHALENE CRYSTALS

- I.Ia.Kucherov & A.N.Faidysh

Introduction

Efficient transfer of electron excitation energy from the host material to certain impurities has been observed in the crystals of a number of aromatic compounds. Some of the characteristics of this energy transfer as well as the splitting of the absorption bands of molecular crystals into a number of bands of unlike polarization[8-10] indicate that in crystals of the given type a significant role is played by nonradiative migration of electron excitation energy (excitons) in the crystal lattice. Energy migration is undoubtedly also important in scintillation processes.

The transfer of energy in anthracene crystals doped with naphthacene and in naphthalene crystals doped with anthracene under photoexcitation has been investigated under different conditions in our laboratory.

All of the samples were prepared by vacuum melting of the appropriate pure materials. The specimens were kept and tested in evacuated vessels in order to obviate photo-oxidation.

The luminescence intensity was measured photoelectrically on a set-up incorporating an electrometer amplifier. In most instances the investigations were performed with total absorption and under identical geometrical conditions, so that the measured luminescence intensities could be used to determine the relative quantum efficiencies.

Concentration dependence of the luminescence yield

The incorporation of naphthacene into an anthracene crystal or of anthracene into a naphthalene crystal strongly reduces the luminescence yield of the host material and enhances the luminescence of the impurity.

Fig.1 shows the concentration dependences obtained at room temperature for the quantum yields of anthracene-naphthacene crystals ($d \approx 0.5$ mm) and powder ($\sim$ 1-3 μ particles) in the case of excitation by 365 mμ light. The quantum yield of pure anthracene is taken as unity. It may be noted that our concentration dependence curves are generally similar to those obtained by Bowen[3].

The quantum yields of the host material and of the impurity become equal at a $2 \cdot 10^{-5}$ mole/mole concentration of naphthacene. Our calculations show that at this concentration the absorption of anthracene luminescence by naphthacene cannot account for the transfer of more than 1-2% of the total excitation energy of the anthracene molecules. Therefore the observed considerable transfer of energy from anthracene to naphthacene must be due almost entirely to migration of excitons in the anthracene crystal and their capture by naphthacene molecules.

The concentration dependence curves for the naphthalene-anthracene system are shown in Fig.2. In this system equality of the quantum yields of the host material and impurity occurs at an anthracene concentration of $4.3 \cdot 10^{-5}$ mole/mole. Here the energy transfer efficiency is considerably lower than in anthracene-naphthacene.

Influence of crystal size on the energy transfer efficiency

It was shown in an earlier contribution[7] that the efficiency of energy transfer from anthracene to naphthacene is considerably lower in the powder than in crystals (~0.5 mm). The variation of energy transfer efficiency over

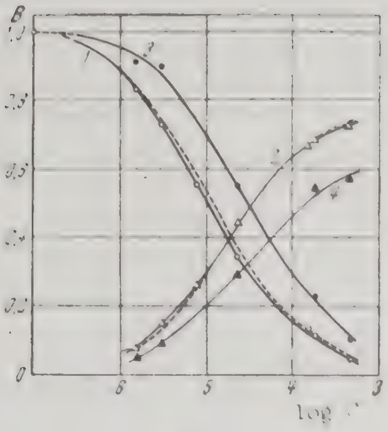

Fig.1

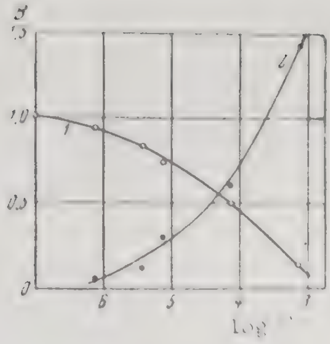

Fig. 2

Fig.1. Variation of the luminescence quantum yield of crystal (○ and △) and powdered (● and ▲) mixtures of anthracene and naphthacene with the concentration of the second component: 1 & 3) anthracene host; 2 & 4) naphthacene host. Crystal thickness 0.5 mm; powder grain size 1-3 μ. Dash lines - theoretical curves.

Fig.2. Same as Fig.1 but for crystals of naphthalene containing anthracene: 1 - naphthalene host; 2 - anthracene host.

a range of specimens from thick crystals to thin films was later investigated in our laboratory at room temperature with 365 mμ excitation. It appeared that for a naphthacene concentration of about $2 \cdot 10^{-4}$ mole/mole the reduction of crystal thickness from 200 μ to 1 μ results in a reduction of the ratio of quantum yields of naphthacene and anthracene (B_n/B_a) by a factor of about three, while a reduction of crystal thickness from 1 μ to 0.2 μ decreases the ratio by a factor of 3 to 3.5. The relatively slow decrease of B_n/B_a as the thickness is reduced to 1 μ and the rapid falling off of this ratio below 1 μ indicate that there exist two different factors affecting the efficiency of energy transfer.

Investigations[12-15] of the luminescence spectra of anthracene crystals have shown that anthracene reabsorbs a very appreciable fraction of its luminescence. Our measurements show that in 0.5 mm diameter crystals the non-reabsorbed fraction of photons is only 0.27. In the case of thin films (1.5 to 0.3 μ) the effect of reabsorption becomes insignificant.

These investigations give reason to infer that the decrease of energy transfer efficiency as we go from thick crystals ($d \approx 0.5$ mm) to thin films of the order of 1 μ is due mainly to diminished reabsorption. Reabsorption means that some of the excitons that ended their lives radiatively in host molecules are regenerated through the absorption of short-wavelength photons. Thus reabsorption increases the effective lifetime of excitons and accordingly extends the luminescence decay time. The reality of the latter effect is substantiated by the measurements of Dirks & Little[16] and Wright[14]. Energy transfer from the host to the impurity will evidently become more efficient as the lifetime of excitons increases.

Since for films thinner than 1 μ reabsorption is insignificant, it is clear that the sharp decrease of B_n/B_a with the reduction of film thickness below 1 μ has a different cause, namely, limitation of exciton mean free path. As the film thickness is reduced, an increasing number of excitons will reach the film surfaces, where most of them will undergo radiative recombination in molecules of the host material. Therefore reduction of the film thickness results in a decrease of the quantum yield ratio B_n/B_a.

Dependence of B_n/B_a on the absorption of the exciting light

As the absorption coefficient of the exciting light increases, the depth at which excitons are generated will decrease, with a consequent increase of the probability that the excitons will emerge to the surface. Since excitons which reach the surface will for the most part terminate radiatively in host molecules, increase of the coefficient of absorption of the exciting light must be associated with an increase of the quantum yield of the impurity. We have in fact observed this effect.

Investigations of the dependence of the quantum yield of thick crystals on the absorption coefficient were performed under excitation by the 365, 313 and 405 mμ Hg lines. The results are shown in Table 1, where B_a is the quantum yield of anthracene for the naphthacene concentration $C_{n1} = 2.3\cdot10^{-5}$ mole/mole and B_{n1} and B_{n2} are the quantum yields of naphthacene when the concentrations of the latter are $C_{n1} = 2.3\cdot10^{-5}$ and $C_{n2} = 1.8\cdot10^{-4}$ mole/mole, respectively.

Table 1

Quantum yields of anthracene and naphthacene with excitation by different Hg lines

Absorption coefficient, cm^{-1}	Quantum yield					
	Measured			Calculated		
	B_a	B_{n_1}	B_{n_2}	B_a	B_{n_1}	B_{n_2}
$K_{365} = 3,1\cdot10^4$	0,34	0,44	0,68	0,375	0,44	0,68
$K_{313} = 0,73\cdot10^4$	0,325	0,49	0,72	0,345	0,52	0,73
$K_{405} = 0,43\cdot10^4$	0,31	0,51	0,77	0,34	0,53	0,74

An analagous effect was observed by Wright[17], who found that when a quenching agent is present on the surface of an anthracene crystal, the luminescence quantum efficiency of a pure anthracene crystal diminishes as the absorption coefficient of the light increases.

Effect of a second impurity on the efficiency of energy transfer

Lattice defects must necessarily curtail the exciton mean free path. Therefore the introduction of a second impurity into a crystal must reduce the lifetime of excitons and thereby lower the efficiency of energy transfer from the host material to the first activator impurity. We have investigated the energy transfer to naphthacene in an anthracene crystal when naphthalene was added as a second impurity. Naphthalene is nonabsorbing in the investigated spectral region.

Table 2 shows the determined values of B_n/B_a for different concentrations of naphthalene in thick crystals at room temperature. Crushing the crystals to a powder and lowering the temperature result in a considerable reduction of the influence of the second impurity (naphthalene).

Table 2

Naphthacene concentration, %	Yield ratio B_n/B_a at indicated naphthalene concentration, %			
	0	1	5	10
$6\cdot10^{-4}$	0,64	0,50	0,39	0,32
$6\cdot10^{-3}$	5,8	4,6	2,9	1,9
$6\cdot10^{-2}$	35,0	27,5	20,0	14,9

The hypothesis that the exciton lifetime diminishes when an impurity is added has been confirmed by direct experiments.[18,6]

Temperature dependence of the quantum yields of the host and impurity

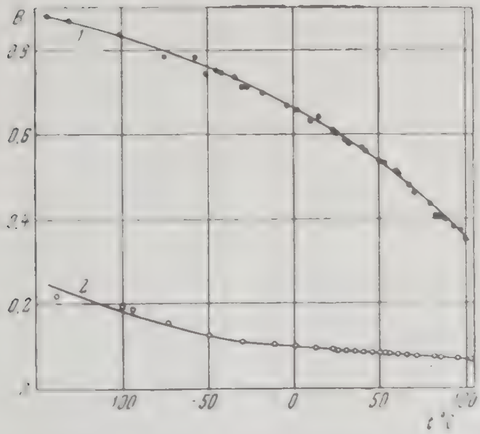

Fig.3. Temperature dependence of the luminescence yield of anthracene: 1) pure anthracene and 2) anthracene containing $1.5 \cdot 10^{-4}$ mole/mole of naphthacene.

The influence of temperature on the luminescence of anthracene crystals was investigated in the temperature range +100° to -140° for pure anthracene and for anthracene containing naphthacene in concentrations of $1.5 \cdot 10^{-6}$, $7.8 \cdot 10^{-6}$, $2.3 \cdot 10^{-5}$ and $1.5 \cdot 10^{-4}$ mole/mole.

Fig.3 shows the temperature dependence of the luminescence yield of anthracene for pure anthracene and for anthracene containing $1.5 \cdot 10^{-4}$ mole/mole naphthacene. It will be seen that the dependences are quite different. With a naphthacene concentration of $1.5 \cdot 10^{-4}$ mole/mole, heating from 30° to 100° reduces the anthracene yield less by a factor of 1.7 than in the case of pure anthracene. This reduction of temperature quenching upon the addition of naphthacene is evidently associated with a decrease of the exciton lifetime (Ref.6, 18). When anthracene crystals containing naphthacene are cooled from -10° to -140° the quantum yield of the anthracene increases considerably more rapidly than for pure anthracene. This rapid rise of the luminescence yield is evidently due to the fact that energy transfer from anthracene to naphthacene is considerably reduced at lower temperatures.

The temperature dependence of the luminescence yield of naphthacene was investigated with excitation by light which is absorbed only by naphthacene (436 mμ) and by light which is absorbed by anthracene (365 mμ). The luminescence intensities of naphthacene excited by the 436 and 365 mμ lines were arbitrarily equated at 100°. The luminescence of naphthacene excited by 436 mμ is enhanced monotonically by cooling (Fig. 4). The temperature dependence with 365 mμ excitation is entirely different. Curve 2 shows that at about -40° the quantum yield passes through a maximum, which results from two effects: 1) less quenching in the naphthacene molecule at lower temperatures, and 2) reduced efficiency of energy transfer at lower temperatures.

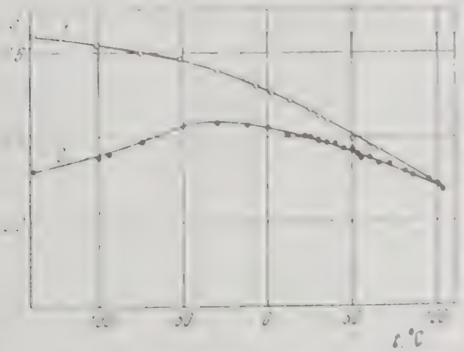

Fig.4. Temperature dependence of the luminescence yield of naphthacene excited by 1) 436 mμ and 2) 365 mμ light.

Reducing the crystal size slows down the decrease of the quantum yield of naphthacene cooled below -40°. The observed decrease in energy transfer efficiency as a result of cooling is presumably due largely to a decrease in reabsorption (Ref. 15).

The decrease of reabsorption leads, as was shown above, to a reduction of energy transfer and of the effective exciton lifetime. Liebson[19] observed a reduction of the luminescence decay time of anthracene crystals as a result of cooling.

Basically similar effects are observed in the naphthalene-anthracene system, although there are considerable quantitative differences from the anthracene-naphthacene system. For example, the temperature dependence of the quantum yield of anthracene as an impurity in naphthalene shows only a broad plateau in the temperature interval -20° to -90° instead of a maximum. For the naphthalene-anthracene system, as was shown in Ref.20, we must take into account the luminescence of the anthracene itself as a result of direct absorption of the incident light.

Calculation of the dependence of quantum yields on impurity concentration and the absorption coefficient for the exciting light

We can now regard it as established that in a number of organic crystals (anthracene, naphthalene, etc.) the primary role in energy transfer is played by excitons. In view of the high efficiency of energy transfer from the host crystal to certain impurities, we can conclude that the excitons pass through tens of thousands of host molecules. It can naturally be assumed that the entire path of an exciton is not a straight line, particularly in the presence of strong molecular vibrations. If the mean free rectilinear path of the excitons is considerably shorter than the total mean free path, the motion of the excitons can be regarded as a diffusion process. This has been assumed in a number of articles (Refs.6,7,21,22). The exciton diffusion equation is

$$D\frac{d^2 f(x)}{dx^2} + \Phi_0 e^{-Kx} - f(x)p = 0,$$

where $f(x)$ is the exciton concentration, D is the exciton diffusion coefficient, Φ_0 is the number of excitons produced per unit volume per second at $x = 0$, K is the coefficient of absorption of the exciting light and p is the combined probability (per second) of exciton disappearance through emission in the host material, trapping by an impurity and quenching.

For thick crystals we can consider[7] the back surface of a crystal to be located at infinity. Excitons that do reach the surface are trapped there[23], so that the boundary conditions can be written as

$$f(\infty) = 0 \text{ and } f(0) = 0.$$

The solution of the diffusion equation gives the exciton distribution function in the crystal. Knowing this function, we can calculate the quantum yields of the host crystal and of the impurity[7,22]. For the quantum yield of the impurity, we obtain

$$B_n = \frac{A_n \cdot C_n}{(\sqrt{1 + \gamma C_n} + l_0 K)\sqrt{1 + \gamma C_n}},$$

where A_n is a constant, C_n is the naphthacene concentration, γ is the ratio of the probability of exciton capture by a unit impurity concentration to the probability of exciton disappearance in the host material and $l_0 = \sqrt{D/p}$ is the exciton diffusion length in a pure anthracene crystal.

The quantum yield of the host crystal is

$$B_a = \frac{1}{\sqrt{1+\gamma C_n} + l_0 K}\left[\frac{A_a}{\sqrt{1+\gamma C_n}} + \rho l_0 K\right];$$

where A_a and ρ are constants.

These formulas characterize the dependence of the luminescence yields on the concentration and on the absorption coefficient. In calculating the concentration dependence of the quantum yields we assumed the following values of the constants:

$$A_n = 7.9 \cdot 10^4,\ \gamma = 10^5,\ l_0 = 1.5 \cdot 10^{-5}\ \text{cm},\ A_a = 1.1 \text{ and } \rho = 0.54.$$

As may be seen from Fig.1, the theoretical curves are in good agreement with experiment.

The dependence of quantum yields on the absorption coefficient was calculated without introducing additional constants. Table 1 shows that the theory correctly indicates the form of the dependence of the quantum yields of both the host material and the impurity on the absorption coefficient and also shows how the observed effect depends on the impurity concentration. In view of the approximate character of the theory and the inaccuracy of the experimental results, the agreement between theory and experiment may be regarded as entirely satisfactory.

In order to obtain the correct concentration dependence of quantum yields it was necessary to set l_0 equal to 0.15 μ. This may be regarded as the approximate exciton diffusion length in anthracene crystals.

In the foregoing calculations we have not taken into account reabsorption and the possibility that two types of excitons exist. A theory which includes these factors is given in Refs.24 and 25.

"T.G.Shevchenko" Kiev State University

References

1. A.N.Terenin, Usp.fiz.nauk., 43, 347 (1951).
2. A.N.Terenin & V.L.Ermolaev, Usp.fiz.nauk., 58, 37 (1956).
3. E.Bowen, E.Mikiewicz & F.Smith, Proc.Phys., A62, 26 (1949).
4. D.Northrop & O.Simpson, Proc.Soc., 234, 136 (1956).
5. O.M.Faidish, Doklady AN Ukrainian SSR, 3, 215 (1953).
6. M.D.Galanin & Z.A.Chizhikova, Opt.i spektr., 1, 175 (1956).
7. I.Ia.Kucherov & O.M.Faidish, Doklady AN Ukrainian SSR, 1, 61 (1956).
8. I.V.Obreimov & A.F.Prikhot'ko, in Symposium in "Memory of S.I.Vavilov", M.-L., 1952.
9. A.S.Davydov, Teoriia pogloshcheniia sveta v molekuliarnykh kristallakh (Theory of light absorption in molecular crystals), Kiev, 1951.
10. A.F.Prikhot'ko, Trudy (Transactions) Institute of Physics, Ukrainian SSR Acad. of Sci., 6, 43 (1955).
11. A.N.Faidysh, I.Ia.Kucherov & A.Ia.Terskoi, Opt.i spektr., 1, 403 (1956).
12. J.B.Birks & G.T.Wright, Proc.Phys.Soc., B 67, 657 (1954).
13. M.D.Galanin & Z.A.Chizhikova, Zhur.eksp.i teor.fiz., 26, 224 (1954).
14. G.T.Wright, Proc.Phys.Soc., B 68, 241 (1955).
15. I.Ia.Kucherov, O.M.Faidish & Z.M.Fesenko, Naukovi povidomlennia KDU, Fizika (Scientific Notes, Kiev State University, Physics), 1, 23 (1956).
16. J.B.Birks & W.A.Little, Proc.Phys.Soc., 66, 921 (1953).
17. G.T.Wright, Proc.Phys.Soc., B 68, 701 (1955).
18. A.Schmillen, L.Smillen & F.Ronde, ZS.Naturforsch, 8a, 213 (1953).

19. S.H.Liebson, Nucleonics, 10, 41 (1952).

20. F.Lipsett & A.Dekker, Nature, 173, 4407 (1954).

21. V.E.Loshkarev & Iu.I.Karkhanin, Doklady AN SSSR, 101, 829 (1955).

22. V.M.Agranovich, I.Ia.Kucherov & A.N.Faidish, Naukovi povidomlennia KDU Fizika (Scientific Notes, Kiev State University, Physics), 1, 25 (1956).

23. A.S.Selivanenko, Izv.AN SSSR, Ser.fiz., 20, 383 (1956). (Trans., Bulletin, 20, No.4, 348.)

24. V.M.Agranovich & A.N.Faidish, Opt.i spektr., 1, 885 (1956).

25. V.M.Agranovich & A.N.Faidish, ibid., 1, 983 (1956).

PLASTIC SCINTILLATORS

- I.M.Rozman

1. Development of plastic scintillators (hereinafter PS) began in 1950. In the first publication on the subject Schorr & Tornay[1] reported that polymerization of a solution of p-terphenyl in styrene yields scintillators suitable for detecting ionizing radiation. Of the various preparation procedures tested by these investigators, the best scintillation phosphor was obtained by low temperature polymerization of styrene with 1% benzoyl peroxide as catalyst. Plastic scintillators were successfully prepared by this procedure with anthracene, stilbene[2] and other materials[3]. The luminescence yield amounted to approximately 10% of that of pure crystalline anthracene. PS having a higher efficiency (~ 30%) were obtained by Pichat & Koechlin[4] using 1, 1', 4, 4' tetraphenylbutadiene as the additive to styrene.[4] In recent years a large number of different luminescing organic materials have been tried for preparing PS based on polystyrene, polyvinyltoluene and other polymers, singly or in combination.[5-8] The best PS have a radioluminescence efficiency equal to about 50% that of anthracene; thus, for example, scintillators with 0.04 g/g p-terphenyl and 0.002 g/g tetraphenylbutadiene (or 0.002 quaterphenyl) in polyvinyltoluene have an efficiency equal to 47% that of anthracene;[4] scintillators with 0.04 g/g p-terphenyl and 0.001 g/g p,p'-diphenylstilbene in polyvinyltoluene have an efficiency of 51%.[9]

In addition to polymerization, a number of other procedures have been tried for preparing PS; these are primarily based on fusing a technical polymer with the luminescing material.[10,11] As a rule these scintillators have a lower efficiency than those prepared by polymerization.

2. Polymerization procedures used for preparing PS may be divided into three groups: a) polymerization at a low temperature (50°) in the presence of a catalyst;[8] b) polymerization at medium temperatures (~140°) without a catalyst but over a prolonged period (several days);[6] and c) polymerization at a high temperature (200°) without a catalyst for a period of 12-15 hours.[5] A considerable increase in the luminescence efficiency in all cases is obtained by preliminary elimination of the oxygen dissolved in the solution subjected to polymerization.[5,6] Thermal polymerization at low pressure is favored for preparing PS of large size.[5,12,13] Scintillators of almost any desired shape and of very large size can be prepared by casting the luminescent plastic. Experiments in our laboratory showed that the decrease in luminescence due to this treatment does not exceed 10%. Pichat et al[8] have prepared PS loaded with up to 9% by weight lead and bismuth.

3. There have been numerous studies of the luminescence of PS under excitation by ionizing radiation. The principal results of these studies are the following. The scintillation spectrum of PS corresponds to the fluorescence spectrum of the impurity rather than to that of the host material.[2,3,5,6,8] The technical (or external) absolute luminescence efficiency as determined by measurements of the brightness of the individual scintillations or of the mean fluorescence intensity increases with increasing activator concentration, attaining a maximum at 1 to 4% activator by weight.[5,6,8,14] In ternary systems consisting of the host plastic and two additives - the second impurity or so-called spectrum shifter in the amount of 0.01 to 0.2% - the luminescence spectrum corresponds to the emission spectrum of the shifter. In the case of large scintillators this leads to an appreciable increase in the technical luminescence yield owing to decrease of self-absorption. The use of a spectrum mixer makes it possible to satisfy more fully two necessary but not always compatible requirements where high efficiency PS are concerned. These requirements are:

1) the luminescence spectrum must correspond to the spectral sensitivity maximum of the radiation receiver (or the human eye in the case of visual observation) and 2) the activator must have a high absorption coefficient in the wavelength region corresponding to the emission of the host material - in the case of ternary systems this applies to the absorption of the spectrum mixer as well. The second requirement corresponds to the familiar relation of a high excitation energy transfer efficiency in the case of solutions of organic substances (Ref.15).

The persistence of PS with excitation by ionizing radiation is not great and generally lies between 10^{-9} and 10^{-8} sec. Thus for example the decay time for PS consisting of 0.015 g/g tetraphenylbutadiene in polystyrene is $7\text{-}8\cdot 10^{-9}$ sec.[16,17] For 0.04 g/g p-terphenyl and 0.001 g/g diphenylstilbene in polyvinyltoluene the decay time is $\leqslant 3\cdot 10^{-9}$ sec.[18,19]

Harrison[20] in studying luminescence of PS under excitation by x-rays observed slowly decaying components whose intensity at saturation amounts to an appreciable fraction of the intensity of the short term (fluorescence) emission. Thus Harrison reports relative intensities of 6% for the luminescence component with $\tau_1 = 0.13\cdot 10^{-6}$, 4% for the component with $\tau_2 = 2.5\cdot 10^{-6}$ sec and 0.3% for the component with $\tau_3 = 50\cdot 10^{-6}$ sec. Rozman[21] found that scintillators of polystyrene with tetraphenylbutadiene at low temperatures exhibit a phosphorescence with a persistence of several minutes and a non-exponential decay.

Like organic crystals, PS are subject to radiation damage by heavy ionizing particles and fast electrons. Rozman & Tsimmer[22] investigated the increase in opacity to their own luminescence and the decrease in luminescence yield of PS irradiated with α- and β-particles. They found that the radiation stability of PS (in the sense of the rate of deterioration of the efficiency) is approximately 50 times higher than that of crystalline anthracene.

4. In investigating radioluminescence of PS, we are immediately faced with the question of the mechanism of excitation energy transfer from the host molecules to the luminescing impurity molecules. That such energy transfer or migration does occur is evident from the following two facts: 1) the luminescence spectrum of PS does not in general contain any luminescence of the host component and 2) the luminescence intensity (or brightness of individual scintillation) of PS is appreciably greater than might be expected on the basis of the fraction of the exciting radiation absorbed directly by the impurity. Koski[2] suggests that the impurity molecules absorb the luminescence of the host component (polystyrene in his case) and emit their own luminescence as a result. This is also the conclusion reached by Birks[23] on the basis of his theory of radioluminescence. Pichat, Pesteil & Clement[8], Swank & Buck[14] and Swank[18] concur in the opinion that reabsorption can account for only about 20% of the luminescence yield of a good PS.

For the purpose of proving the nonradiative character of migration in PS, Swank & Buck[14] carried out the following experiment. They measured the variation of the scintillation intensity with a concentration of tetraphenylbutadiene in polystyrene. In one series of measurements the luminescence of the PS was excited by α- or β-particles, in the second series of measurements by the luminescence photons from a 0.16 mm thick polystyrene disc irradiated with α-particles (approximate range 0.04 mm). If the energy transfer occurred only through absorption of the polystyrene luminescence by the impurity (tetraphenylbutadiene), i.e., radiatively, the impurity concentration dependence of the scintillation intensity would have been the same in both cases. Actually, however, the optimum concentration of tetraphenylbutadiene in the case of excitation via the polystyrene disc proved to be 30 times lower than in the case of direct excitation by α-particles, while the maximum scintillation intensity

proved to be 5 times lower (normalized to zero concentration). Morton[23a] explains these results from the viewpoint of Birks[23] theory as follows: in the case of excitation through the polystyrene disc all the primary photons are absorbed by the polystyrene, while in the case of direct excitation part of the primary photons excite the tetraphenylbutadiene molecules.

Andreeshchev & Rozman[24] carried out a quantitative analysis of the external luminescence spectra of thin PS with a low concentration of triphenylpyrazoline. Comparison of the number of photons in the polystyrene band with the number in the impurity band under excitation by β-particles led them to conclude that the principal energy transfer mechanism is nonradiative.

To evaluate the efficiency of energy transfer from polystyrene to the luminescing impurity (triphenylpyrazoline), Rozman[25] carried out a comparison of the fluorescence intensity with excitation by equal photon fluxes in the absorption band of the impurity and in the absorption band of the polystyrene. He found that if allowance is made for the direct absorption by the impurity, then in the second case the efficiency of energy transfer appreciably exceeds the fluorescence efficiency of the polystyrene, i.e., there obtains sensitized fluorescence of the triphenylpyrazoline. Analogous results were obtained for other PS (polystyrene with p-terphenyl, tetraphenylbutadiene, anthracene and p-terphenyl + triphenylpyrazoline). In addition, Rozman found that the efficiency of energy transfer with excitation by β-particles is close to the efficiency of energy transfer with photoexcitation. The probability of nonradiative transfer here is low ($P \sim 1/\tau_0$, where τ_0 is the mean lifetime of the excited state of polystyrene molecules). It follows that the rate of specifically activation quenching with excitation by ionizing radiation must be appreciably higher than the rate of internal quenching in polystyrene molecules.[26] These deductions conflict with Birks' theory[23] of radioluminescence.

Krenz[28] is of the opinion that the efficient energy migration observed in polystyrene-base PS represents intramolecular rather than intermolecular energy transfer. The luminescent impurity molecules are incorporated into the polystyrene chain (co-polymerization) or linked to the polystyrene molecules as end groups. In particular, this pertains to anthracene at concentrations exceeding 0.1%. Krenz's hypothesis is inconsistent with the results of a study of the infrared spectra of PS[8] and with the results of Pani et al obtained in investigating diverse chemical and physical-chemical properties of polystyrene base scintillators.[29] The last authors, having experimentally disproved copolymerization, infer that in many cases the luminescent impurities form only labile compounds with the polystyrene or are merely distributed in the polystyrene in the form of microcrystals.

5. Plastic scintillators are of practical importance because they possess a number of distinct advantages and positive features. Among these are the following: a) simplicity of preparation, particularly the possibility of preparing large specimens of any desired shape, b) their susceptibility to machining on conventional machine tools, c) good optical properties in conjunction with high mechanical and temperature stability (some types of PS can be used in the temperature range from -198 to +70°), d) the fact that they require no special packaging or treatment to protect them from moisture, e) the possibility of polishing the scintillator surface which in many cases does away with the necessity of using special reflectors or other light collecting devices, f) the possibility of appreciably reducing the internal absorption of luminescence by using two activators, g) the possibility of introducing large amounts of diverse chemical elements into the PS which is important both for increasing the photoeffect probability in recording γ-radiation and for detecting neutrons by the method of activation through threshold reactions and h) the fact that PS can be used inside vacuum equipment.

Plastic scintillators are now widely employed for detecting ionizing radiations. They are used in radiation meters and dosimeters[30-33], for detecting fast neutrons[30] and in coincidence circuit β-spectrometers[34]. The high radiation stability of PS[22] allows of using them for recording very intense radiation fluxes. It has been shown experimentally that the proportionality between the dosage rate of radiation and the scintillation intensity of PS persists at least up to 10^4 roentgen/sec.[35] Recording long-range particles, the lower (as compared with anthracene or NaI(Tl)) luminescence efficiency of PS is to some extent compensated by the possibility of using large scintillators with good optical properties. In addition, PS can readily be made in the form of parallelepipeds with a polished surface, i.e., given the shape which best insures uniformity of a scintillation counter.[36]

6. Investigation of the luminescence of PS is of undoubted practical interest, that is, for the purpose of developing effective radiation detectors. It must be noted, however, that investigation of the luminescence of PS is also of interest from the standpoint of a better understanding of the luminescence of organic materials in general, inasmuch as, in contrast to single crystals, one can readily introduce different components into PS while, in contrast to liquid solutions, internal diffusion of molecules and radicals is virtually precluded in plastic scintillators.

References

1. M.G.Schorr & F.L.Torney, Phys.Rev., 80, 474 (1950).
2. W.S.Koski, Phys.Rev., 82, 230 (1951).
3. T.Carlson & W.S.Koski, Phys.Rev., 85, 697 (1952).
4. L.Pichat & Y.Koechlin, J.Chim.phys., 48, 225 (1951).
5. E.A.Andreeshchev, E.E.Baroni, K.A.Kovyrzina, I.E.Pani, I.M.Rozman & V.M.Shoniia, PTE (Instrumentation & Experimental Technique), 1, 32 (1956).
6. W.L.Buck & R.Swank, Nucleonics, 11, No.11, 48 (1953).
7. M.M.Koton, Zhur.tekh.fiz., 26, 1741 (1956).
8. L.Pichat, P.Pesteil & J.Clement, J.Chim.phys., 50, 26 (1953).
9. D.G.Ott, F.N.Hayes, J.E.Hammel & J.O.Kephart, Nucleonics, 13, No.5, 62 (1955).
10. G.G.Eichholz & I.L.Horwood, Rev.Sci.Instr., 23, 305 (1952).
11. R.M.Kloepper & M.L.Wiedenbeck, Rev.Sci.Instr., 23, 470 (1952).
12. J.Fischer, Nucleonics, 13, 5, 52 (1955).
13. L.Wouters, Nucleonics, 12, 3, 26 (1954).
14. R.K.Swank & W.L.Buck, Phys.Rev., 91, 927 (1953).
15. S.I.Vavilov, Mikrostruktura sveta (Microstructure of light), M., 1950.
16. G.Harding, Nucleonics, 10, 3, 37 (1952).
17. S.F.Kilin, A.A.Pavlov & I.M.Rozman, PTE (Instrumentation & Experimental Technique)., 2, 50 (1956).
18. R.K.Swank, Nucleonics, 12, 3, 14 (1954).
19. R.K.Swank & W.L.Buck, Rev.Sci.Instr., 26, 15 (1955).
20. F.B.Harrison, Nucleonics, 12, 3, 24 (1954).
21. I.M.Rozman, Zhur.eksp.i teor.fiz., 28, 251 (1955).
22. I.M.Rozman & K.G. Zimmer, Atomnaia energiia (Atomic energy), 2, 54 (1957).
23. J.B.Birks, Scintillation Counters (Cited in Russ.trans.), 1955.
23a. G.A.Morton in "Dosimetry of Ionizing Radiations", Geneva Conference Report, 1955.
24. E.A.Andreeshchev & I.M.Rozman, Opt. i spektr., 2, 488 (1957).
25. I.M.Rozman, Opt.i spektr., 2, 480 (1957).

26. I.M.Rozman, Dissertation, Sukhumi, 1957.
27. J.B.Birks, Phys.Rev., 94, 1567 (1954).
28. F.H.Krenz, Trans.Faraday Soc., 51, 172 (1955).
29. E.I.Pani, E.E.Baroni & V.M.Shoniia, Zhur.fiz.khim., 31, 732 (1957).
30. Dosimetry of Ionizing Radiations, Geneva Conference Reports, 1955.
31. F.N.Hayes, R.D.Hiebert, B.Rogers & R.L.Schuch, Nucleonics, 12, 2, 16 (1954).
32. I.M.Rozman & K.G.Zimmer, VR i R, 1, 63 (1955).
33. I.M.Rozman & K.G.Zimmer, ZS.Naturforschung, 11b, 46 (1956).
34. A.Bisi, E.Germagnoli & L.Zappa, Nuovo Cim., 3, 1007 (1956).
35. I.M.Rozman & K.G.Zimmer, Atomnaia energiia (Atomic energy) 2, 70 (1957).
36. D.Brini, L.Peli, O.Rimondi & P.Veronesi, Nuovo Cim., Suppl., 4, 1048 (1955).

SCINTILLATION EFFICIENCY OF CARBO- AND HETEROCYCLIC COMPOUNDS IN PLASTICS

- N.A.Adrova, M.M.Koton, Iu.N.Panov & F.S.Florinskii

At present, in addition to organic and inorganic crystals and liquid solutions, organic compounds incorporated into a plastic are used as scintillators.[1] We carried out an investigation of the scintillation efficiency of substituted anthracenes, polyphenyls, aryl derivatives of dienes, and a number of heterocyclic compounds (oxazoles, oxadiazoles, etc.) in polystyrene. The investigated compounds were added to the styrene monomer in amounts (1-2%) yielding the maximum efficiency and polymerized in the presence of 0.2% benzoyl peroxide by heating at a gradually increasing temperature from 80 to 120° for a period of 4-5 days. The resultant solid masses were machined to standard test cylinders. The scintillation efficiencies were determined by means of a set-up measuring the relative output voltage pulse height of an FEU-19 photomultiplier. The pulse height of a standard sample (2% terphenyl in polystyrene) at a counting rate of 1000 pulses per minute was taken arbitrarily as 100%. If the counting rate is kept at the same level for all the investigated samples by varying the bias voltage on the discriminator input, one obtains a specific cutoff voltage for each sample. Comparison of these values with the cutoff bias voltage for the standard sample yields the comparitive data for evaluating the samples. The pulse height determined from the bias setting for the standard sample equalled 50% of the pulse height for a stilbene crystal, i.e., our 100% rating equals 50% the pulse height from crystalline stilbene.

The data obtained as a result of our investigation indicate a certain correlation between the chemical structure of the organic compounds and their scintillation efficiency. As may be seen from the accompanying table the highest efficiency in polystyrene is given by 1,4-bis-[2-(5-phenyloxazolyl)] benzene (POPOP) (I), quaterphenyl (II) and 9,10-diphenyl-anthracene (III), i.e., by compounds containing 4-5 rings per molecule and conjugate double bonds:

I.

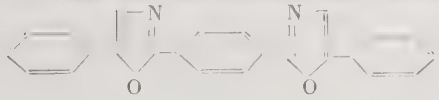

II.

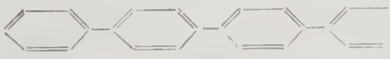

III.

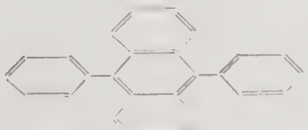

Where the oxazole (IV) and oxadiazole (V) series -

IV.

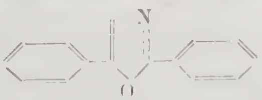

V.

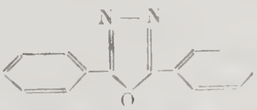

- are concerned, we found that with the same substituting groups (for example, phenyl radicals) the oxazole derivatives have a higher scintillation activity than the oxadiazole ones, which is in agreement with the data of Hayes et al[2] obtained for liquid scintillators.

Scintillation efficiencies of organic compounds added in equal amounts to polystyrene

No.	Organic compound	Concentration in polystyrene, %	Relative pulse height, %
1	1,4-bis-[2-(5-phenyloxazolyl)] benzene (POPOP)	0.5	105
2	quaterphenyl	0.5	95
3	9,10-diphenyl-anthracene	0.5	80
4	2,5-diphenyl-oxazole (PPO)	1.0	105
5	2-(1-naphthyl)-5-phenyl-oxazole (αNPO)	1.0	105
6	2-(ω-styryl)-5-phenyl-oxazole	1.0	67
7	2,5-diphenyl-oxadiazole	1.0	75
8	1,1'4,4'-tertaphenylbutadiene (T.P.B.)	1.0	85
9	1,1',4,4'-tetratolylbutadiene	1.0	75
10	p-terphenyl	2.0	100
11	9,10-bis-(p-methoxyphenyl)anthracene	2.0	96
12	9,10-bis-(m-tolyl)anthracene	2.0	77
13	9,10-bis-(p-tolyl)anthracene	2.0	72
14	9,10-bis-(p-bromphenyl)anthracene	2.0	72
15	9-n-butyl-anthracene	2.0	52
16	9-n-propyl-anthracene	2.0	46
17	9-ethyl-anthracene	2.0	44
18	9,10-diazetaminoanthracene	2.0	38
19	2-methyl-anthracene	2.0	35
20	9-methyl-anthracene	2.0	30
21	anthracene	2.0	30
22	phenanthrene	2.0	15
23	acenaphthene	2.0	10
24	dinaphthylmethane	2.0	31
25	ditolylmethane	2.0	10
26	dixylylmethane	2.0	9
27	dibenzofuran	2.0	15
28	dibenzothiophene	2.0	5
29	dibenzopyrrole	2.0	(2)

A comparatively high scintillation efficiency is also exhibited by 1,1',4,4'-tetraarylbutadiene (VI), where R = H, CH_3) and p-terphenyl (VII):

VI.

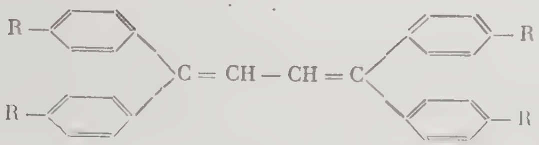

VII.

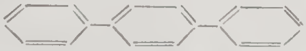

Other compounds having three rings per molecule (anthracene, phenanthrene, acenaphthene, dibenzofuran, dibenzothiophene, etc.) have a low scintillation efficiency in polystyrene.

It is interesting to note that stilbene and diphenyl-acetylene, which exhibit a high scintillation efficiency in the form of single crystals, proved to be inefficient when incorporated in the plastic; 1,4-diphenylbutadiene also proved to be inefficient although it has a relatively high efficiency in solutions.

These data show that in preparing plastic scintillators one cannot indiscriminately use the experimental results obtained for liquid scintillators. The preparation of plastic scintillators has its own idiosyncrasies, possibly stemming from the specific method of preparation by polymerization of the liquid styrene monomer; apparently, the organic scintillators added to the styrene exert their positive or negative influence on the polymerization process and at the same time themselves undergo certain changes affecting their scintillation efficiency in the final product.

For the purpose of increasing the scintillation efficiency of polystyrene scintillators it has proved expedient to introduce two organic scintillators, one of which (terphenyl, diphenyloxazole or some similar relative inexpensive and readily available compound) plays the role of the principal activator, while the second serves as co-activator (quaterphenyl or POPOP). Although added in relatively small amounts, the more expensive co-activator compound has an appreciable enhancing effect on the scintillation efficiency. Thus, for example, 2% terphenyl in polystyrene yields a plastic scintillator with an efficiency of 100%(in our arbitrary units), whereas the addition of 0.01-0.02% POPOP to the same mixture increases the efficiency to 132-134%.

On the basis of our experimental results we worked out a procedure for preparing efficient styrene-base plastic scintillators 30 to 150 mm in diameter and weighing up to 3 kilograms and having an efficiency of the order of 85% relative to crystal stilbene or 50% relative to crystal anthracene.

Institute of High Molecular Compounds,
Academy of Sciences of the USSR

References

1. W.Buck & R.Swank, Nucleonics, 11, 48 (1953); 12, 14 (1954; M.M.Koton, Zhur.tekh.fiz., 1741 (1956); E.A.Andreeshchev, E.E.Baroni, K.A.Kovyrzina, I.E.Pani, I.M.Rozman & V.M.Shoniia, PTE (Instrumentation & Experimental Technique), 1, 32 (1956).

2. F.Hayes, D.Ott, V.Kerr & B.Rogers, Nucleonics, 13, 38 (1955); 14, 42 (1956).

PULSE HEIGHTS FROM PLASTIC SCINTILLATORS WITH DIFFERENT ACTIVATORS

- M.N.Medvedev, E.N.Matveeva & L.Ia.Zhil'tsova

Introduction

Scintillation counters used for experimental work in nuclear physics must satisfy a number of different requirements. Investigations performed on high-energy particle accelerators employ large scintillation counters which are usually incorporated into coincidence circuits and which must possess high time and pulse-height resolution. For this purpose the given scintillator must be highly transparent to its own radiation and have the highest possible ratio of energy yield to light flash duration, B_e/τ.

When light emission from molecules of the scintillator decays exponentially with a time constant τ, the photomultiplier output-current pulse is given by

$$i_{ph}= \frac{B_e}{\tau} \cdot \frac{\eta \alpha E q \bar{k}}{(h\nu)_{av}} \cdot e^{-t/\tau},$$

where η is the photocathode quantum efficiency, $\bar{k}$ is the amplification of the photomultiplier, E is the energy imparted to the scintillator by the recorded particle, α is the fraction of scintillation photons reaching the photocathode, q is the electron charge and $(h\nu)_{av}$ is the average photon energy.

Eq.(1) shows that the output current is proportional to the ratio between the energy yield and the duration of a scintillation. Table 1 gives the values of B_e/τ for a number of organic scintillators with B_e/τ for anthracene taken as unity. These ratios are not very accurate since the values of B_e and τ were taken from different sources.[1,2] They do, however, allow of comparing the B_e/τ values for a number of scintillators that are frequently employed in scintillation counters. It will be evident that B_e/τ for most plastic and liquid scintillators is higher than for the common organic single crystals. Toluene + 8 g/liter PBD and polyvinyltoluene + 4% p-terphenyl + 0.1% DPS exhibit the highest values of B_e/τ. Scintillators with the highest B_e/τ provide the highest time resolution, as has been substantiated experimentally.

The purpose of the present work was to obtain large scintillators, highly transparent to their own radiation and having the highest possible value of B_e/τ.

Plastic scintillator pulse heights

The amplitude of a plastic scintillator pulse depends not only on the activator concentration but also on the purity of both the solvent and the activator. In Ref.3 it was shown that the use of benzoyl peroxide as a polymerizing catalyst leads to the formation of fluorescence-quenching compounds. We have investigated the effect of benzoyl peroxide on plastic scintillator pulse heights. Table 2 gives the data for a number of samples prepared with and without the catalyzer. The data show an increase of pulse heights by ~10% for non-catalyzed plastic scintillators. Non-catalyzed p-terphenyl samples give pulses that are 0.6 as high as those from stilbene, but these samples are poorly transparent to their own radiation. It is therefore not desirable to use p-terphenyl as the principal activator in plastic scintillators larger than 100 mm, intended for use in coincidence circuit scintillation detectors.

We also investigated a number of oxazoles. These were used as the principal activators in plastic scintillators and also are supplements to p-terphenyl and 2,5-diphenyloxazole. The corresponding pulse height data are shown in Table 3.

Table 1

Values of B_e/τ for a number of scintillators

Scintillator	B_e/τ referred to the value for anthracene, taken as unity
Stilbene	3.30
Tolane	2.75
p,p'-Quaterphenyl	4.00
p-Terphenyl	2.64
Phenylcyclohexane + 3 g/l p-terphenyl	3.08
Toluene + 5 g/l p-terphenyl	4.00
Polystyrene + 4% p-terphenyl	3.07
Toluene + 5 g/l p-terphenyl + 0.02 g/l αNPO*	4.35
Polystyrene + 4% p-terphenyl + 0.2% TPB*	3.2
Polyvinyltoluene + 4% p-terphenyl + 0.2% TPB*	3.7
Polyvinyltoluene + 4% p-terphenyl + 0.1% DPS*	5.3
Polystyrene + 1.8% TPB*	2.58
Toluene + 3 g/l PBD*	5.75
Polystyrene + 2% p-terphenyl + 0.02% POPOP*	6.0

---

*αNPO = 2-(1-naphthyl)-5-phenyloxazole; TPB = 1,1',4,4'-tetraphenylbutadiene-1,3; DPS = p,p' diphenylstilbene; PBD = 2-phenyl-5-(4-biphenyl)-1,3,4-oxydiazole; POPOP = 1,4-di[2-(5-phenyloxazolyl)]-benzene

Table 2

Scintillator pulse heights*

Scintillator	Pulse height compared with stilbene (%)
Polystyrene + 0.5% p-terphenyl + 1% benzoyl peroxide	27
Polystyrene + 0.5% p-terphenyl + 0.1% benzoyl peroxide	35
Polystyrene + 2% p-terphenyl + 0.1% benzoyl peroxide	50
Polystyrene + 2% p-terphenyl (without benzoyl peroxide)	60
Polystyrene + 2% PPO + 0.1% benzoyl peroxide	63
Polystyrene + 2% PPO (without benzoyl peroxide)	72
2% p-Terphenyl + 0.2% p,p'-quaterphenyl + 0.1% benzoyl peroxide	66
2% p-Terphenyl + 0.2% p,p'-quaterphenyl (without benzoyl peroxide)	76

---

*All measurements were performed with a FEU-19M photomultiplier; no correction made for spectral sensitivity. Gamma-source - Co^{60}.

Table 3 shows that maximum pulse heights are obtained when the activator concentration for the given materials is 0.5 to 1.0%. The table gives pulse heights from samples polymerized with benzoyl peroxide. The best results were obtained when PBD was used as the activator. A sample of polystyrene + 1% PBD without benzoyl peroxide gave pulses 0.9 as high as those from stilbene. A sample of polystyrene + 1% αNPO without benzoyl peroxide gave pulses which were 0.73 as high as those from stilbene.

Table 3

Pulse heights from scintillators containing oxazole activators

Scintillator	Concentration (%)	Pulse height compared with stilbene
1,4-Di-[2-(5-phenyloxazolyl)]-benzene (POPOP) in polystyrene	0.1	47
	0.5	55
	1.0	62
	2.0	47
2-(1-Naphthyl)-5-phenyloxazole (αNPO) in polystyrene	0.5	57
	1.0	63
	2.0	60
2-(4-Biphenyl)-5-phenyloxazole (BPO) in polystyrene	0.5	70
	1.0	62
	2.0	62
	3.0	61
2-Phenyl-5-(4-biphenyl)-1,3,4-oxadiazole (PBD) in polystyrene	0.5	61
	1.0	71
	2.0	66
	3.0	58
2,5-Diphenyloxazole (PPO) in polystyrene	1.0	70
	2.0	63
	3.0	62
5-Phenyl-2-styryloxazole (PSO) in polystyrene	0.5	47
	1.0	47
2,5-Di-(4-biphenyl)oxazole (BBO)	0.5	69
	1.0	65

The data for scintillators containing oxazoles as supplementary activators are given in Table 4. Benzoyl peroxide was used in preparing only the first five of the listed samples, not the last two. Plastic scintillators containing oxazoles give large pulse heights and have an emission spectrum in the region 3800-5000 Å.

Table 4

Pulse heights from scintillators containing oxazoles as supplementary activators

Scintillator	Pulse height compared with stilbene
Polystyrene + 2% p-terphenyl + 0.1% αNPO	82
Polystyrene + 2% PPO + 0.1% αNPO	77
Polystyrene + 2% p-terphenyl + 0.02% POPOP	86
Polystyrene + 2% PPO + 0.02% POPOP	79
Polystyrene + 1% p-terphenyl + 1% PPO	81
2% p-Terphenyl + 0.1% BBO	86
2% p-Terphenyl + 0.02% BBO	76

Since the concentration of the added luminescent solute is usually at least 0.01%, the persistence of the scintillator is determined principally by the decay time of this activator and, consequently, cannot differ greatly from its (molecular) decay time, i.e., $\sim 3\cdot 10^{-9}$ sec.[4] Therefore plastic scintillators, prepared with p-terphenyl plus POPOP, BBO or αNPO and charac-

terized by good transparency to their own radiation, can be successfully employed in scintillation counters.

In conclusion the authors wish to thank I.N.Chuvilo for his interest in this work.

Joint Institute for Nuclear Research,
Academy of Sciences of the USSR.

References

1. R.K.Swank, Usp.fiz.nauk., 58, 519 (1956).
2. R.K.Swank & W.L.Buck, Rev.Sci.Instr., 26, 15 (1955).
3. Transactions of the Faraday Society, 51, 173 (1955).
4. S.Singer, K.Neher & K.A.Ruehle, Rev.Sci.Instr., 27, 40 (1956).

MECHANISM OF ENERGY TRANSFER IN PLASTIC SCINTILLATORS

- T.P.Belikova & M.D.Galanin

As we showed in an earlier publication[1], excitation energy transfer in luminescing solutions of the type used in physics as liquid scintillators occurs by an inductive resonance (nonradiative) process, with the motion of the solvent molecules during the lifetime of the excited state playing a significant role in the process. It has by now been firmly established that in plastic scintillators energy transfer from the host material to the luminescing impurity also occurs primarily nonradiatively.[2-4] Obviously, in plastics there can be no motion of the molecules through the material during the lifetime of the excited state and, consequently, such energy transfer as does occur must be defined by the theory developed for the given case.[5,6]

In the present work we investigated two series of plastics with different activator concentrations: polystyrene with anthracene and polystyrene with p-terphenyl. The luminescence was excited by ultraviolet light in the region of polystyrene absorption. For determining the probability of resonance transfer and the probability of radiative transfer (i.e., by reabsorption of the polystyrene luminescence) we used the same method as in Ref.1. It was found that the absolute quantum efficiency of pure polystyrene $\eta_p \approx 0.09$, which is in agreement with the results obtained by Rozman.[2]

Table

Absorption coefficients and probabilities of radiative and nonradiative (resonance) energy transfer for different concentrations of anthracene and terphenyl in polystyrene

C, g/g	$\frac{K_p}{K_p + K_s}$	$\eta_p q^{(r)}$	$q^{(t)}$	C, g/g	$\frac{K_p}{K_p + K_s}$	$\eta_p q^{(r)}$	$q^{(t)}$
Anthracene				Terphenyl			
$1 \cdot 10^{-4}$	0,99	0,045	0,001	$1 \cdot 10^{-4}$	1,00	0,045	0,02
$3 \cdot 10^{-4}$	0,99	0,05	0,015	$3 \cdot 10^{-4}$	0,99	0,045	0,05
$1 \cdot 10^{-3}$	0,96	0,05	0,03	$1 \cdot 10^{-3}$	0,98	0,045	0,13
$3 \cdot 10^{-3}$	0,90	0,06	0,08	$3 \cdot 10^{-3}$	0,95	0,045	0,40
				$1 \cdot 10^{-2}$	0,85	0,06	0,50

The accompanying table shows the values of the ratio of the absorption coefficient K_p of the solvent (polystyrene) to the sum of the absorption coefficients $K_p + K_s$ of the solvent and solute (polystyrene and anthracene or terphenyl) for the exciting wavelength (λ = 282 mμ for anthracene and λ = = 266 mμ for p-terphenyl) for different values of the impurity concentration C and the corresponding radiative transfer probability $\eta_p q^{(r)}$ and resonance transfer probability $q^{(t)}$. The factor $q^{(r)}$ was evaluated according to Galanin[7]; in the case when the absorption coefficient for the exciting light is appreciably greater than the absorption coefficient in the region of reabsorption this factor is close to 1/2. The resonance transfer probability $q^{(t)}$ was calculated from the results of measurements of the luminescence intensity in the absorption region of polystyrene and in the region of its transmission as was done in Ref.1. As will be evident from the table, within the range of the investigated concentrations the probabilities of radiative and nonradiative energy transfer in the case of anthracene are comparable, while in the case of p-terphenyl nonradiative transfer predominates.

From the overlapping of the absorption spectra of the luminophors and the luminescence spectrum of polystyrene (Fig.1), we calculated the transfer probability that should be expected according to the theory developed by

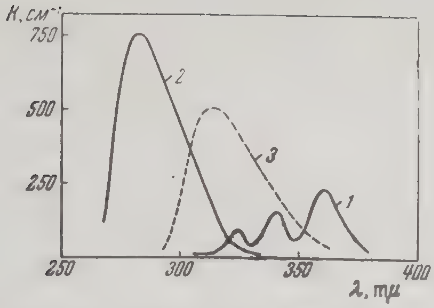

Fig.1. Absorption spectra of 1) anthracene and 2) terphenyl in polystyrene (concentration $3 \cdot 10^{-3}$ g/g) and 3) luminescence spectrum of polystyrene.

Förster[5] and Galanin[6]. The theoretical curves for the concentration dependence of $q^{(t)}$ obtained in this manner are shown in Fig.2; the circle points in the figure are the values deduced from measurements of the luminescence intensity. As follows from Fig.2, these values are in satisfactory agreement with theory*, which substantiates the hypothesis of the inductive-resonance character of nonradiative energy transfer in plastic scintillators. This deduction applies not only to the investigated case of photoexcitation but can also be extended to high energy excitation inasmuch as the concentration dependences of the intensity are identical in both cases.

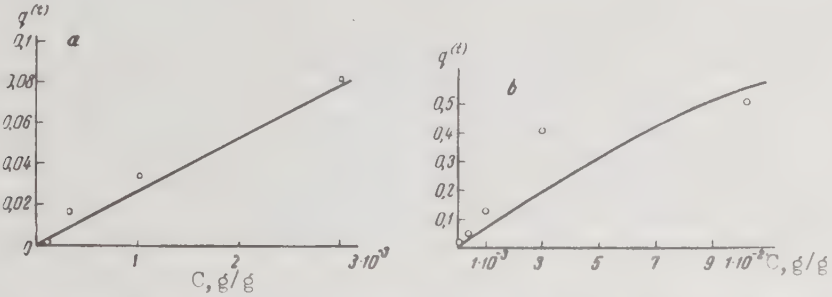

Fig.2. Impurity concentration dependence of the resonance transfer probability: a) anthracene in polystyrene and b) terphenyl in polystyrene.

The writers desire to express their gratitude to M.M.Koton for making available the plastic scintillator samples.

"P.N.Lebedev" Physical Institute,
Academy of Sciences of the USSR

References

1. T.P.Belikova & M.D.Galanin, Opt.i spektr., 1, 168 (1956).
2. I.M.Rozman, Opt.i spektr., 2, 400 (1957).
3. E.A.Andreeshchev & I.M.Rozman, Opt.i spektr., 2, 488 (1957).
4. R.K.Swank & W.L.Buck, Phys.Rev., 91, 927 (1953); Nucleonics 11, 11, 48 (1953).
5. Th.Förster, ZS.f.Naturforsch., 4a, 321 (1949).
6. M.D.Galanin, Zhur.eksp.i teor.fiz., 28, 485 (1955).
7. M.D.Galanin, Trudy (Transactions) Physical Institute of the USSR Acad. of Sciences, 5, 1950.

---

*In the case of p-terphenyl there is some divergence, apparently exceeding the experimental error, the reason for which remains unclear.

TEMPERATURE DEPENDENCE OF THE LUMINESCENCE EFFICIENCY OF POLYSTYRENE PLASTIC SCINTILLATORS

- I.M. Rozman

Introduction

The fluorescence efficiency of organic substances depends on the temperature. In most cases solutions of organic substances have a negative temperature coefficient, i.e., the fluorescence yield increases with decreasing temperature.[1] The extent of temperature quenching depends on the solvent; in some cases the temperature coefficient changes sign at a certain temperature.[2] Investigations of the luminescence of organic compounds in the vapor state have shown that generally the quantum efficiency of molecules decreases with increasing temperature and remains constant only in exceptional cases.[3-6]. Temperature quenching is explained as being due to intramolecular transformation of the electron excitation energy into the energy of molecular vibrations. With increasing temperature the store of vibrational energy increases and, in consequence, the probability of intramolecular deactivation rises.

There are no reports in the literature of analogous investigations of temperature quenching of the luminescence of organic substances with excitation by ionizing radiation (radioluminescence). There have been a number of measurements of the external yield or "technical efficiency" of single crystals and mixed crystals.[7-13] The appreciable reabsorption in such samples and the possible temperature dependence of the reabsorption make it impossible to deduce the true temperature dependence of the luminescence efficiency on the basis of such data.

Experimental Procedure

In our experiments the radioluminescence of the polystyrene[14] plastic scintillators (hereinafter PS) was excited by α- and γ (or β-) radiations and the photoluminescence was excited by monochromatic ultraviolet radiation with $\lambda = 253.7$, 313 or 366 mμ. With excitation by ionizing radiation, the major fraction of the primary activations occur in the polystyrene molecules. Long wave ultraviolet radiation, on the other hand, is absorbed almost entirely by the luminescent impurities. Hence comparison of temperature quenching in the two cases can yield significant information on the mechanism of energy transfer in PS.

The luminescence yield was determined from the mean output current of a FEU-19 photomultiplier viewing the samples. The sensitivity of the photomultiplier was periodically checked and all the measured luminescence intensities normalized to the same photomultiplier sensitivity.

A sectional view of the set-up used for measuring radioluminescence is shown in Fig.1. Temperature changes of the photocathode during an experiment were largely minimized by virtue of the great length of the light pipe 8 (about 230 mm) and the thermal insulation-packing 9. In addition, the photomultiplier was housed in a protective metal casing 12. The temperature of the samples was measured by means of a calibrated thermocouple 4 (copper-constantan or iron-constantan). The hot junction, encapsuled in a thin nickel tube (1.2 mm in diameter), was inserted into a hole drilled to a depth of 4-5 mm in the sample. The sensitivity of the photomultiplier was periodically checked with reference to the luminescence intensity of a standard scintillator 11. The dark current of the photomultiplier was below the sensitivity threshold of the galvanometer used to measure the photomultiplier current.

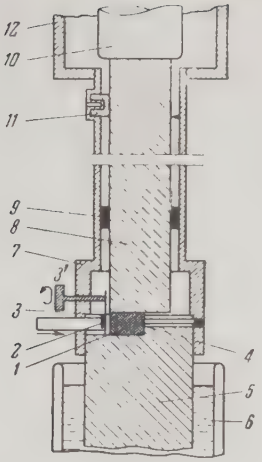

Fig.1

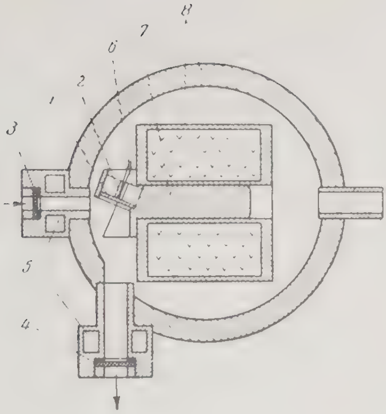

Fig.2

Fig.1. Sectional view of set-up used for investigating radioluminescence: 1) sample, 2) α-particle source, 3) absorbing shield, 3') knob rotating shield, 4) thermocouple, 5) duraluminum sample holder, 6) liquid nitrogen or water, 7) textolite housing, 8) light pipe, 9) insulating packing, 10) FEU-19 photomultiplier, 11) standard scintillator for sensitivity control, 12) metallic housing.

Fig.2. Set-up for measuring fluorescence: 1) PS sample, 2) thermocouple, 3 & 4) windows, 5) circulating water, 6) polished duraluminum or blackened brass, 7) sample holder, 8) metallic Dewar.

Po^{210} (activity 1 millicurie) deposited on a silver disc 5 mm in diameter served as the α-particle source. The source holder had provision for horizontal displacement. In front of the source was a 0.1 mm thick diaphragm with a 4 mm diameter opening. The sample was irradiated only during the time of measurement; at other times it was protected from the radiation by the movable shield 3. The knob 3' rotating the shield was equipped with detents to hold the shield in the open or closed position. This method of excitation 1) minimized α-radiation damage of the samples[15], 2) excluded the influence of luminescence of air[16-18] and 3) allowed of measuring the temperature dependence for both α- and γ-excitation in the same experiment. For γ-excitation a Co^{60} source with an activity of ~7 millicurie in a special holder was inserted into a hole made for this purpose in the sample holder.

A possible source of error in the measurements with γ-excitation could be the luminescence of the light pipe (polymethyl methacrylate). According to our measurements with an FEU-19 photomultiplier, the effective luminescence yield of polymethyl methacrylate amounts to only 1.6% of the yield of PS with 1.5% tetraphenylbutadiene. It will be evident that for some plastic scintillators with a low impurity concentration and, particularly, for pure polystyrene the luminescence of the light pipe may amount to an appreciable fraction of the yield of the PS, particularly since the integral dose of γ-radiation received by the light pipe exceeds the integral dose received by the sample. For this reason we measured the temperature dependence of the luminescence intensity of the light pipe in the absence of a sample and with the sample replaced by an equivalent piece of polymethyl methacrylate or by a duraluminum cylinder. In all three cases the measurements were carried out several times with different rates of temperature change and yielded results in sufficiently close agree-

ment for our purposes. This background, which also includes the background due to direct γ-radiation reaching the photomultiplier, has been subtracted from the experimental data given below.

A diagram of the set-up used for investigating photomulinescence is shown in Fig.2. The sample 1 in a special holder 2 was mounted between the inner and outer walls of the metallic Dewar 8. Two types of holders were used: in one case (as shown in the figure) the luminescence was measured from the excitation side using thin (0.5 mm) samples. In this case the sample was backed by a polished duraluminum or blackened brass insert 6. In the second case the holder was designed for "through" measurements. A flow of water over the quartz entrance 3 and exit 4 windows served to maintain these at a temperature close to room temperature, thus precluding condensation of moisture on them during the low temperature measurements.

The samples were cooled to below room temperature by means of liquid nitrogen. The rate of cooling was regulated by varying the depth of immersion of the sample holder (5 in Fig.1) or the amount of nitrogen poured into the metal Dewar (Fig.2). The large mass of the cooled unit obviated sudden temperature changes. Heating to 5-8° occurred through heat exchange with the room air. In the case of radioluminescence measurements the rate of heating was regulated by means of the Dewar. For the Dewar alone, the warming rate was slow. Further heating was accomplished by water. The rate of change of temperature was usually between 1 and 5 degrees/min and appreciably less during the periods of measurement.

The cylindrical samples were all of standard size - 16 mm in diameter and 10 mm (or 0.5 mm) high. Satisfactory optical contact was obtained by polishing the contacting surfaces. No light pipe was used in the measurements on the set-up shown in Fig.2.

Experimental Results

Most of the measurements were made on PS samples prepared with 1,1',4,4'-tetraphenylbutadiene-1,3, 1,3,5-triphenylpyrazoline-Δ^2 and anthracene. The concentration of these compounds was varied from $1\cdot10^{-4}$ to $3\cdot10^{-2}$ parts by weight. In addition we investigated pure polystyrene. The results obtained for the variation of the technical efficiency as a function of the temperature for some PS samples are shown in Table 1. These results were obtained for 10 mm high samples with the luminescence excited by the γ-rays from Co^{60}. The luminescence intensity was measured by means of an FEU-19 photomultiplier. A more detailed description of the experimental results follows.

Pure polystyrene

The temperature dependence of the luminescence intensity of pure polystyrene samples with excitation by α-particles and γ-rays was measured on the set-up of Fig.1 and by β-particles and the 253.7 mμ ultraviolet line on the set-up of Fig.2. The results obtained with all four excitations were in good agreement.

The observed increase in intensity of emission with decreasing temperature may be associated both with increase in luminescence efficiency and with decrease in self-absorption, which for the investigated samples amounts to about 70%. These two effects were separated and it was shown that the temperature dependences of the photo- and radioluminescence efficiencies of polystyrene are virtually identical.[19] The temperature dependence of the fluorescence efficiency[8] of polystyrene is characterized by the following figures:

T, °K = 110, 130, 170, 210, 250, 290, 330, 350;
q = 0.21, 0.20, 0.17, 0.14, 0.12, 0.10, 0.07, 0.06.

By definition the quantum efficiency

$$q = \frac{K_e}{K_e + K_i},$$

where K_e is the probability of emission of a photon and K_i is the probability of intramolecular nonradiative deactivation. If we assume that K_e is independent of the temperature,[4,20] the temperature dependence of intramolecular quenching can readily be found. Up to $T \approx 280^\circ$K

$$\frac{K_i}{K_e} = Ae^{aT}$$

where A = 2.00 and a = 0.0053 degree^{-1}, which is in accord with the results obtained for organic compound vapors.[4] At higher temperatures the ratio K_i/K_e increases more rapidly. This may either be due to accelerated decrease of K_e as suggested by Stepanov[21] or may be associated with some new physical-chemical effects occurring in polystyrene (see below).

Table 1

Efficiency of plastic scintillators as a function of the temperature

Luminescent impurity	Concentration, 10^{-2} g/g	Relative efficiency at the indicated temperature, °K					
		100	140	190	240	290	340
Pure polystyrene	—	52	41	32	24	17	11
1,1',4,4' Tetraphenylbutadiene-1,3 (TPB)	1,5	98	106	110	108	100	78
p-Terphenyl + TPB	3 & 0,05	134	134	133	132	122	108
1,3,5-Triphenylpyrazoline-Δ^2	1,0	104	103	102	101	100	92
Anthracene	3,0	53	49	43	37	30	23

Plastic scintillators with triphenylpyrazoline (TPP)

The temperature dependence of the luminescence yield of PS with triphenylpyrazoline (TPP) differs substantially from the dependence obtained for pure polystyrene.[19] The $I = f(t)$ curves for scintillators with TPP are flatter than the curve for pure polystyrene (Fig.3); the steepness of the temperature dependence curves decreases with increasing TPP concentration. Moreover the character of the variation of the luminescence intensity as a function of the temperature depends on the type of exciting radiation. The fact that the photoluminescence yield is virtually independent of the temperature in the case of excitation by 366 mμ light[19] indicates that the observed temperature dependence for γ-, α- and λ = 254 mμ excitation must be connected with the temperature dependence of the luminescence efficiency of polystyrene and the mechanism of energy transfer in PS. From the observed influence of concentration, it may logically be inferred that there does occur nonradiative transfer of excitation energy from the polystyrene to the TPP. At the same time the

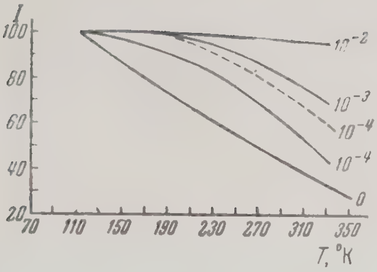

Fig.3

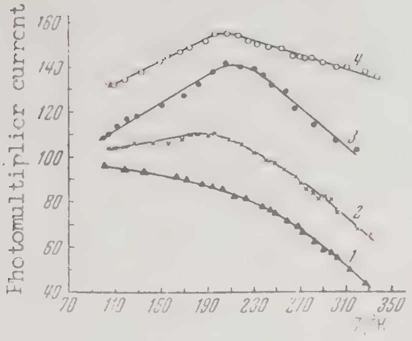

Fig.4

Fig.3. Temperature dependence of the intensity of luminescence of PS with triphenylpyrazoline (TPP) with excitation by γ-rays for different TPP concentrations. Figures at the curves give the proportion of TPP to polystyrene by weight. The dash curve represents the temperature dependence of the luminescence with α-excitation. The intensity values are in arbitrary units with the intensity at 110°K taken as 100.

Fig.4. Temperature dependence of the luminescence intensity of PS with tetraphenylbutadiene (TPB) for different TPB concentrations: 1) $1 \cdot 10^{-4}$, 2) $6 \cdot 10^{-4}$, 3) $1 \cdot 10^{-2}$ and 4) $3 \cdot 10^{-2}$ g/g. Excitation by α-particles.

effect cannot be satisfactorily explained on the assumption of exclusively nonradiative energy transfer; it must be assumed that in addition to the nonradiative mechanism, there also operates a photon mechanism whose relative contribution must increase with decreasing TPP concentration.[19]

PS with tetraphenylbutadiene (TPB)

The temperature dependence of the luminescence intensity of scintillators with tetraphenylbutadiene (TPB), like that of PS with TPP, depends both on the impurity concentration and on the exciting radiation. In this case, in addition, there is observed a definite decrease of radioluminescence intensity in the region of low temperatures, particularly for the scintillators with higher TPB concentrations (Fig.4 and Table 1). Comparison with the results obtained for PS with TPP shows that the temperature dependence of the luminescence intensity of PS with TPB (in the region of temperatures where the intensity begins to decrease with increasing temperature) is appreciably weaker than in the case of pure polystyrene but stronger than for PS with TPP. This stronger dependence is due to the fact that there is appreciable temperature quenching of the fluorescence in the case of the TPB scintillators.

PS with anthracene

In the case of PS with anthracene the concentration effect is weaker than in the two cases discussed above (TPP and TPB). In the temperature region above 180°K the shape of the I(T) curve differs little for α- and γ-excitation (Fig.5). This could be taken as evidence that the mechanism of energy transfer from the polystyrene to the anthracene is predominantly radiative.[22] This deduction, however, would appear to be premature. The photoluminescence yield of anthracene in polystyrene is very strongly dependent on

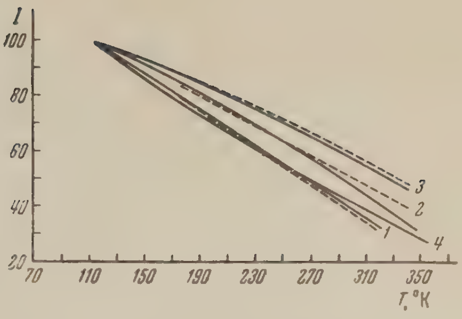

Fig.5. Temperature dependence of the luminescence intensity of PS with anthracene for different anthracene concentrations: 1) $1\cdot10^{-4}$, 2) $1\cdot10^{-3}$, and 3) $1\cdot10^{-2}$ g/g. Solid curves - γ-excitation; dash curves - α-excitation. Curve 4 characterizes the yield of pure polystyrene.

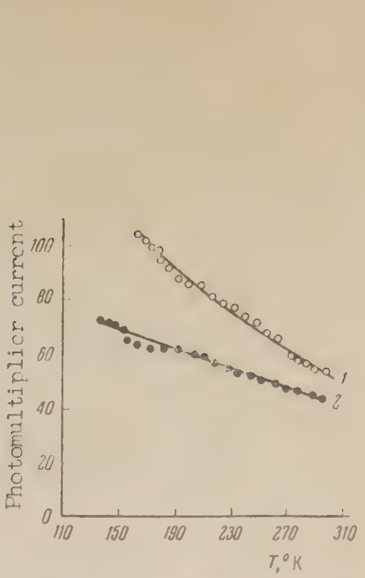

Fig.6. Temperature dependence of the luminescence intensity of PS with anthracene for different anthracene concentrations: 1) $1\cdot10^{-3}$, 2) $3\cdot10^{-2}$ g/g. Excitation with λ = 313 mμ light. "Through" measurement, i.e., sample viewed from the unirradiated side.

the temperature as may be seen from the results of measurement with excitation by 313 mμ light, shown in Fig.6. If the photon energy-transfer mechanism predominated, the temperature dependence of radioluminescence curve should fall off more rapidly with increasing temperature for the PS than for pure polystyrene. Actually this is not the case. The concentration effect obtaining in the case of photoexcitation of anthracene (Fig.6) can be interpreted as follows. At room temperature the major part of the external luminescence at 3% anthracene concentration lies in the λ = 430 mμ region, while at a 0.1% anthracene concentration it occurs in the λ = 410 mμ region. Thus the stronger temperature dependence of the short wavelength bands in the fluorescence spectrum of anthracene[23] leads to the more rapid decrease of luminescence intensity with temperature for PS with a low anthracene concentration.

Further investigation of the temperature dependences

The data given above were obtained in experiments in which the samples were cooled. A number of new effects appear when precooled samples are warmed.

In investigating the temperature dependence of the transmission of polystyrene, it was found that in the case of heating of a precooled sample, the transmission falls off sharply in the 200 to 210°K temperature interval. This decrease is transitory and disappears with further warming. In the first experiments in this series we measured the transmission for λ = 310 mμ. Further experiments showed that the same effect obtains for λ = 410 mμ. In addition to the first transmission drop, there was observed a second one close to 270°K which was evinced only in the case of rapid increase in temperature. It is logical to assume that the decrease in transmission for visible light must be connected with increased internal scattering in the polystyrene. To check this we measured the scattering at 90°. The results substantiated the above assumption. The effect was found to obtain for all the different types of PS studied. The scattering is apparently connected with some sort of phase transformation in the polystyrene. The fact that the effect is not apparent in cooling and appears during heating can be due to different rates of forward and reverse

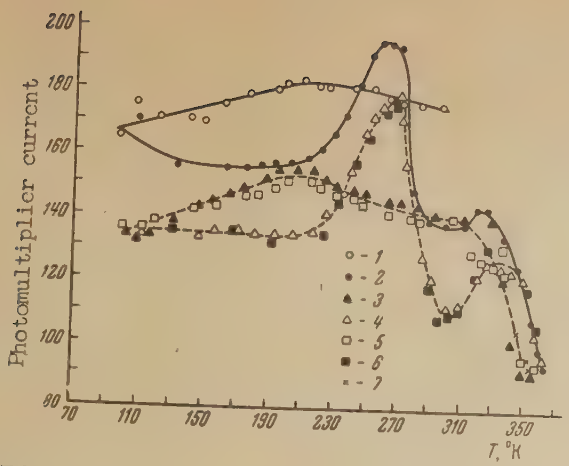

Fig. 7. Variation of the luminescence intensity of PS with 0.03 g/g tetraphenylbutadiene with temperature during heating and cooling cycles: 1) first cooling, 2) first heating, 3) second cooling, 4) second heating, 5) third cooling, 6) third heating and 7) fourth cooling. Excitation by α-particles.

transformation (under our experimental conditions). In any case, any changes in the state of the polystyrene must obviously complicate the entire picture of the temperature dependence of luminescence. By way of illustration, in Fig. 7 we give the results obtained in measurements through three cooling-heating cycles of a PS sample with 3% tetraphenylbutadiene. The luminescence was excited by α-particles. In addition to the appearance of maxima and minima in the I = ƒ(T) curves for rising temperatures, we also have a very sharp decrease in luminescence intensity at temperatures above 340°K. This decrease in luminescence yield after the first heating is not cancelled out by subsequent cooling and therefore results in a permanent decrease of the luminescence yield.

The variations in intensity during the second and third heating-cooling cycles differ little. A similar pattern is obtained with excitation by γ-rays. As a result of experiments in which the range of temperature variation was increased, it was established that the irreversible decrease at temperatures above 340°K is connected only with heating of the sample, i.e., persists whether the sample is or is not cooled to low temperatures. The maximum at 260-270°K and the minimum at ~300°K appear only if the sample is cooled to below ~230°K. In the case of PS with TPB the temperature at which the maximum and minimum develop in the I = ƒ(T) curve and the relative height of the maximum and depth of the minimum are little dependent on the impurity concentration. An analogous situation obtains for PS with TPP. For pure polystyrene the heating curves lie somewhat above the cooling curves and there appears only one clearly pronounced maximum at ~260°K. In the case of pure polystyrene there also occurs an irreversible decrease in the luminescence yield at high temperatures.

Further and more detailed investigations are necessary to clarify the mechanism of the processes in PS responsible for the described effects. Where the scope of the present report is concerned, however, it is significant that although there is an appreciable difference between the absolute values of the luminescence intensity obtained in the first and subsequent coolings, the general character of the I = ƒ(T) curves remains virtually the same. This justifies use of the method of analysis applied to the experimental data above.

Discussion of Results

The experimental results obtained in investigating the temperature quenching of the luminescence furnished incontrovertible evidence that nonradiative energy transfer from the polystyrene to the impurities does occur in the investigated PS. This fact and the fact that the temperature quenching of the luminescence of pure polystyrene is independent of the type of excitation are in conflict with Birks' theory[24,25] of radioluminescence according to which the scintillation process involves primary photons and a subsequent photon cascade.

Table 2

Efficiency of energy transfer from the polystyrene to the luminescing impurity with excitation by β-particles (evaluated for room temperature)

Impurity concentration, g/g polystyrene	Impurity		
	TFP	TFF	Anthracene
$1 \cdot 10^{-4}$	—	0,11	—
$3 \cdot 10^{-4}$	—	0,18	0,18
$1 \cdot 10^{-3}$	0,22	0,23	0,20
$3 \cdot 10^{-3}$	0,32	0,36	0,27
$1 \cdot 10^{-2}$	0,52	0,53	0,43
$3 \cdot 10^{-2}$	0,60	0,60	—

Hence we felt it would be of interest to carry out an independent determination of the efficiency of energy transfer in PS and to compare the results of such determinations with the results obtained in investigating temperature quenching. A detailed description of the procedure used in determining the efficiency (P) of excitation energy transfer from the polystyrene to the luminescent impurity has been given in Ref.26. On the basis of the data given therein we can calculate the efficiency of energy transfer for the PS of interest here with excitation by β-particles. The calculated results for room temperature are given in Table 2. Inasmuch as for the pure photon mechanism $P \leqslant q_1$ (= 0.09), it follows from the table that in the investigated PS there does occur nonradiative energy transfer, the efficiency of which increases with increasing impurity concentration.

At the same time it must be noted that the total transfer efficiency at low impurity concentrations is appreciably less than unity; consequently, in addition to nonradiative energy transfer a significant role must be played by transfer due to absorption by the impurity of photons emitted by the polystyrene. These conclusions are in qualitative agreement with the experimental results on temperature quenching described above. Rigorous quantitative comparison is difficult in view of the temperature dependence of the transfer efficiency (for example, variation due to temperature induced variation of the absorption and emission spectra). This temperature dependence is as yet unknown.

Persistent Luminescence at Low Temperatures

At low temperatures ($T \leqslant 150^{\circ}K$) the luminescence of PS with tetraphenylbutadiene contains slowly decaying components.[27] We carried out measurements of the decay curves for the time interval from 5 sec to 50 min for pure polystyrene and scintillators with different impurities with excitation by γ-rays from Co^{60}. The decay law appears to be independent of the luminescent impurity (similar decays obtained for pure polystyrene and PS with tetraphenylbutadiene, triphenylpyrazoline, anthracene and diphenyloxazole) and differs appreciably from the simple exponential law (Fig.8). The initial luminescence intensity increases with increasing temperature, while the rate of decay decreases (Table 3). Further it was established that heating of the PS samples after prolonged γ-radiation results in the appearance of temperature stimulated luminescence attaining a maximum intensity at $T \approx 120^{\circ}K$ (regardless of the luminescence impurity) (Fig.9).

Table 3

Persistence of luminescence of PS with tetraphenylbutadiene (0.03 g/g) at low temperature and with excitation by Co^{60} γ-rays.

T, °K	Duration of excitation, min	Initial intensity I_0*	Time of decrease by a factor of	
			2	e
129	4	37	0,15	0,58
110	4	70	0,25	0,96
93	4	100	0,46	2,0
83	21	140	0,68	4,3

* Intensity 5 sec after withdrawal of the γ-ray source.

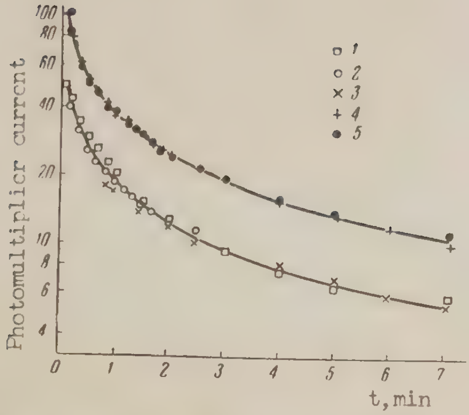

Fig.8. Decay of phosphorescence of PS with excitation by γ-rays for 12 min at 93°K. Luminescent impurities: 1) 0.03 g/g TPB, 2) 0.015 g/g diphenyloxazole, 3) 0.01 g/g anthracene, 4) 0.01 g/g TPP, 5) pure polystyrene. Normalizing factors: 0.06, 0.72, 2.2, 1.8, and 2.0, respectively.

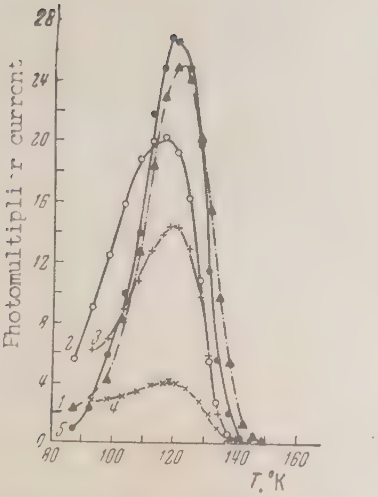

Fig.9. Thermostimulation (glow) curves of PS with excitation by γ-rays for 12 min at 93°K; beginning of heating 7 min after removal of γ-source; rate of heating 8 degree/min. Luminescent impurities: 1) 10^{-4} g/g TPB, (x 0.5), 2) 0.015 g/g diphenyloxazole (x 0.5), 3) 0.01 g/g TPP, 4) 0.01 g/g anthracene, 5) pure polystyrene (after 50 min).

The first deduction to be drawn from the cited data is that the phosphorescence (persistent luminescence) and the thermostimulated emission are caused by some processes in the polystyrene itself rather than in the luminescent impurities. As is known, the phosphorescence of organic substances is usually associated with transitions from a metastable (triplet) state of the molecule to the ground (singlet) state, either directly or through a labile state. In either case the decay law is exponential. The shape of the thermostimulated emission curve is described by the Randall-Wilkins equation.[28] In our case neither the decay laws nor the shape of the glow curves are consistent with the hypothesis of transitions from metastable levels. In this connection it is important to note that prolonged irradiation of the PS with the 253.7 mμ mercury line at 83°K did not lead to any noticeable thermostimulated luminescence, while the phosphorescence died down very rapidly ($\sim$40 sec). The intensity of the luminescence some 10 sec after cessation of excitation amounted to only 0.4% of the intensity of the fluorescence. With excitation by γ-rays the corresponding figure is 3% (even at the higher temperature of 93°K). Consequently, the major portion of the phosphorescence and the temperature stimulated luminescence of PS are connected with the specific characteristics of interaction of ionizing radiation with the PS material. It is possible that these effects are associated in some way with the combination of radicals forming in the polystyrene under the influence of γ-radiation. The lower intensity of the phosphorescence and the thermostimulated emission with excitation by α-particles (Ref.27) can be explained by the hypothesis that the passage of α-particles is followed by a sharp local increase in temperature favoring rapid recombination of the radicals.

References

1. V.L.Levshin, Fotoliuminestsentsiia zhidkikh i tverdykh veshchestv (Photoluminescence of liquid and solid solutions), M.-L., 1951.
2. T.Förster, Fluoreszenz organischer Verbindungen, Göttingen, 1951.
3. G.A.Kundzich & A.A.Shishlovskii, Doklady AN SSSR, 97, 429 (1954).
4. B.S.Neporent, Zhur.fiz.khim. (Journal Phys.Chem.), 21, 1111 (1947).
5. B.S.Neporent, Izv.AN SSSR, Ser.fiz., 15, 533 (1951).
6. B.S.Neporent & N.A.Borisevich, Doklady AN SSSR, 94, 447 (1954).
7. R.S.Classen & R.W.Boom, Phys.Rev., 75, 331 (1949).
8. J.W.Irvine, Nucleonics, 10, 3, 32 (1952).
9. S.H.Liebson & J.W.Keller, Phys.Rev., 78, 305 (1950).
10. S.H.Liebson & R.T.Farrar, Phys.Rev., 79, 733 (1950).
11. S.H.Liebson, Nucleonics, 10, 3, 32 (1952).
12. S.H.Liebson, Nucleonics, 10, 7, 41 (1952).
13. R.K.Sangster & J.W.Irvine, J.Chem.Phys., 24, 670 (1956).
14. E.A.Andreeshchev, E.E.Baroni, K.A.Kovyrzina, I.E.Pani, I.M.Rozman & V.M.Shoniia, PTE (Instrumentational & Experimental Technique), 1, 32 (1956).
15. I.M.Rozman & K.G. Zimmer, Atomnaia energiia (Atomic energy), 2, 54 (1957).
16. J.B.Birks & J.W.King, Proc.Phys.Soc., B66, 81 (1953).
17. J.B.Birks & W.A.Little, Nature, 174, 82 (1954).
18. G.Ortner & S.Salim, Nature, 169, 1060 (1952).
19. I.M.Rozman, Opt.i spektr., 2, 480 (1957).
20. B.S.Neporent & B.I.Stepanov, Usp.fiz.nauk., 43, 380 (1951).
21. B.I.Stepanov, Usp.fiz.nauk., 58, 3 (1956).
22. W.S.Koski, Phys.Rev., 82, 230 (1951).
23. P.Pesteil & M.Barbaron, J.Phys.et Radium, 15, 92 (1954).
24. J.B.Birks, Phys.Rev., 94, 1567 (1954).
25. J.B.Birks, Scintillation Counters (Cited in Russian trans., 1955).
26. I.M.Rozman, Dissertation, Sukhumi, 1957.
27. I.M.Rozman, Zhur.eksp.i teor.fiz., 28, 251 (1955).
28. J.T.Randall & M.H.F.Wilkins, Proc.Roy.Soc., A184, 366 (1945).

RADIATION DAMAGE IN PLASTIC SCINTILLATORS. Part II.*

- I.M.Rozman

1. Ionizing radiation produces a number of chemical transformations in organic substances.[1] In luminescent substances these transformations are accompanied by alteration of the scintillation characteristics, in particular, by a decrease of the luminescence yield. Thus in the case of irradiation of an anthracene crystal with α-particles from Po^{210} the scintillation intensity is characterized by

$$S = \frac{S_0}{1 + A_\alpha N}, \tag{1}$$

where N is the total number of α-particles incident on the surface of the crystal (per 1 cm^2) from the beginning of irradiation and $A_\alpha = 1.0 \cdot 10^{-11}$ cm^2.[2] A similar relationship was obtained for α-bombardment of other organic crystals by Black[3] as well as for irradiation of anthracene by electrons[4,5] and protons[6].

Equation (1) is analogous to the expression describing the quenching of the fluorescence of anthracene by tetracene and acridine[7,8], namely,

$$L = \frac{L_0}{1 + KX}, \tag{2}$$

where X is the relative molecular concentration of the impurity and K is the relative probability of capture of an exciton (migrating quantum of excitation energy) by a molecule of the impurity. Inasmuch as for not excessively large doses of radiation, the relative concentration of damaged molecules (damage products) is proportional to the dosage, Eq.(1) can be explained in a similar fashion.[2]

2. We investigated the kinetics of radiation damage of scintillators of polystyrene with 1,1',4,4'-tetraphenylbutadiene (TPB) and with p-terphenyl (pT) + TPB (Ref.9) as a result of bombardment with α-particles from Po^{210} and β-particles from $Ce^{144} \rightarrow Pr^{144}$. The experimental procedure and the principal results have been described earlier.[10] In the case of all samples there was observed a decrease in the luminescence intensity with increasing radiation dosage. At the same time, although more slowly, there occurs a decrease in transmission of the luminescence light (the samples turn yellow).

The luminescence intensity was measured on the basis of the mean current from a FEU-19 photomultiplier under constant excitation and recording conditions. After the sample has received a radiation dose D, the photomultiplier current is given by

$$I(D) = \text{const} \int n_\lambda(D) f_\lambda d\lambda, \tag{3}$$

where $n_\lambda(D)$ is the external luminescence spectrum of the scintillator and f_λ is the relative quantum sensitivity of the photomultiplier cathode. The difference between the spectrum $n_\lambda(D)$ after the sample has received a dosage D and the zero dose spectrum $n_\lambda(0)$ is in general due to a) decrease in the luminescence yield, B(D), b) additional absorption in the damage products $1 - t_\lambda(D)$ and c) possible alteration of the luminescence spectrum[11].

In the case of our scintillators we detected no noticeable change in the luminescence spectra. Consequently, in our case,

---

*For Part I see Atomnaia energiia (Atomic Energy), 1, 54 (1957).

$$n_\lambda(D) = \frac{B(D)}{B_0} n_\lambda(0)\, t_\lambda(D). \qquad (4)$$

Combining (3) and (4) we obtain

$$\frac{B(D)}{B_0} = \frac{I(D)}{I_0} \cdot \frac{\int n_\lambda(0) f_\lambda d_\lambda}{\int n_\lambda(0) f_\lambda t_\lambda(D)\, d\lambda}.$$

In our tests we measured the quantities I_0, $I(D)$ and $T_\lambda(D)$ the transmission of the full thickness of the samples. The quantitative relationship between t_λ and T_λ is determined by the spatial distribution of damage products and excited luminescence centers. For our experimental geometry there are obtained the following approximate relationships:

a) with excitation by the same radiation as that causing the damage

$$\frac{B(D)}{B_0} \approx \frac{I(D)}{I_0} \cdot \frac{\ln 1/T}{1-T}; \qquad (5a)$$

b) with excitation by Po^{210} α-particles and damage by $Ce^{144} \rightarrow Pr^{144}$ β-radiation

$$\frac{B(D)}{B_0} \approx \frac{I(D)}{I_0} T^{-0,92}; \qquad (5b)$$

c) with excitation by the λ = 254 mμ Hg line regardless of the damaging radiation

$$\frac{B(D)}{B_0} = \frac{I(D)}{I_0} T^{-1}. \qquad (5c)$$

The last equation also applies to the case of excitation of the scintillator with 1.5% TPB by the λ = 366 mμ line. In view of some uncertainty regarding the corrections for additional absorption, hereinafter we shall consider B(D) only for doses for which these corrections are not large.

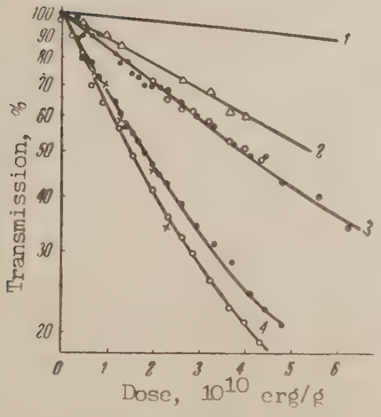

Fig.1. Variation of the light transmission of polystyrene with the α-radiation dosage: 1) for the luminescence of TPB, λ_{max} = 445 mμ, 2) for λ = 366 mμ, 3) for the luminescence of a polystyrene scintillator 5 mm thick, λ_{max} = 340 mμ, 4) same but for a thickness of 0.5 mm and λ_{max} = 310 mμ (+ - transmission for λ = 313 mμ; o & ● points obtained for two different samples.)

3. The additional absorption of light in the irradiated polystyrene decreases with increasing wavelength (Fig.1), which is in qualitative agreement with the results obtained by Fowler & Day[12] in irradiating technical polystyrene with γ and x-rays. For each wavelength the transmission T(D) is characterized by the simple exponential law (for $T \geqslant 0.4$), i.e., the coefficient of additional absorption is proportional to the dosage (see Table 1):

$$\mu_\lambda = K_\lambda D$$

Additional absorption of the luminescence of TPB in polystyrene with impurities is the same as in pure polystyrene. Hence it may be assumed that the processes of radiation damage whose products are responsible for the additional absorption are virtually identical in all polystyrene base scintillators.

The additional absorption in scintillators irradiated with β-particles is also described by the exponential law, in this case, however, two

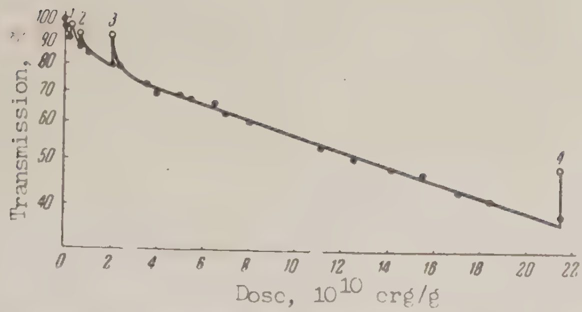

Fig.2. Variation of the transmission of the intrinsic luminescence light in a polystyrene scintillator with 1.5% TPB with the β-radiation dosage. Open circles indicate interruptions in radiation: 1) 18 hours, 2) 16 hours, 3) 73 hours, and 4) 12 days.

new effects are observed (Fig.2). First, during prolonged interruptions in irradiation the transmission is partially re-established (the samples were kept in the dark at room temperature). Second, during the initial irradiation period after an interruption, the transmission falls off somewhat more rapidly.* After attainment of "equilibrium" the coefficient of additional absorption for the luminescence of TPB is given by

$$\mu = K_\beta D,$$

where $K_\beta = 7.6 \cdot 10^{-11}$ g/erg^{-1} cm^{-1}, i.e., is smaller by a factor of 8 than in the case of radiation with α-particles (Table 1).

4. The yield of α-luminescence of polystyrene subjected to an α-particle dose $D \leqslant 5 \cdot 10^{10}$ erg/g is characterized by the expression (Fig.3)

$$B(D) = \frac{B_0}{1 + A_0 D}, \qquad (6)$$

where $A_0 = 2.36 \cdot 10^{-10}$ g/erg, i.e., varies according to the same law as that governing the yield of organic single crystals. The effective radiation stability of polystyrene, however, is approximately 40 times greater than that of anthracene.[3]

The shape of the B_α vs D curves for polystyrene with the luminescent impurities differs substantially from the curve described by Eq.(6). The initial sections of the curves up to about $B = 0.3\ B_0$ or $D \approx 1 \cdot 10^{10}$ erg/g are closely characterized by the exponential expression

$$B_\alpha(D) = B_0 e^{-AD}, \qquad (7)$$

where $A = 7.7 \cdot 10^{-11}$ g/erg for a scintillator with 1.5% TPB (Fig.4, curve 2) and $A = 1.23 \cdot 10^{-10}$ g/erg for a scintillator with 2.5% pT + 0.01 to 12% TPB.

Table 1

Additional absorption of intrinsic luminescence light in polystyrene radiated with Po^{210} α-particles

$\mu_\lambda = K_\lambda D$ (см$^{-1}$)

λ, mμ	313	$\lambda_{max} \approx 340$	336	$\lambda_{max} \approx 445$
K_λ, g erg^{-1} cm^{-1}	$11 \cdot 10^{-9}$	$4.6 \cdot 10^{-9}$	$3.4 \cdot 10^{-9}$	$6.0 \cdot 10^{-10}$

5. The appreciable drop in the luminescence intensity of pure polystyrene with increasing radiation dose (after appropriate corrections for the additional absorption) indicates that the decay products do not merely absorb the photons emitted by the polystyrene. Further, in the case of small doses the concentration of the decay products is clearly insufficient for absorption of a significant fraction

---

*With irradiation by α-particles both effects are appreciably weaker and in many cases are within the limits of the experimental error.

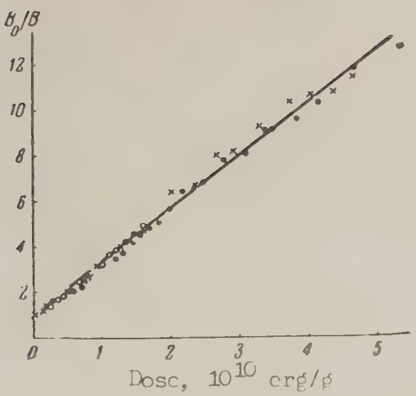

Fig. 3. Variation of the luminescence yield of polystyrene with the α-radiation dosage (points for three different samples).

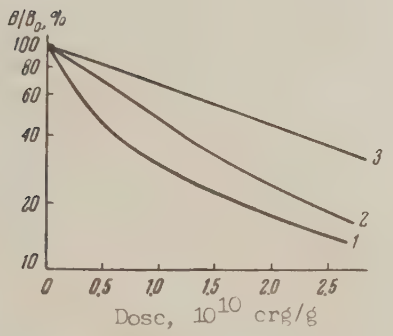

Fig. 4. Comparison of the variation in luminescence yield of polystyrene scintillators with the α-radiation dose and type of excitation: 1) pure polystyrene, α-excitation; 2) scintillator with 1.5% TPB, α-excitation; 3) scintillator with 1.5% TPB, λ = 366 mμ excitation.

of the energy of the exciting ionizing radiation. Consequently, it must be inferred that the damage products produce quenching of the polystyrene luminescence. The observed dosage dependence (6) gives reason to infer that the quenching mechanism in this case is similar to the quenching mechanism in anthracene and consists of competition between the emission of photons by the excited polystyrene molecules and transfer (migration) of excitation energy to the damaged molecules in which the energy is dissipated in the form of thermal vibrations.

The situation is more complicated in the case of polystyrene with luminescent impurities. In this case the efficiency of energy transfer from polystyrene to the damaged molecules is reduced somewhat owing to the operation of the competing process of energy transfer to the impurity molecules. It may be assumed that the quenching of the luminescence of the impurity molecules will be determined primarily by a "static" mechanism in the sense of Peppen's theory[13], inasmuch as the luminescence spectra of the impurities in question lies in the region of relatively weak absorption of the quencher, particularly in the case of tetraphenylbutadiene.

In view of this, the results of the following experiment we performed are of great interest. We determined the effect of increasing doses of α-radiation on the fluorescence intensity of a scintillator with 1.5% TPB under excitation by 366 mμ light. The results after appropriate correction for the additional absorption are shown in Fig. 4 (curve 3); the observed decrease in intensity is characterized by

$$B_1(D) = B_{10}e^{-\alpha_1 D},$$

where $\alpha_1 = 4.1 \cdot 10^{-11}$ g/erg.

Yet according to the above assumptions one should have expected the decrease to be described by

$$B_1(D) = B_{10}\frac{C\varepsilon}{C\varepsilon + C_d\varepsilon_d}e^{-\varkappa C_d},$$

where ε and ε_d are the absorption coefficients for λ = 366 mμ of the luminescent impurity and the damage products and C and C_d are the concentrations of the luminescent impurity and the damage products, respectively (after the scintillator has received a dose D). Inasmuch as according to the additional absorption data C_d is proportional to D and $\varepsilon_d C_d$ is known, while by definition

$$C = C_0e^{-10^{-14}MGD} = C_0e^{-aD}$$

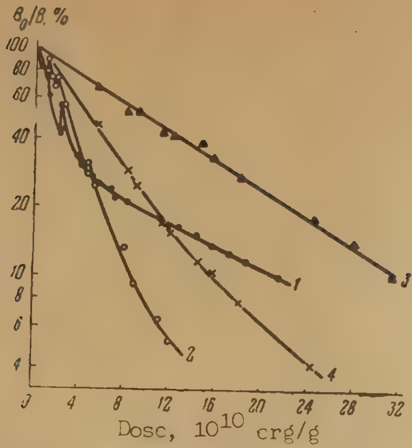

Fig.5. Variation of the relative luminescence yield of a scintillator with 1.5% TPB with the β-radiation dose and the type of excitation: 1) β-particles, 2) α-particles, 3) λ = 366 mμ, 4) λ = 254 mμ. The discontinuities in curves 1 & 2 are connected with interruptions in β-irradiation.

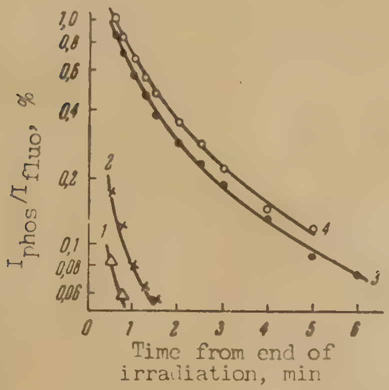

Fig.6. Variation of the ratio between phosphorescence and fluorescence of a scintillator with 1.5% TPB with the β-radiation dose with excitation by β-particles. Doses in 10^{10} erg/g: 1) 0.35, 2) 0.70, 3) 4.0 and 4) 6.5.

(where M is the molecular weight and G is the yield of the radiation damage reaction on the impurity in molecules per 100 ev), we can write

$$B_1(D) = \frac{B_{10}e^{-\alpha_1 D}}{1 + A_1 D e^{aD}}, \qquad (8)$$

where A_1 = $9.1 \cdot 10^{-13}$ g/erg (ε = $2.3 \cdot 10^5$ cm^2/g). For TPB, a = $3.6 \cdot 10^{-12}$ G g/erg. In view of the high radiation stability of such molecules with conjugate double bonds and benzene rings[1] it may be assumed that G ≈ 1 or less. Consequently, for the range of doses of interest to us the denominator in (8) is close to unity, i.e., the results of the above mentioned experiment are not in conflict with our assumption regarding the character of the quenching of the luminescence of TPB.

In Fig.5 we show the variation of the relative luminescence yield of a scintillator with 1.5% TPB with the dose of $Ce^{144} \rightarrow Pr^{144}$ β-radiation under excitation by the same β-particles and also with excitation by Po^{210} α-particles and 254 and 366 mμ light. As might have been expected, with excitation by the 366 mμ line the luminescence yield decreases more slowly than in the case of excitation with α-particles and the 254 mμ line. The decrease is characterized by

$$B_1 = B_{10}e^{-\beta_1 D},$$

where β_1 = $7.3 \cdot 10^{-12}$ g/erg, i.e., is 6 times smaller than in the case of α-irradiation (Fig.4), which is in agreement with the results obtained in investigating additional absorption. With excitation by the 254 mμ line, the yield decreases more slowly than with α-excitation. This is due to partial (~30%) absorption of the ultraviolet light directly by the TPB. For heavier doses the B = f(D) curve in the case of β-excitation is flatter than in the case of 366 mμ excitation. This, however, is not inconsistent with the proposed quenching mechanism. Actually in Fig.5 the horizontal scale is laid off in mean values of the dose according to the effective range of the given exciting radiation. For short-range radiation (α and ultraviolet) the true value of the dose practically does not differ from the mean value. For β-particles, however, the dose in the second half of the scintillator is about 4 times smaller than the dose on the front surface. Hence in the case of nominally high mean dose, the major portion of the luminescence photons will be emitted by parts of the scintillator that have received a dose considerably less than the mean value. If the β-particle irradiation is in-

Table 2

Damage to polystyrene scintillators under irradiation by Po^{210} α-particles

Luminescent impurity	Concentration, %	Dose reducing the luminescence yield by a factor of 2, 10^9 erg/g
Pure polystyrene		4.2
1,1',4,4'-tetraphenylbutadiene-1,3 (TPB)	1.5	9.0
p-Terphenyl + TPB	3 0.02	6.1
p-Terphenyl + TPB	2.5 0.01-0.12	5.6

terrupted for an appreciable period, the luminescence yield is partially re-established (this is indicated by the discontinuities in curves 1 & 2 in Fig.5). When the radiation is resumed, however, the luminescence falls off at a faster rate. An analogous effect has been observed in the case of irradiation with cathode rays.[11]

7. There is one more effect worth mentioning. In the case of excitation with β-particles of a previously irradiated polystyrene scintillator there appears a phosphorescence with a decay time of several minutes. The decay does not follow the exponential law (Fig. 6) and its relative intensity increases with the dose. No such persistent luminescence was observed with excitation by α-particles. If there is phosphorescence with α-particle excitation, its intensity must be less than 1/70 the intensity with β-excitation (based on the same exciting radiation energy absorbed). An analogous effect was observed by Pannel & Manning[14] who explained it by the formation of F-centers.

8. The radiation stability of some of the polystyrene scintillators tested is characterized in Table 2. The good stability of these scintillators together with linear dependence of luminescence intensity on the dosage rate (up to 10^6 erg g^{-1} sec^{-1}) makes them suitable to use for measurements in very strong ionizing radiation fluxes[10].

References

1. H.G.Heal, Atomics, 6, 205, 241 (1955).
2. J.B.Birks & F.A.Black, Proc.Phys.Soc., A64, 511 (1951).
3. F.A.Black, Phil.Mag., 44, 263 (1953).
4. W.Hanle & K.H.Rau, Physik, 133, 297 (1952).
5. K.Hengst, ZS.Naturforsch, 6a, 540 (1951).
6. H.P.Gilfrich, ZS.Physik, 145, 241 (1956).
7. E.J.Bowen & E.Mikiewicz, Nature, 159, 706 (1947).
8. E.J.Bowen, E.Mikiewicz & F.W.Smith, Proc.Phys.Soc., A62, 26 (1949).
9. E.A.Andreeshchev, E.E.Baroni, K.A.Kovyrzina, E.I.Pani, I.M.Rozman & V.M.Shoniia, PTE (Instrumentational & Experimental Technique), 1, 32 (1956).
10. I.M.Rozman & K.G.Tsimmer, Atomnaia energiia (Atomic energy), 1, 54 (1957); 2, 70 (1957).
11. H.Hinrichs, ZS.Naturforsch., 9a, 617, 625 (1954).
12. J.T.Fowler & M.J.Day, Nucleonics, 13, 12, 52 (1955).
13. Th.Forster, Fluoreszenz organischer Verbindungen.-Göttingen, 1951.
14. J.H.Pannel & B.J.Manning, J.Chem.Phys., 23, 1368 (1955).

POLYSTYRENE-BASE PLASTIC SCINTILLATORS

- E.A.Andreeshchev, E.E.Baroni, K.A.Kovyrzina, I.M.Rozman & V.M.Shoniia

The various scintillators tested were prepared in the following manner. A glass vial was half-filled with thoroughly purified distilled (under nitrogen) styrene with a weighed amount of the desired luminescent solute. The vial had a long outlet tube which served as the reflux condenser during polymerization. After elimination of air by prolonged passage of nitrogen through the vial, the outlet tube was sealed off (or closed by means of a valve); the polymerization was carried out in a glycerol bath with the vials mounted on a 50 cps vibrator to insure thorough mixing. During approximately the first hour the temperature of the glycerol was raised to 150°. At the 100-120° point, the mixture was checked for complete solution of the impurity in the styrene. The exothermal process of polymer nuclei formation was allowed to proceed for 2 hours at 150°. Following this the temperature was raised to 200° and the polymerization carried to completion over a period of 10 hours. The average molecular weight of the polymerizers was about 60,000. Finally, the vial was slowly cooled in the bath. In some respects our procedure differed appreciably from the procedures usually employed in preparing plastic scintillators[1-4].

The luminescent organic additives, which were synthesized in our laboratory, were also thoroughly purified. After chromatographic separation using aluminum oxide and evaporation of the solvent, they were subjected to repeated high vacuum distillation.

The luminescence yield measurements were carried out with cylindrical samples 16 mm in diameter and 10 mm high formed by machining on a lathe. The cylinders were polished to a completely smooth surface by means of precipitated calcium carbonate in alcohol. The luminescence was excited by $Ce^{144} \rightarrow Pr^{144}$ β-radiation. The luminescence intensity was determined from the mean FEU-19 photomultiplier current under standard excitation and measurement conditions. The dependence of the luminescence intensity of some plastic scintillators on the concentration of the luminescent solute is shown in the accompanying figure. The indicated values are relative, the yield of the scintillator with 1.5 gram 1,1',4,4'-tetraphenylbutadiene-1,3 per 100 gram polystyrene being taken as 100. The highest efficiency in the case of measurements with an FEU-19 photomultiplier is exhibited by scintillators activated with ~3% p-terphenyl and ~1.3% 2,5 diphenyloxazole.

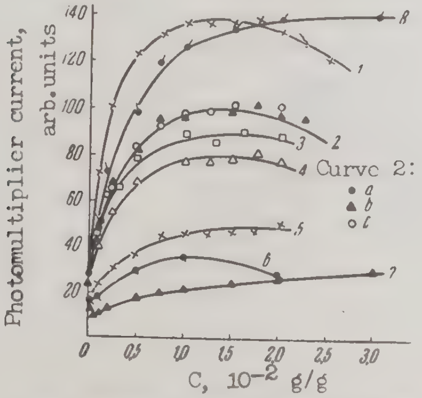

Variation of the efficiency of plastic scintillators with the luminescent impurity concentration (all samples 10 mm thick; excitation by β-particles): 1) 2,5-diphenyloxazole-1,3, 2a) 1,1',4,4'-tetraphenylbutadiene-1,3, 2b) 1,3,5-triphenylpyrazoline-Δ^2, 2c) 1,5-diphenyl-3-n-(metoxyphenyl)-pyrazoline-Δ^2, 3) α,β-diphenyl-o-toluindole, 4) 2,4,5-triphenyloxazole-1,3, 5) 1,5-diphenyl-3-styrylpyrazoline-Δ^2, 6) perylene, 7) anthracene, 8) p-terphenyl.

The cited data do not allow of drawing unequivocal deductions regarding the radioluminescence yield of the scintillator or regarding the fluorescence efficiency of the impurities. For comparison of the radioluminescence efficiencies one must introduce appropriate corrections for the spectral sensitivity

Table 1

Some characteristics of polystyrene scintillators. Cylindrical samples 16 mm in diameter, 10 mm high; excitation of radioluminescence by β- or γ-radiation.

Luminescent impurity	Concentrat. 10^{-2} g per g polystyrene	Luminescence band peak, mμ	Relative yield of luminescence			Quantum fluorescence yield, q	B_{rel} / q
			Effic. photo-multip.	S_{ext}	B_{rel}		
Fluoranthrene	1	470	47	55	1,0	0,52	1,9
Anthracene	3	430	30	21	0,4	0,26	1,7
Perylene	1	485	36	60	1,1	0,57	1,9
Acenaphthalene	1	355	58	26	1,0	0,48	2,1
p-Terphenyl (pT)	3	368	140	64	1,1	0,58	1,8
pT + quaterphenyl	3+0.1	390	147	82	—	—	—
1,1',4,4'-Tetraphenyl-butadiene-1,3 (TPB)	1,5	452	100	100	1,0	0,68	1,5
pT + TPB	3+0.05	438	122	108	—	—	—
2,3-Diphenyl-*o*-tolu-indole	1.6	412	90	58	0,7	0,50	1,5
2,3-Diphenyl-*p*-tolu-indole	1.5	420	84	56	0,7	0,49	1,5
2,3-Diphenylindole	0.5	418	82	54	0,6	0,52	1,2
1,3,5-Triphenylpyrazoline-Δ² (TPP)	1.5	455	100	95	1,1	0,76	1.5
pT + TPP	2+0.06	440	122	102	—	—	—
1,5-Diphenyl-3-(*n*-metoxyphenyl)-pyrazoline-Δ²	1.3	451	100	100	1,2	0,84	1,4
1,5-Diphenyl-3-styryl-pyrazoline-Δ²	1.8	496	49	89	1,2	0,76	1,6
2,5-Diphenyloxazol-1,3	1.3	389	137	70	0,9	0,54	1,6
2,4,5-Triphenyloxazole-1,3	1.5	394	80	45	0,6	0,37	1,6
2,5-Diphenyloxadiazole-1,3,4	1.7	358	104	48	0,9	0,47	2,0
Pure polystyrene	—	310	18	8	0,2	0,09	2,4

of the detecting equipment and for reabsorption in the sample. After making the first correction, we obtain the so-called "technical efficiency" or external scintillation yield S_{ext}. After making the second correction, we obtain the relative radioluminescence yield B_{rel}, giving (with an accuracy to a constant factor) the number of photons emitted in the scintillator per unit excitation energy absorbed. The computed values of S_{ext} and B_{rel} for a number of polystyrene scintillators are listed in Table 1.[5] Scintillators with p-terphenyl as the main luminescent impurity and tetraphenylbutadiene or triphenylpyrazoline as the spectrum shifter apparently have the highest external luminescence yield.

The scintillator formulation exhibiting the highest efficiency depends, of course, to some extent on the size of the scintillator. Thus, for example, in the case of 20 mm thick cylinders, scintillators with 0.02 g/g p-terphenyl and 0.0004 g/g triphenylpyrazoline have a higher efficiency than scintillators with 0.03 g/g p-terphenyl and 0.0002 g/g tetraphenylbutadiene when tested both with an FEU-19 and with an FEU-S photomultiplier. The luminescence band peaks of these scintillators coincide (Table 2).

The fluorescence efficiencies of the impurities in the plastic scintillators (Table 1) were evaluated relative to the scintillator with tetraphenylpyrazoline[6] for which measurements by two procedures[7] yielded q = 0.76.

Table 2

Efficiency of polystyrene scintillators tested with an FEU-S photomultiplier. Cylindrical samples 16 mm in diameter and 20 mm high; excitation by Ce^{144}→Pr^{144} β-radiation.

Luminescent impurity	Concentration 10^{-2} g/g per styrene	Relative efficiency
p-terphenyl (pT)	3	56
pT + quaterphenyl	3 + 0.1	79
pT + tetraphenylbutadiene	3 + 0.02	100
pT + triphenylpyrazoline	2 + 0.04	103
diphenyloxazole	1.3	77

The heterocyclic Δ^2-pyrazoline compounds are characterized by a very high quantum efficiency. Of particular interest in this class of compounds is 1,5-diphenyl-3-styrylpyrazoline-Δ^2 whose luminescence spectrum falls in the region of the maximum sensitivity of the human eye. Consequently, plastic scintillators with this impurity are suitable for visual detection of penetrating radiations.

It is known that for organic single crystals the radioluminescence efficiency is determined primarily by the fluorescence efficiency. (Ref.8 & 9) In the case of plastic scintillators a significant role is also played by the efficiency of energy transfer from the polystyrene to the luminescent impurities. The extent to which B_{rel}/q (Table 1) for scintillators with impurities differs from the value of this ratio for pure polystyrene depends on the efficiency of excitation energy transfer in the scintillator. In Table 2 we have listed the characteristics of a few scintillators that showed the highest efficiency when used in conjunction with an FEU-S photomultiplier.

References

1. W.L.Buck & R.K.Swank, Nucleonics, 11, 11, 48 (1953).
2. L.Pichat, P.Pesteil & J.Clement, J.chim.phys., 50, 26 (1953).
3. L.Wouters, Nucleonics, 12, 3, 26 (1954).
4. M.M.Koton, Zhur.tekh.fiz., 26, 1741 (1956).
5. I.M.Rozman, Dissertation, Sukhumi, 1957.
6. E.A.Andreeshchev, E.E.Baroni, K.A.Kovyrzina, I.E.Pani, I.M.Rozman & V.M.Shoniia, PTE (Instrumentation & Experimental Technique) 1, 32 (1956).
7. I.M.Rozman, Opt.i spektr., 2, 480 (1957).
8. G.T.Wright, Proc.Phys.Soc., A68, 701 (1955).
9. A.Z.Chizhikova & M.D.Galanin, Zhur.eksp.teor.fiz., 30, 187 (1956).

NEW PHOTOMULTIPLIERS

- N.S.Khlebnikov

Our work leading toward the development of new photomultipliers began with an investigation of the properties of FEU-19 since it was our aim to produce multiplier tubes better able to meet the requirements of nuclear physics than the FEU-19. A satisfactory spectrometric multiplier was the primary goal; this would be a tube type consistently possessing high pulse-height resolution, such as is exhibited by only 1-2% of the entire FEU-19 output at present.

We know[1] that the pulse-height resolution of photomultipliers depends primarily on the sensitivity of the photocathode (or, more precisely, on its quantum efficiency in the long wavelength region of scintillators), on the homogeneity of this sensitivity over the photocathode surface and on the efficiency of photoelectron collection by the effective portion of the first dynode's emitting surface (assuming that each dynode collects 100% of the secondary electrons emitted from the previous dynode). These properties were investigated in about 100 tubes taken from several batches of the current FEU-19 production.

The tubes tested showed a wide spread of the sensitivity and efficiency: the sensitivity ranged from 2.5 to 44 microamp/lumen, while quantum efficiency for $\lambda = 4047$ Å ranged from 1 to 12%.

The uniformity of photocathode sensitivity and photoelectron collection on the first dynode were measured by means of a simple set-up consisting of a point incandescent lamp, a Nipkow disk with 9 apertures and a cathode-ray oscilloscope. The Nipkow disk, which was rotated by a synchronous motor, scanned the entire photocathode with 9 lines. The oscilloscope screen registered the photocathode sensitivity distribution (the heights of each of the 9 pulses). Photoelectron collection was shown by the corresponding trace of the current from the photocathode to the first dynode.

Figs.1 and 2 are typical photographs of the oscilloscope screen for two different photocathodes and two scanning directions; in each figure the a trace pertains to the photocathode and the b trace to the first dynode. Fig. 1a shows one of the two common patterns of nonuniform photocathode sensitivity: sensitivity highest in the middle and falling off rapidly towards the edges. The opposite pattern - lowest sensitivity in the middle and highest sensitivity at the edges - is shown in Fig.2a. Both figures also illustrate the change in the pulse height ratios as we go from the photocathode to the first dynode, which indicates that collection is not identical for different portions of the photocathode, but falls off from the center to the edges. A comparison of the traces in Fig.2 is especially interesting. Whereas Fig.1b shows all 9 pulses corresponding to the nine lines of photocathode scanning, in Fig.2b the first, eighth and ninth pulses (counting from left to right) have entirely disappeared, while the seventh pulse, which is the highest in Fig.2a, is barely perceptible.

The difference in experimental geometry in the two cases is that the scanning direction in Fig.1 was parallel to the plane of symmetry of the dynode system, whereas in Fig.2 it was perpendicular to that plane. The associated differences are illustrated in Fig.3, which represents the electron-optical input section of the FEU-19 modeled in an electrolytic bath (the electrolytic tank model differs from the actual FEU-19 by the introduction of two additional lenses between the photocathode and the shield.) The disposition of electrodes, fields and electron trajectories is here shown in the plane of symmetry of the system. Thus Fig.1 corresponds to scanning of the photocathode parallel to the plane of Fig.3. The presence of the two additional lenses in the system in Fig.3 results in photoelectron collection on a very narrow effect-

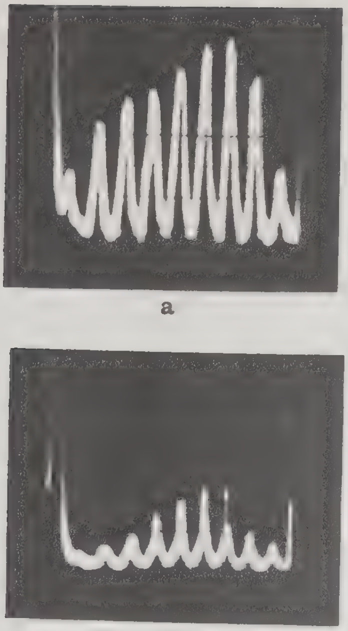

a

b

Fig. 1

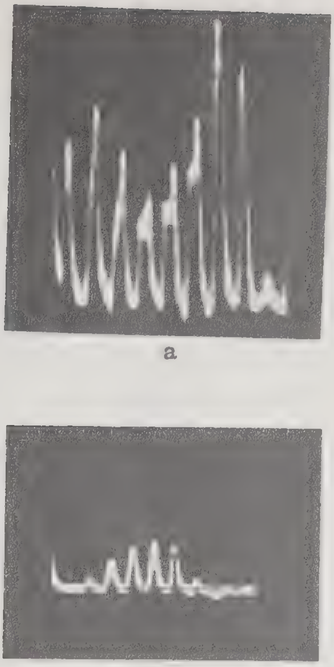

a

b

Fig. 2

Fig.1. Distribution of photocathode sensitivity (A) and of photoelectron collection on the first dynode (b) of an FEU-19 photomultiplier with the scanning direction parallel to the plane of symmetry of the dynode system (the plane of Fig.3).

Fig.2. Same as Fig.1 but for a different FEU-19 photomultiplier tube and with the scanning direction perpendicular to the plane of symmetry of the dynode system.

ive portion (indicated by arrows) of the first dynode (1.5 - 2 mm in actuality). In the absence of these lenses (in a real FEU-19) only a certain fraction of the photoelectrons can be collected by the working part of the first dynode (mainly from the middle of the photocathode, from which they emerge at small angles to the normal). The remaining photoelectrons either strike the reverse side of the third dynode or reach the first dynode outside of the effective area, producing secondary electrons that strike the nonworking section of the second dynode (this section is equal to a little more than half of the dynode guide as reckoned from its upper boundary). In both cases these photoelectrons are "lost" as far as contributing to the multiplication is concerned.

We can now easily understand the differences associated with the direction of the scanning light beam. In the case represented by Fig.1, each line traced by the scanning beam intersects the center line of the photocathode, i.e., the section even from the edges of which the photoelectrons can reach the first dynode (since the dynode extends in this direction). When the scanning lines are perpendicular to the above plane, the outer lines consistently lie outside this section.

The results of the investigation summarized briefly above served as the basis for certain changes in the design of the FEU-19 input section. The same

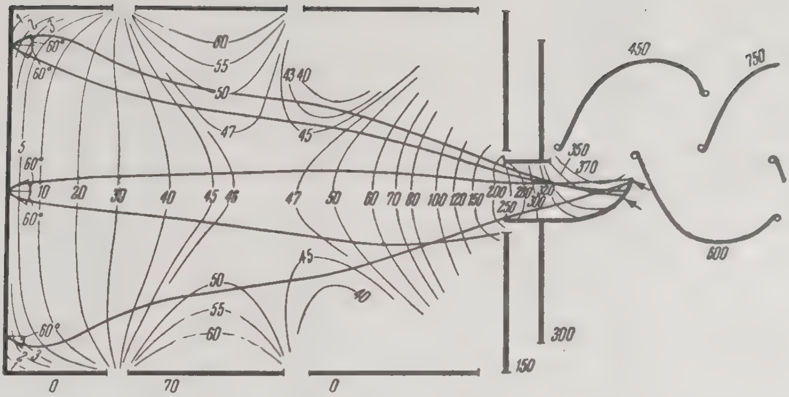
60
55
50
43 40
47
45
60°
5
10
20
30
40
45 46
47
50
60 70 80 100 120 150
200
250
45
50
55
60
40
450
750
350
370
600
300
150
0
70
0

Fig. 3. Electron-optical input section of the FEU-19 photomultiplier modeled in an electrolytic bath. The model differs from the actual photomultiplier in that it has two additional lenses between the photocathode and the shield.

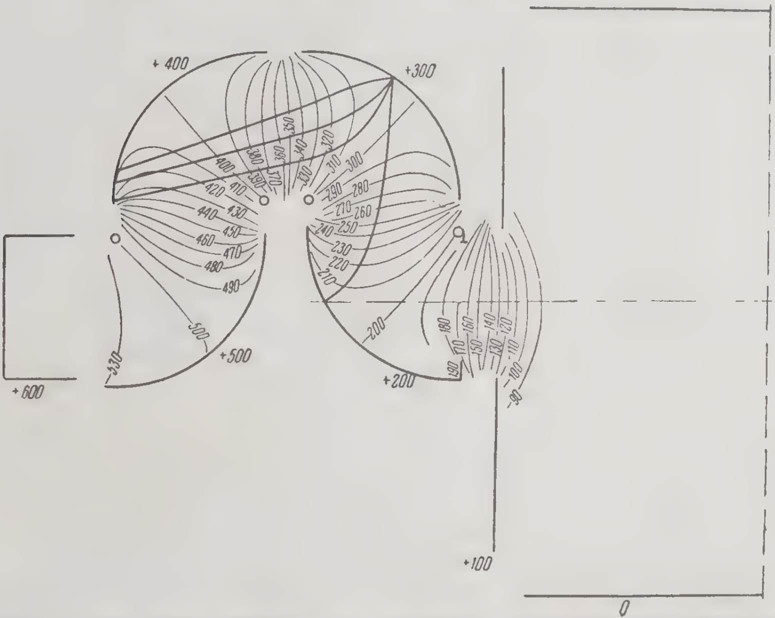
+400
+300
+500
+600
+200
+100
0
500
200

Fig. 4. Shape and arrangement of dynodes. Fields and electron trajectories obtained in electrolytic bath model study.

investigation indicated the problems that had to be solved in designing suitable spectrometric photomultipliers and also pointed up certain technological aspects of tube production that required attention. Our principal conclusion was that any attempt to combine an end-window type photocathode with the FEU-19 dynode system would be inadvisable as regards development of high-grade photomultipliers to be used with scintillation counters, particularly in the case of tubes intended for large scale production, because the present arrangement of the first few dynodes with respect to each other and with respect to the entrance shield requires higher precision forming and assembly than can be attained in practice. It was equally obvious that additional lenses must be used in the input section.

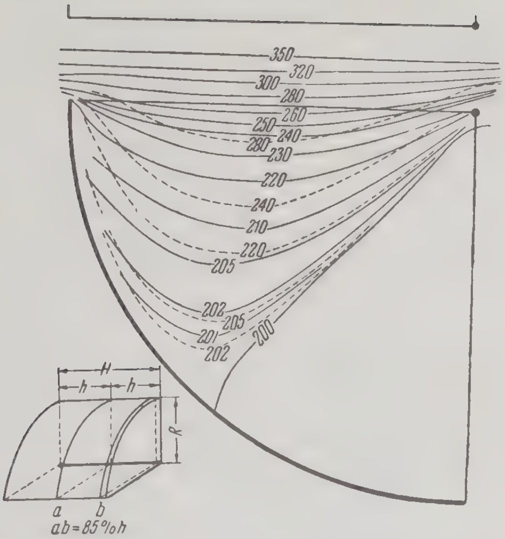
350
320
300
280
260
250
240
280
230
220
240
210
220
205
202
205
201
202
200
H
h
h
R
a
b
ab=85%h

Fig.5. Design of an individual dynode of the new photomultiplier (one-fourth of a right-circular cylinder with H = 1.5 R) and field distribution inside the dynode for two planes: solid lines for plane b and dash lines for plane a.

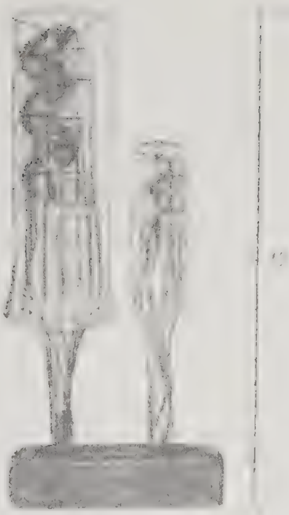

Fig.6. View of mounted dynode systems of the described type: at left - assembly corresponding to Fig.5; at right - reduced scale model.

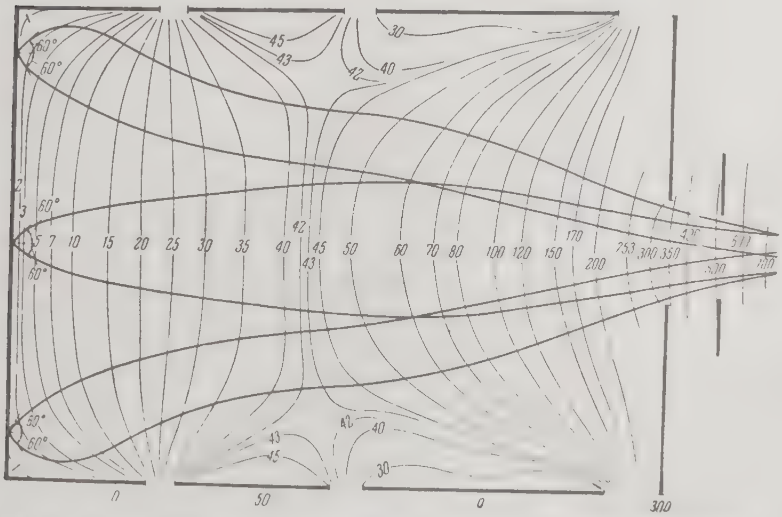
45
43
42
40
30
60°
60°
5
7
10
15
20
25
30
35
40
42
45
43
50
60
70
80
100
120
150
170
200
250
300
350
0
50
0
300

Fig.7. Field distribution and electron trajectories at the entrance of the spectrometric photomultiplier (laboratory type 1S(1C)).

The first problem was thus the selection of a dynode system that could readily be used in conjunction with an end type photocathode. When a number of FEU-19 tubes (from the same batches) were tested for operating stability, most of them were found to be unstable. It was definitely established that the principal cause of the instability was traceable to the antimony-cesium coating on the dynode emitting surfaces. Hence it became necessary to find more stable materials and thus to depart from the existing FEU-19 as regards not only the design but the entire manufacturing process.

The dynode system suitable for a spectrometric photomultiplier was developed from the so-called L-type dynodes which have been described by Zworykin

and his coworkers[2]. We developed this system in 1950; it was announced independently but in a somewhat different form by the DuMont Laboratories. Fig.4 shows the shape and arrangement of the dynodes, the field distribution and a few electron trajectories, found by modeling in an electrolytic tank. Fig.5 shows an individual dynode, which is one-fourth of a right-circular cylinder with H = 1.5 R. Here the field distribution inside the dynode is shown in greater detail for two planes: the center plane (dash lines) and the plane which intersects the dynode at 0.925 of its height above one of its end surfaces (solid lines).

An important feature of this drawing is the low voltage gradient at the working surface of the dynode (about 5 v/mm). This is a shortcoming of the given system which precludes its use when high time resolution is required. In all other respects, as can be seen from Fig.4, the system satisfies the above-enumerated requirements for a spectrometric photomultiplier. When this multiplier system is combined with an end type photocathode, neither the first nor the succeeding dynodes require very precise mounting; the electron-optical input section axis intersects the surface of the first dynode in the positive gradient region. Therefore when the electron flux from

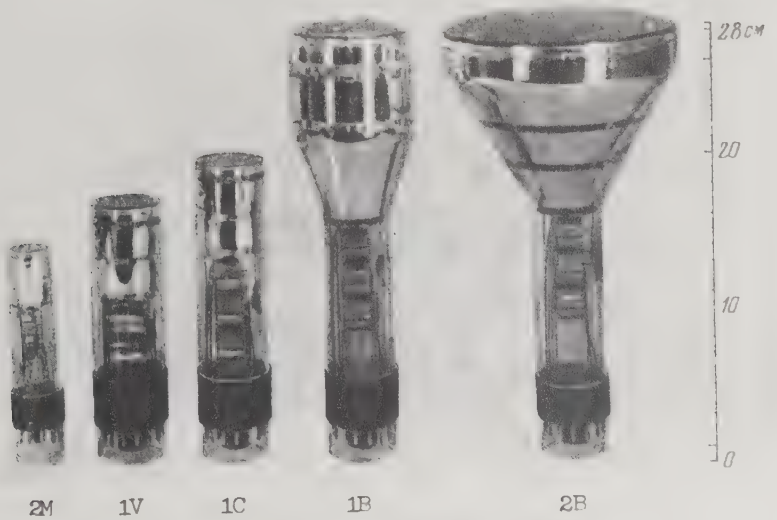
28см
20
10
0
2M
1V
1C
1B
2B

Fig.8. New types of photomultiplier tubes.

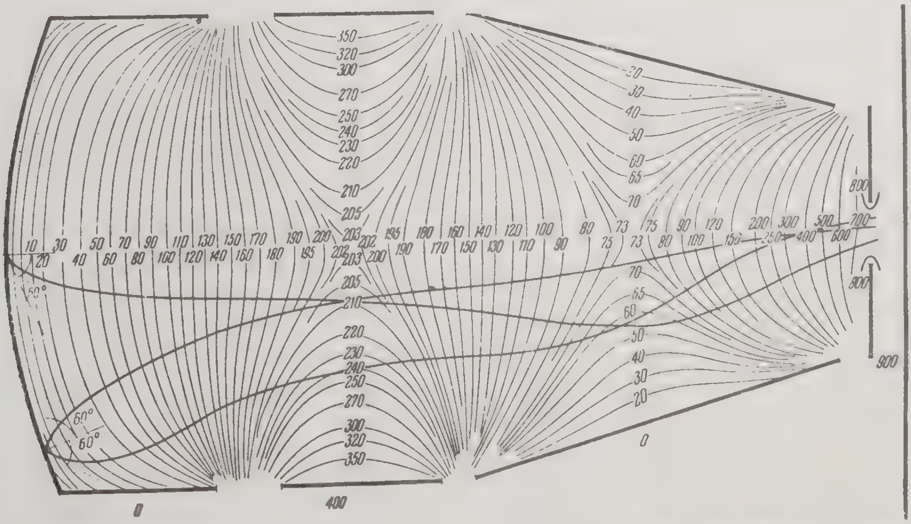
350
320
300
270
250
240
230
220
210
205
203
202
200
10
20
30
40
50
60
70
80
90
100
110
120
130
140
150
160
170
180
190
195
60°
20
30
40
50
60
65
70
73
75
80
90
100
120
150
200
250
300
400
500
600
700
800
900
0
400

Fig.9. The same as Fig.7 but for laboratory Type 1B photomultiplier tube.

the photocathode is sufficiently sharply focused, for which additional electron lenses are required at the entrance, all requirements for the input section design of a spectrometric photomultiplier have been satisfied.

Fig.6 is an external view of the given dynode system mounted under shielding caps. The larger version corresponds dimensionally to Fig.5, while the smaller version consists of dynodes which are half as large.

Since stable photomultipliers require dynode-coating materials other than Sb-Cs, we tested a number of special alloys prepared by E.S.Shpichenetskii and I.L.Rogel'berg at the "Giprotsvetmetobrabotka" Institute (State Research and Design Institute for Nonferrous Metals) and selected an aluminum-magnesium alloy as most suitable from the technological point of view.

Fig.7 shows the input section field distribution and electron trajectories in laboratory Type 1S tube, which was the first of the newly developed spectrometric photomultipliers; a photograph of this tube is shown in Fig.8. This design of the entrance chamber enables the first dynode to collect 95-100% of the electrons (in every tube!) and thus insures uniformly good spectrometric quality with otherwise satisfactory basic characteristics (cathode quantum efficiency, uniform sensitivity and amplification). A similar result (~100% electron collection efficiency) was obtained with all photomultipliers of type 1B (Fig.8), the fields and trajectories of which are shown in Fig.9.

As we have already stated, dynode systems of the type shown in Fig.6 do not furnish high time resolution. We therefore used a circular type of dynode system to obtain a photomultiplier with enhanced time resolution (laboratory Type IV, Fig.8). The principal merit of this system is the possibility of obtaining field gradients at the dynode emitting surfaces which are greater by about one order of magnitude than in the case of the above-described system. This system can be combined entirely satisfactorily with an end-window type photocathode (the entrance chamber in this instance being represented in Fig.7). The time resolution of such photomultipliers is $(1.5\text{-}3)\cdot 10^{-9}$ sec.

Type IV led directly to the development of types 2B (with a cathode 150 mm in diameter) and 2M (with a cathode 27 mm in diameter - see smaller assembly in Fig.6).

We obtained generally good results from our extensive testing of a large number of individual photomultiplier tubes of types 1S, 1B and IV under actual operating conditions. The principal data are given in the table, which also includes similar information on types 2M and 2B based on tests on a considerable number of tubes. Testing of these tubes under actual operating conditions also yielded good results.

In conclusion we wish to mention further directions of photomultiplier development. The present series of spectrometric types with different cathode diameters must be extended to both larger and smaller diameters (partially done in 1956). The fundamental future problem is the designing of new types with improved time-resolution characteristics. Some specific developments we have in mind are: 1) a new circular type of dynode system incorporating a large number of dynodes; 2) a new linear time-resolution type containing annular dynodes (Fig.10 is a photograph of one of the earliest attempts); and 3) high time-resolution photomultipliers with a large cathode area.

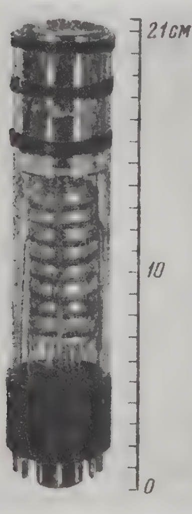

Fig.10. New type of photomultiplier tube with several toroidal dynodes.

A. General data on photomultipliers

Type	Dimensions overall		Type dynode system	Number of dynodes	Dynode material	Cathode diameter	Type cathode
	dia.	length w. base					
1S	48	205	linear	11	AMCK (Al-Mg) alloy	40	Cesium-antimony
1B	80	290	"	11		75	
1V	48	169	circular	10		40	
2M	34	130	linear	10-13		25	
2B	150	310	"	11		145	

B. Basic photomultiplier parameters

Type tube	Integral* sensitivity of phtcathode, μa/lumen	Fluorescence yield (λ = 4047 A), elect/photon.	Inhomogeneity of photocathode sensitivity,%	Electron collection on 1st dynode	Overall voltage, v	Maximum interstage voltage, v	Total amplif.	Dark current in collector circuit, μa	Input capacitance, μμf
1S	30÷90	8÷16	±5	95±5	1800÷2200	170	$5\cdot10^5\div10^6$	0,1	⩽4
1B	30÷90	8÷16	±5	95±5	1800÷2200	170	$5\cdot10^5\div10^6$	0,1	⩽4
1V	30÷90	8÷16	±5	95±5	2300÷2500	190	$\geqslant10^6$	0,05	⩽4
2M	30÷90	8÷16	±5	95±5	1250÷2200	170	10^5	0,1	⩽4
2B	30÷90	8÷16	±10	90±10	1800÷2200	170	10^5	0,1	⩽4

---

*Color temperature source - 2850°K.

C. Operating characteristics

Type	Pulse-height resolution,%, for 861 kev	Intrinsic noise level, kev	Time resolution, sec	Settling time, sec
1S	7-9	10	$5\cdot10^{-8}$	3
1B	7-9	10	$5\cdot10^{-8}$	3
1V	8-11	10	$2\cdot10^{-9}$	3
2M	7-10	10	$3\cdot10^{-8}$	3
2B	8-12	10	------	3

The following persons have taken an active part in the photomultiplier developmental work: A.E.Melamid, E.P.Iurlova, V.I.Bogatyrev, A.M.Potapov, G.E. Levin, Iu.A.Timoshenko, M.F.Adamovich and V.F.Ivanov.

References

1. J.Birks, Scintillation Counters. (Cited in Russian trans., M.1955.)
2. V.K.Zworkyn, G.A.Morton & L.Malter, Proc.IRE, 24, 351 (1936).

PRODUCTION OF PHOTOMULTIPLIERS AND THEIR BASIC PARAMETERS

- A.E.Melamid

The elementary or basic parameters of photomultipliers are understood to be the paramteres that depend directly on the properties of the photocathode, the design of the electron optical input section and the design and characteristics of the dynode system.

The principal basic parameters determining the quality of a photomultiplier cathode are its integral sensitivity and quantum efficiency. The integral sensitivity of a photocathode is defined as the ratio of the photocurrent to the light flux in lumens incident on the photocathode from a source having a color temperature of 2850°K. This quantity is usually expressed in microamp per lumen. The quantum efficiency is understood to be the ratio of the number of electrons ejected from the cathode to the number of quanta incident on it (usually expressed in percent). In the case of semitransparent cesium-antimony cathodes these quantities depend primarily on the thickness of the initial antimony layer and the way it has been cesiated; the dependence on the thickness of the layer, as may be seen from Fig.1, is very pronounced. Inasmuch as with increasing cathode thickness, in addition to the change in quantum efficiency, the maximum of the spectral characteristic is shifted to the long wavelength side of the spectrum (see Fig.2), for determining the quality of a photomultiplier cathode it is not sufficient to know only its integral sensitivity. Thus a comparatively thick cathode with a relatively high integral sensitivity may have a low quantum efficiency. In case the given photomultiplier is intended for use in conjunction with a scintillation counter, i.e., in the rather narrow spectral range of scintillators, the parameter determining the quality of the cathode will be its quantum efficiency in the spectral region of the scintillator's emission. Thus in the case of photomultipliers intended for operation in conjunction with ordinary scintillation counters one could readily dispense with measurement of the integral sensitivity. In other words, where scintillation counter photomultipliers are concerned, the integral sensitivity is a parameter that is more of interest to the production technician than to the ultimate user, inasmuch as the dependence of the quantum efficiency on the integral sensitivity provides a means of controlling the uniformity and constancy of the cathode thickness. Fig.3 shows the variation of the quantum efficiency with the integral sensitivity for about 100 photomultipliers taken off the production line. As may be seen from the figure, all the points fall on a straight line with relatively little scatter. This indicates that the reason for the fluctuation in quantum efficiency and integral sensitivity values lies in the process of activation of the cathode rather than in variations in cathode thickness.

In addition to the quantum efficiency, basic parameters of a photomultiplier that determine its suitability as a scintillation counter component are a) homogeneity of the cathode sensitivity, b) collection of electrons and c) uniformity of electron collection at the first emitter of the dynode system. Homogeneity of photocathode sensitivity is characterized by the ratio of the photocurrent from different individual sections of its surface to the average photocurrent. Collection of electrons is defined as the ratio of the number of electrons arriving at the first dynode to the number of electrons leaving the cathode. Uniformity of electron collection is defined analogously with the difference that the ratio of the number of electrons arriving at the first dynode to the number of electrons leaving the cathode pertains to each individual section of the cathode surface. The homogeneity of sensitivity of an FEU-1B type photomultiplier (cathode 75 mm in diameter) is shown in the form of a "relief map" in Fig.4.

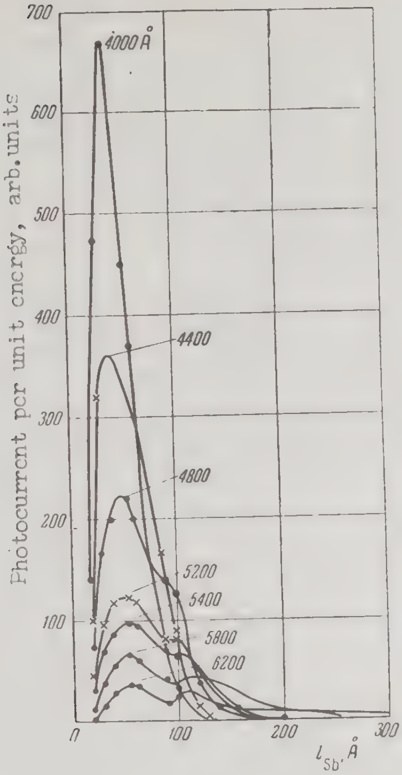

Fig.1. Variation of the monochromatic sensitivity of a photomultiplier cathode with the thickness of the initial antimony layer.

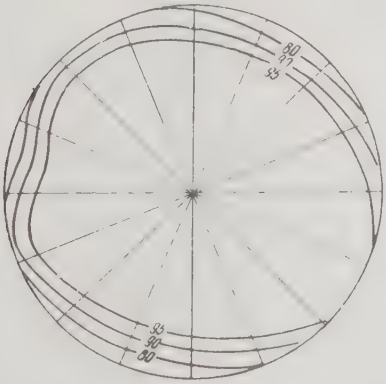

Fig.4. "Relief map" characterizing the degree of homogeneity of sensitivity of a photocathode (the indicated "contour" values are in percent referred to the average sensitivity value).

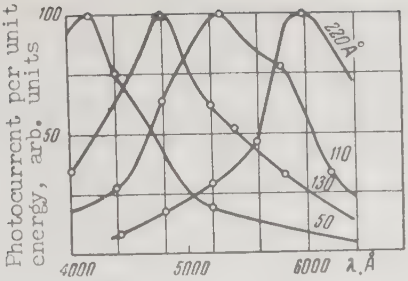

Fig.2. Variation of the spectral sensitivity distribution of a cesium antimony cathode with the thickness of the initial antimony layer.

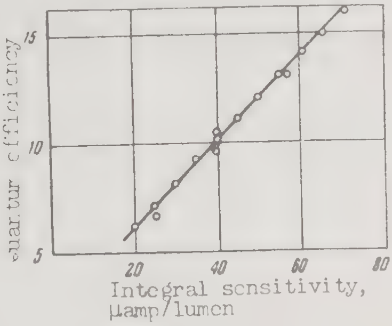

Fig.3. Variation of the quantum efficiency of a photocathode with its integral sensitivity.

Thus determination of the basic parameters of photomultipliers allows of realizing quality control in photomultiplier production both from the viewpoint of efficacy of the individual technological operations and from the standpoint of correct design of the individual tube components and the photomultiplier as a whole.

Obviously, each of the various principal operating parameters of a photomultiplier (the amplitude resolution, the time resolution, etc.) is determined by one or more of the basic parameters. Thus, for example, the quantum efficiency of the photocathode is an important factor where the spectrometric resolution of the photomultiplier is concerned. Fig.5 shows the dependence of the spectrometric resolution on the quantum efficiency. Curve

I was obtained with the photomultiplier viewing an NaI(Tl) crystal irradiated by a Cs^{137} source; curve II was obtained with the photocathode illuminated by light flashes equivalent to 661 kev and having a duration of approximately 0.5 μsec, i.e., flashes closely duplicating the spectral characteristics of the scintillations from an NaI(Tl) crystal. The circle points represent mean values for at least 10 individual tubes. As may be seen from the plot the spectrometric resolution is proportional to the square root of the quantum efficiency, as might have been expected.

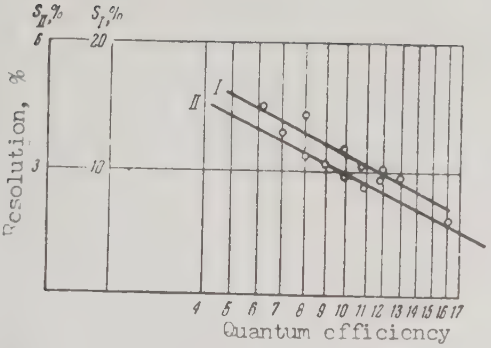

Fig.5. Variation of the spectrometric resolution of a photomultiplier with a quantum efficiency of the photocathode: I) with irradiation of an NaI(Tl) crystal with Cs^{137} γ-rays and II) with illumination of the photocathode by light flashes (661 kev equivalent energy and 0.5 μ sec duration) with spectral characteristics closely duplicating the scintillations of an NaI(Tl) crystal. The points are mean values for at least 10 individual photomultiplier tubes.

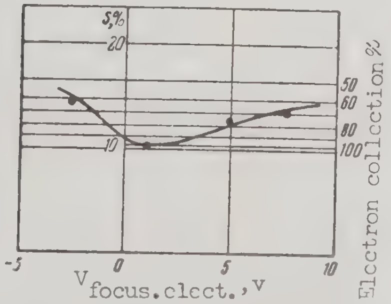

Fig.6. Collection of electrons and spectrometric resolution as functions of the voltage on the second focusing electrode.

It must be noted that the experimentally determined value of the spectrometric resolution of a photomultiplier is greatly dependent on the quality of the crystal employed. In working with different NaI(Tl) crystals produced by the Kharkov Chemical Reagents Plant, we obtained with one and the same photomultiplier spectrometric resolution values ranging from 9 to 20% (for the Cs^{137} photopeak). Hence for inspection and check purposes we consider it more expedient to test photomultipliers not with a radioactive source and scintillation crystal but using equivalent light flashes. The conventional test procedure is still followed, but the radioactive source and scintillator crystal is replaced by a Kerr cell or a special electron beam tube with a minimal-persistence screen.

Such basic parameters as homogeneity of the cathode sensitivity, collection of electrons by the first emitter and uniformity of electron collection - parameters that depend primarily on the design of the tube components - are also very important in determining the suitability of a photomultiplier tube as a scintillation counter component. Fig.6 shows the variation of the photoelectron collection and the spectrometric resolution as a function of the voltage on the second focusing electrode. The points in the figure present quantities proportional to the square root of the electron collection obtaining at the given electrode voltage. As may be seen, the points fall well on the curve.

To obtain the best electron collection values for any given photomultiplier one must find the optimum voltages to be applied to the focusing electrodes. These voltages depend on the design of the input section of the tube and, naturally, differ for different types of photomultipliers. Hence it is desirable to have the optimum voltages for every given type of tube indicated on the manufacturer's certificate accompanying the tube.

Table 1
Secondary emission coefficients of two types of dynodes

Dynode No.	Material: AMGK* alloy (FEU-1S tube)	Material: Cesium-antimony (FEU-19 tube)	Dynode No.	Material: AMGK* alloy (FEU-1S tube)	Material: Cesium-antimony (FEU-19 tube)
1.	3,5	2,6	7	3,3	3,9
2	2,9	2,1	8	2,9	3,6
3	2,7	2,3	9	2,8	6,1
4	2,5	3,5	10	2.6	5,3
5	2,5	4,0	11	2.7	3,8
6	2,6	3,4			

*Aluminum-magnesium alloy

There are two more photomultiplier parameters that we class among the basic ones: the multiplication ratio of the dynode system and the dark current of the tube. The multiplication ratio of the dynode system is the ratio of the output current to the current from the cathode at a given operating voltage. The multiplication ratio is determined by the secondary emission coefficient of the dynode material (on condition that there is no electron loss in the dynode system). Table 1 gives the values of the secondary emission coefficient for each emitter of the dynode system of the FEU-1S tube with a 100 volt differential per stage together with the comparative data for antimony cesium dynodes.

As may be seen from the table the scatter of these coefficients is greater for cesium-antimony dynodes than for aluminum-magnesium alloy dynodes of the type used in the FEU-1S tube.

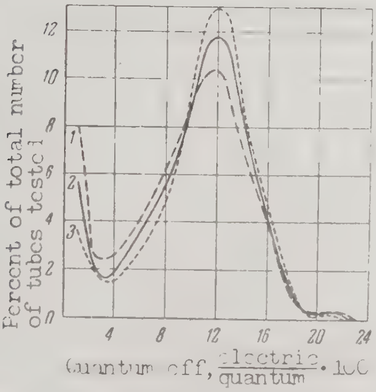

Fig.7. Variation in the production output (relative number) of photomultipliers with a given quantum efficiency as a function of this quantity: 1) FEU-1S tubes, 3) FEU-1B tubes and 2) mean curve.

The dark current of a photomultiplier is understood to be the current in the collector section when there is no illumination of the photocathode. The dark current consists primarily of two components, namely, the leakage current in the collector circuit and the amplified thermal emission current from the cathode and primarily from the first dynodes. In the case of photomultipliers used in scintillation counters, the second component of the dark current is the more important one. This component depends on the type of cathode used, its surface and the ambient temperature. Hence for photomultipliers intended for use in scintillation counters, it is more expedient to specify not the value of the dark current per se but the number of dark pulses and their height.

Inasmuch as most of the operative parameters (performance characteristics) of a photomultiplier are determined by several of the basic parameters taken in conjunction, the probability of obtaining a high quality spectrometric photomultiplier depends on the probability of obtaining the optimal values of the several pertinent basic parameters. The probability of obtaining the requisite (90-100%) values of the collection of electrons and uniformity of electron collection is close to unity inasmuch as this attribute depends primarily on the design of the electron-optical input section of the photomultiplier (and in the case of cesium-antimony cathodes on the arrangement of the antimony evaporator). The probability of obtaining

Table 2

No. tubes in batch	Acceptable, %
500÷600	100
1300÷1400	70
2000÷2100	93
2400÷2500	71
Average	81

optimal values of the quantum efficiency is determined by the technology of fabrication of the cathode. In Fig.7 the number of photomultipliers of types FEU-1S and FEU-1B having a given quantum efficiency is plotted against quantum efficiency. It will be seen that the curve has a sharp maximum at a relatively high efficiency value (12%).

Table 2 gives production test data on the number of photomultipliers found acceptable as regards their spectrometric characteristics referred to the total number of photomultipliers having acceptable basic parameters (quantum efficiency greater than 8%; electron collection 90-100%). As may be seen from the table the relative output of acceptable photomultipliers is over 80% on the average and close to 100% in some batches.

The various parameter correlations and dependences described above, which at first glance may appear trivial, show that one can obtain high quality spectrometric photomultipliers only by satisfying all the requirements set as regards their basic parameters. If rigorous quality control is not exercised where the basic parameters are concerned, the major portion of the tubes produced will be inferior and high quality spectrometric tubes will be obtained only through fortuitous concatenation of circumstances.

USE OF SCINTILLATION COUNTERS WITH TYPE "B" EQUIPMENT

- A.F.Vinogradov

Use of specially designed electronic equipment in conjunction with scintillation counters allows of obtaining a high counting efficiency, a high resolution, a wide range of measurements and good stability.

In some cases, however, in employing scintillation counters it is simpler to use counting equipment designed for operation with Geiger-Müller counters, for example, standard type "B" units[1] in view of the ready availability of such equipment.

Type "B" equipment, however, being designed specifically for use with Geiger-Müller counters, has certain characteristics that are not entirely suitable when it comes to operation with other detectors such as scintillation counters. The type "B" units are equipped with a high voltage rectifier designed to deliver a low current and having relatively poor voltage regulation in view of the fact that Geiger-Müller counters have an extensive plateau.

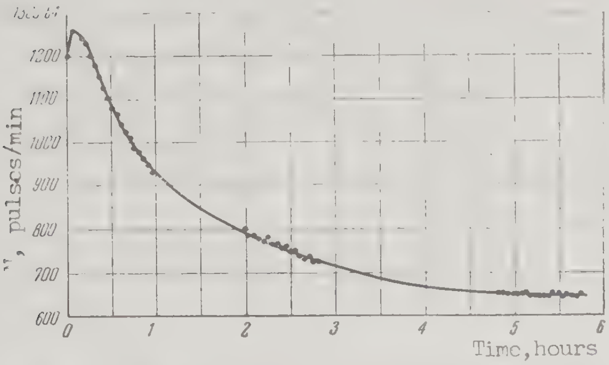

Fig.1. Instability of counting rate with time of a type "B" unit used in conjunction with a scintillation counter. β-particle source - C^{14}; supply voltage - 1500 volts.

In general, the low power of the high voltage source is not a serious difficulty since in the case of general counting (without discrimination in pulse height) one can use a high resistance voltage divider (20-50 megohms overall) to supply the photomultiplier dynodes.

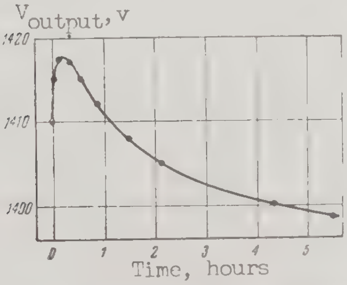

Fig.2. Variation of the output voltage of the VSE high voltage rectifier with time.

The inadequate stability of the high voltage unit presents greater difficulties. Thus when using type "B" equipment with a scintillation counter, there is obtained an appreciable instability in time. The variation of the counting rate with time in such cases is characterized by the curve shown in Fig.1. As may be seen, the counting efficiency falls off with time with the result that an appreciable error may be involved when the measuring period extends to several hours.

It will readily be deduced that the reason for the decrease in efficiency is decrease of the multiplication ratio of the photomultiplier inasmuch as the main amplification occurs in this tube. The decrease in sensitivity is not due to fatigue of the photomultiplier as might be assumed, for the currents involved are too low; the loss in sensitivity is due to falling off of the high voltage supplied to the multiplier. This will be evident from a comparison of the curve characterizing the time variation of the output voltage of the VSE (ВСЭ) high voltage recrifier (Fig.2) with the curve characterizing the decrease in counting rate (Fig.1).

In view of this it is expedient to consider the stability characteristics of the VSE unit in more detail.[2] Fig.3 shows the characteristics of the VSE

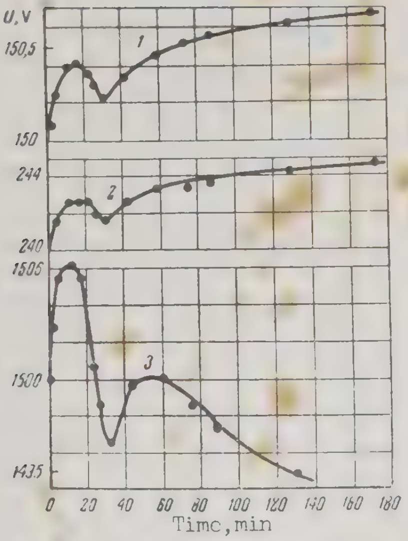

Fig.3. Time characteristics of the VSE unit at different points in the circuit: 1) "reference" voltage on the SG-4 tube, 2) stabilized anode voltage, 3) output voltage.

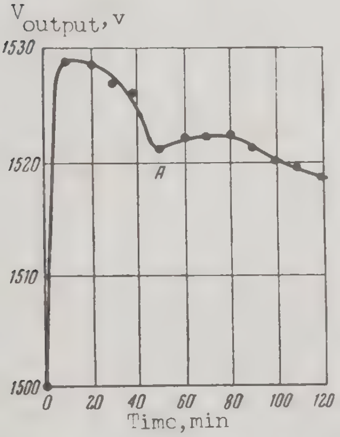

Fig.4. Variation of the high voltage supplied by the VSE unit with time (at point A the trend of the curve is reversed due to decrease of the ambient temperature).

units supplied with type "B" equipment as determined at different points in the VSE circuit with a constant line voltage.

Curve 1 in the figure shows the variation of the "reference" voltage on the SG-4 (СГ-4) [VR] tube; curve 2 shows the variation of the stabilized plate voltage and curve 3 shows the variation of the high output voltage of the unit. It will be evident that the character of the variation of the output voltage is similar to that of the reference and plate voltages only during the initial period of operation of the rectifier unit and that following this initial period the high output voltage continues to decrease despite continued increase of the reference and anode voltages.

From this it may be concluded that the variation in the output voltage of the VSE unit with a constant line voltage is due primarily to heating of the unit. This heating-induced change is so appreciable that it masks the changes due to instability of the reference voltage on the SG-4 tube. This is substantiated by the curve of Fig.4 which shows the variation of the high voltage with time. At point A the trend of the curve reverses due to reduction of the ambient temperature. Thus the stability of the high voltage supplied by this circuit cannot be improved by enhancing the stability of the reference voltage.

Fig.5 shows the variation of the high voltage with changes in the line voltage. This variation is superimposed on the temperature induced voltage drift.

From the above it will be clear that when the VSE unit is used in conjunction with a scintillation counter, it is essential to stabilize the amplification factor of the photomultiplier in order to obtain even reasonably dependable results.

In 1952 Sherr & Gerhart[3] proposed a method of stabilizing the amplification of photomultipliers based on defocusing of the electron beam. The proposed circuit with a uniform voltage divider coupled to the photomultiplier dynodes and one reference voltage was used by the above authors for RCA 5819 and RCA 7151 photomultipliers. An attempt to apply this system of stabilization to an FEU-19 photomultiplier did not yield positive results. Furthermore, for supplying the FEU-19 tube it was found desirable to use a progressive voltage divider for this gave a better signal-to-noise ratio.[4] Hence we used the stabilization circuit with two reference voltages and a progressive divider shown in Fig.6.

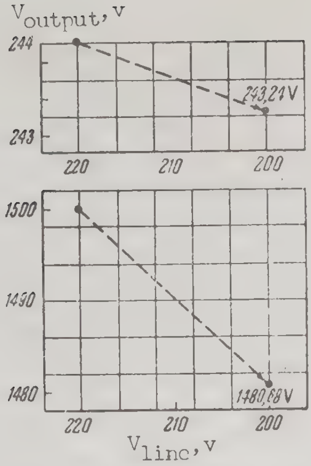

Fig.5. Variation of the high voltage of the VSE unit with line voltage.

The first reference voltage E_{56}, equal to 56-60 v, was connected between the fifth and sixth dynodes; the second reference voltage E_{1011}, equal to 80-94 v, was connected between the tenth and eleventh dynodes of the FEU-19.

We used standard BAS-80 dry cells to supply the reference voltages. Inasmuch as the current drain is virtually nil the operating life of the cells equals the shelf life.

With the usual dynode supply circuit, the amplification factor of the photomultiplier increases with increase in the overall supply voltage. With a constant voltage difference between two pairs of dynodes, the multiplication factor of the other dynodes also increases with increasing voltage on the divider. At the same time, however, due to inhomogeneity (distortion) of the field about the dynodes with the constant potentials, there occurs defocusing of the electron beam which leads to the opposite effect. The defocusing effect in a certain range of voltages on the divider compensates the increase in the multiplication factor on the other dynodes with the result that the overall amplification factor of the photomultiplier remains about the same.

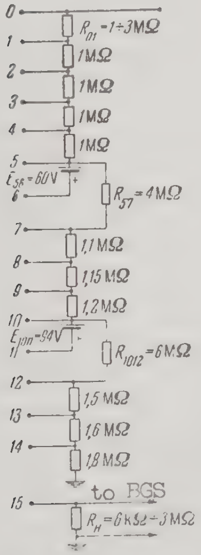

Fig.6. Circuit with two reference voltages used for stabilizing the amplification factor of an FEU-19 photomultiplier.

The circuit with two reference voltages is similar to the circuit proposed by Sherr & Gerhart with the difference that the defocusing effect obtains at two points in the dynode system and thus enters into force more uniformly than in the circuit with one reference voltage. This makes it possible to obtain a longer horizontal section of the current-voltage characteristic of the photomultiplier, i.e., to obtain a "plateau".

In our case the reference voltages were chosen with a view to using standard BAS-80 batteries; they can, however, be varied within a certain range. For example, increasing the first reference voltage E_{56} leads to an increase in the amplification factor of the photomultiplier and at the same time shifts the plateau to the side of higher potentials. We tested three different lots of FEU-19 photomultipliers consisting of 9-10 tubes each. According to our results, the tested multipliers had an excessively great scatter both as regards sensitivity and and the geometry of the dynode system; nevertheless, a 100 to 300 volt plateau was obtained for most of the photomultipliers.

The measurements were made using an MTKh-90 thyraton operated in the relaxation regime with an oscillograph connected to the FEU-19 photomultiplier output. The voltage on the divider was varied and we measured the pulse heights on the oscillograph screen; this height obviously characterized the amplification factor of the FEU-19 with a constant intensity of the MTKh-90 thyraton flashes. The intensity of the flashes was controlled by means of an iris diaphragm so as to preclude pulse limiting due to saturation. The stabilization characteristic recorded in this manner is shown in Fig.7.

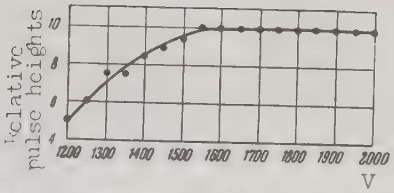

Fig.7. Stabilization characteristic of an FEU-19 photomultiplier recorded by means of thyraton flashes.

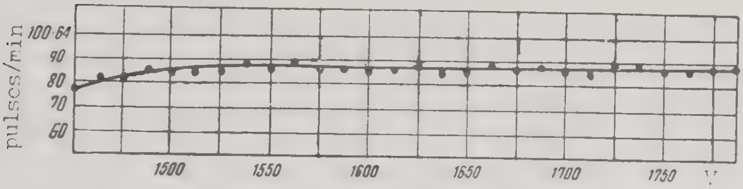

Fig.8. Stabilization characteristic of FEU-19 photomultiplier recorded by means of counting electrons from C^{14}.

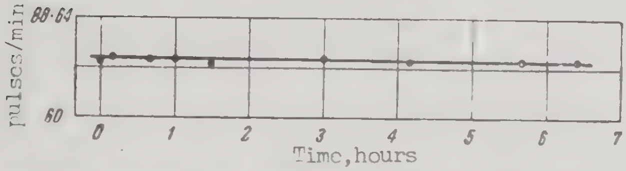

Fig.9. Stability of FEU-19 photomultiplier (sample tube No.13) with diphenyl acetylene crystal. β-particle source - C^{14}.

The circuit diagrammed in Fig.6 was used with scintillation counters for measuring α, β and γ-radiation in conjunction with a type "B" unit having a fixed sensitivity threshold. The stabilization characteristic was checked by counting electrons from C^{14} (Fig.8). The stability of the entire apparatus in time is shown in Fig.9. As will be evident from the figures, use of a scintillation counter in a set-up of this type is entirely feasible from the stability point of view provided the amplification factor of the photomultiplier is properly regulated.

The resolving time of the set-up was 5 to $7\cdot10^{-5}$ sec. The dead time of β- and γ-scintillation counters is 10^{-6} sec or even less, but in conjunction with the described set-up the total resolution is determined by the resolving power of the detecting unit. The sacrifice in resolution, i.e., the difference between the resolution of β- and γ-scintillation counters and the resolution of the recording equipment, is to some extent justified by the fact that in this case the possibility of recording spurious pulses (satellites[5]) originating in the photomultiplier is excluded. As for α-scintillation counters, their resolution is of the same order of magnitude as the resolution of the described recording equipment.

The preamplifier supplied with the type "B" equipment (located before the grid of the input multivibrator tube) is designed for operation from gas counters and has a very steep slope of the frequency response curve at high frequencies. The low amplification coefficient at high frequencies leads to a reduction of the overall counting efficiency particularly in measuring low energy β-radiation. This short-coming can be overcome by using a selected photomultiplier with a high amplification factor.

Almost all FEU-19 tubes can be used, however, if the passband of the preamplifier is extended somewhat to the side of high frequencies. To this end in the case of the "B" type equipment it is desirable to replace the 6Zh7 (= 6J7) tube by a 6Zh4 (= 6AC7) tube in the BGS extension (remote) unit and simultaneously reduce the length of the BGS cable by half. Fig.10 shows a diagram of the BGS unit with a 6Zh4 tube. In making the replacement one should also remove the No.3 resistor in the PS-64 unit[6] and connect a 50 kilohm (0.5 watt) resistor in parallel to the No.5 resistor. Even more effective is replacement of the BGS unit by a BSS unit, a diagram of which is shown in Fig.11.

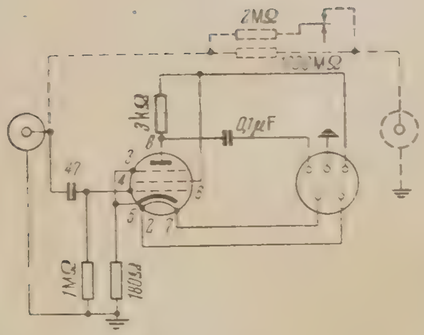

Fig.10. Diagram of BGS unit with 6Zh4 (= 6AC7) tube.

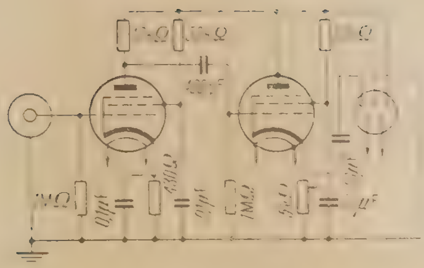

Fig.11. Diagram of BSS unit.

As a result of our experimental work, we constructed a counter set-up consisting of a type "B" unit and three scintillation counters. The β-counter had an efficiency equal to the efficiency of an end counter with a window 25 mm in diameter and having a superficial density of 1 mg/cm^2; the efficiency of the γ-counter exceeded the efficiency of the conventional gas counter by a factor of 15-20; the α-counter had an efficiency somewhat lower than that of a well-adjusted type "D" counter unit.

Conversion from detection of one type of radiation to another is realized by means of two selector switches brought out on the front panel of the instrument. The same two reference batteries (E_{56} & E_{1011} - see Fig.6) supply all three counters.

References

1. Ustanovka tipa "B" (Type "B" equipment) (Description and instructions for use), MPSS, SSSR, Moscow, 1952.

2. Vypriamitel' na 2500 V s elektronnoi stabilizatsiei tipa BSE-2500 (type VSE-2500 2500 v rectifier with electronic stabilization) (Description and instructions for use), MPSS, SSSR, Moscow, 1952.

3. R.Sherr & I.B.Gerhart, Rev.Sci.Instr., 23, 770 (1952).

4. A.A.Markov, Elektronnye metody eksperimental'noi fiziki (Electronic procedures in experimental physics), M., 1954.

5. J.C.Roucayrol & E.Oberhausen, Science, 122, 3161, 201-202 (1955).

6. Pereschetnyi pribor tipa PS-64 (PS-64 scaler) (Description and instructions for use), MPSS SSSR, Moscow, 1952.

THE SG-42 FIELD GAMMA-RADIOMETER

- M.M.Sokolov & N.I.Karabanov

The detection of small amounts of radioactive elements in nature by measuring radioactive radiations rapidly and with adequate accuracy is important in certain types of geological reconnaisance work. By virtue of their high efficiency scintillation counters are more suitable and convenient for such purposes than instruments based on the ionization of gases.

We developed a portable instrument employing a scintillation counter for measuring γ-rays of energies from 50 kev up. This instrument is now in commercial production under the designation "SG-42 ([illegible]) Field Gamma-radiometer".

The radiometer set consists of a tubular housing and a panel-top case connected by a 1.5 meter cable. The housing is a sealed aluminum cylinder 67 mm in diameter and 510 mm in length with 1 mm thick walls. It is equipped with a draw-out carrying handle on the cable lead-in end. The case is made of sheet aluminum and measures 200 x 190 x 90 mm.

The housing contains the phosphor, the photomultiplier and a relaxation relay. The case contains the high voltage source for the photomultiplier (batteries). The appropriate control knobs and pointer indicators for monitoring the power supply and reading the detected radiation are arranged on the top panel.

The detecting component is an NaI(Tl) crystal 30 mm in diameter and 25 mm thick and an FEU-19M photomultiplier. Optical contact between the crystal and the photomultiplier is realized by means of silicone oil.

The electric diagram of the instrument is shown in the accompanying figure.

The instrument has three scales: the first reads from 0 to 50 μr/hour, the second from 0 to 150 μr/hour, the third, 0 to 700-800 μr/hour. The first two scales are linear; the third is nonlinear.

The sensitivity of the instrument with a natural background of 6-7 μr/hour is about 2 μr/hour (triple quadratic error). The sensitivity for a radium source is about 180-200 pulses/min for 1 μr/hour. The time constant of the instrument for the first scale is 4.2 sec; for the second scale - 2.2 sec and for the third scale - 1.2 sec. The relative error may be determined from fluctuation of the indications or by means of the formula

$$\sigma = \frac{1}{\sqrt{2RC\cdot\bar{n}}},$$

where $\bar{n}$ is the mean number of pulses recorded per unit time. For example, at the end of the first scale the uncertainty is about 5%.

The weight of the complete set is 5 kg. Two 2S-L9 batteries are used for supplying the tube filaments and two GB-80 batteries are provided for the plate circuits. The service life of a set of batteries is at least 50 hours. The stability of operation of the instrument in the temperature range from -10 to +40° is satisfactory.

The instrument is intended primarily for geological exploration work, but by replacing the NaI(Tl) crystal with appropriate phosphors the instrument can be used for detecting fast and slow neutrons.

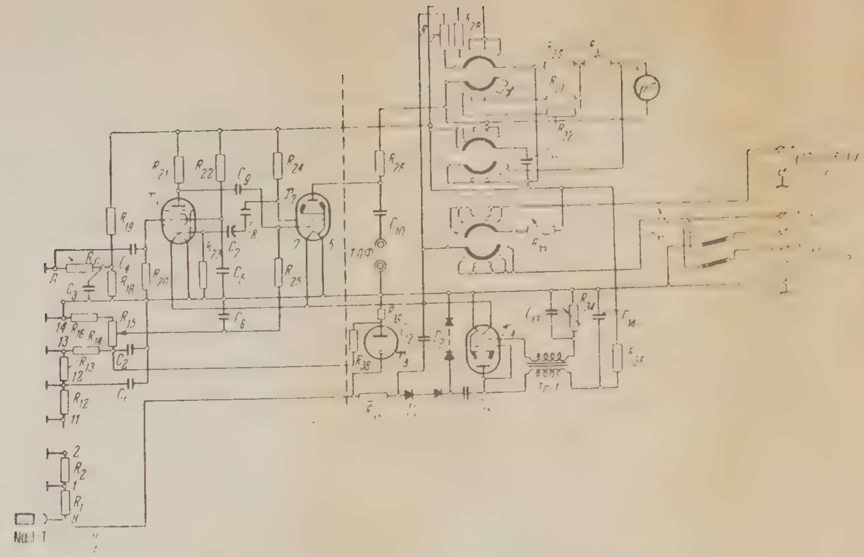
R21
R22
C9
R24
R26
T1
T2
R19
C8
C7
C10
R23
C5
R20
C4
R18
C3
R25
ТПФ
R15
R16
R14
14
13
C6
R13
C2
12
R12
C1
11
R38
T3
R34
C14
2
R2
1
R1
NaJ

Circuit diagram of the Sg-42 gamma-radiometer.

A SCINTILLATION METHOD OF CHECKING β-CONTAMINATION IN THE PRESENCE OF A γ-BACKGROUND

- G.M.Dikareva

The problem of detecting and measuring β-contamination of work surfaces and the apparel and exposed skin of personnel in the presence of an external γ-radiation field is of great practical importance. The difficulty stems from the fact that one must record the β-particles due to the contamination against a background of secondary electrons produced by the γ-background, the number of which may appreciably exceed the β-activity level of interest; moreover, this must be done under circumstances when the spectrum of both the β- and γ-radiations is not known beforehand.

Consequently, the basic criterion in selecting a measurement procedure must be the ratio of the detecting efficiencies for β- and γ-radiation: $K = f\beta/f\gamma$; that is, this ratio must have the highest possible value.

The sensing element capable of measuring allowable levels of β-contamination under conditions of a relatively high γ-background must satisfy the following basic requirements: 1) it must have the maximum possible sensitivity to β-radiation regardless of the β-energy, 2) it must have a low sensitivity to γ-radiation of all energies and 3) it must have a good resolving time.

Of all the available types of radiation detectors now available, these requirements are satisfied to the highest degree by a scintillator-photomultiplier combination.

Obvious measures for reducing the sensitivity of the scintillator to γ-radiation are reduction of its thickness and choice of a scintillator material with a small atomic number Z. Reduction in thickness of the scintillator, however, is limited by the need for obtaining a sufficiently high ratio of the pulse heights from β-particles to the mean noise pulse height of the photomultiplier, for the intensity of the light flashes in a scintillator decreases as a function of the energy lost in the scintillator by the electron traversing it.

Hence it is important to have a scintillator with a high light yield inasmuch as this, other conditions being equal, allows of reducing the thickness. An important advantage of thin scintillators is the weak dependence of their sensitivity on the energy of the radiation.

Some time ago Roesch & Donaldson[1] proposed a radiometer for mixed or separate measurements of β- and γ-radiation doses, based on a scintillator counter with a thin anthracene crystal. Anthracene was chosen in view of the fact that in regard to chemical composition it is equivalent to tissue and of all the known organic crystals has the highest luminescence yield. Such a radiometer has an angular dependence close to that of an extrapolation chamber.

A substantial advantage of scintillation crystal radiometers where measurement of β-contamination in the presence of an appreciable γ-background is concerned is the good resolving time of scintillation counters, which allows of loads three orders of magnitude greater than feasible with radiometers employing STS-5 type counters.

The purpose of our experiments was to find the most suitable scintillator for obtaining the optimal ratio of the detecting efficiencies for β- and γ-radiations. By way of scintillators we tested organic films consisting of a solution of tetraphenylbutadiene in polystyrene, layers of K-5 phosphor (ZnS:Ag) and stilbene single crystals of different thickness.

The measurements were carried out by means of an FEU-19M photomultiplier with the stabilized negative high voltage supplied by a standard VS-9 rectifier. The photomultiplier pulses were fed to an amplifier with a gain of 100,

a pulse height discriminator and a suitable counter. The photomultiplier cathode was protected from stray light by an aluminum foil with a surface density of 4 mg/cm^2. In a special series of experiments we selected the best photomultiplier voltages to obtain an optimum ratio of the amplitude of the pulses due to a standard light signal to the amplitude of the mean noise pulse of the photomultiplier.

By way of β-sources we used thin layers of $Sr^{90} \rightarrow Y^{90}$ uniformly applied to an aluminum backing; the γ-background was produced by Co^{60}. We recorded curves of the counting rate vs the discrimination voltage (bias) for different scintillator thicknesses and from these calculated the detecting efficiency ratio $K = f_{\beta}/f_{\gamma}$.

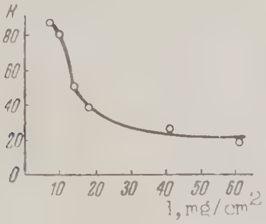

Fig.1

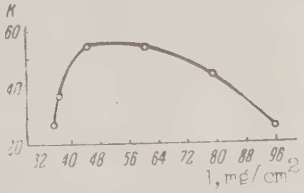

Fig.2

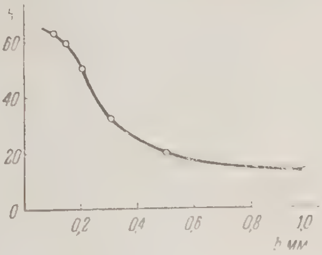

Fig.3

Fig.1. Variation of the detecting efficiency ratio for β- and γ-raditions (K = f_{β}/f_{γ}) with the superficial density d of the tetraphenylbutadiene in polystyrene film.

Fig.2. Same as Fig.1 but for ZnS:Ag layers.

Fig.3. Variation of the detection efficiency ratio K = f_{β}/f_{γ} with stilbene crystal thickness.

In the case of the organic films with tetraphenylbutadiene, we measured the relative efficiencies of detecting β- and γ-radiations with film thicknesses corresponding to superficial densities of 6.5, 7.2, 9.3, 13.7, 18.0, 41.0, 63.7 and 110.0 mg/cm^2. The variation of the efficiency ratio K = f_{β}/f_{γ} with the film thickness is shown in Fig.1. The maximum value of 87 for K was obtained for a film having a superficial density of 7.2 mg/cm^2. It must be noted, however, that the detecting efficiency for β-particles with complete discrimination of the photomultiplier noise amounts to only 4.3%. This may be explained by the low light yield of our films; according to a rough evaluation, their scintillation efficiency did not exceed 20% relative to the efficiency of stilbene. With a thin film, therefore, most of the pulses due to β-particles have a height comparable to the noise level of the photomultiplier.

The use of films as the scintillation component in a radiometer leads to greatly increased time and error of measurement and virtually precludes monitoring at low levels of contamination.

For thin layers of ZnS:Ag phosphor we obtained a clearly discernible maximum in the K vs layer thickness curve (Fig.2). The maximum value of K occurs for a surface density of about 45 mg/cm^2, which is explained by the existence of an "effective thickness" for layers of fine crystal phosphors that have a low transparency to their own radiation.

Satisfactory results were obtained in our experiments with thin single crystals of stilbene kindly made available to us by the personnel of the USSR Academy of Sciences Institute of Crystallography. The results obtained for crystals of different thickness are summarized in Table 1.

Table 1

Detecting efficiency for β- and γ-radiation of stilbene crystals of different thickness

Crystal thickness, μ	Efficiency, %		$K = \frac{f_\beta}{f_\gamma}$
	f_β	f_γ	
100	23,6	0,37	64
150	18,0	0,31	60
200	24,8	0,48	51
300	28,0	0,93	31
500	35,5	1,80	20
1000	52,0	4,20	13

The low efficiency values for β- and γ-radiation obtained for the 150 μ thick crystal may be due to the poor quality of the particular crystal tested.

The curve showing the variation of the detecting efficiency ratio K with the thickness of the stilbene crystal is shown in Fig.3. The highest value of K, equal to 64, was obtained for a crystal having a thickness of 100 μ (superficial density 12 mg/cm^2). The curves characterizing the variation of the counting rate with the bias voltage for this crystal are plotted in Fig.4. With complete discrimination of the photomultiplier noise the detecting efficiency for β-particles is 23.6%, which is far superior to that obtained with the other scintillators. It is obvious that further decrease in the crystal thickness would lead to an increase in K but at a sacrifice of the absolute β-detecting efficiency. It is possible that the 100 μ thickness is not the optimum one, but unfortunately we did not have any thinner crystals available.

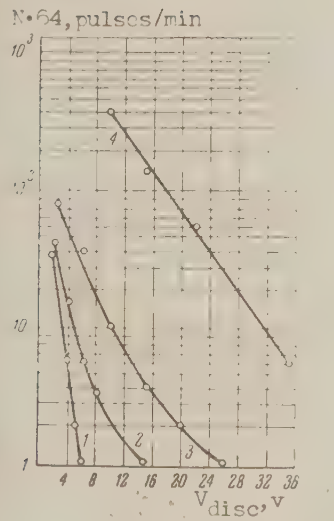

Fig.4. Variation of the counting rate for β- and γ-radiations with the discrimination (bias) voltage: 1) photomultiplier noise, 2) β-contamination, 3) γ-contamination, 4) γ-background (10 μr/sec).

Table 2

Minimal detectable surface β-contamination

Dose rate γ-background μr/sec	Specific β-activity of the checked surface, particles cm^{-2}sec^{-1}
50	36.0
25	24.7
10	16.0
5	11.7
1	5.2

On the basis of the experimental data obtained for the β- and γ-detecting efficiencies of the 100 μ thick stilbene crystal, we calculated the minimum β-contamination levels that could be measured with different γ-backgrounds. The calculations were carried out for a two-channel system with one of the detectors measuring β+γ-radiation and the other only γ-radiation with subsequent compensation. The following numerical values were used: crystal area S = 10 cm^2; time constant of the pulse counting circuit RC = 20 μsec; relative probable error in measuring the β-activity $\epsilon_\beta \leqslant 10\%$. The results of our calculations are listed in Table 2.

References

1. W.C.Roesch & E.E.Donaldson, Portable instruments for β-ray dosimetry. International Conference on the Peaceful Uses of Atomic Energy. Dosimetry of Ionizing Radiations, Geneva, 1956.

PROTOTYPES OF COMMERCIAL THERMAL AND FAST NEUTRON DETECTORS

- V.S.Filonov

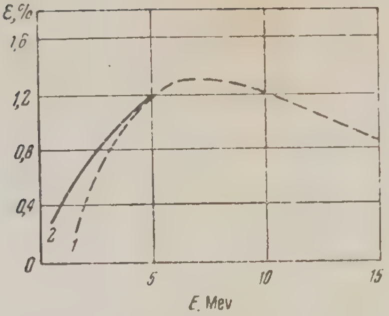

Fig.1. Comparison of the neutron detector efficiency curve (1) with the dose curve (2).

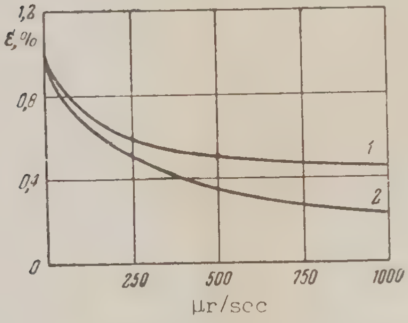

Fig.2. Variation of the neutron detecting efficiency with the strength of the biased-out γ-background: 1) thermal neutron detector, 2) fast neutron detector.

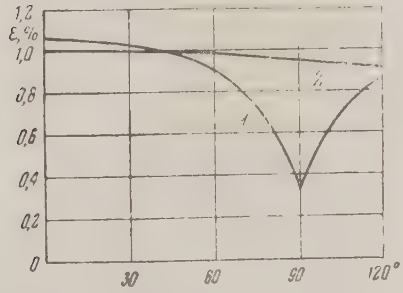

Fig.3. Variation of the efficiency of the neutron detectors with the neutron angle of incidence: 1) thermal neutrons, 2) fast neutrons.

The detectors we shall describe in the present article were prepared for use in commercial type RN-3 and RN-4 slow and fast neutron dosimeters.

Of the various detecting agents tried, the most suitable for fast neutrons, where these instruments are concerned, proved to be the so-called Gorniak wafer[1].

This detector has a sufficiently high efficiency for 0.5 to 14 Mev neutrons in the presence of a strong γ-background (up to 250 μr/sec). According to the data in the literature[1] the detecting efficiency is ~1% for 4 Mev neutrons. The efficiency varies with neutron energy, to some extent following the dose curve (Fig.1*).

The pulses produced by γ-radiation are one order of magnitude lower than the pulses due to neutrons. This allows of realizing reliable discrimination of the γ-background, naturally with some sacrifice in neutron detecting efficiency (Fig.2).

The given detector is nondirectional: the maximum variation in detecting efficiency is 5% with changes in the angle of incidence of the neutrons on the detector (Fig.3). Temperature tests of this detector in conjunction with an FEU-19 photomultiplier showed that in the temperature range from 10 to 60°, a 1% increase in temperature results in 0.6% decrease in counting rate (Fig.4). At the same time, the height of the neutron-produced pulses decreases, while the noise level rises (Fig.5).

The noise spectrum of the FEU-19 and the distribution of pulses produced by Co^{60} γ-radiation and neutrons from a Po-Be source at 20°C are shown in Fig.6. Our tests showed that no individual resistor in the voltage divider used for the FEU-19 photomultiplier should exceed 5 megohm.

---

*Curve 2 in Fig.1 is based on the old data in the literature. In the 5 to 15 Mev region the maximum allowable flux is constant. The dose curve now officially accepted in the USSR does not have a flat section. Measurements of the "variation with hardness" in another laboratory showed that the efficiency of the detector in question for fast neutrons of 14 Mev is 1.5 times higher than shown in Fig.1.

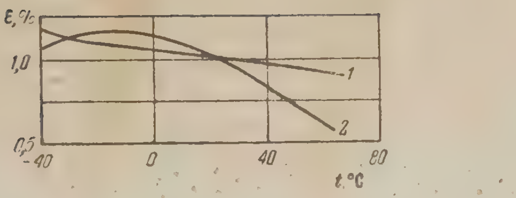

Fig.4. Variation of the detector efficiency with temperature: 1) thermal neutrons, 2) fast neutrons.

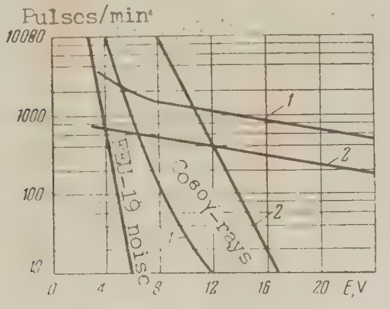

Fig.6. Integral distribution curves of noise pulses of FEU-19 photomultiplier, pulses from Co^{60} γ-rays and neutrons at 20°C: 1) thermal neutron detector, 2) fast neutron detector.

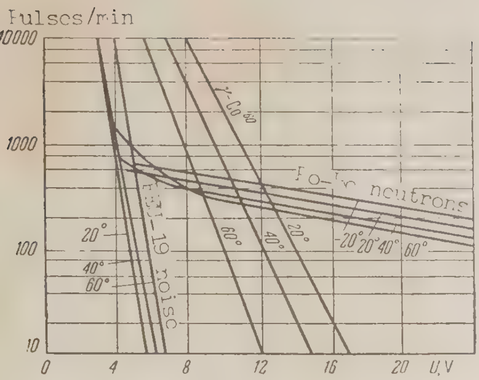

Fig.5. Integral curves characterizing the distribution of pulses from neutrons and Co^{60} γ-rays and the FEU-19 photomultiplier noise pulses at different temperatures.

Increasing the resistance at high γ-field values (~250 μr/sec) leads to a strong redistribution of the potentials on the last dynodes. This raises the requirements as regards the power of the source supplying the photomultiplier. Use of a voltage divider with resistors of 5 megohm at a voltage insuring the maximum signal-to-noise ratio keeps the measurement error within ±3%. The scatter in the efficiencies of the detectors does not exceed ±10%.

Parameters	Fast neutron detector	Thermal neutron detector
Total efficiency, %	1.4	1.2
Efficiency with pulses due to Co^{60} γ-rays (250 μr/sec) cutoff,%	0.7	0.75
Approximation of dose curve, %	±30	--
Directionality within 60%	±1	±10
Change in efficiency with temperature per 1°, %	-0.6	-0.2
γ-Background, μr/sec	1000	1000
Scatter in parameters for different detectors, %	±10	±10

The thermal neutron detector differs from the one described above in that it contains boron oxide. As regards the operating mechanism the difference is that in the first case the heavy ionizing particles are produced by inelastic collisions, while in the second case they are formed by elastic collisions.

Hence as regards their parameters the two detectors are similar to each other (see Figs.2,3,4 & 6 and the table); this makes it feasible to interchange them in the instruments without need for other adjustments.

A shortcoming of the thermal neutron detector is its response to fast neutrons. However, in measuring the maximum allowable thermal neutron flux against the background of the maximum allowable fast neutron flux, the added count due to fast neutrons is less than 1%.

The author wishes to express his gratitude to N.N.Prikhodchenko and E.K. Milovidov for assistance in the work.

References

1. Stsintilliatsionnyi schetchik bystrykh neitronov (Fast neutron scintillation counters) Report LIP AN SSSR, 1954; Rev. Sci.Instr., 23, 6, 264 (1952).

Bulletin of the Academy of Sciences of the USSR - Physical Series
Vol. 22, No.1

Transactions of the First All-Union Conference on the Synthesis and Investigation of Scintillators for Detecting Nuclear Radiation

(Moscow - October 23-25, 1956)

TABLE OF CONTENTS

	Page Orig.	Page Trans.
Technique of growing alkali halide phosphors for scintillation counters - L.M.Shamovskii, L.M.Rodionova & A.S.Glushkova	3	1
Investigation of scintillators containing boron-organic compounds - A.N.Nikitina, M.D.Galanin, P.M.Aronovich, T.A.Shchegoleva & B.M.Mikhailov	12	10
Screens for detecting slow neutrons - T.V.Timofeeva & S.P.Khormushko	14	13
Growth of scintillation crystals by the Kyropoulos procedure - L.Beliaev, V.P.Panova, V.A.Perl'shtein, V.V.Chadaeva & I.N.Tsigler	21	20
On the use of domestic phosphors for scintillation counting (Abstract) - A.N.Pisarevskii & E.D.Terenin	23	21
Impurity quenching of the photoluminescence of stilbene - A.P.Kilimov & N.P.Shimanskaia	24	22
Migration and transfer of electron excitation energy in anthracene and naphthalene crystals - I.Ia.Kucherov & A.N.Faidysh	29	27
Plastic scintillators - I.M.Rozman	36	34
Scintillation efficiency of carbo- and heterocyclic compounds in plastics - N.A.Adrova, M.M.Koton, Iu.N.Panov & F.S. Florinskii	41	39
Pulse heights from plastic scintillators with different activators - M.N.Medvedev, E.N.Matveeva & L.Ia.Zhil'tsova	44	42
Mechanism of energy transfer in plastic scintillators - T.P.Belikova & M.D.Galanin	48	46
Temperature dependence of the luminescence efficiency of polystyrene plastic scintillators - I.M.Rozman	50	48
Radiation damage in plastic scintillators - Part II - I.M.Rozman	60	58
Polystyrene-base plastic scintillators - E.A.Andreeshchev, E.E. Baroni, K.A.Kovyrzina, I.M.Rozman & V.M.Shoniia	67	64
New photomultipliers - N.S.Khlebnikov	70	67
Production of photomultipliers and their basic parameters - A.E.Melamid	78	74
Use of scintillation counters with Type "B" equipment - A.F.Vinogradov	83	79
The SG-42 Field gamma-radiometer - M.M.Sokolov & N.N.Karabanov	88	84
A scintillation method of checking β-contamination in the presence of a γ-background - G.M.Dikareva	90	86
Prototype of commercial thermal and fast neutron detectors - V.S.Filonov	94	89

Translated in 1959 by
Columbia Technical Translations
5 Vermont Ave., White Plains, N.Y.

95

Number 2 Volume 22 1958

BULLETIN

# of the

Academy of Sciences of the USSR

- Physical Series -

(Izvestiia Akademii Nauk SSSR)
(Seriia fizicheskaia)

Reproduction rights reserved

by

Columbia Technical Translations
5 Vermont Avenue
White Plains, New York

Single Issues
$20

Annual Subscription
$215

Transactions
# of the
Eighth All-Union Conference on Nuclear Spectroscopy

(Leningrad - January 27 to February 3, 1958)

(To be continued in Vol.22, Nos. 7 and 8)

ALPHA DECAY OF Cm^{242}

- L.N.Kondrat'ev, V.B.Dedov & L.L.Gol'din

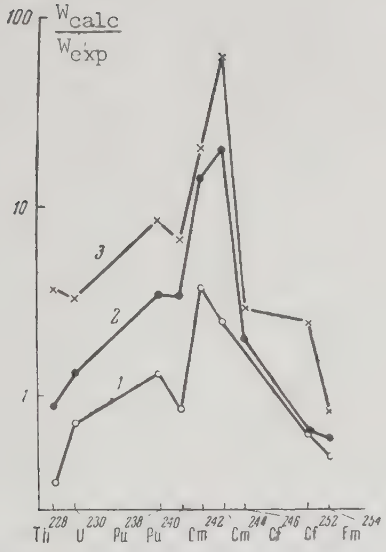

Fig.1. Comparison of the calculated and experimental values of the intensity of α-decay of nonspherical nuclei to the 4+ level: 1) calculated according to Ref.1, 2) according to Ref. 2, 3) according to Ref.3.

The energy of the lower excited levels of nonspherical nuclei is satisfactorily described by the symmetrical rotator formula. The experimental excitation energy values for heavy α-decaying nuclei agree with the rotational formula to within about one percent. This close agreement has prompted a number of authors[1-4] to attempt a calculation not only of the level energies but also of the intensity of α-decay to these levels.

The calculation reduces to evaluating the transparency of the Coulomb barrier surrounding the nonspherical nucleus to α-particles carrying off a certain momentum. The degree of nuclear deformation is determined in such calculations from the relative intensity of the α-transitions to the ground and first excited levels of the daughter nucleus. Having determined the deformation of the nucleus, we have the possibility of calculating the intensity of α-decay to the second excited level (4+) and comparing the calculated with the experimental values. The results of such comparison are shown in Fig.1 for different nuclei. For purposes of comparison we used the formula of Landau[1] and the results obtained by Strutinskii[3] and one of us.[2]

As will be evident from the figure, there is a particularly large divergence between the calculated and measured intensity values of α-decay for Cm^{242} and Cm^{244}. Inasmuch as the intensity of α-decay of curium has been measured only once[5,6], we naturally deemed it desirable first to check the results of the California group.

The measurements were carried out by means of the magnetic α-spectrometer of the USSR Academy of Sciences. A number of exposures of up to one week duration each were made. The resultant α-spectrum is shown in Fig.2. We did not measure the energy of the principal peak but assumed it to be 6110 kev after Asaro, Thompson & Perlman[5]; the energies of all the other α-lines were evaluated relative to this one. The results of our measurements are summarized in the accompanying table where we also give the results obtained by Asaro, Thompson & Perlman[5].

The 5777 kev α-line, clearly discernible in section III of the spectrum, is undoubtedly associated with an admixture of Cm^{243}.

The results of our experiments show therefore that the pronounced divergence between the experimental and calculated values of the intensity of α-decay to the 4+ level actually exists. In the light of the present concepts, this indicates that at least in the case of Cm^{242} the shape of the nucleus cannot be satisfactorily described by an expression of the form

$$r(\vartheta) = r_0 [1 + \alpha_2 P_2 (\cos \vartheta)]$$

(Ref.3) and is certainly not ellipsoidal (Ref.2).

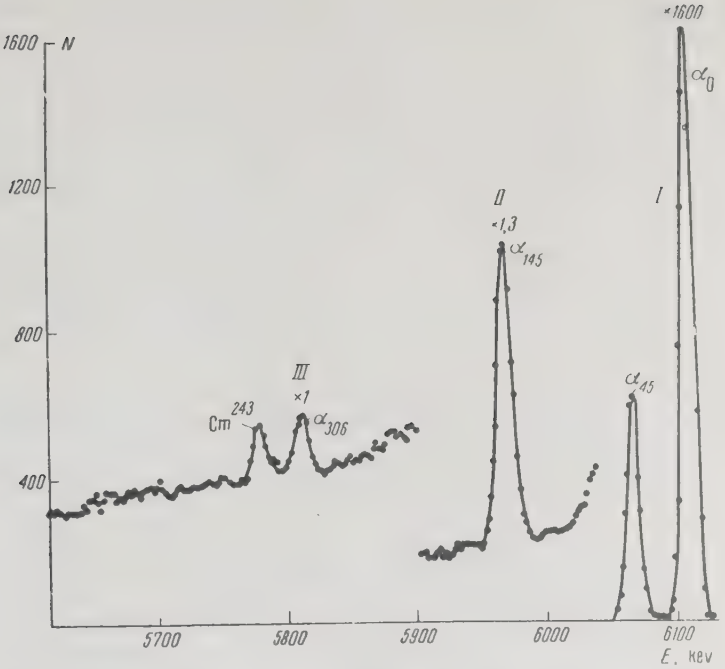

Fig.2. α-Spectrum of Cm^{242}. N - average number of tracks in 0.2 mm wide strip. The different sections of the spectrum (I through III) were obtained with different exposures and using different sources.

Table

Alpha-spectrum of Cm^{242} and levels of Pu^{238}

Line	Energy, kev		Intensity, %	spin & parity	Data of Asaro et al[5]	
	α-particles	excitation of level			α-particle energy kev	Intensity, %
α_0	6110	0	$73,5\pm0,5$	0+	6110	73,7
α_{45}	6065,6+0,5	45,1	$26,5\pm0,5$	2+	6066	26,3
α_{145}	5967 ± 2	145	$(30+1)\cdot10^{-3}$	4+	5965	$35\cdot10^{-3}$
α_{306}	5809 ± 2	306	$(4,6\pm0,5)\cdot10^{-3}$	6+	5811*	$6\cdot10^{-3}$*

*Data obtained in the investigation of Ref.6 by γ-γ coincidence measurements.

In conclusion we desire to express our sincere gratitude to I.I.Agapkin, B.F.Koniaev and Iu.N.Chernov for their assistance in the work and V.N.Kuznetsova for counting the tracks.

References

1. L.D.Landau, Report presented at the Sixth Conference on Nuclear Spectroscopy, Moscow, 1956.
2. G.M.Adel'son-Vel'skii, A.P.Birzgal, N.D.Piliia, L.L.Gol'din & K.A.Ter-Martiresian, Report presented at the Seventh Conference on Nuclear Spectroscopy, Leningrad, 1957.
3. V.M.Strutinskii, Zhur.eksp.i teor.fiz., 32, 1412 (1957).
4. V.G.Nosov, Doklady AN SSSR, 112, 414 (1957).
5. F.Asaro, S.G.Thompson & I.Perlman, Phys.Rev., 92,694 (1953).
6. I.Perlman & J.O.Rasmussen, Alpha-Radioactivity, UCRL 3424.

DECAY OF Tb^{160} AND Ho^{160} AND THE LEVEL SCHEME OF Dy^{160}

- E.P.Grigor'ev, B.S.Dzhelepov, A.V.Zolotavin, O.E.Kraft, B.Kratsik & L.K.Peker

The energy level diagram of Dy^{160} is one of the most complicated known. It is of great theoretical interest inasmuch as the Dy^{160} nucleus is a strongly deformed even-even nucleus with a large quadrupole moment ($Q = 7.8 \cdot 10^{-24}$ cm^2) and a considerable deformation coefficient ($\beta = 0.35$). The unified nuclear shell model allows of explaining a number of experimental facts observed in the case of nuclei of this type.

The levels of Dy^{160} are excited in β^--decay of Tb^{160}, which has been the subject of many investigations, and by β^+-decay and electron capture in Ho^{160}, investigation of which has only recently begun.

1. Description of the Experiments with Tb^{160} and Ho^{160}

In the present work we investigated the radiations from Tb^{160} and Ho^{160}.

Radioactive Tb^{160} was obtained by slow neutron irradiation of chemically pure (99.99%) Tb_2O_3.

The β-spectrum, conversion electron spectrum and photoelectron spectrum were studied by means of a double-focusing ($\pi\sqrt{2}$ angle) β-spectrometer[1], having an equilibrium trajectory radius $\rho = 14$ cm, a transmission factor of 0.6% and an apparatus line half-width of 0.3-0.6%.

The continuous β-spectrum of Tb^{160} was investigated using a source with a superficial density of 1 mg/cm^2, prepared by applying the Tb_2O_3 on a mica backing with a density of $\sim$1.5 mg/cm^2. For the purpose of more dependable determination of the end-point energy and relative intensity of the hardest β component, a source with a superficial density of $\sim$4-5 mg/cm^2 was prepared in a similar manner. The spectrum was resolved into components by the usual Fermi-Kurie analytic procedure on the assumption that the components have the statistical Fermi shape. The results of our measurements are summarized in Table 1; the spectrum is shown in Fig.1.

The relative intensity of the softest component was not determined inasmuch as the source was too thick.

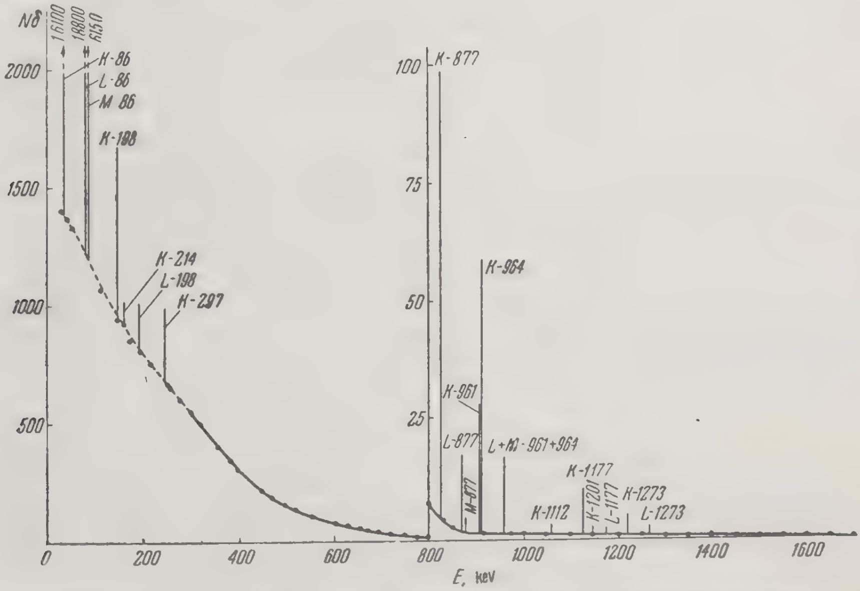

Fig.1. General appearance of the β and conversion electron spectrum of Tb^{160}.

Table 1

β-spectrum of Tb^{160}

$E_{e.p.}$, kev	Relative intensity
350±50	—
562±5	100±2,5
858±5	64±3
1710±10	0,8±0,2

The conversion electron spectrum of Tb^{160} was measured using sources ranging in thickness from 0.03 to 4-5 mg/cm^2. The thin sources were prepared by electrolytic deposition of Tb on an aluminum backing with a superficial density of 0.27 mg/cm^2; the thick ones by applying Tb_2O_3 on a mica or aluminum backing with a superficial density of ~1.5 mg/cm^2.

The positions and relative intensities of 19 lines were carefully determined in the conversion spectrum; most of the lines have been observed earlier by different authors[2-4]. The results are listed in Table 2. What is new here is resolution of the familiar "962 kev" line into two components: 963 and 966 kev. This is illustrated in Fig.2.

Table 2

Conversion lines of Tb^{160}

No.	E_{e^-}, kev	Shell	hV, kev	Relative intensity of conversion lines	K:L
1	32,9±0,5	*K*	86,5±0,5	4600±500	
2	78,6±1,1	*L*	86,4±1,1	5500±500	0,83±0,20
3	85,3±1	*M*	86,6±1	1550±150	
4	144,1±1	*K*	197,9±1	222±10	
5	160 ±2	*K*	214 ±2	37±4	
6	189,9±1	*L*	197,7±1	61±5	3,6±0,5
7	243,0±1	*K*	296,8±1	100	
8	823,6±1	*K*	877,4±1	30,5±0,5	
9	869,6±1	*L*	877,5±1	4,9±0,5	6,2±0,7
10	878 ±2	*M*	879 ±2	1,1±0,2	
11	907,0±1	*K*	960,8±1	8,6±2 *	
12	910,2±1	*K*	964,0±1	18,2±2	
13	963,1±2	*L+M*	961÷964	5,3±0,4	5,1±0.7
14	1058 ±2	*K*	1112 ±2	0,73±0,2	
15	1123 ±2	*K*	1177 ±2	3,2±0,3	
16	1147 ±2	*K*	1201 ±2	0,56±0,07	
17	1171 ±2	*L*	1179 ±2	0,44±0,10	6,0±2
18	1219 ±2	*K*	1273 ±2	1,3±0,1	
19	1264 ±3	*L*	1272 ±3	0,7±0,2	1,7±0,6

*Total intensity 26.8±0.5.

The source in the photoelectron experiments was a copper cylinder 36 mm in length and having an inside diameter of 0.3 mm and an outside diameter of 1.2 mm, filled with Tb_2O_3 powder. The following targets were employed: Ag - superficial density 0.25 mg/cm^2, Bi - 0.65 mg/cm^2 and 3 mg/cm^2, Th - 2 mg/cm^2 and Au - 7.7 mg/cm^2.

The relative γ-transition intensities were determined by dividing the areas under the lines by the corresponding photoelectric absorption coefficients. Appropriate corrections were made for γ-ray absorption in the source itself and in the cylinder walls and for the absorption of photoelectrons in the target and counter windows.

The dependability of this procedure for determining relative γ-transition intensities was demonstrated in earlier experiments in which we compared the relative intensities of γ-transitions in certain radioactive isotopes (for example, I^{131}, Sb^{124} and Co^{60}) known from the literature with the intensities obtained on the basis of such photopeak measurements.

In measurements with a source having an inner diameter of 1 mm, it was found that at energies above 1 Mev the instrument gives the intensities with

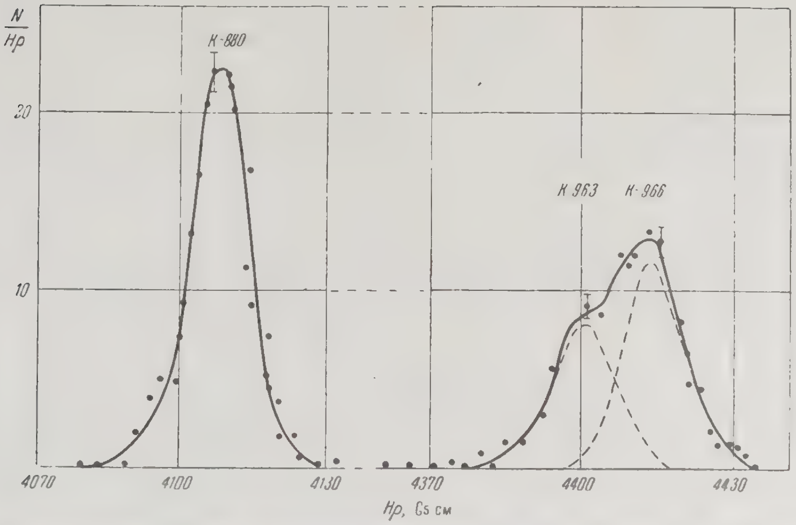

Fig.2. Conversion lines associated with the 880 and 963 + 966 kev transitions in Tb^{160}.

relatively little error, but that in the region of lower energies divergence from the data in the literature becomes appreciable. Thus for 600 kev the difference is about 20%, while in the 200 kev region the divergence mounts to 40%. Use of a 0.5 mm inside diameter source allows of determining relative intensities in a wider range. With this geometry the error in determining relative intensities in the 600 kev region amounts to only a few percent.

As noted above, in the present measurements, the inside diameter of the source was 0.3 mm. Hence it could be assumed that the relative intensity determinations were substantially correct in a wider energy range.

The relative γ-line intensities deduced by us from the photoelectron spectrum are listed in Table 3. They are in agreement within ±20% with the data of Clark & Knowles[5] and Nathan[6].

Table 3

Tb^{160} γ-ray spectrum obtained with targets of Ag, Au, Bi and Th

No.	Energy, kev (mean for all targets)	Shell from which effect is observed	Relative intensity γ-transitions	K/L photolines (Au target)
1	86,2±0,3	K	—	
2	86,8±0,3	$L_I + L_{II}$	—	
3	86,6±0,3	L_{III}	—	
4	196,8±1	K	17±4	
5	297,8±1	K	100±20	
6	295 ±3	L		5,6±2,3
7	878 ±1	K	125±20	
8	878 ±3	L		5,7±2
9	967 ±1	K	162±30*	
10	1178 ±2	K	71±15	
11	1179 ±3	$L + M$		5,1±1,1 $(K/(L+M))$
12	1201 ±2	K	10±2	
13	1273 ±2	K	39±8	

---

*Taking into account the fact that with some targets the L-878 line enters into the K-962 + 965 peak (we assume that the line intensity ratio K/L = 5,6).

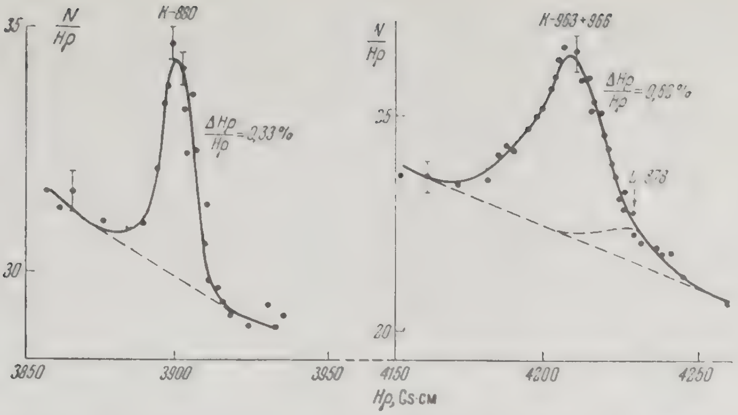

Fig.3. Photoelectron lines from the 880 and 963 + + 966 kev γ-rays of Tb^{160} (Th target).

The 963 + 966 kev doublet was not resolved in the photoelectron spectrum, but it may be noted that while the 880 kev line has an apparatus half-width of 0.33%, the 963 + 966 kev line has a half-width of ~0.62% (Fig.3). This indicates that the components of the γ-doublet are characterized by intensities differing by not more than a factor of 3.

Measurements of the conversion spectrum show that the hard component has twice the intensity of the soft one; since the multipole orders of these transitions are presumably the same, the relative intensities of the two γ-lines must be in the same proportion. Nathan[6] who investigated γ-γ coincidences, came to the conclusion that the ratio of intensities of the 963 and 966 kev lines is 12:23. His deduction is based on the assumption that the 880 kev line is a single one; actually the conversion electron spectrum of Ho^{160} indicates that it is a doublet: 873.1 + 879.9 kev. In the photoelectron spectrum of Tb^{160}, however, the half-width of this line is normal, although the separation in the doublet is one and a half times greater than in the case of the 963 + + 966 doublet and hence it must be concluded that one of the components - presumably the 879.9 kev one - is much more intense than the other. This being the case, Nathan's inference is basically correct.

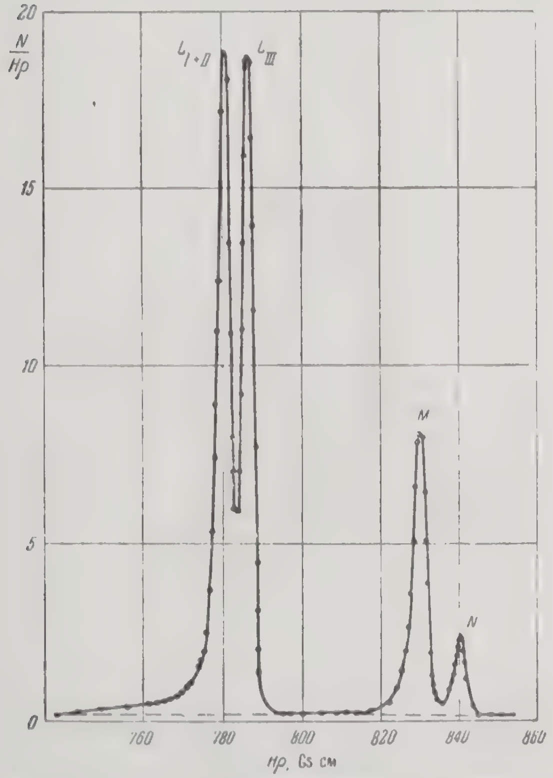

Fig.4. L, M and N conversion lines of the 60 kev transition in Ho^{160}.

The radioactive Ho^{160} was prepared by bombardment of a tantalum target with protons of up to 660 Mev energy. The erbium and holmium fractions were separated from the tantalum chromatographically.

The sources were prepared by applying erbium or holmium lactate to an aluminum foil 5 μ thick with subsequent decomposition of the lactic acid. The holmium fraction was found to contain 5-hour Ho^{160}; the erbium fraction, 29-hour Er^{160}. It was established by Mihelich et al[7] that Er^{160} converts by electron capture to Ho^{160}. The disintegration is accompanied by 60 kev γ-rays associated with the deexcitation of isomeric Ho^{160m} and γ-rays associated with the $Ho^{160} \rightarrow Dy^{160}$ conversion. No other γ-rays or conver-

Table 4

Ho^{160} conversion electrons

No.	E_e, kev	Identification	hν, kev	Relative intensity
1	51,2	$L_{I} + L_{II}$	60,1	1150±120
2	52,05	L_{III}	60,1	1050±100
3	57,9	M	60	480±25
4	59,2	N	59,6	110±8 *
5	33,0	K	86,8	814±150
6	76,3	$L_{I} + L_{II}$	86,2	790±80
7	78,4	L_{III}	86,2	610±60
8	84,5	M	86,3	400±20
9	86,1	N	86,5	100±7
10	53,9	K	107,7	10±1
11	99,3	L	107,2	2,8±0,6
12	142,2	K	196,2	100±5
13	189,7	L	197,0	37±3
14	195,6	M	197,0	8,4±0,8
15	161,0	K	214,8	0,3±0,05
16	243,4	K	297,2	3,0±0,2
17	244,6	K	298,4	
18	290,7	L	298,5	0,9±0,1
19	297,0	M	298,3	0,26±0,05
20	256	K	310	0,16±0,05
21	301	K	365	0,22±0,05
22	339	K	393	0,09±0,04
23	353	K	407	0,4 ±0,06
24	399	L	407	0,06±0,03
25	460,6	K	514,4	0,75±0,04
26	506,1	L	514,8	0,08±0,02
27	485	K	538,9	2,25±0,15
28	531,1	L	540,0	0,4 ±0,06
29	539,4	M	540,6	0,15±0,05
30	593,8	K	647,6	5,25±0,30
31	638,4	L	647,1	0,85±0,10
32	647,0	M	648,3	0,26±0,07
33	675,9	K	729,7	6,9±0,4
34	720,5	L	729,6	1,1±0,1
35	729,4	$M + N$	730,7	0,32±0,08
36	700,9	K	754,7	0,6±0,1
37	713	K	766,7	0,8±0,1
38	819,4	K	873,2	0,92±0,13
39	863,8	L	872,9	0,10±0,05
40	826,0	K	879,8	2,6±0,4
41	871,0	L	880,0	0,40±0,08
42	879,6	M	880,3	0,15±0,06
43	909,6	K	963,4	2,1±0,3
44	912,9	K	966,6	1,8±0,3
45	960,1	L	968,0	0,72±0,15
46	994	K	1048	0,11±0,02
47	1040	L	1048	0,03±0,01
48	1015	K	1069	0,24±0,03
49	1061	L	1069	0,048±0,01
50	1079	K	1133	0,085±0,012
51	1126	K	1180	0,066±0,015
52	1147	K	1201	0,070±0,015
53	1210	K	1264	0,077±0,010
54	1219	K	1273	0,082±0,015
55	1231	K	1285	0,035±0,010
56	1323	K	1377	0,070±0,045
57	1381	K	1435	0,045±0,010
58	14 7	K**	1481	0,034±0,015
59	1665	K	1719	0,0[illegible]3±0,007

---

*The large uncertainties in the intensities of lines Nos.1-9 are connected with the uncertainty in taking account of the number of conversion electrons forming the low-energy tail associated with the thickness of the source (the half-width of the L-60 line is 0.5%; that of the K-196 line - 0.3%).

**The L-1435 line is superimposed on the K-1481 line.

sion electrons have been observed. Hence samples of Er^{160} with Ho^{160} in equilibrium with it can be used for investigating the spectra of the latter.

In a number of cases, primarily to check the radioactive purity of the samples, after the passage of some time the newly formed holmium was again separated from the erbium fraction.

The conversion electron spectrum of Ho^{160} was studied on the same double-focusing spectrometer, but with a line half-width of 0.3%. We confirmed the existence of all the conversion lines of Ho^{160} detected earlier[8] on lens spectrometers and found a number of new lines. The results are listed in Table 4. Figs.4 & 5 show the more intense sections of the conversion spectrum of Ho^{160} including the L_{I+II}, L_{III}, M and N lines associated with the 60.0 kev isomeric transition in Ho^{160} and the 873.1 + 879.9 kev and 963.4 + 966.6 kev doublets.

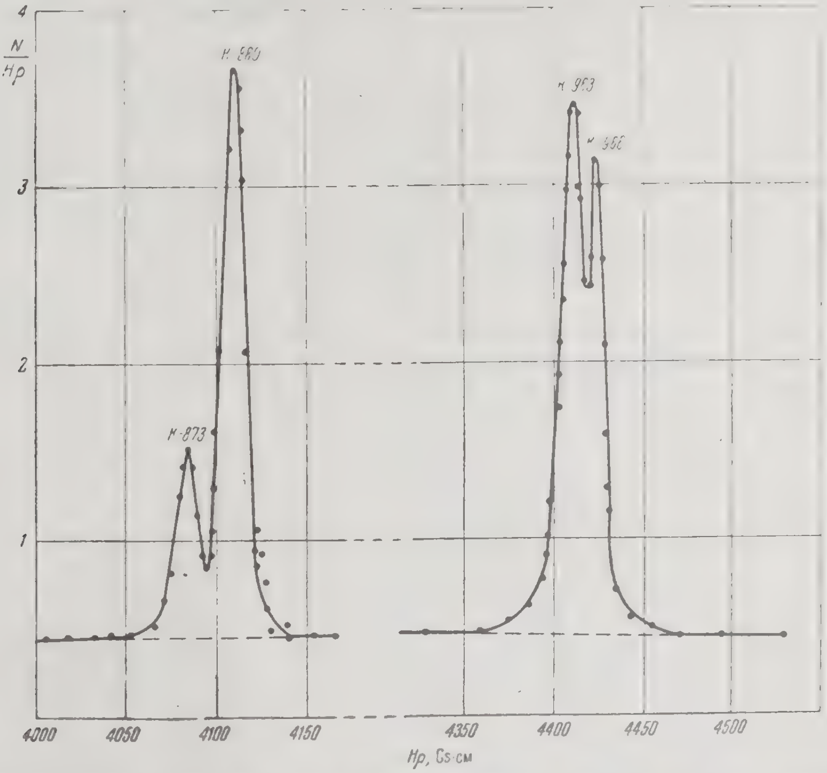

Fig.5. Conversion lines of the 873 + 880 and 963 + 966 kev transitions in Ho^{160}.

A number of different erbium and holmium sources were used in investigating the spectra.

The intensity of all the observed lines fell off with a period corresponding to the half-life of the investigated fraction, namely, 29 hours for the erbium fraction and 5 hours for the holmium fraction. The K - L line energy difference for all the measured transitions equals the difference between the binding energies in the corresponding Dy shells.

The error in determining the line energies varies between 0.1 and 0.3%, depending on their intensity. The statistical error in determining the relative intensities also depends on the counting rate at the lines and amounts to a few percent for the strongest ones.

The β^+-spectrum of Ho^{160} was investigated on an instrument with triple focusing of the electrons in a homogeneous magnetic field[9]. The spectrum

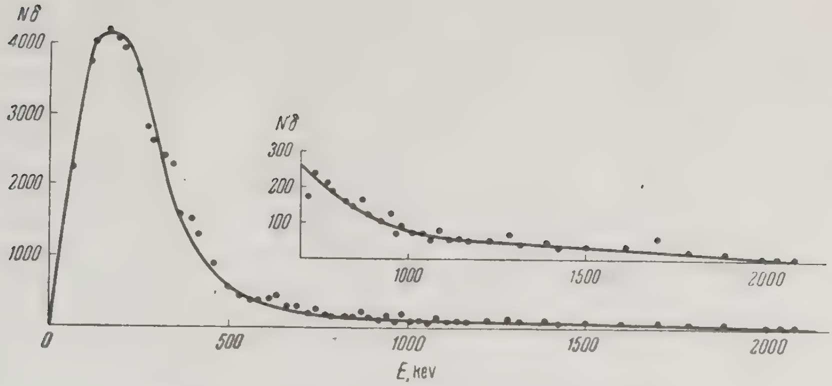

Fig.6. Positron spectrum of Ho^{160}.

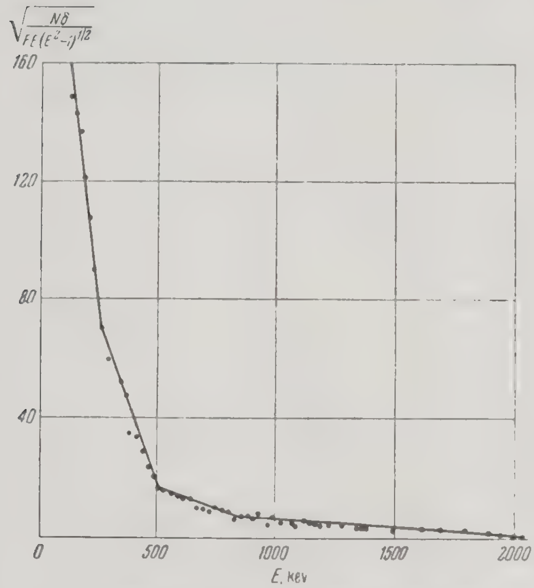

Fig.7. Resolution of the positron spectrum of Ho^{160} (Kurie plot).

Table 5

β^+-spectrum of Ho^{160}

Components end point energies, kev	Relat. intens.	β^+-decay branch, %	log *ft*
300±50	47	0,07	5,1
570±20	100	0,14	6,1
970±30	26	0,04	7,7
1900±100	14	0,02	9,5

proved to be of low intensity and complicated (Fig.6). Fig.7 shows a resolution of this spectrum into its Fermi components (the Kurie plot). The energies and intensities of the components are listed in Table 5.

The same spectrum was obtained in studying both the erbium and holmium fractions; in the latter case a check showed that the half-life is the same for all the components: $T \approx 5.6 \pm 0.7$ hours.

In view of the fact that the number of positrons emitted by the source is thousands or tens of thousands times smaller than the number of decays, it might be suspected that the observed β^+-spectrum is associated with some other Ho isotope, accidentally having a close period. In order to substantiate the identification of the Ho isotope responsible for the positron spectrum we carried out the following two supplementary experiments.

In the first, the holmium was separated from the erbium fraction only 45 hours after separation of the latter. In studying the radiations from this source we obtained the same results as previously, i.e., the same conversion spectrum, the same half-life and the same positron spectrum components. We also obtained the same ratio of the area under the total positron spectrum to the area under the 730 kev conversion line which undoubtedly belongs to Ho^{160}; the area ratio s_{β^+}/s_{e^-730} was found to be 1.6 ± 0.2. If the intensity of the 730 kev line builds up from Er^{160} and the β^+-spectrum from an unknown Er^x isotope, the persistence of the ratio between them indicates closeness of the periods not only of Ho^{160} and Ho^x but also of Er^{160} and Er^x.

In the second auxiliary experiment, we investigated an erbium fraction source held for 110 hours after separation. Again we obtained the same results. The ratio $s_{\beta^+}/s_{e^-_{60}}$ in this case proved to be 1.7 ± 0.2 which agrees with the previous figure within the limits of the experimental error. Yet if there were present in the erbium fraction, in addition to Er^{160}, yet another erbium isotope with a period differing from that of Er^{160} by only 3 hours, the difference in periods would lead to a change of at least 35% in the value of $s_{\beta^+}/s_{e^-_{60}}$ during the 110 hour storage period. It may therefore be concluded that the observed positron radiation belongs to Ho^{160}.

If it be assumed that the observed positrons are produced as a result of pair conversion, the corresponding transition must be rather intense and there should be observed corresponding hard conversion lines. The major group of the positrons (~50%) has an end-point energy of about 550 kev. Even assuming a multipole order of E1 for the transition, the corresponding conversion line (or lines) should have an intensity 100 times greater than observed for all the >1022 kev conversion lines listed in Table 4. Similarly it can be shown that the harder positrons are also not associated with pair production.

Assuming that the hard part of the positrons belongs to the continuous β^+-spectrum of Ho^{160}, we come to the conclusion that the Ho^{160}—Dy^{160} mass difference is not less than 2920 ± 100 kev.

For determining the intensity of the positron spectra (the numbers of positrons per disintegration) we can make use of the measured area ratio

$$s_{\beta^+}/s_{e^-_{60}} = 1.6 \pm 0.2$$

and the data from Table 4:

$$\frac{e^-(K + L\text{-}730)}{e^-(L_{\mathrm{I}} + L_{\mathrm{II}} + L_{\mathrm{III}} + M + N\text{-}60)} = 0.0029;$$

we obtain

$$\beta^+/e^-_{60} = 0.43\,\%.$$

Inasmuch as the 60 kev transition is isomeric, it is strongly converted and e^-_{60} is virtually identical with the number of decays to the ground state of Ho^{160}.

From the intensity balance given in Table 12, it follows that 40% of all decays must be attributed to K capture and β^+-decay from this level. From this we obtain the intensities and log ft values for the β^+-components listed in Table 5.

Thus the transitions to the upper levels are allowed. In view of this it may appear surprising that there are so few positrons per disintegration. This is explained by the fact that at low decay energies, K capture predominates. Assuming that the decay to the upper two levels is allowed, we can approximately determine K/β^+ from Zweifel's tables[10]. The estimated values for K/β^+ are 5400 and 400; although the accuracy of determination is not particularly great, on the basis of these high values it may be asserted that an appreciable fraction of all conversions of Ho^{160} must occur by K capture.

2. Multipole Orders of Transitions

The multipolarity of the transitions in Dy^{160} can be determined from:

1) Values of the relative conversion coefficients K:L and $L_I:L_{II}:L_{III}$ in the conversion spectra of Tb^{160} and Ho^{160}.

2) Values of the absolute conversion coefficients which at present can be obtained only from investigation of the decay of Tb^{160}, for which conver-

Table 6

Multipole orders of the principal transitions in Dy^{160} determined from the K/L ratio in the spectra of Tb^{160} and Ho^{160}

No.	Transition energy, kev	Experimental K/L value		Theoretical K/L values						Assignment*
		Tb^{160}	Ho^{160}	E1	E2	E3	M1	M2	M3	
1	86,5	0,87±0,20	0,58±02	6,5	0,97	0,092	6,2	3,3	0,87	E2, M3**
2	196,6	3,6±0,5	2,7±0,3	7,2	2,8	1,0	6,3	4,6	2,8	E2, M3**
3	297+298	—	3,3±1	7,3	4,1	1,9	6,4	5,2	3,7	E2, M3**
4	407	—	6,7±4	8,1	4,9	2,9	6,5	5,5	4,7	
5	514,6	—	9,4±2,5	8,3	6,6	3,3	7,0	6,6	5,6	E1, M1
6	539,8	—	5,4±1	8,4	6,6	3,9	7,2	6,5	5,6	E2, M2, M3
7	647,3	—	6,2±0,5	8,1	6,8	4,4	7,0	6,4	5,6	E2 M2, M3
8	729,7	—	6,3±0,6	7,6	6,5	4,9	6,7	6,3	5,4	E2, M1, M2
9	873,1	—	9,2±4	7,4	6,5	5,5	6,9	6,3	5,6	
10	879,9	6,2±0,7	6,0±1	7,4	6,5	5,5	7,0	6,2	5,6	
11	962+964	5,1±0,7	5,4±1	7,5	6,7	6,2	7,6	6,2	5,7	
12	1048	—	3,7±2	7,6	6,8	7,0	8,2	6,4	5,9	
13	1069	—	5,0±2	7,6	6,8	7,1	8,2	6,5	5,9	
14	1178	6,0±2,0	—	7,8	6,9	7,7	8,5	6,7	6,1	
15	1272	1,7±0,6	—	7,8	7,0	8,2	8,8	7,0	6,3	

---

*The multipole orders of transitions Nos.9 through 15 have not been determined owing to the large uncertainty in the experimental K/L values. The K/L values are listed for purposes of illustration.

**May also be mixture of E3 + M2.

Table 7

Multipole orders of transitions in the decay of Ho^{160} determined from the values of the $(L_I + L_{II})/L_{III}$ ratio. Values of α_L taken from Rose[11] with corrections according to Andersson & Bergström[12]

Transition energy, kev	Experimental value of $\frac{L_I + L_{II}}{L_{III}}$	Theoretical values of $(L_I + L_{II})/L_{III}$								Assignment
		E1	E2	E3	E4	M1	M2	M3	M4	
60,1	1,1±0,1	3,2	1,29	1,21	0,68	111	3,7	0,63	0,92	E3 (E2)*
86,5	1,3±0,1	4,3	1,3	1,2	1,1	104	5,5	1,14	0,42	E2 (E3, M 3)

* The M4 assignment is excluded by the small value of L_I/L_{II} (<0.3).

Table 8

Multipole orders of transitions in Dy^{160} determined from relative intensities of the conversion and γ-lines averaged from the data of Ref. 5,6,15 & 16 (The 196.6 kev radiation is assumed to be pure E2.)

No.	Transition energy, kev	Experimental value of $\alpha_K \cdot 10^3$	Theoretical value of $\alpha_K \cdot 10^3$						Inferred multipole order
			E1	E2	E3	M1	M2	M3	
1	86,5	1300	380	1600	4600	3100	29000	140000	E2
2	215	43	34	130	430	240	1100	4800	E1
3	297,7	14	15	49	150	98	390	1300	E1
4	878	2,9	1,4	3,4	7,3	6,2	16	33	E2
5	962	2,5	1,1	2,8	5,9	5,0	12	25	E2
6	966	2,5							
7	1178	0,64	0,81	1,9	3,7	3,1	7,5	14	E1
8	1201	0,87	0,79	1,8	3,6	3,0	7,2	13	E1
9	1273	0,54	0,69	1,6	3,2	2,6	6,2	11	E1

sion electron and γ-spectra are also known. In order to relate the scales of these spectra one must have at least one single line associated with radiation of known unmixed multipolarity. By way of such line it is convenient to take the 196.5 kev line; there are no indications that this is not a single line. Moreover, this line is sufficiently intense and according to all available data is associated with the transition between the 4+ and 2+ states of the first rotational band and, consequently, the assignment for it must be pure E2.

The results of multipole order determinations are listed in Tables 6, 7 & 8.

3. Level Diagram of Dy^{160}

The experimental data available to date are as yet inadequate for a consistent step by step systematization of the excited states arising in the decay of Tb^{160} and Ho^{160} and for determination of their exact energies, spins and parities. Consequently, we took recourse to a different procedure. Utilizing all the experimental data, theoretical considerations and analogies with neighboring nuclei, we constructed a level diagram for Dy^{160} which, we feel, is most consistent with the now available data. It is shown in Fig.8.

Below we shall set forth arguments supporting this scheme and list the facts that are either in conflict with it or remain unexplained.

First rotational band

The ground state and the first three excited states of Dy^{160}, having energies of 86.5, 283.1 and 580 kev, form a rotational band composed of the 0+, 2+, 4+ and 6+ states common to even-even nuclei in this region. The first excited level is almost at the same energy as in neighboring even-even nuclei. The values of the constants A and B in the expression giving the level energies,

$$E = AI(I+1) - BI^2(I+1)^2 , \tag{1}$$

are A = 14.51 kev and B = 0.0174 kev.

Almost the same values of A and B are obtained for neighboring even-even nuclei. Transitions between the above mentioned rotational band levels should give rise to γ-rays of energies 86.5, 196.6 and 296.9 kev. All three lines are actually observed in the decay of both Tb^{160} and Ho^{160}.

The following transitions between the levels of the rotational band:

$$6+ \rightarrow 0+ \text{ (580 kev)},\ 6+ \rightarrow 2+ \text{ (494 kev)},\ 4+ \rightarrow 0+ \text{ (283.1 kev)}$$

should be strongly forbidden.

The first two transitions have never been observed in either Tb^{160} or Ho^{160}, but a transition of 282 kev energy in Tb^{160} has been observed twice[2,3]. Apparently this is actually a very weak transition between some two high-lying levels of Dy^{160} (it is not shown in the decay scheme of Fig.8).

All three transitions between the levels of the rotational band must be E2, must give γ-γ coincidences and must be characterized by intensity values falling off with increasing energy.

All these requirements are fulfilled for the first two transitions. For the 86.5 kev level, the conversion ratio determined from measurements with a thin Ho^{160} source is $(K/L)_{exp} = 0.58$, while from theory $(K/L)_{E2} = 0.97$ (the reason for this divergence is not clear); $(L_I:L_{II}:L_{III})_{exp} = (0.2 \pm 0.1):(1.06 \pm 0.10):1.0$, while $(L_I:L_{II}:L_{III})_{E2} = 0.187:1.1:1.0$. The lifetime of

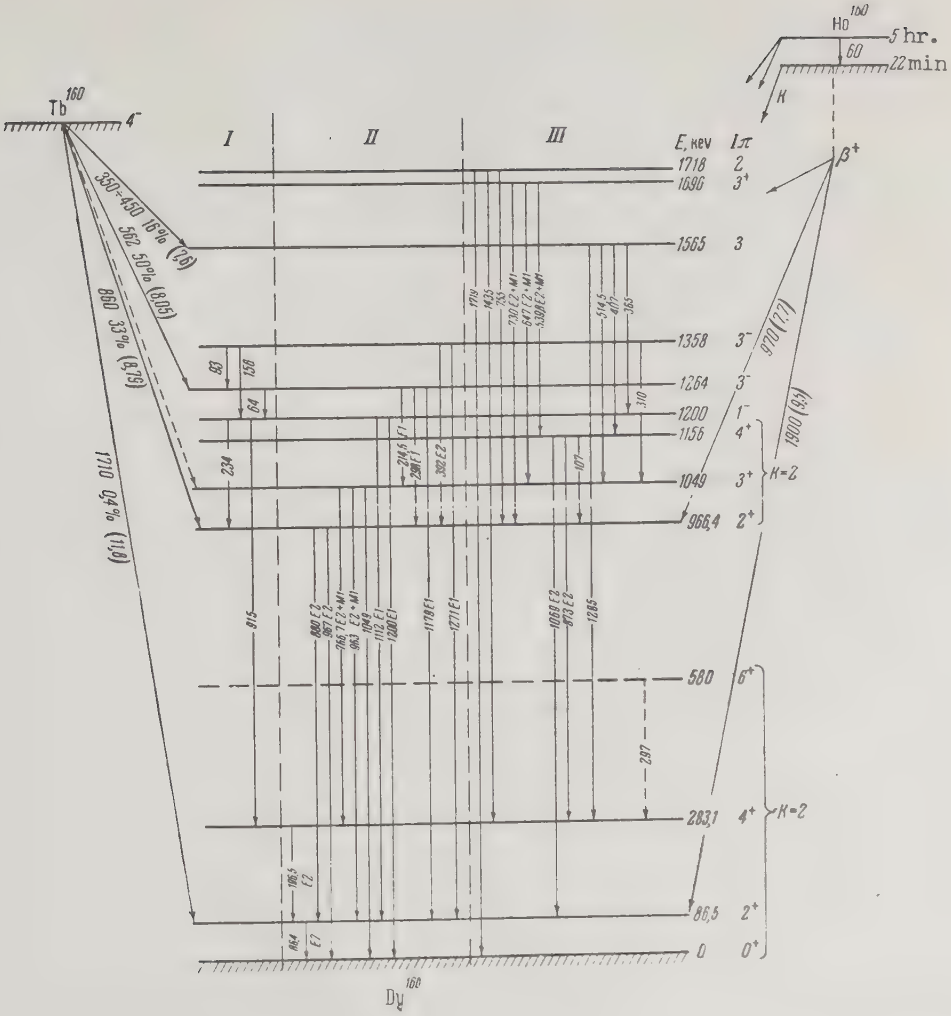
Ho^{160}
5 hr.
60
22min
K
β^+
Tb^{160}
4$^-$
I
II
III
E, кev
Iπ
1718
2
1696
3$^+$
1565
3
1358
3$^-$
1264
3$^-$
1200
1$^-$
1156
4$^+$
1049
3$^+$
966,4
2$^+$
K=2
580
6$^+$
283,1
4$^+$
K=2
86,5
2$^+$
0
0$^+$
Dy^{160}
350÷450 16% (7,6)
562 50% (8,05)
860 33% (8,79)
1710 0,4% (11,8)
970 (7,7)
1900 (9,5)
1719
1435
755
730 E2+M1
647 E2+M1
539 E2+M1
514,5
417
365
310
93
158
64
234
214,5 E1
298 E1
302 E2
107
915
880 E2
967 E2
766,7 E2+M1
963 E2+M1
1049
1112 E1
1200 E1
1178 E1
1271 E1
1069 E2
873 E2
1285
297
196,5 E2
86,4 E2

Fig.8. Decay scheme for Ho^{160} and Tb^{160}: I) lines observed only in the decay of Tb^{160}, II) lines observed in the disintegration of Tb^{160} and Ho^{160} and III) lines observed only in the decay of Ho^{160}.

the 86.5 kev level - $1.8 \cdot 10^{-9}$ sec (Ref.13) - is nearly the same as that of the first 2+ type levels of neighboring even-even nuclei.

For the 196.6 kev transition, we have $(K/L)_{exp} = 2.8$ (average value from Tables 2 & 4 and Refs. 5 & 6) and $(K/L)_{E2} = 2.8$.

Coincidences between the 86.5 kev and 196.6 kev γ-rays are observed; the intensity of the 196.6 kev transition is lower than that of the 86.5 kev transition.

The situation as regards the 296.9 kev line is somewhat more complicated.

First, in the spectrum of Tb^{160} it is 6 times more intense than the 196.6 kev line; this indicates that a transition of this energy occurs not only in the first rotational band but also between some higher-lying levels. It was inferred from analysis of the conversion spectrum of Ho^{160} that this line is a double one with a very small separation (~1 kev) between the components. Moreover, we have the following facts:

a) The experimental value of the conversion ratio K/L = 7.8 for this transition in Tb^{160} is closest to the theoretical value for E1 (rather than E2).

b) The 296.9 kev γ-line in the decay of Tb^{160} yields β-γ coincidences primarily with the soft component of the β-spectrum, whereas the 196.6 kev γ-ray gives coincidences with both components in equal measure.

c) Although 296.9-86.5 and 296.9-196.6 γ-γ coincidences have been observed[6], they are of very low intensity.

All this leads us to conclude that at least in most cases the 296.9 kev γ-ray observed in the decay of Tb^{160} is associated with transitions between high-lying levels and not with the transition between the 580 and 283.1 kev levels of the rotational band.

At the same time this conclusion cannot be drawn for Ho^{160} in whose spectrum the doublet structure of this line has been detected. The total K/L ratio (3.4) is also indicative of a doublet structure; the value of this ratio is closest to the theoretical value for E2.

The double 873+880 kev and 962+966 kev γ-lines

The most intense lines in the γ-spectrum of $Tb^{160} \rightarrow Dy^{160}$ are the 880 and 966 kev lines. These lines are also present in the spectrum of $Ho^{160} \rightarrow Dy^{160}$; here although their intensity is inferior to that of the 730 kev line, these lines are still prominent and of approximately equal intensity.

It was long assumed that these lines are single, but from the measurements of Nathan and our results it became clear that both are at least double. Using all the data of Tables 2, 3 & 4 we deduce that the former doublet consists of lines of 873.1 ± 0.5 kev and 879.9 ± 0.5 kev energy and the latter of 962.1 ± 1.3 kev and 966.4 ± 1.2 kev lines.

How can the 963 and 966 kev transitions be fitted into the level scheme of Dy^{160}? If both these transitions do not go to the ground level, then under them must be another transition having an intensity not inferior to their sum. As may be seen from Table 3 in the decay of Tb^{160} only the hard γ-lines (>800 kev) and the 296.9 kev γ-line have intensities commensurate with the intensity of the 963 + 966 kev doublet. Nathan established, however, that the 963 + 966 kev γ-rays do not yield γ-γ coincidences with either the 873 + 880 kev doublet or with any other hard γ-lines of more than 300 kev energy. Consequently, there can be only low energy transitions under the 963 + 966 kev doublet.

The 296.9 kev transition, as indicated above, must be located in the upper part of the decay scheme, while all the other transitions are weak. It follows that at least one component of this doublet goes to the ground level, which means that at least one level in Dy^{160} is located at either 963 or 966 kev. Let us consider this level further. It would be desirable to determine its spin and parity. For this one must either know the value of K/L or α_K or obtain a reasonable clear picture of the angular correlation of the γ-rays passing through this level. So far we cannot evaluate the K/L ratio since, although the K conversion lines of the 963 + 966 kev doublet have been identified, the L lines have not been resolved.

The coefficient α_K is also unknown, since in order to determine one must know the intensity of the γ-doublet components. Although, as noted above, Nathan did determine the intensity of the γ-doublet (12:23) from γ-γ coincidences, he did this on the assumption that the 876 kev line is single and this apparently is not the case, for, although this line does appear to be single in the photoelectron spectrum of Tb^{160}, in the conversion spectrum of Ho^{160} the doublet structure is clearly discernible.

Although the γ_{300}-$\gamma_{873+880+962+966}$ angular correlation has been investigated, in view of the complexity of the components it can hardly be used for determining the spin of the level in question.

Thus we have no direct data from which one can determine the spin and parity of the 963 or 966 kev level.

Second rotational band

The physical nature of the level of Dy^{160} with 962 or 966 kev energy is not clear. Obviously, this level does not belong in the first rotational band whose levels, as indicated above, are located at 0, 86.5, 283.1 and 580 kev; this level may be a quadrupole or octupole vibrational one or it may be a single-particle level. In any case it can serve as the lowest state of a new, second rotational band whose level energies are given by the expression

$$E = E_0 + A\,[I\,(I+1) - I_0\,(I_0+1)] - B\,[I\,(I+1) - I_0\,(I_0+1)]^2, \tag{2}$$

where I_0 is the momentum of the first level of this band and the constants A and B must have values close to those for the first rotational band.

We provisionally took A and B equal to the values for the first rotational band and calculated the energies of the levels of the second band and of the expected transitions from them on the following assumptions

$K = 0$; $I = 0\pm,\ 2\pm,\ 4\pm,$
$K = 0$; $I = 1\pm,\ 3-,\ 5-,$
$K = 1$; $I = 1\pm,\ 2\pm,\ 3\pm,$
$K = 2$; $I = 2\pm,\ 3\pm,\ 4\pm,$
$K = 3$; $I = 3\pm,\ 4\pm,\ 5\pm,$

and taking the energy of the first level of the band to be 962.1 or 966.4 kev.*

We calculated the positions of the first three levels of the band and determined the energies, relative intensities and multipole orders of the transitions de-exciting these levels. The calculated data are compared with the experimental values and the data from the literature in Tables 2 & 4.

It was found that for one reason or another one can reject all cases except $K = 2$, $I = 2+$, $3+$ or $4+$ and $E_{02} \approx 966.4$ kev. The resultant level energies (assuming the indicated values of A and B) are 966.4, 1052 and 1166 kev. Thus the lowest level of this band has the energy 966.4 kev and spin and parity 2+ ($K = 2$).

There should be transitions of 966.4, 879.9 and 683.3 kev energy from this level to the three lower levels of Dy^{160}, namely, 0+ (ground), 2+ (86.5 kev) and 4+ (283.1 kev).

The first two transitions have been observed in the conversion and photoelectron spectra of Tb^{160}; Keshishian and his co-workers[3] also observed a line of 679 kev energy but the difference between this and 683.3 kev is too great to allow of positive identification. The 966.4 kev (2+)→0 kev (0+) transition must be pure E2. This is not in conflict with the reported experimental values of α_K and K/L.

The 966.4 kev (2+)→86.5 kev (2+) transition of 879.9 kev energy could be of mixed multipolarity, namely, E2 + M1. Evaluation of the relative importance of the components of this mixture is hampered by presence of a transition of

---

*Here K is the projection of the total angular momentum of the nucleus on the nuclear symmetry axis.

close energy (873.1 kev), observed by us in the spectrum of Ho^{160} but not detected in the spectrum of Tb^{160}. However, in investigating the conversion spectrum of Tb^{160}, we determined that the upper bound for the intensity of the 873.1 kev line is 7% relative to the intensity of the higher-energy line.

The photoelectron peak from this transition proved to be single at least within the limits of our measurement error (experimental line half-width 0.33%).

Utilizing the theoretical conversion coefficients for transitions of different multipole orders one can show that the presence of the close line does not alter the experimental conversion coefficient by more than 15% so that it can be unambiguously deduced that the 879.9 kev transition is primarily E2.

If the 966.4 kev and 879.9 kev transitions are pure E2, the ratio of intensities of the corresponding conversion lines can be found according to Alaga's rules:

$$\frac{K\text{-}966{,}4}{K\text{-}879{,}9} = \frac{\langle I_i, L, K_i, \ K_f - K_i \mid I_i, L, I_f, K_f \rangle^2}{\langle I_i, L, K_i, K_{f_1} - K_i \mid I_i, L, I_{f_1}, K_{f_1} \rangle^2} \left(\frac{966}{880}\right)^5 \frac{\alpha_{K\text{-}966.4}}{\alpha_{K\text{-}879.9}} = 0{,}7 \cdot 1{,}6 \, \frac{2{,}8}{3{,}4} = 0{,}9,$$

where the index i corresponds to the initial state and f to the final state of the nucleus.

Experiment yields 0.6 for Tb^{160} and 0.7 for Ho^{160}.

The fact that these values are close to that obtained by means of the above expression indicates that the above assumptions regarding the values of I and K for the 966.4 kev level are substantially correct.

Our calculations show that the second level of the second rotational band must have an energy of about 1051 kev. In the conversion spectrum of Ho^{160} there is a line corresponding to a γ-ray of 1048 kev energy. This could be the 3+ (K = 2)$\rightarrow$0+ (K = 0) transition to the ground state.

Assuming the 1049 kev level to be of the 3+ type there should be transitions to the 2+ (86.5 kev) and 4+ (283.1 kev) level. These transitions should be of the E2 + M1 type (Δ = 1) and have energies of ~962 and ~765 kev. We infer that the first line is the lower energy line in the Tb^{160} and Ho^{160} doublets (962.1 ± 1.3 kev) and the second is the 766.7 kev line detected in the conversion spectrum of Ho^{160}. On the basis of this identification one can refine the positions of the levels, taking the average for the experimental values:

Crossover transition 1048.0
766.7 + 288.1 = 1049.8
962.1 + 86.5 = 1048.6
Average 1048.8 kev

The transition from the 1048.8 kev level to the ground level of Dy^{160} must be 3+$\rightarrow$0+, i.e., M3. One might think that this transition could not compete with E2 + M1 type transitions to the 2+ and 4+ levels of the first band, although the difference in probabilities should be somewhat compensated by the fact that this transition is not inhibited with respect to the K number, while there is some K-forbiddenness for the M1 multipolarity as regards the other transitions. Actually, however, in Ho^{160} the K line corresponding to the 1048.8 kev transition is even more intense than the K line associated with the 766.7 kev transition. The reason for this is not known.

The multipole order of the 962.1 kev transition can be estimated from the experimental data as follows. The photoelectron line from the 962.1 + 966.4 kev γ-rays in the spectrum of Tb^{160} is complicated (anomalously wide), and it may be asserted that the relative intensities of its components do not differ by more than a factor of 3. This deduction agrees with the inference made by Nathan on the basis of γ-γ coincidences. The 966.4 kev γ-line is from a pure

E2 transition. Inasmuch as

$$\frac{K\text{-}962}{K\text{-}966} = \frac{\gamma\text{-}962}{\gamma\text{-}966} = \frac{\alpha_{K\text{-}962}}{\alpha_{K\text{-}966}},$$

it follows from the experimental ratio of K and γ and the theoretical $\alpha_{K\text{-}966}$ value that

$$\alpha_{K\text{-}962} = (1.5\text{-}4)\cdot 10^{-3},$$

which is close to the theoretical value for E2 and M1 type transitions, i.e.,

$$\alpha_K(E2) = 2.8\cdot 10^{-3} \text{ and } \alpha_K(M1) = 5\cdot 10^{-3}.$$

The transition from the 1048.8 kev level to the 966.4 kev (2+) level must be mixed E2 + M1 and have an energy of 82.4 kev. This is, of course, a low intensity transition (due to the low energy) and hence one could hardly expect the doublet structure of the 86.5 kev line to be discernible.

The third level of the second band should, according to our tentative evaluation, have an energy of about 1166 kev and the assignment 4+. One might expect transitions from it to the 86.5 (2+), 283.1 (4+), 966.4 (2+) and 1048.8 (3+) levels and perhaps to the hypothesized 580 kev (6+) level. The respective energies of these transitions should be ~1080, 883, 200 and 117 kev. In the conversion spectrum of Ho^{160} there are lines corresponding to transitions of 1069, 873.1 and 107.3 kev energy; in all these cases the transition energies are approximately 10 kev lower than the calculated values. This circumstance may be utilized for making the energy of the level more precise. If we use all three lines for determining the position of this level, we obtain

$$\begin{aligned} 1069 + 86.5 &= 1155.5 \\ 873.1 + 283.1 &= 1156.2 \\ \underline{107.3 + 1049.8} &\underline{= 1157.1} \\ \text{Average} &= 1155.9 \text{ kev} \end{aligned}$$

The multipole order of the 1069 kev transition should be E2 + M1. The experimental value of K/L is 30% lower than the theoretical value for M1 and 25% lower than the theoretical value for E2. This may be due to experimental errors.

The 873.1 kev level should also be E2 + M1; we have no experimental data for this transition. It is not clear why there is observed a 1155.9 kev (4+, K = 2)→580 kev (6+, K = 0) transition. The transition to the 0+ level is forbidden with respect to spin, while the transition to the 283.1 kev (4+) level is forbidden with respect to the ν number.

Having established the energy positions of the first three levels of the second band, we can determine the corresponding values of A_2 and B_2; we obtain

$$A_2 = 14.16 \text{ kev, and } B_2 = 0.024 \text{ kev.}$$

This value of A_2 is somewhat lower than the value of A for the first band; in other words the effective moment of inertia in the upper band is somewhat greater. This may be regarded as evidence that the base level of this band is a single-particle one; in the case of bands comprised of vibrational levels the moment of inertia is usually smaller than in the lowest band.[14]

Using the values of A_2 and B_2 we can calculate the position of the next level. We find that the energy of this level is 1292 kev. The conversion electron spectrum of Ho^{160} contains a K-1285 line. We are, however, inclined to view this as a fortuitous coincidence since the probability of a cross-over $5+ \rightarrow 0+$ transition is virtually negligible.

The transition from this level to the 86.5 kev level of Dy^{160} must obviously have an energy of 1206 kev; again there is a K-1201 line in the conversion spectrum of Ho^{160}. Here again the close energy value is probably accidental.

Levels in Dy^{160} above 1160 kev

We have introduced the other higher-lying levels of Dy^{160} in cases where one can postulate no less than three transitions from the given level differing in energy from experimentally observed transitions by not more than 3 kev. There are 6 such levels. These are listed below together with the transition energies:

1. 1200 kev level

Direct transition in Tb^{160} & Ho^{160} 1201
86.5 + 1112 (Tb^{160}) = 1198.5
283.1 + 915 (Tb^{160})* = 1198.1
966.4 + 234 (Tb^{160})* = 1200.4
Average 1199.5 kev

2. 1264 kev level

Direct transition in Ho^{160} 1264
86.5 + 1178 (Tb^{160}, substantiated
by γ-γ coincidences = 1264.5
86.5 + 1180 (Ho^{160}) = 1266.5
966.4 + 297.7 (Tb^{160}, Ho^{160}, substantiated by γ-γ coincidences = 1264.1
1048.8 + 214.9 (Tb^{160}, Ho^{160}) = 1263.7
1200 + 64 (Tb^{160}) = 1264.0
Average 1264.4 kev

3. 1358 kev level

86.5 + 1272.5 (Tb^{160}, substantiated
by γ-γ coincidences = 1359.0
86.5 + 1273 (Ho^{160}) = 1359.5
1048.8 + 310 (Ho^{160}) = 1358.8
966.4 + 392 (Tb^{160}) = 1358.4
966.4 + 393 (Ho^{160}) = 1359.4
1200 + 156 (Tb^{160})* = 1356
1264 + 93 (Tb^{160}) = 1357
Average 1358.3 kev

---

*These transitions in Tb^{160} (see also first group on next page) were observed only by Keshishian and his co-worders[3].

4. 1565 kev level

86.5 + 1477 (Tb^{160*}, Ho^{160}) = 1563.5
283.1 + 1285 (Ho^{160}) = 1568.1
1048.8 + 514.5 (Ho^{160}) = 1563.3
1155.9 + 407.0 (Ho^{160}) = 1562.9
1200 + 365 (Ho^{160}) = 1565.0
Average 1564.6 kev

5. 1696 kev level

966.4 + 729.7 (Ho^{160}) = 1696.1
1048.8 + 647.4 (Ho^{160}) = 1696.2
1155.9 + 539.4 (Ho^{160}) = 1695.3
Average 1695.9 kev

6. 1718 kev level

Direct transition in Ho^{160} = 1719
283.1 + 1435 (Ho^{160}) = 1718.1
966.4 + 754.7 (Ho^{160}) = 1721.1
1358 + 364 (Ho^{160}), (other possibility -
see 1565 kev level) = 1722
Average 1718.2 kev

One can introduce yet another level of 1534-1539 kev energy, based wholly on the lines reported by Keshishian and his co-workers:

283.1 + 1250 (Tb^{160}) = 1533.1
966.4 + 569 (Tb^{160}) = 1535.4
1264 + 274 (Tb^{160}) = 1538
1358 + 181 (Tb^{160}) = 1539

We have not, however, shown it in the scheme of Fig.8.

Let us now consider the quantum characteristics of the enumerated levels.

1200 kev level. There are undoubtedly transitions from this level to the 0+ and 2+ levels of the first rotational band; somewhat doubtful are the transitions to the 4+ (K = 0) and 2+ (K = 2).

According to the value of α_K the 1200 kev transition is apparently E1; the spin and parity assignment for the 1200 kev level is therefore 1-.

For a level with I = 1, K may be 0 or 1. Inasmuch as the ratio of intensities of the 1112 and 1200 kev transitions is not known one cannot determine which of the two K values is the true one and hence one cannot at present further characterize this level.

1264 kev level. This level is often excited in the decay of Tb^{160} since the 297.7 kev line is one of the most intense in the γ-spectrum. The transitions from this level to the 2+ (K = 0+), 2+ and 3+ (K = 2+) levels of energies 1178, 297.7 and 214.8 kev, according to the data of Table 8 are all E1. This means that this level is certainly either 2- or 3-. The 2- assignment, however, is excluded in view of the fact that intense β-decay goes to the 1264 kev level. Since (according to Peker[14]) the spin and parity assignment for

---

*See note on preceding page.

the ground state of Tb^{160} is 4-, β-decay to a 2- level would be twice forbidden and would have an incomparably lower probability ($\log ft > 10$), whereas from experiment it follows that $\log ft < 9$. The value of the K number for this level can also be evaluated by means of Alaga's rules since the intensities of the 297.7 and 214.9 kev transitions to the levels of the same rotational band are known from experiment. It may be noted that these intensities were measured independently by Clark and Nathan with nearly identical results. The ratio of the intensity of these transitions normalized to the same energy is 2.92 (Clark & Knowles[5]) or 2.60 (Nathan[6]); the theoretical value of this ratio for K = 2 and I = 2 is 2.0, while for K = 3 and I = 3, the ratio is 2.86. It will be seen that the experimental data on the intensities of the γ-transitions are in better agreement with the assumption that K = 3 (than with K = 2).

1358 kev level. Since there are observed transitions to 2+ (K = 0), 2+ and 3+ (K = 2) and 1- and 3- (K = 3) levels and there is no known transition to the 0+ (K = 0) level it may be inferred that the spin of this level is either 2 or 3. If we accept Nathan's results, according to which the 392 kev transition is E1, and our data, according to which the 1272 kev transition is E1, the most probable spin and parity will be 3-. In this case this level can be fed by β-transitions in Tb^{160}, whereas if one makes the 2- assignment the probability of excitation of this level in β-decay becomes very low.

In view of this spin value the absence of transitions (E3 type) to the ground state (0+) of Dy^{160} becomes understandable.

The transition to the 86.5 kev (2+) level is only 3 times more intense than the transition to the 966.4 kev (2+) level, although from energy considerations it should be 33 times more intense. The low abundance of the 1271 kev γ-transition can be explained by the effect of K forbiddenness which does not affect the 392 kev transition ($\Delta\nu = \Delta K - L \leqslant 0$).

There are certain indications that K = 2 for the 1358 kev level. These include the relatively weak degree of K forbiddenness as regards the 1271 γ-transition and the fact that, according to evaluations, the experimental value of the ratio of the 392 and 310 kev transition intensities (normalized to the same energy) amounts to 0.75, which is in good agreement with the theoretical value of 0.7 deduced on the assumption that K = 2 and I = 3-. If the cited data on the intensities of the 1271, 392 and 310 kev lines are correct, the 1358 kev (3-) level can be interpreted as the first rotational level of a band with K = 2. For reasons that are unclear, however, the "ground" state of this band is not in evidence; it should be located somewhere near the 1264 kev level. It may be that one of the two components of the 298 kev doublet observed in the decay of Ho^{160} is due to deexcitation of a level with an energy close to 1264 kev but with K = 2, in which case this new level will be the "ground" state of the K = 2 band. This hypothesis allows of understanding the doublet structure of the 298 kev line in the decay of Ho^{160} and its singlet structure in the decay of Tb^{160}, since, as noted above, a 1264 kev (I = 2-, K = 2) level cannot be directly excited in β-decay.

1565 kev level. This level is excited only in the decay of Ho^{160}. Inasmuch as there are observed transitions to the 2+ and 4+ (K = 0+), 3+ and 4+ (K = 2+) and 1- (1200 kev) levels, it may reasonably be inferred that the spin of this level is 3. From the value of the K/L ratio for the 514.6 kev transition it may be inferred that the multipole order of the transition to the 3+ level is E1 or M1. Consequently, the parity of this level cannot be determined at present.

1696 kev level. This level is apparently very frequently excited in the decay of Ho^{160}: one of the most intense transitions (729.7 kev) departs from this level.

Since there are transitions to the 2+, 3+ and 4+ (K = 2) levels and no transitions to levels of the lower rotational band, in making the spin assignment we must choose between 3+ and 4+ and $K \geqslant 3$. However, K capture from the 5+ ground state of Ho^{160} to the 3+ level is twice forbidden, while it is allowed to the 4+ level. The K capture transition from the 2- isomeric state of Ho^{160} to the 3+ level should be once forbidden. Hence the probable assignment for the 1696 kev level is 4+.

1718 kev level. Inasmuch as there are observed transitions to the 0+ and 4+ levels of the first band, the 2+ level of the second band and the 1- (1200 kev) level, it may be assumed that the spin of the 1718 kev level is 2.

β-decay of Tb^{160}

According to the rule established by Peker[14], the spin and parity of Tb$^{160}_{95}$ (a deformed odd-odd nucleus) is 4- (for Z = 65, $\Omega_p = 3/2-$; for N = 95, $\Omega_n = 5/2-$; $I = \underline{\Omega_p \pm \Omega_n} = 4-$ or 1-).

If the spin of Tb^{160} were 1, there would be observed an intense β^--transition (once forbidden) to the 0+ ground state of Dy^{160}. The fact that there is no such transition proves that the assignment for the ground state of Tb^{160} is 4-. For this spin value the β-transition to the ground state is strongly forbidden ($\Delta I = 4$, yes) and should not be observed; this is in accord with the experimental data.

β-γ coincidence studies showed that an 856 kev β^--transition feeds the 966 kev level and a 562 kev β^--transition feeds the 1264 kev level. Softer β-components correspond to transitions to the 1359 kev or higher lying levels.

The β^--transition with 1710 kev end-point energy, observed by us and a number of other investigators, must go to the 2+ level at 86.5 kev. In this case this is a unique transition. The large value of log ft (11.9) can be explained if we take into account the fact that this transition is inhibited by a high degree of K forbiddenness ($\Delta \nu = \Delta K - L = 2$), which decreases the probability of an ordinary unique transition with log $ft \approx 7.5$-9 by a factor of 10^4 (which gives log $ft = 11.5$-13). The β^--transition to the 4+ level of the lower rotational band is once forbidden, but it is subject to even stronger K forbiddenness ($\Delta \nu = 3$), which decreases the transition probability by a factor of 10^6. If such a transition does exist, its intensity is very low (inferior to that of the 1710 kev transition), so that it is virtually undetectable against the background of the higher energy transition.

The β^--transition to the 966.4 kev level (2+, K = 2) is an ordinary once forbidden unique type transition not inhibited by K forbiddenness. This inference is consistent with the experimental log ft value of 8.8.

There may also be a β^--transition to the 1049 kev (3+) level. Inasmuch as the 1049 kev level is a rotational one, such a transition must be weaker than the transition to the 966.4 kev level (the "ground" state of the second band). This is connected with the fact that, while in a transition to the "ground" state of the rotational band, part of the wave function in the matrix element does not change, in a transition to higher excited rotational level the wave function does change, which reduces the matrix element of the β-transition and, consequently, lowers the transition probability.

We were not able to distinguish the β-component associated with this transition in the β-spectrum, but the intensity balance for the γ-transitions indicates that it does exist and that it is less intense than the 858 kev transition.

The fact that there is a β-decay to the 1264 kev level and the value of log ft corresponding to it indicate that the spin of this level cannot be less

than 3 (which is in disagreement with the inference made by Nathan[6]). If we assume that the assignment for the 1264 kev level is 3- (as follows from analysis of the γ-transitions), the β-transition to it must be an allowed one ($\Delta I =$ $= 1$, no). In this case it is difficult to understand the large ft value: log $ft = 8.1$.

The same difficulty arises in considering the softest component of the β^--spectrum. If we assume, in agreement with Nathan, that the energy of this transition is approximately 455 kev and that it goes to the 1358 kev (3-) level, we must conclude that it is an ordinary allowed transition which again is inconsistent with the experimental log ft value of 8.1.

Intensity balance in the decay of Tb^{160}

In drawing up the intensity balance for the decay of Tb^{160}, we took the average intensity values of the photoelectron lines from Refs.5,6,15 & 16 and of the conversion lines from Refs.5,6 & 16. For purposes of computation, we took the intensity of the transition to the ground state of Dy^{160} as the 100% value. Further, we assumed that the soft component of the double 963 + 966 kev line accounts for 1/3 the intensity of the doublet in accord with the coincidence measurements of Nathan and our measurement of the photoelectron and conversion lines associated with this transition (see Figs.2 & 3).

The β-spectrum component intensity values are also averages, taken from Refs.4,5,6 & 16.

Table 9 shows that there is no sharp divergence between the abundances of arriving and departing transitions at any level. What minor imbalances there are may be explained, on the one hand, by experimental errors and, on the other hand, that the fact that some low intensity lines that might restore the balance have been neglected.

Table 9

Balance of intensities in the decay of Tb^{160}

No.	Level energy, kev	Transitions to level		Transitions from	Reasons for imbalance
		γ	β		
1	0	100			
2	86,5	90	0,4	68	Errors in determining line intensities
3	283,1	—	—	5,7	Weak transitions to the level may exist
4	966,4	32	33	69	
5	1048,8	3,5	—	14,5	β-decay may exist
6	1200	—	—	2,6	Weak lines
7	1265	—	50	52	
8	1358 & higher	—	16	13,2	β-decay and weak lines

It should be noted that in all investigations devoted to analysis of the β-spectrum, the shape of the components was assumed to be the Fermi one, whereas, for example, the component of 860 kev end-point energy should have the shape corresponding to a unique transition.

Isomerism in Ho^{160}

Analysis of the data on K capture in Ho^{160} is complicated by the fact that this nuclide has two isomeric states having half-lives of approximately 5.2 and 0.5 hours. Very intense lines corresponding to conversion of the 60.1 kev transition on the $L_I + L_{II}$, L_{III}, M and N shells were observed in the conversion spectrum of the erbium and holmium fractions. The integral intensity

of these lines is approximately equal to the intensity of all the other lines in the spectrum of Ho^{160}. Hence it is logical to go along with the assumption of Mihelich et al[7] that these conversion lines are associated with the transition between the two isomeric states of Ho^{160}, although we have no rigorous proof of this. The accuracy of measurement of the differences $L_{II} - L_{III}$ and $L_{III} - M$ is insufficient for identifying the nucleus in which this transition occurs; the difference $K - L_{III}$ would be the most suitable for this purpose but, although the K-60 line has been observed[8], it could not be identified with complete certainty in view of the possible surposition of L Auger electrons.

Inasmuch as the intensity of the L-60 and M-60 lines falls off with a period of about 5 hours, it may be inferred that this period pertains to the upper isomeric state of Ho^{160}.

Experimental data on the multipole order of the isomeric transition. Experimental determination of the multipole order of an isomeric transition can be made by measuring the ratio of intensities of the K and L conversion lines or the ratio of intensities of the L_I, L_{II} and L_{III} lines.

In the present case the K/L ratio cannot be measured with sufficient accuracy in view of the low energy of the K electrons (4.5 kev) and the possible surposition of the L Auger electron group.

The $(L_I + L_{II})/L_{III}$ ratio was measured in the present investigation and the results are listed in Table 7 together with the theoretical values of this ratio for different multipole orders (the values of α_L were taken from Rose's tables as interpolated by Dranitsyna[17]; the correction indicated by Andersson & Bergström[12] was taken into account for $\alpha_{L_{III}}$ E3). The experimental data agree with the theoretical values for E2 and E3 transitions (the theoretical values of L_{II}/L_{III} for these transitions are very close; the choice could have been made if the very weak L_I line had been measured).

One can attempt to make a choice between these two alternatives on the basis of the lifetime of the excited states. The only means now available for comparison are Weisskopf's formulas for single particle transitions. There is of course no certainty that these formulas are exactly applicable to the case in question. It must be noted, however, that the change in lifetime in going from one multipole order to the next is very appreciable - of the order of 10^7 - while the change in lifetime owing to the collective nature of the motion in such cases does not exceed 10^3 times. Hence a rough determination of the multipole order utilizing Weisskopf's formulas is feasible.

The theoretical lifetime values for the 60 kev excited state of Ho^{160} are listed in Table 10.

Table 10

Lifetimes of the 60 kev excited state of Ho^{160} according to
Weisskopf's formulas: $T_{exp} = 5.2$ hours
(It is assumed that β-decay of this state does not occur)

Type of transition	Formula for T (T,sec; E,Mev)	T_γ	T taking conversion into account
E1	$T = 4{,}5\cdot10^{-15}\ A^{-2/3}\ E^{-3}$	$7\cdot10^{-13}$ sec	$1{,}4\cdot10^{-14}$ sec
E2	$T = 4{,}3\cdot10^{-9}\ A^{-4/3}\ E^{-5}$	$6{,}4\cdot10^{-6}$ "	$5{,}9\cdot10^{-7}$ "
E3	$T = 6{,}3\cdot10^{-3}\ A^{-2}\ E^{-7}$	88 "	0,1 "
E4	$T = 1{,}4\cdot10^{4}\ A^{-8/3}\ E^{-9}$	58 yrs	49 hrs
M1	$T = 2{,}5\cdot10^{-14}\ E^{-3}$	$1{,}2\cdot10^{-10}$ sec	10^{-11} sec
M2	$T = 5{,}8\cdot10^{-9}\ A^{-2/3}\ E^{-5}$	$2{,}5\cdot10^{-4}$ "	$1{,}7\cdot10^{-6}$ "
M3	$T = 3{,}8\cdot10^{-3}\ A^{-4/3}\ E^{-7}$	26 min	0,74 "
M4	$T = 4{,}6\cdot10^{3}\ A^{-2}\ E^{-9}$	570 yrs	0,5 yrs

It will be apparent from the values of T_{theo} that the choice between E2 and E3 must be made in favor of the latter (although T_{exp} and T_{theo} in this case differ from each other by a factor of 10^5).

To explain the observed lifetime one can assume a mixture of the E4 + M3 type. Then to obtain the requisite lifetime it would be necessary to take 99.996% E4 + 0.004% M3. However, with such a predominantly E4 mixture one cannot satisfy the experimentally observed value of $(L_I + L_{II})/L_{III}$.

Explanation of isomerism in Ho^{160}

The existence of two isomeric states in Ho^{160} could be foreseen inasmuch as the ground and one of the low-lying excited states of any odd-odd deformed nucleus must have spins described by

$$I = \Omega_p \pm \Omega_n,$$

and identical parities. According to the rule established by one of the present authors[14], Ω_p is equal in the present case to the spin of a nucleus with 67 protons, while Ω_n is equal to the spin of a nucleus with 93 neutrons. According to the data of Ref.14, $\Omega_p = 7/2-$ and $\Omega_n = 3/2-$. It follows therefore that in Ho^{160} there are two close-lying states characterized by 5+ and 2+, one of them being the ground state. The transition between them involves a change in spin by 3 units but no change in parity and hence has the multipolarity M3 + E4.

As we have seen, however, the possibility of the 60 kev transition having this multipolarity mixture is excluded in view of the fact that no M3 + E4 mixture composition yields the necessary value of $(L_I + L_{II})/L_{III}$.

It will be shown below that the ground state of Ho^{160} has spin 5+ and that the assignment for the isomeric state consistent with an E3 transition is 2-.

Apparently, the predicted 2+ level lies somewhat higher and is not evinced in the disintegration inasmuch as it cannot be excited directly in the decay of Er^{160} (K decay to it is twice forbidden).

The experimentally observed 2- level is probably due to excitation of one of the unpaired nucleons, for example, a proton, to the level with $\Omega = 3/2+$. Evidence of the single particle character of the excitation of this level is furnished by the appreciable slowing down of the 60 kev isomeric transition (by a factor of 10^5) which can be explained by the appreciable difference between the inner structures of the ground and isomeric states.

On the excitation of Ho^{160} isomers by electron capture in Er^{160}

Let us now consider the question of spins. The lowest level of Ho^{160} must be either 2+ or 5+. Comparison of the transition abundances in the disintegration of Ho^{160} + Ho^{160m} shows that a very considerable proportion of the decays of Er^{160} goes through the 5-hour level of Ho^{160}. Since the ground state of Er^{160} is 0+; this means that the spin of the upper state of Ho^{160} is in any case lower than that of the lower state.

Gorodinskii, Murin & Pokrovskii[18] carried out a special investigation to determine whether the 22-minute Ho^{160} isomer appears directly in the decay of Er^{160}. To this end the Er^{160} sample was purified of Ho and then several minutes later Ho was again separated from it. The rate of increase of the individual γ-lines indicated that about 10% of the decays of Er^{160} go through the 22-33 min state. This fact is in conflict with the fact of isomerism of Ho^{160}:

if the probabilities of formation of Ho^{160} and Ho^{160m} are close, their spin values must also be close, but the properties of the isomeric transition show that these spins must differ by at least three units.

We consider the last fact to be more reliable and hence are inclined to the hypothesis that the ground state of Ho^{160} is 5+ and the isomeric state is 2-. Where the 2+ level is located remains unclear.

The probability of the 60.1 kev transition is composed of the sum of the probabilities of K, L and M conversion and γ-radiation. If this is an E3 type transition, then

$$\gamma : K : L_I : L_{II} : L_{III} : M = 0.1 : 0.5 : 0.5 : 44 : 35 : 20.$$

Thus K conversion and γ-rays account for only 0.6% of the total intensity, so that one may take the integral intensity of the L and M lines as virtually equal to the total intensity of the transition. In calculating the relative intensities of the other transitions, we used the intensity of the conversion line as the point of departure; the intensity of the transition was calculated from the theoretical conversion coefficient; the mixtures were evaluated on the basis of the corresponding experimental conversion coefficient. In summing up we took into account the positions of the transitions in the Dy^{160} energy diagram. The pertinent data are listed in Table 11.

Table 11

Approximate intensities of different transitions in the decay of Ho^{160}

Transition energy, kev	Intensity of conversion lines	Transition assignments	Conversion coefficient (α_K or α_L)	K + L + M + γ transition intensity**
60	L-2200 $(M+N)$-600	$E3$	380	60
86,5	L-1400	$E2$	1,59	84
196,6	K-100	$E2$	0,17	13,2
298	K-0,8	$E1$	$1,5 \cdot 10^{-2}$	1,1
514,6	K-0,75	$E2+M1$*	$2 \cdot 10^{-2}$	0,8
539,8	K-2,25	$E2+M1$*	$1,5 \cdot 10^{-2}$	3,1
647,3	K-5,25	$E2+M1$*	$1 \cdot 10^{-2}$	10,9
729,7	K-6,9	$E2+M1$*	$7 \cdot 10^{-3}$	21
755	K 0,6	$E2$	$7,7 \cdot 10^{-3}$	2,7
766,7	K-0,8	$E2+M1$*	$4,5 \cdot 10^{-3}$	3,7
873,1	K-0,92	$E2$	$3,4 \cdot 10^{-3}$	5,7
879,9	K-2,6	$E2$	$3,4 \cdot 10^{-3}$	16,3
962	K-2,1	$E2$	$2,8 \cdot 10^{-3}$	15,7
967	K-1,8	$E2$	$2,8 \cdot 10^{-3}$	13,3
1048	K-0,11	$M3$	$2,05 \cdot 10^{-2}$	0,1
1069	K-0,24	$E2$	$2,5 \cdot 10^{-3}$	2,0

---

*The mixture is assumed to be 50% E2 + 50% M1 (the corresponding values of α_K differ by a factor of about 2).

**Referred to the transition intensity to the ground state (taken as 100).

From the data shown in Table 12, it will be evident that 60% of the γ-spectrum of $Ho^{160} + Ho^{160m}$ is associated with the decay of the ground state of Ho^{160} (T = 22 min). Hence the isomeric state of Ho^{160} can undergo K capture or β^+-decay in 30 to 40% of the disintegrations.

We can draw a number of further deductions regarding the character of the decay of both states of Ho^{160} from analysis of the β^+-spectrum of $Ho^{160} + Ho^{160m}$.

The hardest β^+-transition must go to one of the low-lying levels: 0+, 2+ or 4+ (K = 0). If this high energy transition fed one of the high-lying levels of Dy^{160} (966 kev or higher), the total energy of the transition would be

greater than 3900 kev and there would be a high probability of excitation of Dy^{160} levels having energies above 1720 kev. As a result the γ-spectrum of Ho^{160} would be considerably enriched by intense lines that would not fit into the present decay scheme.

This transition cannot pertain to decay of the 5+ ground state of Ho^{160} inasmuch as β-decay to the 0+ or 2+ levels of the lowest rotation band would involve a large spin change (ΔI = 5 or 3, respectively) and, consequently, is strongly forbidden. This is in conflict with the observed log ft = 9.5 value for this transition. β^+-decay to the second rotational level of the lowest band must be of the $5+ \rightarrow 4+$ type. Such decay is allowed by the spin and parity selection rules but strongly forbidden as regards the quantum number K ($\Delta\nu = \Delta K - L = 5 - 1 = 4$).

If a change in ν by one unit leads to a reduction of the transition probability by 10^2, the transition probability for the 4+ level must be decreased by a factor of 10^8 with reference to allowed β-transitions. Inasmuch as for allowed β-transitions log ft = 4-6, the value of log ft for the given transition should be 12-14, which is in conflict with the experimental value of 9.5.

We can therefore only assume that the 1900 kev β^+-transition pertains to decay of the 5-hour Ho^{160} isomer (I = 2-, K = 2). In this case β-transition to the 0+ and 4+ levels of the lowest rotational band would belong to the type of once forbidden unique transitions not inhibited by K forbiddenness ($\Delta\nu = 0$). The transition to the 2+ (K = 0) level would be an ordinary first forbidden transition slowed down by a factor of 100 due to K forbiddenness ($\Delta\nu = \Delta K - L = = 1$). In this case the value of log ft to be expected is close to the experimental one (9.5). Apparently it may be assumed that weak β^+-transitions occur to all three of the 0+, 2+ and 4+ (K = 0) levels.

Analogous considerations lead to rejection of the hypothesis that the β^+-component with end-point energy 970 ± 30 kev, which might be interpreted as a transition to the 966 kev (or 1048 kev) level, pertains to decay of the 5+ ground state of Ho^{160} (such a transition would be strongly forbidden either due to the large spin difference or by K forbiddenness).

The experimental value of log ft = 7.7 can readily be explained if we assume that there occurs β^+-decay of the 2- isomeric state of Ho^{160} to the 966 kev (2+) and 1048 kev (3+) levels of Dy^{160}. These must be once forbidden β-transitions, not inhibited by K forbiddenness ($\Delta K = 0$).

The above high energy β-transitions have a very low intensity ($\beta^+ \approx 0.1\%$, K capture $\approx 1\%$). This is consistent with the fact that a large portion of the decay of the isomeric state is accounted for by the 60 kev isomeric transition.

It is appreciably more difficult to interpret the two soft components of the β^+-spectrum. Despite their relatively low intensity, the total abundance of the corresponding transitions is very high.

It follows from the data of Zweifel[10] that the values of the ratio K/β^+ for $E_{\beta+} = 570$ and $E_{\beta+} = 300$ kev are 540 and ~3800, respectively. Precise calculation of the total intensity of the K and β^+-transitions leads to an absurd value (over 100% of the disintegrations). In any case these data indicate that the abundances of both transitions are very high.

Hence at least one of the soft components of the β-spectrum must be associated with decay of the 5+ ground state of Ho^{160}. Assuming that the hard components of the β^+-spectrum go from the isomeric state of Ho^{160} to the lower band, we infer that the total disintegration energy equals 2900 kev. Presumably the 570 kev β^+-transition must go to the ~1300 kev level of Dy^{160}. If we assume that this transition departs from the isomeric level, the possible assignments for the 1300 kev level are K = 1, 2 or 3 and I = 1-, 2- or 3-, in-

asmuch as in view of the log ft value the β-transition is an allowed one. It will be seen from the level scheme that in the vicinity of 1300 kev there are two levels with values of K and I satisfying these conditions, namely, 1264 kev (I = 3-) and 1358 (I = 3-).

On the other hand, if we assume that the 570 kev β-transition is associated with disintegration of the 5+ ground state of Ho^{160}, the level at 1300 kev must be assigned a spin of 4+, 5+ or 6+. Levels with such spins in the given energy region have not been detected. Hence we assume that the 570 kev β^+-transition pertains to the decay of the isomeric state of Ho^{160}.

The remaining soft component, with $E_{\beta^+} \approx 300$ kev, may be ascribed to the transition from the ground state of Ho^{160} to the ~1700 kev level of Dy^{160}. It will be seen from the level diagram that Dy^{160} does have a level at 1696 kev. The fact that this β-transition is an allowed one (log ft = 5.1) indicates that the spin of this level may be 4+, 5+ or 6+. The 4+ assignment is not in conflict with the data following from the γ-spectrum; the values of the K/L ratio, found for the 730, 647 and 540 kev transitions, do not characterize their multipole orders entirely unambiguously and do not preclude a pure E2 multipole order for the 1696 kev (4+) → 966.4 kev (2+) transition and a mixed E2 + M1 multipolarity for the 1696 kev (4+) → 1048.8 kev (3+) and 1696 kev (4+) → 1155.9 kev (4+) transitions.

Approximate balance of intensities for Ho^{160}

In drawing up the transition intensity balance for each particular level we followed the procedure of taking the relative intensities of the conversion lines and finding the total transition probability by taking into account the conversion coefficient for the multipole order in question as indicated in the decay scheme (Fig.8).

In calculating the probability of the 86.5 kev transition, we used the intensity of the L and M + N conversion lines from Ref.19 and allowed for the contribution from K conversion electrons and γ-rays by means of the theoretical conversion coefficients α_K and α_L. In the case of the 60 kev transition it was assumed, as indicated above, that the K conversion electrons and γ-rays make a very small contribution (~1%) to the total probability of the transformation.

The results of our calculations are summarized in Table 12.

It is interesting to note that the total intensity of the known transitions to the 86.5 kev level is appreciably lower than the intensity of the transitions from this level to the ground state. This discrepancy can be explained if we assume that there occurs very intense K or β^+-decay to this level

Table 12

Approximate balance of intensities in the decay of Ho^{160}

Level energy, kev	% arriving transitions	% departing transitions	difference fr β^+ or K	Level energy, kev	% arriving transitions	% departing transitions	difference fr β^+ or K
0 Ho^{160}	60	60	—	1155,9	3,1	7,7	4,6
0 Dy^{160}	100	—	—	1200	0,4	1,9	1,5
86,5	51	84	33	1265	—	3	3
283,1	11,5	13,2	1,8	1358	—	3	3
966,4	25	30	5	1565	—	1,5	1,5
1048,8	12	19	7	1696	—	35	35
				1718	—	3,3	3,3

or that this level is intensively populated by as yet unknown γ-transitions. Inasmuch as it follows from our experiment that β-decays and K transitions to the 86.5 kev level are very weak, it must be inferred that there exist high-lying excited states from which there occur intense hard transitions to this level.

The region above 1700 kev was not investigated in detail in the present series of experiments, but in some preliminary experiments we observed a conversion line of 2600 kev energy.

Physical Institute
Leningrad State University

Note added in proof: Subsequent to submission of this report to the editor, we carried out an auxiliary series of measurements of the conversion spectrum of Ho^{160} and determined the energies and relative intensities of 48 new conversion lines with energies in the range from 438 to 2700 kev. The observed lines tend to substantiate the proposed level scheme for Dy^{160} and indicate that there exist excited states with energies up to 2900 kev.

References

1. A.V.Zolotavin, Izv.AN SSSR, Ser.fiz., 18, 127 (1954).
2. J.M.Cork, C.E.Branyan, W.C.Rutledge, A.E.Stoddard & J.M.Le Blanc, Phys. Rev., 78, 304 (1950).
3. V.Keshishian, H.W.Kruse, R.J.Klotz & C.M.Fowler, Phys.Rev., 96, 1050 (1954).
4. G.Bertolini, M.Bettoni & E.Lazzarini, Nuovo Cim., 3, 754 (1956).
5. M.A.Clark & J.W.Knowles, Bull.Am.Phys.Soc., 2, 231 (1957).
6. O.Nathan, Nuclear Physics, 4, 125 (1957).
7. J.W.Mihelich, B.Harmatz, I.H.Handley & I.I.Pinajian, Bull.Am.Phys.Soc., 1, 330 (1956).
8. B.S.Dzhelepov, B.K.Preobrazhenskii, I.M.Rogachev & P.A.Tishkin, Izv. AN SSSR, Ser.fiz., 21, 962 (1957). (Trans.Bulletin, 21, No.7, 964.)
9. B.S.Dzhelepov, O.E.Kraft & B.K.Preobrazhenskii, Doklady AN SSSR, 116, 581 (1957).
10. P.F.Zweifel, Phys.Rev., 96, 1572 (1954).
11. Beta and Gamma Spectroscopy. Edited by K.Siegbahn, Amsterdam, 1955.
12. G.Andersson & I.Bergström, Nuclear Physics, 3, 541 (1957).
13. F.K.McGowan, Phys.Rev., 85, 142, 151 (1952).
14. L.K.Peker, Izv. AN SSSR, Ser.fiz., 21, 1029 (1957). (Trans. Bulletin, 21, No.7, 1030.)
15. H.Jaffe, N.S.A., 9, 95 (1955).
16. M.P.Avotina, E.P.Grigor'ev, A.V.Zolotavin & B.Kratsik, Doklady AN SSSR, 118, 6 (1958).
17. G.F.Dranitsyna, Koeffitsienty vnutrennei konversii na L_I, L_{II} i L_{III}-podobolochkakh (L_I, L_{II} and L_{III} internal conversion coefficients), M.-L., 1957.
18. G.M.Gorodinskii, A.N.Murin, V.N.Pokrovskii & B.K.Preobrazhenskii, Izv. AN SSSR, Ser.fiz., 21, 1624 (1957). (Trans.Bulletin, 21, No.12, 1611.)
19. E.P.Grigor'ev, B.S.Dzhelepov, A.V.Zolotavin, B.Kratsik, B.K.Preobrazhenskii & I.S.Ianchevskaia, Doklady AN SSSR, 117, 53 (1957).

CONVERSION ELECTRON SPECTRUM OF A DYSPROSIUM FRACTION

- B.S.Dzhelepov, B.K.Preobrazhenskii, I.M.Rogachev & P.A.Tishkin

1. Introduction

The present work was devoted to an investigation of the conversion spectra of dysprosium isotopes. The dysprosium fraction was separated by chemical and chromatographic procedures from a tantalum target bomberded with fast neutrons in the phasotron of the Joint Institute for Nuclear Research. The irradiation period was several hours and the separation of the rare earths was carried out some 20-30 hours after the irradiation.

Judging from the Table of Isotopes of Seaborg et al, our separated fraction should have contained the following radioactive nuclides:

Dy^{157} T = 8.2 hours; γ = 177 and 325 kev,
Dy^{159} T = 134 days; pure K capture,
Tb^{157} T = 4.7 days; γ = 1400 kev.

Actually the composition of the fraction proved to be considerably more complicated. We observed conversion lines whose intensities fell off with periods of a) 7.5-11 hours, b) 38 hours and c) 4.7 days.

In a parallel investigation of the γ-radiation from the dysprosium fraction Gorodinskii et al[1] detected activities with periods of 8.5 hours, 10 hours, 3 days, 5 days, 8 days and 134 days.

Dzhelepov, Kraft et al[2] observed an activity with a period of 11 hours in the positron spectrum and activities with periods of 11 hours and 4.7 days in the conversion spectrum. Apparently, the proton reaction on Ta yields several Dy isotopes with periods exceeding 4 hours and from them there form isotopes of Tb.

In view of the complexity of the situation in the discussion below, we shall group our results by half-lives.

2. Measurement conditions

The dysprosium fraction was investigated on two magnetic lens β-spectrometers. The activity was applied to a thin lightly aluminized collodion film in the form of 4 mm diameter circles. The measurements were carried out with four sources deriving from three different irradiations, carried out at different times. The counter window of the two-lens β-spectrometer was covered with a 0.025 mg/cm^2 thick collodion film which passed electrons of $>$2.5 kev energy. A transmission curve was obtained for a film of this thickness by means of a suitable accelerator and this was subsequently used to make corrections in the intensity of the recorded electron lines. The film over the window of the counter used in the single lens spectrometer had a superficial density of 1.5 mg/cm^2 and passed electrons of $>$30 kev energy. The measurements were started a day after irradiation of the target so that possible activities with short lifetimes ($<$4 hours) may not have been detected.

3. Conversion electron spectra of the 7.5-11 hour activities

Fifteen electron lines with intensities falling off with a period of 7.5 to 11 hours were observed in the Dy fraction spectrum in the region from 3 to 150 kev. All the lines were repeatedly observed in six series of measurements, carried out with two different sources. The half-life of 7.5 hours was deter-

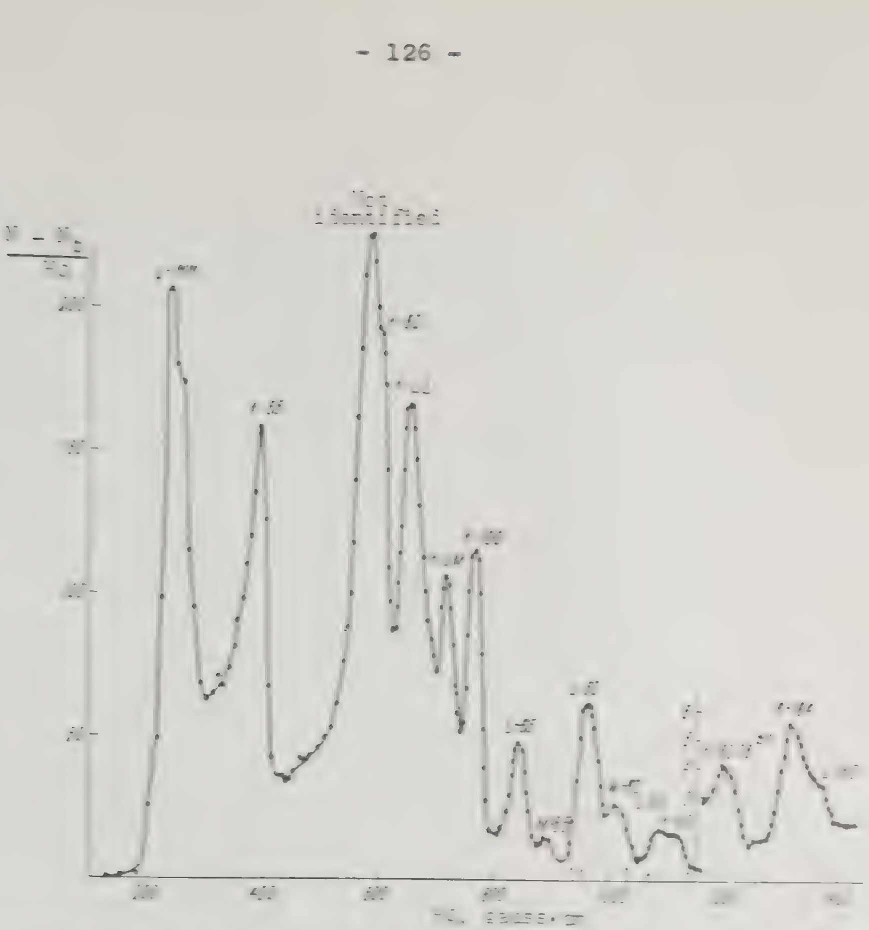

Fig.1. Conversion electron spectrum of the 7.5-11 hour activity in the dysprosium fraction, normalized to the instant t = 6 hours after separation of the Dy. The arrows at the Hρ axis indicate contributions from longer-lived isotopes.

mined from the decrease in intensity of the 74 kev electron line. The other lines had varying periods within the indicated range.

According to Gorodinskii et al[1] the dysprosium fraction contains two isotopes with close periods: T = 8.5 hours (it is assumed that this is Dy^{157}) and T = 10 hours (identified as Dy^{155}). The accuracy of our half-life determinations is not sufficient to attribute each line to one activity or the other.

The results of our measurements are shown in Table 1 and Fig.1. The measurements were carried out only in the energy range under 150 kev.

The 5, 36 and 42 kev electron lines are due to L - MM, K - LL, K - L and M Auger electrons, while the 13.5, 57.5, 64.0, 74.0 and 81.0 kev lines are identified as being due to the K, L and M conversion electrons from the 65.5 and 82.5 kev transitions in Tb (admittedly the accuracy of our experiments was insufficient for unambiguous determination of Z).

The electron lines at 48.0, 92.0 and 142 kev are apparently due to K and L conversion electrons associated with 100 and 150 kev transitions, while the line at 132 kev probably corresponds to K electrons from a 184 kev transition.

All the indicated transitions were observed by us for the first time.

Discussion

A dysprosium activity with a period of 8.2 ± 0.1 hours was discovered in 1953 by Handley & Olson[3] who obtained it by bombarding highly purified terbium oxide with 24 Mev protons. The dysprosium fraction separated by the ion ex-

Table 1

Conversion and Auger electrons from the 7.5-11 hour activity in the dysprosium fraction

No.	$H\rho$, gauss·cm	E_{e^-}, kev	Identification	Relat. intensity	
				Experimental	Corrected*
1	239	5,0±0,5	*L — MM*	—	—
2	392	13,5±0,5	*K*-65,5	100	340
3	582	29,0±1,0	not ident.	360	500
4	598	30,5±1,0	*K*-82,5		
5	651	36,0±1,0	*K — LL*	190	225
6	705	42,0±1,0	*K — LM*	90	100
7	756	48,0±1,0	*K*-100	100	100
8	831	57,5±1,0	*L*-65,5	50	40
9	880	64,0±1,5	*M*-65,5	15	10
10	950	74,0±1,5	*L*-82,5	65	50
11	997	81,0±2,0	*M*-82,5	30	20
12	1068	92,0±2,0	*L*-100	20	15
13	1105	98,0±2,0	*K*-150	12	8
14	1302	132,0±2,0	*K*-184	7	4
15	1356	142,0±2,0	*L*-150	3	2

*Corrected for absorption in counter window (collodion film).

change procedure contained two activities with half-lives of 8.2 hours and 134 days. The latter undoubtedly belongs to the previously known Dy^{159} which is formed by the $Tb^{159}(p,n)Dy^{159}$ reaction. In order to determine the isotope responsible for the 8-hour activity, Handley & Olson investigated the excitation function. The threshold for the formation of this activity proved to be 19 ± 1 Mev, which approximately corresponds to the $Tb^{159}(p,3n)Dy^{157}$ reaction. The cross section for the formation of the 8.2 hour activity also approximately corresponds to the (p,3n) reaction and excludes the possibility that the activity might be formed on some impurity.

Investigating the γ-spectrum, Handley & Olson observed a γ-ray of 325 kev energy as well as 42.5 kev x-radiation from terbium.

Gorodinskii et al[1] detected in their dysprosium fraction (obtained in the same manner as ours) 325 kev γ-rays whose intensity fell off with a period of 8.5 hours. These γ-rays were also observed in the preliminary investigation of the conversion spectrum carried out by Dzhelepov, Kraft et al[2].

The existence of a dysprosium activity with a period of 10 hours was reported for the first time in the above mentioned investigation of Gorodinskii et al[1]. These investigators also observed 227 kev γ-rays whose intensity fell off with the same period. These authors infer that these γ-rays are emitted in the decay of Dy^{155}.

In their investigation, Dzhelepov, Kraft et al[2] observed electron lines corresponding to K conversion of transitions of 230, 270, 320, 370, 450, 515 and 660 kev energy, whose intensity fell off with a period of 11 ± 2 hours.

It must be noted that the identification of the 8.2-hour and 10-hour activities as being due to Dy^{157} and Dy^{155} is only tentative.

Measurements discussed in this section encompassed only the low energy region (up to 150 kev). The work of Dzhelepov, Kraft et al covered the region from 150 to 700 kev. Consequently, more detailed discussion of the decay schemes will be given in Ref.2.

4. Conversion electrons of the ~38-hour activity

In the measurements on the single lens β-spectrometer, in addition to the lines whose intensity fell off with a period of about 10 hours, there were detected about five weak electron lines with half-lives of about 38 hours.

Table 2

Electron lines of ~38-hour activity

No.	Hρ, gauss·cm	E_{e^-}, kev	Identification	Experimental relative intensities
1	936	72	—	160
2	951	74	—	80
3	1027	85,6	*L* - 94	—
4	1068	92	*M* - 94	100
5	1136	103		110

The energies and relative intensities of these lines are listed in Table 2.

So far it has not proved feasible to attribute these lines to any specific isotope.

5. Conversion electrons from the 5-day activity

After disintegration of the 10-hour isotopes, there became discernible a number of weaker conversion lines whose intensity decreased with a period of 4.5±0.2 days. This electron spectrum was investigated by means of both β-spectrometers. The experimental spectra are shown in Figs. 2 & 3; the combined results of measurements on both spectrometers are listed in Table 3.

The spectra shown in Figs.1 & 2 were recorded on the same spectrometer with the same source so that the respective ordinates reflect the falling off of the activity.

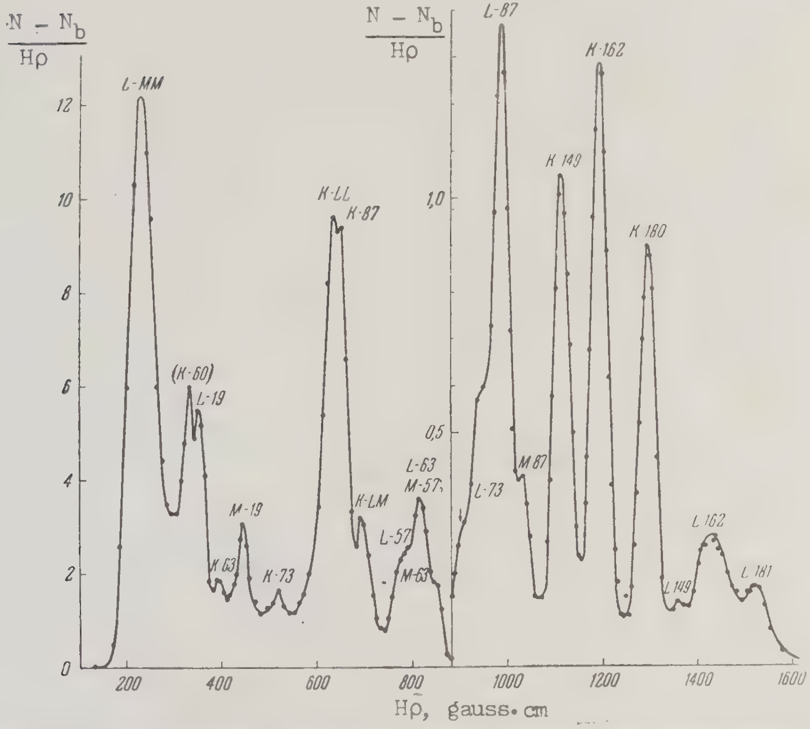

Fig.2. Conversion electron spectrum of the same sample as that of Fig.1 but observed 50 hours after separation of the Dy fraction from the rare earths.

There were detected the K, L and M electrons of transitions of 63 and 87 kev energy, the L and M electrons of a 57 kev transition, the K and L electrons of transitions of 149, 163, 180 and 200 kev energy and the K electrons of transitions of 60 and 262 kev energy. All these transition energies are predicated on the assumption that the conversion occurs in the Gd atom; if it takes place in Tb, then all the listed energies should be increased by 1.8 kev.

The electron line at 113 kev was somewhat wider than the neighboring lines in several series. In measurements with one of the sources there was some indication of splitting of this line.

A number of the observed lines has not been identified.

In another report appearing in this issue of the Bulletin (see next article), Anton'eva et al[4] describe their contemporaneous investigation of the conversion spectrum of a terbium fraction. In this spectrum they detected

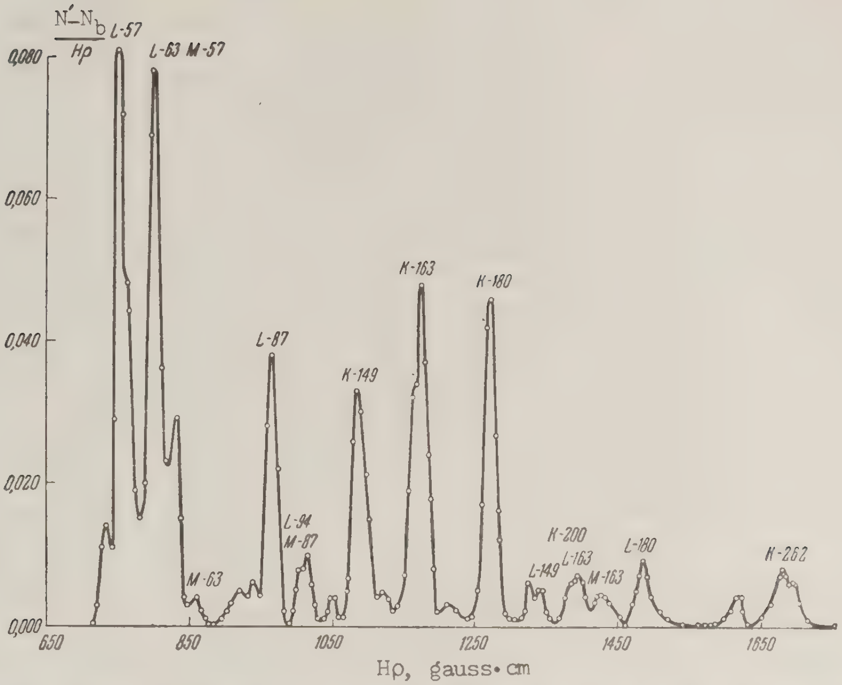

Fig.3. Same spectrum as in Fig.2 but recorded on a lens spectrometer with a resolution of 1.2%.

Table 3

Conversion and Auger electrons from the 4.5-day activity (Tb^{155} + Tb^{157})

No.	Hρ, gauss• cm	E_{e^-}, kev	Identification	Relat. intensity	
				Experi-mental	Correc-ted
1	225	4,5±0,5	*L — MM*	—	—
2	330	9,5±1,0	(*K*-60) Tb^{155}	—	—
3	351	10,7±4,0	*L*-19 Tb^{155}	—	—
4	391	13,3±0,5	*K*-63	180	980
5	443	17,0±0,5	*M*-19 Tb^{155}	300	1260
6	516	23,0±0,5	—	150	470
7	658	36,8±1,0	*K*-87 Tb^{155}, *K-LL*	1440	2850
8	696	41±1,0	*K — LM*	330	590
9	738	45,8±1,0	—		—
10	767	49,3±1,0	*L*-57 Tb^{157}	210	330
11	787	51,8±1,0	—		—
12	816	55,6±0,5	*L*-63	330	500
13	846	59,5±0,5	*M*-57 Tb^{137}	100	150
14	871	61,0±1,0	*M*-63		—
15	980	78,4±0,5	*L*-87 Tb^{155}	150	180
16	1018	84,6±1,0	*M*-87 Tb^{155}	—	—
17	1107	98,3±1,0	*K*-149 Tb^{155}	120	120
18	1195	113±1,0	*K*-163 Tb^{155}	150	150
19	1243	121,6±1,0	—	10	10
20	1292	130±1,0	*K*-180 Tb^{155}	100	100
21	1338	138,6±2,0	—		
22	1353	141±2,0	*L*-149 Tb^{155}	20	20
23	1400	150,0±2,0	*K*-200 Tb^{157}	4	4
24	1417	154,0±2,0	*L*-163 Tb^{155}		
25	1457	161±2,0	*M*-163 Tb^{155}	14	14
26	1518	173±3,0	*L*-180 Tb^{155}	40	40
27	1626	195±2,0	*L*-200 Tb^{157}	7	7
28	1707	212±4,0	*K*-262 Tb^{155}	20	20
29	1712	213±4,0	—	4	4

a number of lines whose intensity fell off with a period of 5 ± 1 days, lines corresponding to eight transitions of energies 86.6, 104.5, 148.0, 160.3, 162.5, 179.2, 260.7 and 337.7 kev. All these transitions except the second and last coincide with those observed by us.

Discussion

None of the known isotopes of dysprosium has a half-life close to 4.5 days; this does not mean, of course, that there are no such Dy isotopes.

On the other hand, there are known to be several terbium isotopes with close periods; some of them could be present in our dysprosium fraction in the form of daughter nuclides. That such Tb daughter isotopes were present in our samples is indicated by the following. The intensity of the electron line located at 113 kev and hence sufficiently far removed from all the lines of the 10-hour and 38-hour activities initially increased during the first 10-13 hours from the beginning of measurement and then began to fall off with a period of 4.5 days. Thus there can be no doubt that this is a line of daughter Tb formed from a short-lived Dy isotope. Unfortunately analogous observations were not carried out for the other lines.

Instead of this, in working with the next source we carried out a separation of terbium from the dysprosium fraction 50 hours after separation of the dysprosium from the other rare earths.

Investigation of the electron spectrum of this Tb fraction showed the presence of a 4.5-day activity. Thus both the half-life and the conversion electron spectrum of this fraction agrees with the data obtained for the 4.5-day activity of the dysprosium fraction. In view of this one can attribute the entire activity falling off with a period of 4.5 days to terbium isotopes.

Further proof of the fact that most of the 8-10-hour Dy isotopes transform into 4.5-day Tb isotopes is furnished by comparison of the intensities of the L - MM line in Figs.1 & 2. Multiplying this intensity ratio by the ratio of the periods and introducing the appropriate correction for decay during the time elapsed between the series of measurements we obtain

$$\frac{205}{12.2} \cdot \frac{9}{120} e^{-0.7 \frac{50}{120}} \approx 0.95.$$

If the Dy were fully converted to ~5-day Tb, the above figure should be 1.

Identification of the mass numbers of the isotopes associated with each of the lines proved to be very difficult.

There are apparently four Tb isotopes with a half-life close to 5 days; these are 5.1-day Tb^{153}, 5.6-day Tb^{155}, 4.7-day Tb^{157} and 6.8-day Tb^{161}.

The neutron-rich Tb^{161} could hardly be present in our sources inasmuch as Dy^{161} is stable; in any case the β-spectrum associated with it was never observed. The presence of $Dy^{153} + Tb^{153}$ was also unlikely inasmuch as the Dy^{153} has too large a neutron deficiency as compared with the main dysprosium isotope.

It may be assumed, however, that Tb^{155} and Tb^{157} were present in our samples.

Terbium 155 was discovered only in 1957 by Ward, Jacob & Mihelich[5]. It has a half-life of 5.6 days and is formed in electron capture by Dy^{155}. Ward et al do not give the period of Dy^{155}; the old determination - 190 days - made by Wilkinson & Hicks[6] is erroneous. Ward et al[5] detected the following transitions in $Tb^{155} \rightarrow Gd^{155}$: 18.9, 26.7, 31.6, 45.6, 60.2, 86.7, 101.4, 105.6, 148.8, 160.8, 161.5, 163.4, 180.4, 181.6, 221.2, 239.7, 262.6, 340.8 and 368.3 kev.

The correctness of their identification is substantiated by the fact that many of these transitions were also detected in the decay of Eu^{155}, which has been studied rather thoroughly. Thus, for example, in a recent investigation devoted to Eu^{155}, Boehm & Hatch[7] reported observing the following transitions in Gd^{155}: 18.9, 26.5, 45.29, 60.00, 86.54 and 105.32 kev. It will be noted that all these transitions appear in the above list of transitions associated with $Tb^{155} \rightarrow Gd^{155}$.

On the basis of the data of Ward, Jacob & Mihelich and the results obtained by different investigators for Eu^{155}, we obtain the decay scheme for Tb^{155} shown in Fig.4. The transitions in the right hand part of the scheme identified by crosses (×) were observed in our experiments.

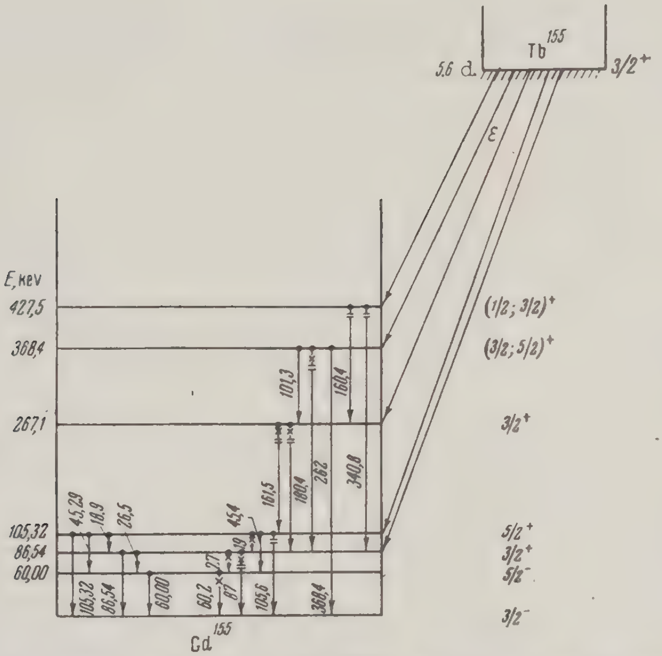

Fig.4. Decay scheme for Tb^{155}. Multipole orders of transitions[7]: 18.9 kev - M1 + E2; 26.5 kev - E1; 45.29 kev - E1; 60.00 kev - M1 + E2; 86.54 kev - E1 and 105.32 kev - E1. The crosses (×) indicate lines observed in the present investigation; double bars (=) identify lines observed in the Tb fraction.

It will be noted that the 31.6, 148.8, 163.4, 181.6, 221.2 and 239.7 kev transitions observed by Ward et al and the 57, 63, 149 and 200 kev transitions listed in Table 3 have not been fitted into the scheme.

In a report published in 1955, Handley & Lyon[8] deny the existence of Tb^{155} with a half-life of ~5 days and establish limits of $T < 10$ min and $T > 5$ years for the half-life of Tb^{155}. They assign the observed ~5 day activities to isomeric states to Tb^{156}. We feel, however, that the coincidence of many lines of 5-day Tb and 1.7-year Eu^{155}, demonstrated above, irrefutably proves the existence of 5-day Tb^{155}. It is not clear, therefore, how the results of Handley & Lyon are to be explained.

Tb^{157} was first mentioned by Butement[9] in 1949 as one of the possible isotopes to which the 5.9-day activity detected by him might belong; it is now clear that the other possibilities suggested by Butement - Tb^{156} and Tb^{158} - are excluded inasmuch as these isotopes have entirely different half-lives.

In 1950 Wilkinson & Hicks[7] unambiguously attributed an activity with a period of 4.7 ± 0.1 days to Tb^{157} obtained by bombardment of Gd with 10 Mev protons and having the following radiation characteristics:

0.09 Mev e^-:0.2 Mev e^-:L x-rays:K x-rays:1.4 Mev γ-rays = 0.2:0.1:0.4:1:0.3.

The mass assignment, however, was not rigorously proved.

In 1953 Handley & Olson[3] attempted to observe Tb^{157} as a daughter nuclide forming in the decay of Dy^{157}. Strange to say, they were not able to detect

Tb^{157} and established very rigorous limits for its half-life: either < 30 min or > 100 years. The latter limit was established on the basis of measurements of the absolute activity of a secondary terbium fraction separated from the dysprosium one after its decay; under the conditions of their experiment Handley & Olson should have been able to detect an activity 8000 times lower than would obtain if the decay were characterized by the chain

$$Dy^{157} \xrightarrow{8.2\text{ hours}} Tb^{157} \xrightarrow{4.7\text{ days}} Gd^{157}.$$

In 1955 Handley & Lyon[8] confirmed this conclusion and attributed the 5.2-day activity to an isomeric state of Tb^{156}. We must emphasize that in any case the activity with this period observed by us could not belong to Tb^{156} inasmuch as Dy^{156} is stable. The fact that Handley & Lyon deny the existence of Tb^{155} with a period of ~5 days, although, as we have seen above, the existence of 5-day Tb^{156} cannot be doubted, puts under question their deductions relative to Tb^{157}.

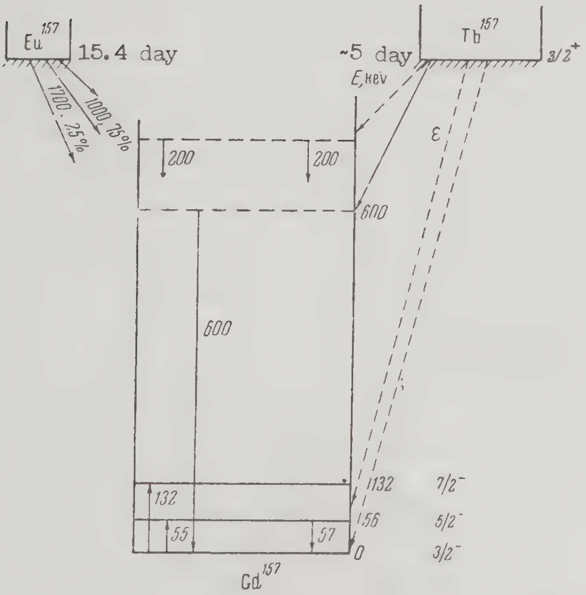

Fig.5. Proposed decay scheme for Tb^{157}.

Hence we consider it to be entirely possible that Tb^{157} has a half-life of ~5 days, that it accumulates from Dy^{157} (8.2 hours) and that it may be responsible for some of the conversion lines decaying with a period of ~5 days, in particular, the lines which cannot be fitted into the decay scheme for Tb^{155} (except, of course, the 149 kev line which undoubtedly belongs to Tb^{155}). Two of these - the 57 and 200 kev lines - coincide closely with lines known from the decay of Eu^{157} and from Coulomb excitation of Gd^{157}. It is not clear, however, why the 57 kev line was not observed by Anton'eva et al[4] in the terbium fraction (the 200 kev line was observed in that investigation but was attributed to Tb^{156}).

The proposed scheme for the decay of Tb^{157} is shown in Fig.5.

The authors desire to thank L.K.Peker for discussion of the decay schemes, K.Ia.Gromov for assistance in organizing the work and students A.Bogdanov and A.I.Iashchuk for assistance in the experiments.

Physical Institute,
Leningrad State University

References

1. G.M.Gorodinskii, V.N.Pokrovskii, A.N.Murin & B.K.Preobrazhenskii, Report presented at the Eighth All-Union Conference on Nuclear Spectroscopy.
2. B.S.Dzhelepov, O.E.Kraft, B.K.Preobrazhenskii & G.F.Iushkevich, Present issue of the Bulletin, p. 205.
3. T.H.Handley & E.Olson, Phys.Rev., 90, 500 (1953).
4. N.M.Anton'eva, A.A.Bashilov, B.S.Dzhelepov & B.K.Preobrazhenskii, Present issue of the Bulletin, p. 134.
5. T.J.Ward, K.P.Jacob & J.W.Mihelich, Bull.Am.Phys.Soc., 2, 259 (1957).
6. G.Wilkinson & H.G.Hicks, Phys.Rev., 79, 815 (1950).
7. F.Boehm & E.N.Hatch, Bull.Am.Phys.Soc., 2, 231 (1957).
8. T.H.Handley & W.S.Lyon, Phys.Rev., 99, 1415 (1955).
9. F.D.S.Butement, Phys.Rev., 75, 1276 (1949).

CONVERSION ELECTRON SPECTRA OF Gd^{151} AND Gd^{153}

- N.M.Anton'eva, A.A.Bashilov, B.S.Dzhelepov & B.K.Preobrazhenskii

1. Introduction

The present work was devoted to investigation of the conversion spectra of some long-lived isotopes of gadolinium obtained as a result of prolonged bombardment of a tantalum target in a scattered beam of 660 Mev protons. First, the rare earth fraction was extracted from the tantalum by conventional chemical procedures and then the pure gadolinium fraction was separated from the rare earths by the ion exchange procedure. This fraction comprised primarily neutron-deficient isotopes decaying by electron capture or positron emission. The active material was collected on a thin aluminum foil.[1]

The conversion electron spectrum was investigated by means of a magnetic spectrometer, the Leningrad State University Ketron[2], adjusted for a resolution of 0.5%. The film over the counter window passed electrons of >7 kev energy.

The spectroscopic measurements were started one month after the end of irradiation and repeated several times over a period of about a year. It was found that the slowly changing part of the conversion spectrum belonged to Gd^{153} and Gd^{151}. In addition there were observed lines attributable to shorter-lived isotopes of gadolinium that had been investigated by us earlier.

2. Conversion Electron Spectrum of Gd^{153}

Survey of the data in the literature on Gd^{153}

Radioactive Gd^{153} was first prepared by Fajans & Voigt[3] in 1941 by means of the Eu(d,2n) reaction. This reaction was subsequently observed in other investigations[4,5]. Ge^{153} can also be obtained by the (n,γ) reaction on Gd^{152} which is present in the amount of 0.2% in natural gadolinium[5-7]. The mass number assignment was subsequently confirmed in a mass spectrometer study by Inghram & Hayden[6].

The half-life of Gd^{153} was carefully measured only in one investigation[5] and found to be 236 days.

The decay of Gd^{153} occurs by capture of atomic K and L electrons and leads to the formation of Eu^{153} in different energy states (the decay scheme is shown below in Fig.3). A number of investigators[7-9] have observed γ-transitions with energies of 70, 97 and 103 kev. Investigation of the decay of Gd^{153} is facilitated by the fact that the final nucleus, Eu^{153}, was also obtained as the result of β^--decay of Sm^{153} which has been thoroughly studied. In the $Sm^{153} \rightarrow Eu^{153}$ decay process there are observed nuclear transitions with energies of 70, 84, 103, 173, 545 and ~600 kev.[10-12] The levels of Eu^{153} have also been investigated by the method of Coulomb excitation.[13-16] Eu^{153} has been found to have a rotational system of levels with energies 82 and 187 kev and γ-transitions having energies of 82, 105 and 187 kev between these levels.

The total disintegration energy of $Gd^{153} \rightarrow Eu^{153}$ has been calculated from the measured value of the L and K capture branching ratio and found to be 190 to 225 kev.[17-20]

Measurements and results for Gd^{153}

It was apparent from the very first series of measurements that the conversion spectrum contained lines belonging to several Gd isotopes characterized by different half-lives. In order to separate these lines according to

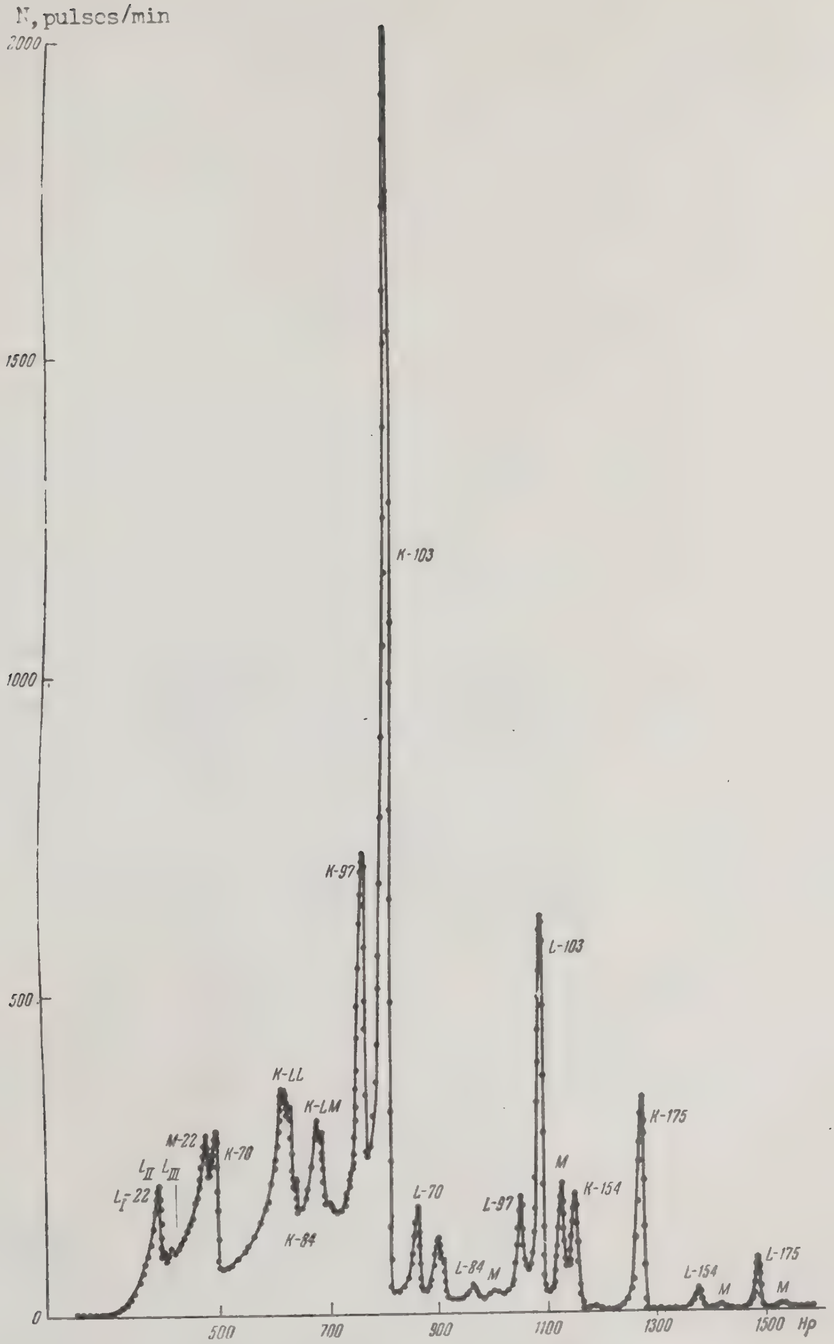

Fig.1. Experimental curve (without correction) of the conversion electrons from the isotopes Gd^{151} and Gd^{153}. Spectrum recorded 13 months after the end of irradiation.

isotopes responsible we carried out repeat measurements of the spectrum over a period of time and observed the variations in the heights of the peaks. The spectrum recorded after the passage of half a year still contained strong K and L conversion lines associated with the 115 and 155 kev transitions excited in

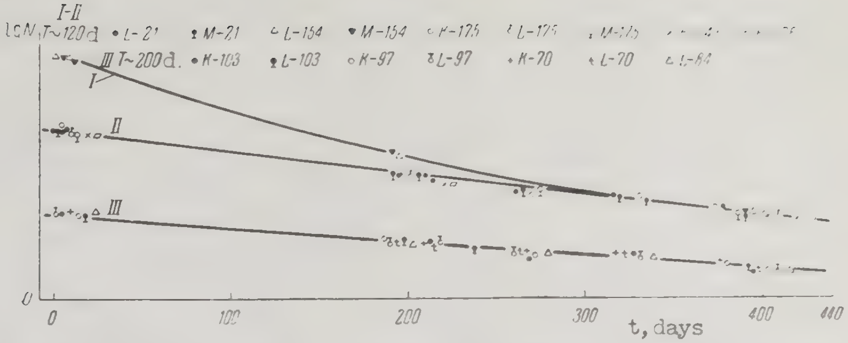

Fig.2. Curves characterizing the decay in intensity of the conversion peaks: I) complex curve of decay with T_1 = 45 days and T_2 = 120 days, II) curve of decay with T = 120 days, III) curve of decay with T = 200 days.

the $Gd^{146} \rightarrow Eu^{146}$ decay with a period of 45 days. In the spectrum obtained a little over a year after irradiation there remained primarily the conversion lines belonging to isotopes with a period of 100 to 200 days. Curves characterizing the decrease in intensity with time of the more persistent peaks are plotted in Fig.2 in semilogarithmic coordinates. It will be clear from this figure that part of the conversion lines are characterized by a half-life of about 200 days. The corresponding transitions have energies of 70, 84, 97 and 103 kev. Comparison with the data in the literature showed that this part of the conversion spectrum belongs to Gd^{153}.

We were able to determine the energy of the listed transitions in Eu^{153} with good accuracy by virtue of the presence in the given region of the spectrum of lines with accurately known energies, namely, the Auger electron lines $K\text{-}L_IL_I$(E = 32.38 kev) and $K\text{-}L_IM_I$(E = 38.64 kev) and the K and L_I conversion

Table 1

Energy of some nuclear transitions in Eu^{153}

Authors, year and Refs.	Method	Transition energy, kev			
		70	84	97	103
Rutledge et al 1952 (22)	Sm^{153},mag.spec.	69,8	—	—	103,4
Graham et al 1954 (23)	Sm^{153},mag.spec.	69,0±0,4	—	—	102,5±0,5
Lee et al 1954 (24)	Sm^{153},mag.lens	69,1±0,2	—	—	102,7±0,3
Church et al 1954 (9)	Gd^{153},mag.spec.	69,4 (±0,5)	—	97,3 (±0.5)	103,1 (±0,5)
Marty 1954-56 (11, 17, 25)	Sm^{153}, Gd^{153} mag. spect.	69	Sm^{153}, 84	98±0,5	103
Andersson 1956 (21)	Sm^{153}, diffract.	—	—	—	103,27±0,02
Present work 1957	Gd^{153},mag.spec.	69,8±0,2	83,6±0.3	97,4±0,1	103,27

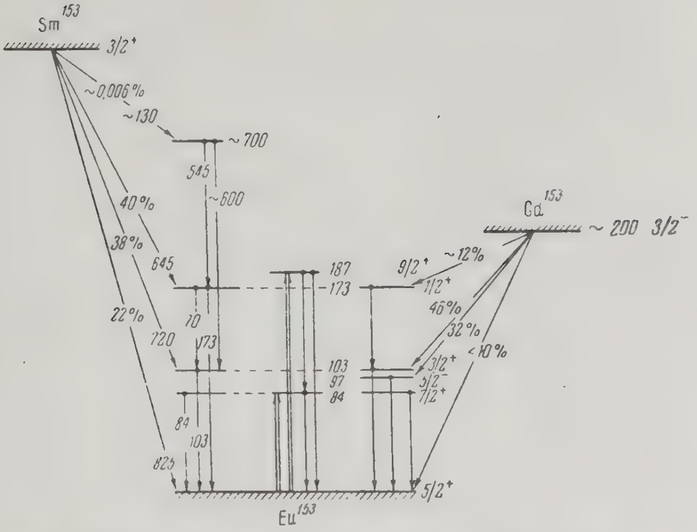

Fig.3. Decay scheme for Gd^{153}→Eu^{153}. The central portion of the diagram shows the levels and transitions observed in Coulomb excitation.

lines of the 103.27 ± 0.002 kev transition.[21] The results of our determination of the transition energies and comparison of these results with the data of other investigators are given in Table 1.

The transitions with energies of 69.8, 97.6 and 103 kev undoubtedly pertain to Eu^{153}. Regarding the 84 kev transition and the transitions with energies 173, 545 and ~600 kev not observed in the present investigation, we must note the following. The 84 kev transition in Eu^{153} was observed by us only from the corresponding weak L and M conversion lines. The K-84 line must be located in the spectrum between the K-LL and K-LM Auger electron groups and, probably due to its low intensity, is not discernible. The above mentioned L and M conversion lines can, of course, have other interpretations. The determination of the half-life in the case of these lines is not very accurate in view of their low intensity (T = 160 ± 40 days). Hence the above interpretation is only tentative and is based primarily on the fact that the 84 kev transition is observed in the decay of Sm^{153}→Eu^{153} (Ref.11) and also in Coulomb excitation of Eu^{153}. One cannot, however, exclude the possibility that this transition belongs to Eu^{151} or to some other isotope.

As for the transition of 173 kev energy, it should be noted that due to its low intensity the conversion electrons corresponding to it have not been observed in any study. According to the evaluation of Dubey et al[12], the total intensity of the 173 kev transition is only 0.07% relative to the intensity of the 70 kev transition. Hence the intense lines associated with the 175 kev transition observed in our conversion spectrum cannot be attributed to Gd^{153}. Accordingly, the lines of the 173 kev transition in Eu^{153} could only make a weak contribution to the spectrum. The 545 and 600 kev transitions cannot be excited in the decay of Gd^{153} (see decay scheme in Fig.3).

The relative intensities of the other conversion lines in our spectrum could not be determined owing to the distortion of the line shape caused by scattering and absorption of electrons. Our results are listed and compared with the data of other investigators in Table 2.

Discussion of results obtained for Gd^{153}

We can draw certain deductions regarding the multipole orders of the transitions of Eu^{153} from the data on the conversion coefficient ratios listed in Table 2. In the case of the 103.3 kev transition, the value of the ratio K/L = 6.4 ± 0.3 shows that this transition is predominantly M1 (possibly with a small admixture of E2) or E1. The ratio L$_1$/(L$_2$+ L$_3$) ≈ 18 found by Mihelich[26], is more consistent with M1 (~10) than with E1 (~3) and is altogether inconsistent with E2 (~0.1). Consequently, on the basis of the cited data, the assign-

Table 2

Relative intensities of conversion lines associated with nuclear transitions in Eu^{153}

Authors, years & Refs.	Method	Transitions			
		70 kev	84 kev	97 kev	103 kev
Mihelich 1952 (26)	Sm^{153}, mag.spec.	$K:L \approx 3,5$ $L_1:L_2:L_3 \approx 20:1:1$	—	—	$K:L \approx 6,5$ $L_1:(L_2+L_3) =$ $= 43:2,3$
Graham et al 1954 (23)	Sm^{153}, mag.spec.	$K:L > 4,6$	—	—	$K:L \geqslant 6,1$
Lee et al 1954 (24)	Sm^{153}, mag.lens	$K:L =$ $= 3,8\left\{\begin{matrix}+2,5\\-1,5\end{matrix}\right\}$	—	—	$K:L =$ $= 6,2 \pm 1,5$
Marty 1954–55 (11,25)	Sm^{153}, mag.spec.	$K:L:M =$ $= > 13:1:0,3$	$K:K_{103} \sim 0,01$ $L:L_{103} \sim 0,04$ $(K:L \sim 1,5)$	—	$K:L =$ $= 6,2 \pm 0,3$ $L:M =$ $= 4,5 \pm 0,5$
Gupta et al 1956 (19)	Gd^{153}, scintil.	—	—	For sum of 2 γ-lines	$K:(L+M) \sim 5$
Marty et al 1956 (17)	Gd^{153}, mag.spec.	— $K:L > 4,5$	—	$K:K_{103} =$ $= 0,25 \pm 0,05$ $K:L$ large	1 $K:L =$ $= 6,0 \pm 0,5$
Present work 1957	Gd^{153}, mag.spec.	$K:K_{103} =$ $= 0,32 \pm 0,07$ $K:L = 6 \pm 1$	$K:K_{103} \leqslant 0,01$ $K:L \leqslant 1$ $L:L_{103} =$ $= 0,05 \pm 0,01$ $L:M =$ $= 4 \pm 1$	$K:K_{103} =$ $= 0,24 \pm 0,03$ $K:L = 6,9 \pm 0,5$	1 $K:L =$ $= 6,4 \pm 0,3$ $L:M =$ $= 5 \pm 1$

ment for the 103.3 kev transition should be M1 (with possibly a small admixture of E2). It is interesting to compare this result with the deductions from analysis of the absolute value of the internal conversion coefficient.

The data of different investigators on the values of α_K for the nuclear transitions in Eu^{153} obtained in investigating the decay of Sm^{153} and Gd^{153} are listed in Table 3. It will be seen that for the 103.3 kev transition, the values of α_K are grouped about 1.2 and 0.65. In this connection it should be noted that the lower values were obtained primarily in experiments with Gd^{153} in which account was not taken of the 97 kev γ-rays. What was actually measured in these experiments was some average value $\bar{\alpha}_K$ (taking $\alpha_{K-103} = 1.2$ and $\alpha_{K-97} = 0.3$ we readily obtain $\bar{\alpha}_K \approx 0.7$). In the case of Sm^{153} the interfering 97 kev γ-line is absent so that the measurements of α_{K-103} are more dependable and hence it may be assumed that the resultant value of 1.2 ± 0.2 is more reliable. The theoretical values of α_{K-103} for different multipole orders according to the tables of Sliv & Band[28] are $\alpha_1 = 0.29$, $\alpha_2 = 1.1$, $\alpha_3 = 4.3$, $\beta_1 = 1.4$ and $\beta_2 = 12$. The closeness of the experimental value $\alpha_{K-103} = 1.2$ to the theoretical value for α_2 and β_1 substantiates the above conclusion that the 103.3 kev transition in Eu^{153} is primarily M1 with an admixture of E2.

In the case of the 97.4 kev transition the value of the ratio K/L = 6.9 ± ± 0.5 shows that the assignment for this transition should be either M1 or E1. On the other hand, the absolute value of the conversion coefficient for this transition listed in Table 3 (0.3 ± 0.1) is consistent with the theoretical value of 0.26 for E1 and altogether inconsistent with the magnetic dipole assignment. The indicated value of α_{K-97} was obtained by Marty & Vergnes[17] who found $I_{\gamma-97}/I_{\gamma-103} = 1.0 \pm 0.3$ by comparing the γ-spectra of Sm^{153} and Gd^{153} and then used this ratio to calculate α_{K-97} from the value of α_{K-103}.

In the case of the 83.6 kev transition the ratio K/L ≈ 1 indicates that the probable assignment is E2 with possibly an admixture of M1. If this trans-

ition belongs to Eu^{153}, we have good agreement here with the results obtained by Coulomb excitation[15,16], according to which the 83.6 kev level in Eu^{153} is the first level of the main rotational band; consequently, the transition from this level to the ground state would be $\Delta I = 1$, no. In their recent investigation of Coulomb excitation of Eu^{153}, Class & Meyer-Berkhout[16], who observed the γ-transitions from the conversion electrons, also obtained a value of ~1 for the K/L ratio for the 83 kev transition. On the basis of this Class & Meyer-Berkhout concluded that this transition is ~25% M1 and ~75% E2.

Table 3

Values of α_K for the 70, 103 and 97 kev transitions in Eu

Author, year & Ref.	Transitions		Method
	70 kev	103 kev	
Lee et al, 1954 (24)	—	0,62±0,15	Sm^{153}, mag. spect.
Graham et al, 1954 (23)	5,7±1,0	—	
McGowan, 1954 (8)	3,8±0,2	1,14±0,20	Sm^{153}, scintil. sp.
Marty 1955 (25)	—	1,2±0,1	
Dubey et al, 1956 (12)	4,4±0,4	1,19±0,15	x-γ coincidence
Cohen et al, 1955 (27)	—	1,2	Gd^{153} scintil. sp.
Bhattecherjee et al, 1956 (18)	—	0,67±0,12	x-γ coinc. or spect.
Gupta et al, 1956 (19)	—	0,61±0,03	
Bisi et al, 1956 (20)	—	0,70±0,03	
Marty et al, 1956 (17)	For the 97 kev trans. $\alpha_K = 0{,}3 \pm 0{,}1$		

In the case of the 69.8 kev transition the value of K/L = 6 ± 1 indicates that this transition is probably a mixture of M1 + E2. This assignment is substantiated by the fact that $L_1:L_2:L_3 = 20:1:1$, inasmuch as the closeness of the values of α_{L_2} and α_{L_3} is typical for electric transitions, while the large value of α_{L_1} is characteristic of M1. The data on the absolute value of α_{K-70} is also evidence in favor of the above assignment. Thus comparison of the mean experimental value $\overline{\alpha_{K-70}} = 4.6 \pm 0.7$ (see Table 3) with the theoretical values from Sliv & Band[28] (70 kev: $\alpha_1 \approx 0.6$, $\alpha_2 \approx 2.8$ and $\beta_1 \approx 4.5$) shows that this transition is probably M1, or, if we allow for an appreciable error in the value of α_K, M1 + E2.

Table 4

Data for determining the multipole orders of the Eu^{153} transitions

Transition energy, kev	Experimental values	Theoretical values					Possible multipolarities	Favored assignment
		*E*1	*M*1	*E*2	*M*2	*E*3		
				K/L				
69,8	6±1	6,6	6,5	0,8	3,2	0,05	*E*1, *M*1, *M*1 + *E*2	*M*1
97,4	6,9±0,5	6,8	6,5	1,4	3,8	0,24		*E*1
103,3	6,4±0,3	6,8	6,5	1,6	3,9	0,30		*M*1 or *M*1 + *E*2
				α_K				
69,8	4,6	0,60	4,5	2,8	44	8,2	*M*1	
97,4	0,3	0,26	1,7	1,2	15	5,0	*E*1	
103,3	1,2	0,22	1,4	1,1	12	4,2	*M*1, *E*2, *M*1 + *E*2	

The above data relating to the multipole orders of the nuclear transitions in Eu^{153} are summarized in Table 4.

Decay scheme for Gd^{153}

The decay schemes of Sm^{153} and Gd^{153} to Eu^{153} (Fig.3) have been considered by a number of investigators and in the main are clearly established.[29] In the present work, we have made certain emendations relative to the intensity of the transitions in the decay of Gd^{153}.

The spin of the ground state of Eu^{153} has been measured and in accord with Nilsson's scheme is 5/2+.

The presence of levels at 103.3, 173 and ~700 kev in Eu^{153} has been reliably established; their existence follows from the conjunction of all the investigations of β- and γ-radiations from Sm^{153}. The existence of the 84 and 187 kev levels of the first rotational band has been established on the basis of investigations of Coulomb excitation of separated Eu^{151} by Heydenburg & Temmer[15]; the spins of these levels are 7/2+ and 9/2+, respectively.

The multipole order of the 103.3 kev transition (M1 + E2) and Nilsson's scheme indicate that the 103.3 level is a successive excitation level with spin and parity 3/2+. The multipole order of the 69.8 kev transition (M1 + + E2) and the very low intensity of the 173 kev cross-over transition to the ground state ($\sim 7 \cdot 10^{-4}$ relative to the intensity of the 70 kev transition[12]) together with comparison with Nilsson's scheme give reason to assume that the 173 kev level is a successive excitation level with spin 1/2+.

The indicated spin systematics are in more or less satisfactory agreement with the data on β^--decay of Sm^{153}, if, from among the spin values possible according to Nilsson's scheme, we assign 3/2+ to the Sm^{153} nucleus. In this case β^--transitions to the 0 kev 5/2+, 103 kev 3/2+ and 173 kev 1/2+ levels will be unfavored allowed transitions ($\Delta I = 0, \pm 1$, no) with relatively high log ft values of 7.3, 7.1 and 6.8, respectively[11,12]. The transition to the 84 kev level will be forbidden.

In the decay of Gd^{153} there is emitted an additional γ-ray of 97.4 kev energy not present in the decay of Sm^{153} (Ref.8). It must correspond to a separate Eu^{153} level of this energy inasmuch as the 97.4 kev γ-rays yield X-γ coincidences but no γ-γ coincidences.[8,17] The parity of this level is opposite to that of the ground state (E1 transition). According to Nilsson's scheme, it may be interpreted as a 5/2- "hole" level. This character of the level explains the absence of γ-transitions to it from higher-lying levels of Eu^{153}. The absence of a β^--transition of any appreciable intensity from Sm^{153} to the 97.4 kev level of Eu^{153} may be explained by the fact that such a transition is a first forbidden one ($\Delta I = 1$, yes).

The energy of $Gd^{153} \rightarrow Eu^{153}$ decay has been determined by different authors from the L and K capture branching ratio inasmuch as the competition between these two processes depends on the liberated energy. There have been obtained the following values for the total disintegration energy: $225 ^{+18}_{-13}$ (Ref.19), ~222 (Ref.17), ~220 (Ref.18) and 187 ± 3 kev (Ref.20).

It was found that the transition to the Eu^{153} ground state is of low intensity. The abundance values given by different authors for this transition are <10% (Ref.27), ~25% (Ref.19), < 3% (Ref.20) and even ~0% (Ref.18). It may be concluded from these data that the intensity of the transition to the ground state is <10% and log $ft > 7.5$. The 173 kev level is excited with an intensity of ~12% (log $ft \approx 4.7\%$). The most readily excited level is the 103.3 kev level for which the intensity is ~46% (log $ft \simeq 5.9$); the intensity for the 97.4 kev level is ~32% (log $ft \simeq 6.2$). The first rotational level of the first

rotational band, located at 84 kev, is the lowest of the known levels of Eu^{153} and is excited with an intensity of only ~0.6%; this level is in all probability fed by nuclear transitions in Eu^{153}.

In order to explain the experimentally observed values of log ft one must assume that the spin of Gd^{153} is 3/2-. The deformation of the Gd^{153} nucleus, which has 89 neutrons, is apparently characterized by $\delta \approx 0.2$ and, according to Nilsson's scheme, this spin value is possible. In this case transitions to the 173 kev 1/2+, 103 kev 3/2+ and ground 5/2+ levels will be first forbidden ones ($\Delta I = 1$, 0 and 1, respectively, yes), while the transition to the 97.4 kev 5/2- level will be allowed ($\Delta I = 0$, no). The observed values of log ft for these transitions lie within the spread of log ft values accepted in the literature for allowed and once forbidden transitions.

3. Conversion Electron Spectrum of Gd^{151}

Survey of the data in the literature on Gd^{151}

Radioactive Gd^{151} was first obtained by Hein & Voigt[5] in 1950 by bombarding europium with 20 Mev deuterons. In addition to a 230-day activity assigned to Gd^{153} produced by the $Eu^{153}(d,2n)$ reaction, Hein & Voigt detected a 150-day activity evinced by 265 kev γ-rays. The authors assigned this activity to Gd^{151} resulting from the $Eu^{151}(d,2n)$ reaction. The ~150-day half-life is based on measurements (absorption) of the ratio of intensities of the 106 (≈103) kev and 265 kev γ-rays carried out over a period of 600 days. Hein & Voigt found that the decay of Gd^{151} occurred by atomic electron capture with the resultant formation of Eu^{151}.

From Sm^{151} decay studies[30-32], Eu^{151} is known to have a level at 19-22 kev, while from Coulomb excitation studies[15] it is known to have levels at 195 and 304 kev and transitions of energies 110, 195 and 304 kev.

After completion of the present work there appeared the communication of Bisi et al[33] who observed 21.3, 80, 144, 155, 176, 240 and 299 kev γ-rays from Gd^{151}. At about the same time, Class & Meyer-Berkhout[16] published their investigation of Coulomb excitation of Eu^{151} substantiating the existence of the earlier detected transitions and reporting an additional nuclear transition of 284 kev energy.

Measurements and results for Gd^{151}

After subtraction of the Gd^{153} lines there still remained a large number of other lines in our conversion electron spectrum of the long period activity contained in the gadolinium fraction.

Fig.4 shows the initial section (up to 23 kev) of the conversion spectrum. The upper and lower curves were recorded at an interval of one year. First, we note that the energies of the first four conversion peaks at 13.6, 14.1, 14.7 and 19.9 kev have differences that are in good agreement with the energy differences of the L_1, L_2, L_3 and M atomic shells of Eu; it may therefore be concluded that the enumerated peaks correspond to conversion of a 21.7 ± 0.3 kev nuclear transition in the indicated shells of Eu. Further, from comparison of the upper and lower curves in Fig.4, it is evident that the heights of the L_1-22 and M_1-22 peaks fall off more rapidly with time than the height of the K-70 peak pertaining to Gd^{153}. The decay curves representing the decrease in the peak height with time are plotted in Fig.2. The points corresponding to the L_1-22 and M_1-22 peaks fall on the curve corresponding to T = 120 ± 20 days, a period that is appreciably shorter than the half-life of Gd^{153} (~200 days). Conse-

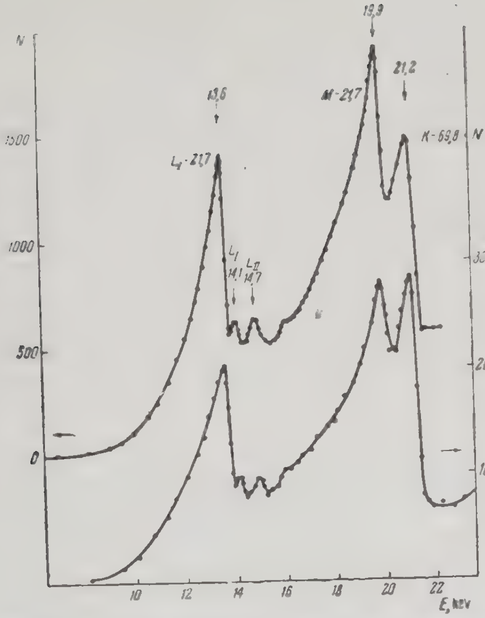

Fig.4. Low-energy section of the conversion electron spectrum of the long period activity in the gadolinium fraction (experimental curve - not corrected). The upper and lower curves were recorded at an interval of one year.

quently, the 21.7 kev transition cannot belong to Gd^{153}. As was noted above, according to the data in the literature[30-32], there is excited a level of 19-22 kev energy in Eu^{151} in the $Sm^{151} \rightarrow Eu^{151}$ decay process. From this we concluded that the 21.7 kev transition evinced by our conversion spectrum is excited in the $Gd^{151} \rightarrow Eu^{151}$ decay. This deduction is in complete agreement with the results of Bisi et al[33] who investigated the decay of Gd^{151} to Eu^{151}. It was very important for us to establish that the 21.7 kev transition belongs to Eu^{151} and to determine the corresponding half-life, inasmuch as this enabled us to complete the analysis of the remaining part of the conversion electron spectrum of the gadolinium fraction and to identify the lines of Gd^{151}.

Our conversion electron spectrum (Fig. 1) contains a group of lines which we have identified as the K, L and M conversion lines of a transition of 154.5 ± 0.5 kev energy in Eu^{151}. Investigation of this transition was hampered by two factors. First, it was found that our spectrum contained conversion lines associated with two transitions of very close energy (~155 kev), one of which belongs to Eu^{155} and the other to Eu^{146}, a decay product of Gd^{146} with a half-life of 45 days. (The data on the decay of Gd^{146} will be the subject of a separate communication.) Second, for a long time the K conversion lines of these transitions were masked by the strong L conversion line of the 115 kev transition in Eu^{146}. Investigation of the variation with time of the heights of the L-155 and M-155 peaks yielded a complicated decay curve (Fig.2). It was found that the initial value of $T \ngtr 50$ days subsequently increased to 100 ± 30 days. From the character of the curve we concluded that the $Gd^{151} \rightarrow Eu^{151}$ decay is accompanied by γ-radiation of 155 kev energy. The conversion spectrum recorded a year after the first measurement (Fig.1) contains the almost pure conversion lines of the 155 kev transition in Eu^{151}.

Further, there are evident in our conversion spectrum (Fig.1) the K, L and M conversion lines associated with a γ-transition of 174.8 ± 0.3 kev energy. The decay curves plotted from the variation with time of the peak heights yields a value of T = 120 ± 20 days and hence we attributed this transition to $Gd^{151} \rightarrow Eu^{151}$. It is possible that there are superposed on these lines the low intensity conversion lines associated with the 173 kev transition in Eu^{153}.

Although we did not detect the 265 kev γ-rays observed by Hein & Voigt (i.e., the rays that led to discovery of Gd^{151}), we found that our conversion spectrum contained weak lines corresponding to transitions of 243 ± 1 and 306 ± 1 kev energy (Fig.5). The half-life determined from the variation of the K-243 and K-306 peaks proved to be 120 ± 30 days and we assigned these transitions to $Gd^{151} \rightarrow Eu^{151}$. Probably the group of γ-rays of 155, 175, 243 and 306 kev energy is identical with the ~265 kev γ-radiation observed by Hein & Voigt. Our data on the energies of the nuclear transitions in Eu^{151} together with the results of other investigators are listed in Table 5.

Table 5

Energies of nuclear transitions in Eu^{151}

γ-transition, kev	$Sm^{151} \rightarrow Eu^{151}$			Coulomb expectation of Eu^{151}		$Gd^{151} \rightarrow Eu^{151}$	
	Ref.30	Ref.31	Ref.32	Ref. 15	Ref. 16	Ref.33	Our work
22	21	19	22	—	—	21,3±0,2	21,7±0,3
80	—	—	—	—	—	80	(84)
110	—	—	—	110	111	—	—
144	—	—	—	—	—	(~144)	—
155	—	—	—	—	—	155	154,5±0,5
175	—	—	—	—	—	176	174,8±0,3
195	—	—	—	195	193	—	—
243	—	—	—	—	—	240	243±1
284	—	—	—	—	284	—	—
300	—	—	—	304	304	299	306±1

As may be seen from this table many of the results obtained in our work are in good agreement with the results reported by Bisi et al[33]. Among the divergences between our data and those of Bisi et al is the interpretation of the 84 kev transition which we initially attributed to Eu^{153} (see Table 1). At present, however, we do not have sufficient data to make a definitive assignment and cannot exclude the possibility that this transition pertains to Eu^{151}. In addition, in our conversion spectrum we did not observe the lines associated with the 144 kev transition. According to our evaluation if this transition does exist the height of the L-144 line would be less than 5% relative to the height of the L-155 peak.

The intensities of the other conversion lines can be evaluated from our conversion spectrum of Gd^{151}. Our results together with those of other investigators are listed in Table 6.

Precise determination of the relative intensities of the conversion lines is, unfortunately, hampered by the necessity of introducing different corrections for each transition. In the case of the 21.7 kev transition the indicated data are only tentative in view of the difficulty of working with low

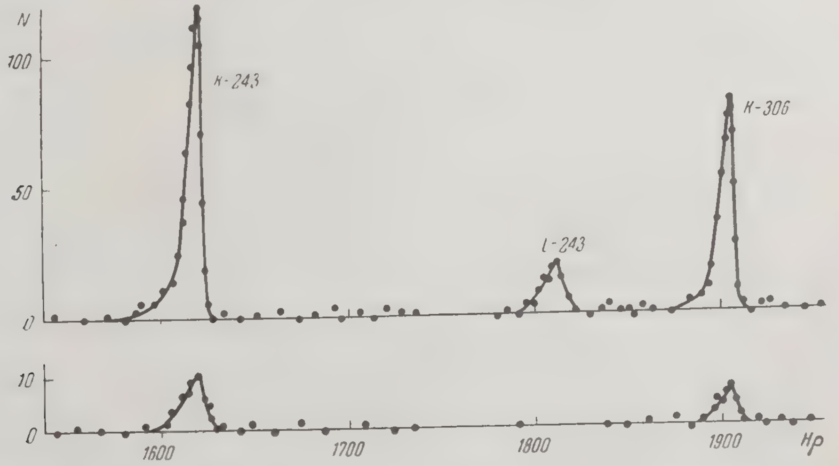

Fig.5. High energy section (200 to 300 kev) of the experimental conversion electron spectrum. The upper and lower curves were recorded with an interval of 1 year.

Table 6

Relative intensities of the conversion lines associated with the nuclear transitions in Eu^{151}

Author, year and Ref.	Method	21.7 kev	155 kev	175 kev	193 kev	243 kev	284 kev	~300 kev
Achor et al, 1957 (32)	Sm^{151}, Mag.spec.	$L:(M+N)==1,8$ $M:N\sim 6$	—	—	—	—	—	—
Bisi et al, 1957 (33)	Gd^{151}, Mag spec.	—	$K:L>10$	$K:L\approx 4,8$	—	$K:L\approx 1$	—	—
Class et al, 1957 (16)	Coul.excit. Eu^{151}, conv. electr.	—	—	—	$K:K_{306}\approx 1$ $K:L=3,1$	—	$K:K_{306}\approx 0,15$ $(K:L>5)$	1,00 $K:L=6,5$
Present work	Gd^{151}, Mag.spec (Ketron)	$L_1:K_{175}\approx 12$ $L_1:L_2:L_3\sim$ $\sim 10:1:1$ $L_1:M_1\approx 2,5$	$K:K_{175}==0,46\pm 0,05$ $K:L=6,5\pm 0,6$	1,00 $K:L=4,9\pm 0,3$	—	$K:K_{175}==0,024\pm 0,005$ $K:L=6,3\pm 1,0$	—	$K:K_{175}==0,013\pm 0,002$

energy electrons and the large corrections involved. In the case of the lines of the 154.5 kev transition there is appreciable interference from other lines. Weak lines associated with the 173 kev transition in Eu^{153} are apparently superposed on the lines associated with the 174.8 kev transition. The lines associated with the 243 and 306 kev transitions are weak and hence their relative intensities cannot be accurately determined. In addition, the L-243 line may also contain the K-294 line.

Discussion of results on Gd^{151}

One can draw certain conclusions regarding the multipole orders of the nuclear transitions from the data on the conversion coefficients listed in Table 6.

In the case of the 21.7 kev transition comparison of the experimental value of the L conversion ratios ($L_1:L_2:L_3 \approx 10:1:1$) with the theoretical indicates that this transition is probably a mixture of M1 + E2, inasmuch as the L_1 peak is appreciably higher than the L_2 and L_3 peaks, while $L_3 \approx L_2$. The only other possible assignment is E1, but in this case we should have $L_1 \approx L_2 \approx L_3$, which is not the case. The fact that the M peak corresponds to conversion on the M_1 shell substantiates the M1 + E2 mixture assignment and is inconsistent with E1. The absolute value of the conversion coefficient $\alpha_L \approx 12$, reported by Achor et al[32], may also be taken as evidence that the multipole order of the 21.7 kev transition is M1 or M1 + E2.

In the case of the 155 kev transition the scatter in K/L values (6.5 ± 0.6) allows of identifying it as E1, M1 or a mixture of M1 + E2.

One can roughly evaluate α_K using the value of α_{L-22}:

$$\alpha_K = \alpha_{L-22} \frac{K : L_{22}}{I_\gamma : I_{\gamma-22}}$$

and the relative intensities of the γ-lines as measured by Bisi et al[33] (Table 7). For the 155 kev transition, we obtain $\alpha_{K-155} \approx 0.4$, which tends to exclude E1 and makes more probable the M1 or M1 + E2 assignments (the theoretical values are $\alpha_2 \approx 0.3$ and $\beta_1 \approx 0.45$).

The experimental value of K/L = 4.9 ± 0.3 for the 175 kev transition is consistent with the assumption that this transition is primarily M2. This is substantiated by the large value of the internal conversion coefficient; this follows from the fact that the conversion lines have

Table 7
Relative intensities of the γ-rays of Gd^{151} according to Ref.33

$h\nu$, kev	$I_{\gamma} : I_{\gamma\text{-}22}$
22	1
155 (+175)	1,3
243	0,87
$\sim$300	0,065

a relatively high intensity, while the intensity of the γ-radiation according to Bisi et al[33] is low.

The spread in the values of K/L for the 243 transition (6.3 ± 1.0) allows of identifying it as E1, M1 or M1 + E2. According to a rough evaluation made as above for $\alpha_{K\text{-}155}$, we have $\alpha_{K\text{-}243} \approx 0.03$, which is most consistent with E1 (the theoretical values are $\alpha_1 \approx 0.02$, $\alpha_2 \approx 0.09$ and $\beta_1 \approx 0.13$).

As regards the 306 kev transition, we did not observe the L-306 line inasmuch as in our spectrum it was masked by the conversion lines from other Gd isotopes. It may be assumed however that the 306 ± 1 kev transition is a transition that occurs in Coulomb excitation of europium; in all investigations of Coulomb excitation there were observed γ-rays of about 300 kev energy[13-16]. Heydenburg & Temmer[15] who had at their disposal enriched europium isotopes observed γ-lines of 110, 195 and 304 kev energy in the spectrum of Eu^{151} and established the existence of levels at 195 and 304 kev. They also found that the intensity of the transition from the 304 kev level to the ground level is 10 times greater than the intensity of the 110 kev transition to the 195 kev level. Consequently, the conversion lines associated with the 110 kev transition should be of relatively low intensity, which explains why they could not be observed in our spectrum against the background of the other, stronger lines. The same thing may be said regarding the conversion lines of the 195 kev transition, if the 195 kev level is not excited indirectly in the decay of Gd^{151}. In their recent Coulomb excitation study, Class & Meyer-Berkhout[16] detected the γ-transitions in Eu^{151} by observing the conversion electrons. Their results substantiate the above deductions; in addition, as was noted above, Class & Meyer-Berkhout observed a new transition of 284 kev energy and found that the ratio of intensities of the conversion lines $K_{284}/K_{304} \approx 0.15$. In our conversion spectrum, the lines associated with the 284 kev transition were not observed. Possibly this is explained by their low intensity and the fact that the K-284 line is close in energy to the L-243 line (the 243 kev transition does not occur in Coulomb excitation).

If the 306 kev transition observed by us is identical with the 304 kev transition observed in Coulomb excitation, the conversion ratio K/L $\approx$ 6.5 (Ref. 16) and the multipole order of the transition must apparently be M1 or M1 + E2. At the same time a rough evaluation of $\alpha_{K\text{-}306}$ made as in the preceding cases and leading to a value of ~0.2 indicates that the multipole order of the transition should be higher (theoretical value - $\beta_1 \approx 0.075$). It should be noted, however, that the accuracy of measuring the intensity of this transition in this case is relatively low and does not allow of unambiguous selection between the two indicated assignments.

It is possible, however, that the difference between the indicated transition energy value, i.e., 306 - 304 = 2 kev, is real and that the transition evinced in our conversion spectrum is not the same transition as occurs in Coulomb excitation. In any case it would appear clearly established that different levels and transitions arise in the decay of Gd^{151} to Eu^{151} as compared with Coulomb excitation of Eu^{151}. The above mentioned data pertaining to the multipole orders of the transitions in Eu^{151} are collected in Table 8.

Finally, we evaluated the relative intensities of the nuclear transitions in Eu^{151} occurring in the decay of Gd^{151} on the basis of our data on the conversion line intensities, the data of Bisi et al on γ-rays and the value of $\alpha_{L\text{-}22}$ reported by Achor et al[32]. With some approximation, we obtained the following total transition intensity ratios:

$$I_{22} : I_{155} : I_{175} : I_{243} : I_{306} \approx 100 : 7 : 9 : 4 : 0.4.$$

Table 8

Data for determining the multipole order of transitions in Eu^{151}

Transition energy, kev	Experimental values	Theoretical values					Possible multipolarities	Favored assignment
		E1	*M1*	*E2*	*M2*	*E3*		
K/L								
154,5	6,5±0,6	7,2	6,6	2,6	4,6	0,88	*E1*, *M1*; *M1* + *E2*	*M1* + *E2*
174,8	4,9±0,3	7,3	6,6	2,9	4,8	1,1	*M2*; *M1*+*E2*	*M2*
243	6,3±1,0	7,5	6,7	3,8	5,2	1,7	*E1*, *M1*; *M1* + *E2*	*E1* *M1* + *E2*
306	(~6,5[16])	7,6	6,8	4,5	5,5	2,2	*M1*	*M1*
α_K								
154,5	(~0,4)	0,075	0,46	0,34	2,9	1,3	*M1* + *E2*	
174,8	High	0,050	0,32	0,23	2,3	0,90	*E2* or higher	
243	(~0,03)	0,020	0,14	0,090	0,61	0,30	*E1*	
306	(~0,2)	0,012	0,076	0,039	0,30	0,11	*M1*, *M2*	
$L_1 : L_2 : L_3$								
21,7	~10 : 1 : 1	~1,5 : :1 : 1,3	~11 : :1:0,14	~0,01 : :1 :0,8	~14 : : 1 : 8	~0,006 : : 1 : : 0,44	*M1*; *M1* + *E2*	*M1* + *E2*

Decay scheme of Gd^{151}

The first decay scheme for $Gd^{151} \rightarrow Eu^{151}$ was proposed by Bisi and his coworkers.[33] Here we shall discuss other versions of the decay scheme and at the same time draw some inferences regarding the probable spins of the levels of Eu^{151} known from Coulomb excitation studies.

Gd^{151} has 87 neutrons and should apparently be classed as a spherical nucleus. Hence it may be assumed that its ground state is described by Mayer's scheme,[34] according to which it may be characterized as $f_{7/2}$ or $h_{9/2}$. We assume that in the case of Gd^{151} there is realized the $f_{7/2}$ state, since, as will be seen from what follows, there occurs fairly intense decay to the excited level of Eu^{151} with spin 3/2. The Eu^{151} nucleus contains 88 neutrons and apparently is also spherical. In view of this it is logical to analyze its system of levels from the viewpoint of the single particle model. The ground state of Eu^{151} has spin 5/2 (experimental value) and is of the $d_{5/2}$ type.

The energy of the first excited level of Eu^{151} is 21.7 ± 0.3 kev. This is most convincingly proved by the data obtained from observing the decay of Sm^{151}. The Sm^{151} nucleus decays by a ~75 kev β^--transition to the ground level of Eu^{151} and by a relatively weak ($<1\%$) β^--transition of 53 kev energy to the 21.7 kev level of Eu^{151} (Ref.32). This 21.7 kev level is strongly excited in the decay of Gd^{151}.

Further in constructing the level diagram of Eu^{151} one must bear in mind the comparatively intense transitions of 154.5 ± 0.5 and 174.8 ± 0.3 kev energy. It must be recalled that the energy difference between these two transitions - 20.3 ± 0.8 kev - is smaller than the energy of the first level (21.7 ± ± 0.3 kev). Hence these two transitions cannot be plotted as departing from the same 174.8 kev level (the 174.8 kev transition leading to the ground state

of Eu^{151} and the 154.5 kev transition leading to the 21.7 kev excited level). Furthermore, V.A. Sergienko et al[35] who investigated e-e coincidences on a double magnetic lens spectrometer found indications that the 22 and 175 kev transitions are in cascade. Thus it would appear that there exists a level with an excitation energy of 196 kev in Eu^{151}.

On the basis of Mayer's single particle level scheme and taking the above mentioned multipole order assignments for the 22 and 175 kev transitions (M1 + + E2 and M2, respectively), we identified the 22 kev level as a $g_{7/2}$ "hole" level and the 196 kev level as a $h_{11/2}$ successive excitation level. As has been noted by Peker & Sliv[36] transitions between "successive excitation" and "hole" levels are strongly forbidden. In this case, however, it must be admitted that our 175 kev M2 type transition to the 22 kev "hole" level can successfully compete with the E3 transition to the ground state.

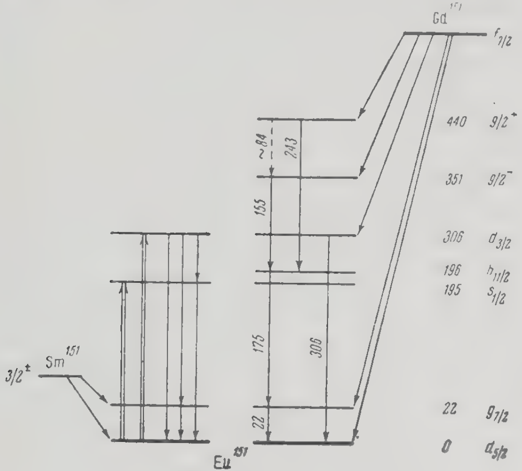

Fig.6

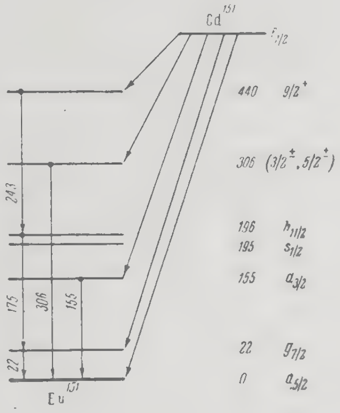

Fig.7

Fig.6. First version of the decay scheme for $Gd^{151} \rightarrow Eu^{151}$. At the left - Coulomb excitation levels and scheme for $Sm^{151} \rightarrow Eu^{151}$.

Fig.7. Second version of the decay scheme for $Gd^{151} \rightarrow Eu^{151}$.

From this point on the construction of the level schemes becomes less certain and we shall examine two possible versions.

First version of decay scheme (Fig.6). Let us turn to the transition next in line in order of intensity, i.e., the 155 kev transition. The fact that the abundances of the 155 and 175 kev transitions are virtually identical shows that these transitions are in cascade. Thus, apparently, all three of the most intense transitions (22, 175 and 155 kev) form one cascade. We assumed, therefore, that Eu^{151} has a level with an excitation level of 351 kev. The spin of this level must be high since the assignment for the 155 kev transition is M1 + E2. However, in the given region according to Mayer's scheme there are no close levels with high values of spin. The level with a suitable value of the spin $h_{9/2}$ already belongs to another shell. Hence it must be inferred that the 351 kev level is not a single particle one but of some other type. In view of the multipole order of the 155 kev transition it must be assumed that this is a 9/2- level.

With the indicated spin, the transition from the given level to the ground state according to the scheme must be M2 and our transition of 155 kev energy (M1 + E2) to the 196 kev level can compete with it successfully. It is difficult, however, to explain the successful competition of the 155 kev transition with an E1 transition (possible according to this scheme) to the

22 kev level. It is of no help here to recall the "hole" character of the lower level because we do know the nature of the level at 351 kev. This difficulty impels us to turn to the second version of the decay scheme which will be discussed below. For the moment, let us continue our description of the first version.

In order to explain the 306 kev transition we assumed, as already noted, that this is the same transition as observed in Coulomb excitation. Accordingly, we hypothesized the existence in Eu^{151} of a discrete level with this energy. In the first version of the decay scheme we will consider it to be a single particle level. According to Mayer's scheme, it can be identified as . Then the 306 kev transition to the ground state must be of the M1 + + E2 type. This is in satisfactory agreement with the experimental data.[16]

Here it is important to note that the 195 kev level, known from Coulomb excitation studies, does not coincide exactly with the level introduced by us at 196 kev. This follows simply from the fact that in Coulomb excitation there does not occur a nuclear transition with 175 kev energy but there is observed an intense transition having an energy of 195 kev. In accord with Mayer's model, the assignment for the 195 kev level appearing in Coulomb excitation should be . Then the transition from the given level to the ground state should be E2 which again is in agreement with experimental data.[16]

The indicated assignment for the low-lying "Coulomb" level makes it possible to explain why the 195 kev level is very weakly excited in the decay of Gd^{151} and why we did not observe the lines associated with this transition in our conversion electron spectrum: first, the spin of the 195 kev level in question differs greatly from the spin of Gd^{151} (ground state) and direct decay to this level is strongly forbidden by the selection rules ($\Delta I = 3$, yes); second, excitation of this level by nuclear transitions from the high-lying levels of Eu^{151} is virtually impossible in view of the large spin difference. An exception in this respect is the sparsely populated level at 306 kev, but in this case the ratio of intensities of the transitions to the 195 kev level ($E_\gamma \fallingdotseq 110$ kev) and the ground level $E_\gamma = 306$, M1 + E2) is very small: the 110 kev (M1 + +2) transition according to our scheme has a very low intensity since it competes with a transition of the same multipole order but with an energy approximately 3 times higher. As was indicated above, experiment fully substantiates this deduction.

It is difficult to make a definitive inference regarding the 243 kev transition. Inasmuch as this transition cannot be fitted between the already introduced levels, in order to explain it, one must introduce a new level. Since all the possible single particle levels have already been utilized in our decay scheme, it must be hypothesized that this new level has a different nature and is located rather high up in the level scheme. The intensity balance suggests that the 243 kev transition feeds either the 196 kev or the 351 kev level. Further, the fact that it proved impossible[33] to detect coincidence between the 155 and 243 kev transitions would indicate that of the two alternatives one must choose the 196 kev level. Then the energy of the new level to be introduced is 440 kev. The spin of this level must be large inasmuch as the multipole order of the 243 kev transition is not greater than E2 and is most probably E1. Moreover, the transition from the ground state of Gd^{151} ( ) to this 440 kev level should not be strongly forbidden inasmuch as the decay probability to this relatively high-lying level is appreciable. Apparently, the spin of this level is 9/2+.

Here it should also be noted that the ~84 kev transition attributed by us to Eu^{153} may at least partially belong to Eu^{151} as well. In the latter case, this transition could be fitted into this scheme between the 440 and 351 kev

levels (the exact energy value of the transition depends on the interpretation given the conversion line). Finally, it must be noted that relatively weak cross-over transitions from the 351 and 440 kev levels could have remained undetected.*

Let us now consider the transitions from Gd^{151} to the levels of Eu^{151}. The characteristics of these transitions according to the first version of the decay scheme are listed in Table 9.

The approximate (experimental) values of the relative transition intensities indicated in the table are based on the assumption that the transitions from Gd^{151} to the 0 and 22 kev levels of Eu^{151} are approximately equally probable inasmuch as both transitions are characterized by equal degrees of forbiddenness and close energies. As may be seen from Table 9 the intensities of the $Gd^{151} \rightarrow Eu^{151}$ transitions are in satisfactory agreement with the level assignments.

Table 9

Characteristics of $Gd^{151} \rightarrow Eu^{151}$ transitions (first version of decay scheme)

Eu^{151} level energy, kev	Type transition	ΔI and parity change	Intensity of transition (% (exper.)
0	$f_{7/2} \rightarrow d_{5/2}$	1,yes (once forbidden)	∼46
22	$f_{7/2} \rightarrow d_{7/2}$	0,yes (once forbidden)	∼46
195	$f_{7/2} \rightarrow s_{1/2}$	3,yes (strongly forbidden)	∼0
196	$f_{7/2} \rightarrow h_{11/2}$	2,no (twice forbidden)	∼0
306	$f_{7/2} \rightarrow d_{3/2}$	2,yes (once forbidden)	∼0,2
352	$f_{7/2} \rightarrow {}^{5}/_{2}^{-}$	1, no (allowed)	∼5
440	$f_{7/2} \rightarrow {}^{9}/_{2}^{+}$	1,yes (once forbidden)	∼2

Table 10

Characteristics of $Gd^{151} \rightarrow Eu^{151}$ transitions (second version of decay scheme)

Eu^{151} level energy, kev	Type transition	ΔI and parity change	Intensity of transition % (exper.)
0	$f^{7}/_{2} \rightarrow d^{5}/_{2}$	1,yes (once forbidden)	∼46
22	$f^{7}/_{2} \rightarrow d^{7}/_{2}$	0,yes (once forbidden)	∼46
155	$f^{7}/_{2} \rightarrow d^{3}/_{2}$	2,yes (once forbidden)	∼4
195	$f^{7}/_{2} \rightarrow s_{1/2}$	3,yes (strongly forbidden)	∼0
197	$f^{7}/_{2} \rightarrow h_{11/2}$	2,no (twice forbidden)	∼0
306	$f^{7}/_{2} \rightarrow {}^{3}/_{2}^{+}$	2,yes (once forbidden)	∼0,2
440	$f^{7}/_{2} \rightarrow {}^{9}/_{2}^{+}$	1,yes (once forbidden)	∼2÷5

For the sake of completeness, we have shown at the left in Fig.6 the levels and transitions in Eu^{151} observed in Coulomb excitation and in the decay of Sm^{151}. It must, apparently, be assumed that the spin of the ground state of Sm^{151} is 3/2±, inasmuch as the β^--transition to the 22 kev level of Eu^{151} is more strongly forbidden than the transition to the ground state.

Second version of the decay scheme (Fig.7). The second version of the decay scheme differs from the first primarily in that in it the 155 kev transition is assumed to go to the ground state of Eu^{151}. Accordingly, there is introduced a 155 kev level which can be identified as a $d_{3/2}$ single particle level. To be consistent with the experimental data the multipole order assignment for this transition should be M1 + E2. Further, in this version the 306 kev level is identified as a first collective level with spin 3/2 or 5/2 and positive parity.

The principal objection to this version is the following. According to this scheme one must expect that in the case of Coulomb excitation of the 195

---

*Note added in proof: Recently student V.Smirnov in our laboratory detected a weak γ-transition of 350 kev energy, the existence of which may be interpreted as substantiation of the first version of the $Gd^{151} \rightarrow Eu^{151}$ decay scheme.

kev level by a nuclear transition of ~40 kev energy (M1) there should also be excited a 155 kev level, and, consequently, there should exist a transition of this energy; no such γ-rays, however, are observed.

Moreover, the total intensity of the 243 kev transition amounts to $\leqslant 50\%$ relative to the total intensity of the 175 kev transition, while the 196 kev level is apparently not directly populated in the decay of Gd^{151}.

The intensities of the transition from Gd^{151} to the levels of Eu^{151} in the second version of the decay scheme are listed in Table 10.

The authors desire to thank V.Il'in and L.Klochkov for aid in the measurements and L.K.Peker for discussion of the decay schemes.

Physical Institute, Leningrad State University

References

1. B.Preobrazhenskii, O.Lilova, A.Dobronravova & E.Teterin, Zhur.neorg. khim., 1, 2294 (1956).
2. B.S.Dzhelepov & A.A.Bashilov, Izv.AN SSSR, Ser.fiz., 14, 263 (1950).
3. K.Fajans & A.Voigt, Phys.Rev., 60, 533 (1941).
4. N.Krisberg, M.Pool & C.Hibdon, Phys.Rev., 74, 44 (1948).
5. R.Hein & A.Voigt, Phys.Rev., 79, 783 (1950).
6. M.Inghram, R.Hayden & D.Hess, Phys.Rev., 71, 643 (1947).
7. J.Cork, R.Schrefler & C.Fowler, Phys.Rev., 74, 240 (1948).
8. F.McGowan, Phys.Rev., 93, 163 (1954).
9. E.Church & M.Goldhaber, Phys.Rev., 95, 626 (1954).
10. J.M.Hollander, I.Perlman & G.D.Seaborg, Table of Isotopes, Revs.Mod. Phys., 25, 469 (1953). (Cited in Russian trans.)
11. N.Marty, C.R., 238, 2516 (1954).
12. V.Dubey, C.Mandeville & M.Rothman, Phys.Rev., 103, 1430 (1956).
13. N.Heydenburg & G.Temmer, Phys.Rev., 100, 150 (1955).
14. H.Mark & G.Paulissen, Phys.Rev., 100, 813 (1955).
15. N.Heydenburg & G.Temmer, Phys.Rev., 104, 981 (1956).
16. C.Class & U.Meyer-Berkhout, Nucl.Phys., 3, 656 (1957).
17. N.Marty & M.Vergnes, C.R., 242, 1438 (1956).
18. S.Bhattecherjee & S.Raman, Nucl.Phys., 1, 486 (1956).
19. R.Gupta & S.Jha, Nuovo Cim., 4, 88 (1956).
20. A.Bisi, E.Germagnoli & L.Zappa, Nucl.Phys., 1, 593 (1956).
21. B.Andersson, Proc.Phys.Soc., 69A, 415 (1956).
22. W.Rutledge, J.Cork & S.Burson, Phys.Rev., 86, 775 (1952).
23. R.Graham & J.Walker, Phys.Rev., 94, 794 (1954).
24. M.Lee & R.Katz, Phys.Rev., 93, 155 (1954).
25. N.Marty, J.Phys.et Rad., 16, 458 (1955).
26. J.Mihelich, Phys.Rev., 87, 646 (1952).
27. S.Cohen, Y.Burde & S.Ofer, Bull.Res.Coun.Israel, 5 A, 87 (1955).
28. L.Sliv & I.Band. Tablitsy Koef.Vnutrennoi Konversii γ-izlucheniia (Tables of internal conversion coefficients), M.-L., 1956.
29. B.Dzhelepov & L.Peker, Skhemy raspada radioaktivnykh izotopov (Decay schemes of radioactive isotopes), M.-L., 1957.
30. G.Scharff-Goldhaber, E.der Mateosian, M.McKeown & A.Sunyar, Phys.Rev., 78, 325 (1950).
31. H.Wilson & G.Lewis, Proc.Phys.Soc., 65A, 656 (1952).
32. W.Achor, W.Phillips, J.Hopkins & S.Haynes, Bull.Am.Phys.Soc., 2, 259 (1957).
33. A.Bisi, E.Germagnoli & L.Zappa, Nucl.Phys., 3, 670 (1957).
34. M.Mayer, Phys.Rev., 78, 16 (1950).
35. B.S.Dzhelepov, B.K.Preobrazhenskii & V.A.Sergienko, Report presented at the Eighth All-Union Conference on Nuclear Spectroscopy.
36. L.Peker & L.Sliv, Izv.AN SSSR, Ser.fiz., 17, 411 (1953).

$Nd^{140} \rightarrow Pr^{140} \rightarrow Ce^{140}$ DECAY SERIES

- K.Ia.Gromov, B.S.Dzhelepov, A.G.Dmitriev & B.K.Preobrazhenskii

1. Survey of data in the literature

In 1935, Amaldi et al[1] in bombarding Pr with neutrons observed a 5-minute activity. Subsequently it was established that an activity with this period (the more accurate value for the half-life is 3.5 min) is formed in the Ce(p,n), Pr(n,2n) and Pr(γ,n) reactions.[1-6] From analysis of these reactions, this activity should be attributed to Pr^{140}. Later it was established that the decay of Pr^{140} is accompanied by the emission of positrons with 2.4-2.5 Mev end-point energy[6-8].

In 1949 Wilkinson & Hicks[7] discovered that in the bombardment of Pr with 19 Mev deuterons there is formed an activity that separates out with the neodymium fraction and has a period of 3.3±0.1 days. Using the absorption procedure and a crude β-spectrometer, these investigators established that the decay is accompanied by β^+-radiation with an end point energy of 2.4-2.5 Mev, K x-rays and γ-rays of ~510 and ~1200 kev energy. According to Wilkinson & Hicks, the relative intensities of the different forms of irradiation are

$$\beta^+ : K : \gamma_{510} : \gamma_{1200} = 0.2 : 1 : 0.2 : 0.01. \qquad (1)$$

The evaluation is approximate and the error in the $\beta^+ : \gamma_{510}$ ratio (the correct value is 1:2, rather than 1:1) may be overlooked. The authors assigned this activity to the isotope Nd^{140}.

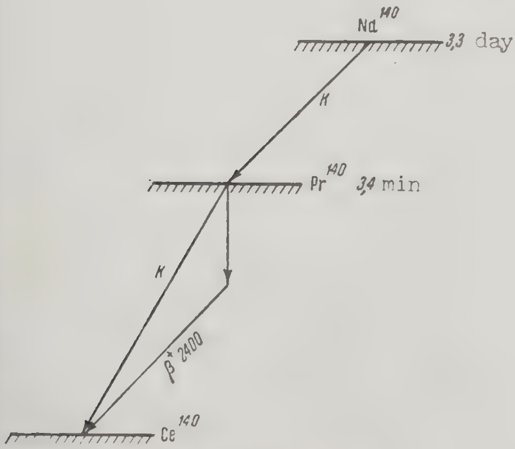

Fig.1. Decay scheme of $Nd^{140} \rightarrow Pr^{140} \rightarrow Ce^{140}$.

The principal arguments in favor of this mass assignment are the coincidence of the positron end-point energy with the end-point energy of positrons from Pr^{140} and the prompt re-establishment of the neodymium fraction activity after rapid separation of Pr from it (the half-life of the daughter activity appears to be 1.5 min).

The decay scheme for $Nd^{140} \rightarrow Pr^{140} \rightarrow Ce^{140}$ inferred by Wilkinson & Hicks is shown in Fig.1. There is virtually always Pr^{140} in equilibrium with the Nd^{140} in the sample.

The $Nd^{140} \rightarrow Pr^{140} \rightarrow Ce^{140}$ chain was investigated by Browne et al.[8] They investigated the electron radiation by means of a double focusing β-spectrometer; the γ-radiation by means of a scintillation spectrometer and a bent crystal x-ray spectrometer. On the basis of their observations the authors constructed a Kurie plot of the β-spectrum which proved to be linear from 1 Mev to the end-point energy value of 2.23 ± 0.02 Mev. The authors do not exclude the possibility of a weak lower energy (~1 Mev) component. In addition to the K x-rays and annihilation radiation, the authors report a meager indication of γ-radiation of 1.0-1.2 Mev energy. Study of the x-ray spectrum by means of the bent crystal spectrometer allowed of determining the relative intensities:

$$\text{Pr } K\alpha_{1,2} : \text{Ce } K\alpha_{1,2} : \text{Pr } K\beta_1 : \text{Ce } K\beta_1 = 100 : 50 : 28 : 11. \qquad (2)$$

Integration of the β^+ and e^- spectra yielded the ratio

$$\beta^+/e^- \approx 50. \tag{3}$$

The above data constitutes virtually all that was known regarding the $Nd^{140} \rightarrow Pr^{140} \rightarrow Ce^{140}$ decay chain at the beginning of 1957.

2. Yield of K Auger electrons

Let us make use of the above data to determine the yield of K Auger electrons e_K/K_Σ, where e_K is the number of K Auger electrons and K_Σ is the number of K captures per disintegration of Nd^{140} and Pr^{140} in equilibrium. The first factor in the equality

$$\frac{e_K}{K_\Sigma} = \frac{e_K}{\beta^+} \cdot \frac{\beta^+}{K_\Sigma}$$

is given by Eq.(3) and the second factor follows from (1):

$$\frac{e_K}{K_\Sigma} = 0.02 \cdot 0.2 = 0.4\%.$$

This figure is unexpectedly small from two points of view:

1. After capture of a K electron there occurs filling of the K shell, which is accompanied either by emission of K fluorescence x-rays or the emission of K Auger electrons.

The fluorescence yield has been investigated repeatedly and carefully. As the survey recently made by Laberrique-Frolow & Radvanyi[9] shows, the data of different authors are in close agreement. For $Z = 58$ and 59, the fluorescence yield is 90%, thus leaving only ~10% for the K Augers. Thus the divergence from experiment amounts to a factor of 25.

Inasmuch as the data on fluorescence are entirely reliable one must seek the source of error in Eqs.(1) or (3).

2. If we assume that the ~10% yield of K Auger electrons is normal, then the small number of Auger electrons observed means that in the given decay chain there occur fewer K captures than β^+-decays: from the ratio $e^-/\beta^+ = 0.02$ there should follow $K/\beta^+ = 1/5$, yet the presence of only one allowed decay of Pr^{140} to the ground level of Ce^{140} requires equality of K and β^+, while the presence of decays of Pr^{140} to other levels of Ce^{140} and $Nd^{140} \rightarrow Pr^{140}$ could only increase the value of the ratio K/β^+.

Attention has been called to the inconsistency of the K Auger yield following from Eqs.(1) and (3) by the authors of Eq.(3) themselves, Browne et al[8], who infer that the smallness of the number of Auger electrons observed may be due to experimental factors (self-absorption and scattering in the source, etc.). In view of this we reinvestigated the radiation of $Nd^{140} + Pr^{140}$.

3. Experimental conditions

The neodymium fraction was separated chromatographically (ion exchange) from a tantalum target bombarded with 660 Mev protons. The separated fraction was applied to an aluminum strip measuring 10 x 1 x 0.05 mm. In the chromatographic process the neodymium is separated without a carrier in the form of neodymium lactate. The salt was deposited on the aluminum strip by evaporation and then heated to volatilize the lactic acid. As a result there was obtained a very thin source; the active layer was barely discernible with the naked eye.

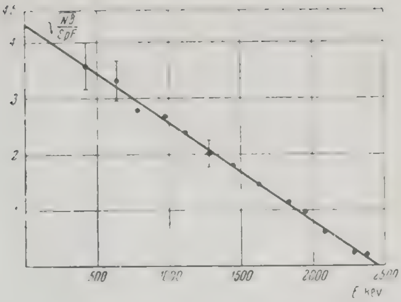

Fig.2. Kurie plot for Pr^{140}.

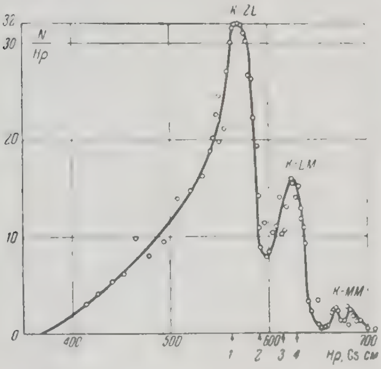

Fig.3. $Nd^{140} \rightarrow Pr^{140}$ Auger electrons. The figures at the arrows along the energy axis indicate the calculated positions of the Auger electron peaks: 1) K-2L with minimal energy $K\text{-}L_IL_I$ for Z = 58, 2) K-2L with maximum energy $K\text{-}L_{III}L_{III}$ for Z = 59, 3) K-LM with minimal energy $K\text{-}L_IM_I$ for Z = 58, 4) K-LM with maximum energy $K\text{-}L_{III}M_V$ for Z = 59. Between 1 and 2 there are 10 more and between 3 and 4 there are 25 more Auger electron peaks of the K-2L and K-LM types, respectively.

Control experiments showed that 120 hours after separation the sample contained only Nd^{140}.

The electron radiation accompanying the decay of Nd^{140} and Pr^{140} was investigated by means of a Ketron type magnetic β-spectrometer. The radius of the central electron trajectory in the instrument was 11 cm; the width of the receiving slit was 0.5 mm. Under these conditions the resolution of the instrument is 0.6%. The film over the counter window passed electrons of > 4-5 kev energy.

We studied the positron spectrum in the range from 0.4 to 3 Mev and the electron spectrum in the range from 12 to 150 kev. The activity of the source used was not high: the counting rate at the maximum of the positron spectrum was 200 pulses/min, while the rate at the peak of the Auger electron line was 180 pulses/min with a background of 70 pulses/min.

On the basis of the results obtained for the positron spectrum we constructed the Kurie plot shown in Fig.2, which proved to be linear in the region above 750 kev. The end-point energy of the positron spectrum is 2470 kev. In the electron spectrum, we observed the K-2L and K-LM Auger electron lines shown in Fig.3. The half-width of these line groups are 9 and 7%. The $K\text{-}L_IL_I$, $K\text{-}L_IL_{II}$, $K\text{-}L_{II}L_{II}$, etc. lines are not resolved with the given instrument resolution. The energies of these lines are not in conflict with those assigned to these electrons from Ce and Pr. No other electron lines were detected. As evaluated from the areas under the peaks, the relative intensities of the Auger electrons and positrons are characterized by

$$I_{K\text{-}2L} : I_{K\text{-}LM} : I_{\beta+} = 10 : 3.2 : 73. \qquad (4)$$

Thus, neglecting $I_{K\text{-}MM}$, we obtain

$$\frac{e_K}{\beta+} = \frac{1.32}{7.3} = 0.182,$$

i.e., a value 9 times greater than that found by Browne et al. From (4) and (1), we obtain 3.6% for the yield of K Auger electrons, i.e., a value ~2.8 times smaller than the expected one.

We agree with Browne et al[8] that the anomalously low number of Auger electrons observed in their experiment was due to apparatus factors. The relatively small number of Auger electrons obtained in our measurements may also be attributed to apparatus error.

As noted above, the source we used was very thin. Still there could be appreciable stopping of electrons in it, which leads to line broadening. A natural source of information on the influence of source thickness is broadening of single conversion lines; unfortunately, no such lines are observed

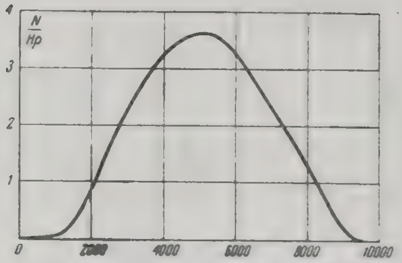

Fig.4. β^+-spectrum of Pr^{140}.

in the decay of Nd^{140} and Pr^{140}. The K-2L Auger group should consist of 12 lines; the separation between the extreme ones is 28 gauss·cm. The experimental line width at half height is 50 gauss·cm. Subtracting 28 gauss·cm, we obtain 22 gauss·cm for the peak located at 570 gauss·cm, i.e., the relative half-width of ~4% The K-2M line is somewhat narrower (~2.2%). Broadening of a line by 2-3% as compared with the apparatus half-width usually does not involve any noticeable change in the area under the line.

Another source of error may be absorption of electrons in the counter window. In our experiments the film over the counter window passed electrons starting with 4-5 kev energy. According to the familiar empirical rule[10], the influence of electron absorption in the counter window can be neglected if the electron energy is 4 times greater than the minimum energy at which electron transmission begins. Thus, according to this rule, electron absorption in the counter window for the K-2L and K-LM lines of Ce and Pr can be considered negligible.

Comparison of the experimental and theoretical values of the K/L intensity ratio for the γ-lines of Er^{168} and Yb^{173}

E_γ	Type transition	K/L ratio	
		exper.	theo.*
79,8 kev Er^{168}	$E2$	0,58	0,76
78,7 kev Yb^{173}	$M1$ ($E2 < 10\%$)	5,2	5,7

*The theoretical K/L values comprise an error of up to 30%. (Refs.11,12)

We carried out an investigation of the isotopes of Tm and Lu under the same conditions as used in investigating the Nd^{140} source.[11,12]

We detected γ-transitions of ~80 kev energy in several of these isotopes. The K conversion lines of these transitions have an energy of about 20 kev, i.e., somewhat lower than the energy of our K-2L electrons. Usually the K line proved to be broadened by 1.5-2% (with an instrument width of 0.6%), but the experimental K/L ratios usually agree with the theoretical values. An appreciable deviation from the theoretical K/L value is observed when the ~20 kev line is not fully separated from the neighboring lines. In two cases the K and L lines were fully resolved from the neighboring lines and hence the experimental K/L ratio obtained in this case can be regarded as the most reliable. We are referring here to the 79.8 kev transition in Er^{168} and the 78.7 kev transition in Yb^{173}.

As will be seen from the accompanying table, the divergences between the experimental and theoretical values of K/L are relatively small. Hence we assume that the probable error in our determination of the e_K/β^+ ratio for $Nd^{140} \rightarrow Pr^{140}$ does not exceed 30%.

The experimental value of e_K/β^+ can be used for determining the yield of K Auger electrons or for determining the value of

1) In order to determine the K Auger yield one must make use of the data of Wilkinson & Hicks that contain a large error; hence the resultant value of the yield - 3.6% instead of 10% - presumably includes a corresponding uncertainty;

2) The value of β^+/K_Σ is determined from the equality $e_K/K_\Sigma = e_K/\beta^+ \cdot \beta^+/K_\Sigma$; solving for β^+/K_Σ and substituting the value of 0.1 for the K Auger electron yield we obtain

$$\beta^+/K_\Sigma = \frac{0.1}{0.182} = 0.55,$$

which agrees within the limits of our apparatus error (~30-40%) with the result that might be expected for the $Nd^{140} \rightarrow Pr^{140} \rightarrow Ce^{140}$ series.

"V.G.Khlopin" Radium Institute,
Academy of Sciences of the USSR

References

1. E.Amaldi, O.D'Agostino, E.Fermi, B.Pontecorvo, R.Rosetti & E.Segre, Proc.Roy.Soc., A149, 522 (1935).
2. B.I.Stover, Phys.Rev., 81, 8 (1951).
3. M.L.Pool & L.L.Quill, Phys.Rev., 53, 437 (1938).
4. I.M.De Wire, M.L.Pool & J.D.Kurbatov, Phys.Rev., 61, 564 (1942).
5. O.Huber, O.Lienhard, P.Scherrer & H.Waffler, Helv.Phys.Acta, 18, 221 (1945).
6. M.L.Perlman, Phys.Rev., 75, 988 (1949).
7. G.Wilkinson & H.G.Hicks, Phys.Rev., 75, 1687 (1949).
8. C.J.Browne, J.O.Rasmussen, I.P.Surls & D.F.Martin, Phys.Rev., 85, 146 (1952).
9. I.Laberrique-Frolow & P.Radvanyi, J.Phys.etRad., 17, 944 (1956).
10. Beta- and Gamm-Ray Spectroscopy, edited by K.Siegbahn, 1955.
11. Iu.Bobrov, K.Gromov, B.Dzhelepov & B.Preobrazhenskii, Izv.AN SSSR, Ser.fiz., 21, 918 (1957). (Trans., Bulletin, 21, No.7, 920.)
12. K.Ia.Gromov, B.S.Dzhelepov & B.K.Preobrazhenskii, Izv.AN SSSR, Ser. fiz., 21, 940 (1957). (Trans., Bulletin, 21, No.7, 942.)

DISTINCTIVE FEATURES OF FORBIDDEN β-TRANSITIONS IN DEFORMED NUCLEI*

- Z.Bokhnatski

As we know, the projection of the total angular momentum of a deformed nucleus on the axis of elongation is a constant of the motion (at least to the extent to which the strong-coupling approximation is valid). Consequently, we have the following selection rules for β and γ transitions with respect to the corresponding quantum number K

$$\Delta K \equiv |K_i - K_f| \leqslant L,$$

where L is the multipole order of the transition. The available experimental data show that K forbiddenness reduces the probability for β or γ transitions by a factor of about 100 ν, where we write $\nu = \Delta K - L$ (for the relative probabilities of K forbidden transitions and an explanation of our notation see Alaga et al[1]).

It is of interest to calculate the probabilities for such transitions by investigating the nondiagonal terms of the nuclear Hamiltonian in the strong-coupling representation. This is of particular interest for forbidden β-transitions, for which K forbiddenness not only reduces the total transition probability, but also changes the shape of the β-spectrum. For an n-fold forbidden β-transition, characterized by operators in which $L = n + 1$, n, and $n - 1$, the K forbiddenness increases the relative contribution to the total transition probability from the operator with $L = n + 1$, which is associated with a unique spectrum. As will be shown using the example of the β^--decay of Er^{171}, this can lead to an almost purely unique spectrum even in cases when the spin and parity selection rules do not place the transition in the class of unique transitions.

In the present article we consider K forbidden β^--decay of nuclei with odd A and odd N. The nucleus is considered to be strictly axially symmetric. This assumption will be discussed at the end of the article.

We write the wave function of the deformed nucleus in the form

$$\Psi^{I_M}_{K\Omega\tau} = \sqrt{\frac{2I+1}{16\pi^2}} \sum_{K'\Omega'\tau'} \varepsilon_{K'\Omega'\tau'} \varphi_{K'\Omega'\tau'} \{\chi_{\Omega'\tau'} D^I_{MK'} + (-1)^{1-\Sigma j'} \chi_{-\Omega'\tau'} D^I_{M-K'}\}.$$

Here φ, χ and D represent vibrational, individual-particle, and rotational motions, respectively. The expansion coefficients $\varepsilon_{K'\Omega'\tau'}$ will be calculated by perturbation theory. (Since we are dealing with the strong-coupling approximation, we may expect that $\varepsilon_{K\Omega\tau} \sim 1$ and that the $\varepsilon_{K'\Omega'\tau'}$ are small for K', Ω' and $\tau' \neq K, \Omega, \tau$.)

The square of the transition matrix element is

$$B(L, I_i \rightarrow I_f) \equiv \sum_{\mu M_f} \left| \langle I_f M_f K_f \Omega_f \tau_f | \hat{\mathfrak{M}}(L, \mu) | I_i M_i K_i \Omega_i \tau_i \rangle \right|^2 =$$

$$= \Bigg| \sum_{K'_f\Omega'_f\tau'_f} \sum_{K'_i\Omega'_i\tau'_i} \varepsilon^*_{K'_f\Omega'_f\tau'_f} \varepsilon_{K'_i\Omega'_i\tau'_f} \left(\int \varphi^*_{K'_f\Omega'_f\tau'_f} \varphi_{K'_i\Omega'_i\tau'_i} \right) \times \Big\{ \langle I_i L K'_i K'_f - K'_i \Big| I_i L I_f K'_f \rangle \int \chi^*_{\Omega'_f\tau'_f} \hat{\mathfrak{M}}'(L, K'_f - K'_i) \chi_{\Omega'_i\tau'_i} +$$

$$+ \langle I_i L K'_i - K'_f - K'_i \Big| I_i L I_f - K'_f \rangle \int \Big[(-1)^{I-\Sigma_j^{-1}} \chi_{-\Omega'_f\tau'_f} \Big]^* \hat{\mathfrak{M}}'(L_1, K'_f - K'_i) \chi_{\Omega'_i\tau'_i} \Big\} \Bigg|^2. \qquad (1)$$

---

*This article was accepted for publication by the Organizing Committee. The paper was not presented at the Conference, since the author was not able to attend.

The matrix elements on the right side of this equation are easily calculated for β^--decay of even-odd nuclei by using Nilsson's[2] wave functions for the odd particle.

It is seen from Eq. (1) that $B(L)$ (and therefore also the transition probability) is determined by the largest $\varepsilon_{K'_f\Omega'_f\tau'_f}\varepsilon_{K'_i\Omega'_i\tau'_i}$ products for which $\Delta K' \leqslant L)$

In calculating the $\varepsilon_{K'\Omega'\tau'}$, therefore we deal only with the perturbation term

$$\hat{U}_1 = -(1-\hat{D})\,E^{(1)}\,(\hat{I}_+\hat{j}_- + \hat{I}_-\hat{j}_+),$$

where $E^{(1)} = \frac{\hbar^2}{2J}$, $\hat{I}_\pm = \hat{I}_1 \pm i\hat{I}_2$, $\hat{j}_\pm = \hat{j}_1 \pm i\hat{j}_2$, $\hat{j}$ is the angular momentum operator of the odd particle and $\hat{D}$ is the projection operator in the $\hat{I}_3\,j_3$ representation. We neglect operators which contain in addition to $\hat{j}$ angular momentum operators $\hat{j}_n$ for other particles outside the last filled shell, as well as terms containing only $\hat{j}_n$ (see, for instance, Ford[3]). These terms excite not only the odd nucleon, but also other particles outside the last filled shell, so that the energy differences $\Delta E \equiv E_{K'\Omega'\tau'} - E_{K\Omega\tau}$ between the levels will be much greater.

The matrix elements of $\hat{U}_1$ are

$$\langle I,\, K\pm 1,\, N,\, \Omega\pm 1,\, \alpha' \,|\hat{U}_1|\, I,\, K,\, N,\, \Omega,\, \alpha\rangle =$$

$$= -E^{(1)}\sqrt{(I\mp K)(I\pm K+1)}\,\langle N,\, \Omega\pm 1,\, \alpha'/\hat{j}\pm|\,N,\, \Omega,\, \alpha\rangle\langle N,\, \Omega\pm 1,\, \alpha'/\hat{j}_\pm\langle N,\, \Omega,\, \alpha\rangle =$$

$$= \sum_{ll'\Lambda\Lambda'\Sigma\Sigma'} a^{\alpha'}_{l'\Lambda'}a^{\alpha}_{l\Lambda}\delta_{ll'}\left\{\sqrt{(l\mp\Lambda)(l\pm\Lambda+1)}\,\delta_{\Sigma,\Sigma'} + \delta_{\Sigma',\pm\frac{1}{2}}\delta_{\Sigma,\mp\frac{1}{2}}\right\}$$

(the notation used here is that of Nilsson[2]).

The value of ΔE is best taken from experiment, but since for the nuclei we shall consider the experimental data are insufficient, we have taken the energy differences between individual-particle levels from Nilsson.

Numerical calculations have been performed for β^--transitions from the 5/2+ ground state of Er^{171} to the 3/2+, 5/2+ and 7/2+ levels of the rotational band of Tm^{171} with K = 1/2 (see accompanying figure). This is a once forbidden β^--transition, since $\Delta I = 0$ or 1 and the parity changes; $\Delta K = 2$, since the ground state of Er^{171} has $K_i = \Omega_i = I_{0i} = 5/2$, while the rotational Tm^{171} have $K_f = \Omega_f = I_{0f} = 1/2$. Therefore for the operators of a once forbidden transition we may write

$$\vec{\sigma}\cdot\mathbf{r}\,(L=0) - \nu = 2; \qquad \mathbf{r},\, \vec{\sigma}\times\mathbf{r},\, \vec{\alpha}\,(L=1) - \nu = 1,\;\; B_{ij}\,(L=2) - \nu = 0.$$

In the first approximation of perturbation theory we obtain

$$\varepsilon_{\frac{5}{2}\frac{5}{2}\alpha=20} = 1, \qquad \varepsilon_{\frac{3}{2}\frac{3}{2}\alpha'=62} = -3.5\cdot 10^{-3} \quad \text{and} \quad \varepsilon_{\frac{3}{2}\frac{3}{2}\alpha'=70} = 4.7\cdot 10^{-3}$$

for Er^{171} and

$$\varepsilon_{\frac{1}{2}\frac{1}{2}\alpha=43} = 1 \quad \text{and} \quad \varepsilon_{\frac{3}{2}\frac{3}{2}\alpha'=42} = 1.9\cdot 10^{-2}.$$

for Tm^{171}.

We take the same $\varepsilon_{K'\Omega'\tau'}$ for the 3/2+, 5/2+ and 7/2+ rotational levels, since the ΔE values for these levels differ little.

The K-allowed matrix element $\int B_{ij}$ gives log ft values of 8.2, 8.5 and 9.2 for the transitions to the 3/2+, 5/2+, and 7/2+ levels, respectively. The contribution from the $\int \mathbf{r}$, $\int \vec{\sigma}\cdot\mathbf{r}$ and $\int \vec{\alpha}$ matrix elements is lower by a factor of about 100, with a log ft value of about 11. The K-twice-forbidden matrix ele-

ment $\int \vec{\sigma} \cdot \mathbf{r}$ contributes virtually nothing to transitions.

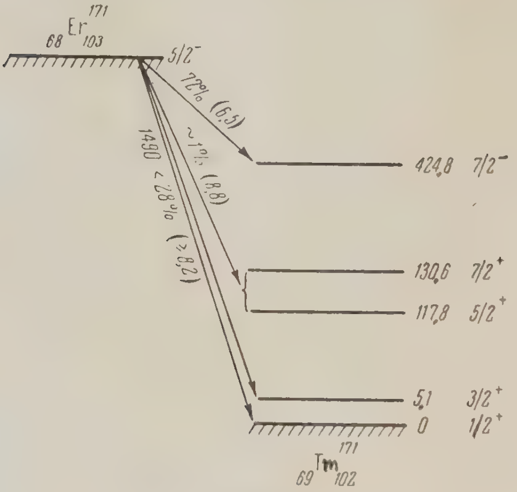

Decay scheme for Er^{171}.

These results are in good agreement with the experimental ft values for the transitions to the 5/2+ and 7/2+ levels.

No experimental data are available on the shape of the spectrum, and it is therefore impossible to verify the prediction that the main contribution to the total transition probability comes from B_{ij}, the operator which leads to the unique spectrum.

An experimental study of the shape of the spectrum would give additional information as to the applicability of the strong coupling approximation.

All possible perturbations which are due to lack of axial symmetry of the nucleus (see, for instance, Ford[3]) connect states in which $|K-\Omega|$ differs by 2. When $|K-\Omega|$ varies by this value, the vibrational energy changes by about 1 Mev and the rotational energy changes by the same order of magnitude. Therefore the energy separations between these levels are of the order of several Mev, which is large compared to the energy separations between the single-particle levels, for which $|K-\Omega|$ remains fixed. In addition, all these perturbations are proportional to the parameter γ (if it is not large) which gives the degree of axial asymmetry; one might therefore expect that they will not greatly influence the probability of the K-forbidden transitions. Rough calculations of the largest values of the product $\varepsilon_{K'_f\Omega'_f\tau'_f}\varepsilon_{K'_i\Omega'_i\tau'_i}$ for which $\Delta K' \leqslant L$ for such perturbations in the case of the β^--decay of Er^{171} give results which are lower by a factor of 100 than the analogous products for $\hat{U}_1$. That means that these perturbations may be neglected. On the other hand, when the K forbiddenness is high, these asymmetric terms may significantly affect the decay probability. This follows from the calculation presented above, since among these terms are operators which change K by two, and for these operators $\Delta K' \leqslant L$ in lower orders of perturbation theory than for $\hat{U}_1$.

In conclusion, I wish to express my deep gratitude to L.A.Sliv, L.K.Peker and V.V.Anisovich for valuable advice as well as to the directors of the Physico-Technical Institute of the Academy of Sciences of the USSR in Leningrad, where the work was performed, for providing the necessary means.

Institute for Nuclear Research,
Polish Academy of Sciences, Cracow

References

1. G.Alaga, K.Alder, A.Bohr & B.Mottelson, Dan.Mat.Fys.Medd., 29, No.9 (1955).
2. S.G.Nilsson, Dan.Mat.Fys.Medd., 29, No.16 (1955).
3. K.Ford, Phys.Rev., 90, 29 (1953).

CONTRIBUTION TO THE THEORY OF INTERNAL CONVERSION. Part I

- V.A.Krutev

1. Introduction

Tralli and Goertzel[1] (hereinafter referred to as TG) have developed a quantum mechanical theory of internal conversion which substantiates earlier results[2] obtained from arguments based on the correspondence principle. The theory has since been improved by taking account of the finite size of the nucleus and screening of the electron wave functions, but this is not related in principle to the theory of internal conversion per se. Taylor and Mott[2] and Davydov[3] have used the correspondence principle to investigate higher perturbation-theory approximations as a means of improving the theory of internal conversion (they included the influence of atomic electrons on the probability for radiative transitions by the nucleus). TG verified these results in their quantum mechanical treatment and showed that an approximation of higher order than the one usually used gives a very small correction (of the order of the fine structure constant) to the probability of γ-radiation. Physically, this correction is due to the internal photoeffect,[2,3] arising from interference between the electromagnetic field of the nuclear transition and the field of the electronic transition.[1] Coish[4] asserts that even this small correction is almost entirely compensated in the internal conversion coefficient (hereinafter ICC) when the approximation for the number of electrons emitted is extended to the same relative order in e^2 as that for the number of photons.

The author again studied the problem of the extent to which higher approximations contribute to the theory of internal conversion. It was found that for low energies and for nuclear transitions of high multipole orders the contributions from higher approximations are not small, as has been asserted, and that the physical interpretation of the correction in terms of the internal photoeffect overlooks the most important process.

In Part I of the present work we investigate the general theory of internal conversion, go to higher approximations of perturbation theory and show certain consequences of the general theory.

In Part II (Ref.5), we shall derive formulas which can be used to calculate the corrections to higher approximations and find the region for which these corrections are substantial.

2. General Theory of Internal Conversion*

Consider a system consisting of a radiation field, a nucleus, and n electrons. In the initial state of the system, the nucleus is in the excited state and the electrons form the ground state of the atom. In the final state, the nucleus is in the ground state and one of the electrons is in the energy continuum. There are no photons in either the initial or final state.

We use i and f to denote the initial and final electron states, write $E_\lambda = E_\lambda^f - E_\lambda^i$, and reckon the energy of the system from $E_0 = \sum_\lambda E_\lambda^i$.

We shall write the wave function of the n-electron system as a product of one-electron wave functions. Indices on these wave functions will denote the complete set of quantum numbers of the electron. We will use the index λ for the initial state and s for the final state; λ will also denote the number of the electron.

---

*The presentation is made as brief as possible where it is similar to that of TG. We will not discuss in detail certain of their omissions which are corrected in this paper.

State	Energy of nucleus	Energy of first electron	...	Energy of n-th electron	Number of quanta	Energy of the system	Probability amplitude
Initial	W_0	E_1^i	...	E_n^i	0	W_0	a_i
Intermediate and final	0	E_1^i	...	E_n^i	1	k	a_{j_0}
Intermediate	W_0	E_1^f	...	E_n^i	1	W_0+k+E_1	a_{j_1}
	W_0	E_1^i	...	E_n^f	1	W_0+k+E_n	a_{j_n}
Final	0	E_1^f	...	E_n^i	0	E_1	a_{f_1}
	0	E_1^i	...	E_n^f	0	En	a_{f_n}

The probability amplitudes are given by the equations

$$i\dot{a}_i = W_0 a_i + \sum_L \int dk \cdot H_{0k}(L) \cdot a_{j_0}(L) + \sum_{\lambda=1}^{n} \sum_{L,s} \int dk \int dE_\lambda H'_{0k}(L,s) \cdot a_{j\lambda}(L,s), \tag{1a}$$

$$i\dot{a}_{j_0}(L) = k a_{j_0}(L) + H_{k0}(L) \cdot a_i + \sum_{\lambda=1}^{n} \sum_{s} \int dE_\lambda \cdot {}^\lambda H_{kE}(L,s) \cdot a_{f_\lambda}(s), \tag{1b}$$

$$i\dot{a}_{j_\lambda}(L,s) = (W_0 + k + E_\lambda)\, a_{j_\lambda}(L,s) + {}^\lambda H'_{k0}(L,s) \cdot a_i + H'_{kF}(L) \cdot \int dE_\lambda \cdot a_{j_\lambda}(s), \tag{1c}$$

$$i\dot{a}_{f_\lambda}(s) = E_\lambda \cdot a_{f_\lambda}(s) + \sum_L \int dk\, {}^\lambda H_{Ek}(L,s) \cdot a_{j_0}(L) + \sum_L \int dk H'_{Ek}(L) \cdot a_{j_\lambda}(L,s), \tag{1d}$$

where the sum $\left(\sum_L\right)$ over the multipoles denotes $\sum_{LM\tau}$ (where τ is the type of multipole). Equations (1c) and (1d) denote a set of *ns* equations.

We will write the matrix elements of H in the same form as did TG. For instance, for the λ-th electron we have

$${}^\lambda H'_{0k}(L,s) = e\left(\frac{2\pi}{k}\right)^{1/2} \int d\tau_\lambda \cdot \Psi^*_\lambda \left[\vec{\alpha}_\lambda A^\tau_{LM}(kr_\lambda) + i\Phi^\tau_{LM}(kr_\lambda)\right] \Psi_s.$$

We apply the Laplace transform[1]

$$L\{a\} = A = \int_0^\infty e^{(i\omega-\eta)t} a(t)\, dt$$

to Eqs.(1a)-(1d) to obtain the following equations (which replace (2a)-(2d) of TG)

$$(W_0-\omega-i\eta)\,A_i=-i-\sum_L\int dk\,H_{0k}(L)\,A_{j0}(L)-\sum_{L\,\lambda s}\int dk\int dE_\lambda\,{}^\lambda H'_{0k}(L,s)\,A_\lambda(L, \tag{2a}$$

$$(k-\omega-i\eta)\,A_{j0}(L)=-H_{k0}(L)\,A_i-\sum_{\lambda s}\int dE_\lambda\,{}^\lambda H_{kE}(L,s)\,A_{f_\lambda}(s), \tag{2b}$$

$$(k+\omega_{0\lambda}-i\eta)\,A_{j\lambda}(L,s)=-{}^\lambda H'_{k0}(L,s)\,A_i-H'_{kE}(L)\int dE_\lambda\cdot A_{f_\lambda}(s), \tag{2c}$$

$$(E_\lambda-\omega-i\eta)\,A_{f_\lambda}(s)=-\sum_L\int dk\,{}^\lambda H_{Ek}(L,s)\,A_{j0}(L)-\sum_L\int dk\,H'_{Ek}(L)\,A_{j_\lambda}(L,s), \tag{2d}$$

where

$$\omega_{0\lambda}=W_0+E_\lambda-\omega.$$

We solve (2a)-(2d) by successive approximation.

In the first approximation for A_j we obtain

$$(k-\omega-i\eta)A_{j0}(L)=-H_{k0}(L)\cdot A_i;$$

$$(k+\omega_{0\lambda}-i\eta)\,A_{j_\lambda}(L,s)=-{}^\lambda H'_{k0}(L,s)\cdot A_i.$$

In the second approximation for A_f we obtain

$$(E_\lambda-\omega-i\eta)\,A_{f_\lambda}(s)=\sum_L {}^\lambda U_{f0}(L,s)\cdot A_i, \tag{3}$$

where (compare with TG)

$${}^\lambda U_{f0}(L,s)=\int dk\left[\frac{{}^\lambda H_{Ek}(L,s)\cdot H_{k0}(L)}{k-\omega-i\eta}+\frac{H'_{Ek}(L)\cdot{}^\lambda H'_{k0}(L,s)}{k+\omega_{0\lambda}-i\eta}\right]-i\pi\,{}^\lambda H^I_{Ek}(L,s)\cdot H_{k0}(L)$$

(here H^I_{Ek} denotes H_{Ek} with the Bessel function in the potential replaced by a Hankel function of the first kind).

Inserting (3) into (2b) and (2c), we obtain A_j in the third approximation, etc.

It is easily shown that A_j in the $(\nu+1)$-st approximation and A_f in the ν-th approximation are given by

$$(k-\omega-i\eta)\,A^{(\nu+1)}_{j_0}(L)=-A_iH^{(\nu+1)}_{k0}(L), \tag{4a}$$

$$(k+\omega_{0\lambda}-i\eta)\,A^{(\nu+1)}_{j_\lambda}(L,s)=-A_i\,{}^\lambda H'^{(\nu+1)}_{k0}(L,s), \tag{4b}$$

$$(E_\lambda-\omega-i\eta)\,A^{(\nu)}_{f_\lambda}(s)=A_i\sum_L {}^\lambda U^{(\nu)}_{f0}(L,s), \tag{5}$$

where

$$H^{(\nu+1)}_{k0}(L)=H^{(1)}_{k0}(L)+i\pi\sum_{\lambda s}{}'H_{kE}(L,s)\sum_{L'}{}^\lambda U^{(\nu)}_{f0}(L',s), \tag{6a}$$

$${}^\lambda H'^{(\nu+1)}_{k0}(L,s)={}^\lambda H'_{k0}(L,s)+i\pi H'_{kE}(L)\sum_{L'}{}^\lambda U^{(\nu)}_{f0}(L',s), \tag{6b}$$

$${}^\lambda U^{(\nu)}_{f0}(L,s)={}^\lambda U^{(2)}_{f0}(L,s)-\pi^2\,{}^\lambda H_{Ek}(L,s)\sum_{\lambda' s'}{}^{\lambda'}H_{kE}(L,s')\sum_{L'}{}^{\lambda'}U^{(\nu-2)}_{f0}(L',s') \tag{6c}$$

$$H^{(1)}_{k0}(L)=H_{k0}(L),\quad U^{(2)}_{f0}(L,s)=U_{f0}(L,s).$$

Inserting (4a) and (4b) into (2a), we obtain A_i in the $(\nu+2)$-nd approximation, namely

$$(W_0 - \omega - i\eta)\, A_i^{(\nu+2)} = -i + A_i \sum_L \int dk \left[\frac{H_{0k}(L)\, H_{k0}(L)}{k - \omega - i\eta} + \sum_{\lambda s} \int dE_\lambda \frac{{}^\lambda H'_{0k}(L, s) \cdot {}^\lambda H'_{k0}(L, s)}{k + \omega_{0\lambda} - i\eta} \right] +$$

$$+ i\pi A_i \sum_{L\lambda s} {}^\lambda U_{0f}(L, s) \sum_{L'} {}^\lambda U_{f0}^{(\nu)}(L', s),$$

where ${}^\lambda U_{0f}$ is obtained from ${}^\lambda U_{f0}$ by taking the complex conjugate and changing the sign of η (compare with Coish4).

The integral over k is calculated in the Appendix. Finally, in the $(\nu + 2)$-nd approximation, we obtain

$$A_i^{(\nu+2)} = -\frac{i}{W - \omega - i(\eta + \gamma_1 + \gamma_2^{(\nu+2)})}, \tag{7}$$

where

$$\gamma_1 + \gamma_2^{(\nu+2)} = \pi \sum_L |H_{0\omega}(L)|^2 + \pi \operatorname{Re} \sum_{L\lambda s} {}^\lambda U_{0f}(L, s) \sum_{L'} {}^\lambda U_{f0}^{(\nu)}(L', s), \tag{8}$$

$$W = W_0 + \delta W,$$

$$\delta W = -\sum_{L\lambda s} \int dk \frac{(k+\omega_{0\lambda}) \int dE_\lambda |{}^\lambda H'_{0k}(L, s)|^2}{(k + \omega_{0\lambda})^2 + \eta^2} + \pi \operatorname{Im} \sum_{L\lambda s} {}^\lambda U_{0f} \sum_{L'} {}^\lambda U_{f0}^{(\nu)}.$$

Here δW is the displacement of the nuclear level due to the presence of the radiation field and the electrons.

Inserting (7) into (4a) and (5) and taking the inverse Laplace transform of the amplitudes, we obtain

$$a_i^{(\nu+2)}(t) = \exp[-iWt - (\gamma_1 + \gamma_2^{(\nu+2)})\, t],$$

$$a_{j0}^{(\nu+1)}(L, t) = \left[\frac{1}{k - W + i(\gamma_1 + \gamma_2^{(\nu+2)})} \right] \cdot H_{k0}^{(\nu+1)}(L) \cdot [e^{-ikt} - a_i(t)],$$

$$a_{f_\lambda}^{(\nu)}(s, t) = \left[-\frac{1}{E_\lambda - W + i(\gamma_1 + \gamma_2^{(\nu+2)})} \right] \cdot \sum_L {}^\lambda U_{f0}^{(\nu)}(L, s) \cdot [e^{-iE_\lambda t} - a_i(t)].$$

Thus N_q, the number of photons, and N_e, the number of electrons, are given by

$$N_q^{(\nu+1)} = \sum_L \int dk\, |a_{j_0}(t = \infty)|^2 = \frac{\pi}{\gamma_1 + \gamma_2^{(\nu+2)}} \sum_L |H_{k0}^{(\nu+1)}(L)|^2, \tag{9a}$$

$$\sum_\lambda {}^\lambda N_e^{(\nu)} = \sum_{\lambda s} \int dE_\lambda\, |a_{f_\lambda}(t = \infty)|^2 = \frac{\pi}{\gamma_1 + \gamma_2^{(\nu+2)}} \sum_{\lambda s} \Big| \sum_L {}^\lambda U_{f0}^{(\nu)}(L, s) \Big|^2, \tag{9b}$$

where $k = E_\lambda = W$ and $\gamma_1 + \gamma_2^{(\nu+2)}$ is given in Eq.(8).

We note here that in contradiction to the assertion made by Coish, the conservation equation $N_q + N_e = 1$ cannot be satisfied in any finite approximation owing to the fact that the method of successive approximations is used to solve the problem.

The probability per unit time that the atom will radiate a photon is given, assuming a narrow level, by

$$\Gamma_\gamma^{(\nu)} = \frac{d}{dt} \sum_L \int dk\, |a_{j_0}^{(\nu)}(L, t)|^2 = 2\pi \sum_L |H_{k0}^{(\nu)}(L)|^2;$$

For instance, for the case of a single multipole, the radiation width is

$$\Gamma_\gamma^{(\nu)} = 2\pi\, |H_{k0}(L)|^2 \cdot \chi(\nu),$$

where

$$\chi(\nu) = \left|1 - \pi^2 \sum_{\lambda s} {}^{\lambda}H_{kE}(L, s)\, {}^{\lambda}H_{Ek}^{I(\nu-1)}(L, s)\right|^2, \qquad (10)$$

$${}^{\lambda}H_{Ek}^{I(\nu)}(L, s) = {}^{\lambda}H_{Ek}^{I}(L, s) - \pi^2\, {}^{\lambda}H_{Ek}(L, s) \sum_{\lambda' s'} {}^{\lambda'}H_{kE}(L, s')\, {}^{\lambda'}H_{Ek}^{I(\nu-2)}(L, s') \qquad (11)$$

$$\chi(1) = 1.$$

Thus χ is a factor which gives the ratio between the probabilities for γ-emission by the atom and by the "bare" nucleus. In the case of isomers, χ may play the role of a noticeable "allowing" factor (see Part II).

3. Discussion of the Results

Physical meaning of the higher approximations

Let us separate out from N_q and N_e the terms corresponding to the usual approximation and divide the higher-order corrections into two parts which we shall call the "interference" part and the "quadratic" part. We thus write

$$\widetilde{N}_q^{(\nu)} = N_q^{(\nu,\nu'')} \frac{\gamma_1 + \gamma_2^{(\nu'')}}{\pi} = \sum_L |H_{k0}^{(1)}(L)|^2 + 2\operatorname{Re} \sum_{L\lambda s} \left\{ i\pi H_{k0}^{(1)*}(L)\, {}^{\lambda}H_{kE}(L, s) \sum_{L'} U_{j0}^{(\nu-1)}(L', s) \right\} +$$
$$+ \pi^2 \sum_L \left| \sum_{\lambda s} {}^{\lambda}H_{kE}(L, s) \sum_{L'} {}^{\lambda}U_{j0}^{(\nu-1)}(L', s) \right|^2, \qquad (12a)$$

$$\sum_{\lambda} {}^{\lambda}\widetilde{N}_e^{(\nu')} = \sum_{\lambda} {}^{\lambda}N_e^{(\nu',\nu'')} \cdot \frac{\gamma_1 + \gamma_2^{(\nu'')}}{\pi} = \sum_{\lambda s} \left| \sum {}^{\lambda}U_{j0}^{(2)}(L, s) \right|^2 -$$
$$- 2\operatorname{Re} \left\{ \sum_{\lambda s} \pi^2 \sum_L U_{j0}^{(2)*}(L, s) \cdot \sum_L {}^{\lambda}H_{Ek}(L, s) \sum_{\lambda' s'} {}^{\lambda'}H_{kE}(L, s') \sum_{L'} {}^{\lambda'}U_{j0}^{(\nu-2)}(L', s') \right\} +$$
$$+ \pi^4 \sum_{\lambda s} \left| \sum_L {}^{\lambda}H_{Ek}(L, s) \sum_{\lambda' s'} {}^{\lambda'}H_{kE}(L, s') \sum_{L'} {}^{\lambda'}U_{j0}^{(\nu-2)}(L', s') \right|^2. \qquad (12b)$$

For simplicity, let us restrict our consideration here to the case of a single multipole and a single K electron.* For the K electron, s-summation becomes the sum over the two possible types of final states. Since the contribution of the second type ($j = l - 1/2$) to U_{j0} is much smaller than that of the first (we are interested in relatively low energies), we may drop $\sum_s$. Then for the third approximation for N_q and the fourth for N_e, we have

$$\widetilde{N}_q = |H_{k0}|^2 \cdot \{1 - 2\operatorname{Re}(\pi^2 H_{kE} H_{Ek}^I) + \pi^4 |H_{kE} H_{Ek}^I|^2\},$$
$$\widetilde{N}_e = |H_{k0}|^2 \cdot \pi^2 |H_{Ek}^I|^2 \cdot \{1 - 2\operatorname{Re}(\pi^2 H_{Ek} H_{kE}) + \pi^4 |H_{Ek}|^2\}.$$

Noting that the integrals over angles are the same in H_{Ek} and H_{Ek}^I and that the radial integrals differ only in that the Bessel function in the potential is replaced by a Hankel function of the first kind, we have

$$H_{Ek} = \operatorname{Re} H_{Ek}^I,$$

---

*A similar analysis for two K electrons is given in Part II.

where the symbol Re (and later also Im) pertains only to the radial integrals.

Writing

$$\delta = \frac{\operatorname{Re} H^I_{Ek}}{\operatorname{Im} H^I_{Ek}}$$

and recalling that the ICC for a single K electron is

$$\beta = \pi^2 \left| H^I_{Ek} \right|^2,$$

we have

$$\widetilde{N}_q = \left| H_{k0} \right|^2 \cdot \left\{ 1 - 2\frac{\beta\delta^2}{1+\delta^2} + \frac{\beta^2\delta^2}{1+\delta^2} \right\}, \tag{13a}$$

$$\widetilde{N}_e = \left| H_{k0} \right|^2 \cdot \beta \cdot \left\{ 1 - 2\frac{\beta\delta^2}{1+\delta^2} + \left(\frac{\beta\delta^2}{1+\delta^2} \right)^2 \right\}. \tag{13b}$$

The processes of photon emission and internal conversion are shown graphically in Fig.1. These diagrams should not be confused, for instance, with diagrams which represent the intrinsic electron energy and the like, since the intermediate state is in our case determinate (it is either the initial or final state of the electron).

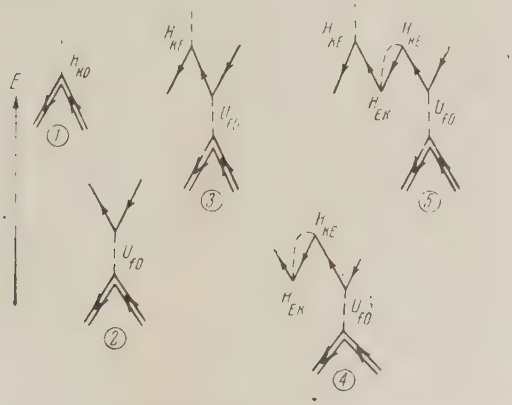

Fig.1.

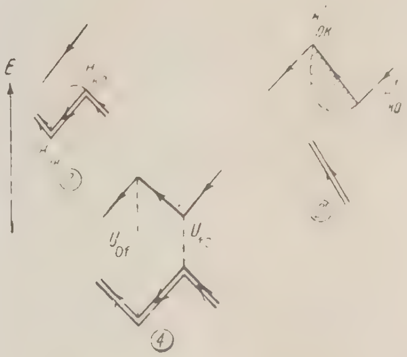

Fig.2.

Fig.1. γ-ray emission and internal conversion. The solid lines represent electrons, the double lines represent nuclei, and the dotted lines represent photons. The E direction denotes excited states, while the opposite direction denotes the ground state. The circled numbers are both the number of the diagram and of the order of the approximation.

Fig.2. Same as Fig.1. The hatched area means that the energy is not definite.

Diagrams 3 and 5 correspond to the correction terms to the fifth order in N_q with the above simplifying assumptions. Diagram 3, for instance, represents the following process: the electron, raised to the energy continuum by interacting with the nucleus (U_{f0}) then drops back to the K shell emitting a photon (H_{kE}). This process leads to two types of correction terms. The second term in (13a) is an interference term (giving the interference between processes 1 and 3) and describes the photon from process 1 absorbed by the electron which is raised to the continuum, and thus characterizes the internal photoeffect (the same graph as 2). The third term in (13a) describes additional emission of γ-rays due to the presence of the electron. Because in the first approximation the internal conversion process is independent of γ-emission by the nucleus, a sort of "electron bridge" is formed, over which the excited nucleus can be de-excited by radiating gammas ("virtual conversion").

If the ICC is small, the corrections are small and the third term in (13a) is much smaller than the second, so that $\tilde{N}_q$ is several times less than $H_{k0}{}^2$. This is the correction due to the photoeffect which was treated both by Taylor and Mott[2] and by Davydov[3].

It is readily seen from (13a), however, that the sign of the correction changes for large conversion coefficients. In Part II we shall evaluate the region in which the additional photon emission may be even greater than the emission of a "bare" nucleus.

The interpretation of the terms in (13b) is similar. For instance, the second term is the effective interference between the electron fields of diagrams 2 and 4, and gives the number of conversion electrons which drop back into the discrete spectrum with the emission of a photon.

It is interesting to note that (13a) and (13b) show that only the interference terms are compensated in the expression for the ICC, Coish to the contrary.

Fig.2 shows diagrams of the processes characterizing the decay amplitude A_i of the initial state up to fourth order. Diagram 2' illustrates a process in which energy is not conserved in the intermediate state. This process contributes only to displacement of the level in energy (see Appendix).

We note that large corrections in the higher approximations do not mean that perturbation theory is inapplicable. The largest corrections come from the addition of the nucleus-electron-field process $H_{kE}U_{f0}$ (diagram 3 of Fig.1) to the nucleus-field process H_{k0} (diagram 1). Process 3 is a process of higher order than 1, but the small value of the fine structure constant α in process 3 can be compensated by the high probability for the nucleus-electron process U_{f0}, i.e., the internal conversion process. Higher-order processes make only relatively minor contributions, since they are merely successive superpositions of the electron-field process H_{kE} in which the smallness of α is not compensated.

"Multipole exchange"

As can be seen from the presence of the sum $\sum_{\lambda'}$ in Eq.(6), the conversion transitions of individual electrons are not independent in higher approximations. There arises a sort of "multipole exchange" of energies (2^L quantum-field exchange) between electron 1 which originally interacts with the nucleus, and another electron 2 of the discrete spectrum (Fig.3). Electron 1 then drops back into the discrete spectrum, while 2 is raised to the continuum.

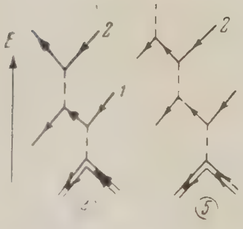

Fig.3. Same as Fig.1, but with "multipole exchange".

This effect can also be treated by the correspondence principle. One considers any electron, assuming that it undergoes transition from the discrete spectrum to the continuum under the influence of the total field due to the original nuclear multipole plus all the additional electromagnetic multipole fields produced in each of the electron transitions. The electrons may be said to "screen" the field of the multipole in the nucleus.

Atomic shell and multipole order

Let us assume that the nuclear selection rules forbid all multipole transitions of the nucleus other than $L = L^{\circ}$ (by L° we denote both the type and angular momentum of the multipole, but we shall not write out $\sum_{M^{\circ}}$ explicitly).

Let us fix the set λ (or s) for some electron. This fixes the z-component of the angular momentum of the electron, which is equivalent to choosing a preferred direction.

Then from (9a) and (6a) we have

$$N_q^{(\nu+1)}(L^0) = \frac{\pi}{\gamma_1 + \gamma_2^{(\nu+2)}} \left\{ \left|\widetilde{H}_{k0}^{(\nu+1)}(L^0)\right|^2 + \sum_{L \neq L} \left| \pi \sum_s^{\lambda} H_{kE}(L, s)^{\lambda} \widetilde{U}_{f0}^{(\nu)}(L^0, s) \right|^2 \right\}, \tag{14}$$

where

$$\left.\begin{aligned} \widetilde{H}_{k0}^{(\nu+1)}(L) &= H_{k0}^{(1)}(L) + i\pi \sum_s {}^{\lambda}H_{kE}(L, s)^{\lambda}\widetilde{U}_{f0}^{(\nu)}(L, s), \\ {}^{\lambda}\widetilde{U}_{f0}^{(\nu)}(L, s) &= {}^{\lambda}U_{f0}^{(2)}(L, s) - \pi^2 \sum_{L'} {}^{\lambda}H_{Ek}(L', s) \sum_{s'} {}^{\lambda}H_{kE}(L', s')^{\lambda}\widetilde{U}_{f0}^{(\nu-2)}(L, s') \end{aligned}\right\} \tag{14a}$$

The second term of (14) gives the contribution from the neighboring multipoles for which L ≠ L^0 to the γ-radiation of the atom (compare Taylor and Mott[2]). The appearance of such an "electronic contribution" is related to electron transitions with the absorption and successive emission of photons $({}^{\lambda}H_{kE}(L, s) \cdot {}^{\lambda}H_{Ek}^{I(\nu)}(L^0, s))$ and is easily explained by the fact that the angular momentum of the electron in both the initial and final states is not uniquely defined by a vector fixed in space.

If we sum or average in (14) over the initial electron states, the contribution from neighboring multipoles vanishes as a result of the orthogonality of the Clebsch-Gordan coefficients in the matrix elements of the electron transitions. Physically this means that the interference of radiation from electrons whose magnetic quantum numbers are of the opposite sign cancels out the admixture (the phase of such radiation, which may be allowed by other selection rules, differs by an odd multipole of π).

It follows from (9b) and (6c) that

$${}^{\lambda}N_e^{(\nu)}(L^0) = \frac{\pi}{\gamma_1 + \gamma_2^{(\nu+2)}} \times \sum_s \left| {}^{\lambda}U_{f0}^{(2)}(L^0, s) - \pi^2 \sum_L^{\lambda} H_{Ek}(L, s) \sum_{s'}^{\lambda} H_{kE}(L, s')^{\lambda}\widetilde{U}_{f0}^{(\nu-2)}(L^0, s') \right|^2,$$

so that these other multipoles contribute also* to N_e in the sense that the final electron state may be formed by emission and absorption $({}^{\lambda}H_{Ek}{}^{\lambda}H_{kE})$ of photons of multipole order L ≠ L^0. What has been said above about the summation is true also about N_e.

Thus the admixture from the other multipoles does not affect the ICC. If there is a preferred direction, however, as for instance in the case of angular γ-γ or γ-e correlation, the electronic admixture may be appreciable.

The author desires to express his gratitude to B.S.Dzhelepov, V.B.Berestetskii, L.A.Sliv, and Iu.V.Novozhilov for discussing the results of this work.

Appendix

Calculating the integral $\int_0^{\infty} dk \left[\frac{H_{0k}(L) H_{k0}(L)}{k - \omega - i\eta} + \sum_{\lambda, s} \frac{{}^{\lambda}H'_{0k}(L, s)^{\lambda}H'_{k0}(L, s)}{k + \omega_{0\lambda} - i\eta} \right]$.

In this integral $H_{0k}H_{k0}$ is the product of nuclear matrix elements, and ${}^{\lambda}H'_{0k} \cdot {}^{\lambda}H'_{k0}$ — is the product of electron matrix elements (the symbol $\sum_s$ also includes $\int dE_{\lambda}$). Therefore the second half of the integral can obviously not be accounted for by extending the lower limit of the first half to $-\omega$, and this

---

*This admixture to N_e has been mentioned by Coish[4]. His expression for the admixture terms (Σ_L) in the ICC is, however, incorrect.

is true also of a similar integral calculated in Appendix B, Section 2 of TG.

Each part of the integral, however, can be calculated separately:

$$\int_0^\infty dk\,\frac{|H_{0k}(L)|^2}{k-\omega-i\eta} = i\pi\,|H_{0\omega}(L)|^2 + \int_0^\infty dk\,\frac{(k-\omega)\,|H_{0k}(L)|^2}{(k-\omega)^2+\eta^2} = i\pi\,|H_{0\omega}(L)|^2 .$$

$$I = \sum_{\lambda s}\int_0^\infty dk\,\frac{|{}^{\lambda}H'_{0k}(L,s)|^2}{k+\omega_{0\lambda}-i\eta} = \sum_{\lambda s}\int_0^\infty dk\,\frac{(k+\omega_{0\lambda})\,|{}^{\lambda}H'_{0k}|^2}{(k+\omega_{0\lambda})^2+\eta^2} + i\sum_{\lambda s}\int_0^\infty dk\,\frac{\eta\,|{}^{\lambda}H'_{0k}|^2}{(k+\omega_{0\lambda})^2+\eta^2} .$$

As $\eta \to 0$, the second integral in I vanishes, and only the real first integral remains. This gives a shift of the energy level, but contributes nothing to the decay probability of the initial state.

We note that in Section 2 we have disregarded integrals in the sense of the principal part. This is valid for energies not too close to the electron binding energy.

Physical Institute
Leningrad State University

References

1. N.Tralli & Goertzel, Phys.Rev., 83, 399 (1951).
2. H.Taylor & N.Mott, Proc.Roy.Soc., A 142, 215 (1933).
3. A.Davydov, Zhur.eksp.i teor.fiz., 10, 865 (1940).
4. H.R.Coish, Phys.Rev., 84, 164 (1951).
5. V.A.Krutov & K.Müller, Present issue of the Bulletin, p.168.

CONTRIBUTION TO THE THEORY OF INTERNAL CONVERSION. Part II*

- V.A.Krutov and K.Müller

To illustrate the possible magnitude of effects described by higher perturbation-theory approximations, let us consider in more detail the case of a single multipole and the K shell.

For N_q and N_e, we have

$$N_q(\nu, \nu'') = Q(\nu'') \cdot \left| 1 - \pi^2 \sum_{\lambda s} {}^{\lambda}H_{kE}(s) {}^{\lambda}H_{Ek}^{I\,(\nu-1)}(s) \right|^2, \tag{1}$$

$$N_e(\nu', \nu'') = Q(\nu'') \cdot \pi^2 \sum_{\lambda s} \left| {}^{\lambda}H_{Ek}^{I}(s) - \pi^2 {}^{\lambda}H_{Ek}(s) \sum_{\lambda' s'} {}^{\lambda'}H_{kE}(s') {}^{\lambda'}H_{Ek}^{I\,(\nu'-2)}(s') \right|^2, \tag{2}$$

where

$$Q(\nu'') = \frac{\pi}{\gamma_1 + \gamma_2^{(\nu'')}} \cdot |H_{k0}|^2.$$

${}^{\lambda}H_{Ek}^{I\,(\nu)}$ is defined in Eq.(11) of Part I; ν, ν', and ν'' denote the order of the approximation, and $|H_{k0}|^2$ infers both summation and averaging over the nuclear states.

The matrix elements which are corrections to the usual expression are H_{Ek}^{I}, H_{Ek}, and H_{kE}. Let us consider these.

For conciseness we shall restrict our consideration to magnetic multipoles (the procedures and results for electric multipoles are similar). Let us choose the potential in agreement with Tralli and Goertzel (hereinafter TG), namely,

$$\mathbf{B}_{LM} = i\sqrt{\frac{2}{\pi}}\,\omega \left[\frac{1}{L(L+1)}\right]^{1/2} h_L(\omega r)\,\mathbf{L} Y_L^M,$$

where

$$\mathbf{L} = -i(\mathbf{r} \times \nabla), \quad h_L = \sqrt{\frac{\pi}{2\omega r}}\, H_{L+\frac{1}{2}}^{(1)}(\omega r),$$

($H_{L+\frac{1}{2}}^{(1)}$ is a Hankel function of the first kind).

Further, we use the notation of Rose[3] to write out the electron wave functions, which are then

$$\Psi(s) = \begin{pmatrix} -if_{\varkappa}\chi_{-\varkappa}^{\mu} \\ g_{\varkappa}\chi_{\varkappa}^{\mu} \end{pmatrix}, \quad \text{and} \quad \Psi(\lambda) = \begin{pmatrix} -if_{\varkappa'}\chi_{-\varkappa'}^{\mu'} \\ g_{\varkappa'}\chi_{\varkappa'}^{\mu'} \end{pmatrix}.$$

Then with Rose we obtain**

$${}^{\lambda}H_{Ek}^{I}(s) = 2i\left[\frac{\alpha\omega}{L(L+1)}\right]^{1/2} \cdot \int d\tau \Psi^*(s) \cdot h_L \boldsymbol{\alpha} \mathbf{L} Y_L^M \cdot \Psi(\lambda) = R(s, \lambda) \cdot T(s, \lambda), \tag{3}$$

where

$$R(s, \lambda) = \int_0^{\infty} (f_{\varkappa} g_{\varkappa'} + g_{\varkappa} f_{\varkappa'})\, h_L r^2\, dr,$$

$$T(s, \lambda) = -2\left[\frac{\alpha\omega}{L(L+1)}\right]^{1/2} \cdot (\varkappa + \varkappa')(-\varkappa\mu \,|\, Y_L^M \,|\, \varkappa'\mu').$$

---

*The present paper is a continuation of the preceding one.[1] All notations not explained herein are the same as in Part I.

**We shall use relativistic units in which $\hbar = m_0 = c = 1$.

For a given shell $R(s, \lambda)$ depends only on the quantum number $\varkappa$.

The matrix element ${}^{\lambda}H_{Ek}(s)$ differs from ${}^{\lambda}H^{I}_{Ek}(s)$ in that the Hankel function of the first kind in the potential is replaced by a Bessel function $(J_{L+1/2})$.

Taking into account the fact that the radial wave functions f and g are real and that

$$J_{L+1/2} = \frac{1}{2}\left[H^{(1)}_{L+1/2} + H^{(1)*}_{L+1/2}\right] = \operatorname{Re} H^{(1)}_{L+1/2},$$

we have

$$ {}^{\lambda}H_{Ek}(s) = \operatorname{Re} R(\varkappa)\cdot T(s, \lambda); \tag{4}$$

${}^{\lambda}H_{kE}(s)$ is obtained from ${}^{\lambda}H_{Ek}(s)$ by interchanging the wave functions and replacing the potential by its complex conjugate, so that

$$ {}^{\lambda}H_{kE}(s) = \operatorname{Re} R(\varkappa)\cdot T^{*}(s, \lambda). \tag{5}$$

Let us also rewrite $\gamma_2^{(\nu'')}$. We have

$$ {}^{\lambda}U_{0f}(s) = i\pi\left({}^{\lambda}H^{II}_{Ek}(s)\right)^{*}\cdot H^{*}_{k0} = i\pi R(\varkappa)\, T^{*}(s, \lambda)\, H^{*}_{k0},$$

where ${}^{\lambda}H^{II}_{Ek}(s)$ denotes ${}^{\lambda}H^{I}_{Ek}(s)$ with the Hankel function of the first kind in the potentials replaced by a Hankel function of the second kind (compare Coish[4]).

Therefore

$$\gamma_2^{(\nu'')} = -\pi\,|H_{k0}|^2\cdot \operatorname{Re}\sum_{\lambda s}\left\{\pi^{2\lambda}\widetilde{H}^{I}_{Ek}(s)^{\lambda}\cdot H^{I\,(\nu)}_{Ek}(s)\right\},$$

where

$$ {}^{\lambda}\widetilde{H}^{I}_{Ek} = R(\varkappa)\cdot T^{*}(s, \lambda). \tag{6}$$

Eqs.(1) and (2) contain a sum of the form

$$\pi^2\sum_{\lambda s}{}^{\lambda}H_{kE}\,{}^{\lambda}H^{I}_{Ek}, \quad \pi^2\sum_{\lambda s}{}^{\lambda}H_{kE}\,{}^{\lambda}H_{Ek}, \quad \pi^2\sum_{\lambda s}{}^{\lambda}\widetilde{H}^{I}_{Ek}\,{}^{\lambda}H^{I}_{Ek}, \quad \pi^2\sum_{\lambda s}{}^{\lambda}\widetilde{H}^{I}_{Ek}\,{}^{\lambda}H_{Ek}. \tag{7}$$

The internal conversion coefficient (hereinafter ICC) in the usual approximation is given by

$$\beta = \pi^2\sum_{\lambda s}\left|{}^{\lambda}H^{I}_{Ek}(s)\right|^2. \tag{8}$$

Thus (7) and (8) differ only in the radial integrals and therefore the summation in (7) can be performed in the same way as is usually done when calculating the ICC (see, for instance, Rose[3]).

Let us separate the ICC into parts, each associated with a different value of the quantum number $\varkappa$. We thus write

$$\beta = \sum \beta_{\varkappa}.$$

Introducing the notation $\delta_{\varkappa} = \frac{\operatorname{Re} R(\varkappa)}{\operatorname{Im} R(\varkappa)}$, we may use (3) and (6) to obtain

$$\left.\begin{aligned}
\pi^2 \sum_{\lambda s} {}^{\lambda}H_{kE}(s)\cdot{}^{\lambda}H^{I}_{Ek}(s) &= \sum_{\varkappa} \beta_{\varkappa} \frac{\delta_{\varkappa}}{\delta_{\varkappa}-i}\,,\\
\pi^2 \sum_{\lambda s} {}^{\lambda}H_{kE}(s)\cdot{}^{\lambda}H_{Ek}(s) &= \sum_{\varkappa} \beta_{\varkappa} \frac{\delta^2_{\varkappa}}{1+\delta^2_{\varkappa}}\,,\\
\pi^2 \sum_{\lambda s} {}^{\lambda}\widetilde{H}^{I}_{Ek}(s)\,{}^{\lambda}H^{I}_{Ek}(s) &= \sum_{\varkappa} \beta_{\varkappa}\cdot \frac{\delta_{\varkappa}+i}{\delta_{\varkappa}-i}\,,\\
\pi^2 \sum_{\lambda s} {}^{\lambda}\widetilde{H}^{I}_{Ek}(s)\,{}^{\lambda}H_{Ek}(s) &= \sum_{\varkappa} \beta_{\varkappa} \frac{\delta_{\varkappa}}{\delta_{\varkappa}-i}\,.
\end{aligned}\right\} \tag{9}$$

Inserting (9) into (1) and (2), we have

$$N_{\mathrm{q}}(\nu,\nu'') = Q(\nu'')\cdot\left|1-\sum_{\varkappa}\beta_{\varkappa}\frac{\delta_{\varkappa}}{\delta_{\varkappa}-i}\sum_{n=0}^{\frac{\nu}{2}-\frac{3}{2}}\left(-\sum_{\varkappa}\beta_{\varkappa}\frac{\delta^2_{\varkappa}}{1+\delta^2_{\varkappa}}\right)^n\right|^2, \tag{10a}$$

$$N_{\mathrm{e}}(\nu',\nu'') = Q(\nu'')\cdot\sum_{\varkappa}\beta_{\varkappa}\cdot\left|1-\frac{\delta_{\varkappa}}{\delta_{\varkappa}+i}\sum_{\varkappa}\beta_{\varkappa}\frac{\delta_{\varkappa}}{\delta_{\varkappa}-i}\sum_{n=0}^{\frac{\nu'}{2}-2}\left(-\sum_{\varkappa}\beta_{\varkappa}\frac{\delta^2_{\varkappa}}{1+\delta^2_{\varkappa}}\right)^n\right|^2, \tag{10b}$$

$$Q(\nu'') = \frac{1}{1-\mathrm{Re}\left\{\sum_{\varkappa}\beta_{\varkappa}\frac{\delta_{\varkappa}+i}{\delta_{\varkappa}-i}-\left(\sum_{\varkappa}\beta_{\varkappa}\frac{\delta_{\varkappa}}{\delta_{\varkappa}-i}\right)^2\sum_{n=0}^{\frac{\nu''}{2}-3}\left(-\sum_{\varkappa}\beta_{\varkappa}\frac{\delta^2_{\varkappa}}{1+\delta^2_{\varkappa}}\right)^n\right\}}\,. \tag{10c}$$

In the case of a single K electron, $\beta_{\varkappa}$ in (10) is everywhere replaced by $\beta_{\varkappa}/2$.

Elimination of the "multipole exchange" effect of two electrons in the K shell leads to replacement of $\beta_{\varkappa}$ by $\beta_{\varkappa}/2$ in $\sum\limits_{n}$ and to insertion of 1/2 in front of $\sum\limits_{n}$ for N_{e} and Q.

As was already noted in Part I, large corrections in higher approximations do not mean that perturbation theory cannot be used to solve the problem. In order again to clarify the situation, let us go to the "infinite order approximation" in (10) (we emphasize that we do this only to illustrate the point, assigning no real meaning to this procedure).

As a rule condition $\sum\limits_{\varkappa}\beta_{\varkappa}\dfrac{\delta^2_{\varkappa}}{1+\delta^2_{\varkappa}} \ll 1$ is fulfilled ($\delta_{\varkappa} \ll 1$). Then the sums over n in Eq.(10) converge (they are a geometric series) and we have

$$N_{\mathrm{q}}(\infty) = Q(\infty)\cdot\left|1-\frac{\sum\limits_{\varkappa}\beta_{\varkappa}\frac{\delta_{\varkappa}}{\delta_{\varkappa}-i}}{1+x}\right|^2 = Q(\infty)\cdot\frac{1+y^2}{(1+x)^2}\,. \tag{11a}$$

$$N_{\mathrm{e}}(\infty) = Q(\infty)\cdot\sum_{\varkappa}\beta_{\varkappa}\left|1-\frac{\frac{\delta_{\varkappa}}{\delta_{\varkappa}+i}\sum\limits_{\varkappa}\beta_{\varkappa}\frac{\delta_{\varkappa}}{\delta_{\varkappa}-i}}{1+x}\right|^2 = Q(\infty)\cdot\left[\sum_{\varkappa}\beta_{\varkappa}-\frac{(x^2+y^2)(2+x)}{(1+x)^2}\right]. \tag{11b}$$

$$Q(\infty) = \frac{1}{1 - \mathrm{Re}\left\{\sum_\varkappa \beta_\varkappa \frac{\delta_\varkappa + i}{\delta_\varkappa - i} - \frac{\left(\sum_\varkappa \beta_\varkappa \frac{\delta_\varkappa}{\delta_\varkappa - i}\right)^2}{1+x}\right\}} = \frac{1}{1 + \sum_\varkappa \beta_\varkappa - 2x + \frac{x^2 - y^2}{1+x}}, \qquad \text{(11c)}$$

where

$$x = \sum_\varkappa \beta_\varkappa \frac{\delta_\varkappa^2}{1+\delta_\varkappa^2}, \qquad y = \sum_\varkappa \beta_\varkappa \frac{\delta_\varkappa}{1+\delta_\varkappa^2}.$$

Simple algebraic operations show that the conservation equation is fulfilled exactly in the infinite order approximation:

$$N_q(\infty) + N_e(\infty) = 1.$$

Let us now evaluate the region in which the higher order corrections may be large.

Let us assume as an approximation that $p \ll \alpha z \ll 1$, where p is the momentum of the electron in the continuum. Then the formulas given by Rose et al.,[5] for the ICC in the K shell can be used to obtain the simple expression*

$$\beta_L \approx 8\pi\alpha \frac{(\alpha z)^{2L+2}}{\omega^{2L+1}} - \frac{[(2L-1)!!]^2}{2L+1} \left\{(L+1)\left|R(\varkappa)\right|^2_{\varkappa=-L} + L\left|R(\varkappa)\right|^2_{\varkappa=L+1}\right\}, \qquad \text{(12)}$$

where

$$\mathrm{Re}\, R(\varkappa)\Big|_{\varkappa=\left\{\begin{smallmatrix}-L\\L+1\end{smallmatrix}\right.} = \frac{\omega}{\alpha z} 2^k \sum_{n=0}^{\infty} \frac{(-2)^n}{n!} \Gamma_0(n)\,(n+k+1-L)\cdot\varphi_n^\pm,$$

$$\mathrm{Im}\, R(\varkappa)\Big|_{\varkappa=\left\{\begin{smallmatrix}-L\\L+1\end{smallmatrix}\right.} = -2^k \sum_{n=0}^{\infty} \frac{(-2)^n}{n!} \Gamma_0(n)\,\tilde{\varphi}_n^\pm,$$

$$\Gamma_0(n) = \frac{(k-L+n)!}{(2k+n)!},$$

$$\varphi_n^\pm = 1 + \frac{k \pm k}{2} - \frac{n+k+2-L}{2k+1+n}, \qquad \tilde{\varphi}_n^\pm = 1 + \frac{k \pm k}{2} - \frac{n+k+1-L}{2k+1+n},$$

$k = |\varkappa|$ and ω is the transition energy.

We note that if αZ is small and $p \ll 1$, we have $\alpha Z \approx \sqrt{2\omega}$. It is seen from (12) that as $\omega \to 0$, the ICC approaches infinity (the "infrared catastrophe" for the ICC). This is verified by the rapid increase of the ICC as Z decreases, observed in the ICC tables for end-point energies.[6] Screening cannot change the essential features of this result, since the same effect is obtained with Z = 1. Higher approximations may, however, change the ICC when there is additional de-excitation by γ-radiation via an "electron bridge". It will be evident from (12) that as ω decreases, $\beta_\varkappa$ increases as ω^{-L}, while $\delta_\varkappa$ decreases as $\sqrt{\omega}$. Thus $\beta_\varkappa\delta_\varkappa$ increases with decrease of ω. According to (10), however, the region in which $\beta_\varkappa\delta_\varkappa$ is not small** compared to unity is the region in which the higher order corrections are large. Thus these corrections may be large for very low energies and for high multipole orders of nuclear transitions.

We note also that in γ-γ and in γ-e correlation even a small additional amount of γ-radiation across the "electron bridge" may be quite important be-

---

*For simplicity we are treating only magnetic multipoles.

**The inequality $\sum_\varkappa \beta_\varkappa \frac{\delta_\varkappa^2}{1+\delta_\varkappa^2} < 1$ must, of course, be fulfilled in this case.

cause of the high sensitivity of the angular correlation method.

The authors express their gratitude to B.S.Dzhelepov, V.B.Berestetskii, L.A.Sliv and Iu.V.Novozhilov for helpful discussion.

Physical Institute,
Leningrad State University

References

1. V.A.Krutov, Present issue of the Bulletin, p. 159.
2. N.Tralli & G.Goertzel, Phys.Rev., 83, 399 (1951).
3. M.E.Rose, Multipole Fields, No.27,-N.Y., 1955.
4. H.R.Coish, Phys.Rev., 84, 164 (1951).
5. M.E.Rose and others, Phys.Rev., 83, 79 (1951).
6. B.I.Spinrad & L.B.Keller, Phys.Rev., 84, 1056 (1951).

GAMMA-SPECTRUM OF La^{140}

- V.P.Prikhodtseva & Iu.V.Khol'nov

The decay scheme of La^{140} is not yet definitively established. In view of the interest attached to ascertaining the level systematics of Ce^{140} (a nucleus with a magic neutron number), we undertook a repeat investigation of the complex γ-spectrum of La^{140} by means of the Ritron[1] operated under new experimental conditions[2] with no gas in the instrument chamber. In the present report we shall give only our experimental results. We carried out two series of measurements with two different La_2O_3 sources weighing ~2 g and having an initial activity of about 1.5 Curie.

Energy and relative intensities of La^{140} γ-rays

No.	E_γ, kev		Relative intensity	No.	E_γ, kev		Relative intensity
	Ref.3	Our data			Ref.3	Our data	
1	328,6	323±6	0,21	8	—	868±5	0,053
2	—	(400)	0,03	9	—	(903)	0,008
3	436	434±7	0,025	10	923	923±5	0,096
4	486,6	491±5	0,419	11	1597	1597±7	1,00
5	—	(643)	0,011	12	1909	—	<0,0015
6	730 751,9	748±7	0,0337	13	—	2343±15	0,0078
7	815,3	815±5	0,196	14	—	2515±15	0,037
				15	—	2890±30	0,0008

A. The results of the first series of measurements - the experimental spectrum with the background subtracted - are shown in the accompanying figure and table.

In determining the relative line intensities, we made appropriate corrections for self-absorption in the source and for absorption in the instrument window. We also took into account the energy dependence of the spectral sensitivity of the instrument.[2]

The principal differences between the present results and the previous ones[3] are the following:

1) Owing to elimination of the gas from the inside of the instrument, the γ-lines became narrower (3.3% instead of 5.5% in the 1 Mev region). Line groups Nos.1, 4 and 6-8 were not resolved in the previous study[4]. Now, instead of a hump, we clearly discern four γ-lines in the 3200-4200 $H\rho$ region.

2) More accurate values for the relative γ-line intensities were obtained. There is some difference in the relative intensity values in the region of soft γ-rays, where the influence of the gas formerly filling the instrument was particularly great.

3) We detected two new γ-lines at 868 and 2343 kev. The lanthanum sources were not purified, hence the assignment of these γ-lines to La^{140} must be based on the fact that their intensity fell off with the ~40 hour period characteristic of La^{140}.

We detected an excess of recoil electrons corresponding to 400, 643 and 903 kev γ-rays, the actual existence of which we cannot regard as definitively established.

4) In the previous investigation we observed a rise in the number of pulses above the background in the energy region above 2700 kev. Accordingly, in Ref.4 we gave an upper limit for the intensity of the hard lines (<0.002 photons/disintegration).

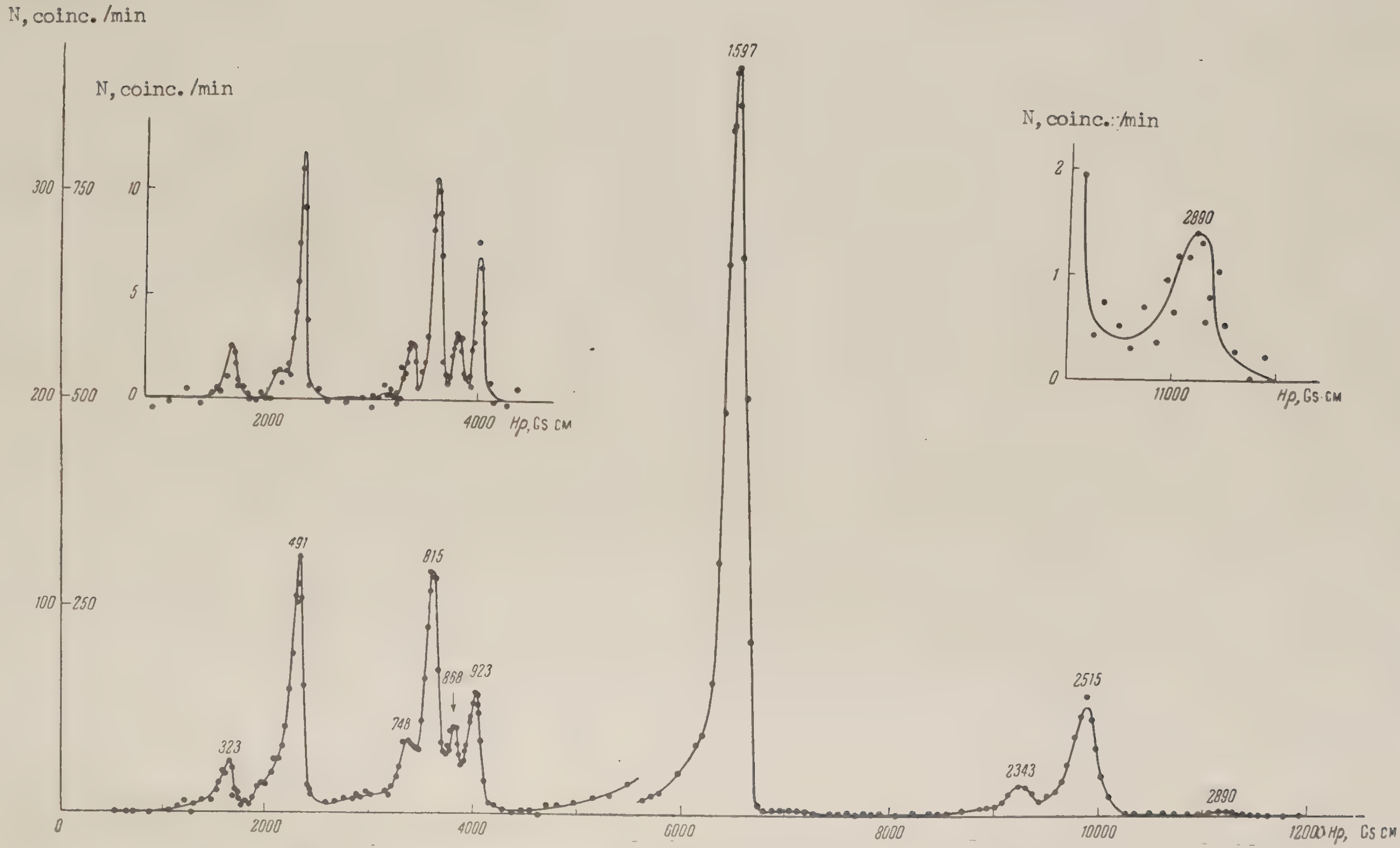

Experimental La^{140} γ-ray spectrum (background subtracted). The right-hand vertical scale pertains to the Hρ = 5600-7400 region; the left-hand scale to the lower spectrum on the left.

This section of the spectrum is shown to an enlarged scale in the insert at the right in the accompanying figure. These data are not statistically accurate but they do indicate that there exists a γ-line of about 2900 kev energy and an intensity of the order of $1 \cdot 10^{-3}$ photons/disintegration. It should be noted that in the investigation of Ref.5 there was detected a distinct conversion line corresponding to a transition of 1909 kev energy. According to our measurements, if there is such a γ-line its intensity does not exceed ~0.1%.

B. The second series of measurements was carried out for the specific purpose of more detailed investigation of the first two sections of the spectrum in the low energy region.

In order to enhance further the resolution of the instrument, we narrowed the focusing slits to 1 mm (from 2 mm) and reduced their height to 18 mm (from 46 mm). We also used a thinner cellophane target (17 μ instead of 50 μ).

The results of this series of measurements are shown at the upper left in the accompanying figure. It will be seen that all the γ-lines observed in the first series of measurements appear here as well but appreciably more clearly. The dips between the lines are deeper and the low-energy tails are shorter. The new line at 868 kev is more clearly discernible in this series.

In determining the γ-line intensities, the results of the second series of measurements were taken into account, but the determination was based primarily on the first series as the statistically more reliable one.

We shall not discuss the decay scheme of La^{140} here, but shall merely note that the two new 868 and 2343 kev lines do not fit into the decay scheme for La^{140} proposed by Peacock et al[3] and by Arkhangel'skii et al[4].

We desire to thank B.S.Dzhelepov for discussion of the results and G.E. Shchukin, V.F.Rodionov & N.Voinova for assistance in carrying out the measurements.

"V.G.Khlopin" Radium Institute,
USSR Academy of Sciences

References

1. B.S.Dzhelepov, N.N.Zhukovskii & Iu.V.Khol'nov, Izv.AN SSSR, Ser.fiz., 18, 599 (1954). (Trans.Bulletin, 18, No.5, 285.)

2. B.S.Dzhelepov, V.P.Prikhodtseva, A.I.Feoktistov & Iu.V.Khol'nov, Izv. AN SSSR, Ser.fiz., 20, 1361 (1956). (Trans.Bulletin, 20, No.12a, 1245); I.B. Golovanov, B.S.Dzhelepov, L.S.Lebedev, V.P.Prikhodtseva & Iu.V.Khol'nov, Izv. AN SSSR, Ser.fiz., 21, 985 (1957). (Trans.Bulletin 21, No.7, 987.)

3. G.Peacock, J.Quinn & A.Oser, Phys.Rev., 94, 372 (1954).

4. L.V.Arkhangel'skii, B.S.Dzhelepov, N.N.Zhukovskii, V.P.Prokhodtseva & Iu.V.Khol'nov, Izv.AN SSSR, Ser.fiz., 19, 251 (1955). (Trans., Bulletin, 19, No.3, 228.)

5. A.A.Bashilov, B.S.Dzhelepov, N.D.Novosil'tseva & L.S.Chervinskaia, Present issue of the Bulletin, p.176.

CONVERSION SPECTRUM OF La^{140}

- A.A.Bashilov, B.S.Dzhelepov, N.D.Novosil'tseva & L.S.Chervinskaia

Introduction

The radiations accompanying the decay of La^{140} have been studied by a number of investigators. A critical analysis of all the work on the subject published up to May 1955 was given by Arkhangel'skii et al[1]. It is evident from this analysis that the spectrum of La^{140} contains an appreciable number of weak conversion lines. The quantum characteristics of the corresponding transitions were unknown and hence it was impossible to establish the spins and parities of the low-lying excited states of Ce^{40}.

Our previous investigation[2] of the conversion spectrum of La^{140} was carried out with neutron irradiated lanthanum; sources prepared in this manner have a low specific activity. As soon as it became feasible to separate La^{140} with a high specific activity from Ba^{140} (T = 12.8 days), we repeated our investigation of the conversion spectrum. The present report is devoted to the results of this study. Recently Prikhodtseva & Khol'nov[23] (see preceding article) reinvestigated the γ-spectrum of La^{140}; their results were utilized in the present work.

1. Experimental Conditions

The conversion electron spectrum of La^{140} was investigated by means of the Ketron[3], a magnetic spectrometer with improved focusing.

The angles of divergence of the electron beam in the spectrometer were such that the width of the principal conversion lines of La^{140} at half-height was 0.5%.

The electrons were detected by means of an ordinary Geiger-Müller counter. To check the operation of the instrument, we used an additional counter located behind the first one and connected in coincidence with it. The counters were filled with argon and alcohol vapor (or methane). The window of the first counter was covered with a collodion film having a superficial density of 0.2 mg/cm^2. In this case electrons from about 10 kev energy were detected.

The La^{140} was separated from a chloride solution of Ba^{140}, in which it was in radioactive equilibrium, by precipitation with ammonium. The precipitate was separated by centrifuging and was repeatedly washed with warm water containing a small amount of ammonium. In order to remove all traces of Ba^{140}, the $La(OH)_3$ precipitate was dissolved in a solution of hydrochloric acid; then barium was added and the La^{140} again precipitated. This operation (solution and precipitation) was repeated several times.

The La^{140} was repeatedly separated from the same initial Ba^{140} solution.

The final La^{140} solution was applied in a thin layer to a collodion film having a thickness of about 0.1 μ. The superficial density of the active layer was minimal as was proved by the coincidence of the experimentally measured line half-widths with the instrument half-width at $E > 200$ kev.

Appropriate corrections were made in the experimental results for electron absorption in the counter window. No correction was made for electron absorption in the source inasmuch as this was negligibly small.

2. Experimental Results

The general β and conversion spectrum of La^{140} is shown in Fig.1. The given curve was obtained as a result of averaging eight series of measurements with five different sources. Approximately 500 experimental points were ob-

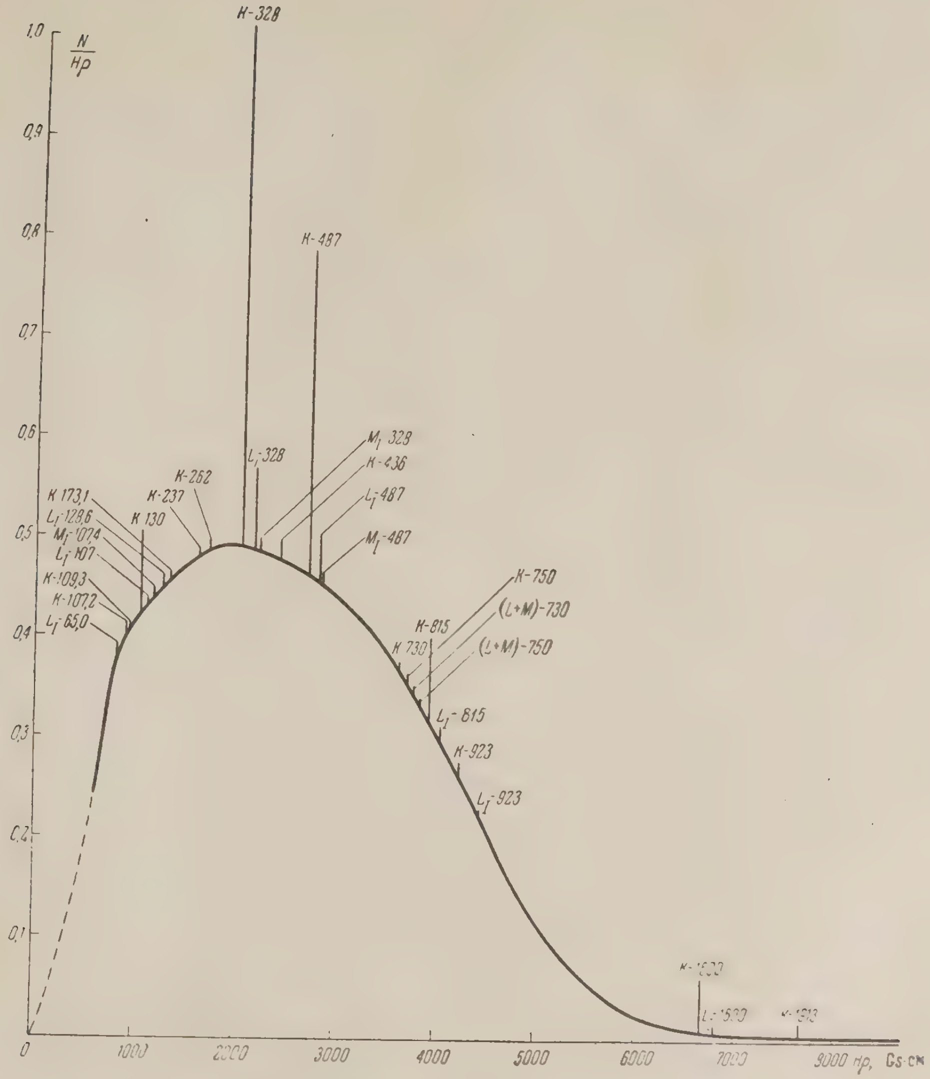

Fig.1. General view of conversion and β-spectrum of La^{140}. The heights indicated by the vertical lines are proportional to the line intensities.

tained in each series. The mean statistical error in measuring the continuous spectrum was about 3%. The conversion lines were measured with a better statistical accuracy.

As a result of our measurements there were detected 28 conversion lines corresponding to 16 nuclear transitions. We found all the conversion lines observed earlier by Cork and his co-workers[4] and in addition weak K and L lines associated with a 730 kev transition.

The low energy region of the spectrum is plotted to a larger scale in Fig.2. At the beginning of the spectrum there was detected a low intensity line of 58.4 kev energy. If it is assumed that this line is due to internal conversion of γ-rays in the L_I shell of Ce^{140}, the energy of the γ-transition comes out to be about 65.0 kev.

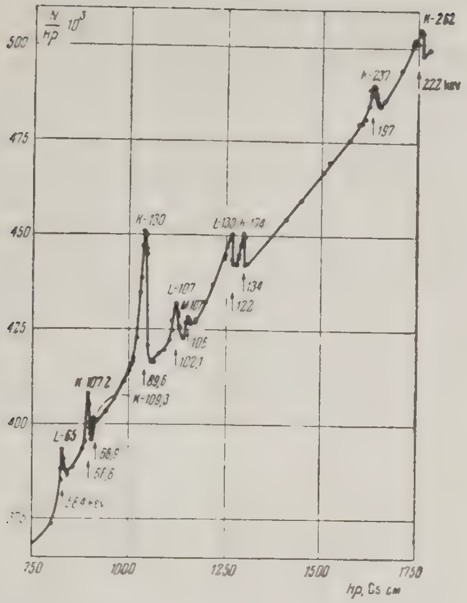

Fig.2. Conversion lines of La^{140} in the low energy region.

The second electron line of 66.8 kev energy was interpreted as the line due to internal conversion in the K shell of a 107.2 kev γ-transition. The energy difference between this line and the 102 kev line corresponds to the energy difference between the K and L_I shells of Ce.

We took the line at 68.9 kev to be due to internal conversion in the K shell of a nuclear transition of 109 kev energy.

The 89.6 kev conversion line is more intense than its neighbors; the energy difference between the 89.6 and 122 kev electron lines clearly indicates that these lines are associated with internal conversion of a 130 kev γ-ray in the K and L_I shells of Ce.

Three conversion lines barely rise above the continuous β-spectrum at 134, 197 and 222 kev. We assume that all three lines are K conversion lines associated with transitions of 174, 237 and 262 kev energy; these cannot be L lines inasmuch as no corresponding lines are discernible.

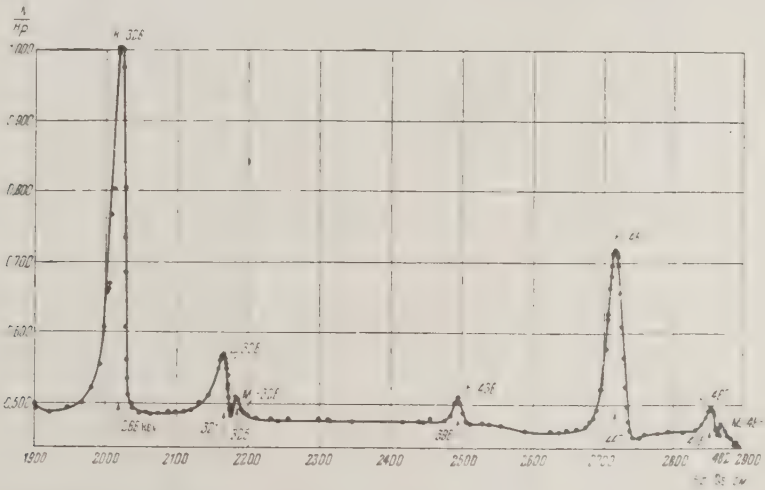

Fig.3. Conversion electron spectrum of La^{140} in the energy region from 320 to 490 kev.

Lines corresponding to internal conversion of nuclear transitions of 328 and 487 kev energy were observed in all investigations of La^{140}. However, all previous investigators, except Cork et al[4], failed to give relative intensity values for these lines. Hence we investigated these lines with particular care. We were able to detect the K, L and M lines associated with the 328 and 487 kev transitions (Fig.3) and determine their relative intensities; the pertinent data are listed in Table 1.

We interpreted the 396 kev line as being the K conversion line of a γ-transition of 436 kev energy.

Table 1

Energies and intensities of conversion lines appearing in the decay of La^{140} to Ce^{140}, according to the data of different investigators

Conversion line energy, kev		Origin shell	Transition energy*, kev		Adopted transition energy value, kev	Relative intensity%		n_e per 100 decays	
Cork et al (4)	Our work		Cork et al (4)	Our work		Cork et al 4	Our work	Ref. 14	Our work
62,1	58,4	L_I	68,7	65,0	68,7	20	1,7	—	0,010
68,9	66,8	K	109,3	107,2	108,3	40	2.2	—	0,013
70,1	68,9	K	110,5	109.3	109,9	10	0,4	—	0,002
90,3	89,6	K	130,7	103,0	130,8	70	17	—	0,100
102,7	102	L_I	109,3	108,7	109,9	40	1,1	—	0,006
108,0	106	M_I	109,4	107,4	109,3	10	0,6	—	0,004
124,3	122	L_I	130,9	128,6	130,8	10	1,9	—	0,011
132,7	134	K	173,1	174	173,1	20	1,8	—	0,011
201,1	197	K	241,5	237	241,5	30	1,3	—	0,008
225,1	222	K	265,5	262	265,5	30	1,8	—	0,011
288,3	288	K	328,7	328	328,6	100	100	1,24	0,59
322,0	321	L_I	328,6	328	328,6	40	16	—	0,094
326,0	325	M_I	327,4	326	328,6	10	3	—	0,018
391,0	396	K	431,4	436	436,4	20	4	—	0,024
446,0	447	K	486,4	487	486,6	70	63	0,4	0,37
480,0	478	L_I	486,6	485	486,6	20	9	—	0,053
484,9	482	M_I	486,3	483	486,6	10	2	—	0,012
—	690	K	—	730	730	—	1,7	—	0,010
711,5	710	K	751,9	750	751,9	10	2,5	—	0,015
—	724	L_I+M	—	731	730	—	1	—	0,006
—	744	L_I+M	—	751	751,9	—	0,7	—	0,004
775,5	775	K	815,9	815	815,3	50	16	0,168	0,094
808,2	808	L_I	814,8	815	815,3	10	2,1	—	0,012
886	883	K	926	923	923	10	2,4	—	0,014
—	916	L_I	—	923	923	—	0,3	—	0,002
1557	1560	K	1597	1600	1597	30	10	0,08	0,059
1591	1596	L_I	1598	1603	1597	10	1,2	—	0,007
1864	1873	K	1904	1913	1909	10	3	—	0,018

*The Ce K-shell binding energy is 40.4 kev, the L_1-shell energy is 6.6 kev, the M_1-shell energy is 1.4 kev.

The section of the conversion spectrum from 700 to 950 kev is shown in Fig.4. In most previous investigations only one γ-ray of 815 kev energy was observed in this region. Cork et al[4], however, detected conversion lines associated with three γ-transitions having energies of 751, 815 and 926 kev in this region. Coleman[5] reports finding two γ-lines having energies of 815 and 893 ± 40 kev. Coleman identifies the last line with the 926 kev line observed by Cork et al[4]. In all our series of measurements, we were able to detect conversion lines corresponding to four γ-transitions. In addition to the K and L lines associated with the well known 815.3 and 926 kev transitions, we observed the K and L line due to transitions of 730 ± 10 and 750 ± 10 kev energy. These lines appear on the steep descending portion of the continuous β-spectrum contour.

We repeatedly measured the conversion electron lines associated with the 1597 kev γ-transition. The results of all series of measurements are in good agreement.

We also detected a conversion line corresponding to a transition of 1913 kev energy (Fig.5), which has hitherto been observed by Cork et al, who give the energy as 1904 kev.

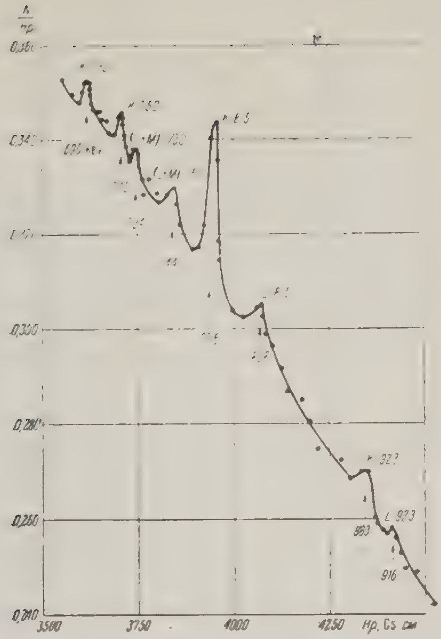

Fig.4. Conversion spectrum of La^{140} in energy region from 700 to 930 kev.

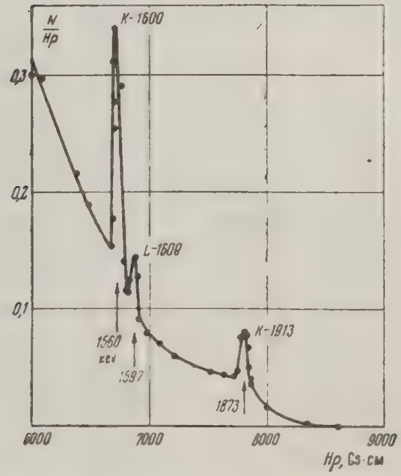

Fig.5. Conversion electron spectrum in the high energy region.

The energy values of the conversion electrons and associated nuclear transitions according to our data and data of Cork et al are listed and compared in Table 1. We chose the results of Cork and his co-workers for purposes of comparison because in our opinion the most accurate values of the transitions energies in Ce^{140} have been obtained by them (spectrometer with photographic recording of conversion electrons) and by Hedgran & Lind[6] (spectrometer with double focusing of photoelectrons). The latter, however, determined the energies of only four transitions: 328.6 ± 0.3 kev, 486.7 ± 0.4 kev, 815.1 ± 0.7 kev and 1596 ± 2 kev.

Comparison of these data with the values given by Cork et al shows that the energies of the soft lines are in agreement to within 0.05% and the energies of the hard lines to within 0.10%. An additional check on the correctness of the values obtained by Cork et al and Hedgran & Lind is furnished by comparison of the energy sum of the cascade transitions with the energy of the direct (cross over) transition. It will be evident from the following table that in the energy region to 1 Mev the divergences between the sum of the cascade transition energies and the energy of the cross-over transition obtained experimentally amounts to 0.2 kev on the average:

$$328.6 + 486.6 = 815.2 \approx 815.3 \text{ kev},$$
$$130.7 + 110.5 = 241.2 \approx 241.5 \text{ kev},$$
$$68.7 + 173.1 = 241.8 \approx 241.5 \text{ kev},$$
$$265.5 + 486.6 = 752.1 \approx 751.9 \text{ kev}$$

(table based on the averaged values of Cork et al and Hedgran & Lind.)

We cannot lay claim to as high an accuracy for our energy values. Our values fluctuate about those given by Cork et al with an average deviation of 3 kev (in the region to 1 Mev); since there is no systematic deviation evident, the absolute scales may be said to agree.

Other determinations of the transition energies made from γ-ray measurements (Refs.5, 7-18) are characterized by a lower accuracy but as a rule agree, within the limits of error indicated by the respective authors, with the data of Cork et al.[4]

We did not include these additional data in Table 1, since they add no new information, except for the two high γ-lines of 2535 and 2700-3000 kev energy which have never been detected in conversion but have been detected by observing photoelectrons[7-9,11,13], Compton recoils[1], photoneutrons and photopro-

tons[7-10,15-18]. Hereinafter we shall use the energy values given by Cork et al to designate the γ-lines except for the 108-109 line for which we have taken the average energy value and the 436, 730 and 923 kev lines whose energies are taken on the basis of our data.

The relative intensities of the conversion lines were determined from the areas bounded by the line contours and the continuous β-spectrum plotted in $N/H\rho$ vs $H\rho$ coordinates. The error in determining the areas and, consequently, the relative intensities is due primarily to the uncertainty in plotting the continuous β-spectrum.

For determining the number of conversion electrons per 100 decays we compared the areas under the lines with the area under the continuous spectrum; in doing so we made no corrections for reflection of electrons from the source backing.

In Table 1 we list the ratios of the number of conversion electrons to the number of β-particles in continuous spectrum and the ratio of the intensity of each of the conversion lines to that of the K-328 line. It will be seen that our values differ very appreciably (sometimes by a factor of 20) from the tentative values as given by Cork et al[4]. These divergences indicate the great error involved in evaluating the intensity of weak lines from the blackening of photographic plates.

For the four most intense conversion lines we have the data of Bolotin, Pruett, Roggenkamp & Wilkinson[14] relative to the number of electrons per β-particle. There is an appreciable divergence between their values and ours for the K-328 and K-815 lines. The values for the other two lines are in better agreement.

3. Determination of the Multipole Order of Nuclear Transitions in Ce^{140}.

K/L ratio

The multipole order of nuclear transitions is commonly determined by comparing the experimental values of K/L with the theoretical values for different multipole orders.

The approximate relative intensities of Cork et al are not suitable for determining the multipolarity of the transitions on the basis of the K/L ratio in view of their low accuracy.

In the work of Bolotin et al[14], K/L was determined only for the 328.6 and 486.6 kev transitions. They give the value as 7.4. They also note that the K/L value for the 815 and 1597 kev γ-rays is very high. Using the data of Table 1 one can determine K/L for the seven principal lines of La^{140}. The experimental values of K/L for six of these γ-rays are listed in Table 2.

Table 2

Multipole order assignments for the nuclear transitions in Ce^{140} based on the experimental and theoretical values of the K/L ratio for the principal lines of La^{140}

Transition energy, kev	Experimental K/L ratio	Theoretical K/L ratios						Assignments
		$E1$	$E2$	$E3$	$M1$	$M2$	$M3$	
109,3	2,0±1	7,0	2,2	0,5	7,0	4,5	1,4	$E2$ ($E3 + M2$)
130,0	9±2	7,4	2,7	1,0	7,0	4,7	1.7	$E1$ or $M1$
328,6	6,2±0,5	7,9	6.2	3,5	7,2	5,3	3.7	$E2$
486,6	7,0±0,5	8,2	6,9	4,7	7,2	5,7	4,8	$M1$, $E2$
815,3	7,6±1	8,2	7,6	6,5	7,5	7,5	6,8	any
923	8±1	8,2	8,6	6,6	7,5	8,0	7,5	any

For calculating the theoretical values of K/L for Z = 58 we used the K conversion coefficient values calculated by Sliv & Band[19] and took the L_I coefficient values from Rose's talbes as interpolated by Dranitsyna[20]. Comparison of the theoretical and experimental ratios shows that the 109.3 kev γ-transition is probably E2 and that the 130 kev transition is either E1 or M1. The 328 kev transition may be identified as E2, while the assignment for the 486.6 kev transition is either E2 or M1. In the case of the 815.3 and 923 kev γ-rays, however, it becomes difficult to determine the multipole order by this method inasmuch as the values of K/L for different multipolarities differ by only 5-10% which is virtually within the limits of the rather large experimental uncertainty. For γ-rays of energies above 1 Mev there are no reliable data for the L conversion coefficients so that determination of the multipole order by this procedure becomes impossible.

Values of α_K

From the work of Prikhodtseva & Khol'nov[23], we now have information on the relative intensities of the γ-rays in the spectrum of La^{140}. This information can be used in conjunction with the conversion electron intensity values for determining the conversion coefficients, provided the scales of the two spectra can be correlated; this can be done if the multipole order of at least one transition is known.

In nuclei with even N and Z, the first excitation level as a rule is 2+. It may, therefore, be assumed that the assignment for the first level of Ce^{140} is 2+. As follows from the analysis of Arkhangel'skii et al[1] there can be no doubt that the first level of Ce^{140} has an energy of about 1597 kev. Hence there is good reason to assume that the 1597 kev transition will be pure electric quadrupole (E2). The experimental data on α_K and angular correlations (see below) are not in conflict with this assumption.

Taking the 1597 kev transition to be pure E2, we readily found α_K for all the transitions for which we know the relative intensities of the γ-rays and conversion electrons. The results of our evaluations are listed in Table 3. In compiling this table we used our data on the conversion electrons and the data of Bolotin et al[14] and Prikhodtseva & Khol'nov[23] on the relative γ-ray intensities.

Table 3

Determination of the multipole orders of the nuclear transitions from the theoretical and experimental values of α_K

Transition energy, kev	Experimental value of $\alpha_K \cdot 10^3$	Theoretical values of $\alpha_K \cdot 10^3$						Multipole order assignment
		E1	*E2*	*E3*	*M1*	*M2*	*M3*	
328	29	8,7	29	93	47	270	380	*E2*
436	10,4	4,8	14	36	19	63	200	(*E2*)
487	9,3	3,7	10	27	15	47	120	*E2*
815	5,0	1,1	2,7	6,0	4,2	11	24	*M1*
923	1,4	0,87	2,1	4,3	3,0	7,8	17	(*E1*, *E2* or *M1*)
1597	0,69*	0,33	0,69	1,3	0,92	19	3,5	*E2**

*Adopted value (see below).

The conversion electron and γ-ray spectra can also be correlated if we know the number of conversion electrons for some line per decay $(e_K^-/\beta)_i$ and the number of γ-rays of the corresponding line per decay $(\gamma/\beta)_i$. The first of these figures is obtained by comparing the areas bounded by the line contour and the continuous β-spectrum.

For the 1597 kev transition, according to Table 1 $(e_K^-/\beta)_{1597} = 0.059$. The second figure cannot be obtained directly from experiment but must be deduced indirectly. The 1597 kev γ-rays give coincidences with all the intense γ-rays of La^{140}.

Analysis[1] shows that the 1597 kev γ-rays appear in 94 ± 9% of the decays; the uncertainty here takes into account the possibility of there being as yet unknown cascades occurring in parallel with the 1597 kev transition. Thus we have

$$\frac{\gamma}{\beta}(1597) = 0.94,$$

whence

$$\alpha_K(1597) = \frac{0.059}{94} = 0.00063.$$

This value is very close to the theoretical one for an E2 transition (0.00069). It is clear, therefore, that the experimental values of α_K for all the lines listed in Table 3, if determined by this method, will be about 10% lower than shown in the table, which will have virtually no effect on the probable multipole order assignment.

Comparison of Tables 2 and 4 shows that there are no explicit contradictions and that in some cases the tables supplement each other and substantiate the inference that the 328.6 and 486.6 kev transitions are almost pure E2 and that the 815.3 kev transition is primarily M1.

So far values of α_K have been given in only two reports: our work[2] and that of Bolotin and co-workers[14]. The values of Bolotin et al for the 328, 487, 815 and 1597 kev γ-rays are 0.0307, 0.00732, 0.00412 and 0.0008, respectively. They differ from our values, which we regard as more accurate, by 25% on the average. As noted, however, the deductions that can be made regarding the multipole order of the transitions on the basis of these data agree with those made above.

γ-γ correlation

We did not investigate the correlation between the γ-rays of Ce^{140}; however, the data obtained in recent years can be of aid in establishing the quantum characteristics and hence we will summarize them here.

γ_{486}-γ_{1597} correlation. Bishop & Perez Y Jorba[21] and Bolotin et al[14] found that this angular correlation is consistent with the spin sequence 4—2—0 for the 2083, 1597 and 0 kev levels of Ce^{140}.

γ_{815}-γ_{1597} correlation. Robinson & Madansky[12] found that this angular correlation is in agreement with the spin sequence 4—2—0. Bishop & Perez Y Jorba[21], however, found that it is in better agreement with the sequence 3—1—0 or 3—2—0. Finally, Bolotin et al[14] consider that it cannot be reconciled with any sequence of pure multipoles but that it is consistent with the mixtures

$$3+(98\%\ M1 + 2\%\ E2)\ 2+\ (E2)\ 0+ \text{ or } 4+(74\%\ E2 + 26\%\ M3)\ 2+(E2)\ 0+.$$

$\gamma_{328}\gamma_{-487}$ and γ_{328}-γ_{1597} correlations. Bolotin et al found that these correlations are compatible with the sequences

3+(M1 + E2) 4+(E2) 2+(E2) 0+ or 4+(M1 + E2) 4+(E2) 2+(E2) 0+.

γ_{923}-γ_{1597} correlation. Coleman[5] found that this correlation is in agreement with the sequence

2+(99% M1 + (0.1-1.0)% E2) 2+(E2) 0+.

4. Spins and Parities of the Excited States of Ce^{140}

1. The first excited state of Ce^{140} (1597 kev) is 2+. This is substantiated by the value of α_K, is not inconsistent with all the angular correlations and is in agreement with the systematics of the first levels of even-even nuclei.

2. The second level of Ce^{140} has an excitation energy of 2083 kev. Only one transition from this level is known: the 486.6 kev transition to the first level. The value of α_K for this transition unambiguously indicates that the multipole order is E2; the experimental value of K/L is almost identical with the theoretical value for E2. This multipole order is consistent with the following spins and parities for the level: 0+, 1+, 2+, 3+ or 4+. The 0+ assignment is excluded, however, in view of the existence of β^--decay to this level together with the absence of a transition to the ground level of Ce^{140}. The 1+ and 2+ assignments are excluded due to the absence of a competing cross-over transition of 2083 kev energy (see first line of Table 4) and, apparently, by the $\gamma_{486.6}$-γ_{1597} angular correlation.

On the basis of the angular correlation data[21,14] one should give preference to 4+ and in what follows we shall adopt this assignment. The 4+ assignment is also consistent with Glaubman's empirical rule according to which the even states of spherical nuclei generally have even spins.

Table 4 shows why a ~2083 kev γ-ray is not observed: with the 2083 kev level being 4+, this ray should be weaker than the 486.6 kev γ-ray by a factor of 160,000.

3. The third excited state has an energy of 2412 kev. There are transitions (815.3 and 328.6) from it to the first and second levels of Ce^{140}, but no transitions to the ground state.

For the 815.3 kev transition the value of α_K according to our data is 0.0050 or 0.0054, depending on the method of calculation used, while according to Bolotin et al[14], $\alpha_K = 0.0041$. All these values are reasonably close to the theoretical value of 0.0042 for M1.

Inasmuch as the first level of Ce^{140} to which the 815.3 kev transition goes has the spin and parity 2+, for the 2412 kev level we must consider 0+, 1+, 2+, 3+ and 4+. As in the preceding case, the 0+ assignment is excluded in view of the existence of β^--decay to this level, while the 1+ and 2+ assignments are precluded due to the absence of a cross-over transition of 2412 kev energy (see second line of Table 4). We are thus reduced to the choice between 3+ and 4+.

Judging by the values of K/L and α_K, the 328.6 kev transition is E2. This transition goes to the 2083 kev level of Ce^{140}, the assignment for which is 3+ or 4+. In this case the possible assignments for the 2412 kev level are 1+, 2+, 3+, 4+, 5+ and 6+; for the above reasons 1+, 2+, 5+ and 6+ are again excluded, so that only 3+ and 4+ remain. The angular correlation data also points to these two assignments.

Table 4

Relative intensities of competing γ-transitions from the 2083, 2412 and 2520 kev levels of Ce^{140}
(Theoretical values calculated according to the single particle model formulas listed in Ref.22; S taken equal to 1)

Level energy, kev	Transition ratio considered	Exp. value probability ratio	Theoretical values of the probability ratios for the indicated spins and parities *[1]				Remarks
			1^+	2^+	3^+	4^+	
2083	$\gamma_{2083}/\gamma_{487}$	<0,15	$1\cdot10^{3}\div8\cdot10^{4}$	$1\cdot10^{3}$	$\underline{6\cdot10^{-6}\div7\cdot10^{-3}}$	$\underline{6\cdot10^{-6}}$	*2
2412	$\gamma_{2412}/\gamma_{815}$	<0,3	$\underline{0{,}6\div9\cdot10^{3}}$	$\underline{0{,}6\div230}$	$\underline{5\cdot10^{-9}\div1\cdot10^{-3}}$	$\underline{2\cdot10^{-6}}$	*3
	$\gamma_{328}/\gamma_{815}$	0,50	$8\cdot10^{-17}\div1\cdot10^{-9}$	$\underline{0{,}01\div3\cdot10^{-5}}$	$\underline{3\cdot10^{-5}\div2}$	$\underline{0{,}01\div20}$	*4
2520	$\gamma_{923}/\gamma_{2520}$	2,2	$\underline{2\cdot10^{-4}\div2}$	$\underline{7\cdot10^{-3}\div2}$	$1\cdot10^{+3}\div2\cdot10^{8}$	$8\cdot10^{5}$	*4
	$\gamma_{436}/\gamma_{2520}$	0,7	$3\cdot10^{-17}\div3\cdot10^{-11}$	$2\cdot10^{-4}$	$\underline{20\div2\cdot10^{7}}$	$2\cdot10^{4}\div2\cdot10^{7}$	*4
	K_{436}/K_{923}	1,7	$2\cdot10^{-14}\div5\cdot10^{-7}$	$\underline{4\cdot10^{-4}\div0{,}2}$	$\underline{4\cdot10^{-4}\div3\cdot10^{2}}$	$\underline{2\cdot10^{-2}\div3\cdot10^{2}}$	
			1^-	2^-	3^-	4^-	
2520	$\gamma_{923}/\gamma_{2520}$	2,2	$\underline{0{,}05}$	$1\cdot10^{4}\div2\cdot10^{6}$	$2\cdot10^{6}$	$\underline{100\div4\cdot10^{8}}$	*4
	$\gamma_{436}/\gamma_{2520}$	0,7	$1\cdot10^{-13}$	$\underline{2\cdot10^{-8}\div4\cdot10^{-2}}$	$2\cdot10^{5}$	$3\cdot10^{10}\div5\cdot10^{13}$	*4
	K_{436}/K_{923}	1,7	$\underline{4\cdot10^{-12}}$	$\underline{1\cdot10^{-5}\div6\cdot10^{2}}$	$\underline{3\cdot10^{-2}}$	$1\cdot10^{5}\div3\cdot10^{8}$	*4

---

*[1] Values underlined in cases when the theoretical value closest to the experimental one differs from it by less than a factor of 100.

*[2] On the assumption that the 486.6 and 1597 kev transitions are E2.

*[3] On the assumption that the 815.3 kev transition can be any mixture of E2 + M1.

*[4] On the assumption that the 2083 and 1597 kev levels of Ce^{140} are 4+ and 2+.

The ratio of intensities of the 328.6 and 815.3 kev γ-rays (Table 4) excludes the 1+ and 2+ assignments, but does not allow of making a choice between 3+ and 4+.

Table 4 shows that the probability of direct de-excitation of the 2412 kev level is low: the 2412 γ-ray should be weaker than the 2521 kev γ-ray by a factor of 30.

4. The fourth level of Ce^{140} has an excitation energy of 2520. It is apparently de-excited to all the lower lying levels - 0, 1597, 2083 and 2412 kev - giving rise to 2520, 923, 436 and 108 kev γ-rays. This indicates that the spin of this level is neither 0 nor greater than 3. Thus the choices to be considered are 1±, 2± or 3±. In order to determine the characteristics of the 2520 kev level, we must utilize the available data pertaining to the 2520, 923

and 437 kev transitions. Use of the data pertaining to the transitions between the 2520 and 2412 kev levels is difficult, first, because we do not know which component of the 107-109 kev doublet is associated with this transition and, second, because we do not know whether the spin of the 2412 level is 3 or 4.

Thus for determining the assignment for the 2520 kev level we can utilize the following data:

a) the K conversion coefficients for the 436 and 923 kev transitions,
b) the γ_{923}-γ_{1597} angular correlation,
c) the relative intensities of the 2520, 923 and 436 kev γ-rays and
d) the relative intensities of the K conversion lines associated with the 923 and 436 kev γ-transitions.

Let us analyze these data and see what conclusions they lead to.

A) For the 923 kev transition the value of α_K is not accurately known, for although the intensity of the 923 kev line has been measured with good accuracy, the K-923 conversion line is very weak so that its relative intensity cannot be measured accurately. The experimental value of α_K lies between the values corresponding to E1 and E2 + M1. The 923 kev transition goes to the 1597 kev level of Ce^{140} which has the spin and parity 2+. Hence the following assignments are possible for the 2520 kev level: 1±, 2+, 3± and 4+.

B) There is also an appreciable uncertainty in the experimental value of the α_K conversion coefficient for the 436 kev transition. In this case the experimental value for α_K is intermediate between the theoretical values for E1 and E2 + M1. This transition goes to the 2083 kev level of Ce^{140} which is characterized by 4+. In light of this assignment, the 2520 kev level may be 2+, 3±, 4±, 5± or 6+. Comparing these possibilities with those under A above, we can eliminate all but 2+, 3± and 4+.

C) Coleman[5] who observed the angular correlation between the 923 kev and 1597 kev γ-rays found that it is most consistent with the sequence 2+ —2+ —0+. This is not in conflict with A and B, but does not necessarily preclude the other possibilities.

D) In Table 4 we have listed the ratios of the intensities of the competing 2520, 923 and 436 kev γ-transitions and the conversion K-436 and K-923 transitions calculated according to the single-particle formulas. Let us compare them with the experimental ratios. In spherical nuclei in which the low-lying levels are vibrational, the probability of a transition from the second excited level to the ground level is usually reduced by a factor of 10 to 100. In Ce^{140}, however, the lower levels are apparently single-particle ones, so that there is no reason to assume an appreciable deviation from the single-particle formulas. We shall consider the agreement between the experimental and theoretical values to be satisfactory if the two values do not differ by a factor of more than 100.

Glancing down all the columns in Table 4 pertaining to de-excitation of the 2520 kev level, we see that there is no satisfactory agreement as regards all three ratios for any value of the spin. Still of all the assignments remaining after the elimination of A and B, the assignments 3- and 4+ can be safely excluded. In order to explain the divergence in Table 4 for the remaining two assignments (2+ and 3+) we must assume that there is a strong inhibition of some of the transitions (for example that either the 923 kev or the 2520 kev transition probability is reduced by a factor of 1000) or that one of the experimental values is wrong. In particular, if the assignment 2+ as proposed by Coleman is correct, the difficulty lies in explaining the $\gamma_{436}/\gamma_{2520}$ ratio: one can hardly infer that the 436 kev γ-line is actually 1000 times weaker, for then α_K would be very large; similarly we cannot assume that the

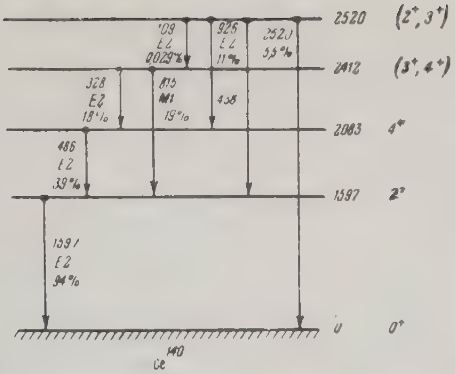

Fig.6. Diagram of transitions between the low-lying levels of Ce^{140}.

2520 kev γ-ray is 1000 times stronger. We must conclude therefore that the theoretical ratio $\gamma_{436}/\gamma_{2520}$ is off and that the 2520 kev γ-line is weakened by a factor of 1000.

The scheme of the transitions between the low-lying levels of Ce^{140} is shown in Fig.6.

The authors desire to thank N.M. Anton'eva for constant help in the work and students L.Chekunova and N.Makhova for assistance in carrying out individual series of measurements.

Physical Institute,
Leningrad State University

References

1. L.V.Arkhangel'skii, B.S.Dzhelepov, N.N.Zhukovskii, V.P.Prikhodtseva & Iu.V.Khol'nov, Izv.AN SSSR, Ser.fiz., 19, 251 (1955) (Trans. Bulletin, 19, No.3, 228.)
2. A.A.Bashilov, B.S.Dzhelepov & L.S.Chervinskaia, Izv.AN SSSR., Ser.fiz., 18, 88 (1954).
3. B.S.Dzhelepov & A.A.Bashilov, Izv.AN SSSR, Ser.fiz., 14, 263 (1950).
4. J.Cork, A.Stoddard, J.LeBlanc, C.Branyan, D.Martin & W.Childs, Phys. Rev., 83, 856 (1951).
5. C.Coleman, Phil.Mag., 46, 1132 (1955).
6. A.Hedgran & D.Lind, Arkiv. f. Fysik, 5, 177 (1952).
7. R.Osborne & W.Peacock, Phys.Rev., 69, 679 (1946).
8. L.Miller & L.Curtiss, Phys.Rev., 70, 983 (1946).
9. W.Rall & R.Wilkinson, Phys.Rev., 71, 321 (1947).
10. L.Beach, C.Peacock & R.Wilkinson, Phys.Rev., 76, 1624 (1949).
11. R.Bannerman, G.Lewis & S.Curran, Phil.Mag., 42, 1097 (1951).
12. B.Robinson & L.Madansky, Phys.Rev., 84, 1067 (1951).
13. C.Peacock, J.Quinn & A.Oser, Phys.Rev., 94, 372 (1954).
14. H.Bolotin, C.Pruett, P.Roggenkamp & R.Wilkinson, Phys.Rev., 99, 62 (1955).
15. A.Mitchell, L.Langer & L.Brown, Phys.Rev., 71, 140 (1947).
16. A.Hanson, Phys.Rev., 75, 1794 (1949).
17. C.Bishop, R.Wilson & H.Halban, Phys.Rev., 77, 416 (1949).
18. A.Wattenberg, Phys.Rev., 74, 497 (1947).
19. L.A.Sliv & I.M.Band, Tablitsy koeffitsientov vnutreniei konversii gamma-izlucheniia (Tables of internal conversion coefficients)., M.-L., 1956.
20. G.F.Dranitsyna, Koeffitsienty vnutrennei konversii na L_I, L_{II} and L_{III} podobolochkakh (L_I, L_{II} and L_{III} internal conversion coefficients), M.-L., 1957.
21. C.Bishop & J.Perez Y Jorba, Phys.Rev., 98, 89 (1955).
22. Beta- and Gamma-Spectroscopy, edited by K.Siegbahn, Amsterdam, 1955.
23. V.P.Prikhodtseva & Iu.V.Khol'nov, Present issue of the Bulletin, p. 173.

PRECISION ENERGY MEASUREMENTS OF SOME LINES IN THE SPECTRA OF Ir^{192}, Eu^{152} AND Eu^{154}*

- V.A.Romanov

Often precise knowledge of transition energies is important in studying the decay schemes of radioactive elements. In addition, most β-spectrometers are calibrated with reference to lines of known energy. Such calibration is feasible only when an adequate number of such lines is available. There are several lines whose energies have been established with considerable accuracy thanks to repeated measurements by different investigators using various appropriate procedures. These are the so-called "standard" lines.[1] Most frequently the conversion lines of RaTh active deposit are used for calibration of spectrometers.

One of the methods of accurate determination of conversion line energies is comparison of these with the energy of a standard line. A convenient instrument for this purpose is a "prism" β-spectrometer: the small line half-width obtained on instruments of this type allows of accurate determination of the line positions in the spectrum. Use of the displacement procedure** in investigating the spectrum allows of excluding the influence of hysteresis and thus makes it feasible to determine the energy separation between conversion lines with high accuracy. The high linear dispersion of β-spectrometers makes for less exacting requirements as regards accuracy of positioning of the sources in the spectrometer.

We used a prism β-spectrometer to determine the energies of some conversion lines in the spectra of Ir^{192} and $Eu^{152,154}$. The energies of the K lines associated with the 296, 308 and 316 kev transitions[3] in the spectrum of Ir^{192} were determined by comparing the positions of these lines with the positions of the I(E - 222.22 ± 0.03 kev) and J(E = 234.61 ± 0.03 kev) lines of a RaTh active deposit. The measurements were carried out with a line half-width of 0.04%. The source dimensions were 1 x 10 mm; the superficial density ~0.48 mg/cm^2. In order to eliminate errors associated with inaccuracy in positioning the source in the spectrometer, the RaTh active deposit was applied directly to the iridium source. With the 0.04% line half-width the line broadening due to application of the RaTh layer was noticeable only after application of a third coat and did not affect the accuracy of measurement. The Ir^{192} spectrum and the RaTh active deposit spectrum were studied simultaneously, i.e., the corresponding ThB and Ir^{192} lines were recorded alternately 8 to 10 times in order to exclude the influence of slow variations of field in the spectrometer, connected, apparently, with temperature fluctuation.

The energy separation between the K-296 and I lines proved to be 4.700 ± ± 0.006 kev. The distance between the K-308 line of Ir^{192} and the $J(M_1)$ line in the ThB spectrum was 4.609 ± 0.005 kev and the separation between the K-316 line and the $J(M_1)$ line of ThB was 3.447 ± 0.004 kev. Thus we obtain the following values for the energies of the enumerated K conversion lines:

---

*This report was presented at the Seventh All-Union Conference on Nuclear Spectroscopy.

**The method of displacement is described in Ref.2. In using this procedure the conversion electron source is insulated from the spectrometer housing. A voltage is then applied between the housing and source. By varying this voltage one can study narrow sections of the spectrum with a constant value of the field in the magnet gap and lenses.

K-296 $E = 217.52 \pm 0.03$ kev,
K-308 $E = 230.00 \pm 0.03$ kev,
K-316 $E = 238.06 \pm 0.03$ kev.

Until now there have been no accurate determinations of the energy of the 374 kev transition since this transition is relatively weak and the K-374 line (conversion in Os) lies in close proximity to the L-316 line. Under our conditions the K-374 and L-316 lines were well separated. We determined the energy of the K-374 line by measuring the separation between it and the L_{II}-316 line; we found the difference to be 2.61 ± 0.01 kev. Accordingly, the energy of the K-374 line is $E = 300.54 \pm 0.04$ kev.

The energy of transitions can readily be calculated by using the tabular values for the electron binding energies in atoms[4]. The uncertainty in electron binding energies is about 0.01 kev. In Table 1 we list the latest data in the literature on the energies of some transitions in Ir^{192} together with the results of our measurements. As may be seen from the table our measurements are in good agreement with the results of Johns & Nablo[5] and Baggerly et al[3] and somewhat inferior accuracy to the measurements of Ryde & Andersson[6].

Table 1

Comparison of the results of measurements of the energy (kev) of some transitions in Ir^{192} obtained on different instruments

From photo-electrons (Ref.5)	Crystal diffraction		From our data
	Ref. 6	Ref. 3	
295,8±0,1	295,96±0,10	295,94±0,09	295,87±0,03
308,4±0,1	308,66±0,06	308,45±0,09	308.35±0,03
316,5±0,1	316,52±0,04	316,46±0,09	316,41±0,03
374 ±2		374,7 ±0,5	374,44±0,04

In the case of the spectrum of Ir^{192}, we carried out measurements of the energy difference of conversion electrons from the subshells of Pt and Os and measurements of the energy difference of the electrons from the K shell of Os for the 201 and 205 kev transitions. The results of these measurements are listed in Table 2, together with the binding energy differences in the L subshells of Pt and Os taken from Ref.4.

Table 2

Energy differences (ev) between the conversion lines in the spectrum of Ir^{192}

Lines	Our measurements	X-ray data
K-201 — K-205	4459±1	—
L_{II}-201 — L_{II}-205	4477±2	—
M_{III}-295— L_{I}-308	1289±10	—
L_{III}- 308 — L_{I}- 316	5724±4	—
L_{I}-316 — M_{III}-308	3176±4	—
L_{I} — L_{II} (Os)	585±4	590
L_{II} — L_{III} (Os)	1519±1	1520
L_{I} — L_{II} (Pt)	609±2	605
L_{I} — L_{III} (Pt)	2311±1	2313

As may be seen from the table the results of our measurements are, in general, in good agreement with those of Hill, Church & Mihelich[4]. From the measured energy separation between the conversion lines associated with the 201 and 205 kev transitions one can accurately determine the energy difference between the transitions. It is 4.477 ± 0.002 kev.

Recently Andersson[7] published new data on the energy of the transitions in Eu^{152} and Eu^{154}; the energy values given by Andersson for the transitions to the ground states of Sm and Gd differ from the values published earlier and also from the energy values obtained by Bobykin & Novik[8] in our laboratory.

Hence we felt it of interest to determine the energy of these transitions more accurately.

Using the prism β-spectrometer we measured the energy separation between the L_{II} 136.33 ± 0.02 kev line (transformation to Pt) in the spectrum of Ir^{192} (Ref.3) and the M_{III} 122 kev line (transformation to Sm) in the spectrum of $Eu^{152,154}$. Measurements were made using 1 x 10 mm sources and a line half-width of the order of 0.07%. The superficial density of the Ir source was 0.2 mg/cm^2; that of the Eu source was 0.05 mg/cm^2. The sources were alternately inserted in the spectrometer and positioned with an accuracy of 0.1-0.2 mm (which corresponds to an error of 5-10 ev in determining the line positions). It was found that the energy difference between these lines was 2.739 ± 0.006 kev. For control purposes we also carried out a measurement of this quantity using two sources (Ir^{192} and $Eu^{152,154}$) mounted at a distance of 3.5 mm from the other. With this set-up we recorded the Sm M_{III} line in the spectrum of $Eu^{152,154}$ and the Pt L_{II} line in the spectrum of Ir^{192}. In this case the magnitude of the displacement is given by $U' = \Delta E + \delta$, where U' is the displacement of the line, ΔE is the energy difference between them and δ is the displacement of the lines due to the difference between the positions of the sources. Then the sources together with their holders were rotated through 180° and the Sm M_{III} and Pt L_{II} lines again recorded. In this case $U' = \Delta E - \delta$. Thus the uncertainty connected with any inaccuracy in positioning the sources in the spectrometer was eliminated. The value of ΔE obtained from these measurements was 2.744 ± 0.009 kev. Using the electron binding energy tables of Hill, Church & Mihelich[4] and the energy separations between the L and M lines in the spectrum of $Eu^{152,154}$ determined by us earlier[2], we calculated the energy of the transitions to the ground states of Sm and Gd. The values so obtained together with the data from the literature are summarized in Table 3.

Table 3

Energies of the most intense transitions in the spectrum of $Eu^{152,154}$ obtained by different authors

Ref.9 (1950)	Ref.10 (1954)	Ref. 11 (1954)	Ref. 7 (1956)	Ref. 8 (1956)	Our data
122,0	121,8	121,2±0,3	122,31±0,04	121,77	121,75±0,03
123,2	123,4	122,4±0,3	123,54±0,09	123,02	123,06±0,03

As may be seen from the table, our data agree within the limits of the experimental error with the results of Bobykin & Novik[8] and differ appreciably from the values reported by Andersson[7].

Leningrad Physical Technical Institute
Academy of Sciences of the USSR

References

1. Beta- and Gamma-ray Spectroscopy, edited by K.Siegbahn, 1955.
2. V.M.Kel'man, V.A.Romanov, R.Ia.Metskhvarishvili & V.A.Koliunov, Zhur. eksp.i teor.fiz., 32, 39 (1957).
3. L.Baggerly, P.Marmier, F.Boehm & J.DuMond, Phys.Rev., 100, 1364 (1955).
4. R.Hill, E.Church & J.Mihelich, Rev.Sci.Instr., 23, 523 (1952).
5. M.W.Johns & S.V.Nablo, Phys.Rev., 96, 1599 (1954).
6. N.Ryde & B.Andersson, Proc.Phys.Soc., 68 B, 1117 (1955).
7. B.Andersson, Proc.Phys.Soc., A 69, 415 (1956).
8. B.V.Bobykin & K.M.Novik, Doklady AN SSSR, 115, 263 (1957).
9. J.M.Cork, H.Keller, W.Rutledge & A.Stoddard, Phys.Rev., 77, 848 (1950).
10. E.L.Church & M.Goldhaber, Phys.Rev., 95, 626 (1954).
11. M.R.Lee & R.Katz, Phys.Rev., 93, 155 (1954).

DECAY OF Rh^{106}*

- E.P.Grigor'ev, A.V.Zolotavin, I.I.Kuz'min & E.D.Pavlitskaia

In the present work we investigated the radiation accompanying the $Ru^{106} \rightarrow Rh^{106} \rightarrow Pd^{106}$ chain by means of the double focusing β-spectrometer described in Ref.1. Prior to the present study, however, the instrument was modified as follows: the slit baffles in the vicinity of the source were removed, the thickness of the other baffles was increased to 8-9 mm (aluminum) and the inner surfaces of the instrument near the source and the edges of the two baffles nearest it were lined with beryllium.

Specifically we studied the conversion lines, the continuous β-spectrum and the photoelectron spectrum.

1. The results obtained for the continuous β-spectrum of Rh^{106} indicated significant differences as regards the relative intensities of the β-spectrum components from the data obtained by Alburger[2] by means of a lens spectrometer. With a view to clarifying the reason for the differences, we carried out a series of control measurements of the β-spectra of P^{32}, As^{76} and K^{42}; the results of these led us to conclude that our spectrometer correctly renders the shape of β-spectra up to 3 Mev, but that above this energy there may be distortions of the line shape, probably caused by variations of the field configurations at high values of induction in the magnet, i.e., changes causing impairment of the focusing. The effect, however, does not appear to have any great influence on the position of the spectrum end-point. From our measurements, we determined the end-point energy of the hard β-component to be 3.55 ± ± 0.01 Mev.

In view of the possible instrument distortion of the shape of the hard component, we shall not give our analysis of the composition of the β-spectrum here. The principal difference between our results and the best data in the literature[2] (see figure) is that the hard component, according to our evaluations, has a higher intensity (90%), while the components with end-point energies of 3.1 and 2.4 Mev have lower intensities (3 and 5% respectively).

We made an attempt to determine the intensity of the soft β-spectrum accompanying the decay of Ru^{106}. In view of the appreciable thickness of our source, however, the accuracy of our determination is rather low. We obtained 39.6 ± 0.3 kev for the end-point energy and a value of $0.6^{+0.5}_{-0.1}$ for the intensity of this component relative to the total intensity of the Rh^{106} spectrum.

2. It is difficult to observe internal conversion in Pd^{106} since Z is small and the continuous spectrum is very intense. We succeeded in measuring the K and L conversion lines of the 513 and 623 kev transitions. The results are summarized in the accompanying table in which E_e is the energy of the conversion electrons in the indicated shells, n_e is the ratio of the number of K conversion electrons to the number of electrons in the continuous Rh^{106} spectrum and α_K and α_L are the conversion coefficients in the K and L shells of Pd^{106}. For purposes of comparison, the data of Alburger[2] are also listed in the table.

As may be seen the conversion line intensities as evaluated by Alburger and ourselves are in good agreement. The L-623 line was observed only in our experiments.

The experimental values of K/L for the 513 and 623 kev transitions are very close to the theoretical ones for electric quadrupole radiation. That

---

*Report presented at the Seventh All-Union Conference on Nuclear Spectroscopy.

Table

Experimental data on the internal conversion lines of Rh^{106}

Line	E_{e^-}, kev	Our data			Alburger's data[2]			K/L* for E2
		hν, kev	n_{e^-}	K/L	hν, kev	n_{e^-}	K/L	
K	489	513	$(8.0\pm0.5)\cdot10^{-4}$	7.1 ± 1	511	$(7.5\pm1)\cdot10^{-4}$	7.8 ± 1	7.[illegible]
L	509							
K	582	623	$(3.2\pm1.0)\cdot10^{-4}$	5 ± 2	621	$(2.3\pm1)\cdot10^{-4}$	-	6.4
L	620							

*The values of α_K were taken from Sliv & Band[3]; the values of α_L from Dranitsina[4].

these two cascade transitions are E2 was deduced earlier on the basis of investigation of the angular correlation between these two γ-rays[5], experiments on Coulomb excitation of these levels[6] and other measurements. Our results substantiate this deduction.

3. We studied the γ-spectrum of Rh^{106} by observing photoelectrons; the source used had cylindrical symmetry[1]. In the earlier investigation[1] we studied the photoelectron spectrum produced by the γ-rays from Sb^{124}. For the strong and well separated 603 and 1694 kev γ-lines of Sb^{124}, the evaluated intensity ratio was 1.94, (this value comprises a statistical uncertainty amounting to several percent). This result was substantiated by measurements on the Elotron.[7] The geometry of these experiments was the following: diameter of target 3 mm; diameter of radioactive source 0.5 mm. Experiments were also made in which the diameter of the radioactive source was increased to 1 mm. Under these conditions the intensity ratio of the 603 and 1694 kev γ-lines of Sb^{124} increased by 20%. Thus it proved inexpedient to vary the geometry of the source in this direction. In connection with evaluation of the relative intensities of the γ-rays in the low energy region (100 to 400 kev), it must be noted that we did not carry out any special experiments for determining the most suitable geometry of the source or for calibrating the spectrometer. Hence our data on the relative intensities of the low energy γ-transitions may comprise appreciable errors.

In observing the photoelectron spectrum of Rh^{106}, we experimented in two directions.

First, we measured the photoelectrons produced by the 513, 623 and 1052 kev γ-rays and from the data thus obtained determined the transition intensities. The measurements were carried out with targets (radiators) of Pb, Bi and Th. Energies and relative intensities were averaged for all series of measurements. The following results were obtained:

γ-rays, kev	513 ± 0.5	623 ± 1	1052 ± 2
I	1.00	0.53 ± 0.03	$0.04^{+0.03}_{-0.01}$

These results agree with the data obtained by other procedures and published in Refs. 8 & 9. The transitions of energies above 1052 kev are appreciably weaker and could not be satisfactorily observed under our conditions.

Second, we searched the region from 100 to 400 kev, where, according to the available decay scheme, we could expect to find transitions of 150, 220, 240, 345 and 390 kev energies. The difficulties encountered in carrying out these experiments stemmed from the very appreciable Compton recoil background and the low energy and intensity of the γ-rays. We did not observe any photopeaks in this region and evaluated the upper bound of the intensity of possible γ-transitions as $3\cdot10^{-3}$ relative to the intensity of the γ-rays of 513 kev energy. True, we did detect a peak corresponding to a 156 ± 2 kev trans-

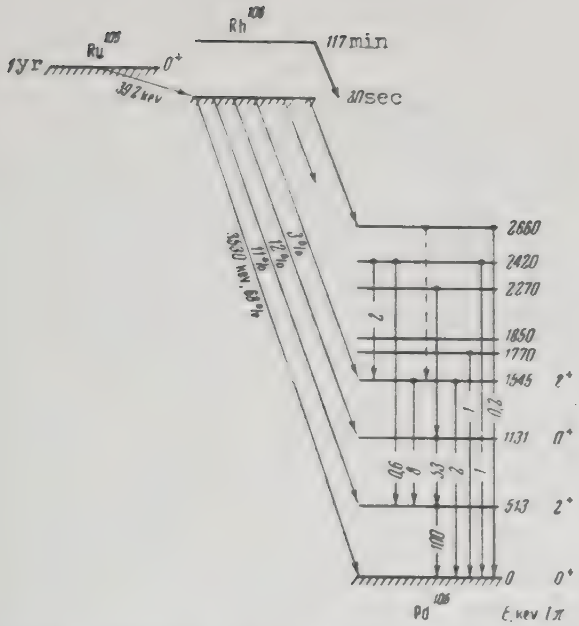

Decay scheme for $Ru^{106} \rightarrow Rh^{106} \rightarrow Pd^{106}$ taken from Dzhelepov & Peker[10]. The intensities of the β-transitions are taken from Alburger[2]; the relative intensities of the γ-transitions indicated in the break of the transition arrows are taken from Refs.2,6 & 11 and our work.

ition (in Bi and Th) with a relative intensity of $(6 \pm 3) \cdot 10^{-3}$. Further experiments are necessary, however, to substantiate the existence of γ-rays of this energy from Rh^{106} inasmuch as our data were obtained at the limit of the experimental sensitivity. The 156 kev γ-rays can correspond to a transition between the 2.42 and 2.27 Mev levels.

4. In the decay scheme proposed by Alburger there is inconsistency between the intensities of the β-spectrum components and the relative intensities of the γ-transitions: specifically, the conversion coefficient for the 513 kev transition calculated on the basis of the decay scheme differs greatly from the theoretical value for E2, which is the assignment for the 513 kev transition. Thus, if we accept the Alburger scheme (see figure) and take the number of conversion electrons per disintegration to be $8 \cdot 10^{-4}$, we obtain $\alpha_K = (2.7 \pm 1) \cdot 10^{-3}$, whereas the theoretical value for E2 is $4.87 \cdot 10^{-3}$ (Ref.3).*

In order to reconcile these two values, we must assume that the intensity of the β-component with end-point energy 3.53 Mev is close to 83%, that of the 3.1 Mev end-point energy component is 6% and that of the 2.4 Mev end-point energy component is 9%. The relative intensities of the 513 and 623 kev γ-transitions have been determined with good accuracy, as is evinced by the agreement of the values given in Ref. 2, 8 & 9 and those obtained by us. The other higher energy transitions are of very low intensity so that any errors in determining their intensities will have no appreciable effect on the result of the evaluation.

With the above intensity values the conversion coefficient for the 623 kev transition is found to be $(3.5 \pm 1) \cdot 10^{-3}$, if one uses our value of $n_{e^-} = (3.2 \pm 1) \cdot 10^{-4}$. This value of the conversion coefficient is not far from the value of $2.85 \cdot 10^{-3}$ given by Sliv & Band for E2 transitions.

Physical Institute,
Leningrad State University

References

1. A.V.Zolotavin, E.P.Grigor'ev & M.A.Abroian, Izv.AN SSSR, Ser.fiz., 20, 289 (1956). (Trans. Bulletin, 20, No.7, 271.)
2. D.E.Alburger, Phys.Rev., 88, 339 (1952).

---

*In Ref.2 the value is erroneously given as $\alpha_K = (3.5 \pm 1) \cdot 10^{-3}$ instead of $(2.5 \pm 1) \cdot 10^{-3}$.

3. L.A.Sliv & I.M.Band, Tablitsy koeffitsientov konversii (Tables of conversion coefficients), M.-L., 1956.

4. G.V.Dranitsina, Koeffitsienty vnutrennei konversii na L_I, L_{II}, L_{III} podobolochkakh (L_I, L_{II} and L_{III} internal conversion coefficients), M.-L., 1957.

5. Kraucher, Phys.Rev., 85, 727 (1952).

6. G.M.Temmer & D.E.Alburger, Phys.Rev., 98, 1308 (1955).

7. B.S.Dzhelepov, N.N.Zhukovskii & V.G.Nedovesov, Report presented to the Fifth Conference on Beta- and Gamma-ray Spectroscopy, M., 1956.

8. D.C.Lu, W.H.Kelly & M.L.Wiedenbeck, Phys.Rev., 97, 139 (1955).

9. B.Kahn & W.S.Lyon, Phys.Rev., 92, 902 (1953).

10. B.S.Dzhelepov & L.K.Peker, Skhemy raspada radioaktivnykh izotopov (Decay schemes of radioactive isotopes), M.-L., 1957.

11. D.E.Alburger & B.J.Toppel, Phys.Rev., 100, 1357 (1955).

TWIN MAGNETIC LENS SPECTROMETER WITH IMPROVED FOCUSING FOR RECORDING COINCIDENCES

- V.A.Sergienko

Introduction

Observation of β-e and e-e coincidences in the decay of radioactive isotopes yields direct data on the correlation between β and γ-transitions and between different γ-transitions. Together with measurements of the energy and relative intensities of γ-transitions, investigation of coincidences allows of establishing the decay schemes.

The principal advantages of magnetic spectrometers as compared with double-coincidence scintillation spectrometers are their higher spectral resolution and better resolving time characteristics. In view of this, magnetic spectrometers can be successfully used for determination of decay branching ratios, absolute conversion coefficients and lifetimes of excited nuclear states.

The most important characteristics of a double coincidence spectrometer are its transmission factor and its resolution as regards energy and time. These characteristics determine the ratio of the number of true to the number of chance coincidences. The higher the transmission factor and the better the resolution as regards energy and time, the higher will be this ratio and hence the more dependable and accurate the ensuing determination of the decay scheme of even complex nuclear disintegrations.

To date, there have been published a number of articles[1-3] describing spectrometers with a high value of the ratio of the number of true to accidental coincidences for investigating β-γ coincidences and one report[4] describing an instrument for investigating β-e and e-e coincidences. In contrast to earlier investigations[5-13], in which spectrometers with 180° focusing and spectrometers with thin lenses were used for studying β-e and e-e coincidences, the instrument described in Ref.4 is a spectrometer with thick lenses. At the same resolution, spectrometers with thick lenses have an appreciably higher transmission factor than spectrometers with thin lenses and spectrometers with 180° focusing. Of great interest from the standpoint of coincidence measurements are spectrometers with toroidal lenses[1,14] characterized by a high transmission factor and good resolution. The theory of double coincidence magnetic spectrometers is discussed in detail in the work of Gerholm[15].

In the present report we shall describe a spectrometer designed for investigation of β-e and e-e coincidences and characterized by a good ratio of the numbers of true to chance coincidences. This instrument was constructed in the Department of Nuclear Spectroscopy of Leningrad State University.

General descroption of the spectrometer

A diagram of the twin magnetic lens spectrometer is shown in Fig.1. The two symmetrical spectrometers have a common vacuum chamber 240 cm in length and 25 cm in diameter. The source is introduced into the chamber without disturbing the vacuum through a special lock. The distance from each counter to the source is 125 cm. Each 30 cm lens consists of 10^4 turns of 1.8 mm diameter wire.

To determine the position of the focus and its dimensions, we measured the variation of the magnetic field of the lenses with r and z, where r is the distance from the instrument axis and z is the distance from the central plane of the lens.

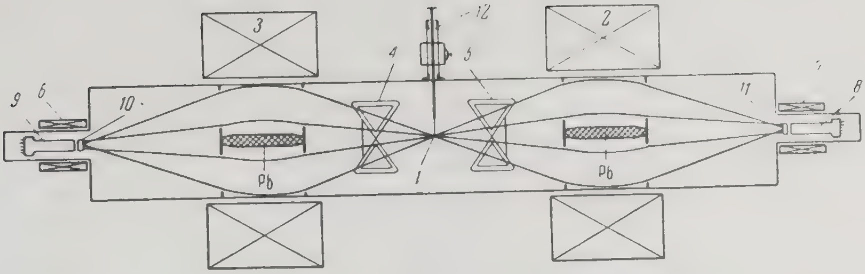

Fig.1. Diagram of twin magnetic lens spectrometer: 1) source, 2 & 3) magnetic lenses, 4 & 5) correcting coils, 6 & 7) compensating coils, 8 & 9) photomultipliers, 10 & 11) crystals, 12) blocking device.

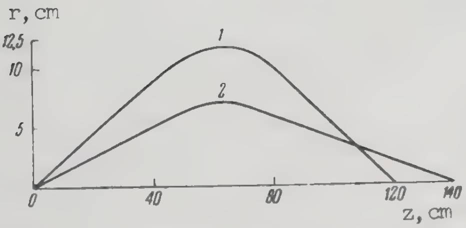

Fig.2. Electron paths calculated for angle of emergence of 1) 13° & 2) 7°.

The field was investigated by the ballistic procedure with intervals of 2 cm between points. The relative error in these measurements was 0.1-0.5%. Using the field configuration determined in this manner, we calculated the electron trajectories by the method of Goddard & Klemperer[16] for different electron emergence angles in the interval from 13 to 7°. The electron trajectories obtained for angles of emergence of 13 and 7° are shown in Fig.2. The diameter of the electron "image" on the spectrometer axis for a point source and a divergence angle of 6° is 25 mm; the electron image is, naturally, somewhat larger with a source 5-10 mm in diameter.

The maximum obtainable angle of divergence in the electron beam is 8° in both parts of the spectrometer. The solid angle defined with this divergence angle is 2% of 4π. The electron beam in each spectrometer is defined by two annuli mounted at 48 and 80 cm from the source. The half-width of the ThB F conversion line in the absence of correction of the lens field is 3% with a 2° angle of divergence and 8% with an 8° angle of divergence.

The number of true coincidences per unit time in a twin spectrometer is proportional to the product of the transmission factor of the first instrument by the transmission factor of the second. Obviously, increase in the transmission factor of each spectrometer (without sacrifice of resolution) leads to an increase in the number of true coincidences. In order to enhance the transmission factors of the spectrometers, we used the procedure for improving the focusing properties of lens spectrometers described in Ref.17. The application of an additional toroidal magnetic field made it possible to compensate to an appreciable extent the spherical aberration of the lenses and to increase the angle of divergence of the electron beam in each spectrometer from 2 to 8° without impairing the resolution. With the correcting field applied, the diameter of the electron image with an angle of divergence of 8° (and a source 5 mm in diameter) is 12 mm; the half-width of the ThB F conversion line under these conditions does not exceed 3.5%. The shape of the ThB F conversion line recorded with and without correction with a counter having a 6 mm diameter window is shown in Fig.3. The use of an additional toroidal magnetic field for improving the transmission factor of a lens spectrometer and the results obtained thereby are described in detail in Ref.17a.

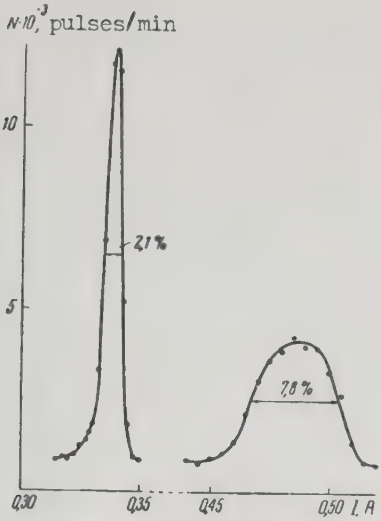

Fig.3. ThB F conversion line recorded with (1) and without (2) correction of the spectrometer field by a weak toroidal magnetic field; counter window diameter 6 mm.

Tests showed that the magnetic coupling between the lenses is negligible. If with one lens operating the other lens is switched on, the current in the former need only be adjusted by about 5% to refocus the electrons. The two spectrometers are provided with separate power sources (Ref.17a) and operate independently, i.e., each focuses electrons of a given energy regardless of the electrons being detected by the other instrument.

With an optimum ratio of the current through the lens and correction coil windings (1:1.5), each spectrometer is capable of discriminating electrons of up to 1.2 Mev energy. For investigating electrons of higher energy, the correcting coils are connected in series with the lenses. In this case, although the resolution is somewhat impaired, the spectrometers can focus electrons of up to 2.5 Mev.

In view of the large distance between the source and counters, the Earth's magnetic field in the absence of compensation has an appreciable influence on low energy electrons and distorts the proportionality between the current and the lenses and the momentum of the recorded electron. Hence six special rectangular section coils are provided for compensating the Earth's field; these are located about 2 m from the spectrometer chamber; four of the coils measure 6 x 4 meters, while the other two measure 4 x 4 meters. The coils consist of some 100 to 200 turns and carry a current of from 0.2 to 1 amp. The residual field in the spectrometer as measured by means of a search coil and ballistic galvanometer does not exceed 1-5% of the normal Earth's field.

Adjustment of the lens spectrometer consists of aligning the magnetic axis of the lens with the geometric source-counter axis. The spectrometer may be regarded as adjusted when electrons with a given energy are focused with the same value of the current in the lens winding regardless of its direction and the counting rate does not differ by more than 5-10% when the current through the lenses is reversed. In practice, we adjusted the spectrometers separately with reference to the ThB F line. Alignment of the magnetic axes with the geometric source-counter axis was realized by successive displacement of the lenses. The requisite direction of displacement of the spectrometer lenses was determined from the shape of the electron image by means of an auxiliary 1 x 2 x 4 cm magnet located in the chamber in the vicinity of the counter. Only the current in the lenses was reversed during the adjustment; the current through the correcting coils was always in the same direction.

Scintillation counters

The accuracy obtainable in measuring β-e and e-e coincidences is determined by the true coincidence counting rate and the ratio of the number of true to the number of chance coincidences. In investigating low intensity decay branches it is obviously necessary to use sources with a high activity. In order to obtain a good value of the ratio N_{true}/N_{ch} (where N_{true} is the number of true coincidences and N_{ch} is the number of chance coincidences) with

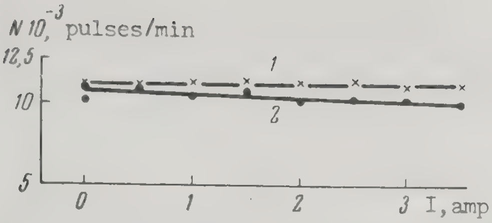

Fig.4. Variation of the number of pulses recorded by the counters to the current in the lenses: curve 1 pertains to the first counter; curve 2 to the second counter.

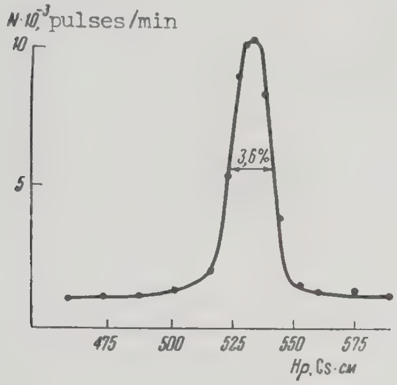

Fig.5. ThC A conversion line recorded with one half the spectrometer (24 kev electrons).

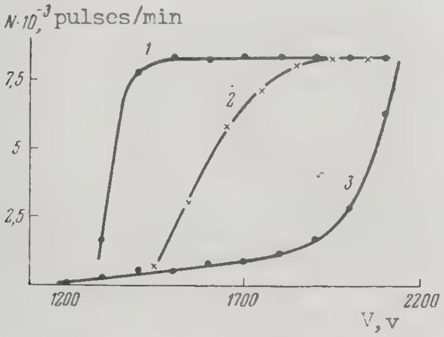

Fig.6. Variation of the efficiency of the scintillation counter in detecting 24 and 148 kev electrons and of the background pulse counting rate as a function of the operating voltage of the photomultiplier: 1) counting rate for 148 kev electrons, 2) for 24 kev electrons, 3) number of background pulses per min. In the region of saturation the detecting efficiency is virtually 100%.

a high activity source one must discriminate the β-e and e-e coincidences by means of a coincidence circuit with a short resolving time. Miniature Geiger-Müller counters filled with an appropriate gas mixture can be used in coincidence circuits with a minimal resolving time of $(4\text{-}5)\cdot 10^{-8}$ sec. With a shorter resolving time, a part of the true coincidences are missed due to lag of the beginning of development of the discharge in the counter with reference to the instant of entry of the particle into the counter.[18-21]

Hence we used scintillation counters with FEU-19M type photomultipliers and stilbene crystals in our instrument. Both the photomultipliers and crystals were located in the vacuum.

In the region of the counters the magnetic field due to the lenses ranges from 0 to 30 oersted as the lens current is increased from 0 to 3 amp. Since a field of a few oersted noticeably affects the electrostatic focusing of electrons in the FEU-19M photomultiplier, additional compensating coils 15 cm in length and 10 cm in diameter were provided to obviate the disturbing influence of the magnetic field of the lenses. These compensating coils are mounted inside the respective photomultiplier housings and surround the photocathode and all the dynodes. With a 1 to 20 ratio of the current through the compensating coils to the current through the lenses, the influence of the magnetic field on the operation of the photomultipliers is eliminated throughout the operating range of the spectrometers. The variation of the counting rate with the current in the lenses (with external loading of the counters) is shown in Fig.4.

Installation of the scintillation counters in the vacuum of the instrument with compensation of the lens field by means of the auxiliary coils does away with the need of using light pipes, which makes it possible to detect electrons of low energy. The spectrometer can be used for detecting electrons of energies from 5 kev; the efficiency in recording electrons of 25-30 kev energy is close to 100%.

The "dark pulse" counting rate with an operating voltage of about 2 kev is approximately 1000 pulses/min. To illustrate the operation of the scintillation counters,

we reproduce in Fig.5 the record of the ThC A conversion line (electron energy 24 kev) and in Fig.6 curves characterizing the variation of the counting efficiency for 24 and 148 kev electrons and of the "dark pulse" counting rate as a function of the operating voltage.

Recording system

The principal component of the recording system of the twin spectrometer is the coincidence circuit. Its resolving time determines the chance coincidence rate. By employing additional wide-band amplification of the signals one can obtain a higher resolving power with an efficiency of the coincidence circuit close to 100%.

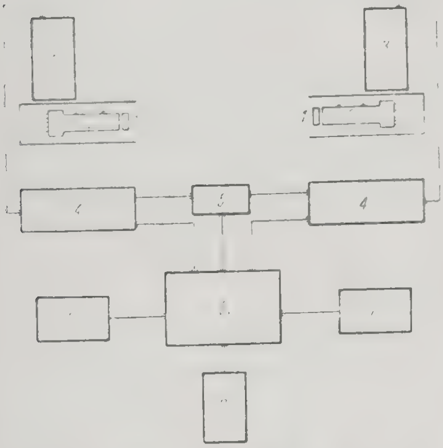

Fig.7. Block diagram of the spectrometer recording system: 1) scintillation counters, 2) FEU-19M photomultipliers, 3) pre-amplifiers, 4) main amplifiers, 5) double coincidence circuit, 6) triple coincidence circuit, 7) scalers.

The recording system of the spectrometer is essentially a slow-fast coincidence network. A block diagram of the system is shown in Fig.7. The pre-amplifiers receiving the output pulses of the scintillation counters are mounted directly on the photomultiplier housings. Pulses going to the fast coincidence circuit are amplified by wide-band amplifiers.

Each pre-amplifier consists of a 3-tube amplifier with distributed amplification and two matching output stages with 150 ohm plate loads. The passband of the pre-amplifiers is 100 Mc; the transmission factor about unity.

Each main amplifier consists of a matching input stage with a plate load and two stages of distributed amplification, employing 4 and 5 tubes. The two amplifiers are identical, have a passband of 130 Mc and a gain of 25. Two signals are taken off each amplifier by means of a buffer tube: one goes to the fast double coincidence circuit, the other to the slow triple coincidence circuit. The grid and plate circuits of the amplifiers with distributed amplification incorporate M-filter sections. The characteristic impedance of all the lines is the same and equals 460 ohm. The total inductance of each coil is 1.3 μH, the inductance of each half of the coil is 0.533 μH and the mutual inductance between the coil sections is 0.117 μH.

All the amplifying and coupling stages are designed about 6Zh1P tubes. High frequency RK-50 cable is used for connecting the various components. The output matching cascades in the pre-amplifiers and amplifiers serve as pulse limiters which makes it possible to obtain pulses with a steep front. Two parallel output stages in the pre-amplifiers serve for checking the entire recording system and evaluating the efficiency of the double coincidence system.

The fast coincidence system is assembled about DGTs-4 diodes. The pulses are shaped (limited in duration) by short-circuited lines, much as outlined in Ref.22. The triple coincidence circuit is a standard "Iablonia" unit. Use of a controlling triple coincidence circuit improves selection of coincidences, increases the efficiency of the double coincidence circuit and enhances the stability of the operation of the entire system.

The optimum operating conditions for the photomultipliers were selected with both photomultipliers viewing the same crystal and connected into the coincidence circuit. The voltage distribution to the electrodes was selected so as to obtain a maximum pulse height after the coincidence circuit and a maximum counting rate.

The resolving time of the recording system as determined from the number of chance coincidences with independent loads on the counters and by the method of delayed coincidences, using a suitable cable, was found to be $(1-2)\cdot 10^{-8}$ sec. The efficiency of the coincidence circuit for electrons of >40 kev energy is about 95%. With the FEU-19M photomultiplier tubes it proved impossible to obtain a higher resolving power without sacrifice of efficiency. Reducing the length of the short-circuited lines led to a rapid decrease of the recording efficiency.

The settling time of the recording system with a 100 Mc passband is $(5-4)\cdot 10^{-9}$ sec. By limiting the pulses in height at the output of the wideband amplifiers, one can obtain pulses with a leading edge rise time of about 10^{-9} sec. Hence, by employing photomultipliers with better time parameters than the FEU-19M, it should be possible to obtain a coincidence circuit resolving time of the order of 10^{-9} sec.

Calibration of the spectrometer

In investigating β-e and e-e coincidences in radioactive isotopes by means of a twin spectrometer, correlation between β-γ and γ-γ transitions can be regarded as definitely established when the ratio $N_{true}/N_{ch} > 1$. If this ratio is smaller than unity, one can only infer the possibility of correlation. The magnitude of the ratio N_{true}/N_{ch} depends on the parameters of the spectrometer and decay scheme of the isotopes.

Let us assume that the lines under investigation do not overlap, that the photomultiplier background and the background due to scattering of electrons and γ-rays are small as compared with the loads on the respective counters and that the lifetime of the intermediate state between the two transitions in question is much shorter than the resolving time of the coincidence circuit. Let us further assume that the electron detecting efficiency is 100%, that the source has a high specific activity and that multiple electron scattering in the source and source backing is negligible.

If the first spectrometer selects a conversion line corresponding to the first transition and the second a line corresponding to the second transition, then the counting rate in each channel is described by the following general expression[15]

$$N = N_0 \varphi(p) \eta p \omega + N \delta \alpha \omega, \tag{1}$$

where N_0 is the number of disintegrations per unit time, $\varphi(p)$ is a function characterizing the electron distribution in the continuous spectrum, p is the momentum of the detected electrons, η is the relative line half-width, ω is the effective solid angle (as a fraction of 4π), δ is the probability of the given γ-transition (referred to the total number of disintegrations) and α is the probability of conversion of the given transition in the K, L or other shell of the atom.

The coincidence counting rate is given by the expression

$$N_{true} = \{N_0 \delta_1 \alpha_1 \omega_1 \delta_2 \alpha_2 \omega_2 \eta_1 q_2 + N_0 \varphi(p_1) \eta_1 p_1 \omega_1 \delta_2 \alpha_2 \omega_2 \eta_2 q_2 + \tag{2}$$

$$+ N_0 \varphi(p_2) \eta_2 p_2 \omega_2 \delta_2 \delta_1 \alpha_1 \omega_1 \eta_1 q_1\} \varepsilon, \tag{3}$$

[illegible]

where q is the probability that the γ_2-transition follows the γ_1-transition or that the γ_1 and γ_2-transitions follow the β-transition, ε is the coincidence recording efficiency and 2τ is the resolving time of the coincidence circuit.

Then for N_{true}/N_{ch} we can write

$$\frac{N_{true}}{N_{ch}} = \frac{\varepsilon}{2N_0\tau}\cdot\frac{{}_1q_2 + {}_\beta q_1\chi_1 + {}_\beta q_2\chi_2}{1+\chi_1+\chi_2+\chi_1\chi_2}, \tag{4}$$

where $\chi = \frac{\varphi(p)\,p\eta}{\alpha\delta}$ is the ratio of the number of detected electrons of the continuous spectrum to the number of conversion electrons.

It will be evident from the above equalities that N_{true} is proportional to the activity of the source and the product of the transmission factors of the first and second spectrometers and that N_{ch} will be the smaller, the better the resolving power of the coincidence circuit. The ratio N_{true}/N_{ch} is determined by the efficiency of detecting coincidences, the relative intensities of the β-γ and γ-γ decay branches and the number of conversion electrons were detected in each channel.

For any given double-coincidence magnetic spectrometer there exist limiting values of the relative intensity of the β-e and e-e chains for which the β-γ and γ-γ branches are still susceptible of investigation. With a view to determining these values in the case of the described spectrometer, we investigated the most intense decay branches of the isotopes ThB, Au^{198} and Ce^{141} and the coincidences between some of the converted γ-transitions in the decay of Yb^{169}.

In all cases the first spectrometer separated and detected the conversion electrons of a given γ-transition, while the second detected electrons of the continuous spectrum or the conversion electrons of other energies. From the total number of electrons detected by the first and second counters, the coincidence circuit selected the electron pairs corresponding to the investigated β-γ or γ-γ decay branch.

The decay scheme of Au^{198} has been thoroughly studied. Its β-spectrum consists of three elementary spectra, two of which lead to excited states of Hg^{198}. We investigated the most intense decay branch, namely, the partial spectrum with an end-point energy of 960 kev and the 411 kev γ-transition following it. The relative intensity of the partial spectrum is 98.66% and the K shell conversion coefficient is 0.0307. Consequently, the relative intensity of this chain is approximately $27.4\cdot10^{-3}$.

The coincidence measurements in this case were carried out before installation of the auxiliary toroidal coil for correction of the lens field. The diameter of the source was 2 mm. The transmission factors of the first and second spectrometers were 0.6 and 1.3%, respectively. The half-width of the conversion line in the first spectrometer did not exceed 2.5%; the second 4%. The resolving time 2τ of the coincidence circuit was $6\cdot10^{-8}$ sec.[29]

The partial spectrum of Au^{198} and its Kurie plot are shown in Fig.8. The end-point energy value obtained is in good agreement with the data of other investigators[24-31]. The ratio N_{true}/N_{ch} varied over the spectrum within the range from 1.5 to 2; the true coincidence counting rate near the maximum of the β-spectrum was 150-160 counts/hour.

The partial spectra of ThB and Ce^{141} were recorded with the lens field correcting coils installed. In this case the transmission factor of each spectrometer was 2% of 4π and the half-width of the conversion line 3.5%. The sources used were 5mm in diameter. The resolving time of the coincidence circuit was $2\tau = (2\text{-}3)\cdot10^{-8}$ sec.

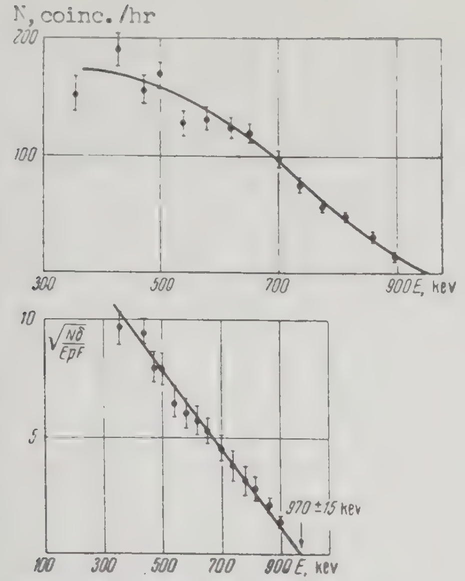

Fig.8. Partial spectrum of Au^{198} and Kurie plot.

In the case of ThB we studied the most intense decay branch: the partial spectrum of end-point energy ~340 kev and the 238 kev γ-transition; in the case of Ce^{141} we studied the partial spectrum with end-point energy 430 kev and the 145 kev γ-transition. The relative intensities of the β-e_K branches are, respectively, $\sim 21\cdot 10^{-2}$ and $1\cdot 10^{-2}$ per decay.

The partial spectrum of ThB and the corresponding Kurie plot are shown in Fig.9; the coincidence spectrum of Ce^{141} and the corresponding Kurie plot - in Fig. 10. The value of the N_{true}/N_{ch} ratio in the vicinity of the maximum in the ThB spectrum was 100 and in the vicinity of the maximum of the Ce^{141} spectrum, 50; the true coincidence counting rates were about 600 and 200 coincidences/hour, respectively. The end-point energies as determined by extrapolation of the Kurie plots to the energy axis were 338 ± 5 kev for ThB and 431 ± 5 kev for Ce^{141}. These end-point energy values are in good agreement with the data in the literature (Refs. 5,8,32 & 33).

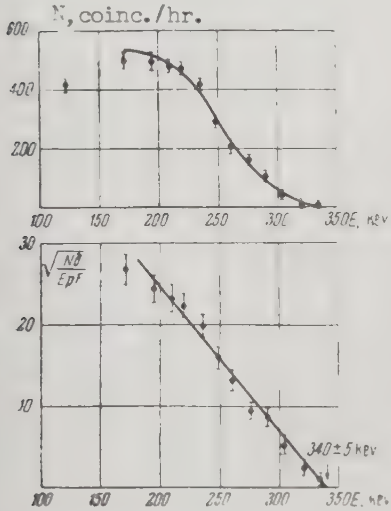

Fig.9. Partial spectrum of ThB and its Kurie plot.

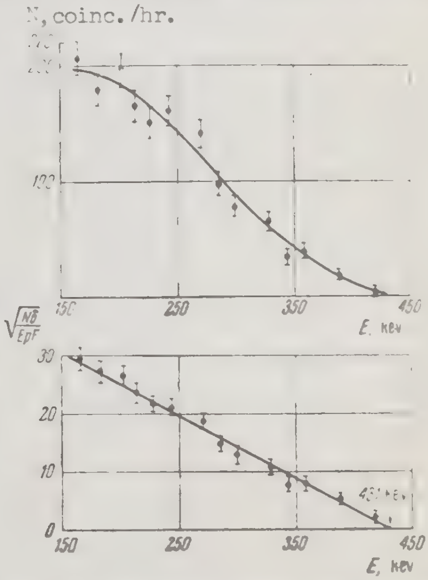

Fig.10. Partial spectrum of Ce^{141} and its Kurie plot.

The conversion electron spectrum of Yb^{169} and the correlation between the γ-transitions in Tm^{169} have been investigated by Kondajan[32] and Cork et al[35]. We separated the e-e coincidences of the 177 and 130 kev transitions. For preparing the source, active Yb^{169}, obtained by chromatographic separation from the fraction of neutron-deficient Lu isotopes, was deposited on a thin lightly aluminized collodion film. The first spectrometer detected the K conversion electrons from the 177 kev γ-transition; the second, the electrons associated

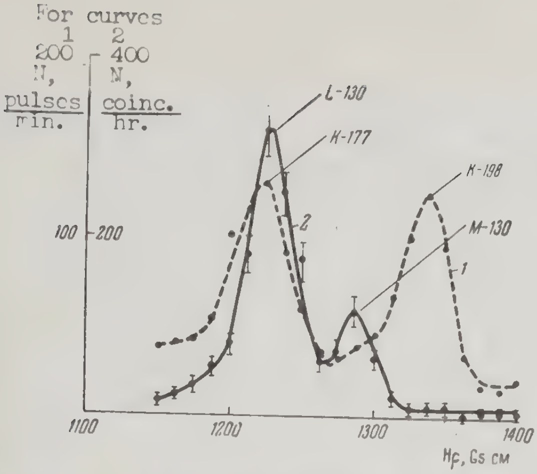

Fig.11. e-e Coincidence of the 177 kev γ-transition with the 130 and 198 kev transitions in the decay of Yb^{169}. 1) conversion electron spectrum; 2) coincidence spectrum.

with the 130 and 198 kev transitions. The K conversion lines of the 177 and 198 kev transitions and of the coincidence-discriminated L and M lines associated with the 130 kev transition are shown in Fig.11. No coincidences between the K conversion electrons of the 177 and 198 kev transitions were observed. These data are in agreement with the decay schemes for Yb^{169}. The results of an investigation of e-e coincidences for neutron-deficient isotopes of Lu, Tm, Gd, Eu and Tb will be described in a separate report.

By virtue of the correction of the lens field by the weak toroidal magnetic field and the use of auxiliary wide-band amplification of the signals from the scintillation counters, the present spectrometer as regards its spectral and time characteristics virtually does not differ from the double coincidence spectrometer with thick lenses described by Gerholm[4] and is appreciably superior to the thin lens and 180° focusing spectrometers described in the literature[5-13].

In our measurements the counting rate for true coincidences at the maximum of the partial spectrum of ThB was more than 10 times higher than the counting rate obtained in studying this spectrum by other authors[5,8] by means of similar thin lens spectrometers, while the N_{true}/N_{ch} ratio was more than 50 times higher. Clearly, the minimal relative intensity of the β-e and e-e branches susceptible of investigation by means of our spectrometer is approximately 100 times smaller than in the case of other similar spectrometers.

From Eq.(4) and the experimental results obtained for β-e coincidences in the decay of radioactive ThB, Ce^{141} and Au^{198} and the e-e coincidences in the decay of Yb^{169}, one can conclude that the described twin spectrometer can be used to study 1) β-e decay branches whose relative intensity is not less than 10^{-3} per disintegration with the end-point energy of the β-spectrum of the order of 0.5-1 Mev and 2) e-e decay branches having a relative intensity of not less than 10^{-5} per disintegration.

The described spectrometer was constructed at the suggestion of B.S.Dzhelepov. The initial design calculations were carried out by P.A.Tishkin. G.S. Kvater participated in the early work on the spectrometer.

I take this occasion to express my gratitude to B.S.Dzhelepov, A.A.Bashilov, G.S.Kvater and P.A.Tishkin for their constant interest in the work and to I.V. Tupitsin for his assistance in building the amplifiers with distributed amplification and adjustment of the recording system.

Physical Institute,
Leningrad State University

References

1. O.B.Nielsen & O.Kofoed-Hansen, Kgl.Danske Videnskab, Nat.Fys.Medd., 29, 6, 19 (1955).
2. R.T.Nichols & A.V.Pohm, Rev.Sci.Instr., 26, 580 (1956).
3. C.Bertolini, C.Bettoni & E.Lazzarini, Nuovo Cimento, 2, 273, (1955).
4. T.R.Gerholm, Rev.Sci.Instr., 26, 1069 (1955).
5. L.V.Groshev & L.Ia.Shavtvalov, Doklady AN SSSR, 68, 257 (1949).
6. E.E.Berlovich, Izv.AN SSSR, Ser.fiz., 16, 314 (1952).
7. R.E.Bell & R.L.Graham, Phys.Rev., 86, 212 (1952).
8. K.Siegbahn, Arkiv Fys., 4, 223 (1952).
9. S.Kageyama, J.Phys.Soc., Japan, i, 689 (1953).
10. J.Kyles, C.G.Campbell & W.J.Henderson, Proc.Phys.Soc.Lond., A 66, 519 (1953).
11. C.Fowler & R.Shreffler, Rev.Sci.Instr., 21, 740 (1950).
12. R.Katz, R.Hill & M.Goldhaber, Phys.Rev., 78, 9 (1950).
13. C.G.Campbell & J.Kyles, Proc.Phys.Soc.Lond., A 66, 911 (1953).
14. V.V.Vladimirskii, E.K.Tarasov & Iu.V.Trebukhovskii, PTE (Instruments & Experimental Techniques), 1, 13 (1956).
15. T.R.Gerholm, Arkiv. Fys., 11, 55 (1956).
16. L.S.Goddard & O.Klemperer, Proc.Phys.Soc., 56, 378 (1944).
17. V.A.Sergienko, PTE (Instruments & Experimental Techniques), 4, 13 (1957).
17a. B.S.Dzhelepov, No Sen Chan & P.A.Tishkin, Izv.AN SSSR, Ser.fiz., 20, 947 (1956). (Trans., Bulletin, 20, No.8, 857.)
18. Alden Stevenson, Rev.Sci.Instr., 23, 93 (1952).
19. C.E.Mandeville, Rev.Sci.Instr., 23, 94 (1952).
20. W.E.Ramsey, Rev.Sci.Instr., 23, 95 (1952).
21. W.C.Porter & W.E.Ramsey, Rev.Sci.Instr., 23, 95 (1952).
22. S.De Benedetti & H.J.Richings, Rev.Sci.Instr., 23, 37 (1952).
23. V.B.Ustinov & V.A.Sergienko, PTE (Instruments & Experimental Techniques), 1, 76 (1958).
24. N.M.Anton'eva, A.N.Bashilov, B.S.Dzhelepov & A.V.Zolotavin, Izv.AN SSSR, Ser.fiz., 14, 299 (1950).
25. L.Elliot & J.Wolfson, Phys.Rev., 82, 333 (1951).
26. L.Elliot, M.Prestom & J.Wolfson, Canad.J.Phys., 32, 153 (1954).
27. P.Levy & E.Grenlind, Phys.Rev., 73, 83 (1948); 75, 819 (1949).
28. O.Saxon, Phys.Rev., 73, 811 (1949).
29. R.Steffen, O.Huber & F.Humbel, Helv.Phys.Acta, 22, 167 (1949).
30. L.Langer & H.Price, Phys.Rev., 76, 641 (1949).
31. C.Fan, Phys.Rev., 87, 252 (1952).
32. E.Kondajan, Arkiv.Fys., 4, 81 (1952).
33. J.T.Jones,Jr. & E.N.Jensen, Phys.Rev., 97, 1031 (1955).
34. A.E.Wen & A.E.Johansson, Phys.Rev., 100, 835 (1955).
35. J.Cork, M.Brice, D.Martin, L.Schmid & R.G.Helmer, Phys.Rev., 101, 1042 (1956).

POSITRON SPECTRUM OF A DYSPROSIUM FRACTION

- B.S.Dzhelepov, O.E.Kraft, B.K.Preobrazhenskii & G.F.Iushkevich

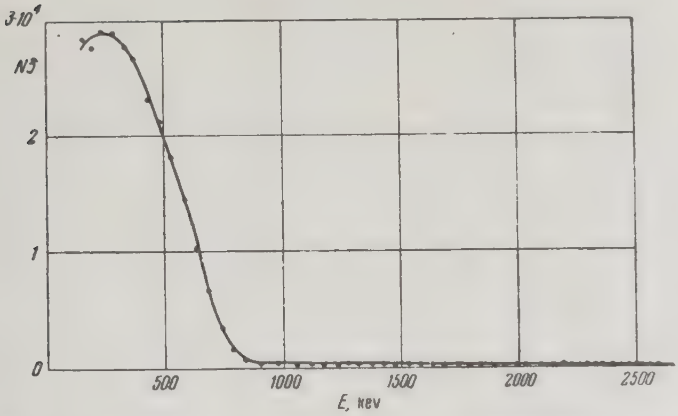

Fig.1. Positron spectrum of the dysprosium fraction recorded 9 hours after separation.

The dysprosium fraction was separated from a tantalum target bombarded with 660 Mev protons and was applied in the form of a thin layer to a 5 μ thick aluminum foil backing. The positron spectrum was observed by means of the triple focusing β-spectrometer described in Ref.1.

The positron spectrum obtained 9 hours after separation of the dysprosium fraction is shown in Fig.1. Observation of the spectrum over a period of time showed that the number of pulses per unit time in different parts of the spectrum fell off with different periods. It was found that the spectrum shown in Fig.1 consists of a surposition of two spectra: a hard component with a period of ~20 hours and a soft component with a period of 11 ± 2 hours. Using these values and having recorded the spectrum several times, we were able to resolve it completely. The Kurie plots of both components are shown in Figs.2 & 3. The end-point energies are 2800 ± 200 and 850 ± 50 kev. It will be evident from Fig.3 that the Kurie plot of the soft spectrum is not rectilinear, but exhibits a break at about 400 kev. It cannot be asserted, however, that this break is a consequence of complexity of the β^+-spectrum inasmuch as in this energy region one must make very appreciable corrections for scattering in the case of our instrument.

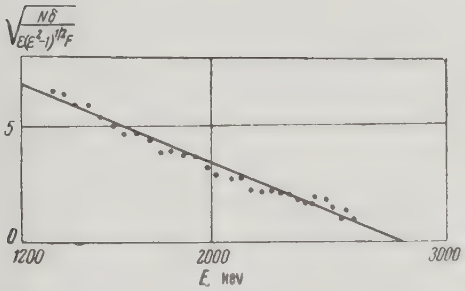

Fig.2. Kurie plot of the positron spectrum with a period of 11 ± 2 hours.

There is no information in the literature concerning a dysprosium isotope with a half-life of 20 hours. A half-life of 8 hours has been encountered and was ascribed to Dy^{157} by Handley & Olson[2]. From the work of Dzhelepov, Preobrazhenskii, Rogachev & Tishkin[3] it is apparent that there exists Dy^{155} with a period of about 10 hours.

In order to determine what isotopes were present in our sample, we investigated its conversion spectrum. Obviously, this investigation was of a tentative or exploratory character inasmuch as our instrument has a low resolution ($\Delta H\rho/H\rho \geqslant 3.5\%$) and is not particularly adapted for the study of line spectra.

We found 11 conversion electron peaks in the spectrum of our dysprosium fraction. Six of them fell off with the same period of 11 ± 2 hours. The observed electron energies were 180 ± 10, 270 ± 15, 320 ± 20, 400 ± 25, 465 ± ± 30 and 610 ± 30 kev. Assuming that all these are K electrons, we obtain the following energies for the corresponding transitions: 230, 320, 370, 450, 515 and 660 kev. These transitions apparently occur in Dy^{155} or Dy^{157}.

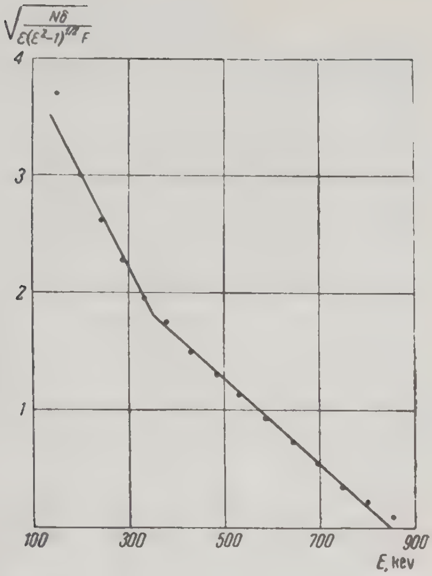

Fig.3. Kurie plot of the hard component of the positron spectrum with a period of ~20 hours.

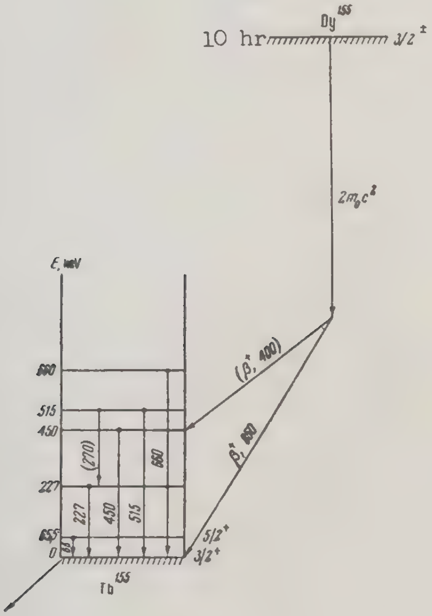

Fig.4. Proposed decay scheme for Dy^{155}.

It is impossible, however, to compare our data with the results of Dzhelepov et al[3] since in their work the conversion electron measurements extended only up to 150 kev energy. In the list of lines recorded by Anton'eva et al[4] for a terbium fraction with a period of 18 hours only two transitions - 442 and 616 kev - have energies close to any of those listed above; in the list of lines obtained for the 8-hour fraction there are no lines of close energies.

We therefore attribute the detected lines to Dy^{155} and Dy^{157}; the tentative decay scheme for Dy^{155} is given in Fig.4.

The intensity of the 220 kev conversion line fell off with a period of ~20 hours. No other lines with this period were observed. Careful repeat investigation of this section of the spectrum showed that here there are located two close lines whose intensities decrease with periods of ~11 hours and ~5 days. The corresponding 270 kev transition can be fitted into the decay scheme shown in Fig.4.

We evaluated the ratio of the number of positrons with end-point energy of 850 kev to the number of conversion electrons from the 515 kev transition and found it to be 37.5.

Four groups of conversion electrons observed at 98, 112, 132 and 162 kev in the conversion spectrum of the dysprosium fraction fell off in intensity with a period of 4.7 days. Comparison of these with the conversion spectrum of the dysprosium fraction described by Dzhelepov et al[3] enabled us to identify these electron groups as K-148, K-162, K-182 and K-210 lines originating in the decay of Tb^{155} (the first three). These substances formed in the decay of Dy^{155} and Dy^{157}. In repeat measurements of the positron spectrum made 240 hours after separation, we did not observe any component with a period close to 5 days. If such a component does exist its intensity relative to the component of the positron spectrum with the 11-hour period is less than 0.3% referred to the time of beginning of measurement (approximately 9 hours after separation).

We can as yet say nothing definite regarding the origin of the 20-hour activity observed by us in the dysprosium fraction.

In the measurements on the terbium fraction carried out by means of the Ketron by Anton'eva et al[4] there were observed positrons with an end-point energy of ~2800 kev and a period of 18 hours. This energy value agrees with

the end-point energy of the hard positron spectrum which we observed in the dysprosium fraction and which has, according to our measurements, a period of ~20 hours. It is possible that this positron spectrum belongs to Tb with a period of 18 hours.

The authors express their gratitude to L.K.Peker for discussion of the decay scheme and to K.Ia.Gromov for organizational assistance.

Physical Institute,
Leningrad State University

References

1. B.S.Dzhelepov & E.O.Kraft, Izv.AN SSSR, Ser.fiz., 20, 318 (1956). (Trans., Bulletin, 20, No.3, 293.)
2. H.Handley & E.Olson, Phys.Rev.; 90, 500 (1953).
3. B.S.Dzhelepov, B.K.Preobrazhenskii, I.M.Rogachev & P.A.Tishkin, Present issue of the Bulletin, p.125.
4. N.M.Anton'eva, A.A.Bashilov, B.S.Dzhelepov & B.K.Preobrazhenskii, Present issue of the Bulletin, p.134.

HIGH-ENERGY GAMMA-RADIATION FROM Na^{24}

- L.V.Gustova, B.S.Dzhelepov, P.F.Ermolov & O.V.Chubinskii

Introduction

As a result of numerous investigations[1-15], we now know the principal features of the decay scheme of Na^{24}: the energies of the β- and γ-transitions, the multipole orders of the γ-transitions, the spins and parities of the levels, etc. (Fig.1). Most of the decays of Na^{24} go to the 4.12 Mev level of Mg^{24}.

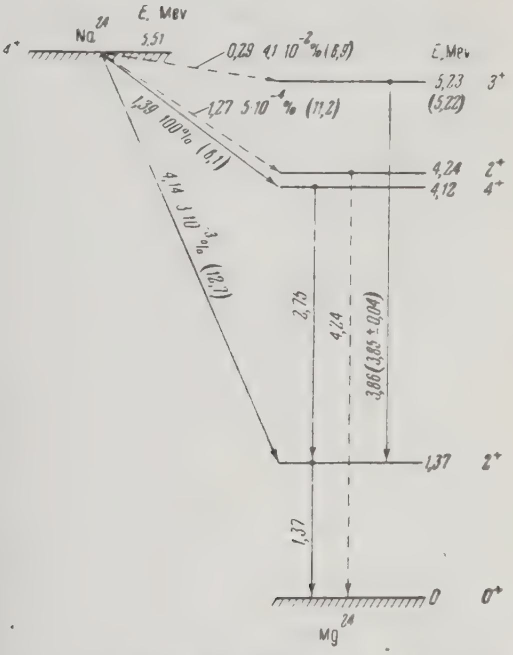

Fig.1. Decay scheme of Na^{24}. The figures in () are the energy values obtained in the present investigation.

The most accurate values for the energy of the cascade γ-transitions were obtained in the work of Hedgran & Lind[12]: 1.3672 and 2.7535 Mev. The intensities of these γ-rays are approximately equal.

In 1951 Turner & Cavanagh[8] detected γ-rays of 3.9-4 Mev energy in the spectrum of Na^{24}; the intensity of these γ-rays according to the determination of these investigators is $5\cdot10^{-4}$ photons per disintegration. The authors inferred that they detected a cross-over transition from the 4.12 Mev level to the ground level of Mg^{24}. In the same year, Beghian, Bishop & Halban[9] also observed hard γ-radiation from Na^{24}; they evaluated its energy as 3.6-3.8 Mev and intensity as $(4.0 \pm 0.4)\cdot10^{-4}$ photons per disintegration. They established that if there does occur a cross-over γ-transition from the 4.12 Mev level of Mg^{24} its intensity is less than $2\cdot10^{-6}$ photons per disintegration. It remains unclear between which levels the 3.6-3.8 Mev transition occurs.

In 1954 Newton[15], investigating the γ-rays from the $Na^{23}(p,\gamma)Mg^{24}$ reaction, discovered a triple cascade transition: 7.6 Mev—3.86 Mev—1.37 Mev. He inferred that the 3.86 Mev γ-rays are emitted in a transition from the 5.33 Mev level to the first excited 1.37 Mev level of Mg^{24} and indicated the possibility of this line originating in β-decay of Na^{24}. It follows from correlation experiments carried out by Newton that the spin of the 5.33 Mev level is 3.

It has been established by a number of researchers (see, for example, Refs.11 & 15), investigating the excited states of Mg^{24} by the method of nuclear reactions, that there exists a level of 4.24 Mev energy which is not evinced in β-decay of Na^{24}.

The present work was concerned with investigation of the γ-radiation from Na^{24} in the energy region above 3 Mev by means of the gamma-hodoscope. The hodoscope and the experimental procedure employed are described in Refs.16 & 17. Most of the results described in the present report were obtained by us in 1955-1956.[18]

Description of the experiment

In investigating the high energy γ-radiation from Na^{24}, we carried out a number of experiments using different sources and different magnetic fields. The sources were primarily preparations of NaCl and Na$_2$Co$_3$ irradiated with slow neutrons. The mean activity of the sources used in different experiments varied in the range from 15 to 200 millicuries. In the experiments the glass tube containing the radioactive material was suspended at a distance of 50 mm from the opening of the collimator.

Our experiments may be subdivided into two groups.

The first group of experiments was devoted to a detailed investigation of the energy composition of the γ-radiation of Na^{24} in the region from 3 to 5.6 Mev. The strength of the hodoscope magnetic field was chosen so that the intense 2.75 Mev line would not be detected at all by the instrument. The measurements were carried out with H = 1520 oersted, using cylindrical counters with cellophane windows, and with H = 1360, 1500 and 1675 oersted, using rectangular counters.

The geometry of the gamma-hodoscope (i.e., the relative arrangement of the source, target and counters) is such that with H = 1360 oersted the instrument records the section of the γ-spectrum in the range from 3.1 to 5.7 Mev (the maximum spectral sensitivity lies in the range from 4.0 to 4.9 Mev); with H = 1500 oersted the instrument records the section from 3.5 to 6.3 Mev (maximum sensitivity - from 4.5 to 5.4 Mev); with H = 1675 oersted the instrument records the γ-spectrum from 3.9 to ~7.0 Mev (maximum sensitivity - 5.0 to 6.0 Mev). The measurements with each value of the magnetic field were carried out twice with different sources. In all cases the reproducibility of the results was satisfactory.

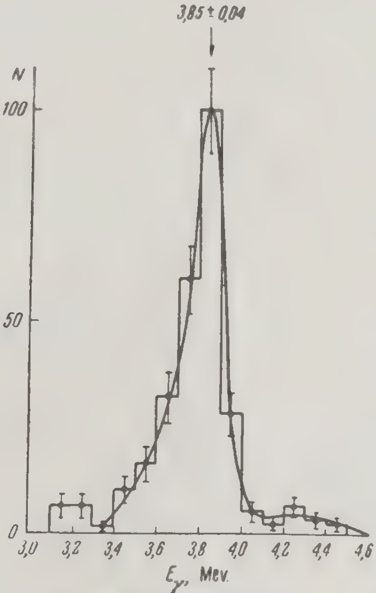

Fig.2. Result of measurements of the γ-radiation from Na^{24} with H = 1360 oersted.

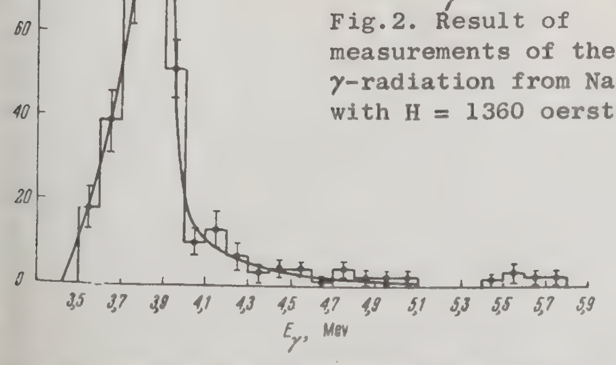

Fig.3. Same as Fig.2 but with H = 1500 oersted.

In processing the results of all measurements, we took into account only the frames (photographs of the neon bulb array coupled to the hodoscope counters) corresponding to recoil electron trajectories with a Compton angle $\varphi \leqslant 6^{\circ}$. This selection process was necessary in order to reduce the distortion introduced into the experimental results by electrons scattered through large angles in the target, counter walls, etc. As a result of this rejection of frames corresponding to $\varphi \leqslant 6^{\circ}$, the "transmission factor" (efficiency) for $h\nu$ = 4 Mev is reduced by 5 to 15%.

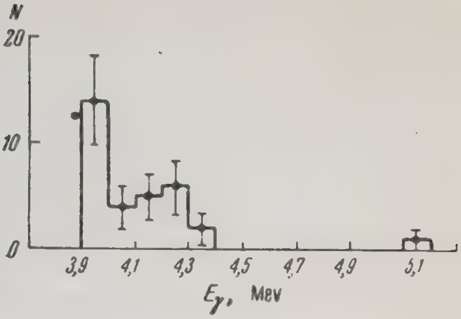

Fig.4. Same as Fig.2 but with H = 1675 oersted.

The experimental results obtained with the rectangular counters are shown in Figs. 2, 3 & 4. The horizontal axes are scaled in γ-ray energies; the vertical axes, in terms of the number of frames contained in the given 100 kev wide spectral interval.

A γ-line of 3.85 Mev energy is clearly discernible in the plot of Figs.2 & 3. The counting rate for this line in both cases fell off in accord with the half-life of Na^{24}: 15 hours. The line has the shape commonly obtained in the hodoscope. The position of the line peak has been determined in both cases with an accuracy of ±0.04 Mev.

The line has a very long high-energy tail. From the shape and magnitude of this tail it can be inferred that the spectrum of Na^{24} contains low intensity γ-rays of 4.1-4.3 Mev energy. In view of the relatively poor experimental statistics and appreciable background due to electron scattering, however, this inference cannot be regarded as definite.

One can determine the upper bounds for the intensity of the possible (in the light of the decay scheme for Na^{24}) 4.12, 4.24 and 5.22 Mev transitions relative to the intensity of the 3.85 Mev transition (Fig.1). Taking into account the spectral sensitivity of the instrument and attributing to the 4.12, 4.24 and 5.22 Mev γ-rays the maximum number of frames consistent with experiment, we obtain the values shown in the accompanying table.

Table

Upper bounds for the intensities of the 4.12, 4.24 and 5.22 Mev γ-lines relative to the intensity of the 3.85 Mev line

H, oersted	Upper bounds of line intensities		
	4.12 Mev	4.24 Mev	5.22 Mev
1360	$2\cdot10^{-2}$	$1.2\cdot10^{-2}$	—
1500	$4\cdot10^{-2}$	$2\cdot10^{-2}$	$6\cdot10^{-4}$
1675	$2\cdot10^{-2}$	$1\cdot10^{-2}$	$5\cdot10^{-4}$

Analogous results were obtained in the experiments with H = 1520 oersted in which cylindrical counters were used.

Thus the first group of experiments leads to the following results: 1) there is a line of 3.85 ± 0.04 Mev energy in the γ-spectrum of Na^{24} and 2) the upper bounds of the possible 4.12, 4.24 and 5.22 Mev transitions are as indicated in the accompanying table.

The second group of experiments was carried out for the purpose of determining the intensity of the 3.85 Mev γ-rays relative to the intensity of the 2.75 Mev γ-rays, the intensity of which is almost exactly 1 photon per disintegration. The experimental conditions were selected so that the gamma-hodoscope would simultaneously record both lines, with the sensitivity with respect to the 3.85 Mev line being much higher than the sensitivity for the 2.75 Mev line. These conditions were realized with H = 1240 oersted with the cylindrical and with H = 1220 oersted with rectangular counters. The results of the measurements with H = = 1220 oersted, after subtraction of the background, are shown in Fig.5.

The line corresponding to γ-rays of 2.75 Mev is asymmetric and the maximum is somewhat displaced to the high energy side inasmuch as with H = 1220 oersted the instrument records mainly the high energy side of this line. The 3.85 Mev line has the "standard" shape.

The results of these experiments lead to a value of $(4.1 \pm 0.9)\cdot10^{-4}$ photons per disintegration for the intensity of the 3.85 Mev γ-line. The

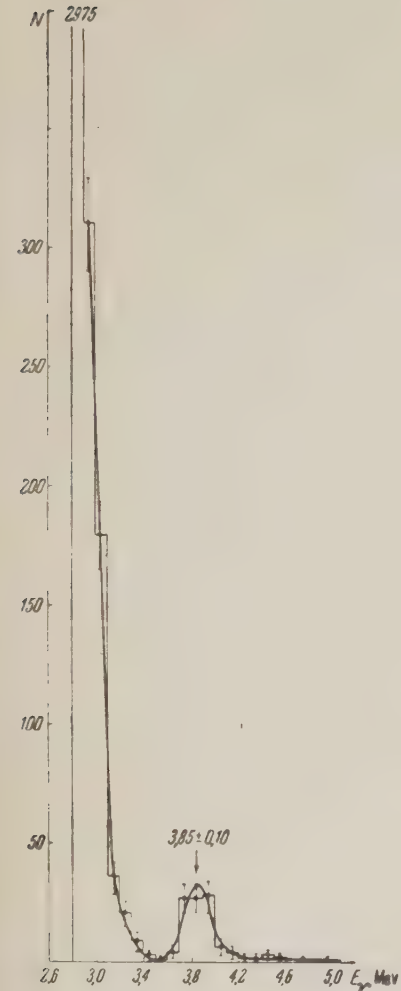

Fig.5. Same as Fig.2 but with H = 1220 oersted.

indicated uncertainty is associated with the uncertainty in determining the spectral sensitivity of the instrument and the inferior statistics of measurement.

Using this last result we obtained the following upper bounds for the intensities of the possible γ-transitions: $I_{4.12} \leqslant 9\cdot10^{-6}$, $I_{4.24} \leqslant 5\cdot10^{-6}$ and $I_{5.22} \leqslant 2\cdot10^{-7}$ photons per disintegration.

Discussion

From the results of the present investigation we can draw certain deductions regarding the character of the β-decay of Na^{24}.

If there occurred β-decay of Na^{24} to the 4.24 Mev level (end-point energy ≈ 1.27 Mev), there would be observed a 4.24 Mev γ-line having an intensity comparable to the intensity of the β-spectrum. According to our data $I_{4.24} \leqslant 5\cdot10^{-6}$ photons per disintegration. Assuming that the intensity of the β-spectrum with end-point energy 1.37 Mev is $5\cdot10^{-6}$, we obtain log ft = 11.3 (Ref.19). This log ft value indicates a twice forbidden β-transition. This deduction is in agreement with the data of earlier investigations (see, for example, Refs.15 & 20) to the effect that the spin and parity of the 4.24 Mev level are 2+.

Our data indirectly substantiates Newton's inference[15] of the possibility of β-decay of Na^{24} to the 5.22 Mev level of Mg^{24} with subsequent emission of 3.85 Mev γ-rays. The other hypothesis regarding the origin of the 3.85 Mev γ-rays is that they are emitted in a transition between the 4.12 Mev level and a new ~0.27 Mev level or between a new 3.85 Mev level and the ground state of Mg^{24}. In order to reconcile these assumptions with the available experimental data on the β- and γ-transitions in the decay of Na^{24} one must assign a spin value of $\geqslant 7$ to these hypothetical (0.27 or 3.85 Mev) levels. Beghian, Bishop & Halban[9] came to the same conclusion. So large a spin value for any of the first excited levels of an even-even nucleus appears little plausible and hence the existence of these levels appears doubtful. On the other hand, the hypothesis of the existence of a 5.22 Mev level is not in conflict with the known data on the β-decay of Na^{24}.

The intensity of the soft β-spectrum of end-point energy ~300 kev is apparently of the same order of magnitude as the intensity of the 3.85 Mev γ-transition, i.e., $\sim 4\cdot10^{-2}\%$, inasmuch as no other γ-transitions from the 5.22 Mev level are observed. Whence we obtain for the soft β-transition log ft = = 6.9. This is apparently an allowed β-transition slightly inhibited due to K forbiddenness (the probable value of K for the 5.22 Mev level of Mg^{24} is 2 — Ref.21). (K is the projection of the total angular momentum of the nucleus of the nuclear symmetry axis.) It follows that the possible spin values are 3, 4 or 5. With I = 4 or 5, γ-de-excitation of the 5.22 Mev level would go

through the 4.12 Mev (4+) level, but no γ-rays of 1.10 Mev have been observed. Hence it is probable that I = 3 in agreement with the deductions of Newton[15].

T.V.Poleshchuk participated in the measurements of the γ-radiation from Na^{24} and processing of the results.

References

1. D.Fermi, E.Amaldi, O.D'Agostino, F.Rasetti & E.Segré, Proc.Roy.Soc., 146, 483 (1934).
2. M.Sampson & W.Bleakney, Phys.Rev., 50, 732 (1936).
3. J.Lawson, Phys.Rev., 56, 131 (1939).
4. L.Elliott, M.Deutsch & A.Roberts, Phys.Rev., 63, 386 (1943).
5. K.Seigbahn, Phys.Rev., 70, 127 (1946).
6. C.Cook, E.Jurney & L.Langer, Phys.Rev., 70, 985 (1946).
7. E.Brady & M.Deutsch, Phys.Rev., 78, 558 (1950).
8. J.Turner & P.Cavanagh, Phil.Mag., 42, 636 (1951).
9. L.Beghian, G.Bishop & H.Halban, Phys.Rev., 83, 186 (1951).
10. S.Blom, Phys.Rev., 88, 312 (1952).
11. H.Hausman, A.Allen, J.Arthur, R.Bender & C.McDole, Phys.Rev., 88, 1296 (1952).
12. A.Hedgran & D.Lind, Arkiv.Fysik, 5, 177 (1952).
13. E.Bellamy & K.Smith, Phil.Mag., 44, 33 (1953).
14. E.Lockett & R.Thomas, Nucleonics, 11, 3, 14 (1953).
15. J.Newton, Phys.Rev., 96, 241 (1954).
16. B.S.Dzhelepov, Izv.AN SSSR, Ser.fiz., 21, 1580 (1957). (Trans.Bulletin, 21, No.12, 1569).
17. O.V.Chubinskii, Izv.AN SSSR, Ser.fiz., 21, 1583 (1957). (Trans.Bulletin, 21, No.12, 1572.)
18. L.V.Gustova, B.S.Dzhelepov, P.V.Ermolov & O.V.Chubinskii, Report presented at the Sixth All-Union Conference on Nuclear Spectroscopy, 1956.
19. B.S.Dzhelepov & L.N.Zyrianova, Vliianie elektricheskogo polia atoma na β-raspad (Influence of the atomic electric field on β-decay), M.-L., 1956.
20. J.Calvert, A.Jaffe, A.Litherland & E.Maslin, Proc.Phys.Soc., A 68, 1008 (1955).
21. L.K.Peker, L.V.Gustova & O.V.Chubinskii, Izv.AN SSSR, Ser.fiz., 21, 1013 (1957). (Trans.Bulletin, 21, No.7, 1014).

CONCERNING THE DECAY SCHEMES OF CERTAIN ODD-ODD NUCLEI

- L.K.Peker

By now there has been accumulated a large amount of experimental data on the γ- and β-spectra of odd-odd deformed nuclei. In most cases, however, investigators have not been able to determine the energies and spins of levels above the lowest rotational band in the even-even daughter nuclei. In the few cases when investigators attempted to construct a diagram of such levels, it usually proved to be inconsistent with the current concepts regarding the attributes of the levels of deformed nuclei (except for the level diagrams of W^{182}, Os^{186}, Os^{188}, and Pu^{238}). By way of illustration, one may cite the level diagrams for Sm^{152}, Gd^{154}, Dy^{160}, W^{180}, Os^{190}, Th^{228}, Th^{230}, U^{232}, U^{234} and Pu^{240} given in Ref.1.

Recently, the level diagrams of some of the enumerated nuclei have been revised. In particular, new measurements have been made of the γ-spectra of Tb^{160} (Refs.2 & 3), Ho^{160} (Ref.3) and Ac^{228} (Ref.4). The level schemes of Dy^{160} and Th^{228} proposed as a result of these investigations tend to substantiate the theoretical concepts in Ref.5 regarding the excited levels of such nuclei up to energies of 1200-1300 kev.

In the present work we have attempted to construct, on the basis of the known experimental data on the β- and γ-spectra, the level diagrams of some deformed even-even nuclei, with a view to bringing these diagrams into agreement with present-day theoretical concepts.

Level diagram of Gd^{154}

As a result of his investigation of the β- and γ-spectra of Eu^{154} by means of a scintillation spectrometer, Stephens[6] proposed the decay scheme shown in Fig.1. According to Stephens, the 996.6 and 1128.4 kev* levels of Gd^{154} form a rotational band with $K = 2+$ and hence have the spins and parities 2+ and 3+, respectively. (K is the projection of the total angular momentum on the nuclear symmetry axis.)

It can readily be seen, however, that these assumptions lead to inconsistencies. Inasmuch as the spin of Eu^{154} is 3 (Ref.8) ($K = 3-$), β-decay to the 996 and 1128 kev levels should be once forbidden and log ft should not exceed 8-8.5, inasmuch as in this case there is no K forbiddenness[9].

There are no direct experimental data on the intensity of the β-transitions to the 996 and 1128 kev levels, but even if 100% of the β-transitions went to these levels log ft would be $\geqslant 12$.

This inconsistency can be eliminated if we assume that the characteristics of the 996 and 1128 kev levels are 1- and 3- ($K = 0-$). In this case, β-decay to 996 (1-) level would be twice forbidden by the spin and parity selection rules and in addition would be inhibited by K forbiddenness ($\Delta\nu = \Delta K - L = 1$, where L is the multipole order of the transition). This deduction is consistent with the data of Stephens who did not detect β^--decay to the 1128 (3-) level is allowed by the spin and parity selection rules ($\Delta I = 0$, yes), but is strongly inhibited with respect to the quantum number K ($\Delta\nu = 3$ or 2). Thus the value of $K = 0-$ for the 1128 kev level cannot explain the observed value of log $ft \geqslant 12$.

---

*The cited energy values are taken from the precision measurements of B.V.Bobykin.[7]

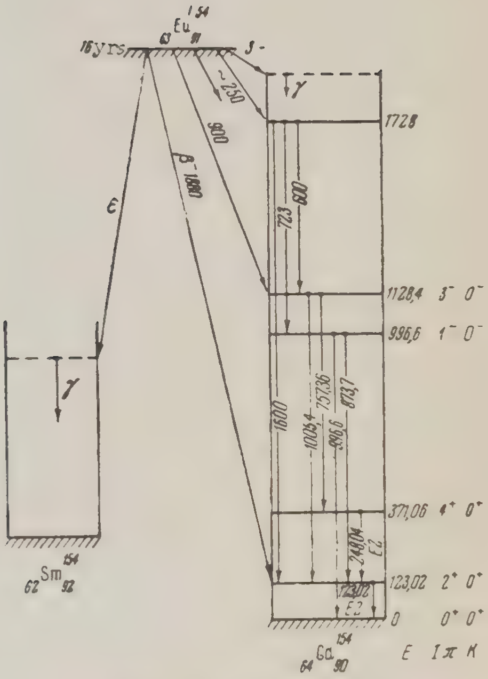

Fig.1. Decay scheme for Gd^{154}.

We can choose between K = 0- and K = = 2+ only if we know the precise multipole order of at least one of the four γ-rays: 1005.4, 996.6, 873.7 and 757.36 kev, inasmuch as in the case of K = 0- all these radiations must be E1, while in the case of K = 2+ they must all be E2.

Owing to the inadequate resolution of extant spectrometers, however, the intensities of these γ-rays cannot be precisely determined (the 996 and 1005 kev lines, as well as the 873.7 and 868.5 kev lines ⟨from Eu^{152}⟩ are not separated). Hence at present we cannot determine the precise values of the corresponding internal conversion coefficients and, consequently, the multipole orders of the transitions in question.

Nevertheless, the data on the relative intensities of the γ-lines can be utilized for evaluating K if we make certain specific assumptions regarding the multipolarity.[9]

An even more convincing argument in favor of a given value of K is obtained from comparison of the relative intensities of the K conversion lines, inasmuch as these are known with appreciably higher accuracy than the intensities of the γ- lines. Here again one must make certain specific assumptions regarding the multipole order - (E1) or (E2) - and utilize the corresponding theoretical values of the internal conversion coefficients.

Table 1 gives the theoretical and experimental values of the ratio B_1/B_2 reduced to the same transition energy values. It will be seen from the table that comparison of the intensities of the 996 and 873 kev γ-lines does not enable us to choose between the two alternative values of K inasmuch as the values of B_1/B_2 for both K values are close.

From the data on the intensities of the K conversion lines and γ-transitions from the 1128 kev level, it clearly follows, however, that for this level K = 0- and that the alternative K = 2+ is excluded.

All other values of K, such as 0+, 1±, 2- and 3+ need not be considered inasmuch as they are inconsistent not only with the quantitative data on the intensity of the γ-transitions but also with the very fact of the existence (or absence) of the transitions.

In accord with the above deduction, the lowest (996 kev) level of the rotational band must have K = 0- and, consequently, spin and parity 1-. It may therefore be characterized as an octupole vibrational level with $\lambda = 3$ and $\nu = 0$, where λ is the quantum number characterizing the symmetry of the vibrations and ν is its projection on the nuclear symmetry axis.

It is interesting to note that in Sm^{152} - a nucleus with the same number of neutrons as Gd^{154} - the corresponding 1- level ($\nu = 0$, K = 0-), found by Grodzins[13], has a somewhat lower excitation energy, namely, 976 kev.

At present we can draw no definite deductions regarding the higher lying levels of Gd^{154}.

Table 1

Theoretical and experimental values of the ratio B_1/B_2*

Ratio	From data on intensity of		Theoretical values	K
	γ-lines	K-conversion lines		
$\frac{B_1(996;\ E1;\ 1^- \to 0^+)}{B_2(873;\ E1;\ 1^- \to 2^+)}$	—	—	0,5	0^-
$\frac{B_1(996;\ E2;\ 2^+ \to 0^+)}{B_2(873;\ E2;\ 2^+ \to 2^+)}$	—	—	0,7	2^+
$\frac{B_1(1005;\ E1;\ 3^- \to 2^+)}{B_2(753;\ E1;\ 3^- \to 4^+)}$	$\frac{13\pm2}{10\pm4}$	1,14	0,75	0^-
$\frac{B_1(1005;\ E2;\ 3^+ \to 2^+)}{B_2(753;\ E2;\ 3^+ \to 4^+)}$	$\frac{8\pm2}{10\pm4}$	0,7	2,5	2^+

---

*E = 1005 kev: $I_\gamma = 29\pm2$, $I_{e_K} = 1.6$, $\alpha_{E1} = 9.7\cdot10^{-4}$, $\alpha_{E2} = 2.32\cdot10^{-3}$; E = 753 kev: $I_\gamma = 10\pm4.1$, $I_{e_K} = 1.0$, $\alpha_{E1} = 1.68\cdot10^{-3}$, $\alpha_{E2} = 4.25\cdot10^{-3}$; the γ-line intensities are taken from Ref.10; the intensities of the K conversion lines are taken from Ref.11 and the values of α_{E1} and α_{E2} are taken from Ref.12.

Level diagram of Gd^{156}

In "New Nuclear Data" for the first quarter of 1957 there appear new data on the composition of the γ-spectrum[14] accompanying β-decay of Eu^{156}. There are also available some tentative data on the γ-spectrum of Tb^{156}.[15]

A level diagram of Gd^{156}, which includes most of these new data, is shown in Fig.2. Inasmuch as no information except for the transition energies is given in the cited references, we constructed the decay scheme on the basis of the theoretical concepts regarding the attributes of levels of deformed even-even nuclei. Presumably the 88.97, 199.19 and 360 kev γ-rays are emitted in transitions between the 0 (0+), 88.97 (2+), 288.16 (4+) and 650 kev (6+) levels of the first rotational band. The existence of levels of a different type with energies under 1000-1200 kev is improbable inasmuch as an energy in excess of 1000 kev is necessary for excitation of single particle or vibrational levels.

The position of the first level with an excitation energy above 1000 kev can be established if we assume that the 1240 kev and 1150 kev γ-rays are emitted in transitions from this level to the 0+ ground state or the 2+ lowest level. Accordingly, the energy of this level must be 1240 kev and its spin 1± or 2+. In this case, the 1270 and 1075 kev γ-rays can be readily interpreted. If we assume that there exists a level at 1360 kev, we can postulate that these γ-rays originate in transitions from this level to the lower-lying 2+ and 4+ levels. The fact that there is no 1360 kev γ-line corresponding to a transition to the 0+ ground state indicates that if the 1360 kev level does exist its spin must be $\geqslant$ 3±.

The relative positions of the 1240 and 1360 kev levels suggest that they pertain to the same rotational band. If this is the case, we can draw certain specific deductions regarding the spins and parities of both these levels. The requirement that the spin of the 1240 level be 1 or 2 and the spin of the 1360 kev level be $\geqslant 3$ is compatible only with two values of K, namely, 0- and 2+. In the first case, the spins and parities of the two levels must be 1- and 3-; in the second case, 2+ and 3+.

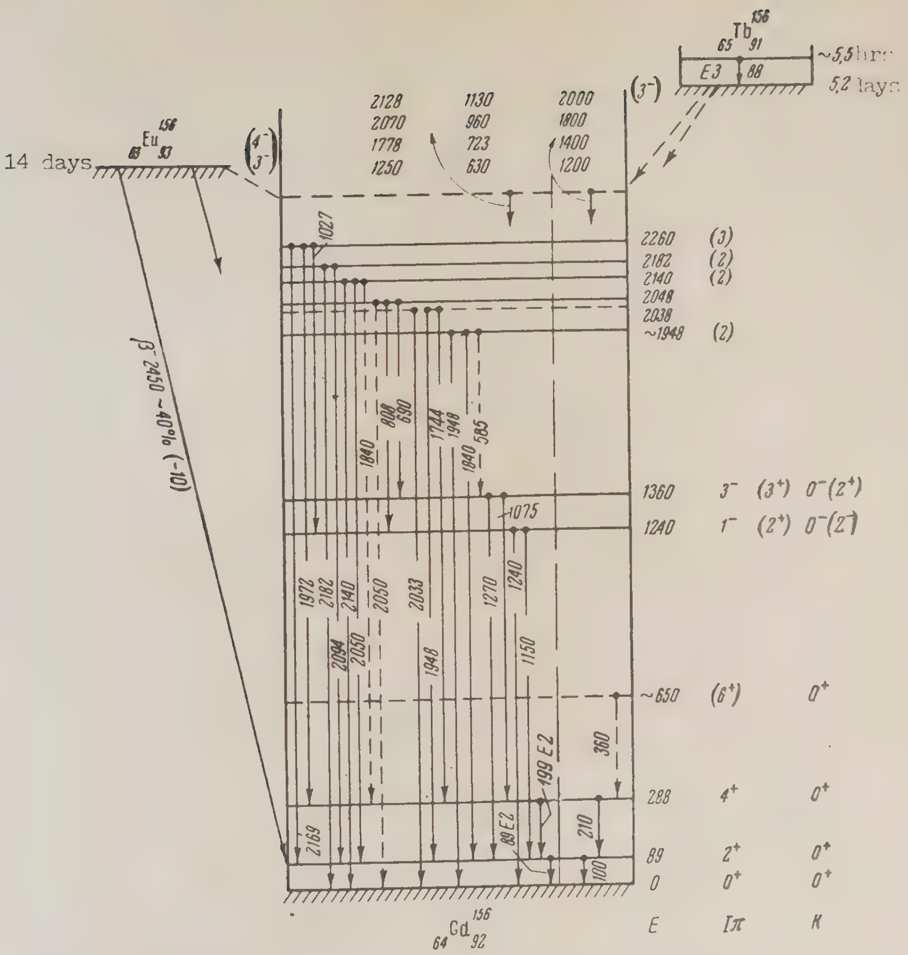
Tb 156 65 91
~5,5 hrs
5,2 days
E3
88
(3⁻)
2128
2070
1778
1250
1130
960
723
630
2000
1800
1400
1200
Eu 156 63 93
14 days
(4⁻ 3⁻)
β⁻ 2450 ~40% (-10)
1027
2260 (3)
2182 (2)
2140 (2)
2048
2038
~1948 (2)
1840
808
690
1744
1948
1840
585
1360 3⁻ (3⁺) 0⁻(2⁺)
1075
1240 1⁻ (2⁺) 0⁻(2⁻)
1972
2182
2140
2050
2033
1270
1240
2094
2050
1948
1150
~650 (6⁺) 0⁺
199 E2
360
288 4⁺ 0⁺
2169
89 E2
210
89 2⁺ 0⁺
100
0 0⁺ 0⁺
Gd 156 64 92
E Iπ K

Fig.2. Level diagram of Gd^{156}.

The moment of inertia of the 1240 kev level in the K = 2+ case is somewhat smaller and in the K = 0- case, somewhat larger than the moment of inertia of the ground state, which is characteristic for vibrational levels[9] of the octupole or quadrupole type.

We could choose between the two indicated values of K if we knew the multipole order of at least one of the four γ-transitions (1270, 1240, 1150 and 1075 kev) or if we had accurate data on the relative intensities of the γ-lines of the K conversion lines associated with the 1270 and 1075 kev transitions (see above under Gd^{154}).

The existence and positions of each of the higher lying levels indicated in the diagram is inferred from at least two or three γ-transitions.

The 2182 and 2260 kev levels may comprise yet another rotational band; the spin values are 2+ and 3+. If this assumption is correct the moment of inertia of the 2182 kev level is somewhat greater than the moment of inertia of the ground state, which may indicate that this is a single particle level.

It should be noted that Ewan, Knowles & McKenzie[16] observed additional γ-transitions which indicate the existence of levels at 1940 and 2140 kev; the spins of these should be 2 or 1.

Energy diagram of Er^{168}

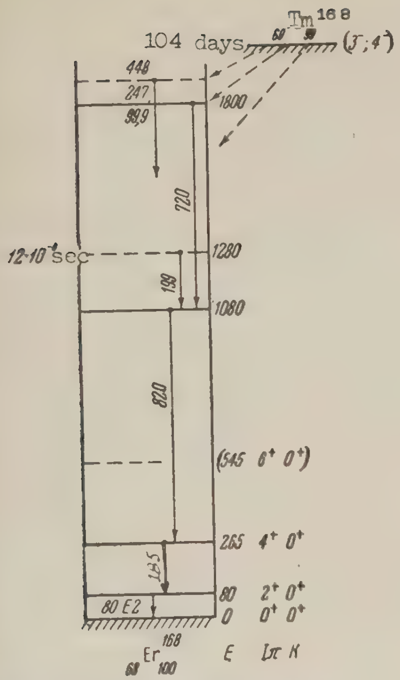
Tm^{168}
69
99
104 days
(3⁻;4⁻)
448
247
99,9
1800
720
12·10⁻⁹ sec
1280
199
1080
820
(545 6⁺ 0⁺)
265 4⁺ 0⁺
185
80 2⁺ 0⁺
80 E2
0 0⁺ 0⁺
$_{68}Er^{168}_{100}$
E
Iπ K

Fig.3. Level diagram of Er^{168}.

According to the data of Mihelich et al[17], the γ-spectrum accompanying the decay of Tm^{168} consists of lines of the following energies: 820, 720, 448, 247, 199, 185, 99.9 and 80 kev; the 820 kev γ-rays yield coincidences with the 720 kev γ-rays. These authors give the tentative decay scheme for Tm^{168} shown in Fig.3.

Noteworthy is the absence of any γ-rays that could be interpreted as due to transitions from a high level with spin 2+ or 1. It may therefore be assumed that there is no such level up to an excitation energy of 1600 kev and that, consequently, the vibrational level with 2+ in Er^{168} is situated higher.*

Level diagram of W^{184}

Levels of W^{184} (Fig.4) are excited in β-decay of Ta^{184} and β^+- and ϵ-decay of Re^{184}.

Below we give data on the γ-spectra of Ta^{184} (obtained on a scintillation spectrometer) and Re^{184} (obtained by observing internal conversion electrons).

The spectrum of Ta^{184} comprises γ-lines of the following energies (intensity values in parentheses): 1180(50), 890(90), 780(17), 405(100), 300(35), 240(60), 210(10), 160(10) and 110(30) kev, as well as K x-rays (40).[20]

The γ-spectrum of Re^{184} is reported to comprise lines of the following energies: 890, 784, 244, 206 and 159 kev (Ref.21) and 286, 205, 159 and 43 kev (Ref.22).

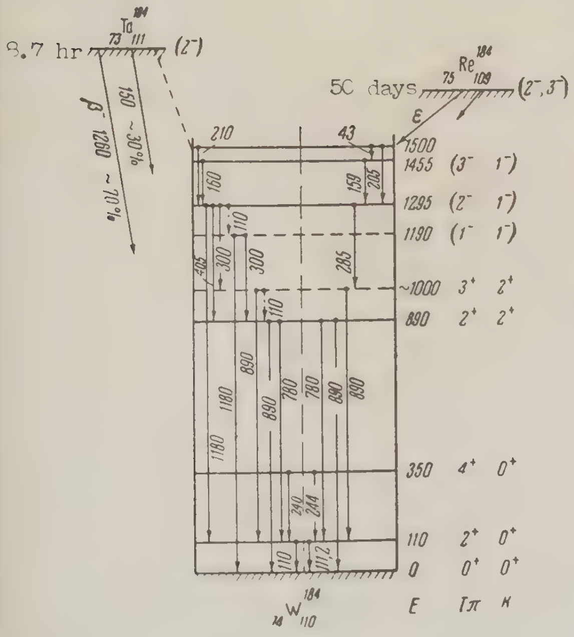
$_{73}Ta^{184}_{111}$
8.7 hr
(2⁻)
β⁻
150 ~30%
1260 ~70%
$_{75}Re^{184}_{109}$
5C days
(2⁻,3⁻)
ε
210
43
1500
1455 (3⁻ 1⁻)
160
159
205
1295 (2⁻ 1⁻)
110
1190 (1⁻ 1⁻)
405
300
300
285
~1000 3⁺ 2⁺
110
890 2⁺ 2⁺
1180
890
1180
890
780
780
890
890
350 4⁺ 0⁺
240
244
110 2⁺ 0⁺
110
111,2
0 0⁺ 0⁺
$_{74}W^{184}_{110}$
E
Iπ
K

Fig.4. Level diagram of W^{184}.

---

*In the γ-spectrum accompanying the Er(n,γ)Er reaction there were observed γ-lines of 188, 280, 730 and 820 kev energy.[18] They can all be fitted into the level diagram of Er^{168}.

It is interesting to note that the possible values of the spin and parity of Tm^{168}, namely, $\Omega_p \pm \Omega_n$ = 3- or 4- (Ref.19) are the same as for Er^{168}, which forms as a result of capture of a thermal neutron by Er^{168}, namely, [(7/2-) ± (1/2+)] = 4- or 3-. Hence it may be assumed that the most probable transitions in both processes lead to excitation of the same level and that consequently the γ-spectra accompanying both processes will be similar. As may be seen from the cited data the inferred similarity of the γ-spectra does actually obtain.

From Coulomb excitation experiments it follows that the first rotational level of W^{184} has the assignment 2+ and an energy of about 110 kev. The corresponding values for the second rotational level are 4+ and 360 kev. Apparently, the 240 kev γ-ray corresponds to the 4+→2+ transition. If it is assumed that there exists a level at 890 kev, then the 890 and 780 kev γ-rays are emitted in transitions to the low-lying 0+ and 2+ levels. The relatively high intensity of the 890 kev line precludes all spin and parity assignments for the 890 kev line except 1+ and 2+.

Comparing its characteristics of the similar 730 kev 2+ level in Os^{186} (a nucleus with the same number of neutrons)[1], we infer that the spin and parity of the 890 kev level of W^{184} are also 2+.

In order to explain the other γ-rays, we introduce levels at 1000, 1190, 1295, 1455 and 1500 kev. In this scheme the 890 kev γ-ray can correspond to two transitions: a) transition between the 890 kev and 0 kev levels and b) between the 1000 kev and 110 kev levels. This apparently can explain the fact that the ratio of the intensities of the 890 and 780 kev γ-lines is appreciably greater than that predicted by theory for K = 2+ (~3 instead of 0.7).

If the inferred 1000 kev level does exist, it may be interpreted as the first level of the rotational band with K = 2+ and I = 3+.

We note that the energies of the 1190, 1295 and 1455 kev levels are satisfactorily described by a formula of the type

$$E = A\left[I(I+1) - I_o(I_o+1)\right],$$

if $K = I_o = 1-$; it must be noted, however, that the very existence of these levels has not been definitively established.

Level diagram of W^{186}

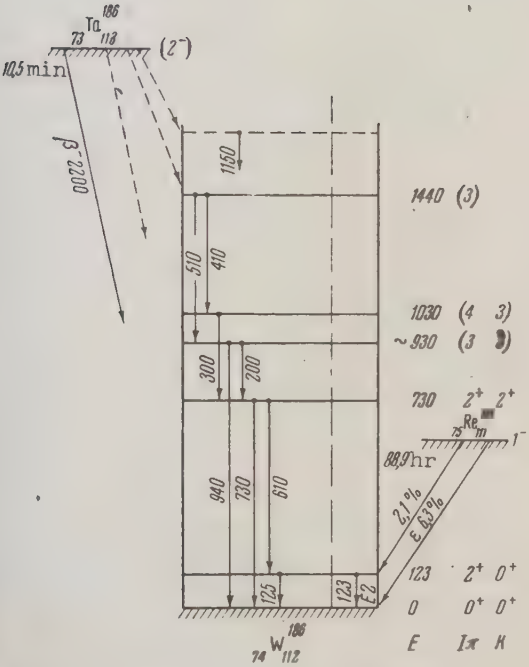

Fig.5. Level diagram of W^{186}.

The γ-spectrum accompanying β^--decay of Ta^{186} was investigated by Poë[23]; it consists of the following lines: 1150(10), 940(15), 730(65), 610(45), 510(45), 410(20), 300(25), 200(100) and 125(25) kev (values in parentheses = relative intensities).

It follows from Coulomb excitation experiments and the data on the decay of Re^{186} that the 125 kev line corresponds to a 2+→0+ γ-transition and that the first excited level of W^{186} lies at 125 kev and has spin and parity 2+ (Fig.5).

By analogy with Os^{188} (Ref.1), which has the same number of neutrons, it may be assumed that W^{186} has a 2+ level at 730 kev from which γ-transitions of 730 and 610 kev energy proceed to the 0+ and 2+ levels (K = 0+).

Accepting this hypothesis and knowing the relative intensities of both γ-transitions, we obtain for their ratio (after normalization to the same energy) a value of 0.6, which is in good agreement with the theoretical value of 0.7

for K = 2+ (for K = 0- and I = 1-, the theoretical ratio, however, is not very different, namely, 0.5, in view of which the validity of the K = 2+ assignment will be definitively proved only after determination of the multipole order of these transitions).

In order to explain the other lines we have introduced levels at 930, 1030 and 1440 kev. Where the 1150 kev transition fits into the scheme is not clear.

Level diagram of U^{232}

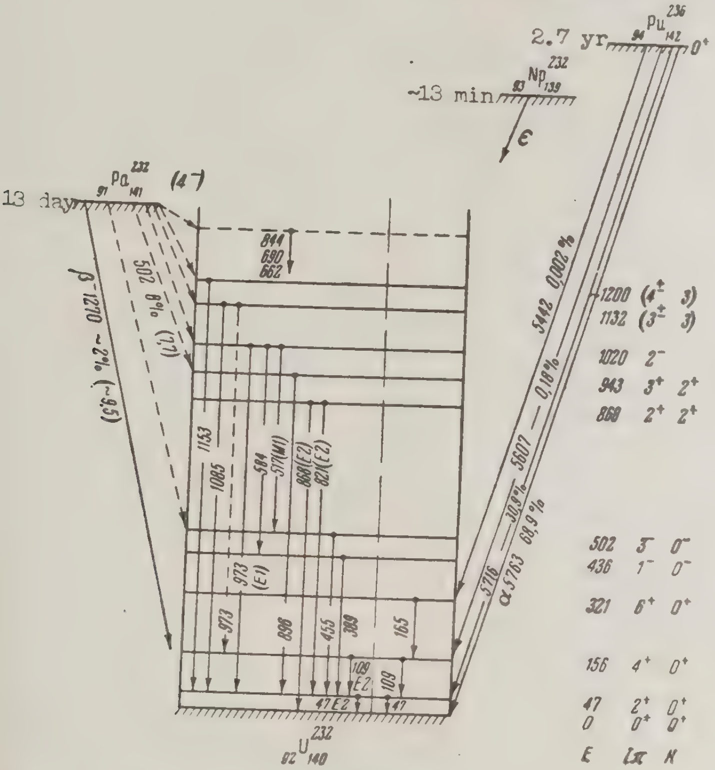
2.7 yr
$_{94}Pu^{236}_{142}$
0^+
~13 min
$_{93}Np^{232}_{139}$
ε
13 day
$_{91}Pa^{232}_{141}$
(4⁻)
β⁻ 1270 ~ 2% (~9,5)
502 8% (7,7)
844
690
662
5442 0,002%
0,18%
5607
30,9%
68,9%
5716
α 5763
1153
1085
584
517(M1)
868(E2)
821(E2)
973 (E1)
973
896
455
389
165
109 E2
109
47 E2
47
$_{92}U^{232}_{140}$
1200 (4± 3)
1132 (3± 3)
1020 2⁻
943 3⁺ 2⁺
868 2⁺ 2⁺
502 3⁻ 0⁻
436 1⁻ 0⁻
321 6⁺ 0⁺
156 4⁺ 0⁺
47 2⁺ 0⁺
0 0⁺ 0⁺
E Iπ K

Fig.6. Level diagram of U^{232}.

Levels of U^{232} are excited in β^--decay of Pa^{232}, ε-capture in Np^{232} and α-decay of Pu^{236} (Fig.6). In the last process the α-transitions proceed to the 47(2+), 156(4+) and 321(6+) kev levels of U^{232}; these levels form a rotational band with K = 0+.[24] The γ-spectrum accompanying ε-capture in Np^{232} has not been investigated. The data from Ref.25 on the γ-spectrum of Pa^{232} are listed in Table 2.

In constructing the level diagram of U^{232}, we proceeded by analogy with the diagrams for nuclei such as Th^{228} (Ref.4), Pu^{238} (Ref.1) etc.

The 389 and 455 kev γ-rays may correspond to two levels of the rotational band with K = 0-: a 436(1-) and a 502 kev (3-) level. The 868 and 943 kev levels (if they

Table 2

γ-spectrum of Pa^{232} from Ref.25

E_γ	K/L	$L_I:L_{II}:L_{III}$	Intensity of conversion line I_{e^-}	E_γ	K/L	$L_I:L_{II}:L_{III}$	Intensity of conversion line I_{e^-}
47,2	—	0:1:0,9	Strong	821	4		Strong
109,3	—	1:0:0,4	Very strong	844	—		Weak
389	2		Strong	868	4		Strong
455	4		Very strong	896	>6		Strong
517	8,5		Strong	973	6		Strong
584	~1,5		Very weak	1085	—		Weak
662	<1		Very weak	1153	—		Very weak
690	—		—				

actually exist) may belong to a rotational band with K = 2+. The K/L value for the 868 and 821 γ-rays is not inconsistent with the expected multipole order - E2.

In order to explain the 973, 584 and 517 kev γ-lines we introduced a 1020 kev level, while for accomodating the 1153, 1085 and 973 kev γ-rays we plotted levels at 1132 and 1200 kev. Data on the multipole orders of the γ-transitions obtained from analysis of the K/L values are highly unreliable and hence cannot be utilized for determining the spins and parities of the levels.

Nothing definite can be said at present regarding the origin of the weak γ-rays of 844, 690 and 922 kev energy.

In the diagram of Fig.6 we have listed the assumed spin and parity values. If the assumptions made above are correct, the 436 kev level is an octupole vibrational level with ν = 0, while the 868 kev level may be a quadrupole γ-vibrational level.

Level diagram of Pu^{240}

In α-decay of Cm^{244} there are excited Pu^{240} levels of energies 42, 87(2+), 141.77(4+) and 292 kev (6+) constituting a rotational band with K = 0+ and levels of energies 600 (1-) and 640 (3-) belonging to a rotational band with K = 0-.[24] Apparently, the 600 kev level of Pu^{240} is an octupole vibrational level with ν = 0 (Fig.7).

β-decay of the isomeric state of Np^{240} (T = 7.3 min; I = 0-) is accompanied by the emission of γ-rays of 1400, 900 and 560 kev energy[24], while ε-capture in Am^{240} (I = 2-) is accompanied by γ-rays of 1400, 1020, 920, 98.9 and 42.87 kev energy[26,27]. In order to fit in these γ-transitions, we have, by analogy with Pu^{238}, assumed that there exists in Pu^{240} a 940 kev(0+) level (quadrupole β-vibrational level) and 1020 and 1060 kev levels belonging to a rotational band with K = 2+ and having spins and parities of 2+ and 3+, respectively. The presence of a line of 1400 kev energy in the γ-spectra of Np^{240} and Am^{240} indicates the existence of a 1400 kev (1-) level. This spin assignment is explained by the fact that transitions from the 0- state of Np^{240} and 2- state of Am^{240} proceed to this level. Analysis of the β-spectrum of Np^{240} and K capture in Am^{240} substantiates the above assumptions (based only on analogy with the level diagram of Pu^{238}).

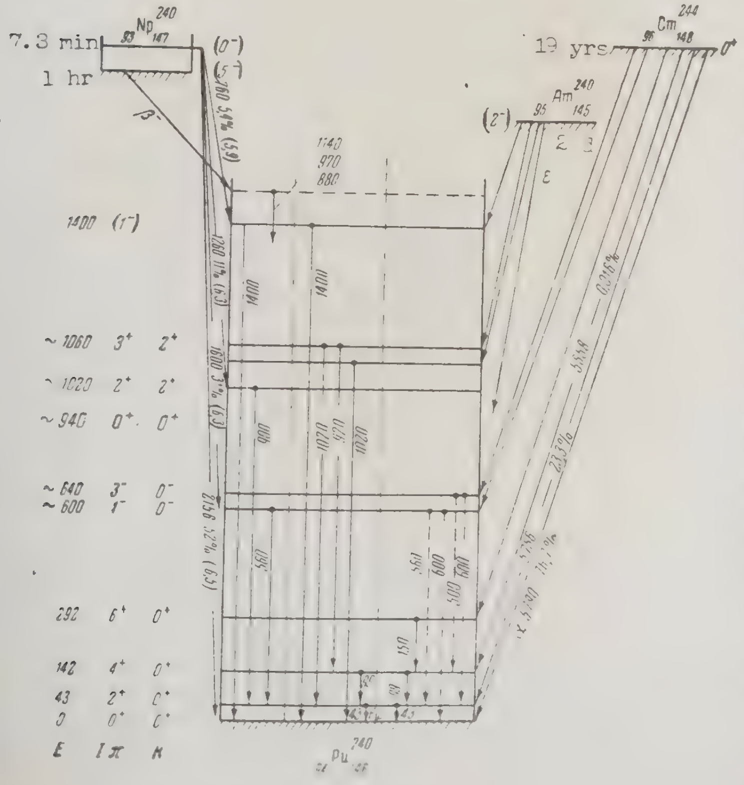

240 Np 93 147
7.3 min
1 hr
(0⁻)
(5⁺)
β⁻
760 54% (5.9)
1140
970
880
1400 (1⁻)
1280 11% (6.3)
1400
1400
~1060 3⁺ 2⁺
~1020 2⁺ 2⁺
~940 0⁺ 0⁺
1600 3% (6.3)
900
1020
970
1020
~640 3⁻ 0⁻
~600 1⁻ 0⁻
2156 32% (6.3)
560
561
600
500
1400
292 6⁺ 0⁺
150
142 4⁺ 0⁺
98
43 2⁺ 0⁺
0 0⁺ 0⁺
42
E Iπ K
Pu 240 94 146
19 yrs
Cm 244 96 148
0⁺
Am 240 95 145
(2⁻)
ε
0.016%
5.55
23.3%
5.76
76.7%
5.800

Fig.7. Level diagram of Pu^{240}.

Table 3

β-Vibrational levels of the quadrupole type; K = 0+

Nucleus	Level energy, kev	
	$I = 0+$	$I = 2+$
${}_{68}\mathrm{Er}^{166}_{98}$	1460	
${}_{90}\mathrm{Th}^{232\star}_{142}$	~720	770
${}_{92}\mathrm{U}^{234\star}_{142}$	~805	—
${}_{94}\mathrm{Pu}^{238\star}_{144}$	~935	986
${}_{94}\mathrm{Pu}^{240}_{146}$	~940	—

Table 4

γ-Vibrational levels of the quadrupole type; K = 2+

Nucleus	Level energy, kev		Nucleus	Level energy, kev	
	$I = 2+$	$I = 3+$		$I = 2+$	$I = 3+$
Sm^{152}	1086	1235?	Th^{228} [4]	964	—
Gd^{156}	1240?	1360?	Th^{230}	1060?	—
W^{182} [9]	1222	1332	U^{232}	868	943
W^{184}	890	1000	Pu^{238}[1]	1030	1076
W^{186}	730	—	Pu^{240}	~1020	1060
Os^{186} [1]	764	—	$\mathrm{Cm}^{246\star}$	~1300	—
Os^{188} [1]	633	—	$\mathrm{Cf}^{250\star}$	~1200	—
Os^{190} [29]	586	—	Fm^{254}	~ 700	—

Table 5

Vibrational levels of the octupole type (K = 0-, λ = 3, ν = 0)**

Nucleus	Level energy, kev			
	$I = 1^-$	$I = 3^-$	ΔE $(3^-) \to (1^-)$	ΔE $(2^+) \to (0^+)$
Sm^{152}	976	—	—	122
Gd^{154}	996	1128	132	123
Gd^{156}	1240?	1360?	120	90
Er^{166}	1610 (or 1690)	—	—	80
Ra^{222} [1]	242	—	—	112
Ra^{224} [1]	217	289	72	84
Ra^{226} [1]	253	320	67±5	68
Th^{226} [1]	232	—	—	73
Th^{228} [1, 4]	326	392	66	58
U^{232}	436	502	66	47
Pu^{238} [1]	605	656	51	44
$\mathrm{Pu}^{240\star}$	600	643	43±5	43

According to Ref.19 the spin and parity of the isomeric state of Np^{240} are 0- and of the ground state of Am^{242} 2-. The value of log $ft < 7$ for all the β^--transitions indicates that the spins of the Pu^{240} levels to which the β-decay proceeds may be either 0± or 1±. It is evident from the diagram that β-decay goes to the ground state (0+) and the 600(1-) and 940 kev (0+) levels; there are no β-transitions to the 1020(2+) and 1060 kev (3+) levels.

At the same time, in the decay of Am^{240} there are excited the 1020 and 1060 kev levels but not the 940 (0+), 600 (1-) and 640 kev (3-) levels evinced in the disintegration of Cm^{244}. Electron capture to these levels is forbidden by the selection rules as regards spin and parity or the quantum number K.

In β^--decay of the ground state of Np^{240} (T = 1 hour) there are emitted γ-rays of 1440, 970 and 880 kev energies (Ref.28). It is not clear at present how these fit into the level diagram of Pu^{240}.

Discussion

In Tables 3, 4 & 5 we have assembled the experimental data on the excited levels characterized by 0+ (K = 0+), 2+ (K = = 2+) and 1- (K = 0-), which may be interpreted as vibrational levels of the quadrupole (K = 0+ or 2+) and octupole type.

Fig.8 shows the variation of the energy of these levels with the number of neutrons in the nucleus and, consequently, with the deformation parameter. It will be evident from the figure that the energy of the vibrational levels increases with the deformation parameter and that this increase is particularly noticeable in the case of rare earth nuclei. In view of this dependence of the energy on the deformation parameter, the energy of the 1-, 0+ and 2+ vibrational levels in nuclei with A = 158 to 180 will probably exceed 1500-2000 kev, so that these levels will be difficult to observe in radioactive decays.

---

*According to the data of Mottelson (1957).

**In the fourth and fifth columns we list the excitation energies of the first rotational level in the bands with K = 0- and K = 0+.

This deduction is in agreement with the experimental data on the spectra of nuclei in this A region, namely, Er^{166}, Er^{168}, Hf^{176}, Hf^{178}, Hf^{180} and W^{182}.

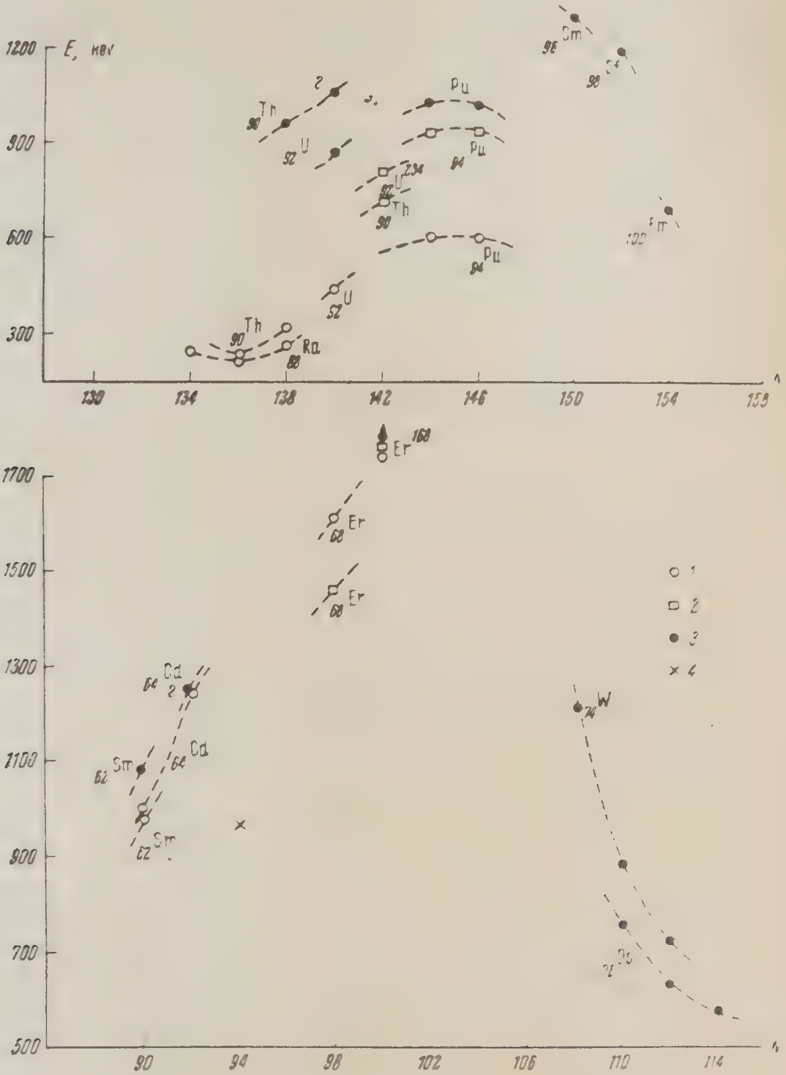

Fig.8. Variation of the energy of the vibrational levels of deformed even-even nuclei with the number of neutrons in the nucleus: 1) quadrupole γ-vibrational levels with K = 2+ and I = 2+; 2) quadrupole β-vibrational levels with K = 0+ and I = 0+; 3) octupole vibrational levels with λ = 3, ν = 0, K = 0- and I = 1-; 4) the 966 kev 2+ (K = = 2+)[3] level of Dy^{160} which, apparently, is not a γ-vibrational level.

The indicated variation of the energy of vibrational levels of quadrupole type with the deformation parameter is explicable from the standpoint of the unified shell model. A detailed discussion of the properties of such levels will be published elsewhere.

In conclusion I desire to express my gratitude to B.S.Dzhelepov for discussion of the decay schemes appearing herein.

Library,
USSR Academy of Sciences

References

1. B.S.Dzhelepov & L.K.Peker, Skhemy raspada radioaktivnykh izotopov (Decay schemes of radioactive isotopes), M.-L., 1957.
2. O.Nathan, Nuc.Phys., 4, 125 (1957).
3. E.P.Grigor'ev, B.S.Dzhelepov, A.V.Zolotavin, O.E.Draft, B.Kratsik & L.K.Peker, Present issue of the Bulletin, p. 99.
4. O.Nathan & M.A.Waggoner, Nucl.Phys., 4, 3 (1957).
5. K.Alder, A.Bohr, T.Huus, B.Mottelson & A.Winther, Rev.Mod.Phys., 28, 432 (1956).
6. F.S.Stephens, Nucl.Phys., 2, 548 (1957).
7. B.V.Bobykin, Tezisy VII Soveshchaniia po iadernoi spektroskopii (Abstracts of Reports presented at the VII Conference on Nuclear Spectroscopy), L., 1957.
8. R.W.Kedzie, M.Abraham & C.D.Jeffries, Bull.Am.Phys.Soc., 1, 390 (1956).
9. G.Alaga, K.Alder, A.Bohr & B.Mottelson, Kgl.Danske Math.Fys.Medd., 29, No. 9 (1955).
10. B.S.Dzhelepov, N.N.Zhukovskii, V.G.Nedovesov & G.E.Shchukin, Izv.AN SSSR, Ser.fiz., 21, 966 (1957). (Trans., Bulletin, 21, No.7, 968.
11. O.Nathan & M.A.Waggoner, Nucl.Phys., 2, 548 (1957).
12. L.A.Sliv & I.M.Band, Tablitsy koeffitsientov vnutrenei konversii (Tables of internal conversion coefficients), M.-L., 1956.
13. L.Grodzins, Bull.Amer.Phys.Soc., 1, 329 (1956).
14. F.Boehm & E.N.Hatch, N.S.A., 11, No. 6B, (1957).
15. T.H.Handley & W.S.Lyon, Phys.Rev., 99, 1415 (1955).
16. G.T.Ewan, J.W.Knowles & D.R.McKenzie, Bull.Am.Phys.Soc., 2, 259 (1957).
17. J.W.Mihelich & B.Harmatz, Phys.Rev., 106, 1232 (1957). K.P.Jacob, J.W. Mihelich & B.Harmatz, Bull.Am.Phys.Soc., 2, 260 (1957).
18. C.A.Fenstermacher, R.L.Hickock & H.L.Schultz, Bull.Amer.Phys.Soc., 2, 41 (1957).
19. L.K.Peker, Izv.AN SSSR, Ser.fiz., 21, 1029 (1957). (Trans.Bulletin, 21, No.7, 1030.)
20. F.D.S.Butement, & A.J.Poë, Phil.Mag., 46, 482 (1955).
21. G.Wilkinson, (1952), Rev.Mod.Phys., 25, 465 (1953).
22. G.Wilkinson & H.G.Hicks, Phys.Rev., 77, 314 (1950).
23. A.J.Poë, Phil.Mag., 46, 1165 (1955).
24. I.Perlman & J.O.Rasmussen,"Alpha Radioaktivity", Handbuch der Physik. - Springer, Berlin, 1956.
25. Ong Ping Hok & G.J.Sizoo, Physica, 20, 77 (1954).
26. R.A.Glass (1954), Phys.Rev., 105, 1514 (1957).
27. W.G.Smith, W.M.Gibson & J.M.Hollander, Phys.Rev., 105, 1514 (1957).
28. H.W.LeFevre, E.M.Kinderman & H.H.Van-Tuyl, Bull.Am.Phys.Soc., 1, 62 (1956); N.S.A., 11, No.613 (1957).
29. L.K.Peker, Present issue of the Bulletin, p. 224.

ON THE CHARACTERISTICS OF NUCLEI WITH SMALL DEFORMATION PARAMETERS. PROPERTIES OF Os^{190}

- L.K.Peker

As a result of a large number of investigations many of the properties of spherically symmetric nuclei and nuclei with large deformation parameters are relatively well known and readily interpreted by means of the unified shell model.[1]

In contrast, we still have very little information on ellipsoidal nuclei with small deformation parameters ($\beta \approx 0.15$-0.20). Yet these nuclei are located in a transition region, so that an understanding of their characteristics might prove highly useful in further development of our concepts of nuclear structure. Examples of such transition effects are furnished by the new type of isomerism in Eu^{152} and the characteristic ratios of K capture and β^--decay in the ground and isomeric states of this nucleus[2].

Below we shall discuss the properties of a nucleus located at the other end of this same region of deformed nuclei, namely, Os^{190}. Os^{190} is of particular interest since this nucleus has the lowest known deformation parameter ($\beta \approx 0.15$). Hence it may be assumed that in this case the deviations from the properties peculiar to ellipsoidal nuclei will be maximum and, consequently, most clearly evinced.

We have re-examined all the experimental data pertaining to Os^{190} and constructed a decay scheme taking all of them fully into account (see accompanying figure).

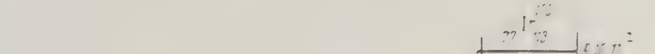

Level diagram of $_{76}Os^{190}_{114}$.

The scheme is based on the following considerations.

There have been observed in the γ-spectrum accompanying the decay of 10-min Os^{190m} four γ-lines (E2) of approximately the same intensity - 614, 500, 359 and 187 kev - which yield coincidences with each other.[3-4] In addition there has been observed a 39 kev line identified as M2.[5]

The spin sequence 0+, 2+, 4+, 6+ and 8+ following from the data on the multipolarities and coincidences of the γ-rays and the obvious regularity in the successive energies of the γ-transitions give reason to assume that in Os^{190} there exists a rotational band comprised of the above mentioned levels (energies: 0, 186, 546, 1046 and 1660 kev) and that the 39 kev transition is an isomeric M2 type transition from the 1669 kev (10+) to the 1660 kev (8+) level.

Of the enumerated five lines associated with the rotational band, there is observed in the γ-spectrum of Re^{190} only the 186 kev line and in the γ-spectrum of 11-day Ir^{190} only the 186 and 360 kev lines; in addition there

appear in these spectra a number of other lines: in the spectrum of Re^{190} γ-lines of the following energies (and relative intensities)[6]: 830(~25), 569(~75), 392(~75) and 191 kev (~75) and in the spectrum of Ir^{190} lines of the following energies (and relative intensities)[5,7]: ~1330(2), ~800(17), ~580(80), ~540(65), 400(55), 360(30) and 186 kev (75). In the spectrum of Ir^{190} the 186 kev γ-rays yield coincidences with the 360 and 400 kev γ-rays.

There is no record in the literature of attempts to fit these γ-rays into the decay scheme of Os^{190}. We made an attempt to do so. First, we determined the possible values of the spins and parities of the ground states of Re^{190} and Ir^{190}. According to Ref.8, the assignment for the ground state of Re^{190} is either 2- or 7-; that for Ir^{190} (T = 11 days) is either 3- or 0-.

Analysis of the characteristics of γ-vibrational levels of deformed nuclei showed that one should expect such a 2+ level in Os^{190} at an energy of 550-600 kev.

We assumed that in Os^{190} the 2+ γ-vibrational level has an excitation energy of ~580 kev and that this level is connected with the ground level in the first rotational 186 kev level by γ-transitions of 580 and ~400 kev energy (in Re^{190} 569 and 392 kev, respectively). The high intensities of the γ-lines indicate that this γ-vibrational level is directly excited in the disintegration of Re^{190} and Ir^{190}. This determines the spins of Re^{190} and Ir^{190}, namely, 2- and 3-, respectively. In this case for β^-- and K-transitions to the 580 kev level there is no K forbiddenness ($\Delta\nu = \Delta K - L \leqslant 0$, where L is the multipole order of the radiation) and hence these transitions can occur with high probability.

Recently there has appeared a report describing experiments on Coulomb excitation of Os^{190}. These experiments furnish direct proof of the existence of a 2+ level with an energy of 570 kev.[9]

Turning to the other levels of Os^{190}, we must note that the 360 and 540 kev γ-rays are observed only in the decay of Ir^{190}. The 580 kev γ-line is apparently a doublet. This is indicated by the fact that the intensity ratio $I_{\gamma 580}/I_{\gamma 400}$ in Ir^{190} equals 1.5, while in Re^{190} it is ~1, and in Coulomb excitation of Os^{190} it is 0.6.[9]

In order to explain the presence of the 360 and 540 kev γ-lines and one of the components of the 580 kev γ-line, we introduced a level at 1126 kev; we have adopted the assignment 4+ for it, since the other possible spin and parity values (1±, 2± and 3±) are less probable inasmuch as this level is not observed in β-decay of the ground state of Re^{190} (2-). It is interesting to note that the excitation energy of this level is almost two times greater than the energy of the first vibrational level of Os^{190} — 586 kev (2+). Possibly this is the second vibrational level in Os^{190}.

To explain the weak lines of ~800 and 1330 kev energy, we introduced a level at ~1380 kev. Our assignment for this level is 2-. The odd parity is dictated by the ~4.7 value for log ft, which is characteristic for an allowed β-transition to the level from the ground state of Re^{190}. A spin value of 1 is less probable in view of the presence of a K transition from the ground state of Ir^{190} (3-). A spin of 3- is less probable than 2- inasmuch as in addition to a ~800 kev transition to the 2+ level, there is observed a 1330 kev transition to the ground state of Os^{190} (0+), the intensity of which is only eight times lower than the intensity of the 800 kev transition. Let us compare the data on the levels of Os^{190} with deductions from the unified shell model.

1. The energy of rotational levels differs appreciably from the energy values following from the formula

$$E_{rot} = AI(I + 1).$$

According to this formula

$$E_{2+} : E_{4+} : E_{6+} : E_{8+} = 1 : 3.33 : 7 : 12$$

whereas the experimentally determined ratios are 1 : 2.94 : 5.6 : 9.

Taking into account a term of the $BI^2(I + 1)^2$ type[1], reflecting the interaction between the rotation and vibration of the nuclear surface, leads to an increase of the divergence between theory and experiment.

We note that an appreciable deviation of the energy of rotational levels from the theoretical value is characteristic not only for nuclei with $\beta \leqslant 0.2$ but also for nuclei with large deformation parameters up to $\beta \approx 0.25$ (see, for example, Sm^{152}, Gd^{154} & Ra^{122})[10,11].

2. In nuclei with a large deformation parameter, K (the projection of the total angular momentum of the nucleus on its symmetry axis) is a good quantum number: β- and γ-transitions for which $\Delta\nu = \Delta K - L > 0$ are strongly inhibited[12]; analysis shows that a one-unit change in $\Delta\nu$ leads to a change of approximately 100 in the transition probability.[13]

In Os^{190} there must be very strong K forbiddenness ($\Delta\nu = \Delta K - L = 8$) as regards the 39 kev (M2) isomeric γ-transition, so that one might assume that compared with an allowed single particle transition this transition will be retarded by a factor of 10^{16}. Experiments, however, show a reduction by a factor of only 10^6, i.e., for $\Delta\nu = 1$ there occurs only a 5-6-fold diminution of the transition probability.

3. Let us compare the relative intensities of the γ-transitions from the level with K = 2+ and I = 2+ to the levels of the lower rotational band with K = 0+ and I = 0+ and 2+ with the theoretical data.[12]

It will be seen from the accompanying table that as the deformation of the nucleus decreases, the deviation of the experimental values from the theoretical increases, attaining a maximum for Os^{190}. The decrease in the value of B_1/B_2 with decreasing deformation is probably connected with the fact that in going to spherical nuclei, vibrational levels, according to Bohr & Mottelson[1], transform into two-phonon vibrational levels with I = 2+, i.e., levels of the type cross-over transitions from which to the ground state have a low probability.

Variation of the relative intensities of γ-transitions B(E2) to levels with K = 0+ & I = 0+ and 2+ with the magnitude of the nuclear deformation parameter β

Nucleus	$\frac{B_1(E2;\, 2^+ \to 0^+)}{B_2(E2;\, 2^+ \to 2^+)}$ experimental (theor.=0.7)	$\beta \approx \frac{\Delta R}{R}$
${}_{62}Sm^{152}_{90}$	0,6 [14]	0,28 [1]
${}_{66}Dy^{160}_{94}$	0,6 [15]	0,35 [1]
${}_{74}W^{182}_{108}$	0,62 [16]	0,31 [1]
${}_{74}W^{186}_{112}$	0,6 [17]	0,24 [1]
${}_{76}Os^{186}_{110}$	0,37 [18]	0,20 [1]
${}_{76}Os^{188}_{112}$	0,4 [18, 19]	0,18 [1]
${}_{76}Os^{190}_{114}$	$\sim$0,1 [3, 6, 9]	0,15 [9]

We conclude from the above that in nuclei with a small deformation parameter, such as Os^{190}, many of the assumptions fundamental to the theory of deformed nuclei no longer hold. Thus in Os^{190} K ceases being a good quantum number since K forbiddenness is virtually no longer evident. The deviation of B_1/B_2 from the value of 0.7 obtained according to the rule of Alaga et al[12] indicates that in Os^{190} one cannot satisfactorily separate rotational and internal motions.

I desire to acknowledge my indebtedness to L.A.Sliv and B.S.Dzhelepov for helpful discussions.

Library, USSR Academy of Sciences

References

1. K.Alder, A.Bohr, T.Huus, B.Mottelson & A.Winther, Revs.Mod.Phys., 28, 432 (1956).
2. L.K.Peker, Zhur.eksp.i teor.fiz., 33, 291 (1957).
3. A.H.Aten, G.D.de Feufer, M.J.Sterk & A.N.Wapstra, Physica, 21, 740, 990 (1955).
4. G.Scharff-Goldhaber, D.E.Alburger, G.Harbottle & M.McKeown, Bull.Am. Phys.Soc., 2, 25 (1957).
5. G.Scharff-Goldhaber, D.E.Alburger, G.Harbottle & M.McKeown, N.S.A., 11, No. 6B (1957).
6. A.H.Aten & G.D.de Feyfer, Physica, 21, 543 (1955).
7. G.J.Nijgh, L.T.M.Ornstein & A.H.Wapstra,(1954). See Physica, 21, 740 (1955).
8. L.K.Peker, Izv.AN SSSR, Ser.fiz., 21, 1029 (1957). (Trans. Bulletin, 21, No.7, 1030.)
9. R.Barloutaud, P.Lehmann & A.Leveque, C.R., 245, 523 (1957).
10. B.S.Dzhelepov & L.K.Peker, Skhemy raspada radioaktivnykh izotopov (Decay schemes of radioactive isotopes), M.-L., 1957.
11. B.S.Dzhelepov & L.K.Peker, Skhemy raspadov radioaktivnykh iader (Decay schemes of radioactive nuclei), M.-L., 1958.
12. G.Alaga, K.Alder, A.Bohr & B.Mottelson, Kgl.Danske Mat.Fys.Medd., 29, No. 9 (1955).
13. L.K.Peker, Tezisy VII Soveshchaniia po iadernoi spektroskopii (Abstracts of Reports presented at the Seventh Conference on Nuclear Spectroscopy), M.-L. 1957.
14. L.Grodsins, H.Kendall, N.S.A., 10, No.24 B (1957); B.S.Dzhelepov, N.N. Zhukovskii & B.O.Bobykin, Abstracts of Reports Presented at the Seventh Conference on Nuclear Spectroscopy, Leningrad, 1957; O.Nathan & M.A.Wagonner, Nucl. Phys., 2, 548 (1957).
15. E.P.Grigor'ev, B.S.Dzhelepov, A.V.Zolotavin, O.E.Kraft, B.Kratsik & L.K.Peker, Present issue of the Bulletin, p.99.
16. J.J.Murray, F.Boehm, P.Marmier & J.DuMond, Phys.Rev., 97, 1007 (1955).
17. A.J.Poë, Phil.Mag., 46, 1165 (1955).
18. M.W.Johns, C.C.McMullen, I.R.Williams & S.V.Nablo, Can.J.Phys., 34, 69 (1956).
19. V.R.Potnis, V.S.Dubey & C.E.Mandeville, Phys.Rev., 102, 459 (1956); W.G.Smith & J.M.Hollander, Phys.Rev., 98, 1258 (1955).

Vol.22, No.2 NUCLEAR SPECTROSCOPY

BULLETIN of the Academy of Sciences of the USSR - Physical Series
- Transactions of the Eighth All-Union Conference on Nuclear Spectrsocopy -

TABLE OF CONTENTS

	Page Orig.	Page Trans.
Alpha-decay of Cm^{242} - L.N.Kondrat'ev, V.B.Dedov & L.L.Gol'din	99	97
Decay of Tb^{160} and Ho^{160} and level scheme of Dy^{160} - E.P. Grigor'ev, B.S.Dzhelepov, A.V.Zolotavin, O.E.Kraft, B.Kratsik & L.K.Peker	101	99
Conversion electron spectrum of a dysprosium fraction - B.S. Dzhelepov, B.K.Preobrazhenskii, I.M.Rogachev & P.A.Tishkin	126	125
Conversion electron spectra of Gd^{151} and Gd^{153} - N.M.Anton'eva, A.A.Bashilov, B.S.Dzhelepov & B.K.Preobrazhenskii	135	134
$Nd^{140} \rightarrow Pr^{140} \rightarrow Ce^{140}$ decay series - K.Ia.Gromov, B.S.Dzhelepov, A.G.Dmitriev & B.K.Preobrazhenskii	153	151
Distinctive features of forbidden β-transitions in deformed nuclei - Z.Bokhnatski	158	156
Contribution to the theory of internal conversion. Part I. - V.A.Krutov	162	159
Contribution to the theory of internal conversion. Part II. - V.A.Krutov & K.Müller	171	168
Gamma-spectrum of La^{140} - V.P.Prikhodtseva & Iu.V.Khol'nov	176	173
Conversion spectrum of La^{140} - A.A.Bashilov, B.S.Dzhelepov, N.D.Novosil'tseva & L.S.Chervinskaia	179	176
Precision energy measurements of some lines in the spectra of Ir^{192}, Eu^{152} and Eu^{154} - V.A.Romanov	191	188
Decay of Rh^{106} - E.P.Grigor'ev, A.V.Zolotavin, I.I.Kuz'min & E.D.Pavlitskaia	194	191
Twin magnetic lens spectrometer with improved focusing for recording coincidences - V.A.Sergienko	198	195
Positron spectrum of a dysprosium fraction - B.S.Dzhelepov, O.E.Kraft, B.K.Preobrazhenskii & G.F.Iushkevich	208	205
High-energy gamma-radiation from Na^{24} - L.V.Gustova, B.S. Dzhelepov, P.F.Ermolov & O.V.Chubinskii	211	208
Concerning the decay schemes of certain odd-odd nuclei - L.K.Peker	216	213
On the characteristics of nuclei with small deformation parameters. Properties of Os^{190} - L.K.Peker	228	224

Translated in 1959 by
Columbia Technical Translations
5 Vermont Ave., White Plains, N.Y.

Subscriptions: $215 per annum.
Single issues: $20 each.
Individual articles: $8 each.

Number 3 Volume 22 1958

BULLETIN

of the

Academy of Sciences of the USSR

- Physical Series -

(Izvestiia Akademii Nauk SSSR)
(Seriia fizicheskaia)

Reproduction rights reserved

by

Columbia Technical Translations
5 Vermont Avenue
White Plains, New York

Single Issues
$20

Annual Subscription
$215

NONFERROELECTRIC DIELECTRICS WITH A HIGH DIELECTRIC CONSTANT (Abstract*)

- G. I. Skanavi, Ia.M.Ksendzov, V.M.Trigubenko &
V.G.Prokhvatilov

The basic properties of ferroelectric materials are connected with the presence of spontaneous polarization in the temperature region below the Curie point. From the conditions of thermodynamic equilibrium it follows that at the Curie point, which corresponds to a phase transition, the specific inductive capacity attains a very high value (theoretically an infinitely high one). There is, however, a possibility of increasing the dielectric constant of solid dielectrics by means of relaxation polarization produced by a relative large displacement of the ions and not associated with a phase transition at the Curie point. Conjunction of large ionic displacement with a polarization-favoring local field in a crystal lattice of the perovskite type may lead to a very high value of the dielectric constant without ferroelectric properties. Experimental data show that "loosening" of a perovskite type lattice (strontium titanate, solid solutions of strontium titanate and lead titanate, or barium titanate) by partial replacement of the bivalent cations by cations with a higher valence (bismuth or cerium) does yield a great increase in the dielectric constant (up to a factor of several thousand) together with a change in the temperature and frequency dependences of the constant without significant alteration of the structure or increase in conductivity. The temperature and frequency dependences of ϵ and tan δ observed in such cases indicate that the polarization is associated with relaxation effects. Analysis of the experimental data from the standpoint of the hypothesis of ionic relaxation polarization allows of evaluating a number of quantities characterizing the polarization process (relaxation time, activation energy, displacement of the ions participating in the relaxation polarization, internal field, etc.). The results show that the basic hypothesis is consistent with the experimental data and not in conflict with phenomenological theory.

The replacement of the bivalent cation in the perovskite type lattice by cations of higher valence leads to the formation of deficiency solid solution. It follows from conditions of electric neutrality of the lattice that there must form vacant sites in the cation part of the lattice. Experimental x-ray diffraction data and specific weight measurements show that with increasing bismuth ion concentration in strontium titanate and barium titanate the number of cations per unit cell actually does decrease; the number and intensity of the Debye lines also decrease in a regular manner. It may be assumed that the vacant sites are formed at the expense of bivalent cations (strontium or barium). The presence of vacancies and trivalent cations in the perovskite type lattice must lead to distortion of the oxygen octahedra surrounding the titanium ions and, consequently, to a greater freedom for displacement of the latter. As a result there is superposed on the usual elastic (electronic and ionic) polarization, a relaxation polarization that effectively enhances the dielectric constant.

"P.N.Lebedev" Physical Institute
Academy of Sciences of the USSR

---

*Complete article in Zhur.eksp.i teor.fiz., 33, 320 (1957).

INFLUENCE OF IMPURITIES ON THE ELECTRIC PROPERTIES OF RUTILE

- Ia.M.Ksendzov

Experimental part

The experiments were carried out on specially purified titanium dioxide; the results of chemical and spectroscopic analyses of the material are given in Ref.1. Additional careful spectroscopic analysis showed the absence of P, Ta, Nb, Sb, V, Mo, W and U. The limiting sensitivity of the spectroscopic procedure for the listed impurities in TiO_2, according to the data of M.P.Atroshenko, ranges from 0.0005% for Sb to 1% for Ta; in the case of the most probable impurity, Nb, the sensitivity does not exceed some hundredths of a percent, which is approximately in agreement with the data of Ref.2.

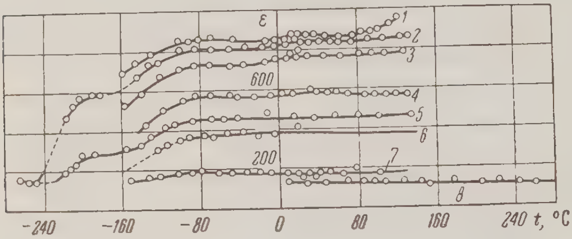

Fig.1. Temperature dependence of the dielectric constant ϵ of spectroscopically pure TiO_2 at different frequencies: 1) $2 \cdot 10^2$, 2) $1 \cdot 10^3$, 3) $1 \cdot 10^4$, 4) $7.5 \cdot 10^4$, 5) $1.5 \cdot 10^5$, 6) $3.5 \cdot 10^5$, 7) $2.5 \cdot 10^6$, 8) $2.3 \cdot 10^7$ cps.

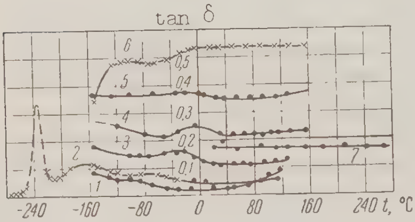

Fig.2. Temperature dependence of the dielectric loss tangent of spectroscopically pure TiO_2 at different frequencies: 1) $2 \cdot 10^2$, 2) $1 \cdot 10^3$, 3) $1 \cdot 10^4$, 4) $7.5 \cdot 10^4$, 5) $3.5 \cdot 10^5$, 6) $2.5 \cdot 10^6$ and 7) $2.3 \cdot 10^7$ cps.

The electric properties of polycrystalline rutile of the indicated purity after sintering at 1400-1450° are listed in Ref.1 and are characterized by an anomolously high value of ϵ (up to 2000) and tan δ, with dispersion in the 10^5 to 10^7 cps region. Additional data on the temperature dependences of ϵ and tan δ at different frequencies are shown in Figs.1 & 2. As may be seen from the figures, at temperatures below -240° the values of ϵ at different frequencies become identical and equal to ~140-150. With increasing temperature, ϵ at low frequencies increases in two successive steps; with increasing frequency, the increase of ϵ with temperature slows down and at a frequency of $\sim 2 \cdot 10^7$ cps the value of ϵ remains virtually constant up to about 400°. The value of tan δ at low frequencies goes through a maximum at the temperatures characterized by the rise in ϵ, while at radiofrequencies tan δ at first increases and then remains virtually constant in a wide temperature range.

The presence of oxides of alkali metals (Li & K), of alkaline earth metals (Ca, Sr, Ba & Mg) and of Cu, Co and Ni in amounts from 0.03 to 2% does not significantly alter ϵ and tan δ or their temperature and frequency dependences. The electric conductivity of TiO_2 with an admixture of Cu_2O, Li_2O or K_2O increases appreciably in the temperature range below 200°; the activation energy in the same interval is sharply reduced.

The contrast, Al_2O_3 and Fe_2O_3 have a marked effect on the electric properties of TiO_2. The addition of even a few hundredths of a percent of iron or aluminum oxide liquidates the anomolous properties of TiO_2; it increases tan δ and ϵ to the usual value for ordinary rutile ($\epsilon \approx 105$). Addition of the oxides of the tetravalent metals Zr and Sn shifts the beginning of the anomolous rise of ϵ and tan δ into the region of higher temperatures.[1] The

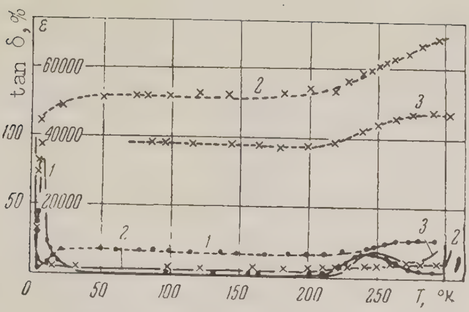

Fig.3. Temperature dependences of the dielectric loss tangent (solid lines) and the dielectric constant (dash lines) of spectroscopically pure TiO_2 doped with uranium and niobium oxides: 1) TiO_2 + 0.03% U_3O_8, 2) TiO_2 + 0.1% U_3O_8, 3) TiO_2 + + 0.15% Nb_2O_5.

presence of La_2O_3, SiO_2 and ThO_2 only slightly decreases the absolute value of ϵ. The substantial difference between the influence of La, Si and Th impurities and that of Fe, Al, Zr and Sn is due to the marked difference between the size of the ions of the first three compared to that of Ti^{4+} ions. The radii of Al^{3+}, Fe^{3+}, Zr^{4+} and Sn^{4+} ions are little different from the radius of the Ti^{4+} ion and hence these ions can occupy the titanium positions in the lattice; on the other hand, replacement of Ti^{4+} ions by La^{3+}, Th^{4+} and Si^{4+} is unlikely.

A particularly strong influence on the electric properties of TiO_2 is exerted by the oxides of metals in columns 5 and 6 of the Periodic Table, having a maximum valence greater than four. Thus small amounts of the oxides of Nb, Ta, W and U increase ϵ to several tens of thousands. For example, the addition of 0.03% of U_3O_8 increases ϵ to 10,000, while the addition of 0.1% Nb_2O_5, Ta_2O_5 or U_3O_8 increases ϵ to 40,000. The temperature dependences of ϵ and tan δ for TiO_2 with 0.03 and 0.1% U_3O_8 and 0.15% Nb_2O_5 are shown in Fig.3. The introduction of these impurities not only increases ϵ but also reduces the temperature rise of ϵ and the maximum value of tan δ as compared with pure TiO_2.

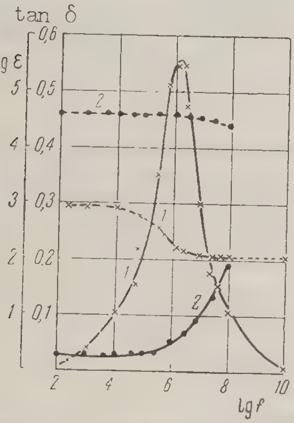

Fig.4. Frequency dependences of the dielectric loss tangent (solid lines) and the dielectric constant (dash lines) of spectroscopically pure TiO_2 (curves 1) and TiO_2 + + 0.1% U_3O_8 (curves 2).

At temperatures in the range from -40 to -20° there is another rise in ϵ and a maximum of tan δ, which becomes more pronounced with decreasing impurity concentration.

The dispersion frequency in TiO_2 with U, Nb and Ta impurities is higher than the dispersion frequency for pure TiO_2 (Fig.4); at a U_3O_8 concentration of 0.1%, for example, the dispersion frequency goes to above 10^9-10^{10} cps. The addition of WO_3 to TiO_2 increases not only the value of ϵ but also the temperature of the beginning of growth of ϵ.

Uranium, niobium, titanium and tungsten impurities also produce a noticeable change in the color of TiO_2; after sintering the TiO_2 specimens with these impurities have a dark color similar to that of reduced TiO_2. Admixtures of V_2O_5 and Cr_2O_3 have approximately the same effect on ϵ and tan δ as Al and Fe oxides (Fig.5). Specimens with V_2O_5 impurity have the same dark color as reduced TiO_2. The temperature dependence of tan δ of TiO_2 with V_2O_5 and Cr_2O_3 corresponds almost exactly to the temperature dependence of the electric conductivity. Additions of U, Nb, Ta and W have a pronounced effect on the electric conductivity of TiO_2, whereas V, Cr and Mo influence the conductivity very little. Fig.6 shows the variation of the conductivity σ with the temperature for pure TiO_2 and TiO_2 with different concentrations of U_3O_8 as recorded in a field of 200 v/cm. One can distinguish three sections in all the curves: a region of low temperatures in which σ changes insignificantly, a

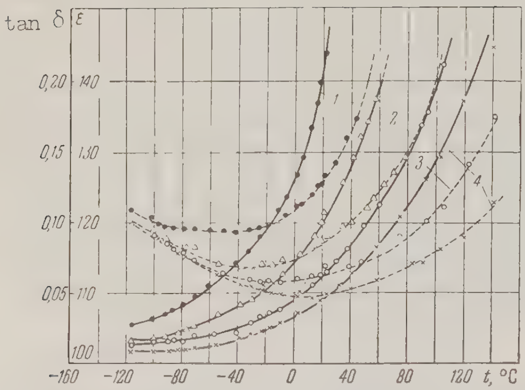

Fig.5. Temperature dependences of the dielectric loss tangent (solid lines) and the dielectric constant (dash lines) of TiO_2 + 0.15% Cr_2O_3 at different frequencies: 1) $2\cdot 10^2$, 2) 10^3, 3) $3\cdot 10^3$, 4) 10^4 cps.

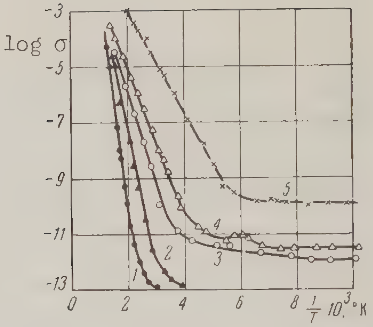

Fig.6. Temperature dependences of the electric conductivity of chemically pure TiO_2 and TiO_2 with different amounts of U_3O_8: 1) chemically pure TiO_2, 2) TiO_2 + 0.03% U_3O_8, 3) TiO_2 + 0.065% U_3O_8, 4) TiO_2 + 0.1% U_3O_8, 5) TiO_2 + 0.16% U_3O_8.

region of medium temperatures with an appreciable temperature dependence of σ, and a region of high temperatures in which the temperature dependence of σ is the same as in pure TiO_2. The temperature dependence of the electric conductivity may be characterized by the following three-term formula:

$$\sigma = A_1 f(t) + A_2 \exp(-\Delta E_2 / 2kT) + A_3 \exp(-\Delta E_3 / 2kT), \tag{1}$$

where $\Delta E_2 < \Delta E_3$.

Table 1

Activation energy of TiO_2 with different amounts of U_3O_8

Activation energy, ev	TiO_2	TiO_2+0.06 %U_3O_8	TiO_2 + 0.1 %U_3O_8	TiO_2+0.16 %U_3O_8
ΔE_2	—	1.33	1.0	0.75
ΔE_3	3.6	3.4	3.6	3.2

In the region of low temperatures the form of the function $f(t)$ cannot be accurately determined inasmuch as log σ does not vary linearly with 1/T; the value of σ in this region increases with increasing impurity concentration. The values of the activation energy ΔE_2 and ΔE_3 as determined from the curves of Fig.6 are listed in Table 1. The activation energy ΔE_2 in the second section decreases with increasing impurity concentration, while the value of ΔE_3 is approximately the same for all specimens.

The temperature dependence of the electric conductivity of TiO_2 with V, Cr and Nb impurities (Fig.7) consists only of two sections: a high temperature section with an activation energy approximately equal to that for pure TiO_2 and a low temperature section with an activation energy ΔE_1, that varies with the type and amount of impurity. At equal impurity concentrations, the value of ΔE_1 in TiO_2 containing Nb_2O_5 is appreciably lower than in TiO_2 containing

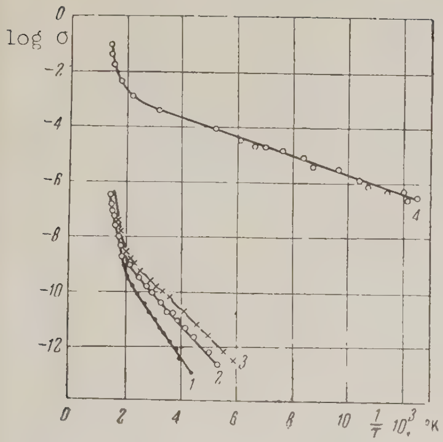

Fig.7. Same as Fig.6 but for TiO_2 with different impurities: 1) TiO_2 + 0.15% V_2O_5, 2) TiO_2 + 0.15% Cr_2O_3, 3) TiO_2 + 0.5% V_2O_5, 4) TiO_2 + + 0.15% Nb_2O_5.

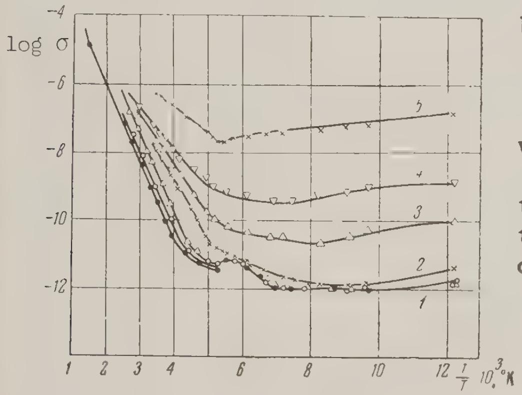

Fig.8. Temperature dependences of the electric conductivity of TiO_2 + 0.1% U_3O_8 at different field intensities: 1) 800, 2) 2000, 3) 2400, 4) 3200, 5) 4000 v/cm.

V_2O_5 or Cr_2O_3. Thus, for example, at a concentration of 0.3% of V or Cr, $\Delta E_1 = 0.59$ or 0.50 ev, respectively, while with a concentration of 0.3% Nb, $\Delta E_1 \approx 0.15$ ev, i.e., is smaller by a factor of 3-4.

The electric conductivity of TiO_2 specimens with U, Nb, Ta and W impurities is markedly dependent on the field intensity. Fig.8 shows the temperature dependences of log σ at different field intensities for a TiO_2 sample containing 0.1% U_3O_8. With increasing field gradient F, the dependence of σ on the temperature becomes increasingly similar to that in metals. The temperature range characterized by metallic type conductivity increases with increasing field intensity.

Fig.9a shows the variation of the volumetric resistivity ρ with the field intensity F at liquid nitrogen temperature; Fig.9b shows the variation of the activation energy ΔE_2 with F.

At liquid nitrogen temperature Ohm's law holds up to 2000 v/cm; at higher field gradients the conductivity is closely characterized by the expression

$$\sigma = \sigma_o \exp(-\beta/F)$$

with the coefficient $\beta = 5.5 \cdot 10^4$ v/cm.

The deviation from Ohm's law at room temperatures begins at lower field intensities and the F dependence of σ is closely characterized by

$$\sigma = \sigma_o \exp\left[-(\Delta E_2 - \alpha\sqrt{F})/2kT\right].$$

The maximum experimental field intensity was limited by the possibility of heating of the specimens. The maximum rate of heating (power dissipation ~0.02 watt) occurred at F = 4000 v/cm in a TiO_2 specimen with 0.1% U_3O_8. Determination of the sign of the thermo-emf showed that all specimens with U,

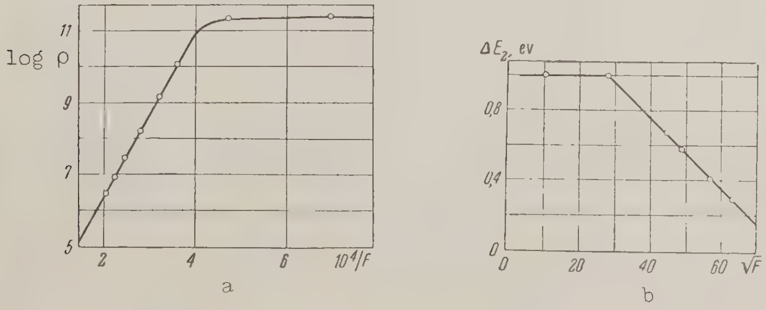

Fig.9a) Variation of the volumetric resistivity of TiO_2 + 0.1% U_3O_8 with the electric field intensity at liquid nitrogen temperature; b) variation of the activation energy ΔE_2 with the field intensity.

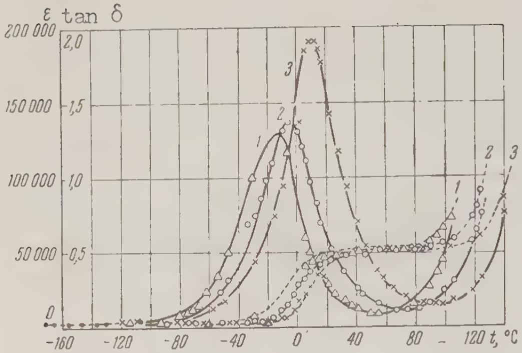

Fig.10. Temperature dependences of the dielectric loss tangent (solid lines) and the dielectric constant (dash lines) observed for TiO_2 with 0.16% U_3O_8 + 0.25% Fe_2O_3 at different frequencies: 1) $2\cdot 10^2$, 2) $1\cdot 10^3$, and 3) $1\cdot 10^4$ cps.

Nb, Ta and W impurities had n-type conductivity.

The electric conductivity of TiO_2 specimens with V, Cr and Mo impurities is independent of the field gradient up to 8000 v/cm in the entire investigated temperature range.

Upon introduction into TiO_2 in equal concentrations of two oxides the valence of whose cations adds up to 8, for example, $UO_3 + MgO$, $Nb_2O_5 + Al_2O_3$ or $Ta_2O_5 + Fe_2O_3$, the value of ϵ goes to its normal value of $\sim$105-110, tan $\delta \approx (3\text{-}5)\cdot 10^{-4}$ and the electric conductivity decreases by 5-6 orders of magnitude as compared with that of TiO_2 containing only Nb, Ta or U oxides.

If the sum of the valences of the impurities is greater than 8, for example, if one adds $UO_3 + Fe_2O_3$ or $Ta_2O_5 + ZrO_2$, the anomalous properties of TiO_2 persist and the temperature of the beginning of the rise of ϵ may be appreciably increased (Fig.10). In the case of different concentrations of impurities with a total valence of 8, the effect evinced is that of the excess impurity with the greater valence.

It might be assumed that the anomalously high value of ϵ and the sharp field dependence of σ are due to the existence of barrier layers at the electrode interfaces. To check this assumption, we measured the distribution of potentials by means of probes and an electrometer and compared the conductivity values determined by the bridge and compensation procedures. The potential distribution in specimens with U, Nb and Ta impurities proved to be linear, while the values of σ determined by the compensation and bridge procedures differed by less than 3-5%. We also found that the magnitude of ϵ does not depend on the sample thickness in the range from 0.5 to 6 mm. Hence the anomalously high value of ϵ and the sharp variation of σ with the field intensity are not due to effects at the electrode interfaces but are, rather properties intrinsic to the given composition.

Discussion of the experimental results

1. Exceptionally high values of the dielectric constant for rutile have been observed repeatedly in purified specimens[1,2], in different types of technical raw material[4] and in technical grade rutile doped with alkaline earth oxides[5]. The differences between the experimental data obtained in the investigations referred to are due primarily to differences in the range of temperatures and frequencies in which the anomalous electric properties of rutile were observed.

In view of our experimental data it may be hypothesized that the anomalously high values of ϵ in pure and technical grades of TiO_2 are connected with the presence of Nb or Ta oxide impurities. The influence exerted by Al and Fe on the electric properties of pure TiO_2 can be understood if we assume that there were already present in the TiO_2 Nb and Ta impurities. Inasmuch as the sensitivity of spectroscopic analysis as regards these impurities is not great and the experimental data show that it is sufficient to add as little as 0.01% of either of these oxides to obtain a sharp enhancement of the "anomalous" properties, the reported spectroscopic analysis data do not invalidate our hypothesis.

In natural minerals and technical grade TiO_2 there are present in a dissolved state impurities with different valences in the compensated tetravalent state. Chemical purification, even when carried out with utmost care, disturbs the compensated state between the impurities inasmuch as some of them, for example, Fe_2O_3 and Al_2O_3 are removed much more easily than others such as P_2O_5 and Ta_2O_5. By virtue of this, the "anomalous" electric properties are more clearly evinced in "purified" TiO_2. The compensated state of the impurities may also be altered because of their different solubility in the vitreous material that forms during sintering. Thus, increasing the sintering temperature of TiO_2 specimens prepared from technical grade material, as our experiments have shown, or the introduction into technical grade TiO_2 of alkaline earth metal oxides[5] which tend to facilitate glass formation, leads to the appearance of anomalously high values of ϵ and tan δ. It may also be hypothesized that in absolutely pure TiO_2 there may appear anomalously high values of ϵ due to lattice defects.

2. Careful examination of the curves of Figs.1, 2 & 3 and of the data reported in Refs.1 & 5 shows that the temperature and frequency dependences of ϵ and tan δ differ significantly from the classical picture for relaxation processes. In the wide temperature range in which ϵ has an anomalously high value, it also exhibits a strong dependence on the frequency, while at frequencies above $2 \cdot 10^7$ cps the usual value of $\epsilon \approx 110$ persists to 400°. Maxima of tan δ are observed only at technical and audio frequencies; at radiofrequencies tan δ increases at low temperatures and has a constant value over the entire higher temperature range (if one takes into account conductivity losses). Analogous variation of ϵ and tan δ with temperature and frequency is observed in TiO_2 with admixtures of U_3O_8, Nb_2O_5 and Ta_2O_5. Consequently, the frequency of dispersion of ϵ, associated with the time constant of the polarization process, is a constant, temperature independent quantity. Thus the polarization responsible for the anomalously high values of ϵ and tan δ in pure TiO_2 and TiO_2 with impurities is connected not with thermal relaxation but with vibrations having definite natural frequencies.

3. As follows from the experimental data the anomalous electric properties of TiO_2 are connected with an excess uncompensated valence of the impurities and, consequently, are determined by the state of their excess valence electrons; this state depends on the type of solid solution formed. The solution of impurities with a cation valence greater than that of the cation of the main oxide may occur in two ways:

(a) In a reaction between the impurity and the main oxide, accompanied by formation of vacant sites in the cation part of the lattice, there is formed a deficiency type solid solution. In this case all the valence electrons are bound:

$$(1-x)\,\mathrm{TiO_2} + x\,\mathrm{M_2O_5} \rightarrow [\mathrm{Ti}_{1-x},\ \mathrm{M}_{2x},\ \overset{\square}{\mathrm{Ti}}_{x/2}],\mathrm{O}_{2(1+x/2)},$$

where the □ over the element designation indicates a vacant site.

(b) In a reaction accompanied by partial dissociation of the oxygen, there is formed a substitutional solid solution, for example:

$$(1-x)\,\mathrm{TiO_2} + x\,\mathrm{M_2O_5} \rightarrow [\mathrm{Ti}_{1-x},\ \mathrm{M}_{2x}]\,\mathrm{O_2} + \frac{x}{2}\,\mathrm{O_2}\uparrow + 2xe$$

or for hexavalent impurities

$$(1-x)\,\mathrm{TiO_2} + x\mathrm{M'O_3} \rightarrow [\mathrm{Ti}_{1-x},\ \mathrm{M'}_{x}]\,\mathrm{O_2} + \frac{x}{2}\,\mathrm{O_2}\uparrow + 2xe,$$

where e are excess valence electrons of the impurity.

There are no vacant sites in the crystal lattice of such a solid solution. The formation of an interstital solid solution is little probable in view of the necessity in this case of complete dissociation of the impurity oxide. Let us consider the probabilities of formation of solid solutions of types (a) and (b).

The energy W_H of formation of a vacant site can be approximately evaluated by means of the formula[6]:

$$W_H = W_L - \frac{1}{2} e\varphi,$$

where W_L is the lattice energy per titanium ion and φ is the electrostatic potential developing as a result of formation of a vacant site. The lattice energy per molecule of TiO_2 is

$$W_0 = A_m e^2 z^2 (1 - 1/n) / R_0, \qquad (2)$$

where A_m is Madelung's constant, equal to 4.816 for rutile, R_o is the distance between the Ti^{4+} and O^{2-} ions. With $R_o = 1.96$ Å, $n = 9$ and $z = 2$, we obtain $W_o = 125$ ev and $W_L = W_o/2 = 62.5$ ev.

The value of φ is obtained from the equality

$$\varphi = \frac{4e}{r_0}\left(1 - \frac{1}{\varepsilon}\right).$$

The minimum value of r_0 is 0.64 Å - the radius of the Ti^{4+} ion. In this case the value of φ is maximum and equals 90 v and the minimum energy of formation of a vacant site in the titanium part of the lattice equals ~20 ev. The maximum energy of formation of a substitutional solid solution by the (b) reaction is equal to either the energy of formation of a vacant site in the oxygen part of the lattice, which site is then occupied by an excess oxygen ion of the impurity, or to the energy of dissociation of the impurity oxide. For the free energy of the reaction

$$2TiO_2 \rightleftarrows Ti_2O_3 + {}^1/_2 O_2 \uparrow,$$

from the data on the reduction of TiO_2 in a stream of oxygen Breckenridge[12] obtained

$$\Delta F = 71{,}600 - 22.21\ T,$$

whence for the equilibrium constant we have

$$K_p = P_{O_2^{1/2}} = 6.3 \cdot 10^4 \exp(-35800/T).$$

Inasmuch as the primary product of the reduction of TiO_2 is Ti_3O_5, the reduction reaction taking into account the formation of vacant sites (O_V) and excess valence electrons e may be written

$$2TiO_2 \rightleftarrows {}^2/_3 Ti_3O_5 + {}^1/_3 O_2 \uparrow + {}^2/_3 O_V + {}^4/_3 e.$$

The equilibrium constant for the reaction is

$$K_p = P_{O_2^{1/3}} XO_V^{2/3} Xe^{4/3},$$

where XO_V and Xe are the concentrations of vacant sites and the excess valence electrons.

In view of the fact that $XO_V = {}^1/_2 Xe$, we obtain

$$XO_V = {}^1/_2 Xe = K_p^{1/2} P_{O_2}^{-1/6} = 10^2 [\exp(-35800/2T)] P_{O_2}^{-1/6}. \tag{3}$$

Thus the energy of formation of vacant sites in the oxygen part of the lattice (~3.1 ev) is appreciably lower than the energy of formation of vacancies in the titanium part of the lattice (~20 ev); hence as a result of the reaction there is formed a substitutional solid solution (type (b)).

It also follows from Eq.(3) that the number of excess valence electrons and, consequently, the electric conductivity vary exponentially with the temperature at an activation energy of 3.1 ev and in inverse proportion to the oxygen pressure to the 1/6 power; this is in agreement with the experimental data.[7]

The excess valence electrons of the impurity may have two bound states. In one, the basic state, the electrons are in the shell of the impurity ions. In the second bound state, the excess valence electrons are located at an appreciable distance from the impurity ions but are coupled to them by the Coulomb energy of the resultant excess charge and the impurity ions. Transition of the impurity electrons from the first to the second state is connected with an appreciable energy gain due to polarization and reduction of the size of the ion with increasing ionic charge. It must be borne in mind that tetravalent Nb, Ta, U and other ions have a radius exceeding the ionic radius of Ti^{4+} (the Ti^{4+} radius is 0.64 Å) and their solution gives rise to elastic stresses in the lattice. Transition of such ions to a higher valence decreases their size and, consequently, reduces the energy of the elastic stresses. The magnitude of the elastic energy associated with the solution of ions of different radius may be calculated from an expansion of the energy in terms of the parameter r characterizing the displacement of the ions from their equilibrium position

$$W(r_0 + \Delta r) = -W_0 + \frac{\alpha}{2}\Delta r^2 - \frac{\beta}{3}\Delta r^3. \tag{4}$$

Limiting the expansion to the quadratic term from Eq.(2), we obtain for the elastic energy:

$$\Delta W = n(\Delta r / R_0) W_0 / 2.$$

If we bear in mind that

$$R_0 = r_{O^{2-}} + r_{Ti^{4+}} \text{ and } \Delta r / R_0 = 0.326 \Delta r / r_{Ti^{4+}},$$

where $\Delta r = r_k - r_{Ti^{4+}}$, then for the elastic energy in the TiO_2 lattice we obtain

$$\Delta W \approx 66 \left(\frac{\Delta r}{r_{Ti^{4+}}}\right)^2 \text{ev}.$$

When the radius of the impurity ion differs from the radius of Ti^{4+} by 5%, we have $\Delta W = 0.15$ ev; if the difference is 10%, $\Delta W = 0.66$ ev, and if the difference is 15%, $\Delta W = 1.5$ ev.

Thus a difference between the radius of the impurity cation and the radius of the Ti^{4+} ion leads to an accumulation of an appreciable elastic energy, which is the principal factor limiting the concentration of solid solutions. Transformation of ions of elements having an ionic radius greater than 0.64 in the tetravalent state to a state with a higher charge reduces the energy of the system, thereby facilitating transition of the excess valence electrons to the second bound state.

The Nb^{4+}, Ta^{4+}, W^{4+} and U^{4+} ions have radii greater than the radius of Ti^{4+}

(the radii are 0.69, 0.69, 0.68 and 1.08 Å, respectively); consequently, in the TiO_2 lattice they go over into the pentacharged state (Nb^{5+} and Ta^{5+}) or the hexacharged state(U^{6+} and W^{6+}). Va^{4+}, Cr^{4+}, P^{4+} and As^{4+} ions have radii smaller than 0.64 and their transition to states with a higher valence, on the contrary, could only produce an increase of elastic energy and hence is unlikely.

It may be assumed that it is energetically more advantageous for some of these ions to go to the trivalent state, which is evinced in the case of the oxides of V and Cr. If we take into account that the formation of a Ti^{3+} ion is connected with an increase of the lattice energy by 0.4 due to increase of its radius from 0.64 to 0.69 Å, it becomes obvious that the most probable state for Nb, Ta, U and W ions in the TiO_2 lattice is their maximum valence with retention of the tetravalent state of the Ti ions.

4. In the second bound state the excess valence electrons of the impurity are located in a medium with a dielectric constant ϵ and an index of refraction n in a field U(r) due to the excess charge Ze of the impurity. The energy state of the electrons of pentavalent ions is determined from Schrödinger's equation, in which, in order to take into account the periodic potential of the lattice, the electron mass is replaced by the effective mass[2], by analogy with the problem for a hydrogen atom, and in the case of hexavalent ions, in the same way as for a helium atom.

For pentavalent ions the excess charge is $+e$ and the energy of the electron and the radius of the electron orbit in the basic state are, respectively,

$$E_{1s} = E^0_{1s}\frac{m^*}{m\varepsilon^2}, \text{ and } a = a_0\frac{\varepsilon m}{m^*},$$

where m^* is the effective electron mass, $E^0{}_{1s}$ = 13.55 ev, the energy of the hydrogen atom electron in the ground state, and a_0 = 0.523 Å is the radius of the first Bohr orbit.

For hexavalent ions the excess charge is $+2e$; the ionization energy of the first excess electron and the radius of the electron orbit are

$$I = 0.903e^2/\varepsilon a_1 = 1.806E_{1s}, \text{ and } a_1 = a.$$

For purposes of approximate calculation, it may be assumed that ϵ is determined only by the electronic part of the polarization and that the effective electron mass is equal to the mass of a free electron. Then, $E_{1s} = 13.55/n^4 = 13.55/57 = 0.24$ ev and $a = 4.2$ Å for a quintuply charged ion and I = 0.43 ev and $a = 4.2$ for a sextuply charged ion. From the data on electrical conductivity we have $\Delta E \approx 0.15$ ev for Nb and Ta impurities and $\Delta E \approx 1$ for uranium oxide; it must be noted that these values agree only as regards order of magnitude with the calculated values. The frequency $\nu = E_{1s}/h$ is greater than 10^{13} sec^{-1}, i.e., is appreciably greater than the natural vibration frequencies of ions, and, consequently, cannot be used for calculating $n^2 = \epsilon$.

5. The polarizability α of such a quasiatom, as follows from classical and quantum mechanical considerations[10], is proportional to the cube of the radius of the electron shell, i.e.,

$$\alpha = \frac{9}{2}a^3.$$

To calculate the dielectric constant we have recourse to the procedure used by Odelevskii[11], i.e., we juxtapose our medium, in which $\epsilon_o = 114$, with an auxiliary medium in which the dielectric constant is ϵ_o times smaller. With a statistically uniform distribution of impurity atoms one can apply the

Lorentz method of calculation. For the polarizaing field, we have

$$E_{\mathrm{p}} = E_{\mathrm{av}} + 4\pi \frac{P}{3} = E_{\mathrm{av}} + 6\pi N a^3 E_{\mathrm{p}} = \frac{E_{\mathrm{av}}}{1 - 6\pi N a^3},$$

where N is the number of impurity atoms per cm^3.

From the equality $D = E_{\mathrm{av}} + 4\pi P$ for the auxiliary medium with impurities we obtain

$$\varepsilon_{\mathrm{II}} = 1 + \frac{18\pi N a^3}{1 - 6\pi N a^3};$$

the dielectric constant of the actual medium with impurities is obtained by multiplying ϵ_{II} by ϵ_o, i.e.,

$$\varepsilon = \varepsilon_0 \left[1 + \frac{18\pi N a^3}{(1 - 6\pi N a^3} \right].$$

Now $\epsilon \to \infty$, as $6\pi N a^3 \to 1$, which corresponds to an impurity concentration of ~2.5%; a change in ϵ by a factor of 2, as follows from the above equality, can be expected at an impurity concentration $\leqslant 1\%$. The experimental data show that even at an impurity concentration of the order of 0.1%, $\epsilon > 10{,}000$, i.e., ϵ increases by more than two orders of magnitude as compared with ϵ_o.

It must be noted also that the dispersion frequency obtained from experiment is many orders of magnitude lower than the frequency determined from the relationship $\nu = E_{1s}/h$ and the dispersion frequency of ϵ_o of the medium. It has also been determined experimentally that the dispersion frequency increases with increasing impurity concentration, while the relationship $\nu = E/h$ either yields concentration independence of ν or leads to a decrease of the frequency, inasmuch as usually E decreases with increasing impurity concentration. Thus taking into account the polarization of separately considered impurity centers leads to values of ϵ and a frequency dependence of ϵ differing appreciably from the experimental data.

6. The rapid increase of ϵ with increasing impurity concentration and its frequency dependence are probably connected with the interaction of the impurity center electrons. It is known that this interaction, just as that of hydrogen atoms, leads to the appearance of exchange energy. Neglecting terms containing the factors $\exp(-2R/a)$ and $\exp(-1.5\,R/a)$ and taking ϵ of the medium into account one can obtain the following expression[9] for the exchange energy A when $R/a \gg 1$ (where R is the distance between the impurity atoms):

$$A = \frac{e^2}{n^2 a} \left(1 + \frac{R}{3a}\right) \left(1.7 + 1.2 \lg \frac{R}{a}\right) \exp\left(-\frac{R}{a}\right).$$

For a = 4.2 Å and n^2 = 7.6, the values of the exchange frequency $\nu = 2A/\pi h$ as a function of the impurity concentration in TiO_2 are listed in Table 2.

The variation of the exchange frequency is in qualitative agreement with the impurity concentration dependence of the frequency of dispersion of ϵ. Moreover the exchange energy and exchange frequency depend only on the separation between the impurity atoms and the radius of the electron shell and do not depend on the temperature, which is consistent with the experimentally observed constancy of the frequency of dispersion of ϵ in a wide temperature range. The exchange frequency may change as a result of transition of an electron from one state of the atom to another or transition of an electron to an excited level within the limits of the transformed state of the atom. This leads to an increase in the radius of the electron orbit, which is apparently what determines the observed increase in ϵ and $\tan \delta_{max}$ in the region of low temperatures. An appreciable increase in ϵ is apparently caused by a

Table 2

Values of the exchange energy A and exchange frequency ν as functions of the impurity concentration in TiO_2

Concentration of impurity atoms, %	N, number of impurity atoms, cm^{-3}	Distance between impurity atoms, A	$\frac{R}{a}$	Exchange energy A, ergs	Exchange frequency, sec^{-1}
0,001	$3,2 \cdot 10^{17}$	145	34,5	$2 \cdot 10^{-26}$	2,0
0,01	$3,2 \cdot 10^{18}$	68	16,15	$8 \cdot 10^{-19}$	$8 \cdot 10^{7}$
0,1	$3,2 \cdot 10^{19}$	31,5	7,5	$2 \cdot 10^{-15}$	$2 \cdot 10^{11}$
0,3	$9,6 \cdot 10^{19}$	21,8	5,2	$1,5 \cdot 10^{-14}$	$1,5 \cdot 10^{12}$

large polarizability of the electrons during exchange due to the possibility of their being located anywhere in the volume between the impurity atoms. It follows from the data of Table 2 that the effect of "anomalous" polarization in pure TiO_2 may be produced by an impurity atom concentration of only ~0.01%.

The possibility of electron exchange between impurity centers means that the potential barrier formed by the Coulomb field of the impurity atoms can be penetrated by the electrons (tunnel effect). The total electric conductivity associated with the presence of impurities will therefore consist of two parts: the electric conductivity due to thermal ionization with transition of electrons into the conduction band, which depends on the temperature, and the electric conductivity due to the tunnel effect, which is independent of the temperature. The electric conductivity associated with the tunnel effect will be evinced at low temperatures when the number of electrons in the conduction band is small. In TiO_2 with U_3O_8 impurity the ionization energy is high (~1 ev) and the number of electrons in the conduction band rapidly falls off with decreasing temperature; consequently, in this case one can experimentally observe the part of the electric conductivity associated with the tunnel effect. In the case of impurities consisting of pentavalent elements with an activation energy ~0.2 ev, this part of the conductivity must, obviously, be evinced at lower temperatures than were attained in our experiments.

An electric field lowers the potential barrier, which is manifested by a decrease of the thermal ionization energy, and reduces the width of the barrier, which is evinced in a sharp decrease of the "metallic" part of the conductivity (see Figs.8 & 9). The variation of the part of the electric conductivity that is of the metallic type with the electric field can be approximately calculated from the change in the width of the potential barrier. In an electric field the potential energy of an electron between two impurity centers, a distance R apart, is given by

$$U = -\frac{e^2 R}{\varepsilon a (R - a)} - eFr,$$

while the width of the potential barrier l at the level E (with some simplifying assumptions) is given by the expression:

$$l = \frac{R}{1 + \frac{eFR}{U_m - E}},$$

where U_m is the depth of the potential well.

Replacing the "true" potential barrier by a rectangular one, we obtain the following expression for the coefficient of penetration (transparency):

$$D = D_0 \exp\left[-\frac{2}{h}\sqrt{2m^*(U_m - E)}\,\frac{R}{1 + \frac{eFR}{U_m - E}}\right].$$

With $eFR > U_m - E$, we obtain for the conductivity

$$\sigma = \sigma_0 \exp\left[-\frac{2\sqrt{2m^*}}{h}\frac{(U_m - E)^{3/2}}{eF}\right],$$

where m^* is the effective electron mass. Comparison of the above with the experimentally obtained dependence $\sigma = \sigma_0 \exp(-\beta/F)$ yields

$$\beta = \frac{2\sqrt{2m^*}}{h}(U_m - E)^{3/2}.$$

With $U_m - E$ = 0.5 ev (the value obtained by calculation for a sextuply charged impurity ion), we obtain $\beta = 1.2 \cdot 10^5$ v/cm. This is in fair agreement with the value of $\beta = 5.5 \cdot 10^4$ v/cm obtained from experiment.

Sharp deviation from Ohm's law should begin at a field value F given by the expression $eFR = U_m - E$. For an impurity concentration of 0.1% (R ≈ 31 Å) we find $F \approx 5 \cdot 10^3$ v/cm, which as regards order of magnitude is in agreement with the value of $2 \cdot 10^3$ v/cm given by experiment.

The absence of anomalous dispersion in the frequency dependence of ϵ in connection with the resonance character of the effects limiting polarization is apparently a consequence of strong slowing down of the electrons by the medium.

Conclusions

1. Only impurities that have a valence and an ionic radius greater than that of titanium exert a strong influence on the values of ϵ, tan δ and the conductivity σ of TiO_2. Such impurities form F-centers and the energy spectrum of the excess valence electrons can be calculated in the same way as for hydrogen or helium atoms. The high value of the index of refraction leads to the formation of large orbits of the excess valence electrons and appreciable polarizability. This effect alone, however, cannot explain the sharp increase of ϵ and the observed dependence of the dispersion of ϵ on the temperature, frequency and impurity atom concentration.

2. The polarization introduced by impurity centers is characterized by a resonance rather than a relaxation mechanism. The resonance frequency corresponds to the electron exchange frequency between impurity centers and depends only on the concentration of impurity atoms and the electron orbit radius. The experimental data are in satisfactory agreement with approximate calculations taking into account the interaction of impurity center electrons.

References

1. Ia.M.Ksendzov, Zhur.tekh.fiz., 20, 117 (1950).
2. I.V.Melamed, Zavodsk. labor. (Industrial laboratory), 9, (1955).
3. L.Nicolini, Nature, 170, 938 (1952).
4. I.N.Beliaev, N.S.Novosil'tsev et al, Zhur.tekh.fiz., 21, 547 (1951).
5. G.I.Skanavi & A.I.Demeshina, Zhur.eksp.i teor.fiz., 19, 3 (1949).
6. N.F.Mott & R.W.Gurney, Electronic Processes in Ionic Crystals. (Cited in Russian trans., M. 1950.)
7. K.Hauffe, H.Grunewäld & R.Trenckler-Gresse, Electrochem, 56, 937 (1952).
8. S.I.Peker, Issledovaniia po elektronnoi teorii kristallov (Investigations in the electronic theory of crystals), 1951.
9. H.Bethe, Quantum Mechanics of Simple Systems (Cited in Russ.trans.,1935).
10. G.Castellan & F.Seitz, Semiconducting Materials (" " " 1954).
11. V.I.Odelevskii, Zhur.tekh.fiz., 21, 667 (1951).
12. R.G.Breckenridge & W.R.Hosler, Phys.Rev., 91, 793 (1953).

RELAXATION THEORY OF ELECTRIC POLARIZATION

- N.S.Fastov & B.N.Finkel'shtein

The use of thermodynamics in treatment of electric polarization is usually based on the implicit assumption that the variation of the induction or electric field in the medium is quasistatic, i.e., it is assumed that the rate of change of these quantities is infinitesimal. It is only on this assumption that one may consider the substance to be in thermodynamic equilibrium during the process of polarization. If, on the other hand, the field varies at a finite rate (for instance when it is periodic) there will occur deviations from thermodynamic equilibrium that may give rise to one or more relaxation processes with their associated relaxation times.

It then becomes necessary to introduce new independent parameters characterizing the deviations from thermodynamic equilibrium and to derive the appropriate kinetic equations.

It is known that for small deviations from equilibrium the fundamental relations of thermodynamics remain in force.[1] In the case of interest to us the relation

$$E_i = 4\pi \frac{\partial F}{\partial D_i}, \tag{1}$$

remains valid; here E_i and D_i are the components of the electric field strength and induction, and F is the free energy per unit volume.

Without restriction of generality, let us consider the case of isothermal electric polarization of an isotropic homogeneous dielectric. If the rate of change of D_i is nonzero, the free energy in the isothermal process will depend, in addition to D_i, on a new relaxation variable, which we shall designate as the vector ξ_i. The free energy per unit volume of such a dielectric can in the first approximation be represented by a quadratic invariant form in D_i and ξ_i, namely,

$$F = F_0 + \frac{1}{2} a_1 D_j^2 + a_2 D_j \xi_j + \frac{1}{2} a_3 \xi_j^2 \tag{2}$$

(summation is implied over repeated indices), where F_0 is the free energy of the dielectric for zero field, a_1, a_2, and a_3 are constants for the substance and j takes on the values 1, 2 and 3.

Let us find the vector $\bar{\xi}_i$ which gives the minimum free energy for a given value of the induction. From the condition

$$(\partial F / \partial \xi_i)_{D_j} = 0 \tag{3}$$

we obtain

$$a_2 D_i + a_3 \bar{\xi}_i = 0,$$

and this gives

$$\bar{\xi}_i = -\frac{a_2}{a_3} D_i. \tag{4}$$

Let us find the time dependence of ξ_i.

The kinetic equation for this variable may be written

$$\dot{\xi}_i = -\frac{1}{\tau}(\xi_i - \bar{\xi}_i), \tag{5}$$

where τ is the relaxation time of the polarization process.

Comparing (5) and (2), we obtain the new form

$$\xi_i = -b \frac{\partial F}{\partial \xi_i}, \tag{6}$$

for this kinetic equation, where $b = \frac{1}{\tau a_3}$.

Integrating (5) and using (4), we obtain

$$\xi_i(t) = -\frac{a_2}{a_3} D_i(t) + \frac{a_2}{a_3} \int\limits_{-\infty}^{t} e^{\frac{t'-t}{\tau}} \dot{D}_i(t')\, dt'. \tag{7}$$

We now use this equation in combination with (1) and (2), arriving at

$$E_i(t) = 4\pi \left\{ \left(a_1 - \frac{a_2}{a_3} \right) D_i(t) + \frac{a_2}{a_3} \int\limits_{-\infty}^{t} e^{\frac{t'-t}{\tau}} \dot{D}_i(t')\, dt' \right\}. \tag{8}$$

If the time dependence is periodic of the form

$$D_i = D_i^{(0)} \exp(i\omega t)$$

Eq.(8) becomes

$$E_i(t) = 4\pi \left(a + \frac{i\omega\tau}{1 + i\omega\tau} \cdot \frac{a_2^2}{a_3} \right) D_i(t) \tag{9}$$

or

$$E_i(t) = 4\pi \frac{a + i\omega\tau a_1}{1 + i\omega\tau} D_i(t), \tag{9'}$$

where we have introduced the notation

$$a = a_1 - \frac{a_2^2}{a_3}.$$

It can be shown by using the extermal properties of the free energy that a_1, a_2, and a_3 are real and positive.

Equ.(9') shows that there is a phase difference between the electric field strength and the induction.

It follows from (9') that

$$D_i(t) = \frac{1}{4\pi} \cdot \frac{1 + i\omega\tau}{a + i a_1 \omega\tau} E_i(t).$$

If, therefore, the dielectric constant $\varepsilon(\omega)$ is complex, we obtain

$$\varepsilon(\omega) = \frac{1}{4\pi} \cdot \frac{a + a_1(\omega\tau)^2}{a^2 + a_1^2(\omega\tau)^2} - \frac{i}{4\pi} \cdot \frac{\frac{a_2^2}{a_3}\,\omega\tau}{a^2 + a_1^2(\omega\tau)^2}. \tag{10}$$

Let us deal separately with the real and imaginary parts.

We denote the former by ε:

$$\varepsilon = \frac{1}{4\pi} \cdot \frac{a + a_1(\omega\tau)^2}{a^2 + a_1^2(\omega\tau)^2} \tag{11}$$

and go to the limits

$$1) \quad \omega = 0 \qquad \varepsilon(0) = 1/4\pi a, \tag{12}$$

$$2) \quad \omega = \infty \quad \varepsilon(\infty) = 1/4\pi a_1. \tag{12'}$$

Then $\varepsilon(0)$ represents the "relaxed" dielectric constant, which characterizes the equilibrium state.

The quantity $\varepsilon(\infty)$, on the other hand, is the "unrelaxed" dielectric constant. Using (12) and (12'), we can write (11) in the form

$$\varepsilon = \varepsilon_0 \frac{1+\frac{\varepsilon(0)}{\varepsilon(\infty)}(\omega\tau)^2}{1+\left[\frac{\varepsilon(0)}{\varepsilon(\infty)}\omega\tau\right]^2}. \tag{13}$$

This equation can be rewritten

$$\varepsilon = \varepsilon(\infty) + \frac{\varepsilon(0)-\varepsilon(\infty)}{1+(\varepsilon(0)/\varepsilon(\infty))^2(\omega\tau)^2}. \tag{14}$$

The dielectric loss is given by the angular phase difference δ between E_i and D_i, for which

$$\tan\delta = \frac{\operatorname{Im}\varepsilon(\omega)}{\operatorname{Re}\varepsilon(\omega)}$$

or

$$\tan\delta = \frac{\Delta_\varepsilon\omega\tau}{1+\frac{\varepsilon(0)}{\varepsilon(\infty)}(\omega\tau)^2},$$

where the quantity

$$\Delta_\varepsilon = \frac{\varepsilon(\infty)-\varepsilon(0)}{\varepsilon(\infty)}$$

may be called, by analogy with elastic relaxation, the "defect in the dielectric constant". We note that $\Delta_\varepsilon < 0$.

The dielectric loss attains a maximum at the frequency given by

$$\omega_0 = \frac{1}{\tau}\sqrt{\frac{\varepsilon(\infty)}{\varepsilon(0)}}. \tag{15}$$

For the maximum absorption we obtain

$$(\tan\delta)_{\max} = \frac{\Delta_\varepsilon}{2}\sqrt{\frac{\varepsilon(\infty)}{\varepsilon(0)}} = \frac{\varepsilon(\infty)-\varepsilon(0)}{2\sqrt{\varepsilon(0)\varepsilon(\infty)}}. \tag{16}$$

The theory here developed is easily extended to the case of an anisotropic medium, as well as to the case in which there occur several relaxation processes in the dielectric during polarization.

Institute of Metallography and Metal Physics Institute
TsNIIChermet
"I.V.Stalin" Moscow Steel Institute

Reference

1. M.A.Leontovich, Vvedenie v termodinamiku (Introduction to thermodynamics) M.1950.

POLARIZATION AND DIELECTRIC LOSS IN SOLID SOLUTIONS OF THE FIRST AND SECOND KINDS (Abstract*)

- G.A.Smolenskii, V.A.Isupov, A.I.Agranovskaia & E.D.Sholokhova

1. The report gives the results of an investigation of the polarization and dielectric loss in polycrystalline samples of solid solutions of the first and second kinds.

2. The report gives the results obtained in a study of the $(Sr,Ca)(Ti,Zr)O_3$ system of solid solutions.

3. The $BaTiO_3$-$LaAlO_3$ system was also investigated.

4. A study was made of the solid solutions of the first kind based on strontium pyrotantalate: $(Sr,Ca)_2Ta_2O_7$, $(Sr,Ba)_2Ta_2O_7$ and $Sr_2(Ta,Nb)_2O_7$.

5. The report also gives the results of a preliminary investigation of the solid solutions of two systems of the second kind: $BaTiO_3$-$BaTa_2O_6$ and $BaTiO_3$-$BaNb_2O_6$.

Institute of the Chemistry of Silicates,
Academy of Sciences of the USSR

---

*For complete report see Zhur.tekh.fiz., 27, 2528 (1957); Doklady AN SSSR, 113, 803, 1053 (1957).

* * * * * *

DISCUSSION FOLLOWING THE PRECEDING FOUR REPORTS

N.S.Novosil'tsev: In connection with the report presented by Skanavi and his co-workers on the development of new nonferroelectric substances with a high dielectric constant, I should like to mention that in the treatment of structurally sensitive dielectric properties the concept of a real crystal with defects of various types is being found increasingly useful. In 1950-1951 we obtained[1] barium titanate crystals with a single wide maximum of the dielectric constant. In investigating these crystals it was established that by proper heat treatment[2] their lattices can gradually be made to approach the equilibrium state. In the process the normal ferroelectric properties also gradually become manifest.

In 1952-1953 investigators in our laboratory and other authors (Smolenskii & Verbitskaia) found, in studying single crystals and solid solution ceramics, that when "extraneous" ions are incorporated into the barium titanate lattice the temperature dependence of the dielectric constant is altered. The maximum at the Curie point is broadened and the phase transition points move closer together and finally merge. Both Smolenskii and we explained this phenomenon as being caused by the narrowing of the temperature range in which the tetragonal phase obtains (Zhur.tekh.fiz., 26, 312 (1956)). This view, however, hardly corresponds to reality. As long ago as 1954 I pointed out (in a report to a seminar at the Crystallography Institute of the Academy of Sciences, USSR) that in certain solutions such as $BaSnO_3$-$BaTiO_3$ and $BaZrO_3$-$BaTiO_3$, when the stannate or zirconate content is sufficiently high, the temperature dependence of the dielectric constant is very similar to that in barium titanate crystals in which the lattice order was disturbed during crystal growth. Disorder and deviations from an ideal lattice, whether due to dislocated ions or to the introduction of extraneous ions into the solution lattice, should affect structurally sensitive properties such as ferroelectricity in the same way. All the transition points should merge and there should be one broad maximum.

What is the nature of this "transition merging"? Analysis of some x-ray diffraction studies performed in our laboratory by Fesenko, Slabchenko, Mozgovaia and others, gives reason to suppose that in this case there actually occurs no phase transition on passing through the maximum, i.e., the cubic lattice is retained. Clearly, disordering should lead to some amorphization, an increase in the degree of symmetry and disappearance of spontaneous polarizability, i.e., should result in a cubic nonferroelectric modification.

The maxima observed in the dielectric constant curve should in this case be regarded as relaxation maxima.

I would also like to touch on the question of whether the Curie transition in barium titanate is a transition of the first or second order. It is easy to see from what I have said that this question has meaning only for a single-domain crystal. In any real crystal the transition does not take place instantaneously; in fact, in different crystals it occurs in different temperature intervals. This is what leads to thermal hysteresis. This is verified by studies of domain transitions in multiple domain crystals.

K.B.Tolpygo (on the report by Ia.M.Ksendzov): There have been objections raised here to the model proposed by Ksendzov for the purpose of explaining the increase in the dielectric constant of TiO_2 resulting from the addition of a small amount of Nb_3O_5.

The question of the behavior of ions of a different valence when introduced as an impurity into a crystal has often arisen in semiconductor physics and has been discussed in detail. In germanium, for instance, Sb impurity enters the lattice, with Sb atoms replacing Ge atoms; four of the five Sb valence electrons form covalent bonds with the four nearest Ge atoms. The fifth electron moves off to a considerable distance from the Sb nucleus, and is in a state similar to that of the electron in a hydrogen atom. Such a state has the lowest energy and the radius of the orbit is several times greater than the lattice constant, so that the medium between the electron and the Sb nucleus may be treated as a continuum.

An entirely analogous situation arises in the case of ionic semiconductors when an impurity ion of different valence has dimensions similar to that of the lattice ions (for instance, the Ca^{2+} ion in the NaCl lattice). In the case of ionic crystals, however, the field acting on the outer electron of the impurity ion will no longer be equal to $-e^2/\epsilon r$, for the electron causes an inertial polarization of the medium, so that it is influenced by the field of dielectric which it itself has polarized. The result is the formation of not a hydrogen-like atom, but a so-called F-center. The theory of the F-centers has been discussed in detail by Pekar. His theory leads to quantitative results which differ from those presented by Ksendzov.

Thus for the reciprocal of the radius of the state one obtains

$$\frac{1}{r} = \frac{m^* e^2}{3{,}2\hbar^2}\left(\frac{1}{n^2} + \frac{2}{\varepsilon}\right).$$

While, for the F-center dissociation energy we have

$$E = \frac{3}{56} \cdot \frac{m^* e^4}{\hbar^2}\left(\frac{1}{n^2} + \frac{2}{\varepsilon}\right)^2;$$

here n is the index of refraction, and m^* is the effective electron mass. The polarizability of the F-center has been calculated by Perlin. It can also be expressed in terms of ε, n^2 and m^*.

I agree with Ksendzov's qualitative inferences, but would like to note that they can be subjected to a more thorough quantitative verification in accordance with Pekar's formulas. There are two unknown quantities: m^* and the F-center concentration N_F. The experimental data, however, include the value of the conductivity σ, the slope of the curve of $\ln \sigma$ as a function of $1/T$, and the variation of ϵ and $\tan \delta$. Such a quantitative verification is highly desirable. From the point of view of the general theoretical considerations, however, the model presented in the paper cannot be criticized.

G.I.Skanavi (on the report of Fastov and Finkel'shtein): The equations obtained for ϵ' and ϵ'' by the use of nonequilibrium thermodynamics are the same as the familiar Debye formulas and analogous ones.

It is important that these formulas, derived by the authors without the use of special models, contain the polarization time constant, which differs from the relaxation time by the factor $\epsilon_0/\epsilon_\infty$. In model theories, however, the ratio between these two times depends on the form of the internal field, and can be written

$$\frac{\varepsilon_0 - 1 + 4\pi / \beta_1}{\varepsilon_\infty - 1 + 4\pi / \beta_1},$$

where β_1 is the proportionality constant between the relaxational polarization and the field which it produces.

The reason for the indicated discrepancy should be investigated.

References

1. I.N.Beliaev, N.S.Novosil'tsev, A.L.Khodakov & E.G.Fesenko, Doklady AN SSSR, 78, No.5 (1951).

2. N.S.Novosil'tsev & A.L.Khodakov, Doklady AN SSSR, 85, No.6 (1952).

THEORY OF SYSTEMS COMPRISING NONCENTRALLY INTERACTING PARTICLES

- A.E.Glauberman

A rigorous statistical theory of systems of interacting particles is being developed successfully using the methods due to N.N.Bogoliubov.[1] Bogoliubov's theory has facilitated a consistent description of equilibrium properties of systems with short-range central forces and systems of charged particles and the treatment of many kinetic problems.

The present paper is an attempt, based on Bogoliubov's principles, to construct a general theory of systems of interacting particles for which not only central interaction but also orientation-dependent interaction is important.

1. General Theory of Systems with Noncentral Interaction in the Absence of Crystal Ordering.

Consider a gas or liquid whose particles interact according to a potential which depends on the distance between the centers of gravity of the two particles under consideration, on the orientation of their line of centers and on the orientations of their "axes". For simplicity we shall consider all the particles to be of one and the same kind.

We introduce the particle "complex" or cluster distribution function

$$F_s(\mathbf{q}_1, \ldots, \mathbf{q}_s, \vartheta_1, \ldots, \vartheta_s, \varphi_1, \ldots, \varphi_s) = (4\pi V)^s \int D_N(\mathbf{q}_1, \ldots, \varphi_N)\, d\mathbf{q}_{s+1} \ldots d\Omega_N, \tag{1}$$

where D_N is the Gibbs configuration function for the system, q_i is the radius vector of the center of gravity of the i-th molecule and ϑ_i and φ_i are the angles defining the orientation of the molecular axis. Further, $d\mathbf{q}_i$ is the element of volume about the center of the i-th molecule, and $d\Omega_i$ is the element of solid angle.

On going formally to the limit

$$V \to \infty, \quad N \to \infty, \quad V/N = \mathrm{const},$$

where V is the volume of the system and N is the total number of particles, we find that the F_s are given by the set of integro-differential equations

$$\begin{gathered}\frac{\partial F_s}{\partial q_1^\alpha} + \frac{1}{\theta} \cdot \frac{\partial U_s}{\partial q_1^\alpha} F_s + \frac{1}{4\pi v\theta} \int \frac{\partial}{\partial q_1^\alpha} L(1, s+1) F_{s+1} d\mathbf{q}_{s+1} d\Omega_{s+1} = 0, \\ (\alpha = 1, 2, 3), \\ \frac{\partial F_s}{\partial \vartheta_1^\alpha} + \frac{1}{\theta} \cdot \frac{\partial U_s}{\partial \vartheta_1^\alpha} F_s + \frac{1}{4\pi v\theta} \int \frac{\partial}{\partial q_1^\alpha} L(1, s+1) \cdot F_{s+1} d\mathbf{q}_{s+1} d\Omega_{s+1} = 0, \\ (\alpha = 1, 2),\end{gathered} \tag{2}$$

where

$$q_1^\alpha (\alpha = 1, 2, 3) = (x, y, z) \quad \vartheta_1^\alpha (\alpha = 1, 2) = (\vartheta_1, \varphi_1), \quad \theta = kT$$

and

$$U_s = \sum_{1 \leqslant i < j \leqslant s} L_{ij} + \sum_{1 \leqslant i \leqslant s} \varphi_i,$$

the L_{ij} are the interaction potentials and are given by

$$L_{ij} = L_{ij}(|\mathbf{q}_i - \mathbf{q}_j|, \vartheta_i, \varphi_i, \vartheta_j, \varphi_j, \vartheta_{ij}, \varphi_{ij}), \tag{3}$$

and $\varphi(\vartheta_i, \varphi_i) = \varphi_i$ is the potential energy of the i-th particle in the external field.

Eqs.(2) are to be treated together with the normalization condition

$$\lim_{V\to\infty} \frac{1}{4\pi V} \int F_1(\mathbf{q}, \vartheta, \varphi)\, d\mathbf{q}\, d\Omega = 1 \tag{4}$$

and the boundary conditions

$$F_s(\mathbf{q}_1, \ldots, \mathbf{q}_s, \vartheta_1, \ldots, \vartheta_s, \varphi_1, \ldots, \varphi_s) \to \prod_{1\leqslant i\leqslant s} F_1(\mathbf{q}_i, \vartheta_i, \varphi_i), \tag{5}$$

which state that the correlation vanishes in the limit as all the $|\mathbf{q}_i - \mathbf{q}_j| \to \infty$.

We shall consider a system having a density such that the desired F_s functions may reasonably be expanded in powers of the density (more accurately, in powers of the dimensionless parameter r_0^3/v, where r_0 is the "effective radius" of the molecule, associated with the short-range part of L_{ij}). We thus write

$$F_s = F_s^0 + \frac{1}{v} F_s^1 + \frac{1}{v^2} F_s^2 + \cdots \tag{6}$$

When we solve the equations giving the various approximations for F_s, we obtain

$$F_s^0 = C_s^0 \exp(-U_s/\theta),$$

where

$$C_s^0 = (C_1^0)^s, \qquad C_1^0 = \left(\frac{1}{4\pi}\int e^{-\frac{\varphi}{\theta}}\, d\Omega\right)^{-1}. \tag{7}$$

Further, writing F_s^1 in the form

$$F_s^1 = C_s^1 \exp(-U_s/\theta),$$

we find that

$$C_s^1 = \frac{1}{4\pi}\int (C_1^0)^s \prod_{1\leqslant i\leqslant s} (1 + f_{i,\, s+1})\, F_1^0(s+1)\, d\mathbf{q}_{sn}\, d\Omega_{s+1} + K_s', \tag{8}$$

$$K_s^1 = -\frac{(C_1^0)^s}{4\pi} \int\left\{1 + \frac{1}{4\pi} \sum \int f_{i,\, s+1} F_1^0(i)\, d\Omega_i\right\} F_1^0(s+1)\, d\mathbf{q}_{s+1}\, d\Omega_{s+1}, \tag{9}$$

where $f_{ij} = \exp(-L_{ij}/\theta) - 1$ and where we have abbreviated $F_1^0(\mathbf{q}_1, \vartheta_1, \varphi_1)$, etc. by $F_1^0(1)$, etc. It is not particularly difficult to obtain higher approximations, but the calculations become quite cumbersome.

In the special case of a dipole gas in uniform external electric field, we write $\varphi = PE\cos\vartheta$ (where P is the dipole moment of the molecule, and E is the field strength); L_{ij} is then the interaction potential of two molecules with dipole moments. For such a potential we may choose the expression (obtained by Stockmayer):

$$L_{ij} = \chi_{ij} + \frac{\mathbf{P}_i \cdot \mathbf{P}_j}{r_{ij}^3} - \frac{3(\mathbf{P}_i \cdot \mathbf{r}_{ij})(\mathbf{P}_j \cdot \mathbf{r}_{ij})}{r_{ij}^5}, \tag{10}$$

where χ_{ij} is the short-range central potential, or the simpler expression (proposed by Keesom)

$$\left.\begin{aligned} L_{ij} &= \frac{\mathbf{P}_i \cdot \mathbf{P}_j}{r_{ij}^3} - \frac{3(\mathbf{P}_i \cdot \mathbf{r}_{ij})(\mathbf{P}_j \cdot \mathbf{r}_{ij})}{r_{ij}^5}, \qquad && r > d, \\ L_{ij} &= \infty. \qquad\qquad\qquad\qquad\qquad\qquad , && r < d. \end{aligned}\right\} \tag{11}$$

In the latter case the mean potential energy is

$$\bar{U}_N = -\theta N\beta L(\beta) + \frac{Np^2}{3(4\pi^2)}\left(\frac{\beta}{\operatorname{sh}\beta}\right)^2 \sum_{n=1}^{\infty} \frac{(-1)^{n+1}}{n(n+1)!}\left(\frac{P^2}{d^3\theta}\right)^n \times$$
$$\times\left[\beta L(\beta)\lambda(n+1,\beta) - \frac{n+1}{2}\lambda(n+1,\beta) - \frac{1}{2}\frac{d}{d\beta}\lambda(n+1,\beta)\right] + \cdots, \tag{12}$$

if the first approximations to the unary and binary distribution functions are used, i.e., if we include terms containing r_0^3/v up to the first power. In (12) $L(\beta)$ is Langevin's function, $\beta = PE/\theta$ and

$$\lambda(n,\beta) = \int (\psi_{13})^n \exp\beta(\cos\vartheta_1 + \cos\vartheta_3)\, d\Omega_1\, d\Omega_3\, d\Omega_{13},$$

where the ψ_{ij} are related to the L_{ij} by

$$L_{ij} = \chi_{ij} + \Phi_{ij}(r)\cdot\psi_{ij}(\vartheta_i, \vartheta_j, \varphi_i, \varphi_j, \vartheta_{ij}, \varphi_{ij}).$$

This can be used as a basis for a consistent and rigorous theory of a dipole gas. Without going into the quantitative aspects, we remark that our proposed general theory readily encompasses systems consisting of axially symmetric molecules with constant quadrupole moments or axially symmetric molecules with zero moment and having a weak orientation-dependent interaction (ellipsoidal molecules, etc.).

In the latter case the interaction potential can be written

$$L_{ij} = \Phi_{ij}(|\mathbf{q}_i - \mathbf{q}_j|)\,[1 + \lambda\psi_{ij}(\vartheta_i, \vartheta_j, \varphi_i, \varphi_j, \vartheta_{ij}, \varphi_{ij})], \qquad \lambda \ll 1 \tag{13}$$

and the equilibrium properties of the system can be found. The second virial coefficient, for instance, is found to be

$$B = B_c\left\{1 - \lambda\bar{\psi}\frac{d}{d\theta}\ln\beta_1 + \lambda^2\bar{\psi}^2\theta\frac{d}{d\theta}\ln\beta_1 + \frac{\lambda^2\bar{\psi}^2\theta^2}{2}\frac{d}{d\theta}\ln\beta_1\frac{d}{d\theta}\left(\ln\frac{d\beta_1}{d\theta}\right)\right\}, \tag{14}$$

where B_c is the second virial coefficient for pure central forces in which only the Φ_{ij} appear, β_1 is the first irreducible integral for the case of pure central interaction, and $\bar{\psi} = (1/4\pi)^3\int \psi_{ik}\, d\Omega_i\, d\Omega_k\, d\Omega_{ik}$.

Comparison with experiment for gaseous CO_2 and C_2H_6 with $\bar{\psi} = 0$ shows that with the appropriate choice of $\lambda^2\bar{\psi}^2 = \text{const}$, one can fit the experimental results with satisfactory accuracy. The calculations should also be performed with a potential in which the angular dependence - unlike the situation in (13) - is contained only in the short-range attraction term.

Theory of Dipole Crystals

The second system that we propose to treat by Bogoliubov's method is a dipole crystal consisting of molecules with dipole moments $\mathbf{P}_i\ (i = 1, \ldots, N)$. We shall assume the centers of gravity of the dipoles fixed at the lattice sites and shall treat the crystal as a system of different kinds of particles. The particles will be classified by the vectors specifying the sites at which they are located. We shall choose the two-particle interaction potential in the usual form for the interaction of two dipoles.

Inasmuch as

$$|\mathbf{r}_{a_i} - \mathbf{r}_{a_k}| = |\mathbf{r}_{a_i a_k}| = d e_{a_i a_k}^{1/2} \tag{15}$$

(where the a_i specify the kind of particle, d is the lattice constant, and the $e_{a_i a_k}$ are numbers), the different characteristics of the different kinds of particles will enter the interaction potential in terms of the $e_{a_i a_k}$ and the angles $\vartheta_{a_i a_k}$ and $\varphi_{a_i a_k}$ which determine the orientation of the line of centers.

We introduce the distribution functions $F_{a_1, \ldots, a_s}(\theta_1, \ldots, \theta_s)$ and $\theta_1 = (\vartheta_1, \varphi_1)$ normalized so that

$$\left(\frac{1}{4\pi}\right)^s F_{a_1, \ldots, a_s}(\theta_1, \ldots, \theta_s)\, d\Omega_1 \ldots d\Omega_s$$

gives the probability that in a fixed group of s dipoles of kinds specified by $a_1, \ldots, a_s$ the dipole moments lie within the solid angles $d\Omega_1, \ldots, d\Omega_s$.

Consider the functional

$$L_N = \int D_N \prod_{1 \leqslant a_i \leqslant N} (1 + 4\pi U_{a_i}(\theta_i))\, d\Omega_1 \ldots d\Omega_N, \tag{16}$$

defined on an arbitrary class of regular functions $U_{a_1}(\theta_1), \ldots, U_{a_N}(\theta_N)$ on the unit sphere. This functional is analogous to that introduced by Bogoliubov for a system of centrally interacting particles and can be used to construct equations involving variational derivatives, from which it is a simple matter to proceed to the equations for the distribution functions.

Introducing the notation

$$\frac{1}{kT}\Phi_{a_i a_k} = \frac{P^2}{d^3 kT}\psi_{a_i a_k}(\theta_i, \theta_k, \theta_{ik}) = \gamma\psi_{a_i a_k},$$

where the $\Phi_{a_i a_k}$ represent the interaction potential for two dipoles, we can write

$$\frac{\partial F_{a_1, \ldots, a_s}}{\partial \theta_1^\alpha} + \gamma \cdot \frac{\partial U^*_{a_1, \ldots, a_s}}{\partial \theta_1^\alpha} F_{a_1, \ldots, a_s} + \frac{\gamma}{4\pi} \int \sum_{\substack{a_{s+1} \\ a_{s+1} \neq a_1, \ldots, a_s}}^{N} \frac{\partial \psi_{a_1 a_{s+1}}}{\partial \theta_1^\alpha} F_{a_1, \ldots, a_{s+1}} d\Omega_{s+1} = 0, \tag{17}$$

where

$$U^*_{a_1, \ldots, a_s} = \sum_{a_1 \leqslant a_i < a_k \leqslant a_s} \psi_{a_i a_k}.$$

Let us assume that $\gamma \ll 1$ and perform the expansion

$$F_{a_1, \ldots, a_s} = F^0_{a_1, \ldots, a_s} + \gamma F^1_{a_1, \ldots, a_s} + \cdots \tag{18}$$

after which we find the functions $F^0_{a_1, \ldots, a_s}$, $F^1_{a_1, \ldots, a_s}$, etc.

In the presence of an external field E, we must add the term

$$-\frac{1}{kT} F_{a_1, \ldots, a_s} \frac{\partial}{\partial \theta_1^\alpha}\Big(\sum_{a_1 \leqslant a_i \leqslant a_s} (\mathbf{P}_{a_i} \cdot \mathbf{E})\Big).$$

to the left side of (17).

The set of equations obtained after the expansion is solved under the normalization conditions

$$\left.\begin{aligned} \left(\frac{1}{4\pi}\right)^s \int F^0_{a_1, \ldots, a_s} d\Omega_1 \ldots d\Omega_s = 1, & \\ \left(\frac{1}{4\pi}\right)^s \int F^k_{a_1, \ldots, a_s} d\Omega_1 \ldots d\Omega_s = 0, & \qquad k > 0. \end{aligned}\right\} \tag{19}$$

The zeroth and first approximations for the distribution function of a cluster of s particles in a uniform external electric field are then

$$F^0_{a_1,\ldots,a_s} = \left(\frac{\beta}{\operatorname{sh}\beta}\right)^s \exp\Big\{\sum_{a_1\leqslant a_i\leqslant a_s} (\mathbf{P}_{a_i}\cdot\mathbf{E})/kT\Big\}, \qquad \beta = PE/kT,$$

$$\begin{gathered} F^1_{a_1,\ldots,a_s} = F^0_{a_1,\ldots,a_s}\Big[\left(\frac{1}{4\pi}\right)^s \int F^0_{a_1,\ldots,a_s}\cdot U^*_{a_1,\ldots,a_s} d\Omega_1,\ldots,d\Omega_s + \\ + \left(\frac{1}{4\pi}\right)^{s+1} \sum_{\substack{1\leqslant a_{s+1}\leqslant N \\ a_{s+1}\neq a_1,\ldots,a_i}} \sum_{a_i}^{a_s} \int \psi_{a_i a_{s+1}} F^0_{a_1,\ldots,a_{s+1}} d\Omega_1,\ldots,d\Omega_{s+1} - \\ - \frac{1}{4\pi} \sum_{a_{s+1}} \sum_{a_i} \int \psi_{a_i a_{s+1}} F^0_{a_{s+1}} d\Omega_{s+1} - U^*_{a_1,\ldots,a_s}\Big]. \end{gathered} \tag{20}$$

The higher approximations can be calculated similarly.

Using the expressions for $F^0_{a_1,\ldots,a_s}$ and $F^1_{a_1,\ldots,a_s}$, we can calculate the mean potential energy in the form[2]

$$\begin{gathered} \frac{\overline{U}_N}{N} = -kT\,\beta L(\beta)\,[1+\gamma(L^2+2L/\beta-1)\,\sigma_1] + \gamma\frac{kT}{2}L^2\sigma_1 + \\ + \gamma^2\left\{\frac{kT}{2}[L^4-(1-2L/\beta)^2]\,\sigma_2 - \frac{L^3}{\beta}\sigma_3 + L^2(L^2+2L/\beta-1)\,\sigma_4 - \right. \\ \left. - (L^2/\beta^2)\,\sigma_5 - (L/\beta)(1-2L/\beta)\,\sigma_6\right\}, \end{gathered} \tag{21}$$

where the σ_1 are the structure factors of the crystal lattice. To show their general form, we note that the first is

$$\sigma_1 = \sum_{a_i}^{N} \gamma_{a_i}/N, \tag{22}$$

where

$$\gamma_{a_i} = \sum_{\substack{a_j \\ a_j\neq a_i}}^{N} \gamma_{a_i a_j}, \quad \text{and} \quad \gamma_{a_i a_j} = \frac{1-3\cos^2\vartheta_{a_i a_j}}{e^{3/2}_{a_i a_j}}.$$

In order to avoid cumbersome expressions, we shall give the free energy up to terms containing the parameter γ to the first power. This is

$$F = -\theta N \ln\frac{\operatorname{sh}\beta}{\beta} - \frac{P^2}{d^3}\sigma_1\left\{-\frac{1}{2} - \frac{\Gamma(\beta)}{\beta} - \frac{L(\beta)}{\beta} - \frac{L(\beta)}{\beta}\left(\frac{1}{2}+\beta L(\beta)\right)\right\}. \tag{23}$$

To the same approximation the polarization P is

$$P = -\frac{1}{V}\cdot\frac{\partial F}{\partial E} = nPL(\beta) + \frac{np^3}{d^3kT}\sigma_1\left\{\lambda(\beta) - \frac{1}{2\beta}\cdot\frac{dL}{d\beta} - 2L\frac{dL}{d\beta}\right\}, \tag{24}$$

where the transcendental function $\lambda(\beta) = \frac{d}{d\beta}\left(\frac{\Gamma(\beta)}{\beta}\right)$ may be written

$$\lambda(\beta) = \sum_{k=1}^{\infty} \frac{2^{2k+3}}{(2k+1)!} B_{k+1}\left\{\frac{k}{2k+1} + \frac{1}{6}\frac{B_k}{B_{k+}} + \sum_{m=1}^{\infty}\frac{2^{2m}B_m}{(2m)!}\cdot\frac{k+m}{2(k+m)+1}\beta^{2m}\right\}\beta^{2k-1},$$

in which the B_k are the Bernoulli numbers.

Evaluation of the structure factors σ_i for different crystal structures allows of carrying out specific numerical computations. When $\beta < 0.3$, we may approximate $L(\beta)$ by a linear function, and then in our approximation the polarization is given by the simple formula

$$P = \frac{np^2}{3kT}\left(1 - \frac{\gamma\sigma_1}{3}\right)E, \tag{25}$$

where E is the external field. Setting $E = (\varepsilon + 2/3)E_{av}$, where E_{av} is the average macroscopic field in the dielectric, we find that the dielectric constant, due only to the orientational effect, is given by

$$\frac{\varepsilon - 1}{\varepsilon + 2} = \frac{4\pi}{3} \cdot \frac{np^2}{3kT}\left(1 - \frac{\gamma\sigma_1}{3}\right) + \cdots \tag{26}$$

We note that the use of the above first approximation makes sense only if the crystal structure is such that σ_1 is nonzero. Thus for cubic crystals, for instance, the calculation must be extended to the second approximation.

The general theory presented above is obtained by Bogoliubov's rigorous methods, which makes it preferable to that of Kirkwood[3] and the later results obtained by Pople.[4]

Our method can in principle be used to take into account any type of interaction.

The theory may be generalized to dipole liquids. To do this the σ_i should be taken as appropriately averaged structure factors. Without going any further into this concept, we note in conclusion that the rigorous solution obtained can be used only if the temperature is sufficiently far from the temperature of orientational melting, as specified by $\gamma = p^2/d^3kT$ being sufficiently small. Thus problems involving orientational melting cannot be solved in this way.

As is shown by calculations, the superposition approximation involves much smaller errors in our dipole crystal model than it does in the liquid state problem. This situation may be utilized in constructing an approximate theory for temperatures at which the small parameter does not exist.

"Ivan Franko" L'vov State University

References

1. N.N.Bogoliubov, Problemy dinamicheskoi teorii v statisticheskoi fizike (Problems of dynamic theory in statistical physics), M. 1946.
2. A.E.Glauberman, Doklady AN SSSR, 108, 49 (1956).
3. J.G.Kirkwood, Jour.Che.,Phys., 7, 911 (1939); 8, 205 (1940).
4. J.A.Pople, Phil.Mag., 44, 1276 (1953).

IONIC DISPLACEMENT POLARIZATION IN COMPLEX IONIC CRYSTALS*

- A.E.Glauberman and I.M.Spitkovskii

In treating the properties of ionic crystals, in particular, of barium titanate crystals, from the standpoint of molecular theory, one must have expressions and numerical estimates for the ionic displacement polarizability of the different kinds of ions in the crystal.[1,2]

The calculations are simple for symmetric binary systems such as NaCl, but for more complicated crystals they become very difficult. In this short note we present a simple and general method for calculating the ionic displacement polarizability for crystals of any structure and with any number of different kinds of ions.

We shall consider an ionic crystal composed of several kinds of ions in a constant external electric field. Each kind of ion is displaced from its equilibrium (zero field) position in the lattice. We shall treat the displaced ion and the "hole" left by it as a "dipole" and consider that the aggregate of these dipoles determines the ionic displacement polarization.

Let us consider an elementary cell consisting of l ions, and let U_k be the energy of the k-th ion when the ions are displaced. The U_k are functions of the ionic displacements. We shall choose our coordinate system so that the x-axis lies along the principal crystallographic axis and assume that the external field is directed along the same axis. Further we assume that the displacements are parallel or antiparallel to the field.

The U_k are composed of two parts: the part which gives the Coulomb interaction between the given kind of ion and the surroundings, and the part which gives the energy of short-range forces. The first part can be calculated according to Ewald,[3] while in calculating the second part account is taken of the neighbor ions within the unit cell.

We assume the displacements to be small, so that we can expand the U_k in powers of these displacements and retaining only terms through the second order. We then have

$$U_k = (U_k)_0 + \sum_{i=1}^{n} \left(\frac{\partial U_k}{\partial \xi_i}\right)_0 \xi_i + \frac{1}{2} \sum_{i,\, j}^{n} \left(\frac{\partial^2 U_k}{\partial \xi_i \partial \xi_j}\right)_0 \xi_i \xi_j,$$

where n is the number of ions in a cell and the index zero denotes the value of the quantity evaluated at the non-displaced equilibrium position. Since at the equilibrium position $(\partial U_k / \partial \xi_i)_0 = 0$, we may write

$$U_k = (U_k)_0 + \frac{1}{2} \sum_{i,\, j}^{n} \left(\frac{\partial^2 U_k}{\partial \xi_i \partial \xi_j}\right)_0 \xi_i \xi_j. \tag{1}$$

Under the external field $\mathcal{E}$ the charges e_k are displaced a distance ξ_k. The total potential energy of the system of charges (per unit cell) is

$$\sum_{l=1}^{n} \left[\frac{1}{2} U_l - e_l \mathcal{E} (r_{lx}^0 + \xi_l)\right].$$

The equilibrium conditions in the external field are

---

*In presenting their work at the Conference the authors mistakenly used the effective, rather than the external, field values on the left side of the equations for the equilibrium values of the ionic displacements. This error was pointed out by K.B.Tolpygo, and in preparing the paper for print the authors have taken this into account.

$$\frac{\partial}{\partial \xi_k} \sum_{l=1}^{n} \left[\frac{1}{2} U_l - e_l \mathscr{E} (r^0_{lx} + \xi_l) \right] = 0, \tag{2}$$

and these, using the notation $(\partial^2 U_l / \partial\xi_i \partial\xi_j)_0 = U^l_{ij}$, lead to the following set of equations:

$$e_k \mathscr{E} = \frac{1}{2} \sum_{l=1}^{n} \frac{\partial}{\partial \xi_k} \frac{1}{2} \sum_{i,\, j}^{n} U^l_{ij} \xi_i \xi_j. \tag{3}$$

Solving these for the $\xi_k = \Phi_k (\mathscr{E}, e_1, \ldots, e_n, U^1_{11}, \ldots, U^n_{nn})$, we find the polarizabilities to be given by

$$\alpha_k = \frac{e_k \mathscr{E}}{E_k D} \sum_{l=1}^{n} e_l A^k_l, \tag{4}$$

where D is the determinant of (3), the A^k_l are the minors of the determinant D_k (which is defined by $\xi_k = D_k / D$), $\mathscr{E}$ is the external field, and E_k is the effective field acting on the k-th ion.

The equations obtained for the α_k can be used to solve the equations for the effective fields (first obtained by G. I. Skanavi[1]) as well as the equations figuring in the theory for barium titanate, developed by Glauberman & Lubchenko.[2]

Let us now consider a somewhat different computational procedure. We write the equilibrium condition for the lattice in an external field using only the effective fields acting on the different kinds of ions. We then have

$$e_i E_i = \sum_l \left(\frac{\partial U^{*l}}{\partial \xi_i} \right)_0 + \frac{1}{2} \cdot \frac{\partial}{\partial \xi_i} \sum_l \sum_{i,\, j} U^{*l}_{ij} \xi_i \xi_j, \tag{5}$$

where U^{*l} differs from U^l in that it does not contain the energy of the Coulomb interaction between the -th ion and its surroundings.

We then find that the polarizabilities are given by

$$\alpha_k = \frac{e_k}{E_k D^*} \sum_{l=1}^{n} e_l E_l A^{*k}_l + \frac{e_k B^*_k}{E_k D^*}, \tag{6}$$

where D^* is the determinant of (5), and the determinants with the replaced column are separated into the parts containing the effective fields and those not containing them.

In the equations of Skanavi[1] and those of Glauberman and Lubchenko[2] for the effective fields the $\bar{\alpha}_k$ enter multiplied by the corresponding effective fields, so that the second term on the right in (6) enters the equations in a form convenient for numerical evaluation.

The first term

$$\alpha'_k = \frac{e_k}{E_k D^*} \sum_{l=1}^{n} e_l E_l A^{*k}_l \tag{7}$$

can be evaluated numerically only by replacing all the effective fields in it by some mean effective field.

Eqs. (4) and (6) may be useful in developing a quantitative theory of the dielectric properties of ionic crystals.

"Ivan Franko" L'vov State University

References

1. G. I. Skanavi, Zhur. eksp. i teor. fiz., 17, 399 (1947).
2. A. E. Glauberman & A. F. Lubchenko, Zhur. eksp. i teor. fiz., 23, 188 (1952).
3. P. P. Ewald, Ann. de Phys., 4, 253 (1921).

Discussion following the reports of A.E.Glauberman and A.E.Glauberman & I.M.Spitkovskii

K.B.Tolpygo: I wonder whether the energy of the dipole is properly expressed; shouldn't the external field be replaced by the effective field?

Since the effective field includes part of the molecular interaction, and since this interaction is explicitly included in the theory here developed, it is clear that it should not be included twice and that the author has expressed properly the energy of the particle in the external field.

This method cannot be used, however, to proceed as far as one would like toward including the interaction. In Bogoliubov's method the correlation between the orientations of different molecules is not taken into account in the zeroth approximation. This correlation enters only in the higher approximations. The expression for the dielectric constant is therefore obtained as a power series in $\alpha = np^2/3kT$. One thus requires that $\alpha \ll 1$.

When using the effective field in its simplest Lorentz form, $E_{eff} = E + 4\pi P/3$, on the other hand, we have

$$\varepsilon = 1 + \frac{4\pi\alpha}{1 - \frac{4\pi}{3}\alpha}.$$

This formula, valid even if $4\pi\alpha/3$ is close to unity, cannot be written as a power series in α with just a few terms. This restricts the applicability of Bogoliubov's method; it cannot be used for the most interesting materials, those with large ε.

I think that the most reasonable thing would be to combine Bogoliubov's method with the concept of the effective field. Then the "average" long-range forces between molecules could be treated by means of the effective field, while deviations from the average and the short-range forces could be included in the interaction potential. Then Bogoliubov's expansion should be applied only to this part of the interaction. Such an approach could be used to proceed toward the treatment of substances with large values of ε.

G.I.Skanavi (on the paper by A.E.Glauberman): The use of Bogoliubov's method would be very interesting if it could lead to any new concrete results. It is not clear, however, why the theory here developed is better, when applied to polar liquids, than Kirkwood's theory, since in order to obtain numerical results one seems in the final analysis to have to use some kind of specific model.

THERMAL IONIC POLARIZATION AND SLOW PROCESSES IN SOLID DIELECTRICS

- V.N.Lozovskii

1. All real crystals have structural distortions and defects. They may be of different origin, nature and size, but they all cause the energies of the individual parts of a solid to be unequal. For this reason the potential configuration for conduction ions is somewhat different in different regions of a solid dielectric. The conduction ions (or vacant sites) moving towards the electrodes are delayed for longer times in the vicinity of higher potential barriers than they are in other regions of the dielectric. This results in local concentrations of ions, production of reverse fields, and a decrease in the current. The concept of various factors delaying ions moving in a dielectric has on occasion been used to explain related experimental data.

It is possible to give a mathematical interpretation of this "absorption" mechanism in terms of the theory of thermal ionic polarization.[2] The first step in this direction was taken by Venderovich[3] who considered the model of a dielectric with cylindrical "defects" oriented parallel to the field, with three potential wells per defect along the defect axis. In the present paper we treat a dielectric with "defects" having an arbitrary number of potential wells.

2. Let us assume that the "defective" regions - for instance, regions in which the potential barriers for conduction ions are depressed - are cubes with edges oriented along the field and that they contain m^3 identical potential wells. Let us also assume that a) the weakly bound ions are acted upon by the mean macroscopic field $\overline{\mathrm{E}}$, which is time independent; b) the "defective" regions are surrounded by high potential barriers, holding back ionic diffusion out of these "defects"; c) the number n_i of weakly bound ions in each layer of potential wells is small compared with m^2, the number of wells in the layer; d) the ions move within a "defect" only by jumps through a single potential barrier.

If these conditions are fulfilled, the redistribution of the ions in the "defects" of the dielectric when a field is suddenly applied is given by a set of linear homogeneous differential equations with constant coefficients. This set is

$$\left.\begin{aligned}
\frac{dn_1}{dt} &= -n_1\delta\beta + n_2\frac{\delta}{\beta},\\
\frac{dn_2}{dt} &= n_1\delta\beta - n_2\frac{\delta}{\beta} - n_2\delta\beta + n_3\frac{\delta}{\beta},\\
&\cdots\cdots\cdots\cdots\cdots\cdots\cdots\cdots\\
\frac{\partial n_i}{dt} &= n_{i-1}\delta\beta - n_i\frac{\delta}{\beta} - n_i\delta\beta + n_{i+1}\frac{\delta}{\beta},\\
&\cdots\cdots\cdots\cdots\cdots\cdots\cdots\cdots\\
\frac{dn_{m-1}}{dt} &= n_{m-2}\delta\beta - n_{m-1}\frac{\delta}{\beta} - n_{m-1}\delta\beta + n_m\frac{\delta}{\beta},\\
\frac{dn_m}{dt} &= n_{m-1}\delta\beta - n_m\delta\beta,
\end{aligned}\right\} \tag{1}$$

where t is the time, and n_i is the number of ions in each layer of potential wells perpendicular to $\overline{\mathrm{E}}$.

In Eq.(1) we use the notation

$$\delta = \frac{\nu}{3}\exp\left(-\frac{U}{kT}\right), \quad \beta = \exp\left(\frac{\Delta U}{kT}\right),$$

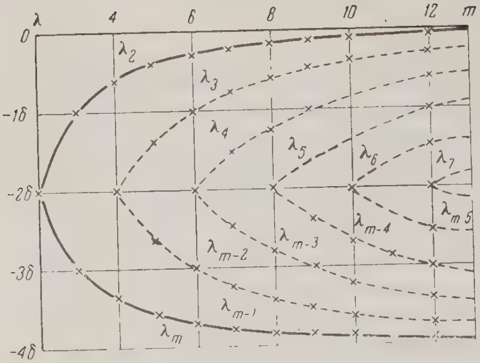

Fig.1. Roots of the characteristic equation of the redistribution of ions in the "defects" of the dielectric.

where ν is the vibration frequency of the weakly bound ions, U is the height of the potential barriers, $\Delta U = aq\mathrm{E}/2$ is the energy the ion acquires in moving a distance $a/2$ in a field E, a is the distance between two potential wells, and q is the ion charge.

It can be shown that a) the roots of the characteristic equation of (1) are all real and different; b) one root, which we call λ_1 vanishes for all m; c) all the other roots are negative; d) as $m \to \infty$, the greatest of the negative roots, λ_2, tends to zero, while λ_m, the smallest, tends to -4δ. This is illustrated in Fig.1, where the solid curve shows how λ_2 and λ_m depend on m and the dotted curves show the m-dependence of all the other roots. The general solutions of our initial set of equations are then

$$n_i = A_{i1} + \sum_{k=2}^{m} A_{ik} \exp(\lambda_k t), \qquad (i = 1, 2, 3, \ldots, m). \tag{2}$$

The charge redistribution process in the "defects" described by Eq.(2) is manifested on the macroscopic scale in the form of an absorption current, a "high-voltage" polarization emf, and relaxation losses.

3. It can be shown that the expression for the high-voltage polarization emf is of the form

$$P = 2\pi aqNd_{mn_0} \frac{[(m-1)\beta^{2(m-1)} - (m+1)\beta^{2m} + (m+1)\beta^2 - (m-1)]}{[1 + \beta^2 + \ldots + \beta^{2(m-1)}](1-\beta^2)^2}, \tag{3}$$

where N is the number of defects per unit volume and d is the thickness of the sample.

When $m = 3$ this expression agrees, up to a constant factor, with that obtained by Venderovich[3] (without taking diffusion into account). Keeping terms only up to second order in the expansion of β in powers of $\gamma = aqE/2kT$, we obtain

$$P = \frac{\pi a^2 q^2 N n_0 m (m^2 - 1) d}{3kT} \cdot E \frac{1}{1 + \gamma + \frac{1}{3}(m-1)(2m-1)\gamma^2}. \tag{4}$$

According to this equation, the high-voltage polarization emf increases with N and m (the latter being a measure of the size of the "defects"), as well as with the concentration $n = Nmn_0$ of weakly bound ions in the dielectric. The field-strength dependence of P given by (4) is also in qualitative agreement with experiment. Assuming that the nonlinearity in the E-dependence of P becomes noticeable at a value of $E = E_{\mathrm{cr}}$, when the factor multiplying E in Eq.(4) differs from unity by 10%, we find that

$$E_{\mathrm{cr}} = \frac{0.45kT}{(2m-1)aq}. \tag{5}$$

This formula gives agreement with experiment[4] for NaCl if we set $m = 6$. The lack of agreement between experiment and Venderovich's calculations may be due to his assumption that $m = 3$.

When the concentration of weakly bound ions is constant, Eq.(3) gives an experimentally verified temperature dependence of the high-voltage polarization emf.

In order to obtain the correct temperature dependence for the case in which n increases with rising temperature, one must take into account the diffusion of ions out of the defects.[3]

The physical meaning of the temperature and gradient dependences of this emf, interpreted from the standpoint of the given model of a dielectric is the following. As the field strength increases, the asymmetry in the charge distribution within the "defects" also increases, so that P gets larger. In large fields, however, when most of the ions have already been removed to the "defect" boundary by the field, further increase of the emf is damped and saturation occurs. Simultaneously with the increase in the concentration of weakly bound ions at the boundary of the "defect", their diffusion out of the "defect" increases, and this is aided by stronger fields. In very strong fields, therefore, P begins to decrease as E is raised. An increase in the temperature disrupts the asymmetry in the ion distribution within the defects and enhances the outgoing diffusion. This causes a decrease in P.

4. The absorption current can be expressed in the form

$$j = \frac{aqN\delta}{\beta} \sum_{k=2}^{m} [1 + (-1)^k \beta^m] A_{1k} \exp\left(-\frac{t}{\tau_k}\right), \tag{6}$$

where $\tau_k = -\frac{1}{\lambda_k}$.

Eq.(6) shows that the absorption current is not given by a simple exponential even in the idealized model in which all the "defects" have a stringently fixed number of identical potential wells. An exponential dependence is obtained only when $m = 2$. Inserting into (6) the value for A_{12} found from a direct solution of (1) with $m = 2$ and going only to terms of second order in the expansion of β in powers of $aqE/2kT$, we obtain

$$j_m = \frac{a^2q^2n\nu}{6kT} \cdot \exp\left(-\frac{U}{kT}\right) E \exp\left(-\frac{t}{\tau_2}\right), \tag{7}$$

where $n = Nmn_0$ is the number of weakly bound ions per unit volume of the dielectric.

This is in agreement with Skanavi's[2] expression for the absorption current.

Fig.2 gives the time dependence of the absorption current for $m = 2, 3, 4$ and 5. In constructing these curves it was assumed that $E = 10^4$ v/cm, $n = 10^{18}$, $a = 10^{-7}$ cm, $\nu = 10^{12}$ sec^{-1}, $T = 300^\circ$K and $U = 10^{-12}$ erg.

As may be seen from the figure, for small values of m the current decrease curve is close to exponential. This is because the coefficient of the exponential with the longest time constant τ_2 is large compared to the others.

As m increases the contributions from the other exponentials also increase and the dependence deviates further from the simple exponential. This makes the theoretical curve approach the experimental one, which is characterized by a more rapid initial decay.

5. Fig.3 shows that as m increases, so does τ_2/τ_k ($k = 3, 4, \ldots, m$). Therefore the exponential with the longest time constant τ_2 will determine the shape of the "tail" of the absorption current decay curve for large values of m. Thus τ_2 plays a special role in the discrete spectrum of the relaxation times τ. It can be shown that

$$\tau_2 = \frac{0{,}3 \exp\frac{U}{kT}}{\nu} (m^2 + 1). \tag{8}$$

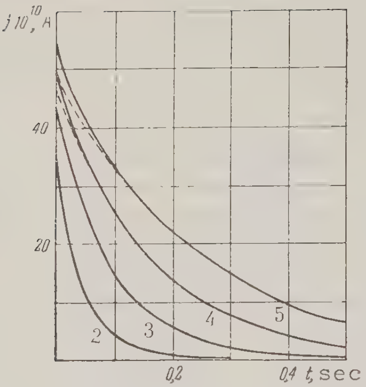

Fig.2. The absorption current j_m as a function of time and the number of potential wells m. The m values are indicated at the curves. The dash curves are exponentials.

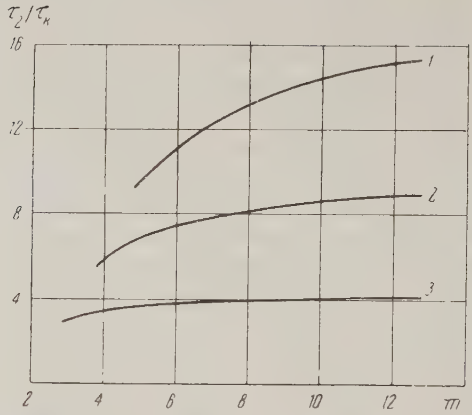

Fig.3. τ_2/τ_k as a function of m:

$1 - \frac{\tau_2}{\tau_5}, \quad 2 - \frac{\tau_2}{\tau_4}, \quad 3 - \frac{\tau_2}{\tau_3}$

6. Eq.(8) shows that a long decay time for the absorption current can be due not only to a large activation energy U, but also to large dimensions of the localization volume of the weakly bound ions.

The number m of potential wells is, of course, independent of the temperature. Therefore Skanavi's equation for finding the activation energy of the relaxing ions from the temperature induced displacement of the peak loss frequency remains valid also for our model (for values of m that are not very large).

Eq.(6) can also be used to find the temperature and gradient dependences of the absorption current. As the temperature is raised, the absorption current at any given instant decreases because of the sharp drop in the relaxation time (the absorption-current curve "drifts" toward small values of the time) and because of the increased diffusion of the weakly bound ions out of the "defects". As the field strength is increased the absorption current first increases for weak fields, then passes through a maximum, and finally decreases for strong fields. The field strength corresponding to the maximum of the absorption current is about 10^5-10^6 v/cm. Experimentally, however, a decrease of the current with increasing field strength is observed even for weaker fields.[5] This is probably because ionic diffusion out of the "defects" increases in strong fields, and this also leads to a decrease in the absorption current.

7. Finally, it should be noted that in spite of the artificiality of our model and all our simplifying assumptions, we obtain qualitative agreement with experiment.

Where we were able to obtain quantitative results, they, too showed reasonable agreement. Consequently, a process akin to thermal ionic polarization must play a significant role in absorption phenomena in solid dielectrics with ionic conductivity. This is entirely natural inasmuch as internal defects necessarily exist in all real dielectrics.

References

1. V.I.Arkhanov, Zhur.tekh.fiz., 24, No.3 (1954).
2. G.I.Skanavi, Fizika dielektrikov (Physics of dielectrics). M.-L.,1949.
3. A.M.Venderovich, Zhur.tekh.fiz., 23, 297 (1953).
4. B.M.Gorelik & V.G.Dmitriev, Zhur.tekh.fiz., 23, 297 (1953).
5. V.A.Pesnov, Zhur.tekh.fiz., 22, 956 (1952).

ORIENTATIONAL POLARIZATION OF DIPOLE GASES, SOLUTIONS AND LIQUIDS TAKING INTO ACCOUNT THE INTERNAL FIELD

- A. A. Borgardt

Debye's concept of an internal field in liquids served as the basis for the first theory of polarization of liquids that yielded reasonable agreement with experiment.[1,2] Attempts at a similar treatment of polarization were made by the author in collaboration with Finkel'shtein.[3-5]

If one makes use of the fact that the molecules themselves give rise to a statistical internal field F with a distribution $W(F)$, the polarization P becomes

$$P(\alpha, \beta) = n\int_0^\pi d\vartheta\, w(\vartheta) \int_0^\infty df \mu_\beta(\vartheta, \alpha f')\, \mathbf{W}(f), \tag{1}$$

where

$$\beta = \frac{\mu E^{(ef)}}{kT}, \quad \alpha = \frac{\mu \langle F \rangle}{kT}, \quad f = \frac{F}{\langle F \rangle}, \quad f' = f\,(1 + (\beta/\alpha f)^2 + 2\,(\beta/\alpha f)^2 \cos\vartheta)^{1/2},$$

and ϑ is the angle between $\mathbf{E}^{(ef)}$ and $\mathbf{F}$.

The assumption that every dipole undergoes rotational diffusion about the direction of $\mathbf{F}' = \mathbf{E}^{(ef)} + \mathbf{F}$ gives

$$\mu_\beta(\alpha f') = \mu L(\alpha f') \cos\vartheta', \tag{2}$$

where ϑ' is the angle between $\mathbf{E}^{(ef)}$ and $\mathbf{F}'$.

Using the fact that $\beta/\alpha \ll 1$, we find in the linear approximation that

$$P(\alpha, \beta) = (n\mu\beta/3)\,(1 + \langle\cos\vartheta\rangle_\vartheta \int_0^\infty df L(\alpha f)\, W(f) - 3\,\langle\cos^2\vartheta\rangle_\vartheta \int_0^\infty df L^2(\alpha f)\, W(f)). \tag{3}$$

If we assume that

$$\langle\cos\vartheta\rangle_\vartheta = 0 \quad \text{and} \quad \langle\cos^2\vartheta\rangle_\vartheta = 1/3, \tag{4}$$

we arrive at Debye's theory with the statistical nature of the internal field taken into account.[3] It was pointed out by Ansel'm[6] that it is incorrect to neglect $\langle\cos\vartheta\rangle_\vartheta$. When one calculates $\langle\cos\vartheta\rangle_\vartheta$ on the assumption that the internal field is produced by nearest neighbors of the molecule under consideration, this error is eliminated.[4]

Most important for the whole theory is the form of $W(F)$ or $W(f)$. As a first approximation this problem can be stated as a Markov problem for the probability $W(F)\,(dF)$ that the resultant of N random vectors $\mathbf{F}_i$ (the field strengths due to the individual molecules) will lie between $\mathbf{F} - dF$ and $\mathbf{F} + dF$ We then have[7]

$$W_N(\mathbf{F}) = (2\pi)^{-3} \int_{-\infty}^{+\infty} \exp(i\vec{\xi}, \mathbf{F})\, K_N(\vec{\xi})\,(d\vec{\xi}), \tag{5}$$

where the kernel $K_N(\vec{\xi})$ of the Fourier transformation is given by

$$K_N(\vec{\xi}) = \Big(\int_{-\infty}^{+\infty} p(\mathbf{x}) \exp(-i\vec{\xi}, \vec{\varphi}(\mathbf{x}))\,(d\mathbf{x})\Big)^N, \tag{6}$$

in which

$$\vec{\varphi}(\mathbf{x}) = -\nabla(\vec{\mu}, \mathbf{x}/x^3), \tag{7}$$

or, when the number N of molecules is allowed to increase without bound,

$$K_N(\vec{\xi}) \to \exp(-nC(\vec{\xi})), \tag{8}$$

where

$$C(\vec{\xi}) = \int_{-\infty}^{+\infty} p(x)(1 - \exp(i\vec{\xi}, \vec{\varphi}(x)))(dx). \tag{9}$$

The absolute values of F divided by the mean internal field $\langle F \rangle$ are distributed according to the well-known Holtsmark distribution[8]

$$W_2(f) = (1/2\pi^2 \langle F \rangle^3 f^3) \int_0^{\infty} x \sin x \exp(-x/f)\, dx, \tag{10}$$

or

$$W_2(f) = (4/\pi) f^2 / (1 + f^2)^2, \tag{11}$$

where

$$f = F / \langle F \rangle \quad \text{and} \quad \langle F \rangle = 4{,}54\ n\mu. \tag{12}$$

This distribution is obtained on the assumption of zero correlation between the orientations of neighboring molecules, which is its most serious shortcoming (see below). Taking into account the finite volume of the molecular dipoles is quite complicated, but it leads to a simple correction factor for (11). The corrected expression is[9]

$$W_2(f, v_0) = W_2(f)(1 + 4v_0(3 - f^2)/(1 + f^2)). \tag{13}$$

In any case, it should be mentioned that the dielectric constant of a liquid only very weakly depends on any of the molecular constants other than $n\mu$. This is probably because of the similarity in the values of v_0 for different substances (all liquids have $v_0 \approx 0.435$).

The effect of the external field on the distribution of the internal one is in general unimportant, at least in the approximation that the orientational polarization is linear in β. This question has been investigated[10] for the case of an alternating field (we shall here be concerned with the limit as $\omega \to 0$), and it is found that

$$W_2(\beta, f) \approx W_2(f)[1 - (10/9\sqrt{15})\beta f/(1 + f^2)(1 + \omega^2/\omega_0^2)]. \tag{14}$$

where ω_0 is the Debye frequency.

If this distribution is used in the theory, we obtain corrections to $P(\alpha, \beta)$ quadratic in β. At high frequencies, i.e., as $\omega \to \infty$, the correction tends to zero.

More important is the polarization of the molecules by the internal field. According to the estimates of Frenkel'[11] and the results obtained with the Holtsmark distribution ($\langle F \rangle = 4.54\ n\mu$), this field may attain a strength of 10^8 v/cm. Because of elastic polarization, the dipole moment of molecules in liquids is always greater than the value obtained from analysis of the polarization of the corresponding vapor or by extrapolating the results of polar solution studies to infinite dilution. The expression

$$\langle \cos\vartheta \rangle = L(\alpha f) \tag{15}$$

therefore, is not exact, and must be replaced by a new one. The energy of elastic polarization of a molecule in the internal field is

$$U = -kT(\alpha f \cos\vartheta + (\gamma \langle E \rangle / \mu)\alpha f^2 \cos^2\vartheta). \tag{16}$$

where γ is its elastic polarization.

The distribution in angles ϑ is now obtained in the form

$$dw(\alpha, \gamma, f, \vartheta) = N^{-1} \exp(\alpha f \cos\vartheta + (\gamma \langle F \rangle / \mu) \cdot \alpha f^2 \cos^2\vartheta) \cdot \sin\vartheta \, d\vartheta, \tag{17}$$

where

$$N = \int_{-1}^{+1} \exp(\alpha f \cos\vartheta + (\gamma \langle F \rangle / \mu) \alpha f^2 \cos^2\vartheta) \sin\vartheta \, d\vartheta. \tag{18}$$

The calculation is made somewhat simpler by the fact that γ is small, in view of which we have

$$\exp(\alpha f \cos\vartheta + (\gamma \langle F \rangle / \mu) \alpha f^2 \cos^2\vartheta) \approx (1 + (\gamma \langle F \rangle / \mu) \alpha f^2 \cos^2\vartheta) \exp(\alpha f \cos\vartheta). \tag{19}$$

In this approximation we have

$$\langle \cos\vartheta \rangle \approx ((1 + 3B/\alpha) L(\alpha f) - B) / (1 - BL(\alpha f)), \tag{20}$$

or, to the same accuracy,

$$\langle \cos\vartheta \rangle \approx (1 + 3B/\alpha) L(\alpha f) + BL^2(\alpha f) - B, \tag{21}$$

where

$$B(\alpha, f, \gamma) = 2\gamma \langle F \rangle f^2 / (\mu + \gamma \langle F \rangle \alpha f^2). \tag{22}$$

The value of $\langle \cos\vartheta \rangle$ obtained in this way satisfies the necessary conditions in the limits

$$\begin{array}{ll} \langle \cos\vartheta \rangle \to 0 & \text{as} \quad \alpha \to 0, \\ \langle \cos\vartheta \rangle \to 1 & \text{as} \quad \alpha \to \infty, \\ \langle \cos\vartheta \rangle \to L(\alpha f) & \text{as} \quad \gamma \to 0, \end{array}$$

and can be used in the theory.

The resulting corrections are not large, but they do make for somewhat better agreement with experiment.[12]

Let us now attempt to determine the limits of applicability of our theory.

The derivation of the Holtsmark distribution is based on the assumption that all the dipoles, including nearest neighbors, are oriented entirely at random. The validity of this assumption is limited, of course, owing to the very fact of dipole interaction of the molecules. Under this assumption each dipole can be regarded as a statistically independent entity, if it approaches no closer to any of its neighbors than

$$x \approx 0{,}4 n^{-1/3} \alpha. \tag{23}$$

The separation between nearest neighbors, as calculated from the nearest neighbor distribution (the Hertz distribution[13]), is

$$\langle x \rangle_{\mathrm{H}} = \Gamma(4/3) / (4\pi n/2)^{1/3} \approx 0.554 n^{-1/3}. \tag{24}$$

It follows from these calculations that one may assume the dipoles to be distributed entirely at random only if $\alpha \leqslant 1.4$.

The situation is somewhat different in solutions with a non-polar solvent. In these the dielectric constant of the solvent weakens the interaction, and, therefore, the correlation as well.

Comparison with experiment carried out for some dozens of polar liquids,[12] shows that good agreement is obtained even if $\alpha \approx 5$; for instance, when t = = 20°, the theory gives ϵ = 12.8 for benzophenone (experiment gives 13.3), 16.8 for acetophenone (18.1 from experiment), 18.2 for ethyl nitrate (19.6 from experiment), and 27.0 for ethyl thiocyanate (29.7 from experiment).

The reasons for this are probably the following.

a) Correlation between the orientations of nearest neighbors is to a large extent distrupted by thermal motion. This may be why the theory gives poorer results at low temperatures.[4]

b) Molecules whose internal correlation is so great that one must practically treat them as binary systems never stop producing an internal field. In this case, in fact, two antiparallel dipoles form a quadrupole whose moment Q is of the order of $3\,\mu a$, where a is the separation between the dipoles. In the absence of correlation, such formations produce an internal field with a Holtsmark distribution of the form

$$W_3(f) = (1/2\pi^2 \langle F\rangle^3 f^3) \int_0^\infty x \sin x \cdot \exp\,[-(x/f)^{3/4}]\, dx, \tag{25}$$

where the mean field is

$$\langle F\rangle = 8.2 n^{4/3} Q. \tag{26}$$

If we compare this with intensity of the mean field produced by the dipoles, we find that, if α_D is of the order of unity, there is little difference $(\alpha_Q \approx \alpha_D$ when the dipole separation $a \approx 0.35 \langle x\rangle_{\mathrm{H}})$

The most satisfactory results are obtained when the theory is used for solutions of dipole liquids in non-polar solvents.[5] For this reason we have performed some more accurate calculations for this case, but without changing the basic premises of the theory. What we did was to take into account the volume of the molecules and its influence on the polarization. The molecular dipole moment in the solution was found to equal not its nominal value but

$$\mu' = \mu\varphi_0(v_0 - q), \tag{27}$$

where

$$\varphi_0(v_0 - q) = 1 - e^{v_0 - q} E_i(v_0 - q), \tag{28}$$

$$q = [8\pi n(c)/3]\,\gamma(\varepsilon_l - 1)(1 - c)/c(2\varepsilon_l + 1); \tag{29}$$

v_0 is the volume, γ is the polarizability of a solvent molecule and c is the concentration of the substance.

Because the quantity q appears in the above expressions, we were forced to introduce the concept of the effective dielectric constant of the solvent. By this we understand that value of the dielectric constant which the solution of the given concentration would have, if all of the solute were removed without changing the total volume. This is

$$\varepsilon_l(c) = \frac{(1 + 2R_0 n(c)(1 - c)/N_0 c)}{(1 - R_0 n(c)(1 - c)/N_0 c)}, \tag{30}$$

where R_0 is the refractivity of the solvent.

For pure liquids the effective field was chosen as the Lorentz field

$$E^{(ef)} = ((\varepsilon + 2)/3)\,E, \tag{31}$$

because of its simplicity and also because the theory, when applied to pure liquids is less accurate, so that the approximation implied by (31) is sufficiently close.

For solutions we used the Onsager relation[14] as being more accurate, correcting it to take account of the molecular volume. The resulting expressions are

$$E^{(ef)} = [3\varepsilon_l / (2\varepsilon_l + 1)]\, \varphi_0 (v_0 - q)\, E, \tag{32}$$

$$F^{(ef)} = 4{,}54 \cdot [3\varepsilon_l / (2\varepsilon_l + 1)]\, \varphi_0^2 (v_0 - q)\, n(c)\, \mu. \tag{33}$$

Comparison of theory with experiment gives good results and allows of evaluating the proportion of molecules associated into complexes (alcohols, fatty acids, etc.). One of the interesting implications of the theory, which is related to the introduction of ε_l is the fact that P_∞ depends on the dielectric constant ε_0 of the solvent. This dependence is given by

$$P_\infty = (4\pi / 9)\, [3\varepsilon_0 / (2\varepsilon_0 + 1)]\, \varphi_0^3 (v_0 - q)\, N_0 \mu^2 / kT, \tag{34}$$

and has been observed experimentally (the so-called Müller effect[15]).

Finally, we may note the following concerning Kirkwood's theory,[16] which explains the polarizability of dipole liquids without making use of the concept of an internal field. One of the fundamental aspects of his theory is the use of some clever tricks to calculate directly the integral over states of the polarized dipole liquid. The final result can be written in the form

$$P = (4\pi n / 3)\, (\gamma + \vec{\mu}, \langle\vec{\mu}\rangle / kT)\, E, \tag{35}$$

where $\langle\vec{\mu}\rangle$ is the dipole moment induced by the molecule in its immediate vicinity (in the macroscopic sense). This can also be expressed by the formula

$$(\varepsilon - 1)(2\varepsilon + 1) / 3\varepsilon = 4\pi n\, [\gamma + \mu^2 (1 + z \langle\cos\zeta\rangle)/kT], \tag{36}$$

where z is the number of nearest neighbors of the molecule and ζ is the angle between the moments of a pair of molecules.

The following comments may be made concerning the existence of the above two theories treating the same phenomenon, yet based on different premises:

1. If there is no contradiction between the premises, there can be no contradictions between the theories themselves. The two theories merely represent two different points of view which are neither contradictory nor mutually exclusive. Thus Kirkwood's theory is statistical; Debye's is stochastic.

2. This implies that the two theories are equivalent. No one has yet studied this situation, but the equivalence cannot be doubted, and Kirkwood's equation (36) can be reduced to a factor which is a function of the internal field:

$$\vec{\mu}, \langle\vec{\mu}\rangle = \mu^2 \varphi(\alpha). \tag{37}$$

3. Further extension of Kirkwood's theory by introducing concrete models (i.e., introducing z and $\cos\zeta$) does not appear to improve it. This is, first, because these parameters can not be directly determined (the estimates of their magnitudes obtained by analysis of x-ray scattering data cannot be considered particularly reliable) and, second, because the experimental data seem quite unequivocally to imply that the dielectric constant of a dipole liquid depends only on the value of $n\mu^2/kT$ and on the elastic polarizability γ (only very weakly on the latter).[17]

For this reason any structural parameters introduced into the theory of polar liquids must necessarily be of a conventional nature, in the sense of "effective" as contrasted with "real" parameters. This means that in the final analysis they can all be written as functions of the internal field, so that

$$\alpha = \mu \langle F \rangle / kT, \quad \langle F \rangle \approx n\mu. \tag{38}$$

An attempt to do this within the framwork of the Kirkwood theory would be of great interest from the methodological point of view.

These remarks show why we have unhesitatingly used Debye's theory in its corrected form, although we do not doubt the validity of Kirkwood's. There are great mathematical difficulties involved in taking account of correlation when obtaining $W(F)$, but if this is done one obtains an accurate theory of the electrical properties of strongly polar liquids, and no unnecessary structural parameters are involved. Any ordering that may obtain in ordinary dipole liquids will have no influence on their electrical polarization.

Dnepropetrovsk State University

References

1. P.Debye, Phys.ZS., 36, 100, 193 (1935).
2. Ia.I.Frenkel', Kineticheskaia teoriia zhidkostei (Kinetic theory of liquids), M. 1946.
3. A.A.Borgardt & B.N.Finkel'shtein, Doklady AN SSSR, 67, 981 (1949).
4. A.A.Borgardt & B.N.Finkel'shtein, Zhur.eksp.i teor.fiz., 20, 887 (1950).
5. A.A.Borgardt, Zhur.eksp.i teor.fiz., 21, 436 (1951).
6. A.I.Ansel'm, Zhur.tekh.fiz., 18, 1905 (1948).
7. S.Chandrasekar, Stochastic problems in physics and astronomy. (Cited in Russian trans., M. 1947.)
8. J.Holtsmark, Phys.ZS., 20, 162 (1919).
9. J.Holtsmark, Phys.ZS., 25, 73 (1924).
10. A.A.Borgardt, Otchet (Report), Dnepropetrovsk State Univ., 1950.
11. Ia.I.Frenkel',Statisticheskaia fizika (Statistical physics), M. 1948.
12. A.A.Borgardt, Teoriia orientatsionnoi poliarizatsii dipolnykh zhidkostei i gazov (Theory of orientational polarization of dipole liquids and gases) Dnepropetrovsk State Univ. 1948.
13. P.Hertz, Math.Ann., 67, 387 (1909).
14. J.Onsager, Jour.Amer.Chem.Sci., 58, 1486 (1936).
15. C.Smyth, Dielectric behavior and structure, N.Y. 1953.
16. J.Kirkwood, Jour.Chem.Soc., 7, 911 (1939).
17. Ia.K.Syrkin, Doklady AN SSSR, 35, 45 (1942).

DISCUSSION

V.I.Odelevskii: In 1935 Debye introduced the concept of the "attenuating molecular field" to remove the contradiction resulting from the application of the Clausius-Mosotti equation to the calculation of the polarization and statistical dielectric constant of dipole liquids in weak and strong fields.[1] This modified theory was called "the new Debye theory".

As was already noted in the work of Ansel'm,[2,3] "the new Debye theory" is incorrect. Ansel'm's criticism of this theory is, however, given in a somewhat veiled, polite form and, as a result, attempts are still being made to improve this inconsistent theory. The paper we have been listening to is such an attempt, as are the earlier works of Borgardt and Finkel'shtein[4-6] and Borgardt's present contribution.

The basic error involved in this theory and all its modifications lies in the incorrect treatment of the influence of the so-called "molecular field" on the dipole polarization.

In a dipole liquid the polarization due to a constant external electric field is composed of a) the polarization associated with the redistribution of the dipole molecules, or, more accurately, the reconstruction of the microvolumes of the liquid as a result of thermal motion (this is the main term in the expression for the polarization), b) a moment depending on the elastic rotation of the molecules by the external field and c) polarization due to the elastic displacement of the nuclei and electron shells, also, by the external field.

For clarity let us consider a simplified model of dipole polarization in the spirit of Frenkel's ideas concerning the transfer of individual molecules from one local equilibrium position to another neighboring one.[7] The corresponding energy diagram is shown in the figure.

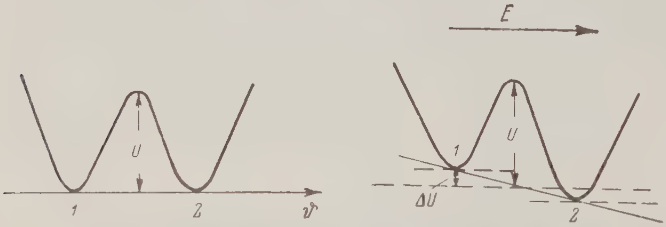

Energy diagram of dipole polarization.

An increase in the "internal molecular field will cause an increase in the height U of the energy barrier and therefore of the corresponding time constant τ. The static dipole polarizability, of course, does not depend on U or τ.

The "internal field" and the energy U affect the polarization associated with elastic rotation of the dipoles; the larger U, the lower the associated polarizability. This polarization, however, is very small (a few percent) compared to the normal thermal orientational polarization.

Confusion of these two types of polarization is what led Debye and his followers astray.

It should be remarked that in the rigorous theory of dipole polarization developed by Kirkwood, there is no room for the concept of any additional molecular field acting on "an equal footing" with the external polarizing field.

The attempt to "improve" the calculations in this theory as undertaken by Borgardt and Finkel'shtein does not alter the fact that the physical concepts at its basis are erroneous, as is therefore the entire theory.

M.P.Tonkonogov: One should differentiate between Borgardt's statement of the problem, which is entirely correct, and the solution, which is a very rough approximation.

Debye's internal molecular field correctly characterizes the interaction between molecules of a dielectric, although Debye assumed incorrectly that it is isotropic when an external field is applied. Ansel'm calculated the molecular field with the anisotropy taken into account. When this was done, the results of his theory were the same as those obtained from Kirkwood's more general considerations.

Borgardt solves the problem of calculating the molecular field more consistently and more rigorously than did Ansel'm, since the average is taken over both the magnitudes and directions of the field.

I therefore see no reason to reproach Borgardt for an incorrect statement of the problem. As for his solution, the results are quite unpretentious because of the rough approximations made at the start to simplify the calculation (the use of the Lorentz formula, for instance, for the effective field). Nevertheless, it is very valuable to have a calculation of the dielectric constant which does not involve undetermined parameters.

E.M.Fradkina: I have no objections to the essence of Borgardt's theory. Odelevskii's objections, on the other hand, reduce to stating that Kirkwood's theory is the only correct theory. That seems to be his opinion.

G.I.Skanavi: Odelevskii's criticism is based on a subjective conviction that the interaction between molecules can not change their polarizability. I believe that this conviction is not entirely well-founded.

A.A.Borgardt: The assertion that the new Debye theory is "incorrect", bolstered by reference to the work of Ansel'm, bears absolutely no relation to reality. As anyone taking the trouble to read his contributions can see, Ansel'm's work is devoted to correcting the new Debye theory not by subjecting to criticism the concept of the internal field itself, but the assumption that it is isotropic.

It is also difficult to understand what motives would, as so emphatically stated by Odelevskii, lead Ansel'm to criticize Debye's theory in a "veiled, polite form".

Our work is based on Ansel'm's corrected version of the Debye theory. In my opinion, the model presented by Odelevskii has no direct relation to the problem being discussed. The most that can be inferred from it is that all orientations of dipole molecules in dielectrics are not equally probable, which is obvious. This was realized, by the way, by Ia.I.Frenkel' himself; yet by no means did he imply that such concepts contradict the Debye theory.[7]

It should be mentioned anyway that the action of an internal field on the polarization of a dipole substance is a necessary consequence of the stochastic model together with some elementary electrodynamic considerations. There is for this reason no necessity to use models and concepts of a qualitative nature when the problem can be stated rigorously and based on general considerations of the stochastic theory.

As for Kirkwood's theory, it is certainly true that the internal field does not appear in it; nevertheless it does involve an effective dipole moment, and this reflects the same concepts from another point of view. The advantage of our theory is that it does not involve arbitrary parameters, which do occur in Kirkwood's.

References

1. P.Debye, Phys.ZS., 36, 100 (1935).
2. A.I.Ansel'm, Zhur.eksp.i teor.fiz., 12, 274 (1942).
3. A.I.Ansel'm, Zhur.tekh.fiz., 18, 1095 (1948).
4. A.A.Borgardt & B.N.Finkel'shtein, Doklady AN SSSR, 67, 981 (1949).
5. A.A.Borgardt & B.N.Finkel'shtein, Zhur.eksp.i teor.fiz., 20, 887 (1950).
6. A.A.Borgardt, Znur.eksp.i teor.fiz., 21, 436 (1951).
7. Ia.I.Frenkel', Kineticheskaia teoriia zhidkostei (Kinetic theory of liquids) M-L, 1945.

MECHANISM OF RELAXATION DIELECTRIC LOSS IN CRYSTAL HYDRATES

- I.Ts.Liast

Dielectric losses in a substance containing polar molecules may be caused not only by simple rotation of these molecules. Relaxation dielectric losses must occur also in the case of translational motion of polar molecules, inasmuch as the orientation of the molecules also obviously changes as a result of translation. For the purposes of the present discussion, we assume that polar molecules in the crystal occupy certain definite positions in which they cannot rotate. Because of lattice defects, however, the molecules are capable of moving inside the crystal. Such displacement of the molecules is essentially diffusion but, in view of the fact that the moving molecules have a dipole moment, such motion also leads to relaxation polarization. Thus the diffusion and polarization are characterized by the same relaxation time τ.

In crystal hydrates water molecules are weakly bound and hence the number of diffusing molecules in hydrates is comparatively large and the polarization due to displacement of the water molecules may play a significant role. In order to obtain expressions for the real and imaginary parts of the dielectric constant we must solve the kinetic equation. In the general case, when there are molecules with different bonding energies in the crystal hydrate, one must solve a set of kinetic equations. The dielectric loss occurring in the general case has been examined by the author in Ref.1.

If we limit our consideration to the particular case of equally strongly bound molecules, we obtain the kinetic equations in the form

$$\frac{dn^{\mathrm{I}}}{dt} = -\frac{n^{\mathrm{I}}\left(\frac{1}{2}N - n^{\mathrm{II}}\right)}{\frac{1}{2}N} \cdot \frac{1}{\tau}\left[1 + \frac{\varepsilon+2}{3} \cdot \frac{\mu}{kT}\,\mathbf{l}_0\left(\mathbf{l}_6 - \mathbf{l}_{\mathrm{I}}\right)\right] +$$

$$+ \frac{n^{\mathrm{II}}\left(\frac{1}{2}N - n^{\mathrm{I}}\right)}{\frac{1}{2}N} \cdot \frac{1}{\tau}\left[1 + \frac{\varepsilon+2}{3} \cdot \frac{\mu}{kT}\,\mathbf{l}_0\left(\mathbf{l}_6 - \mathbf{l}_{\mathrm{II}}\right)\right], \qquad (1)$$

where N is the total number of lattice sites at which there can be water molecules, $n^{\mathrm{I}} + n^{\mathrm{II}} = n$ is the number of water molecules in the lattice and μ is the dipole moment of a water molecule.

For the sake of simplicity let us assume that at half the sites that can be occupied by water molecules the dipole moments of these molecules are directed along a certain unit vector $\mathbf{l}_{\mathrm{I}}$ and that in the other half of the possible sites the direction of the dipole moment is $\mathbf{l}_{\mathrm{II}} = -\mathbf{l}_{\mathrm{I}}$; n^{I} is the number of molecules whose dipole moment is aligned with $\mathbf{l}_{\mathrm{I}}$ and n^{II} is the number of molecules whose dipole moment is aligned with $\mathbf{l}_{\mathrm{II}}$. We shall characterize the direction of the dipole moment of a molecule at the instant it passes through the top of the potential barrier by the unit vector $\mathbf{l}_6$. Eq.(1) was obtained on the assumption that the molecules are acted on by a Lorentz field.

Solving the kinetic equations (1), we obtain, after averaging, the following equation for tan δ for a polycrystalline sample:

$$\tan\delta = \frac{\varepsilon+2}{\varepsilon} \cdot \frac{\mu^2}{9kT} \cdot \frac{n(N-n)}{N} \cdot \frac{\omega\tau}{1+(\omega\tau)^2}. \qquad (2)$$

The values of n and N are per unit volume of the crystal. Eq.(2) was deduced without taking into account the interaction of the moving molecules. In the case of crystal hydrates one can neglect the interaction of the molecules inasmuch as the contribution to the polarization from this interaction is small compared with the total polarization.

As is evident from the work of Vodop'ianov and his colleagues[2-5], an interesting distinctive feature of the dielectric loss in crystal hydrates is the presence of a so-called concentration maximum in the plot of tan δ as a function of the water of crystallization content. The expression for tan δ deduced above explains this distinctive characteristic. The concentration maximum occurs when the number of vacancies $(N - n)$ becomes equal to the number of remaining water molecules.

The presence of a concentration maximum can be explained not only in terms of the indicated mechanism. A concentration maximum will also obtain when some relaxation process occurs next to the site vacated by a water molecule. Such a relaxation process can be rotation of the water molecules, rotation of OH radicals, motion of ions between potential wells, etc. Although such relaxation processes are possible, they do not appear particularly probable inasmuch as it is not clear why or how the absence of a water molecule could lead to any relaxation processes in neighboring unit cells.

The given mechanism allows of determining the relaxation time τ from the diffusion coefficient D. For a cubic lattice the diffusion coefficient D is related to the relaxation time τ by[6]

$$D = \frac{d^2}{6\tau}, \tag{3}$$

where d is the distance between water molecules. For crystal hydrates the diffusion coefficient D can be determined from the rate of hydration or dehydration of the crystal. Solving the diffusion equation for a spherical specimen, we obtain the following relationship between the relaxation time τ and the time t during which the crystal absorbs 1/e of the total amount of water absorbed (e is the base of natural logarithms):

$$\tau = \frac{\pi^2 d^2}{6R^2} t, \tag{4}$$

where R is the radius of the specimen. Using the data of Budnikov[7] on the hydration of gypsum, we obtain $\tau = 4 \cdot 10^{-9}$ sec at $T = 413^\circ K$. Extrapolating the relaxation time determined for gypsum from the position of the tan δ maximum[2] at the same temperature, we obtain $\tau = 2 \cdot 10^{-9}$ sec. Thus diffusion and electric measurements yield a value of the same order of magnitude for τ. This is convincing evidence that the high frequency dielectric loss in gypsum is due to translational motion of the water molecules.

The bonding energy of water molecules can be determined from the rate of dehydration. For gypsum ($CaSO_4 \cdot 2H_2O$) we obtain the following value for the energy of the weakly bound molecules:

$$U = 1.1 \cdot 10^{-12} \text{ erg.}$$

Knowing the bonding energy U, one can determine, in the case of static equilibrium, the number of water of crystallization molecules by means of the following modification of Langmuir's adsorption formula[6]:

$$n = \frac{N}{1 + \frac{N}{m} e^{-\frac{U}{kT}}}, \tag{5}$$

where m is the number of water vapor molecules per unit volume.

Finally, substituting the number of water molecules in the lattice determined in this manner in (2), we can calculate the value of tan δ_{max}. Rough computations showed that the value of tan δ_{max} evaluated in this manner agrees as regards order of magnitude with its experimental value.

In crystals whose lattice is constructed of polar molecules (ice, solid hydrochloric acid, etc.) there should also obtain losses due to displacement of molecules, inasmuch as in these crystals, by virtue of presence of defects therein, the polar molecules also have the ability to diffuse. Using Eq.(3), one should be able to determine from the diffusion coefficient D the approximate position of the corresponding loss maximum.

Inasmuch as the number of defects is usually very small, the corresponding value of tan δ should also be very small; hence the described mechanism cannot be used for explaining the comparatively large dielectric loss observed in these substances.

I take this occasion to thank G.I.Skanavi and M.P.Tonkonogov for valuable discussions.

Karagandinsk Mining Institute

References

1. I.Ts.Liast, Zhur.tekh.fiz., 26, 2293 (1956).
2. K.A.Vodop'ianov, Zhur.tekh.fiz., 24, 25 (1954).
3. K.A.Vodop'ianov, Zhur.tekh.fiz., 19, No.9 (1949).
4. M.P.Tonkonogov, Dissertation, Tomsk, 1953.
5. A.P.Izergin, Dissertation, Tomsk, 1955.
6. Ia.I.Frenkel', Statisticheskaia fizika (Statistical physics), M., 1948.
7. P.P.Budnikov, Gips (Gypsum), M., 1933.

STRUCTURAL LOSS IN AMORPHOUS DIELECTRICS

- V.Kh.Kozlovskii

The dielectric loss in amorphous dielectrics (specifically, in glasses) may be thought of as comprised of 1) the conductance loss, the relaxation loss and 3) the structural loss.

The relaxation loss is due to the presence of certain impurity ions, for example, alkali ions; the nature of this loss has been investigated in the experimental and theoretical work of Skanavi.[1]

As for the structural loss, it has been noted that losses of this type are dependent on the nature of the glass-forming oxide. In studying the structural loss, therefore, one can disregard the losses of the first two types and neglect the presence of the ions responsible for them. Rigorously speaking, the existence of relaxation centers is inevitable because of thermal ionic dislocations; their contribution to the loss, however, will be noticeable only in crystals, while in amorphous dielectrics it will be masked by the stronger effects that we shall consider below.

Under these conditions it is reasonable to assume that the potential energy of an amorphous dielectric at temperatures well below the softening point may be represented in the form of a quadratic function of the ionic displacements with the same degree of accuracy as for ordinary crystals (nonferroelectric materials). If there were present relaxation ions, characterized by a potential energy with a hump, it would be necessary to take into account anharmonic terms. In their absence the absorption of electromagnetic energy by an amorphous dielectric must in principle be of the same nature as the absorption by a crystal, i.e., it must be associated with the dynamics of the atoms and not with their relaxation, and the loss in glass must be of the resonance type. In this case the loss cannot be dependent on the temperature.

Actually, however, resonance absorption in crystals obtains only at certain frequencies in the infrared region, while in glasses it occurs in a wide frequency range. Hence we have here a difference in principle, the reason for which requires clarification. If there is propagated a plane electromagnetic wave through a crystal, then, as follows from Born's[2] theory, the forced vibrations of the lattice are also characterized by a plane wave of the same frequency and the same value of the wave vector. As a result, only such normal vibrators of the crystal can be excited and absorb the field energy as correspond to vibrations with the frequency and wave vector equal to the frequency and wave vector of the electromagnetic wave.

In ideal crystals absorption is associated with resonance both as regards frequency and wave vector. Hence infrared rays are absorbed only by the limiting vibrations of the lattice. In an amorphous structure, however, the forced vibrations are not plane waves and hence the wave vector concept and the limitations connected with it fall away. If we vary the frequency of long electromagnetic waves over a wide range, there will in turn be excited all the normal vibrations of the amorphous dielectric and not only the limiting ones as in an ideal crystal.

Lifshits[3] considered the absorption of electromagnetic energy by a crystal with a weakly disturbed periodicity, such as obtains in any real crystal consisting of a randomly distributed mixture of isotopes. Calculations showed that disturbance of the periodicity leads to absorption of energy in a range of frequencies which in an ideal crystal would be inactive. Although one cannot consider the disturbance of periodicity in an amorphous dielectric to be weak, the above result is qualitatively applicable to this case. In the crystallization of glass at room temperature there develop limitations on the excitation of normal vibrators connected with the appearance of long-range order which leads to an appreciable diminution of the loss.

Let us formulate these considerations in mathematical terms. To this end let us consider a particle of an amorphous dielectric; we use E to denote the energy of its ordered motion and R to denote the dissipation function. In the simplest case R is proportional to the kinetic energy W:

$$R = \frac{1}{\tau} W. \tag{1}$$

According to available thermostructural analysis data,^{4} the silicon-oxygen groups in silicate glass form chains of up to 100 Å in length. Hence let us choose a cube with an edge of 10^{-4} cm, containing up to 10^{12} ions. We shall consider electromagnetic vibrations of wavelengths much greater than the dimensions of the cube, i.e., not less than 10^{-2} cm, which corresponds to frequencies not exceeding 10^{12} cps. Using $\vec{\rho}_s$ (with components ξ_s, η_s, ζ_s) to denote the vectors describing the displacement of the ions from the positions they would occupy if thermal motion ceased and introducing normal coordinates of χ_j by means of the relationship

$$\vec{\rho}_s = \sum_j \vec{\alpha}_{sj} \chi_j, \tag{2}$$

we can represent the kinetic and potential energy of the cube as

$$W = \frac{1}{2} \sum_j \dot{\chi}_j^2; \text{ and } U = \frac{1}{2} \sum_j \omega_j^2 \chi_j^2. \tag{3}$$

The quadratic approximation for the potential energy is applicable for temperatures well below the softening point.

The ion energy in an electric field $\mathbf{E} = \mathbf{E}_0 e^{i\Omega t}$ is given by

$$U_E = - e^{i\Omega t} \sum_j (\mathbf{E}_0 \mathbf{Q}_j) \chi_j, \tag{4}$$

where

$$\mathbf{Q}_j = \sum_k q_k \vec{\alpha}_{kj}. \tag{5}$$

The equations of motion have the form

$$\frac{d}{dt}\left(\frac{\partial W}{\partial \dot{\chi}_j}\right) + \frac{1}{\tau} \frac{\partial W}{\partial \dot{\chi}_j} + \frac{\partial U}{\partial \chi_j} = - \frac{\partial U_E}{\partial \chi_j}. \quad j = 1, 2 \ldots \tag{6}$$

Eqs. (6), being classical, are valid only at not very low temperatures. The forced vibrations are described by

$$\chi_j = \frac{\mathbf{E}_0 \mathbf{Q}_j}{\omega_j^2 - \Omega^2 + i \dfrac{\Omega}{\tau}} e^{i\Omega t}. \tag{7}$$

The dipole moment of our specimen is

$$\delta \vec{\mathbf{P}} = \sum_k q_k \vec{\rho}_k + \sum_k \alpha_k \mathbf{E} = \sum_j \mathbf{Q}_j \chi_j + \sum_k \alpha_k \mathbf{E}, \tag{8}$$

where the α_k are the electronic polarizabilities of the ions. If the vibration spectrum is sufficiently dense, we can, combining the terms into groups, write

$$\sum_j Q_j \chi_j \approx \sum_{\Delta j} \mathbf{Q}_j \varkappa_j \Delta_j \approx \sum_{\Delta\omega} \mathbf{Q}(\omega) \chi(\omega) \delta n(\omega) \, \Delta\omega \approx \int_0^\infty \mathbf{Q}(\omega) \, \chi(\omega) \, \delta n(\omega) \, d\omega. \tag{9}$$

Here $\delta n(\omega)\,\Delta\omega = \Delta j$ is the number of vibrations in the frequency interval $\Delta\omega$ and δn is the frequency density. Obviously, δn is proportional to the volume δV:

$$\delta n = u(\omega)\,\delta V.$$

Setting $\varkappa_e = \frac{1}{\delta V}\sum\limits_k \alpha_k$ and substituting (8) in Eq.(7), we obtain the following expression for the complex amplitudes

$$\mathbf{P} = \varkappa_e \mathbf{E} + \int\limits_0^\infty \frac{\mathbf{Q}(\mathbf{QE})\,u}{\omega^2 - \Omega^2 + i\,\frac{\Omega}{\tau}}\,d\omega. \tag{10}$$

Inasmuch as the amorphous structure is isotropic, clearly the tensor in Eq.(10) can have only equal diagonal components, so that the complex dielectric constant is represented by the scalar

$$\varepsilon = \varepsilon_\infty + \frac{4\pi}{3}\int\limits_0^\infty \frac{|\mathbf{Q}|^2 u}{\omega^2 - \Omega^2 + i\,\frac{\Omega}{\tau}}\,d\omega. \tag{11}$$

The variation of $|\mathbf{Q}|^2 u$ with the frequency ω is not known, but we can attempt to represent it by the function

$$|\mathbf{Q}|^2 u = \beta\omega^s. \tag{12}$$

In view of the fact that the number of degrees of freedom is limited, the function $u(\omega)$ vanishes above a certain frequency ω_m, lying in the infrared region, but with $\Omega \ll \omega_m$ we can integrate to infinity if the integral exists, which is the case for $0 < s < 1$.

It can be shown that the integral J in (11) has the following real and imaginary parts:

$$\begin{array}{l}\operatorname{Re}(J)=\\ \\ -\operatorname{Im}(J)=\end{array} \frac{\pi}{2(\sqrt{2})^{s-1}\cos\frac{\pi s}{2}}\left(\sqrt{R^2\Omega^2+\frac{1}{\tau^2R^2}}\right)^{s-1}\begin{array}{c}\cos\\ \\ \sin\end{array}\left[(1-s)\operatorname{arctg}\frac{1}{R^2\tau\Omega}\right], \qquad \begin{array}{r}(13')\\ \\ (13'')\end{array}$$

where

$$R^2 = \sqrt{1 + \frac{1}{\tau^2\Omega^2}} - 1. \tag{14}$$

With $\Omega \gg \frac{1}{\tau}$, R^2 asymptotically approaches $\frac{1}{2\tau^2\Omega^2}$ and (13') and (13") are proportional to Ω^{s-1}, so that for values of s close to unity the real and imaginary parts of ε slowly decrease with increasing frequency so their ratio may remain approximately constant in a wide frequency range. With $s = 1$, extending the integration to a certain frequency ω_m, we obtain asymptotically for $\Omega \ll 1/\tau$

$$\varepsilon = \varepsilon_\infty + \frac{4\pi\beta}{3}\ln\omega_m - \frac{4\pi\beta}{3}\ln\Omega - \frac{4\pi^2\beta}{3}\,i. \tag{15}$$

The imaginary part becomes frequency independent and the real part very slowly (logarithmically) decreases. This result is close to what actually happens.

If the dissipation function differs somewhat from that represented by the simple relationship (1), then from (6), we obtain

$$\ddot{\chi}_j + \frac{dR}{dW}\dot{\chi}_j + \omega_j^2\chi_j = (\mathrm{E}_0\mathrm{Q}_j)\, e^{i\Omega t}. \tag{16}$$

Let us replace $\frac{dR}{dW}$ by the mean value $\overline{\frac{dR}{dW}}$ (averaged over time). Then from (16) we obtain Eq.(7), but τ will be a function of the temperature. With $\Omega \gg 1/\tau$, however, τ drops out of Eqs.(13') and (13'') and the temperature dependences are eliminated. Thus some variation of the dissociation law does not affect the dependences deduced above.

We note that for explaining the temperature independent component of the loss in glasses Frenkel'[5] proposed a mechanism involving conversion of the electromagnetic field energy into acoustic vibrations of the medium through the agency of the metallic ions therein. Evaluation of the energy lost by an acoustic vibrator[6] showed, however, that acoustic radiation makes a very small contribution to the loss. Apparently, the loss is connected primarily with dissipative processes. V.A.Ioffe suggested[4] that the loss in glasses in the region of ultrahigh frequencies is caused by the presence of a large number of resonators with different intrinsic frequencies; these may but need not necessarily be actual material formations.

Leningrad Institute of Semiconductors
Academy of Sciences of the USSR

References

1. G.I.Skanavi, Dielektricheskaia poliarizatsiia i poteri v steklakh (Dielectric polarization and loss in glasses), M.-L., 1952.
2. M.Born & M.Geppert-Mayer, Solid State Theory (Cited in Russ.trans., L.-M., 1938).
3. I.Lifshits, Zhur.eksp.i teor.fiz., 12, 117 (1942).
4. Stroenie stkla (sbornik) (Structure of glass - collected articles), 1955.
5. Ia.I.Frenkel', Izv.AN SSSR, Ser.fiz., No.3, 287 (1937).
6. E.Lysenko, Zhur.tekh.fiz., 8, 1637 (1938).

DISCUSSION

K.B.Tolpygo (on the report by Kozlovskii): It must be emphasized that the specific frequency dependences of ϵ and tan δ, which are of primary interest to experimenters, can be obtained only if we know $u(\omega)$, the frequency distribution in the liquid and $Q_j(\omega)$, the dipole moments of the vibrations. It is doubtful whether the last quantity can be calculated theoretically. In the presence of long range order $Q_j(\omega)$ will be a δ-function with a maximum for the limiting frequency and with diminution of order this maximum will undergo broadening.

Kozlovskii assumed that $|Q_j|^2 u(\omega) \sim \omega^s$. This assumption however appears to be entirely arbitrary and has no experimental or theoretical justification. Yet the specific attributes of any given liquid are to be found precisely in the values of Q and $u(\omega)$.

In view of this, any explanation of the observed regularities from the standpoint of the proposed theory it must necessarily be illusory to some extent.

V.Kh.Kozlovskii: Our purpose was not to calculate the frequency dependences of ϵ and tan δ that could be compared with experiment. This is impossible at present inasmuch as not enough is yet known regarding the structure of glasses and the bonding forces in them. In our work we only attempted to bring out the fact that one can remove the limitation on the excitation of normal vibrations in the case of absence of translational symmetry in considering structural losses. In the case of an ideal crystal there actually remain in the sum $P = \sum_j Q_j \chi_j$ several terms corresponding to limiting vibrations, from which there is obtained the general infrared dispersion. In the absence of long-range order all the Q_j are nonzero, which alters the picture qualitatively. Our calculations are intended to have only an illustrative value. They show that the absorption will not be concentrated in narrow frequency bands as in crystals. Naturally, my report does not negate the existence of other points of view on the nature of structural losses.

DIELECTRIC LOSS AT HIGH FREQUENCIES IN MUSCOVITE WITH INCLUSIONS OF LIMONITE AND BIOTITE

- K.A.Vodop'ianov & I.G.Vorozhtsova

Introduction

In studying the electric properties of mica one must bear in mind its physical-chemical characteristics, which in most cases are determined by the composition, distribution and shape of diverse inclusions. A certain amount of water of crystallization is generally present both in the host mica and in the inclusions. Depending on the amount of such water present and the degree of binding of the water molecules, there may be evinced effects due to orientation of the polar molecules (or their radicals) in the applied alternating electric field.

One of the present authors[1-3] has shown that the dielectric loss observed in phlogopite is due to orientation of the polar molecules of the crystallization water and that the mechanism involved is a relaxation one. Measurements carried out by A.P.Izergina[4] in our laboratory showed that dielectric losses associated with relaxation effects also occur at low and audio-frequencies in pure muscovite mica subjected to heat treatment.

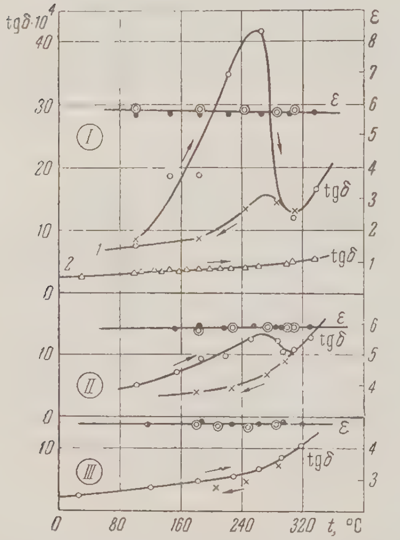

Fig.1. 1) Variation of the dielectric loss tangent and dielectric constant with the temperature for the muscovite sample with limonite inclusions and 2) variation of the dielectric loss tangent with the temperature for a sample of pure muscovite (from the Chuisk mine, vein No.66) at $F = 10^6$ cps; ◎ - forward (increasing temperature) variation of ϵ, ● - reverse (decreasing temperature) variation of ϵ; I, II & III - first, second and third cycle measurements for the same samples.

We felt it would be of interest to clarify the dielectric loss mechanism at high frequencies in muscovite with inclusions of limonite and biotite before and after heat treatment. As is known, muscovite with biotite inclusions contains a large amount of Fe_2O_3 and relatively little crystallization water, whereas muscovite with limonite inclusions, on the contrary, has an appreciably higher crystallization water content and little Fe_2O_3.

Thus in investigating muscovite with the two types of inclusion we have the possibility of clarifying the roles of water of crystallization and Fe_2O_3 where the dielectric loss is concerned.

In addition to their theoretical interest these investigations are of value from the standpoint of developing an efficient technology for the preparation of insulating materials and various mica products from spotty muscovite.

Specifically, we investigated the dielectric loss in muscovite with inclusions of limonite and biotite from the Chuisk and Kolotovsk mines (East Siberia), which we obtained from the Irkutsk Mica Plant.

Experimental Results

Muscovite with limonite inclusions

The temperature dependence of tan δ of muscovite with limonite inclusions is characterized by a curve going through a maximum, which is located in the 240 to 280° temperature interval for all the investigated samples. The maxi-

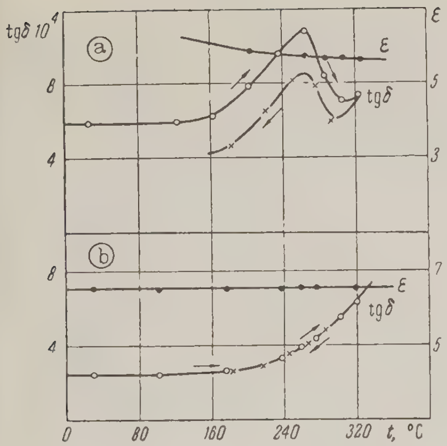

Fig.2. Influence of heating of a muscovite sample with limonite inclusions and a sample with 40% spottiness on the temperature dependences of the dielectric loss tangent and dielectric constant at F = 10^6 cps: a) sample not heated, b) sample heated at 400° (sample from Chuisk mine, vein No.58).

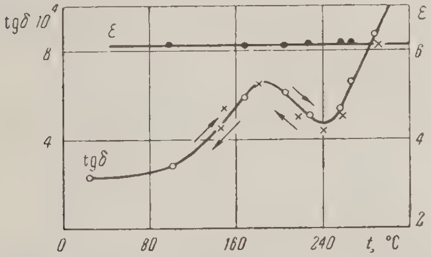

Fig.3. Same variation as in Fig. 2 but for sample heated to 600°.

Correlation between the temperature maximum of tan δ and the degree of spottiness of the sample

Degree of spottiness	Tan δ maximum
5.4	None
25.0	5.8
37.2	9.3
40.9	11.0

mum value of tan δ depends on the amount of crystallization water present. In all cases the dielectric constant varies with the temperature.

As may be seen from Fig.1, heating and cooling the mica samples through three temperature cycles leads to a reduction of tan δ and a marked change in the character of its temperature dependence: in the second heating-cooling cycle the absolute value of the tan δ maximum is significantly reduced, while in the third cycle the maximum is no longer in evidence, i.e., there is obtained almost the same kind of dependence as for mica without limonite inclusions. It is interesting to note that the forward (i.e., heating) temperature variation of tan δ in the second and third heating-cooling cycles virtually repeats the reverse (i.e., cooling) variation observed in the first and second cycles.

The decrease and gradual disappearance of the temperature maximum of tan δ can be explained if we bear in mind that in the temperature range from 200 to 300° an appreciable part of the water of crystallization is driven off from limonite ($Fe_2O_3 \cdot nH_2O$).

The absolute value of the temperature maximum also depends on the degree of spottiness. As may be seen from the accompanying table, the greater the area occupied by these spots, the greater the absolute value of tan δ. In the case of spottiness of the order of 5%, no temperature maximum of tan δ is observed. In contrast, for mica with 40.9% spottiness, we have a clearly pronounced temperature maximum of tan δ which, however, disappears upon heating at 400° for four hours (see Fig.2). In the case of the sample heated at 400°, the experimental points for the forward and reverse (heating and cooling) temperature variations of tan δ virtually coincide. As follows from Fig.3, however, heat treatment of this same mica at a higher temperature (600°) again yields a temperature maximum of tan δ; in this case the forward and reverse curves are virtually identical which indicates that no further crystallization water is eliminated.

Summarizing the experimental data, we see that in the case of unheated muscovite with limonite inclusions there is observed a temperature maximum of

$\tan\delta$ and that the heating and cooling curves for $\tan\delta$ to not coincide. There is no maximum of $\tan\delta$ in the case of samples heated at 400° but there is one in samples heated to 600°. In both cases the heating and cooling curves are virtually identical. These effects, in our opinion, are due to the properties of the polar molecules of the water of crystallization. In the case of the unheated mica sample, in recording the temperature variation of $\tan\delta$, i.e., during the heating up to 320°, both elimination of the weakly bound polar molecules and weakening of the bonds of the others occur. In the process of prolonged heat treatment at 400°, most of the polar molecules are driven off from the limonite; the remaining molecules apparently have strong bonds and are not capable of being oriented at the given temperature and frequency conditions, to give a temperature maximum of $\tan\delta$. Heating the samples to 600° weakens the bonds between the molecules initially strongly held both in the limonite and in the host mica; orientation of these now weakly bound polar molecules of crystallization water presumably gives rise to the temperature maximum of $\tan\delta$ observed in the case of the sample characterized in Fig.3.

Muscovite with and without biotite inclusions

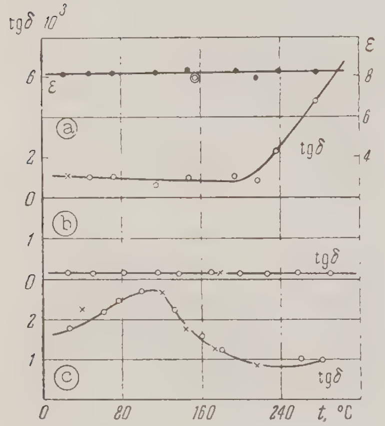

Fig.4. Influence of heating (4 hours) on the temperature dependences of the dielectric loss tangent of pure muscovite (sample from Kolotovsk mine, vein No.68): a) unheated sample, b) sample heated at 400°, c) sample heated at 600°. Curve at top of figure - temperature dependence of ϵ of pure unheated muscovite sample. Open circles - points obtained in heating; solid dots - points obtained in cooling.

Samples with and without biotite inclusions were prepared from the same chunk of mica obtained from the Kolotovsk mine (vein No.68). By comparing the temperature and frequency dependences of $\tan\delta$ and ϵ for pure muscovite and muscovite with biotite inclusions, we can evaluate the role played by these inclusions.

The area of the biotite spot in the investigated sample was greater than the area of the test capacitor electrodes.

The results of measurements of the temperature dependences of ϵ and $\tan\delta$ for pure mica before and after heating at 400 and 600° for 4 hours are shown in Fig.4. It will be seen that $\tan\delta$ of the unheated sample is independent of the temperature in the range from 25 to 200° and that at higher temperatures $\tan\delta$ begins to increase with the temperature. In contrast, the dielectric constant remains virtually constant throughout the entire temperature range. These results are in agreement with the experimental data for pure muscovite from other mineral deposits[5].

Heating of the muscovite at 400° leads to the reduction of the absolute value of $\tan\delta$ (Fig.4,b) and to its becoming temperature independent up to 300°, which is apparently connected with elimination of hygroscopic water. After heating of the mica at 600°, there appears a maximum in the temperature variation of $\tan\delta$ at 100° (Fig.4,c). The $\tan\delta$ maximum is probably due to orientation of weakly bound polar molecules of crystallization water.

The following results were obtained in measuring the temperature and frequency dependences of ϵ and $\tan\delta$ for muscovite with biotite inclusions before heating and after heating at 400 and 600°. As may be seen from Fig.5, the tan δ vs temperature curve obtained for the unheated sample has a diffuse maximum in the region from 100 to 260°. The curves obtained in cooling and heating differ. The absolute value of tan δ_{max} decreases appreciably with increasing frequency. Owing to the diffuse character of the tan δ maxima, their displacement with variation in frequency is obscured. The dielectric constant in the region of high temperature is appreciably reduced.

As a result of heating at 400°, as may be seen from Fig.6, the temperature maxima of tan δ become sharper, but the absolute values of tan δ_{max} are lower than for the unheated mica. The tan δ vs temperature curves obtained in heating and cooling nearly coincide. In the case of mica samples heated at 600 and 800°, there is observed a continuous growth of tan δ with increasing temperature. The experimental points in heating and cooling lie on the same curve. The dielectric constant does not vary with the temperature.

The observed effects of heat treatment of pure muscovite and muscovite with biotite and limonite inclusions on the temperature dependence of tan δ are in good agreement with the results obtained in measurements of the weight loss incident to heating. The loss in weight of muscovite was determined in the temperature range from 20 to 850° by weighing on a torsion balance with the samples heated in a crucible furnace. The length of each measurement cycle was 1.2-2 hours. For pure muscovite from the Kolotovsk mine as well as for the muscovite with limonite inclusions from the Chuisk mine there was obtained a sharp decrease in weight in the temperature range from 700 to 850°, while for the samples containing biotite there was observed an almost continuous reduction in weight in the entire range of temperatures up to 800°. This is in agreement with the lower thermal stability reported for biotite by Lashev[6].

Thus, the water of crystallization in pure muscovite is bound more strongly than in muscovite with biotite inclusions. This is probably the reason why an unheated sample of pure muscovite has no temperature maximum of tan δ, while a heated sample of muscovite with biotite does have a noticeable if somewhat diffused maximum.

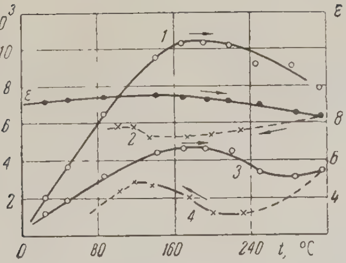

Fig.5. Temperature dependences of tan δ and ϵ of unheated muscovite sample with biotite inclusions (sample from Kolotovsk mine): curves 1 & 2 - tan δ at $f = 10^5$ cps; curves 3 & 4 - tan δ at $f = 10^6$ cps.

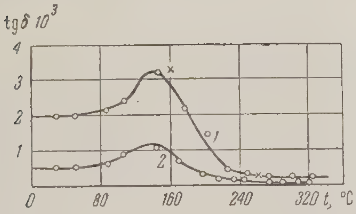

Fig.6. Temperature dependences of the dielectric loss tangent of a muscovite sample with a biotite inclusion (sample from Kolotovsk mine) heated at 400° at different frequencies: 1) 10^5 cps and 2) 10^6 cps (o - points obtained during heating; X - points obtained during cooling).

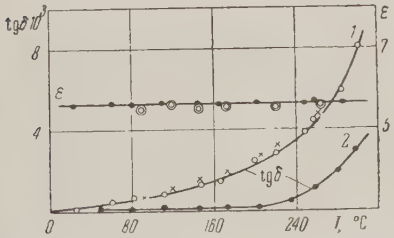

Fig.7. Influence of the heating temperature on the temperature dependence of the dielectric loss tangent of muscovite with a biotite inclusion measured at a frequency of 10^6 cps: 1) sample heated to 600°, 2) sample heated to 800°.

Structural changes in muscovite incident to heat treatment

That the atomic structure of muscovite and biotite changes in the direction of formation of a looser mosaic structure has been noted on the basis of x-ray diffraction studies by Wood[7] and Hidnert & Dickson[8]. In connection with our research we also carried out x-ray studies of some of our samples: we recorded Laue diffraction patterns of samples of pure muscovite from the Kolotovsk mine after heating to different temperatures.

The diffraction patterns show that after heating to 400° there were no noticeable changes in the structure of the mica. The diffraction patterns show only a minor displacement of the Laue spots, which indicates a minor rotation of the atomic planes. Heating to 600° leads to more appreciable twinning of the spots with gradually increasing asterism, which indicates a considerable disorientation of the individual mica crystallites, i.e., a noticeable disarrangement of the structure. Heating to 800° results in clear asterism of the patterns; this is undoubtedly associated with more appreciable disorientation of the atomic planes or, as Wood puts it, with the formation of a mosaic structure.

Conclusions

1. The observed regularities in the variation with temperature and frequency of the dielectric loss tangent in muscovite with and without inclusions of limonite and biotite can be explained on the basis of the quantitative and qualitative characteristics of molecules of crystallization water and their orientation in an alternating high frequency electric field.

2. Heat treatment of low grade muscovite with biotite inclusions at 600 to 800° and of muscovite with limonite inclusions at 400° results in significant improvement of the dielectric characteristics of the material; material treated thus can therefore be recommended for use in powdered form for the fabrication of diverse mica products.

Students L.M.Dubinina, G.M.Kosiachenko and G.V.Shpatenko participated in the experimental part of the work.

Siberian Physico-Technical Institute
"V.V.Kuibyshev" Tomsk State University

References

1. K.A.Vodop'ianov, Tr.Sib.fiz.-tekhn. in-ta. (Proceedings of the Siberian Phys.Rech.Inst.) 7, No.2 (1947).
2. K.A.Vodop'ianov, Zhur.tekh.fiz., 19, No.9 (1949).
3. K.A.Vodop'ianov, Doklady AN SSSR, 84, No.5 (1952).
4. A.P.Izergin, Tr.Sib.fiz.-tekhn.in-ta (Proceedings of the Siberian Phys.Tech.Inst.) No.32 (1953).
5. K.A.Vodop'ianov, ibid., No.2 (1947).
6. E.K.Lashev, Sliuda (Mica), 1948.
7. W.A.Wood, Proc.Roy.Soc.A, 163, N 913 (1937).
8. P.Hidnert & G.Dickson, Jour. of Res. of the Nat.Bur.Standards, 35, No.4 (1945).

DIELECTRIC LOSS AT HIGH FREQUENCIES IN PURE AND MIXED ALKALI HALIDE CRYSTALS

- K.A.Vodop'ianov and G.I.Galibina

It has been found that the dielectric loss angle of alkali halide crystals (NaCl, KCl, KBr and KI) is associated with the basic physical and chemical parameters of these crystals such as the lattice energy, melting point, activation energy, heat of formation, etc.[1]. The dielectric properties of natural rock salt have been investigated as a function of temperature, frequency, annealing, x-irradiation and additive coloration.[2] Similar studies have been performed on compressed powder samples.

On the basis of these investigations Vorob'ev and one of the present authors[1] proposed a mechanism of the dielectric loss in pure alkali halide crystals. With a view to verifying this mechanism and determining whether it applies to all alkali halide crystals, we felt it would be of value to continue the work on dielectric loss, extending the measurements to include a larger number of different crystals. The work on dielectric loss and the dielectric constant which is reported here was performed on a number of pure crystals as well as on solid solutions of several systems and on crystals doped with bivalent ions.

Dielectric loss in simple alkali halide crystals

The crystals were grown by the Kyropoulos technique[3] from melts of chemically pure materials. The dielectric loss angle at 10^6 cps and room temperature was measured in the following crystals: LiF, NaCl, KCl, KBr, KI, NaBr, CsBr and RbCl. The results are shown in Table 1.

Table 1

Dielectric losses in alkali halide crystals

Crystal	$\tan\delta\cdot10^4$	$(r_k + r_a)$, Å	Lattice energy Kcal/mole	Melting point °C
LiF	0,45	2,11	242,0	870
NaCl	0,64	2,79	183,5	800
NaBr	0,80	2,94	174,3	740
KCl	0,80	3,14	163,0	770
KBr	1,00	3,29	155,6	730
KJ	1,25	3,53	145,0	686
RbCl	1,15	3,30	155,0	715
CsBr	1,40	3,61	141,0	627

The table shows that the variation of the loss angle is consistent with the variation of certain physical and chemical properties of the crystals. The loss angle increases with increase of the distance between ions and, consequently, with decrease of the crystal energy and and melting temperature. In other words, the variation of $\tan\delta$ with the physical and chemical properties of the crystals is governed by the regularities established by Unzhakov.[4]

The variation of the loss angle as a function of temperature and frequency must be known before the dielectric loss mechanism can be understood. The frequency dependence of the loss angle in NaCl and KCl was obtained for the range from $3\cdot10^5$ to 10^8 cps. and the temperature dependence was determined for all the crystals under study in the interval from 20 to 240°. At 10^6 cps the loss tangent of all of the crystals shows the same variation with temperature. Very little temperature dependence is found in the wide temperature interval from 20 to 180°, but a considerable increase of the loss tangent is observed in the range of higher temperatures.

The variations of $\tan\delta$ were measured over a wider temperature range in the case of NaCl and KCl. Fig.1 shows the frequency dependence of the loss tangent of these crystals; Figs.2 & 3 show the temperature dependence at 10^6 cps.

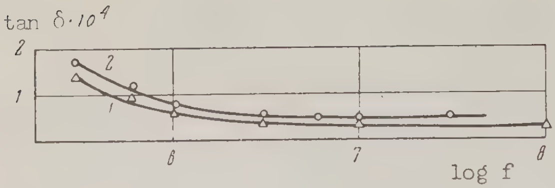

Fig.1. Variation of the dielectric loss tangent as a function of the frequency in 1) NaCl and 2) KCl.

The points plotted in Figs.2 and 3 are for two samples of each kind of crystal; it will be seen that they are well fitted by a single curve. Good agreement is also evident between the heating and cooling runs.

Just as in the case of the loss tangent measurements for KI, KBr and CsBr for the temperature range from 20 to 220°, the tan δ vs temperature curves for KCl and NaCl, obtained in the wider range from 20 to 300° showed no tan δ maximum for measurements at 10^6 cps.

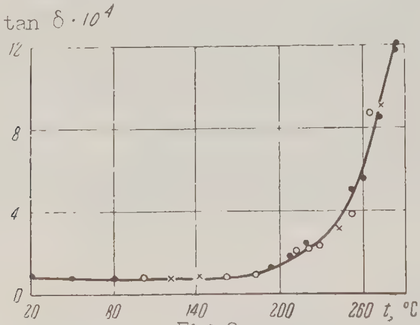

Fig.2

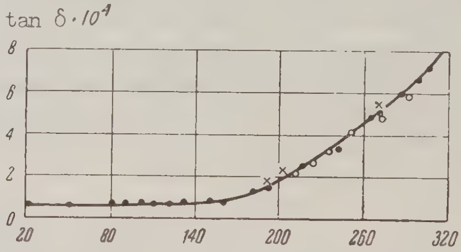

Fig.3

Fig.2. Variation of the dielectric loss tangent in KCl as a function of temperature at $f = 10^6$ cps. The open and closed circles are for two different samples as the temperature was increased; the crosses are the points obtained in cooling.

Fig.3. The same as Fig.2, but for NaCl.

The electric conductivity of KCl and NaCl crystals was measured in the range from 150 to 300° in order to determine its role in the process of energy loss. The loss tangent due to conduction was computed from the measurements. Table 2 shows the directly measured values of the loss tangent compared with the values computed from the conductivity.

Table 2

Dielectric loss tangents as measured and calculated from electrical conductivity

t, °C	NaCl		KCl	
	$\tan\delta_{meas}\cdot10^4$	$\tan\delta_{calc}$	$\tan\delta_{meas}\cdot10^4$	$\tan\delta_{calc}$
100	0,80	$1\cdot10^{-6}$	0,90	$1\cdot10^{-6}$
150	1,00	$1\cdot10^{-6}$	1	$9\cdot10^{-5}$
200	1,48	$1\cdot10^{-5}$	1,80	$1,34\cdot10^{-4}$
240	3,16	$1,4\cdot10^{-4}$	3,20	$3,18\cdot10^{-4}$
290			20	$1,92\cdot10^{-3}$
310	9	$10\cdot10^{-4}$		

At temperatures up to 150° the loss angle calculated from the conductivity is 2-3 orders smaller than the directly measured value. At 200-300° the calculated and measured values are usually of the same order of magnitude. A similar relation between total losses and conduction losses was observed for NaCl, NaBr, CsCl and CsBr by Bogoroditskii and Fridberg.[5] These results indicate that in such crystals other types of losses are superposed on conduction losses.

In addition to conduction, there may develop in alkali halide crystals in an electric field relaxation processes associated with the displacement of loosely bound ions in limited regions; these processes naturally involve an additional expenditure of energy.

Assuming that energy losses in alkali halide crystals are associated with conduction and the oscillations of loosely bound ions, the temperature and frequency dependences of the loss tangent in pure alkali halide crystals can be accounted for as follows. Conduction losses at low temperatures are small, so that we cannot observe the exponential temperature dependence of tan δ which is characteristic of ohmic losses. The relative importance of conduction losses increases with temperature, so that at high temperatures tan δ exhibits strong growth with temperature. The frequency dependence exhibits similar behavior; at high frequencies conduction losses are small and are masked by the dominant relaxation losses. With decreasing frequency the conduction losses become more significant and tan δ is found to increase with diminishing frequency.

Dielectric loss of solid solution crystals

It is well known that either solid solutions or eutectics[6] can be formed when two alkali halide salts are mixed, the determining factor being the ratio between the lattice constants of the interacting components.[4,6-8]

In the present work we investigated NaCl-NaBr, KCl-KBr and KCl-RbCl solid solutions, which are known to be the most stable. X-Ray diffraction patterns obtained for most of the investigated crystals showed that they were actually solid solutions. Measurements of the loss angle at room temperature at different frequencies revealed dependence of tan δ on the solid solution composition (Fig.4). The dependence is similar for the systems NaCl-NaBr, KCl-KBr and KCl-RbCl, as well as for KI-KBr system previously investigated at two frequencies. The loss tangent vs composition curve shows a maximum located in the region of approximately equal component concentrations. The highest peak is obtained at low frequencies ($3 \cdot 10^5$ cps) and decreases with rising frequency until at 10^7 cps the loss tangent becomes almost independent of the composition. In addition to the loss angle, we measured the dielectric constant. The dielectric constant of all the investigated crystals is almost independent of frequency and shows only minor variation as a function of the composition of the solid solutions.

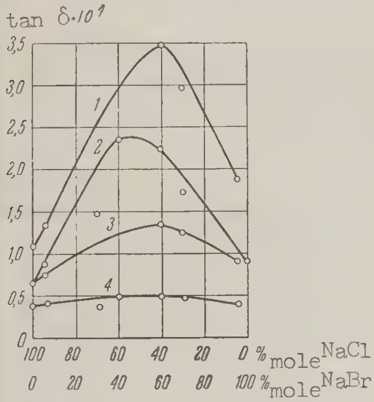

Fig.4. Variation of the dielectric loss angle as a function of the composition of NaCl-NaBr solid solutions at different frequencies: 1) $5 \cdot 10^5$, 2) $1 \cdot 10^6$, 3) $1.5 \cdot 10^6$, 4) $3 \cdot 10^6$ and $1 \cdot 10^7$ cps.

The temperature dependence of the loss tangent for KCl-KBr crystals is shown in Fig.5. Analogous curves were obtained for NaCl-NaBr and KCl-RbCl solid solutions. As is evident from Fig.5, the temperature dependence of the loss tangent in a solid solution is similar to the corresponding dependence in pure crystals of each of the components, the only difference being that the rise in tan δ is evinced at a lower temperature for the mixed crystal. This temperature is lowest when the two components are present in approximately equal amounts, and for any given composition rises with the frequency of the applied field (Fig.6).

In order to evaluate the role of conduction in the energy loss occurring in our crystals, we measured the conductivity of some of the solid solutions At low temperatures the loss tangent calculated from the conductivity proved to be smaller than the directly measured value, while at high temperatures the two values were found to be approximately equal.

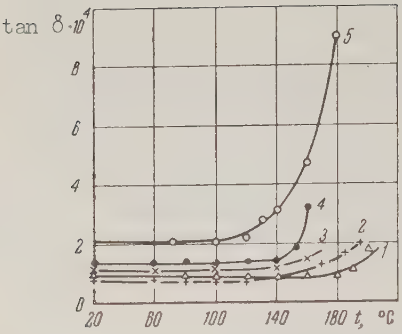

Fig.5

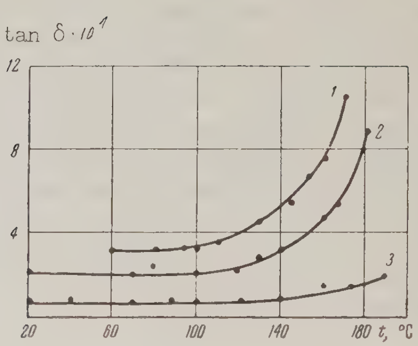

Fig.6

Fig.5. Variation of the dielectric loss tangent as a function of the temperature at 10^6 cps in the KCl-KBr system with different molar percentages KCl: 1) 100%, 2) 95%, 3) 90%, 4) 70%, 5) 50%.

Fig.6. Variation of the dielectric loss tangent as a function of the temperature in a 50% KCl + 50% KBr (molar %) crystal at different frequencies: 1) $3 \cdot 10^5$, 2) 10^6 and 3) 10^7 cps.

The frequency dependence of the loss tangent in mixed crystals, like the temperature dependence, is similar to the analogous dependence in pure crystals of the components, differing only in the steeper rise of the loss tangent with diminishing frequency. Neither the frequency nor the temperature dependence of the loss tangent of solid solutions or of pure crystals exhibited a maximum in the investigated frequency range ($3 \cdot 10^5$ to 10^8 cps) and temperature interval (20 to 240°). This is an indication that the loss mechanism is the same in pure single crystals and their solid solutions. However, the solid solutions do show a higher absolute value of the loss tangent as compared with the pure crystals as well as a steeper rise of tan δ with decreasing frequency and rising temperature. Spectroscopic analysis of the mixed crystals revealed only the same impurities that were contained in the original components. Therefore the differences between the mixed and pure crystals with regard to the frequency and temperature dependences of the loss angle must be associated with distinctive features of the crystal structure.

The lattice of solid solutions is characterized by the presence of a large number of microdeformations[9], which result from the fact that the lattice sites are occupied by ions of different radii. The number of microdeformations, which favor the formation of lattice defects, increases with the concentration of the second component.[10]

As was shown by Frenkel,[11] the presence of lattice distortions leads to a reduction of the activation energy for "loosening" of the lattice. This in turn leads to an increase in the number of ions participating in conduction as well as in the number of loosely bound ions capable of moving within a limited region. The increased conductivity and losses in mixed crystals, as compared with pure crystals, can thus be understood. The fact that the conduction loss is small at room temperature, while composition dependence of the loss tangent definitely obtains, indicates that mixed crystals contain a considerably larger number of loosely bound ions giving rise to relaxation processes. The sharper earlier rise of tan δ with increasing temperature or decreasing frequency is associated with an increase of the relative contribution of the conduction loss to the total energy loss.

Consequently, the same loss mechanism operates in both pure and mixed crystals. The larger loss tangent in mixed crystals and the more pronounced temperature and frequency dependences are connected with the structural characteristics of these crystals. It should be noted that similar relations are obtained for the loss tangent in solid solution ceramics.[12]

Dielectric loss in doped crystals

We know that small amounts of impurities greatly modify the mechanical properties of crystals.[13] The conductivity of crystals is also appreciably influenced by impurities.[14] The influence of impurities on dielectric loss has been investigated mainly in the frequency range from 10 to 10^5 cps.[15,16] There have been no systematic studies of the effect of impurities on dielectric properties at high frequencies. In this section we shall consider the effects of small amounts (<2 molar %) of $CaCl_2$, $BaCl_2$ and $MgCl_2$ on the dielectric properties of KCl and NaCl.

The doped crystals were grown from melts and the impurity concentrations were determined by quantitative chemical analysis.[17] Table 3 shows the crystal compositions and the values of the loss tangent measured at room temperature and a frequency of 10^6 cps.

Table 3

Loss tangent in KCl and NaCl crystals doped with $CaCl_2$, $BaCl_2$ and $MgCl_2$ at 10^6 cps (impurity concentrations given in molar percent)

Composition of crystal	$\tan \delta \cdot 10^4$	Composition of crystal	$\tan \delta \cdot 10^4$
KCl	0.84	KCl + 0.59% $BaCl_2$	2.32
KCl + 0.003% $CalCl_2$	0.84	KCl + 0.03% $MgCl_2$	0.84
KCl + 0.03% $CaCl_2$	0.90	KCl + 0.13% $MgCl_2$	0.89
KCl + 0.11% $CaCl_2$	1.10	KCl + 0.55% $MgCl_2$	1.79
KCl + 0.40% $CaCl_2$	7.25	NaCl	0.64
KCl + 0.85% $CaCl_2$	14.5	NaCl + 0.03% $CaCl_2$	0.64
KCl + 0.99% $CaCl_2$	23.1	NaCl + 0.10% $CaCl_2$	1.20
KCl + 0.12% $BaCl_2$	0.88	NaCl + $CaCl_2$	2.30
KCl + 0.4% $BaCl_2$	1.68		

Since $CaCl_2$ concentrations of the order of hundredths of a percent could not be determined by chemical analysis, the low values listed in the table are based on the proportions used in synthesis. The loss tangent in NaCl crystals doped with $CaCl_2$ was measured in the frequency range from $3 \cdot 10^5$ and 10^8 cps; the range for the other crystals was $3 \cdot 10^5$ to 10^7 cps. The frequency dependence of the loss tangent for NaCl crystals doped with $CaCl_2$ is shown in Fig.7. Similar curves were obtained for the other crystals and impurities.

Analyzing the data in Table 3 and the frequency dependence curves for the doped crystals, we note the following: 1) $CaCl_2$ induces the largest change in the loss tangent in KCl, 2) all the impurities increase the losses with decreasing frequency, and 3) impurities in the amount of a few thousanths or hundredths of a percent do not affect the loss tangent at room temperature.

We detected no change of the dielectric constant as a result of doping with $BaCl_2$, $MgCl_2$ or $CaCl_2$, except in the KCl + 0.99 molar % $CaCl_2$ crystal, which had a dielectric constant of 6.0 compared with 4.8 for KCl.

For the purpose of determining the loss mechanism in doped crystals we measured the loss angle as the temperature was increased. Figs.8 and 9 show typical $\tan \delta$ vs temperature dependence curves at 10^6 cps for different im-

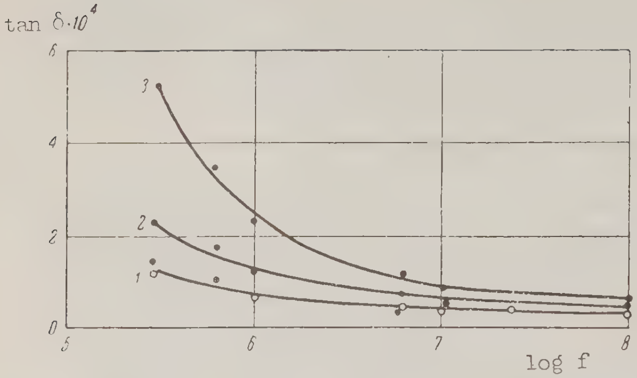

Fig.7. Frequency dependences of tan δ for NaCl crystals doped with $CaCl_2$: 1) NaCl, 2) NaCl + 0.10% $CaCl_2$, 3) NaCl + 1.6% $CaCl_2$

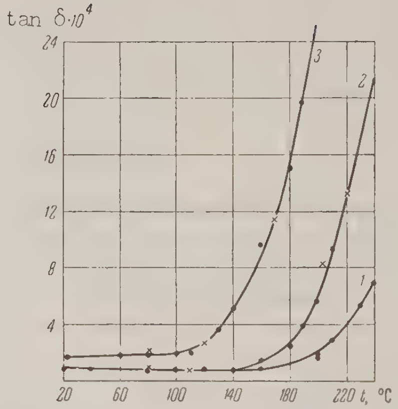

Fig.9. Temperature dependence of tan δ at 10^6 cps for KCl crystals doped with $BaCl_2$: 1) KCl, 2) KCl + 0.12% $BaCl_2$, 3) KCl + 0.40% $BaCl_2$.

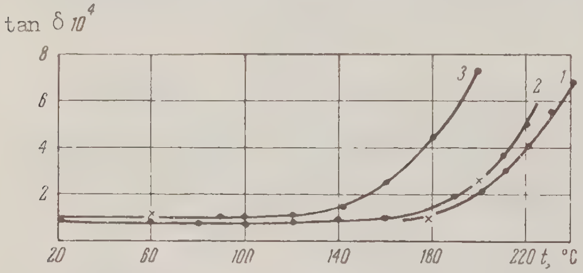

Fig.8. Temperature dependence of tan δ at 10^6 cps for KCl crystals doped with $CaCl_2$: 1) KCl, 2) KCl + 0.003% $CaCl_2$, 3) KCl + 0.03% $CaCl_2$.

purity concentrations. While impurities amounting to hundredths of a percent do not affect the absolute value of the loss tangent at room temperature, the shape of the tan δ vs temperature curve is considerably modified (Fig.8). Similar curves were obtained for KCl crystals doped with small amounts of $CaCl_2$ and for the KCl + 0.03% $MgCl_2$ and NaCl + 0.03% $CaCl_2$ crystals.

Thus a small amount of impurity, which does not noticeably affect the loss tangent at room temperature, can change the loss tangent very appreciably at high temperatures.

KCl crystals doped with about 0.1 molar percent of $BaCl_2$ (Fig.9) or $MgCl_2$ also exhibit almost no change of the loss tangent at room temperature but again show a large increase of tan δ at high temperature.

The figures show that the temperature dependences of tan δ for doped crystals resemble the dependences for pure crystals, but are generally characterized by a steeper rise with temperature. The temperature at which this steep rise begins is lowered as the concentration of a given impurity is increased, and for a fixed concentration is lowered with diminishing of the frequency.

As noted, the temperature and frequency dependences of tan δ for the doped crystals are similar to those for pure crystals and differ from these only in a steeper rise of tan δ with decreasing frequency or increasing temperature. Therefore the same mechanism must be responsible for the losses in both pure and doped crystals. The larger loss tangent in doped crystals results from the fact that the impurity distorts the lattice by large disruptions of the periodic potential field, thus providing favorable conditions for a larger number of ions to participate in the conduction or at least move in limited regions of the lattice. Larger impurity concentrations naturally distort the lattice of the host material to a greater extent, and the loss angle increases with the number of weakly bound ions and conduction ions.

As already mentioned, $CaCl_2$ affects the loss tangent of KCl crystals more strongly than do other impurities. Similarly, the mechanical properties of pure crystals are influenced most by $CaCl_2$ and $PbCl_2$ and least by $BaCl_2$ and $MgCl_2$.[13]

CONCLUSIONS

1. The values of the loss tangent in pure crystals vary in accordance with the different physical and chemical properties of the crystals.

2. The dielectric losses in pure crystals, solid solutions and crystals doped with $CaCl_2$, $BaCl_2$ and $MgCl_2$ are a combination of relaxation and ohmic losses; the relative contribution of the latter increases with diminishing frequency and rising temperature.

3. The influence of impurities on the loss tangent becomes more pronounced as the frequency is reduced and the temperature is increased.

4. An impurity content of the order of some hundredths of a molar percent (as introduced into the melt) has a very marked effect on the temperature dependence curve of tan δ, i.e., appreciably increases the value of tan δ at high temperatures.

Siberian Physical-Technical Institute,
"V.V.Kuibyshev" Tomsk State University

References

1. A.A.Vorob'ev & K.A.Vodop'ianov, Doklady AN SSSR, 94, No.3 (1954).
2. M.A.Krivov, Trudy (Proceedings) Siberian Phys.Tech.Inst., No.27 (1949) and No.35 (1956).
3. V.D.Kuznetsov, Kristally i kristallizatsia (Crystals and crystallization), M.1954.
4. G.M.Unzhakov, Doklady,AN SSSR, 90, No.1 (1953).
5. N.P.Bogoroditskii & I.P.Fridberg, Zhur.tekh.fiz., 24, No.7 (1954).
6. N.S.Kurnakov & S.D.Zhemchuzhnyi, Sobr.soch.Akad.Kurnakova (in Collected works of Academician Kurnakov), Vol.1, p.186, M. 1939.
7. A.J.Tobolsky, Jour. Chem. Phys., 10, No.3 (1942).
8. V.P.Radishev, Zhur.fiz.khim., No.4 (1935).
9. J.A.Wasastjerna, Phys.Rev., 55, No.10, 986 (1939).
10. G.Z.Miessner, Z.Physik, 134, 576 (1953) & 134, 606 (1953).
11. Ia.I.Frenkel', Kineticheskaia teoriia zhidkostei (Kinetic theory of liquids) M. 1945.
12. A.I.Avgustinnik & N.S.Antselevich, Zhur.fiz,khim, 27, No.7 (1953).
13. V.D.Kuznetsov, Fizika tverdogo tela (Solid state physics), Vol.II, Tomsk, 1941.
14. W.Lehfeld, Z.Physik, 85, 717 (1933).
15. R.G.Breckenridge, Jour.Cehm.Phys., 16, No.10 (1948).
16. Y.Haven, Jour.Chem.Phys., 18, No.7 (1950).
17. E.V.Alekseevskii et al, Kolichestvennyi analiz (Quantitative analysis), M.1948.

DIELECTRIC CONSTANT, DIELECTRIC LOSS AND ELECTRIC CONDUCTIVITY OF ALKALI HALIDE SINGLE CRYSTALS

- B.N.Matsonashvili

Introduction

Until recently it was generally assumed that the nature of dielectric loss in alkali halide crystals was adequately understood. Thus the work done by Bogoroditskii and Malyshev[1] as well as by other investigators seemed to show that dielectric loss in NaCl type crystals was an ohmic effect.

In 1948 Breckenridge[2] stated that the curve of the temperature dependence of tan δ (at constant frequency) in rapidly quenched "pure" alkali halide crystals exhibits a relaxation maximum. Later Breckenridge[3] observed a few additional maxima in the curves for crystals containing impurities. He attributed the maximum in pure crystals to reorientation of "pairs" of oppositely charged vacancies and the additional maxima to reorientation of complexes consisting of bivalent impurity ions and cation vacancies. There were many shortcomings in Breckenridge's work: he investigated the dielectric losses in air, he presumably was able to observe shifts of the relaxation maxima at all but the lowest frequencies, etc. In view of their obvious significance many investigators tried to reproduce Breckenridge's results; so far as we know, however, no one succeeded in doing so.

In 1953 Haven[4] succeeded in observing a relaxation maximum in the low frequency region of the frequency dependence curve of tan δ (T = const) for NaCl crystals doped with bivalent impurity ions. Haven attributed this maximum to the reorientation of complexes consisting of bivalent ions and vacancies. He was unable to detect any relaxation maxima in the temperature dependence curves of tan δ. Unlike Breckenridge, however, he detected regular shifts of the relaxation maxima, and his results were subsequently reproduced by others[5-10]. A theoretical explanation of Haven's results was given by Lidiard,[11] who showed that combinations of bivalent impurity ions and vacancies can explain only one relaxation maximum of tan δ.

The foregoing shows that we still have no reliable experimental data to confirm the existence of relaxation losses in pure crystals and that we still do not know how many relaxation maxima are to be found on the tan δ curves of crystals with impurities. We are in the dark regarding the mechanism of the additional relaxation maxima (if these exist) in the tan δ curves for doped crystals. It is also necessary to determine whether all alkali halide crystals exhibit relaxation losses. Investigation of relaxation losses in pure and doped isomorphic crystals is of particular interest.

The principal purposes of the present research were to clarify the character of the dielectric loss in alkali halide crystals and to determine the nature of the relaxation losses and the factors that affect them. For the purpose of eliminating all doubts regarding the possible existence and character of the effects, we investigated the temperature and frequency shifts of the relaxation maxima over broad frequency and temperature ranges. Unlike previous investigators, we measured the dielectric losses in vacuum and we obtained the frequency and temperature dependences of tan δ and of the electric conductivity γ for the same samples.

Experimental Part

Growth and preparation of samples

We used the Kyropoulos technique to grow single crystals of NaCl, KCl, KBr, KI, CsBr and isomorphic KCl-KBr crystals with different component proportions, both without impurities and with Ag^+, Cu^+, Tl^+, Cd^{2+} and Pb^{2+} in different amounts. The crystals were grown in porcelain, glazed, fireclay, corundum and quartz crucibles in order to determine the possible effect of these materials on the crystal properties. The temperature conditions of crystal growth were varied over a wide range. In addition to the above listed crystals, we also investigated crystals of LiF, LiF(In), KRS-5 and natural NaCl, obtained from other sources.

Slabs 2.5-3 mm thick were first sawed from the crystals by means of a water-wetted wire saw and then these were carefully ground and polished, using dehydrated alcohol, to the shape of disks, 0.26 to 1 mm thick (a few were somewhat thicker) and 15 to 20 cm^2 in area. The samples were planeparallel to within 1-2 μ.

It was very difficult to prepare thin isomorphic KCl-KBr crystals and crystals containing a relatively large amount of thallium impurity; the least trace of moisture caused these crystals to split along the cleavage planes.

It is easier to cut and grind thick samples, but reliable measurements require samples with the smallest possible capacitance. Thick samples must also be heated in the vacuum for a longer period which, of course, makes the study of the temperature dependences more onerous.

The samples were transparent and crossed polaroids revealed no perceptible internal stresses.

Application of electrodes

We tested different methods of applying electrodes; silver and platinum fired-on pastes, cemented foils, Aquadag coating and vacuum sputtering of silver, gold and aluminum. These techniques are suitable for samples that are not very highly hygroscopic (LiF, KCl and NaCl). It was found that the lowest dielectric losses are observed when silver is used, if care is taken to obviate contamination and moisture. With NaCl crystals we began by using the method of Bogoroditskii and Malyshev[1]: the end faces were coated with silver, the sample was heated to 200° and the lateral surfaces before cooling were coated with a film of heated paraffin. This procedure was later abandoned.

At times electrodes consisting of mercury or low melting point alloys were used. For precision measurements this method suffers from the fact that contact resistance is high and that at high temperatures the crystal may react with the electrode material. (Artsybashev[12] has shown that at sufficiently high temperatures alkali halide crystals react with almost all metals except chemically pure iron and platinum.) Therefore in our investigation of ϵ, tan δ and γ in vacuum we used the so-called optical contact technique which we regard as closest to ideal. The finished ground samples were clamped between chemically pure iron electrodes of suitable shape. The electrodes were polished to a mirror finish, the "wedge" tolerance being 1-2 μ. Before the beginning of measurements the electrode surfaces were usually cleaned by vacuum heating and kept under vacuum thereafter. With gradual and uniform heating the electrodes retained their plane surfaces. Careful measurements performed by this method yield the same results for tan δ and γ as in the case of silver-coated samples. At times the latter exhibited somewhat higher values of tan δ, possibly as the result of contamination in the process of silvering. Ground and polished samples exhibited identical values of tan δ regardless of difference in thickness and area.

Measuring apparatus

The frequency and temperature dependences of ϵ and tan δ were measured by means of a 716-V audio-frequency bridge and a Boonton Q-meter with good voltage stabilization. LiF and KCl crystals were studied in atmospheric air at temperatures ranging from -170° to +330° and frequencies from 10^2 to 10^7 cps. All other crystals and some LiF and KCl samples were investigated in vacuum at temperatures ranging from -140° to +550° and frequencies from 10^2 to 10^6 cps. The frequency and temperature dependence curves of ϵ and tan δ in vacuum were obtained under identical conditions and for the same samples. For more precise measurements of the dielectric loss angle at room temperature, we constructed a special apparatus*, which permitted measurements of small values of tan δ at frequencies of the order of 10^7 cps by the equivalent resistance method in air (the standard platinum and silver wire resistances were measured very accurately by means of a Thomson double bridge). For some NaCl and KCl samples tan δ was measured by means of a resonator set-up at $f = 10^{10}$ cps in the range from 20 to 125°.

A mirror galvanometer was used to measure the dc conductivity in vacuum.

Experimental Results and Discussion

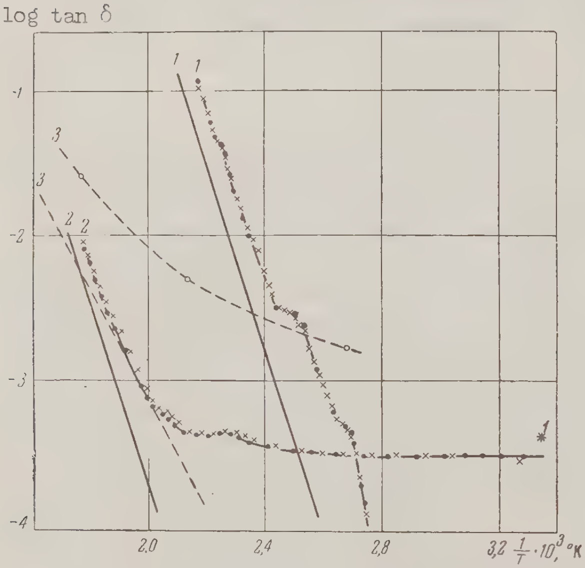

Fig.1. Variation of tan δ with temperature in CsBr crystals at the following frequencies: 1) 1 kc and 2) 750 kc (our data, in vacuum); 3) 1 kc (P.N.Bogoroditskii, in air). ● - heating run; ✕ - cooling run. The asterisk denotes the value of log tan δ for the crystal before evacuation. The straight lines represent the corresponding functional relations as calculated from the dc conductivity.

It was established that tan δ for hygroscopic samples is independent of pressure in an evacuated system (10^{-3} to 10^{-5} mm Hg), but is strongly affected by traces of moisture. Oil vapor and any contamination of the crystal surface also influence tan δ to some extent. Therefore moisture and oil vapor were frozen out for vacuum measurements. The values of tan δ obtained by other investigators at different temperatures are compared with our vacuum results in Figs.1 and 2. It will be seen that for hygroscopic samples tan δ measured in air is appreciably higher than in vacuum at all temperatures up to 200° in the frequency range to 10^6 cps.

The tan δ curve as a rule showed only one relaxation maximum for all pure crystals (and KRS-5 crystals) that were not subjected to additional heat treatment after growth (Figs.2-4). Excellent re-

---

*D.G.Lebedev constructed, assembled and adjusted the first laboratory version of the set-up.

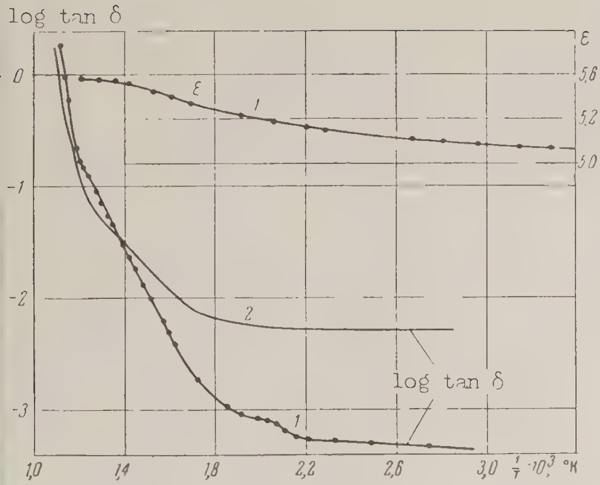

Fig.2. Variation of tan δ and ϵ with temperature in KCl crystals: 1) 750 kc (our vacuum data); 2) 3 Mc (Suita, in air).

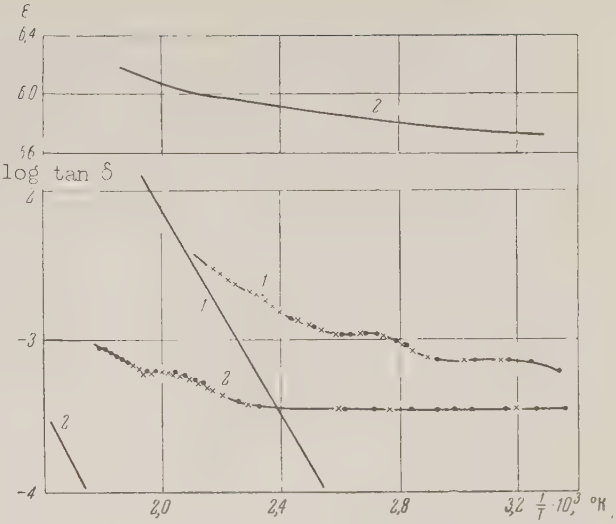

Fig.3. Variation of tan δ and ϵ with temperature in NaCl crystals: 1) 1 kc, 2) 850 kc. Designations same as in Fig.1.

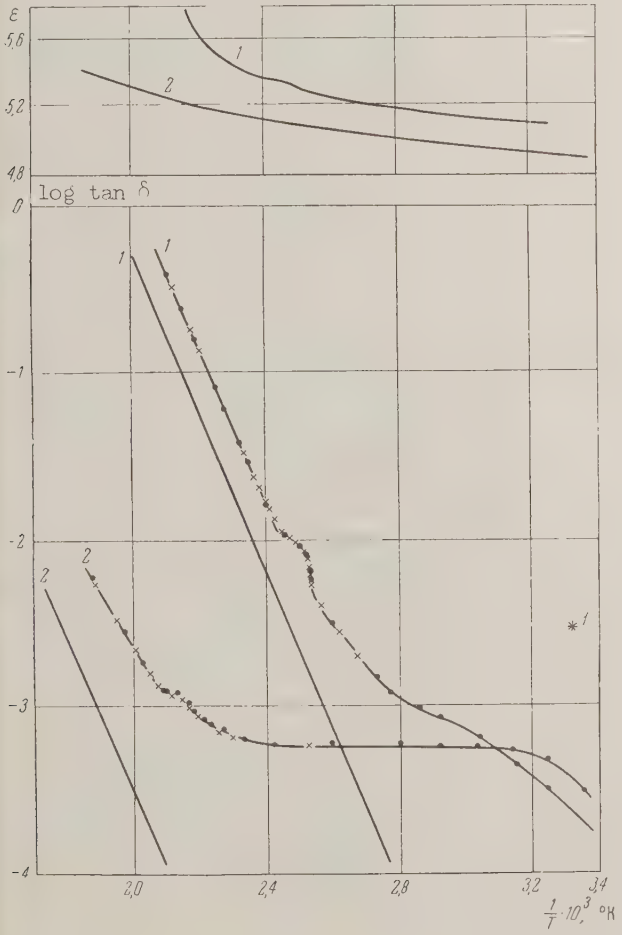

←Fig.4. Variation of tan δ and ϵ with temperature in KBr crystals: 1) 1 kc, 2) f = 950 kc. Designations same as in Fig.1.

---

producibility of the values of tan δ was obtained in the vacuum measurements in the temperature range from -140° to +300°. Different samples cut from the same single crystal sometimes yielded different values of tan δ (and γ), presumably because of nonuniform distribution of impurities. Such differences were especially marked in samples taken from single crystals of the same material grown in different crucibles. For example, the tan δ curve of KCl crystals grown in a quartz crucible shows a weak additional maximum possibly as the result of impurities entering from the crucible (Fig.5).

Additional relaxation maxima are evident in the tan δ curves of all the impurity containing crystals. Examples are shown in Figs.6 through 11.

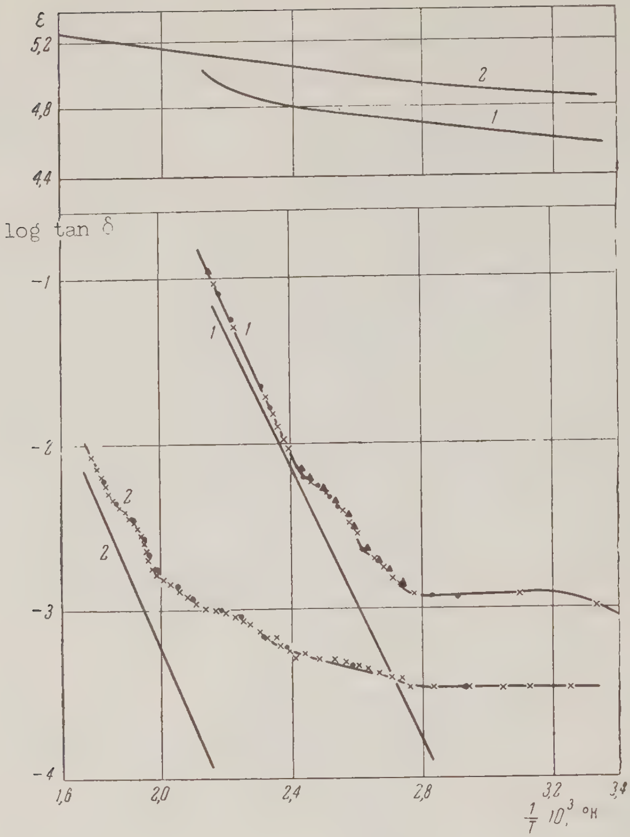

←Fig.5. Variation of tan δ and ε with temperature in KCl crystals grown in a quartz crucible: 1) 1 kc, 2) 850 kc. Designations same as in Fig.1; the triangles represent a repetition of the heating run.

We were able to determine the temperature and frequency shifts of all the relaxation maxima in many of the crystals; for some types of crystals, however, the available instrumental temperature and frequency ranges were inadequate. Most of the relaxation maxima are observed at temperatures for which tan δ is of the order of 10^{-3} to 10^{-1}. Such losses can be measured accurately by means of a Q-meter and audio-frequency bridge.

In some cases it was impossible to make precise measurements of tan δ at $\sim 10^6$ cps in the temperature region below 150° with a Q-meter inasmuch as the losses were below the sensitivity threshold of the instrument ($2\text{-}3 \cdot 10^{-4}$). Hence the tan δ curves obtained with a Q-meter for this temperature region have an apparent "plateau". We were also unable to measure tan δ precisely at very low temperatures (under -170°). Our vacuum measurements for all of the investigated crystals show that tan δ at

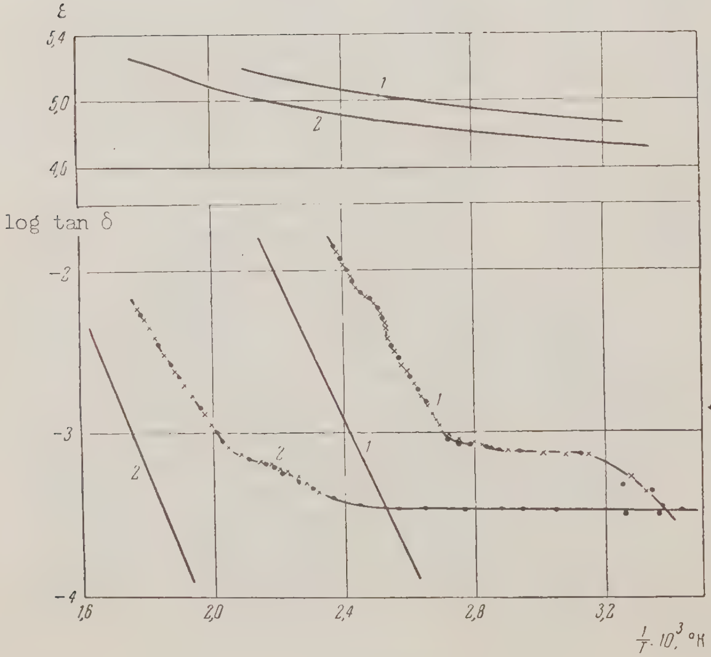

←Fig.6. Variation of tan δ and ε with temperature in crystals having the composition 180 g KCl + 1 g CuI: 1) 1 kc, 2) 850 kc. Designations same as in Fig.1.

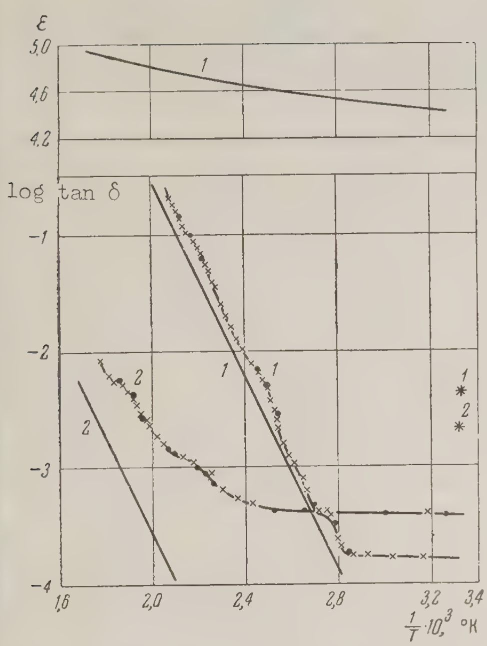

Fig.7. Variation of tan δ and ϵ with temperature in crystals having the composition 270 g KBr + + 1 g PbI_2: 1) 1 kc, 2) 1 Mc. Designations same as in Fig.1.

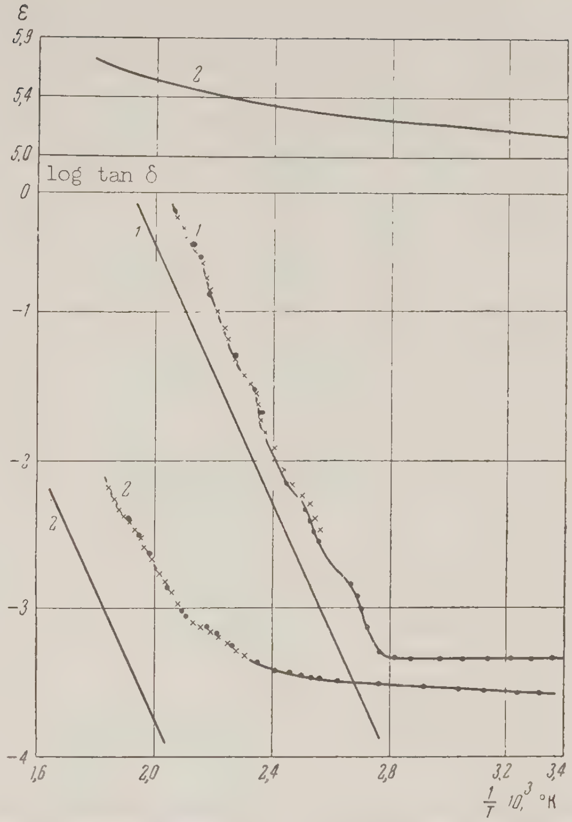

Fig.8. Variation of tan δ and ϵ with temperature in crystals having the composition 260 g KBr + 2 g TlI: 1) 1 kc, 2) 950 kc. Designations same as in Fig.1.

temperatures from +20 to -170° does not exceed its value at room temperature. This disagrees with the results obtained by Breckenridge, who for highly hygroscopic iodide crystals obtained values of tan δ which are as much as three orders of magnitude too high.

The usual methods[13] were employed to calculate the activation energy V_{rel} of the relaxing groups and the relaxation time τ from the family of frequency and temperature curves for tan δ. Table 1 gives the results for a few crystals.

V_{rel} is between 0.7 and 1 ev for different single crystals and can be calculated from a single temperature vs tan δ curve if the intrinsic vibrational frequency of the ions is known (or can be estimated approximately). V_{rel} determined in this way from the experimental data is about 0.5-0.8 ev. Two different temperature dependence curves of tan δ yield different values of V_{rel} for the same complex. The calculated value of V_{rel} is smaller for higher frequencies (and, therefore, higher temperatures). This can be accounted for by the temperature dependence of the energy of activation of the complexes.

It is interesting to note that consideration of the temperature dependence of V_{rel} enables us to explain the experimentally observed fact that the half-widths of the relaxation maxima in the temperature dependence curves of tan δ, in contrast to those in the frequency dependence curves, are smaller than the half-widths predicted by the general theory of relaxation losses.

The values of V_{rel} obtained from different pairs of tan δ curves for LiF and KCl agree to within ± 0.1 ev, as shown by Table 1, which also lists the

Table 1

Relaxation times τ and activation energies V_{rel} of relaxing groups, calculated from the temperature dependence (a) and frequency dependence (b) of tan δ. The activation energies V_{γ} of the same samples were calculated from the residual conductivity.

a

No.	Crystal	Frequency, kc	Max. tan δ at °K	τ, sec	V_{rel}, ev	V_{γ}, ev
1	LiF	1	318	$1{,}6\cdot10^{-4}$	0,806	1,195
		160	384	$1\cdot10^{-6}$		
2	NaCl (natural)	1	366	$1{,}6\cdot10^{-4}$	0,835	1,07
		800	489	$1{,}98\cdot10^{-7}$		
3	KCl	1	351	$1{,}6\cdot10^{-4}$	0,814	0,96
		3000	471	$5{,}3\cdot10^{-8}$		
4	CsBr	1	376 400 446	$1{,}6\cdot10^{-4}$	1,33	0,98
		900	448 484	$1{,}77\cdot10^{-7}$	1,35	

b

No.	Crystal	Max. tan δ	Temperature, °K	τ, sec	V_{rel}, cv	V_{γ}, ev
1	LiF	40 2000	335	$2{,}5\cdot10^{-3}$ $7{,}94\cdot10^{-4}$ $3{,}54\cdot10^{-4}$ $1{,}32\cdot10^{-4}$	0,69 0,39	1,195
		450 12000	373			
2	NaCl (natural)	120	407	$1{,}32\cdot10^{-3}$ $3{,}23\cdot10^{-4}$ $1{,}06\cdot10^{-4}$	0,68 0,87 0,85	1,07
		500	438			
		1500	457			
3	KCl (after heat treatment)	100 800	419	$1{,}59\cdot10^{-3}$ $2\cdot10^{-4}$ $2{,}45\cdot10^{-4}$ $4{,}2\cdot10^{-5}$	0,8 0,67	0,855
		650 3800	460			
4	CsBr	20 200	413	$7{,}94\cdot10^{-4}$ $7{,}94\cdot10^{-3}$ $2{,}65\cdot10^{-3}$ $3{,}19\cdot10^{-5}$	1,33	0,98
		600 5000	453		1,26	

values of the activation energy V_{γ} calculated from the conductivity of the same samples.* The calculations show that the concentration of the relaxing groups is of the order of 10^{17} per cm^3, whereas the concentration N of the defects which determine the conductivity is about one to two orders of magnitude lower (a calculation of N from tan δ for 1 kc gives 10^{18} per cm^3.

---

*The "true values" of V_{γ} can be deduced from the "initial" conductivity or slope of the tan δ plot in the range of high temperatures at high frequency.

We checked the influence of heat treatment near the melting point on the dielectric loss tangent and conductivity γ of several samples. Fig.12 shows the values of tan δ and γ for the same KCl sample before and after heat treatment. The samples were heated at 735° for 2 hours, cooled to 500° over the period of one hour and then slowly cooled down to room temperature. The experimental values of tan δ and calculated values of γ are seen to be considerably reduced after the heat treatment, while the dielectric loss maxima, which appear in the same temperature region, are smoothed out. These results can be attributed to reduced vacancy density after heat treatment (enhanced ordering). The ratio between the measured and calculated (from the conductivity) values of tan δ is retained on the whole.

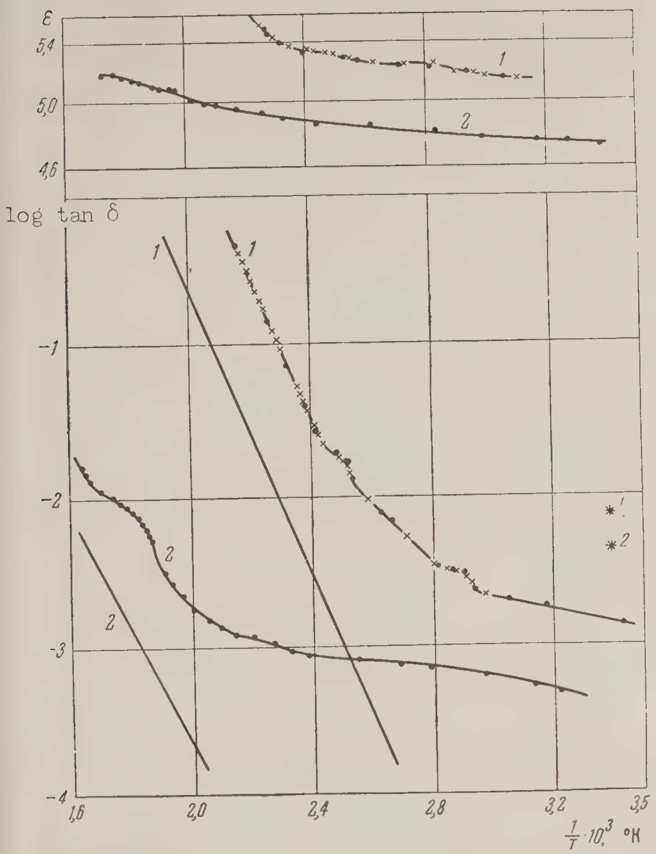

Fig.9. Variation of tan δ and ε with temperature in crystals having the composition 120 g KCl + 69 g KBr: 1) 1 kc; 2) 950 kc. Designations same as in Fig.1.

Analysis of the results shows that tan δ and γ in isomorphic KCl-KBr crystals are of the same order of magnitude as in the pure crystals (see Fig.9). The values for crystals doped with thallium, however, are sharply reduced.

It follows from our data (Fig.13) that for many crystals the relaxation $TK\epsilon = CT^{3/2}$ is fulfilled; here T is the absolute temperature and C is a characteristic crystal constant. (This empirical relation was recently suggested by

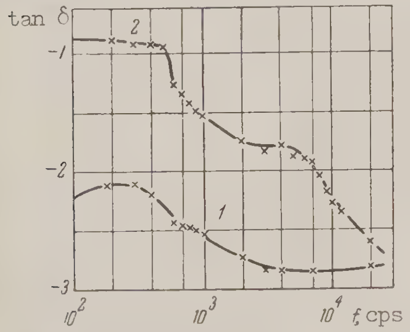

Fig.10. Variation of tan δ with frequency in CsBr crystals: 1) 140°, 2) 180°. Designations same as in Fig.1.

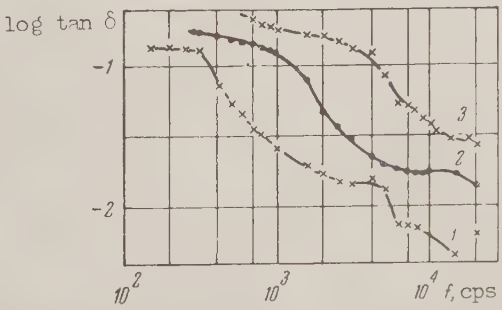

Fig.11. Variation of tan δ with frequency in crystals composed of 180 g KCl + 10 g KBr + 0.2 g AgCl: 1) 158°, 2) 181°, 3) 207°. Designations same as in Fig.1.

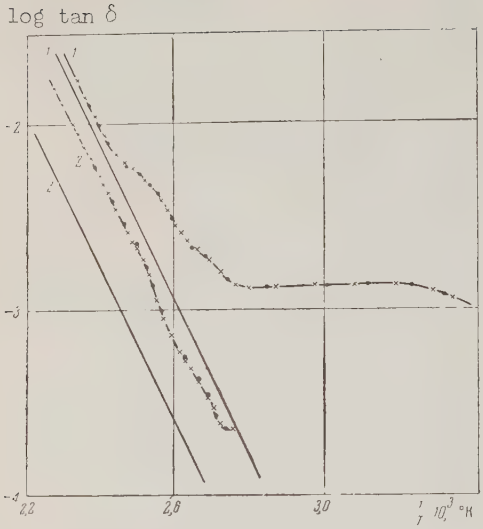

Fig.12. Variation of tan δ and γ with temperature in KCl before (1) and after (2) heat treatment, measured at 1 kc. The KCl crystal was grown in a quartz crucible. Designations same as in Fig.1.

Narasimhan[14] from a study of the temperature dependence of ϵ in LiF and NaCl crystals at 1 Mc.)

A comparison of the experimental values $\tan\delta_e$ with $\tan\delta_c$ calculated from the conductivity (represented by straight lines in the figures) for the same samples shows that at audiofrequencies and temperatures above ~50° and at high frequencies in the temperature range above ~150°, the losses are basically ohmic. The curve of $\tan\delta_c$ calculated from the conductivity always lies somewhat below the experimental curve of $\tan\delta_e$. At lower temperatures $\tan\delta_c$ is much smaller than $\tan\delta_e$. (This discrepancy is considerably reduced if we take the time dependence of the conductivity into account and calculate $\tan\delta_c$ from the initial rather than from the residual conductivity.)

At $f = 10^{10}$ cps in the temperature interval from 20 to 125° the dielectric loss in the KCl and NaCl crystals was found to be of the order of $3 \cdot 10^{-4}$. Possibly the true values are lower, but we were unable to determine this owing to the inadequate sensitivity of our equipment.

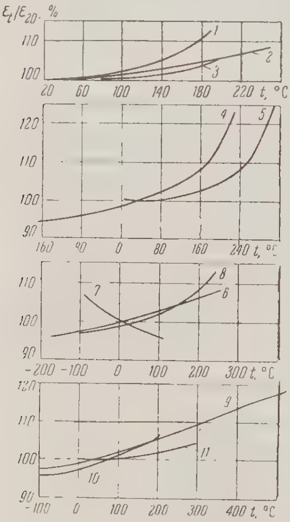

Fig.13. Variation of ϵ with temperature: 1) KBr, f = 1 kc; 2) KI+TlI, f = 1 kc; 3) CsBr, f = 1 kc; 4) KCl, f = 1 kc; 5) NaCl, f = 1 kc; 6) LiF, f = 2.5 Mc; 7) KRS-5, f = 600 kc; 8) KI+TlI, f = 850 kc; 9) NaCl, f = 750 kc; 10) KBr, f = 950 kc; 11) CsBr, f = 850 kc.

We determined tan δ for many single crystals at room temperature using the above mentioned special apparatus designed for the measurement of small dielectric losses in air. The samples were sometimes preheated and were kept in a vacuum prior to the measurements in order to minimize the effect of moisture, which, contrary to common belief, strongly distorts measurements even around 10^7 cps. In these crystals, tan δ was of the order of 3 to $5 \cdot 10^{-5}$.

Most of the hygroscopic samples, tested by means of the aforementioned apparatus, did not absorb an appreciable amount of moisture in 1 to 1.5 minutes (the time required to remove a sample from the vacuum in which it had been kept and to perform the measurements). Tan δ increased appreciably only after a few minutes.

We were unable to measure the "true" values of tan δ in highly hygroscopic samples such as KCl + KRS-5 because when these samples were taken out of the vacuum system, tan δ increased rapidly in the course of a few seconds; this effect could be observed easily with a Q-meter through measurements before and after evacuation of the system. Values of tan δ obtained in air must therefore be regarded with great caution. Otherwise one may well deduce "regularities" that are actually caused by hygroscopicity rather than by the structural characteristics of the crystals. When the hygroscopic effect is eliminated at high temperatures these same "regularities" are not observed this is easily verified through comparison of tan δ for different crystals at the same temperature and frequency.

Polarographic analysis* readily detected the 6-10% impurities by weight which had been especially introduced into the melt. Appreciable quantities of additional contaminating impurities were often detected in addition (Table 2).

Table 2

Activator concentrations determined by polarographic analysis

Batch composition	Activator	Activator concentration, %		C/C_o, %	Remarks
		in batch	in crystal		
180 g KCl + 20 g TlI	Tl	6.1	0.47	7.7	
180 g KCl + 1 g CuI	Cu	0.185	0.0048	2.6	
180 g KCl + 0.1 g PbI_2	Pb	0.16	0.018	11	
180 g KCl + 1 g PbI_2	Pb	0.25	0.025	10	
180 g KCl + 0.1 g $CdCl_2$	Cd	0.034	0.0022	6.2	
180 g KCl + 4.5 g $CdCl_2$	Cd	1.52	0.008	0.53	0.005% Tl detected in crystal
210 g KBr + 2 g TlI	Tl	0.6	0.063	10.5	
210 g KBr + 7 5 g TlI	Tl	2.1	0.12	5.7	
260 g KBr + 1 g CuI	Cu	0.12	0.00125	1.04	
270 g KBr + 1 g PbI_2	Pb	0.16	0.018	11	
270 g KBr + 0.1 g $CdCl_2$	Cd	0.024	0.0018	7.3	0.002% Tl detected in crystal
180 g KCl + 10 g KBr + 0.1 g TlI	Tl				
180 g KCl + 10 g KBr + 1 g TlI	Tl	0.32	0.029	9.0	
130 g KCl + 50 g KBr + 20 g TlI	Tl	6.1	0.37	6.05	
180 g KCl + 10 g KBr + 0.1 g CuI	Cu	0.018	0.0056	31	
180 g KCl + 10 g KBr + 1 g CuI	Cu	0.18	0.0040	2.2	
CsBr + TlBr	Tl				
KI + TlI	Tl	—	0.16	—	

According to Seitz low-temperature losses can be attributed to the presence of complexes with low activation energies and almost temperature-independent mobility.

The relaxation losses observed in crystals grown without especially introduced impurities evidently resulted from the reorientation of "pairs" of oppositely charged vacancies. Relaxation losses in doped crystals can be interpreted as follows. In addition to the single relaxation maximum produced by the existence of "dipoles" formed by pairs of oppositely charged vacancies, the presence of impurities gives rise to additional maxima due to complexes consisting of impurity ions and vacancies as well as nuclei of edge dislocations and vacancies of appropriate polarity.

The activation energies of different complexes are very close in value. It is therefore hardly possible to classify the maxima as is done by Breckenridge[3] if we take into account the strong dependence of the activation energy on the previous history of samples.[11]

In analyzing the data it is necessary to keep in mind the assumptions that were made in calculating the activation energies of different complexes theoretically.[15-20]

The dislocation mechanism can also be used to account for the experimentally observed fact that in crystals subjected to additional high temperature heat treatment tan δ and γ decrease and the relaxation peaks are smoothed out.[21]

---

*The author is indebted to Z.L.Morgenshtern and N.V.Kostina for the polarographic analyses.

In conclusion I wish to thank Scientific Director G.I.Skanavin for his interest and for a discussion of the results.

"P.N.Lebedev" Physics Institute,
Academy of Sciences of the USSR

References

1. N.P.Bogoroditskii & V.N.Malyshev, Zhur.tekh.fiz., 4, 1306 (1934).
2. R.G.Breckenridge, J.Chem.Phys., 16, 959 (1948).
3. R.G.Breckenridge, J.Chem.Phys., 18, 913 (1950).
4. Y.Haven, J.Chem.Phys., 21, 171 (1953).
5. E.Burstein, J.V.Davisson & N.Sclar, Phys.Rev., 96, 819 (1954).
6. G.Jacobs, Naturwiss., 42, 575 (1955).
7. J.Meinnel, Conf. on Defects in Crystal. Solids (Bristol, 1954), Phys. Soc. (London), 428 (1955).
8. J.S.Dryden & N.Rao, J.Chem.Phys., 25, 222 (1956).
9. M.Ishiguro, F.Oda & T.Fiyno, Phys.Rev., 95, 1347 (1954).
10. T.Suita, Phys.Rev., 94, 1497 (1954).
11. A.B.Lidiard, Phil.Mag., 46, 815; 46, 1218 (1955). Conf.on Defects in Cryst. Solids (Bristol, 1954), Phys.Soc. (London), 283, 1955.
12. S.A.Artsybashev, Zhur.eksp.i teor.fiz., 7, 903 (1937).
13. G.I.Skanavi, Fizika dielektrikov (Physics of dielectrics), M.-L. 1949.
14. P.T.Narasimhan, Proc.Nat.Inst.Sci., India, A 21, 133 (1955).
15. N.F.Mott & M.Littleton, Trans., Faraday Soc., 34, 485 (1938).
16. G.J.Dienes, J.Chem.Phys., 16, 620 (1948).
17. E.S.Rittner, R.A.Hunter & F.K.du Pré, J.Chem.Phys., 17, 198; 204 (1949); 18, 379 (1950).
18. J.R.Reitz & J.L.Gammel, J.Chem.Phys., 19, 894 (1951).
19. F.Bassani & F.G.Fumi, Phil.Mag., 45, 228 (1954); Nuovo Cimento, 11, 274 (1954); 1, 114 (1955).
20. F.Bassani & R.Thomson, Phys.Rew., 102, 1264 (1956).
21. B.N.Matsonashvili, Zhur.eksp.i teor.fiz., 31, 1110 (1956).

Discussion of the reports presented by K.A.Vodop'ianov & I.G.Vorozhtsova, K.A. Vodop'ianov & G.I.Galibina and B.N.Matsonashvili:

G.P.Mikhailov (on the report of K.A.Vodop'ianov and I.G.Vorozhtsova): The frequency range covered in the work was too narrow to allow of drawing any deductions regarding relaxation processes in mica.

G.P.Fedoseev (on the report of K.A.Vodop'ianov and I.G.Vorozhtsova): The conclusions arrived at in this report are unconvincing. The mica industry and factories making mica products have for a long time followed the practice of heating mica (the so-called "thermalizing" process). This practice is recommended for the purpose of improving the separation and cleavage of industrial mica but not for the purpose of improving its dielectric properties. Spotted muscovite contains very little limonite compared with other compounds giving rise to spottiness. Therefore there is insufficient practical value in the annealing of mica for the purpose suggested in the paper, which is the conversion of limonite into goethite.

It is also doubtful whether heat treatment can improve the quality of muscovite containing biotite to such an extent that the final mica product can be used like muscovite free of biotite. It is known that the character of heated biotite does not change so much that its dielectric characteristics approach those of muscovite. Hence there is no basis for recommending the heating of muscovite containing biotite. The authors should have paid more attention to the fact that the mechanical properties of any form of mica suffer from heating, which ultimately reduces the dielectric strength of mica and of mica insulators.

There is no sense in annealing muscovite containing limonite to obtain micanite and micalex, for the following reasons. The dielectric characteristics of micanites depend to a large extent on the quality of the binder as well as on the quality of the mica. We know that the dielectric characteristics of mica are much higher than those of the binder; micanite contains a large amount of the latter. A possible insignificant improvement of mica quality through the conversion of limonite into goethite does not effectively improve the dielectric properties of mica products. On the other hand, products made of heated mica will show considerable loss of mechanical strength.

There is also no need for pre-heating mica for the production of micalex, which is made by prolonged heating at 700-730° of a mixture of finely ground mica and special glass. Moreover, the manufacture of micalex makes use of high-grade muscovite waste from the stamping of mica parts for radio tubes and from the trimmings of high-grade capacitor mica. There is no appreciable amount of limonite in these waste products.

The paper is valuable for its explanation of the mechanism which causes variation of the dielectric constant and loss tangent in mica, but additional work is needed for convincing proof of the relaxational character of the processes occurring in mica.

G.I.Skanavi (on the reports of B.N.Matsonashvili and K.A.Vodop'ianov & G.I.Galibina): The work done by Vodop'ianov and Galibina and the work done by Matsonashvili in our laboratory disagree in two essential respects: a) Matsonashvili observed relaxation maxima of the tan δ curves for alkali halide crystals, which were not found by Vodop'ianov and Galibina; b) Vodop'ianov and Galibina state that when the lattice energy of alkali halide crystals is increased tan δ decreases at room temperature and high frequencies, whereas this behavior was not observed by Matsonashvili.

The first disagreement results from the fact that Vodop'ianov and Galibina obtained the temperature dependence of tan δ from measurements over a wide temperature range in air but not in vacuum. Therefore although the general form of the dependence was found approximately correctly (especially at high temperatures) the experimenters failed to observe the weak maxima of tan δ. It must also be noted that the relaxation maxima of tan δ were found not only by Matsonashvili but in the work of other experimenters (although the maxima observed by others were admittedly less distinct).

The second disagreement results from the fact that at room temperature the true losses in alkali halide crystals are very small, but that the hygroscopicity of many of these crystals causes a rapid rise of the losses if suitable precautions are not observed. Matsonashvili observed lower values of tan δ at room temperature than those reported by Vodop'ianov and Galibina. This favors the results of the former, because we can consider that the losses as measured by Vodop'ianov and Galibina differ greatly from the very low true losses.

At sufficiently high temperatures, the losses in alkali halide crystals are essentially ohmic, with the superposition of another type of loss. At room and at low temperatures, the value of tan δ due to ohmic loss is very small and cannot be measured by even the most sensitive apparatus. If the sensitivity of the measurements is increased by one or two orders of magnitude and if the samples are prepared with extreme care, we may find that even at low temperatures the value of tan δ for alkali halide crystals results essentially from ohmic losses and that the low-temperature portions of the curves of log tan δ vs 1/T, which are rather flat, do not reflect the true state of affairs.

M.S.Chmutin (on the reports of K.A.Vodop'ianov & G.I.Galibina and B.N.Matsonashvili): It was stated that in NaCl and KCl ϵ is almost invariable at low temperatures and that tan δ rises rapidly above 200°. Matsonashvili gave values of tan δ of the order of a few hundredths in the 200-250° region. We have measured ϵ and tan δ in NaCl, KCl and KBr using a modified Wien bridge from room temperature to 650°. Up to 300° ϵ rises linearly and TKϵ has the following values: $3.45 \cdot 10^{-4}$ in NaCl, $3.06 \cdot 10^{-4}$ in KCl and $3.15 \cdot 10^{-4}$ in KBr. Above 300° ϵ increases more rapidly especially near 640-660°. The variation of ϵ during cooling lags somewhat behind the variation during heating. The character of these changes is generally reproduced in repeated heating and cooling.

Tan δ has values of the order of hundredths at 350-400°. Above these temperatures, it increases rapidly and reaches a value of 2 to 3 at 650°. The variation of tan δ also lags somewhat during cooling.

A tentative extrapolation of tan δ to high temperatures using the data of Vodop'ianov and Galibina agrees with our experimental results. Although Matsonashvili performed his experiments with samples kept in vacuum, his results extrapolated to high temperatures yield values higher than those obtained by us.

Ia.M.Ksendzov: The lower values of tan δ, which were obtained by Matsonashvili, are more reliable.

B.N.Matsonashvili: The results obtained by Vodop'ianov and Galibina have the shortcoming that they were obtained in air and hence were influenced by the hygroscopicity of the samples, which has a strong effect even at frequencies of 10^7 cps. This is shown by the results, wherein for equal concentrations of the components the most hygroscopic samples exhibit the highest losses. With increasing frequency this effect is reduced, as might be expected. These investigators also observed a rapid rise of the dielectric loss in crystals containing large impurity concentrations. This could also result from high hygroscopicity of the crystals. In fact, it may be said that Vodop'ianov and Galibina observed the dependence of tan δ on the degree of hygroscopicity of the crystals rather than on the lattice energy.

These authors also noted that no relaxation maxima were observed in the tan δ curves. This can be accounted for by the large spread of values obtained in air and by the sparsity of experimental points. M.S.Chmutin has remarked that we obtained "excessively high" values of tan δ for some crystals and that his own measurements are in better agreement with extrapolations from the results of Vodop'ianov and Galibina. It was shown in our paper that dielectric properties depend on the previous history of the samples. Therefore one can only compare results obtained for the same or identical samples.

Finally, I wish to emphasize the special need for a comprehensive study of different properties of alkali halide single crystals (electrical, optical, mechanical and other properties), using the same uncontaminated samples.

F.I.Kolomoitsev: We can infer that there is no fundamental disagreement between the experimental results obtained in the laboratories of G.I.Skanavi and K.A.Vodop'ianov, because differences in the previous histories of the samples can result in different values of tan δ.

K.A.Vodop'ianov: The experimental procedure is a decisive factor in work such as ours and that of Matsonashvili. The technique used and the results obtained in Skanavi's laboratory cannot disprove the existence of a correlation between tan δ and the lattice energy. Skanavi's statements concerning the ohmic character of losses at low temperatures have no experimental basis. We can infer that losses in alkali halide crystals are ohmic only at very high temperatures, while at lower temperatures both ohmic and nonohmic losses occur.

With regard to the remarks made by G.P.Fedoseev I wish to emphasize that the work done by Vorozhtsova and myself did not involve the determination of the practical expediency of subjecting mica to heat treatment.

DIELECTRIC CONSTANT OF ROCK SALT AT HIGH TEMPERATURES

- M.S.Kosman & N.A.Petrova

Investigations of the dielectric constant ϵ of a number of substances at elevated temperatures has shown that this constant tends to increase with increasing temperature. For example, Chmutin[1] found that ϵ of rock salt, measured at a frequency of 10^6 cps, increases at temperatures above 400°. Most investigators assume that absorption effects in dielectrics occur so slowly that they cannot affect measurements at high frequencies; these investigators fail to take into account the fact that at elevated temperatures these processes may proceed much more rapidly. Measurements carried out by means of conventional bridge circuits do not allow of separating polarization processes from absorption effects. In the present work we investigated the dielectric constant of rock salt by a procedure that allows of such separation. The results showed that with increasing temperature the rate of absorption processes increases and that at temperatures of the order of 300° they may appreciably increase ϵ even at frequencies of only 100 cps.

Measurements

The circuit employed in our measurements is shown in Fig.1. The voltage was applied to the sample by means of the pendulum switch M. At the initial instant the sample circuit is open. The requisite voltage is set by means of a potentiometer. Upon release of the pendulum, this voltage is applied to the sample when the end of the pendulum makes contact with plate B. The charging is determined by the rate of motion of the pendulum and the dimensions of plate B; it can readily be varied from 10^{-1} to 10^{-3} sec. When the pendulum contact leaves plate B and before it touches plate A the sample circuit is open and the sample (and stray capacitance) discharges through its own resistance (self-discharge). When the end of the pendulum makes contact with plate A the sample discharges through the ballistic galvanometer with a sensitivity of $5 \cdot 10^{-10}$ coulomb mm. The self-discharge time and the discharge time of the sample could readily be varied within the same limits as the charging time.

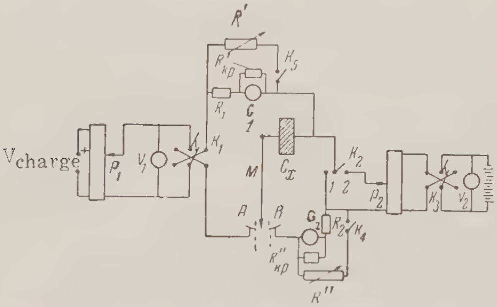

Fig.1. Set-up for measuring ϵ of crystals.

In addition to the ballistic galvanometer the voltage from an auxiliary battery, opposed to the charging voltage, could be connected into the discharge circuit. By varying the magnitude of this compensating voltage so that the throw of the galvanometer would be zero one could readily determine the voltage on the sample at the time of discharge. The dimensions of the investigated samples in most cases were such that the geometric capacitance did not exceed 20 cm and was smaller than the stray capacitance. This made accurate determination of the capacitance of the sample at low temperatures difficult and, consequently, in the present experiments such measurements were not made. At higher temperatures the resistance of the samples was reduced and during a self-discharge time of the order of 0.01 sec the stray capacitance was virtually fully discharged, while the absorption capacitance, which exceeded the geometric capacitance of the samples and the stray capacitance of the circuit, discharged little. Hence beginning with temperatures at which the resistance of the samples became equal to about 10^{-8} ohm (or under), the stray capacitances virtually did not interfere with investigation of the absorption capacitances. The principal results of our investigation of these capacitances are given below.

Experimental results

Fig.2 shows the variation of the residual differences of potential with the self-discharge time as measured for one of the samples. Curve 1 was obtained with the sample at 180°; curve 2 with the sample at 211° and curve 3 with the sample at 246°.

The charging voltage was 100 v and the charging time was $2 \cdot 10^{-2}$ sec in all three cases. It will be evident from the results that in this temperature range there is no need for shorting the sample in order to exclude the influence of the geometric (and stray) capacitance, as was done in earlier investigations[2].

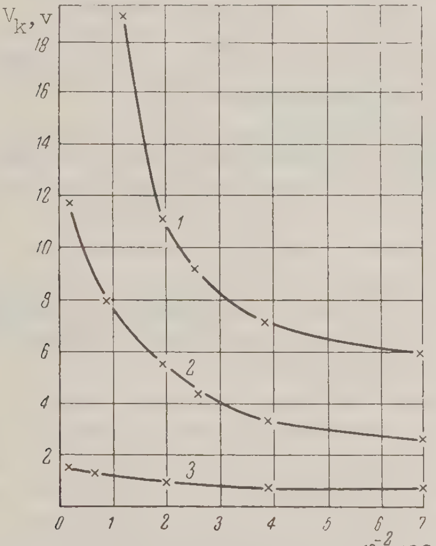

Fig.2

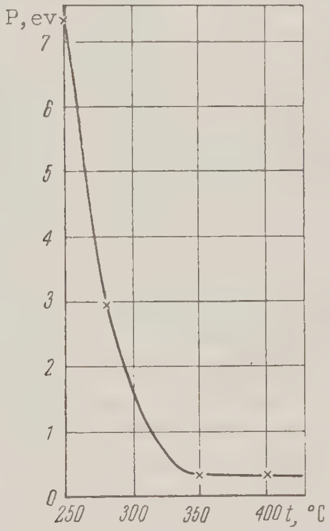

Fig.3

Fig.2. Residual potential difference V_k as a function of the self-discharge time of the sample.

Fig.3. Variation of the high voltage polarization emf (absorption emf) P with the temperature for one of the samples. Charging time $2.5 \cdot 10^{-2}$ sec; charging voltage 300 v.

The results of determination of the "high voltage" emf (it is preferable to call it the absorption emf) by the self-discharge method at different temperatures are given in Fig.3. As will be evident from the curve the polarization emf falls off sharply with increasing temperature to about 370° and then instead of going to zero remains virtually constant. The temperature region in which the sharp diminution of the "high voltage polarization" emf occurs depends on the conductivity of the investigated sample: the greater the conductivity, the lower the temperature at which the decrease begins.

Some of the other characteristics of absorption charges in rock salt are illustrated by the curves of Figs.4 & 5.

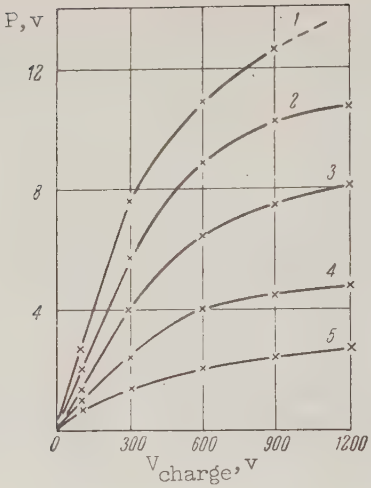

Fig.4

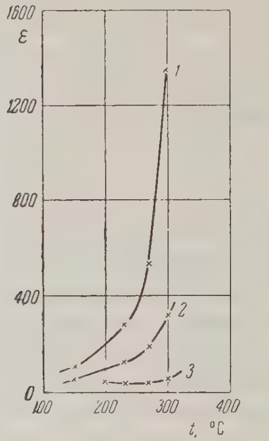

Fig.5

Fig.4. Variation of the high voltage polarization emf at different temperatures: 1) 198°, 2) 216°, 3) 238°, 4) 251°, 5) 290° C.

Fig.5 Variation of the dielectric constant with temperature. Discharge times of: 1) $t_p = 7.5 \cdot 10^{-2}$ sec, 2) $2.5 \cdot 10^{-2}$ sec, 3) $5 \cdot 10^{-3}$ sec. In all cases charging voltage = 300 v; self-discharging time = $2 \cdot 10^{-3}$ sec.

Fig.4 shows the variation of the "high voltage polarization" emf with the charging voltage for five different temperatures, with the charging time in all cases being 10^{-2} sec. In weak fields the dependence proved to be close to linear with a transition to saturation in strong fields.

Fig.5 shows the variation of the dielectric constant of rock salt, as determined from the throw of the galvanometer and the magnitude of the charging voltage, with the temperature for discharge times of $7.5 \cdot 10^{-2}$, $2.5 \cdot 10^{-2}$ and $5 \cdot 10^{-3}$ sec, which is approximately equivalent to measurements with alternating current at frequencies of 13, 40 and 200 cps. It may be seen from these curves that the effective emf due to absorption processes increases rapidly with temperature, so that the higher the temperature, the higher will be the frequency at which absorption processes can be evinced.

Discussion of results and conclusions

As the results of our experiments show, "high voltage polarization" in rock salt does not vanish at high temperatures, as has been assumed hitherto, but rather degenerates into low voltage polarization (Fig.3); it is noteworthy that the increase in the absorption capacitance with increasing temperature proceeds more rapidly than the decrease in voltage so that the absorption charges increase with increasing temperature. The rate at which absorption processes proceed increases with increasing temperature so that at sufficiently high temperatures their effect may be evinced in the high voltage characteristics. It follows that one cannot neglect absorption processes in measurements at high temperatures (without appropriate control experiments), even if the measurements are carried out at relatively high frequencies.

The nature of absorption processes in rock salt and other dielectrics has not been definitively established, but the fact that these processes are observed in all substances without exception, provided they can be heated to a sufficiently high temperature without decomposition or melting, favors the hypothesis that these are electronic rather than ionic in character.

Recently experiments have shown that the potential distribution in rock salt, contrary to established opinion, is nonlinear: potential discontinuities that give rise to absorptive capacitance, are concentrated near both electrodes. One can establish the existence of such discontinuities at high temperatures only after a certain self-discharge time of the sample, inasmuch as the magnitude of the potential discontinuities is too small for them to affect appreciably the potential distribution in the presence of a field. The existence of these discontinuities or jumps can be of practical importance inasmuch as strong fields in the vicinity of the electrodes can have an appreciable influence on ionic processes and may even give a false impression of the type of conductivity of the material.

In Fig.5 we give the effective values of ϵ calculated taking into account the magnitude of the charging voltage. The actual potential difference across the sample at the instant of discharge is much smaller. Hence one can speak of the value of ϵ calculated on the basis of this voltage. At sufficiently high temperatures, ϵ calculated in this manner proves to be exceptionally large even with a short term discharge: for example, for one of the samples at 350^o and a discharge time of $2.5 \cdot 10^{-2}$ sec, ϵ calculated in this manner proved to be $3 \cdot 10^5$. Contrary to commonly held views, these superhigh values of ϵ have a definite physical meaning: the relaxation time of charges in self-discharge of any material $\tau = \epsilon\rho/4\pi$ and, consequently, if the voltage on the sample decreases due to self-discharge by a factor of e in 100 sec with resistivity of the sample equal to 10^8 ohm/cm, this means that the dielectric constant of the sample is not less than 10^7. The values cited in the above example correspond to experimental data and are observed in the case of substances with a macroscopically linear distribution of potential (with no noticeable discontinuities at the electrodes) for which the resistivity is reliably known, for example, such as barium titanate and zirconium dioxide.

"A.I.Gertsen" Leningrad State Pedagogical Institute

References

1. M.S.Chmutin, Zhur.eksp.i teor.fiz., 26, 640 (1954).
2. O.Beran & F.Quittner, ZS.f.Phys., 64, 760 (1930).

DIELECTRIC CONSTANT OF ZINC OXIDE WITH AN ADMIXTURE OF BISMUTH OXIDE

- M.S.Kosman & I.A.Gesse

The present investigation was concerned with the electric properties of mixtures of an n-type semiconductor - zinc oxide - with a p-type semiconductor - cupric oxide, cuprous oxide or bismuth oxide. The most interesting property of such mixtures is their high dielectric constant; for example, in the case of $ZnO + Cu_2O$, ϵ may be as high as 1000 to 1500. At present many materials with a high value of the dielectric constant are known; most of them, however, contain rutile which in pure form has $\epsilon \approx 100$, while the dielectric constant of the above-mentioned oxides is of the order of 10. Our tests were concerned primarily with mixtures of ZnO and Bi_2O_3.

1. Sample preparation and experimental procedure

The samples for investigation were prepared from a mechanical mixture of the appropriate powdered materials. The samples were compressed in the form of pellets at a pressure of 10^4 kg/cm^2 and then sintered at a temperature from 800 to 1100° for 15 minutes, 1 hour and 3 hours. Either graphite or silver electrodes (applied by evaporation) were used; the results with both types of electrodes were the same. All measurements were carried out in air at atmospheric pressure and at room temperature.

Measurements of inductive capacitance by means of a bridge circuit do not give sufficiently accurate results owing to large losses. Hence in our capacitance measurements we used the procedure and set-up proposed by M.S.Kosman. The circuit is shown in Fig.1, where C is a variable air gap capacitor, C_x is the test capacitor, M is a source of square pulses, O is an oscillograph and R and R are equal resistances.

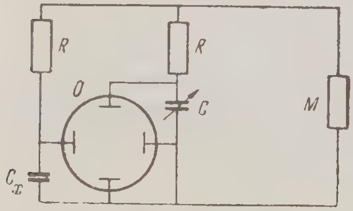

Fig.1. Diagram of set-up used for inductive capacitance measurements.

If the pulse rise time τ is less than the relaxation times of RC and RC_x, the change of potential on each pair of oscilloscope plates is determined by the change in potential on the capacitors and depends on the time constant of the corresponding circuit branch. These conditions were fulfilled in the given set-up ($\tau \approx 10^{-7}$ sec, $R \approx 10^4$-10^6 ohm, $C \approx 10^2$-10^3 cm).

When $RC = RC_x$ or $C = C_x$, the change in potential occurs at the same rate and the display on the oscilloscope screen is a straight line. If $C \neq C_x$, a loop appears on the oscilloscope screen which by appropriate adjustment of C can be transformed to a straight line. This circuit allows of measuring the capacitance of samples with an appreciable conductivity.

Measurements by means of this circuit correspond to measurements at a frequency $f = 1/RC$.

The limits of variation of the resistances R are limited, on the one hand, by the pulse rise time τ and, on the other hand, by the resistance of the sample R_x (a necessary condition is $R_x > R$, for otherwise, as can readily be shown, misleadingly low capacitance values are obtained). The accuracy of capacitance measurements by means of the described set-up is not less than 10%.

2. Results of measurement

We investigated the variation of ϵ with the Bi_2O_3 content, the temperature, and the firing time. In calculating ϵ, we used the capacitance data obtained by means of the oscillograph circuit; consequently, the values of ϵ obtained may be somewhat low (underestimates). Each value of ϵ given below is the average for a batch consisting of a number of samples prepared under identical conditions; deviations from the mean in most cases were less than 10%.

The dielectric constant of the samples did not change spontaneously with time as was shown by measurements carried out several days and five months after preparation.

The values of ϵ obtained for samples with different percentages of Bi_2O_3 fired at different temperatures for different times are listed in the accompanying table.

Dielectric constant of ZnO with different amounts of Bi_2O_3 sintered at different temperatures for different periods

Bi_2O_3, %	15 min at °C				1 hr. at °C				3 hrs. at °C		
	800°	870°	970°	1060°	800°	870°	970°	1060°	800°	870°	970°
0	20	20	10	10	20	10	10	10	20	10	10
0.5	140	175	480	660	113	170	660	1280	130	530	850
1.0	135	290	530	970	150	250	590	1100	102	530	880
3.0	127	253	620	1010	190	340	840	1180	200	500	960
5.0	280	280	760	—	222	460	750	1270	400	520	420
10	250	380	960	1220	265	390	950	1200	410	590	1190
15	346	670	920	1080	526	920	1270	—	492	700	—
20	360	560	830	960	540	760	880	—	—	—	900
30	290	570	840	820	530	730	920	—	—	—	700
40	260	—	310	—	—	—	—	—	—	—	—
50	260	—	51								

It will be obvious from the table that ϵ is strongly dependent on the Bi_2O_3 concentration in the mixture. The Bi_2O_3 content was varied over a wide range, but it was found that mixtures containing over 30% Bi_2O_3 tended to fuse during heating.

Even under conditions of "weak" sintering (heating for 15 minutes at 800°C) the addition of 0.5% Bi_2O_3 to pure ZnO increases ϵ from 10 to ~120. The dielectric constant continues to increase up to a Bi_2O_3 concentration of about 20%. Then, with further increase in Bi_2O_3 concentration, ϵ begins to decrease slightly. This variation of ϵ with Bi_2O_3 concentration is in general characteristic for all sintering conditions. It will be noted from the table, however, that with increasing sintering temperature the maximum value of ϵ occurs in samples with a lower Bi_2O_3 concentration (Fig.2).

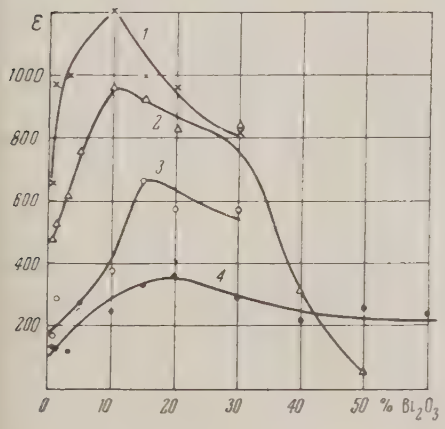

←Fig.2. Variation of the dielectric constant with the Bi_2O_3 content of zinc oxide samples sintered for 15 minutes. Sintering temperatures: 1) 1060°, 2) 970°, 3) 870°, 4) 800°.

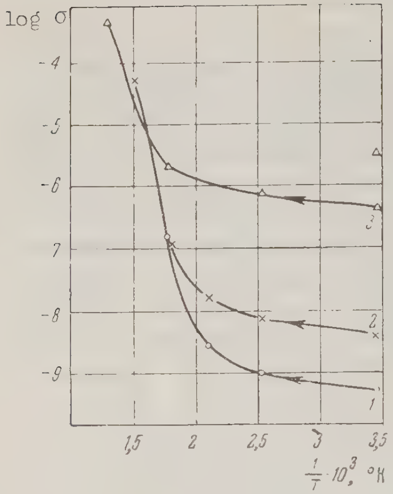

Fig.3. Variation of the conductivity σ of a sample with the heating temperature: 1) to 300°, 2) to 390°, 3) to 500°. Arrows indicate the direction of the process.

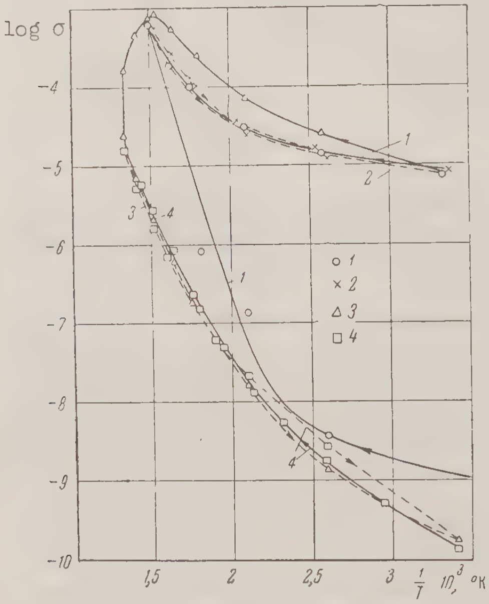

Fig.4. Variation of the conductivity of a sample with the cooling conditions: 1 & 2) heating to ~400° followed by rapid cooling; 3 & 4) heating to ~500° followed by slow cooling. The arrows indicate the direction of the process.

The data in the table also show that the dielectric constant is strongly dependent on the sintering temperature, the increase with increasing sintering temperature being more marked for samples with a lower Bi_2O_3 content. (Samples fired at temperatures above ~1100° have so low a resistivity that their dielectric constant cannot be measured.

Increasing the sintering time also tends to increase the dielectric constant.

The capacitance of samples having a resistance greater than 10^7 ohm was measured not only on the oscillograph set-up but by means of a UM-2 bridge. It was found that for many samples ϵ was frequency independent in the range from 10^3 to 10^6 cps. In the case of some samples ϵ decreased with increasing frequency. No correlation between the sintering conditions and the frequency dependence was observed.

The addition of Bi_2O_3 to ZnO also changes some of the other electric properties of the material: in addition to an increase of ϵ, there is observed a decrease of conductivity as compared with that of pure ZnO. This decrease may attain 3-4 orders of magnitude: thus, for example, the addition of 0.5% Bi_2O_3 reduces the conductivity of ZnO from 10^{-4} mho/cm to 10^{-8} mho/cm. However, the resistivity of none of the specimens became so great that they could be classed as true dielectrics and utilized for practical purposes.

At room temperature the resistance of the samples remains constant over a long period (months), but it can readily be changed by heat treatment. The extent of change in resistance depends on the initial state, the heating temperature and the cooling conditions. In general, the higher the heating temperature, the greater the change in conductivity. Fig.3 shows the change in conductivity of a sample after heating to 300, 390 and 500°, followed by rapid cooling. After heating to 400-700° and rapid cooling, the conductivity may be increased 4-5 orders of magnitude. This new state is also stable and persists indefinitely at room temperature.

By repeat heating to the same temperature followed by slow cooling, one can return the sample to the initial low conductivity state. The influence of cooling conditions is shown in Fig.4. Curves 1 & 2 pertain to heating to ~400° and rapid cooling; curves 3 & 4 were obtained after heating to ~500° and slow cooling.

Regardless of the mode of treatment, however, we were not able to reduce the conductivity of the samples to less than 10^{-10} mho/cm.

In all probability the variation in conductivity is connected with the influence of oxygen. Presumably, in heating the ZnO is partially decomposed and in the case of rapid cooling the excess Zn atoms do not have time to oxidize. It must be noted, however, that this simple mechanism does not fully explain all the variations in conductivity observed incident to heat treatment.

Changes in conductivity incident to heat treatment are accompanied by changes in inductive capacitance: an increase in conductivity is accompanied by an increase in capacitance and vice versa. Conductivity of the ZnO plus Bi_2O_3 samples was of the n-type (determined from the sign of the thermo-emf).

At present we can only speculate regarding the nature of the large dielectric constant exhibited by samples of ZnO with Bi_2O_3.

The samples showed no dependence of ϵ on the voltage and no piezoelectric effect. It may be inferred therefore that the ZnO plus Bi_2O_3 mixture is not ferroelectric.

X-ray diffraction studies showed that up to 15% Bi_2O_3 content, the mixture retains the ZnO lattice. Weak frequency dependence of ϵ in the frequency region above 10^3 cps would appear to disprove the hypothesis that the high value of the dielectric constant is due to insulating layers between the individual crystallites. The possibility is not precluded that the high value of ϵ is associated with relaxation processes of an electronic character. Indirect evidence in favor of this assumption is furnished by the observed parallelism in the variation of the capacitance and the conductivity as a result of heat treatment.

It is possible that these processes are analogous to the effects observed by Ia.M.Ksendzov in TiO_2 with small amounts of impurities. This hypothesis, however, requires further verification.

"A.I.Gertsen" State Pedagogical Institute

DIELECTRIC CONSTANTS OF BISMUTHATES OF SOME METALS

- A.M.Kashtanova & G.I.Skanavi

Chemically bismuth trioxide, Bi_2O_3, has weakly pronounced basic properties. These properties are evinced both in solutions, where Bi^{3+} ions are present, and at high temperatures. Until now, there have been no reports of compounds in which Bi manifested acid properties. It is known that acid-basic properties of some elements such as Al, Cr, Cu and Zn, in many cases, are determined by the influence of the "other" component, i.e., depending on the medium, these elements may enter into compounds either as anions or as cations.

We made an attempt to obtain by sintering compounds which by analogy with titanates may be called bismuthates, i.e., compounds prepared from a batch consisting of equimolar proportions of Bi_2O_3 and oxides with strongly pronounced basic properties as well as from mixtures of Bi_2O_3 with such oxides as CuO, ZnO and Al_2O_3.

We succeeded in obtaining well-sintered ceramic specimens with an internal porosity not exceeding 5% by firing bismuth trioxide with the oxides of Be, Mg, Ca, Zn, Sr and Ba.

The bismuthates were prepared in the following manner. The appropriate chemically pure initial products were thoroughly dried and very finely powdered. The barium oxide was obtained from the appropriate hydroxide. CaO and SrO were obtained by heating the corresponding carbonates. The powder mixtures of the initial components were stirred with ethyl alcohol to form a paste. The samples were fired in a Silit furnace on a bed of Al_2O_3. The sintering temperature for bismuthates is lower than the sintering temperature for the corresponding titanates and lies in the range from 700 to 900°. Technologically, the sintering of bismuthates is more difficult inasmuch as the sintering interval is only about 10°. The sintering interval can be widened somewhat by the introduction into the batch of 2 to 4% of such oxides as ZrO_2 and Al_2O_3. The Debye diffraction patterns of Ca, Zn, Sr and Ba bismuthates are very complex and entirely different from the x-ray diffraction patterns obtained from the initial products. The Debye diffraction patterns of Be and Mg bismuthates do not contain the lines characteristic of Be and Mg oxides. The Debye patterns of Be and Mg bismuthates as regards the number of lines almost fully coincide with the pattern obtained for Bi_2O_3; however, the intensities of some of the lines differ.

The dielectric properties of the bismuthates were investigated by means of an audiobridge and a Q-meter. The data on the dielectric properties and resistivity of our bismuthates are listed in the accompanying table.

Dielectric constant, loss tangent and resistivity of different bismuthates

Composition	Firing temp. °C	Firing time, min.	f = 1 Mc; t = 20°		ρ_{av}, ohm·cm
			ε_{av}	tan δ_{av}	
$ZnO \cdot Bi_2O_3$	770	50	76	0,005	$5 \cdot 10^9$
$BaO \cdot Bi_2O_3$	775	15	32	0,03	$2 \cdot 10^{10}$
$BeO \cdot Bi_2O_3$	820	90	28	0,0003	$3 \cdot 10^{11}$
$CaO \cdot Bi_2O_3$	870		25	0,005	$7 \cdot 10^{12}$
$MgO \cdot Bi_2O_3$	760	30	22,5	0,0005	$3 \cdot 10^{12}$
$SrO \cdot Bi_2O_3$	850	90	17	0,02	$5 \cdot 10^{11}$

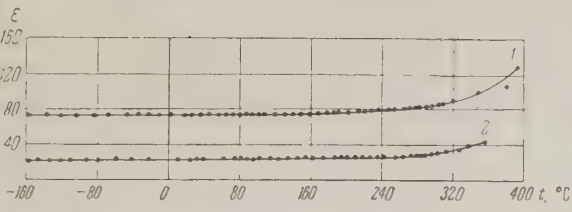

Fig.1. Temperature dependence of the dielectric constant of bismuthates measured at a frequency of 1 Mc: 1) $ZnO \cdot Bi_2O_3$ and 2) $BeO \cdot Bi_2O_3$.

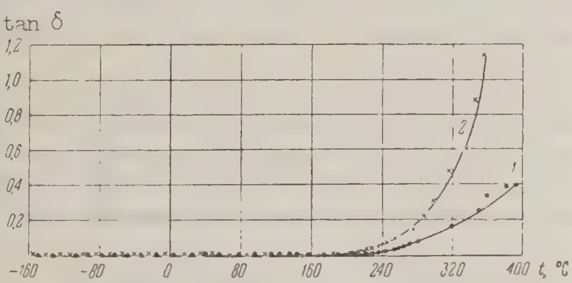

Fig.2. Temperature dependence of the dielectric loss tangent measured at 1 Mc: 1) $ZnO \cdot Bi_2O_3$ and 2) $BeO \cdot Bi_2O_3$.

Bismuthates are characterized by a high value of the dielectric constant, which decreases somewhat with frequency. The dielectric constants of Be, Mg and Zn bismuthates are somewhat greater than the dielectric constants of the corresponding titanates. In general these ceramics have a relatively high resistivity, the values lying in the range characteristic of good dielectrics (an exception is Zn bismuthate).

In contrast to titanates and rutile, bismuthates have a positive $TK\varepsilon(\frac{1}{\varepsilon} \cdot \frac{d\varepsilon}{dT})$ characteristic. The temperature dependences of ϵ and tan δ of Zn and Be bismuthates measured at a frequency of 1 Mc in the temperature range from -160 to +400° are shown in Figs.1 & 2. The value of $TK\varepsilon$ of bismuthates is relatively large (for example, in the case of Be bismuthate, $TK\varepsilon$ in the temperature range from -160 to +300 is $4 \cdot 10^{-4}$, while for Zn bismuthate the corresponding value is $3 \cdot 10^{-4}$).

No hysteresis loops were observed in investigating the variation of the charge on the plates of the test capacitor as a function of the voltage applied to the bismuthate sample. The explanation of the high value of the dielectric constant must await determination of the structure of bismuthates and accumulation of more extensive data on the temperature and frequency dependences of ϵ and tan δ.

"P.N.Lebedev" Physical Institute
Academy of Sciences of the USSR

INFLUENCE OF GRINDING ON THE DIELECTRIC PROPERTIES OF POLYCRYSTALLINE BARIUM TITANATE

- G.M.Kovalenko

Introduction

Many of the recent advances scored by science and technology would have been impossible without the aid of high-speed computers. Within the last decade Soviet scientists have created a number of new types of such machines. The computer known in the literature as the BESM, designed under the supervision of Academician S.A.Lebedev, performs 7-8 thousand arithmetic operations in 1 second. Modern computers are actually a complex of several separate units: a) the data storage unit ("memory"), b) a data reduction unit that performs the mathematical operations, c) a controlling section and d) data input and output units.

As time goes on each of these individual units and, consequently, computers as a whole, are being improved and simplified. Thus for example the first electronic computer, the ENIAK, was very bulky, consumed a great deal of power and had about 18,000 vacuum tubes, while modern computers employing semiconductor and magnetic components occupy much less space and require considerably less power.

Recently there has been considerable discussion in the literature[1] regarding the possibility of using ferroelectric materials, including polycrystalline ones, as memory components. Ferroelectric materials intended for such purposes must meet a number of special requirements (have a rectangular hysteresis loop, low coercivity, etc.). One of these requirements is that polarization processes in the material must occur at relatively low electric field intensities; this can be attained by reducing the thickness of the material.

Research has been carried on in the Electrophysical Laboratory of the "P.N.Lebedev" Physical Institute of the USSR Academy on the possibility of using certain polycrystalline ferroelectrics as memory components. Samples with a thickness of the order of 0.01-0.02 cm were obtained by grinding down from an initial thickness of 0.05-0.1 cm. In the course of the study it was noted that specimens obtained in this manner have certain distinctive characteristics.

Below we give the experimental results obtained for $BaTiO_3$ and propose a qualitative explanation of the observed effect.

Description of specimens

The polycrystalline ferroelectric ceramics were prepared by the conventional technological procedure. According to the requirements for memory components the ferroelectric specimens should be fairly uniform over the entire area and have a thickness of 0.01-0.02 cm. Inasmuch as such plates of polycrystalline ferroelectrics cannot always be directly obtained by sintering, we initially prepared specimens 0.05-0.1 cm thick and reduced them to the requisite thickness by grinding. The specimens had the form of discs about 1 cm in diameter. The silver electrodes were fired on and had an area of about 0.75 cm^2 (electrodes were applied a small distance in from the edges of the specimen).

Measurement procedure and results

The dielectric hysteresis loops were recorded for all specimens on a Sawyer-Tower set-up[2]. We then calculated the values of the maximum and spontaneous and residual polarizations and the values of the coercive force and rectilinearity coefficients. Since, as is known, dielectric hysteresis loops attain a stable shape only after the passage of some time, all the dielectric hysteresis loops were recorded 30 minutes after applying the electric field. We investigated the loops of specimens having thicknesses of 0.2, 0.1, 0.05, 0.02 and 0.01 cm. It was found that specimens with thickness of 0.01, 0.02 and 0.05 cm have an appreciably lower polarization than thicker specimens at the same field intensity (6 kv/cm) - see curve 1 in the accompanying figure.

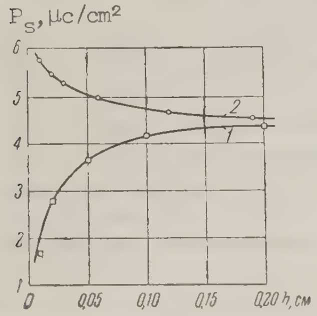

Variation of the spontaneous polarization P_s with the thickness h of the $BaTiO_3$ specimen: 1) ground, 2) not ground.

For purposes of control and comparison we prepared specimens of the same mass and approximately the same thicknesses directly by sintering, i.e., without grinding. Curve 2 shows that for these specimens as the thickness is reduced the quality is not only not impaired but on the contrary is somewhat improved. This effect can be understood if we take into account the fact that in both cases we were dealing with triple layer dielectrics: in the case of ground specimens the electrodes are applied to surfaces subjected to grinding, while in the case of unground specimens they are applied to "fire-polished" surfaces having a dense fine-crystalline structure. In both cases between these superficial layers there is an intermediate layer of similar material.

Obviously, the presence of these surface layers, which are characterized by different values of the dielectric constant, in one case reduces and in the other case increases the effectiveness of the electric field. Polishing with fine (NO.240) emery and heating of the ground specimens to temperatures close to the sintering temperature diminishes but does not entirely remove the influence of grinding.

Conclusions

1. It was established that grinding of polycrystalline specimens of $BaTiO_3$ having thicknesses of 0.2, 0.1, 0.05, 0.02 and 0.01 cm has the effect of reducing the polarization as we progress to thicknesses of 0.05 cm and less.

2. It was established that specimens of the same thickness and mass with "fire polished" surfaces (not ground) exhibit a noticeable increase in polarization as one goes to thinner specimens.

I take this occasion to thank A.M.Cherepanov under whose supervision the specimens were prepared and S.V.Bogdanov for discussion of the experimental results.

References

1. F.Charles & Pulvari, Proc.Western Computer Conference, 140-149, N.Y., Feb., 1953.
2. C.B.Sawyer & C.H.Tower, Phys.Rev., 35, 269 (1930).

DIELECTRIC LOSS AND POLARIZATION IN POLYMERS (Abstract*)

- G.P.Mikhailov & A.M.Lobanov

1. Investigation of dielectric loss and polarization in a wide range of frequencies and temperatures showed that these properties are mainly associated with relaxation effects.

2. From observation of the electric, mechanical and other properties it was established that polymers can exist in three physical states: glass-like, ultra-elastic and viscous-fluid.

3. Investigation of the dielectric losses in polymers in the glass-like and ultra-elastic states showed that these losses are characterized by a number of distinctive features. For example, where the losses observed in the ultra-elastic state are concerned, the relaxing element may be a segment, i.e., a group of monomeric links of the main chain; in the glass-like state the relaxation element may be a monomer link or a side group of atoms in the macromolecular chain.

4. Accordingly, in determining the relaxation times from temperature-frequency dependences of the losses, both dielectric and mechanical, there is not infrequently observed a correlation between the two series of values.

5. Polymers, both synthetic and natural, as regards structure may be crystalline or amorphous. The specific characteristics of the frequency and temperature dependence of the losses and polarization naturally depend on whether the material is crystalline or amorphous. Some polymers, such as for example, polyethylene tetraphthalate and polytrifluoroethylene, etc. can exist either in the crystalline or in the amorphous state.

6. Crystallization sharply reduces the dielectric loss associated with segmental thermal motion. On the other hand, the relaxation dielectric loss, associated with thermal motion of the monomer links or polar radicals changes little with crystallization.

7. Determination of the effective dipole moments of monomer links in polymer macromolecules showed that the theories developed for monomer systems are applicable to calculation of the polarization of polymers.

8. The values of the effective dipole moments, calculated per monomer link of a polymer molecule, indicate that the predominate change in the value of this moment is due to intramolecular interaction.

Institute of High Molecular Compounds,
Academy of Sciences of the USSR

---

*The more important aspects of the work covered by the present report are described in the article by G.P.Mikhailov in Usp.khim., 23, 875 (1955).

THEORY OF DIPOLE MOMENTS OF POLYMER MOLECULES (Abstract*)

- O.B.Ptitsyn, T.M.Birshtein & Iu.A.Sharonov

1. We proposed a theory of dipole moments of polymer molecules that relates the mean square dipole moment of polymer chains with their chemical structure, stereoisomerism and suppression of internal rotation. The theory pertains to polymers of the types $(\text{-Cr}_2\text{-})_n$, $(\text{-CH}_2\text{-CR}_2\text{-})_n$, $(\text{-CH}_2\text{-CHR-})_n$ and $(\text{-CHR-})_n$, where R is the polar pendant group.

In addition to the first approximation of the theory taking into account only interaction between neighboring groups of chains, we have derived a second approximation taking into account interaction between more widely separated groups.

2. We show that the dipole moment is strongly dependent on the stereoisomerism of the chain: for chains of the $(\text{-CH}_2\text{-CHR-})_n$ type and particularly of the $(\text{-CHR-})_n$ type with rigidly attached dipoles, the dipole moment is appreciably smaller with the *dl-* than with the *dd-*arrangement of the polar groups (under equal conditions of internal rotation in the chain). We also show that in chains of the $(\text{-CH}_2\text{-CHR-})_n$ type with rigidly attached dipoles, the dipole moment depends on which pendant groups - polar or nonpolar - repel each other more strongly (in the former case the dipole moment is appreciably smaller than in the latter). If internal rotation is realized in the polar pendant groups, the dipole moment in the first approximation does not depend on the chain structure.

3. Comparison of the theory with experimental data on poly-p-halogenostyrenes and polyvinyl chloride shows that in the chains of these polymers the phenyl groups or chlorine atoms repel each other more strongly than the hydrogen atoms. The degree of suppression of rotation in these polymers as determined from the experimental data on the dipole moments is approximately in agreement with the data obtained from evaluations of molecular dimensions and the photoelastic effect.

Institute of High Molecular Compounds,
Academy of Sciences of the USSR

---

*For more details, see T.M.Birshtein & O.B.Ptitsyn, Zhur.tekh.fiz., 24, 1998 (1954) and O.B.Ptitsyn & Iu.A.Sharonov, Zhur.tekh.fiz., 27, 2744 (1957).

DIELECTRIC LOSS IN CRYSTALLINE NON-POLAR POLYMERS

- S.P.Kabin & G.N.Mikhailov

Polyethylene is the high molecular product of polymerization of ethylene in the presence of a suitable catalyst.

A polyethylene molecule is essentially a more or less branched chain of successively linked CH_2 groups. Polyethylene owes its ability to crystallize to the presence of appreciable sections with linear structure. Owing to the presence of crystallites, that melt completely only at temperatures of 110 to 140°, objects fabricated of polyethylene are resistant to plastic deformation in a wide temperature range. On the other hand, the presence of amorphous sections enables polyethylene to maintain its elasticity down to temperatures of about -70°. These characteristics in conjunction with high chemical stability and low dielectric loss make polyethylene invaluable in many industrial fields.

The number of practical applications of polyethylene is constantly increasing; it is used for household wares, in medicine, for preparing corrosion resistant balloon envelopes, as an insulating material for high frequency cables (where it often replaces much more expensive coatings), etc.

The purpose of the present report is to give the results of an investigation of the dielectric properties of non-polar crystallizing polymers: polyethylene and teflon (polytetrafluoroethylene)[1]. These results are not only of practical value but also of scientific interest inasmuch as both these polymers are typical representatives of the class of crystallizing polymers, the regularities and characteristics of which often differ substantially from those of amorphous substances.

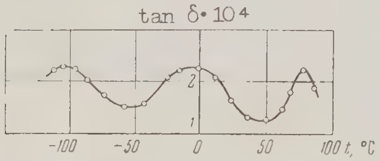

Fig.1. Temperature dependence of the dielectric loss tangent of polyethylene measured at a frequency of 50 kc.

The investigations of Refs.2-5 were concerned with the dielectric properties of polyethylene at different frequencies and at different temperatures as a function of its structure.

The temperature dependence of tan δ of polyethylene at a frequency of 50 kc is shown in Fig.1. It will be evident from the curve that in the case of this polymer we observe three relaxation dielectric loss regions of the type usually associated with the presence of polar radicals in the polymer macromolecules. With increasing temperature, these loss maxima are displaced so that at $t = 20^{\circ}$ the most probable relaxation times have values of $\tau_1 = 10^{-2}$ sec, $\tau_2 = 10^{-5}$ sec and $\tau_3 = 10^{-9}$ sec. As was noted in a previous contribution by one of the present authors[6], amorphous polymers (such as those of the polyvinyl acetate series) are characterized by only two relaxation loss regions. One is observed in the interval of high elasticity of the polymer; the other in the region below the temperature of vitrification. In crystalline polyethylene we observe the presence of a third region of losses which have come to be called low frequency relaxation losses.[4,5] A series of experiments was carried out with a view to clarifying the nature of these losses; the results of these experiments are described in Ref.3.

Fig.2. shows the temperature dependence of tan δ obtained for polyethylene rapidly cooled from the molten state, i.e., with a low degree of crystallinity. It will be evident that there is no low frequency relaxation loss where this polymer is concerned. This loss appears upon slow cooling of polyethylene from the molten state. At the same time there is evident an increase in the medium

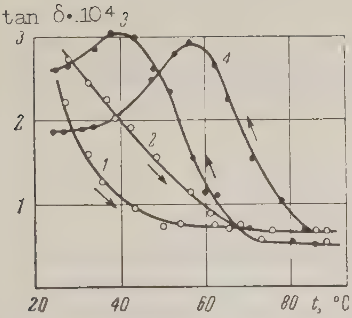

Fig.2. Temperature dependence of the dielectric constant measured at a frequency of 10 kc for polyethylene rapidly cooled from the molten state. The arrows show the direction of change in temperature. The curves pertain to two different samples.

frequency relaxation loss ($\tau_2 = 10^{-5}$ sec at $t = 20^{\circ}$). In view of the above, it may be hypothesized that the low frequency relaxation loss is due to polar radicals linked with those amorphous sections whose state changes substantially with changes in the degree of crystallinity.

As is known, the monomer link of the polyethylene molecule is non-polar. Yet, as was noted above, the polyethylene exhibits relaxation dielectric losses associated with the presence of polar radicals. Cross et al[7] investigated the infrared absorption spectrum of polyethylene subjected and not subjected to heat treatment. They found that the number of polar C═O radicals in the molecule increases with oxidation of the polyethylene. No other significant changes were detected.

It was shown in the investigations of Refs. 2 & 4 that as a result of heat treatment of polyethylene the relaxation dielectric losses increase in magnitude without changing their position as regards frequency and temperature. From this it may be assumed that the relaxation dielectric losses in polyethylene are due to the presence of polar C═O radicals, a small number of which may enter during polymerization into the polyethylene molecule, particularly, if the polymerization process is carried out at elevated temperatures in the presence of oxygen.

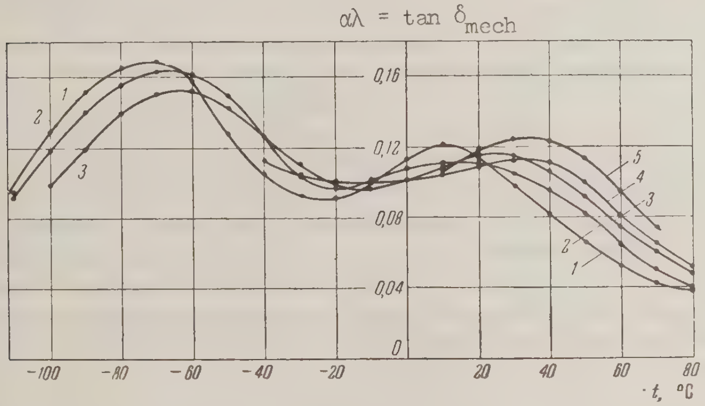

Fig.3. Temperature dependence of $\alpha\lambda = \pi \tan \delta_{mech}$ for polyethylene.

For the purpose of more detailed investigation of the nature of the dielectric losses in polyethylene, we carried out measurements of the mechanical losses in this polymer in the range of ultrasonic frequencies. Measurements were carried out by the pulse method in a liquid bath. From the change in the amplitude of the ultrasonic impulse of the longitudinal mechanical vibrations after passage through the sample, we calculated the amplitude absorption coefficient α. The velocity v of sound in the polyethylene could be calculated from the delay of the pulse passing through the sample. The mechanical loss tangent was calculated by means of the formula

$$\tan \delta_{mech} = \frac{\alpha v}{\pi f}$$

where f is the frequency of the ultrasonic vibrations.

Fig.3 shows the temperature dependence of $\alpha\lambda = \pi \tan \delta_{mech}$ for polyethylene. It will be seen from the curves that where mechanical losses are concerned, in this case there are observed two relaxation loss regions, which as regards position in the temperature scale are analogous to the high frequency and medium frequency relaxation dielectric losses.

Fig.4 shows the variation of log f_{max} with 1/T for the mechanical and dielectric losses in polyethylene. It will be evident from the curves that the relaxation times for both mechanical and electrical losses are well characterized by the relationship

$$\frac{1}{\tau} = f_{max} = f_o \cdot e^{-U/RT}$$

where f is the frequency corresponding to the maximum loss, U is the activation energy, R is the universal gas constant and T is the absolute temperature. This shows that in a given case the polar radicals are linked with the sections of the macromolecule of the polymer whose motion also determines the mechanical relaxation losses. The values of the activation energy for the low frequency, medium frequency and high frequency relaxation losses are $U_1 = 25$ Kcal/mole, $U_2 = 16$ Kcal/mole and $U_3 = 11$ Kcal/mole, respectively.

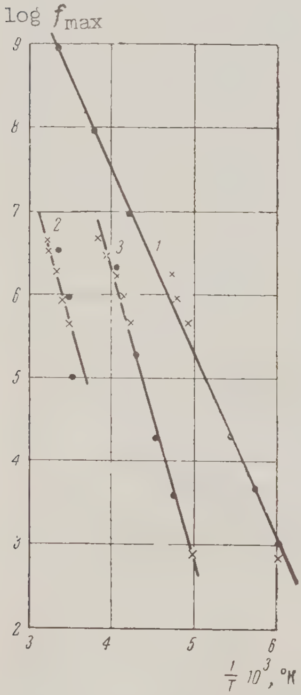

Fig.4. Variation of log f_{max} as a function of 1/T for polyethylene (curves 1 & 2) and teflon (curve 3). Solid points - data for dielectric losses; crosses - mechanical losses.

Another crystallizing non-polar polymer is teflon. This polymer combines high dielectric properties elasticity and chemical inertness with exceptionally high heat stability (up to 350°), which makes it irreplaceable in certain special cases. Production of this polymer is, however, at present limited in view of its high cost. The results of our investigation of the dielectric properties of teflon are given in Ref.8. It was found in this investigation that only one relaxation dielectric loss region is observed in teflon in the temperature range from -60 to +300°. The dielectric losses were found to decrease with increasing degree of crystallinity of the polymer. This gave reason to assume that the relaxation dielectric losses are associated with a small number of polar radicals entering into the amorphous regions of the teflon macromolecules. This assumption is substantiated by the fact that the relaxation times for the mechanical and dielectric losses in teflon are virtually identical.

Conclusions

Investigation of the dielectric properties of the non-polar crystalline polymers, polyethylene and teflon (polytetrafluoroethylene) showed the following:

1. In both polymers there are observed relaxation dielectric losses associated with extraneous polar radicals entering into the polymer macromolecule.

2. In the case of polyethylene there are observed three relaxation processes, which distinguishes this polymer from amorphous polymers.

3. The magnitude of the medium frequency relaxation loss increases with decreasing degree of crystallinity of the polymer, while the magnitude of the low frequency relaxation loss decreases.

4. In both polyethylene and teflon the relaxation processes are evinced

at frequencies from 10^4 to 10^7 cps and can be characterized by identical relaxation times and one and the same activation energy for mechanical and dielectric losses. This equality of the relaxation times and activation energies substantiates the hypothesis that a common molecular mechanism underlies the dielectric and mechanical relaxation processes.

"M. I. Kalinin" Leningrad Polytechnical Institute
and
Institute of High Molecular Compounds,
Academy of Sciences of the USSR

References

1. A.I.Dintses & I.P.Losev, Usp.khimi, 20, 430 (1951).
2. G.P.Mikhailov & T.I.Borisova, Zhur.tekh.fiz., 12, 2154 (1953).
3. G.P.Mikhailov, A.M.Lobanov & B.I.Sazhin, Zhur.tekh.fiz., 24, 9 (1954).
4. G.P.Mikhailov, S.P.Kabin & B.I.Sazhin, Zhur.tekh.fiz., 25, 4 (1955).
5. G.P.Mikhailov, B.I.Sazhin & S.P.Kabin, Vestnik, Leningrad Polytechnic Institute, 81, 1955.
6. G.P.Mikhailov, Usp.khimi, 24, No.7 (1955).
7. Cross, Richards & Willies, Disc.Faraday Soc., 9, 30 (1952).
8. G.P.Mikhailov, S.P.Kabin & A.L.Smolianskii, Zhur.tekh.fiz., 25, 12 (1955).

DISCUSSION FOLLOWING THE REPORTS OF G.P.MIKHAILOV & A.M.LOBANOV AND C.P.KABIN & G.P.MIKHAILOV

M.P.Tonkonogov: The work of Professor Mikhailov's group is a very complete and exhaustive investigation of dielectric losses in polymers. The experimental results can be qualitatively explained on the basis of the theory of Debye & Kirkwood, which allows of carrying out quantitative evaluations (for example, calculating the dipole moments of molecules). It would, however, be more consistent and fruitful to apply to polymers the kinetic equation for orientation of dipoles in an external field, regarding which we heard in the report by Comrade Liast. For crystals, solution of this equation in the first approximation allows of finding tan δ, which in this case depends not only on the frequency, temperature, and molecular constants but also on the number of dipoles per unit volume and on the number of vacant sites per unit volume. The results (i.e., solution of the kinetic equation) allow of explaining the following experimental facts which formerly seemed puzzling.

1. If there is superposed on the process of dielectric relaxation a process of degradation, the maximum in the temperature dependence of the loss angle with increasing frequency may be displaced, under certain conditions, to the side of lower temperatures (experiments of A.P. Izergin with crystal hydrates). This effect can be explained if we bear in mind that in the hydration of crystal hydrates the number of dipoles per unit volume decreases, while the number of vacant sites increases. Because of the surposition of these two competing factors, the maximum in the temperature dependence of the loss angle may with increasing frequency be displaced to the side of lower temperatures; it is also possible for the maximum to be evinced at one and the same temperature with increasing frequency. This effect, however, has not been observed. It may eventually be manifested in the experiments described in the report of K.A.Vodop'ianov and I.G.Vorozhtsova.

2. It is known that the dielectric constant of inorganic crystals containing polar molecules changes little with frequency and temperature in the region of the loss angle maxima. Rigorous calculations show that the part of the dielectric constant that is due to orientation effects is very small; changes in this part amount to only an insignificant part of the total value of the dielectric constant.

G. I. Skanavi (on the report of Kabin & Mikhailov): It is regrettable that the procedure of measuring very small losses (of the order of 10^{-5}) was not employed in the work. The authors were therefore forced to investigate the losses in polytetrafluoroethylene (teflon) only in a very narrow temperature interval close to the relaxation maximum. It must be noted, however, that the discovery of relaxation maxima of $\tan \delta$ in teflon is in itself of great interest.

PREPARATION AND PROPERTIES OF NEW ELECTRETS OF INORGANIC DIELECTRICS

- A.N.Gubkin & G.I.Skanavi

1. Over 60 different dielectrics have been investigated from the standpoint of the possibility of obtaining them in the form of electrets; for the most part the dielectrics studied have been organic substances: waxes, rosins, hydrocarbons, different types of rubber, polymers, solid acids and alcohols, etc.[1-6]

Inorganic substances have been far less extensively studied from this viewpoint and what information we have on them is often conflicting. There have been investigations of glass, sulfur, naphthalene, calcium sulfate, sodium chloride and a few other substances.[4,5,7] At the 1953 annual meeting of the American Physical Society, Thickens & MacDonald[8] presented a report on the electret-like behavior of barium titanate ceramic polarized in an electric field. However, the authors tend to associate the observed effect with the ferroelectric properties of $BaTiO_3$.

Hitherto no one had undertaken the preparation and investigation of the properties of electrets of inorganic polycrystalline dielectrics (so-called ceramic dielectrics) not possessing ferroelectric properties.

Most of the known electrets are prepared of dielectrics containing polar groups and the heterocharges in these are apparently due to "frozen" dipole polarization. An obvious question is whether one can prepare an electret from an ionic dielectric and what would be the properties of such an electret? Furthermore, it would seem to be of interest to investigate the possibility of preparing stable electrets in general and to investigate the factors affecting this stability. No less interesting is the question of the maximum possible value of the charge of an electret and the possibility of experimentally determining the magnitude of the heterocharges and homocharges* separately. These are some of the questions we sought to answer in undertaking this investigation, whose primary purpose was to prepare electrets of inorganic dielectrics not containing polar groups and to investigate their properties.

2. We investigated the following polycrystalline dielectrics with different values of the dielectric constant: magnesium, calcium, strontium, zinc, bismuth and strontium-bismuth titanates, barium metatitanates and barium tetratitanate, steatite and porcelain (type M-23). In addition to these polycrystalline materials, we investigated a number of solid amorphous and single crystal dielectrics, namely, KBr single crystals, ordinary glass, pyrex glass and fused quartz. A brief characterization of the investigated materials is given in Table 1. It was assumed that investigation of these materials should give an answer to the question of which class of inorganic dielectrics is capable of yielding electrets.

After polarization we measured what might be termed the effective charge density σ on the sample surfaces. The measurements were made by the electrostatic induction procedure which is described in detail in the literature on electrets. The charge density was measured on two opposite surfaces of each electret; hereinafter we shall designate the surface turned to the negative polarizing electrode as the negative side and the other as the positive side. As a rule, the charges on the two opposite surfaces did not differ appreciably.

The electrets after polarization were wrapped in lead foil and stored in desiccators at a relative humidity of 35%.

---

*Here and in the following articles "homocharge" means that the polarity of the electret surfaces is the same as that of the polarizing electrodes; "heterocharge" means opposite polarities. Translator's note.

Table 1

Characterization of materials tested for their ability to form electrets

Material	Dielectric constant & conductivity at room temperature		Type conductivity	Type of polarization
	ε	λ,mho/cm		
$MgTiO_3$	16	$10^{-13}-10^{-14}$	Electronic to 800°	Electron & ion displacement
$ZnTiO_3$	22	$10^{-12}-10^{-13}$	Electronic to 800°	
$BaO \cdot 4TiO_2$	28	$10^{-13}-10^{-14}$	Electronic to 800°	
Bismuth-titanate	80	$10^{-12}-10^{-13}$	-	Electron & ion displacement; relaxati
$CaTiO_3$	150	$10^{-12}-10^{-13}$	Electronic to 800°	Electron & ion displacement
$SrTiO_3$	175	$10^{-10}-10^{-12}$		
Strontium-bismuth titanate	750	$10^{-13}-10^{-15}$	-	Electron & ion displacement; relaxation
$BaTiO_3$	1200	$10^{-10}-10^{-12}$	Electronic to 800°	Ferroelectric
Steatite	4-5	$10^{-14}-10^{-15}$	Electronic and ionic	Electron & ion displacement
Porcelain (M-23)	4-6	$10^{-12}-10^{-13}$		
Glass, ordinary	7-8	$10^{-10}-10^{-11}$	Ionic and electronic (after molding)	Electron & ion displacement; weakly evinced relaxation type
Glass, pyrex	5.8	10^{-14}		
Quartz, fused	3.7	10^{-15}	Electronic & ionic	
KBr, crystalline	4.7	10^{-14}	Ionic	Electron & ion displacement

The surface charge density measurements were carried out at the following intervals: during the first month after polarization σ was measured every day; during the second and third months, once a week; and once a month thereafter. As will be evident from what follows the measured values of σ are affected to some extent by the order and frequency of measurement.

In the first series of experiments the following "standard" polarization conditions were employed for all the samples: the sample was placed in an electric field having the strength of 20 kv/cm; it was held for 30 minutes at room temperature, then the temperature was raised over a period of two hours to 200°; the sample was held at this temperature for 2 hours, then the temperature was reduced to 60-80° over a further period of 2 hours. The diameter of the carefully ground samples was about 60 mm; the thickness about 5.0 mm; the electrodes were ground brass discs 30.0 mm in diameter.

The experimental results obtained with polarization under the above conditions are given in Table 2. As indicated in the notes under the table some of the materials could not be polarized under the "standard" conditions inasmuch as they lacked adequate stability with respect to thermal breakdown.

Table 2

Results of polarization under "standard" conditions

Material	Maximum current during polarization, amps	$\sigma \cdot 10^3$ (C/cm^2) after polarization (on negative side of electret)				
		30 min	10 days	1 mo.	3 months	7 months
$MgTiO_3$	$4,0 \cdot 10^{-8}$	—1,9	—1,4	—0,5	—0,5	—0,5
$ZnTiO_3$	$3,4 \cdot 10^{-6}$	—0,3	—0,2	—0,3	—0,4	None
$BaO \cdot 4TiO_2$	$1,6 \cdot 10^{-7}$	—1,1	—2,8	—0,2	—1,6	—1,4
Bismuth titanate[1]	$1,2 \cdot 10^{-4}$	—10,0	—6,8	—3,9	—4,2	—1,8
$CaTiO_3$	$5,0 \cdot 10^{-8}$	—5,3	—10,5	—5,8	—9,6	—4,2
$SrTiO_3$	$3,4 \cdot 10^{-7}$	—1,7	—2,2	—0,1	—0,7	—0,7
Strontium-bismuth titanate[2]	$7,0 \cdot 10^{-7}$	—3,4	—0,2	—0,8	No data obtained	
$BaTiO_3$[1]	$5,9 \cdot 10^{-4}$	—15,4	—2,0	—0,04	—1,2	—1,1
Steatite	$3,5 \cdot 10^{-7}$	—0,3	—2,1	—1,5	No data obtained	
Porcelain (M-23)[3]	$5,0 \cdot 10^{-4}$	None	None	None		
Glass, ordinary[4]	$15 \cdot 10^{-6}$	»	»	»		
Glass, pyrex[1]	$1,0 \cdot 10^{-4}$	—00,7	»	»	None	None
Quartz, fused	$3,5 \cdot 10^{-9}$	None	»	»	»	No data obtained
KBr (crystallized)[1]	$1,5 \cdot 10^{-5}$	»	»	»	»	

---

1) Samples polarized in 10 kv/cm field. 2) Sample thickness 3.55 mm.
3) Samples polarized in 10 kv/cm field; heated to 175°. 4) Sample heated to 50°.

Polarizing conditions as close as possible to the standard ones were used for these substances. The results of measurements of σ are given only for the negative side of the electret. In the table a negative sign before the value of σ indicates a homocharge; a positive sign (Table 3) indicates a heterocharge. As will be evident from Table 2, electrets with homocharges were obtained from all the materials under the above described polarizing conditions.

Next, samples of all the investigated materials were polarized at a field intensity of 5 kv/cm, the other conditions remaining as above. The results are listed in Table 3, from which it will be seen that in this case electrets with a heterocharge are obtained from many of the materials.

It will be evident from Tables 2 & 3 that not all the investigated materials become electrets when polarized under the described conditions. Such materials as ordinary glass, pyrex glass, KBr single crystals, fused quartz and porcelain either acquire no charge or at most a charge that disappears within a few days. Hereinafter we shall discuss only the materials that retain charges of opposite polarity for an appreciable time.

Here it must be noted that even prior to being subjected to the influence of the electrostatic field samples usually have a surface charge; this is induced by friction incident to grinding, handling, etc. These pre-polarization surface charges are particularly appreciable in the case of substances with a large resistivity (for example, quartz). These charges, however, are relatively small in magnitude and are of the same polarity on opposite sides of the sample, therefore the error introduced by them in the measured value of σ is virtually negligible. We assumed that if together with a low absolute value of the charge the polarity on both sides of the sample was the same, the sample did not have the type of charge characteristic of an electret; in this case we have written "None" in σ columns in Tables 2 & 3.

Fig.1 shows the variation with time during the first month for steatite samples polarized in the 20 kv/cm field. It will be seen from the curve that σ fluctuates with time, and shows a general tendency to decrease. Apparently, the jumps in the curve are connected with changes in the ambient temperature

Table 3

Results of polarization in a 5 kv/cm field

Material	Maximum current during polarization, amps	$\sigma \cdot 10^3$ (C/cm²) after polarization (on negative side of electret)				
		30 min	10 days	1 month	3 months	7 months
$MgTiO_3$ (P-15)	$0,26 \cdot 10^{-10}$	+1,8	0,0	—0,5	—0,8	No data obtained
$ZnTiO_3$	$0,11 \cdot 10^{-6}$	—1,5	—0,3	—0,3	—0,3	—0,2
$BaO \cdot 4TiO_2$	$0,24 \cdot 10^{-7}$	—1,3	—0,3	No data obtained		
Bismuth titanate	$13 \cdot 10^{-6}$	—2,6	—0,9			
$CaTiO_3$	$0,33 \cdot 10^{-8}$	—6,3	—3,3	—0,7	—1,8	—0,2
$SrTiO_3$	$0,07 \cdot 10^{-7}$	—4,4	No data obtained			
Strontium-bismuth titanate	$0,15 \cdot 10^{-6}$	—9,5	None	None	None	No data obtained
$BaTiO_3$	$89 \cdot 10^{-6}$	—1,3	—1,7	No data obtained		
Steatite	$0,05 \cdot 10^{-6}$	+2,2	—0,9	—0,6	—1,0	No data obtained
Porcelain (M-23)	$8 \cdot 10^{-4}$	None	None	None	No data obtained	
Glass, ordinary	$0,43 \cdot 10^{-6}$	—0,06	»	No data obtained		
Glass, pyrex	$52 \cdot 10^{-6}$	+0,08	»			
Quartz, fused	$7 \cdot 10^{-6}$	+3,0	»	None	No data obtained	
KBr (crystallized)	$3,5 \cdot 10^{-6}$	None	»	»		

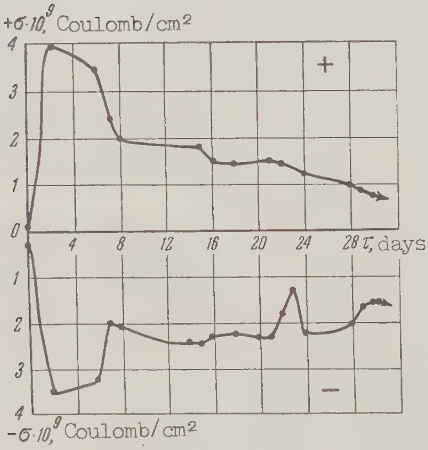

Fig.1

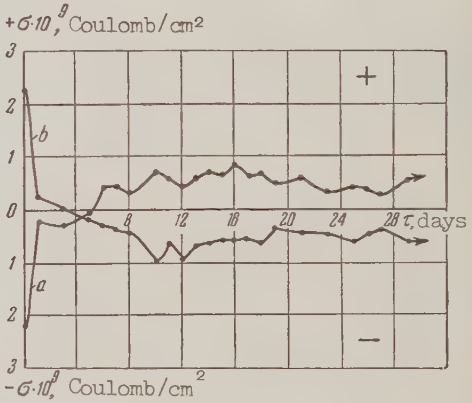

Fig.2

Fig.1. Variation of the surface charge density with time during the first month in the case of a steatite electret polarized in a 20 kv/cm field (sample thickness 5.0 mm). The upper curve (+) corresponds to the positive side of the sample; the lower (−) to the negative side.

Fig.2. Same as Fig.1 but for steatite sample polarized in a 5 kv/cm field. Curve a is for the positive side of the sample; curve b is for the negative side.

and humidity, while the overall decrease in σ is associated with the frequency of measurement (Fig3.5-10). Analogous results for polarization in a 5 kv/cm field are shown in Fig.2. It will be seen that in this case the heterocharge of the steatite electret falls off to zero in about 5 days and then becomes a

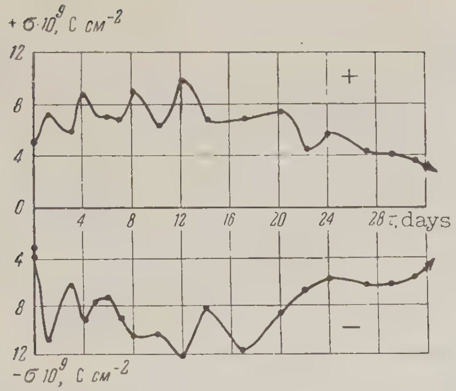

Fig.3. Same as Fig.1 but for a calcium titanate electret.

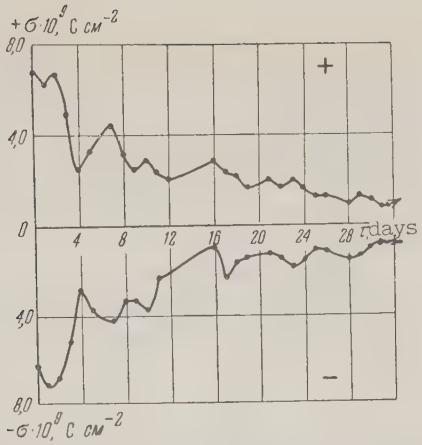

Fig.4. Same as Fig.2 but for a calcium titanate electret.

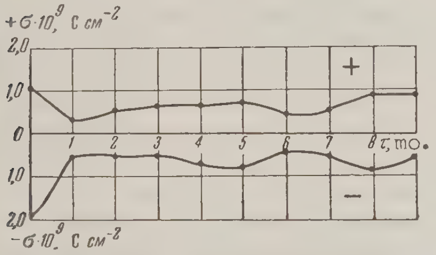

Fig.5. Variation of the surface charge density with time (in months) for an electret of magnesium titanate polarized in a 20 kv/cm field.

homocharge that exhibits little further change with time. Similar dependences for samples of $CaTiO_3$ are shown in Figs. 3 & 4. Analogous results were obtained for the other investigated materials, but reversal of the sign of the charge was observed only in the case of the $MgTiO_3$(M-40 & R-15 type) and steatite samples. The other substances, after polarization at both 20 kv/cm and 5 kv/cm, acquired only homocharges, which, it is true, differed in magnitude for the different materials.

Figs.5 through 9 show how σ varied with time over a period of months for some of the tested electrets. The other electrets investigated exhibited analogous dependences. For purpose of comparison, in Fig.10 we give the variation of σ with time over a period of a few months for an electret of $CaTiO_3$ after polarization in the 5 kv/cm field (Table 3). It should be noted that control samples of electrets prepared earlier of $MgTiO_3$ retained their charge for over two years.

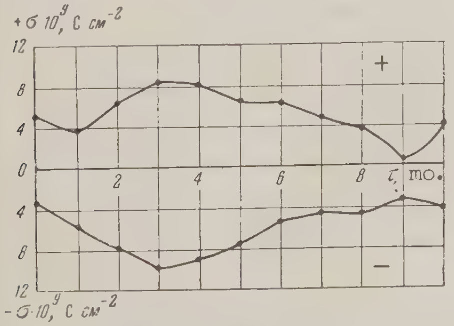

Fig.6. Same as Fig.5 but for a calcium titanate electret.

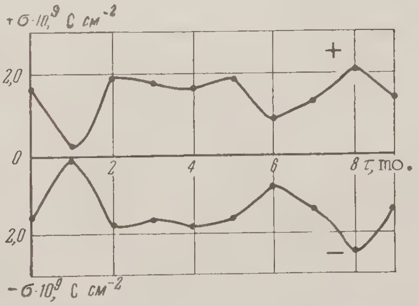

Fig.7. Same as Fig.5 but for a barium tetratitanate electret.

By way of illustration, in Fig.11 we give results of measurements of the current during polarization of a $CaTiO_3$ sample. From Fig.11 and from the data on the variation in current during polarization obtained for the other dielectrics (not given here), it is evident that there are no anomalies in the curve

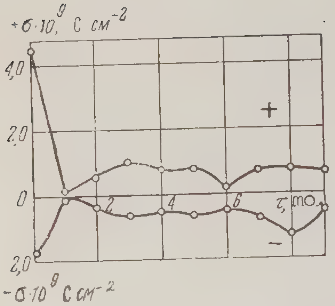

Fig.8. Same as Fig.5 but for a strontium titanate electret.

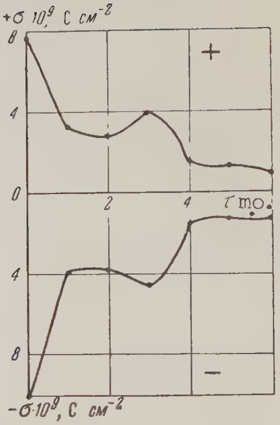

Fig.9. Same as Fig.5 but for a bismuth titanate electret (polarizing field = 10 kv/cm).

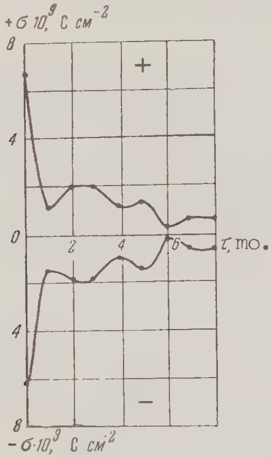

Fig.10. Variation of the surface charge density σ with time for a calcium titanate electret polarized in a 5 kv/cm field.

characterizing the variation of the current with time and temperature.

3. The next part of the work was devoted to determining the optimum conditions of polarization for obtaining electrets. To this end we determined how the properties of the electret vary with the holding (polarization) time, the temperature, the field intensity and the thickness of the samples. In these investigations the sample was first heated to the holding temperature without a field, i.e., the field was applied only when the sample had been heated to the holding temperature.

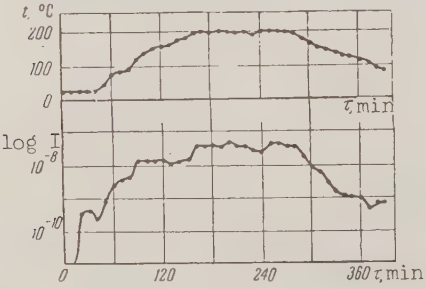

Fig.11

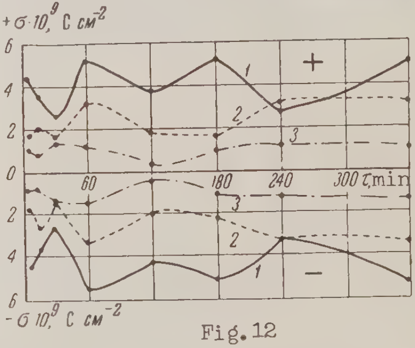

Fig.12

Fig.11. Variation of the polarization current I (in amps) with the time and temperature for a sample of calcium titanate (E = 20 kv/cm).

Fig.12. Variation of σ with holding time for polarization of electrets of barium tetratitanate (E = 20 kv/cm). Time lapse between polarization and measurements: 1) Δτ = 30 min, 2) Δτ = 10 days, 3) Δτ = 30 days.

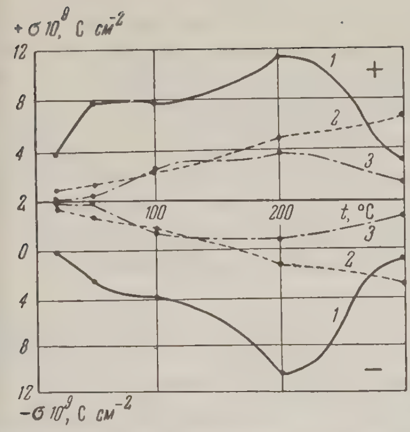

Fig.13. Variation of σ with the polarization temperature for electrets of calcium titanate (E = 20 kv/cm). Curve designations same as in Fig.12.

Variation of the surface charge density σ acquired by electrets of $BaO\cdot 4TiO_2$ during polarization with the holding time is shown in Fig. 12. The holding time at 200° was varied from 5 min to 6 hours; in every case the field intensity was E = 20 kv/cm and the cooling time was 4 hours. Thus the total polarization time for the samples varied from 4 to 10 hours. As will be evident from Fig.12 the duration of polarization (the holding time) does not have an appreciable effect on the magnitude of the surface charge density or on its time dependence. Apparently 5 min heating followed by 4 hours cooling is sufficient for the samples to acquire the maximum charge at the given field strength.

Fig.13 shows how the surface charge density σ of electrets of $CaTiO_3$ varies with the polarization temperature. The holding temperature was varied from room temperature to 300°; the field intensity in all cases was 20 kv/cm; the holding time 30 minutes; the cooling time 4 hours. It will be evident that σ is somewhat dependent on the polarization temperature; apparently 200° is the optimum temperature for calcium titanate. It must be noted that 300° appears to be the limiting temperature for this type of material inasmuch as at higher temperatures, we either have thermal breakdown at E = 10-20 kv/cm or chemical alteration of the material connected with increasing conductivity.

It was obviously also important to determine how the surface charge density varies with the strength of the applied field. The pertinent data for $MgTiO_3$ (R-15) and $CaTiO_3$ are shown in Figs.14 & 15. The field intensity was varied from 100 v/cm to 40-60 kv/cm. In all cases the sample thickness was 5.0 mm, the holding time at 200° was 2 hours and the cooling time 4 hours.

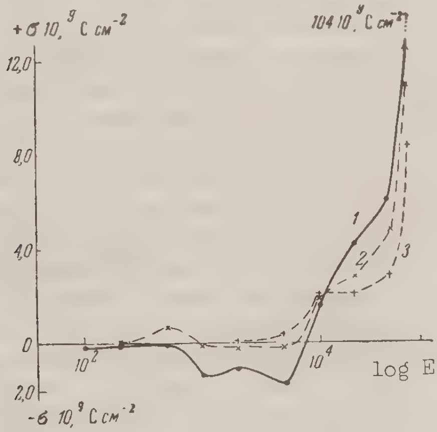

Fig.14

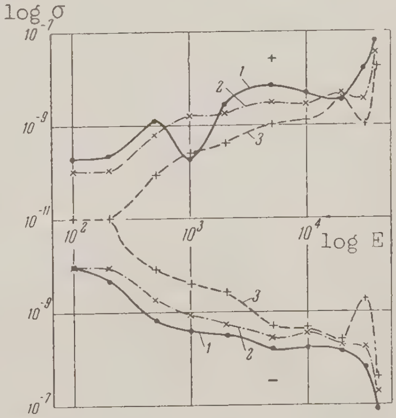

Fig.15

Fig.14. Variation of σ with the polarizing field strength (in v/cm) for electrets of magnesium titanate (the results are given only for the positive side of the electret). Curve designations same as in Fig.12.

Fig.15. Same as Fig.14 but for electrets of calcium titanate.

It follows from Figs.14 & 15 that in the homocharge region σ, in general, increases with increasing field strength E. With $E < 10$ kv/cm in the case of $MgTiO_3$ electrets there is observed a heterocharge which transforms to a homocharge (at E = 5 kv/cm) or falls off to zero (for $E < 5$ kv/cm). Initially, after the transformation, the homocharge has an appreciably higher value than follows from extrapolation of the field intensity curve, but then with time goes down and σ increases with increasing E. In the case of $CaTiO_3$ electrets, no heterocharge was obtained even at low field values down to E = 100 v/cm. This is apparently connected with the fact that the dielectric constant of this material is large ($\epsilon \approx 150$), while the dielectric constant of magnesium titanate is only ~15.

It must be noted that at field strengths under 5 kv/cm $MgTiO_3$ "electrets" are very unstable: their"lifetime" is a matter of days. Hence, in our opinion, they cannot be regarded as electrets in the commonly accepted sense. Very large charges ($\sigma \approx 100 \cdot 10^{-9}$ coulomb/cm^2) were observed in the case of $MgTiO_3$ samples polarized in a field of 60 kv/cm; these charges, however, fell off by a factor of about 10 in a few days.* In the case of $CaTiO_3$ electrets, we observed no gradual growth of the homocharge with increasing E, although at E = = 60 kv/cm there were also obtained large charges (2 to $4 \cdot 10^{-8}$ coulomb/cm^2) which did not noticeably change over a period of a month.

In a brief communication Yamanaka[9] reports that electrets prepared of Carnauba wax in fields of different intensity but with the same field gradient exhibit different properties. The field gradient in Yamanaka's experiments was 7 kv/cm: at an overall potential of 1 kv there was obtained a heterocharge which rapidly fell off with time; at potentials of 1-3 kv there were obtained heterocharges that transformed into homocharges; at higher potentials homocharges resulted. Yamanaka assumes that the field distribution inside the electret has an appreciable influence on the formation of the homocharge.

For a more complete characterization of the new electrets we undertook an analogous investigation of samples of $CaTiO_3$. The results obtained are shown in Fig.16. It will be seen that we found no significant dependence of the electret properties on the applied potential with E = const.

In order to determine the influence of heating in the preparation of electrets a number of samples were polarized at room temperature. It was found that in this case too, one can obtain appreciable surface charges. The magnitude of these charges, however, is somewhat lower than when the sample is heated. In addition, the charge falls off more rapidly with time without going through a homocharge maximum characteristic of true electrets.

Fig.17 characterizes the variation of σ with time for an electret-like sample of $CaTiO_3$ polarized at room temperature with E = 20 kv/cm; the polarization time was 6.5 hours (compare with Fig.6). Fig.18 shows how the value of σ varies with the time the $CaTiO_3$ samples are held in the electric field (E = = 20 kv/cm) at room temperature. The indicated values of σ were measured 30 minutes after polarization. It follows from Fig.18 that to obtain appreciable charges at room temperature, the sample must be held for a considerable time (1 hour or more) in the polarizing field.

Finally, we note that one can obtain inorganic electrets by means of an intermittent voltage (full wave circuit without a filter). Properties of electrets prepared in this manner differ little from the corresponding properties of electrets polarized in a constant (dc) field. As might be expected, electrets are not obtained with an alternating voltage.

---

*The diameter of the electrodes used in polarizing the samples in the 60 kv/cm field was 10 mm, whereas in all the other cases the electrode diameter was 30 mm.

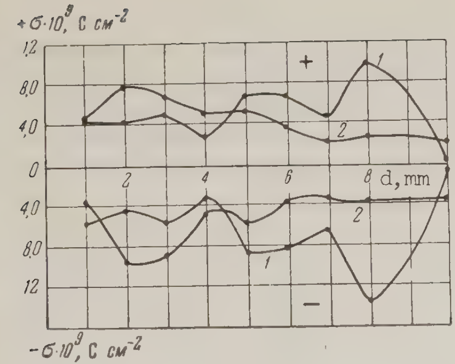

Fig.16

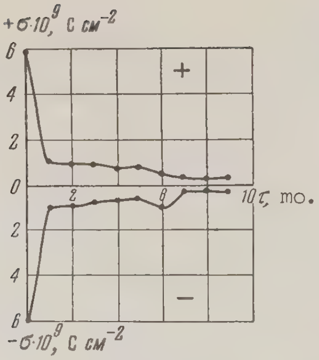

Fig.17

Fig.16. Variation of σ with the thickness d of calcium titanate electrets polarized with a constant field gradient E = 10 kv/cm. Lapse of time between polarization and measurements: 1) Δτ = 30 min and 2) Δτ = 10 days.

Fig.17. Variation of σ with time for an "electret" of calcium titanate obtained at room temperature (E = 20 kv/cm).

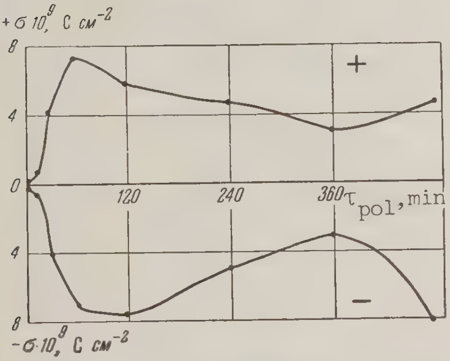

Fig.18. Variation of σ with the time calcium titanate samples are held in a polarizing field (E = 10 kv/cm) at room temperature; σ measured 30 min after polarization.

4. According to the hypothesis of Gross[10], homocharges in electrets are formed by transfer of charges from the electrodes to the sample during polarization. This transfer is realized, according to Gross, by means of local breakdowns of the air between the electrode and the surface of the sample. This hypothesis can be checked by using appropriate electrodes; an attempt in this direction was made by Baldus[11].

In our work we also tried to check Gross' hypothesis. In order to eliminate the air gap between the electrode and the sample surface, the electrets were polarized in a silicone oil. Under these conditions the insulating liquid completely filled the gap between the electrode and the dielectric so that there could be no penetration of charge into the dielectric due to local breakdowns of the air in the gap.

Electrets prepared in this manner from $MgTiO_3$ (M-40) had homocharges the magnitude of which is appreciably lower than the case of $MgTiO_3$ electrets prepared "in air": $\sigma = (0.1\text{-}0.3)\cdot 10^{-9}$ coulomb/cm^2 in the case of silicone insulation and $\sigma = (0.5\text{-}2.10)\cdot 10^{-9}$ coulomb/cm^2 in the case of air. The life of these electrets, however, ran to months. Consequently, there was no essential qualitative difference between electrets obtained with an air gap and electrets obtained with a silicone oil filled gap. Apparently, in the latter case there may accumulate at the liquid-dielectric solid interface appreciable charges due to a difference between the conductivities of the liquid and solid dielectric. These charges may partially return into the depth of the dielectric and form a homocharge.

In addition we made an attempt to obtain higher homocharges in an electret on one side of which we introduced an artificial 0.57 mm wide air gap between the electrode and the sample surface (the other electrode was the usual closely fitting ground brass disc). In this case there was obtained on the side with the air gap a homocharge about 20% higher than the homocharge on the opposite side.

These results show that the process of formation of a homocharge is more complex than assumed by Gross.

It has been established by a number of investigators that both homocharges and heterocharges in electrets are space charges; in contrast to heterocharges, homocharges are distributed only in a thin layer close to the electrodes.

In our work we made an attempt to substantiate these results using the new electrets. We prepared a sample of magnesium titanate consisting of a stack of two ground

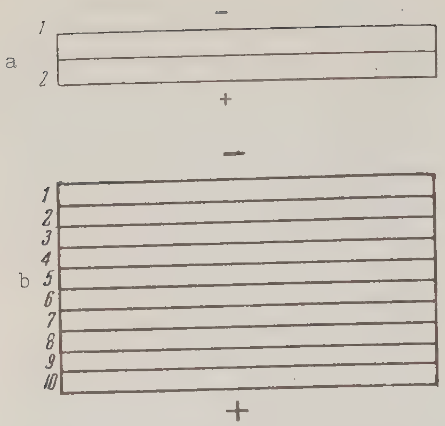

Fig.19. a) sample of two ground discs of magnesium titanate (see Table 4); b) sample of 10 ground discs of calcium titanate (see Table 5).

Table 4

Two-disc sample of $MgTiO_3$ (sample thickness 10mm)

$\sigma \cdot 10^9$ C/cm² after polarization	Disc 1		Disc 2		Stack	
	neg. side	pos. side	neg. side	pos. side	neg. side	pos. side
After 30 min.	—4,1	+4,6	+0,8	—0,8	—2,6	+2,1
After 8 mos.	—2,3	+2,7	None	None	—2,1	+1,8

Table 5

Sample of $CaTiO_3$ consisting of 10 disc (total thickness - 10 mm)

Disc. No.	$\sigma \cdot 10^9$ C/cm² 30 minutes after polarization		$\sigma \cdot 10^9$ C/cm² 8 months after polarization	
	negative side	positive side	negative side	positive side
1	+ 7,5	— 4,7	None	None
2	—15,4	+15,9	—0,3	+2,9
3	—14,4	+ 8,6	—0,9	+0,5
4	+ 6,5	— 6,3	—0,1	+0,2
5	— 6,1	+ 1,2	—1,2	+1,2
6	+ 3,5	— 2,6	—0,4	+0,3
7	—38,0	+32,5	None	None
8	— 2,6	+ 2,4	—0,4	+0,8
9	—13,0	+14,4	—0,7	+0,5
10	— 0,4	+1,0	—0,8	+0,1
Stack as a whole	—7,7	+6,7	—0,2	+0,2

discs and a sample of calcium titanate consisting of 10 ground discs (Fig.19). The stacks were polarized in the usual manner after which we measured the surface charges on the stacks as a whole and on the individual discs. Some of the results are given in Tables 4 & 5. In view of the fact that despite the careful grinding there are still air gaps present between the surfaces of the discs, charges accumulate at the air-dielectric interfaces; these charges can partially penetrate into the dielectric, thereby complicating the charge distribution in the dielectric. Hence, one cannot affirm as Wieder & Kaufman did[6], that the presence of long persistent charges on the surfaces of the individual discs unambiguously indicates volume distribution of the charges in the electret.

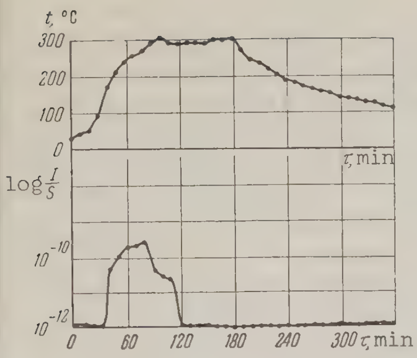

Fig.20. Depolarization current of a magnesium titanate (R-15) electret polarized in a field E = 2 kv/cm (S is the area of the polarized part of the electret). The upper curve shows the variation in the temperature of the sample during the same period.

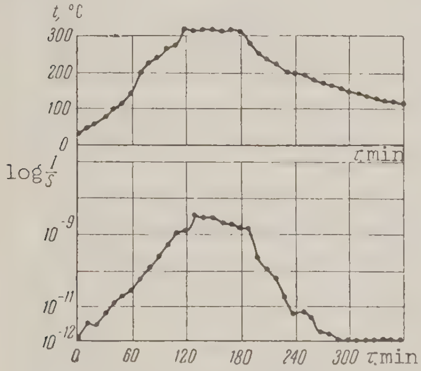

Fig.21. Same as Fig.20 but for a magnesium titanate electret polarized with E = 20 kv/cm.

In the process of polarization of an electret there is stored in it a certain amount of electricity from the external source owing to the displacement current if only a heterocharge is formed; the situation is more complicated in the case of formation of a homocharge.

If one depolarizes the sample by heating the electricity stored in it is released. The experimental results obtained in depolarization of samples of $MgTiO_3$ are shown in Figs.20 & 21. In Fig.20 we have the depolarization current for an electret having a heterocharge, i.e., $\sigma = \sigma_{het} - \sigma_{hom} > 0$, while Fig.21 is for an electret having a homocharge, i.e., $\sigma = \sigma_{het} - \sigma_{hom} < 0$. From the area between the current curve and the time axis one can evaluate the magnitude of the heterocharge: $\sigma_{het} = q/S$ (S is the area of the surface of the polarized part of the electret), if we neglect the dissipation of the homocharge through the internal volume of the dielectric during the period of polarization.

We performed the calculations and obtained a value of $\sigma_{het} = 90\cdot10^{-9}$ coulomb/cm^2 (Fig.20). The value of σ measured in the conventional manner before depolarization was $2.5\cdot10^{-9}$ coulomb/cm^2.

These results indicate that the $MgTiO_3$ electret polarized under the given conditions (E = 20 kv/cm and t = 200°) has both a heterocharge and a homocharge $\sigma_{hom} = 87.5\cdot10^{-9}$ coulomb/cm^2, which together appreciably exceed the measured value of σ. Analogous calculations were carried out for the $MgTiO_3$ electret having a homocharge $\sigma = -4.0\cdot10^{-9}$ coulomb/cm^2 (Fig.21). The results obtained were the following: $\sigma_{het} \approx 2\cdot10^{-5}$ coulomb/cm^2 and $\sigma_{hom} \approx 2\cdot10^{-5}$ coulomb/cm^2. These results show that there may exist in an electret large charges of opposite polarity, but of almost the same magnitude.

Gross[10], neglecting the diffusion of the homocharge through the dielectric and the current through the electrode-dielectric gap, determined separately the values of the hetero- and homocharges for an electret of Carnauba wax (the electret had a heterocharge). Both values under Gross' conditions were about $10\cdot10^{-9}$ coulomb/cm^2.

If the heterocharge of an electret is due to "freezing" of dipoles and ions displaced under the influence of the electric field, this should to some degree be evinced in the change in the value of the dielectric constant and the loss tangent of the electret. True, it appears probable that the dipoles or ions subject to freezing, are the dipoles or ions that at room temperature have enormous relaxation times (years). According to this view, there should be observed no change in ϵ and tan δ provided there is no correlation between the dipoles (ions) with "normal" relaxation times (which determine ϵ and tan δ) and the dipoles (ions) with very large relaxation times.

Wikstrom[13] found that in electrets of Carnauba wax there is no change in ϵ and tan δ as compared with the usual values for nonpolarized samples. In contrast, Chatterjee & Bhadra[14] found an enormous temporary increase in ϵ (by a factor of 1000) and tan δ in a polarized cylindrical capacitor with Carnauba wax. These changes of ϵ and tan δ are evinced not immediately after polarization but only after a couple of days; then after the passage of a certain time they return to their initial values.

We also carried out measurements of the changes of ϵ and tan δ in electrets of $CaTiO_3$ and $SrTiO_3$ over a period of 20 days, comparing the values with ϵ and tan δ for control samples. We observed no changes in ϵ in electrets as compared with ϵ of nonpolarized samples and no variation of ϵ with time. The dielectric loss tangent increased somewhat with time with decreasing superficial charge density.

Before concluding, we want to touch on the interesting question of the effect of shorting the surface of electrets in storage. All previous investigators, beginning with Eguchi and Gemant, insist that the surfaces of electrets must be shorted during storage and assert that if this is not done there is formed a double electric layer at the surface of the electret and this layer prevents deposition of ions on the electret surface; significant here is that in the process the field inside the electret goes to zero.

Our experiments have shown, on the contrary, that a nonshorted inorganic electret is more stable than a shorted one. It may be assumed that in such an unshorted electret there form in some manner surface charges opposite in polarity to the charges of the electret itself, i.e., there form double electric layers and the electret is "self-shorted". It may be that some role here is played by a very thin film of moisture condensing over the entire surface of the hydrophilic ceramic dielectric. In measurement of the surface charge of the electret, at the instant of grounding of its surfaces, these double layers apparently break down. We advance the above only as a tentative hypothesis which does not appear wholly satisfactory to us. Further investigation is underway.

V.S.Mitronina, Z.N.Kalganova, and during the early stages P.Kh.Mukhamedieva, participated in the work.

"P.N.Lebedev" Physical Institute,
Academy of Sciences of the USSR

References

1. M.Eguchi, Phil.Mag., 49, 178 (1925).
2. A.Gemant, Phil.Mag., 20, 929 (1935).
3. E.Padgett, Radio Electronics, 20, 20 (1949).
4. G.Wiseman & E.Linden, Electr.Eng., 72, 10 869 (1953).
5. F.Gutman, Revs.Mod.Phys., 20, 457 (1948).
6. H.Wieder & S.Kaufman, J.Appl.Phys., 24, 156 (1953); Electr.Eng., 72, 511 (1953).
7. F.Binder, ZS.Naturf., 6a, 714 (1951).
8. R.Thickens & R.MacDonald, Phys.Rev., 90, 375 (1953).
9. C.Yamanaka, J.Phys.Soc., Japan, 9, 3, 425 (1954).
10. B.Gross, J.Chem.Phys., 17, 866 (1949). Phys.Rev., 66, 26 (1944); B. Gross & F.Denard, Phys.Rev., 67, 253 (1945); B.Gross, Brit.J.Appl.Phys., 1, 259 (1950).
11. W.Baldus, ZS.f.augew,Phys., 6, 11, 481 (1954).
12. P.Thiessen, A.Winkel & K.Herrman, Phys.ZS, 37, 511 (1936).
13. S.Wikstrom, Ark.f.Physik, 7, 3, 213 (1954).
14. S.Chatterjee & T.Bhadra, Phys.Rev., 98, 1728 (1955).

INVESTIGATION OF THE ELECTRIC AND OPTICAL PROPERTIES OF ELECTRETED POLYMERS

- K.B.Filippova

Introduction

A number of scientists, including Heaviside, advanced hypotheses regarding the possibility of creating electric analogs of permanent magnets. The Japanese physicist Eguchi[1] was the first, however, to obtain permanently polarized dielectrics which, at the suggestion of Heaviside, have come to be called electrets.

Eguchi's discovery was followed by a large number of studies devoted to this interesting effect and by now there have been published about 100 investigations in this field. In view of the complexity of the electret effect, however, we still have no fully satisfactory theory for this phenomenon.

An important role in the development of the theory of electrets was played by the hypothesis of Mikola, according to which all the observable manifestations of an electret are the result of a combination of two different processes which have been termed internal and external polarization. The first, according to Mikola, results in a heterocharge, the second in a homocharge.

Modern interpretations of internal and external polarization have been given by a number of authors[2-4]. It is assumed that internal polarization may arise as a result of "frozen" dipole polarization, macroscopic inhomogeneities and ionic charged layers due to ionic conductivity of the material.

The mechanism of external polarization first proposed and substantiated experimentally by Gross[2,3] consists of a transfer of charges from the electrodes to the sample and adsorption of these charges on the surface of the dielectric.

All investigators in the field associate the transition of samples from the heterocharge state to the fact that heterocharges and homocharges have different relaxation times.

This mechanism of the electret effect apparently correctly characterizes the physical nature of this phenomenon. There can be no doubt, however, that it requires further refinement and elaboration particularly as regards the formation and the conditions of stability of homocharges.

Despite the considerable number of experimental studies, the physical properties of electrets have not as yet been fully investigated. Thus, for example, no one has investigated the optical properties of electrets. This may be explained by the fact that until recently electrets were prepared exclusively of opaque waxes and resins.

The structure of wax electrets has been studied only in the work of Nakata[5], Swing[6] and Good & Stranathan[7]. These authors came to the conclusion that while crystalline orientation may obtain in electrets, it is evident from comparison of the results of x-ray diffraction analysis and electric measurements that crystalline orientation is not a necessary condition for the formation of electrets.

In 1953 Wieder & Kaufman[8] published the results of their work in which they reported successful preparation of electrets of a transparent material: polymethyl methacrylate. This made it possible to proceed to investigation of the optical properties of electrets.

Inasmuch as there was reason to assume that the optical properties of a dielectric may change a result of electreting, the present work was undertaken with a view to investigating the optical properties of electrets; our specific aim was to detect and investigate optical anisotropy developing in an amorphous dielectric as a result of electreting and to establish the relation between this effect and the electric characteristics of electrets.

1. Experimental procedure

By way of primary subject of our investigation we chose polymethyl methacrylate. Inasmuch as in the process it became clear that an important characteristic in polymers as regards formation of electrets is the degree of polarity of the monomolecules, we also took two other materials, namely, non-polar polystyrene and the highly polar copolymer of acrylonitrile with methyl methacrylate.

For the electric measurements we used samples in the form of discs. Inasmuch as numerous experiments showed, however, that for optical purposes this shape is not suitable, we used samples of the shape shown in Fig.1 for the optical studies. For the purpose of separating the anisotropy due to the electric field from the anisotropy due to the presence of metallic electrodes on the surface of the sample (we noted that this effect does obtain), in all the optical studies we used the illustrated system of two pairs of identical electrodes applied in the same manner to the sample. One pair of electrodes was the active one, i.e., the one through which the high voltage was applied; the other pair consisted of control or dummy electrodes.

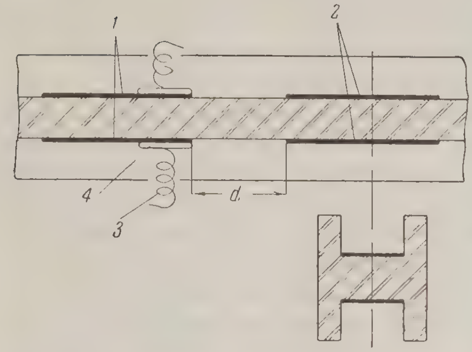

Fig.1. Diagram showing application of electrodes and high voltage leads: 1) active foil electrodes, 2) control electrodes, 3) high voltage contacts and leads, and 4) cushions of foil. Distance d = 60-70 mm.

In preparing the electrets we followed the procedure described by Wieder & Kaufman[8] for electreting polymethyl methacrylate. It consisted essentially of heating the polymer to $T > T_g$, followed by cooling it in a strong constant electric field.

The optical properties of the samples were investigated visually by means of an MP-3 polarizing microscope and photometrically by photographing the polarization microscope image on film and then scanning the photographs by means of an MF-2 microphotometer.

Since it was found that the optical anisotropy of the electret volume of a sample is comprised of the anisotropy due to the influence of the electric field, (i.e., the sought quantity) and the anisotropy due to other factors, as the measure of the sought anisotropy, we took the difference between the anisotropies of the electreted and control sections of the sample. In photometric parameters this difference is given by

$$B_e - B_c = \log \frac{I_e}{I_c} ,$$

where I_e and I_c are the intensities of the light passing through the electreted and control sections of the sample under "crossed polarizing optics" conditions. The values of $\log (I_e/I_c)$ were averaged over the central portion of the sample.

2. Investigation of the electric properties of electrets of polymethyl methacrylate

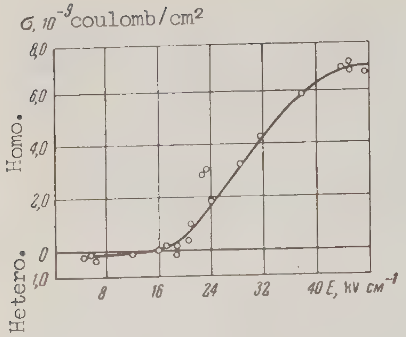

Fig.2. Variation of the surface charge density σ with the density of the polarizing field E. Heating time 2 hours.

For the purpose of investigating variation of the properties of polymethyl methacrylate electrets with the magnitude of the polarizing electric field, we prepared a series of electrets in a wide range of field strengths, namely, from 4 to 46.5 kv/cm (Fig.2.)

It was found that under the given conditions in the region of weak fields ($E < 16$ kv/cm) there are formed heteroelectrets, while in the region of strong fields ($E > 18$ kv/cm), other experimental conditions being equal, there are formed homoelectrets. These two regions are separated by a narrow region of "threshold" potential gradients (16-18 kv/cm) at which the resultant samples exhibit no electret properties at all.

In the region of weak fields, increasing E from 4 to 16 kv/cm results in a decrease of the surface charge density σ of the heteroelectrets from about $(0.1\text{-}0.2)\cdot 10^{-9}$ coulomb/cm² to 0.

In the strong field region, increasing E from 18 to 44 kv/cm results in an increase of the superficial charge density σ of the homoelectrets from 0 to values of the order of $7\cdot 10^{-9}$ coulomb/cm².

Above about 44 kv/cm there obtains a region of saturation of the surface charge density σ of the homoelectrets, inasmuch as increasing the field strength up to 46.5 kv/cm did not yield any increase in σ.

From the above described experimental data it may be concluded that the character of electrets of polymethyl methacrylate is determined by the strength of the electric polarizing field E in which the electret is formed and that, depending on the value of E, there may be obtained either homoelectrets or heteroelectrets; the magnitude of the surface charge density σ of both types is a function of the electric field strength and can be varied over a rather wide range by varying E.

Further observation of the electrets over a period of time showed that for all homoelectrets prepared in the range of fields from 18 to 46.5 kv/cm there is always observed a more or less slow decrease of the surface charge density σ to zero with no indications of polarity reversal (Fig.3). Analogous properties were exhibited by the heteroelectrets prepared in fields from E = 4 to 8 kv/cm. In the case of these samples there was observed only a slow decrease of the surface charge density to zero and no evidence of reversal of charge polarity thereafter.

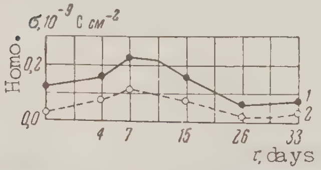

Fig.3. Variation of the surface charge density with time: 1) positive side of sample, 2) negative side of sample. Polarizing field strength E = 19 kv/cm.

The heteroelectrets prepared in fields from E = 10 to 16 kv/cm exhibited the usual transition from the heterocharge state to the homocharge state (Fig.4), characteristic of electrets of waxes and resins.

Further observations showed that the behavior of these electrets during their life is also strongly dependent on the strength of the electric field in which the electret is formed.

The electret effect in polymethyl methacrylate can be explained by means of the hypotheses of Mikola and Gross. In view of what is know regarding the structure of polymethyl methacrylate and the mechanism of dielectric polarization, it may be inferred that the internal electret effect is due primarily to thermal orientational polarization of the dipole $O{=}\overset{|}{C}OCH_3$ radicals. During cooling of the polymer in an electric field, the dipole polarization is so to say "frozen" in the dielectric and persists in it for a long period after termination of the electreting process. Thus we have a stable internal electret effect.

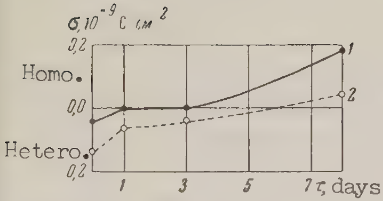

Fig.4. Same as Fig.3 but for a polarizing field strength E = = 11 kv/cm.

As for the external effect, in the case of polymethyl methacrylate we tentatively suggest that it is due to adsorption of charges on the surface of the sample.

3. Investigation of the optical properties of polymethyl methacrylate electrets

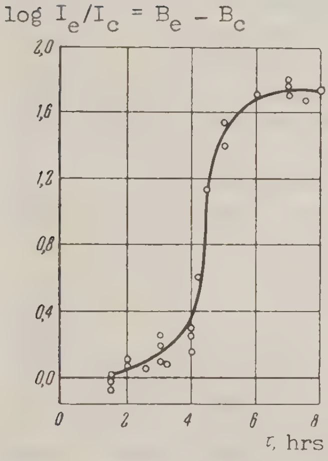

Fig.5. Variation of the optical anisotropy of samples with the heating time τ. Polarizing field strength E = 35 kv/cm.

For investigating the optical properties, we prepared a series of electrets in the form of rods under the same temperature and time conditions as used for the disc electrets. In all cases the electric field strength was 35 kv/cm. Thus we deliberately selected the optimal preparation conditions yielding fairly strong and stable homoelectrets with charge densities of $(4\text{-}7)\cdot 10^{-9}$ coulomb/cm^2.

Visual examination of these electrets, carried out immediately after termination of the electreting, showed that the anisotropy of the electret section of the sample only slightly exceeded the anisotropy of the control section.

The negligible value of the optical anisotropy effect due to rearrangement of the polymethyl methacrylate structure in the process of electreting with a 2 hour heating time, led us to vary the experimental conditions over a wide range. In doing so we found that the anisotropy increases sharply with increasing heating time. The results are shown in Fig.5.

With 1.5-2 hours heating the quantity $B_e - B_c = \log(I_e/I_c)$ has a weakly negative or zero value. In the interval of 2 to 4 hours heating time, this quantity gradually increases to about 0.4. Then we have a region of sharp increase and in the 4 to 6 hour interval $B_e - B_c$ increases to 1.7, after which it enters a region of saturation.

Comparison of the results of investigation of the electric and optical properties of polymethyl methacrylate samples shows that the electret effect and the birefringence effect are not directly related, inasmuch as a short (1.5-2 hours) polarization period is sufficient for the formation of a stable electret state, whereas an appreciably longer time is necessary for optical

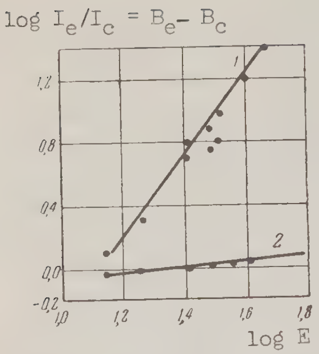

Fig.6. Variation of the optical anisotropy $B_e - B_c$ with the polarizing field strength E(kv/cm) for different times τ : 1) τ = 6 hrs., and 2) τ = 4 hrs.

anisotropy to be evident. Thus we found that optical anisotropy need not appear in the formation of a stable electret.

Despite the fact that our experiments do not allow of drawing any definite deductions regarding the mechanism of the detected optical effect, it may be assumed that the nature of the electret effect differs from that of the optical effect inasmuch as it follows from the experimental data that these effects are not necessarily correlated.

It is possible that the optical effect is connected with orientation at $T > T_g$ of principal sections of the polymer chain of the polymolecules due to the initial orientation of the dipole $O{=}\overset{|}{C}OCH_3$ groups.

In order to clarify the dependence of the optical anisotropy $B_e - B_c$ on the intensity of the polarizing electric field E, we carried out two series of experiments in which the electric field strength was varied from 13.7 to 46.5 kv/cm. In other respects the preparation procedure and the method of optical measurement remained the same as in the experiments described above. The results obtained in this case are shown in Fig.6. The heating time of the samples in the first series was 6 hours; that for the samples of the second series was 4 hours.

It will be seen from the curve that in both cases there is a direct proportionality between $\log (I_e/I_c)$ and log E; for the 6 hours heating time samples the straight line plot is characterized by

$$\overline{\log(I_e/I_c)} = 3 \log E + \log C_1,$$

while the 4 hour series

$$\overline{\log(I_e/I_c)} = 0.2 \log E + \log C_2.$$

4. Variation of the electric properties of electrets with the heating time

The above described experiments showed that in the process of electreting the structure of the polymer changes in the sense of transition from the amorphous state to the oriented state.

In view of the above inferences regarding the nature of the electret and optical effects, we had reason to assume that increase in the degree of ordering of the structure should be accompanied by an increase in the dielectric polarization P. In other words, we assumed that with increasing heating time, there would occur an increase of the "frozen" polarization P and that the properties of the electrets, primarily the surface charge density σ would vary accordingly.

In order to check this we investigated the variation of the electret properties of polymethyl methacrylate samples with the electreting heating time.

It was found that the superficial charge density σ does vary with the heating time.

In the case of homoelectrets formed in a strong field (46.5 kv/cm), increasing the heating time from 2 to 7 hours reduces the surface charge density

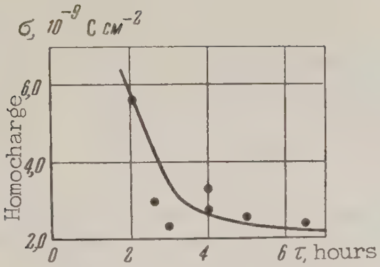

Fig.7. Variation of σ with heating time τ. E = 46.5 kv/cm.

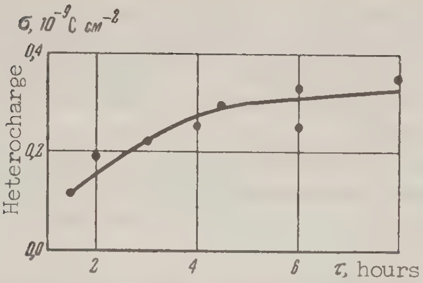

Fig.8. Same as Fig.7 but with E = 5 kv/cm.

σ from $6 \cdot 10^{-9}$ to $2 \cdot 10^{-9}$ coulomb/cm^2 (Fig.7). In the case of preparation of heteroelectrets in weak fields (5 kv/cm), a corresponding increase in the heating time increases σ from $0.1 \cdot 10^{-9}$ to $0.3 \cdot 10^{-9}$ coulomb/cm^2 (Fig.8).

Actually all the described changes in the magnitude of the surface charge can be explained by increase of the heterocharge, which in turn can be explained by increase of the "frozen" polarization P.

5. Relation between the electric and optical properties of electreted polymethyl methacrylate

Investigation of the relaxation of surface charges or what is the same thing "frozen" dipole polarization and the optical anisotropy at $T = 25^o$ showed that the relaxation time of optical anisotropy is much greater than the relaxation time of the dipole polarization. The maximum "life" of an electret was 60 to 80 days, whereas the optical anisotropy retained an appreciable magnitude for at least 7 to 10 months.

This lack of correlation between the dipole polarization and optical relaxation times substantiates our earlier inference that the mechanisms of these effects are different. The difference in relaxation times indicates that the electret and optical effects are associated with orientation of different sections of the polymolecules.

If it be assumed that the electret effect is connected with orientation of dipole radicals, one may hypothesize that the optical effect is associated with orientation of larger sections of the polymer chain, for example, segments. In this case the short relaxation time of the electret effect can be explained by the relative ease of disorientation of dipoles having a certain freedom of motion relative to a fixed segment at $T < T_g$. Relaxation of the optical effect is hindered inasmuch as at $T < T_g$ the segments are relatively rigidly held.

6. Investigation of electretic polystyrene and acrylonitrile copolymerized with methyl methacrylate

In view of our inference that the electret state of polymethyl methacrylate is determined by the "frozen" polarization of dipole $O{=}\overset{|}{C}OCH_3$ radicals and that this "frozen" polarization is also responsible for the change in the structure of the polymer, we felt it would be of decisive interest to carry out analogous measurements on a polymer whose molecules, in contrast to those of polymethyl methacrylate, do not possess a dipole moment.

Accordingly we chose polystyrene whose monomolecules do not contain a polar group.

Investigation of the electric properties of polystyrene electreted in fields from 24 to 40 kv/cm with variation of the heating time from 2 to 7 hours showed that in all cases immediately after electreting there is a homocharge on the surface of the samples. The surface density σ of this homocharge is independent of the heating time and varies from $1 \cdot 10^{-9}$ to $3 \cdot 10^{-9}$ coulomb/cm^2.

Continued observations showed that in all cases without exception this homocharge disappears entirely within 2-3 days.

In view of the instability of these charges it may be concluded that in the case of polystyrene the charges are free charges adsorbed on the surface of the sample and that they vanish as a result of internal and surface conductivity of the material. The fact that these charges disappear is explained by the absence of "frozen" dipole polarization, inasmuch as electronic polarization is not subject to "freezing", while dipole polarization is absent in the case of polystyrene. Optical investigation of polystyrene electreted in fields of 35-40 kv/cm showed that for all heating times from 2 to 8 hours the anisotropy of the electreted volume does not exceed the anisotropy of the control area, which indicates the absence of a positive anisotropic difference $B_e - B_c$.

From the absence of a positive anisotropic difference between the electret ed and control sections of the sample, on the one hand, and the absence of a stable electret effect, on the other, it may be inferred that in polystyrene there cannot occur an appreciable rearrangement of the structure under the influence of a constant electric field owing to the absence of polar moments in the polystyrene molecule. What dipole moments may be induced by the field are too weak to overcome the great viscosity of the polymer and rotate sections of the macromolecular chain.

In electreting the copolymer of acrylonitrile with methyl methacrylate in fields of 2-4 kv/cm, we obtained heteroelectrets with surface charge densities about 10 times greater than the surface charge density on polymethyl methacrylate samples electreted in equal fields. The stability of the copolymer electrets, however, proved to be inferior to that of polymethyl methacrylate electrets. The greater values of surface charge of the copolymer electret may be explained by the greater dipole polarization of the copolymer due to the greater dipole moment of the CN group.

Conclusions

1. It was established experimentally that the optical properties of electrets of polymethyl methacrylate differ from the optical properties of the initial nonelectreted material. Electreted polymethyl methacrylate, which is amor phous in the initial state, may acquire properties of an optically anisotropic substance.

2. It was found that the magnitude of the optical anisotropy produced by the electric field depends on the electreting time (time of heating in an electric field. It was established that there is virtually no optical anisotropy produced in the case of 1.5-2 hour heating. In the 4 to 6 heating interval there occurs a sharp increase in optical anisotropy, which reaches a maximum value at about 4 hours heating. Further increase in the heating time to 8-9 hours results in no appreciable increase of the optical anisotropy, which indicates that after the initial ~6 hour period no further alterations occur in the structure of the initially amorphous polymethyl methacrylate under the influence of a constant electric field at $T > T_g$. We also investigated the variation of the optical anisotropy with the electric field strength.

3. We investigated the variation of the electret properties of polymethyl methacrylate samples with the duration of heating in the electreting process. We found that the surface charge density σ of the resultant electret varies with the heating time. In the case of formation of homoelectrets in strong fields, increasing the heating time reduces the surface charge density σ, whereas in the formation of heteroelectrets in weak fields, increasing the heating time increases the surface charge density. The observed variations in the magnitude of the surface charge density of electrets may be explained by increase the heterocharge, which in turn can be explained by increase of the "frozen" dipole polarization.

4. We investigated the relaxation of the electret effect and optical anisotropy. The fact that there is no correlation between these relaxation processes indicates that the mechanisms of the two effects are different.

5. There is reason to assume that the decisive factor in the electret effect in polymethyl methacrylate is thermal orientational polarization of the $O{=}\overset{|}{C}OCH_3$ dipole radicals. This, too, may be the primary cause of the optical effect. The last effect, however, should probably be associated with orientation of larger sections of the polymer chain than dipole radicals.

6. From analysis of the experimental data it may be concluded that the optical anisotropy appearing in the process of electreting is not a necessary conditions for the electret effect. This deduction is in agreement with the results of investigation of the crystal structure of wax electrets[5-7].

7. In order to check the decisive role of dipole polarization in the electret effect and optical anisotropy in electreted polymethyl methacrylate, we investigated the optical and electric properties of electreted polystyrene and the copolymer of acrylonitrile with polymethyl methacrylate. Electric measurements of the polystyrene and the copolymer yielded results that substantiate our inference regarding the decisive role played by dipole polarization in the electret effect in polymers. The negative results of optical investigation of electreted polystyrene may be taken as evidence in favor of the proposed mechanism of optical anisotropy in polymethyl methacrylate.

"V.P.Potemkin" Moscow City Pedagogical Institute

References

1. M.Eguchi, Phil.Mag., 49, 178 (1925).
2. B.Gross, J.Chem.Phys., 17, 866 (1949).
3. B.Gross, Brit.J.Appl.Phys., 1, No.10, 259 (1950).
4. A.Gemant, Direct Current, 1, (1953).
5. K.Nakata, Proc.Phys.Math.Soc.Japan, 9, 179 (1927).
6. M.Swing, Phys.Rev., 36, 378 (1930).
7. M.Good & J.D.Stranathan, Phys.Rev., 56, 810 (1939).
8. H.H.Wieder & S.Kaufman, J.Appl.Phys., 2 (1953).

ON THE PHOTOELECTRET AND THERMOELECTRET STATES IN SULFUR SINGLE CRYSTALS

- I.S.Zheludev & V.M.Fridkin

The effect of conditions of polarization on the charge of a photoelectret and the persistence of residual polarization in a sulfur single crystal have been investigated. The temperature dependence of the rate of depolarization of a sulfur single crystal has been determined. The concept of a thermal photoelectric state is introduced.

Introduction

Nadzhakov[1] (Nadjakoff) published his pioneering work on constant internal photopolarization in 1937. It was shown that a plate of pure polycrystalline sulfur polarized in the process of photoconduction is capable of retaining its polarization unchanged for an appreciable time (over 15 hours) and is, consequently, an analog of the electrets discovered and investigated by Eguchi back in 1921.

As is known, the formation of the heterocharge of Eguchi electrets is due to changes in the temperature of the dielectric in the process of its polarization, which in turn is associated with the temperature dependence of the ion mobility and dipole relaxation time.

Accordingly, it may be assumed that the formation of the photoelectrets discovered and investigated by Nadzhakov is associated with photoconductivity of the dielectric and fixing or "freezing" of displaced charges at local levels.

On the basis of the above analogy, Nadzhakov suggested calling this new type of electret "photoelectrets" and the Eguchi electret "thermoelectrets". As subsequent investigations[2-4] showed, this approach to the photopolarization phenomenon proved to be fruitful.

In the present report we give new results of our investigation of the photoelectret state in single crystals. In our opinion, the question of the possibility and the conditions of creation in single crystals of a stable or a slowly decaying polarization is of considerable interest from the standpoint of crystal physics. It is of interest also to compare the conditions governing the appearance and existence of internal polarization in single crystal and polycrystalline media.

The appearance of constant internal polarization in a polycrystalline specimen should be regarded as the formation of a polar texture with $\infty \cdot m$ symmetry (designation according to Shubnikov). The stability of such texture has been experimentally proved by Nadzhakov in the case of pure polycrystalline sulfur. The formation of residual polarization in a single crystal should be regarded as the creation in it of a distinctive polar direction which, in the general case, means alteration of the initial symmetry of the crystal to one of the symmetry subgroups of $\infty \cdot m$ symmetry. From this standpoint, it is of interest to compare the conditions governing the appearance and the persistence of polarization in non-polar, polar and, particular, polar-directed crystals. It may be assumed that the conditions for creation of polarization in these geometrically different directions will be different. The persistence of the artificially induced internal polarization in the crystal should be regarded as an indication of the time the crystal remains in the given state with unaltered symmetry. On the other hand, it is of interest to investigate the anisotropy, the photopolarization and its persistence for one and the same crystal.

Below we give the results of an investigation of the conditions of appearance of photopolarization and the duration of photopolarization in sulfur single crystals as well as the results of some experiments on the temperature dependence of depolarization of photoelectrets.

Experimental procedure

Measurements were made on plates cut from natural rhombic sulfur crystals. The crystal plates having an area of about 1 cm^2 and a thickness of 1-1.5 mm were cut at right angles to the bisector of the acute or obtuse angle between the optical axes. In some cases the specimen was cut in the form of a cube with edges perpendicular to the two axes. The samples were polished to mirror smoothness on cloth moistened with kerosene.

The measurements were carried out by means of a vacuum tube electrometer similar to that described in Ref.5.

For measurements, the sulfur plate was placed in the test capacitor which was mounted in a thermostatic chamber and had provision for illumination of the specimen by a horizontal light beam (parallel to the polarizing field). The available temperature range was from room temperature to 100°. The parallel light beam was directed by means of a special collimator onto a quartz window in the test capacitor. The illumination on the specimen was measured by means of a luxmeter with known spectral characteristics. There was provision in the thermostatic chamber for swinging the capacitor plates aside during these measurements.

The thermostat together with the light source were mounted on an optical bench. The light source was a PRK-4 mercury vapor tube. This made it possible to illuminate the specimen during polarization with either "white" or monochromatic light. The latter was obtained by means of an appropriate set of selective light filters. For polarization we used a high voltage rectifier with electronic stabilization, employing a conventional circuit. The measurements were carried out by the constant deflection procedure.

In most cases the voltage was applied to the specimen simultaneously with illumination. After the passage of a certain time, the light was cut off, after which the voltage was removed and the transparent electrode grounded. The polarized sulfur plate (photoelectret) was kept for a certain time in the dark with short-circuited electrodes. The charge of the photoelectret was measured by depolarization of the specimen under repeat illumination. To this end, we recorded the variation with time of the discharge current (the depolarization current). Usually the polarization of the photoelectret (numerically equal to the surface charge density) was evaluated from the initial value of the discharge current. The procedure employed also allowed of integrating the depolarization current over the discharge time, thereby determining the total depolarization charge. We could also measure the variation of the charging current (polarizing current) with time.

Influence of some polarization conditions on the photoelectret charge

We carried out an investigation of the "lifetime" of the internal polarization in single crystal and in polycrystalline sulfur. The single crystal specimen was a sulfur plate having an area of 1 cm^2 and a thickness of 1.5 mm, cut normal to the bisector of the acute angle between the optical axes. The polycrystalline specimen of approximately the same dimensions was obtained by melting the single crystal plate and allowing the melt to recrystallize by the procedure described by Nadzhakov[6].

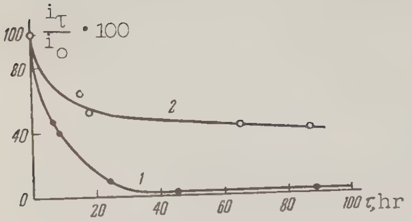

Fig.1. Decrease of residual polarization in sulfur specimens: 1) single crystal, 2) polycrystalline.

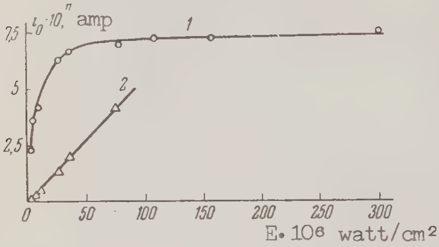

Fig.2. Variation of the initial depolarization current (1) and the initial charging photocurrent (2) with the illumination intensity in the process of polarization.

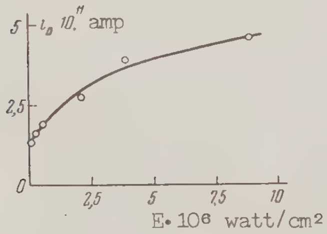

Fig.3. Variation of the initial depolarization current i_o with the illumination intensity in the process of polarization (for low light intensities).

The sample was polarized under illumination with "white" light for 10 min at a potential of 200 v, after which the electrodes were shorted and it was kept in the dark for a certain time. The charge was measured by the depolarization procedure described above.

The results obtained are shown in Fig.1, where the horizontal time axis is scaled in hours and the vertical axis in terms of the ratio (in percent) of the initial discharge current i_τ, obtained a time τ after termination of polarization, to the initial value of the discharge current i_o, obtained immediately after the polarization. It will be seen from the curves that after about 50 hours storage in the dark the polarization of the single crystal specimen falls off virtually to zero. In contrast, the polycrystalline specimen retains about 40% of its initial polarization at the end of 90 hours storage.

This result can be explained by the different conditions of "fixing" of the electrons at the local levels in polycrystalline and single crystal specimens. Obviously, the activation energy which determines the "sticking" of the electrons on the local levels is much higher in the polycrystalline specimen than in the single crystal one. The question of whether the polarization of a polycrystalline specimen tends to a value differing from zero requires special examination.

The curves of Fig.2 show the variation of the initial discharge current i_o with the intensity of illumination incident on the surface of the specimen during polarization.

Single crystal specimens, similar to that described above, were polarized with "white" light from the mercury tube for 10 minutes with an applied potential of 200 v. The intensity of illumination on the surface of the crystal could be varied both by moving the source and by interposing metallic screens (neutral filters) between the source and the specimen. Five minutes after the end of polarization, the specimen was depolarized and the discharge current measured. In each case the polarization was carried out with the same light intensity equal to $3 \cdot 10^{-4}$ watt/cm^2.

Curve 2 in Fig.2 shows the variation of the initial direct (i.e., during polarization) photocurrent with the illumination intensity. It will be seen that whereas the photocurrent during polarization is directly proportional to the illumination, the illumination dependence of the polarization (the initial depolarization current) is characterized by saturation beginning at $E = 5 \cdot 10^{-5}$ watt/cm^2.

Fig.3 shows a separate plot of the variation of the initial discharge current with the illumination intensity (for low values of illumination). In the case of polarization induced under an illumination of only $2.4\cdot10^{-8}$ watt/cm^2, the initial discharge current i_o was $1.3\cdot10^{-11}$ amp. It must be borne in mind that the initial discharge current i_o corresponding to dark polarization induced in the specimen during the same time amounted to $0.5\cdot10^{-11}$ amp. Thus, even at such low illumination intensities, the photopolarization noticeably differed from the effect of dark polarization. Nevertheless, separation of the total polarization of the sulfur crystal into dark polarization and photoseparation, from the standpoint of the persistence of polarization is hardly worthwhile since with time the entire polarization falls off to zero. Such separation is, however, expedient for polycrystalline sulfur inasmuch as in this case depolarization in the dark leads with time to a complete decay of the dark polarization, but does not fully do away with the photopolarization[2]. Variation of the polarization of a photoelectret (as characterized by the initial value of the discharge current) with the illumination time is shown in Fig.4. The single crystal specimen was polarized with "white" light from the mercury lamp at an applied voltage of 200 v and an illumination intensity of $3\cdot10^{-4}$ watt/cm^2. The voltage was in all cases applied for 10 min, while the time of illumination was varied. The depolarization was effected with "white" light ($3\cdot10^{-4}$ watt/cm^2) 5 min after the end of polarization.

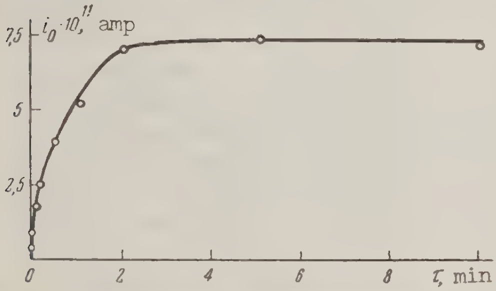

Fig.4. Variation of the initial depolarization current i_o with the illumination time τ during polarization.

It will be seen from the figure that in this case there is obvious saturation, i.e., further increase in illumination time leads to no further increase of the residual polarization.

In the case of illumination of the specimen for 1 sec (a photographic camera shutter was used for short exposures), there was obtained a polarization characterized by an initial discharge current $i_o = 0.8\cdot10^{-11}$ amp, whereas with dark polarization for a period of 10 min, the initial discharge current, as before, did not exceed $0.5\cdot10^{-11}$ amp. With shorter exposure times (for example, 0.2 sec), however, the total polarization proved to be virtually equal to the dark polarization; in other words, the photopolarization effect could not be detected. In order to determine the effective photopolarization of polycrystalline sulfur, induced in the range of short illumination times, one must, according to Nadzhakov & Kashukeev[2], initiate depolarization after the lapse of sufficient time for the dark polarization to disappear completely so that only photopolarization remains. In the case of sulfur single crystals, however, this procedure is not suitable inasmuch as in this case the entire residual polarization of the crystal rapidly falls off to zero.

From a comparison of the curves of Figs.4 and 2 it may be inferred that the law of interchangeability (of illumination intensity and time) does not hold as regards internal polarization in a single crystal. This means that with a constant value of E·τ (where E is the illumination on the surface of the specimen and τ is the illuminating time), the magnitude of the residual polarization depends on the time during which the specimen is illuminated in the electric field.

The saturation effect observed in investigating the variation of the polarization of a photoelectret with the light intensity and the illuminating time in the process of polarization, in both cases, apparently, is connected with filling of the entire finite number of electron traps participating in the polarization process. Using monochromatic light and knowing the quantum efficiency, one can on this assumption calculate from the experimental curves the number of traps involved in polarization.

Temperature dependence of the rate of depolarization of photoelectrets

We carried out a series of experiments aimed at determining the rate of depolarization of sulfur single crystals at different temperatures.

To this end the test capacitor with the specimen was placed in a pumped quartz container equipped with a heater. The container could be lowered into a Dewar with liquid nitrogen. Thus we could measure the polarization and depolarization in the specimen in vacuum at different temperatures and also observe the effects connected with continuous variation of temperature. The temperature of the specimen was measured by a copper-constantan thermocouple.

The specimen was polarized at a potential of 300 v, with illumination by "white" light from the mercury vapor tube at room temperature for 10 min. Immediately after polarization, the container was lowered into the Dewar with liquid nitrogen and the apparatus brought to the requisite temperature. Then the specimen was depolarized by illumination with "white" light of the same intensity as employed during polarization.

A typical depolarization curve for a sulfur single crystal is shown in Fig.5. Illumination of the specimen at -103° led to only partial depolarization (initial falling portion of the curve). It will be seen from the curve that 10 minutes after the beginning of illumination the depolarization process virtually terminated and further illumination led to no additional discharge of the photoelectret. At this time the heater was switched on and the specimen was gradually warmed with continued illumination.

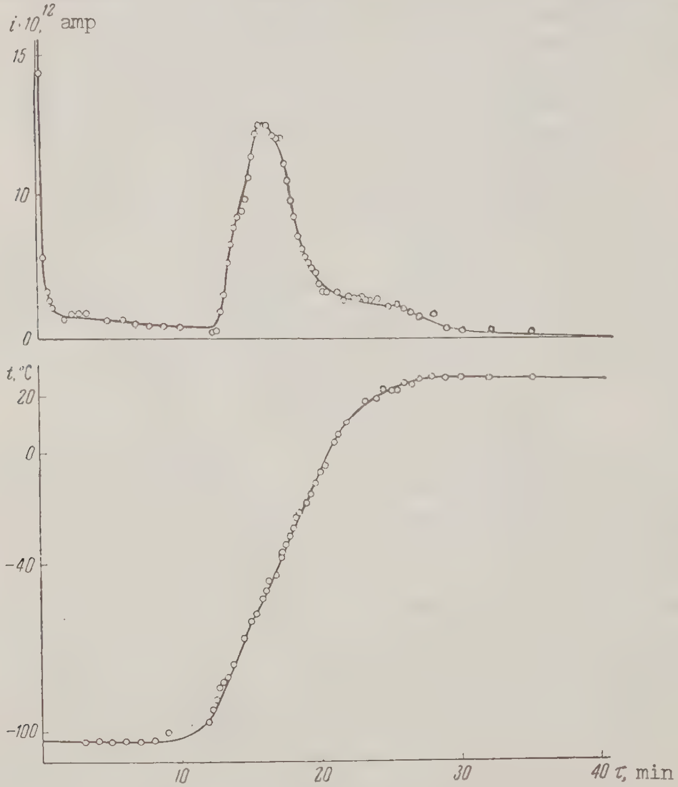

Fig.5. Curve characterizing the discharge current during depolarization of a sulfur single crystal photoelectret in the process of illumination and heating (above) and the corresponding temperature curve (below).

It will be evident from Fig.5 that heating of a photoelectret gives rise to a characteristic discharge current peak so that the discharge current falls off to zero only some time after the specimen has been heated to room temperature. The shape and height of the discharge current peak depend on the rate of change of temperature of the photoelectret. The temperature variation in the above described experiment is shown by the lower curve in Fig.5. Similar discharge current curves were obtained for other initial depolarization temperatures.

The depolarization curves for photoelectrets obtained with simultaneous illumination and heating are similar to the depolarization curves for thermoelectrets obtained in a number of earlier investigations (see, for example, Ref.5). In these investigations depolarization of the thermoelectrets by heating and subsequent integration of the discharge current over the discharge time were carried out for the purpose of determining the total charge of the electret.

Thus the photoelectret state obtained under the above described conditions is also a thermoelectret state inasmuch as illumination of the photoelectret at low temperature results only in its partial discharge and complete depolarization is realized only when the specimen is heated to the temperature at which it was polarized (in our case to room temperature). It is obvious, too, that the state of the sulfur specimen realized in our experiments is not a purely thermoelectret one, inasmuch as for complete depolarization of the electret, both heating and illumination are required. Experiments showed that heating of the photoelectret without simultaneous illumination is not accompanied by a measurable (under our experimental conditions) discharge current, although the total charge of the photoelectret is somewhat reduced. Thus the above described state of the polarized sulfur single crystal may be termed a thermophotoelectret state.

It is apparent that the thermophotoelectret state in a sulfur single crystal is due, on the one hand, to trapping of electrons at certain local levels and, on the other hand, to the presence of a thermal barrier separating the excitation level from the conduction band. Depolarization of the sulfur single crystal under the influence of illumination is connected with transition of the electrons to an excitation level from which the electrons can go over into the conduction band, the probability of the last transition being temperature dependent. This mechanism, which was proposed by Mott & Gurney[7] for explaining the temperature dependence of photoconductivity in alkali halide crystals, can, obviously, serve to explain the thermophotoelectret effect and, consequently, the appearance of a transitional discharge current peak in the process of depolarization of a photoelectret during simultaneous illumination and heating.

The authors are grateful to Academician A.V.Shubnikov and Academician (Bulgarian Academy of Sciences) G.Nadzhakov for discussion of the work and the results obtained and to Iu.N.Martyshev and A.I.Delovaia for assistance in carrying out the measurements.

References

1. G.Nadjakoff, Phys.Zs., 36, 226 (1938).
2. G.Nadzhakov & N.T.Kashukeev, Izv.Bulg.AN, Ser.fiz., 2, 321-337 (1951).
3. G.Nadzhakov & N.T.Kashukeev, ibid., 3, 103 (1952).
4. H.Kallmann & B.Rosenberg, Phys.Rev., 97, 1596 (1955).
5. A.I.Froiman & V.M.Fridkin, Kristallografiia (Crystallography), 1, 342 (1956).
6. G.Nadjakoff, ZS.phys.Chem., 36, 4, 314 (1937).

7. N.F.Mott & R.W.Gurney, Electronic Processes in Ionic Crystals. (Cited in Russian trans., M. 1950).

DISCUSSION FOLLOWING THE REPORTS OF K.V.FILIPPOVA AND I.S.ZHELUDEV & V.M.FRIDKIN

G.P.Mikhailov: The experimental results obtained by K.V.Filippova are of great interest. The experiments themselves have been carried out carefully and accurately, but the molecular explanation of the electret state of polymethyl methacrylate does not follow from the data obtained. It must be borne in mind that a "segment" is only a hypothetical unit, a concept introduced in order to explain the thermal motion of molecules. Hence one must be more careful in operating with this concept: one cannot make the segment responsible for the observed effects.

G.I.Skanavi: Filippova showed in her work not only that the electret effect in polymethyl methacrylate is connected with the rise of optical anisotropy, which in itself is important, but also that the relaxation time of the electret charge at room temperature is appreciably shorter than the optical anisotropy relaxation time.

One can agree with Filippova that the dipole groups are responsible for the electret effect. These groups are connected with larger formations, for example, segments, whose orientation in turn produces the optical anisotropy. At room temperature the disorientation time of the segments, as follows from the experimental data, exceeds the disorientation time of the dipole groups. Contrary to the assertions of G.P.Mikhailov this interpretation at this stage of the work is legitimate and is not in conflict with the experimental data.

K.B.Tolpygo (on the report of Zheludev & Fridkin): It seems to me that the experimental work is now at the stage where one can risk proposing a definite model and energy scheme for the electron levels. Apparently, one can hypothesize the presence of principal impurity levels and "sticking" levels. One can treat the experimental results on the basis of a definite model and determine, in particular, the energy separation of the local levels from the conduction band. In this connection I would like to take this occasion to summarize the discussions regarding the band theory of solids, that have recently been going on among theoretical physicists in the Soviet Union.

Most solid state theorists are now in agreement that the concept of a "lower wholly filled band" is antiquated. Inasmuch as the electrons of a crystal interact strongly with each other, one cannot speak of the energy of each electron. Only the concept of the energy of the entire system of electrons has any meaning. The separation of this quantity into the energies of individual electrons involves a certain degree of arbitrariness. Hence in speaking of the "structure of the filled band", we are speaking not of subjective reality but of interpretation of one of the methods of calculating the electron states. If there is present in the dielectric one excess electron, the state of the dielectric is represented by a band of allowed energy values. The energy of the crystal is presented as a function of the velocity (or wave vector) of thie "excess" electron. Analogously a dielectric with one electron removed also has continuous energy spectrum. In this case one can speak of a "hole band" in which the energy is a function of the "hole" wave vector. In the case when both free electrons and holes are absent, the normal state of the dielectric is represented by one discrete energy level for the entire system of electrons. In addition, there may exist in the crystal excited currentless states, so-called "excitons", for which there is no place in the conventional band scheme. Apparently, however, a number of processes occurring in solids cannot be properly understood without recourse to the exciton concept.

Further, in speaking of the internal photoeffect from local electron levels, we often have in mind direct electron transitions into the conduction band. Actually, the probability of such transitions is very low. Appreciably more probable are transitions under the influence of light from the ground state of the impurity center to an excited state. Subsequent transition of the electron into a conducting state requires a small activation energy: of the order of 0.1-0.15 ev. As a result we have temperature dependence of the internal photoeffect. "Additional excitation" of an electron into the conduction band can also be realized by means of infrared illumination at low temperature. This procedure has the advantage that with it only the electrons of interest to us, i.e., the electrons on shallow levels or trapping levels, are subject to the external influence. In contrast, change of temperature, i.e., heating, affects a number of different properties of the crystal.

MULTIPLE COMPONENT ORGANIC ELECTRETS

-Iu. Ia. Ianson

We prepared electrets from mixtures of organic substances. Our investigations show that the best electrets, i.e., electrets having the strongest and most stable electric field, are obtained from a mixture of 40% Carnauba wax, 40% rosin and 20% beeswax. This mixture was melted, introduced between electrodes to which a potential of 10 kv/cm was applied and allowed to cool slowly. After solidification, the potential was removed and charges appeared on surfaces of the sample. For a certain period, these charges varied and then attained a constant value, which in the immediate proximity of the surfaces amounted to an electrostatic field intensity of 24 kv/cm; this remained constant with minor fluctuations over a period of more than 1 year. We prepared electrets having a thickness $d = 3$ mm and a surface area $s = 30$ cm^2.

The electric field intensities of the electrets were measured by the method of electrostatic induction by means of a quadrant electrometer. Appropriate electrodes were applied to the electret; the lower electrode was grounded and the upper connected to one of the quadrant pairs of the electrometer. Initially both quadrant pairs were grounded, then the quadrant pair connected to the electret was disconnected from the ground and the electrode lifted off the electret. The induced charge then leaped to the electrometer. This allowed of determining the charge $q = CV = \sigma s$, where C is the total capacitance of the system, V is the potential to which the electrometer was charged, σ is the surface charge density and s is the area of the electrode. Having measured σ, one can calculate the electric field strength by means of the formula $E = 4\pi\sigma$.

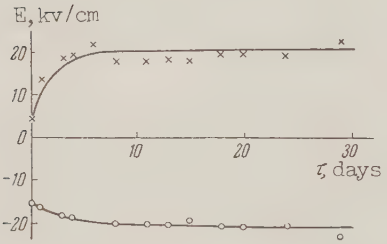

Fig.1. Variation of the electric field E of homocharges with time τ for electrets prepared by slow cooling.

Most of the experiments were carried out with electrets prepared of a mixture of 40% Carnauba wax + 40% rosin + 20% beeswax. It was found that with slow reduction of the temperature in the process of preparation of the electret (2.5 hours) there were obtained electrets with homocharges (charges having the same polarity as the forming electrodes), which gradually increased and after 15 days attained a constant value. The results of measurements on one of the samples are shown in Fig.1.

In the case of rapid cooling of the same mixture (40 min), there were obtained electrets with heterocharges (charges opposite in polarity to that of the forming electrodes), which gradually decreased. At the end of 5 days these charges fell off to zero and then the polarity was reversed, i.e., there appeared homocharges which gradually increased over a period of 6 months to a final field intensity of $E = 21$ kv/cm. Thereafter the homocharges remained constant. Variation of the electric field intensity of one of these electrets as a function of time over a period of 30 days is shown in Fig.2.

We also carried out experiments on the preparation of electrets from substances that do not naturally form electrets with small additions of materials that do.

Thus we added 0.5% of the mixture of Carnauba wax (40%), rosin (40%) and beeswax (20%) to pure paraffin which, as is known, does not itself form electrets. In this case we obtained an electret with homocharges, which after 30

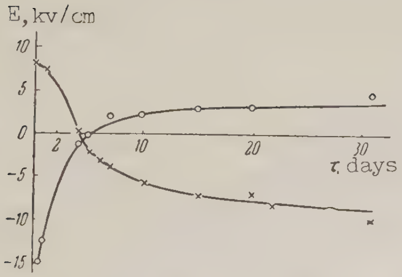

Fig.2. Variation of E with time τ of an electret prepared by slow cooling.

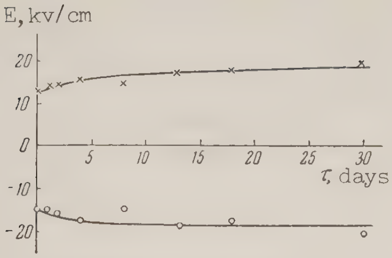

Fig.3. Variation of E with time τ obtained for a mixture of paraffin with 0.5% of a substance forming electrets.

days exhibited a field strength of 21 kv/cm at the surface. The results of measurements on this sample are shown in Fig.3.

As a result of all our experiments (not all of which have been described above), we came to the conclusion that the principal roles in the formation of electrets are played by orientation of dipoles in the electric field, external polarization, i.e., transfer of charges from the electrodes to the material forming the electret, and internal polarization, i.e., accumulation of space charges at the electrodes due to a certain conductivity of the sample.

Work on determining the relative importance of these different factors in the formation of electrets is continuing.

Faculty of General Physics,
Kazan State University

References

1. Problemy sovermennoi fiziki (Problems of modern physics), Series 3, No.17 (1951).
2. V.G.Nazarov, Elektrety i ikh primenenie v elektrotekhnike (Electrets and their application in electrical engineering) Elektrichestvo (Electricity), 7 (1954).
3. M.Eguchi, Phil.Mag., 49 (1925).
4. J.Euler, ETZ (1950).

Bulletin of the Academy of Sciences of the USSR - Physical Series
Vol. 22, No.3

Transactions of the All-Union Conference on the Physics of Dielectrics

TABLE OF CONTENTS

	Page	
	Orig.	Trans.
Nonferroelectric dielectrics with a high dielectric constant (Abstract) - G.I.Skanavi, Ia.M.Ksendzov, V.A.Trigubenko & V.G.Prokhvatilov	235	233
Influence of impurities on the electric properties of rutile - Ia.M.Ksendzov	237	234
Relaxation theory of electric polarization - N.S.Fastov & B.N.Finkel'shtein	249	246
Polarization and dielectric loss in solid solutions of the first and second kinds (Abstract) - G.A.Smolenskii, V.A. Isupov, A.I.Agranovskaia & E.D.Sholokhova	236	249
Theory of systems comprising noncentrally interacting particles - A.E.Glauberman	254	252
Ionic displacement polarization in complex ionic crystals - A.E.Glauberman & I.M.Spitkovskii	260	258
Thermal ionic polarization and slow processes in solid dielectrics - V.N.Lozovskii	263	261
Orientational polarization of dipole gases, solutions and liquids taking into account the internal field - A.A.Borgardt	268	266
Mechanism of relaxation dielectric loss in crystal hydrates - I.Ts.Liast	276	274
Structural loss in amorphous dielectrics - V.Kh.Kozlovskii	279	277
Dielectric loss at high frequencies in muscovite with inclusions of limonite and biotite - K.A.Vodop'ianov & I.G.Vorozhtsova	283	282
Dielectric loss at high frequencies in pure and mixed alkali halide crystals - K.A.Vodop'ianov & G.I.Galibina	288	287
Dielectric constant, dielectric loss and electric conductivity of alkali halide single crystals - B.N.Matsonashvili	296	294
Dielectric constant of rock salt at high temperatures - M.S.Kosman & N.A.Petrova	311	308
Dielectric constant of zinc oxide with an admixture of bismuth oxide - M.S.Kosman & I.A.Gesse	315	312
Dielectric constants of bismuthates of some metals - A.M.Kashtanova & G.I.Skanavi	319	316
Influence of grinding on the dielectric properties of polycrystalline barium titanate - G.M.Kovalenko	321	318
Dielectric loss and polarization in polymers (Abstract) - G.P.Mikhailov & A.M.Lobanov	323	320
Theory of dipole moments of polymer molecules (Abstract) - O.B.Ptitsyn, T.M.Birshtein & Iu.A.Sharonov	324	321
Dielectric loss in crystalline non-polar polymers - S.P.Kabin & G.N.Mikhailov	325	322
Preparation and properties of new electrets of inorganic dielectrics - A.N.Gubkin & G.I.Skanavi	330	327

Investigation of the electric and optical properties of electreted polymers - K.V.Filippova	343	340
On the photoelectret and thermoelectret states in sulfur single crystals - I.S.Zheludev & V.M.Fridkin	352	348
Multiple component organic electrets - Iu.Ia.Ianson	359	356

Translated in 1959 by
Columbia Technical Translations
5 Vermont Ave., White Plains, N.Y.

TRANSACTIONS OF THE ALL-UNION CONFERENCE
ON THE
PHYSICS OF DIELECTRICS

Dnepropetrovsk, August 1956

(Continued from Vol.22, No.3)

BEHAVIOR OF GERMANIUM-TYPE VALENCE CRYSTALS IN STRONG ELECTRIC FIELDS

- V.A.Chuenkov

Let us consider a valence crystal of the germanium type, the width of whose conduction band is at least twice as great as the width of the forbidden band* (here we shall consider only crystals with n-type conductivity).

The distribution of conduction electrons in a strong electric field taking into account electron scattering by optical and acoustic mode vibrations of the lattice, ionization by electron impact, generation (thermal generation, the Zener effect and the Frenkel effect) and recombination may be characterized by a function of the form

$$f(\varepsilon, \theta) = f_0(\varepsilon) + f_1(\varepsilon)\cos\theta \tag{1}$$

where $\varepsilon > \hbar\omega_0$ (where ε is the electron energy and ω_0 is the frequency of the optical vibrations of the lattice). Whence we obtain

$$f_0(\varepsilon) = \exp\left(-\int_{\varepsilon_p}^{\varepsilon} \frac{b(\varepsilon)}{a(\varepsilon)}\, d\varepsilon\right)\cdot\left[C_1 - \int_{\varepsilon_p}^{\varepsilon} \frac{j(\varepsilon)\, d\varepsilon}{2\pi\left(\frac{2}{m^*}\right)^{3/2} a(\varepsilon)} \exp\left(\int_{\varepsilon_p}^{\varepsilon} \frac{b(\varepsilon)}{a(\varepsilon)}\, d\varepsilon\right) d\varepsilon\right], \tag{2}$$

$$f_1(\varepsilon) = -\frac{eE\sqrt{\frac{2}{m^*}}}{\frac{1}{4}\frac{a_0 k_0 T}{m^* u^2} + \frac{8 b_0 c_0}{3\hbar\omega_0}\varepsilon + \varepsilon^{-1/2} W_i(\varepsilon) + \varepsilon^{-1/2} W_{rec}(\varepsilon)}\frac{df_0}{d\varepsilon}. \tag{3}$$

In calculating the distribution function it was assumed that the probability of electron scattering by the acoustic and optical modes is given by[2]:

$$P_a^{ac,op} = \frac{4\pi}{9} C^2_{ac,op} \sigma^2 \frac{N_\sigma}{MN\hbar\omega_\sigma}\delta(\xi) \tag{4}$$

in the case of absorption of a phonon by the electron, and by

$$P_e^{ac,op} = \frac{4\pi}{9} C^2_{ac,op} \sigma^2 \frac{N_\sigma + 1}{MN\hbar\omega_\sigma}\delta(\xi) \tag{5}$$

in the case of emission of a phonon by the electron.

The ionization cross section was assumed to be

$$Q(\varepsilon, \varepsilon^*) = S_0(\varepsilon - I - \varepsilon^*), \tag{6}$$

where ε is the energy of the ionizing electron, I is the width of the forbidden band, ε^* is the energy of an electron in the valence band referred to its upper edge and S_0 is a constant. Assuming that the density of states in the valence band as a function of ε^* is given by

$$n_b(\varepsilon^*) = \beta\varepsilon^{*1/2}, \tag{7}$$

we obtain the following expression for the probability of ionization by an electron of energy ε:

$$W_i(\varepsilon) = S_0\beta\sqrt{\frac{2}{m^*}}\int_0^{\varepsilon - I} \varepsilon^{1/2}(\varepsilon - I - \varepsilon^*)\,\varepsilon^{*1/2}\, d\varepsilon^* = \gamma_0 \varepsilon^{1/2}(\varepsilon - I)^{5/2}. \tag{8}$$

---

*Germanium and silicon generally satisfy this condition. The width of even the valence band in germanium is about 20 ev[1] (the width of the conduction band is still greater), whereas the width of the forbidden band is only 0.75 ev.

We have used the following notation in Eqs. (1)—(5):

$$a(\varepsilon) = \frac{\frac{2e^2E^2}{3m^*}\varepsilon}{\frac{1}{4}\frac{a_0k_0T}{m^*w^2} + \frac{8b_0c_0}{3\hbar\omega_0}\varepsilon + \varepsilon^{-1/2}W_{\mathrm{i}}(\varepsilon) + \varepsilon^{-1/2}W_{\mathrm{rec}}(\varepsilon)} + \left(b_0c_0\hbar\omega_0 + \frac{a_0k_0T}{2}\right)\varepsilon^2, \qquad (9)$$

$$b(\varepsilon) \doteq \left(\frac{a_0}{2} + 2b_0\right)\varepsilon^2, \qquad a_0 = \frac{16\sqrt{2}C_{\mathrm{ac}}^2\Delta m^{*5/2}}{9\pi M\hbar^4}, \qquad (10)$$

$$b_0 = \frac{4\sqrt{2}C\Delta m_{\mathrm{op}}^{2\,*5/2}}{9\pi M\hbar^4}, \qquad c_0 = \frac{e^{\frac{\hbar\omega_0}{k_0T}} + 1}{e^{\frac{\hbar\omega_0}{k_0T}} - 1}, \qquad (11)$$

$$N_\sigma = \frac{1}{e^{\frac{\hbar\omega_\sigma}{k_0T}} - 1}, \qquad \gamma_0 = \frac{4}{15}\sqrt{\frac{2}{m^*}}\,S_0 3, \qquad (12)$$

where e is the electron charge, m^* is the effective electron mass, θ is the angle between the direction of the electric field and the electron velocity vector, E is the electric field intensity, k_0 is Boltzmann's constant, T is the absolute temperature, w is the speed of sound, M is the mass of the atoms composing the lattice, $\hbar$ is Planck's constant, Δ is the volume of a unit cell, $W_{\mathrm{rec}}(\varepsilon)$ is the probability for recombination, C_{ac} and C_{op} are constants, σ is the phonon wave number, N is the number of unit cells in the crystal, C_1 and ε_p are arbitrary constants, ω_σ is the lattice vibration frequency ($\omega_\sigma = w\sigma$ for the acoustic mode and $\omega_\sigma = \omega_0$ for the optical mode), $\delta(\xi)$ is the δ-function of the argument

$$\xi = \varepsilon_{\mathbf{k}'} - \varepsilon_{\mathbf{k}} \pm \hbar\omega_\sigma,$$

where $\varepsilon_{k'}$ and k' are, respectively, the energy and momentum of the electron after scattering and ε_k and k the energy and momentum before scattering; $j(\varepsilon) = N_i^0(\varepsilon) + G_T(\varepsilon) - R(\varepsilon) - N_i(\varepsilon)$ is the electron flux in energy space with $N_i^0(\varepsilon)$ and $G_T(\varepsilon)$ being the number of electrons entering the region from 0 to ε per unit time as a result of ionization and generation, respectively, and $R(\varepsilon)$ and $N_i(\varepsilon)$ being the number of electrons leaving the region from 0 to ε per unit time as a result of recombination and ionization, respectively.

We note that one can discard the term with $W_{\mathrm{rec}}(\varepsilon)$ in Eqs. (3) and (9) even with a very high concentration of recombination centers.

Let us first consider the values of E at which ionization by electron impact and the Zener and Frenkel effects play no significant role (the electron concentration is independent of E) so that $j(\varepsilon) = 0$. In this case

$$f_0(\varepsilon) = C_1^0 \exp\left[-\int_0^{\varepsilon} \frac{\left(\frac{a_0}{2} + 2b_0\right)\varepsilon^2 d\varepsilon}{\frac{2e^2E^2/3m^*\cdot\varepsilon}{\frac{1}{4}\frac{a_0k_0T}{m^*w^2} + \frac{8b_0c_0}{3\hbar\omega_0}\varepsilon} + \left(b_0c_0\hbar\omega_0 + \frac{a_0k_0T}{2}\right)\varepsilon^2}\right], \qquad (13)$$

$$f_1 = -\frac{eE\sqrt{\frac{2}{m^*}}}{\frac{1}{4}\frac{a_0k_0T}{m^*w^2} + \frac{8b_0c_0}{8\hbar\omega_0}\varepsilon}\,\frac{df_\theta}{d\varepsilon}. \qquad (14)$$

Let us consider some limiting cases.

1. The electric field is weak and the mean electron energy is low so that $\frac{1}{4}\frac{a_0k_0T}{m^*w^2} \gg \frac{8b_0c_0}{3\hbar\omega_0}\bar{\varepsilon}$, and in Eq. (13) one can disregard the term containing E. Then

with $k_0T > \hbar\omega_0$

$$f_0(\varepsilon) = C_1^0 e^{-\frac{\varepsilon}{k_0T}}, \quad f_1 = -\frac{4m^* u^2 e \sqrt{\frac{2}{m^*}}}{a_0k_0T} E \frac{df_0}{d\varepsilon}, \tag{15}$$

and the electron mobility

$$\mu_0 = 3\sqrt{\frac{\pi}{2}} \frac{e\hbar^4 M u^2}{C_{\text{ac}}^2 \Delta m^{*5/2} k_0^{3/2}} T^{-3/2}. \tag{16}$$

2. The electric field intensity is such that in the denominator of the expression under the integral in Eq.(13) we can disregard the term not containing E. The mean electron energy, however, is not very great so that as before $\frac{1}{4} \cdot \frac{a_0k_0T}{m^*u^2} \gg \frac{8b_0c_0}{3\hbar\omega_0} \bar{\varepsilon}$. Under these assumptions we obtain (in this case the condition $k_0T > \hbar\omega_0$ is not necessary inasmuch as in a strong field $\bar{\varepsilon} > \hbar\omega_0$ and at low temperatures):

$$f_0 = C_1^0 \exp\left[-\frac{3}{32} \cdot \frac{a_0^2 k_0 T}{e^2 w^2 E^2}\left(1 + \frac{C_{\text{op}}^2}{C_{\text{ac}}^2}\right)\varepsilon^2\right], \quad f_1 = -\frac{4\sqrt{2m^*}\, e w^2}{a_0k_0T} E \frac{df_0}{d\varepsilon}, \tag{17}$$

$$\mu = \frac{\sqrt{2\pi}}{3^{3/4}\Gamma\left(\frac{3}{4}\right)(m^*k_0T)^{1/4}} \left(1 + \frac{C_{\text{op}}^2}{C_{\text{ac}}^2}\right)^{1/4} \left(\frac{elw}{E}\right)^{1/2}, \tag{18}$$

where $\Gamma\left(\frac{3}{4}\right)$ is a γ-function and the free path length is

$$l = \frac{9\pi M \hbar^4 w^2}{4C_{\text{ac}}^2 \Delta m^{*2} k_0 T}. \tag{19}$$

The electric field at which Eq.(16) transforms into Eq.(18) is approximately

$$E_1 = \frac{4}{\sqrt{\pi}} \cdot \frac{w}{\mu_0} \cdot \frac{\left(1 + \frac{1}{2} \cdot \frac{\hbar\omega_0}{k_0T} c_0 \frac{C_{\text{op}}^2}{C_{\text{ac}}^2}\right)}{\left(1 + C_{\text{op}}^2 / C_{\text{ac}}^2\right)^{1/2}}. \tag{20}$$

The field E_1 was determined from the equation (see Eq.(13))

$$\frac{8}{3} \cdot \frac{e^2w^2E^2}{a_0k_0T} = \left(\frac{a_0k_0T}{2} + b_0c_0\hbar\omega_0\right)\varepsilon_{m1},$$

where ε_{m1} is the energy satisfying the condition for a maximum of $\varepsilon^{1/2} f_0(\varepsilon)$, $f_0(\varepsilon)$ being taken in the form (13), bearing in mind the inequality

$$\frac{1}{4} \cdot \frac{a_0k_0T}{mw^2} \gg \frac{8b_0c_0}{3\hbar\omega_0} \varepsilon.$$

3. The electric field and the mean electron energy are so great that in addition to the first condition under paragraph 2 above the condition

$$\frac{8b_0c_0}{3\hbar\omega_0} \bar{\varepsilon} \gg \frac{1}{4} \cdot \frac{a_0k_0T}{m^*u^2};$$

is fulfilled; in this case

$$f_0(\varepsilon) = C_1^0 \exp\left[-\frac{2}{3} \cdot \frac{a_0b_0c_0m^*}{\hbar\omega_0 e^2 E^2}\left(1 + \frac{C_{\text{op}}^2}{C_{\text{ac}}^2}\right)\varepsilon^2\right];$$

$$f_1(\varepsilon) = -\frac{3e\sqrt{\frac{2}{m^*}\hbar\omega_0}}{8b_0c_0\varepsilon} E\frac{df_0}{d\varepsilon}, \tag{21}$$

and μ and the electron drift velocity are given by

$$\mu = \left(\frac{3\hbar\omega_0}{2\pi m^* c_0}\right)^{1/2} \left(1 + \frac{C^2_{\rm ac}}{C^2_{\rm op}}\right)^{1/2} \frac{1}{E} \quad \text{and} \quad v_{\rm dr} = \mu E = \left(\frac{3\hbar\omega_0}{2\pi m^* c_0}\right)^{1/2} \left(1 + \frac{C^2_{\rm ac}}{C^2_{\rm op}}\right)^{1/2}. \tag{22}$$

The electric field E_2 at which Eq.(18) transforms into Eq.(22) is approximately

$$E_2 = \frac{\hbar\omega_0}{\sqrt{\pi m^* c_0\mu_0 w}} \left(1 + \frac{C^2_{\rm op}}{C^2_{\rm ac}}\right)^{1/2} \frac{C^2_{\rm ac}}{C^2_{\rm op}}. \tag{23}$$

The field E_2 is determined from the equation (see Eq.(13))

$$\frac{1}{4}\cdot\frac{a_0k_0T}{m^* w^2} = \frac{8b_0c_0}{3\hbar\omega_0}\varepsilon_{m2},$$

where ε_{m2} is the energy satisfying the condition for the maximum of the function $\varepsilon^{3/2}f_0(\varepsilon)$, $f_0(\varepsilon)$ being taken in the form (13), discarding the term not containing E in the denominator of the expression under the integral.

The variation of the electron mobility with the electric field strength E characterized by Eqs.(16), (18) and (22) was observed experimentally in the work of Ryder[3], who also gives values of E_1, E_2 and $v_{\rm dr}$.

Let us now select values of the parameters $C_{\rm ac}$, $C_{\rm op}$ and m^* so that the four equations, Eqs.(16), (20), (22) & (23), will yield the best agreement of theory with experiment. The results are given in the accompanying table.

Material	E_1, v/cm		E_2, v/cm		$v_{\rm dr}$, cm/sec		$\frac{C^2_{\rm op}}{C^2_{\rm ac}}$	m^*
	theory	exper.	theory	exper.	theory	exper.		
n-type germanium	888	890	$5{,}1\cdot10^3$	$3{,}8\cdot10^3$	$4{,}6\cdot10^6$	$6{,}3\cdot10^6$	6,2	$0{,}53m_0$
n-type silicon	$4{,}5\cdot10^3$	$3{,}2\cdot10^3$	$2{,}7\cdot10^4$	$2{,}0\cdot10^4$	$7{,}2\cdot10^6$	$8{,}9\cdot10^6$	4	$0{,}8\,m_0$

Let us now examine the value of E at which ionization by electron impact plays a substantial role $(j(\varepsilon) \neq 0)$ and let us try to determine the critical field $E_{\rm cr}$ at which multiplication of electrons begins (recombination cannot compensate for the increase in number of electrons due to ionization) and electric breakdown of the material is initiated.

Let us introduce the quantity $\varepsilon_{\rm p}$, i.e., the value of the energy at which an electron on the average receives as much energy from the field as it gives up to the lattice. From Eqs.(2) & (3) we obtain, according to Ref.4, the following expression for $\varepsilon_{\rm p}$:

$$\frac{3m^*\varepsilon_{\rm p}b(\varepsilon_{\rm p})}{2e^2E^2}\left(\frac{a_0k_0T}{2} + b_0c_0\hbar\omega_0\right)\left[\frac{1}{4}\frac{a_0k_0T}{m^*w^2} + \frac{8b_0c_0}{3\hbar\omega_0}\varepsilon_{\rm p} + \gamma_0(\varepsilon_{\rm p} - I)^{5/2}\right] = \frac{j(\varepsilon_{\rm p})}{2\pi\left(\frac{2}{m^*}\right)^{3/2}C_1}. \tag{24}$$

Inasmuch as in valence crystals the probability of electron scattering by lattice vibrations increases with increase in electron energy (this may be shown by integrating Eqs.(4) & (5) over the wave numbers σ) all the electrons having an energy $\varepsilon < \varepsilon_{\rm p}$ will on the average be accelerated by the field, while electrons with $\varepsilon > \varepsilon_{\rm p}$ will on the average be slowed down by the lattice; we note that in general

$$\frac{d\varepsilon_p}{dE} > 0.$$

Let us denote through ε_1 the value of the energy at which the probability of ionization is equal to the probability of scattering by lattice vibrations. At $\varepsilon < \varepsilon_1$ scattering of lattice vibrations predominates, while with $\varepsilon > \varepsilon_1$ ionizing collisions are more probable; it may be noted that the transition from one case to the other is rather sharp (see Eq.(26)).

From what has been said above it is obvious that with $\varepsilon_p < \varepsilon_1$ electrons coming into the energy range $0 \leqslant \varepsilon \leqslant \varepsilon_p$ due to ionization cannot on the average attain an energy high enough to be capable of again ionizing (at $\varepsilon < \varepsilon_1$ scattering by lattice vibrations is more probable). In this case only a relatively small number of electrons enters into the $\varepsilon > \varepsilon_1$ region by fluctuation. Clearly under these conditions an electron avalanche cannot develop. On the contrary, with $\varepsilon_p > \varepsilon_1$, electrons raised to the $0 \leqslant \varepsilon \leqslant \varepsilon_p$ region due to ionization are accelerated by the field through such values of ε where they can again ionize. Thus, in this case, there are created conditions for an electron avalanche and electric breakdown of the crystal. In view of the above, a criterion for electric breakdown of valence crystals of the germanium type may be the condition

$$\varepsilon_p(E_{cr}) = \varepsilon_1, \tag{25}$$

where the quantity ε_1 is to be found, in accord with the above definition, from the following equation (see Eqs.(3) & (8)):

$$\frac{1}{4} \cdot \frac{a_0 k_0 T}{m^* w^2} + \frac{8 b_0 c_0}{3\hbar\omega_0} \varepsilon_1 = \gamma_0 (\varepsilon_1 - I)^{5/2}. \tag{26}$$

Now with $\varepsilon_p = \varepsilon_1$ the value of ε_p must approximately satisfy yet another equation. Thus, it may be assumed that in a strong electric field the distribution function falls off only at such values of ε, where ionization begins to play a significant role, i.e., at $\varepsilon > \varepsilon_1$ (numerical evaluations substantiate this assumption). With $\varepsilon < \varepsilon_1$ the value of $f_0(\varepsilon)$ changes slowly with increasing ε; here, however, the probability of ionization is low. Consequently, under these conditions the maximum number of ionizations is attributable to electrons with energy $\varepsilon \approx \varepsilon_p = \varepsilon_1$.

Thus the quantity ε_p must also satisfy the following equation (see Eqs. (2) and (8)):

$$\frac{d}{d\varepsilon} [W_i(\varepsilon) f_0(\varepsilon) \varepsilon^{1/2}]_{\varepsilon = \varepsilon_p} = 0, \tag{27}$$

whence

$$\frac{j(\varepsilon_p)}{2\pi \left(\frac{2}{m^*}\right)^{3/2} \cdot C_1} = \frac{\frac{7}{2}\varepsilon_p - I}{\varepsilon_p(\varepsilon_p - I)} a(\varepsilon_p) - b(\varepsilon_p). \tag{28}$$

Combining (24), (28) and (25) leads to the following expression (after simplification) for the critical field intensity E_{cr} at which electric breakdown occurs

$$E_{cr} = \frac{16}{3} \sqrt{\frac{2}{7\pi}} \cdot \frac{C_{op}^2}{C_{ac}^2} \cdot \frac{m^{*1/2} w^2}{\mu_0 (k_0 T)^{3/2} (\hbar\omega_0)^{1/2}} \varepsilon_1 (\varepsilon_1 - I)^{1/2} \left(\frac{e^{\frac{\hbar\omega_0}{k_0 T}} + 1}{e^{\frac{\hbar\omega}{k_0 T}} - 1} \right)^{1/2}, \tag{29}$$

where μ_0 is the mobility in a weak field (see Eq.(16)). There is one unknown parameter - $S_0\beta$ (see Eq.(12)) - in Eqs.(26) and (29).

Experiments on the breakdown of wide p-n junctions[5] yield $E_{cr} = 9\cdot10^4$ c/cm for germanium at room temperature. From this we obtain $S_0\beta = 1.65\cdot10^{35}$ (in cgs units). If the ionization cross section at $\varepsilon \approx 3I$ is taken to be 10^{-16} cm^2, then $S_0 \approx 10^{-4}$ (see Eq.(6) and $\beta \approx 1.8\cdot10^{39}$. Knowing β, we obtain for the width of the valence band in germanium a value of about 20 ev which is in agreement with other data[1]. For silicon taking the same $S_0\beta$, we obtain at T = 300°K, the critical energy value $E_{cr} = 6.6\cdot10^5$ v/cm.

Calculations show that E_{cr} increases with increasing temperature linearly which is in agreement with the experimental data[6,7]. Theory, however, yields a sharper increase of E_{cr} with temperature. For example, for germanium in the temperature range from 120 to 340°K theory indicates a change of E_{cr} by a factor of 2.3, while experiment indicates a 1.3-fold increase;[6] in the case of silicon in the interval from 100 to 400°K theory shows an increase of E_{cr} by a factor of 1.7, whereas experiment[7] yields a factor of 1.15. The slower increase of E_{cr} with temperature observed in experiment is explained by the fact that the available experimental data were obtained for the breakdown of narrow p-n junctions wherein higher values of E are possible than in a homogeneous semiconductor to which our calculations apply. Actually at higher values of E the influence of temperature on breakdown is weaker. This is confirmed by the data of McKay[7] who reports that in junctions in which very high values of E are possible ($\sim10^6$ v/cm) no discernible temperature dependence of E_{cr} is observed. The value of ε_1 at T = 300°K proves to be 2.6 ev for germanium and 4 ev for silicon. This indicates one of the reasons why in bombardment of a semiconductor with electrons there is expended on the production of an electron-hole pair an energy ε^* appreciably exceeding the width of the forbidden band (at $\varepsilon < \varepsilon_1$ scattering by lattice vibrations predominates). The experimental value of ε^* is ~3-4 ev.

Thus theory allows of explaining some otherwise puzzling experimental data on the behavior of semiconductors in a strong electric field on the assumption that the electron has a certain scalar effective mass m^*, the value of which is intermediate between that of the longitudinal mass and that of the transverse mass.

"P.N.Lebedev" Physical Institute,
Academy of Sciences of the USSR

References

1. T.Sugita & E.Yamaka, Reports Electr.Commun.Lab., Nippon Telegr. & Teleph.Public Corp., 2, 8, 24 (1954).
2. W.R.Heller, Phys.Rev., 84, 1130 (1951).
3. E.J.Ryder, Phys.Rev., 90, 766 (1953).
4. V.A.Chuenkov, Izv.(Bulletin) Tomsk Polytechnic Institute, 91, 45 (1956).
5. B.M.Vul & A.P.Shotov, Radiotekhn.i elektronika 2, 1080 (1956).
6. A.P.Shotov, Zhur.tekh.fiz., 26, 1634 (1956).
7. K.McKay, Phys.Rev., 94, 877 (1954).

TOWARDS DERIVATION OF A CRITERION OF ELECTRIC BREAKDOWN OF IONIC CRYSTALS FROM THE KINETIC EQUATION

- V.A.Chuenkov

At present, on the basis of ample experimental data, it may be assumed that electric breakdown of solid dielectrics occurs due to ionization of atoms (or ions) of the dielectric by electron impact and formation of an electron avalanche.

Akhiezer & Lifshits[1] showed that the most rigorous condition for electric breakdown of a dielectric can be found from solution of the corresponding kinetic equation.

In an earlier paper[2], on the basis of physical considerations, using the distribution function for conduction electrons in a strong electric field deduced from solution of the kinetic equation, the author formulated a criterion for electric breakdown of ionic crystals, giving satisfactory agreement with experiment. This criterion, however, did not follow directly from solution of the kinetic equation.

Below, on the basis of a more rigorous solution of the kinetic equation, explicitly taking into account recombination processes, we shall attempt to show that the breakdown criterion formulated in Ref.2 follows directly from the kinetic equation.

Let us consider a homogeneous dielectric whose conduction band is at least twice as wide as the forbidden band (only in this case can one apply the method of effective masses). Let the electric field be directed along the z axis. We write the stationary integro-differential equation for the distribution function in the form

$$eE\frac{\partial f}{\partial P_z} = (b-a)_{\text{lat}} + (b-a)_{\text{ion}} + (b-a)_{\text{rec}} + g_T(\varepsilon). \tag{1}$$

Here f is the distribution function, e is the electron charge, P_z is the electron momentum component along the z axis, E is the strength of the external electric field and $(b-a)_{\text{lat}}$, $(b-a)_{\text{ion}}$ and $(b-a)_{\text{rec}}$ are the changes in the number of electrons per unit time in the given region of phase space due to scattering by lattice vibrations, to ionization and to recombination collisions, respectively. We understand $g_T(\varepsilon)$ to mean the change in number of electrons per unit time in the given region of phase space due to thermal generation and the Zener and Frenkel effects (hereinafter these three effects will be referred to simply as generation). For reasons outlined in Ref.2, we shall not take into account the change in number of electrons in phase space due to collisions leading to the rise of excited states.

We write the distribution function in the form

$$f = f_0(\varepsilon) + f_1(\varepsilon)\cos\theta, \tag{2}$$

where ε is the electron energy and θ is the angle between the electron velocity and the electric field vectors.

We separate the sets of possible values of ε into two regions:
1) $0 \leqslant \varepsilon \leqslant I$ and 2) $\varepsilon \geqslant I$.

Let us first consider the region $0 \leqslant \varepsilon \leqslant I$, where I is the ionization potential or the width of the forbidden band. In this case we obtain (the method of calculation of $(b-a)_{\text{lat}}$ is analogous to that given in Refs.2 & 3) with $\varepsilon \gg \hbar\omega$:

$$f_0(\varepsilon) = \exp\left(-\int\limits_{\varepsilon_p}^{\varepsilon} \frac{b(\varepsilon)}{a(\varepsilon)}\, d\varepsilon\right)\left[C_1 - \int\limits_{\varepsilon_p}^{\varepsilon} \frac{N_i^0(\varepsilon) + G_T(\varepsilon) - R(\varepsilon)}{2\pi\left(\frac{2}{m^*}\right)^{3/2} a(\varepsilon)} \exp\left(\int\limits_{\varepsilon_p}^{\varepsilon} \frac{b(\varepsilon)}{a(\varepsilon)}\, d\varepsilon\right) d\varepsilon\right], \tag{3}$$

$$f_1 = -\frac{\sqrt{\frac{2}{m^*}}\, eE\varepsilon}{g + \varepsilon^{1/2} W_{\mathrm{rec}}(\varepsilon)} \frac{df_0}{d\varepsilon} \quad \text{for } \varepsilon \leqslant \varepsilon'', \tag{4*}$$

$$f_1 = -\frac{\sqrt{\frac{2}{m^*}}\, eE\varepsilon^2}{q + \varepsilon^{3/2} W_{\mathrm{rec}}(\varepsilon)} \frac{df_0}{d\varepsilon} \quad \text{for } \varepsilon \geqslant \varepsilon''. \tag{5}$$

where

$$a(\varepsilon) = \frac{2e^2E^2\varepsilon^3}{3m^*\, g} + r \ln \frac{4\varepsilon}{\hbar\omega}; \qquad b(\varepsilon) = p \ln\left(\frac{4\varepsilon}{\hbar\omega}\right) \text{ for } \varepsilon \leqslant \varepsilon'', \tag{6}$$

$$a(\varepsilon) = \frac{2e^2E^2\varepsilon^3}{3m^*\, q} + r \ln\left(\frac{2\pi L_0}{\omega} \sqrt{\frac{2\varepsilon}{m^*}}\right); \qquad b(\varepsilon) = p \ln\left(\frac{2\pi L_0}{\omega} \sqrt{\frac{2\varepsilon}{m^*}}\right) \text{ for } \varepsilon \geqslant \varepsilon'', \tag{7}$$

$$\varepsilon'' = \left(\frac{3}{4\pi}\right)^{2/3} \frac{h^2}{8m^* a^2}, \tag{8**}$$

$$p = \frac{\pi\sqrt{2m^*}\, e^2 e^{**2}}{Ma^3}; \qquad r = \frac{\pi\sqrt{m^*}\, e^2 e^{**2}\hbar\omega}{\sqrt{2}\, Ma^3} \, \frac{e^{\frac{\hbar\omega}{k_0T}} + 1}{e^{\frac{\hbar\omega}{k_0T}} - 1}, \tag{9}$$

$$g = \frac{\pi\sqrt{2m^*}\, e^4}{Ma^3\hbar\omega_t} \, \frac{e^{\frac{\hbar\omega_t}{k_0T}} + 1}{e^{\frac{\hbar\omega_t}{k_0T}} - 1}; \qquad q = \frac{\pi^3 e^4 \hbar L_0^2}{\sqrt{2m^*}\, Ma^3\omega_t} \, \frac{e^{\frac{\hbar\omega_t}{k_0T}} + 1}{e^{\frac{\hbar\omega_t}{k_0T}} - 1}, \tag{10}$$

$$L_0 = \left(\frac{3}{4\pi}\right)^{1/3} \frac{1}{a}, \tag{11}$$

$W_{\mathrm{rec}}(\varepsilon)$ is the probability of recombination of an electron, m^* is the effective electron mass, a is the lattice constant, M is the reduced mass of the ions, k_0 is Boltzmann's constant, T is the absolute temperature, h is Planck's constant, ω_t is the frequency of the transverse optical vibrations of the lattice, ω is the effective frequency of the longitudinal optical mode and e^{**} is the effective charge of the ions. In contrast to what was done in Ref.2, here we have not subdivided the region of integration over wave numbers L into two regions: a long wave one and a short wave one. Consequently, the value of ω in Eqs.(6), (7) & (9) lies between ω_t and ω_0, determined in Ref.2 by Eq.(25) and the value of e^{**} lies between e and e^*, determined in Ref.2 by Eq.(24). This, without introducing any significant changes in the numerical calculations allows of simplifying computation of the distribution function. Further, $N_i^0(\varepsilon)$ and $G_T(\varepsilon)$ are the numbers of electrons entering the region from 0 to ε per unit time due to ionization and generation, respectively, and $R(\varepsilon)$ is the number of electrons leaving the region from 0 to ε due to recombination.

We note that there enter into the expression for $N_i^0(\varepsilon)$ both electrons that have undergone a transition due to ionization from the valence band to the conduction band and electrons that have undergone a transition due to ionization from the region $\varepsilon \geqslant I$ to the region $0 \leqslant \varepsilon \leqslant I$ (ionizing electrons), so that

---

*In Eqs.(4) & (5) the terms containing $W_{\mathrm{rec}}(\varepsilon)$ are small compared to g and q even at concentrations of recombination centers of the order of 10^{22} per cm^3.

**For alkali halide crystals $\varepsilon'' < I$, if $m^* \geqslant m_0$.

$$N_i^0(\varepsilon \to \infty) = 2N_i, \tag{12}$$

where N_i is the total number of ionizations per unit time. We assume here that the ionization cross section is isotropic, which is entirely allowable at low energy values $(\varepsilon \approx I)$ of the ionizing electrons[4]. We note further that generation of electrons is significant only at low values of ε (where $\varepsilon < 0.1$ ev), inasmuch as the probability of all three effects responsible for electron generation falls off rapidly with increasing ε.[2] The same observation applies to recombination of electrons.[2,5,6] Consequently, for $\varepsilon \geqslant 0.1$ ev, we have

$$\begin{gathered} G_T(\varepsilon) \approx G_T^0, \quad \frac{dG_T(\varepsilon)}{d\varepsilon} \approx 0, \\ R(\varepsilon) \approx R^0, \quad \frac{dR(\varepsilon)}{d\varepsilon} \approx 0, \end{gathered} \tag{13}$$

where G_T^0 is the total number of generations and R^0 is the total number of recombinations of electrons per unit time.

Quantities C_1 and ε_p in Eq.(3) are arbitrary constants.

Evaluations show that in solving the kinetic equation in the region $\varepsilon \geqslant I$, we can limit ourselves to taking into account the influence of the external field and the departure of electrons to the $0 \leqslant \varepsilon \leqslant I$ region due to ionization (this is valid for $E \geqslant 10^5$ v/cm). Then the expressions for f_0 and f_1 become

$$\frac{d}{dx}\left[\frac{x^3}{1 + a_0 x^2 (x-1)} \frac{df_0}{dx}\right] - \frac{b_0}{E^2} x(x-1) f_0 = 0, \tag{14}$$

$$f_1 = -\frac{\sqrt{\frac{2}{m^*}}\, eE\varepsilon^2}{q + \sqrt{\frac{2}{m^*}}\, NS_0 \varepsilon^2 (\varepsilon - I)} \frac{df_0}{d\varepsilon}, \tag{15}$$

where

$$x = \frac{\varepsilon}{I}; \quad a_0 = \sqrt{\frac{2}{m^*}} \frac{1}{q} NS_0 I^3; \quad b_0 = \frac{3m^{*1/2} q N S_0 I}{\sqrt{2}\, e^2}, \tag{16}$$

and N is the number of negative ions per unit volume (in alkali halide crystals ionization by electron impact consists of detachment of an electron from a negative ion); it is assumed above that the effective ionization cross section

$$Q(\varepsilon) = S_0(\varepsilon - I). \tag{17}$$

Substituting the new variable

$$y = \int \frac{1 + a_0 x^2 (x-1)}{x^3} dx, \tag{18}$$

in Eq.(14) we obtain

$$\frac{d^2 f_0}{dy^2} - \frac{b_0}{E^2} \frac{x^4 (x-1)}{1 + a_0 x^2 (x-1)} f_0(y) = 0, \tag{19}$$

where x in the factor next to $f_0(y)$ must be expressed in terms of y, according to Eq.(18).

The factor in front of $f_0(y)$ in the interval $1 \leqslant x \leqslant 3$, (the function f_0 begins to decrease sharply from $x = 2$) can be approximated with fair accuracy (within 5%) by

$$\frac{x^4(x-1)}{1+a_0x^2(x-1)} \approx \gamma_{10}(y-y_0)^\alpha, \tag{20}$$

where

$$y_0 = a_0 - \frac{1}{2}, \qquad \gamma_{10} = \frac{8{,}4}{(1+2{,}6a_0)(0{,}35+0{,}21a_0)^\alpha},$$

$$\alpha = \frac{\ln\left(20{,}25\,\dfrac{1+0{,}29a_0}{1+2{,}6a_0}\right)}{\ln\dfrac{0{,}35+0{,}21a_0}{0{,}15+0{,}02a_0}}. \tag{21}$$

Substituting (20) in (19) and taking into account the fact that in the stationary case $f_0 \to 0$ as $y \to \infty$ (at the same time $\varepsilon \to \infty$), we obtain

$$f_0 = C_2 \cdot \varkappa^{1/2} K_{\frac{1}{\alpha+2}}(\xi), \tag{22}$$

where $K_{\frac{1}{\alpha+2}}(\xi)$ is a cylindrical function of the third kind of order $\frac{1}{\alpha+2}$ of the argument

$$\xi(\varepsilon) = \frac{2c_0}{(\alpha+2)E}\,\varkappa(\varepsilon)^{\frac{\alpha+2}{2}}, \tag{23}$$

$$\varkappa(\varepsilon) = \frac{1}{2} - a_0 - \frac{I^2}{2\varepsilon^2} + a_0\left(\frac{\varepsilon}{I} - \ln\frac{\varepsilon}{I}\right); \quad c_0^2 \approx b_0\gamma_0. \tag{24}$$

Joining the functions (3) and (22) and their first derivatives at $\varepsilon = I$ yields two relationships:*

$$\frac{N_i^0(I) + G_T(I) - R(I)}{2\pi\left(\dfrac{2}{m^*}\right)^{3/2}} = C_2 \cdot \frac{\pi}{2\sin\dfrac{\pi}{\alpha+2}}\left[\frac{a(I)}{I\cdot\Gamma\left(\dfrac{\alpha+3}{\alpha+2}\right)}\left(\frac{c_0}{(\alpha+2)E}\right)^{\frac{1}{\alpha+2}} - \right.$$

$$\left. - \frac{b(I)}{\Gamma\left(\dfrac{\alpha+1}{\alpha+2}\right)}\left(\frac{c_0}{(\alpha+2)E}\right)^{-\frac{1}{\alpha+2}}\right], \tag{25}$$

$$C_1 = C_2\,\frac{\pi\cdot a(I)}{2I\cdot b(I)\cdot\Gamma\left(\dfrac{\alpha+3}{\alpha+2}\right)\sin\dfrac{\pi}{\alpha+2}}\left(\frac{c_0}{(\alpha+2)E}\right)^{\frac{1}{\alpha+2}}\exp\left(\int_{\varepsilon_p}^{I}\frac{b(\varepsilon)}{a(\varepsilon)}\,d\varepsilon\right) -$$

$$- \frac{N_i^0(\varepsilon_p) + G_T(\varepsilon_p) - R(\varepsilon_p)}{2\pi\left(\dfrac{2}{m^*}\right)^{3/2} b(\varepsilon_p)} - \int_{\varepsilon_p}^{I}\frac{\dfrac{dN^0_i(\varepsilon)}{d\varepsilon}}{2\pi\left(\dfrac{2}{m^*}\right)^{3/2} b(\varepsilon)}\exp\left(\int_{\varepsilon_p}^{\varepsilon}\frac{b(\varepsilon)}{d(\varepsilon)}\,d\varepsilon\right)d\varepsilon. \tag{26}$$

Further the function (22) can with sufficient accuracy (the error does not exceed 10%) be approximated in the form

$$f_0 \approx C_2\alpha_0 e^{-\beta_0\left(\frac{\varepsilon}{I}-1\right)^{\gamma_0}}, \tag{27}$$

where

$$\alpha_0 = \frac{\pi}{2\sin\dfrac{\pi}{\alpha+2}\cdot\Gamma\left(\dfrac{\alpha+1}{\alpha+2}\right)}\left(\frac{c_0}{(\alpha+2)E}\right)^{-\frac{1}{\alpha+2}}, \tag{28}$$

$$\beta_0 = \frac{2c_0}{(\alpha+2)E}\,\varkappa(\varepsilon=2I)^{\frac{\alpha+2}{2}} -$$

$$- \ln\left[\left(\frac{1}{\pi}\right)^{1/2}\sin\frac{\pi}{\alpha+2}\cdot\Gamma\left(\frac{\alpha+1}{\alpha+2}\right)\varkappa(\varepsilon=2I)^{-\frac{\alpha}{4}}\left(\frac{c_0}{(\alpha+2)E}\right)^{-\frac{\alpha}{2(\alpha+2)}}\right], \tag{29}$$

---

*We used expansion of $K_{\frac{1}{\alpha+2}}(\xi)$ into a series for small values for ξ.

$$r_0 = 1{,}1\left[\ln\beta_0 - \ln\ln\frac{\alpha_0}{\sqrt{\varkappa(\varepsilon = 1{,}4I)\cdot K_{\frac{1}{\alpha+2}}(\varepsilon = 1{,}4I)}}\right]. \tag{30}$$

Assuming further that the ionizing and ejected electrons after ionization have the same energy ε and utilizing Eq.(27), we obtain for $N_i^0(\varepsilon)$ (see Eqs.(3) and (12))

$$N_i^0(\varepsilon) = C_2\frac{64\pi N S_0\alpha_0}{m^{*2}}\int_0^{\varepsilon}\varepsilon(I+2\varepsilon)\,e^{-\beta_0\left(\frac{2\varepsilon}{I}\right)^{r_0}}d\varepsilon. \tag{31}$$

Thus Eqs.(3), (4), (5), (15) and (27) determine the function characterizing the electron distribution in energy and angle (see Eq.(2)) in the stationary case.

In order to find the field intensity E_{cr} (at which the stationary solution of the kinetic equation becomes impossible and electric breakdown of the dielectric occurs), let us introduce two characteristic quantities having definite physical meaning in the stationary case:

1) $\varepsilon_{1/2}$, which we define as an energy value in the region above and below which there arrive per unit time equal numbers of electrons due to ionization and

2) ε_p, which we define as the energy value at which an electron obtains from the field per unit time on the average as much energy as it gives up to the lattice. (If the electric field accelerated even the electrons which undergo maximum slowing down by interaction with the lattice vibrations, the stationary state would be disturbed; whence it is understandable that there exist in the stationary case certain definite values of ε_p at each given value of E.)

Using our solution of the kinetic equation (see Eqs.(3), (4), (5), (15) & (27)), we obtain the following expressions for determining $\varepsilon_{1/2}$ and ε_p:

$$r_0\beta_0^{\frac{3}{r_0}}x_{1/2}^2 e^{-\beta_0 x_{1/2}^{r_0}}\left[K_1(x_{1/2}, E) + \frac{2}{3}x_{1/2}K_2(x_{1/2}, E)\right] - \Gamma\left(\frac{3}{r_0}\right) - \beta_0^{\frac{1}{r_0}}\Gamma\left(\frac{2}{r_0}\right) = 0, \tag{32}$$

$$\frac{2e^2E^2\varepsilon_p^2}{2e^2E^2\varepsilon_p^2 + 3m^*gr\cdot\ln\left(\frac{4\varepsilon_p}{\hbar\omega}\right)}\cdot\left[1 + \frac{N_i^0(\varepsilon_p) + G_T(\varepsilon_p) - R(\varepsilon_p)}{2\pi\left(\frac{2}{m^*}\right)^{3/2}p\ln\left(\frac{4\varepsilon_p}{\hbar\omega}\right)C_1}\right] - 1 = 0, \tag{33}$$

for $\varepsilon_p \leqslant \varepsilon''$ and

$$\frac{2e^2E^2\varepsilon_p^3}{2e^2E^2\varepsilon_p^3 + 3m^*qr\ln\left(\frac{2\pi L_0}{\omega}\sqrt{\frac{2\varepsilon_p}{m^*}}\right)}\times\left[1 + \frac{N_i^0(\varepsilon_p) + G_T(\varepsilon_p) - R(\varepsilon_p)}{2\pi\left(\frac{2}{m^*}\right)^{3/2}p\cdot\ln\left(\frac{2\pi L_0}{\omega}\sqrt{\frac{2\varepsilon_p}{m^*}}\right)}\,\frac{1}{C_1}\right] - 1 = 0 \tag{34}$$

for $\varepsilon_p \geqslant \varepsilon''$, where

$$K_1(x_{1/2}, E) = 1 + \frac{\beta_0}{1+\frac{2}{r_0}}x_{1/2}^{r_0} + \frac{\beta_0^2}{\left(1+\frac{2}{r_0}\right)\left(2+\frac{2}{r_0}\right)}x_{1/2}^{2r_0} + \ldots;$$

$$x_{1/2} = \frac{2\varepsilon_{1/2}}{I};$$

$$K_2(x_{1/2}, E) = 1 + \frac{\beta_0}{1+\frac{3}{r_0}}x_{1/2}^{r_0} + \frac{\beta_0^2}{\left(1+\frac{3}{r_0}\right)\left(2+\frac{3}{r_0}\right)}x_{1/2}^{2r_0} + \ldots, \tag{35}$$

and C_1 is determined by means of Eq.(26).

We note that with increasing field intensity the mean energy of the electrons after ionization increases. Consequently, $\varepsilon_{1/2}$ must increase with increasing E. On the contrary, ε_p must decrease with increasing E, inasmuch as in ionic crystals the probability of electron scattering by lattice vibrations increases with decrease of their energy (expressions for the probability of scattering are given in Ref.2). Incidentally, it follows from the above that electrons with $\varepsilon > \varepsilon_p$ are in general accelerated by the field, while electrons with $\varepsilon < \varepsilon_p$ are on the average slowed down by the lattice.

Thus the stationary solution of the kinetic equation has significance only at values of E at which Eqs.(32)-(34), which are consequences of this solution, lead to the conditions

$$\frac{d\varepsilon_{1/2}}{dE} > 0 \text{ and } \frac{d\varepsilon_p}{dE} < 0. \tag{36}$$

Evaluations show that in a strong electric field $\varepsilon_{1/2} \approx 1$ ev, i.e., is much greater than 0.1 ev. Consequently, in accord with what has been said above $G_T(\varepsilon_{1/2}) \approx G_T^0$, the total number of generation events per unit time and $R(\varepsilon_{1/2}) \approx R^0$, the total number of recombinations per unit time. In addition, by definition, $N_i^0(\varepsilon_{1/2}) = N_i$, the total number of ionizations per unit time. Inasmuch as in the stationary case the total number of particles created (the number of ionizations plus the number of generations) must equal the total number of recombinations, we have

$$N_i^0(\varepsilon_{1/2}) + G_T(\varepsilon_{1/2}) - R(\varepsilon_{1/2}) = 0. \tag{37}$$

We note that the coefficient C_1 (see Eqs.(26), (33) & (34)) can only be positive, inasmuch as with $C_1 \leqslant 0$ the distribution function becomes negative or zero in some ε interval, which is devoid of physical meaning. Hence it follows that Eqs.(33) and (34) can be satisfied only by the values of $\varepsilon_p > \varepsilon_{1/2}$, since with $\varepsilon_p \leqslant \varepsilon_{1/2}$, we would have $N_i^0(\varepsilon_p) + G_T(\varepsilon_2) - R(\varepsilon_p) \leqslant 0$ (see (37)).

Now using the relationship (see (31) & (37))

$$N_i^0(\varepsilon_p) + G_T(\varepsilon_p) - R(\varepsilon_p) = C_2 \frac{64\pi N S_0 \alpha_0}{m^{*2}} \int_{\varepsilon_{1/2}}^{\varepsilon_p} \varepsilon(I + 2\varepsilon)\, e^{-\beta_0\left(\frac{2\varepsilon}{I}\right)^{r_0}} d\varepsilon, \tag{38}$$

and Eqs.(26) & (31), we can from Eqs.(32), (33) & (34) obtain the dependences of $\varepsilon_{1/2}$ and ε_p on the electric field intensity E. Qualitative plots of these dependences as given by Eqs. (32), (33) & (34) are shown in Fig.1. It will be seen that with $E > E_{cr}$, $\frac{d\varepsilon_p}{dE} > 0$, which is in conflict with one of the conditions (36), which has definite physical significance.

Contrary to physical actuality, too, is the circumstance that at $E > E_{cr}$ with increasing field intensity there come to be slowed down electrons which in weaker fields are ostensibly accelerated (for example, electrons with an energy ε_1 can be accelerated with $E = E_1$ - see Fig.1 - and slowed down with $E = E_2 > E_1$).

Thus with $E > E_{cr}$ the stationary state assumption (37) is unjustified inasmuch as it leads to physically impossible consequences. The field intensity $E = E_{cr}$, determined from the condition

$$\frac{d\varepsilon_p}{dE} = 0, \tag{39}$$

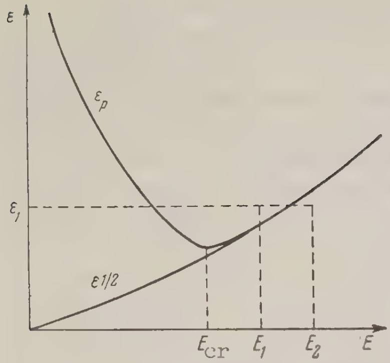

Fig.1. Qualitative dependences of $\varepsilon_{1/2}$ and ε_p on E.

is the field intensity above which the stationary condition becomes impossible (the balance between ionization and recombination is disturbed) and electric breakdown occurs. Eqs. (32), (33), (34) & (39) taken together allow of determining E_{cr} and the values of $\varepsilon_{1/2}$ and ε_p at the instant of electric breakdown.

Let us apply the above results to alkali halide crystals.

Except for the parameter S_o (see Eq.(17)) all the quantities in Eqs.(32), (33), (34) & (39) are known. Substituting the experimental values for the breakdown voltage at room temperature in these equations we obtain

$$S_o = 3\cdot 10^{-6}\ \sec^2 g^{-1} \text{ for KBr and}$$
$$S_o = 3.8\cdot 10^{-6}\ \sec^2 g^{-1} \text{ for NaCl.}$$

At these values of S_o the ionization cross section for an electron of energy $\varepsilon \approx 3I$ is approximately 10^{-16} cm^2, which appears to be reasonable. Increase or decrease of S_o by one order of magnitude results in an increase or decrease of E_{cr} by a factor of less than 2.

Consequently, the theory yields values of E_{cr} in agreement with experiment for alkali halide crystals with a reasonable value of the ionization cross section. The temperature dependence of E_{cr} for KBr following from the theory is also in agreement with the experimental data obtained in breakdown experiments using pulses of 10^{-6} sec duration (Fig.2) i.e., under conditions when the breakdown is purely electrical and not complicated by the effects of heating and high voltage polarization. The temperature dependence of E_{cr} for other crystals is similar.

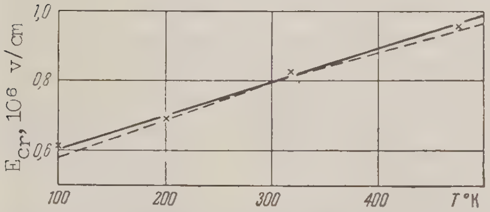

Fig.2. Temperature dependence of E_{cr} for KBr: solid lines - experimental[7]; dash lines - theoretical plot. The experimental curve was obtained using pulses of 10^{-6} sec duration (also see Ref.8).

Regarding the dependence of E_{cr} on the parameters of the lattice one can infer the following: E_{cr} increases with decrease of the reduced ionic mass M, the lattice constant a, the frequency of oscillation ω of the lattice and decreases with decreasing effective electron mass m^*. These inferred dependences appear to us to be physically reasonable.

We note that at E = E_{cr} the values of $\varepsilon_{1/2}$ and ε_p are approximately 1-2 ev, while the difference $\varepsilon_p - \varepsilon_{1/2} \approx 0.05$ ev. This means that at the instant of electric breakdown $\varepsilon_p \approx \varepsilon_{1/2}$. This condition agrees with the criterion for breakdown of ionic crystals deduced by the author earlier[2] from purely physical considerations. Consequently, the breakdown criterion formulated earlier* has now been more rigorously substantiated directly on the basis of the kinetic equation.

In concluding we note that in calculating E_{cr} the expanded expression for the variation of the distribution function due to electron scattering by vibrations of the lattice was invoked only for electrons with energy

---

*The physical meaning of the breakdown criterion is discussed in detail in Ref.2.

$\varepsilon \gg \varepsilon_{1/2}$, the approximate value of $\varepsilon_{1/2}$ being 1-2 ev. The free path length of such electrons $l(\varepsilon) \gg \lambda$, where λ is the wavelength of the electron. This means that in calculating the scattering of such electrons by lattice vibrations one can make use of perturbation theory in the first approximation.

Further evaluations carried out on the basis of the deduced electron distribution function show that ionization of impurities exerts an appreciable effect on the electric strength of a dielectric only when the impurity concentration $N_{imp} \geqslant 10^{18}$ per cm^3.

"P.N.Lebedev" Physical Institute,
Academy of Sciences of the USSR

References

1. A.Akhiezer & I.Lifshits, Doklady AN SSSR, 27, 785 (1940).
2. V.A.Chuenkov, Izv. (Bulletin) Tomsk Polytechnic Inst., 91, 45 (1956).
3. B.I.Davydov & I.I.Shmushkevich, Zhur.eksp.i teor.fiz., 10, 1043 (1940).
4. L.D.Landau & E.M.Lifshits, Kvantovaia mekhanika (Quantum mechanics), Part 1, 1948.
5. D.I.Blokhintsev, Zhur.eksp.i teor.fiz., 6, 1053 (1936).
6. E.I.Adirovich, Nekotorye voprosy teorii liuminestsentsii kristallov (Some problems in the theory of the luminescence of crystals), 1951.
7. E.A.Konorova & L.A.Sorokina, Zhur.eksp.i.teor.fiz., 32, 143 (1957).
8. A.von Hippel & R.S.Alger, Phys.Rev., 76, 127 (1949).

POLARON THEORY OF BREAKDOWN OF IONIC DIELECTRICS

- Iu.I.Gorkun & K.B.Tolpygo

The theory of breakdown in ionic crystals must be based on polaron concepts of conductivity. The present treatment is based on the von Hippel criterion for breakdown. The energy transferred by a polaron to the lattice is calculated on the assumption that the shape of the polaron is independent of its velocity and taking into account this dependence. In the first case there result excessively high values of the breakdown voltage. The more accurate theory leads to satisfactory agreement with experiments for crystals in which the polaron radius is relatively large and overestimates for crystals with a small polaron radius.

1. Basic presmises

All extant theories of breakdown of ionic dielectrics are based on band concepts.[1,2] The authors treating the subject generally consider a band electron moving in a strong electric field and the balance between the energy acquired and given up by the electron. Thus the interaction of the electron with the lattice vibrations, leading to a loss of energy by the electron, is regarded as a perturbation.

The unsatisfactory nature of this approach in the theory of slow electrons has been convincingly demonstrated by Pekar[3,4]. We need only note that the free path length of an electron in ionic crystals according to the band theory is estimated to be only about 1 Å, i.e., appreciably shorter than the de Broglie wavelength.[5] Thus the uncertainty as regards the electron's energy proves to be several times greater than the energy itself and, consequently, the band state cannot even be approximately regarded as a stationary one.

As has been shown by Pekar, the energetically most advantageous state in ionic crystals is the so-called polaron state. In this state the field of a conduction electron polarizes the surrounding dielectric and the electron is situated on a discrete level in a potential well formed by the polarized dielectric. In alkali halide crystals this discrete level lies 0.15-0.2 ev below the bottom of the conduction band. Thus no activation energy is necessary for transition of the electron from the band state to the polaron state. Hence the preponderant number of conduction electrons must be in the polaron state (for example, in NaCl at room temperature the proportion should be 1 band electron to 10^6 polarons).

As has been shown by Pekar[3], such a self-consistent state of the electron and dielectric can move through the crystal and carry current. The mobility of polarons, as calculated by Pekar, proves to be of the same order of magnitude as that deduced from measurements of the Hall effect. Thus polarons prove to be the majority carriers in ionic crystals. Consequently, the theory of breakdown in ionic dielectrics must be based on polaron concepts. The present work is an attempt to elaborate such a theory.

The theory of stationary and slowly moving polarons has been worked out most fully.[3] Hence it is expedient to start our consideration of breakdown neglecting possible deformation of the polarons in strong electric fields. Calculations show, however, that the energy lost by a fast polaron depends on its shape and therefore, in order to obtain satisfactory quantitative results, we must take into account the deformation of the polaron with increasing velocity. This problem was solved by one of us on the basis of the adiabatic approximation method developed by Bogoliubov.[6] As might have been expected this variant of the theory gave better agreement with experiment.

Our purpose is to find the value of the breakdown field E_{br} from the condition that the energy evE (v is the drift velocity) acquired by a conduction electron in the field with increasing field strength begins to increase more rapidly than the energy $\mathscr{E}(v)$ lost by the electron per unit time due to interaction with the lattice. From the energy balance with $E \leqslant E_{br}$ we find the relationship between the velocity and field:

$$E = \frac{\mathscr{E}(v)}{ev}\,. \tag{1}$$

At small values of E and v , $\mathscr{E}(v)$ is a monotonically increasing function. The unstable state is attained at the point $v_{\max}$, where

$$\left.\frac{dE}{dv}\right|_{v=v_{\max}} = 0, \text{ i.c. } \frac{1}{v}\cdot\frac{d\mathscr{E}}{dv} - \frac{1}{v^2}\mathscr{E}(v) = 0. \tag{2}$$

At $v > v_{\max}$ the electron is further accelerated despite the fact that the field may even decrease. Obviously, breakdown occurs at $E = E(v_{\max})$. According to Eq.(2) this will be the point where the curve of $\ln\mathscr{E}$ vs $\ln v$ has unit slope. Thus determination of E_{br} reduces to finding $\mathscr{E}(v)$ for polarons.

2. Determination of the energy lost by polarons to the lattice

Let $\psi_0(r)$ be the wave function of the stationary polaron and

$$D_0(\mathbf{r}) = -e\int\frac{(\mathbf{r}-\mathbf{r}')\,|\,\psi_0(\mathbf{r}')\,|^2}{|\,\mathbf{r}-\mathbf{r}'\,|^3}\,d\tau'$$

be the mean electric field produced by the polaron.

For a moving polaron $\mathrm{D} = \mathrm{D}(\mathrm{r}, t)$. At not excessively high polaron velocities, when the frequencies of the greater part of the Fourier components of this field are small compared with the intrinsic frequencies $\omega_{\alpha K}$ of the crystal, ψ and D are equal to $\psi_0(\mathbf{r}-\mathbf{v}t)$ and $\mathrm{D}_0(\mathbf{r}-\mathbf{v}t)$, respectively.*

Let us denote through $\mathbf{p}_s^l$ and $\mathbf{P}_s^l$ the dipole moments due to displacement and electronic polarization of the s-th site in the l-th cell. We can introduce the normal coordinates $q_{\alpha K}$ of the crystal by means of the formulas[7]:

$$\begin{gathered}\mathbf{p}_s^l = ea\sum_{\alpha K}\mathbf{p}_s^{\alpha\mathbf{K}}e^{i\mathbf{K}\cdot\mathbf{r}_s^l}\,q_{\alpha\mathbf{K}},\\ \mathbf{P}_s^l = ea\sum_{K}\Big(\sum_{\alpha}\mathbf{P}_s^{\alpha\mathbf{K}}q_{\alpha\mathbf{K}} + \mathbf{R}_s^{\mathbf{K}}\Big)\cdot e^{i\mathbf{K}\cdot\mathbf{r}_s^l},\end{gathered} \tag{3}$$

where $\mathbf{p}_s^{\alpha\mathrm{K}}$ and $\mathbf{P}_s^{\alpha\mathrm{K}}$ are the orthonormalized amplitudes of the intrinsic vibrations of the lattice, K is the wave vector, α is the mode number, a is half the lattice constant and e is the elementary charge. Then

$$\sum\mu_s\mathbf{p}_s^{\alpha\mathbf{K}}\,\mathbf{p}_s^{\alpha'-\mathbf{K}} = \delta_{\alpha\alpha'};\qquad \mu_s = \frac{m_s}{\mu}\,, \tag{4}$$

where μ for binary crystals is the reduced mass of an ion pair, $\mu = \frac{m_1\cdot m_2}{m_1+m_2}$; $\mathbf{R}_s^{\mathbf{K}}$ is the part of the electronic polarization due directly to the influence of the field and $\sum_{\alpha} \mathbf{P}_s^{\alpha\mathbf{K}} q_{\alpha\mathbf{K}}$ is the electronic polarization due to displacement of the ions.

---

*Energy transfer will occur due to the "tail" of the Fourier expansion $\mathrm{D}(\mathrm{r}, t)$. These components will not appreciably effect the form of the polaron ψ-function.

Let the external field be expanded in a Fourier series:

$$\mathbf{D}_0(\mathbf{r}) = \sum_{\mathbf{K}} \mathbf{D}_{\mathbf{K}}^0 e^{i\mathbf{K}\cdot\mathbf{r}}; \text{ then } \mathbf{D}_0(\mathbf{r}-\mathbf{v}t) = \sum_{\mathbf{K}} \mathbf{D}_{\mathbf{K}}^0 e^{i\mathbf{K}(\mathbf{r}-\mathbf{v}t)}. \tag{5}$$

As shown by Tolpygo & Uritskii[8], equations for forced vibrations in terms of the variables $q_{\alpha\mathbf{K}}$ may be written

$$\ddot{q}_{\alpha\mathbf{K}} + \omega_{\alpha\mathbf{K}}^2 q_{\alpha\mathbf{K}} = Q_{\alpha\mathbf{K}}(t) = \frac{e}{\mu a} \sum_s (\mathbf{p}_s^{\alpha-\mathbf{K}} + \mathbf{P}_s^{\alpha-\mathbf{K}}) \mathbf{D}_{\mathbf{K}} = Q_{\alpha\mathbf{K}}^0 e^{-i\mathbf{K}\cdot\mathbf{v}t}, \tag{6}$$

here

$$Q_{\alpha\mathbf{K}}^0 = \frac{e}{\mu a} \sum_s (\mathbf{p}_s^{\alpha-\mathbf{K}} + \mathbf{P}_s^{\alpha-\mathbf{K}}) \cdot \mathbf{D}_{\mathbf{K}}^0 .$$

The energy transferred to the lattice during the time 0 - t, on the assumption that with t = 0, $q_{\alpha\mathbf{K}} = 0$ and $\dot{q}_{\alpha\mathbf{K}} = 0$, will be

$$A(t) = N\mu a^2 \int_0^t \sum_{\alpha\mathbf{K}} Q_{\alpha\mathbf{K}} \dot{q}_{\alpha\mathbf{K}}\, dt = 2\mu a^2 N \sum_{\alpha\mathbf{K}} Q_{\alpha\mathbf{K}}^0 Q_{\alpha_1-\mathbf{K}}^0 \times \frac{\sin^2 \frac{1}{2}(\omega_{\alpha\mathbf{K}} - \mathbf{K}\cdot\mathbf{v})t}{(\omega_{\alpha\mathbf{K}} - \mathbf{K}\cdot\mathbf{v})^2} . \tag{7}$$

For polarons of large radius expansion (6) involves primarily long wavelengths $\mathrm{K} \ll 2\pi/a$, for which one can neglect the dependence of $\omega_{\alpha\mathbf{K}}$ on K in the optical modes and in the acoustic modes take $\omega_{\alpha\mathbf{K}} = |\mathbf{K}| \cdot c_{\alpha}$, where c_{α} is the speed of sound for the α-th mode. Then, going over in (7) from summation to integration in polar coordinates with the axis in the v direction, we obtain for the energy lost per unit time

$$\mathscr{E}(v) = \frac{dA}{dt} = \frac{\mu a^2 V N}{4\pi v} \sum_{\alpha} \int K\,dK\, |Q_{\alpha\mathbf{K}}^0 (K, \vartheta_{\alpha})|^2, \tag{8}$$

where $\cos\vartheta_{\alpha} = \frac{\omega_{\alpha}}{\mathbf{K}\cdot\mathbf{v}}$ and c_{α}/v are taken, respectively, for the optical and acoustic modes and V is the volume of the crystal. (In Ref.8 the corresponding equations - (25) and (26) - erroneously give half the correct values.)

3. Breakdown voltage on the assumption of a "rigid" polaron

In Ref.8 one of us in collaboration with Uritskii calculated $\mathscr{E}(v)$ for all six modes for NaCl, KCl and KBr crystals when the state of the polaron is characterized by the Gaussian function

$$\psi_0(r) = \left(\frac{2}{\pi}\right)^{3/4} \alpha^{3/2} e^{-\alpha^2 r^2}; \qquad \alpha = \frac{m^* e^2}{3\sqrt{\pi}\,\hbar^2} c; \qquad c = \frac{1}{n^2} - \frac{1}{\varepsilon} . \tag{9}$$

Here ε and n^2 are the static and high frequency dielectric constants and m^* is the effective mass of a band electron.

Analogous calculations were carried out by Iasinskii & Nosar, students at Kiev State University, for the more precise polaron functions

$$\psi_0(r) = \sqrt{\frac{\alpha^3}{7\pi}} (1 + \alpha r) e^{-\alpha r}; \qquad \alpha = \frac{m^* e^2 c}{2\hbar^2}, \tag{10}$$

$$\psi_0(r) = 0{,}1229\alpha^{3/2}(1 + \alpha r + 0{,}4516\alpha^2 r^2) e^{-\alpha r}; \quad \alpha = 0{,}6585\frac{m^* e^2 c}{\hbar^2} . \tag{11}$$

As in all other cases, at high polaron velocities, generation of vibrations of the longitudinal optical mode occurs 10 to 100 times more intensively than generation of vibrations for the other modes so that interaction with the last can be neglected.

Curves 1,2,3 & 4 of Fig.1 show the variation of the dimensionless rate of energy transfer with the dimensionless polaron velocity

$$u = \frac{v}{r_0\omega}\left(\text{where } r_0 = \frac{\hbar^2}{m^* e^2 c}\right)$$

plotted in double logarithmic coordinates for the functions $e^{-\alpha r}$ (9), (10) & (11); $\frac{m^* e^4 c^2 \omega}{16\hbar^2}$ is taken as the unit rate of energy transfer. These data were used to compute $u_{\max}$ and E_{br} by means of Eqs.(1) and (2). The resultant values are listed in columns 1 through 4 of Table 1.

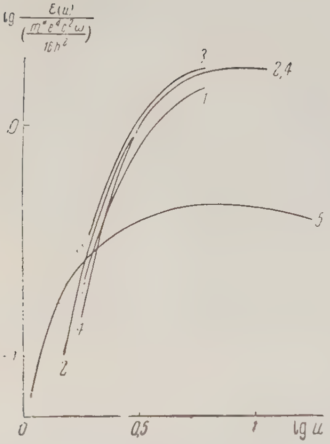

Fig.1. Variation of with for 1,2,3 & 4 "rigid" polarons and 5) a deformable polaron.

Table 1

Values of $u_{\max}$ and E_{br} calculated on the basis of the variation of $\mathcal{E}(u)$ with u (Fig.1) (values of E_{br} in V/cm)

	$\psi\sim e^{-\alpha r}$	$\psi\sim(1+\alpha r)e^{-\alpha r}$	$\psi\sim(1+\alpha r+\beta r^2)e^{-\alpha r}$	$\psi\sim e^{-\alpha^2 r^2}$	$\psi\sim(1+\beta^2 r_2 p_2(\theta))e^{-\alpha r}$
E_{br}	$2.4\cdot10^{-9}\frac{c}{r^2_0}$	$2.91\cdot10^{-9}\frac{c}{r^2_0}$	$3.12\cdot10^{-9}\frac{c}{r^2_0}$	$2.8\cdot10^{-9}\frac{c}{r^2_0}$	$1.26\cdot10^{-9}\frac{c}{r^2_0}$
$u_{\max}$	3.94	3.80	3.71	3.98	1.88

Table 2

Calculated values of $v_{\max}$ and calculated and experimental values of E_{br} for alkali halide crystals

Crystal	$v_{\max}$, 10^{-5} cm/sec 1	E_{br}, 10^{-6} v/cm 2	$v_{\max}$, 10^{-5}cm/sec 3	E_{br}, 10^{-6}v/cm 4	E_{br}, 288°K 5	$10r_0$, Å 6	a, Å 7
RbJ	10,9	3,23	5,4	1,4	0,49	13,6	3,66
RbBr	12,51	3,69	6,2	1,6	0,63	13,5	3,42
RbCl	14,13	5,77	7,0	2,5	0,83	11,3	3,27
KJ	13,12	2,91	6,5	1,26	0,57	13,6	3,53
KBr	15,13	3,69	7,5	1,6	0,7	13,0	3,29
KCl	17,35	5,77	8,6	2,5	1,0	11,4	3,145
KF		24,2		10,5	1,9	6,69	2,66
NaJ		7,85		3,4	0,8	8,5	3,23
NaBr		12		5,2	0,81	7,85	2,97
NaCl	13,52	13,6	6,7	5,9	1,5	7,4	2,82
NaF	16,75	33,2	8,3	14,4	2,4	5,805	2,315
LiF	12,51	162	6,2	70	3,1	2,705	2,013

Excluding the function $e^{-\alpha r}$, which is a poor approximation in polaron theory, we find that all the other three functions - (9), (10) & (11) - yield very close values of E_{br}. The values of $v_{\max}$ and E_{br} for specific crystals, calculated in this manner, are listed in columns 1 & 2 of Table 2. The theoretical values of E_{br} proved to be appreciably (6-7 times) greater than the experimental values (the experimental data listed in column 5 are taken from Chuenkov's review[2]). This is apparently connected with the excessively large values of $\mathscr{E}(v)$ at high polaron velocities. There is reason to assume that taking into account the dependence of $\psi(r)$ on the polaron velocity and, in particular, the increase of the radius of the polaron state with velocity will lead to an appreciable reduction of $\mathscr{E}(v)$ at high polaron velocities and hence to better agreement with experiment.

4. Variation of the shape of the polaron with its velocity and determination of E_{br} for a deformable polaron

As a result of separating the translational motion of polarons, Bogoliubov[6] obtained the following zeroth approximation equation for finding the wave function of the fluctuational motion of an electron:

$$\left(-\frac{\hbar^2}{2m^*}\Delta + U(\mathbf{r}) - E\right)\psi = 0, \tag{12}$$

wherein

$$U(\mathbf{r}) = -\frac{4\pi e^2 c}{V}\sum_{\mathbf{K}}\frac{\omega_k^2}{\mathbf{K}^2}\,\frac{\int e^{-i\mathbf{K}\mathbf{r}'}\,|\psi(\mathbf{r}')|^2\,d\tau'}{\omega_{\mathbf{K}}^2 - (\mathbf{K}\cdot\mathbf{v})^2}\,e^{i\mathbf{K}\mathbf{r}}. \tag{13}$$

Here it is assumed that the electron interacts only with one mode (the longitudinal optical mode).

Eq.(12) was approximately solved by one of us by the variational method, neglecting the dependence of ω_{K} on K. In selecting the approximating function account was taken of the fact that at high polaron velocities the polarization of the environs is described not by the static formula $\mathrm{P} = \frac{c}{4\pi}\mathrm{D}$, but by the dynamic one $\frac{c}{4\pi}\cdot\frac{\mathrm{D_K}}{1-\left(\frac{\mathrm{Kv}}{\omega_{\mathrm{K}}}\right)^2}$ for each Fourier component $\mathrm{D_K}$ and thus becomes dependent on the angle θ between r and v. Consequently, the shape of the polaron will differ from the spherical. It is natural to limit the expansion of the ψ-function in Legendre polynomials to the first term

$$\psi(r,\theta) = \sqrt{\frac{\alpha^3}{\pi\left(1+\frac{9\beta^2}{2\alpha^4}\right)}}\,[1+\beta r^2 P_2(\cos\theta)]\,e^{-\alpha r}. \tag{14}$$

Here α and β are approximation parameters.

As a result of substitution of (14) in (13) and (12) and minimization of the corresponding functional with respect to α and β, by numerical methods there were obtained the dependences of α and β (in $1/r_0$ and $1/r_0^2$ units, respectively) on the dimensionless velocity $u = v/\omega r_0$ shown in Fig.2. With increasing velocity the polaron at first shrinks and then diffuses. In the process it undergoes contraction in the direction of motion analogous to the Lorentz contraction in the theory of relativity.

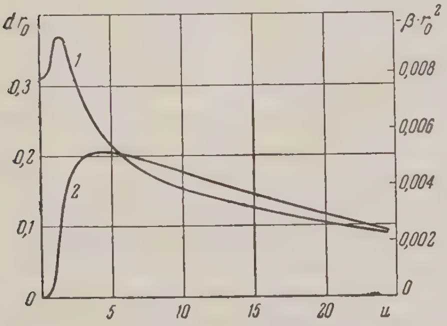

Fig.2. Curve 1 - variation of α with u; curve 2 - variation of β with u.

Curve 5 in Fig.1 shows the energy lost by the polaron as a function of the dimensionless velocity u. The corresponding values of $u_{\max}$ and E_{br} are listed in column 5 of Table 1. For E_{br} on the basis of Fig.1 there was deduced the formula

$$E_{br} = 1.26 \cdot 10^{-9} \frac{c}{r_0^2} \text{ v/cm} \tag{15}$$

where

$$r_0 = \frac{\hbar^2}{m^* e^2 c}.$$

Dimensional values of $v_{\max}$ and E_{br} for specific crystals are given in Table 2 (columns 3 & 4).

Owing to increase of the polaron radius with velocity (Fig.2), $\mathcal{E}(u)$ for a deformable polaron increases with u more slowly than for a "rigid" polaron and the maximum of $\mathcal{E}(u)$ is shifted to the side of lower velocities (Fig.1, curve 5). This leads to somewhat better agreement of theory with experiment. For RbI, RbBr, RbCl, KI, KBr and KCl crystals, wherein the polaron radius is relatively large, the theoretical values of E_{br} are only 2-3 times larger than the experimental ones (Table 2). For KF, NaI, NaBr, NaCl, NaF and, particularly, LiF crystals, wherein the polaron radius is small, the divergence is appreciably greater; in the case of the former group the theoretical values of E_{br} are 6-7 times greater than the experimental ones, while for LiF the theoretical value exceeds the experimental one by a factor of about 20.

It should be noted that Pekar[3] gives the criterion $10 \; r_0 \gg a$ for applicability of the macroscopic theory. Comparison of columns 6 & 7 in Table 2 shows that for the first group of substances $10 \; r_0$ is 3-4 times greater than a (i.e., the criterion holds), while for the second group it is 2-2.5 times greater and for LiF only 1.5 times greater. Thus the more applicable the macroscopic method of calculation of the polaron, the better the agreement with experiment.

There is another reason for the excessively high theoretical values of E_{br}. For breakdown in an actual crystal to occur, not all the current carriers need have the velocity $v_{\max}$. It is sufficient for some relatively small fraction of the polarons to have this velocity; these may, for instance, be the polarons whose random velocity at a given instant coincides in direction with the drift velocity. For example, for KCl the thermal polaron velocity at room temperature amounts to about 10^6 cm/sec, which is close to $v_{\max}$. This effect may appreciably lower the effective E_{br}.*

More precise results for E_{br} may be obtained from more rigorous calculations by means of the kinetic equation. It is clear from the cited data, however, that this theory must be constructed on the basis of polaron concepts and must take into account deformation of the polaron as a function of its velocity.

Physical Institute,
Academy of Sciences of the Ukrainian SSR

References

1. A.S.Zingerman, Usp.fiz., nauk, 46, 450 (1952).
2. V.A.Chuenkov, Usp.fiz.nauk, 54, 185 (1954).
3. S.I.Pekar, Issledovaniia po elektronnoi teorii kristallov (Investigations in the electronic theory of crystals), 1951.
4. S.I.Pekar, Usp.fiz.nauk, 50, 197 (1953).
5. N.F.Mott & R.W.Gurney, Electronic Processes in Ionic Crystals. (Cited in Russian trans., M. 1950.)

---

*It should be noted that the present theory, which does not take into account the random motion of the polaron, should be compared with experiments at T = 0°K.

6. N.N.Bogoliubov, Ukrainsk. matematicheskii zh. (Ukrainian Mathematical Journal), 2, No.2, 3 (1950).

7. K.B.Tolpygo, Matematicheskii sb. (Mathematical collection), Kiev State University, No.5, 99 (1951).

8. K.B.Tolpygo & Z.I.Urithkii, Zhur.eksp.i teor.fiz., 30, 929 (1956).

DISCUSSION OF THE REPORTS OF V.A.CHUENKOV AND IU.I.GORKUN & K.B.TOLPYGO

G.I.Skanavi: The speakers have touched on a number of problems that have been discussed in reports presented at earlier conferences and published in scientific journals. Questions having to do with the role of impact ionization in breakdown and the relation between the breakdown voltage and the lattice energy have been discussed last Septamber in Tomsk and at earlier conferences.

I would like to make a few general remarks. There can be no doubt that the breakdown of a solid dielectric comprises two stages. Unfortunately, we have no experiment that would clearly separate these two stages, inasmuch as the technique for such an experiment would necessarily be complex and has not yet been developed.

In experimental investigation of electric strength we must first direct our attention to the first stage of breakdown - impairment or failure of electric strength.

Among classical theories, one might mention the theories of Rogovskii, Gorovits and Ioffe. The first theory of rupture of an ionic lattice is inconsistent not only because it gives an excessively high value for the breakdown voltage but also because one cannot deduce from this theory the dependence of the breakdown voltage on the sample thickness at small thicknesses and on the temperature. The microfissure theory of Gorovits leads to certain results that are not in agreement with experiment, but this theory may be of value in interpreting the breakdown of technical materials. The basic premises of Ioffe's theory of impact ionization by ions are questionable because in general ions in solid dielectrics are not sufficiently mobile to produce impact ionization. The idea of impact ionization in solid dielectrics was developed by von Hippel & Fröhlich, but on the premise that electric breakdown occurs as a result of ionization by electron impact. Their theories are more complex inasmuch as in them the behavior of the electron is treated from the standpoint of quantum mechanics.

Zener made an attempt to explain breakdown by means of tunneling of electrons from the valence band to the conduction band. The theory of Vol'kenshtein is closely allied to this theory.

In contrast to the cited authors, Frantz, Heller and Chuenkov in considering the question of electric breakdown investigated the behavior of a collective of electrons in a strong electric field. Their work is based on solution of the kinetic equation. At present there can be no doubt that the initial stage of breakdown is due to electronic processes.

Today we heard a report having a different approach (Gorkun & Tolpygo), one based on examination of the polaron states of the electron. In this work use has been made of the von Hippel criterion, which can hardly now be utilized inasmuch as we cannot consider only one electron but must take into account the collective system of electrons and, consequently, the distribution function. This work is of interest, however, inasmuch as it is the first attempt to take into account polaron states in the process of electric breakdown.

As for the work of Chuenkov, it has been repeatedly discussed; attractive in it is the clear physical formulation of the breakdown criterion. The difficulty here is, first, that the ionization cross section is unknown and must be found from experimental values of E_{br} (i.e., a purely theoretical evaluation is impossible) and, second, recombination must be taken into account not in the kinetic equation but somewhat indirectly. However, Chuenkov makes fewer arbitrary assumptions than do other authors.

I.E.Balygin: The striving to improve extant theories is understandable. To this end Tolpygo & Gorkun introduced the polaron state of the electron into their treatment of electric breakdown. The assumptions made by them, however, are so rough that the resultant polaron theory of greakdown gave even greater divergence from experiment than earlier theories.

There is an obvious objection to Chuenkov's theory where valence crystals are concerned, for it follows from the theory that the energy loss of an electron in scattering by lattice vibrations is independent of its velocity, which is impossible. Obviously, the energy loss by an electron in scattering by lattice vibrations must depend on the electron velocity and the function characterizing this dependence must have a maximum.

The theories we have heard proposed today do not give a temperature dependence of the breakdown voltage. We know from experiment, however, that the breakdown voltage at first increases with temperature and then decreases. In order to explain the falling section of the temperature dependence curve, Fröhlich takes into account, at high temperatures, interaction of conduction electrons with electrons localized on impurities. It may be noted, incidentally, that in taking into account statistical fluctuations, the criteria of von Hippel & Fröhlich overlap.

K.B.Tolpygo: In discussing our report some speakers indicated that the basic criterion for the validity of a theory is agreement with experiment and that better agreement with experiment is given by von Hippel's earlier theory.

Agreement of theory with experiment is a convincing criterion, provided the theory is not internally inconsistent. Otherwise, agreement with experiment is an illusion, an indication that somewhere in the theoretical calculations there was an undetected and possibly misleading error.

In the case of ionic dielectrics there exists a breakdown theory based on socalled band concepts. This theory, however, involves internal contradictions. According to this theory in the zeroth approximation it is assumed that the ions are fixed at the lattice sites and that the potential acting on an electron is periodic. The electron wave function has the form

$$\psi_k = e^{ikr} u_k(r).$$

Variation of the potential due to vibration of the ions is regarded as a small perturbation that is the cause of scattering of the electron waves. Calculations of Fröhlich & Mott show, however, that the free path length of a band electron is only 1 Å. This is appreciably less than the de Broglie wavelength for an electron: $2\pi/K$.

Can one represent the state of an electron even approximately by a wave so much shorter than the de Broglie wavelength? Is it meaningful in general in this case to speak of a definite wavelength? Obviously the zeroth approximation of the theory is altogether invalid. But then the calculations of energy loss in this approximation can hardly be correct.

In the polaron theory of S.I.Pekar an appreciable part of the interaction of the electron with lattice vibrations is introduced in the Hamiltonian of the zeroth approximation. The electron in the zeroth approximation moves in a polarizing potential well and migrates over the crystal together with this well. Inasmuch as the band state of the electron is not stable - stationary - every electron injected into the crystal or produced therein as a result of impact ionization or the internal photoeffect, very quickly - within a time of the order of 10^{-12} sec (the period of the lattice vibrations) - loses its initial velocity and transforms into a polaron. Calculations show that in an NaCl crystal the number of polarons is 10^6 times greater than the number of band electrons. A polaron has a large effective mass (of the order of 100 or more electron masses) and an appreciable free path length. Hence the polaron theory is free of the internal contradictions of the band theory that I have just mentioned.

It was correctly noted here that fast electrons capable of ionizing atoms of the host material cannot be polarons and that, consequently, it should be possible to describe them in the framework of the band scheme and to characterize their behavior on the basis of band theory.

One may ask how does the breakdown process develop in time? Fast electrons do not appear immediately upon the application of a field. Initially all electrons are in the polaron state. These electrons are gradually accelerated by the field to energy values at which impact ionization is possible and at which polaron effects can be neglected. Thus the first stage in the breakdown process is acceleration of polarons. If the field is not sufficiently strong for such acceleration, breakdown cannot occur.

As was noted in our report, with increase in field and polaron energy there is reached a point or instant of "disruption" at which the energy received by the polaron exceeds the energy given up by it. It is only after this instant that the polarons can be accelerated without limit by the field and transform into band electrons. From this point on, the breakdown process develops in accordance with the theory based on the band scheme and will be determined by its own criteria. If the critical field, according to polaron theory, is greater than the band theory field, it will play the role of the breakdown field. In the contrary case, the band theory criterion will apply. Then the polaron theory should be used only for describing the pre-breakdown states. Possibly one case or the other applies to different crystals.

As one of the shortcomings of the proposed theory G.I.Skanavi remarked that in it we consider the behavior of only an "average" electron and do not take into account the statistical scatter of electron velocities. This is admittedly true. In further development we intend to consider breakdown by the kinetic equation method. In the first stage of our work, it was essential to use the simple von Hippel criterion in order to see whether the order of magnitude of the breakdown field given by polaron theory is reasonable. It must be noted that calculation of the energy loss by a deformable polaron is rather cumbersome. There is no reason to assume, however, that application of the kinetic equation method will lead to very different results.

V.A.Chuenkov remarked that in the statistical approach a decisive role will be played by a small number of band electrons with energies 0.15-0.2 ev greater than the energy of a stationary polaron. These will be the electrons accelerated by the field up to energies at which impact ionization becomes possible. The situation is somewhat more complicated. It must be recalled that a band electron having a small energy, i.e., 0.15-0.2 ev above the polaron ground state, is not stable. Such a state simply does not exist. One can arrive at the band state only by considering all the faster polarons. With increasing polaron velocity v the polarization well should gradually disappear, but this will occur not at 0.15-0.2 ev but at an appreciably higher energy, possibly at 0.5-1.0 ev. In Pekar's theory only stationary or very slow polarons were considered. Iu.I.Gorkun examined the deformation of a polaron with velocity and extended the treatment to higher velocities. At polaron velocities of 10^6 cm/sec and energies of 0.1 ev the polarization well is still sufficiently deep. To resolve the argument one must investigate the behavior of yet faster polarons with energies of 0.5 ev and establish the bound beyond which the electrons can be regarded as band electrons and polaron effects can be neglected. Up to this bound the energy balance must be treated on the basis of polaron theory.

I would like to call attention to certain advantages of the polaron theory. It operates only with well-known crystal parameters: ε, n^2_0, ω_0 and m^*, where ω_0 is the limiting frequency of the optical mode and m^* is the effective mass of a band electron. All these parameters can be determined from experiments not involving breakdown effects. For example, m^* can be determined from comparison with the experimentally observed position of the maximum in the F absorption band. In contrast, in band theory one is forced to operate with an unknown interaction constant

$$C = \int (\nabla U_k)^2 \, dT,$$

where U_k is the periodic part of the electron wave function. Furthermore, the cross section for excitation and ionization of the crystal by an electron are unknown.

It must be emphasized that in the treatment presented in our report there was not a single "free" parameter that could be used for fitting the calculated results to experiment. All the quantities utilized in the treatment were taken from earlier work on the theory of polarons and F-centers. Taking this into account, one cannot say that the agreement with experiment is so very poor. It is possible, for example, that the effective mass taken from the theory of F-centers is an overestimate inasmuch as the macroscopic theory of F-centers of small radius is not very precise. Inasmuch as $E_{br} \sim m^{*2}$ an error of 1.4 in the value of m^* may obviously be responsible for the theoretical breakdown voltage being approximately twice the experimental value.

Finally, I want to note that the correlation between the lattice binding energy and the breakdown field, which has been the subject of so much discussion, is taken into account if not directly, at least indirectly, in the polaron breakdown theory. The polaron theory gives $E_{br} \sim m^{*2} C^3$ where

$$C = \frac{1}{n_0^2} - \frac{1}{\varepsilon}.$$

If we examine a number of crystals with decreasing binding energy from the lightest to the heaviest, for example, the series LiF, NaCl, KCl and RbI, we see that in this series the values of m^* and C and, consequently, E_{br} as well, decrease monotonically. This makes itself felt even though the polaron theory does not explicitly treat the lattice energy.

V.A.Chuenkov: A number of critical remarks have been made concerning our theory in the course of the discussion. I.E.Balygin indicated that our theory of electric breakdown in valence (atomic) crystals is incorrect because it follows from the theory that the electron energy loss due to interaction with lattice vibrations is independent of the electron energy. This is simply a misunderstanding: it definitely follows from the theory that in valence crystals the electron energy loss in scattering by lattice vibrations is $B = a_1 \varepsilon^{1/2}$ at low energies and $B = a_2 \varepsilon^{3/2}$ at high energies (here ε is the electron energy).

The maximum electron energy loss, to which Seitz calls attention in his work, occurs in germanium and silicon at energies much greater than the ionization potential (width of the forbidden band), where the distribution function virtually equals zero. Hence the existence of this maximum has virtually no significance in calculating the electric strength of germanium and silicon.

I also fail to understand the remark of Balygin regarding the temperature dependence of the electric strength. It is obvious from the formulas given in our report that we can calculate the temperature dependence of the breakdown voltage. We even have plots of this dependence.

Now as for the remark that the proposed theories only obscure the question of electric breakdown as compared with the theories of von Hippel & Fröhlich. The theories of von Hippel & Fröhlich are inconsistent for the following reasons:

1) As has been noted many times in the literature, the most rigorous criterion for electric breakdown may be obtained on the basis of solution of the kinetic equation; the theories of von Hippel & Fröhlich are based not on solution of the kinetic equation but on consideration of the behavior of one electron in the conduction band.

2) Account is not taken in the cited theories of the process of impact ionization, i.e., of the process that essentially determines electric breakdown.

3) Account is not taken of recombination of electrons.

4) The criteria of von Hippel & Fröhlich do not follow from the theory but are introduced formally.

5) In the case of more precise calculation of electron scattering by lattice vibrations the theories of von Hippel and Callen disagree with experiment.

In our work we attempted to eliminate the listed short-comings and as a result obtained a criterion for electric breakdown which gives agreement with experiment as regards the numerical values of the breakdown voltage and its temperature dependence in breakdown under pulse conditions when thermal effects are obviated. The theory gives a physically correct dependence on the lattice parameters.

Now a few words regarding the remarks of G.I.Skanavi. In the presented variant of the theory, recombination is taken into account directly. As regards the effective cross section for ionization we can note the following. In the entire range of values of $\epsilon \geqslant I$ (ϵ is the electron energy and I is the ionization potential), important to us are the values of ϵ at which $\epsilon - I \ll I$, inasmuch as at $\epsilon - I \approx I$, the distribution function virtually vanishes; it follows, therefore, that the ionization cross section can be written as

$$Q(\epsilon) = S_o(\epsilon - I),$$

(where S_o is a constant), i.e., in the expansion of the ionization cross section in a series in terms of the difference $(\epsilon - I)$ we can limit our consideration to the first term.

As for the influence of polaron states of the electron on electric breakdown, this has been touched upon by Comrade Tolpygo, but I must further emphasize that only electrons with very low energy can be in the polaron state. The polaron state of an electron is possible only when the time of flight of an electron past an ion is much greater than the period of vibration of the lattice, i.e., when

$$\frac{l}{v} \gg \frac{2\pi}{\omega},$$

where l is the size of the ion, v is the velocity of the electron and ω is the lattice vibration frequency.

For $l = 5 \cdot 10^{-8}$ cm and $\omega \approx 10^{14}$ sec^{-1}, we find that the electron state is possible at an electron velocity $v < 10^6$ cm/sec and an energy $\epsilon < 0.1$ ev (we take the effective mass of the electron equal to 200 free electron masses). In a weak electric field at room temperature most of the electrons are in the polaron state inasmuch as in this case the mean electron energy $\bar{\epsilon} = 3kT/2 \approx 0.04$ ev. Owing to fluctuations, however, even in this case part of the electrons (albeit a small fraction) will have energies $\epsilon > \bar{\epsilon}$, at which the polaron state is impossible. With increasing external field strength the average electron energy increases and with it the number of electrons in the band state, so that at the same time the number of electrons in the polaron state decreases. At fields close to the breakdown value the overwhelming majority of the electrons is in the band state ($\bar{\epsilon} \approx$ 1-2 ev with $E = 10^6$ v/cm). At the same time, in such fields the number of electrons with $\epsilon \gg I$ becomes appreciable and hence ionization by electron impact begins to play a significant role.

In our report we proposed a criterion according to which the electric strength of an ionic dielectric breaks down when at least half the total number $2N_i$ (N_i is the number of ionizations per unit time) of electrons (ionizing plus ejected) appearing in the region $0 \leqslant \epsilon \leqslant I$ due to ionization are accelerated by the field and therefore are able to reionize.

The characteristic quantities ϵ_p and $\epsilon_{1/2}$ introduced by us for mathematical formulation of the breakdown criterion are equal to about 1 ev in fields close to the breakdown value, i.e., lie in the region of energy values at which the polaron states play no significant part. Consequently, in our approach to the problem of electric strength one can literally do without taking into account polaron states.

Further, we cannot agree with the remarks of Comrade Tolpygo that every electron injected into an ionic crystal, owing to impact ionization of the photoeffect, very quickly (within 10^{-12} sec) loses its initial velocity and is transformed into a polaron. This observation is valid only in the absence of an external electric field.

In the presence of a strong electric field, an electron after ionization acquires an energy (at $E = 10^6$ v/cm, an energy of the order of 1 ev) at which it is, first, in the band state, and, second, is accelerated by the field. Obviously, such an electron cannot be in the polaron state inasmuch as this is precluded by the influence of the external electric field which accelerates the electron.

Since, as calculations indicate, in a strong electric field most of the electrons after ionization are raised to band states, the "polaron stage" of electron acceleration cannot play a significant role in the breakdown of the electric strength.

Thus everything depends on the behavior of the electrons that appear in the region $\epsilon \leqslant I$ as a result of ionization. If due to acceleration by the electric field more electrons enter the $\epsilon \geqslant I$ region than leave it due to ionization, we have the condition leading to breakdown. If the electric field does not accelerate more electrons into the $\epsilon \geqslant I$ region than leave it through ionization, no breakdown occurs. Clearly, in view of situation we can disregard the behavior of the electrons that are in the polaron state. Taking into account the polaron states is necessary only in detailed calculation of the number of recombinations (only slow electrons recombine). In our case, however, there was no necessity for carrying out this calculation inasmuch as the contribution from recombination is negligible.

As for the criterion for the applicability of perturbation theory, in our case it is fulfilled. Calculations show that the wavelength of an electron with an energy 1-2 ev is less by an order of magnitude than its free path length.

ELECTRIC STRENGTH OF POLYETHYLENE AT HIGH FREQUENCIES

- S.M.Bragin

1. Introduction

In recent years polyethylene has been finding increasing use as an insulating material for high voltage cables, special capacitors and other high voltage equipment. The principal obstacle to even more extensive use of polyethylene in high voltage engineering is the deterioration of its electric strength with time, which limits the useful service life of polyethylene insulation particularly at high frequencies.

It has been established in a number of studies that the principal reason for the decrease in the electric strength of polyethylene is the destructive effect of ionization of air inclusions under the influence of an applied voltage.

The electric strength of many such high quality insulating materials as polyethylene decreases rapidly with increasing frequency. According to experiments carried out in the Cable Laboratory of the Department of Electric Materials and Cables of the Moscow Power Institute, the electric strength of cables with polyethylene insulation at frequencies of 30-38 Mc does not exceed 7.5 kv/mm, whereas at 50 cps the electric strength of the same cables (RK-3 - PK-3) is 43 kv/mm. In an investigation[1] of polyethylene discs about 3 cm in diameter and 0.05 to 0.1 cm thick, having a 0.0008 to 0.03 cm deep recess in the center of one face, it was found that at high frequency the surface of the disc undergoes considerable disintegration (erosion) and "resinification" as a result of chemical decomposition of the insulation.

Microscopic examination of the surface of polyethylene cable insulation showed that there are present in it cavities 0.001 to 0.03 cm in depth extending in the radial direction. Ionization processes developing in these gaseous inclusions (cavities) at high frequencies and relatively high voltages lead to intensive disintegration of the polyethylene, starting from the surface, heating and finally breakdown of the sample.

It was hypothesized that there should exist a "safe" discharge level in the cavities. It was suggested that the border-line discharge level may be $2 \cdot 10^{-12}$ coulomb. At high frequencies, however, this level must be appreciably lower. The discharge produces erosion of the material. It is reported[2] that a discharge of $10 \cdot 10^{-12}$ coulomb causes the transport (disintegration) of about 10^{-15} cm^3 polyethylene.

The role of ionization of gaseous inclusions in the dielectric is very important inasmuch as it determines the possibility of utilizing the given material for engineering purposes and the useful life of the material at high voltage.

In view of the fact that the physical action of the ionized gas on the dielectric is proportional to the frequency one can, at high frequencies, obtain accelerated disintegration of the material, i.e., produce accelerated aging.

2. Experimental procedure

For the purpose of investigating the breakdown strength of high frequency materials we constructed a special high frequency, high voltage set-up consisting of a high-frequency oscillator, a control circuit and appropriate measuring equipment.[3]

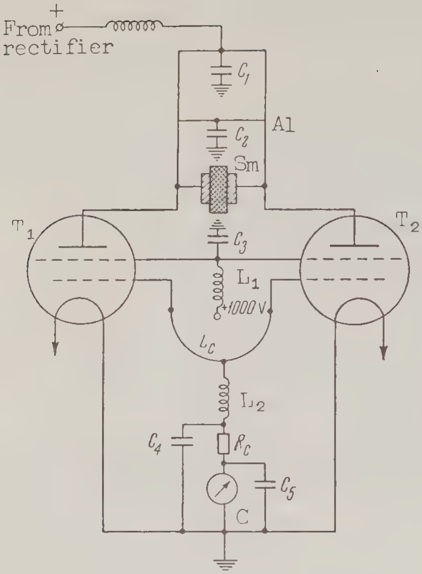

Fig.1. Circuit of high-frequency oscillator: T_1 & T_2 - oscillator tubes, S_m - sample, C_1, C_2 & C_3 - 3500 μμf decoupling capacitors, C_4 & C_5 - 1000 μμf and 3500 μμf, respectively, blocking capacitors, AL - plate line, L_c - grid circuit plug-in inductance, L_1 & L_2 - 20 μH chokes, R_c - 100 ohm resistor.

The high-frequency oscillator operated at frequencies from 30 to 100 Mc with a crest voltage of about 4 kv. The operation of the oscillator was stable in testing capacitors of up to 20 μμf.

Power for the oscillator was supplied from a special three-phase rectifier, designed about VG-236 tubes and connected through a booster transformer to the 220 volt line.

The high frequency oscillator employed a push-pull circuit with a grounded cathode and GU-27-B tubes (Fig.1).

A short-circuited line was employed as the plate circuit, while the grid circuit was a conventional network. The frequency was varied by replacing the grid circuit plug-in inductances and appropriate tuning of the plate line by means of a variable short-circuiting bridge.

To insure stable operation of the oscillator in the region of high frequencies the plate line was adjusted to 3/4 the wavelength, while in the low frequency region the plate line was operated as a quarter-wave short-circuited line.

The sample was mounted at the voltage antinode. Variation of the high frequency voltage amplitude on the sample was realized by regulating the plate voltage.

Two methods were used for measuring the high frequency voltage: one of them amounted to measuring the current through a high voltage lossless capacitor (vacuum type), the second to measuring the rectified voltage by means of an electrostatic voltmeter.

3. Breakdown of polyethylene samples and insulated cables

Polyethylene samples 1-1.5 mm thick were punctured in a discharger with disc electrodes 20 mm in diameter, equipped with springs and sealed into a glass envelope (Fig.2); with this set-up the disruptive discharge always occurred at the edge of the electrodes. In addition, we investigated the influence on the disruptive strength of conducting coatings on the surface of the samples with disc electrodes and also with 16 mm diameter spherical electrodes. A layer of vacuum-sputtered silver in the form of a circle 12 mm in diameter or a layer of graphite of the same diameter was applied to both sides of the samples. Further, we also tested tinfoil electrodes of the same diameter applied by means of a drop of mineral oil rubbed into the sample surface.

In all cases, breakdown of the samples with tinfoil electrodes occurred at the edges of the electrodes with some melting of the polyethylene.

Breakdown of samples with the silvered and graphited surfaces occurred at the minimal voltage, for example, at 2 kv for a sample thickness of 1.44 mm; the puncture always occurred under the electrodes. This reduction of the electric strength could not be explained by the presence of weak areas under

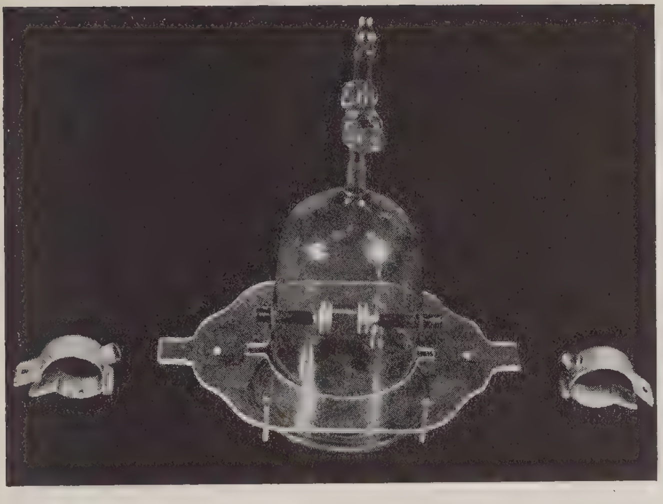

Fig.2. Glass envelope with electrodes for testing disruptive strength.

the metallized or graphite surface inasmuch as all the samples were tested beforehand at a frequency of 40 cps and successfully withstood a voltage of 15 kv.

It was found that in the case of breakdown between 16 mm diameter spherical electrodes the disruptive voltage is greatly dependent on the state of the surface of the samples. Thus when the surfaces were metallized or graphited the breakdown voltage was reduced to well below the value observed for samples with clean surfaces (from 3-4 kv/mm to about 2 kv/mm).

Increasing the frequency to 80 Mc also reduces the breakdown voltage somewhat. The breakdown voltage between disc electrodes is generally some 25% lower than between spherical electrodes. The disruptive discharge always occurs at the edge of the electrodes, whereas with spherical electrodes the puncture occurs in the center of the metallized or graphited area.

Table 1 gives the results of tests of samples of polyethylene and teflon (fluoroplastic) at the same frequency with electrodes of different shape without metallization or graphiting of their surfaces in air and in carbon tetrachloride vapor.

Table 1

Measured breakdown voltages V_{br} and field strength E_{br} for polyethylene and teflon

Material	Thickness, mm	Electrodes					
		Disk, 20 mm dia		Spherical, 16 mm dia		20 mm long needle and 20 mm dia disc	
		V_{br}, kv_{max}	E_{br}, kv_{eff}/mm	V_{br}, kv_{max}	E_{br}, kv_{eff}/mm	V_{br}, kv_{max}	E_{br}, kv_{eff}/mm
Polyethylene	0.75-0.78	3.6	3.4	4.4	4.1	2.1	2.0
Teflon	1.8	---	---	---	---	3.5	1.4
Polyethylene in CCl_4 vapor	0.75	4.2	4.0	---	---	---	---

In a nonuniform field (i.e., with a point-disc electrode set) the electric strength is reduced approximately to the value observed for graphited or metallized samples.

The breakdown strength in CCl_4 vapor was increased by about 20% due to increase of the ionization voltage of the gaseous medium surrounding the electrodes.

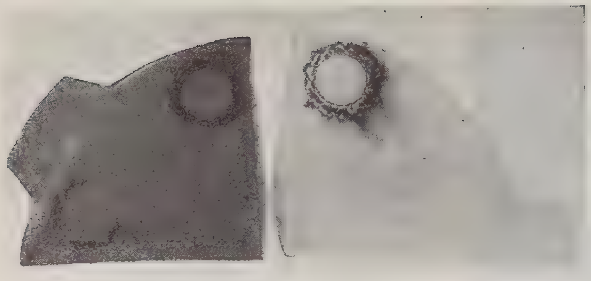

Fig.3. Appearance of disrupted polyethylene samples: strong traces of corona.

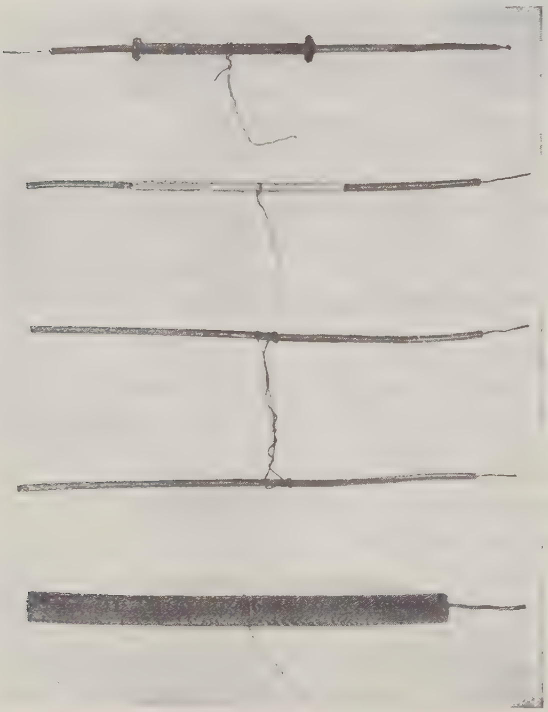

Fig.4. Samples of conductors with polyethylene insulation prepared for breakdown tests.

After breakdown the polyethylene samples showed clear evidence of the corona effect (Fig.3) very similar to that observed after prolonged testing at high voltage and 50 cps. The effect of the corona is particularly clearly evident on samples tested in CCl_4 vapor and in freon (CCl_2F_2), i.e., samples disrupted at a comparatively high voltage. The time of action of the high voltage in these cases was a matter of seconds whereas according to earlier studies the same type of corona damage of polyethylene was obtained only after several hundred hours subjection of the sample to 50 cps current at a voltage gradient of 8-9 kv/mm. Several hours are necessary to produce the same effect at a frequency of 10^5 cps.

It follows that the cause of breakdown of polyethylene and teflon is disintegration of the samples at the electrode edge owing to the influence of ionized air. Naturally, at a frequency 10^6 times higher this aging process is accelerated by approximately the same factor.

Reduction of the disruptive gradient at high frequency can be explained by the fact that in this case the ionization of the gas begins at a lower voltage than at the low (50 cps) frequency. Breakdown tests were also carried out at high frequency on short sections of single wire conductors with polyethylene insulation. The results are summarized in Table 2 and the samples are shown in Fig.4.

Table 2

Values of breakdown voltage V_{br} of conductors with polyethylene insulation

Sample	Diameter, mm		Thickness of insulation, mm	Outer electrode		
	wire	insulation		graphite	copper braid	tinfoil
Conductor with polyethylene insulation	0.7	2.5	0.9	2	3.7	2.2
Conductor in copper wire braid	1.4	9.3	4	3	No breakdown	---

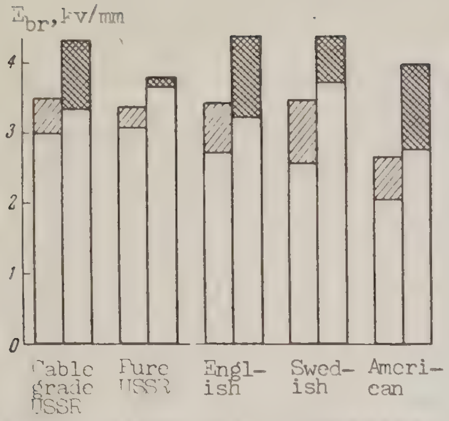

Fig.5. Diagram of comparative disruptive strength of polyethylene samples of different brands and types: ▨ in air and ▩ in freon.

It will be evident from the table that graphiting and even application of a layer of tinfoil greatly reduces the strength of the insulation as compared with copper braid. The indicated disruptive strength values, however, characterize not so much the actual breakdown strength of the material as primarily the intensity of ionization of the surrounding gas.

Finally, we carried out a series of comparative tests for disruptive strength at high frequency (30 Mc) in air and in freon at atmospheric pressure and room temperature of polyethylene samples of domestic and foreign manufacture. In these tests all the electrodes were 20 mm diameter discs.

The results of these tests are shown in Fig.5. It will be evident from the diagram that the disruptive strength at high frequency does not depend on the quality of the material itself, but depends primarily on the aging of the material under the influence of ionization of the ambient gas.

Thus it may be assumed that the disruptive strength and useful life of polyethylene insulation can be increased by suitably protecting the polyethylene insulation from the disruptive influence of ionization of the surrounding gaseous medium.

In absence of an ionized gaseous medium the electric strength of polyethylene will be appreciably higher. It also follows that it is expedient to use polyethylene insulation primarily for high voltage dc cables.

References

1. J.H.Mason, Proc.Inst.Electr.Engr., 98, 1 (1951).
2. Dakin, Philofsky & Divens, Electr.Engng., 73, NO.9 (1954).
3. S.M.Bragin & V.A.Golubtsova, Otchet MEI (Report, Moscow Power Institute) 1956.

ON CERTAIN PROCESSES INVOLVED IN THE ELECTRIC BREAKDOWN OF SOLID DIELECTRICS

- A.A.Vorob'ev & G.A.Vorob'ev

1. Discharge formation time

We determined experimentally the variation of the electric strength of NaCl, KCl, KBr and KI single crystals with the time the crystal is exposed to the influence of the voltage.[1] With exposure times of $1 \cdot 10^{-7}$ sec and less there is observed an increase of the breakdown strength due to lag of the discharge.

We carried out experiments on the breakdown of x-irradiated rock salt with a view to establishing the existence of a statistical time lag in such solid dielectrics. At the minimum exposure time of $2\text{-}3 \cdot 10^{-8}$ sec there were obtained virtually equal values of breakdown strength for noncolored rock salt and colored salt tested under strong illumination. This shows that in rock salt and, apparently, in the other investigated dielectrics at voltage transient times of $2\text{-}3 \cdot 10^{-8}$ sec and greater there is virtually no statistical delay time and the lag is wholly due to the time of formation of the discharge. Knowing the value of the electric strength at a given exposure and the value of the static breakdown strength, we determined the discharge formation time from the voltage oscillograms. For the static electric strength we took the value of the breakdown strength at an exposure of $3 \cdot 10^{-7}$ to $6 \cdot 10^{-6}$ sec, when the discharge formation time is much shorter than the exposure time and the influence of space charge is absent.

It should be noted that when the discharge lag becomes noticeable, there is an appreciably greater scatter of the breakdown strength values than in the case of exposures from $3 \cdot 10^{-7}$ to $6 \cdot 10^{-6}$ sec; this is illustrated by the data of Table 1.

Table 1

Exposure (to voltage) time, t, sec	Scatter of electric breakdown values relative to mean value in kv/cm			
	NaCl	KCl	KBr	KJ
$3 \cdot 10^{-7}$—$6 \cdot 10^{-6}$	340	335	275	235
$6 \cdot 10^{-8}$—$1{,}4 \cdot 10^{-7}$	695	470	540	265
$2 \div 3 \cdot 10^{-8}$	790	710	520	575

At exposures in the $3 \cdot 10^{-7}$ to $6 \cdot 10^{-6}$ sec interval the scatter of the electric strength values is due to structural defects in the samples: microfissures, mechanical stresses, etc. At exposures of $1.4 \cdot 10^{-7}$ sec and less to this spread there is added the scatter due to differences in the discharge formation time for different samples. From the experimental data one can roughly evaluate the bounds of fluctuation of the discharge formation time. Curves characterizing the variation of the electric strength of KBr with the exposure time are shown in Fig.1. It may be assumed that the increase in breakdown strength according to the law characterized by curve 1 is due to the maximum value of the discharge formation time, while the increase according to the law characterized by curve 2' is associated with the minimum value of the discharge formation time. Accordingly, employing the procedure described in Ref.1, we determined the maximum discharge formation time $t_{f\ max}$ and the minimum formation time $t_{f\ min}$ as well as the corresponding mean discharge propagation velocities

$$v_{av\ min} = \frac{d}{t_{f\ max}} \text{ and } v_{av\ max} = \frac{d}{t_{f\ min}},$$

where d is the thickness of the dielectric.

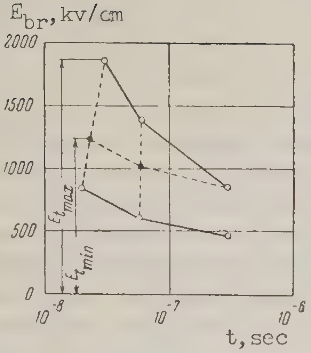

Fig.1. Variation of the electric strength of KBr single crystals with the time of application of the voltage: 1) upper curve - curve for a breakdown probability of 90%, 2) lower curve - envelope of minimal values, 2') middle (dash line) curve - curve drawn parallel to lower curve 2. Crystal thickness d = 0.15 mm.

The calculated data are listed in Table 2.

The average velocity of discharge propagation in the investigated dielectrics is of the order of 10^6 cm/sec. This value of v may tentatively be taken in calculating the voltage-time characteristics of a solid homogeneous insulating material with a breakdown strength of about 10^6 v/cm.

The discharge formation time decreases with increasing overvoltage. In the case of NaCl the discharge formation time increases with increasing sample thickness.

The rates of discharge development obtained by us for KCl are appreciably greater than the values given by Inuishi & Suita^2. These investigators divide the discharge lag in KCl crystals and sulfur into the statistical delay time and the discharge formation time. On the basis of the discharge formation time, they determined the mean electron velocity, which more accurately should be termed the mean discharge propagation rate. If we take the full discharge time, then according to the data of Inuishi & Suita, the average discharge propagation velocity in KCl comes out to be $0.67 \cdot 10^5$ cm/sec, i.e., one order of magnitude lower than our value.

In their work, von Hippel & Alger^3 also observed an increase of the breakdown strength of KBr with decreasing exposure (transient rise time), which can be explained by lagging of the discharge. Unfortunately, von Hippel & Alger do not give the thickness of their samples. For purposes of approximate calculation, we assumed this to be 0.1 mm; then according to the data of von Hippel & Alger, we find that $t_f = 0.5 \cdot 10^{-8}$ sec and the mean discharge propagation velocity

$$v_{av} = \frac{d}{t_f} = \frac{0.01}{0.5 \cdot 10^{-8}} = 2 \cdot 10^6 \text{ cm/sec.}$$

This value is close to our data.

Table 2

Discharge formation time t_f and average discharge propagation velocity v_{av} in different dielectrics

Dielectric	Exposure $6 \cdot 10^{-8}$–$1.4 \cdot 10^{-7}$ sec					Exposure 2–$3 \cdot 10^{-8}$ sec				
	Over-voltage, %	t_f, 10^{-8} sec		v_{av}, 10^6 sec		Over-voltage, %	t_f, 10^{-8} scc		v_{av}, 10^6 scc	
		max	min	min	max		max	min	min	max
NaCl d=0,15 mm	14,0	1,7	0,6	0,88	2,5	46,1	1,5	0,45	1,0	3,33
KCl d=0,15 mm	16,1	1,6	0,6	0,94	2,5	54,0	1,37	0,3	1,095	5,0
KBr d=0,15 mm	29,5	2,2	0,5	0,68	3,0	55,8	1,2	0,25	1,25	6,0
KJ d=0,15 mm	28,4	2,1	0,6	0,72	2,5	53,8	1,1	0,23	1,36	6,5
NaCl d=0,3 mm	17,9	3,0	1	1	3,0	No data				

2. Two discharge stages

The arithmetic mean values of the time of falling off of the voltage across the sample upon breakdown are $7 \cdot 10^{-9}$ sec for NaCl, $5 \cdot 10^{-9}$ sec for KCl and $4 \cdot 10^{-9}$ sec for KI.

The falling off of the voltage across the dielectric sample should be regarded as the second stage of the discharge - the stage of completion of the discharge. The first stage is the formation of the discharge, i.e., the process leading to formation of a discharge channel with a high electric conductivity. Such separation of the discharge into two stages is applicable to all dielectrics. In the case of breakdown of large air gaps, the first or forming stage is what is termed the leader stage and the completion stage is the stage of the principal discharge. The processes occurring in the stage of completion of discharge in solid dielectrics are still far from clear. Possibly in this case there occurs compensation of the excess space charge produced in the discharge channel during formation, much as occurs in the case of a long spark.

3. Completion of discharge stage

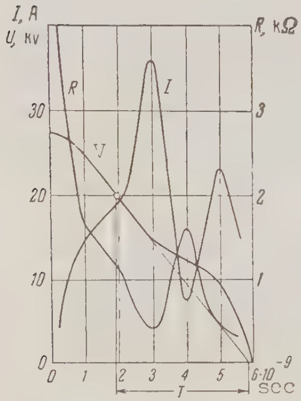

Fig.2. Variation of the voltage V, the current I and the resistance R of the discharge channel with time in a rock salt sample in the completion of discharge stage.

Calculations[4] show that the energy stored in the capacitance of the sample prior to breakdown is sufficient for disruption of the dielectric in the volume of the discharge channel.

If we take for NaCl $E_{br} = 2700$ kv/cm with an exposure of $2\text{-}3 \cdot 10^{-8}$ sec, a sample thickness of $d = 0.15$ mm, a sample capacitance $C = 6$ μμf, the diameter of the disrupted breakdown channel as 0.1 mm and the time of the completion of discharge stage as $7 \cdot 10^{-9}$ sec, we obtain a value of 600 megawatts/cm^3 for the average power of the discharge at this stage.

The voltage fall-off incident to breakdown may tentatively be regarded as discharge of the sample capacitance. The length of the subtangent at every point of the curve characterizing the falling off of the voltage (Fig.2) is constant and equals $T = RC$, where R is the resistance of the discharge channel.

Thus we have the possibility of plotting the curve $R = f(t)$ as well as the current curve $I = f(t)$, each point on which is given by $i = V/R$. The $V = f(t)$, $R = f(t)$ and $I = f(t)$ curves for rock salt are shown in Fig.2. The maximum current density, if we assume the diameter of the breakdown channel to be 0.1 mm is 445 kiloamp/cm^2.

4. Discharge formation stage

Approximately, the discharge formation energy is

$$W_f \approx \int_{t_0}^{t_0+t_f} U^2 g_t \cdot dt,$$

where t_o is the time from the beginning of the voltage pulse to the instant it attains the statistical breakdown value, t_f is the discharge formation time and g_t is the electric conductivity at the time t.

For variation of the voltage during the rise of the pulse, we have the expression

$$V = A(e^{\beta t} - 1),$$

where $A = 12.66$ kv and $\beta = 3.5\cdot10^7$ sec^{-1}.

If we assume that the increase in the electric conductivity in the discharge formation stage is due to impact ionization, we can write

$$g_t = g_0 e^{\gamma(t-t_0)},$$

where g_0 is the conductivity at the beginning of the discharge formation stage.

The value of the pre-breakdown current in KCl measured at constant voltage[5] attains 10^{-8} amp. Taking the sample thickness to be 0.1 mm and the breakdown voltage $V = 10$ kv, we obtain $g_0 = 10^{-12}$ mho. The value of the conductivity at the end of the formation stage, according to the curves of Fig.2, may approximately be taken as $g_{tf} = 10^{-4}$ mho.

We obtained the following values for γ:

NaCl	KCl	KBr	KI
1.23	1.53	1.67	$1.84\cdot10^9$ sec^{-1}.

Bearing in mind that $\gamma \gg \beta$, we obtain the following expression for the discharge formation energy

$$W_f \approx \frac{A^2 g}{\gamma}\left[e^{2\beta(t_0+t_f)} - 2e^{\beta(t_0+t_f)} + 1\right],$$

whence we obtain the following values for W_f:

NaCl	KCl	KBr	Ki
4.27	3.72	2.12	$1.52\cdot10^{-5}$ J.

The values of W_f are proportional to the lattice energy.

It is known that the impact ionization coefficient in air is 17.5 cm^{-1}. Taking the ionization potential of a nitrogen molecule to be 15 ev and the breakdown field to be $E_{br} = 32.5$ kv/cm, we find that only 15 x 17.5/32,500 or 1/124th part of the electrons energy is expended on ionization; the remainder goes for radiation and heating of the gas.

If we assume that in a solid dielectric in the formation of a discharge a major portion of the energy is expended on melting the dielectric, we can determine the radius of r of the discharge channel: calculations yield

NaCl	KCl	KBr	KI
12.6	16	13.5	$13.2\cdot10^{-4}$ cm.

Presumably not all the energy is expended on melting the dielectric; part of the energy probably is lost in the form of radiation. Assuming that only 0.01 W_f is expended on fusing the dielectric, even then we obtain a value of the order of 1 μ for r.

5. On the possibility of mechanical disruption

In her work, Zavadovskaia[6] gives the calculated values of the mechanical stresses developing in alkali halide crystals at breakdown fields and the experimental data on the magnitude of the ultimate (disruptive) mechanical stresses in such crystals; she shows that these values are close and suggests that there may occur mechanical disruption of solid dielectrics under the influence of high electrostatic forces. In the case of breakdown of solid dielectrics by a steep pulse there is a sharp increase in the electric strength and in the mechanical forces involved; hence the probability of mechanical disruption under the influence of electrostatic forces also increases.

Evidence in favor of this assertion is furnished by the fact that in breakdown by pulses with a short rise time alkali halide crystals are commonly fragmented, i.e., split into several parts, whereas in the case of long exposures with the same current-limiting resistance this does not occur. From this it may be inferred that the discharge formation time for an ionization process will be greater than the values we have calculated above.

In order to be able to judge of the character of breakdown in solid dielectrics by transient voltages with short rise times, additional photographic investigations of the development of discharges in solid dielectrics and studies of the variation with time of current in solid dielectrics are necessary.

Conclusions

1. In the process of breakdown of solid dielectrics, just as in the case of breakdown in gases, we can distinguish between two stages: the stage of discharge formation and the stage of completion of the discharge.
2. In the discharge formation stage there occurs partial destruction of the solid structure of the dielectric, which explains the appearance of incomplete punctures in solid dielectrics. Hence division of the breakdown of solid dielectrics into a stage of loss of electric strength and a stage of destruction is somewhat arbitrary. Most of the destruction of a solid dielectric does occur in the stage of completion of the discharge.
3. Owing to the enhanced electric strength of solid dielectrics in the case of short voltage pulses, the probability of mechanical destruction of the dielectric under such conditions increases.

"S.M.Kirov" Tomsk Polytechnic Institute

References

1. G.A.Vorob'ev, Izv. (Bulletin), Tomsk Polytechnic Institute, 91, 79 (1956).
2. J.Inuishi & T.Suita, J.Inst.El.Eng.Eng.Japan, 74, 150 (1954).
3. A.von Hippel & R.S.Alger, Phys.Rev., 76, 1, 127 (1949).
4. A.A.Vorob'ev & A.F.Kalganov, Izv. (Bulletin) Tomsk Polytechnic Institute, 91, 97 (1956).
5. A. von Hippel, Phys.Rev., 54, 1096 (1938).
6. E.K.Zavadovskaia, Doklady AN SSSR, 81, 541 (1951).

INVESTIGATION OF THE BREAKDOWN OF ROCK SALT CONTAINING COLOR CENTERS

- A.A.Vorob'ev & G.A.Vorob'ev

The influence of color centers, which are sources of weakly bound electrons, on the electric strength of alkali halide crystals has been repeatedly investigated (Table 1).

A decrease in the electric strength of colored crystals under static test conditions has been observed in the presence of photoconduction. In the dark, however, the breakdown strength of colored crystals remains equal to that of colorless ones.[1-3]

Inuishi & Suita[3] tested weakly x-irradiated KCl crystals with an alternating voltage and found no decrease of the electric strength due to photoconduction.

It has been noted that in the case of impulse breakdown, discharges in rock salt crystals are propagated primarily through regions of high electron concentration.

Vul & Gol'dman[2], Walter & Inge[5] and Inuishi & Suita[3] failed to detect any significant influence of photoconductivity and color centers as regards the impulse breakdown voltage. On the other hand, von Hippel & Alger[6] indicate that photoconduction reduces the electric strength in the case of pulsed voltages when the exposure time (transient rise time) exceeds 10^{-5} sec.

Reduction of the breakdown strength due to photoconduction has been explained by the influence of the positive space charge persisting in colored crystals after removal of the electrons. A positive space charge may produce emission of electrons from the cathode[3] or appreciably increase the local electric field intensity as compared with the mean value[2]. Both processes may favor the development of breakdown in dielectrics.

The absence of a noticeable influence of photoconductivity on the breakdown strength in the case of short voltage pulses, reported by some investigators, is explained by the appreciable time required for a space charge to form.

Vul & Gol'dman[2] indicate that in rare cases they observed in samples of colored rock salt at pre-breakdown voltages an increase in current by a factor of several thousand. This could result in thermal breakdown.

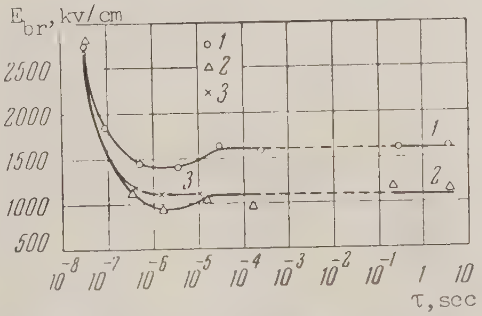

Variation of the electric strength of rock salt crystals at the time of exposure to the voltage (breakdown probability - 90%): 1) non-x-rayed samples, 2) x-rayed samples disrupted with strong illumination, 3) x-rayed samples disrupted in the dark. Sample thickness - 0.15 mm.

The reduction in breakdown voltage in the presence of photoconductivity, observed by some investigators, is explained as a result of secondary effects: the influence of space charge or thermal processes.

We determined the variation of the breakdown strength of colored and non-colored rock salt crystals with the time of application of the voltage. The crystals were colored by x-rays, the exposure time being about 4 hours with the x-ray tube operated at 150 kv and 10 ma.

Colored samples were tested for breakdown partially under strong illumination and partially in the dark. The results are shown in the accompanying figure. The indicated breakdown voltages are for a breakdown probability of 90%.

Table 1

Effect of coloring on the electric strength of crystals*

Type of investigation and Ref.	Conditions	Voltage					
		dc		ac		pulse	
		kv/cm or kv**	%	kv/cm or kv**	%	kv/cm or kv**	%
X-rayed rock salt in weakly non-uniform field. Ref.1	In dark	---	100	---	100	---	---
	In light	---	70	---	70	---	---
	Non-x-rayed	---	100	---	100	---	---
X-rayed rock salt in highly non-uniform field with point electrode positive. Ref.4	In dark	---	---	---	---	---	100
	In light	---	---	---	---	---	<100
Additively colored rock salt in uniform field. Ref.2	In dark	2100	100	1800	100	1900	100
	In light	830	40	840	47	1900	100
KBr single crystals in uniform field. Ref.6	In dark	---	100	---	---	---	100
	In light	---	<100	---	---	---	<100 at 10^{-5} sec
X-rayed rock salt plates in non-uniform field. Ref.5	In light:						
	point -	---	---	---	---	---	100
	point +	---	---	---	---	---	100
	Non-x-rayed						
	point -	---	---	---	---	---	100
	point +	---	---	---	---	---	100
X-rayed KBr single crystals in weakly non-uniform field. Ref.3	In dark	30	105	25	102	19	90
	In light	10	37	28	118	18	86
	Non-x-rayed	27	100	24	100	21	100

---

*In compiling the table we took as 100% the electric strength or breakdown voltage of non-colored crystals. Where such data were lacking we took the electric strength or breakdown voltage of colored crystals in the dark as 100%.

**Different authors give either breakdown voltages or field intensities; hence one can only compare data in the same row.

It will be seen from the figure that in the case of voltage pulses of $2\text{-}3\cdot10^{-8}$ sec duration, the breakdown strength in all three cases is virtually the same, which indicates that the same breakdown mechanism obtains in all cases. With this mechanism the discharge delay time is $1\text{-}2\cdot10^{-8}$ sec. The mechanism itself is considered to be an electronic process.[7]

In colored crystals we have yet another mechanism which comes into operation when the voltage is applied for a period of $3\text{-}4\cdot10^{-7}$ sec or more.

With transient times of $3\text{-}4\cdot10^{-7}$ sec the electric strength of colored and illuminated samples is somewhat greater than with a transient time of $1.6\cdot10^{-6}$ sec, which, it may be assumed, is due to a lag in the operation of the second mechanism. Assuming tentatively that the voltage rise is linear for a pulse of $4\cdot10^{-7}$ sec duration and that the difference in electric strength for pulse durations of $4\cdot10^{-7}$ and $1.6\cdot10^{-6}$ sec is

$$\frac{1120 - 930}{1120} \cdot 100 = 17\%$$

we obtain for the breakdown formation time in colored crystals: t_f colored = $= 4\cdot10^{-7}\cdot0.17 = 6.8\cdot10^{-8}$ sec.

With the scanty experimental data available so far it is difficult to determine the nature of the breakdown mechanism in colored crystals under the influence of transients of more than 10^{-7} sec duration.

Table 2

Breakdown voltages of rock salt under different conditions

Field		Breakdown voltage					
		Non-x-rayed samples		x-irradiated samples			
				in light		in dark	
		kv	%	kv	%	kv	%
Non-uniform	point −	42.4	100	36.3	86	38.2	90
	point +	44.4	100	43.8	98	51	115
Uniform		--	100	---	67	---	77.3

We also carried out experiments on the breakdown of colored and noncolored crystals of rock salt in a nonuniform field under the influence of voltage pulses of about 10^{-6} sec. Conical hollows were made in the crystals to obviate edge discharges.

The results of these tests are given in Table 2 together with the data on the breakdown of rock salt in a uniform field for purposes of comparison.

Table 3

Direction of discharges in rock salt samples with positive polarity of the point electrode

Samples	Total No. of samples	No. of samples with discharge along indicated direction		
		[100]	[110]	[111]
Nonirradiated	16	1	15	---
X-irradiated; in dark	11	4	7	---
X-irradiated; in light	12	4	5	3

With negative polarity of the point electrode, there were obtained the same regularities as in a uniform field, but with less pronounced differences. With positive polarity of the needle electrode, there was obtained a noticeable increase of the breakdown voltage in the case of samples tested in the dark as compared with those tested under strong illumination.

With negative polarity of the point electrode the discharges were oriented in the [100] crystallographic direction in both colored and non-colored crystals, whereas with positive polarity of the point there are distinct differences in the paths followed by the discharges in colored and non-colored crystals (Table 3).

The variation in the direction of the discharge in x-irradiated samples is apparently connected with the influence of photoelectrons on the space charge near the point electrode.

Conclusions

1. Under the influence of voltage pulses of $4 \cdot 10^{-7}$ sec duration and greater, the breakdown strength of colored rock salt crystals is lower than that of non-colored crystals. In the case of transients of $2\text{-}3 \cdot 10^{-8}$ sec duration approximately equal values of electric strength are observed.
2. The breakdown formation time in colored crystals subjected to voltage pulses with a rise time of more than 10^{-7} sec is approximately $6.8 \cdot 10^{-8}$ sec.
3. Photoelectrons in colored crystals alter the direction of the discharge path when the needle point is the positive electrode.

"S.M.Kirov" Tomsk Polytechnic Institute

References

1. A.A.Vorob'ev, Doklady AN SSSR, 3, 424 (1934).
2. V.M.Vul & I.M.Gol'dman, Doklady AN SSSR, 1, 363 (1935).
3. I.Inuishi & T.Suita, J.Phys.Soc.Japan, 9, 431 (1954).
4. A.A.Vorob'ev, Doklady AN SSSR, 26, 780 (1940).
5. A.F.Walther (Val'ter) & L.O.Inge, Doklady AN SSSR, 2, 65 (1949).
6. A.vonHippel & R.S.Alger, Phys.Rev., 76, 127 (1949).
7. G.A.Vorob'ev, Zhur.eksp.i teor.fiz., 30, 256 (1956).

TEMPERATURE DEPENDENCE OF THE ELECTRIC STRENGTH OF KBr AND KCL CRYSTALS

- E.A.Konorova & L.A.Sorokina

Until recently it has been assumed that the breakdown strength of crystals is temperature independent. In the work of Inge et al[1] it is shown that in NaCl electric (disruptive) breakdown occurs up to 200° and that above this temperature we have thermal breakdown characterized by a sharp decrease of the electric strength with temperature.

In a number of recent investigations[2-6], the results of which are plotted in Fig.1, it has been demonstrated that in the case of alkali halide crystals electric strength does not remain constant in the region of electric breakdown: all the authors report a maximum in the variation of the electric strength with temperature in tests with dc voltage. The results of different investigators are not in agreement, however, as regards the results for impulse breakdown. Thus von Hippel & Alger[4] report that for KBr the maximum in the temperature dependence is gradually smoothed out with reduction of duration of the applied voltage and that in the case of transients with rise times of 10^{-6} sec there is observed a weak increase of the electric strength with increasing temperature. Inuishi & Suita[5] in testing KCl crystals with voltage pulses of 10^{-6} sec duration did not observe temperature dependence of E_{br}, but found that the absolute value of E_{br} is lower than with dc voltage. Finally, in the work of Calderwood & Cooper[7] the results of measurements with pulses of 10^{-6} sec duration agree with the results obtained with dc voltage and show a maximum in the temperature dependence of the electric strength of KCl and NaCl crystals.

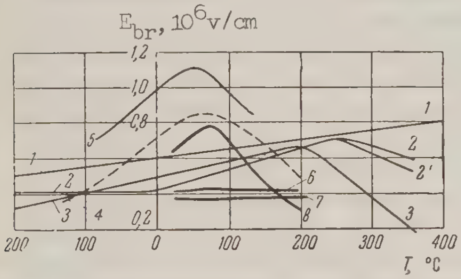

Fig.1. Experimental data on the temperature dependence of E_{br} for alkali halide crystals: 1,2 & 3) according to the data of von Hippel & Alger[4] for KBr with pulses (rise times) of 1) 10^{-6} sec, 2) 10^{-4} sec, 2') 10^{-3} sec, and 3) dc voltage, 4) according to Buehl & von Hippel[2] and von Hippel & Maurer[3] for KBr, 5) according to Callen[6] for KCl, 6,7 & 8) according to Inuishi & Suita[5] for KCl.

Nor is there agreement in the results of different investigators as regards the position of the temperature maximum. Thus, according to the data of most authors the breakdown-voltage maximum of KBr lies in the vicinity of 50°, whereas, according to von Hippel & Alger[4], the maximum occurs at 200°.

The actual temperature dependence of the electric strength of alkali halide crystals is of undoubted interest from the standpoint of the physics of electric breakdown. Hence we undertook the present investigation for the purpose of determining this dependence of KBr and KCl crystals in the temperature range from -170° to +200°. The experiments were carried out with dc voltage and linearly rising pulses of 10^{-2}, 10^{-4} and 10^{-6} sec duration. The voltage on the sample in the case of dc voltages and 10^{-6} sec pulses was measured by means of an electrostatic voltmeter with an accuracy within 5%. For recording the amplitude of the 10^{-4} and 10^{-6} sec pulses we used a high voltage KO-20 oscillograph, the voltage pulse being applied to the oscillograph plates through an appropriate divider. The error of measurement in this case did not exceed 10%.

The samples were prepared of KBr and KCl single crystals grown by the Kiropoulos technique. A recess was drilled in each crystal plate after which, for relief of mechanical stresses, the samples were heated for 3 hours at a temperature 50-70° below the melting point, followed by cooling at the rate of 1° per min. After the heat treatment, the thickness of the sample (bottom of recess to opposite face) was reduced to 0.1-0.2 mm by grinding and polishing; finally silver electrodes were applied by vacuum sputtering. To obviate cracking, the rate of heating and cooling of the samples before breakdown was kept to less than 1° per min.

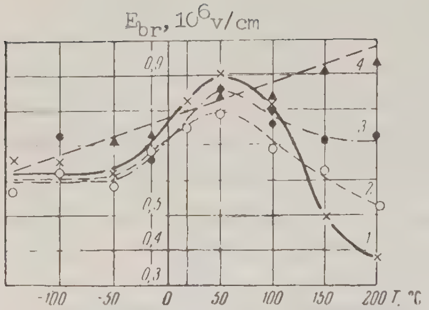

Fig.2. Temperature dependence of E_{br} for KBr with different durations of the applied dc voltage (1) and with pulses of 10^{-2} sec duration (2), 10^{-4} sec (3) and 10^{-6} sec (4).

The temperature dependences of E_{br} obtained for KBr are shown in Fig.2. Each point in the figure represents the average value from measurements on 12 to 20 samples. The root mean square error in the case of dc voltages did not exceed 8% and in the case of pulses 12%. It will be seen that in the temperature dependence of E_{br} with dc there is observed a maximum at 50°, which is gradually flattened out with decreasing duration of the applied voltage. There is no maximum evident in the case of pulses of 10^{-6} sec; instead there is observed a slow but constant increase of electric strength with temperature. In the temperature region below 0° the electric strength does not depend on the temperature for dc voltage and pulses of 10^{-2} and 10^{-6} sec duration.

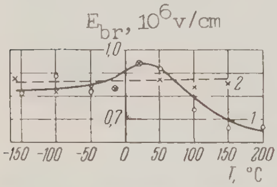

Fig.3. Temperature dependence of E_{br} for KCl with 1) dc voltage, 2) pulses of 10^{-6} sec duration.

The results obtained for the temperature dependence of E_{br} for KCl crystals are shown in Fig.3.

Conclusions

1. We have established experimentally that the temperature dependence of the dc breakdown strength of alkali halide crystals has a maximum which is flattened out with decreasing time of application of the dc voltage. Present-day theories of electric breakdown[8-10] associate failure of electric strength with electronic impact ionization. Hence in the entire temperature range regardless of the duration of application of the voltage (in any case for pulses of 10^{-6} duration) there should be observed a slow increase of electric strength with temperature.

In the "high temperature" breakdown theory of Fröhlich an attempt is made to explain the appearance of the maximum in the temperature dependence of E_{br}: however, even from the standpoint of this theory one cannot explain why the maximum that is so clearly evident in the case of a dc voltage is entirely absent in the case of 10^{-6} sec pulses.

2. The observed dependences indicate that the appearance of the maximum in the temperature dependence of E_{br} is associated with relatively slow processes initiated in the dielectric upon the application of a field. Hence the most promising hypothesis for explaining the observed dependences is that advanced by von Hippel & Alger[4], according to which the reduction in breakdown strength is due to distortion of the field because of formation of space charges: at low temperatures, a negative (electronic) space charge due to

field emission from the cathode and at high temperatures, a positive (ionic) space charge due to conductance of the crystal. At some temperature, presumably, the two charges compensate each other so that the field is relatively undistorted and the breakdown strength attains a maximum. The observed increase in strength with decreasing time of application of the voltage at high temperatures indicates that a time greater than 10^{-6} is necessary for the formation of an ionic space charge.

3. The magnitude of the electronic space charge, apparently, depends on the rate of electron emission from the cathode and, consequently, on the one hand, on the material of the cathode and the state of the contact surface and, on the other hand, on the concentration of electron traps in the crystal, i.e., on the amount of impurities present, previous heat treatment, etc.

Inasmuch as one can hardly expect these factors to be identical in all experiments, it is not surprising that the results of different investigators disagree, particularly as regards the position of the E_{br} maximum.

Definitive deductions regarding the factors involved in the temperature dependence of E_{br} in electric breakdown, we feel, can be made only on the basis of more detailed study of the currents in the region of pre-breakdown fields.

The present work was carried out under the supervision of G.I.Skanavi, whom the authors take this occasion to thank.

"P.N.Lebedev" Physical Institute,
Academy of Sciences of the USSR

References

1. L.D.Inge, N.Semenoff & A.F.Walther, Z.Phys., 32, 373 (1925).
2. R.C.Buehl & A.Hippel, Phys.Rev., 56, 7/12, 941 (1939).
3. A.Hippel & R.J.Maurer, Phys.Rev., 59, 820 (1941).
4. A.Hippel & R.S.Alger, Phys.Rev., 76, 127 (1949).
5. Y.Inuishi & T.J.Suita, Phys.Soc.Japan, 8, 567 (1953).
6. H.Callen, Phys.Rev., 76, 1394 (1949).
7. J.H.Calderwood & R.Cooper, Proc.Phys.Soc., B, 66, 2, 74 (1953).
8. A.Hippel, J.Appl.Phys., 8, 815 (1937).
9. H.Fröhlich, Proc.Roy.Soc., A, 160, 230 (1937).
10. V.A.Chuenkov, Usp.fiz.nauk, 14, 185 (1954).
11. H.Fröhlich, Proc.Roy.Soc. A, 188, 521 (1947).

TEMPERATURE DEPENDENCE OF THE ELECTRIC BREAKDOWN STRENGTH OF IONIC CRYSTALS

- V.D.Kuchin

At present, investigators are taking renewed interest in the temperature dependence of the electric strength of ionic crystals as regards electric (rather than "thermal") breakdown. There are a number of theoretical investigations proving that the electric strength of ionic crystals is temperature dependent. In Fröhlich's[1] theory of electric breakdown, a significant role is played by the critical temperature T_c at which the material transforms from the crystalline state to the amorphous. According to this theory, at temperatures below T_c the electric strength of the dielectric with increasing temperature must increase according to the equation

$$E_{br} \approx 0{,}8\, E_0 G\,(kT_0 / \hbar\omega), \tag{1}$$

where the function $G(kT/\hbar\omega)$ varies from 2/3 to 1 as $kT/\hbar\omega$ goes from 0 to ∞. Above T_c, when the material becomes amorphous, Fröhlich[2] gives the following condition for characterizing the electric strength

$$\ln E = \text{const} + \frac{\overline{\Delta e}}{2kT}, \tag{2}$$

where Δe is the mean energy required for raising an electron located at the excited heterogeneity levels into the conduction band.

According to the impact ionization theory of Franz[3], which takes into account collisions of electrons with acoustic modes of the lattice, the breakdown field is given by

$$E_{br} = \frac{30}{a_0^3} \cdot \frac{30}{A} \cdot \frac{4 \cdot 10^5}{V_S} \sqrt{\frac{T}{300}}, \tag{3}$$

where A is the atomic weight and V_s is the velocity of sound.

In the impact ionization theory developed by Callen[4], which takes into account electron collisions with optical vibrations, a complicated temperature dependence of E_{br} is obtained. In the region of low temperatures the electric strength of alkali halide compounds should presumably increase linearly at the rate of about 1 kv/cm per degree.

According to Zener's theory of electrostatic ionization by the field, E_{br} for ionic crystals is described by the formula

$$E_{br} = 0{,}1\, \frac{a_0 (\Delta W)^2}{n}, \tag{4}$$

where ΔW is the width of the energy gap. According to this formula the electric strength is temperature independent.

Vorob'ev & Zavadovskaia[6] showed that a linear relationship exists between E_{br} and the lattice energy of ionic crystals. According to Zavadovskaia[7] the lattice energy is only weakly dependent on the temperature. Accordingly, one should expect only a small variation of E_{br} in ionic crystals with changes in temperature. It has been shown[8] that the electric strength of alkali halide crystals as a function of the temperature is described by the formula

$$E_{br} = \frac{U_0 \sqrt{m}\, V_S}{e a_0 \sqrt{kT}}. \tag{5}$$

where U_0 is the height of the potential barrier, e is the electron charge, m is the electron mass and a_0 is the lattice constant. In light of these considerations the electric strength of solid dielectrics should vary little with temperature. In fact, it should vary so little that it is doubtful whether the changes can be detected experimentally[9].

As a result of theoretical calculations Chuenkov[10,11] found that E_{br} of ionic crystals increases with temperature from 100 to 500°K at a rate of approximately 2 kv/cm per degree.

The validity of the different theories of electric breakdown of dielectrics is generally evaluated primarily from the standpoint of correct prediction of the temperature dependence of the electric strength. Inasmuch as the temperature dependence of E_{br} for ionic crystals predicted by different theories is different, in order to choose between the different theories it is of interest to investigate the temperature variation of E_{br} in ionic crystals experimentally and compare the results with the predictions of the different theories.

We measured the electric strength of NaCl, KCl, KBr and KI at temperatures from -130 to +150° both with dc voltages and pulses of 10^{-4} to 10^{-8} sec duration. The results obtained for NaCl in the form of arithmetic mean values of E_{br} are given in Fig.1. It will be seen that in the case of NaCl in the temperature range below 0° the electric strength increases with increasing temperature linearly at the rate of approximately 1.75 kv/cm per degree for dc and pulses of up to 10^{-7} sec.

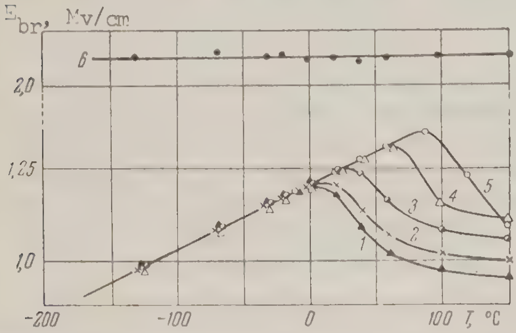

Fig.1. Temperature dependence of the electric strength of NaCl. Pulse durations: 1) 10^{-6} sec, 2) 10^{-5} sec, 3) 10^{-4} sec, 4) 10^{-7} sec, 5) dc voltage, 6) 10^{-8} sec.

Similar results were obtained for KCl, KBr and KI (Figs.2,3 & 4). It was found that for all times of application of the voltage there persists a definite correlation between the electric strength and the lattice energy: the greater the energy of the crystal lattice, the higher the electric strength. The observed temperature dependence of E_{br} in the region below 0° in the case of ionic crystals can be explained from the standpoint of Fröhlich's theory as follows. It is known[12] that at breakdown the electron density attains 10^{17} per cm^3. Fröhlich showed that even at an electron density of about 10^{-4} per cm^3 in a dielectric the interaction between electrons is stronger than between electrons and lattice vibrations.[1] With increasing temperature the number of interelectron collisions increases and, consequently, the energy lost by elec-

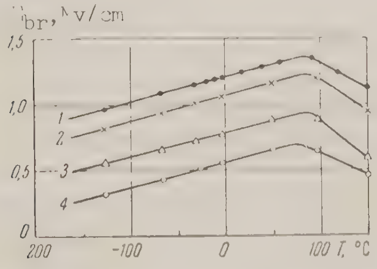

Fig. 2. Temperature dependence of the dc electric strength: 1) NaCl, 2) KCl, 3) KBr and 4) KI.

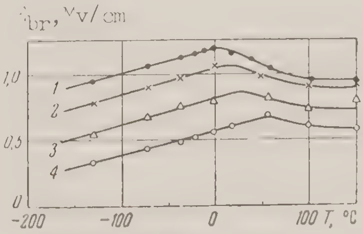

Fig.3. Temperature dependence of the electric strength with pulses of 10^{-6} sec duration: 1) NaCl, 2) KCl, 3) KBr and 4) KI.

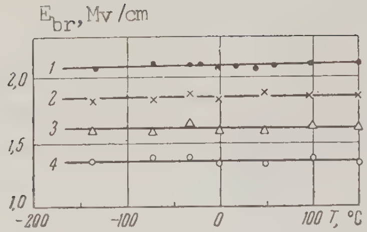

Fig.4. Temperature dependence of the electric strength of pulses of 10^{-8} sec duration: 1) NaCl, 2) KCl, 3) KBr and 4) KI.

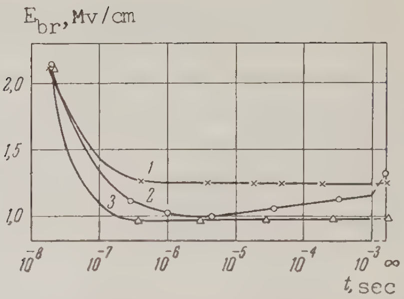

Fig.5. Voltage-time characteristics of NaCl at different temperatures: 1) 0°, 2) 100°, 3) -130°.

trons in such collisions increases accordingly. This means that E_{br} must increase with rising temperature.

At temperatures above 0° the lowest values of E_{br} are observed for voltage pulses of 10^{-6} sec duration. The voltage-time characteristic of ionic crystals at high temperatures (above 0°) have a dip (Fig.5) which, apparently, should be explained by the influence of space charge in the case of voltage pulses of more than 10^{-6} sec duration. We assume that the space charge in ionic crystals has an ionic origin and enhances the electric strength. Thus the discharge lag in a dielectric is of the order of 10^{-8} sec,[12] while the time required for the space charge to become evident is greater than 10^{-6} sec (Fig.5). With increasing temperature the number of ions contributing to the space charge increases. Consequently, with increasing temperature the influence of the space charge should become stronger.

The high electric strength of ionic crystals with pulse times of 10^{-8} sec as compared with the value of the strength with 10^{-6} sec pulses is connected with the lag of the discharge in the dielectric. The temperature dependence of E_{br} at $t = 10^{-8}$ sec is neither qualitatively or quantitatively in agreement with any of the extant theories of electric breakdown in solid dielectrics. Apparently, with pulses of 10^{-8} sec duration there occurs mechanical disruption of the dielectric under the influence of the strong electric field with no preliminary or preparatory processes involved. That such mechanical disruption of a dielectric in a strong electric field is possible has been indicated earlier by Zavadovskaia[14] and Cooper & Wallace.[15] In particular, Zavadovskaia calculated that at field strengths close to the breakdown value there develop in a dielectric mechanical stresses comparable with the ultimate (disruptive) stress for the material.

The fact that there are mechanical stresses in the dielectric in a strong electric field has been experimentally proved by Cooper & Wallace.[15] True, under their experimental conditions the mechanical stresses in the investigated KCl crystals could not be large inasmuch as the applied field was relatively weak. It may be assumed, however, that at voltages 2-3 times greater than the breakdown value the mechanical stresses in a crystal under the influence of an applied electric field may appreciably exceed its mechanical strength and hence that the dielectric can be mechanically ruptured. Experiments to check this are being planned.

In view of what has been said above it is obvious that in theoretical evaluations of the temperature dependence of E_{br} in ionic crystals one must take into account the time of application of the voltage (pulse duration or transient rise time) and at temperatures above 0° the appreciable influence of space charge in the case of pulses of 10^{-6} sec and more duration.

In conclusion I desire to thank A.A.Vorob'ev for his great assistance in carrying out the work and for valuable suggestions in discussing the results.

"S.M.Kirov" Tomsk Polytechnical Institute

References

1. H.Fröhlich & B.V.Paranjape, Proc.Phys.Soc., B, 69, 433, 21 (1956).
2. H.Fröhlich, Proc.Roy.Soc., A, 160, 230 (1937).
3. W.Franz, Z.Phys., 113, 607 (1939).
4. H.B.Gallen, Phys.Rev., 76, 1394 (1949).
5. C.Zener, Proc.Roy.Soc. A, 145, 523 (1934).
6. A.A.Vorob'ev & E.K.Zavadovskaia, Doklady AN SSSR, 81, 375 (1951).
7. E.K.Zavadovskaia, Doklady AN SSSR, 82, 656 (1952).
8. A.A.Vorob'ev & E.K.Zavadovskaia, Izv. (Bulletin) Tomsk Polytechnic Institute, 71, 3 (1952).
9. A.A.Vorob'ev & E.K.Zavadovskaia, Izv. (Bulletin) Tomsk Polytechnic Institute, 71, 7 (1952).
10. V.A.Chuenkov, Usp.fiz.nauk., 54, 185 (1954).
11. V.A.Chuenkov, Izv. (Bulletin) Tomsk Polytechnic Institute, 91, 45 (1956).
12. A.Rose, Phys.Rev., 97, 1538 (1956).
13. G.A.Vorob'ev, Zhur.eksp.i teor.fiz., 30, 256 (1956).
14. E.K.Zavadovskaia, Thesis, Tomsk.
15. R.Cooper & A.A.Wallace, Proc.Phys.Soc., B, 66, 1113 (1953).

TEMPERATURE DEPENDENCE OF THE PULSE ELECTRIC STRENGTH OF CERTAIN POLYCRYSTALLINE DIELECTRICS

- E.A.Konorova, V.V.Krasnopevtsev & G.I.Skanavi

In the first researches undertaken with a view to determining the possible influence of the dielectric constant ϵ on the electric strength of solid dielectrics, this (expected) dependence was explained in terms of the influence on electric breakdown of a local field dependent on ϵ.[1,2] Later, when the concept of electronic impact ionization was formulated, it was hypothesized that the decisive factor in breakdown is the mean field and hence that there is no reason to expect the electric strength to be dependent on the dielectric constant.[3]

In modern theories of electric breakdown in solid dielectrics, in accord with experiment, it is assumed that breakdown is caused by the behavior of conduction electrons in the crystal lattice under the conditions of a strong electric field.[4-6] Consequently, it may be assumed that the motion of the conduction electrons and in the final analysis the electric strength must be influenced by the dielectric polarization of the lattice, which is characterized by the dielectric constant. In view of the weak (in the absence of secondary effects) temperature dependence of electric breakdown, one may reasonably attempt to find the relation between the electric strength and the dielectric constant for a material with a sufficiently great (several fold) variation of ϵ with temperature, thus excluding the uncertainty connected with differences in structure of different materials. In general the strongest temperature dependence of the dielectric constant is observed in ferroelectrics (Rochelle salt, barium titanate, etc.). Unfortunately, however, in fields approaching the breakdown value this temperature dependence of ϵ in ordinary ferroelectrics is attenuated.

Recently there were synthesized in our laboratory new dielectrics, namely, strontium-bismuth titanate - SBT - with a high dielectric constant ($\epsilon \approx 800$ at room temperature) devoid of ferroelectric properties. The temperature dependence of ϵ for SBT is shown in Fig.1. Furthermore, ϵ is independent of the electric field intensity (up to the breakdown value). Consequently, this dielectric has the properties requisite for investigating the influence of ϵ on the breakdown strength.[7]

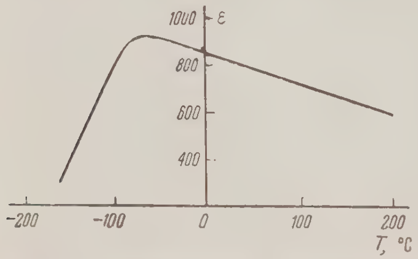

Fig.1. Temperature dependence of the dielectric constant of strontium-bismuth titanate (SBT) at a frequency of 50 kc.

Accordingly, we undertook an investigation of the temperature dependence of E_{br} in the region of electric breakdown for solid dielectrics having different values of the dielectric constant.

We investigated dielectrics with different types of polarization, with different values of ϵ and different temperature dependences of ϵ, namely, zinc titanate - $ZnO \cdot TiO_2$ ($\epsilon = 30$), calcium titanate - $CaTiO_3$ ($\epsilon = 130$), barium titanate - $BaTiO_3$ ($\epsilon \approx 1000$) and SBT ($\epsilon \approx 800$). (The indicated values of ϵ are for room temperature and a frequency of 1 kc.) The samples had the shape commonly employed in measuring the breakdown voltage under conditions of a uniform field (plates with a spherical recess on one side). The electrode material in each case was selected to assure a maximum breakdown voltage and a minimum scatter of the experimental points. As a result of preliminary experiments, we chose aquadag for all the dielectrics, except zinc titanate for which we used vacuum sputtered silver electrodes. The thickness of the sample at the thinnest point (between the bottom of the recess and the opposite flat face) was measured by means of a mechanical indicator to within $\pm 2 \cdot 10^{-4}$ cm. In order to exclude the possible influence of thickness on the breakdown voltage, the thickness was kept within fixed limits, namely, 0.30 to 0.50 mm for $BaTiO_3$ and between 0.10 and 0.30 mm for all the other dielectrics.

The breakdown tests were carried out with dc, 50 cycle ac and single pulses with different rise times (to 10^{-7} sec). The breakdown voltage with dc and 50 cycle ac was measured by means of an electrostatic voltmeter; an oscillograph was used in the pulse measurements.

The temperature measurements were carried out in the range from $+150^{\circ}$ to that of liquid nitrogen temperature.[8] The breakdown temperature was recorded by means of a copper-constantan thermocouple mounted in the immediate proximity of the sample. The holding time necessary to insure equalization of temperature between the sample and thermocouple and the rate of cooling were selected experimentally. The last did not exceed 1.5° per min which insured the absence of cracks and deformations that might affect the electric strength. The samples tested at liquid nitrogen temperature were immersed in liquid nitrogen; at all the other temperatures the tests were carried out on samples suspended in silicone oil. The maximum error in these tests did not exceed 12%.

The mean and maximum values of the breakdown strength of zinc, calcium and barium titanate and SBT at room temperature for the different forms of applied voltage are shown in the accompanying table.

Mean and maximum values of the breakdown voltage for some polycrystalline dielectrics for dc, 50 cycle ac and pulse voltages at room temperature (τ - pulse duration; η - number of samples tested)

Dielectric	50 cycle ac		dc voltage		$\tau = 1{,}0 \cdot 10^{-2}$ sec		$\tau = 1{,}0 \cdot 10^{-4}$ sec	
	n	E_{br}, 10^6 v/cm	n	E_{br}, 10^6 v/cm	n	E_{br}, 10^6 v/cm	n	E_{br}, 10^6 v/cm
$ZnO \cdot TiO_2$	19	0,275 0,360	20	0,490 0,635	8	0,495 0,615	19	0,485 0,660
$CaTiO_3$	16	0,195 0,230	20	0,380 0,495	16	0,325 0,460	14	0,370 0,450
CBT	32	0,120 0,143	56	0,200 0,280	10	0,250 0,310	21	0,290 0,355
$BaTiO_3$	25	0,0675 0,090	27	0,110 0,170	10	0,135 0,150	17	0,125 0,175

Dielectric	$\tau = 0{,}8 \cdot 10^{-5}$ sec		$\tau = 1{,}5 \cdot 10^{-6}$ sec		$\tau = 3{,}0 \cdot 10^{-7}$ sec		$\tau = 7{,}0 \cdot 10^{-8}$ sec	
	n	E_{br}, 10^6 v/cm	n	E_{br}, 10^6 v/cm	n	E_{br}, 10^6 v/cm	n	E_{br}, 10^6 v/cm
$ZnO \cdot TiO_2$	19	0,550 0,755	27	0,550 0,760	24	0,510 0,650	— —	— —
$CaTiO_3$	16	0,405 0,515	23	0,355 0,525	22	0,365 0,540	— —	— —
CBT	18	0,220 0,290	29	0,220 0,315	27	0,230 0,310	36	0,255 0,335
$BaTiO_3$	15	0,150 0,180	24	0,135 0,170	26	0,150 0,205	20 —	0,160 0,210

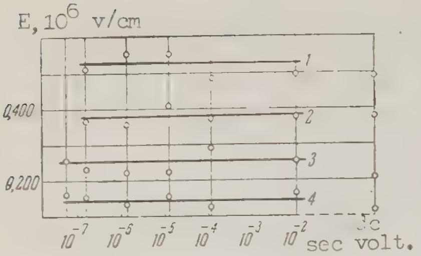

Fig.2. Variation of the breakdown voltage of polycrystalline dielectrics with the time of application of the dc voltage at room temperature: 1) $ZnO \cdot TiO_2$, 2) $CaTiO_3$, 3) SBT, 4) $BaTiO_3$.

Each experimental point is an average for not less than 12 samples. The scatter of breakdown voltage values from sample to sample was no greater than common in tests of this type. The root mean square deviation did not exceed 7%.

At room temperature the electric strength of the investigated polycrystalline dielectrics does not vary with the time of application of the voltage (Fig.2).

The temperature dependences of the breakdown voltage for some of the dielectrics tested are shown in Figs.3 and 4. It will be seen that in the case of SBT there is evinced a minimum value of the electric strength. This minimum is most pronounced in the case of pulses with a rise time of 10^{-4} sec. The breakdown strength for dc and 50 cycle ac does not vary with the temperature in the region above room temperature (according to the data of Sarafanova[9]) and increases with decreasing temperature below room temperature. There is some correlation between the temperature dependence of ϵ and the temperature dependence of the breakdown voltage (compare Figs.3 and 1). The highest breakdown voltage corresponds to low values of ϵ, but the temperature minimum of E_{br} and the temperature maximum of ϵ do not coincide.

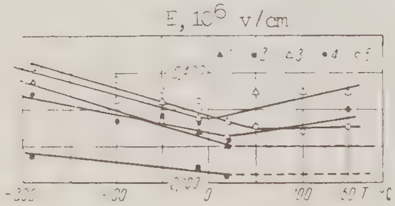

Fig.3. Temperature dependences of the breakdown voltage of SBT: 1) dc voltage, 2) 50 cycle ac, 3) 10^{-4} sec pulses, 4) 10^{-6} sec pulses, 5) 10^{-7} sec pulses.

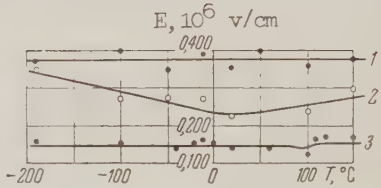

Fig.4. Temperature dependences of the breakdown voltage of dielectrics with single pulses having a rise time of $1.5 \cdot 10^{-6}$ sec: 1) $CaTiO_3$, 2) SBT and 3) $BaTiO_3$.

The electric strength of calcium and barium titanates is virtually temperature independent (Fig.4). Extant theories of electric breakdown in solid dielectrics are based on the concept of impact ionization by electrons moving in a mean electric field. Breakdown follows an avalanche-like build-up of conduction electrons in the crystal lattice. The condition for formation of an electron avalanche is determined, on the one hand, by the process of acquisition of energy by a conduction electron from the external field and, on the other hand, by energy losses of the electron as a result of collision with lattice vibrations and possibly with other electrons, particularly, in fields close to the breakdown one when the electron concentration becomes appreciable.[10]

Theoretical evaluations show that the ionization free path of a conduction electron in a breakdown field is about 100 lattice constants. Hence, in view of averaging over this path, the influence of the effective field (and, consequently, of ϵ) on the conduction electron must be nullified so that the acceleration of the electron is realized by the mean macroscopic field.

There may however be a relation between electric breakdown and polarization effects in the crystal (vibration frequency, effective ionic charge, etc.) realized through energy losses of the conduction electrons in interacting with the lattice vibrations.

Gallen[11] was able in the case of alkali halide crystals to relate the breakdown field strength, in addition to other characteristics of the material, with the polarization associated with elastic displacement of the ions. The variation of the electric strength of alkali halide crystals with variations in ϵ is not great, probably, in view of the small difference between the values of ϵ for different alkali halide crystals and the weak influence of external factors on ϵ for a given alkali halide crystal. For a material with a very high dielectric constant (for example, SBT and barium titanate) the influence of different types of polarization on the energy loss of conduction electrons, and in the final analysis, on electric breakdown strength may apparently be more strongly evinced.

Thus the influence of polarization on the electric strength of dielectrics must be realized through energy losses of the conduction electrons in exciting vibrations not only of the principal ions (atoms) of the lattice but also of the ions that produce polarization accompanied by a very high dielectric constant. Furthermore, a very strong effective field may alter the frequency of vibration of the principal ions which will naturally affect the energy loss by the conduction electrons.

To obtain an analytic expression characterizing the dependence of the electric strength on the dielectric constant, from this viewpoint, is extremely difficult and lies beyond the scope of the present work.

The proposed interpretation of the relation between the electric strength and the dielectric constant must be checked in the case of pure single crystals. Our experiments were carried out on polycrystalline samples. Hence in our case, unfortunately, the dependence in question is complicated by secondary effects associated with macroscopic inhomogeneity of the material (crystallites, vitreous layers, pores, etc.).

SBT and other polycrystalline materials of this type consist of individual minute crystals and vitreous interlayers with a small number of pores disseminated through them. The individual crystals in SBT are very small (they cannot be discerned even with 400-fold magnification); the vitreous interlayers apparently make up not more than 5% of the total crystal phase; the concentration of pores which have the form of fairly regular spheres with a maximum diameter of 0.013 mm does not exceed 10^5 per mm^3. At first glance it might be assumed that the breakdown voltage is determined by breakdown of the pores, but since the field in a spherical pore inside a material with a dielectric constant ϵ is

$$E_i = \frac{3\epsilon}{2\epsilon + \epsilon_p} \cdot E,$$

where ϵ_p is the dielectric constant of the pores and E is the mean field, dependence of the breakdown voltage on ϵ should not obtain if $\epsilon \gg \epsilon_p$. This condition is fulfilled in SBT ($\epsilon \approx 800$) and, consequently, the results obtained cannot be explained by the presence of pores in the dielectric.

Another possible explanation of the temperature dependence of the electric strength of SBT might be sought by picturing the macroscopic field distribution in a stratified dielectric consisting of a crystal phase with a very large value of ϵ and a vitreous phase with a small value of ϵ. The vitreous interlayers, which account for less than 5% of the total mass of the dielectric, may be represented in the form of thin boundary layers enveloping the individual crystals. In the very simplest case the system may be thought of as a two-layer capacitor consisting of a thin (5%) layer d_1 with a small value of ϵ_1 (10-12) and a thick layer d_2 with a high value of ϵ_2 (800-1000) (Fig.5). Under pulse conditions the field in these layers is inversely proportional to ϵ, i.e.,

$$E_2/E_1 = \epsilon_1/\epsilon_2,$$

where E_1 is the field intensity in layer d_1 and E_2 is the field intensity in layer d_2.

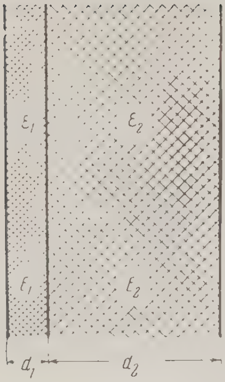

Fig.5. Simplified "capacitor" model of SBT.

If we use the known temperature dependence of ϵ of the crystal phase (Fig.1) and assume that the breakdown of a two-layer capacitor is determined by breakdown of the thin vitreous phase (breakdown field 10^6 v/cm), we can calculate the breakdown voltage at different temperatures. The curve calculated in this manner is reminiscent of the experimental curve for SBT (Fig.3). (The experimental results for barium titanate and calcium titanate are also not in conflict with such calculations.) However, the temperature minima in the experimental and calculated curves (Fig.6) differ by approximately 100°. A satisfactory explanation of this discrepancy from the standpoint of the proposed simple model does not appear feasible.

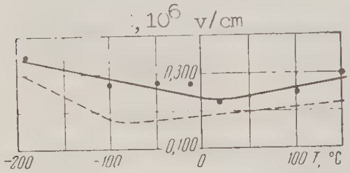

Fig.6. Comparison of the temperature dependence of the breakdown voltage calculated for a two-layer capacitor model (Fig.5) (dash line) with the experimental dependence of SBT (points). Pulse duration - $1.5 \cdot 10^{-6}$ sec.

Apparently the question of the nature of the variation of the electric strength with the dielectric constant for SBT can be resolved only by carrying out experiments on single crystals.

"P.N.Lebedev" Physical Institute,
Academy of Sciences of the USSR

References

1. B.V.Gorelik, Zhur.tekh.fiz., 10, 369 (1940).
2. N.A.Prikhod'ko, Trudy (Transactions), Siberian Phys.Tech.Inst.,6 114, (1942).
3. B.M.Vul, Sb., posviashch. 70-letiiu akad. A.F.Ioffe (Symposium dedicated to the 70th anniversary of Academician A.F.Ioffe), p.182, M., 1950.
4. A.von Hippel, J.Appl.Phys., 8, 815 (1937).
5. F.Seitz, Phys.Rev., 76, 1176 (1949).
6. V.A.Chuenkov, Usp.fiz.nauk, 54, 185 (1954).
7. G.I.Skanavi & E.N.Matveeva, Zhur.eksp.i teor.fiz., 30, 1047 (1956).
8. V.N.Kostriukov, R.A.Alikhaniants, B.N.Samoilov & P.G.Strelkov, Zhur. fiz.khim., 28, 650 (1954).
9. V.N.Sarafanov, Zhur.eksp.i teor.fiz., 27, 590 (1954).
10. H.Fröhlich & B.V.Paranjape, Proc.Phys.Soc., 69, 21 (1956).
11. H.B.Callen, Phys.Rev., 76, 1394 (1949).

DISCUSSION FOLLOWING THE PRECEDING SIX REPORTS

V.F.Pisarenko (on the report by Vorob'ev & Vorov'ev): In the report on the breakdown of colored rock salt, account was not taken of space charges due to freeing of F-centers. With pulses of 10^{-6} sec and sufficiently strong illumination the space charge developing must be sufficiently great to affect the breakdown strength.

I.E.Balygin: The experiments carried out by S.M.Bragin are exceptionally important inasmuch as hitherto, unfortunately, this field has been inadequately studied. In the report of A.A.Vorob'ev and G.A.Vorob'ev division of breakdown into two stages appear to be rather arbitrary. The measuring procedure used in the work of L.A.Sorokina cannot be regarded as sufficiently reliable inasmuch as samples of only 0.1-0.2 mm thickness were used and at such small thicknesses any minute cracks and fissures in the material may seriously affect the results. In addition, compressed gas should have been used as the medium.

G.P.Fedoseev: The report of S.M.Bragin stands out against the other papers that we heard today by its practical value. The possibility of using polyethylene insulation for high-voltage, high-frequency cables instead of impregnated paper and rubber insulation is of great economic importance. The purpose of Bragin's extensive work was to determine the possibility of using a new form of cable insulation for high voltage cables. It is known that the type of insulation now used for such cables can no longer fully satisfy the increasingly exacting requirements of present-day high-voltage technology and high-frequency engineering. The new requirements primarily concern aging of the insulation. The high-voltage, high-frequency set-up developed by Bragin is of interest for it can also be utilized for testing other forms of insulation at high frequencies and voltages.

Of particular interest in the experiment is the fact that the conditions of application of the simple metallic electrodes approach the conditions of possible operation of the conductor-and-polyethylene-insulation complex in cables of recent design. Consequently, the results obtained are of great practical interest. Unfortunately, the research has not yet been carried far enough to allow of making specific technological recommendations that would be of aid to cable design engineers.

M.P.Tonkonogov: The report of Prof.Bragin is very valuable from the standpoint of clarifying the relation between dielectric loss and breakdown. It would be of great interest to carry out experiments on breakdown at high frequency on samples with different losses, to determine how the ratio of the breakdown strength with dc voltage (or 50 cycle ac) to the breakdown strength at high frequencies varies. It may be predicted that this ratio will increase with increasing loss tangent of the material.

If one solves the kinetic equation for orientational polarization in the second approximation, rough evaluations show that the loss angle begins to depend on the intensity of the applied field. It may therefore be assumed that large dielectric losses favor development of breakdown. This influence is evinced not only in heating of the dielectric in high frequency fields but also, apparently, in the creation of more favorable conditions for development of electron avalanches.

I.D.Fridberg: Prof.Bragin noted that the corona effect seriously hampered obtaining dependable results. In this connection I would like to share the experience gained in our institute where for such tests we used shielded electrodes obviating edge discharges. The shape of flat and cylindrical samples is shown in the figure (see next page).

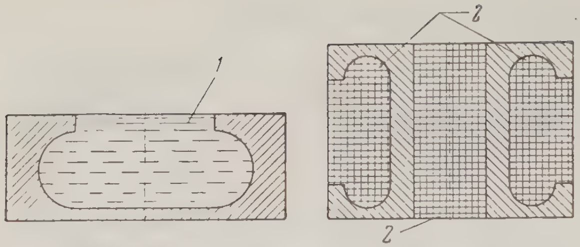

Shielded electrodes precluding edge discharges: at left - flat and at right - cylindrical sample; 1 - mercury, 2 - solid electrodes.

K.B.Tolpygo: In connection with the report of Krasnopevtsev, Konorova & Skanavi, I would like to note that according to the polaron theory the dependence of E_{br} on ϵ is given by $E_{br} \sim 1/n^2 - 1/\epsilon$, where n is the index of refraction and ϵ is the static dielectric constant. This theoretical dependence of E_{br} on ϵ does not agree with the result given in the report.

E.A.Konorova: Comrade Balygin raised the following objections to our procedure: 1) in connection with the small thickness of the samples there is a probability of appearance of cracks and 2) the medium was incorrectly selected (Balygin pointed out the desirability of using compressed gas). In order to avoid the appearance of cracks, we especially selected cooling and heating conditions guaranteeing the absence of cracking; this also applies to the other conditions involved in preparing the samples. The small spread of electric strength values indicates that the quality of the samples was good. As for the medium, we used silicone oil, which has very good insulating properties, and worked in the temperature range from 100 to 300°. Hence flashover in our experiments was precluded. The difference between the test procedure employed by von Hippel and ourselves and the techniques used in the 1930-ies consists in improvement in the quality of the investigated samples - the purity of the initial materials and the preliminary treatment - and on the accuracy of measuring the pulse breakdown voltages.

G.I.Skanavi: Of particular interest in the work of G.A.Vorob'ev & A.A. Vorob'ev is the attempt to obtain definite data on the second stage of breakdown and, especially, on the rate of propagation of the discharge. Their approach to these problems merits attention.

The latest investigations on the temperature dependence of breakdown, including recent work in our laboratory and in the Tomsk Laboratory, proved that there is a maximum in the temperature dependence of the dc electric strength, even though not very long ago A.A.Vorob'ev attempted to explain the presence of the apparent maximum by cracking of the samples. We checked this very carefully and carried out experiments to find appropriate cooling and heating regimes for the samples. At present there can be no doubt that the temperature maximum exists and is due to physical effects rather than to possible defects in the sample. The hypothesis advanced by von Hippel regarding the causes of this maximum obviously requires experimental verification.

Some divergences between the experimental data on the temperature dependence can be explained (on the basis of von Hippel's hypothesis) by different values of the field emission current from the cathode. It is difficult to reproduce identical conditions in this respect. V.D.Kuchin obtained a maximum of E_{br} even with very short pulses (of the order of 10^{-6} sec); according to his data, the strength of samples decreases at high temperatures. Possibly this is due to insufficiently careful preparation of the samples.

The variation of the breakdown strength of ceramics with the dielectric constant was investigated in the work of Vul, Gol'dman & Razbash who found that no dependence exists for barium titanate. This, however, could be explained by the ferroelectric properties of barium titanate. We repeated the experiments of Vul et al using strontium-bismuth titanate (SBT), a material which has a comparatively strong temperature dependence of the dielectric constant but which is not ferroelectric; we obtained a minimum for the electric strength somewhat shifted relative to the maximum for ϵ. Our experimental results were checked repeatedly on a large number of different samples. That such a maximum exists we cannot doubt. The observed dependence, however, may be due not only to variation of the electric strength of the crystal phase with ϵ but also to macroheterogeneity of the polycrystalline samples. Definitive answers can only be obtained by investigating SBT single crystals.

OSCILLOGRAPHIC INVESTIGATION OF THERMAL BREAKDOWN OF ROCK SALT IN DC FIELDS

- G.A.Andreev

The distinction commonly made between electric and thermal breakdown of solid dielectrics is based on the difference between the effects accompanying these two forms of breakdown, including, for example, the temperature dependence of the electric strength. As has been shown by a number of investigators (Ref.1-4), the dc breakdown strength of alkali halide crystals first increases with increasing temperature (region of electric breakdown) and then, above a certain temperature, begins to decrease (region of thermal breakdown).

The processes occurring in crystals in strong electric fields are satisfactorily explained by the theories of electronic impact ionization, while the effects occurring in the breakdown of solid dielectrics at high temperatures are satisfactorily described by thermal theories[5,6], which have certain practical applications.

In 1956 Fröhlich & Paranjape[7] proposed a new theory explaining the temperature dependence of the electric strength in the region of high temperatures from the standpoint of impact ionization by electrons; until now this theory has not been verified experimentally.

We note that experimental verification of the thermal theories of breakdown, carried out by Walther & Inge, must be supplemented by data on the current flowing through the dielectric prior to breakdown. This was the purpose of the present investigation.

Equipment

We investigated the breakdown of rock salt in a uniform dc field of increasing voltage by means of a double oscillograph. The electric diagram of the set-up is shown in Fig.1.

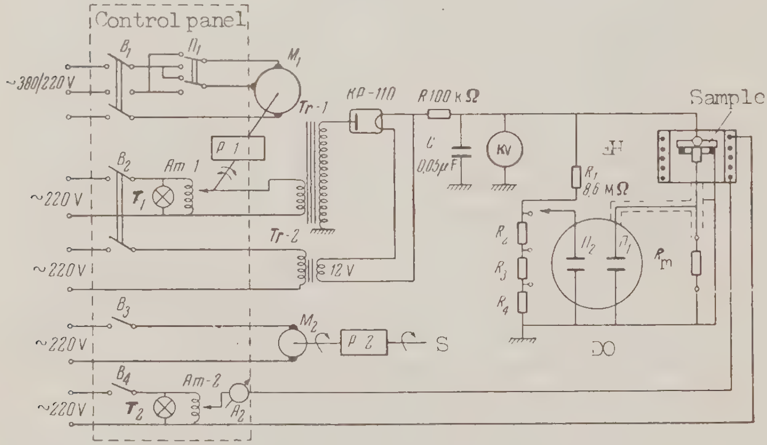

Fig.1. Diagram of set-up for recording the voltage-current-time characteristics of solid dielectrics at different temperatures: DO - oscillograph, S - shaft of camera, EH - electric heater.

The voltage proportional to the current flowing through the sample was applied to one pair of vertical deflection plates (Π_1) of the oscillograph through resistor R_m. At the same time a high voltage (up to 40 kv) was applied to the second pair of vertical deflection plates (Π_2) through the voltage divider, R_2, R_3 & R_4. A special device provided for uniform increase of the high voltage at a constant rate of 630 v/sec. The width of the oscillograph screen was 9 cm; the sensitivity of the oscillograph was 3.3 v/mm.

The vertical deflections of the beam were recorded by means of a conventional camera with an attachment providing for uniform horizontal feed of the film during the exposure. Particular pains were taken to ensure stability of R_m, the value of which was varied in the experiments from 10^5 to 10^9 ohm.

Fig.2 shows the size and shape of the samples used in experiments; the dark areas in the figure represent graphite electrodes. The investigated samples had a flat to bottom-of-recess thickness (d) of 50, 100 and 200 μ. Glass tube shields were cemented to the 100 and 200 μ thick samples to prevent edge breakdown.

The samples were heated during the tests by means of an electric heater, the temperature being measured by means of a mercury thermometer with a range up to 800°.

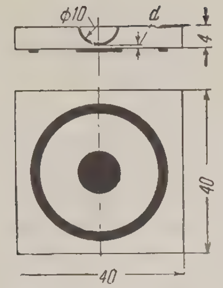

Fig.2. Shape and size of rock salt samples with applied electrodes.

A typical breakdown oscillograph obtained by means of the described set-up is shown in Fig.3: U_n characterizes the variation of the voltage and U_i the variation of the current flowing through the sample. The overall error in determining the voltage and current values from the oscillogram did not exceed ±5%.

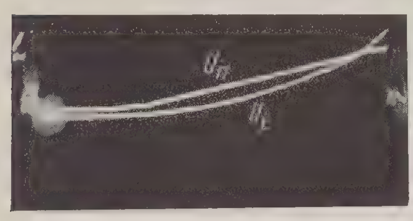

Fig.3. Typical thermal breakdown oscillogram: U_n - variation of voltage on sample; U_i - variation of current through sample.

Experimental results and discussion

The experimental work consisted of obtaining the voltage-time and current-time characteristics of rock salt at different temperatures. Some of the results following from analysis of the oscillograms are given below.

Fig.4 gives the temperature dependence of the electric strength E_{br} of rock salt for samples of different thickness. It will be seen from the curves that there is a maximum of E_{br} at about 40°; with further increase of temperature E_{br} falls off rapidly. Above 150° E_{br} increases with decreasing sample thickness, which can be explained by better heat conduction in thinner samples. This effect is in agreement with the thermal theory proposed by V.A.Fok.

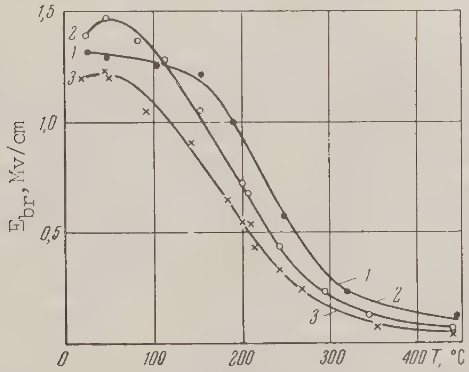

Fig.4. Temperature dependence of E_{br} of rock salt for samples of different thickness d (see Fig.2): 1) 50 μ, 2) 100 μ and 3) 200 μ.

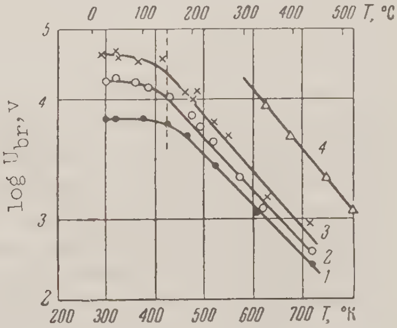

Fig.5. Variation of log U_{br} with the temperature for rock salt samples of different thickness: 1) 50 μ, 2) 100 μ, 3) 200 μ and 4) 4 mm (Ref.8).

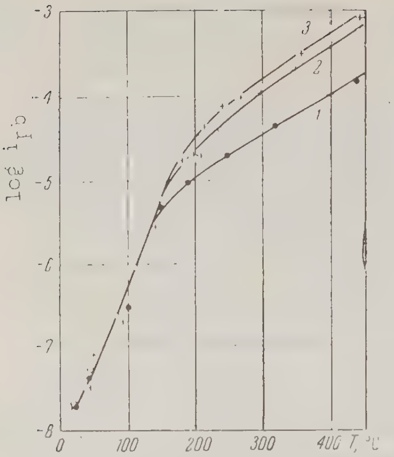

Fig.6. Temperature dependence of the prebreakdown current i_{pb} in rock salt samples of different thickness: 1) 50 μ, 2) 100 μ and 3) 200 μ.

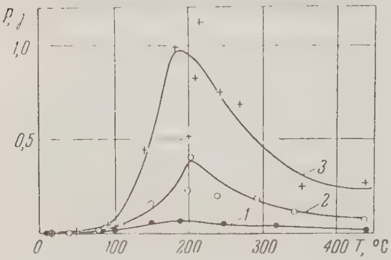

Fig.7. Temperature dependence of the total electric energy P dissipated prior to breakdown in rock salt samples of different thickness: 1) 50 μ, 2) 100 μ and 3) 200 μ.

The thermal nature of breakdown at temperatures above 150° is substantiated by the fact that the plot of the logarithm of the breakdown voltage vs the initial temperature of the ambient medium (air) is a straight line (Fig.5); it has the same slope as the plot obtained earlier by Walther & Inge[8].

Fig.6 shows the variation of the average value of the current passing through the rock salt samples prior to breakdown. It will be seen that in the case of our samples there is a strong increase of the prebreakdown current with increasing temperature characterized (in the semilogarithmic coordinates used) by two straight lines with different slopes. The change in slope occurs at about 150° and is explained by the effect of high voltage polarization which tends to reduce the current in the range of low temperatures.[9] It will be seen from Fig.6 that up to 150° the prebreakdown current is independent of the sample thickness, at least in the investigated range from 50 to 200 μ. Above 150° the prebreakdown current is appreciably greater in thicker samples. This can be explained from the standpoint of the thermal theory of V.A.Fok by nonuniform heating of the sample in thickness upon the application of a slowly increasing electric field. Inasmuch as the rate of heat transfer from the sample to the electrodes must depend on the thickness of the sample, the rate of heating of the sample in the central interelectrode region must be greater in the case of samples of greater thickness. Hence the resistance of thicker samples must be lower and the current accordingly greater than in thin samples.

From analysis of the oscillograms we obtained the variation with temperature of the total energy dissipated prior to breakdown in the rock salt samples (Fig.7). It will be seen that the curves characterizing the dependence have a maximum at about 200°, which is obviously connected with the transition from electric to thermal breakdown. An obvious explanation of the maximum is that the increase in energy is connected with rapid increase of the current flowing through the sample as the temperature is increased to 200°. In the region of thermal breakdown, i.e., above 200°, increased heating of the sample leads to a reduction of the electric energy required for fusing the material, i.e., for providing a breakdown path.

It will also be seen from Fig.7 that with increasing thickness the amount of electric energy dissipated prior to breakdown increases almost in proportion to the sample thickness.

Conclusions

Using the set-up and procedure developed by us, we obtained the voltage-time and current-time characteristics for samples of rock salt having thicknesses of 50, 100 and 200 μ in the temperature range from 20 to 440° in a uniform dc field. Analysis of the oscillograms obtained shows that there is a maximum of E_{br} at about 40°; with further increase of temperature E_{br} of rock salt decreases sharply; above 150° the requirement of V.A.Fok's thermal breakdown theory is fulfilled, i.e., the plot of log $U_{br} = f(T)$ is a straight line.

The observed decrease in resistance of the samples prior to breakdown and the decrease of the prebreakdown current with decreasing sample thickness above 150° indicate that above this temperature the breakdown of rock salt is thermal breakdown (rather than electric).

In conclusion I wish to express my gratitude to A.A.Vorob'ev for his help and guidance in carrying out the work.

"S.M.Kirov" Tomsk Polytechnic Institute

References

1. A.Hippel & R.C.Alger, Phys.Rev., 76, 127 (1949).
2. R.C.Buehl & A.Hippel, Phys.Rev., 56, 941 (1939).
3. J.H.Calderwood & D.R.Cooper, Proc.Phys.Soc.B, 66, 398, 74 (1953).
4. G.I.Skanavi, Izv. (Bulletin) Tomsk Polytechnic Inst., 91, 7 (1956).
5. K.W.Wagner, AJEE, 41, 1034 (1922).
6. V.A.Fok, Trudy (Proceedings), LFTL, 5, 52 (1928).
7. H.Fröhlich & B.V.Paranjape, Proc.Phys.Soc.B, 69, 433, 21 (1956).
8. A.F.Val'ter (Walther) & L.D.Inge, Zhur.tekh.fiz., 8, 295 (1938).
9. A.F.Val'ter (Walther) & B.M.Gokhberg (Hochberg), ZhRFKhO (Journal of the Russian Physical and Chemical Society), Physics section, 62, 399 (1930).

IMPULSE BREAKDOWN OF THICK LAYERS OF ICE

- A.V.Astafurov

Breakdown of solid dielectrics has commonly been investigated on samples having a thickness not exceeding 1-2 mm; in fact, most studies have been made on samples less than 1 mm thick. It is known that in inhomogeneous fields the electric strength increases with decreasing thickness of the dielectric and that the effect of polarity becomes vanishingly small.[1] The purpose of our work was to obtain the voltage-time characteristics of solid dielectrics with a large thickness, determine the thickness dependence of the breakdown voltage and clarify the effect of polarity.

By way of test material we chose river ice formed under natural conditions. Investigation of ice is of scientific interest inasmuch as knowledge of the electric characteristics of ice is essential in connection with investigation of the properties of dielectrics containing water.

The high voltage source was a pulse generator yielding pulses of up to 1440 kv. For measuring the high voltage, we used a fast oscillograph designed about a 13 LO-2S cathode ray tube. The measured pulses were applied to the oscillograph plates through a capacitive voltage divider.

The samples measuring 40 x 200 x 200 to 60 x 450 x 450 mm^3 were cut from ice floes in the direction normal to the free surface. For the uniform field tests the spherical recess in the samples was made by heating with a spherical electrode, while the conical recess for the nonuniform field tests was made by drilling. The recess surfaces were coated with a colloidal suspension of carbon black in toluene.

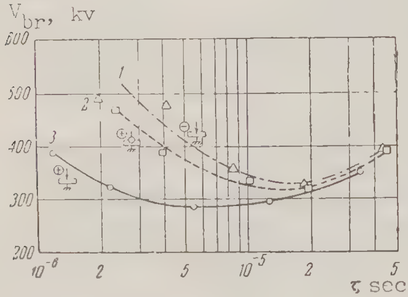

Fig.1. Voltage-time characteristics of ice. Sample thickness d = 15 mm for the tests in an inhomogeneous field with negative (1) and positive (3) polarity of the point electrode and d = 10 mm in tests with a uniform field (2).

The breakdown tests were performed with the sample immersed in transformer oil with the ice at -8 to -12°, the corresponding temperatures of the oil being -2 to +2°. The polished aluminum electrodes had the following diameters: plate - 120 mm, hemisphere - 100 mm; the point electrode was a 15 mm diameter cylindrical rod tapered at an angle of 30°.

The samples were subjected to single pulses having rise times of 2 to 40 microsec and amplitudes over 500 kv. The breakdown in each case occurred during the rise of the pulse. Each experimental point represents the breakdown of from 7 to 20 individual samples.

Fig.1 shows the voltage-time characteristics of ice in a nonuniform field for samples 15 mm thick and both polarities of the point electrode and for 10 mm thick samples in a uniform field (flat and hemispherical electrode).

Fig.2 shows the variation of the breakdown voltage with the sample thickness d for pulses with a rise time of 10 microsec. Fig.3 shows the same dependence for pulses with the steepest leading edge (rise time - 2 microsec). All the curves are plotted on the basis of statistical processing of the experimental dtat for a breakdown probability of 90%. Fig.4 shows the actual distribution of experimental points obtained in recording $V_{br} = f(d)$ for pulses having rise times of up to 10 microsec and an amplitude of 550 kv.

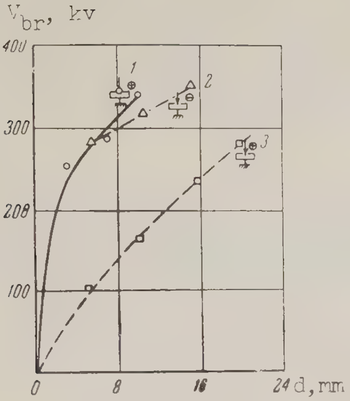

Fig.2. Variation of the breakdown voltage with the thickness of the ice sample for a pulse rise time of 10 microsec and a pulse amplitude of 550 kv in a uniform field (1) and in a nonuniform field with the point electrode negative (2) and positive (3).

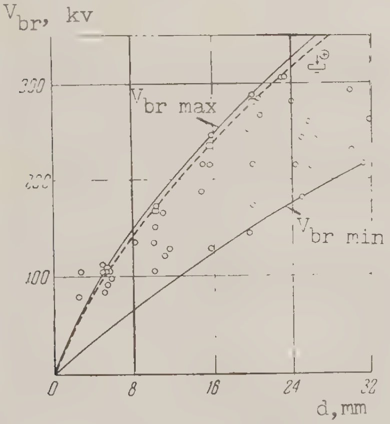

Fig.4. Experimental points for the variation of the breakdown voltage with the thickness of the ice samples with pulses having leading edge times to 10 microsec and an amplitude of 550 kv. Nonuniform field; point electrode positive (curve 3 in Fig.2).

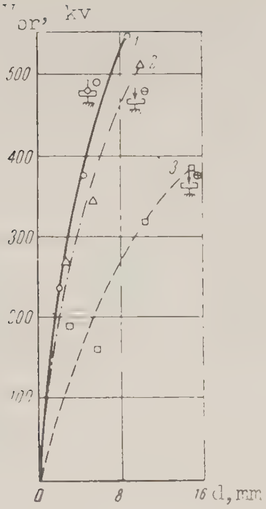

Fig.3. Variation of the breakdown voltage with the thickness of the ice sample with pulses having a rise time of 2 microsec and an amplitude of 550 kv, measured in a uniform field (1), in a nonuniform field with the point electrode negative (2) and positive (3).

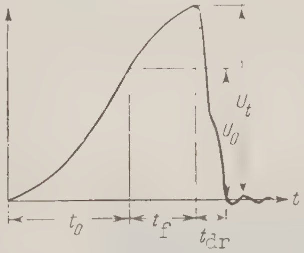

Fig.5. Diagram used in determining the pulse formation time.

The voltage-time characteristics for ice in uniform and nonuniform fields have the appearance commonly observed for other dielectrics^2. A sharp increase in the electric strength becomes apparent starting with exposure times of under 5 microsec.

From the recorded voltage-time characteristics for ice one can evaluate discharge formation time and the rate of development of the discharge. The method of determining the discharge formation time proposed by Vorob'ev^4 is clarified in Fig.5, where U_t is the breakdown voltage with a short exposure (rise time), U_o is the minimum measured breakdown voltage at which the discharge lag is not evident, t_o is the time corresponding to U_o, t_f is the discharge formation time and t_{br} is the voltage drop time during breakdown of the dielectric.

The statistical voltage delay time in x-irradiated rock salt is virtually nil.[4] Determinations of the electric strength with pulse rise times of $2 \cdot 10^{-8}$ sec for x-irradiated and non-irradiated rock salt yielded identical values of electric strength which allowed of neglecting the statistical discharge delay time in calculating the discharge formation time in solid dielectrics.[5] The rate of development of a discharge is given by the formula

$$R = \frac{d}{t_f},$$

where R is the rate of development of the discharge, d is the sample thickness and t_f is the discharge formation time. The results of evaluation of the discharge formation time and the rate of development of the discharge in ice are given in the accompanying table.

Calculated discharge formation time and rate of discharge development in ice

Type of field	d, cm	U_t kv	U_o, kv	t_o, 10^{-8} sec	t_f, 10^{-7} sec	R, 10^6 cm/sec
Positive sphere; grounded flat	1,0	455	324	4,35	6,9	1,45
Positive point; grounded flat	1,5	385	280	14,80	3,8	3,96
Negative point; grounded flat	1,5	540	336	15,15	9,2	1,63

In ice, as in air, the rate of discharge development with the point electrode positive is higher than in the case of negative polarity of the point electrode.[2] From this it may be inferred that the discharge in solid dielectrics of great thickness may be of the streamer type.

Under the influence of high voltage ice exhibits strong luminescence. Fig.6 is a photograph of a luminescing ice sample maintained at a temperature of -15° with a pulse voltage of 100 kv, the point electrode being positive and the flat electrode opposite it being grounded. The distance between electrodes was 70 mm; the sample was cylindrical, 120 mm in diameter and 380 mm in length; the iron point electrode was frozen into the sample in preparing it. All visible luminescence vanishes a few seconds after removal of the voltage. The intensity of luminescence at a given voltage increases with decreasing temperature.

Fig.6

Conclusions

1. The voltage-time characteristics of ice in layers 10 to 15 mm thick are similar to the voltage-time characteristics of solid dielectrics of small thickness.

2. The breakdown voltage of ice with increasing thickness in the range from 5 to 30 mm increases somewhat more slowly than in direct proportion to the thickness.

3. With large thicknesses of the dielectric the rate of discharge development is appreciably greater than in the case of small thicknesses.[4]

The writer wishes to express his heartfelt gratitude to A.A.Vorob'ev for suggesting the subject of the investigation, for guidance and constant interest in the work and to G.A.Vorob'ev for discussion of the results and valuable suggestions.

"S.M.Kirov" Tomsk Polytechnic Institute

References

1. A.A.Vorob'ev & N.Prikhod'ko, Trudy (Transactions), Physical-Technical Institute, 4, No.3 (1936).
2. A.F.Val'ter (Walther) & L.D.Inge, Zhur.tekh.fiz., 3, 6 (1933).
3. Tekhnika vysokikh napriazhenii (High voltage engineering), edited by L.I.Sirotinskii, Part 1, M., 1953.
4. G.A.Vorob'ev, Zhur.eksp.i teor.fiz., 30, 256 (1956).
5. G.A.Vorob'ev, Izv. (Bulletin), Tomsk Pedagogical Institute, 91 (1956).

ON THE DISCHARGE DELAY TIME IN IONIC CRYSTALS

- K.K.Sonchik

The physical processes involved in electric breakdown have different development times in different dielectrics and under different experimental conditions. The breakdown lag is characteristic of the material and from it one can evaluate the mean rate of propagation of the discharge.

When a solid dielectric is subjected to an increasing voltage, breakdown occurs not at the instant when the voltage reaches the static breakdown value V_{st} but somewhat later. In the case of slowly rising pulses (i.e., a gradually increasing voltage) this lag is much shorter than the rise time and is usually not taken into account. In the case of transient rise times of the order of 10^{-7}-10^{-8} sec or less for samples having the thickness common in breakdown tests (~0.1 mm) the discharge delay time becomes comparable with the time of application of the voltage and the breakdown of the dielectric occurs at a voltage appreciably higher than the static breakdown value. We define the static breakdown voltage as the breakdown voltage when the effective time of application of the voltage is $6 \cdot 10^{-6}$ to $3 \cdot 10^{-7}$ sec, i.e., the breakdown voltage in the range of transient rise times for which there is no noticeable lag of the discharge and the influence of space charge is absent.

The discharge delay times calculated by Whitehead, Simpson and others[1] for solid dielectrics differ appreciably. Experimental data on discharge delay times are scanty and often contradictory.

The shortcomings of breakdown experiments have been analysed by Vorob'ev[2], who determined the discharge lag in solid dielectrics as a function of the rise time of the applied voltage pulses. The discharge delay time obtained with a varying (increasing) voltage can only serve indirectly to characterize the breakdown process. If we assume that upon attainment of the static breakdown voltage there begins to form an electron avalanche, it is obvious that with further increase in the voltage, conditions for its development become increasingly favorable and the time necessary for breakdown is shortened. From this viewpoint it would be of greater interest to determine the delay time when a nearly square pulse with a very steep leading edge and flat top is applied to the dielectric. The duration of the leading edge should be as short as possible so that breakdown will not occur during the rise and the height of the pulse must equal but not exceed the static breakdown voltage. Under these conditions breakdown will occur at a constant voltage (flat part of the square pulse) and the time from the instant of attainment of the static breakdown voltage V_{st} to breakdown can be taken as approsimately equal to the discharge delay time t_{lag} (Fig.1). In the oscillogram breakdown is evinced by the sharp voltage drop.

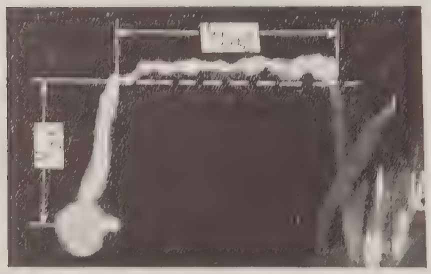
Fig.1. Determination of the discharge delay time t_{lag} from an oscillogram

Measurements of the discharge delay time by means of square pulses have been made by a number of investigators in gases[3] and liquids[4,5]. More recently, Inuishi & Suita[6] carried out similar studies on solid dielectrics. They investigated the breakdown lag in KCl and sulfur using square pulses with a rise time of $5 \cdot 10^{-8}$ sec. The shortcomings of their procedure were use of aquadag electrodes which have an appreciable resistance and recording the time by means of a Zeit-transformer instead of an oscillograph.

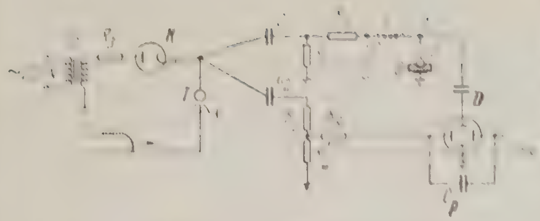

Fig.2. Diagram of set-up for determining discharge delay times in solid dielectrics.

Kavamura et al[7] applied a series of square pulses to their dielectric sample until breakdown occurred; they determined the statistical delay time as NT, where N is the number of pulses to breakdown and T is the pulse duration. The shortcoming of this technique is that the electric strength of the dielectric is reduced by some extent by each successive pulse.

Taking the above-mentioned shortcomings into account, we developed a procedure and set-up for determining the discharge delay time in solid dielectrics under the influence of a single rectangular voltage pulse, using a high-speed, high-voltage oscillograph and samples with metallic electrodes having a low resistance.

In recording processes having a duration of the order of 10^{-8} sec and less, synchronization of the time sweep and the investigated effect by means of a spark relay[8] (in view of the large scatter of tripping times) could not be regarded as satisfactory.

Accordingly, we employed a rigid synchronization circuit without switching units based on a suggestion of G.A.Vorob'ev. The circuit is shown in Fig.2. The capacitors C_1 (through R_1) and C_2 (through $R_2 + R_{2'}$) were charged from the high-voltage transformer T_p through the charging resistor R_3 and the Kenotron K to the desired voltage (regulated from the low voltage side). The gap between the electrodes of the trigatron T was set so it would not discharge at the set voltage. The test pulse triggered the trigatron and the capacitor C_1 discharged through R_1 and C_2 through $R_2 + R_{2'}$ producing steep pulses. The voltage pulse on $R_{2'}$ served as the time base; to realize recording of the pulse leading edge the capacitor C_p was connected in parallel with the time plates of the oscillograph. The sweep rate could therefore be varied by adjusting C_p. The resistor R_g in the time plate circuit served to damp out parasitic oscillations. For more efficient utilization of the tube screen the electron beam prior to oscillographing was deflected to the edge of the screen by applying a 1 kv negative bias to one of the deflecting plates.

The voltage pulse from the resistor R_1 was applied through the limiting resistor R_0 to the sample 0 and the capacitive voltage divider D, part of which was comprised by the "effect" plates of the oscillograph. The steepness of the leading edge of this pulse depended on the value of R_0 and on the stray capacitance C and inductance L of the associated circuit. In assembling the circuit these were reduced to a minimum by using short direct leads for all connections; the leading edge pulse time proved to be $3\text{-}4 \cdot 10^{-8}$ sec.

The error in time measurement connected with propagation of the electromagnetic wave from point 1 to point 2 and back was of the order of 10^{-10} sec and was accordingly neglected.

By virtue of the rigid synchronization, time straggling between the beginning of the time sweep and the investigated effect was eliminated. The pulse always appeared at the same point on the oscillograph screen. The time scale was calibrated by means of a high-frequency oscillator.

We determined the discharge delay time in natural rock salt single crystals from the Artemov (Ukrainian SSR) region. The samples measuring 20 x 20 x x 3 mm were cleaved from suitable single crystals and polished. A hemispheric recess 8-10 mm in diameter was made in one side of the samples. The flat and hemispherical electrodes were applied by vacuum sputtering of tin and assured an adequately uniform field in the test area. The thickness of the samples (bottom of recess to opposite flat) was 0.12 mm. During the tests the samples were immersed in dehydrated transformer oil. Tests at a given pulse height were carried out on 20 to 30 samples and the delay times for the punctured samples determined. After which the pulse amplitude was increased somewhat, the breakdown tests repeated, etc. If one plots the number of nonpunctured samples in percent along the y axis to a logarithmic scale and the delay time t_{lag} along the X axis, the resultant dependences are characterized by straight lines described by

$$\varphi = \frac{n_t}{n_o} = e^{-t_{lag}/\tau},$$

where n_t is the number of nonpunctured samples by the instant t_{lag}, n_o is the number of samples tested and τ is the averaged delay time.

We determined the delay time for $\varphi = 37.5\%$, i.e., when $t_{lag} = \tau$.

As a result of the measurements, it was established that with increasing overvoltage on the sample the discharge delay time is reduced. For rock salt samples having a thickness of 0.12 mm ($V_{st} = 16.1$ kv) and a rectangular pulse amplitude of 19.2 kv, the discharge delay time $t_{lag} = 4.6 \cdot 10^{-8}$ sec, while with a pulse amplitude of 20.4 kv, $t_{lag} = 2.6 \cdot 10^{-8}$ sec. The mean rates of discharge propagation are $2.6 \cdot 10^5$ cm/sec and $4.62 \cdot 10^5$ cm/sec, respectively. The question of division of the discharge delay time into a static delay time and a discharge formation time in the region of exposure times of the order of 10^{-8} sec has not been definitively resolved.

In the work of Inuishi & Suita[6] this resolution is carried out graphically and purely formally. The experiments of Vorob'ev[2] with x-irradiated samples showed that with exposure times of 10^{-8} sec and a sample thickness of 0.15 mm the statistical delay time is virtually zero.

Preliminary experiments also showed no appreciable reduction of the discharge delay time in x-rayed and illuminated (during the experiment) samples as compared with non-irradiated samples, which also indicates that the statistical delay time in rock salt is either zero or very short.

I take this occasion to thank A.A.Vorob'ev for his constant attention and interest in the work and G.A.Vorob'ev for a number of valuable suggestions.

Tomsk Polytechnic Institute

References

1. S.Whitehead, Dielectric Breakdown of Solids, Oxford, 1951.
2. G.A.Vorob'ev, Thesis, Tomsk, 1956.
3. C.G.Morgan & D.Harcombe, Proc. Phys. Soc., 66, 404 B, 665 (1953).
4. S.D.Edwards, Canad.J.Phys., 29, 310 (1951).
5. D.W.Goodwin & K.A.Macfadyen, Proc.Phys.Soc., 66, 398 B, 85 (1953).
6. Y.Inuishi & T.Suita, J.IEE Japan, 74, 2, 150 (1954).
7. H.Kawamura, H.Ohkura & T.Kikuchi, J.Phys.Soc.Japan, 9, 4, 541 (1954).
8. I.S.Stekol'nikov, Impul'snaia ostsillografiia i ee primenenie (Pulse oscillography and its applications), M., 1949.

ELECTRIC BREAKDOWN OF A TITANIUM CERAMIC HAVING A DIELECTRIC CONSTANT OF 80

- I.E.Balygin

Some interesting regularities have been brought out in recent years in investigations of the electric strength of barium titanate and the titanates of metals in Group II of the periodic table.[1-3] It was not clear, however, whether these regularities are characteristic for other titanium containing ceramics. With a view to clarifying this we carried out experiments on Tikond T-80. This titanium ceramic material has the following composition: ~89% TiO_2, ~3% SiO_2, ~2% Al_2O_3, 3.9% ZrO_2 plus minor amounts of other oxides.

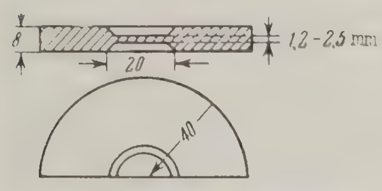

Fig.1. Shape of samples used in the experiments.

The shape of the samples used in our experiments is shown in Fig.1. The electrodes were applied by three-fold firing on of silver at 800°. All the samples were checked for adequate sintering by measuring the value of tan δ before and after boiling in distilled water.

The tests were carried out with pulse voltages using the circuits pictured in Figs.2 a,b & c. The respective resistance values were $R_0 + r = 1.9 \cdot 10^4$ ohm, $r_0 = 167$ ohm and $R = 3.2 \cdot 10^5$ or $5 \cdot 10^5$ ohm. In order to minimize the inductance of the set-up connections were made as short and direct as feasible. From 7 to 15 samples were measured under each set of conditions. Reproducibility of the oscillograms within the limits of the statistical deviations was satisfactory.

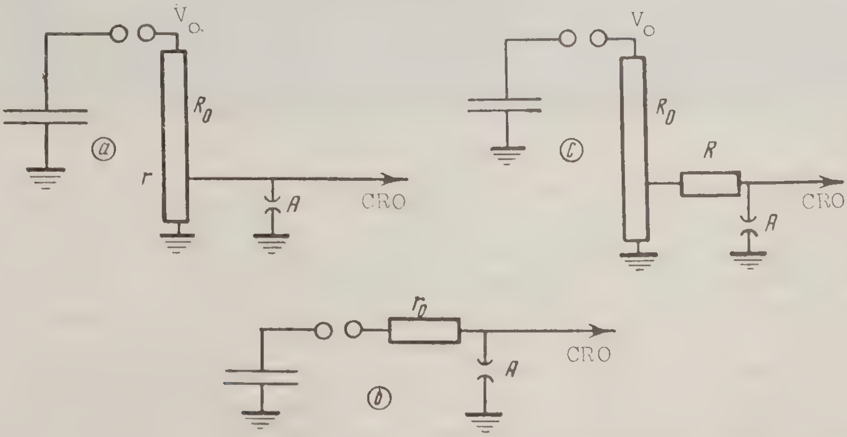

Fig.2. Diagrams of experimental set-ups. CRO - cathode ray oscillograph.

A series of oscillograms obtained at 20°C using circuits a and b is shown in Fig.3. The thickness of the samples was 1.2 to 2.5 mm. The period of the time scale sinusoidal oscillations recorded along the horizontal axis of the oscillograms is $4.5 \cdot 10^{-7}$ sec. In recording the oscillograms I, II and III, the amplitude of the pulses was gradually increased to the point of breakdown. Some oscillograms show the repeated breakdowns of previously disrupted samples. After the first breakdown, without altering anything in the test circuit, we applied a voltage of the same amplitude as the first time. This repeat breakdown oscillogram was recorded on the same photographic plate. Oscillograms IV and V were recorded with a faster rise of the voltage pulses (1.7--2.2 microsec) to the breakdown value. Oscillogram VI is a calibration oscillogram; it was recorded for the breakdown of a 10 mm air gap between 6.25 cm diameter spherical electrodes.

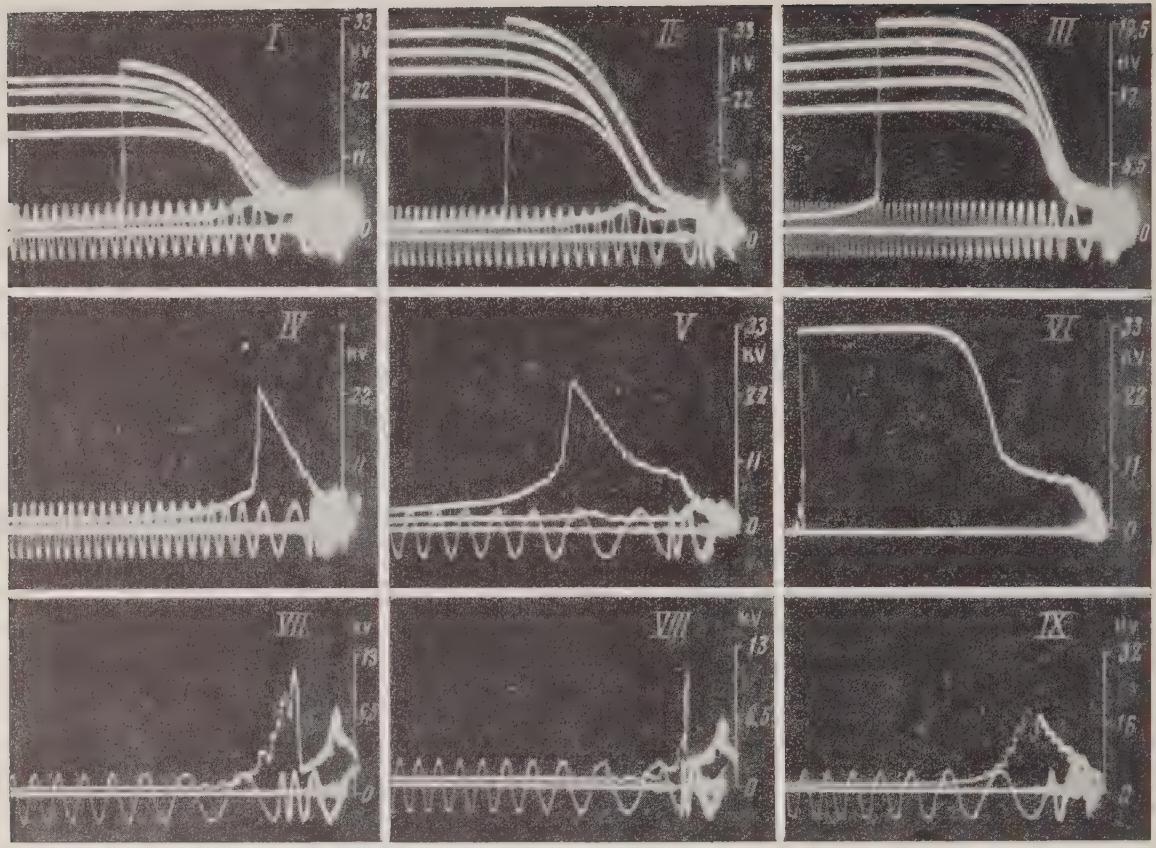

Fig.3. Oscillograms of breakdown of Tikond T-80 at 20°.

Oscillograms VII, VIII & IX were recorded using circuit b (r_0 = 167 ohm) with even steeper pulses (shorter rise times). It will be seen that in this case there was recorded a somewhat unusual effect of pre-breakdown voltage drop. Some of the numerical data pertaining to oscillograms I through V of Fig.3 are given in the upper half of Table 1; the data for oscillograms VII through IX are summarized in Table 2. The mean breakdown field strength E_{br} according to oscillograms I-V proved to be 11 kv/mm. For the second and third breakdowns of the same samples E_{br} decreased to 1.4 kv/mm and 0.6 kv/mm, respectively.

At a constant (dc) voltage, the value of E_{br} for the initial breakdown was the same. It is obvious from the cited data that the insulating properties of T-80 ceramic are not re-established after the first breakdown. There apparently occur irreversible changes in the discharge channel involving the formation of a conducting bridge, probably of reduced titanium. It will be seen from the oscillograms that the so-called static breakdown delay time in the absence of an overvoltage is relatively great. It may be assumed, therefore, that there are certain factors tending to counteract breakdown in the T-80 ceramic. This inference is substantiated by the data obtained for certain liquid dielectrics by Balygin[4]. In oscillograms I and II (Fig.3) there are clearly discernible two thickenings of the voltage drop trace, indicative of points where development of the breakdown is slowed down or temporarily halted. This slowing down, just as in the case of breakdown of airgaps (oscillogram VI), is apparently caused by space charges forming after passage of the electronic avalanche.[5]

Table 1

Data pertaining to the oscillograms of Figs.3 & 4

Oscillog No.	Thickness of sample, mm	Breakdown voltage, kv/mm		Time, microsec		Fig. No.
		First breakdown	Second breakdown	from zero to begin. of formation of breakdown	formation of breakdown	
I	2,26	11,7	1,5	5,8	0,01—0,02	3
II	2,54	14,0	1.3	6,2	0,01—0,02	3
III	2,0	10,0	—	10,3	0,01—0,02	3
IV	2,44	9,5	—	2,2	0,15	3
V	2,5	9,5	1.7	1,7	0,5—0,55	3
IV	1,35	7,5	—	3,0	0,3	4
V	2,2 & 2,14	6,5 & 6	—	1,8 & 1,6	0,56 & 0,6	4
VI	2,16	6,3	—	1,8	0.6	4
VII	1,44 & 1,4	6,7 & 5,5	—	3,5 & 2,7	0,3 & 0,33	4
VIII	2,35 & 2,2	8 & 7,5	—	1,6 & 1,6	0,5 & 0,5	4
IX	2,5	8,3		0,6	0,5	4

Table 2

Data pertaining to the oscillograms of Fig.3

Oscillogr. No.	Sample thickness, mm	Beginning of voltage drop E_1, kv/mm	Minimum voltage at end of drop kv/mm	Breakdown voltage kv/mm	Time from zero to begin. of drop, µsec	Time of voltage drop, microsec	Breakdown formation time, microsec
VII	1,25	6,2	1,6	9,4	0,3	0,5	0,7
VIII	1,3	5	1,5	8,3	0,3	0,5	0,6
IX	2,15	8,2	5,2	9·	0,8	0,04	0,28

According to oscillograms I, II & III of Fig.3, the time of formation of breakdown is a few hundredths of a microsecond when the pulse rise time from zero voltage to the breakdown value is 5.8 to 10.3 microsec. In the case of a steeper pulse (rise times - 1.7 and 2.2 microsec), the formation time increases to 0.15-0.55 microsec. With even shorter rise times, there occurs the distinctive prebreakdown voltage drop mentioned above. It is obvious, therefore, that pre-breakdown processes have a strong influence on the dynamics of the discharge.

In order to follow the variations in the discharge with a relatively slow increase of the pulse (long rise time), we recorded the breakdown process by means of circuit c (Fig.1). Oscillogram I in Fig.4 was recorded with R = $3.2 \cdot 10^5$ ohm; oscillograms II and III with R = $5 \cdot 10^5$ ohm. The discharge current in these tests was strongly limited. The discharge voltages according to oscillograms I, II and III were 10.7, 12 and 10 kv/mm, respectively. The period of the time scale sinusoidal wave in oscillograms I, II and III is 50 microsec; in the others - 0.45 microsec. It will be seen from oscillograms I, II & III that with slowing down of the pulse rise nothing substantial occurs as regards the magnitude of E_{br} and the formation time, but sometimes there is evinced partial breakdown of the ceramic. These partial breakdowns are particularly clearly evident in oscillogram III. The greatest voltage drop in this case is 8 kv/mm. It is clear that the discharge in this case was interrupted at the streamer stage of its development. It must be noted, however, that such partial breakdowns were rarely observed.

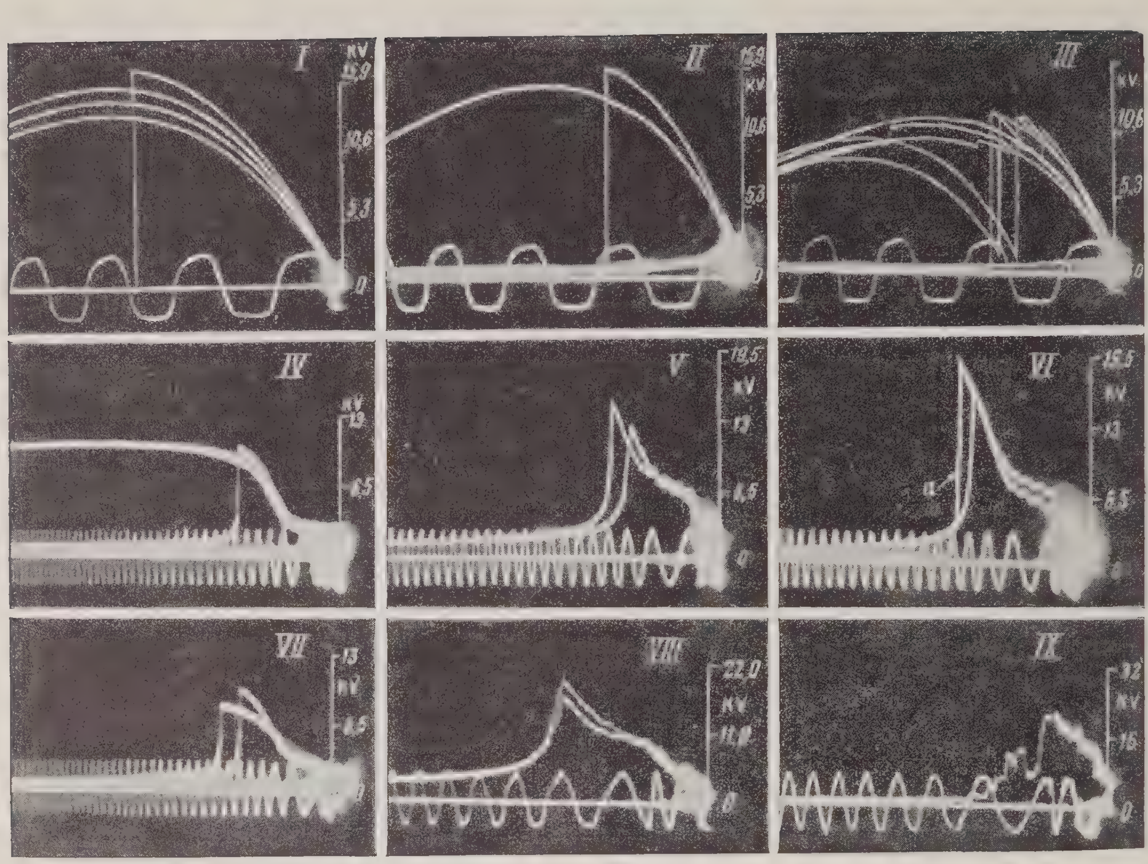

Fig.4. Oscillograms characterizing the breakdown of Tikond T-80 at different temperatures: I-III - at 20°, IV-VI - at 300° and VII-IX - at 400°.

Oscillograms IV, V & Vi of Fig.4 show the breakdown record for the ceramic samples at t = 300°. One of the oscillograms, VI (a) was recorded in the case of flashover (edge discharge). Such flashovers can be distinguished from true breakdown by the relatively small amplitude after the voltage drop. Both oscillograms in photograph VI were recorded under identical conditions, but it will be seen that the duration of formation of the processes recorded differed appreciably.

Oscillograms VII, VIII & IX of Fig.4 were recorded at t = 400°. Some of the numerical data pertaining to oscillograms IV through IX of Fig.4 are given in the lower half of Table 1. It will be seen from the oscillograms and the table that the time of formation of the breakdown at the indicated temperatures is little dependent on the pulse rise time. In the case of a rise time of 0.6 microsec from zero to 8.3 kv/mm, as may be seen from oscillogram IX, the pre-breakdown voltage drop again becomes evident.

Upon increase of the temperature to 300° (from 20°) the value of E_{br} was appreciably reduced, but no further decrease in E_{br} is observed in the temperature range from 300 to 400°. For purposes of comparison it may be noted that at constant dc voltage and 300°, E_{br} = 8.3 kv/mm and that at 400° Tikond T-80 becomes a semiconductor. Inasmuch as every semiconductor becomes a dielectric at temperatures close to absolute zero[6] and most dielectrics become semiconductors at higher temperatures (specifically, T-80 becomes a semiconductor at 400°), certain considerations applicable to semiconductors can be extended and applied to our ceramic.

It is generally known, for example, that in solid and liquid dielectrics E_{br} depends on the material of the electrodes.[7-10] Consequently, the magnitude of E_{br} must to some extent be determined by field emission or thermionic emission of the electrodes. Given the dielectric constant of Tikond ($\epsilon = 80$), conditions for such emission will be favorable particularly from the fine silver filaments formed as a result of diffusion of the silver during the firing on process.

Agglomeration of the finely powdered particles of T-80 paste occurs at 1350°, i.e., at a temperature below that of fusion of the principal oxides. Hence it must be assumed that the atoms of the dielectric do not occupy minimum potential energy positions and that the system is not in equilibrium. In view of this, there may occur processes involving spontaneous recrystallization and changes in the electric properties of the ceramic.[11] The dislocations that are formed in the initial process of grinding undoubtedly persist in the sintered particles. Furthermore, additional dislocations may form[12] as a result of shrinkage and the possible outward flow of vacancies.[13] All this can give rise to considerable distortions in the regular structure of the crystal phase and the appearance of numerous energy levels that may act as electron trapping centers.

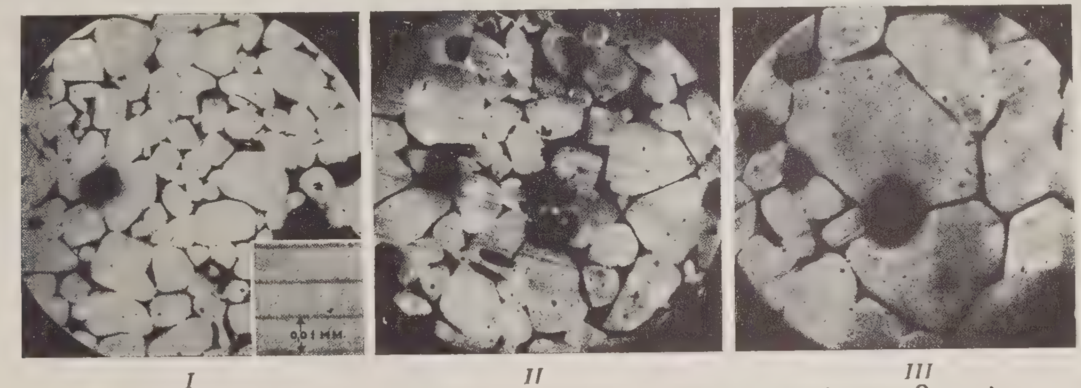

Fig.5. Microphotographs of Tikond T-80 sintered at I) 1350°, II) 1400° and III) 1460°. Note scale in I.

During sintering there form in T-80 individual crystalline cells whose size depends on the firing temperature. Microphotographs of T-80 ceramic fired at different temperatures are shown in Fig.5. Amorphous layers between the crystalline cells also exhibit structural irregularities. It is not impossible that the surfaces of these crystalline cells also serve as electron trapping centers.[14]

When the voltage pulse rises slowly and the electrons emitted from the cathode fill the trapping centers in the region surrounding this electrode, relatively little time is required for formation of the breakdown. With a rapid rise of the pulse, however, when the number of such electrons is small the formation of the discharge occurs under relatively unfavorable conditions and part of the electrons of the forming avalanche settle into the trapping centers and are lost to the process. With an even more rapid rise of the voltage pulse the trapping of the electrons becomes so great that the developing breakdown is suppressed and we obtain the prebreakdown voltage drop mentioned above.

With increasing temperature the disturbances in the regular structure of the crystal lattice increase as does the electronic conductivity[15] of T-80 and, consequently, the influence of emission from the cathode is less pronounced and the dependence of the discharge formation time on the steepness of the pulse front becomes weaker. There is some reason to assume that the partial discharges recorded in oscillograms II & III of Fig.4 occurred due to breakdown of the amorphous interlayers between the crystalline cells at appropriate increases of the potential due to settling of electrons on the surface of these cells.

References

1. B.M.Vul, in Sb. posviashchennom semidesiatiletiiu akademika A.F.Ioffe (Symposium dedicated to the Seventieth Anniversary of Academician A.F.Ioffe) p. 182, M.-L., 1950.
2. G.I.Skanavi & V.I.Sarafanov, Zhur.eksp.i teor.fiz., 27, 595 (1954).
3. V.I.Sarafanov, Zhur.eksp.i teor.fiz., 27, 590 (1954).
4. I.E.Balygin, Zhur.eksp.i teor.fiz., 30, 464 (1956).
5. I.E.Balygin, Zhur.tekh.fiz., 27, 580 (1954).
6. A.F.Ioffe, Poluprovodniki v sovremennoi fizike (Semiconductors in modern physics), M.-L., 1954.
7. A.Hippel & R.Alger, Phys.Rev., 76, 127 (1949).
8. J.K.Bragg, A.H.Sharbough & R.W.Growe, J.Appl.Phys., 25, 382 (1954).
9. Zener, Proc.Roy.Soc.A. 145, 523 (1934).
10. W.Franz, ZS. Phys., 113, 607 (1939).
11. N.P.Bogoroditskii & T.N.Verbitskaia, Doklady AN SSSR, 89, 447 (1953).
12. V.A.Ivensen, in Voprosy poroshkovoi metallurgii (Problems in powder metallurgy), p.130, Kiev, 1955.
13. B.A.Pines, in ibid., p. 74.
14. I.M.Livshits & S.I.Pekar, Usp.fiz.nauk., 6, 531 (1955).
15. S.I.Gorelik, Zhur.eksp.i teor.fiz., 7, 826 (1951).

SOME REGULARITIES OF ELECTRIC BREAKDOWN OF LIQUID DIELECTRICS

- I.E.Balygin

Investigations of certain liquid dielectrics carried out in recent years have brought to light a number of interesting regularities.[1-4] The mechanicsm of breakdown, however, has not been fully investigated and many of the effects connected with breakdown are still obscure. Below we give some new data obtained by us in investigating discharges in some liquid dielectrics.

Rather heavy currents flow through the conducting channel formed in breakdown; these currents disrupt and "burn" the dielectric and therefore mask details of what occurs immediately after puncture of the interelectrode gap. One can, however, counteract the obscuring effect of these currents by limiting them through the use of a series-connected resistance. Our experiments showed that under such limiting conditions variations in voltage after completion of breakdown in many liquid dielectrics are characterized by consistent regularities.

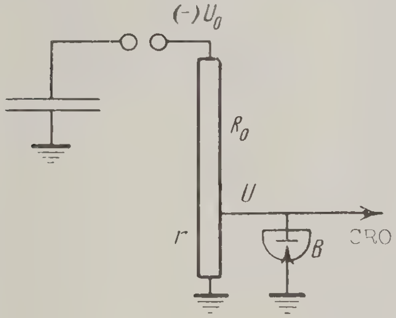

Fig.1. Diagram of experimental set-up. CRO - cathode ray oscillograph.

The experiments were carried out in a porcelain vessel with one steel point electrode and a steel disc electrode 40 mm in diameter with rounded edges. Whenever the test liquid was changed, both the vessel and the electrodes were carefully washed and dried. A diagram of the set-up is shown in Fig.1. The constant (dc) voltage ($U_0 = -90$ kv) was applied to the resistance $R = R_0 + r = 8 \cdot 10^4$ ohm. The voltage to the disc electrode in the test vessel B was taken off part of this resistance so that the resistance R_0 served as the voltage limiting resistance. The distance between electrodes was kept constant at 1 mm. Nothing except the voltage U was varied in the set-up. The maximum current through the discharge channel did not exceed 1.3 amp.

In Fig.2 we reproduce a series of oscillograms characterizing the breakdown of different liquid dielectrics including transformer (capacitor) oil,

Table 1

Data pertaining to the oscillograms of Fig. 2

Oscillogram No.	Dielectric	Initial breakdown voltage, kv	Time to first voltage peak μsec	Peak height, kv	Time to cessation of discharge μsec	Voltage at cessation of discharge kv
I	Transformer oil	12	370	4.5	—	—
II	Vaseline	12	375	4.7	—	—
III	Benzene	16	525	4.5	1430	0.9
IV	1) Transformer oil	12	350	5.4	1500	—
	2) Same	12	—	—	350	5.4
V	Vaseline	12	375	—	—	5.9
VI	Carbon tetrachloride	10	—	—	1050	1.5
VII	Toluene	10.3	—	—	396	4.5
VIII	Silicone oil	11.3	330	6.0	1500	—
IX	Xylene	14.0	—	—	390	6.0

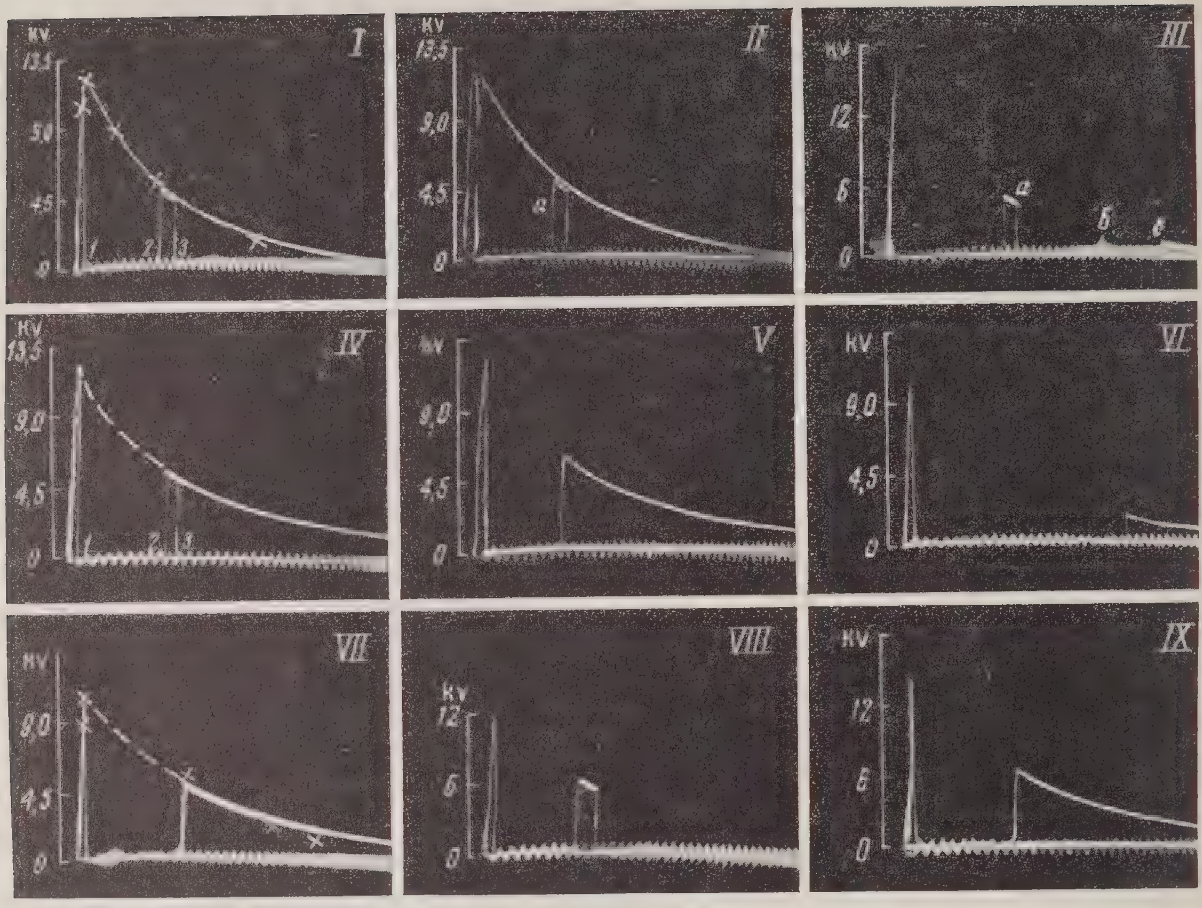

Fig.2. Oscillograms of breakdown of different insulating liquids.

natural (capacitor) vaseline (at 40°) and nonchlorinated silicone oil. The highly purified (with 30% sulfuric acid) transformer oil was filtered and vacuum dried at 100°. The highly purified vaseline and silicone oil were vacuum dried under the same conditions. The other liquids were distilled and filtered twice. The lighter fractions of the xylene were driven off at 120-129°. The period of the time-scale sinusoidal trace in the oscillograms of Figs.2 & 3 is 44 microsec. Some of the data taken from the oscillograms of Fig.2 are summarized in Table 1. The time was reckoned from the instant of completion of the initial breakdown.

It will be evident from Table 1 that the quantities characterizing the variations in voltage after breakdown differ for the different investigated liquids. Noteworthy features in some of the oscillograms are the sharp terminations of the discharges and the voltage peaks which indicate very sudden - almost jump-like - and very intense de-ionization of the discharge channel. As a result of this de-ionization the dielectric strength of the disrupted liquid is re-established and the voltage on the electrodes increases accordingly. In some cases, after such re-establishment, a repeated puncture of the interelectrode gap occurs. Such repeated breakdowns were observed in transformer oil, vaseline, benzene and silicone liquid (oscillograms, I, II, III, IV and VIII in Fig.2).

Oscillogram IV in Fig.2 is the record of two breakdowns of transformer oil. In one case there occurred a repeat breakdown, while in the other, after the jump-like de-ionization, the discharge terminated completely. This behavior is characteristic of transformer oil and vaseline (oscillograms II and V). The probabilities of repeat puncture and of complete cessation of discharge after the jump-like de-ionization appear to be approximately equal. This ratio of probabilities remained the same when the temperature was increased to 80°. In the case of benzene (III), in addition to the first peak $\bar{a}$, among the series of low-intensity discharges one can distinguish another peak $\bar{b}$ with an amplitude appreciably inferior to $\bar{a}$. The discharge terminated at point $\bar{c}$ after 1430 microsec, the voltage at this point being 0.9 kv (Table 1). The discharge duration in carbon tetrachloride (oscillogram VI) was 1050 microsec; during this period no secondary peaks were observed.

The differences between the discharge patterns obtained for the investigated liquid dielectrics lie in the time of appearance of the jump-like de-ionization and of the corresponding secondary peaks in cases where formation of repeat breakdown occurred. In addition, there are differences in the amplitudes and widths of the peaks and in the time to termination of the discharges as well as in the values of the voltage as the end of the discharge is approached. These differences are undoubtedly connected with the chemical composition of the insulating liquids and their physical structure.

It was noted in the experiments that at the instant of breakdown in some of the liquids there occurs ejection of the liquid from the interelectrode gap. The intensity of this ejection depends on the magnitude of the discharge current.[5]

It is obvious that the time - $1\text{-}2 \cdot 10^{-7}$ sec - during which formation of the breakdown occurs[6] is insufficient for such ejection and that the ejection actually occurs somewhat later. It is reasonable to assume that this ejection in some cases is connected with the jump-like de-ionization when nonionized molecules from the surrounding medium penetrate into the region of the discharge channel. In the case of such liquids as carbon tetrachloride, however, the cause of the jump-like de-ionization is apparently different. There is reason to assume that in such cases the de-ionization is caused by reduction of the spark temperature to some critical value at which there occurs rapid recombination of charged particles and association of molecules that initially decompose under the influence of the high temperature of the spark during the earlier stages of the discharge.

The breakdown process with limiting of the discharge current may, on the basis of the oscillograms reproduced in Fig.2, be roughly divided into several stages. In the first stage, there occurs shorting of the interelectrode gap by a streamer (breakdown); the second stage may be characterized by variation of the radius and temperature of the discharge channel and by processes preparatory to the jump-like de-ionization (1-2 in oscillograms I and IV); in the third stage, if the discharge has not terminated, there occurs formation of a secondary discharge (2-3 in oscillograms I and IV) after de-ionization of the discharge channel. The fourth stage after the second breakdown is essentially a repetition of stage two.

It may be assumed that the very noticeable lag in the ejection of the liquid is connected with the fact that during the very short time interval of the discharge the plastic properties of the insulating liquids could not be manifested,[7] while the available energy was insufficient for rupture of the molecular bonds. If this hypothesis is correct the duration of the second stage should depend both on the strength of the molecular bonds and on the way the plastic properties of the liquid are manifested in time. Hence one may assume that the character of the de-ionization should depend on the viscosity of the liquid.

In order to check this hypothesis, we carried out the following experiments. We investigated breakdown in 1 to 6% solutions of ethyl cellulose in toluene. The oscillograms are shown in Fig.3; data from the oscillograms and on the viscosity of the solutions are given in Table 2. The breakdown voltage of the solutions was the same within the limits of the statistical scatter. From oscillogram I and Table 2 it will be seen that at a viscosity of $1.8 \cdot 10^4$ degrees Engler there was no ejection or jump-like de-ionization at the instant of discharge, if we do not count the small voltage peak k with amplitude 0.7 kv which appeared 374 microsec after completion of the breakdown. Upon reduction of the viscosity to $2.2 \cdot 10^3$ degrees Engler (other conditions being the same) jump-like de-ionization appeared at the expiration of the same interval, namely, 374 microsec. The discharge was completely interrupted. Further decrease of the viscosity to 37 degrees Engler did not bring any further noticeable change in the discharge pattern or its parameters as may be seen from oscillograms III and IV.

With increase of the discharge current the amount of heat evolved in the discharge channel within an equal time interval was greater and hence the pressure in the channel could increase. Therefore ejection of liquid could be expected within a shorter interval after completion of the initial discharge. Inasmuch as formation of the breakdown with the point electrode positive usually occurs with some lag, one can in practice apply a voltage considerably exceeding the minimal breakdown value for the given gap.

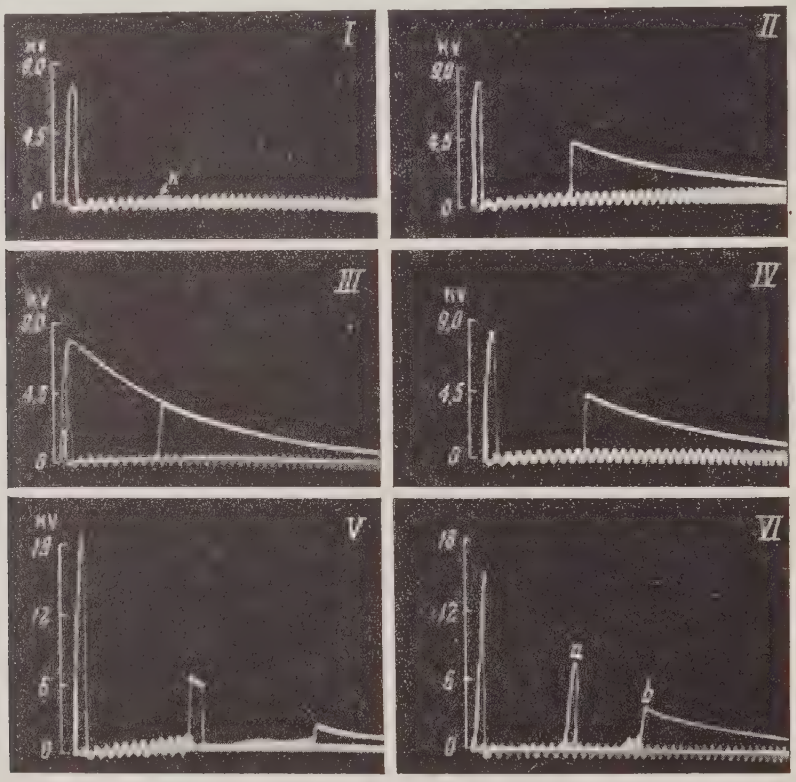

Fig.3. Oscillograms characterizing the breakdown of solutions of ethyl cellulose in toluene (I-IV) and the breakdown of benzene (V) and xylene (VI).

Table 2

Data pertaining to the oscillograms of Fig. 3

Oscillogram No.	Dielectric	Solution, %	Initial breakdown voltage, kv	Time to first voltage peak, µsec	Peak height, kv	Time to cessation of discharge µsec	Voltage at cessation of discharge µsec	Viscosity in Engler degrees
I	Ethyl cellulose in toluene	6	8	374	0.7	> 1600	—	$1.8 \cdot 10^4$
II	Same	3	8.2	—	—	374	3.6	$2.2 \cdot 10^2$
III	Same	1	8	—	—	374	3.6	37
IV	Same	1	8.2	—	—	374	3.6	37
V	Benzene	—	19	480	6	1230	1.8	—
VI	Xylene	—	15.5	350	7.5	750	3.6	—

In order to obtain some information on this, we carried out experiments with benzene and xylene. The oscillograms obtained are shown in Fig.3 (IV and VI) and the pertinent data are listed in Table 2. From a comparison of the data in Tables 1 and 2 for benzene it will be seen that with increase of the breakdown voltage by 18%, the time of appearance of the first discharge peak was reduced by 45 microsec. Approximately the same reduction occurred in the case of xylene with an increase of E_{br} by 11% (oscillogram VI).

The amplitude of the voltage during the jump-like de-ionization as compared with oscillogram IX in Fig.2 increased by 1.5 kv. A voltage of 7.5 kc proved to be sufficient for formation of a new breakdown of the well-ionized spark gap. Hence there appeared the peak a in oscillogram VI of Fig.3. Termination of the discharge occurred at point b at a voltage of 3.6 kv.

References

1. D.W.Goodwin & K.A.Macfadden, Proc.Phys.Soc.B., 66, 85 (1953).
2. W.R.LePage & L.A.DuBridge, Phys.Rev., 58, 61 (1940).
3. D.R.Young, J.Appl.Phys., 21, 222 (1950).
4. R.W.Growe, J.H.Bragg & A.H.Sharbaugh, J.Appl.Phys., 25, 392 (1954).
5. I.E.Balygin, Zhur.eksp.i teor.fiz., 25, 738 (1953).
6. I.E.Balygin, Zhur.tekh.fiz., 24, 337 (1954).
7. V.P.Vnukov, Fizika i oborona strany (Physics and national defense), p. 68, M., 1936.

DISCUSSION FOLLOWING THE PRECEDING FOUR REPORTS

V.A.Chuenkov: I.E.Balygin noted that the magnitude of the breakdown voltage depends on the electrode material. However, the experiments of Krasin carried out in Tomsk showed the opposite. Inasmuch as the results of Balygin's and Krasin's experiments are contradictory the question still remains unresolved. The experiments of Astafurov in which he discovered the luminescence of ice are very interesting. This suggests that there may be similarity between the breakdown of solid dielectrics and compressed gases.

A.V.Astafurov (on the report of I.E.Balygin): The two-fold and three-fold successive breakdown of liquids under the influence of a single pulse with the successive breakdowns occurring at lower voltages appears very strange. Possibly this effect is connected with shortcomings of the test circuit.

The breakdown oscillograms we have been shown were obtained by oscillographing the first, second or third breakdowns of the liquid. It is known that the first breakdown of a degassed liquid occurs with subsequent increase of the breakdown strength. In view of the fact that apparently Balygin did not degas his liquids he obtained misleadingly low values of the breakdown voltage, while the physical process recorded in the oscillograms was distorted due to the gas inclusions.

E.A.Konorova: The experimental results of Andreev are not in conflict with our results on electric breakdown. The shortcoming in the work of Astafurov is the poor contact provided between the ice and the electrodes.

Iu.V.Koritskii: In regard to the report of Andreev I would like to note that in investigating the regularities of thermal breakdown one must take into account the variation of the electric strength with the time of application of the voltage (the exposure). This was not done in Andreev's experiments. According to his report the voltage rose in all cases at a constant rate. But the breakdown voltages of the different samples were different and, consequently, so were the exposure times. This should be taken into account in analyzing the experimental data. Taking this factor into account would remove the internal contradiction in the report: the electric strength would prove to be independent of the retarding resistance, while the pre-breakdown current and the resistance of the discharge channel before breakdown depend upon it. The contradiction in the report is that the factor influencing the value of the current before breakdown did not have any effect on the electric strength in thermal breakdown.

Now as regards Balygin's work on the breakdown of liquid dielectrics I would like to note that a serious shortcoming of this investigation is that the liquids used were not sufficiently purified, that the degree of purity was not taken into account. It is well known that the electric strength of liquid and the breakdown mechanism are strongly effected by even traces of water, any air dissolved in the liquids and other contaminations. One cannot investigate the nature of breakdown of liquids without taking these factors into account.

V.A.Odoevskii: The same assertions in different variants are made in the work of A.A.Vorog'ev and his colleagues, without analysis of the physics of the mechanism involved. Some of their assertions have long ago been disproved; for example, one can hardly agree that the breakdown criterion is to be found in the second stage. This only obscures our concepts of the mechanism of breakdown.

Transactions of the Eighth All-Union Conference on Cathode Electronics

FROM THE EDITORIAL BOARD

The Eighth All-Union Conference on Cathode Electronics, dedicated to the Fortieth Anniversary of the Great October Revolution, was held in Leningrad from the 17th to the 24th of October, 1957.

The conference heard over one hundred reports at plenary and section meetings.

Some of the reports on secondary electron emission are being printed in the present issue of the Bulletin. Part of the reports on other topics will be published in No. 5 of the Bulletin as well as in Radiotekhnika i elektronika (No. 8 for 1958), Zhurnal tekhnicheskoi fiziki (No. 6 for 1958) and other technical journals.

REFLECTION OF ELECTRONS AND SECONDARY ELECTRON EMISSION FROM SOME METAL SURFACES AT LOW PRIMARY ELECTRON ENERGIES

- I.M.Bronshtein

1. What is commonly called "secondary electron emission" from metals actually consists of elastically and inelastically reflected primary electrons and true secondary electrons. Experimental data[1-7] show that the ratio between the true secondary and elastically reflected primary electrons depends on the primary electron energy. At very low primary energies - E_p of the order of a few electronvolts - most of the "secondaries" are actually elastically reflected primary electrons. With increase of E_p, in addition to the elastically and inelastically scattered primaries, there appear true secondary electrons, the proportion of which in the total emission increases with increasing E_p. As for the fraction r of elastically reflected electrons in the emission, offhand one might assume that it will monotonically decrease with increasing E_p in accord with the approximate theory of the one dimensional model with a constant potential inside the metal and an image force barrier outside it.[8] Recent data[2,4,9] show, however, that actually r decreases for some substances with increasing E_p, increases indefinitely for others, and rises to a saturation value for yet a third group.

This difference in the primary energy dependences of r is apparently connected with differences in the energy structure of the diverse substances inasmuch as the coefficient of reflection of electrons should, it seems to us, depend in a consistent manner on the density of electron states in the material.

2. In the present report we give the results of our investigation of secondary emission and reflection of electrons from Ni, Pt, Al, Ag, Au, Cu, W, Mo and Ta in the region of primary energies from 0.4 to 30 ev. Here under the energy of the primary electron we understand the excess energy over and above the energy of thermal motion and the energy due to non-equipotentiality of the cathode. The energy spread in our beam was of the order of 0.8-1 ev.

The measurements were carried out in a vacuum of $\sim 10^{-8}$ mm Hg in the setup with a spherical capacitor and moveable target, described earlier.[10-11] This apparatus allowed of measuring the coefficients σ and r and the cathode-target and cathode-collector contact potential differences, of applying the investigated layers by evaporation on a nickel or tantalum base and of investigating the energy spectrum of the secondary electrons.

The local magnetic field in the vicinity of the apparatus was compensated by Helmholtz coils.

The electron gun, consisting of a Wehnelt cylinder, an accelerating anode and two focusing annuli yielded a well-focused beam of 0.2-0.4 ev electrons.

The emission from Ni, Pt, W, Ta and Mo was investigated using solid heated targets, that from Ag and Cu using solid heated targets and layers obtained by evaporation and that from Al and Au only employing layers applied to Ni and Ta supports.

3. The $\sigma = f(E_p)$ and $r = f(E_p)$ curves proved to be different for different metals. For Ni and Pt the $r = f(E_p)$ curves were monotonic, with r decreasing with increasing E_p in accord with the approximate (Nordheim-MacColl) theory of electron reflection.[8]

The $r = f(E_p)$ curves for Al, Ag, Au and Cu are not monotonic, but exhibit maxima and minima of r at certain E_p values. Thus for Al there is a maximum of r at $E_p = 4$ ev, while for Ag, Au and Cu r rises to a maximum at $E_p = 10$-12 ev. For all the enumerated metals, except Pt, near zero E_p $r \approx 0.1$, while for Pt, $r \approx 0.2$.

In our opinion the nonmonotonic character of the reflection curves for Al, Ag, Au and Cu is due to the influence of the periodic field of the lattice, i.e., the existence of energy bands in the metal. Thus comparison of the electron reflection curves and the level density distribution for copper[11,12] shows that the minimum level density corresponds to the maximum value of the reflection coefficient r and vice versa.

4. The secondary emission characteristics of W, Mo and Ta have been investigated by Shul'man & Miakinin[3,9], and Morgulis & Gorodetskii[4] and Hobson[13]; in the work of Refs.4 & 9, in addition to the $\sigma = f(E_p)$ curves, there were obtained the curves for $r = f(E_p)$. For Mo, r monotonically decreases from 0.6 near $E_p \fallingdotseq 0$ to 0.15 at $E_p = 13$ ev;[9] while for W, r increases from 0.07 to 0.14 in the interval from 2 to 4 ev and then remains constant in the range from 4 to 10 ev[4]. According to Hobson[13], in the case of Ta, $r = 0.05$ at $E_p \fallingdotseq 0$.

Thus according to the data of the above investigators, not only are Mo, W and Ta characterized by values of r differing from each other by more than an order of magnitude but also their $r = f(E_p)$ curves have an entirely different appearance. This appears strange and is difficult to understand. In view of this we undertook an investigation of the secondary emission characteristics of W, Mo and Ta under identical conditions in a wider range of energies (from 0.4 to 30 ev).

The experimental procedure has been described earlier.[2] Just as in the case of Ag, Au, Cu, Al, Ni and Pt, we recorded the $\sigma = f(E_p)$ curves and the retarding potential curves from which we deduced the curves for $r = f(E_p)$. The curves σ, $\delta = \sigma - r$ and r as functions of E_p are shown in Figs.1,2 & 3, while the retarding potential curves are reproduced in Figs.4-10.

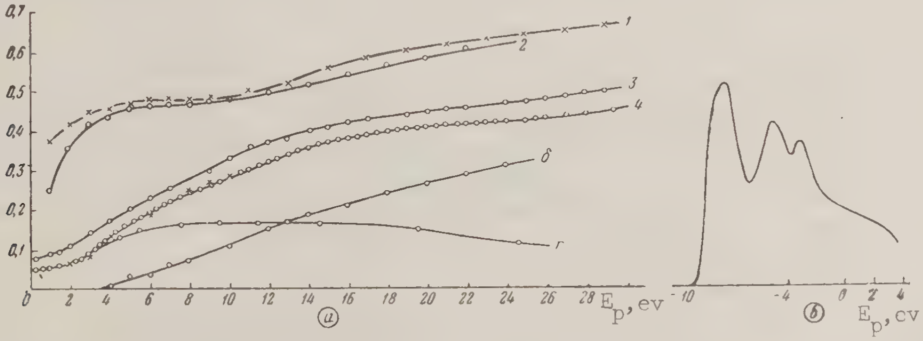

Fig.1. a) $\sigma = f(E_p)$, $r = f(E_p)$ and $\delta = \sigma - r = f(E_p)$ curves for W: 1) target not degassed, 2) target degassed for 30 min at ~2000°K, then held two weeks at $\sim 10^{-5}$ mm Hg, 3) target heated 5 min at ~1800°K at a pressure of 10^{-6} mm Hg (during measurement with a hot target $p \approx 10^{-7}$ mm Hg), 4) target heated about 10 hours at ~2000°K (crosses indicate points taken from Ref.4); b) curve characterizing level density distribution in W.

It will be evident from Figs.1,2 & 3 that the $\sigma = f(E_p)$ curves for W, Mo and Ta have the same appearance: σ monotonically increases from 0.05 at $E_p \approx 0$ to 0.35-0.4 at $E_p \approx 30$ ev. The $r = f(E_p)$ curves for all three metals are also similar. The reflection coefficients near zero primary voltage are ~0.05; at first they increase with increasing E_p, then remain approximately constant over a primary energy interval of ~10 ev and finally monotonically decrease.

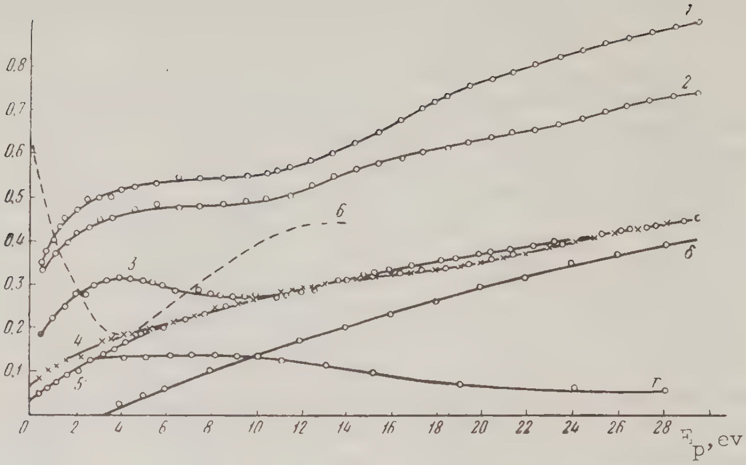

Fig.2. $\sigma = f(E_p)$, $r = f(E_p)$ and $\delta = f(E_p)$ curves for Mo: 1) target not degassed, 2) target heated 1 min to 1000°, 3) target heated 30 min at ~1500° K (all points obtained with target hot), 4) target heated for 4 hours at ~1700°K, 5) target heated an additional 8 hours at ~2000°K; 6) $\sigma = f(E_p)$ curve from Ref.3.

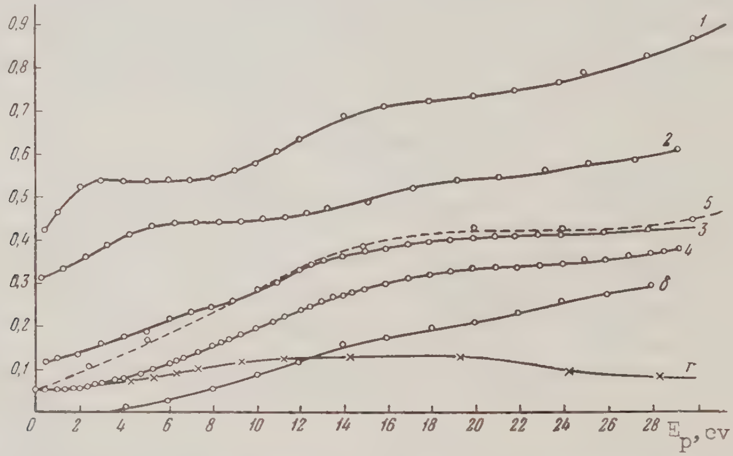

Fig.3. $\sigma = f(E_p)$, $r = f(E_p)$ and $\delta = f(E_p)$ curves for Ta: 1) target not degassed, 2) target heated 2 hours at ~1000°K, 3) target heated 5 min at ~1800°K, 4) target heated 10 hours at ~2000°K; 5) curve obtained at a vacuum of 10^{-9} mm Hg in the investigation of Ref.13.

Assuming, as in Ref.11, that the $r = f(E_p)$ curve is approximately a mirror image of the curve characterizing the density of electron states in the region of positive energies, one can expect that the density of states will at first decrease slowly with increasing electron energy and then more rapidly, finally tending to a more or less constant value.

The density of energy states in W was calculated by Manning & Chodorow[14] and is shown in Fig.1,b. Unfortunately, the calculated curve extends only 3.2 ev into the region of positive energies. It will be seen that in this energy interval at any rate the electron reflection curve is actually a mirror image of the density of states curve. Apparently, a similar distribution of level densities obtains in Ta and Mo as well.

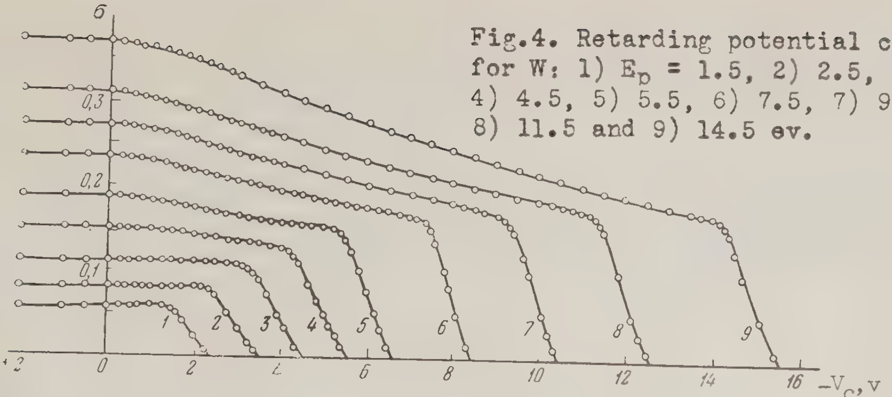

Fig.4. Retarding potential curves for W: 1) E_p = 1.5, 2) 2.5, 3) 3.5, 4) 4.5, 5) 5.5, 6) 7.5, 7) 9.5, 8) 11.5 and 9) 14.5 ev.

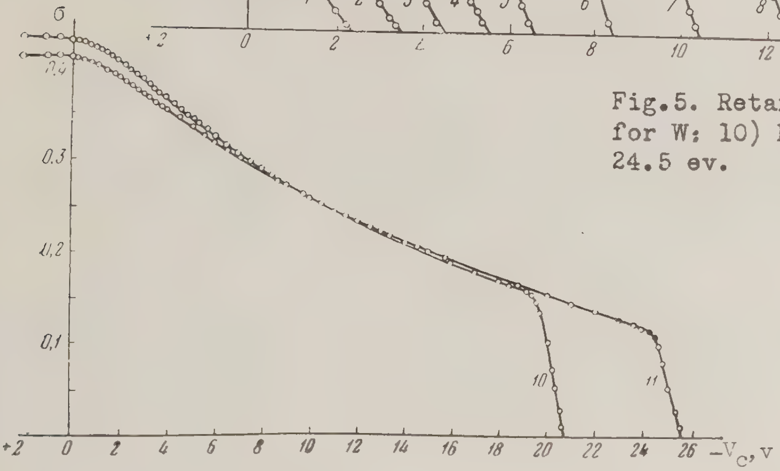

Fig.5. Retarding potential curves for W: 10) E_p = 19.5 and 11) 24.5 ev.

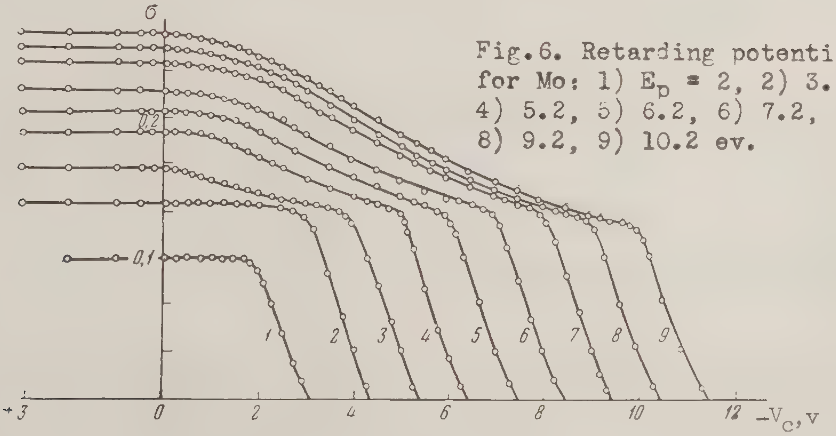

Fig.6. Retarding potential curves for Mo: 1) E_p = 2, 2) 3.2, 3) 4.2, 4) 5.2, 5) 6.2, 6) 7.2, 7) 8.2, 8) 9.2, 9) 10.2 ev.

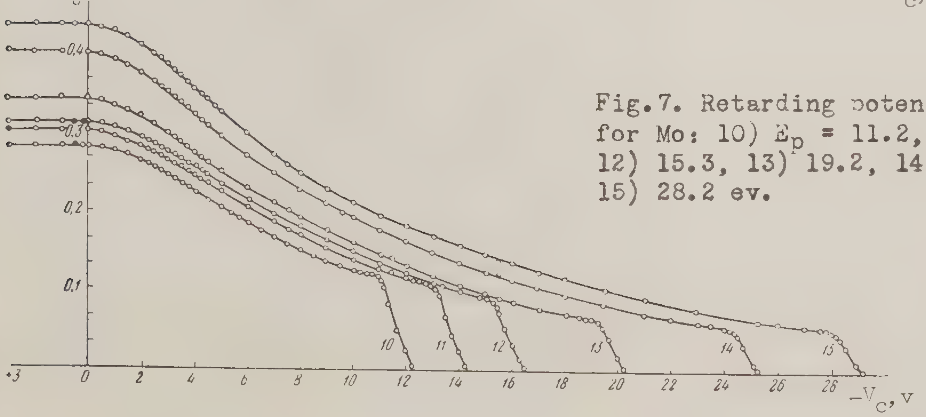

Fig.7. Retarding potential curves for Mo: 10) E_p = 11.2, 11) 13.2, 12) 15.3, 13) 19.2, 14) 24.2 and 15) 28.2 ev.

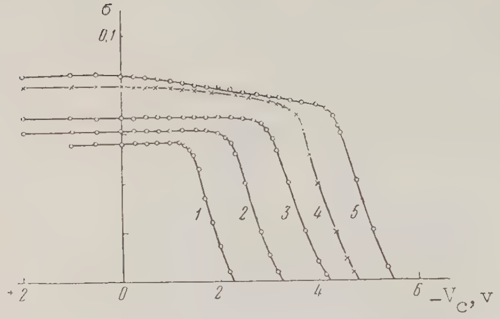

Fig.8. Retarding potential curves for Ta: 1) E_p = 1.3, 2) 2.3, 3) 3.3, 4) 3.8, 5) 4.3 ev.

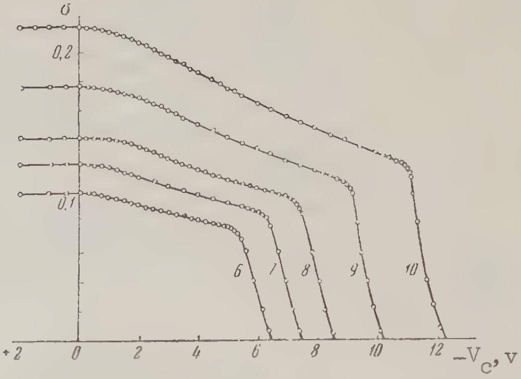

Fig.9. Retarding potential curves for Ta: 6) E_p = 5.3, 7) 6.3, 8) 7.3, 9) 9.3, 10) 11.3 ev.

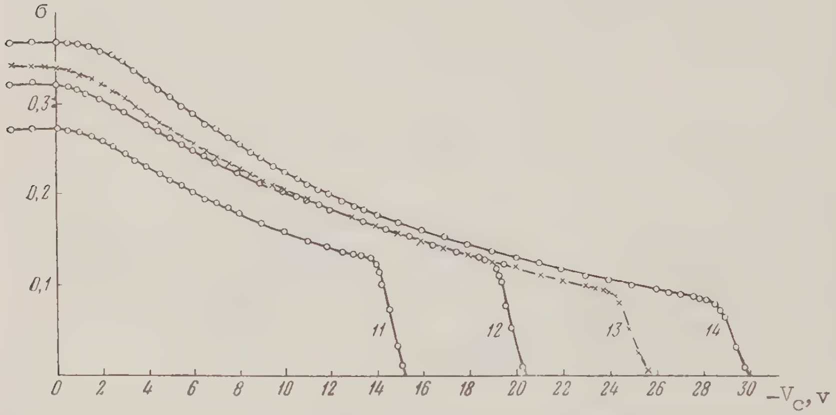

Fig.10. Retarding potential curves for Ta: 11) 14.3, 12) 19.3, 13) 24.3, 14) 28.3 ev.

5. In Figs.1,2 and 3, in addition to the curves characterizing the variation of σ and r as functions of E_p, we have also plotted $\delta = \sigma - r = f(E_p)$, i.e., the variation of true secondary and inelastically scattered primary electrons as a function of the primary voltage. It will be evident from these curves that in our experiments elastically scattered primary electrons appeared in detectable amounts only at primary voltages above 3-3.5 ev. True secondary electrons appear at somewhat higher values of E_p. We cannot, however, affirm that the secondary emission threshold corresponds exactly with the work function in view of the fact that our primary electron beam was not sufficiently monoenergetic. The same observation applies to other investigations. The data of Shul'man & Miakinin[3], who assert that the values of the secondary emission threshold for Ni and Mo coincide (to within 0.15 ev) with their work functions, and the data of Morgulis & Gorodetskii[4], who report observing a tendency of the secondary emission threshold to vary with variation of the work function, cannot be taken as proof that the secondary emission threshold - if such a threshold does exist - exactly corresponds to the work function φ. We feel that to obtain such proof one must carry out high-precision experiments using a rigorously monoenergetic beam. Judging by the retarding potential curves given in Ref.3 & 4, the energy spread of the primary electron beams was 1.5 to 2.5 ev. In this case the threshold cannot be determined with an accuracy better than 1-2 ev.

In addition, in such experiments, one must exclude insofar as possible other sources of error such as, for example, local magnetic fields in the laboratory (as is known, such local fields may appreciably distort the retarding potential curves). Moreover, in order to establish definitively correspondence between the secondary emission threshold and the work function of a given substance one must measure the work function and the reflection of electrons in the same set-up under rigorously identical conditions.

An appreciable portion of this work - investigation of Ni, Pt, Al, Ag, Au and Cu - was carried out in collaboration with V.V.Roshchin.

References

1. I.Gimpel & O.Richardson, Proc.Roy.Soc. A182, 17 (1943).
2. H.Myers, Proc.Roy.Soc. A215, 329 (1952).
3. A.R.Shul'man & E.I.Miakinin, Zhur.tekh.fiz., 26, 2223 (1956).
4. N.D.Morgulis & D.A.Gorodetskii, Zhur.eksp.i teor.fiz., 30, 667 (1956).
5. P.I.Lukirskii & N.N.Semenov, ZhRFKhO, 55, 107 (1923).
6. Iu.A.Nemilov & E.I.Fedorova, Tekh.telev., 5, 64 (1951).
7. G.A.Harrower, Phys.Rev., 104, 52 (1956).
8. L.A.MacColl, Phys.Rev., 56, 699 (1939).
9. A.R.Shul'man & E.I.Miakinin, Doklady AN SSSR, 91, 1075 (1953).
10. I.M.Bronshtein & V.V.Roshchin, Zhur.tekh.fiz., 28, 9 (1958).
11. I.M.Bronshtein & V.V.Roshchin, Zhur.tekh.fiz, 28, 10 (1958).
12. E.Rudberg & J.C.Slater, Phys.Rev., 50, 150 (1936).
13. J.P.Hobson, Canad.J.Phys., 34, 1089 (1956).
14. M.F.Manning & M.J.Chodorow, Phys.Rev., 56, 787 (1939).

DISCUSSION

L.N.Dobretsov: According to your data the secondary emission coefficient tends to zero for Pt at primary electron energies of 4 ev, for Ag at 3 ev, for Mo at 3 ev; in other words, the secondary emission "thresholds" do not coincide with the work functions.

I.M.Bronshtein: I feel that with a spread of 1 ev in the energy of the primaries one cannot establish whether the values coincide. The intersection of the $\sigma = f(E_p)$ curve with the x axis should rather be called the threshold of inelastic reflection.

L.N.Dobretsov: The density of states curves pertain to all directions of electron motion. In your experiments, however, you have a directed beam. In view of this, is a comparison such as you have made justified?

I.M.Bronshtein: I think that it is, taking into account the polycrystalline character of the target.

A.Ia.Viatskin: The density of states curves not only for Cu, but for other metals have a maximum. Why then do not the $r = f(E_p)$ curves exhibit maxima?

I.M.Bronshtein: One cannot speak of lack of correspondence between the experimental $r = f(E_p)$ curves and the density of states curves inasmuch as these have not yet been calculated for the other metals.

N.D.Morgulis: What was the energy spread in the primary beam?

I.M.Bronshtein: About 0.8-0.9 ev.

A.A.Mostovskii: With such an energy spread can one begin measurements from 0.5 ev?

I.M.Bronshtein: One can, always bearing in mind the non-monoenergetic character of the beam.

N.D.Morgulis: Your apparatus was not sealed off. Can one trust your results?

I.M.Bronshtein: Yes, one can, inasmuch as for a number of materials our curves are identical with yours.

A.I.Piatnitskii: What is the difference in reflection coefficients for annealed (heated) and sputtered on materials?

I.M.Bronshtein: For Ag and Cu the reflection coefficient is about 10% higher for sputtered on targets, apparently due to greater contamination of the surface.

D.G.Bulyginskii: Why do your curves for Ni lie lower than those in the work of A.R.Shul'man?

I.M.Bronshtein: Probably because our Ni was purer.

INVESTIGATION OF THE STRUCTURE AND PROPERTIES OF Ge, Cr AND Bi FILMS TAPERING IN THICKNESS IN CONNECTION WITH THEIR SECONDARY EMISSION CHARACTERISTICS

- N.G.Nakhodkin & A.I.Novosel'skaia

1. Investigation of the variation of the secondary emission coefficient δ with the thickness d of the emitting film can be instrumental in clarifying certain aspects of secondary emission. Thus, we and a number of other authors[1-3] have shown that the secondary emission coefficient varies with d up to a certain thickness d_{eff} which has been called the effective depth (of origin) of secondary emission.

Investigations of the effective depth of secondary emission of different substances, both metals and semiconductors (germanium, Sn-Cs and Sb-Cs cathodes)[2,3] has shown that the effective depth d_{eff} varies little with changes in the primary electron energy in the range from 200 to 3000 ev. From this it could be inferred that d_{eff} is determined primarily by the kinetics of motion of the secondary excited electrons.

2. Our earlier investigations[3], however, had one shortcoming. The fact is that the values of d_{eff} of most substances proved to be commensurate with the limiting aggregation thickness of the film.[4,5] From the absence of anomalies in the variation of the optical properties of films with thickness (in the thickness interval in question) it could be inferred that in the case of germanium[6], chromium[4,7] and cesium-antimony and cesium-tin cathodes[8] the layer is continuous with $d \geqslant d_{eff}$. Inasmuch as conditions of preparation have an appreciable influence on the structure of layers, it appeared of interest to investigate the structure of films prepared under conditions close to those employed in our earlier investigation of the secondary emission properties of films[3].

3. The present work was concerned with vacuum condensed films of germanium and chromium and bismuth. The films were deposited on carefully cleansed glass backing plates with silver strip electrodes for measuring resistance and on collodion backings for investigating the structure by means of an electron microscope and an electron diffraction camera. The thickness of the film at any given point of the wedge-like layer was determined from the geometry of the evaporating-condensing system and the weight of the deposited material.[9] In calculating the thickness, it was assumed that the film was continuous and that its density was the same as that of the bulk metal. The coated collodion strips were exposed to air only while being transferred to the electron microscope. The layers on the glass backings were divided into strips by means of a graduating machine and the resistance of each section was measured with an MOM-1 megohmmeter.

4. Germanium films from 3 to 10 mμ appeared to be continuous under the electron microscope, i.e., no inhomogeneities were distinguishable on the microscope screen or in photographs (resolution of the instrument <100 Å).

As may be seen in Fig.1, electron diffraction patterns of freshly applied germanium layers, obtained by the transmission procedure, exhibit three very diffuse rings. The lines in the electron diffraction patterns of germanium films on a glass support, obtained by reflection, proved to be even more diffuse and much less contrasty. Hence, according to the data in the literature (Ref.10), it may be asserted that such freshly deposited germanium layers are amorphous. Increasing the intensity of the electron beam in the microscope induces structural changes in the film. By way of illustration, in Fig.2 we show an electron microphotograph and the electron diffraction pattern of a germanium film (the same as that of Fig.1) obtained after a period of exposure to the electron beam. Apparently, heating of the film by the beam produces crystallization; the distribution of surface tension forces at the

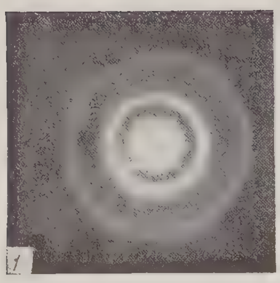

Fig.1. Electron diffraction pattern of freshly sputtered Ge layer.

germanium-backing interface is altered and the film breaks up into individual aggregates. The size and shape of the aggregates depend on both the thickness of the film and the intensity of the incident electron beam.

From the appearance of the diffraction patterns obtained from germanium layers before and after exposure to an electron beam, it may be asserted that a short-range order persists in the amorphous germanium film. Reduction of the film thickness leads to broadening of the diffraction lines. For example, increase in thickness from 3 to 73 mμ resulted in a change of the line half-width by a factor of almost 2. If for purposes of rough evaluation we take as the natural line width the width of the diffraction reflex from a standard MgO sample, the size of the individual crystals, as calculated by means of Eq.(IX,6) from Ref.11 is found to be between 5 and 12 Å. Under the influence of the electron beam, there are formed in the layer crystals with the diamond type lattice, the parameter of which is about 5.8 Å. With increase in thickness the half-width of the lines in the electron diffraction patterns decreases so much that it becomes commensurate with the half-width of the MgO line, i.e., the size of the scattering crystals in the germanium film increase to 100 Å or more.

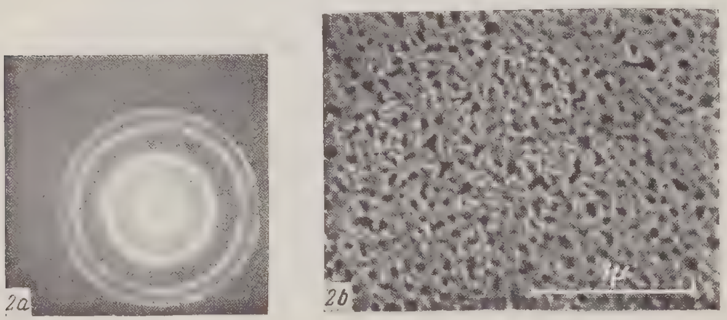

Fig.2. a) Electron diffraction pattern of the same (as in Fig.1) Ge layer recrystallized under electron bombardment; b) electron microphotograph of 53 mμ thick Ge layer after exposure to an electron beam.

In addition to the techniques employed in earlier similar investigations, we also used the method of profile photographs. A coating of germanium of the requisite thickness was applied by vacuum evaporation to fine, smooth glass wool. Then the profile of a glass filament bearing the germanium layer was examined by means of the electron microscope. It was found that the initial smooth layer (Fig.3,a) recrystallizes under the influence of the electron beam with the formation of a characteristic petal-like structure (3,b). Formation of this structure is favored by the appreciable tension existing in a freshly deposited germanium film.

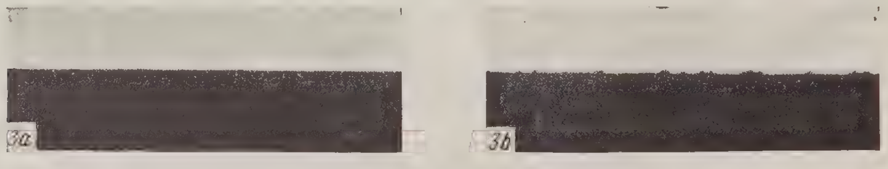

Fig.3. Profile photographs of 53 mμ thick germanium coating on a glass filament: a - before and b - after electron bombardment. Magnification 36,000 X.

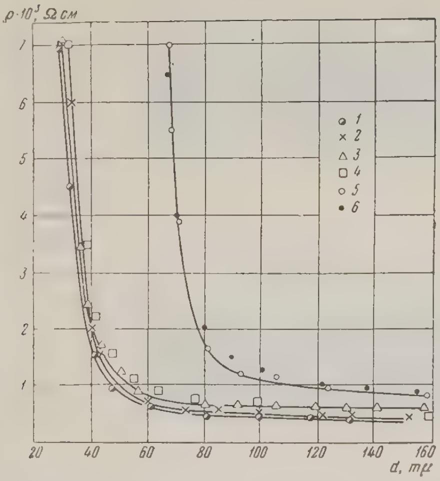

Fig.4. Variation of the resistivity of germanium layers as a function of thickness; layers obtained by evaporation 1) for 1 min, 2) for 15 min, 3) for 40 sec; 4) after heating at 200° for 15 min, 5 & 6) after heating at 450° for 1 hour.

We also investigated the variation of the resistivity of condensed layers as a function of thickness. Some of the observed dependences are plotted in Fig.4. It will be seen that the resistivity of even comparitively thick layers is at least two orders of magnitude greater than that of bulk germanium. All the layers proved to be p-type semiconductors. In the range of thicknesses less than 40 mμ the increase in resistivity with decreasing d is less than observed for other metals. Incidentally the thickness at which a sharp increase in resistance is observed decreases noticeably (down to 10 mμ) with improvement of the vacuum during application of the film.

Heating of such films under vacuum for 15 minutes at temperatures of about 200° does not lead to any noticeable change in the conductivity (curve 4 in Fig.4). As a result of heating at 450° for 1 hour, however, the increase in resistivity begins at greater thicknesses (~80 mμ) regardless of the original rate of condensation of the film (curves 5 & 6).

These variations are in agreement with deductions drawn from the electron microphotographs; for thicknesses greater than 30-40 mμ one can safely consider freshly applied germanium films to be continuous. The shift of the point marking the beginning of a sharp increase in resistivity to the side of greater thicknesses as a result of heating can be explained by aggregation of the film; this effect is actually observed under the microscope after a period of exposure to the electron beam.

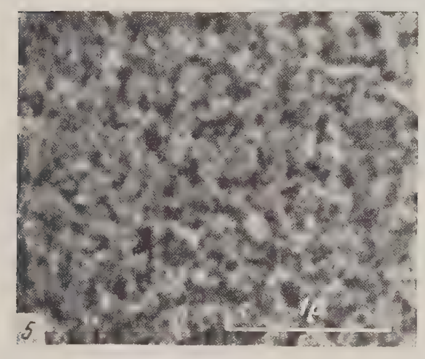

Fig.5. Electron microphotograph of freshly deposited 10 μ thick Bi layer.

5. The range of bismuth film thicknesses found suitable for electron microscope studies proved to be 6 to 60 mμ. Thicker layers were opaque to electrons. Fig.5 shows the characteristic structure of a bismuth layer. In the entire investigated thickness range, the films were discrete with not quite sharp light and dark spots, which is in agreement with the data of other investigators.[5,12]

We assumed that in this case the bismuth layers must consist of single crystal needles; then the faces for which the first Bragg reflection is not limited by the diaphragm aperture must yield light spots. This view was confirmed by profile photographs of a bismuth layer deposited on a smooth glass filament. It was found that the bismuth coating consists of individual distinct needles, decreasing in size with the layer thickness and inclined at an angle to the substrate corresponding to the angle of incidence of the molecular beam. Electron microscope photographs of profiles of freshly desposited bismuth layers taken with the electron beam normal to and at an angle to the glass substrate are shown in Fig.6,a & b.

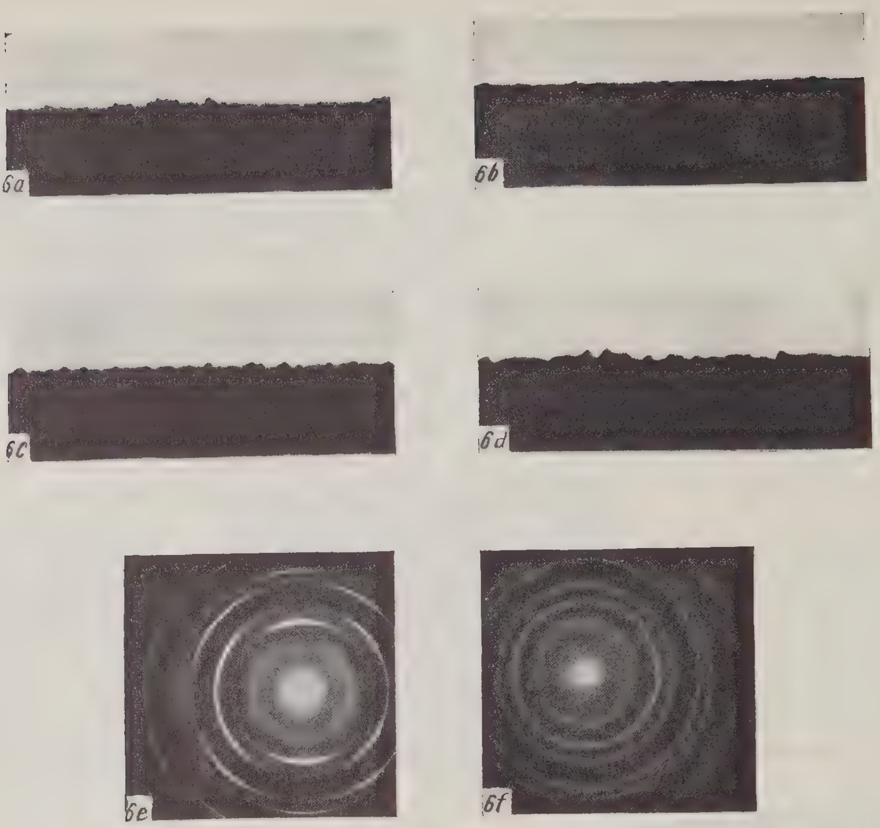

Fig.6. a-d) Profile microphotographs of ~40 mμ bismuth layer deposited on a glass filament: a & b - freshly deposited layer obtained with normal and oblique incidence of the molecular beam, c & d - same layer after a period of exposure to the electron beam (all magnifications 36,000 X); e & f - electron diffraction patterns freshly deposited Bi layer before and after exposure to electron beam.

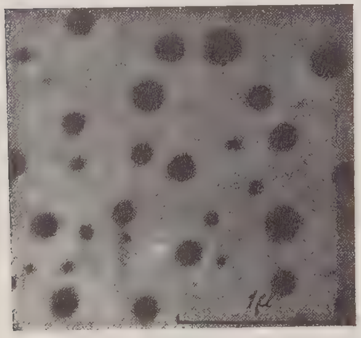

Fig.7. Electron microphotograph of bismuth layer (same as in Fig.5) after exposure to electron beam.

Under the influence of heating by the electron beam the film undergoes recrystallization, apparently passing through a liquid phase. The appearance of the film after the period of electron bombardment is shown in Fig.7; the corresponding profile photographs are reproduced in Fig.6, c & d. Exposure to the electron beam smooths out the film: the initial needle-like structure is transformed into a granular one.

Electron diffraction patterns confirm the deduction that the bismuth needles are individual single crystals. This is evident from the pronounced texture, which changes with the angle of inclination of the sample relative to the electron beam. After recrystallization under electron bombardment there forms a fine crystalline layer and the texture disappears.

The sharp increase in the resistivity of bismuth layers is observed for smaller thicknesses than in the case of germanium, namely, at d < 10 mμ, as may be seen in Fig.8. We are not able, however, to distinguish any qualita-

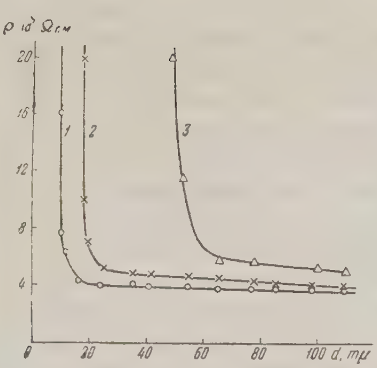

Fig.8. Variation of the resistivity of bismuth layers as a function of the thickness: 1) freshly deposited layer, 2) layer heated in vacuum at 180° for 1 hour, 3) layer heated in vacuum at 300° for 1 hour.

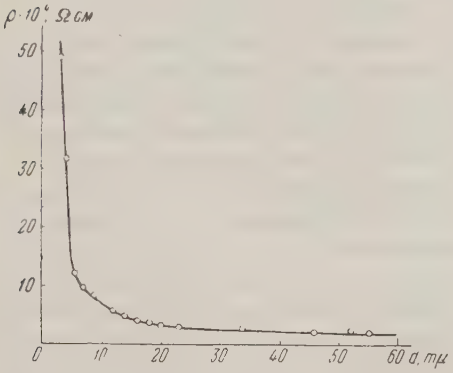

Fig.9. Variation of the resistivity of a freshly deposited chromium layer as a function of its thickness.

tive differences in the structure of the films having thicknesses greater and less than ~10 mμ, either from the electron microscope photographs or the diffraction patterns. Heating of the films in vacuum up to about 180° did not noticeably change the appearance of the resistivity vs thickness curves. Apparently, the alterations in the structure of bismuth films as the thickness is reduced to below 10 mμ lie below the resolving power of the electron microscope. Bismuth layers having thicknesses greater than 60 mμ may safely be regarded as continuous.

6. Next we investigated chromium films. Freshly deposited chromium coatings from 3 to 70 mμ thick appear continuous under the electron microscope. This ability of chromium to form continuous solid films is well known[6] and is extensively utilized in electron microscopy for structureless backing of certain objects.

From the appearance of the electron diffraction patterns it may be asserted that the chromium films were polycrystalline. Under the influence of the electron beam the initially continuous chromium films aggregate with the formation of a fine grain structure. This aggregation is markedly facilitated with increasing film thickness. No noticeable corresponding changes in the electron diffraction patterns were observed.

Increase in the resistivity of chromium layers with decreasing thickness begins at thicknesses of less than 10 mμ, as may be seen in Fig.9. Consequently, it may be assumed that at thicknesses greater than ~10 mμ chromium films are continuous; this is substantiated by our electron microphotographs.

7. Concurrently with the above experiments, we determined the variation of the coefficients of transmission (τ) and reflection (r) for monochromatic light as a function of the layer thickness d. The optical characteristics of all three investigated materials are shown in Figs.10 & 11. It was found that freshly deposited films did not exhibit any of the anomalies characteristic of aggregated silver layers.[4]

Heating of the bismuth layers in vacuum at a temperature of ~180° caused no noticeable changes in their optical properties and electric conductivity. In the case of germanium layers in the thickness range from 80-100 mμ heating in vacuum at a temperature of ~450° resulted in a decrease of the reflection coefficient r for wavelengths shorter than 720 mμ. A particularly large change in r was observed at wavelength of 540 mμ, whereas at $\lambda \approx 850$ mμ, the reflection curves for heated layers of all thicknesses virtually coincided with the corresponding curves for unheated layers. Unfortunately, owing to the

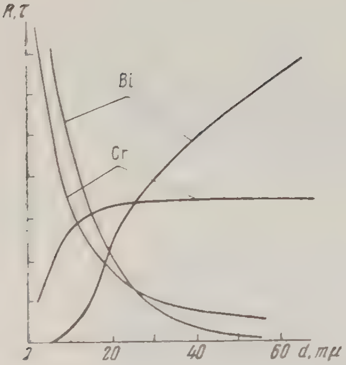

Fig.10. Variation of the coefficients of reflection and transmission as a function of the thickness of freshly deposited Bi and Cr layers.

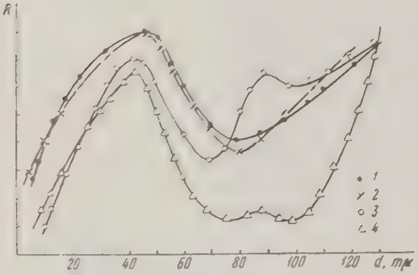

Fig.11. Variation of the coefficient of reflection as a function of the thickness of a germanium layer. Curves 1 & 3 were recorded for a freshly deposited layer at λ≈850 and ~540 mμ; curves 2 & 4 were obtained for layers heated in vacuum at 450° for 1 hour for the same wavelengths.

strong absorption of light in this range of thicknesses and wavelengths we were not able to measure the absorption coefficient.

These variations of the reflection coefficient can be related with the structural characteristics of the heated film. If we assume, in accord with the conductivity and electron microscope data, that after heating germanium layers up to 80-100 mμ thick are aggregated with a volumetric filling ratio close to unity, the structural light absorption maximum (or reflection minimum), similar to that observed in the case of silver, gold and analogous materials, must appear when $k^2 \rightarrow n^2 > 0.5$, where k is the coefficient of absorption and n is the index of refraction of the material.[4] If we take the values of $k(\lambda)$ and $n(\lambda)$ from the work of Brattain & Briggs[6], we find that the structural maximum should be observed at wavelengths of the order of 500 mμ, which, as will be seen from Fig.11, is in agreement with experiment.

8. In view of the above described results, it may be asserted that germanium films prepared under the conditions used in our earlier experiments on secondary emission[3] are amorphous and continuous and have a finite resistivity. Freshly deposited chromium films become continuous and conducting beginning with a thickness of the order of 5-10 mμ. Consequently, the "thickness" properties of films, including the thickness dependence of the secondary emission coefficient δ, in the case of germanium at all thicknesses greater than 30 mμ should not be complicated by structural factors associated with aggregation. Hence the thickness at which the δ vs d curves for germanium and chromium are flattened out (60-70 mμ for Ge and 7-10 mμ for Cr) may be regarded as the effective depth of origin of secondary emission.

The same assertion cannot be made in the case of bismuth. The rapid increase of the resistivity at the thickness values at which the δ vs d curve first flattens out, the complex needle-like structure that is clearly dependent on the thickness of the film and, finally, the complicated variation of the secondary emission coefficient as a function of the primary electron energy, all hamper unambiguous determination of the effective secondary emission depth.

Thus it would appear that the effective depth of secondary emission of metal (in our case chromium) is less than the effective depth in a semiconductor (for example, germanium). This could reasonably be expected inasmuch as in metals there must occur appreciable slowing down of the emerging secondary electrons by conduction electrons. The value of the coefficient of secondary emission in both cases, however, is almost the same. Apparently, the character of the energy losses of the primary and secondary electrons is rather complicated, i.e., the excitation probability is small in inefficient secondary emitters with large effective depths of emission. It may be noted that the intensity of excitation processes inside ordinary semiconductors (for example, germanium) will be appreciably lower than the intensity not only in efficient semiconductors but also in certain metals such as chromium. It may be concluded, therefore, that the character of one of the processes fundamental to secondary emission - excitation of secondary electrons - depends in a complex way on the material of the emitter.

In conclusion the authors wish to acknowledge their gratitude to N.D. Morgulis for constant interest in the work.

"T.G.Shevchenko" Kiev State University

References

1. A.V.Afanas'eva, P.V.Timofeev & A.Ignatov, Zhur.tekh.fiz., 6, 1649 (1936); A.F.Pes'iatskii, Zhur.tekh.fiz., 9, 188 (1939); P.L.Copeland, Phys. Rev., 58, 604 (1940); A.E.Hastings, Phys.Rev., 57, 695 (1940); V.M.Lovtsov & S.V.Starodubtsev, Trudy (Transactions), Physical-Mathematical Institute, Uzbek SSR Academy of Sciences, 3, 57 (1950); M.M.Vudynskii, Doklady AN SSSR, 82, 705 (1952); I.M.Bronshtein, Zhur.tekh.fiz., 13, 173 (1943); I.M.Bronshtein & T.A.Smorodina, Zhur.eksp.i teor.fiz., 27, 215 (1954); 29, 495, 500 (1955).

2. B.I.Diatlovitskaia, Doklady AN SSSR, 63, 641 (1948).

3. N.G.Nakhodkin, Naukovi zap. KDU (Scientific notes, KDU), 14, No.8, 209 (1955); N.D.Morgulis & N.G.Nakhodkin, Doklady AN SSSR, 94, 1029 (1954).

4. P.Morozob & M.Butslov, Zhur.tekh.fiz., 16, 857 (1946); R.Sennet & G.Scott, JOSA, 40, 203 (1950).

5. R.Picard & O.Duffenduck, J.Appl.Phys., 14, 291 (1943); H.Levinstein, J.Appl.Phys., 20, 306 (1949).

6. W.H.Brattain & H.B.Briggs, Phys.Rev., 75, 1705 (1949); N.V.Rapp, Uch.Zap.(Scientific notes) Phys.Math.Faculty, Kharkov University, 2, 105 (1950).

7. Elektronnaia mikroskopiia (Electron microscopy), edited by A.A.Lebedev, 1954; C.Calbick, Bell.System Tech., 30, 798 (1951).

8. P.Borziak, Trudy (Transactions) Physical Institute AN Ukrainian SSR, No.2, 3 (1952); N.Morgulis, P.Borziak & B.Diatlovitskaia, Izv.AN SSSR, Ser.fiz., 12, 126 (1948).

9. N.D.Morgulis, Dopovidi sichnevoi sesii AN URSR (Reports of the January session of the Ukrainian RSR Academy of Sciences) No.2, 285 (1942); S.A.Vekshinskii, Novyi metod metallograficheskogo issledovaniia splavov (A new method of metallographic investigation of alloys), 1944.

10. E.Fischer & H.Richter, Ann.Phys., 16, 193 (1955); H.Konig, Reichberichte f.Phys., 1, 7 (1944); A.Verma, Proc.Phys.Soc.,B,67,359 (1954); M.Dunover, J. Phys.et radium., 12, 602 (1951).

11. Z.G.Pinsker, Diffraktsiia elektronon (Electron diffraction), 1949.

12. R.Williams & R.Wyckoff, J.Appl.Phys., 15, 712 (1944); P.Bryant, H. Rhoads & A.Weber, J.Appl.Phys., 25, 1343 (1954).

DISCUSSION

V.N.Lepeshinskaia: What was the density of the electron flux in the microscope when aggregation began and is the energy of the electron beam important?

N.G.Nakhodkin: Increasing the intensity above the normal leads to aggregation. The electron energy was constant - 40 kev.

L.N.Dobretsov: What were the coefficients of adhesion?

N.G.Nakhodkin: For thick layers the adhesion coefficient is close to unity, while for thin layers it is not know precisely.

L.N.Dobretsov: From what does it follow that the difference in the conditions of secondary electron excitation by the primary beam is important?

N.G.Nakhodkin: In germanium and SbCs the depth of emergence of secondary electrons is the same, while the values of σ are different. Apparently, the conditions of motion of the secondary electrons are the same, while the values of σ differ due to different conditions of secondary excitation. It has been shown that the effective depth of emergence of secondary electrons varies little with the primary electron energy. Hence it may be assumed that the effective depth is determined only by the motion of the secondary electrons.

I.M.Bronshtein: In order to obtain reliable results one must use substrates for which the coefficient of secondary emission is appreciably lower than for the applied layer.

B.N.Popov: It would be of interest to try lanthanum boride as the base; lanthanum boride has metallic conductivity and $\sigma_{max} = 0.95$.

VARIATION OF THE SECONDARY EMISSION COEFFICIENT OF KCl WITH THE LAYER THICKNESS

- N.G.Nakhodkin & V.A.Romanovskii

The depth of origin of secondary emission can be determined from the variation of the secondary emission coefficient with the thickness of the emitting layer. There are diverse empirical data relative to the variation of the effective depth of secondary emission as a function of the primary electron energy.[1] In 1948 Diatlovitskaia[2] first employed the wedge ⟨tapering coating thickness⟩ technique in investigating an Sb-Cs cathode and showed that the effective depth d_{eff} of secondary emission does not depend on the primary electron energy V_p. Later this result was shown to hold for a large number of different metals and semiconductors in our experiments[3], in which the same technique was employed, and, subsequently, in the work of Bronshtein & Smorodina[4]. In view of these results, we were able to infer that the effective depth of secondary emission in the range of medium primary energies is directly related with the kinetics of motion of excited secondary electrons inside the solid.

Nevertheless, we felt it would be of interest to determine the causes that led a number of investigators[1] to observe a strong dependence of the effective depth d_{eff} of secondary emission on the primary energy V_p.

Earlier, one of us[3] found that the secondary emission coefficient δ in the range $V_p > 2000$ ev increases slightly with thickness even in the case of layer thicknesses greater than d_{eff}. This increase of δ ceases at a certain thickness $d_2 > d_{eff}$, which depends on the energy of the primary electrons and the substrate material. It was hypothesized that this second rise of the secondary emission coefficient is associated with secondary electrons produced by so-called "back diffusion" of primary electrons. Inasmuch, however, as this second increase in δ was small in the case of metals and the primary energy interval in which it was observed was comparatively narrow, we remained somewhat doubtful about this interpretation of the effect.

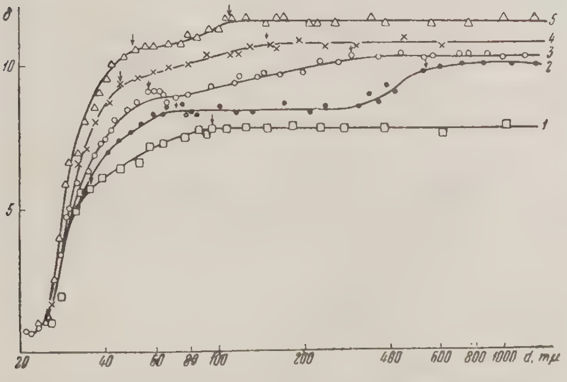

Fig.1. Variation of δ with the layer thickness d for different primary energies V_p: 1) 480 v, 2) 6000 v, 3) 4900 v, 4) 4000 v and 5) 3000 v.

We investigated the thickness dependence of the secondary emission coefficient of KCl in the primary energy range from 480 to 6000 ev. The backing for the KCl films was a layer of beryllium sputtered on glass under vacuum (10^{-8} mm Hg). The difference between the secondary emission coefficient δ of the backing and δ of the layer was large, so that the measurements could be made with an adequate degree of accuracy. The measurements were carried out with single pulses ($\tau = 2.5$ microsec) using very low currents, which made it possible to exclude the effect of surface charge[5] even at room temperature. The thicknesses were determined by the interferometric technique.

The characteristic dependences of the secondary emission coefficient on the thickness d of the layer for several primary electron energies are shown in Fig.1. It will be seen that the thickness dependence of δ has two flats

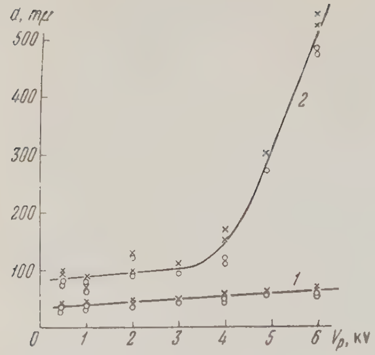

Fig.2. Variation of d_1 (1) and d_2 (2) with the primary electron energy V_p.

at d_1 and d_2, indicated in Fig.1 by arrows. The observed experimental variation of δ with d allows of explaining the persisting disagreement regarding the dependence of d_{eff} on V_p. If the experimental points are not taken sufficiently close together in the interval from d_1 to d_2, the first plateau will not be discernible in the experimental curve.

We identify the value of d_1, which in our experiments was of the order of 50 mμ, with the effective depth of secondary emission. As will be evident from the curves reproduced in Fig.2, this effective depth in a very appreciable primary interval (480 to 6000 ev) is independent of the primary energy and, consequently, may be related with the kinetics of motion of the secondary electrons in the emitting solid. As will be seen from Fig.2, d_2 is consistently greater than d_1 and depends on the primary electron energy. The increase in the coefficient of secondary emission in going from thickness d_1 to d_2 is of the order of 15-20%. Hence it is logical to assume that the thickness d_2 must to some extent characterize the range of the primary electrons in the solid.

Electronics Faculty
"T.G.Shevshenko" Kiev State University

References

1. P.L.Copeland, Phys.Rev., 58, 604 (1940); A.Hastings, Phys.Rev., 57, 695 (1940); M.Vucynskii, Doklady AN SSSR, 82, 705 (1952); V.Lovtsov & S.Starodubtsev, Trudy (Proceedings) Phys.-Technical Institute, AN Uzbek SSR, 3, 57 (1952); M.Knoll, O.Hachenberg & J.Randmer, Z.Phys., 122, 137 (1944).
2. B.Diatlovitskaia, Doklady AN SSSR, 63, 641 (1948).
3. N.Nakhodkin, Naukovi zap.KDU (Scientific notes, KDU), 14, 209 (1955); N.Morgulis & N.Nakhodkin, Doklady AN SSSR, 94, 1029 (1954); N.Nakhodkin, Dissertation, Kiev State University, 1953.
4. I.Bronshtein & T.Smorodina, Zhur.eksp.i teor.fiz., 27, 214 (1954); Zhur.eksp.i teor.fiz., 29, 495 (1955).
5. A.Shul'man & V.Makedonskii, Zhur.tekh.fiz., 22, 1540 (1952).

PASSAGE OF ELECTRONS THROUGH THIN GLASS FILMS

- A. I. Piatnitskii

Introduction

Thin glass films transparent to electrons are finding increasing application in electronic technology, inasmuch as glass is one of the most convenient materials for preparing large but thin, continuous, defect free films that can be used as targets or as base layers for emitters and photocathodes.

Hence investigation of the passage of electrons through such glass films and their behavior under electron bombardment is of considerable interest. Such investigation was the purpose of the present work.

Preparation of the glass films

For preparing the films we used primarily the glasses designated as No.23 and BD-1 (БД-1). We also tested other kinds of glass, but the best results were obtained with these two types.

In preparing the films we used tubes 25-30 mm in diameter inasmuch as smaller diameter tubing did not yield sufficiently large sections of thin film. A drop of glass was formed by heating one end of the tube in a burner and then puffed into a large bubble with walls having a thickness of a few microns. As usual, the thinnest section of the film formed at the end of the bubble. A hole was melted in the bubble by a fine point flame, and then, while continuing to blow into the tube (to prevent collapse of the bubble and curling up of the film), pieces of the finer film were broken off by means of tweezers introduced through the hole. Only the thinnest interferometric sections were used in the measurements.

Despite their minimal thickness ($\sim 1\ \mu$) such films are extremely fragile and the least breath of air causes them to flutter and break. If one film chances to come into contact with another piece, they commonly adhere so strongly that it is virtually impossible to separate them. Hence for purposes of measurements the films were mounted on special holder rings of 47-N-5KhB alloy whose thermal expansion coefficient is close to that of the No.23 and BD-1 glasses.

Good results were also obtained in using rings with a platinum wire rim, mounted at a distance of 2.5 mm from a nickel base. The films were attached to the mounts in a muffle furnace at a temperature of $\sim 650^{\circ}$. Once sealed to the holder the films were sufficiently strong to be readily mounted in the measuring tube. In some cases we were able to interchange the mounted films and reuse the same film a number of times.

Experimental equipment and procedure

A diagram of the tube used in performing the measurements is shown in Fig.1. In the center of the spherical section we have a glass diaphragm with an opening designed to receive the test film in its mount. The experimental tubes had no demountable joints but were completely sealed. The branch tube had to be opened for removing and inserting the sample films. The Faraday cup had to be lifted off its suspending hooks for installation of a film; after which the Faraday cup was replaced and the branch tube resealed. Both hemispheres of the experimental tube were coated with gold on the inside.

The design of the electron gun provided for rapid replacement of the cathode heater and cathode electrode, which allowed of varying the diameter

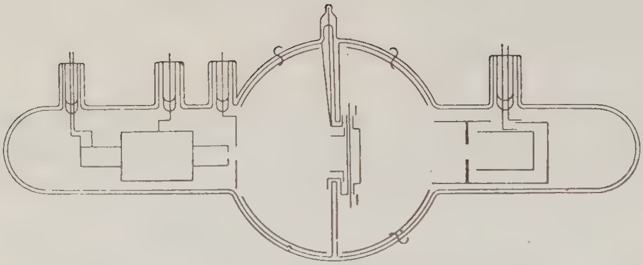

Fig.1. Experimental tube used in investigating the passage of electrons through the glass films.

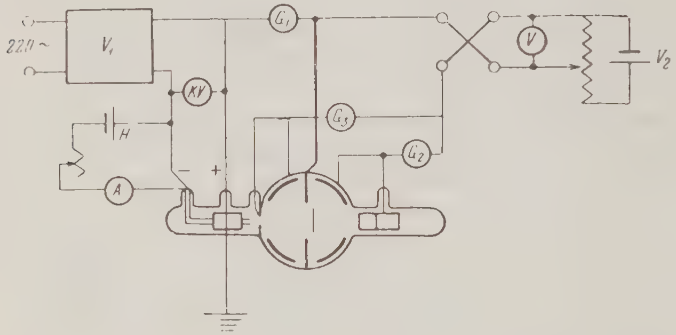

Fig.2. Diagram of the experimental set-up.

of the electron beam from 1 to 7 mm at the film surface.

The frame holding the film could be moved by means of an electromagnet, which was supplied with alternating current to obviate magnetization of the nickel components. Thus the test film could be moved over the opening in the central diaphragm, i.e., into the path of the primary electrons, or shifted to the side so that the primary electrons were free to pass into the other half of the tube.

All the measurements were performed with the tube being continuously pumped; a vacuum of 10^{-6} mm Hg was maintained with the heater of the electron gun in operation.

A circuit diagram of the set-up is shown in Fig. 2. Here V_1 is a rectifier yielding an accelerating potential of up to 30 kv, V_2 is a battery supplying a voltage of up to 150 v on the collector and H is the film and heater battery.

During the measurements the gun anode was grounded. The primary electron current could be determined in two ways: from the indications of galvanometer G_1 or from the indications of galvanometer G_2 with the opening in the diaphragm open, i.e., with the film moved out of the way. The galvanometer G_3 indicated the number of electrons reflected from the film and collected in the front (left) hemisphere. As will be evident from the circuit diagram, both hemispheres were at the same potential. The Faraday cup served for measuring the distribution in energy of the electrons that passed through the film without appreciable scattering. The current-voltage curves for the entire electron flux passing through the film were determined from the current in the back (right in the figure) hemisphere with the Faraday cup connected to it; in this case the Faraday cup served as an auxiliary electrode.

The films were not cleaned in any way prior to installation in the tube. In preparing the films, however, we took appropriate measures to insure a clean surface and the prepared films were stored in tightly covered dust-free containers.

Experimental results and discussion

The thickness of the investigated film was determined by weighing either before measurement, using a piece of film broken off the edge of the selected section before attaching it to the ring holder, or after measurement, using a piece of the actually tested film. The thickness of the film was found as d = P/gs, where P is the weight, s is the area and g is the specific gravity of the glass of which the film is made. Measurements of the specific gravity of the types of glass used in the experiment yielded average values of g = = 2.55 for the No.23 glass and g = 2.51 for the BD-1 glass.

The accuracy of determining obviously depended on the accuracy of weighing the film and measuring its area. The uncertainty in the case of both measurements was approximately 3% so that in most cases the thickness of the film was determined to within 10%.

In the course of the measurements we also considered the effects connected with the influence of the electrons incident on the film and the charge built-up on the film.

The electron transmission curve for a No.23 glass film 1.3 μ thick is shown in Fig.3. Prior to the measurements, the tube of the film was degassed at 380° for 1 hour. Measurements were performed with a primary electron current $i_1 = 5 \cdot 10^{-8}$ amp. The diameter of the beam at the film was 7 mm. The horizontal axis is scaled in terms of the voltage applied to the anode, i.e., the electron velocity in kilovolts; the vertical axis, in terms of the transmission coefficient $\eta = i_2/i_1$, where i_2 is the electron flux passing through the film and i_1 is the electron flux incident on the film. The potential on the collector was +70 v.

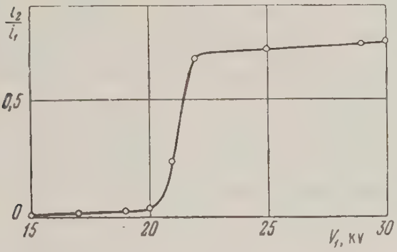

Fig.3. Electron transmission by a 1.3 μ thick film of BD-1 glass.

As will be evident from Fig.3, at values of V_1 less than 20 kv the transmission is small and amounts to only a few percent of the total number of electrons incident on the film. At a primary voltage above a certain critical value V_{cr}, the transmission is greatly increased and a large fraction of the primary electrons passes through the film. Measurements of the reflection of primary electrons from the film showed that at normal incidence ($\varphi = 0^\circ$) the number of reflected electrons is small and the major part of the loss is due to absorption of electrons by the film.

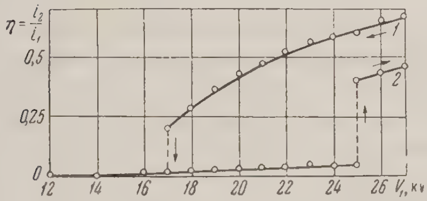

Fig.4. Electron transmission characteristics of a film of No.23 glass: 1) with decrease of the electron velocity V_1 and 2) with increase of V_1 ($d \approx 1$ μ).

The curve of Fig.3 was obtained while gradually decreasing the velocity of the primary electrons from 29 kv. Measurements performed while increasing the electron velocity yield a different curve. By way of illustration the transmission curves obtained for a 1 μ thick film of No.23 glass with increasing and decreasing voltage are shown in Fig.4. In this case a discontinuity in the rising voltage curve is observed at a primary electron voltage of 25 kv. Here, as in the case of many other measurement runs, when the voltage was increased to a value somewhat greater than V_{cr} the transmission coefficient η began to increase and in the course of a few minutes rose from 4 to 40% after which it remained constant (at the given value of V_1).

Further increase of the primary voltage led to continued increase of the transmission coefficient. It should be noted that the decreasing voltage curve 1 was obtained first; as the voltage was decreased from the initial high value the coefficient monotonically fell off down to 17 kv, where the coefficient dropped abruptly almost to zero.

Thus the electron transmission curves for glass films exhibit a distinctive kind of hysteresis, namely, when the primary voltage is increased there is observed a sudden rise of the transmission coefficient at a value of V_1 appreciably higher than that at which the coefficient drops as the primary voltage is decreased.

A similar hysteresis effect was observed by Owen & Cook[1] in the case of Zapon foils. This effect is closely associated with another experimentally observed phenomenon: the dependence of the transmission coefficient on previous electron bombardment of the film. In general, our experiments showed that the transmission coefficient η was greater if the film was previously exposed to the influence of electrons of energy greater than V_{cr} and, on the contrary, η was lower if the film was previously bombarded with electrons of less than V_{cr} energy. This explains the difference between the values of η for curves 1 and 2 in Fig.4 in the 25 to 28 kv interval. Prior to the measurements characterized by curve 1, the glass film was irradiated for some time by electrons of 27 kv energy, while before the measurements characterized by curve 2, it was bombarded for some time by 12-14 kv electrons; this preliminary treatment is responsible for the difference between values of η in the region of high electron velocities.

In most cases, however, the influence of preliminary bombardment of the film is not as clearly evident as in Fig.4; nevertheless, the effect is always present and should be taken into account in comparing the results of different series of measurements.

An effect analogous in principle - increase of the conductivity under the influence of light, electron bombardment or current - has been observed for a number of other dielectrics and semiconductors. There are a number of reports[2-4] in the literature devoted to investigations of bombardment induced conductivity.

We also found that the shape of the η vs V_1 curve is influenced by the state of the film surface. Thus, for example, transmission measurements carried out on a film that was kept in the vacuum set-up for several days showed a monotonic increase of the transmission coefficient with increasing primary electron energy. Only after heating the evacuated tube containing the film at 380° for 1 hour and subsequent cooling was there observed a jump in the η vs V_1 curve. This effect must be attributed to the presence of condensed oil vapor on the film (presumably from the grease used in the valve connecting the measurement tube to the vacuum pump). Heating eliminated this oil film from the surface of the glass.

The position of the sharp rise in the transmission curve depends on the thickness of the film and on its conductivity. Fig.5 shows the transmission characteristics obtained for a film of No.23 glass with the electrons incident normal to the film ($\varphi = 0^\circ$) (curve 1) and with the beam incident at an angle somewhat greater than 45° (curve 2). Electrons incident on the film of thickness d at an angle φ travel a distance $l = d/\cos\varphi$ through the glass. For an angle of incidence of 45°, $l = 1.4$ d. As may be seen from curves 1 & 2 in Fig.5 this increase in the electron path length in the glass resulted in a proportional decrease in the transmission of electrons having an initial velocity greater than V_{cr} and a shift of the break in the curves (and, consequently, in the value of V_{cr}) to the side of higher energies.

It should be noted that for thinner films ($\sim 0.15\ \mu$) the hysteresis effect is much weaker and the transmission curves obtained with increasing or decreasing voltage lie considerably closer together.

Hysteresis of the $\eta = f(V_1)$ curves might have been expected in the light of current concepts concerning the mechanism of electron transmission through dielectric films.

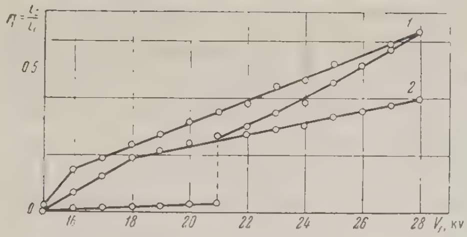

Fig.5. Transmission of the electrons through a film of No.23 glass: 1) electron beam incident at an angle $\varphi = 0^{\circ}$, 2) angle of incidence $\varphi = 45^{\circ}$.

The passage of electrons through matter in the region of energies above 10 kv can be described by the Widdington-Bethe formula

$$W_0^2 - W^2 = bd,$$

where W_0 is the initial (primary) electron energy, W is the energy of electrons after passage through the layer of thickness d, and b is a constant dependent on the material.

If the thickness d of the film is such that the electrons have just enough energy to traverse it, the emerging electrons will have zero energy. With increasing initial energy, the emerging electrons will possess a certain energy and the number of emergent electrons will increase inasmuch as additional electrons that have lost more than the minimal energy will be able to emerge. Actually, the position of the discontinuity in the transmission characteristics, i.e., the value of V_{cr}, does not indicate the energy just sufficient for traversing the film. Thus in the case of incidence on the film of a beam of electrons of energy less than V_{cr} the electrons, being unable to traverse the layer, will be absorbed by it and owing to the low conductivity of the film will accumulate in it. The magnitude and polarity of the accumulated charge will depend on the velocity of the primary electrons, the coefficient of secondary emission and the electric conductivity of the layer. Thus at a value of V_1 corresponding to $\delta > 1$, as a result of emission, there will develop on the surface a positive charge and in the limiting case the bombarded section of the film may attain a potential somewhat greater than the collector potential. At a value of V_1 corresponding to $\delta < 1$, there will build up on the surface a negative charge and the potential of the bombarded section may build up to the potential of the electron gun cathode. Then with increasing primary energy the electrons will be slowed down by the retarding field due to the negative charge and, consequently, passage of the electrons through the film and hence the abrupt rise in the η vs V_1 curve will occur at a value of $V_1 > V_{cr}$, inasmuch as part of the electron energy will be expended on overcoming the retarding field.

In contrast, when measurements of η are started at a high energy, the primary electrons do not have to lose energy on overcoming the negative charge in their path and hence the η vs V_1 curve will lie higher than in the former case. Moreover, in view of the observed variation of η with time of bombardment by fast electrons, it may be inferred that passage of electrons through the film produces favorable conditions for the passage of subsequent electrons; hence with decreasing velocity of the primary electrons the abrupt decrease of η, i.e., the discontinuity in the transmission curve, occurs not at V_{cr} but at a somewhat lower primary energy.

A certain fraction of the electrons passes through the film even when the energy of the beam is appreciably lower than V_{cr}. The number of such electrons is not great and they are not scattered electrons or primary electrons that have slipped through defects in the film. Their appearance does not contradict the Widdington-Bethe law according to which in the absence of charges a glass film 1 μ thick should be transparent to electrons of energy greater than 7 kev.

As was noted above, reflection of primary electrons from the surface of a glass film is small, amounting to only a few percent of the primary flux. Curves 1 & 2 is Fig.6 characterize the electron transmission and reflection by a glass film as a function of the primary energy. The variation of the primary voltage is indicated by the arrow. The measurements were made with the electron beam incident normal to the surface ($\varphi = 0^{\circ}$).

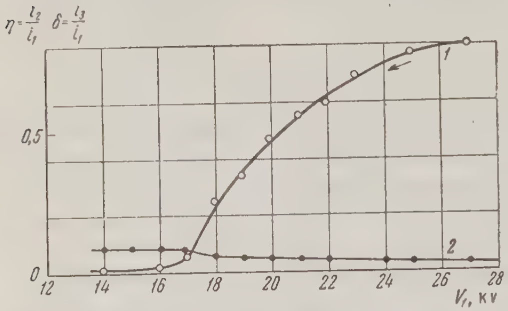

Fig.6. Transmission and reflection of electrons by a glass film: 1) transmission η and 2) reflection δ.

It is interesting to note that the reflection coefficient δ remains constant at primary energies up to 17 kv, decreases from 9 to 6% at 18 kv and then continues to decrease slowly to a value of 3% at 27 kv. The rapid reduction in the number of reflected electrons in the 17 to 18 kv interval is connected with the change in the number of electrons passing through the film, i.e., with increase of the transmission coefficient, the number of reflected electrons is somewhat reduced.

From these characteristics we can deduce some information regarding the state of films subjected to electron bombardment. Having the transmission and reflection curves, we can determine the absorption. We find that at primary beam energies less than V_{cr}, 90% of the incident electrons are absorbed by the film; the increase in the number of electrons passing through the film with increasing energy of the primary beam apparently occurs at the expense of electrons absorbed earlier by the film. Thus we have direct proof of the existence of a negative space charge in the glass film, inasmuch as absorption of an appreciable number of electrons by the dielectric cannot but lead to the formation of a space charge in it, for the presence of a large surface charge would lead to an increase in reflection, which is not observed.

Very important from the practical standpoint is the question of the velocity of the electrons penetrating a glass film. A current-voltage plot characterizing the electrons passing through a 1 μ thick film of BD-1 glass is shown in Fig.7. The primary electron energy in this experiment was 28 kv. The vertical axis is laid off in the number of electrons reaching the collector; the horizontal axis is scaled in values of the retarding potential V_2.

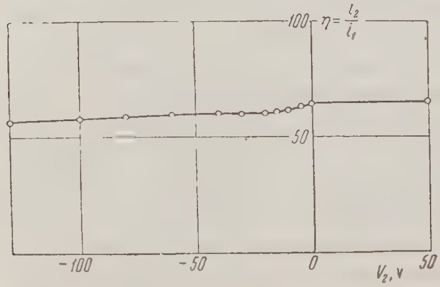

Fig.7. Retarding potential curve for electrons passing through a 1 μ thick film of BD-1 glass.

It will be seen that the $\eta = f(V_2)$ curve dips slightly at a potential of 10-20 v on the collector and then very slowly goes down with increasing V_2, which indicates that most of the electrons passing through the glass film still have a very appreciable energy. If we use the section of the current-voltage curve shown in Fig.7, we obtain upon differentiation of the curve only a very small maximum in the 0 to 20 v region. The number of slow electrons is very small: only 3% of the total number of electrons passing through the film have an energy of less than 5 ev, whereas ~90% of the electrons have an energy of over 150 ev. In other words,

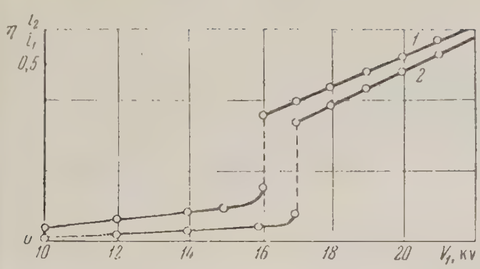

Fig.8. Transmission characteristics for a 0.85 μ thick film of BD-1 glass: 1) +65 v potential on collector and 2) -65 v on collector.

most of the electrons pass through a film of this type without appreciable loss of energy.

While fast electrons predominate in the transmitted component, the exact energy distribution varies somewhat with the velocity of the primary beam. The transmission curves for a 0.85 μ thick film of BD-1 glass are shown in Fig.8. Curve 1 was obtained with an electron collecting potential of +65 v; curve 2 with a retarding potential of -65 v on the collector. Thus from curves 1 & 2 we can determine the ratio between the number of electrons arriving at the collector with an accelerating and with a retarding potential for any energy of the primary beam from 10 to 21 kv.

It will be obvious from Fig.8 that there is a difference between the two curves both for primary energies lower than 17 kv and for energies above this value. In the lower energy range, changing from an accelerating to a retarding potential resulted in an almost parallel displacement of the curve over the entire interval from 10 to 16 kv, so that at 10 kv η fell to 0, while at other energies (up to 16 kv) the transmission coefficient was reduced to approximately 2/3 its initial value.

It follows that in the low energy region the flux of electrons passing through the film is made up primarily of slow electrons that have lost most of their energy in traversing the film. In contrast, in the high primary energy region the coefficient η decreased by only a relatively small amount as a result of change of the potential on the collector from +65 to -65, in accord with what has been said above regarding the energy distribution of the transmitted electrons. The curves very clearly indicate this change in relative energy distribution, i.e., the decrease in the relative number of slow electrons with increasing energy of the primary beam.

Thus at primary electron energies lower than V_{cr} only a small number of electrons passes through the film and these emerge with a low velocity. In contrast, at primary electron energies greater than V_{cr}, most of the electrons pass through the film and upon emerging retain a high velocity.

In order to check the validity of the Widdington-Bethe law for electrons passing through glass films, we evaluated the coefficient b in the formula

$$W_o^2 - W^2 = bd$$

from the beginning of the transmission curve, i.e., at a primary beam energy less than V_{cr}. Obviously, in view of the charging of the surface by the electron beam and the ensuing difficulties in determining the actual beginning of the transmission curve, one cannot expect exact agreement of the measured value of b with the calculated one. The divergence, however, turned out not to be excessive. Measurements yielded a value of $6.5 \cdot 10^{11}$ for b, whereas the calculated value for this type of glass is $5.2 \cdot 10^{11}$. This indicates that the Widdington-Bethe law is applicable to electrons in the 10 to 30 kv energy range passing through glass films.

All-Union Electrotechnical Institute

References

1. P.H.Owens & C.S.Cook, Phys.Rev., 86, 961 (1952).
2. M.M.Vudynskii, Zhur.eksp.i teor.fiz., 15, 187 (1945).
3. S.M.Ryvkin, B.M.Konovalenko & Iu.S.Smetannikova, Zhur.tekh.fiz., 24, 961 (1954).
4. F.Ausbacher & W.Ehrenberg, Proc.Phys.Soc., A,64, No.375, 362 (1951).
5. L.Pensak, Phys.Rev., 75, 472 (1949).
6. K.G.McKay, Phys.Rev., 74, 1606 (1948).
7. W.E.Spear, Proc.Phys.Soc., B68, N432, 991 (1955).
8. V.A.Arkhangel'skaia & A.M.Bonch-Bruevich, Doklady AN SSSR, 77, 229 (1951).
9. S.S.Anitov & M.S.Kosman, Zhur.eksp.i teor.fiz., 9, 1495 (1939).

SECONDARY ELECTRON EMISSION OF CESIUM-ANTIMONY EMITTERS "FROM THE BACK"

- A. I. Piatnitskii

Two types of experimental tubes were used for the measurements. The tubes of the first type had a glass diaphragm with an opening for the investigated film, sealed into the center of the glass sphere forming the body of the tube (see Fig.1 in Ref.1 - the preceding article). In the tubes of the second type, the application of antimony to the glass film and the formation of the cesium-antimony emitter were realized in a branch tube, after which the frame holding the film was moved to the center of the measuring tube by means of an external magnet. A general view of the second type of tube is given in Fig.1. All the measurements were carried out with continuous pumping at a vacuum of the order of 10^{-6} mm Hg. The measurements were made using the earlier described circuit (see Fig.2 in Ref.1) by means of which one could measure either the primary electron current i_1 passing through the film or the secondary electron current i_2 "from the back" and the current i_3 of reflected electrons. The tube was equipped with an exhaust stem by means of which it could be connected to or disconnected from the rest of the system without disturbing the vacuum.

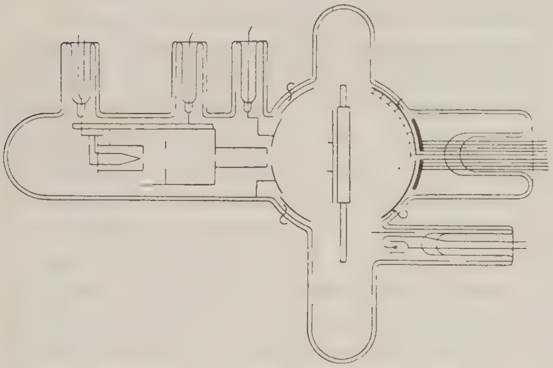

Fig.1. Tube for measuring secondary emission "from the back".

Experimental results and discussion

The antimony layers were applied to the surface of films of No.23 and BD-1 glass by evaporation of the metal from a tungsten spiral. The cesium-antimony emitters were prepared in the usual manner.

The results of the first measurements are shown in Fig.2. The electron transmission by a 0.15 μ thick film of BD-1 glass is characterized by curve 1. After measurement of the electron transmission, a layer of antimony was applied to the film and the transmission again measured (curve 2). Measurements after the application of a second antimony layer yielded curve 3. The total thickness of the antimony coating in this case was about 2000 Å.

After treatment of the antimony layer with cesium at 200° (to obtain a maximum photocurrent), we obtained curve 4 characterizing the transmission of electrons by the cesium-antimony layer.

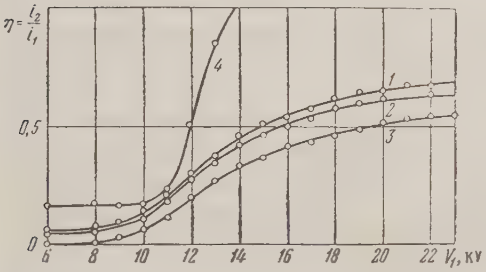

Fig.2. Transmission of electrons by a 0.15 μ thick film of BD-1 glass without and with a layer of antimony and secondary emission from the formed Cs-Sb emitter from the back: 1) bare glass film, 2) glass film with single layer of antimony, 3) glass film with double layer of antimony, 4) secondary emission from Cs-Sb emitter.

Obviously, more detailed information

could be obtained by measuring the transmission of electrons through a glass film with a cesium-antimony layer of varying thickness. Hence we prepared films of BD-1 glass mounted in a holder frame measuring 10 x 30 mm. The amount of antimony deposited on the film in preparing the emitter was calculated from the weight of the antimony pellet and the distance between the film and the vaporizer. The thickness of the glass film in this case was about 0.75 μ, while the thickness of the antimony "wedge" tapered from 0.2 to 0.01 μ. Before cesiation we measured the electron transmission of the bare glass film and the film with the antimony layer. Then the antimony film was cesiated to obtain a cesium-antimony emitter. The electron transmission characteristic of the glass film is shown by curve 1 in Fig.3. The general appearance of this curve is similar to that of curves obtained earlier. The value of the critical primary velocity V_{cr} is less than 12 kv. Curves 2 & 3 in Fig.3 show the transmission after application of the antimony layer. The measurements were made at a point 14 mm from the beginning of the film, i.e., at the point where the thickness of the antimony layer was about 0.03 μ. Curve 1 was obtained with a potential of +75 v on the collector; curve 3 was obtained with no voltage on the collector.

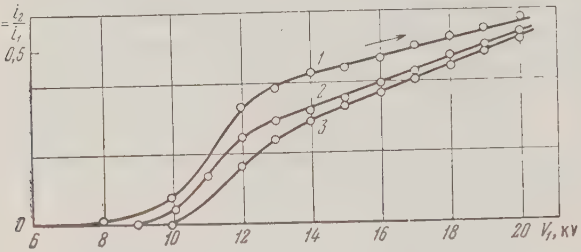

Fig.3. Transmission of electrons by a film of glass and the same film with a layer of antimony: 1) 0.75 μ thick film of BD-1 glass, 2) same film with a 0.03 μ thick layer of antimony; collector potential V_2 = +70 v, 3) same but with V_2 = 0.

It will be evident from a comparison of the curves that the reduction in transmission as a result of application of the antimony layer depends on the velocity of the primary electrons. The greatest decrease of the transmission coefficient η is observed at primary electron energies close to V_{cr}, i.e., 12-14 kv; with increasing primary velocity the relative decrease in the transmission coefficient becomes smaller and the transmission curves for the bare glass film and the film with a layer of antimony approach each other.

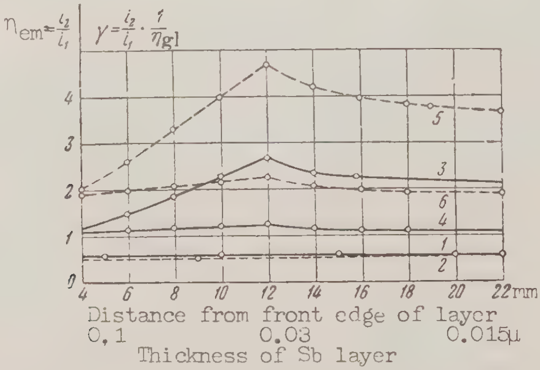

Fig.4. Variation of the secondary emission coefficient from the back of a Cs-Sb emitter as a function of the layer thickness: 1) transmission of electrons by the bare 0.75 μ thick film of BD-1 glass; primary electron energy 20 kv, 2) transmission of electrons by the glass film with a layer of antimony of varying thickness on it, 3) variation of the secondary emission coefficient $\eta_{em} = i_2/i_1$ of the Cs-Sb emitter with the layer thickness, 4) same for air poisoned emitter, 5) variation of the coefficient γ of the secondary emission from the Cs-Sb emitter with the layer thickness, 6) same for air poisoned emitter. $\eta_{em} = i_2/i_1$; $\gamma = (i_2/i_1)(1/\eta_{gl})$.

The difference between curves 2 and 3 shows the relative number of slow electrons comprised in the electron current characterized by curve 2. The proportion of slow electrons is very small in the region of primary velocities of the order of 20 kv and increases somewhat with decreasing primary energy. From a comparison of curves 2 and 3 in the region of primary velocities smaller than V_{cr} it becomes obvious (also see Fig.2) that the transmission is here composed mainly of slow electrons which are absorbed to an appreciable extent by the additional metal layer. The application of a thicker metal coating entirely cuts off the slow electrons that were initially able to pass through the bare glass film.

Curve 1 in Fig.4 shows the results of measurement of the electron transmission coefficient at different points across a 0.75 μ thick film of BD-1 glass subsequently used as the substrate for an antimony-cesium emitter. The measurements showed that the value of η is virtually constant and that the film itself is fairly uniform. Curve 2 shows the electron transmission at V_1 = 20 kv of the film with a tapering-thickness layer of antimony applied to it. As follows from curves 1 & 2, in agreement with the previous results, the decrease in the transmission coefficient as a result of application of the antimony layer is relatively small for electrons of 20 kv energy. Nevertheless, a certain decrease, roughly proportional to the thickness of the antimony layer, was observed in all the experiments. Curves 3 and 4 characterize the behavior of the cesium-antimony emitter prepared by cesiation of the tapering-thickness antimony layer. These curves were obtained at a primary electron energy V_1 = 20 kv and a potential V_2 = +75 v on the collector. Curve 3 pertains to a cesium-antimony emitter cesiated to a maximum value of the photocurrent and measured immediately after preparation. Curve 4 was obtained for the same emitter after prolonged exposure of the emitter to air in the set-up as a result of which it had almost completely lost its photosensitivity.

A significant feature of these characteristics is the maximum in the value of η observed at the point about 12 mm in from the front (thick) edge of the layer. At this point the thickness of the initial antimony layer was evaluated to be 0.04 μ, which is equivalent to approximately 140 atomic layers of Sb.

The decrease in the emission coefficient η in the region of small thicknesses is explained by incomplete utilization of the primary beam energy. As will be seen from what follows, this inference is substantiated by the somewhat larger number of fast electrons among the secondary electrons emerging from the thin emitter layer. In the case of relatively thick emitter layers, the thickness of which exceeds the optimal value, the secondary emission coefficient decreases due to absorption of secondary electrons in it. Consequently, the thickness of the emitter layer corresponding to the maximum in the curve determines the effective depth of secondary emission, i.e., the depth (in the case of ordinary emission) from which a secondary electron generated at this point with average initial energy is capable of overcoming the potential barrier and emerging from the emitter.

Finally, let us turn to curves 5 and 6 in Fig.4. These curves have been computed from the characteristics 3 and 4 so as to show the ratio of the secondary current to the current of the primary electrons passing through the bare glass film. Hereinafter we shall denote this ratio by $\gamma = (i_2/i_1)(1/\eta_{gl})$. (In contrast, curves 3 and 4 characterize the ratio of the number of secondary electrons to the number of primary electrons incident on the glass film, which we have been denoting by $\eta = i_2/i_1$.) Here η_{gl} is the coefficient of transmission of the bare glass film. Hence γ is the true coefficient of secondary emission "from the back". As may be seen from the curves it is relatively small and equals only 4.7 at the maximum.

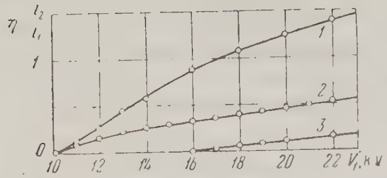

Fig.5. Secondary emission "from the back" of a cesium-antimony emitter as a function of the primary electron energy. BD-1 glass; thickness of glass film d_{gl} = 0.75 μ; thickness of initial antimony layer d_{Sb} = 0.1 μ. 1) collector potential V_2 = +70 v, 2) V_2 = 0 and 3) V_2 = -70 v.

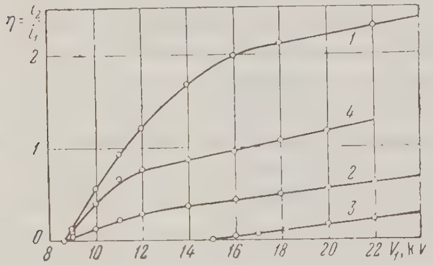

Fig.7. Same as Figs. 5 & 6 but for d_{Sb} = 0.015 μ. 1) V_2 = +70 v, 2) V_2 = 0, 3) V_2 = -70 v and 4) for an air poisoned emitter with V_2 = = +70 v.

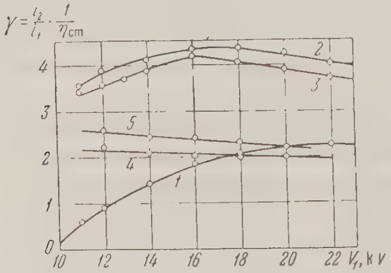

Fig.8. Variation of the coefficient γ of secondary emission from a Cs-Sb emitter as a function of the primary electron energy: 1) for an emitter with an initial Sb layer 1000 Å thick; 2) same for an initial 300 Å layer, 3) same for an initial 150 Å layer, 4) for an emitter with an initial 150 Å thick Sb layer poisoned by air, 5) same but for an initial 300 Å thick layer.

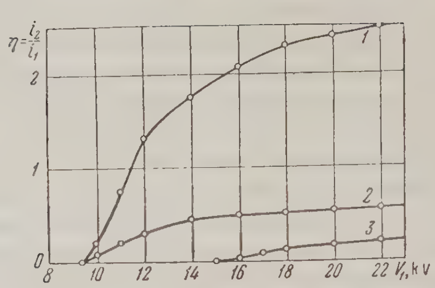

Fig.6. Same as Fig.5, but for d_{Sb} = = 0.03 μ. 1) V_2 = +70 v, 2) V_2 = 0 and 3) V_2 = -70 v.

Curves characterizing the variation of the total secondary emission coefficient η as a function of the primary electron energy V_1 for cesium antimony emitters are given in Figs.5,6 & 7. These curves were determined for points on the emitters located 6, 12 and 21 mm from the front (thick) edge of the layer. The thicknesses of the initial antimony layer applied to the 0.75 μ thick glass film were, respectively, about 0.1, 0.03 and 0.015 μ or about 350, 100 and 50 atomic layers of Sb. In comparing the curves of Figs.5,6 & 7 we note an appreciable difference in the values of η for different points of the tapering-thickness film, consistent with what has been said above in discussing the curves of Fig.4. This difference is due primarily to the number of slow electrons drawn out of the cathode by the accelerating field. The values of η given in Figs. 5,6 & 7 were determined as the ratio of the electron current from the Cs-Sb layer to the primary electron current incident on the glass film. If we take into account the transmission of primary electrons by the glass and recalculate the curves to obtain the ratio of the true secondary current to the current of primary electrons passing through the glass film, we obtain the characteristics that are shown in Fig.8.

Curves 1,2 and 3 in Fig.8 were obtained from curves 1 in Figs.5,6 & 7, respectively. All the curves exhibit maxima whose position varies with the thickness of the layer. Thus for the Cs-Sb emitter prepared by cesiating the

150 A thick antimony layer the secondary emission maximum was observed at a primary energy of about 16 kv, while the maximum for the layer having an initial thickness of 1000 Å lies at about 22 kv. Hence the secondary emission maximum is shifted to the side of higher primary energies approximately linearly with increasing layer thickness.

Curve 4 & 5 in Fig.8 characterize the secondary emission coefficients of emitters that were poisoned by air and virtually lost their sensitivity. Curve 4 was obtained from curve 4 in Fig.7. Curve 5 was obtained for the point of the Cs-Sb variable thickness layer close to the maximum of the $\gamma = f(d_{Sb})$ curve (d_{Sb} is the thickness of the initial antimony layer). Exposure of the emitter to air (poisoning) resulted in so great a leftward shift of the maxima in both curves (similar to the shift resulting from decrease in the layer thickness) that only the linear sections of the characteristics appear in the figure. The same tendency to linear variation is evinced by the characteristics 2 and 3 to the right side of the maximum.

The slow decrease in the number of secondary electrons after the current maximum may be due to a number of causes; these include a change in the conditions of excitation of the secondary electrons inside the emitter layer, in particular, a possible decrease in the probability of excitation with increasing primary electron energy. The apparent decrease may also be due to an increase in the fraction of fast electrons among the primaries passing through the glass film and into the Cs-Sb layer, inasmuch as increasing the velocity of the primary beam not only increases the number of electrons passing through the glass film but also alters the spectrum of the transmitted beam to some extent. The relative number of fast electrons among the secondaries must therefore increase with increasing energy of the primary beam; this is evidenced in the experimental results.

The relative number of fast secondary electrons emitted with different thicknesses of the Cs-Sb layer was determined by measuring the secondary emission coefficient with a retarding potential (-70 v) on the collector (curves 3 in Figs.5,6 & 7). Curves characterizing the ratio of the number of secondary electrons with an energy greater than 70 ev to the total number of secondary electrons are shown in Fig.9. Curves 1, 2 & 3 in Fig.9 pertain to points on the emitter having initial Sb layer thicknesses of 0.1, 0.03 and 0.015 μ, respectively. All the characteristics after the break exhibit a linear increase of the fraction of fast secondary electrons with increasing primary energy. The slope of these straightline plots depends on the thickness of the layer, the steepest slope being that for the thinnest emitter layer (curve 3). It must be noted, however, that the difference between the values of the ratio $\gamma_{+70}/\gamma_{-70}$ for layers of different thickness is not great, which substantiates our earlier inference that the difference in the value of the true secondary emission coefficient γ is determined primarily by the number of slow electrons.

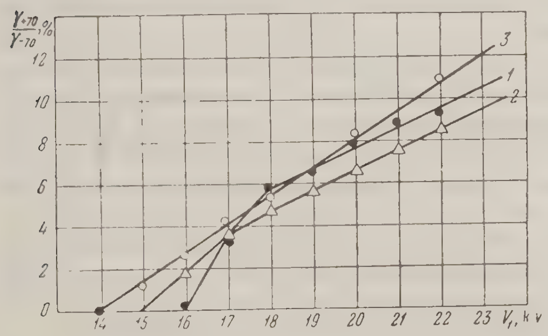

Fig.9. Relative number of secondary electrons with energy greater than 70 ev: 1) for an emitter prepared by cesiating an initial Sb layer 1000 Å thick, 2) same for a 300 Å layer, 3) same for a 150 Å layer.

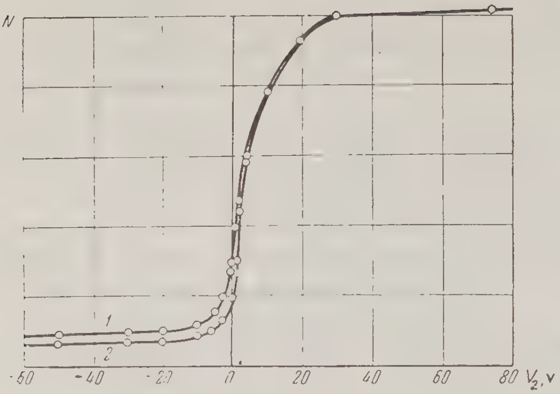

Fig.10. Retarding potential curves. Cs-Sb emitter on a 0.75 μ thick film of BD-1 glass. Primary electron energy 20 kv. V_2 = potential on collector; N = number of electrons: 1) for emitter prepared by cesiating an antimony layer having an initial thickness of 150 A, 2) same for a layer having an initial thickness of 300 A.

To get a clearer picture of the energy distribution of the electrons emerging from the emitter, we recorded the current-voltage characteristics (retarding potential curves) for the same emitter thicknesses. These characteristics are shown in Fig.10. Curve 1 pertains to an initial Sb thickness of 0.015 μ; curve 2 to an initial thickness of 0.03 μ. The curve for the point with an initial Sb thickness of 0.1 μ is not given here inasmuch as comparison of all the characteristics showed that they differed little. We only note that for a thin emitter layer, in agreement with the results described above, there is observed a somewhat larger fraction of fast electrons. All the curves show evidence of an appreciable group of electrons emerging from the layer under the influence of the collecting field and the points of saturation on these curves are shifted far into the region of positive values of the collector potential.

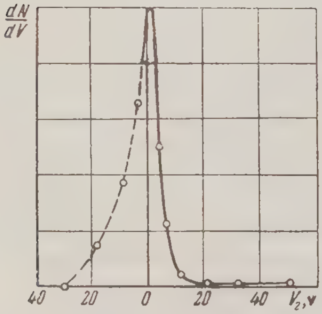

Fig.11. Energy distribution of the secondary electrons from an emitter produced by cesiation of an antimony layer 150 Å thick on a 75 A thick film of BD-1 glass. Primary electron energy V_1 = 20 kv.

It should be noted that in this case one can expect distortion of the shape of the current-voltage curves and a shift of the point of saturation to the side of positive collector potentials as a result of the influence of the resistance of the layer and other factors. Measurements of the current-voltage characteristics of a cesium-antimony layer carried out earlier[2] showed that under conditions of good contact of the Cs-Sb layer with the metallic base and a small amount of cesium, the shift of the saturation point in the current-voltage curve is very small and in individual cases altogether unnoticeable. A distinctive feature of the present experiment is that we had a Cs-Sb emitter with a high resistance deposited on a thin dielectric film, which can lead to "extension" of the current-voltage characteristics as has been demonstrated by Iasnopol'skii[4].

The distribution in energy of the secondary electrons is found by differentiation of the current-voltage curves. Fig.11 shows the distribution in energy of the secondaries for a Cs-Sb emitter prepared from an antimony layer having an initial thickness of 0.015 μ.

In view of what has been said above, the left side of the curve cannot be considered as reliably determined and is therefore shown by a dash line. The energy maximum for a layer of the given thickness (0.015 μ) lies at about 2 ev, while the maximum for a layer with an initial Sb thickness of 0.03 μ is shifted about 0.8 ev to the side of lower electron energies. From this it follows that the most probable energy of the electrons emerging "from the back"

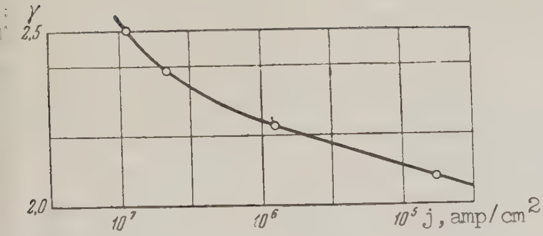

Fig.12. Influence of the primary electron current density on the magnitude of the secondary emission coefficient "from the back". Thickness of the initial antimony layer - 120 Å. Primary electron velocity V_1 = 20 kv; collector potential V_2 = +70 v. Coefficient of electron transmission by the glass η_{gl} = 0.57. Thickness of BD-1 glass film d_{gl} = 0.75 μ.

of a Cs-Sb emitter bombarded by a beam of 20 kv primary energy equals 1-2 ev, i.e., is of the same order of magnitude as in the case of "normal" secondary emission from a cesium-antimony emitter.

Pes'iatskii[4], who investigated secondary emission of metal films "from the back", also indicates that the distribution in energy of the secondary electrons emitted "from the back" of metal films is close to that observed in the case of ordinary secondary emission from metals.

The magnitude of the secondary emission from a Cs-Sb emitter "from the back" proves to be dependent on the current density of the primary beam. Fig.12 shows the results of measurements of the variation of the emission coefficient γ with the density of the primary electron current for a Cs-Sb emitter prepared from a 0.12 μ thick layer of antimony on a 0.75 μ thick glass film. It will be seen from the figure that for currents of the order of a microampere γ monotonically increases with decrease of the primary current density. Measurements carried out on a Cs-Sb emitter of different thickness gave a similar dependence of γ on the primary current density. This result is not connected with passage of the electrons through the glass film inasmuch as the transmission coefficient of glass films does not depend on the density of the primary beam in this current range; this was substantiated by control measurements.

It may be noted that measurements of the secondary emission coefficient δ as a function of the primary current density for oxygen-silver-cesium photocathodes, carried out some time ago by us[5], showed a similar variation of δ as a function of the current density. In the case of secondary emission from good magnesium emitters there is also observed a decrease of the secondary emission coefficient with increasing primary current density. It may be concluded, therefore, that this effect is common to all efficient emitters and is apparently connected with variation in the probability of excitation of secondary electrons.

The results of measurement of the angular distribution of secondary electrons emitted "from the back" will be discussed in detail in a separate article. Here we need only note that these measurements showed that the angular distribution depends substantially on the thickness of the Cs-Sb layer. In the case of thin layers, an appreciable number of secondary electrons is emitted in the direction perpendicular to the surface, while for thick layers most of the electrons, having undergone collisions in the emitter, emerge at different angles.

From a comparison of the characteristics of secondary emission with different layer thicknesses one can also draw certain deductions regarding the transfer of primary energy in the emitter. The primary electrons entering the emitter layer are slowed down and transfer part of their energy to the secondary electrons, with most of the secondary electrons being generated in the immediate proximity of the point of incidence of the primaries. As one goes deeper into the emitter, the number of primary electrons and their mean energy decrease rapidly. Thus with a primary beam energy of about 20 kv, after passing through a layer 150 Å thick (based on the thickness of the initial antimony layer) only about 8% of the electrons retain an energy greater than 150 ev, while after passage through a 300 Å layer only 5% of the electrons retain an energy greater than 150 ev.

From the experimental results one can approximately evaluate the energy loss of the secondary electrons. Measurements of the energy distribution for layers having an initial antimony thickness of 0.015 μ and 0.03 μ showed a difference of about 0.8 ev in the most probable energy of the secondaries. Inasmuch as in both cases the velocity of the primary electrons was the same, the difference was obviously due to the difference in energy loss through the thickness of the emitter. The secondary electrons emerging from a thin layer have a somewhat greater energy than electrons emerging from a thicker layer, for in the latter case the electrons expend a greater amount of energy in passing through the thicker layer. Dividing the difference between the energies at the maxima of the distribution curves by the difference in layer thickness, we obtain the energy loss over the given thickness difference. Here the actual thickness of the emitter layer becomes important. Above, in speaking of the layer thickness we gave its value in terms of the thickness of the initial antimony layer calculated from the weight of the antimony pellet, assuming the density of the layer to be equal to that of bulk Sb. This is not quite correct inasmuch as the density of a vacuum sputtered metal may differ as much as 25% from the density of the bulk metal. Furthermore in preparing the emitter an appreciable amount of cesium is introduced into the layer. Preliminary measurements of the coefficient of "swelling" of a Cs-Sb emitter showed that the actual thickness of a Cs-Sb emitter is approximately 2.5-3.5 times greater than the thickness of the initial antimony layer. Accepting this approximate value, we find that the energy loss of the secondary electrons is about 0.02 ev/mμ, which is close to the value of the loss obtained by Morgulis and Diatlovitskaia[6] for the secondary emission from Cs-Sb cathodes "from in front".

Above we noted the correlation between the effective depth of emergence of secondary electrons and the position of the maximum in the $\gamma = f(d)$ curve. The thickness of the antimony layer at the maximum was evaluated to be 400 Å. Assuming the thickness of the cesium-antimony layer to be approximately three times the initial thickness of the antimony, we obtain a value of the order of 1200 Å for the effective depth of secondary emission for Cs-Sb emitters, i.e., a value close to that obtained by Morgulis and his co-workers[7] for the secondary emission from Cs-Sb emitters "from in front".

The results of the work, apparently, corroborate the previously expressed view that (disregarding the influence of charge fields on the emergence of secondary electrons) the secondary emission of efficient emitters is determined primarily by the character of the secondary electron excitation processes in the emitter and to an appreciable extent by the ratio of the ranges of the primary and secondary electrons in the given material.

In conclusion I wish to acknowledge my indebtedness to P.V.Timofeev for suggesting the subject and constant interest in the work.

All-Union Electrotechnical Institute

References

1. A.I.Piatnitskii, Present issue of the Bulletin, p. 459.
2. A.I.Piatnitskii, Radiotekh.i elektronika (Radio engineering and electronics), 2, 714 (1957).
3. N.L.Iasnopol'skii, Zhur.tekh.fiz., 10, 1813 (1940).
4. N.F.Pes'iatskii, Zhur.tekh.fiz., 9, 188 (1939).
5. P.V.Timofeev & A.I.Piatnitskii, Zhur.tekh.fiz., 10, 1 (1940).
6. B.I.Diatloviskaia, Doklady AN SSSR, 53, 641 (1948); Zhur.tekh.fiz., 22, 84 (1952); N.D.Morgulis, Zhur.tekh.fiz., 9, 853 (1939).
7. N.D.Morgulis & N.G.Nakhodkin, Doklady AN SSSR, 94, 1029 (1954); N.D. Morgulis, P.G.Borziak & B.I.Diatlovitskaia, Izv.AN SSSR, Ser.fiz., 12, 126 (1948).

DISCUSSION

N.L.Iasnopol'skii: What portion of the electrons is transmitted?

A.I.Piatnitskii: That depends on the thickness of the glass film. With a thickness of 1 μ more than half of all the primary electrons having an energy of about 20 kv pass through the film.

N.D.Morgulis: What slowing-down law obtained in your experiments and how rapidly did the mean electron energy change with changes in thickness?

A.I.Piatnitskii: Slowing down was very abrupt. With a linear law we would have a larger number of secondary electrons emerging from the upper layers of the emitter. The mean energy of the secondary electrons changed by 0.8 ev in going from an initial antimony layer thickness of 150 to 300 Å.

P.G.Borziak: Slow electrons must still be reflected regardless of whether the charge is on the surface or in the depth of the film.

A.I.Piatnitskii: If the charge is in the depth, the reflection must be appreciably less.

Krasovskii: We also investigated the secondary emission "from the back" of a Sb-Cs_3 emitter, but in our case we used a metal base so that the complication due to charges did not arise. We did not observe a maximum in the $\sigma_{max} = f(d)$ curve, where d is the thickness of the Sb-Cs_3 emitter. We also established that with increasing thickness of the Sb-Cs_3 layer, the maximum in the secondary emission curve is displaced slightly to the side of greater accelerating potentials. Measuring the same areas of the emitter with regard to emission "from the back" and reflection we found 1) that the curves are similar and 2) that σ_{max} "from the back" is as a rule smaller than σ_{max} "from in front". This difference is explained by the fact that the primary spectrum is greatly extended. Hence in the case of "from the back" emission not all the electrons can participate with the same intensity in the formation of secondaries. It is not surprising therefore that in this case the secondary emission coefficient is smaller. The greatest secondary emission coefficient we obtained was ~7.

Bulletin of the Academy of Sciences of the USSR - Physical Series
Vol.22, No. 4

TABLE OF CONTENTS

Transactions of the All-Union Conference on the Physics of Dielectrics

	Page	
	Orig.	Trans.
Behavior of germanium-type valence crystals in a strong electric field - V.A.Chuenkov	363	363
Towards derivation of a criterion of electric breakdown of ionic crystals from the kinetic equation - V.A.Chuenkov	369	369
Polaron theory of breakdown of ionic dielectrics - Iu.I.Gorkun and K.B.Tolpygo	377	377
Electric strength of polyethylene at high frequencies - S.M.Bragin	387	389
On certain processes involved in the electric breakdown of solid dielectrics - A.A.Vorob'ev and G.A.Vorob'ev	392	394
Investigations of breakdown of rock salt containing color centers - A.A.Vorob'ev and G.A.Vorob'ev	397	399
Temperature dependence of the electric strength of KBr and KCl crystals - E.A.Konorova and L.A.Sorokina	401	403
Temperature dependence of the electric breakdown strength of ionic crystals - V.D.Kuchin	404	406
Temperature dependence of the pulse electric strength of certain polycrystalline dielectrics - E.A.Konorova, V.V.Krasnopevtsev and G.I.Skanavi	408	410
Oscillographic investigation of thermal breakdown of rock salt in DC fields - G.A.Andreev	415	418
Impulse breakdown of thick layers of ice - A.V.Astafurov	419	422
On the discharge delay time in ionic crystals - K.K.Sonchik	423	426
Electric breakdown of a titanium ceramic having a dielectric constant of 80 - I.E.Balygin	427	429
Some regularities of electric breakdown of liquid dielectrics - I.E.Balygin	433	435

Transactions of the Eighth Conference on Cathode Electronics

Reflection of electrons and secondary electron emission from some metal surfaces at low primary electron energies - I.M.Bronshtein	441	442
Investigation of the structure and properties of Ge, Cr and Bi films tapering in thickness in connection with their secondary emission characteristics - N.G.Nakhodkin and A.I.Novosel'skaia	448	449
Variation of the secondary emission coefficient of KCl with the layer thickness - N.G.Nakhodkin and V.A.Romanovskii	454	457
Passage of electrons through thin glass films - A.I.Piatnitskii	456	459
Secondary electron emission of cesium-antimony emitters "from the back" - A.I.Piatnitskii	464	467

Translated in 1959 by
Columbia Technical Translations
5 Vermont Ave., White Plains, N.Y.

TRANSACTIONS ON THE EIGHTH ALL UNION CONFERENCE ON CATHODE ELECTRONICS

(Continued from Vol.22, No.4)

From the Editorial Board

The Eighth All-Union Conference on Cathode Electronics, dedicated to the Fortieth Anniversary of the Great October Revolution, was held in Leningrad from the 17th to the 24th of October, 1957.

The Conference heard over one hundred reports presented at plenary and section meetings.

The publication of reports on secondary electron emission, photoelectron emission, field emission, photoconductivity and thermionic emission is being continued in the present issue (see Bulletin - Physical Series Vol.22, No.4). Part of the reports not appearing in the Bulletin will be published in Radiotekhnika elektronika (Radio Engineering and Electronics), No.8, 1958, Zhurnal technicheski fiziki (Journal of Technical Physics), No.7, 1958 and other journals.

INVESTIGATION OF DISCRETE ENERGY LOSSES OF ELECTRONS IN Mg, MgO, BeO and Ge

- N.B.Gornyi

Introduction

In recent years a number of investigators have reported observing discrete energy losses of slow (~100 ev) electrons in various solids: Cu_2O (Ref.1), Ni and Mo (Ref.2), MoO_2 (Ref.3), and GeO_2(Ref.4).

According to the theory of Viatskin[5], the energy losses, corresponding to the discrete loss peaks, can be explained by the fact that interaction of the incident electrons with the lattice electrons can lead to a transition of the latter from the filled band to higher levels in accord with the momentum selection rules. According to Viatskin's theory the transition energy is given by

$$W = \frac{h^2}{2m}\left(\frac{n}{d}\right)^2, \qquad (1)$$

where h is Planck's constant, m is the electron mass and $\left(\frac{n}{d}\right)^2$ is determined by the interplanar distance in the lattice of the given solid.

In applying Eq.(1), however, many discrete losses are identified with lattice planes for which the structure factor is zero; moreover, part of the discrete losses remain unexplained.

Our earlier experimental data[3,4] led us to conclude that the discrete electron energy losses are better described by the formula

$$W = \frac{h^2}{8m}\left(\frac{n}{d}\right)^2. \qquad (2)$$

Later we learned that Eq.(2) was independently derived by the Japanese physicist Hayasi.

According to Hayasi (see Ref.6), the discrete energy losses are explained by the fact that part of the energy of the incident electron is utilized for raising a lattice electron to "quasistationary" states and are described by Eq.(2).

Bohm & Pines[7] hypothesized that the discrete energy losses are due to excitation by the incident electrons of collective oscillations of the electron-gas plasma in the metal with a frequency

$$\omega_p = \sqrt{\frac{4\pi ne^2}{m}}, \qquad (3)$$

where n is the concentration of free electrons, e is the charge and m is the mass of a free electron.

For some metals (Mg, Al and Be) the theoretical value of the energy

$$W = \frac{h\omega_p}{2\pi} \qquad (4)$$

is in good agreement with the discrete energy losses of comparatively fast (~10^4 ev) electrons in passing through thin films. For a number of other substances, however, the observed discrete losses differ from the values calculated by means of Eq.(4).[8]

On the basis of the hypothesis of excitation of valence electrons accompanied by transitions to "quasistationary" states, Hayasi carried out calculations for the discrete energy losses of electrons incident to passage through thin films of nickel and copper.[9] The results of these calculations are in good agreement with the experimental data.

Later, Marton et al[6], comparing the discrete energy losses of electrons in several materials with the fine structure of the x-ray K absorption edge, found a correlation between the two phenomena. These authors are of the opinion that many of the discrete energy losses may be due to excitation of valence electrons to higher allowed energy levels.

Thus it must be assumed that there exist at least two possible mechanisms of electron energy loss in matter: one mechanism due to interband transitions; the other associated with excitation of collective oscillations of the electron plasma.

Apparently, one cannot resolve the question of the validity of the theory of single electron transitions or the theory of plasma oscillations simply by comparing the experimental values of the discrete energy losses with the loss values given by the respective theoretical equations. The difficulty stems from the fact that, on the one hand, the theoretical discrete loss values as obtained from both theories are close and, on the other hand, the experimental values obtained by different investigators with the same material differ to an appreciable extent. In view of this there has been obvious interest in experiments that would allow of determining the discrete loss mechanism in each particular case. Experiments of this type that led to substantiation of the plasma mechanism for certain discrete losses have been carried out by Watanabe[10], Gabor & Jull[11] and Jull[12].

Watanabe[10] found that for Be, Mg and Al some discrete energy loss values increase with increasing scattering angle. This increase is satisfactorily explained by the dispersion relationship of Bohm & Pines based on the plasma mechanism of discrete losses in metals. Investigations of the discrete losses in the passage of electrons through solid films of Au[11] and Al[12] and films with interlayers of an extraneous material also appear to favor the plasma mechanism. On the other hand, it is clearly desirable to carry out experiments that would allow of unambiguously resolving the question of discrete losses due to interband transitions. An experiment of this type would be parallel investigation of the discrete energy losses of incident electrons and the distribution in energy of true secondary electrons for some particular material. The presence among the true secondary electrons of a group of discrete energy values not varying with V_p and definitely correlated with the discrete loss values would furnish definite evidence of single electron excitation. We undertook an investigation of this type on Cu_2O.

Experimental data

In the present work we investigated the discrete losses of reflected electrons and the distribution in energy of true secondary electrons from Mg, Mo, BeO and Ge by the electric differentiation technique described earlier[13,14].

All the enumerated substances were investigated in separate sealed tubes. The magnesium and germanium layers were obtained by vacuum (10^{-7} mm Hg) evaporation in the experimental vessels.

The BeO layer was deposited on a beryllium plate 0.4 mm thick. The beryllium plate was thoroughly washed in hot soapy water, distilled water, ether and alcohol and then etched in concentrated nitric acid followed by washing in distilled water and alcohol. Next the plate was mounted in the vacuum apparatus and heated for a long time at $\sim 450^\circ$.

The MgO layer was obtained on a magnesium plate 0.5 mm thick. The magnesium plate was washed in the same way as the beryllium plate, then etched in 20% nitric acid and in a 15% solution of NaOH. Then the treated plate after careful washing was heated for a long time in vacuum at 350°.

The aging and outgassing of the apparatus has been described in Ref.13. The pressure in the bulbs before sealing off and flashing of the getter at 450° was lower than 10^{-6} mm Hg.

All the important measurements were made at night when the extraneous noise level was minimal.

Tests of the amplifying part of our circuit showed that in all the measurement ranges the amplification factor in each given range remained constant. The Earth's magnetic field was compensated by two 1 meter diameter coils.

The true secondary electron distribution in energy curves were not corrected for the contact difference of potential.

A. Magnesium

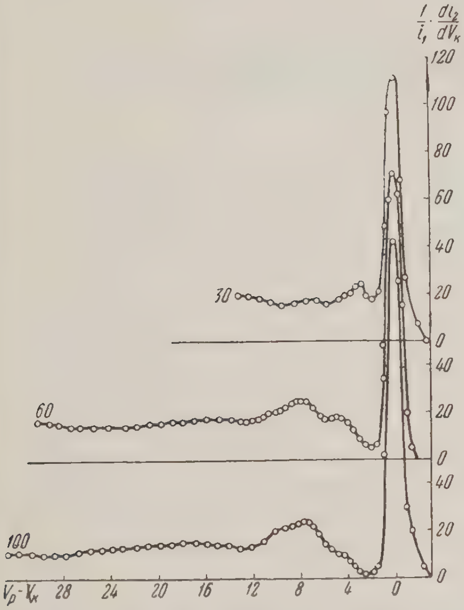

Fig.1. Distribution in energy curves of inelastically reflected electrons obtained for M_g at different values of V_p (indicated at the curves) at t = 20°.

The energy distribution curves for inelastically reflected electrons obtained for magnesium at room temperature are shown in Fig.1. It will be apparent that the discrete loss energy values do not depend on the energy of the incident electrons (except for the discrete losses with $V_p =$ = 30 v). It will also be evident from the figure that the intensity of the high energy discrete losses increases with increasing V_p.

The discrete loss energy values $V_p -$ $- V_k$ (V_k = collector voltage) obtained in our experiments are listed in column 1 of Table 1; the theoretical values of W calculated according to Eq.(2) are listed in column 3. For magnesium, which crystallizes in a hexagonal lattice,

$$\left(\frac{n}{d}\right)^2 = \frac{4}{3} \cdot \frac{h^2 + k^2 + hk}{a^2} + \frac{l}{c^2},$$

where a and c are the lattice constants.

The values of W were calculated for the Millerian indices h, k and l listed in column 2 of Table 1. The agreement of our experimental values of $V_p - V_k$ with the theoretical values of W is good. The theoretical values W = 14.7, 19.6, 20.2 and 22.2 ev, apparently, correspond to our wide experimental maximum extending from 14 to 23 ev.

In column 4 of Table 1 we list the fine structure peaks of the K absorption edge of Mg, taken from the table in Ref.6. Our experimental values of the discrete loss peaks agree much better with the fine structure absorption peaks than do the discrete loss values given in the literature for electrons of relatively high energies (Table 2). It must be noted, however, that the good agreement of our experimental data with the fine structure peaks does not appear convincing to us inasmuch as one of the absorption peaks is taken from the work of Sandström[15], while the other values are taken from the work of Munier et al[16]; the corresponding values of the peaks for Mg given in the two references are in rather poor agreement.

Table 1

Discrete energy losses in Mg

$(V_p - V_{k}, v)$,	(hkl)	W, ev	Peak in x-ray fine structure
1	2	3	4
4,5	100	4,9	
7,5	101	6,3	7,4
10,5	102	10,5	11,8
14—23	110	14,7	13,9
	200	19,6	17,9
	112	20,2	20,1
	004	22,2	23,3
25,5	202	25,2	27,9
31,5	203	32,1	33,4

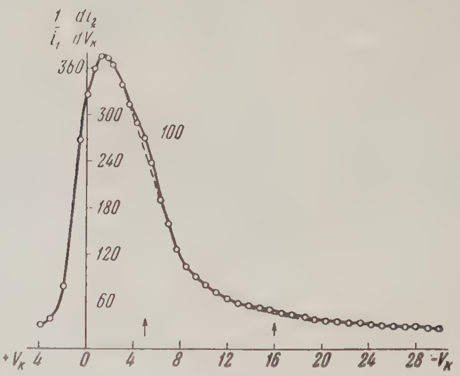

Fig.2. Energy distribution curve obtained for the true secondary electrons from Mg at V_p = 100 v and t = 20°.

Table 2

Values of discrete energy losses of electrons in Mg at high primary energies

Investigators	$(V_p - V_k)$, v						
Marton & Leder (18)			9,7		20,3		
Watanabe (19)			10,3		20,7		31,2
Jull (12)			10,0		20,3		
Blackstock, Ritchie and Birkhoff (20)			10,5		21,5		31,6
Kleinn (21)	4,7		10,3	19,0	22,1		
Our data	4,5	7,5	10,5	14—23		25,5	31,5

In order to make sure that the discrete loss mechanism observed by us is connected with interband electron transitions, we investigated the energy distribution of the true secondary electrons. The experimental energy distribution curve is shown in Fig.2. It will be seen that in addition to the principal maximum there are two bulges (see arrows) in the curve indicating the presence of two additional groups of true secondary electrons with discrete energy values of about 5 and 16 ev. Inasmuch as the true secondary electron group peaks appear against the strong background of the continuous spectrum of secondary electrons, the discrete structure of the true secondary electron spectrum naturally stands out much less clearly than the discrete structure in the spectrum of inelastically reflected electrons. If we take the work function of magnesium to be 3.6 ev (from Ref.17), we obtain 8.6 and 19.6 ev for the energies of the two true secondary electron groups inside the metal. These values agree well with the mean values of the two groups of discrete energy losses observed at V_p = 100 v, namely 8 and 19 ev.

There have been several investigations of the discrete energy losses incident to passage of relatively high energy (~10^4 ev) electrons through magnesium films.[12,18-20] Kleinn[21] investigated the discrete energy losses in the reflection of electrons from the surface of magnesium. The discrete energy losses taken from Refs.12, 18, 19 & 20, listed in Table 2, show good agreement. The average values of the discrete losses are 10.3 and 21.1 ev. Only in the reflection experiments of Kleinn[21] was there obtained yet another discrete energy loss value (4.7 ev) close to the lowest value obtained by us (4.5 ev).

It is noteworthy that the highest discrete energy loss peak in our curve (7.5 v - Fig.1) was not observed in any of the listed investigations (Refs.12, 18-21).

Watanabe[10] from his investigation of the variation of the discrete losses with increasing scattering angle established that the mechanism of discrete losses with 10.3 ev energy is excitation of plasma oscillations.

Thus from analysis of all the available experimental material we come to the conclusion that in our investigations, carried out at low energies (~100 v) of the incident electrons, the discrete loss mechanism in magnesium is excitation of interband electron transitions. In contrast, at comparatively high (10^4 ev) electron energies, the discrete loss mechanism is, apparently, excitation of plasma oscillations.

B. Magnesium oxide

The distribution in energy curves for electrons inelastically reflected from MgO are shown in Fig.3. A number of discrete loss peaks are evident. At low values of V_p (30 v), the discrete loss peaks are shifted to the side of lower energies. With increasing energy of the incident electrons, the curves become smoother and the discrete energy peaks increasingly diffuse.

The experimental values of the discrete energy losses together with the values of W calculated by means of Eq.(2) are listed in Table 3. For MgO, which crystallizes in the face-centered cubic lattice,

$$\left(\frac{n}{d}\right)^2 = \frac{h^2 + k^2 + l^2}{a^2},$$

where h, k and l are the Millerian indices and a is the lattice constant. It will be seen that the agreement between the experimental values of $V_p - V_k$ and the calculated values of W is satisfactory.

It should be noted that for MgO with its face-centered cubic lattice the factor for the (210) and (411) planes is zero so that the corresponding values of W, namely, 10.7 and 12.8 v, should not be observed. Actually, however, we obtained discrete energy values of 10 and 13, reasonably close to the indicated values of W.

The distributions in energy of the true secondary electrons obtained by us for MgO are shown in Fig.4. In addition to the principal peak there are two bulges indicating the presence of two

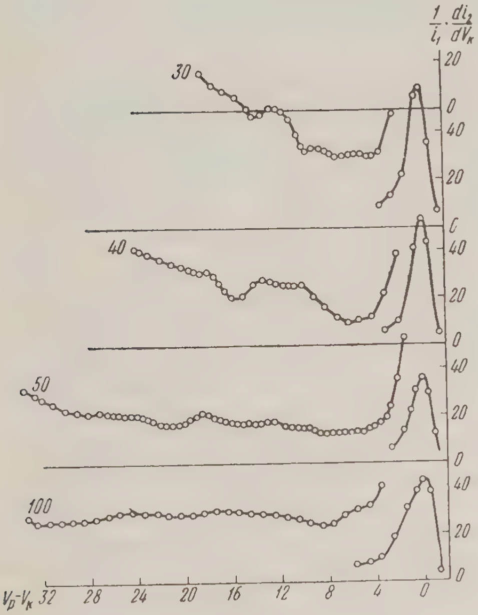

Fig.3. Distribution in energy curves for inelastically reflected electrons obtained for MgO at t = = 350°. The peak due to elastically scattered electrons is plotted to 1/4 the scale indicated for the other curves.

Table 3

Discrete energy losses of electrons in MgO

V_p, v	$(V_p - V_k)$, v						
30	5,0		8,5		12		
40	5,0	6,5		10	13	18,5	25
50							
100							
(hkl)		111	200	210	411	220	311 222
W, ev	—	6,42	8,56	10,7	12,8	17,1	23,5 25,7

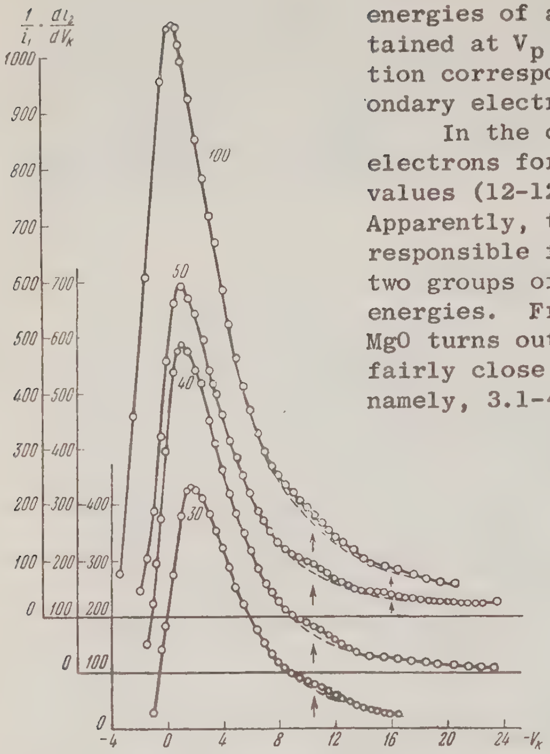

Fig.4. Energy distribution curves for true secondary electrons from MgO obtained at t = 350°.

discrete groups of true secondary electrons with energies of about 10 and 16 ev. In the curves obtained at V_p = 40 and 30 v there is only one inflection corresponding to a discrete group of true secondary electrons having an energy of ~10 ev.

In the curves of Fig.3 there are two groups of electrons for which the mean discrete energy loss values (12-12.5 and 18-18.5 ev) also differ by 6 ev. Apparently, these two groups of discrete losses are responsible for the appearance of the above mentioned two groups of true secondary electrons with discrete energies. From the above, the work function $e\varphi$ for MgO turns out to be approximately 2.5 ev, which is fairly close to the values given in Ref.17 for MgO, namely, 3.1-4.4 ev.

Rather interesting where the emission from MgO is concerned is the following fact. With increasing primary energy V_p, the peak associated with the first (~10 ev) group of true secondary electrons, which is clearly evident in all the curves of Fig.4, is displaced to the side of lower values. We did not observe this type of displacement for Mg. This decrease of the secondary electron energy for MgO, although not very great, is clearly noticeable. It can be explained as follows.

Our investigation of the secondary emission from the MgO sample showed an appreciable decrease of the secondary electron yield with increasing temperature and indicated that the secondary electrons on their way to the surface are subject to appreciable phonon drag. With increasing V_p the mean depth of origin of the secondary electrons increases and, consequently, so does the phonon drag loss for these secondary electrons in view of the fact that they must travel a greater distance from their point of origin to the surface. Hence the energy of the discrete group of secondary electrons must decrease with increasing V_p, which is what our experimental data show.

We must also note the increase in the width of the elastically scattered electron peak with increasing V_p (Fig.3); this is most noticeable at V_p = 100 v. Further, as has already been noted, with increasing V_p the discrete loss peaks in the curves of Fig.3 diffuse, the diffusion being greatest for V_p = 100 v. These two effects are apparently due to the same mechanism, namely, increase of the phonon drag for the part of the elastically and inelastically reflected electrons arriving from a greater depth as V_p is increased. These variations were not observed in the case of the curves obtained for magnesium (Fig.1). Thus on the basis of our experimental data we have come to the conclusion that phonon drag in MgO plays a significant role both where true secondary and reflected electrons are concerned.

To facilitate comparison of the data obtained by other investigators for MgO with our results, we list the discrete loss values of Refs.12, 22 & 23 in Table 4. We note that only Rudberg[23], who also used relatively low primary energies, observed a discrete loss with an energy value (17.5 v) close to

Table 4

Discrete energy losses of electrons in MgO at large values of V_p

Investigators	V_p	$(V_p - V_k)$, v					
Jull (12)	10 kv	5,0		12		22,5	
Watanabe (22)	16—24,5 kv	5,3		11,4		25	
Rudberg (23)	100—500 v		6,9	11,7	17,5	22,7	33,8
Our data	100 v	5,0	6,5	10 13	18,5	25	

that of the 18.5 v peak obtained by us. As regards the other discrete loss values, however, the data obtained by different investigators are in fairly good agreement.

Turning to the question of the mechanism responsible for the discrete losses, it must be noted that Wanatabe, on the basis of his investigation of the variation of the discrete losses with the scattering angle[10], came to the conclusion that the discrete losses in MgO at an energy of 11.4 ev are not due to excitation of plasma oscillations. Our data on the distribution in energy of secondary electrons indicate that the discrete losses with energies of 12 and 18.5 ev are associated with interband transitions.

C. Beryllium oxide

Table 5

Discrete energy losses of electrons in BeO

$V_p - V_k$, v	4	8			15,5 (12–19)	24,5
(hkl)	—	100	002	101	102	103
W, ev	—	7	7,92	9	14,9	25

The energy distribution curves for inelastically reflected electrons obtained for BeO are shown in Fig.5. In contrast to the case of the other investigated substances, the discrete loss values obtained for BeO do not vary with V_p, even down to $V_p = 30$ v. Our experimental values of $V_p - V_k$ and the values of W calculated according to Eq.(2) are listed Table 5. For BeO, which crystallizes in a hexagonal lattice,

$$\left(\frac{n}{d}\right)^2 = \frac{4}{3} \cdot \frac{h^2 + k^2 + hk}{a^2} + \frac{l^2}{c^2},$$

The values of W were calculated for the Millerian indices listed in the second line of the table. It will be seen that our experimental values are in good agreement with the calculated ones except for one, namely, $V_p - V_k = 4$ ev; for which there is no corresponding value of W.

The curve characterizing the distribution in energy of the true secondary electrons is shown in Fig.6. There are two bulges in this curve, indicating the presence of two groups of true secondary electrons with discrete energies of about 4 and 18.5 ev. Taking the value of the work function for BeO

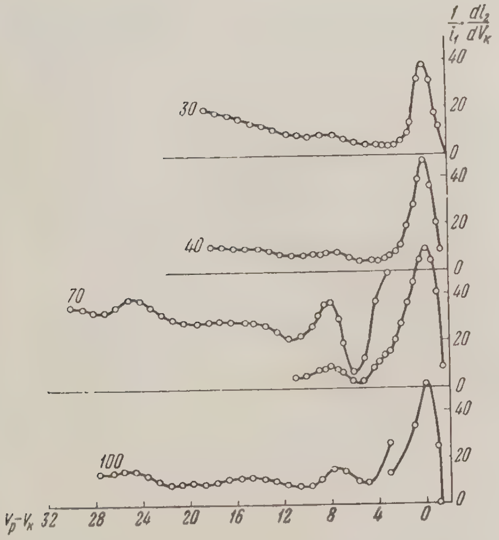

Fig.5. Energy distribution curves for inelastically reflected electrons obtained for BeO at t = 350°.

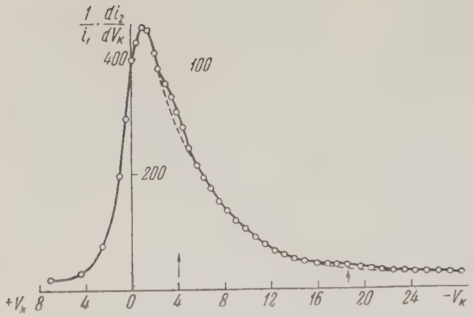

Fig.6. Distribution in energy of true secondary electrons from BeO at t = 350°.

as 3.8-4.7 ev (Ref.17), we obtain 7.8-8.7 ev and 22.3-23.2 ev for the energies of these electron groups inside the oxide. There values are in agreement with the values of the most intense discrete losses, namely, 8 and 24.5 ev (Fig.5). Hence we conclude that these discrete loss peaks are due to interband transitions.

In Table 6 we list for comparison the discrete energy values obtained by us and by other investigators[12,14] at high values of V_p. It will be seen that the values of $V_p - V_k$ obtained in other investigations are close to ours. Hence we infer that the discrete energy losses in BeO at high primary electron energies are due to the same mechanism (interband transitions) as in the case of low energies.

Table 6

Discrete energy losses of electrons in BeO at high values of V_p

Investigators	V_p	$(V_p - V_k)$, v			
Jull (12)	10kv	6,5		23	45
Watanabe (24)	22kv	5,7	16,5	28	57
Our data	100v	4,8	15,5	24,5	

D. Germanium*

The energy distribution curve for inelastically scattered electrons obtained for a vacuum evaporated layer of germanium is shown in Fig.7. It will be seen from the figure that the heights of the discrete loss peaks increase with increasing V_p but that the energy positions of the peaks remain unchanged.

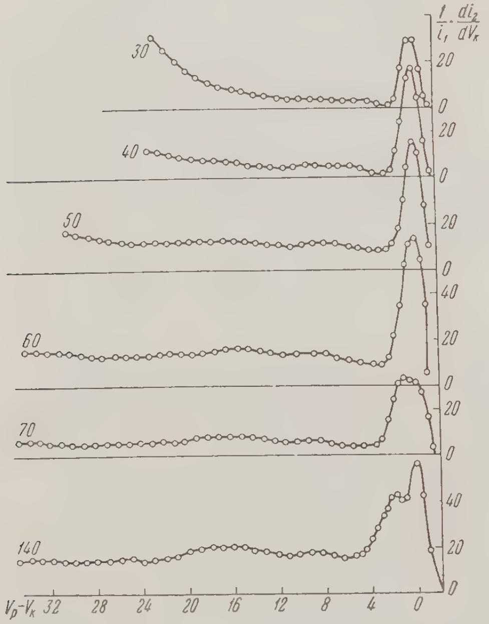

Fig.7. Energy distribution curves for inelastically scattered electrons obtained for Be at t = 350°.

A distinctive feature of the curves obtained for germanium, as compared with the curves for the other investigated substances, is the marked increase of the discrete loss at 2 ev with increasing primary voltage. The intensity of this discrete energy loss is greatest at $V_p = 70$ ev. On the other hand, at the lowest value of V_p used (30 v), the 2 ev discrete loss peak is not evident at all.

In the first line of Table 7 we list our experimental values for the discrete energy losses. In the third line we give the theoretical values of the discrete losses calculated for Ge (cubic lattice) by means of the formula

$$W = \frac{h^{2**}}{8m} \cdot \frac{h^2 + k^2 + l^2}{a^2}$$

---

*S.F.Skirko participated in the germanium measurements.

**Planck's constant.

Table 7

Discrete energy losses of electrons in Ge

$(V_p - V_k)$, v	2	4	9	16 (12–21)		25	32	
(hkl)	—	111	220	311	400	420	422	333
W, ev	—	3,6	9,6	13,2	19,2	24	28,7	32,3

for the Millerian indices listed in the second line of Table 7. The theoretical values W = 13.2 and 19.1 ev apparently correspond to the broad experimental peak extending from 12 to 21 v. As may be seen from the table, our experimental values of $V_p - V_k$ agree well with the theoretical values of W. It should be noted that there is no theoretical value corresponding to the $V_p - V_k = 2$ v peak.

A number of authors[25-27] have investigated the fine structure of the K absorption edge of germanium. Unfortunately, there is great divergence between the energy values reported for the fine structure peaks; hence it is impossible to make a satisfactory comparison of the discrete energy losses with the x-ray absorption data.

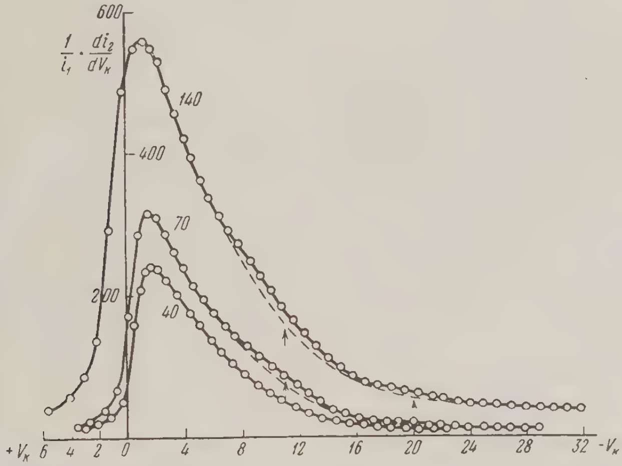

Fig.8. Energy distribution curves for true secondary electrons obtained for Ge at t = = 350°.

As in the case of the other investigated substances, in order to clarify the mechanism of discrete losses in Ge, we investigated the distribution in energy of the true secondary electrons. The resultant curves are shown in Fig.8. In the curves for V_p = 70 and 140 v there are bulges corresponding to a group of true secondary electrons with a discrete energy of 20 ev. If we take the work function of Ge to be 4.8 ev (Ref.28), we obtain a value of 24.8 ev for the electrons of this group in the germanium, which is very close to the energy of the fifth discrete loss peak - 25 ev (Fig.7). There is also evident an irregularity in the true secondary electron energy curves, i.e., a certain rise of the curves in the interval from 7 to 16 v (mean value ~11 v), which, apparently, corresponds to the group of inelastically reflected electrons with discrete losses in the range from 12 to 21 ev (maximum at about 16 v - Fig.7). Neither the bulge nor the irregularity is evident in the energy distribution curve obtained at V_p = 40 v.

Table 8

Discrete energy losses of electrons in Ge at high values of V_p

Investigators	V_p, kv	$(V_p - V_k)$, v				
Marton & Leder(18)	30			16,0		30,1
Watanabe (24)	22			16,4		33,8
Our data		4	9	16	25	32

In Table 8 we list the discrete energy values obtained for Ge by other investigators at relatively high values of V_p together with our data. It will be seen that our loss values of 16 and 32 ev are in good agreement with the corresponding energies reported by Marton & Leder[18] and Watanabe[24]. The peaks found by us at 4.9 and 25 ev were not observed in the work of Sandström[15] and

Watanabe[22]. The existence of true secondary electron groups with energies corresponding to the discrete losses of 16 and 25 ev indicate that these losses may be attributed to the interband transition mechanism.

Conclusions

1. Our investigation of the discrete energy losses in the reflection of comparatively slow (~100 v) electrons and of the discrete groups of true secondary electrons from Mg, MgO, BeO and Ge showed that the discrete losses are due to interband transitions and are satisfactorily described by Eq.(2). With increasing incident electron energy the probability of high energy discrete losses increases.

2. We observed discrete losses with minimal energy values (3 ev for Mg, 5 ev for MgO, 4 ev for BeO and 2 ev for Ge) which are not satisfactorily described by Eq.(2). Presumably a different mechanism i.e., excitation of plasma oscillations is responsible for these discrete losses.

References

1. N.B.Gornyi, Zhur.eksp.i teor.fiz., 27, 649 (1954).
2. A.R.Shul'man & I.I.Farbshtein, Doklady AN SSSR, 104, 56 (1955).
3. V.N.Gornyi, Zhur.eksp.i teor.fiz., 31, 132 (1956).
4. N.B.Gornyi & A.Iu.Reitsakas, Zhur.eksp.i teor.fiz., 33, 571 (1957).
5. A.Ia.Viatskin, ibid., 20, 557 (1950).
6. L.B.Leder, H.Mendlowitz & L.Marton, Phys.Rev., 101, 1460 (1956).
7. D.Pines, Revs.Mod.Phys., 28, 184 (1956).
8. L.Marton, L.H.Leder & H.Mendlowitz, Advances in Electronics and Electron Physics, Vol.7, 183 (1955).
9. T.Hayasi, Sci.Repts.Tŏhoku Univ., 39, 1 (1955).
10. H.Watanabe, J.Phys.Soc.Japan, 11, 112 (1956).
11. D.Gabor & G.W.Jull, Nature, 176, 718 (1955).
12. G.W.Jull, Proc.Phys.Soc., 69, 1237 (1956).
13. N.B.Gornyi, Zhur.eksp.i teor.fiz., 27, 171 (1954).
14. N.B.Gornyi, ibid., 30, 160 (1956).
15. A.E.Sandström, Arkiv.Mat.Astron.Fysik, 23A, 1 (1942).
16. J.Munier, J.A.Bearden & C.H.Shaw, Phys.Rev., 58, 537 (1940).
17. B.M.Tsarev, Kontaktnaia raznost' potentsialov (Contact difference of potential), Moscow, 1955.
18. L.Marton & L.B.Leder, Phys.Rev., 94, 203 (1954).
19. H.Watanabe, J.Phys.Soc., Japan, 9, 1035 (1954).
20. A.M.Blackstock, R.H.Ritchie & R.D.Birknoff, Phys.Rev., 100, 1078 (1955).
21. W.Kleinn, Optik., 11, 226 (1954).
22. H.Watanabe, Phys.Rev., 95, 1684 (1954).
23. E.Rudberg, Proc.Roy.Soc.A, 127, 111 (1930).
24. H.Watanabe, J.Phys.Soc., Japan, 9, 920 (1954).
25. W.W.Beeman & H.Friedman, Phys.Rev., 56, 392 (1939).
26. H.Hulubei & J.Cauchois, Compt.rend.Acadm.sci. (Paris), 211, 316 (1940).
27. D.G.Doran & S.T.Stephenson, Phys.Rev., 105, 1156 (1957).
28. L.Apker, E.Taft & J.Dickey, Phys.Rev., 74, 1462 (1948).

SECONDARY ELECTRON EMISSION FROM ALKALI HALIDE SINGLE CRYSTALS AT LOW PRIMARY ENERGIES

- S.A.Fridrikhov & G.N.Goriacheva

Introduction

Investigation of the interaction of slow electrons with the surface of solids is obviously of scientific interest and practical utility. Whereas there have been notable advances in recent years in the study of the interaction of slow electrons with metallic surfaces,[1,2] one cannot say the same thing as regards semiconductors and, particularly, dielectrics.

Secondary emission from dielectrics at low primary energies has been investigated in the work of Hilsh[3], Krenzien[4], Maurer[5] and Jacobs & his coworkers[6]. All these investigators used sputtered films of alkali halide compounds.

In order to understand the true physical significance of the variation of σ as a function of E_p in the range of small values of E_p one must have data on the energy spectrum of the secondary electrons. Such data were not obtained in the listed investigations. Only Krenzien[4] attempted to separate the elastically reflected electrons from the total emission current; some of the retarding potential curves obtained by him, however, have peaks, which is evidence of the inadequacy of his technique. So far no one has investigated the shape of the σ vs E_p curve for a dielectric target in the form of a single crystal. It must also be noted that all the above-mentioned investigators bombarded their dielectric samples under static conditions and this could lead to distortion of the results both due to charging of the surface and because of the influence of the bombarding beam on the properties of the superficial layer.

The most dependable method of investigating secondary emission from dielectrics, that of single pulses developed by Shul'man and his colleagues[7], has so far not been used for investigating the emission from dielectrics at low primary energies. Hence the purpose of the present investigation was to fill in the blank spot in the literature as regards the secondary emission coefficients of single crystal dielectrics at low primary energies.

Experimental Procedure and Equipment

We used a set-up which allowed of investigating the secondary emission of single crystal dielectrics under the influence of low energy (3 to 50 ev) single and periodic voltage pulses. Inasmuch as we employed a spherical apparatus, in addition to obtaining the $\sigma = f(E_p)$ curves, we had the possibility of analyzing the energy distribution of the secondary electrons.

A diagram of the experimental set-up is shown in Fig.1. It is in general similar to the pulse measurement circuit developed and used by Shul'man et al[7-9]. In our experiments we used square pulses of 2 to 5 microsec duration. The Earth's magnetic field in the vicinity of the apparatus was compensated by means of a Helmholtz coil. The targets were freshly cleaned single crystal plates of NaCl, KCl, KBr and KI, having an area of 25 x 25 mm and a thickness of 1.0 to 0.3 mm, mounted on a nickel base.

The electron beam was directed perpendicularly to the (100) cleavage plane. The low energy beam was monitored by several procedures: 1) by observation of the spot on a willemite target in conjunction with after-acceleration, 2) by means of a split target and 3) by measuring the primary and difference currents upon deflection of the beam from the target by means of a magnetic coil. These

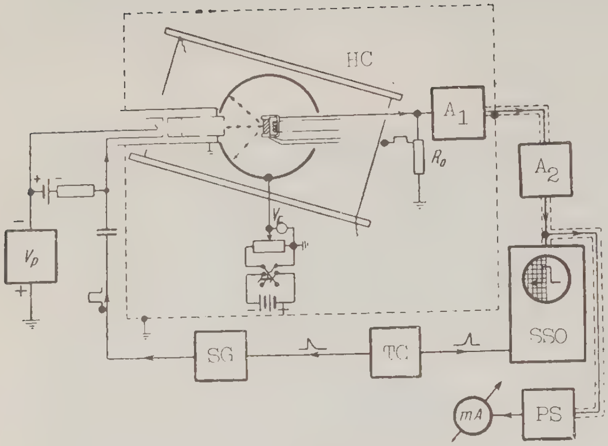

Fig.1. Diagram of experimental set-up: V_p - accelerating voltage source, TG - trigger generator, SG - square pulse generator, A_1 & A_2 - amplifiers, SSO - slave sweep 25-I oscillograph, PS - pulse stretcher, HC - Helmholtz coil.

measurements showed that the beam had a diameter of 5-8 mm in the plane of the target and that its position on the target did not vary significantly with changes in V_p and V_c in the entire measurement range.

The vacuum in the tube during measurements was $2\cdot10^{-7}$ mm Hg. Inasmuch as we worked with dielectric targets and in view of the fact that most of the measurements were made at relatively high (for the investigated substances) temperatures (300-400°)*, the indicated vacuum could be regarded as adequate. The values of the accelerating potential V_p were corrected for the cathode-target contact difference of potential.

The primary electron energy corrected for the target-cathode contact potential difference is hereinafter denoted by E_p. The contact difference of potential between the target and collector, which could be evaluated from the shift of the elastically scattered electron peak with reference to E_p, was negligibly small in our case. The accuracy of measurement in using periodic pulses was of the order of 3-5%. Most of the measurements were carried out at a pulse repetition rate of ~50 per sec.

Experimental Results

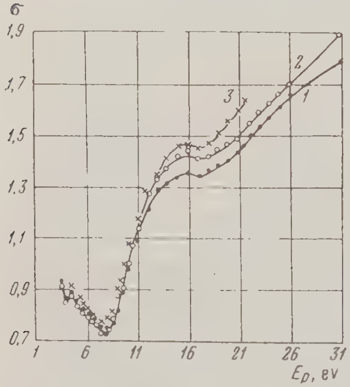

Fig.2. Variation of the secondary emission coefficient σ as a function of the primary electron energy E_p for NaCl single crystals. Curves 1 & 2 were obtained in successive measurements on the same crystal (No.1); curve 3 was obtained for a different crystal (No.2).

The $\sigma = f(E_p)$ curves obtained for artificially grown NaCl single crystals in the primary energy range from 3.5 to 31 ev are shown in Fig.2. It will be seen that there is good reproducibility of the readings for the same crystal (curves 1 & 2) and that going from one crystal to another does not result in any significant changes in the character of the curve (curve 3). It will be seen that the $\sigma = f(E_p)$ curve has a principal minimum at $E_p \approx 7$ ev and two auxilliary minima located at ~4 ev and ~17 ev. The value of σ increases most rapidly in the primary energy range from 8 to 11 ev.

Concurrently with the $\sigma = f(E_p)$ curves, we recorded the retarding potential curves for the secondary current i_2 at different values of E_p.

---

*In a series of special experiments we established that in the investigated primary energy range, going from room temperature to 300-400° does not involve any changes in the measured values exceeding the usual experimental error.

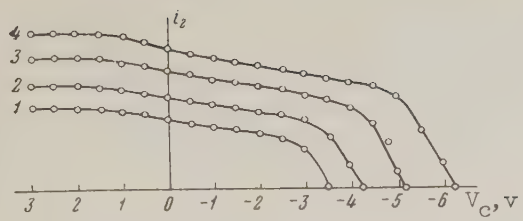

Fig.3. Secondary current retarding potential curves for an NaCl single crystal: 1) E_p = 3.5 ev, 2) 4 ev, 3) 5 ev abd 4) 6 ev.

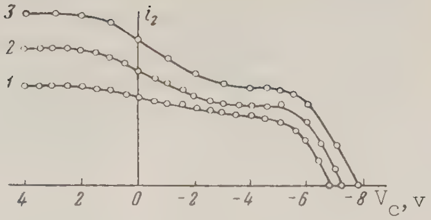

Fig.4. Retarding potential curves for NaCl single crystal: 1) E_p = 6.5 ev, 2) 7 ev and 3) 7.5 ev.

By way of illustration, the retarding potential curves obtained for an NaCl single crystal are reproduced in Figs.3 & 4. As may be seen from Fig.3, the retarding potential curves for low values of E_p initially have a fairly constant slope and then fall off rapidly. This falling off corresponds to stopping of elastically reflected electrons. Turning to Fig.4 we see that the curve recorded at E_p = 6.5 ev is similar to the curves shown in Fig.3. At E_p = 7 ev we note a change in the character of the retarding potential curves: there appears a dip in the curves in the region of low retarding potentials; this is presumably associated with a maximum in the distribution of slow true secondary electrons. It is noteworthy that the character of the secondary electron spectrum changes at precisely the value of E_p that corresponds to the beginning of the rapid growth of σ, following the principal minimum in the $\sigma = f(E_p)$ curve. The start of saturation of the retarding potential curves is shifted some 1.5-2 v to the side of positive collector potentials.

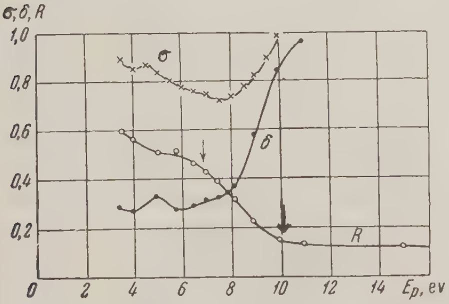

Fig.5. Variation of σ, δ and R as functions of the primary electron energy E_p for an NaCl single crystal. The interval between the arrows corresponds to the region of intrinsic optical absorption of NaCl.

Having the distribution in energy of the secondary electrons, we can resolve the $\sigma = f(E_p)$ curves into two curves: $R = f_1(E_p)$ and $\delta = f_2(E_p)$, where R is the coefficient of elastic deflection of the electrons and δ is the coefficient of emission of slow (inelastically reflected and true secondary) electrons.

The functional dependences of σ, δ and R on E_p in the primary energy range from 3 ev to 5 ev for an NaCl single crystal are shown in Fig.5. Here the arrows indicate the boundary of the interval of values of E_p corresponding to the region of intrinsic absorption of rock salt[10]. It will be seen from the curves that 1) a sharp increase in the value of δ begins at the energy corresponding to the long wavelength edge of the intrinsic absorption band of the crystal, i.e., at $E_p \approx 7$ ev (the peak of the exciton absorption band lies at about 7.8 ev), 2) the value of E_p at which $d\delta/dE_p$ is maximal lies between 8 and 10 ev, 3) an appreciable change in the reflection coefficient R (by about 35%) occurs in the rather narrow primary energy interval between 6 and 10 ev, corresponding to the region of intrinsic optical absorption of NaCl, 4) δ has an appreciable magnitude (at least 25% of σ) all the way down to $E_p \approx 3$ ev, and 5) there is a small increase in the value of δ at $E_p \approx 4$ ev.

In addition to artificially grown single crystals, we also investigated natural NaCl crystals; no significant difference was observed between the $\sigma = f(E_p)$ curves and the distribution in energy curves for the secondary electrons, except for the part of the $\sigma = f(E_p)$ curve lying to the left of the principal minimum, where, in addition to the persisting singularity at $E_p \approx 4$ ev, there appeared a new singularity at $E_p \approx 5$ ev (in the curves for natural crystals).

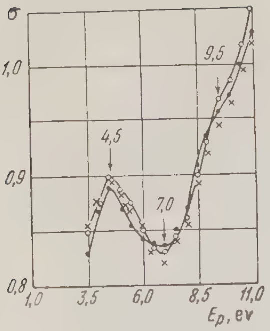

Fig.6. Results of repeated measurements of the variation of σ with E_p for KCl single crystals.

We also obtained $\sigma = f(E_p)$ curves and the secondary electron energy distribution curves for KCl, KBr and KI single crystals. The basic regularities obtained for these crystals are similar to those observed in the case of NaCl. Results of repeated measurements of σ for KCl single crystals in the primary electron energy range from 3.5 to 11 ev are shown in Fig.6. It will be seen that the reproducibility of the σ vs E_p curves is good.

The averaged σ vs E_p curves for all four types of investigated single crystals are shown in Fig.7. The arrows in the figure indicate the position of the long wavelength edge of the first intrinsic absorption band of the respective crystals[10]. It will be seen that in each case σ begins to rise rapidly at a value of E_p close to that identified by the arrows. The value of E_p at which $\sigma = 1$ is 10 ev for NaCl, KCl and KBr and 13 ev for KI. It is possible that there are singularities in the σ vs E_p curves for the investigated crystals in the energy region below 3.5 ev, but unfortunately our measurements did not extend into this region.

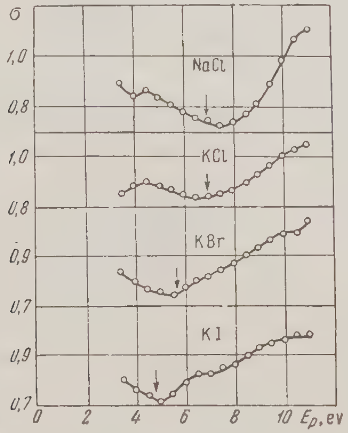

Fig. 7

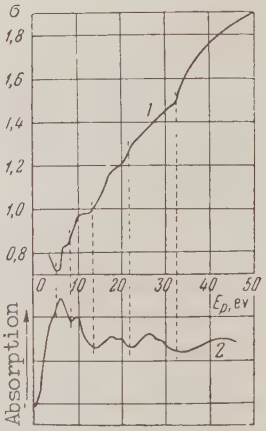

Fig.8

Fig.7. Variation of the secondary emission coefficient σ with the primary electron energy E_p for NaCl, KCl, KBr and KI single crystals. The arrows indicate the position of the long wavelength intrinsic optical absorption limit of the respective crystals.

Fig.8. Fine structure of $\sigma = f(E_p)$ (1) and the K absorption edge (2) of x-rays of KI. The absorption is given as a function of the energy reckoned from the K edge.

As in the case of NaCl single crystals, the character of the secondary electron spectrum for KCl, KBr and KI changes at values of E_p (hereinafter denoted by E_p^*) close to those indicated by the arrows in Fig.7.

The $\sigma = f(E_p)$ curves of the investigated alkali halide crystals also have a number of local irregularities, apparent up to the maximum values of E_p (~50 ev) utilized in our experiments. The character of the $\sigma = f(E_p)$ curves in this region is illustrated in Figs.2 and 8.

Discussion

1. Analysis of the $\sigma = f(E_p)$ curves and the secondary electron energy spectra indicates that there is a correlation between the primary energy E_p^* necessary for the appearance of a peak corresponding to slow true secondary electrons in the curves characterizing the distribution in energy of the secondaries and the position of the long wavelength optical (ultraviolet) absorption edge of alkali halide crystals. The value of σ corresponding to E_p^* is close to that at the principal minimum in the $\sigma = f(E_p)$ curve. Above E_p^* the coefficient σ (or more accurately δ) begins to increase rapidly. The accompanying table shows the variation in E_p^* with displacement of the first (exciton) intrinsic absorption peak (E_e) into the long wavelength region.

Substance	E_e, ev	E_p^*, ev
NaCl	7.8	7.0
KBr	6.5	6.0
KI	5.6	5.0

It will be seen that E_p^* is somewhat smaller than E_e, i.e., the sharp increase in the number of slow electrons in the secondary electron spectrum actually begins at primary energies approximately corresponding to the low-energy limit of the intrinsic absorption in the crystals. This result is reminiscent of the data obtained by Apker & Taft[11] on the photoemission of alkali halide compounds containing F-centers. It follows from the work of Apker & Taft that excitons produced in such substances, in moving through the crystal, can transfer some of their energy to F-center electrons which are then observed as photoelectrons. According to Dekker[12], a similar process can also occur in secondary emission from dielectrics if it is assumed that the primary electrons also produce excitons. Theoretically the production of excitons by the primary electron beam can be expected to occur particularly in crystals with strong exciton peaks, i.e., in alkali halide crystals.[10]

The results obtained in the present investigation apparently substantiate Dekker's hypothesis. It must be noted, however, that we investigated non-colored single crystals. In view of this, in order to explain the observed facts, one must assume the presence in the investigated crystals of a considerable number of defects. This assumption is in accord with the fact that at small values of E_p all the effects of interest occur in the thin superficial layer of the crystal, in which the number of defects may be very appreciable.

2. Analysis of the $\delta = f_2(E_p)$ curves shows that the sharpest increase of the slow electron emission coefficient δ, i.e., the position of the $d\delta/dE_p$ maximum, corresponds to a value of E_p equal approximately to the width ΔE_e of the forbidden band. Thus, for NaCl for which $\Delta E_e = 9.4$ ev, $d\delta/dE_p$ has a maximum at $E_p \approx 9$ ev (see Fig.5). Hence the principal contribution to the secondary emission, at least in the region of low primary energies, is made by electrons from the filled band of the crystal.

3. The small local rise of δ for NaCl and KCl crystals at $E_p \approx 4$ ev is apparently connected with the removal of electrons from some impurity or defect levels. In this connection one may recall the experiments of Tartakovskii[13] on the determination of the threshold of the external photoeffect in

NaCl. In these experiments the surface of an NaCl crystal was bombarded with slow (5-100 ev) electrons and then the threshold of the external photoeffect was determined. It was found that it lies at about 4.2 ev. Tartakovskii associates this value with the presence of surface states.

4. Fine structure of the $\sigma = f(E_p)$ curves for alkali halide compounds in the region lying to the right of the principal minimum has been observed earlier by Hilsh[3], Maurer[5] and Shul'man[14]. According to the data of Shul'man, the fine structure region extends to values of E_p of the order of several hundred electron volts. The question of the origin of this structure is still unclear. In considering the question it would be of obvious interest to compare the fluctuations of the secondary emission coefficient with data on the absorption of soft x-rays. Unfortunately the requisite data are not available in the literature. There is only information[15] on the fine structure of the K absorption edge connected with the transition of K shell electrons to some allowed states lying above the first unoccupied level. It has been shown experimentally that the energy intervals between the elements of this structure are approximately inversely proportional to the squares of the lattice constant. Theoretical analyses[16] of the fine structure of the K absorption edge lead to the same deduction.

Let us attempt to compare the regularities observed in the x-ray fine structure with the fine structure of the $\sigma = f(E_p)$ curves for alkali halide single crystals. It will be seen from the curves of Fig.8 that the distances between the minima in both cases are approximately the same and that consequently the singularities in the $\sigma = f(E_p)$ curves for different alkali halide crystals (as in the case of x-ray spectra) can be matched by introducing a normalizing factor $1/a^2$, where a is the lattice constant. Although the effects being compared differ as regards the nature of the causative agent and as regards the initial state of the lattice electrons, inasmuch as the transitions in both cases are related in a definite manner with the distribution in energy of the final states, the observed correspondence is probably not fortuitous. The fact that the fine structure of the $\sigma = f(E_p)$ curves is related in some way with the lattice constants gives reason to assume that this structure is connected with the periodic field of the crystal. It is interesting to note that regularities of the same nature are observed in the absorption of light in the visible and ultraviolet regions. Theoretical considerations[17] and numerous experimental facts indicate that the energy position E_F of the peak of the F-center absorption band in alkali halide crystals depends only on the lattice constant: in all alkali halide compounds the product $E_F a^2$ is a constant.

5. One of the interesting results of the present work is the observed character of the variation of the elastic reflection coefficient R with the primary electron energy. It follows from the curve for R in Fig.5 and from similar curves obtained for other alkali halide compounds that an appreciable change in R (amounting to 35-40%) occurs in a narrow interval (~4 ev) of primary energies and that this interval corresponds to the region of intrinsic optical absorption of the crystal. Thus we have detected a correlation between the optical and electronic absorption in alkali halide crystals. This is theoretically plausible in view of the fact that the electron affinity in such crystals is close to zero.

6. Finally, one should note two distinctive features of the experimental retarding potential curves, namely, 1) the steep slope of the curves at $E_p < E_p^*$ and 2) the leveling off (saturation) of the curves in the region of positive collector potentials of the order of 1.5-2 v.

As regards the slope of the retarding potential curves (continuous background in the distribution curves) at small primary energies, it may be assumed that it is due to inelastic scattering of slow primary electrons. Inasmuch as there are no free electrons in dielectrics, this scattering probably occurs as a result of interaction of primary electrons with phonons or lattice defects, for it is known that analogous processes occur in the case of slow secondary electrons.

The shift of saturation into the region of positive values of V_c cannot be explained either by the contact difference of potential or by charging of the surface in the usual sense. A possible explanation of this effect is the following: during bombardment of the dielectric, even during the brief time a single pulse, there forms a localized charge patch of irregular cross section; this leads to the appearance of a patch field that interferes with the normal removal of the slowest electrons. In order to compensate this field and extract the electrons one must apply to the spherical collector a positive potential greatly exceeding the potential of the charge patch.[18,19]

Conclusions

1. The present work was devoted to the investigation of the secondary emission from alkali halide single crystals at low primary electron energies. We used the pulse technique which made it possible to reduce to a minimum the effects connected with surface charges and variation in the properties of the target under bombardment.

2. We showed that true secondary electrons appear in appreciable amounts in the secondary spectrum at primary energies corresponding to the long wavelength limit of the first intrinsic absorption band of the crystals.

3. Starting with this energy the coefficient δ of emission of slow electrons increases sharply. The region of the steepest rise of δ corresponds to the interval between the first and second intrinsic absorption peaks.

4. We found that one can establish a correlation between the fine structure of the $\sigma = f(E_p)$ curves of alkali halide single crystals with the periodic field of the crystal lattice; by introducing the normalizing factor $1/a^2$, where a is the lattice constant, the singularities in the $\sigma = f(E_p)$ curves for the given class of substances can be brought into approximate alignment.

5. It was found that there is a correspondence between the intrinsic optical absorption and the electronic absorption of alkali halide crystals. This is further evidence that the electron affinity of such crystals is very small or zero.

The authors desire to express their deep gratitude to A.R.Shul'man for suggesting the subject, constant interest in the work, useful suggestions and helpful discussion.

"M.I.Kalinin" Leningrad Polytechnic Institute

References

1. A.R.Shul'man & E.I.Miakinin, Doklady AN SSSR, 91, 1075 (1953).
2. N.D.Morgulis & D.A.Gorodetskii, Zhur.eksp.i teor.fiz., 30, 4 (1956).
3. R.Hilsh, Z.Phys., 77, 427 (1932).
4. O.Krenzien, Wiss.Keroff a.d.Simens Werken, 20, 91 (1941).
5. G.Maurer, Z.Phys., 118, 122 (1941).
6. H.Jacobs, J.Martin & F.Brand, Phys.Rev., 85, 441 (1952).
7. A.R.Shul'man & V.L.Makedonskii, Zhur.tekh.fiz., 22, 1542 (1952).
8. A.R.Shul'man & B.P.Dement'ev, ibid., 25, 2256 (1955).
9. A.R.Shul'man, I.R.Zakirova, Iu.A.Morozov & S.A.Fridrikhov, Elektronika i radiotekhnika (Electronics and Radioengineering), 3, 3 (1958).

10. R.Hilsh & R.W.Pohl, Z.Phys., 59, 812 (1930); H.Fesefeldt, Z.Phys., 64, 623 (1930); E.G.Schneider & H.M.O'Bryan, Phys.Rev., 51, 293 (1937).
11. L.Apker & E.Taft, Phys.Rev., 82, 814 (1951).
12. A.J.Dekker, Physica, 22, 361 (1956).
13. P.S.Tartakovskii, Z.Phys., 58, 394 (1929).
14. A.R.Shul'man, Doklady AN SSSR, 20, 9 (1956).
15. G.A.Lindsay, Z.Phys., 71, 735 (1931); S.Kiyono, Sci.Rep.Tohoku Univ., 36, 1 (1952).
16. R.L.Kronig, Z.Phys., 70, 317 (1931); Ibid., 75, 191 (1932); T.Hayasi, Sci.Rep.Tohoku Univ., 33, 129 (1949); Ibid., 34, 185 (1950).
17. H.Fröhlich, Z.Phys., 80, 819 (1933).
18. V.Ia.Upatov, Elektronika i radiotekhnika (Electronics and Radioengineering), 2, 193 (1957).
19. I.R.Zakirova & S.A.Fridrikhov, Present issue of the Bulletin, p. 547.

DISCUSSION

N.D.Morgulis: What is the difference between the data for the artificial and natural crystals? Can this difference be used for determining impurities?

S.A.Fridrikhov: There is an additional singularity in the σ vs V_p curves for natural crystals at very low energies.

L.N.Dobretsov: What is the magnitude of your experimental errors?

S.A.Fridrikhov: From 3 to 5% for periodic pulses and about 10% with single pulses.

L.N.Dobretsov: In view of this uncertainty can you be sure of your minima?

S.A.Fridrikhov: Yes, I think one can in view of the good reproducibility of the curves.

L.N.Dobretsov: Were there singularities at energies close to the heat of dissociation?

S.A.Fridrikhov: We did not notice any.

A.Ia.Viatskii: Why did you carry out the comparison with data on hard x-rays?

A.S.Fridrikhov: There are no experimental data on the absorption of soft x-rays. The indication correlation would probably also obtain inasmuch as the final electron states are the same in both cases.

L.N.Rakhovich: Did you observe charging of the surface?

S.A.Fridrikhov: No, we did not.

SECONDARY EMISSION FROM THORIUM OXIDE ACTIVATED WITH BARIUM

- B.N.Popov and V.F.Koliverdov

Introduction

In recent years secondary emitters have found increasing application in different types of electronic devices: receiving and amplifying tubes, electron multipliers and microwave magnetrons.

The fundamental requirements set for magnetron emitters are the following:

1) The coefficient of secondary emission must be as high as possible; in any case not lower than 2.

2) The current density must be of the order of tens or hundreds of amperes per square centimeter.

3) The emitter should have a thermionic emission (at the operating temperatures) of the order of a microampere or more per square centimeter.

4) The emitter must have a sufficiently long life (in any case hundreds of hours) at the operating temperatures obtaining in the tube as a result of operation of the heater, electron back bombardment and flow of current[1]; the operating temperatures in actual magnetrons range between 700 and 1500°.

5) The emitter must be capable of withstanding severe electron and ion bombardment.

There are other subsidiary requirements which we shall not mention here inasmuch as they are not fundamental.

No emitters available now satisfy all the enumerated requirements. Hence an urgent research problem is the development of stable emitters capable of efficient operation under the conditions obtaining in magnetrons.

The most direct approach to solution of the problem is search for new compounds, in particular, oxides, possessing the necessary characteristics. Another approach consists in modifying the properties of present emitters by appropriate treatment.

To help clarify the means that might be used for obtaining better emitters let us review the general attributes of the energy structure of secondary emitters. All efficient secondary emitters are semiconductors or dielectrics with a rather wide energy gap. This wide forbidden band, as has been shown by de Baer[2] and Morgulis[3], is responsible for the small energy loss of the secondary electrons on their way from the point of origin to the surface. By virtue of this, the emergence of electrons from the depth of hundreds of atomic layers is possible in the case of semiconductors and dielectrics, whereas in the case of metals the depth of emergence does not exceed some tens of atomic layers.[4] These considerations largely define the class of substances capable of satisfying the first of the above listed requirements. It would seem that substances capable of meeting the second and third requirements must have a narrow energy gap. At first glance these requirements are contradictory. There is, however, a way of reconciling these contradictions. The concentration of conduction electrons necessary for meeting the second and third requirements can be obtained by creating a system of local levels in the forbidden zone. The requisite concentration of impurities, as is known from experiment, may be so small that it does not significantly reduce the secondary emission, while the conductivity of the emitter is sharply increased and the work function decreased. Appreciable increase of the number of conduction electrons in itself, however, cannot influence the magnitude of the secondary emission coefficient. Proof of this is the fact (for example, Ref.5) that the secondary emission coefficient is temperature independent in most semiconductors and dielectrics with impurities.

Tazulakhov[6] made an attempt to produce efficient emitters by holding the oxides of different metals in barium vapor at a certain pressure. The mechanism of the emitters produced by Tazulakhov has not, unfortunately, been fully investigated. The author attributes the enhanced emission primarily to a film of barium atoms on the surface of the oxide. It is also possible, however, that actually the barium atoms penetrate into the oxide lattice forming a new emitter. In any case the excellent results obtained by Tazulakhov merit attention and further study with a view to development, on this basis, of efficient and more convenient emitters capable of operating at higher temperatures (in practice one cannot continuously expose the emitter to barium vapor).

The purpose of the present research, therefore, was to develop an emitter of this type and clarify its operative mechanism.

The principal difficulty in realizing a high temperature emitter with impurities is that at high temperatures the concentration of local centers near the surface of the emitter rapidly decreases with time. In order to compensate for the loss one must continually replenish the supply of impurity atoms, i.e., prepare an emitter with a continuously renewing surface. We decided to provide for surface renewal on the principle of the porous metal cathode[7], utilizing flow of the activator through the sponge pores and its migration over the internal surfaces of the emitter.

By way of the basic material we chose thorium oxide inasmuch as this oxide has a high melting point and is therefore suitable for fabricating heat resistant emitters. At the same time the substance has already gained acceptance as a cathode material for magnetrons so that in choosing it we were dealing with a proven material that only needed further improvement (rather than with an entirely new untried substance).

Experimental Part

1. Experiments with a ceramic cathode with a supply of barium

The cathode in these experiments was a tube compacted of a mixture of powdered tungsten and thorium oxide and then sintered in hydrogen at 1700°.[8] After this treatment the ceramic has a bulk porosity equal to that of porous metal cathodes. Using this ceramic, we prepared tubes with a wall thickness of 1.1 mm. Tantalum caps with tightly rolled in edges were fitted over the ends of the ceramic tubes (Fig.1). The cathode tube was filled with barium carbonate with some reducing agent (we tried carbon, titanium and tantalum). The filler opening was sealed and the cathode mounted in the test bulb.

The cathode was directly heated; the variation in temperature over its length did not exceed 10% (the cathode temperature was measured by means of a micropyrometer). After decomposition of the carbonates, the temperature of the cathode was slowly increased further and, simultaneously with continuous pumping, we carried out measurements of the thermionic emission of the cathode by the pulse procedure. The error in measurement was certainly less than 10%. At some temperature T_0 the measured value of the thermionic emission current began to increase sharply (at constant temperature) up to a certain equilibrium value I_0. All the processes and the current values were characterized by good reproducibility. The results of these experiments are summarized in the accompanying table.

The following inferences may be drawn from the data in the table:

1. The change in the properties in the cathode is apparently connected with the appearance of free barium, inasmuch as no current rise is observed when the cathode is filled with barium oxide alone.

Values of the equilibrium current and temperature corresponding to the rise of emission for cathodes with different reducing agents

Material inside cathode	Temperature T_0 of beginning of current rise (brightness temperature), °C	Density of emission current at 1100°, amp/cm^2
BaO + C	990	3.5
BaO + Ti	1100	2.0
BaO + Ta	1225	0.8
BaO	No rise up to 1500°	$\sim 1.10^{-4}$
No filler		

2. The amount of free barium necessary to obtain the desired emitter characteristics is obtained only when such reducing agents as Ti, C and Ta are employed. As is known,[9] the amount of free barium present in such cases is much greater than in ordinary porous metal cathodes.

Measurements of the secondary emission coefficient σ showed the following:

1) After activation σ increases very rapidly with the temperature, whereas in the case of a nonactivated emitter no such growth is observed;

2) At 900° $\sigma_{max} = 4.5$ instead of 2.4, the value for pure thorium oxide.

Brief life tests (about 100 hours) showed that the stability of the cathode (within the indicated limit) is satisfactory. In view of the fact that further work on the given cathode without an understanding of its mechanism might have proved long-drawn out and unrewarding, we undertook a detailed investigation of secondary emission from thorium oxide with sputtered on barium.

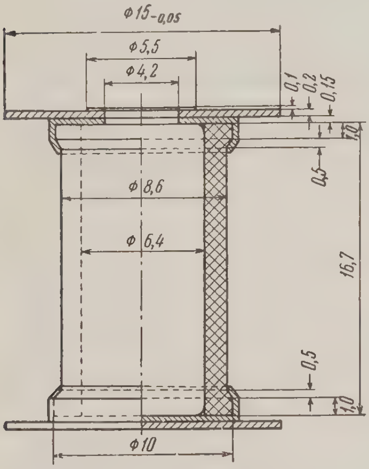

Fig.1. Sectional view of the experimental cathode.

2. Secondary emission of thorium oxide with sputtered on barium

A. Measurement procedure and experimental tube

The experimental tube (Fig.2) consisted of an electron gun, two targets pivoted about a common axis perpendicular to the axis of the gun and a molecular gun with a device for regulating the amount and purity of the sputtered barium.

The first target was a tantalum cup 6 mm in diameter and 7 mm deep. The thorium oxide was applied to a tantalum sponge which was baked onto the bottom of the cup.

The second target was made of pure tantalum. Either of the targets could be brought in front of either the electron or the molecular gun by rotating the tube. The amount of sputtered on barium was monitored and regulated by Becker's technique[10]. For this purpose a tungsten filament 0.15 mm in diameter was mounted at a fixed distance from the target on the side of the molecular gun; the distance from the filament to the target, facing towards the molecular gun, did not exceed 2 mm. The barium source was a 0.8 Feb getter, placed in a chamber formed by two tantalum cups. The density of the sputtered on material at the edges of the target did not differ from the density at the center of the target by more than 1%.[11] A special shutter and limiting diaphragm allowed of beginning and stopping sputtering at predetermined instants.

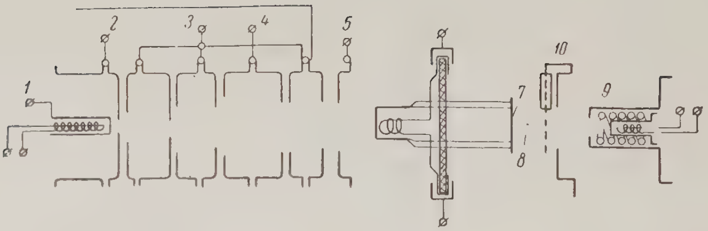

Fig.2. Experimental tube: 1) gun cathode, 2) control electrode, 3) first anode of gun, 4) second anode of gun, 5) secondary electron collector, 6) target with thorium oxide, 7) tantalum target, 8) tungsten wire for measuring rate of sputtering, 9) molecular gun, 10) shutter and limiting diaphragm.

The secondary emission coefficient was measured by the pulse technique.[12] The vacuum at all stages of the experimental procedure was no worse than $1 \cdot 10^{-5}$ mm Hg, and as a rule was better than $1\text{-}2 \cdot 10^{-6}$ mm Hg. All the electrodes of the measurement tube were degassed at temperatures higher than those of measurement. By virtue of the simultaneous effect of the vacuum gage tube and the evaporating barium, the vacuum in the experimental tubes at the time of measurements was $2\text{-}5 \cdot 10^{-7}$ mm Hg. No measures were taken to obtain a higher vacuum inasmuch as it was desired to simulate the operating conditions in commercial tubes.

The temperature of the target was monitored by means of a micropyrometer and controlled by regulating the filament current. The horizontal scale in Fig.4 shows the temperature of the target at different values of the current greater than 800 ma (at higher current values measurements of the temperature by means of the pyrometer were impossible). The temperature variation is, of course, not linear with the current.

For control purposes we measured the secondary emission from a clean tantalum target; these measurements yielded values within 5% of the reputedly reliable data of Warnecke[13]. The values obtained with pulse measurements differed from those obtained with dc by less than 1-2%. In the measurements with clean thorium oxide we also obtained results agreeing well with the data in the literature[14,15], namely, we obtained $\sigma_{max} = 2.3\text{-}2.5$ and found that σ was temperature independent in measurements with single pulses. With repetitive pulses the influence of surface charge disappears at a temperature of about 600°.

To check the purity of the tungsten filament and the sputtered on barium, we measured the work function of the tungsten and an optimum barium coating. The observed work function values did not differ from those cited in the literature by more than 5%.[16,17]

In addition we measured the secondary emission coefficient of a thick layer of barium sputtered on the tantalum target. The value obtained for σ_{max} was 0.83 (in agreement with Bruining & Baer[18]) and did not change up to a coating thickness of more than 20 monolayers (by "monolayer" here and below we understand the amount of barium sputtered on the target within the time required to reach the maximum filament current with the filament at constant temperature).

B. Experimental results

In the case of a barium coated tantalum plate we obtain at room temperature first an increase of σ corresponding to a decrease of the work function of the cathode and then σ begins to decrease tending to a value of 0.83. In the case of a barium coating on thorium oxide, however, no such gradual transition is observed. Frequently, the values of σ for two successively deposited layers do not differ from each other: however, the final value of σ attained after the application of about 50 sputtered layers goes to 0.3 as might be expected.

This value persists even after the target has been kept for 20 hours at room temperature.

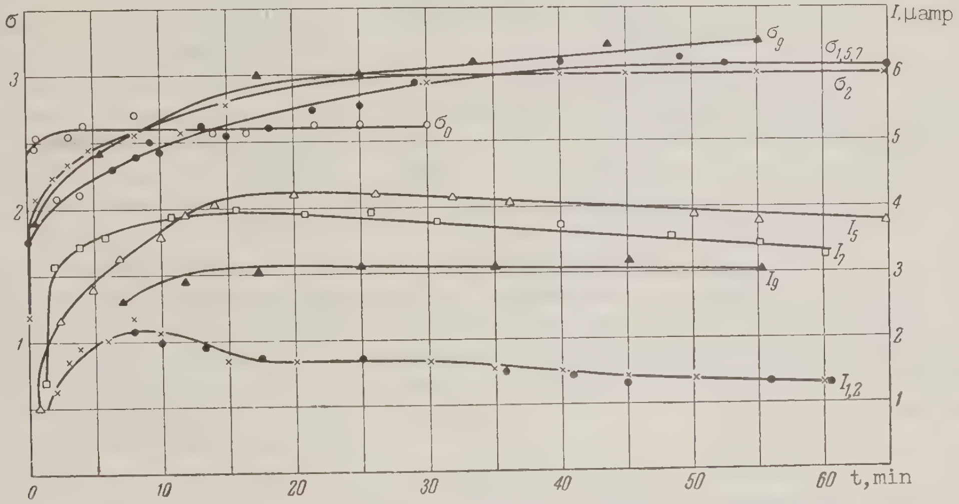

Fig.3. Variation of σ and the thermionic current for different numbers of monolayers: ⊙ - no barium coating, ● - one layer, × - two layers, △ - five layers, □ - seven layers, ▲ - nine layers. The subscripts at σ and I indicate the number of sputterings (monolayer coats).

We began our study of the behavior of targets at elevated temperatures with investigation of the variations with time at constant temperature. To facilitate measurements, we selected the temperature at which surface charge disappears. The observed variation of σ and the thermionic current with the heating time are shown in Fig.3. We have given the dependences for a clean target and for targets with 1, 2, 5, 7 & 9 monolayers, which we selected as being most typical of all those tested. Examining the variation of σ with time for clean thorium oxide, we see that the time required for attainment of temperature equilibrium is 2-2.5 min. Even if we disregard the variation during this period, we see that σ for a target with barium sputtered on it is initially lower than for clean thorium oxide. With passage of time the coefficient of secondary emission of the target with barium increases and finally levels off at a constant value of about 3.5.

The thermionic emission of such emitters also at first increases with time, goes through a maximum (for a small number of layers) and then tends to a constant value at a considerably greater thickness of the coating (9 or more layers).

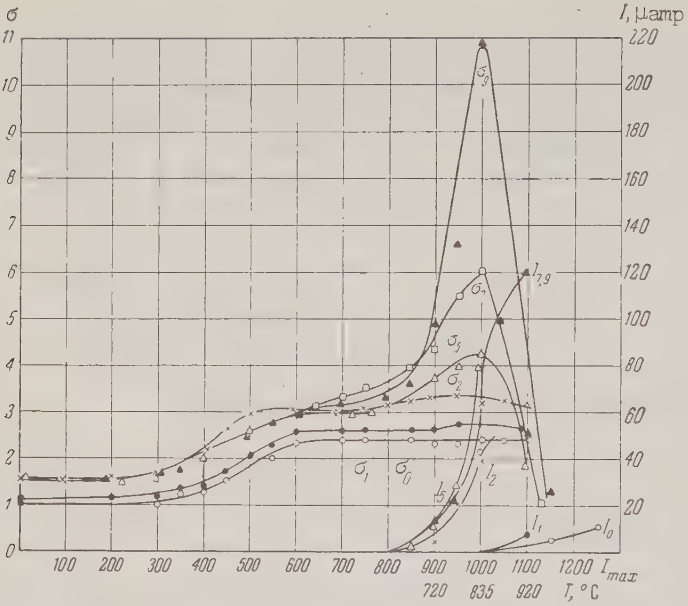

Fig.4. Variation of σ and the thermionic current with temperature (the horizontal scale is laid off in values of the heater current and the measured temperature of the target). Designations same as in Fig.3.

In investigating the behavior of targets at higher temperatures, after attainment of the equilibrium state, the emitter was heated to successively higher temperatures. The behavior under these conditions is shown by the curves of Fig.4. In the case of targets with one or two monolayers of barium σ increases by 10-12%, remaining constant with increasing temperature, as in the case of thorium oxide.

With increasing number of layers the variation with temperature becomes more evident; σ sharply increases with increasing temperature attaining a value of 6 to 12. The maximum values of σ are attained at temperatures between 740 and 830°, with most of the maxima falling within the 790 to 830° interval. The maximum value of σ increases markedly with the thickness of the coating. At higher temperatures σ decreases, falling to 1 at 970°. In repeat measurements, carried out without replenishment of the barium, the character of the curves remained the same but the respective maxima were shifted to the side of higher temperatures and reduced in height. After 3 hour heating of a barium sputtered target at 1300° its emission and σ fell off to the values observed for uncoated thorium oxide.

The thermionic current at first increases with number of layers and beginning with about 6 layers levels off.

Qualitatively, the reproducibility of the results described above is good. The absolute values of σ, however, show a scatter within a range of 1 at 600° and over a range of as much as 4 at higher temperatures.

In the course of heating a target coated with barium, the vacuum is always worsened, the impairment being the greater the thicker the barium layer; thus in the case of a coating consisting of 50 layers the vacuum decreased by a whole order of magnitude. In contrast, in the case of heating a clean target and targets coated with barium oxide there was little or no noticeable impairment of the vacuum.

We also prepared tubes with two molecular guns and sputtered on pure barium oxide. The temperature dependence of σ of such targets was close to that obtained for heated targets with a barium coating.

Discussion and Conclusions

Examining the temperature dependence of σ shown in Fig.4, we note that such an unusually rapid growth of σ with temperature is reminiscent of the temperature dependence of the secondary emission coefficient of barium oxide.[19,20]

In fact, in our experiments with barium oxide coatings we obtained a qualitatively similar temperature dependence of σ. In our opinion the metallic barium is transformed into barium oxide as a result of reaction with the residual oxygen in the tube.

The time over which σ varies in this case was determined not by the time of adsorption of the gases, which does not exceed a few dozen seconds, as by the rate of the barium oxidation reaction. The rate of this reaction is strongly dependent on temperature. It has been noted, at room temperature, the reaction, if it occurs at all, is extremely slow (no change in σ after 20 hours), while at 300-400° σ increases by 25% within 5-6 min. At a temperature of 600° the reaction goes to completion within a few minutes.

We were not able to establish whether this reaction occurs at all temperatures (even though slowly in the low range) or whether there is some minimum temperature below which the reaction is completely inhibited. We plan to investigate this problem in the future.

Research now being carried out by one of the present authors in collaboration with B.Ch.DuBois on films of barium on titanium and tungsten substrates indicates that barium does not adsorb residual gases only at a vacuum better than $5 \cdot 10^{-8}$ mm Hg; at higher pressures such adsorption obtains and this means that chemical reaction is possible either in general or at elevated temperatures.

The oxidizing reaction either did not occur on tungsten and tantalum bases or was compensated by the reducing influence of these metals. We are not asserting, of course, that there were no metallic barium atoms or even aggregations of barium atoms on our targets. Probably there was free barium present in amounts depending on the conditions obtaining in the particular tube; we feel safe in asserting, however, that most of the deposited barium was converted to barium oxide.

From our point of view the dependence of σ on the layer thickness (see above) is of particular interest. This increase of the secondary emission coefficient is difficult to explain solely in terms of increase of the range of the primary electrons in the emitter.

Nor can one accept the hypothesis of break-up of the continuity of the coating and the formation of thicker clots or conglomerates of barium oxide. In this case the bare (barium oxide free) part of the target should have $\sigma =$ $= 2.5$, so that the coefficient of secondary emission averaged over the target surface would be close to 2.5.

According to Johnson[21], the increase of σ of barium oxide with increasing temperature is actually due to increase of the thermionic activity of the oxide under the influence of electron bombardment. The rise time of the enhanced activity is shorter than (or equal to) the rise time of the primary current pulse.

If we accept this mechanism (enhanced thermionic emission) for the increase of σ of barium oxide with temperature, the observed increase of σ with layer thickness can readily be explained by the lesser (relative) poisoning of the layer by the residual gases with increasing thickness of the layer[22]. The existence of this activation with very thin coatings, we feel, merits attention.

The falling off of the secondary emission coefficient at temperatures above 835° (Fig.4) is, according to Johnson[23], due to the influence of space charge. This view is substantiated by the fact that the thermionic current from the target at coating thicknesses greater than 5 monolayers proves to be thickness independent. This is possible when only a fraction of the thermal electrons are attracted to the collector, i.e., in the presence of a potential minimum near the cathode.

If we consider the mechanism of the emitters developed by Tazulakhov[6] in the light of the above described experimental results, it becomes clear that Tazulakhov's emitters were actually not films of barium on oxides but surface films of barium oxide (possibly with an admixture of barium). We also obtained a difference in secondary emission coefficients for different bases. Thus, for example, σ for a target with a very "loose" (patchy) thorium oxide surface was equal to about 1.9. In this case σ with barium sputtered on the target did not exceed 6-7 (instead of the usual 9-12).

What has been said above makes questionable the assertion of certain investigators regarding the presence of free atoms of alkali and alkaline earth metals on the surface of heated nonmetallic targets.

Can some other processes explain the observed facts?

Among the possibilities are the following phenomena:

1) Removal of residual gases from the layer, resulting in a change of σ.

2) Oxidation of the barium as a result of the chemical reaction $ThO_2 + 2\,Ba = Th + 2BaO$.

3) Diffusion of the barium into the thorium oxide lattice.

4) Alteration of the layer under the influence of electron bombardment during measurement of σ.

It is known that the secondary emission coefficient of nonmetallic targets always increases when these are thoroughly outgassed.[5]

If the thickness of the sputtered on barium is increased to 40-50 layers, the target darkens. After being heated, however, it again becomes white and this color persists even if it is exposed to the action of residual gases at appreciably higher pressure than initially. In view of this it is obvious that the first of the above enumerated effects cannot be wholly responsible for the change in σ.

The second suggestion must also be discarded. Numerous calculations (see for example Refs.23 & 24) show that this reaction proceeds in the opposite direction (from right to left). Evaporation of the thorium from the reaction space, which might cause the reaction to proceed in the indicated (left to right) direction[24], will be appreciably less in the indicated temperature range than the evaporation of the barium, which will tend to reverse the reaction.

Some diffusion of barium into the thorium oxide lattice probably does occur. In certain cases, changes of many characteristics of semiconductor targets have been attributed to diffusion processes.[26,27] In the present case, however, the temperature must be appreciably higher to assure the requisite barium concentration within so short a time. Admittedly, however, the diffusion hypothesis cannot be definitively discarded without analysis of the emitting layer.

The influence of electron bombardment on the secondary emission coefficient has been noted by many authors, in particular by Kul'varskaia[26] and Woods & Wright[27]. In all cases electron bombardment, however, tends to decrease (or at least does not increase) the secondary emission coefficient. In our experiments all the measurements were carried out by the pulse technique; consequently, the influence of electron bombardment was minor if not negligible. Hence the observed increase in σ cannot be explained by electron bombardment of the target.

Therefore, our assumption regarding oxidation of the metallic barium to barium oxide by the residual oxygen appears to us to be the most plausible explanation for the observed increase of σ.

The results of our experiments are not encouraging from the standpoint of practical utilization of the developed emitter in view of the dependence of its characteristics on the presence of residual gases and the appreciable expenditure of barium involved (greater than in the case of porous metal cathodes). Still it may be feasible to use such emitters in certain specific cases.

For final resolution of the question one must carry out experiments under conditions of superhigh vacuum with admission of gases of known composition. Such work is underway and the results will be published when the research is completed.

The authors express their deep gratitude to A.R.Shul'man for his constant attention to the work and valuable discussions.

References

1. Magnetrony santimetrovogo diapazona (Microwave magnetrons), Sovetskoe radio (Soviet radio, 1950).
2. H.Bruining, Die Sekundäre Elektron Emission fester Körper, 1942.
3. N.D.Morgulis, Zhur.tekh.fiz., 9, 853 (1939).
4. N.D.Morgulis & N.G.Nakhodkin, Doklady AN SSSR, 94, 1029 (1954).
5. A.R.Shul'man, Dissertation, L, 1956.
6. B.D.Tazulakhov, Zhur.tekh.fiz., 20, 773 (1950).
7. Lemmens, Jansen & Loosjes, Phil.techn.Rev., 11, 341 (1950).
8. J.Fan, Appl.Phys., 20, 682 (1949).
9. N.D.Morgulis and others,Otchet po metalloporistym katodam (Reports on porous metal cathodes), Kiev, 1956.
10. Becker, Trans.Amer.Electrochem.Soc., 55, 153 (1929).
11. S.A.Vekshinskii, Novyi metod metallograficheskogo issledovaniia splavov (A new method of metallographic investigation of alloys), M.-L., 1944.
12. A.R.Shul'man & V.L.Makedovskii, Zhur.tekh.fiz., 22, 1540 (1952).
13. J.Warnecke, Phys.et radium, 7, 278 (1936).
14. A.R.Shul'man & I.D.Iaroshetskii, Zhur.tekh.fiz., 24, 845 (1954).
15. B.N.Popov, Dissertation, Moscow, 1954.
16. A.H.Warner, Proc.Nat.Acad.Sci., 13, 56 (1927).
17. V.M.Gavriliuk, Trudy (Proceedings), Phys.Inst., Acad.of Science, Ukrainian SSSR, 5, 87 (1954).
18. H.Bruining & I.H.deBaer, Physica Holl, 5, 17 (1938).
19. N.D.Morgulis & I.A.Nagorskii, Zhur.tekh.fiz., 5, 848 (1938).
20. A.V.Morozov, Dissertation, M., 1950.
21. I.B.Johnson, Phys.Rev., 83, 49 (1951).
22. N.G.Nakhodkin & A.E.Kulik, Izv.AN SSSR, Ser.fiz., 20, 1096 (1956). (Trans., Bulletin, 20, No.10, 989.)
23. O.Kubashevskii & E.Evans, Termokhimiia v metallurgii (Thermochemistry in metallurgy), M., 1954.
24. V.A.Pazukhin & A.Ia.Fisher, Vakuum v metallurgii (Vacuum in metallurgy), Moscow, 1956.
25. C.E.Moore, J.Chem.Phys., 9, 427 (1941).
26. B.S.Kul'varskaia, Dissertation, M., 1956.
27. I.Woods & D.A.Wright, Brit.J.Appl.Phys., 3, 56 (1952).

DISCUSSION

N.L.Iasnopol'skii: What was the value of σ?

B.N.Popov: The maximum value of σ was 12.

A.V.Morozov: Consequently, sputtering of pure barium yields a value of σ of the order of 9?

B.N.Popov: Yes. The indicated temperature variation is obtained only for barium oxide but not for the other oxides. This is not the true temperature variation but rather rapid activation of the cathode under the influence of electron bombardment.

A.V.Morozov: What does the activation amount to?

B.N.Popov: We plan to undertake a special investigation of this problem.

V.N.Lepeshinskaia: How would you characterize the temperature stability of the cathode?

B.N.Popov: In our case the surface of the emitter was continuously renewed. After 100 hours this was actually not the same emitter as initially.

I.M.Bronshtein: What happens if one doesn't heat the sample?

B.N.Popov: In this case $\sigma = 0.83$. The variation of σ obtained is the same as for ordinary coated cathodes.

O.G.Sarbei: The secondary emission of films of germanium and tantalum with sputtered on barium oxide was investigated in the Physical Institute of the Ukrainian SSR Academy of Sciences. As a result of sputtering on of barium oxide, σ at room temperature increases from 1.1 (for pure germanium) to 5.5 at an optimal number of barium oxide layers, then falls off slightly (to 4.6) with increasing barium oxide thickness.

BEHAVIOR OF COMPOSITE SECONDARY EMITTERS IN EXTENDED OPERATION

- E.G.Kormakova & V.G.Pavlovskaia

The present report is concerned with the behavior of oxygen-magnesium emitters in extended operation in electron multipliers. Of all the composite emitters known at present the oxygen-magnesium emitter is the most suitable for use in vacuum tubes employing secondary emission.

Oxygen-magnesium emitters have a fairly large secondary emission coefficient: $\sigma = 8\text{-}10$ at a primary energy of 300-400 v. The permissible current density for these emitters is about 10 ma/cm^2. Oxygen-magnesium emitters are comparatively stable: an increase of temperature (up to 600°) results in no appreciable change in the secondary emission; these emitters do not lose their secondary emission as a result of exposure to air provided moisture is absent[1].

At present oxygen-magnesium emitters are prepared by appropriate activation of alloys of magnesium with Ag, Al, Cu and other metals.[2,3] The technology of preparing these emitters with the appropriate alloy is very simple and convenient to use in fabricating such emitters for operation in electron multipliers and similar tubes.

1. Measurements

We investigated the emitter behavior in VEI (ВЭИ) multiplier tubes by testing the "stability" of the tubes, i.e., by measuring the output current over an extended period of operation with a constant primary current.

The VEI multipliers use a cylindrical emitter with a central directing grid made in the form of a cone, mounted concentric with the cylinder formed by the emitters. The number of emitters is 13. These multipliers are produced with a hot cathode or a photocathode. The photocathode is semitransparent and is mounted on the hemispherical part of the envelope of the photomultiplier tubes. The thermionic cathode, made in the form of a bronzed tungsten filament, is mounted along the transverse slit in the control cylinder which is aligned with the opening in the multiplier annulus.

The secondary electron emitters in these multiplier tubes are oxygen-magnesium surfaces obtained by activation of an aluminum-magnesium alloy (Al-Mg or Al-Mg-Si) containing 1-4% magnesium. In the hot cathode multipliers these are pristine oxygen-magnesium surfaces, while in the photomultipliers they are oxygen-magnesium surfaces treated with cesium vapor and therefore have a trace layer of Cs_2O-Cs.

The activation of these alloys in the multiplier tubes consisted of preliminary heating followed by oxidation of the alloy in an atmosphere of dry oxygen at a pressure of ~1 mm Hg and a temperature of 400-450°. The adequacy of oxidation was gaged from the drop in oxygen pressure in the system.

Fig.1 shows the variation of the secondary emission coefficient σ of an oxygen-magnesium emitter prepared according to the above described technique as a function of the primary electron velocity. Curve 1 pertains to a "pure" oxygen-magnesium emitter; curve 2 is for an emitter exposed to the influence of cesium vapor during treatment of the photocathode. It will be seen from the curves that the coefficient of a cesium treated oxygen-magnesium emitter is 10-15% higher than that of an untreated one.

The conventional photomultiplier test circuit was used for the stability tests. The time over which the stability was measured was one working day and in some cases 20-30 hours. We measured both the plate current and the currents in the individual emitters. Knowing the primary current, we determined the amplification factors, overall and for the individual emitters.

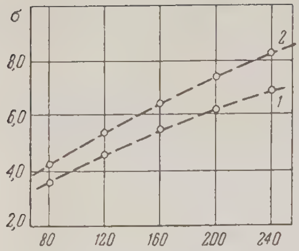

Fig.1. Variation of the secondary emission coefficient of oxygen-magnesium emitters obtained by activation of an Al-Mg alloy as a function of the primary electron energy: 1) "pure" oxygen-magnesium emitter and 2) same emitter after treatment with Cs vapor.

The conditions under which the multipliers were kept prior to measurement were as nearly identical as possible.

During the stability measurements on both the hot cathode and photocathode multipliers, the primary current was monitored and kept constant throughout each test. The measurements were carried out with plate currents of the order of 3 to 5 ma, which corresponds to a current density on the last emitters of about 1-1.5 ma/cm^2. This current density is entirely permissible for oxygen-magnesium emitters.

2. Results and Discussion

In the case of the hot cathode multipliers the plate current in the stability tests was about 5 ma and the overall voltages on the multiplier were 850, 1200 and 1400 v; the corresponding primary electron velocities are 60, 85 and 100 v; respectively.

Fig.2. shows the variation with time of the overall multiplication of two multipliers over a period of 5 hours continuous operation at a potential of 850 v. For the first multiplier (curve 1) the increase in amplification amounts to about 3.5%; for the second (curve 2) - about 8%. As may be seen from the figure, in the case of the second tube the greatest change in amplification occurred during the first 30 minutes of operation (about 7.5%) after which the emission was stabilized and increased only by 0.5% over the ensuing 4.5 hours.

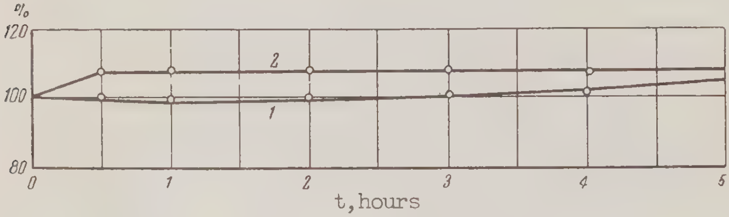

Fig.2. Variation of the total amplification with time for two hot cathode multipliers; voltage on multiplier - 850 v.

The curves of Fig.3 show the variation of the total amplification of a multiplier over 4 hours of operation with a potential of 1200 v (curve 1) and 1400 v (curve 2) on the tube. Here again the greatest change in amplification occurred during the first 30 minutes and then by only 3% during the following 3.5 hours; the respective values for curve 2 are 29% and 16%.

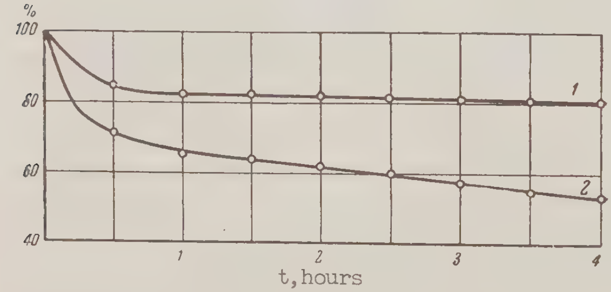

Fig.3. Variation of the total amplification with time for a hot cathode multiplier; voltage on tube 1) 1200 v and 2) 1400 v.

It will be evident from the illustrated curves that in the case of a potential of about 850 v on the multiplier, the change in amplification with time is very small; for most of the tubes tested the gain tends to increase with time; as shown in Fig.2. In the case of higher potentials the amplification tends to decrease with time, the amount of decrease being greater for higher potentials. The tube characterized by curve 2 in Fig.3 exhibited a particularly marked decrease of amplification with time.

Figs.4 & 5 show the variation of the total amplification and the amplification at individual emitters over a period of 4-5 hours continuous operation of the multiplier tube. By the amplification at an individual emitter we mean the amplification of all the preceding emitters of the multiplier including the given emitter. The curves of Fig.4 (voltage on tube - 850 v) show only minor variation of both the total amplification and the individual amplifications; for the first five emitters there is a small increase in amplification, while for the ninth and twelfth there is a minor decrease.

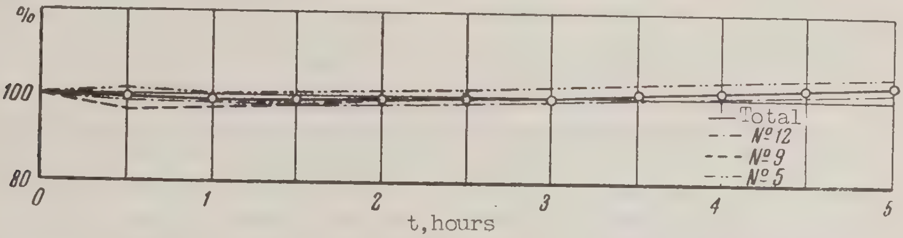

Fig.4. Variation of the total amplification and amplification at the individual emitters with time for a hot cathode multiplier operated at 850 v.

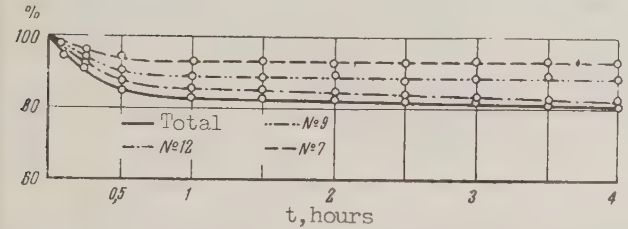

Fig.5. Variation of the total amplification and amplification at the individual emitters with time for a hot cathode multiplier operated at 1200 v.

The curves of Fig.5 (voltage on tube - 1200 v) show a decrease both of the total amplification and of the amplification at the individual emitters. The greatest decrease, as might have been expected, is observed for the twelfth emitter and the relative decrease in amplification at the 7th and 9th emitters is less, which may be explained by the fact that the current density on these emitters is lower: whereas the current density on the 12th emitter is about 1 ma/cm^2, it is only some hundredth of a milliampere per cm^2 on the 9th and 7th emitters.

As will be evident from the figures, the curves characterizing the variation in amplification at the individual emitters differ. For the first emitters there is observed an increase in amplification in some cases, whereas for the last there is commonly a decrease. From this it may be inferred that the character of the variation in multiplication with operating time is determined primarily by the magnitude or density of the emitter current, inasmuch as the energy of the primary electrons in a given photomultiplier tube is the same for all the emitters.

Hence we can tentatively assume that the observed impairment of stability of amplification with increasing operating voltage on the multiplier (Fig.3) occurs not due to increase in the velocity of the primary electrons bombarding the emitter but due to increased output of the emitter.

Investigation of the operation of a photomultiplier with a thermionic cathode over a period of 20 hours showed that the main decrease in amplification occurs during the first hours of operation, after which the amplification becomes stabilized. The variation of the total amplification of a multiplier

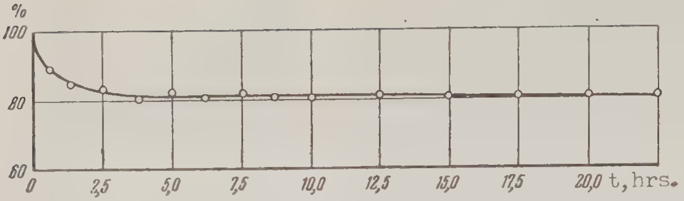

Fig.6. Variation of the total amplification of a hot cathode multiplier over a period of 20 hours; voltage - 1200 v, plate current - 5.7 ma.

over a period of 20 hours operation at a voltage of 1200 v and a plate current of 5.7 ma is shown in Fig.6. During the first 2.5 hours of operation the total amplification fell off by 18% (12.5% during the first 30 min), while during the remaining 17.5 hours of the test the further decrease amounted to only 2%.

Thus for an oxygen-magnesium emitter operated in a hot cathode multiplier at a current density of 1-1.5 ma and a primary electron energy of 60 v the variation of the secondary emission over 6-8 hours continuous operation amounts to a few percent. The greatest change in emission occurs during the initial period of operation (30 min to 2 hours), after which the emission becomes stabilized or changes very little. The emitter is "formed" during the initial period of operation: this forming process consists primarily of elimination of the oxygen adsorbed on the emitter surface and some alteration in the structure of the emitter incident to passage of current through it. The formation time necessarily depends on the operating conditions.

Measurements of the stability of oxygen-magnesium emitters treated with cesium vapors were carried out in photomultipliers with cesium-antimony photocathodes at different values of the plate current and a voltage of 800 v on the tube.

The variation with time of the overall amplification of two extreme photomultiplier tubes operated continuously for four hours is shown in Fig.7. Curve 1 characterizes the behavior of the tube having the lowest amplification; curve 2 characterizes the behavior of the tube having the highest total amplification of all the tubes tested. For tube 1 the decrease in amplification factor is 8% within the first 30 minutes and 13% over the 4 hour period of the test; for tube 2 the corresponding values are 15 and 35%.

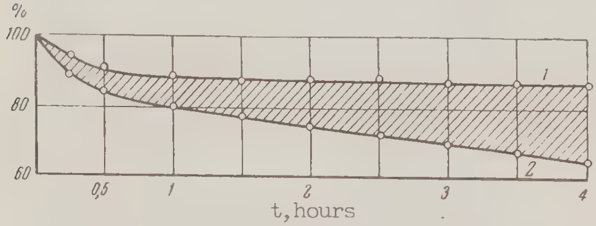

Fig.7. Variation with time of the amplification of two photomultiplier tubes (tubes with the highest and lowest amplification factors of all those tested); voltage - 800 v; plate current - 4 ma.

We see therefore that for some photomultiplier tubes operated with a plate current of 4-5 ma the decrease in amplification is large and attains 35%. Moreover, the amplification does not become stable over the entire test period. From this it may be inferred that a plate current of 4-5 ma (corresponding current density at the last emitters = 1-1.5 ma/cm^2) is excessive for oxygen-magnesium emitters treated with cesium.

We assume that as a result of treatment with cesium vapor there forms on the surface of the oxygen-magnesium emitter in the photomultiplier tube a trace layer of Cs_2O-Cs. The secondary emission of the oxygen-magnesium emitter in this case increases (as compared with an untreated emitter), but the permissible current density and amplification stability decrease.

In photomultipliers the amplification factor depends to an even greater extent (than in hot cathode multipliers) on the magnitude of the plate current.

Both the character and height of the amplification vs time curves vary with changes in the magnitude of the plate current.

Fig.8 shows the variation of the total amplification of a photomultiplier tube with different values of the plate current I_a (the operating potential in all cases was 800 v).

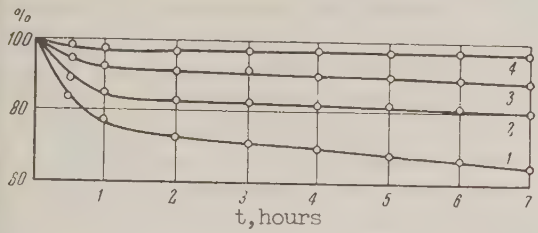

Fig.8. Variation with time of the amplification of a photomultiplier operated at 800 v with different plate currents: 1) I_a = 4 ma, 2) I_a = 0.35 ma, 3) I_a = 70 μa, 4) I_a = 0.8 μa.

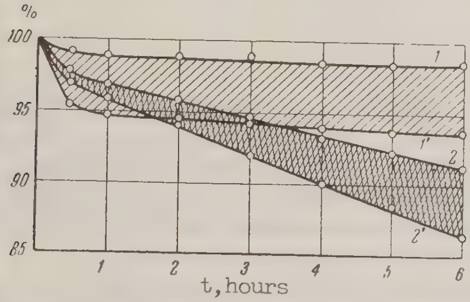

Fig.9. Variation of amplification with time for photomultipliers operated at 800 v and having different amplification factors; the area between 1 and 1' pertains to photomultipliers with an amplification factor of $0.5\text{-}3\cdot10^4$; the area between 2 and 2' pertains to amplifiers with a mean amplification of $3\cdot10^4$.

In the case of the photomultipliers, too, we investigated the variation of the amplification at the individual emitters. Here, as in the case of the hot cathode multipliers, we observed different variations of the amplification: for the first emitters there occurs an increase in amplification in some photomultiplier tubes; at the last emitters there is always a decrease of the amplification with time.

Where the photomultiplier tubes were concerned, we observed a correlation between the stability and magnitude of amplification: the greater the magnification the less stable its value with time. This is illustrated by the curves of Fig.9. The area between curves 1 and 1' characterizes photomultipliers having an amplification of $0.5\cdot10^4$ to $1.3\cdot10^4$ at an operating voltage of 800 v. The decrease in amplification over an operating period of 6 hours for these tubes amounts to 1 to 6% with almost the entire decrease occurring during the first hour of operation. The area between curves 2 and 2' characterizes photomultipliers with an average amplification of $3\cdot10^4$, and in this case the decrease in amplification over a period of 6 hours is 8 to 14%. Here, even with so minor a difference between the amplifications of the photomultipliers, there is a marked difference as regards their stability. The reproduced curves were recorded at plate currents from 20 to 50 microamp.

We observed a similar correlation for the hot cathode multipliers, but in the case of these tubes it was less noticeable inasmuch as for them the decrease in amplification at plate currents of 4-5 ma was comparatively small. Consequently, one cannot explain the correlation between the stability of amplification and its magnitude in photomultipliers solely by the fact that in these tubes the oxygen-magnesium emitter was treated with cesium.

In one of the earliest reports[4] on silver-magnesium alloy emitters, it was noted that emitters having a high secondary emission coefficient σ are characterized by lower stability compared with emitters having an average value of σ.

Thus where a primary requirement is good stability of the amplification factor in the case of multipliers with oxygen-magnesium emitters and, particu-

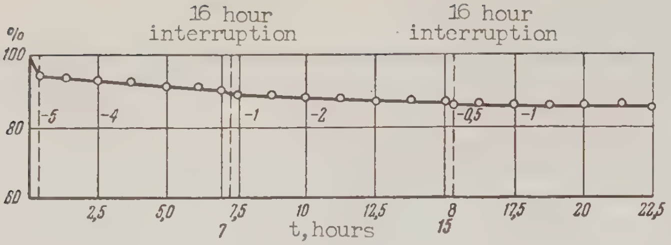

Fig.10. Variation of amplification of a photomultiplier over three days operation for 7-8 hours a day.

larly, in the case of cesiated oxygen-magnesium emitters, we recommend aging of the multiplier prior to measurements (or operation) at current values of the order of the operating current or not more than 10-100 times greater than the normal operating current.

In our opinion an appreciable increase of the output current during the aging does not lead to an increase of the amplification stability of the multiplier in subsequent operation at lower (normal) currents.

Fig.10 shows the variation of the amplification of a photomultiplier operated for 7-8 hours at a stretch on three consecutive days.

As may be seen, the decrease in amplification during the third day was very small (~1%). It is also noteworthy that upon being switched-on on the second and third days the photomultiplier immediately begins to operate in a stable fashion, i.e., without an initial decrease of the amplification factor.

Conclusions

1. In thermionic cathode multipliers at a current density of 1-1.5 ma/cm^2 at the last emitters and a primary electron energy of 60 v, the variation of the secondary emission of an oxygen-magnesium emitter obtained by activating an appropriate Al-Mg alloy amounted to a few percent over 6-8 hours of operation. The greatest change (decrease) in emission occurs during the initial period of operation (30 min to 2 hours), after which the emission becomes stabilized or changes very little. During the initial operating period the emitter is formed; this process consists primarily of removal of the oxygen adsorbed on the emitter surface and some alteration of the emitter structure incident to passage of current through it.

The character and magnitude of the change in emission with time depends primarily on the plate current or current density at the given emitter. The emission stability decreases with increasing energy of the primary electrons and accordingly with increasing operating potential.

2. In photomultipliers with a photocathode, the stability of the emission of an oxygen-magnesium emitter treated with cesium is lower than the emission of a "pure" (untreated) oxygen-magnesium emitter in a hot cathode multiplier.

As a result of cesiation of the photocathode there forms, in our opinion, a trace layer of Cs_2O-Cs on the surface of the oxygen-magnesium emitter.

In this case the secondary emission of the emitter increases, while the permissible current density on the emitter and its stability are reduced. In multipliers with a photocathode (as compared with multipliers with a hot cathode) the variation of amplification with time depends to an even greater extent on the magnitude of the plate current: both the magnitude and character of change in amplification of the photomultiplier vary with increasing current.

3. The stability of an oxygen-magnesium emitter in a photomultiplier depends on the magnitude of the secondary emission coefficient of the emitter: the higher the secondary emission coefficient, the lower the stability. A similar correlation was also observed for untreated oxygen-magnesium emitters in hot cathode multipliers.

4. Where a high amplification stability is a primary requirement we recommend aging of the emitters prior to measurement or operation.

5. In conclusion we must note that VEI photomultipliers with oxygen-magnesium emitters have been tested by purchasers and, according to their reports, satisfied exacting amplification stability requirements. Over periods of 6-8 hours of continuous operation with plate currents of 10^{-6}-10^{-7} amp and different illuminating conditions (both continuous and intermittent) the change in current amounted to less than 1%.

VEI photomultipliers are now in test operation in Moscow motion picture theatres. Prototype photomultipliers were operated in two motion picture theatres for an average of more than 10,000 hours at a mean current of 1 ma and a plate voltage of 300 v; tests after this period of operation showed no significant alteration of the tube parameters.

References

1. P.O.Chechnik, S.M.Fainshtein & T.M.Livshits, Elektronnye umnozhiteli (Electron multipliers), M., 1957.
2. B.S.Kul'varskaia, Dissertation, IRE AN SSSR, Moscow, 1955.
3. P.Rappoport, J.Appl.Phys., 25, 288 (1954).
4. V.K.Zworykin, G.E.Ruechs & E.W.Pixe, J.Appl.Phys., 12, 696 (1941).

DISCUSSION

G.S.Vil'dgrube: What is the operating current density and do your measurements pertain to aged multipliers or to tubes freshly taken off the exhaust unit?

E.G.Kormakova: The average current was 1 ma, that is, equivalent to a current density of 0.2-0.5 ma/cm^2. All of the multipliers had been operated for several hours before the measurements.

L.G.Leiteizen: Was one aging enough or must each tube be checked and aged again after a period of storage?

E.G.Kormakova: Multiplier tubes should be rechecked immediately before being put into operation only when it is necessary to assure a high amplification stability (less than 0.5-1%).

G.S.Vil'dgrube: One can obtain optimum operating conditions for alloy emitters. As a rule heating at 100-300° does not result in a change of the secondary emission coefficient, while heating at a lower or a higher temperature may bring about either a decrease or an increase of σ. The change in σ is usually reversible at a current density of 1 ma/cm^2; at this load the multiplier usually operates in a stable manner. If desired, the load can be increased to 4 ma/cm^2, resulting in a decrease of σ, but the stability remains good. Thus our data are not in conflict with the results reported by E.G. Kormakova.

SOME CHARACTERISTICS OF NEW COMMERCIAL PHOTOMULTIPLIER TUBES

- L.G.Leiteizen, A.G.Berkovskii, B.M.Glukhovskoi, O.S.Korol'kova & E.I.Tarasova

In 1956-1957 there were developed and put into batch production a number of new types of multiple stage photomultipliers, which are now finding increasing use in various fields of physical research. Below we give some data characterizing these new photomultipliers.

1. Characteristics of new photomultipliers

The thirteen-stage FEU-29 photomultiplier with a flat semitransparent cesium-antimony cathode 34 mm in diameter is intended for use in nuclear spectrometry. In the first eleven stages these multipliers have cesium-antimony dynodes; in the two last stages emitters of Al-Mg alloy. At the recommended voltage distribution, which is the same for all tubes of this type, the energy resolution at the standard Cs^{137} line is 8-10% with the multiplier viewing an NaI(Tl) crystal 30 mm in diameter and 15 mm thick. The noise level in energy units in the scale of the same crystal, measured with an output resistance of 50 kilo ohm, a stray capacitance of 10 μμf and an amplifier pass band of 3-4 Mc is of the order of 1.5-2 kev. The linearity of the light characteristic (with the above output circuit parameters) extends to output pulses of 7-8 v amplitude. The sensitivity of the FEU-29 cathodes is not less than 30 μa/lumen; the amplification is 10^7-10^8.

The FEU-24 type photomultiplier is also intended for use in scintillation counters and spectrometers but has a larger cathode (75 mm diameter). Focusing of the photoelectrons on the first dynode is realized by means of a cathode lens which comprises a metallic ring sputtered on the inner surface of the envelope and a metal cylinder electrically connected with the shield. The leads from the cathode and ring are brought out to a button terminal on the side of the envelope. This multiplier has thirteen stages of multiplication; the emitters are made of Al-Mg alloy. At the recommended voltage distribution, the energy resolution of the FEU-24 is 8-11% for any section of the cathode in measurements with a 30 mm diameter crystal under the experimental conditions specified for the FEU-29 tube. The energy equivalent of the intrinsic noise is 2-4 kev on the average. The light characteristic is linear to an output pulse height of 7-8 v.

The FEU-33 photomultiplier is developed specifically for the investigation of processes separated by very short time intervals (10^{-9}-10^{-10} sec). As regards dimensions, as well as the area and sensitivity of the cathode, this tube is identical with the FEU-29. The good time resolution of the FEU-33 tube was realized by the introduction of an accelerating cylinder into the cathode lens and the use of a special multiplying system with accelerating grids operated at twice the stage potential. The new multiplying system allows of obtaining pulse currents of the order of 0.5 amp at the output and an amplification of about 10^8.

In addition to the above three mentioned photomultipliers, which are intended primarily for investigation in the field of nuclear physics, there were also developed a number of other photomultiplier tubes.

The field of application of the new photomultiplier with a bismuth-silver-cesium cathode is determined by its specific spectral characteristics. The spectral characteristics of this multiplier are compared with those of tubes with Sb-Cs and Sb-Na-K cathodes in Fig.1. The multiplier has a flat

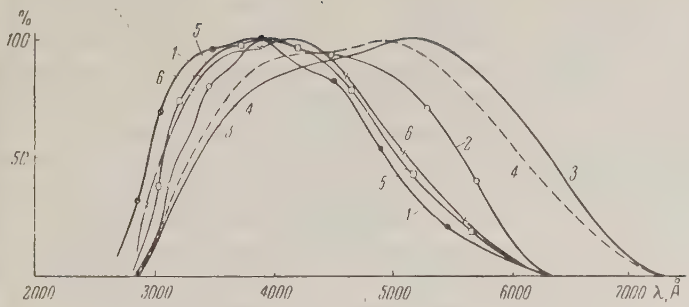

Fig.1. Spectral characteristics of photomultipliers: 1 & 2) with cesium-antimony cathode, 3 & 4) with bismuth-silver-cesium cathode and 5 & 6) with antimony-sodium-potassium cathode.

cathode 25 mm in diameter and 11 stages of amplification (with emitters of Al-Mg alloy). All the leads are brought out through the base. The maximum diameter of the envelope is 30 mm; the length (less pins) is 90 mm.

In developing the tube special attention was given to the sensitivity threshold, which on the average lies at $(1\text{-}3)\cdot 10^{-11}$ lumens with an amplifier pass band of about 20 cps. The sensitivity of the cathode is not less than 30 μa/lumen; the amplification of the multiplier is 10^6-10^7. The tube is vibration and shock resistant.

A special miniature multiplier with a cesium-antimony semitransparent cathode (effective diameter 18 mm) was developed for use in portable equipment.

The overall length of the multiplier (less pins) is 70 mm; the maximum diameter of the envelope is 23.5 mm. The multiplying system consists of 8 cesium-antimony emitters of the "box" type. The average sensitivity threshold with an amplifier pass band of 20 cps is $(3\text{-}4)\cdot 10^{-11}$ lumens. The amplification at an operating potential of 1.0-1.3 kev is 10^5-10^6. The variation of the sensitivity threshold with the applied voltage for a typical multiplier tube with bismuth-silver-cesium cathodes and the miniature photomultiplier with a semitransparent cathode is shown in Fig.2.

There was also developed a miniature amplifier having a massive cesium-antimony cathode and a side optical input.[1] As regards external appearance these multipliers resemble bantam (button) radiotubes and have a standard nine pin base (6NIP, 6PIP, etc.). Both the miniature photomultipliers are of vibration resistant design.

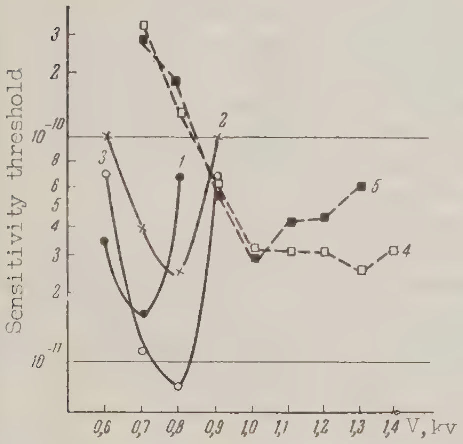

Fig.2. Variation of the sensitivity threshold with voltage for different photomultiplier tubes: 1,2 & 3) for the miniature photomultiplier with semitransparent cathode, 4 & 5) for photomultiplier tubes with bismuth-silver-cesium cathode.

2. Stability of the photomultipliers

A very important characteristic of any photomultiplier is its stability. It must be emphasized that, in contrast to other photomultiplier parameters, the stability of a photomultiplier tube depends on the operating conditions and the measurement procedure employed. There is as yet no general agreement regarding which specific operating conditions are most important from the standpoint of stability. By varying the current load, pulse height, counting

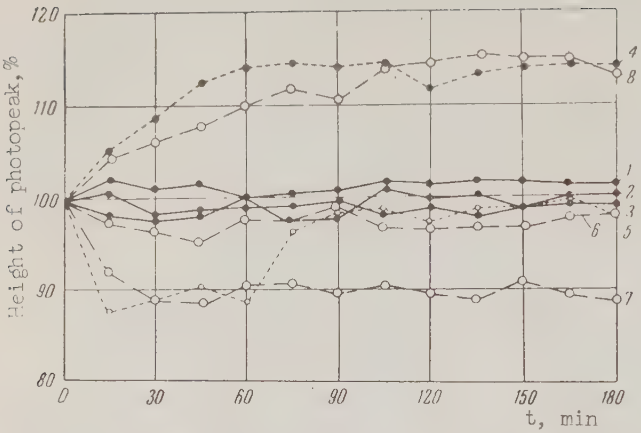

Fig.3. Variation with time of the photopeak height for different photomultipliers: 1,2 & 3) FEU-29 and FEU-33, 4) photomultiplier with Bi-Ag-Cs cathode, 5) photomultiplier with Sb-Na-K cathode, 6,7 & 8) RCA-6810 photomultiplier.

rate and other conditions one can obtain very different stability ratings for the same multiplier tube. Hence one can compare the stability characteristics of different photomultipliers only on the basis of tests carried out under rigorously identical conditions.

We checked the stability of samples of photomultipliers under two different sets of conditions: 1) under scintillation counter conditions with respect to position of the photopeak with the multiplier viewing an NaI(Tl) crystal exposed to Cs^{137} radiation, and 2) under conditions of a constant output current. In the first case the position of the photopeak was determined every 15 minutes by means of a single channel pulse height analyzer. The supply voltage for all the amplifiers was selected so that the pulse height at a load of 50 kilohm would be 4 v. The counting rate was 2000 pulses/sec, which corresponded to a mean output current of 1.5-2 microamp. The accuracy of measurement did not exceed 2-3%.

In the second case the photomultiplier cathode was illuminated by a constant output luminophor and the output current of the photomultiplier (the initial value of the current was about 100 microamp for all the tubes) was measured by means of a recording SG-6 galvanometer.

In addition to the above enumerated photomultipliers, we prepared and tested sample photomultipliers with a cesium-antimony cathode and emitters of Al-Mg, Cu-Mg and Cu-Be alloys as well as sample tubes with Sb-Na-K cathodes and Al-Mg emitters (based on the FEU-29 tube).

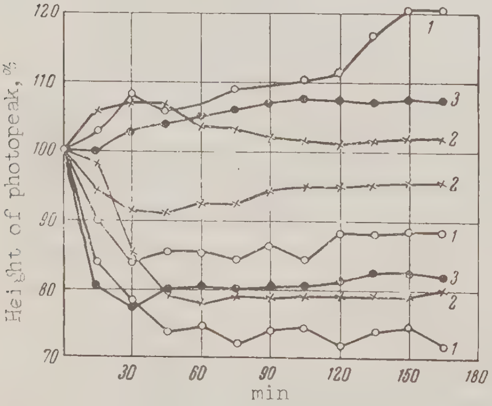

Fig.4. Variation with time of the photopeak height of photomultipliers with emitters of different alloys: 1) Cu-Be, 2) Al-Mg, 3) Cu-Mg.

Several photomultiplier tubes of each type were tested under the pulse conditions and larger batches of several dozen tubes were tested under the constant current conditions. It must be noted that in both cases we found both more and less stable individual tubes among the multipliers of each type.

Curves characterizing the variation of the photopeak height (in percent of the initial height) for different types of photomultipliers are reproduced in Figs.3 & 4. For purposes of comparison in Fig.3 we also give the curves obtained for American RCA-6810 photomultipliers tested under the same conditions. It will be seen from the figure that changes in the material of the cathode does not affect the photomultiplier stability. This is further evidence that the variation in the sensitivity of photomultipliers is determined not by processes occurring on the cathode, where the current density is very low, but is rather due to changes in the secondary emission coefficient of the emitters (particularly the last ones), where the current density is highest. It will be seen from the curves that the settling time for most of the multipliers does not exceed 30 min. It will be seen from Fig.4 that no single alloy emitter is outstandingly superior. The stability of the multiplier tubes with Sb-Cs emitters proved to be equal to that of multipliers with alloy emitters.

As was noted above, measurements at constant current were carried out on a larger number of photomultipliers. For evaluating the stability we calculated for each group of photomultipliers the average value of the relative change in output current in percent:

$$\frac{100}{n}\sum_{i=1}^{n}\left|\frac{\Delta I_i}{I_{\text{irit}}}\right|.$$

where n is the number of tubes of the given type tested.

The results for different times of operation after a 30 minute aging period are summarized in the table.

Emitter type	Number	Average percent change over a period of		
		0.5 hrs	1.5 hrs	3.5 hrs.
11Sb-Cs + 2Al-Mg	51	2,7	6,0	10,5
Al-Mg	127	2.5	3.8	5.2
Cu-Be	34	2.4	5,6	7,9
Cu-Mg	19	4.4	8,8	12,9

It will be apparent from the listed data that in the case of tests by the constant current procedure no single type of emitter exhibited marked superiority to the others, although the stability performance of Al-Mg emitters was somewhat better. RCA-6810 multipliers, tested under the same conditions, on the whole exhibited inferior stability characteristics.

References

1. A.G.Berkovskii & L.G.Leiteizen, Radiotekhnika i elektronika (Radio Engineering and Electronics), 3, 421 (1958).

DISCUSSION

G.S.Vil'dgrube: On the basis of the illustrated curves characterizing the stability of photomultipliers with trough-shaped dynodes of Sb-Cs or Al-Mg alloy Leiteizen concludes that photomultipliers with alloy emitters become fatigued in the same way that photomultipliers with cesium-antimony emitters. In my opinion one cannot generalize the results obtained for these alloy emitters to all types of photomultipliers in general. In our stability tests photomultipliers with a louvre system of dynodes prepared of Cu-Al-Mg alloy invariably exhibited good stability with variation of the output current in the wide range from 50 microamp to 30 milliamp.

I believe that the instability of the photomultipliers, fabricated by the MELZ, detected by Leiteizen and his co-workers is due to instability of the cesium-antimony cathode applied directly to glass and to the design of the dynode system, characterized by sharp electron focusing, as a result of which there may occur local fatigue of the emitters. The instability of the photomultipliers may also be due to charging of the side mica insulators by stray electrons.

One can agree with the fact that the instability of the photomultiplier tubes with alloy emitters, observed by Leiteizen and his co-workers, is an attribute of the photomultipliers of the MELZ design, but one cannot extend this deduction indiscriminately to all photomultipliers including those with louvre type dynodes.

N.S.Khlebnikov: I would like to say a few words in connection with all the reports on photomultipliers. One would not get a complete picture of state of development of photoelectronic multipliers in the Soviet Union if in addition to the data on the excellent photomultipliers given in the preceding reports (G.S.Vil'dgrube, N.K.Dalinenko and L.G.Leiteizen) no mention was made, however brief, of a number of new tubes of this type developed in our laboratory for the purposes of nuclear physics, for measurement of extremely weak light fluxes (tubes for optical spectroscopy and astronomy), as well as of electron multipliers intended both for use in nuclear spectroscopy and in mass spectroscopy. The basic data on these photomultipliers have been given by Khlebnikov & Melamid[1].

The spectrometric group of tubes comprises six types; the time group - three, the measurement group - two. All the multipliers have cesium-antimony cathodes (not sensitized with oxygen) and dynode systems of AMGK alloy - a special aluminum-magnesium alloy developed by E.S.Shpichenetskii and I.L. Rogel'berg. Use of very high evacuation insures a high degree of stability in operation, a low intrinsic noise and a short settling time.

Production of some of these tubes started in the second quarter of 1955 and an appreciable number of these tubes has already been supplied to various agencies and organizations.

The electron multipliers developed in our laboratory also have dynode systems of AMGK alloy. The type of dynode system was selected in accord with the resolving time requirements and the design of the output section to meet the exigencies of each specific research problem. The requisite amplification is also determined by the requirements of the user or research problem and usually lies in the range from 10^4 to 10^9.

References

1. N.S.Khlebnikov & A.E.Melamid, PTE (Instruments and experimental techniques, 6, 6 (1957).

SECONDARY EMISSION FROM COMPOSITE EMITTERS IN THE RANGE OF HIGH SECONDARY EMISSION COEFFICIENT VALUES

- R.M. Aranovich & A.I. Piatnitskii

Introduction

A distinctive feature of field emission is the appreciable "inertia" or time lag of the secondary field current with respect to variations of the primary current. Thus in individual cases Malter[1] observed detectable field emission persisting days after removal of the primary beam. So great an inertia of the current precludes practical utilization of this effect; hence there naturally arose the idea of finding methods of preparing emitters of an intermediate type in which the "normal" secondary emission would be enhanced by partial utilization of the electric field produced by positive charges on the emitter surface.

The possibility of realizing emitters of this type was demonstrated by Aranovich & Timofeev[2]. In preparing his early emitters Aranovich[3] used two methods of applying magnesium oxide to a metal base: evaporation of the magnesium in an atmosphere of oxygen and spraying finely dispersed magnesium oxide. These emitters had an appreciable secondary emission coefficient - about 80 - with relatively little inertia (lag) in the audiofrequency range. Serious shortcomings of these emitters were their instability in operation and the technological difficulty of preparing coatings intended for operation in conjunction with a cesium photocathode.

The present investigation was concerned with effective emitters of thin layers of magnesium oxide applied to a nickel base in the form of the carbonate which was then decomposed to the oxide by vacuum heating in a high frequency furnace.

Preparation of emitters and measurement procedure

The magnesium carbonate layers were applied by the cataphoresis procedure which allows of obtaining uniform layers with the desired density and consisting of particles of known size. It is known that in the preparation of secondary emitters of this type a decisive factor is the structure of the oxide layer. Thus, for example, in forming emitters of metallic magnesium, deposited by evaporation in an oxygen atmosphere on a metal base, the best results are obtained with a "loose" structure of the coating. In our case a loose structure was obtained as a result of decomposition of the magnesium carbonate and elimination of CO_2 from the layer. In the process, the thickness of the layer on the metal base was reduced several fold. The thickness of the layers varied from sample to sample but remained within the range from 1 to 2 μ.

The measurements were made in two types of tubes; the primary electron source was an electron gun or a photocathode. The investigated emitter was mounted in the center of the bulb, while the collector grid was mounted in front of it at a distance of 1.5-2.0 mm. Most of the measurements were made in photocathode tubes inasmuch as the presence of cesium has a favorable effect on the emission properties of emitters of this type; it facilitates and stabilizes the emission process. The conventional three-electrode circuit was employed in the measurement set-up.

A serious shortcoming of early investigations of emitters of the field emission type is that determinations of the emitter characteristics were usually carried out under static conditions, i.e., with a constant primary electron current. Only a few earlier investigators supplemented their static measurements with dynamic ones, i.e., employed pulse techniques. This approach to investigation of emitters is justified in the case of metals, but for emitters of the field emission type one must consider both the variation of the total current and of its alternating component in the case of modulation of the primary electron beam.

In order to bring out the characteristics of our emitters, we recorded secondary emission curves of two types: curves characterizing the variation of the total secondary emission coefficient δ_{tot} and curves characterizing the variation of the coefficient δ_{ac} of the alternating* component of the secondary emission. To this end in the case of measurements with the electron gun an alternating voltage from an audiofrequency oscillator was applied to the control electrode of the gun, while in the case of measurements with photocells the light beam incident on the photocathode was modulated by means of a rotating shutter (disc with apertures). In both cases measurements were carried out in the frequency range from 20 to 10,000 cps. The total current was measured by means of a sensitive galvanometer in the collector circuit. The galvanometer was connected in series with a load resistance which served for measurement of the ac component. The galvanometer was shunted by a large capacitance (to pass the ac component of the total current). An oscilloscope and vacuum tube voltmeter were coupled to the resistance; these instruments gave us the shape of the current curve and the value of the ac component.

Even our preliminary measurements showed that there was a radical difference between the curves characterizing the total secondary emission current as measured by the galvanometer and the ac component of this current as indicated by the voltmeter and oscillograph.

Results and discussion

Fig.1 shows the δ vs V_1 curves obtained for emitter No.336; it will be seen that there is an appreciable difference between the shape of the total secondary emission current curve (curve 1) and the ac component curve (curve 2). Significant here is the fact that the maximum of the δ_{tot} curve lies at appreciably higher values of V_1 than the maximum of the δ_{ac} curve: whereas the maximum for δ_{tot} occurs at a primary voltage of about 600 v, the δ_{ac} maximum lies in the range between 150 and 200 v. Further measurements showed that position of the maxima and the appearance of the curves depend on the thickness of the oxide layer and other factors; in all cases, however, the maximum of δ_{ac} lies at appreciably lower values of V_1 than the maximum of δ_{tot}. The ratio k of the total current to its ac component depends primarily on the primary voltage V_1. Thus for a given emitter at $V_1 = 50$ v, $k = \delta_{ac}/\delta_{tot} = 0.62$; at $V_1 = 100$ v, $k = 0.59$; at $V_1 = 200$ v, $k = 0.26$ and at $V_1 = 650$ v, $k = 0.04$. This ratio also depends on the collector potential V_2 pulling the electrons away from the emitter and on the frequency and density of the primary current. The δ vs V_1 curves obtained at different values of the collector voltage for emitter No.313 are shown in Figs.2 & 3. In this case the maximum in all the total current curves occurs at $V_1 = 350$ v, while the ac component curves peak at 200 v.

The curves for δ_{ac} have a rather sharp peak, whereas the δ_{tot} maxima are comparatively flat. Increase of the attracting (collector) voltage V_2 always increases the total secondary emission current. In the given case δ_{tot} attained a value of 145 at $V_2 = 110$ v, whereas the ac component attained an

---

*"Alternating" as used here and below should be understood to mean "variable" or "modulated" rather than "ac" in the conventional sense.

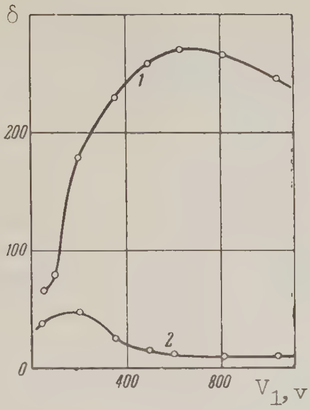

Fig.1

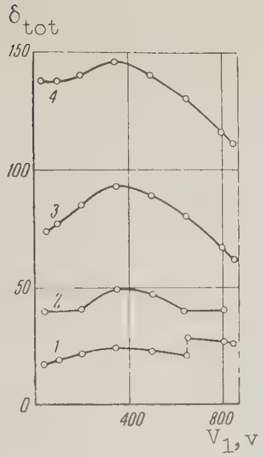

Fig.2

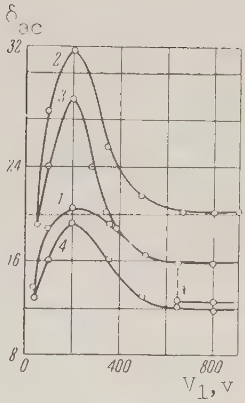

Fig.3

Fig.1. Variation of the secondary current with the primary electron voltage V_1: 1) total current measured by means of a galvanometer and 2) ac component of the secondary current measured by means of an oscillograph. Collector potential, $V_2 = 120$ v.

Fig.2. Variation of the total secondary current δ_{tot} with the primary voltage V_1: 1) $V_2 = 80$ v, 2) $V_2 = 90$ v, 3) $V_2 = 100$ v, 4) $V_2 = 110$ v. Frequency 300 cps.

Fig.3. Variation of the ac component of the secondary current δ_{ac} with the primary voltage: 1) $V_2 = 80$ v, 2) $V_2 = 90$ v, 3) $V_2 = 100$ v, 4) $V_2 = 110$ v. Frequency 300 cps.

optimum value at $V_2 = 90$ v and further increase of V resulted in a decrease of δ_{ac}. Change in the thickness of the active layer alters the shape of the total current curves. With increasing collector potential V_2, the secondary emission coefficient δ_{tot} in this case may monotonically increase, which leads finally to a great increase of the total current and breakdown of the dielectric film. Curves characterizing the total secondary emission current from an emitter with a thick coating of magnesium oxide are shown in Fig.4; the corresponding curves for δ_{ac} are given in Fig.5.

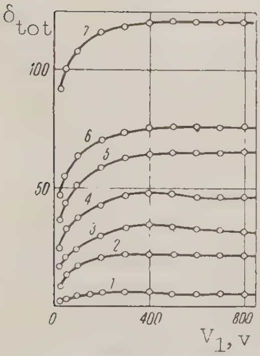

Fig.4. Variation of the total secondary emission current with the primary voltage V_1: 1) $V_2 = 50$ v, 2) 70 v, 3) 80 v, 4) 90 v, 5) 100 v, 6) 110 v, 7) 140 v. Frequency 350 cps.

The δ_{tot} and δ_{ac} curves in Figs.2 & 3 exhibit discontinuities at $V_1 = 650$ v. It is noteworthy that the direction of the jumps in the respective characteristics is different. In this case δ_{tot} and δ_{ac} were measured simultaneously and the discontinuities are evidence of a simultaneous change in both currents, namely, an abrupt increase of the total current and a decrease of its ac component. Repeat measurements yielded identical curves at $V_2 = 80$ v. Jumps in the characteristics were again observed at $V_1 = 650$ v and the increase in the total current was accompanied by a decrease of its ac component. The curves were obtained with a gradual increase of the primary voltage. Determination of these characteristics in the re-

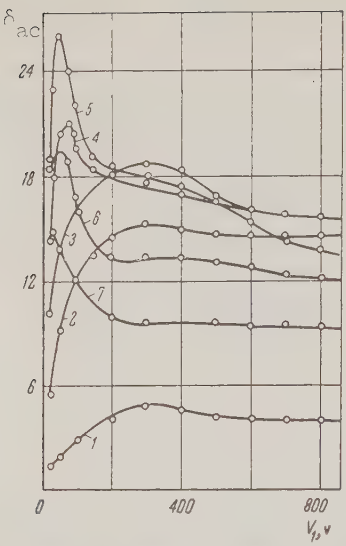

Fig.5. Variation of the ac component of the secondary emission current with the primary voltage V_1: 1) V_2 = 50 v, 2) 70 v, 3) 80 v, 4) 90 v, 5) 100 v, 6) 110 v, 7) 140 v. Frequency 350 cps.

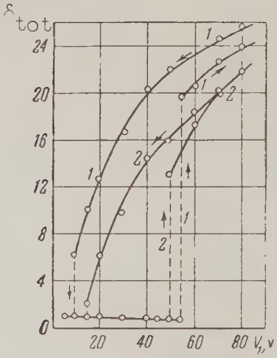

Fig.6. Hysteresis of the δ_{tot} = = $f(V_1)$ curves: 1) primary current $i_1 = 200 \cdot 10^{-8}$ amp, 2) $i_1 = 20 \cdot 10^{-8}$ amp. V_2 = 130 v.

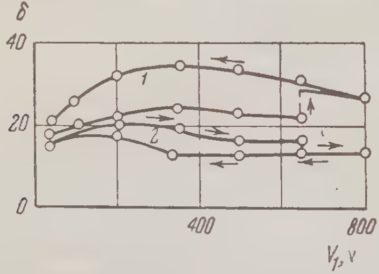

Fig.7. Hysteresis of the $\delta = f(V_1)$ curves: 1) total current δ_{tot}, 2) ac component δ_{ac}. V_2 = 80 v; frequency 300 cps.

verse direction, i.e., with a gradual decrease of V_1, leads to the appearance of hysteresis loops in the $\delta = f(V_1)$ curves, which is common to all emitters with a large transverse resistance, as has been shown by Iasnopol'skii[4]. A number of such curves are shown in Figs.6 & 7. It will be seen in Fig.7 that there is an appreciable difference between the forward (1) and reverse (2) curves, due to the jumps at V_1 = 650 v. Such discontinuities occur only at low values of the accelerating collector potential V_2 and are not observed at higher values of V_2. The observed discontinuities and hysteresis loops are not consistent with the scheme proposed by Iasnopol'skii and are apparently connected with processes involving charging of the surface or charge redistribution in the emitter.

The effective emitters exhibit a strong dependence of δ on the attracting collector voltage V_2; this is a direct consequence of the mechanism of these emitters. The curves of Fig.8 show the variation of the secondary emission with V_2 for emitter No.313 at a primary current frequency of 1700 cps. Here again we see that the total current and ac component characteristics are entirely different. The δ_{ac} curves exhibit a small but distinct dependence on V_2. At small values of V_1, the $\delta_{ac} = f(V_2)$ characteristics have a maximum in the region of small values of V_2 - usually between 90 and 110 v for our tubes used in which the collector grid was located 2 mm from the target. With increasing primary energy, the maximum in the δ_{ac} vs V_2 curve shifts to the side of smaller values of V_2 and at values of V_1 close to 1000 the δ_{ac} vs V_2 curve becomes a monotonically falling one. Thus at high primary energies only a relatively weak attracting (collector) field is necessary to obtain an optimal value of δ_{ac}.

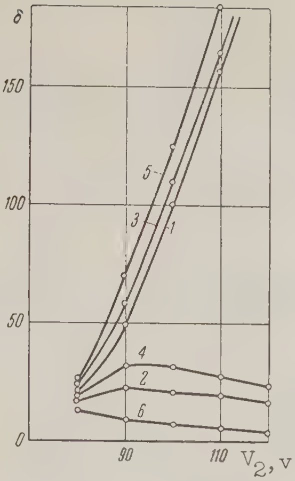

Fig.8. Variation of the secondary current as a function of the collector potential V_2: 1) total current at $V_1 = 50$ v, 3) total current at $V_1 = 200$ v, 5) total current at $V_1 = 1000$ v; 2) ac component at $V_1 = 50$ v, 4) ac component at $V_1 = 200$ v, 6) ac component at $V_1 = 1000$ v. Frequency 1700 cps.

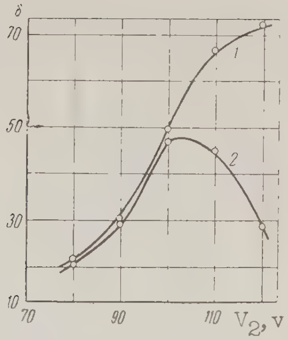

Fig.9. Influence of frequency on the shape of the δ_{ac} vs V_2 curves: 1) 100 cps, 2) 3000 cps. $I = 10^{-6}$ amp; $V_1 = 50$ v.

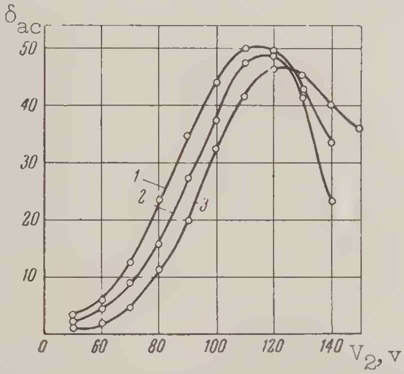

Fig.10. Influence of frequency on the shape of the $\delta_{ac} = f(V_2)$ curves: 1) 210 cps, 2) 1000 cps, 3) 5000 cps. $V_1 = 50$ v.

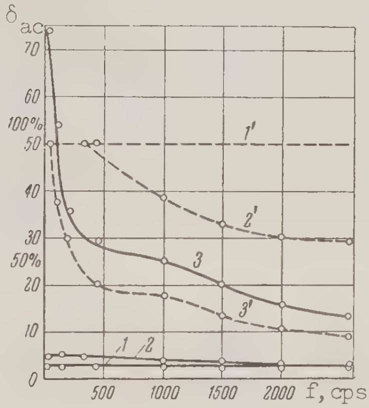

Fig.11. Influence of the collector voltage V_2 on the shape of the δ vs frequency curves 1) $V_2 = 80$ v, 2) $V_2 = 90$ v, 3) $V_2 = 120$ v. $V_1 = 50$ v.

In contrast, the characteristic of the total current is almost always a monotonically rising curve; for a few individual emitters, however, we obtained δ_{tot} vs V_2 curves with a maximum in the region of 120-140 v, followed by a small decrease and an almost horizontal section extending to 200-220 v. Further increase of the voltage led to a sharp increase of the current, breakdown and disintegration of the emitter.

In a number of cases a change in frequency alters the character of the variation of δ_{tot} as a function of V_2. Two δ_{ac} vs V_2 curves obtained at different frequencies of the primary current for emitter No.545 are reproduced in Fig.9. It will be seen that the curve obtained at a frequency of 3000 cps has a maximum shifted far to the side of lower values of V_2 as compared with the curve recorded at 100 cps. It is interesting to note that the positions of the maxima in the δ_{ac} vs V_2 curves obtained at different frequencies apparently depend on the thickness of the oxide layer. Measurements carried out on emitters with a thin oxide coating (~1μ) showed a displacement of the maximum of δ_{ac} to the side of larger values of V_2 with increasing frequency (Fig. 10). Thus the position of the maximum of δ_{ac} depends on both the frequency of the primary current and the thickness of the oxide layer.

One of the attributes of field emitters of this type is decrease of the secondary emission coefficient with increasing frequency of the primary current. As follows from Fig.11 the extent of the decrease of δ_{ac} with increasing frequency depends largely on the value of the collector potential V_2. Curves 1', 2' and 3' are percentile curves, plotted taking the value at 50 cps as 100%.

It follows from these curves that the degree of inertness of the secondary current for effective emitters is determined by the value of the attracting collector potential. Thus for $V_2 = 80$ v the $\delta_{ac} = \varphi(f)$ curve extends parallel to the horizontal axis, i.e., there is not the slightest decrease of the current up to 3000 cps. At $V_2 = 90$ v, the curve bends down at 350 cps, while at $V_2 = 120$ v, the secondary current begins to fall off sharply at 50 cps. It must be noted, however, that the absolute values of the current increase with increasing collector voltage V_2. Thus, for example, at a frequency of 1000 cps and $V_2 = 80$ v, $\delta_{ac} = 3$, its value at 50 cps as well; whereas with $V_2 = 120$ v, $\delta_{ac} = 74$ at 50 cps and 25 at 1000 cps, i.e., decreases by 65%. Nevertheless, its absolute value at 1000 cps is still appreciably greater than the value for all frequencies at $V_2 = 80$ v. The curves reproduced in Fig.11 characterize emitter No.285 in which the described dependence was particularly strong; other emitters exhibit a somewhat weaker frequency dependence of the secondary current.

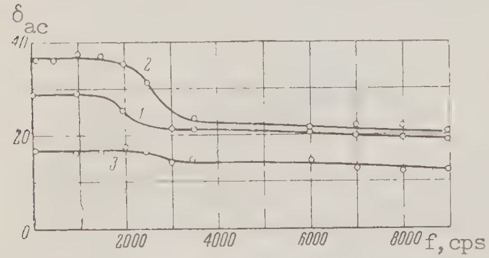

Fig.12. Frequency characteristics of the secondary current δ_{ac}: 1) $V_1 = 50$ v, 2) 200 v, 3) 800 v.

The frequency dependences of the secondary emission at different values of the primary voltage are shown in Fig.12. Here the horizontal axis is scaled in terms of the frequency of interruption of the light beam incident on the photocathode, i.e., in terms of the frequency of the primary current; the vertical axis is laid off in values of δ_{ac}. As will be seen from the figure, there is no significant difference in the shape of these curves for different primary energies. The variation in the magnitude of δ_{ac} in the range of low frequencies is determined wholly by the shape of the $\delta_{ac} = f(V_1)$ curve (curve 1 in Fig.5). As might have been expected, with increase of the primary voltage to 200 v, which corresponds to the maximum in the $\delta_{ac} = f(V_1)$ curve, the secondary emission coefficient increased and at $V_1 = 800$ v, again decreased. Highly significant, however, is the fact that the variation in the secondary emission incident to variation of the primary electron energy proves to be different for different frequencies. These variations of δ_{ac} are evinced most strongly in the region of low frequencies (50 to 2500 cps), while in the region of higher frequencies δ_{ac} remains virually constant.

The decrease in the secondary current with increasing frequency depends on the energy of the primary electrons. Comparing the coefficient of secondary emission at frequencies of 900 and 50 cps, we find that the ratio of the secondary emission coefficients at these frequencies is 0.69 at $V_1 = 50$ v, 0.57 at $V_1 = 200$ v and 0.77 at $V_1 = 800$ v. The sharp decrease in the frequency interval from 1500 to 3000 cps exhibited by the curves shown in Fig.12 is

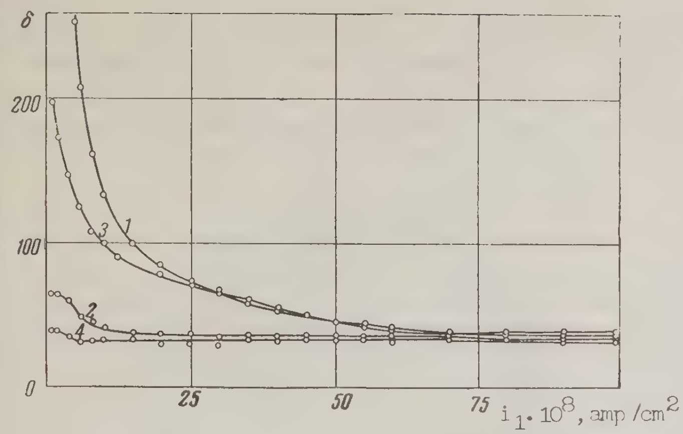

Fig.13. Variation of the secondary emission with primary current density: 1) total secondary current δ_{tot} at f = 300 cps, 2) ac component at f = 300 cps, 3) secondary current δ_{tot} at f = 1700 cps, 4) its ac component at f = 1700 cps, V_1 = 50 v, V_2 = = 90 v.

not observed for all emitters. The frequency position of the falling section in the curves depends primarily on the structure of the emitter. A number of the tested emitters exhibited an appreciable decrease of the secondary emission coefficient in the initial frequency interval from 50 to 500 cps; in the case of these emitters there was no significant decrease in the range from 1500 to 9000 cps, although in general the lag (of the secondary current behind the primary current) in these emitters is greater than in most emitters of this type.

The behavior of the emitters at different densities of the primary current is a very important characteristic, which yields auxiliary information for determining the emission mechanism. This characteristic plays a particularly important part in the case of effective emitters, the character of whose emission depends substantially on the primary beam density. For all emitters there exists a unique threshold, i.e., a minimum current density, which must be exceeded for them to operate as effective emitters. The relation between the total secondary emission current and its ac component at different values of primary current density is shown in Fig.13. Here curves 1 and 3 characterize the total current; curves 2 and 4 the ac component. All the curves were obtained with V_1 = 50 v, and V_2 = 90 v.

It is noteworthy that the ac component remains virtually constant in a wide primary current range and rises to a maximum only in the region of very weak currents, whereas the total current curve falls off in this region with increasing primary beam density. Measurements made on other samples yielded $\delta = f(i_1)$ curves with a sharp maximum in the region of low current densities. It may be assumed that for the emitter characterized in Fig.13 this maximum lies in the region of still lower current densities. The curves for the ac component indicate that such a maximum exists. It will also be evident that the ratio $k = \delta_{ac}/\delta_{tot}$ is not constant but varies with the primary current density. The ratio attains a value of 0.9 in the region of large current densities (with a small value of the primary voltage and with low collector potentials) and gradually decreases with decreasing primary current density.

The lowest value of k is obtained in the region of the maximum of $\delta = = f(i_1)$. Thus at a current density $i_1 = 1 \cdot 10^{-8}$ amp/cm^2, δ_{tot} attained 500 (upper part of curve 1) and the ratio k for this point (i.e., the ratio of the height of curve 1 to curve 2 in Fig.13) fell off to 0.13 as compared with the values approaching unity (~0.9) in the region of current densities of the order of $1 \cdot 10^{-6}$ amp/cm^2.

We obtained another interesting result from analysis of the curves shown in Fig.13; inasmuch as curves 1 & 2 were determined at a primary current frequency of 300 cps, while curves 3 & 4 were recorded at a frequency of 1700 cps, comparison of these curves allows of determining the "inertia" or lag of these emitters at different densities of the primary electron beam. It follows from Fig.13 that the lag of the ac component is only weakly dependent on the primary beam density in a rather wide range. At a primary current density greater than $15 \cdot 10^{-8}$ amp/cm^2 the ratio of the ac components at 300 and 1700 cps remained constant and equal to 0.9; only in the region of weak currents does the inertia of the secondary emission increase, attaining a maximum value at the peak of the $\delta_{ac} = f(V_1)$ curves. The value of δ_{ac}/δ_{tot} for the given emitter in this region was 0.6. At primary current densities greater than $25 \cdot 10^{-8}$ amp/cm^2, the total secondary current curves for 300 and 1700 cps virtually coincide. At low current densities the ratio where the total current curves are concerned decreases which must be ascribed to decrease of the surface charge on the emitter when it is irradiated at a higher frequency by a low intensity beam. The general appearance of the $\delta = f(V_1)$ characteristics remains approximately the same for other primary electron energies. The variation of the total secondary current and its ac component as a function of the primary current for two values of V_1 is shown in Fig.14.

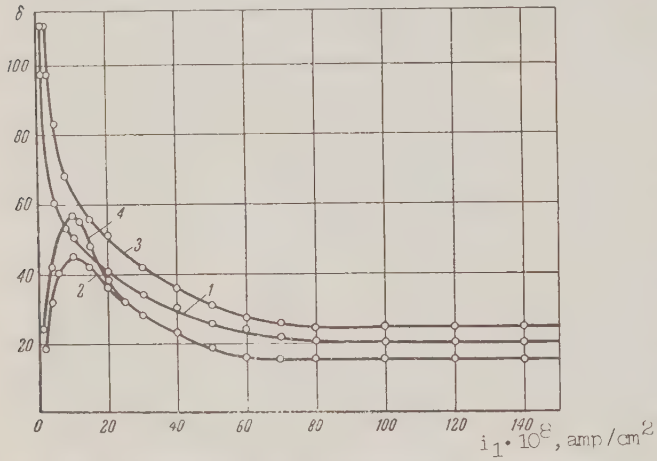

Fig.14. Variation of secondary emission with primary current density i_1: 1) total current at $V_1 = 50$ v, 2) its ac component, 3) total current at $V_1 = 100$ v, 4) its ac component. Frequency 1000 cps; $V_2 = 80$ v.

In connection with the above, it must be noted that the decrease of the secondary emission with increasing primary beam density does not mean a decrease of the collector current I_2. Results similar to ours for the total current were obtained by Zernov, Elinson & Levin[5] in studying field emission from Al_2O_3 layers. Our observations, however, established the presence of a maximum in the $\delta_{tot} = f(i_1)$ curve in the region of weak currents, which was not noticed earlier. The presence of a maximum in the $\delta_{tot} = f(i_1)$ curve should have been expected in view of the fact that at low current densities all the electrons incident on the target in ejecting secondaries produce a positive charge. With increasing primary beam density, part of the electrons will fall on positively charged sections of the emitter. This will lead to a relative decrease in the number of autoelectrons entering the vacuum under the influence of the positive charges.

The above described experimental results allow of drawing a number of deductions fundamental to an understanding of field emitters of the given type. First, we must note the consistent radical difference between the ac component characteristics and the total current curves. This was evident in almost all cases when both curves were recorded.

In the case of field emitters of the given type, we are dealing with two entirely different groups of electrons, the ratio between which may vary depending on the density of the primary current, the primary electron energy, the collector potential, the structure of the layer and other factors. In some cases the difference is so great that one can scarcely speak of the secondary emission characteristics of the given emitter or surface but must rather consider separately the total secondary current (more accurately the nonmodulated part of the emission) and the alternating component of the current, although actually emission of both groups of electrons occurs simultaneously. So great a difference as was actually observed between the ac component and total current characteristics was unexpected, although the presence of two groups of electrons in the total current obviously followed from the very mechanism of emission from cold cathodes.

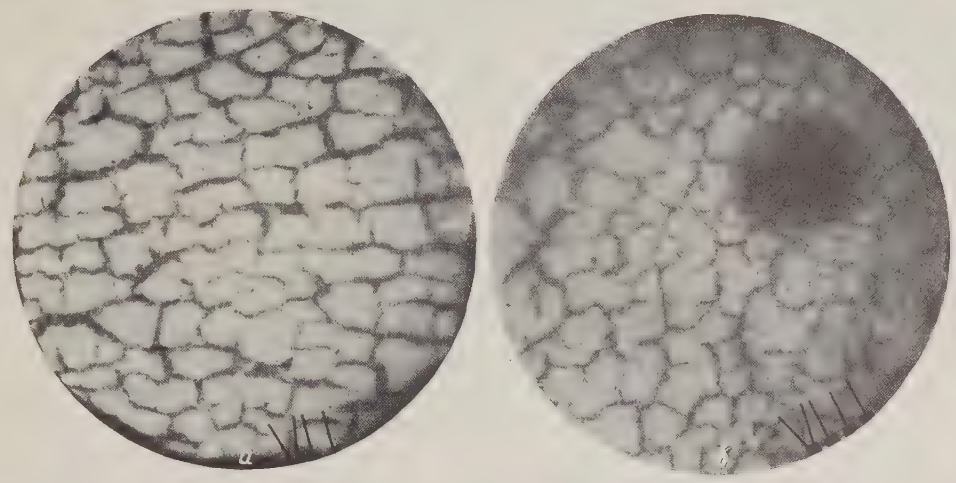

Fig.15. Microphotographs of emitter surfaces: a) thin coating, b) thicker coating (~2 μ). The dark patch is due to metallic particles from the base condensed on the oxide coating.

The presence of two electron groups in field emission of this type has been noted by a number of earlier investigators[6-10]. Comparing their results with ours, we come to the conclusion that the nonmodulated component of the current must consist of autoelectrons emerging from the metal base of the emitter into the vacuum without appreciable loss of energy. The alternating component of the current cannot, however, be wholly attributed to the so-called "true secondary" electrons, i.e., to electrons which are emitted from the coating in the absence of a field. The alternating current component is composed both of these true secondary electrons and of electrons with "insufficient energy", i.e., electrons which could not have emerged from the depth of the layer without the help of the field, as well as autoelectrons, drawn from the atoms of the dielectric. This difference in the origin of the two groups of electrons determines the difference between their characteristics. The magnitude of the alternating component is determined by processes occurring in the emitter in the region close to its surface and on its surface. The shape of the total current curves depends not only on the charge on the emitter surface and the work function, but also on the field distribution inside the dielectric layer and on the character and height of the potential barrier at the metal-dielectric interface. It must be noted, however, that in addition to the primary process of emission of autoelectrons from the metal through the dielectric into the vacuum, there is a considerable probability of direct emission of the autoelectrons into the vacuum, bypassing the dielectric. Formation of numerous cracks in the emitter incident to heating in the vacuum not only facilitates the emergence of electrons but also modifies the character of the emission to some extent. In a number of cases these cracks in the emitting layer are areas of intense emission; in fact, sometimes the field induced emission is so intense that upon examination under a microscope one can observe areas with an appreciable amount of metal "pulled" out of the base and deposited on the oxide in the vicinity of an emission center (see, for example, Fig.15).

Our final deduction, which follows from analysis of our experimental results, is that in investigating secondary emission with a modulated primary electron beam one cannot in general consider the characteristics so obtained as curves characterizing the secondary emission properties of the given emitter. As we demonstrated, the alternating component characteristics are neither the total current characteristics nor the characteristics of the so-called true secondary electron current. Actually, the alternating component curves characterize only the alternating component of the secondary electron current which should not be confused (as has sometimes been done) with the true secondary electron current.

References

1. L.Malter, Phys.Rev., 50, 48 (1936).
2. P.V.Timofeev & R.M.Aranovich, Zhur.tekh.fiz., 10, 32 (1940).
3. R.M.Aranovich, Izv.AN SSSR, Ser.fiz., 8, 346 (1944).
4. N.L.Iasnopol'skii, Zhur.tekh.fiz., 10, 1813 (1940).
5. D.V.Zernov, M.I.Elinson & N.M.Levin, Izv.AN SSSR, Otd.tekh.nauk., No.3, 166 (1944).
6. H.Mahl, Phys.Z.38, 935 (1937).
7. D.V.Zernov & B.S.Kul'varskaia, Zhur.tekh.fiz., 16, 711 (1946).
8. M.S.Kosman, N.E.Zalkind & M.E.Zelkind, Uch.zap. (Scientific notes), Leningrad University, No.57, 40 (1940).
9. D.V.Zernov, Zhur.tekh.fiz., 15, 447 (1945); ibid., 16, 931 & 935 (1946); Izv.AN SSSR, Ser.fiz., 8, 352 (1944); ibid., 14, 866 (1950).
10. H.Jacobs, T.Freely & F.Brand, Phys.Rev., 88, 492 (1952); D.Dobischek, H.Jacobs & J.Freely, Phys.Rev., 91, 804 (1953); H.Jacobs, Phys.Rev., 85, 441 (1952).
11. V.N.Favorin, Zhur.tekh.fiz., 20, 916 (1950).
12. M.I.Elinson & D.V.Zernov, Radiotekhnika i elektronika (Radio Engineering and Electronics), No.1, 75 (1957).

DISCUSSION

E.A.Krasovskii: What is the value of the coefficient δ in the absence of lag at 10,000 cps?

R.M.Aranovich: At 50 v, $\delta = 40\text{-}80$ in the absence of lag.

I.F.Pes'iatskii: What was the magnitude in percent of the current "bumps"?

R.M.Aranovich: Generally the current "throws" did not exceed 1%, but there were jumps incident to breakdown of the layer which grealy exceeded the mean current.

O.M.Sorokin: For what reason does a single primary 50 v electron give rise to 50 secondaries?

R.M.Aranovich: Due to field induced emission.

L.N.Dobretsov: What was modulated, the collector voltage or the primary current?

R.M.Aranovich: We modulated the primary current. One cannot modulate the collector potential inasmuch as the secondary emission is strongly dependent on V_2.

SOME FEATURES OF THE RETARDING POTENTIAL CURVES OF SURFACE ACTIVATED CATHODES

- V.N.Lepeshinskaia & T.M.Sukova

It has been repeatedly noted in connection with investigations of secondary electron spectra that the retarding potential curves obtained in a spherical capacitor attain saturation in the region of positive potentials on the collector, i.e., there are observed what Piatnitskii[1] and others have termed "electrons with insufficient energies". In earlier investigations with dielectric targets, Bruining & DeBoer[2] also observed saturation of the retarding potential curves at large values of V_c; this saturation, however, occurred due to charging of the surface. In going over to the single pulse measurement technique[3] the $I_2 = f(V_c)$ curves once more became "normal" and saturation was observed at $V_c \approx 0$.

As has been noted in Refs.4 & 5, where the current-voltage curves for activated magnesium and beryllium alloys are concerned, saturation occurs at a positive collector potential in the range from a few to several tens of volts. Leaving aside for the moment the physical aspects of this effect, let us first consider a number of incidental causes that might be responsible for it. The four principal ones in our opinion are 1) the presence in the current of tertiary electrons from the collector, 2) charging of the surface in the case of low electric conductivity of the target leading in some cases even to appearance of a Malter type effect, 3) the presence of resistance in the target-collector circuit (this resistance includes the resistance of the active layer on the target, the transverse resistance of the collector and the external resistance in the measurement circuit) and 4) distortion of the field within the vicinity of the target due to unsatisfactory experimental geometry.

In our experiments we repeatedly checked the influence of these factors. The presence of tertiary electrons was eliminated by the introduction of an antidynatron grid to which we applied a negative bias of 60 volts relative to the conducting silver coating on the inside surface of the spherical glass bulb. The collector potential, negative or positive with respect to the target, was applied to the same grid for analyzing the secondary electron energies. Fig.1 shows the retarding potential curve obtained for an activated magnesium alloy with no potential on the antidynatron grid (curve 1). It will be seen that in the presence of a potential on the grid (curve 2) the experimental points fall on the same curve. In both cases the measurements were carried out under static conditions.

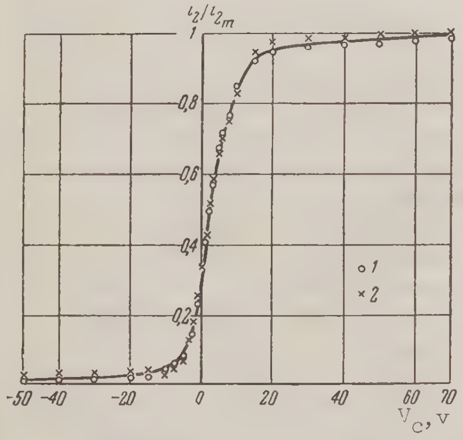

Fig.1. Retarding potential curve for activated magnesium alloy in the presence of an antidynatron grid and without it: 1) for the case when $V_g = V_c$; 2) for the case when $V_g = -60$ v.

In order to check for the possible influence of surface charge, we recorded the retarding potential curve for the same alloy by the method of single pulses (2 microsec duration) with heating in the interval between pulses. The experimental points all fell on the curve obtained by the static (dc) technique.

We checked for the presence of resistance in the target-collector circuit and the resultant voltage drop by recording retarding potential curves for metals: gold, heated nickel, etched copper and nonactivated alloy. The resultant curves are shown

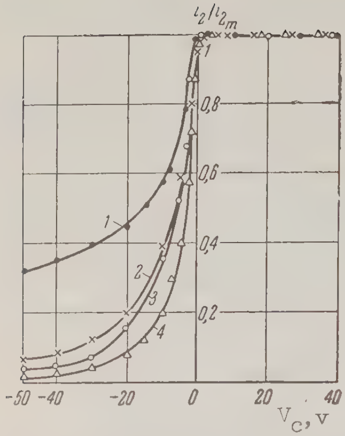

Fig.2. Retarding potential curve for metals: 1) gold, 2) nickel, 3) copper, 4) nonactivated alloy.

in Fig.2. For all the metals saturation of the secondary current occurred at virtually zero potential on the collector. There still remained the possibility of a voltage drop in the activated layer itself. It was shown earlier[4], however, that bombardment with beam currents in the range from 10^{-7} to 10^{-11} amp did not alter the nature of the retarding potential curve. Consequently, the active target coating has a relatively low resistance; moreover, the Malter effect is absent.

The effect of the geometry of the set-up on the retarding potential curves was checked by comparing the results obtained for spherical and flat targets with different ratios of the diameters of the target and collector; in all cases for attaining saturation of the secondary current a positive voltage on the collector was necessary; this was the higher, the greater the size of the target.

In view of the absence of these possible sources of error, it may be assumed that a stopping field exists at the surface of the target so that an additional positive voltage must be applied to the collector in order to compensate it. The localization of such a stopping field at the surface of the target is substantiated by the following experiment. We introduced into our apparatus a nickel screen cage (grid) in the form of a 30 mm diameter sphere surrounding the target and connected electrically to the substrate (the base alloy under the active coating). We then analyzed the energy of the secondary electrons in the drift space between this spherical grid and the collector. In this case normal retarding potential curves were obtained, i.e., saturation occurred close to $V_c = 0$ rather than +40 v, the collector voltage at the onset of saturation for the same sample in the absence of the screen.

Most investigators who have worked with magnesium and beryllium alloys assume (and some support the assumption by means of electron diffraction patterns) that in an activated target the surface layer responsible for the high secondary emission is an oxide of the light component (i.e., is MgO or BeO). In view of this we prepared a number of targets using different procedures to apply the oxide to a nickel base; specifically, we employed mechanical application of a suspension of MgO in alcohol, evaporation of magnesium in an atmosphere of oxygen and vacuum evaporation of metallic magnesium with subsequent oxidation by a glow discharge in oxygen. We recorded retarding potential curves for all these targets and since the coatings on them were appreciably thicker than those obtained on alloys, charges were present on the surface of these magnesium oxide layers. Upon removal of the charges by heating or through use of the single pulse measuring technique, saturation of the secondary current occurred close to zero collector potential. No anomalies in the retarding potential curves were observed, as may be seen in Fig.3.

In the case of a layer of MgO obtained on a piece of magnesium by heating it in the residual gases at a pressure of 10^{-3} mm Hg (i.e., by a procedure similar to that employed in activating magnesium alloys), the retarding potential curves were distorted (Fig.4) and saturation occurred at +10 v even though the measurements were carried out using single pulses. Thus these "activated" solid magnesium targets approached activated alloys as regards their properties.

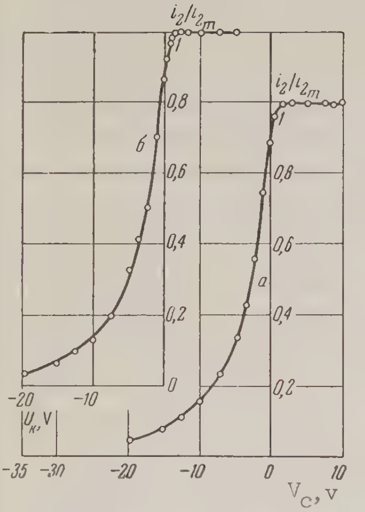

Fig.3. Retarding potentials for MgO films: a) obtained by evaporation of magnesium on a nickel base under vacuum with subsequent oxidation by a glow discharge in oxygen and b) obtained by evaporation of magnesium on a nickel base in an atmosphere of oxygen (oxidation in flight).

In view of the above results we made an attempt to develop a hypothesis that would allow of explaining all the experimentally observed facts. In an earlier publication[5] one of us put forward the suggestion that there exists over the surface of an emitter a patch field which slows down the emitted secondary electrons. This assumption, however, does not yield a satisfactory explanation for the change in the retarding potential curve as a result of heating of the target to 400° (i.e., shift of the curve to exhibit saturation of the secondary current at $V_c = 0$ (see Fig.5)) and, particularly, the reversibility of this effect.

Hence we suggest that the following interpretation is more plausible. Let us assume that we have an activated target of a copper-magnesium alloy, as shown schematically in Fig.6. In the process of activation the magnesium diffuses towards the surface and is oxidized, forming a thin magnesium oxide coating on the layer. The surface of contact between the base and the oxide is not homogeneous inasmuch as the magnesium in diffusing towards the surface does not emerge uniformly: the diffusion will obviously be easier between the alloy grains than through the crystal faces. In addition, the oxidation of the magnesium will not proceed at the same rate in different areas. As a result there will be formed at the alloy base-oxide film interface a patchy surface with a work function differing in value from one microscopic area to another. These areas or patches apparently consist partially of nonactivated alloy

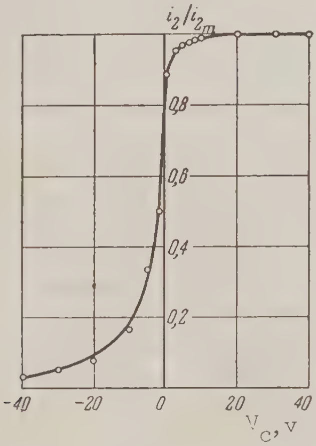

Fig.4

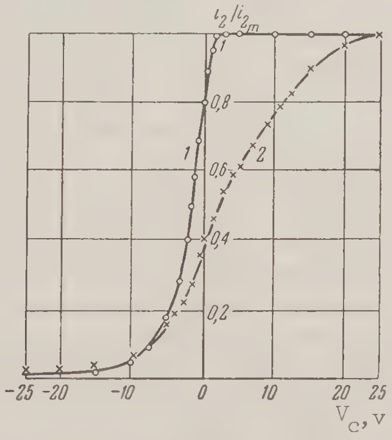

Fig.5

Fig.4. Retarding potential curve for MgO film formed on a piece of magnesium by heating it in the residual gases at a pressure of 10^{-3} mm Hg for 10 min at 600°.

Fig.5. Retarding potential curves for an activated Cu-Al-Mg alloy ($\sigma = 12.4$): 1) at a temperature of 450° and 2) at 20°.

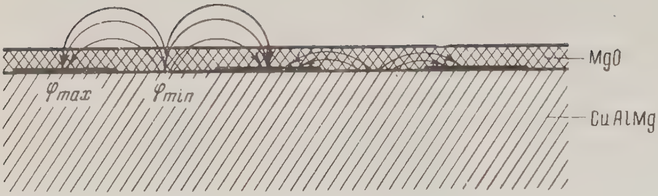

Fig.6. Schematic section through target of activated Cu-Al-Mg alloy.

(work function $\varphi_1 \approx 4.1$-4.2 ev), partly of pure nonoxidized magnesium (work function $\varphi_2 \approx 3.5$-3.8 ev), partly of magnesium oxide of stoichiometric composition ($\varphi_3 \approx 2.2$ ev) and partly of magnesium oxide with varying amounts of interstital magnesium atoms (work function variable, depending on the amount of impurity present). The contact differences of potential between the individual components produce a patch field which we shall call the "internal" patch field to distinguish it from the patch field that may form on the external surface of the oxide (see above).

Although it is difficult to establish the size of the patches, it may be assumed that they are larger than the thickness of the dielectric oxide film which most investigators in the field evaluate to be about 1000 Å. In view of the fact that the work function of the different areas varies from some tenths of a volt to about two volts and that the dimensions of the patches are of the order of tenths or hundredths of a millimeter, we obtain a field gradient of some tens of volts per centimeter for the patch field.

This "internal" field penetrates the thin dielectric layer, in which the Debye-Huckel radius is fairly large, and extends out over the surface of the emitter, giving rise to a stopping field over the microscopic areas with a small work function. To compensate this field and draw out all the secondary electrons one must therefore have a suitable additional positive potential on the collector. This is why in practice saturation of the secondary current is observed at appreciable positive collector potentials.

When the target is heated, the thin active layer becomes more conducting and screens the internal patch field so that the experimental retarding potential curve goes to saturation at $V_c \approx 0$. In this case the lines of force of the patch field close in the oxide layer without emerging out over the surface, as indicated in Fig.6. The effect is reversible, i.e., the local fields reappear upon cooling of the target. It must be noted that the character of the retarding potential curve is affected not only by the thickness of the active coating but also by its composition which determines its conductivity. The magnitude of the secondary emission coefficient σ is also connected with the composition and thickness of the active coating, although no direct correlation between the magnitude of σ and the stopping field is observed.

L.N.Dobretsov advanced the hypothesis that the stopping field over the surface of the target is produced by the patch field of the base itself, i.e., of the metallic alloy. Although retarding potential curves recorded for a nonactivated alloy exhibit saturation close to zero collector potential, nevertheless the patch field may exist due to polycrystallinity of the surface, but not be evinced in the retarding potential curve inasmuch as the secondary electrons have higher energies and a broader energy spectrum. When such a metal is covered with an oxide coating, then by virtue of the dielectric nature of the surface film, the energies of the secondary electrons will be substantially reduced (Fig.7) and the patch field of the base may produce a field over the surface of the emitter, stopping the secondary electrons.

True retarding potential curves, reflecting the actual secondary electron energy spectrum of activated alloys, can be obtained either with targets heated

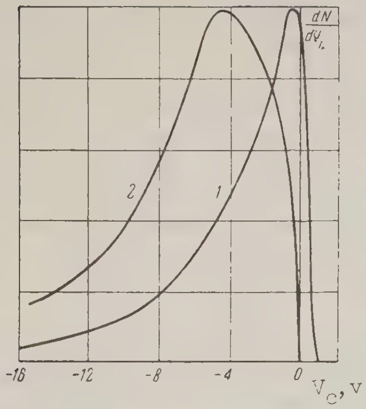

Fig.7

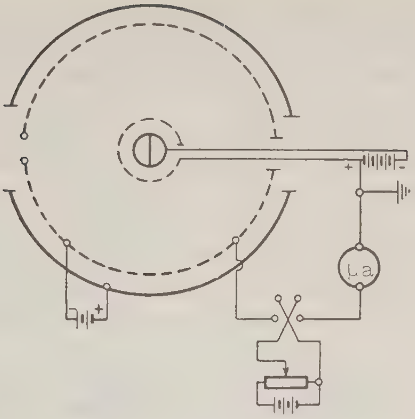

Fig.8

Fig.7. Secondary electron energy distribution: 1) for a dielectric, 2) for a metal.

Fig.8. Diagram of apparatus with two grids.

to 400° or by means of the apparatus shown in Fig.8 with a large positive potential on the second grid. Here the velocity analysis is carried out in the space between the grids.

Fig.9 shows the retarding potential curves obtained for Cu-Al-Mg alloy (1) with the target heated to 450° and (2) at room temperature with a positive potential on the second grid. The deviation of saturation from zero collector potential is due solely to the contact difference of potential between the target and collector. The difference in the shape of the curves obtained in heating the target and with a potential on the second auxiliary grid is due to the distortion of the field produced by the geometry of the apparatus: the diameter of the grid cage was 30 mm so that the velocity analysis is not based on the full energies. The curve obtained with a heated target gives a better charac-

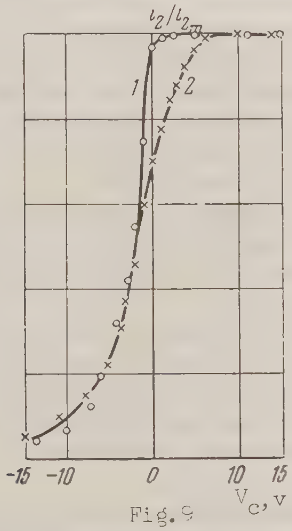

Fig.9

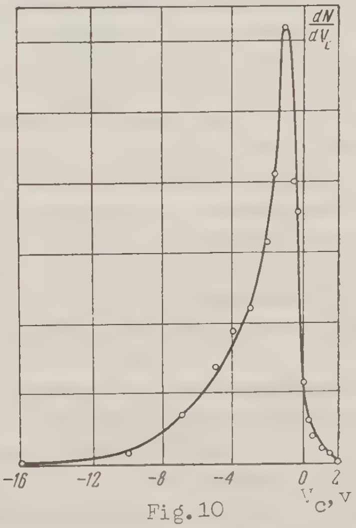

Fig.10

Fig.9. Retarding potential curves for activated Cu-Al-Mg alloy: 1) recorded at t = 450°, 2) recorded in the presence of the inner grid as illustrated in Fig. 8 and t = 20°.

Fig.10. Secondary electron energy distribution curve for Cu-Al-Mg alloy.

terization of the true secondary electron spectrum. Differentiation of this curve yields the curve shown in Fig.10, the appearance of which (half-width and location of the peak) is indicative of the semiconductor character of the active layer.

The authors wish to acknowledge their indebtedness to L.N.Dobretsov and A.R.Shul'man for valuable discussions and to V.L.Borisov for assistance in the work.

"M.I.Kalinin" Leningrad Polytechnic Institute

References

1. A.I.Piatnitskii, Zhur.tekh.fiz., 8, 1014 (1938).
2. H.Bruining and J.H.DeBoer, Physica, 6, 823 (1939).
3. A.R.Shul'man and V.L.Makedonskii, Zhur.tekh.fiz, 22, 1540 (1952).
4. V.N.Lepeshinskaia & V.M.Tumorin, ibid., 24, 1933 (1954).
5. V.N.Lepeshinskaia, Izv.AN SSSR, Ser.fiz., 20, 1025 (1956). (Trans. in Bulletin, 20, No.9, 927).

DISCUSSION

N.M.Politova: What were the geometric parameters of the apparatus?

V.N.Lepeshinskaia: The ratio of the diameters of the collector and target spheres was 10 to 16.

N.I.Ionov: What values of σ correspond to the retarding potential curves at 20° and 450°?

G.S.Vil'dgrube: If the temperature influences the retarding potential curve due to change in resistance of the layer should not σ also change for the same reason?

V.N.Lepeshinskaia: At V_p less than 300 v, σ does not change with temperature, at higher primary energies there is a weak temperature dependence.

V.G.Butkevich: It would appear that in the case of the effects in question the coating thickness is important?

V.N.Lepeshinskaia: Obviously. With thin films (coatings) the patch field penetrates further (through the coating and into the vacuum) and saturation occurs at higher positive potentials; with thick films, even at low temperatures, the patch field does not emerge from the coating and saturation will occur close to zero potential.

N.B.Gornyi: What is the field formed in the layer?

V.N.Lepeshinskaia: Probably a patch field due to inhomogeneities of the work function at the metal-oxide layer interface.

N.M.Politova: What was the thickness of the coating and the magnitude of the field in the layer?

V.L.Makedonskii: Doesn't the field in the coating attain the breakdown value?

V.N.Lepeshinskaia: The thickness of the layer is in the neighborhood of 1000 Å; the field strength in the layer is far from the breakdown value.

Lifshits: Did you try oxidizing magnesium single crystals?

V.N.Lepeshinskaia: No.

Pes'iatskii: Data obtained by Kozina support the conclusions reached in the report. In oxidizing aluminum one can obtain oxide coatings containing grains of the metal. These grains are negatively charged and act as a negatively charged grid in a vacuum tube, that is, reduce σ. Saturation of the current from such a coating was obtained at 100-200 v.

SECONDARY EMISSION CHARACTERISTICS OF MAGNESIUM AND BERYLLIUM ALLOY CATHODES AFTER SHORT-TERM ACTIVATION

- V.L.Borisov & V.N.Lepeshinskaia

Introduction

Owing to their high secondary emission coefficient magnesium and beryllium alloys are finding increasing application in photomultipliers and other electron tubes employing secondary emission.

While there have been numerous investigations devoted to activation of these alloys, so far there has not been developed a procedure fully adapted to commercial production of such emitters. Some of these studies have been concerned with the activation of specific individual alloys. Thus, for example, Zworykin and his coworkers[1] and Rappaport[2] give data pertaining only to a silver-magnesium alloy. Jenny[3] worked with the same alloy. All these authors report that they did not succeed in obtaining stable operation of the activated emitters or satisfactory resistance to the influence of air and current.

Ioshida and his colleagues[4] worked primarily with nickel-beryllium and copper-beryllium alloys. As a result of the activation procedure proposed by them there were obtained emitters having a relatively low secondary emission coefficient (at best $\sigma_{max} = 7$) and the procedure developed was applicable only under laboratory conditions.

Bobenrieth and his co-workers[5] investigated the activation of nickel-beryllium alloys containing from 2.8 to 5% Be. Their treatment requires many hours and leads to the formation of layers exhibiting the Malter effect; it is therefore not suitable for practical production purposes.

Kul'varskaia[6,7] developed a method of "dosed" oxidation (oxidation with a carefully metered amount of oxygen) for a number of alloys. According to this procedure, for each square centimeter heated to a given temperature there must be absorbed 15-20 μg oxygen for the formation of a magnesium or beryllium oxide coating. This activation technique, while it has a number of merits, is not always convenient inasmuch as the process requires an appreciable amount of time; the resultant oxide layer is rather thick (up to 3000 Å) which frequently leads to charging of the surface under electron bombardment and in some cases gives rise to the Malter effect. Inasmuch as for the dynodes used in multiplier tubes one must have emitters with no time lag, i.e., emitters whose surface would not acquire a charge in the process of operation, further research aimed at developing suitable activation procedures is indicated. At present Wargo and his co-workers[8] and Hirashima and his co-workers[9] are engaged in work in this direction, that is, are seeking ways of enhancing the air and current stability of alloy emitters and prolonging their useful life.

The specific aim of our research was to develop an activation procedure which, on the one hand, would yield a high secondary emission coefficient particularly at small primary energies and, on the other hand, would be rapid, simple and suitable for industrial use. The activated emitters had to be able to withstand prolonged exposure to air and be capable of re-establishing their properties after simple reactivation. A final requirement was that the emitters must remain stable over a prolonged period. Although the stability requirement is of paramount importance from the standpoint of practical utilization, in the present report we shall not dwell upon it. This question will be the subject of a separate publication. Here we shall give the results of our investigation of the secondary emission characteristics of alloy emitters activated under conditions satisfying the above requirements.

We investigated the following alloys: Cu-Al-Mg (94%, 6% & 1%), Cu-Si-Mg, Cu-Al-Be (97.5%, 0.5% & 2%) and Cu-Be (98% & 2%). The aluminum and silicon were introduced for the purpose of improving the mechanical properties of the alloys and did not affect the magnitude of the secondary emission coefficient. This choice of alloys was dictated by the practical aims involved. We determined the variation of σ as a function of V_p in the primary range from 20 to 1750 v. Particular attention was paid to the initial sections of these characteristics, i.e., from 20 to 150 ev. We also investigated the temperature dependence of the secondary emission coefficient, the influence of air on the emitter at different pressures, the effect of different reactivation conditions and the reproducibility of the results. We obtained curves characterizing the energy distribution of the secondaries for all the investigated emitters. These results are of particular interest inasmuch as they allow of drawing a number of deductions regarding the nature of the active layer. The measured variation of the secondary current as a function of the collector potential, as has been shown in Ref.10 (preceding article), reflects the true distribution of secondary electrons. The distribution in energy curves were obtained from samples heated to 400°, or under conditions where the retarding patch fields over the emitter surface (fields which distort the V_c dependence of I_2) were compensated.

Apparatus and measurement circuit

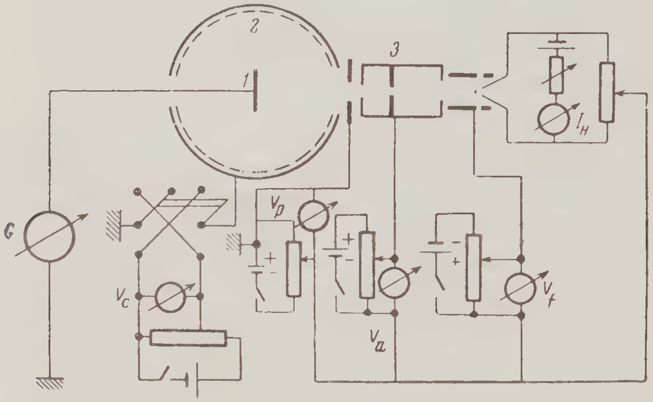

Fig.1. Diagram of apparatus and measurement circuit: 1 - target, 2 - collector, 3 - electron gun; G - galvanometer for measuring primary and difference current; V_p - voltmeter indicating primary electron velocity; V_c, V_a & V_f - voltmeters indicating voltages on collector, accelerating cylinder and focusing cylinder, respectively; I_H - ammeter indicating heater current.

All the measurements were carried out in the demountable apparatus with a spherical capacitor incorporating an antidynatron molybdenum grid (see Ref. 10). The inside surface of the glass bulb was coated with a layer of aquadag. The collector was the composite system composed of the aquadag layer and the grid. The analyzing field was applied between the grid and the target. The current was measured by means of an M-91 galvanometer with a sensitivity of $0.8 \cdot 10^{-8}$ amp per scale division. The primary current was measured with a bias of -100 v on the grid relative to the target which was grounded. Then applying +100 v to the grid, we measured the difference current $I_1 - I_2$ (or the secondary current I_2 by means of a meter in the collector circuit). The maximum value of the secondary current was $(2\text{-}4) \cdot 10^{-7}$ amp. A potential of 60 v was applied between the antidynatron grid and the aquadag layer to hold back tertiary electrons. The electron gun was of the usual four-electrode design and allowed of obtaining a well-focused electron beam with energies from 60 to 1750 v. For investigating the 10 to 150 v region we used a special Mayers type electron gun. The measurement circuit is diagrammed in Fig.1.

The vacuum during the measurements was 10^{-7}-10^{-6} mm Hg; this was obtained by means of an oil diffusion pump and two liquid nitrogen traps. Thermocouple and ionization pressure gages were used for measuring the pressure. The target temperature was monitored by means of a W-Ni thermocouple.

Copper-Magnesium Alloy

For our first experiments we chose magnesium alloys inasmuch as these are the alloys now commonly used in the production of secondary emission vacuum tubes.

A. Activating conditions and σ vs V_p curves

Aiming at utmost simplification of the activation procedure and maximum reduction of the treatment time, we carried out a series of experiments in which we varied the oxidizing medium, the pressure and the temperature and time of heating. Approximately the same results as regards secondary emission coefficient can be obtained with different combinations of the enumerated factors. In particular, the temperature and time of treatment are in inverse dependence; hence, desiring to minimize the treatment time, we found it expedient to increase the temperature for each alloy to the point of beginning of intense evaporation of the light component. In general the rate of heating must be as high as possible so that the copper, which forms the base of all the investigated alloys, would not have time to oxidize, i.e., will be quickly protected by a layer of magnesium or beryllium oxide.

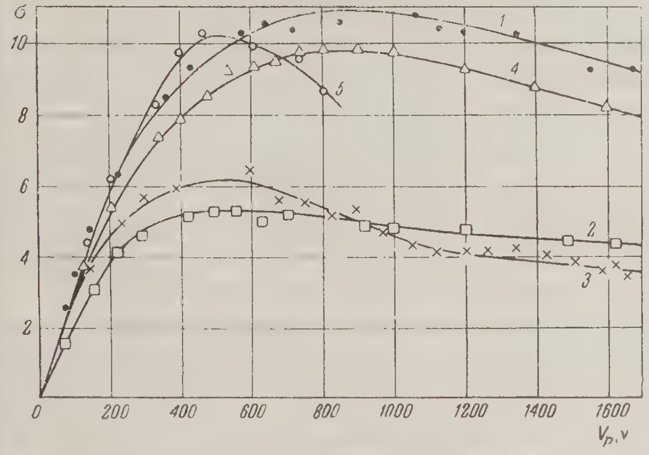

Fig.2. Variation of σ with V_p for Cu-Al-Mg alloy emitters activated in different media: 1) in carbon dioxide (measurements at 250°), 2) hydrogen, 3) oxygen, 4) water vapor, 5) "residual gases" (curves 2,3,4 & 5 recorded at 20°).

The preliminary treatment of the alloys consisted of electric polishing or mechanical cleaning (rubbing with fine abrasive paper followed by washing in alcohol). After cleaning, the samples were mounted in the experimental apparatus which was evacuated to 10^{-5} mm Hg. We experimented with activation of the Cu-base alloys in oxygen, hydrogen, water vapor, carbon dioxide and "residual gases". Samples activated in hydrogen had low values of σ; approximately the same results (Fig.2) were obtained with activation in water vapor, oxygen, carbon dioxide and "residual gases". In almost all cases by appropriate selection of the pressure, temperature and heating time we were able to obtain a maximum value of the secondary emission coefficient (8 to 13). Inasmuch as no one of these media showed clear cut advantages over the others, we decided upon activation in the "residual gases" as the most simple procedure. The term "residual gases" is admittedly ambiguous; in our cases this was air plus a certain amount of CO and CO_2 released from the aquadag coating the inside surfaces of our experimental collector bulb. This composition, however, does not appear to be "essential" for activation. Minor variations in the composition of the air in the laboratory had no appreciable influence on the quality of the activated samples. In addition, virtually identical results were obtained by activation in other experimental equipment provided there was an aquadag coated surface present.

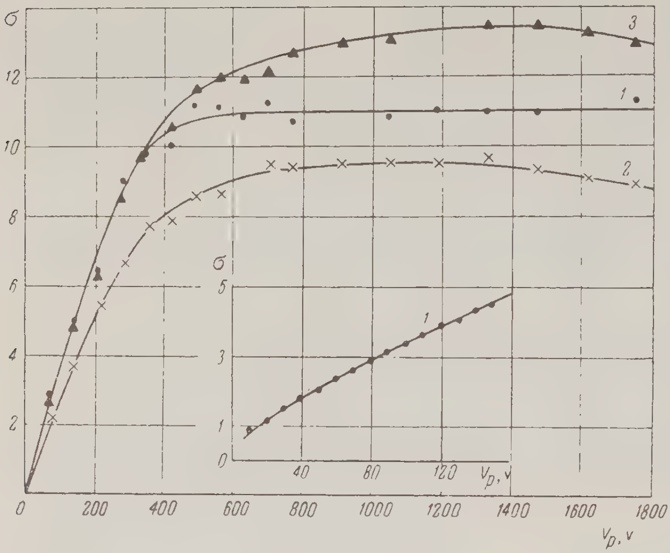

Fig.3. Variation of σ with V_p for Cu-Al-Mg alloy: 1) freshly activated sample, 2) after exposure of the activated sample to air for 2 hours, 3) after reactivation.

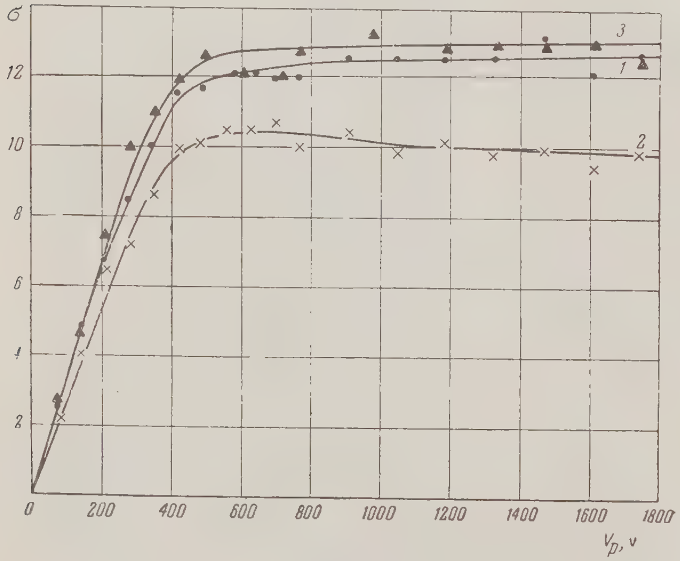

Fig.4. Variation of σ with V_p for Cu-Si-Mg alloy: 1) freshly activated sample, 2) after exposure to air for 2 hours, 3) after reactivation.

The "residual gas" pressure remained between $2 \cdot 10^{-3}$ and $6 \cdot 10^{-3}$ mm Hg during the activation process. The samples were heated at 600-620° for 8-10 min. More prolonged activation or introduction of a larger amount of oxygen leads to formation of a relatively thick magnesium oxide coating (several thousand ångstroms according to Kul'varskaia[7]) as a result of which a surface charge builds up when the target is bombarded with electrons. Charging of the surface was not observed with the thickness and conductivity of the magnesium oxide layers formed in the activation procedure described above. The σ vs V_p curves obtained show that the scatter of data for samples of the same alloy activated under identical conditions is not large: for the initial section of the curve (up to V_p = 300 ev) the spread does not exceed 10-12%; after attainment of the maximum secondary emission coefficient, however, the characteristics do differ. We obtained curves with pronounced peaks, curves with a flat maximum as well as curves with intermediate shape. This variation may be attributed to variations in the thickness of the active coatings and the number of defects therein, which is inevitable in the case of individual activation of each sample.

The section of the σ vs V_p curve in the primary energy range from 20 to 150 ev was investigated in more detail inasmuch as for practical purposes it is particularly important to know the value of the secondary emission coefficient at low primary energies. The characteristics obtained for Cu-Al-Mg alloy in the primary energy range to 1750 ev are shown in Fig.3. Similar characteristics for Cu-Si-Mg alloy are reproduced in Fig.4. As may be seen from the curves, the maximum value of the secondary emission coefficient is attained in the primary electron energy interval from 550 to 650 ev. At $V_p =$ $= 100$ ev the values of σ fluctuate between 3.2 and 3.6. The variation of σ as a function of V_p in the initial portion of the curve (up to $V_p = 300$ ev) is almost linear for all the investigated alloy samples.

B. Reactivation conditions and their effect of the σ vs V_p curves

In view of the fact that activated emitters must come into contact with air for some period (for example, while being mounted in tubes), the effect of air on their secondary emission characteristics is important. It is known that contact with air generally reduces the secondary emission coefficient of alloy cathodes by 10 to 50%. Hence we investigated the efficacy of reactivation treatments suitable for use under industrial conditions. Further, we investigated the influence of time of exposure to air, the air pressure and the composition of the atmosphere. The principal decrease of the secondary emission coefficient occurs during the first fraction of an hour; following this the sample may remain in air for many hours with little additional decrease of σ. It is important, however, that the surface of the sample be protected from extraneous contaminants, particularly water vapor. Samples stored at air pressure in a closed container (for example, the experimental tube or a dessicator) show a smaller decrease of σ than emitters held in the open.

We found on the basis of our experiments that fully satisfactory results as regards reactivation are obtained by simple heating at 450-500° at a pressure of 10^{-5}-10^{-6} mm Hg. Curves 2 & 3 in Figs.3 & 4 show the influence of air on σ and the restoring effect of 2 hours heating in vacuum. If the sample after activation is held for several hours in air at atmospheric pressure, the coefficient σ is reduced over the entire primary electron energy range. On the other hand, if the sample is held under poor vacuum conditions, i.e., in air at a pressure of 10^{-2} mm Hg, it exhibits little or no decrease of σ in the low primary energy region.

As a result of such reactivation heating the value of the coefficient σ is fully restored; in fact, in some cases the σ vs V_p curve for the reactivated sample lies somewhat higher than the original curve. The initial section of the curve up to $V_p = 300$ ev remains linear.

C. Temperature dependence of σ

There are only scanty data in the literature on the temperature dependence of the secondary emission coefficient of alloy emitters. Kul'varskaia[6,7] gives the results of rather detailed measurements; however, in view of the activation procedure used, the magnesium oxide coating formed in Kul'varskaia's experiments was relatively thick and a surface charge built up on it during electron bombardment. The observed increase in σ with increase of temperature to 250° may, apparently, be explained by the increase in the conductivity of the layer with resultant decrease of charging of the surface. The shape of the curve above 250° indicates a decrease of σ with increasing temperature and is consistent with the true temperature dependence of σ owing to increased energy loss of the secondary electrons as a result of collisions with the lattice.

Johnson & McKay[11] measured the variation of σ with temperature for an MgO single crystal; Dekker[12] attempted to explain their results on the basis of a simple model and obtained good agreement with experiment.

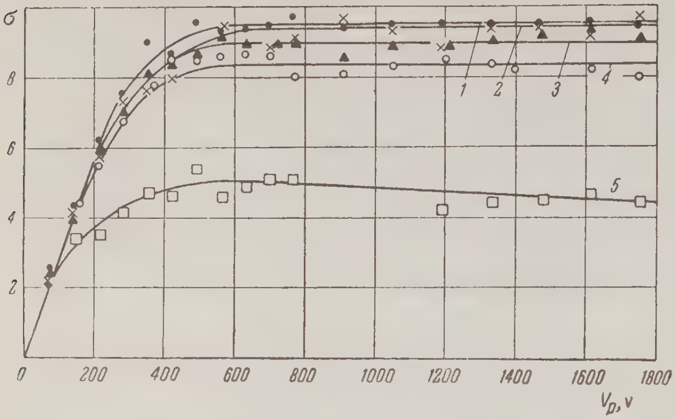

Fig.5. Variation of σ as a function of V_p for Cu-Al-Mg alloy at different temperatures: 1) 20°, 2) 100°, 3) 250°, 3) 350° and 5) 475° C.

In the present investigation the temperature dependence of σ of activated magnesium alloys was studied in fair detail. The experimental results show that with increasing temperature, there occurs a monotonic (but reversible) decrease of σ (see Fig.5). In the range of primary energies greater than 500-600 ev dσ/dt remains virtually constant. We calculated the theoretical temperature dependence of σ in the range from 290 to 750°K making use of the formula

$$\frac{\sigma_1}{\sigma_2} = \left[\frac{2n_{\nu_2}+1}{2n_{\nu_1}+1}\right]^{1/2},$$

derived by Dekker[12]; here $n_\nu = \frac{1}{e^{h\nu/kT}-1}$, the value of $h\nu$ for MgO from optical data being $1300k$ (k is Boltzmann's constant). The calculated data were compared with our experimental results for activated copper-magnesium alloys. As will be seen from the accompanying table up to 400° the agreement is satisfactory.

T°,K	σ_T/σ_{273}, calculated	σ_T/σ_{273}, exper.	T°,K	σ_T/σ_{273}, calculated	σ_T/σ_{273}, exper.
293	1	1	598	0,905	0,88
373	0,982	0,99	623	0,895	0,88
473	0,950	0,96	673	0,876	0,87
523	0,931	0,94	698	0,862	0,77
548	0,923	0,92	723	0,856	0,75
573	0,912	0,90	748	0,848	0,50

This agreement gives reason to assume that a layer of magnesium oxide forms on the surface of the activated alloy. At higher temperatures, however, the reduction of σ in the case of the actual alloy is somewhat greater than given by calculation; this indicates that there is another factor affecting σ, a factor that begins to prevail in the region of higher temperatures. Apparently, there are superposed on the "normal" temperature dependence of σ changes in the coefficient connected with alteration of the state of the active coating at temperatures above 400°.

For repeatedly oxidized samples (when the thickness of the magnesium oxide coating increases), we obtained a temperature dependence analogous to that reported by Kul'varskaia. Heating of samples to 450° with simultaneous electron bombardment leads to irreversible changes of σ, presumably connected with permanent alterations of the coating composition.

D. Energy distribution of secondary electrons

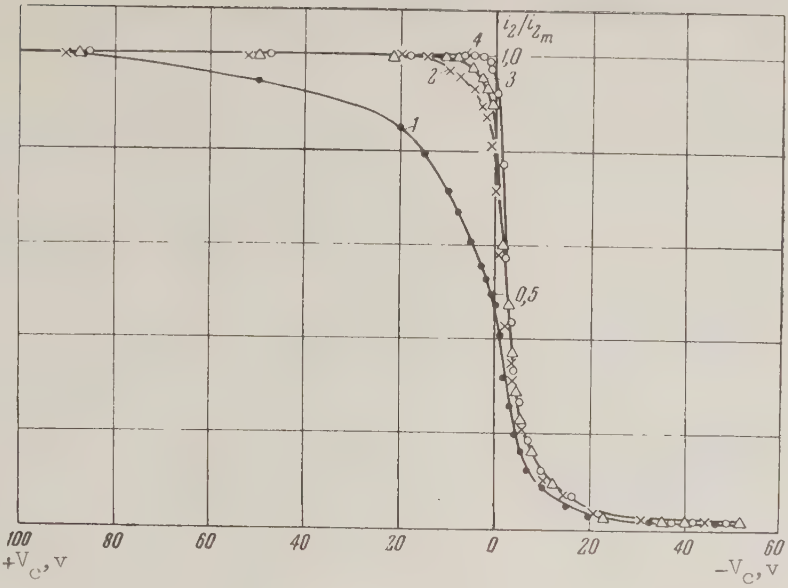

Fig.6. Series of retarding potential curves for Cu-Al-Mg alloy obtained at different temperatures: 1) 20°, 2) 250°, 3) 350° and 4) 400°C.

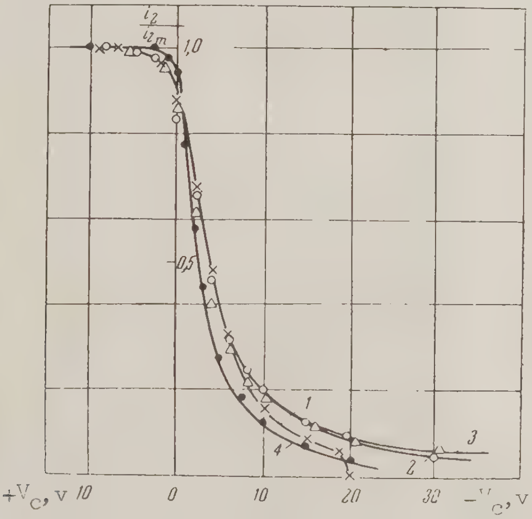

Fig.7. Series of retarding potential curves for Cu-Al-Mg alloy obtained at different primary electron energies (target temperature - 400°): 1) V_p = 20 ev, 2) 50 ev, 3) 70 ev, 4) 280 and 500 ev.

The secondary current vs collector potential curves, as was noted in an earlier contribution[13], do not exhibit saturation near zero collector potential. The secondary current approaches saturation at a collector potential of 30-50 v or higher, which indicates that there are present at the surface of the emitter retarding fields, concerning which there are diverse hypotheses[10,14]. Naturally, such retarding potential curves do not reflect the true distribution in energy of secondaries. If, however, the samples are heated to about 400°, the collector potential at which saturation occurs approaches zero. The series of σ vs V_c curves obtained at different temperatures is shown in Fig.6. Retarding potential curves obtained at different primary electron energies for targets heated to 400° are reproduced in Fig.7. Differentiation of the $I_2 = f(V_c)$ curves obtained for heated targets yields true energy distribution of the secondary electrons; distribution curves obtained in this way on the basis of our data are shown in Fig.8.

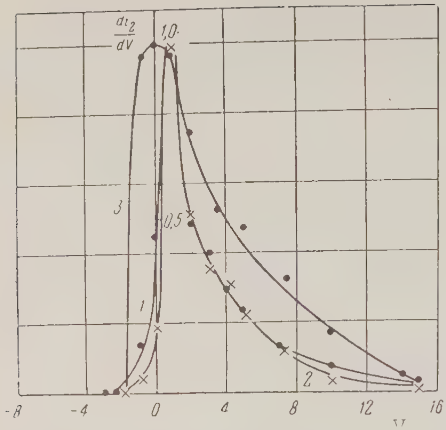

Fig.8. Energy distribution of secondary electrons: 1 & 2) for Cu-Al-Mg alloy (V_p = 280 v and 600 v, respectively), 3) for Cu-Al-Be (V_p = 330 v).

Copper-Beryllium Alloys

We established that the following procedure for activating copper-beryllium alloys, yielding relatively high values of the secondary emission coefficient. After preliminary cleaning of the alloy (in the same way as outlined above for copper-magnesium alloys), the samples are heated for 8-10 min at 800° in the "residual gases" at a pressure of $(2\text{-}5)\cdot 10^{-3}$ mm Hg. After such activation the maximum value of the secondary coefficient is 9-11 and at V_p = 100, σ is about 3.5-4.0.

The variation of the secondary emission coefficient σ with the primary electron energy for copper-beryllium emitters is shown in Fig.9. A common feature of these curves is a pronounced maximum. This maximum is shifted by 100 v to the side of lower primary energies as compared with its position for copper-magnesium alloys. In most cases the initial section of the σ vs V_p curves for beryllium alloys lies higher than the corresponding section for magnesium alloys.

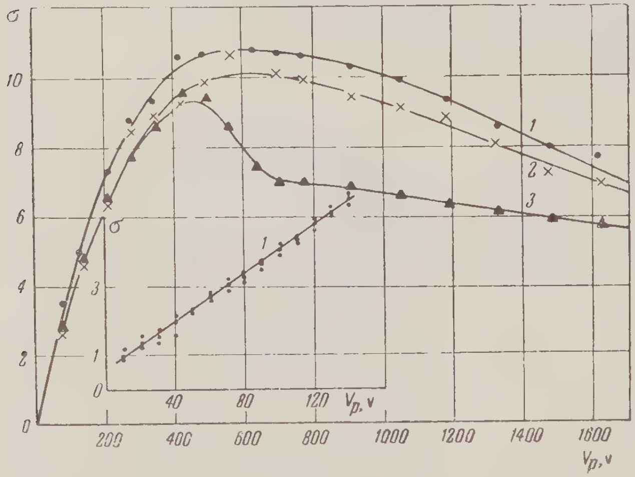

Fig.9. Variation of σ with V_p for Cu-Al-Be alloy: 1) freshly activated sample, 2) after exposure to air for 2 hours, 3) after reactivation.

The influence of air on the secondary emission coefficient of activated copper-beryllium emitters is weaker than in the case of copper-magnesium ones. The coefficient of secondary emission is reduced very little by exposure to air. Reactivation of the copper-beryllium emitters, however, at temperatures of 400-500° does not fully re-establish the initial properties, as may be seen from Fig.9. The reactivation temperature for beryllium alloys must be higher owing to the fact that beryllium diffuses less intensely than magnesium.

Fig.10 shows the σ vs V_p curves obtained at different temperatures for Cu-Al-Be alloy.

The variation of the secondary electron current with the collector potential at different temperatures of the emitter is shown in Fig.11. As may be seen, saturation of the secondary current occurs at an appreciably higher value of V_c when the emitter is at room temperature. At 500° the retarding potential curves become "normal" (allowing for the target-collector contact difference of potential). The energy distribution of secondary electrons obtained by graphic differentiation of the high temperature retarding potential curve is shown in Fig.8.

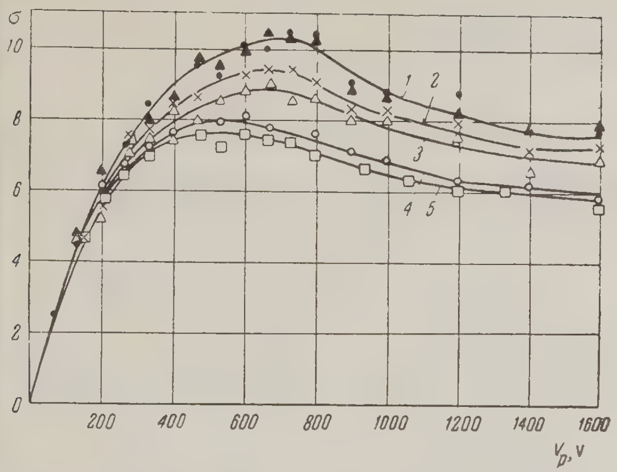

Fig.10. Variation of σ with V_p for Cu-Al-Be alloy at different temperatures: 1) T = = 20°, 2) 100°, 3) 250°, 4) 400°, 5) 500°C.

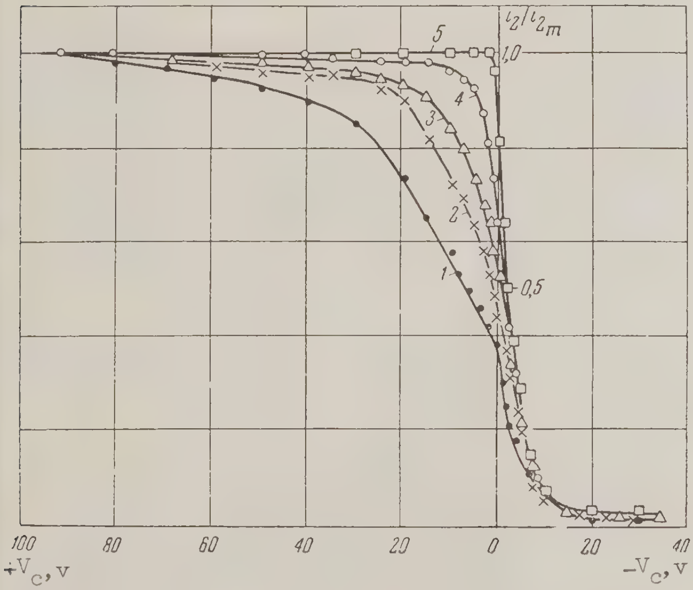

Fig.11. Series of retarding potential curves obtained for Cu-Al-Be alloy at different temperatures: 1) T = 20°, 2) 120°, 3) 320°, 4) 450° and 5) 500°C.

Conclusions

The activating procedure developed by us for a number of alloy emitters allows of reducing the activating time to a few minutes (8-10 min). This procedure does not require the use of any special oxidizing medium: the entire process is carried out in the "residual gases" in the apparatus. The resultant maximum value of the secondary emission coefficient σ changes from 9 to 13; at V_p = 100, σ equals 3.2-3.6 for copper-magnesium alloys and 3.5-4.0 for copper-beryllium alloys. The proposed activation technique allows of using a relatively simple method of reactivation of copper-magnesium alloy emitters whose secondary emission properties have been lowered due to exposure to air.

We investigated the character of the variation of σ with V_p and the temperature dependence of σ. The temperature coefficient of σ proved to be negative and equal to between -0.02 and -0.03% per degree.

We obtained curves for the variation of the secondary current as a function of the collector potential and then by graphic differentiation determined the curves characterizing the secondary electron energy distribution for all the investigated alloys.

Graduate students N.N.Khristoforov and T.A.Kuz'mina participated in the investigation.

"M.I.Kalinin" Leningrad Polytechnic Institute

References

1. V.K.Zworykin, J.E.Ruedy & E.W.Pike, J.Appl.Phys., 12, 696 (1941).
2. P.Rappaport, J.Appl.Phys., 25, 288 (1954).
3. D.A.Jenny, Secondary Emission at High Current Densities. - Zürich, 1951.
4. Sh.Ioshida, J.Takeda, Y.Igarashi & Y.Arata, J.Phys.Soc.Japan, 8, 318 (1953).
5. A.Bobenrieth, J.Millet & S.Teszner, Compt.Rend., 239, 794 (1954).
6. B.S.Kul'varskaia, Izv.AN SSSR, Ser.fiz., 20, 1029 (1956). (Trans., Bulletin, 20, No.9, 931.)
7. B.S.Kul'varskaia, Radiotekhnika i elektronika, (Radio Engineering and Electronics), 1, 512 (1956).
8. P.Wargo, B.Haxby & W.G.Shepherd, J.Appl.Phys., 27, 1311 (1956).
9. M.Hirashima & S.Miyashiro, J.Phys.Soc.Japan, 12, 770 (1957).
10. V.N.Lepeshinskaia & T.M.Sukova, Present issue of the Bulletin, p.631.
11. J.B.Johnson & McKay, Phys.Rev., 91, 582 (1953).
12. A.J.Dekker, Phys.Rev., 94, 1179 (1954).
13. V.N.Lepeshinskaia & V.A.Tumorin, Zhur.tekh.fiz., 24, 1933 (1954).
14. V.N.Lepeshinskaia, Izv.AN SSSR, Ser.fiz., 20, 1025 (1956). (Trans. Bulletin, 20, No.9, 927.)

DISCUSSION

I.M.Bronshtein: What were the conditions of measurement? Were the temperature induced changes reversible? Which σ vs V_p curves correspond to the thinner coatings - those with a sharp peak or those with a flat maximum? What was the secondary emission coefficient of the nonactivated alloy?

V.L.Borisov: The measurements were made under static conditions (i.e., not with pulses). The temperature induced changes are reversible. Generally curves with a peak were obtained for the thinner films. For nonactivated alloys $\sigma_{max} \approx 2$ at $V_p = 350$ v.

A.I.Piatnitskii: Did you observe charging of the surface?

V.L.Borisov: In the case of overactivation we observed a time lag of the emission, indicating building up of a surface charge.

D.B.Diiatroptov: What were the vacuum conditions?

V.L.Borisov: The work was carried out in an apparatus that had two joints; the vacuum was between $5 \cdot 10^{-7}$ and $7 \cdot 10^{-7}$ mm Hg.

V.A.Astrin: What was the reproducibility from sample to sample and how would you characterize the uniformity of the sample surfaces?

V.L.Borisov: The initial sections of the σ vs V_p curves were reproducible; that is, virtually identical for different samples. We did not investigate the uniformity of the surface.

N.A.Iasnopol'skii: What was the thickness of the oxide layer? What is the difference between your work and that of B.S.Kul'varskaia?

V.L.Borisov: The coating thickness was of the order of 1000 Å. The difference between our work and that of Kul'varskaia lies mainly in the technique employed for activating the alloys; the results are generally in agreement.

Iaskovskaia: Does the method of preparation of the surfaces (polishing, cleaning with abrasive paper) prior to oxidation affect the results?

V.L.Borisov: Polishing and cleaning with abrasive paper yielded approximately the same results.

KINETICS OF CHARGE BUILD-UP ON A DIELECTRIC SURFACE UNDER ELECTRON BOMBARDMENT

- I.R.Zakirova & S.A.Fridrikhov

Introduction

When charged particles fall on the surface of a dielectric or an insulated metal body these objects become charged. The rate of charge build-up and its magnitude under equilibrium conditions depend on a number of factors: the properties of the given surface (its secondary emission characteristics, conductivity, etc.) and the number of particles incident on and leaving the surface.

To a greater or lesser extent the charging effect is encountered in all electronic vacuum devices inasmuch as in every tube charged particles may be incident on the surfaces of the bulb and various mounting components. Generally, in such cases the charge is an undesirable effect inasmuch as it alters the configuration of the electric field in the device and therefore interferes with its normal operation (see, for example, Ref.1).

On the other hand, a number of electronic devices are based precisely on utilization of the charging effect.[2,3] In view of this, investigation of the behavior and the mechanism of formation of a charge spot or patch on the surface of a dielectric is of great interest.

In most investigations devoted to the problem no account is taken of the specific properties of the dielectric: the charging of the dielectric surface is regarded as equivalent to the charging of an insulated metallic target and therefore is considered as essentially charging of a certain capacitance. Highly typical in this respect is the work of McKay[4]. Iasnopol'skii[5] was the first to note the distinctive features of charging of an insulated metallic target in the presence of edge effects. Iasnopol'skii showed that under such conditions the equilibrium potential to which the insulated metallic target is charged may differ appreciably from the potential of the electron collector and depends on the distance between the target and the collector.

Upatov[6] calculated the electric field in the vicinity of a charge spot. In his work Upatov took into account the nonuniform charge distribution over the surface of the dielectric and the influence of charges induced by the charge patch on other electrodes and showed that the potential at the center of the charge patch produced by an electron beam with a Gaussian current density distribution over its cross section is a slowly varying function of time that is strongly dependent on the ratio between the beam radius and the distance from the target surface to the collector.

The time dependence of the potential on the surface of a dielectric bombarded by an electron beam was investigated by Hinterberger[7]. Inasmuch as, however, Hinterberger did not take into account the specific characteristics of a dielectric target the results of his work do not have general significance.

Thus until now the kinetics of formation and dissipation of charge on a dielectric surface has not been adequately studied. At the same time it must be noted that there is still no convenient and dependable technique for monitoring the variations in the state of a charge patch, occurring over a given time interval, particularly a short one (of the order of a microsecond).

In the present report we describe a pulse technique for investigating the kinetics for charging and discharging of a dielectric surface and give the results of measurement carried out by this procedure on a number of dielectric surfaces.

This report was originally presented at an interdepartmental seminar in April 1957.

Measurement Procedure and Equipment

For investigation of the kinetics of appearance and disappearance of charges on the surface of dielectrics under electron bombardment we used a pulse technique based on analysis of the influence of the charged dielectric surface on the secondary electron flux.

Fundamental to development of the technique were the following considerations. The kinetics of charging is determined primarily by the magnitude of the charging current, i.e., by the number of electric charges settling on the target surface by the end of successive time intervals. For a given dielectric target the magnitude of the charging current depends not only on the properties of the target but also on the conditions under which secondary emission occurs. These are necessarily determined by the electric fields in the proximity of the target surface.

Let us consider in more detail the actual electric field obtaining over the target surface. The field over the bombarded area of the dielectric is determined by the potentials and arrangement of the surrounding electrodes and by the potential distribution in the charge patch itself and over the entire surface of the dielectric in general. Hereinafter we shall refer to the field produced by the electrodes surrounding the target (specifically, the collector) as the collector field E_c. The field due to the potential distribution over the charge patch we shall refer to as the charge patch field E_p; finally, we shall designate the field due to edge effect as the edge field E_{ee}.

The normal component of the total field then is

$$E_{tot\ x} = E_{c\ x} + E_{p\ x} + E_{ee\ x}. \tag{1}$$

Obviously, in the case of a nonuniform potential distribution over the patch and the presence of edge effects, $E_{tot\ x}$ will differ at different points over the target surface.

Here we shall consider the specific case of appearance of a positive charge patch ($\sigma > 1$). As long as the field $E_{tot\ x}$ over the entire target accelerates the secondary electrons, pulling them away from the target, the maximum charging current will flow through the target circuit. We can call this stage of formation of the patch "charging under conditions of complete collection of the current". As the charge on the target surface builds up there will arrive a time τ, when over some point above the patch $E_{tot\ x}$ becomes zero; then the field at this point is transformed from an accelerating to a retarding one. Obviously, the secondary current from this section of the target will decrease, which will lead to a decrease of the total charging current. With time these conditions spread to the other parts of the charge patch, in consequence of which the charging current will be further reduced with accompanying equalization of the potential over the surface of the dielectric. At some instant, therefore, the charging current i_3 will fall off virtually to zero. As a result, further alteration of the potential distribution over the dielectric surface will proceed very slowly. Let us designate the time to establishment of this quasi-stationary state on the dielectric surface by t_{qs}.

From the variation with time of the secondary electron current one can judge of the changes in the charging current and, consequently, of the state of the target surface. It is simpler, however, to determine directly the variations in the magnitude of the charging current by measuring the difference current (difference between secondary and primary currents) in the target circuit, inasmuch as this difference current is the charging current (provided leakage can be neglected).

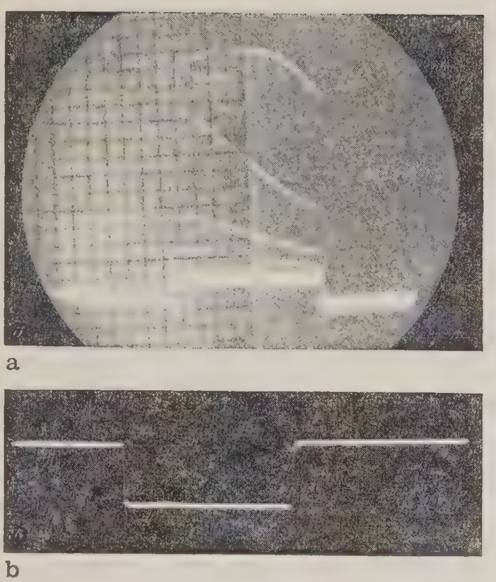

Fig.1. Oscillograms of current pulses: a) difference, b) primary current. Pulse duration - 100 μsec; interval between pulses - 1 sec.

By applying one or more single pulses of known height and width to an initially uncharged dielectric surface and measuring the charging (difference) current pulses one can determine the value of τ and t_{qs}, characterizing the kinetics of charging.

Our experimental data are consistent with the above concepts. By way of illustration, characteristic oscillograms of the primary and difference currents obtained in bombardment of a mica surface are reproduced in Fig.1. Fig.1,a shows the succession of difference current pulses obtained with 100 microsec primary pulses at intervals of 1 sec. It will be seen that for some time (approximately 60 microsec) the amplitude of the upper (first) pulse remains constant (complete collection of secondary persists); then there follows a characteristic break at the pulse peak and a slow decrease of the charging current which continues for 5-6 pulses (500-600 microsec). After this there is no further appreciable change in the current (bright trace in Fig.1,a), which corresponds to establishment of the quasistationary state on the surface. Thus from these oscillograms we can determine both τ and t_{qs}.

Making use of difference current oscillograms similar to the one shown in Fig.1,a, one can also determine the charge built up on the target at any given instant.

The amount of electricity Q accumulated on the surface of the dielectric at the time t in the absence of leakage can be determined as the area under the pulses, i.e.,

$$Q = \int_{0}^{t} i(t)\,dt, \tag{2}$$

where i(t) is the amplitude of the charging current. As may be seen from Fig.2, the initial amplitude of each succeeding pulse is virtually equal to the final amplitude of the preceding pulse, i.e., leakage is virtually negligible during the interval between pulses (1 sec) and therefore entirely insignificant during the pulse duration time (100 microsec). This enables us to calculate the amount of electricity accumulated on the surface by any given time t by means of Eq.(2), i.e., by graphic integration of $i = f(t)$.

If we now determine the capacitance of the target (under our conditions this was easy inasmuch as in most cases the electron beam covered the entire target surface), then knowing the charge accumulated at any given instant, we can readily determine the mean surface potential of the target due to this charge at any given instant including the instants τ and t_{qs}.

Finally, utilizing the described pulse technique we can evaluate the time t_d for the complete discharge of the target, initially charged to any

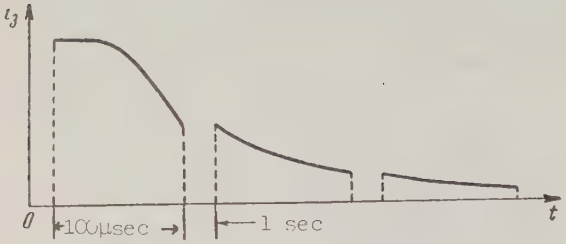

Fig.2. Succession of difference (charging) current pulses obtained for mica at a temperature of 20° and a potential V_c = 100 v on the spherical collector.

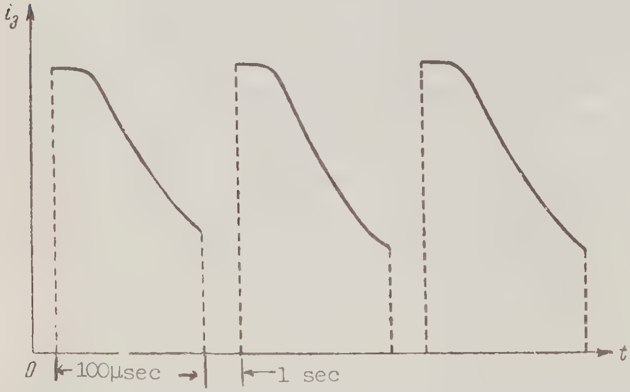

Fig.3. Succession of almost identical difference current pulses. Target - mica; target temperature - 500°.

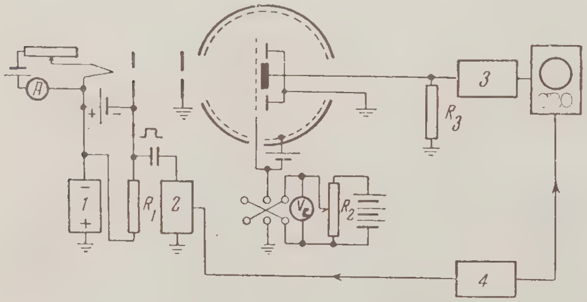

Fig.4. Block diagram of set-up: 1) accelerating voltage source, 2) square pulse generator, 3) pulse amplifier, 4) triggering pulse generator, CRO) slave sweep oscillograph.

given potential. Applying a series of primary pulses to the target and appropriately varying the interval between them, one can obtain complete duplication of the shape and height of the successive pulses. This will occur when the charge accumulated by the target during the period of the pulse is fully dissipated in the interval between pulses. Hence the minimal time between successive pulses necessary to obtain difference current pulses of identical height and shape gives us t_d.

The above said may be clarified by the following examples. It will be seen in the oscillograms of Fig.1,a and the drawing of Fig.2 that the amplitude of the beginning of the second, third, etc. pulses approximately equals the final amplitude of the preceding pulse. This is due to the fact that under the given specific conditions (target at room temperature) the leakage from the surface was virtually negligible during the interval between pulses (1 sec), i.e., the interval between pulses was appreciably smaller than t_d. The succession of pulses shown in Fig.3, however, was taken under conditions (target temperature - about 500°), where each succeeding pulse virtually repeated the shape of the preceding one. In other words, t_d in the latter case is approximately equal to the interval between successive pulses, i.e., t_d = 1 sec in this case.

To investigate the kinetics of charging, we used the set-up diagrammed in Fig.4. This set-up is similar in type to that used by Shul'man et al [8,9] for investigating secondary electron emission by the single pulse procedure. Our set-up differed from that of Shul'man et al as regards design of the target and collector; also we used pulses of greater duration (100-250 microsec).

A standard electron gun, yielding a medium energy electron beam, served as the primary electron source. We carried out a series of special measurements which showed that the current density distribution across the beam is nearly Gaussian. The current density across the central part of the beam could therefore be regarded as essentially uniform. Hence separating this part of the beam, one can carry out investigations under conditions of uniform current density. This was realized by using a target design in which only the central 6 mm diameter portion of the defocused 12-15 mm diameter (at the dielectric surface) beam was utilized. The peripheral portion of the beam fell on a grounded metallic ring surrounding the target. It could be assumed that under these conditions edge effects would exert the greatest influence on the process of patch formation. For control purposes, we also carried out measurements under conditions when the diameter of the electron beam was smaller than that of the target and the metallic ring was removed.

Aside from the usual spherical collector, we also utilized a fine-mesh grid from a television tube as collector; by means of a special device this collecting grid could be positioned at different distances from the dielectric surface.

All the measurements were carried out at a pressure of 10^{-6} mm Hg. The investigated dielectrics were mica and different kinds of glass.

Experimental Results

According to the concepts of McKay[4], which do not take into account the specific features of charging of a dielectric, the charging current pulse should have the shape shown in Fig.5. Conditions for current collection should persist until the potential of the target surface becomes equal to the collector potential after which there may be a short period of additional charging of the target at the expense of the initial velocities of the secondary electrons. In other words, the time t_s to establishment of the stationary state is very close to τ.

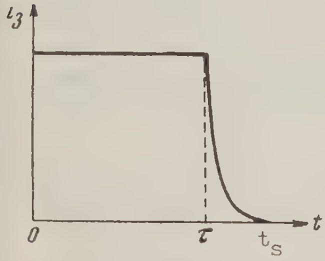

Fig.5. Schematic representation of the process of charging of an insulated metallic target, neglecting edge effects.

Thus, according to McKay, the charging of a dielectric surface to the collector potential V_c (in the virtual absence of leakage) may be regarded as charging of a certain capacitance by a charging current of constant value. The time τ is then given by

$$\tau = \frac{\epsilon V_c}{4\pi l j(\sigma-1)} \tag{3}$$

where ϵ is the dielectric constant of the dielectric, l is the thickness of the dielectric, σ is the secondary emission coefficient and j is the primary current density.

Our very first measurements showed, however, that this idealized description does not correspond to reality. Fig.2 shows the succession of difference (charging) current pulses obtained for mica at room temperature and with a potential $V_c = 100$ on the collector. The mean charging current density was $2\cdot10^{-6}$ amp/cm^2; the target subtended only the central portions of the defocused beam (experiment with metallic ring - see description above).

It will be seen from Fig.2 that, in contrast with the idealized case pictured in Fig.5, conditions for complete collection of the secondary current breakdown comparatively soon, i.e., the experimentally determined time τ

is appreciably shorter than the value given by Eq.(3). At the same time the additional charging of the target to the stationary state continues over an appreciable period. Thus actually $\tau \ll t_s$.

Numerical calculation of the magnitude of the charge built up on the surface by the times τ and t_{qs} showed that the surface obtains an appreciable portion of the total charge built up on the surface by the time t_{qs} after breakdown of the condition for complete collection of the secondary current, i.e., during the time $t_{qs} - \tau$.

Determination of the mean surface potential of the charge patch, by the procedure described above, showed that at the instant τ the potential of the surface differs appreciably from the potential of the positive electrode (collector). In fact, the complete charge accumulated by the surface at the instant of attainment of the quasi-stationary state, i.e., by the time t_{qs}, is also insufficient for the target to come up to the collector potential.

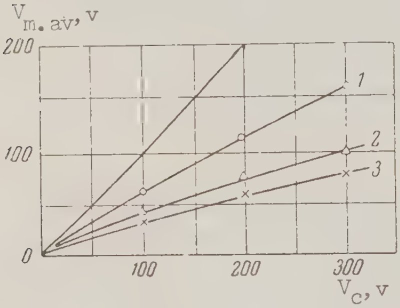

Fig.6. Variation of the mean potential $V_{m.av}$ acquired by the dielectric surface during the time t_{qs} as a function of the collector potential V_c for different distances d between the surface of the target and the collector. The straight line at 45° corresponds to the ideal case when $V_{m.av} = V_c$; 1) d = 1 mm, 2) d = 2 mm, 3) sphere of radius r = 60 mm.

Fig.6 shows the variation of the average potential $V_{m.av}$ of the dielectric surface (calculated for the time t_{qs} from the amount of charge accumulated by the surface and the capacitance of the target) with the collector potential V_c for different distances d between the target surface and the collector. The straight line plotted at 45° is for the ideal cases when $V_{m.av} \approx V_c$. The experimental curves show that the mean surface potential of the dielectric lags behind the collector potential and that it depends on the geometry of the apparatus.

These results can be explained from the standpoint of the above description of charge build-up on the surface of the dielectric, i.e., by taking into account the fields due to appearance of the charge patch. If due to the presence of the charge patch $E_{tot\ x} < E_{c\ x}$, obviously, the time τ will be reduced compared with the value of τ calculated according to Eq.(3) and, consequently, the potential at the given instant will differ from V_c. For the same reason the quasi-stationary state of the target surface will be established at a potential smaller than V_c. The transition from the quasi-stationary state to the stationary one can be extremely drawn out; where this is the case leakage will begin to play a significant role and the surface of the dielectric (even if the beam density distribution over the entire surface of the target is fairly uniform) may never attain the collector potential. In other words, the condition for equality of the number of electrons arriving at and leaving the surface will be determined by the magnitude of $E_{tot\ x}$ and the leakage current, and will only partially depend on the collector potential V_c inasmuch as this potential determines only one of the components of $E_{tot\ x}$.

Now we must determine the conditions affecting the rate of charge build-up and its magnitude.

Fig.7 shows the variation of the time τ of persistance of complete collection of the secondary current with the magnitude of the charging current i_3. This curve is characterized by the hyperbolic law

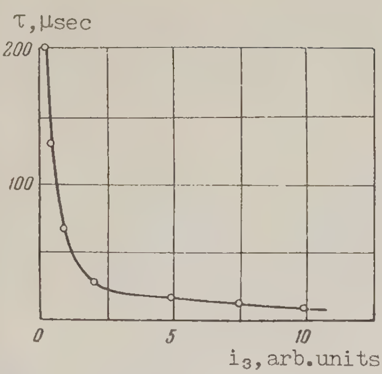

Fig.7. Variation of the time τ of persistance of complete secondary current collection with the magnitude of the charging current i_3.

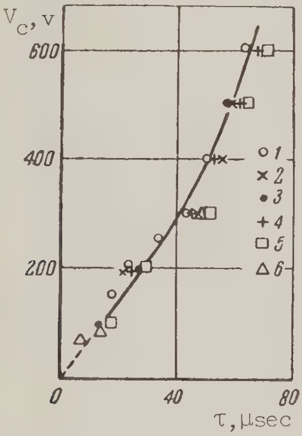

Fig.8. Variation of the time τ of persistance of complete collection of the secondary current with the collector potential V_c (collector - sphere of radius r = 60 mm): 1) V_p = = 300 ev, 2) 500 ev, 3) 700 ev, 4) 800 ev, 5) 1000 ev, 6) 2000 ev.

$$i_3\tau = Q = \text{const.}$$

An analogous relation obtains for i_3 and t_{qs}. On the basis of these results one can normalize the experimentally determined charging times to the same charging current value. This allows of comparing τ and t_{qs} measured at different values of the primary electron energy V_p (different values of σ) other conditions being equal.

Let us call the functional dependence of τ on V_c for a given set of conditions the target charging characteristic. The charging characteristics for different values of V_p obtained with a spherical collector of radius r = 60 mm are shown in Fig.8. It will be seen that within the limits of experimental accuracy one cannot establish dependence of τ on V_p. Similar experiments carried out with different substances at different collector-to-target distances showed that for all the utilized primary electron energies (50 to 2000 ev) and the given collector field E_c, the magnitude of τ is independent of V_p (normalized to the same current density) and is determined only by the time of accumulation of a certain definite amount of electricity on the target surface.

At the same time it will be seen from Fig.8 that the variation of τ with the collector potential V_c is nonlinear. This shape of the charging characteristic may be explained by the fact that at higher values of V_c, at the instant τ the surface accumulates a larger amount of electricity in consequence of which there are formed stronger local fields, the influence of which increases more rapidly than the direct influence of the collector potential. This effect of a stronger influence of local fields becomes clearly evident if we analyze the dependence of the charging process on geometric factors.

We also investigated the charging characteristics for different distances d between the surface of the dielectric and the collector. The functional dependences of τ and t_{qs} on V_c are shown in Fig.9. Characteristics 1 and 1' were recorded with the spherical collector of radius r = = 60 mm; curves 2 & 2' were obtained with a target-to-collector (grid) distance of 2 mm; curves 3 & 3' with a distance of 1 mm.

Fig.10 shows the variation of the time τ of persistance of complete collection with the distance d between the target surface and the collector for different values of the collector potential V_c. From these curves (knowing l and ε), we can calculate the variation of τ as a function of the collector field intensity. This collector-field dependence of τ is shown in Fig.11. It will be seen that τ and, consequently, surface potential at the instant τ are proportional to E_c. The slope of the τ = $f(E_c)$ plot depends on the

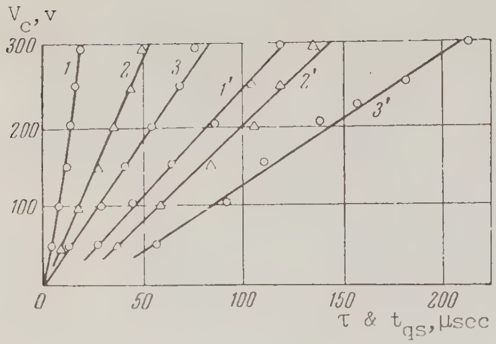

Fig.9. Variation of τ and t_{qs} with the collector potential V_c; 1,2 & 3) variation of τ with V_c for a sphere (r = = 60 mm) and collector-to-target distances d = 2 mm and d = 1 mm, respectively; 1',2' & 3') corresponding dependences of t_{qs} on V_c.

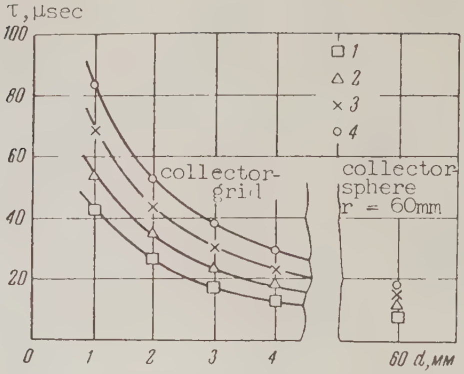

Fig.10. Variation of the time τ of persistance of total collection of the secondary current with the distance d between the target surface and the collector (grid), 1) V_c = = 150 v, 2) 200 v, 3) 250 v, 4) 300 v.

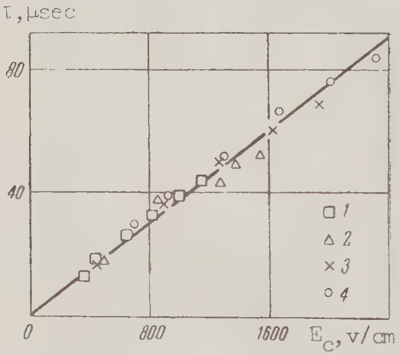

Fig.11. Variation of τ as a function of the collector field E_c: 1) V_c = 150 v, 2) 200 v, 3) 250 v, 4) 300 v.

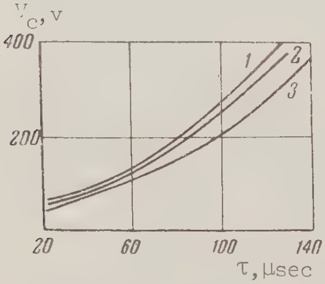

Fig.12. Temperature dependence of the charging characteristics. Target - ZS-5 glass. Curves 1,2 & 3 recorded at 20°, 200° & 500°, respectively.

capacitance of the target, the density of the charging current and the density distribution in the bombarding beam.

For the purpose of determining the temperature dependence of charging we carried out measurements at different temperatures from 20 to 500°. It was found that with increasing temperature, the charging characteristics, other conditions being equal, are shifted to the side of longer times τ (Fig.12). For glass and particularly for mica this effect is small at small values of V_c. At first glance this may appear surprising: one might expect a greater increase of τ. If we recall, however, that at the temperatures in question there is only a barely noticeable increase in leakage, we see that the variation is not abnormal. Obviously, with further increase of temperature the effect will become appreciably stronger. The temperature dependence becomes more pronounced with increase of V_c. With increase of temperature there probably occurs not only an increase of leakage through the target material but also a decrease of the local field, inasmuch as surface leakage tends to equalize the potential distribution. Both these factors lead to an increase of τ. It may be assumed that at not very high target temperatures the second factor predominates. Indirect substantiation of this is the fact that measurements of the charging characteristics of samples of mica coated with willemite carried out at different temperatures showed that in this case the temperature dependence is appreciably more pronounced. Inasmuch as the application of willemite cannot substantially alter the bulk resistivity of the samples, it may be assumed that the presence of such a coating leads to smoothing out of the potential topography, which becomes particularly noticeable at elevated temperatures.

Conclusions

1. We investigated the kinetics of appearance and dissipation of charges on the surface of dielectrics under electron bombardment by means of a new pulse technique.

2. We found that after a certain time (i.e., from the instant of cessation of complete collection of the secondary current), the rate of charge build-up on the dielectric surface decreases, which is explained by the influence of fields due to the appearance of the charge patch or spot itself. Owing to the influence of these fields the surface of the dielectric does not receive the amount of electricity necessary for charging of the target surface to the collector potential during the time τ of persistance of complete secondary current collection or even during the longer time t_{qs}, the time to attainment of the quasi-stationary state. In fact the target may never attain the collector potential in view of the very slow charge accumulation after establishment of the quasi-stationary state and the appreciable role played under these conditions by leakage.

3. We found that the time τ of persistance of complete secondary current collection increases linearly with the intensity of the collector field. Consequently, the amount of electricity accumulated on the dielectric surface at instants τ and t_{qs} at a given collector potential depends on the geometry of the apparatus.

Although according to commonly held opinion the purpose of the "barrier grid" used in many electron beam tubes is to shield the peripheral areas of the target from secondary electrons, such a "barrier grid" also serves to increase the time τ, i.e., to accentuate the potential topography and accelerate the charging to a given potential of the dielectric under electron bombardment.

4. It was found that the values of τ and t_{qs}, which characterize the kinetics of charging, in the region of medium bombarding electron energies are independent of the electron energy and depend under any given set of conditions on the magnitude of the accumulated charge.

The authors take this occasion to express their gratitude to A.R.Shul'man for suggesting the subject, constant attention and valuable advice and to thank students V.V.Bashenko and T.A.Koriakina who participated in the measurements.

"M.I.Kalinin" Leningrad Polytechnic Institute

References

1. N.V.Cherepnin, Elektronika i radiotekhnika (Electronics and Radio Engineering) 1, 1 (1956).

2. M.Knoll & B.Kazan, Storage tubes and their basic principles. (Cited in Russian trans.)

3. V.N.Laut & L.A.Liubovich, Zepominaiushchee ustroistvo na elektronnoluchevykh trybkakh bystrodeistvuiushchei elektronnoi schetnoi mashiny Akademii nauk SSSR (Electron beam tube memory used in the high-speed computer of the Academy of Sciences), 1957.

4. J.G.McKay, J.Appl.Phys., 22, 89 (1951).

5. N.L.Iashnopol'skii, Trudy (Proceedings) Institute of Automatics and Telemechanics, USSR Academy of Sciences, 2, 70 (1952).

6. V.Ia.Upatov, Radiotekhnika i elektronika (Radio Engineering and Electronics), 2, 193 (1957).

7. H.Hinterberger, Z.Phys., 114, 98 (1939).

8. A.R.Shul'man & V.L.Makedonskii, Zhur.tekh.fiz., 22, 1542 (1952).

9. A.R.Shul'man & B.P.Dement'ev, Zhur.tekh.fiz., 25, 2257 (1955).

DISCUSSION

V.Ia.Upatov: How did the surface potential vary as the beam was swept over the target?

I.R.Zakirova: The low intensity probing beam 0.5 mm in diameter was deflected by means of plates to which single sawtooth voltage pulses were applied. At the same time a certain dc potential was applied to the collector. The current in the target circuit drops to zero at the instant when the beam passes over an element of the surface with a potential equal approximately to that of the collector. During each sawtooth pulse, i.e., each scan of the target, therefore values are obtained for all the points on the surface lying on a straight line, that is, with the same potential value.

A.V.Morozov: In the case of a positively charged patch, outside its boundaries where there impinge slow secondary electrons ejected from the area of the patch or deflected there by the patch field, there should be an area with negative charges (potentials). Do these negative areas appear in your potential distribution curves?

I.R.Zakirova: Our experimental curves do not have sections with a negative potential.

Zernov: The periphery of the target will not be negatively charged inasmuch as the secondary electrons are pulled away by the electric field.

L.N.Dobretsov: The field of a positively charged spot holds back secondary electrons within the region of the spot, but outside the spot the direction of this field will be reversed, i.e., the field will tend to drive away the electrons from the surface to the collector. This field together with the collector field will prevent secondary electrons from impinging on the target area outside the spot.

A.A.Mostovskii: In view of the Gaussian current density distribution in the primary beam, rigorously speaking it covers the entire surface of the target and with a sufficiently long bombardment time the positive charge patch will occupy the entire target.

I.R.Zakirova expressed agreement with the views of Dobretsov and made some critical observations regarding the potentialities of the method of measuring the potential distribution on the surface of dielectrics employed in the work of Upatov.

ENERGY DISTRIBUTION OF SECONDARY ELECTRONS FROM OXIDE-COATED SURFACES

- M.L.Kapitsa

Introduction

It is a recognized fact that the secondary electron spectrum, particularly in the region of low primary energies, depends substantially on the state of the bombarded surface. This dependence is evinced in the different regions of the electron spectrum corresponding to slow true secondary electrons, fast electrons and elastically reflected electrons. The dependence is most pronounced, however, in the part of the spectrum due to slow true secondary electrons.

The energy distribution of slow electrons emitted by clean metal surfaces differs markedly from the distribution in the corresponding emission from dielectrics: for dielectrics the distribution has a peak with a half-width of 1.5-2 v in the region from 0 to 2 v, while for metals the maximum of the distribution curve lies in the region from 4 to 6 v and may have a half-width of more than 10 v.[1]

It has been reported that upon contamination of a metal surface, the slow electron part of the spectrum is altered and begins to approach the secondary electron spectrum characteristic of dielectrics.[1] This observation calls for careful checking. If this effect really obtains, it can be utilized for monitoring the cleanness of metal surfaces and in fact opens the possibility of drawing certain inferences regarding the state of the metal surface from the shape of the energy distribution curve for slow secondary electrons.

The purpose of the present work was to investigate in detail the difference between the spectra of slow secondary electrons emitted by clean metal surfaces and metal surfaces coated with films of oxides of the same metals. A further purpose was to clarify the possibility of utilizing this difference for checking the degree of cleanness of metal surfaces.

The very interesting question of the reason for the change in the appearance of the spectrum as a result of contamination of the surface lies beyond the scope of the present investigations.

Procedure

The measurements were carried out in a continuously pumped spherical capacitor at a vacuum no worse than $5 \cdot 10^{-7}$ mm Hg.

We used the method of electric differentiation of the retarding potential curves. The measurement circuit allowed of obtaining the secondary electron velocity distribution curves directly on the screen of the oscillograph. The patterns on the screen were recorded photographically.[2] The primary electron energy V_p was varied in the range from 20 to 100 ev; it was found that the shape of the distribution curves is independent of V_p in the indicated range.

Results

We investigated nickel, copper, molybdenum and tantalum. All the observed regularities for these metals proved to be qualitatively similar. Therefore, below we shall give only the principal results obtained for nickel which was investigated in most detail.

The following samples were chosen for investigation.

1. Samples of N-1 (H-1) nickel cut from a 0.1 mm thick ribbon of the type commonly used in the fabrication of vacuum tubes; the samples were not subject to any mechanical, chemical or heat treatment prior to measurement. Hereinafter we shall refer to this material as untreated nickel.

2. Samples of the same ribbon but subjected to intense heat treatment (heating to above 1000°) under high vacuum. Hereinafter we shall refer to these samples as clean nickel inasmuch as it is known that such heat treatment yields a clean metallic surface. As the standard of cleanness for nickel we took such nickel ribbon heated at 850-900° in a vacuum of about 10^{-7} mm Hg. A temperature of this order is necessary to eliminate the influence of adsorption of residual gas.

3. Samples of nickel covered with a film of adsorbed gas; the samples were treated in the same way as to obtain clean nickel (i.e., as described above) and then cooled and held in an atmosphere of residual gases until a constant, stable state was attained.

4. Samples covered with a layer of oxide; these were prepared of nickel treated in the same way as for obtaining clean nickel and then heated at the forevacuum pressure or in air to a temperature of 500-600°. We also used the electrolytic method of oxidizing the surface.

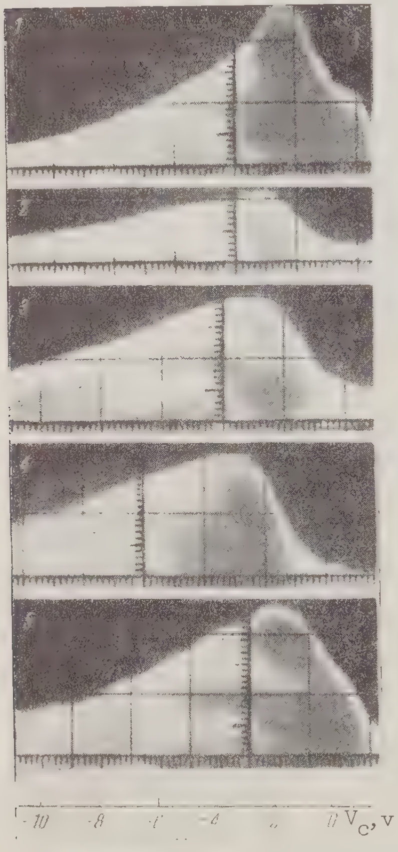

Figs.1--5.

A typical photograph of part of the secondary electron velocity distribution curve for untreated nickel is reproduced in Fig.1. The peaks in this and the following photographs are the maxima of the curves characterizing the distribution in energy of slow true secondary electrons. As may be seen from Fig.1 most of the secondary electrons have energies in the range from 1.0 to 1.5 ev. The half-width of the peaks varies between 3.5 and 4.5 v. Clearly evident in this distribution is a group of electrons with "insufficient energies", i.e., electrons which are drawn out into the vacuum only when a certain accelerating potential is present.

Figs.2 and 3 give the distribution curves for nickel subjected to light heating (600-700°). As compared with the curve for untreated nickel, there are evident the following alterations: the maximum is displaced to the left (the number of fast electrons is increased), the half-width of the peak is increased and the number of electrons with "insufficient energies" is reduced.

Fig.4 shows the distribution curve obtained for a nickel sample heated six hours at 900°. In this case the measurements were carried out with a hot target to obviate adsorption of residual gases. Most of the secondary electrons have an energy of the order of 4 ev. The half-width of the distribution curve is 10 v. Here there are virtually no electrons with "insufficient energies", i.e., the retarding potential curve shows saturation at $V_c \approx 0$ v. Further heating of the sample for 30 hours resulted in no significant modification of the curve.

Artificial oxidation of clean nickel brought the distribution curve back to the shape characteristic of untreated nickel (Fig.1). From this it may be inferred that an oxide film is normally present on the surface of untreated nickel.

The following deductions may be drawn from a comparison of the curves reproduced in Figs.1 and 4: the energy distribution curves for slow secondary electrons emitted by a clean and a contaminated (oxide-coated) surface differ as regards a) the position of the principal peak in the distribution curve, b) the half-width of this peak and c) the presence (or absence) of a group of electrons with "insufficient energies". Each of these indications can serve as a criterion for evaluating the cleanness of a metallic surface.

However, in order to use these indications to judge of the presence of an oxide film on the metal we must be sure that a film of adsorbed gas on the metal surface does not produce the same effects.

In order to check the influence of adsorbed gases on the secondary electron distribution in energy curve, we first brought our nickel target to the state corresponding to a clean surface. Then the heating was stopped and while the target cooled distribution curve oscillograms were photographed at intervals. We found that 5 minutes holding in the vacuum brought the distribution curve to the stable shape (Fig.5). This appearance of the secondary electron energy spectrum can be attributed to a clean nickel surface covered with a film of adsorbed gas. It may be noted that very brief heating of the sample sufficed to bring the curve to the shape characteristic of a clean surface.

Let us compare Figs.1, 4 & 5 which represent, respectively, nickel covered with an oxide film, clean nickel and clean nickel with a layer of adsorbed gas on its surface. We see that in the presence of a gas layer on the clean nickel surface the energy distribution curve becomes similar in some respects to the curve for nickel with an oxide film. Specifically, the position of the maximum approximately coincides with the position of the maximum for oxidized nickel and there is evident the group of electrons with "insufficient energies". At the same time, however, there are substantial differences: the half-width of the maximum in the case of an oxide film (Fig.1) is appreciably less than in the case of the adsorbed gas layer (Fig.5); the principal maximum is considerably more pronounced in the former case (Fig.1).

Thus these indications can be utilized to distinguish between an oxide coating and a layer of adsorbed gas.

The group of electrons with "insufficient energies" (i.e., insufficient energies to emerge from the target without an attracting collector field) merits further consideration. As is known such electrons have been observed in a number of previous investigations; often the energy necessary for drawing them into the vacuum exceeded some tens of volts. It was shown in the investigation of Ref.3, carried out in our laboratory, that if one prevents charging of the surface of alkali halide single crystals, the retarding potential curves goes to saturation close to zero collector potential and electrons with such "insufficient velocities" are absent. More detailed investigation showed that even when charging was obviated there were present in our films electrons with "insufficient energies" of the order of several volts.

Apparently, the reason for the appearance of electrons with low "insufficient energies" in our films is the presence on the surface of micropoles either created during bombardment of the coating or appearing owing to heterogeneities of the surface.[4]

Conclusions

1. It has been established that the curve characterizing the distribution in energy of secondary electrons in the region corresponding to true secondaries is very sensitive to the state of the surface. The reason for this requires further and separate investigation.

2. There is present in the spectrum of the secondary electrons emitted from surfaces coated with oxide film or adsorbed gas a group of electrons with low "insufficient energies" even under conditions when charging of the surface is precluded.

3. There are a number of indications or parameters (the position and half-width of the slow secondary electron peak and the presence or absence of electrons with "insufficient energies") which differ for a clean metal surface as compared with a metal coated with an oxide film. From the half-width of the peak one can also distinguish between metal surfaces coated with oxide and surfaces covered with adsorbed gases.

4. The experimental data provided the basis for the design of an apparatus for monitoring the cleanness of metal surfaces.

The writer wishes to acknowledge his gratitude to A.R.Shul'man for suggesting the subject, constant attention to the work and valuable advice.

References

1. A.R.Shul'man, Izv.AN SSSR, Ser.fiz., 20, 1008 (1956). (Trans. in Bulletin, 20, No.9, 912.)
2. A.R.Shul'man & I.I.Farbshtein, Doklady AN SSSR, 104, 56 (1955).
3. A.R.Shul'man, Zhur.tekh.fiz., 25, 2150 (1955).
4. V.N.Lepeshinskaia, Izv.AN SSSR, Sr.fiz., 20, 1025 (1956). (Trans. in Bulletin, 20, No.9, 927.)

DISCUSSION

I.M.Bronshtein: How was the contact difference of potential measured?

M.L.Kapitsa: It was not measured.

I.M.Bronshtein: How then can one draw any conclusions regarding the displacement of the maxima in the curve without taking into account the contact potential difference?

M.L.Kapitsa: The maximum was displaced by about 4 v: for a contaminated surface it was located at 1-1.5 v; for a clean surface at 4.5-5 v. The contact difference of potential could not change so appreciably.

N.B.Gornyi: In your opinion then heating to 900^o results in complete elimination of the oxide film and all contamination?

M.L.Kapitsa: Yes.

G.P.Prudkovskii: Did you try cleaning the surface by cathode sputtering?

M.L.Kapitsa: No.

V.S.Gusel'nikov: Why do there appear electrons with "insufficient velocities" after cooling of the sample?

M.L.Kapitsa: This question requires further investigation.

A.R.Shul'man: The secondary electron energy distribution curves for metals and dielectrics differ markedly. A dirty metal gives curves of the same shape and appearance as dielectrics. Curves obtained after cooling of the surface, i.e., after adsorption of residual gases on it, are intermediate between the curves obtained for clean and contaminated metals.

SOME PROPERTIES OF MULTIALKALI PHOTOCATHODES

- A.A.Mostovskii, O.B.Vorob'eva & K.A.Maiskaia

Within the last few years there have been developed several new types of efficient photocathodes; from among these Bi-Ag-Cs photocathodes have already come into industrial use and their properties have been fairly thoroughly studied.

Multialkali photocathodes, which appeared about two years ago and were first described by Sommer[1,2], have not yet been extensively studied. In the present report we give the principal results of an investigation of such multialkali photocathodes. We evaluated diverse methods of preparing such cathodes, studied their properties and compared these with the properties of other cathodes, particularly cesium-antimony and bismuth-silver-cesium photocathodes.

The photocathodes were prepared by successive treatment of the antimony base layer with the alkali metals. The most efficient proved to be treatment of the antimony layer first with potassium and then with sodium and cesium.

We made an attempt to replace the potassium with lithium, but this did not result in any significant advantages as regards either the integral or the spectral sensitivity. It was subsequently discovered that our lithium contained sodium and potassium in amounts sufficient for the formation of ordinary Sb-K-Na-Cs photocathodes (instead of Sb-Li-Na-Cs as expected).

An important consideration in forming multialkali photocathodes is proper dosage of the alkali metals. Usually we controlled and monitored the dosage by observing the photocurrent but sometimes by measuring the conductivity of the photocathode layer (the conductivity is more sensitive to variations in the amount of alkali metals). Usually minimum conductivity precedes maximum photocurrent. Initially for rigorous control of the amount of alkali metals we used capillaries; subsequently, however, the dosage was realized by varying the size of the branch tubes (containing the evaporated metals) and control of the furnace temperature.

We succeeded in obtaining photocathodes with sensitivities ranging from 80 to 150 microamp/lumen, and in the case of individual samples up to 200 microamp/lumen (color temperature - 2854°K).

We recorded the spectral characteristics of the photocathodes in the wavelength range from 400 to 1000 mμ. The spectral characteristics are shown in Fig. 1 together with the characteristics for Sb-Cs and Bi-Ag-Cs photocathodes for purposes of comparison.

The quantum efficiency of Sb-K-Na-Cs photocathodes at a wavelength of 400 mμ attains 1/5 electrons per quantum for the best samples which is approximately equal to the quantum efficiency of the best Sb-Cs cathodes. Nevertheless the sensitivity of multialkali photocathodes in the 400-500 mμ interval remains inferior to that of the best samples of cesium-antimony photocathodes. The higher sensitivity of the new photocathodes is due primarily to their better response in the 550 to 850 mμ range.

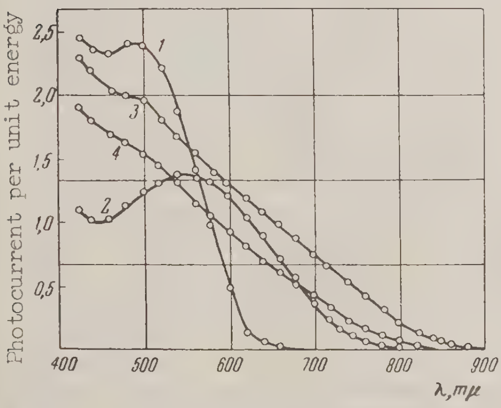

Fig.1. Spectral characteristics of photocathodes: 1) Sb-Cs, ε = = 75 μamp/lumen, 2) BiO-Ag-Cs, ε = 92 μamp/lumen, 3) Sb-K-Na-Cs, ε = 200 μamp/lumen, 4) Sb-K-Na-Cs, ε = 100 μamp/lumen.

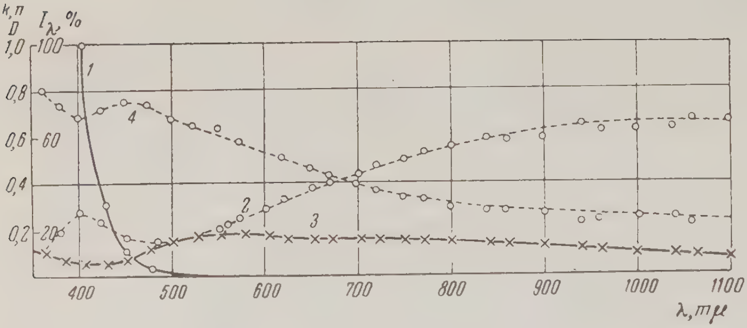

Fig.2. Photoelectric and optical properties of Sb-K photocathodes: 1) spectral photosensitivity, 2) transparency, 3) reflection, 4) absorption.

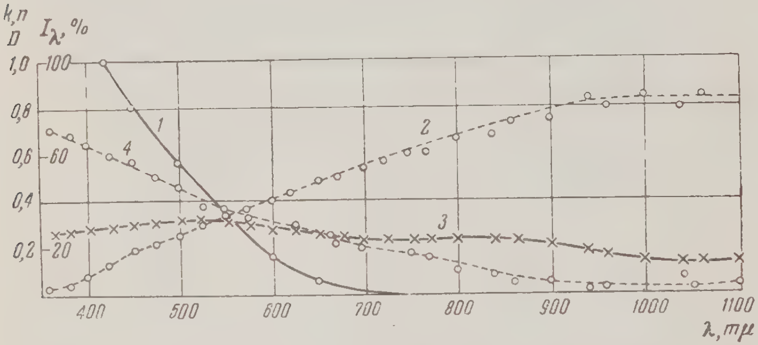

Fig.3. Photoelectric and optical properties of Sb-K-Na photocathodes: 1) spectral photosensitivity, 2) transparency, 3) reflection, 4) absorption.

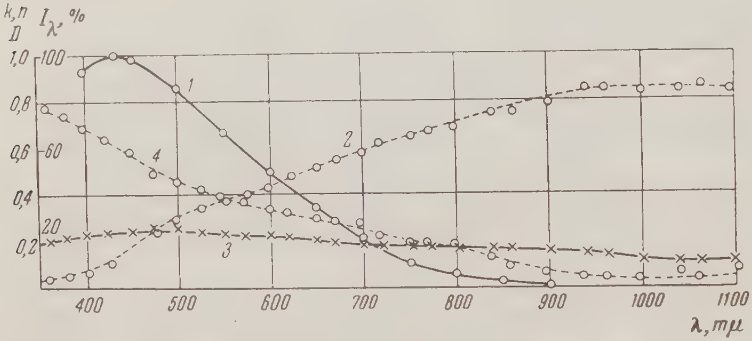

Fig.4. Photoelectric and optical properties of Sb-K-Na-Cs photocathodes: 1) spectral photosensitivity, 2) transparency, 3) reflection, 4) absorption.

In addition to the spectral sensitivity, we also determined the optical properties of the cathode at all stages of preparation. The optical properties at successive stages of treatment of the antimony base are shown in Figs. 2, 3 & 4.

As will be evident from the curves, treatment with sodium after potassium leads to an appreciable change not only of the spectral sensitivity but also of the optical properties. The color of the layer viewed in transmitted light changes from violet to yellow. Treatment of Sb-K-Na photocathodes with cesium modifies only the spectral response but does not alter the optical attributes (Figs.3 & 4).

As will be evident from the curves, as a result of cesiation, the "external" work function is changed by 0.4-0.5 ev, while the "internal" work function, judging from the absorption limits, is not changed.

This change in the height of the potential barrier at the photocathode-vacuum interface can be realized not only by cesiation but also by sensitization with oxygen. As a rule, the Sb-K-Na-Cs photocathodes were prepared without sensitization with oxygen inasmuch as the most sensitive multialkali photocathodes were poisoned by small amounts of oxygen. In the course of the work it was found, however, that in a number of cases cesium did not yield an adequate increase in sensitivity of Sb-K.Na photocathodes; in these cases we realized an excess of cesium in the layer and carried out oxygen sensitization. By this means we were able to obtain photocathodes with a sensitivity better than 100 microamp/lumen and spectral characteristics typical of multialkali photocathodes.

Unfortunately, this procedure resulted in a substantial increase of the dark current, thereby negating one of the principal advantages of photocathodes of this type. The dark current of regular Sb-K-Na-Cs photocathodes is comparatively small, amounting to about 10^{-16} amp/cm^2 at room temperature. The thermionic work function varies between 1.1 and 1.2 ev for different samples (Fig.5).

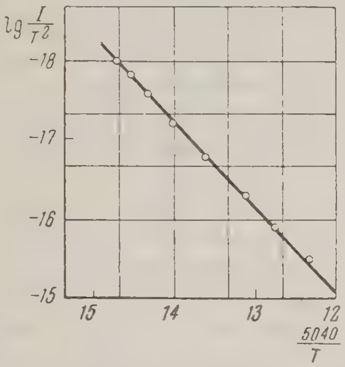

Fig.5. Temperature dependence of the thermionic emission of Sb-K.Na-Cs photocathodes: ϵ = 100 μamp/lumen, φ_T = 1.1 ev.

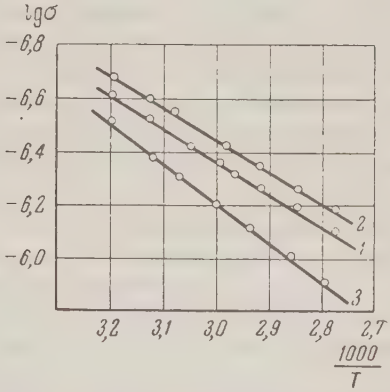

Fig.6. Temperature dependence of the conductivity: 1) Sb-K-Na, Q = 0.57 ev, 2) Sb-K.Na-Cs, Q = 0.52 ev, 3) Sb-Cs, Q = 0.60 ev.

The electric conductivity of multialkali photocathodes is typical for semiconductors. The activation energy, as determined from the slope of the temperature vs conductivity plots, lies between 0.4 and 0.6 ev for different samples (Fig.6). The current carriers, as indicated by the polarity of the thermo-emf, are holes.

The activation energy has approximately the same value for both Sb-K-Na and Sb-K-Na-Cs photocathodes, which also indicates that the role of cesium is restricted to altering the potential barrier at the surface of the photocathode and that the influence of the cesium does not extend to the volume properties of the material.

Multialkali photocathodes layers have a certain photoconductivity which, however, is characterized by appreciable "inertia"; the time lag for establishment (or disappearance) of photoconductivity after the light is switched on (or off) runs to minutes or even an appreciable fraction of an hour.

From the practical standpoint, the question of stabilization of these photocathodes is important. So far we have only preliminary data which indicates that fatigue of multialkali photocathodes is relatively minor. We tested such photocathodes over a period of 100 hours under illumination of 50 lux and V = 450 v (Fig.7).

Thus the cited data on multialkali photocathodes show that the photoemission mechanisms of Sb-K-Na-Cs and cesium antimony photocathodes have much in common and that Barton's model is equally applicable to both types.

The higher sensitivity of Sb-K-Na-Cs photocathodes in the long wave-

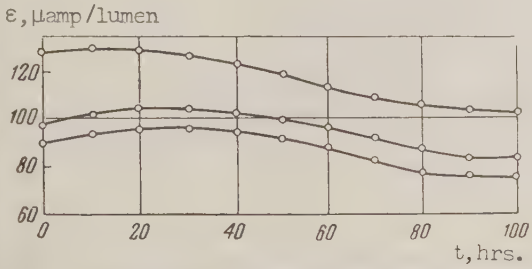

Fig.7. Fatigue of Sb-K-Na-Cs photocathodes: variation of the integral sensitivity over a period of 100 hours operation.

length region as compared with the sensitivity of cesium-antimony photocathodes is connected with the greater absorption of the former. The increase in sensitivity of Sb-K-Na-Cs photocathodes over Sb-K-Na photocathodes, in view of their equal absorption, is probably due to decrease of the "external" work function.

So far we have not established the stoichiometry of multialkali photocathodes. The ratio of sodium to potassium as evaluated for efficient cathodes proved to be close to that cited by Sommer[1,2]. This ratio varied from 1.5 to 1.9 in our photocathodes. This ratio is apparently realized in the layer with our method of preparation as a result of a substitution reaction, if it is assumed that during treatment with potassium there forms a compound of the Sb-K_3 type and that in efficient cathodes the stoichiometry must be SbM_3.

According to Men'shikov[3] in cesiation of antimony there occur three phases: Sb_3Cs_5, Sb_3Cs_7 and $SbCs_3$. However, only the last compound is photosensitive. If it be hypothesized that such intermetallic compounds are also formed in successive treatment with potassium and sodium and that replacement of one metal with the other does not occur, then the ratio of sodium to potassium should differ from 2:1, which is contrary to the experimental results.

On the other hand, if our assumption is correct, then the technology of preparation of multialkali photocathodes can be greatly simplified.

The authors desire to thank V.I.Safronova and L.I.Biserkina for assistance in preparing some of the samples and constructing the experimental equipment.

References

1. A.Sommer, Rev.Sci.Instr., 26, 725 (1955).
2. A.Sommer, Trans. IRE on Nuclear Science, 3,4,8-12 (1956).
3. M.Men'shikov, Zhur.tekh.fiz., 5, 579 (1947).

DISCUSSION

V.S.Gusel'nikov: Can you express an opinion regarding the structure of the photosensitive layers?

A.A.Mostovskii: I have no particular observations. One must bear in mind the size of the ions comprising the lattice. As for antimony, we do not know what type of lattice it has.

Shcheglov: Did you study field emission from your photocathodes?

A.A.Mostovskii: No, we did not.

PHOTOELECTRON EMISSION FROM SOME SEMICONDUCTOR AND METAL CATHODES WITH A REDUCED WORK FUNCTION

- P.G.Borziak, V.F.Bibik & O.G.Sarbei

Physicists are currently giving increasing attention to electronic processes in semiconductors. Hence investigation of all phenomena in this category, including photoelectron emission, is currently of interest. Where photoelectron emission is concerned, measurements in the widest possible spectral interval are important. A difficulty here, however, is that clean semiconductors, like clean metals, are characterized by large value of the work function which limits the range of possible investigation to a comparatively narrow interval. Going over to vacuum ultraviolet, in addition to technical complications, is also inconvenient because in this case it is impossible to assure the requisite vacuum conditions. Some time ago one of us[1] had the idea of widening the effective spectral interval by reducing the work function of the investigated photocathodes.

Morgulis & Gavriliuk[2] showed that the work function of metallic cathodes can be substantially reduced by adsorption of a BaO film. Gavriliuk and the present authors[3] demonstrated the effectiveness of this method as regards germanium, as a typical semiconductor. In the present research we extended this method to other emitters.

In our experiments we used tubes of the type pictured in Fig.1. Here the movable carriages 11 and 12, made of tungsten or tantalum, are suspended on the guide rails 10 extending the length of the cylindrical evacuated glass tube 1. We did not attempt to attain complete cleanness of the carriage surfaces, but aged them only for the purpose of providing a sufficiently high vacuum in the tube. The size and number of carriages in different experiments varied: usually one of the carriages was a control one (its surface remained unchanged during the entire experiment); the second carriage received an

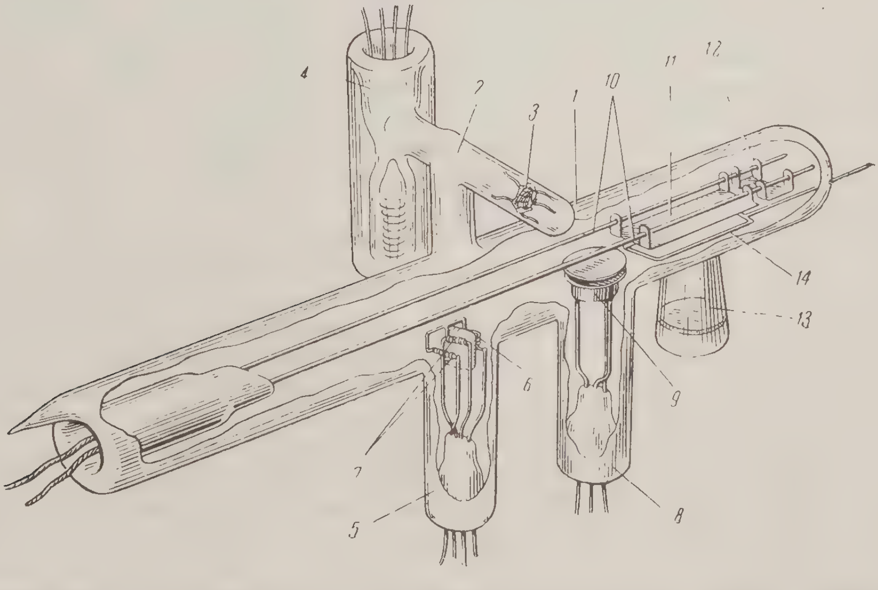

Fig.1. Experimental apparatus: 1 - glass envelope; 2 - branch tube for attaching tube with getter (3) and ionization pressure gage (4); 5 - branch for evaporator of semiconductor (6) and barium oxide (7); 8 - branch tube with electron gun (9); 10 - molybdenum rails for suspended carriages (11 & 12); 13 - branch tube with uviol insert; 14 - electron collector.

evaporated coating of the investigated semiconductor; the third carriage served as the metallic cathode for comparative measurements.

The investigated semiconductor was vaporized from the evaporator 6 in branch tube 5. In view of the possibility of partial thermal decomposition, in some experiments we vaporized the entire batch of semiconductor in order to provide conditions close to stoichiometry in the sputtered-on film.* The BaO evaporator 7 was located either in the same branch tube or in another one; in either case the BaO evaporator was well shielded from the semiconductor vaporizer. In order to insure uniform distribution of the BaO over the surface of the semiconductor or metal, the evaporator was located as far as possible from the guide rails. In this case we used the method of successive additional evaporation of BaO, carrying out a series of measurements after vaporization of each portion of the oxide. In other cases, we applied a BaO film of tapering thickness to a long carriage previously coated with the investigated semiconductor. In these cases the evaporator was located close to one end of the carriage. In other experiments, we carried out simultaneous evaporation of BaO (uniform or tapering thickness coatings) on semiconductor and metallic surfaces located next to each other.

The requirements of photoelectric measurements were provided by the uviol insert in branch tube 13 and the metallic frame 14 which served as the anode (photoelectron collector).

After the initial assembly, the experimental tube was attached to the vacuum system and pumped continuously for several days concurrently with the requisite aging of the envelope, the internal metallic components, getter and evaporators. Partially before and partially after sealing off the tube the getter 3 in branch tube 2 was vaporized; after this the pressure in the tube was reduced to $\lesssim 10^{-9}$ mm Hg by means of the Alpert ionization gage 4.

Next the semiconductor film was applied by evaporation, generally without impairment of the vacuum. In some cases the pressure in the tube in the process went to $\sim 10^{-8}$ mm, but it generally returned to the initial value after termination of the evaporation. After formation of the semiconductor film, we recorded the current-voltage characteristics of the thermionic current with the electron beam from gun 5 directed successively on the control and investigated plates (carriages). As a result we obtained the contact potential difference between these surfaces (coated and metallic). The uniformity of the contact potential along the semiconductor surface was checked in every case; no significant variation was observed.

Next, under substantially constant vacuum conditions, we carefully evaporated successive amounts of barium oxide onto the investigated surfaces. After application of each BaO coat, we checked the invariance of the contact potential difference relative to the control plate and then determined the change in the work function of the investigated surface by the method of shift of the current-voltage characteristics. After each successful evaporative application of BaO the entire procedure was repeated. By way of illustration of the results obtained, the curves for InSb and Ta are shown in Fig.2.

At the right in the figure are the characteristics pertaining to the initial semiconductor (InSb) and metal (Ta) surfaces; at the left are the characteristics as displaced after successive (simultaneously for the two surfaces) depositions of evaporated BaO. The Roman numerals identify curves pertaining to the semiconductor; the Arabic numerals, curves pertaining to the metal. The results show that in the case of the given metal (Ta) there is a greater reduction of the work function than for the semiconductor. After the first application, there is observed a maximum for the displacement of the characteristics. As a result of the fifth coating the characteristic is shifted in the reverse direction (to the right) and with further increase of the BaO coating approaches the extreme position characteristic, apparently, of BaO films, the work function of which is, consequently, somewhat greater than for the optimum Ta-BaO system.

---

*Four of the InSb films produced in this manner were given to R.M.Khaikina for electron diffraction analysis; this showed that the compound formed in all cases was InSb.

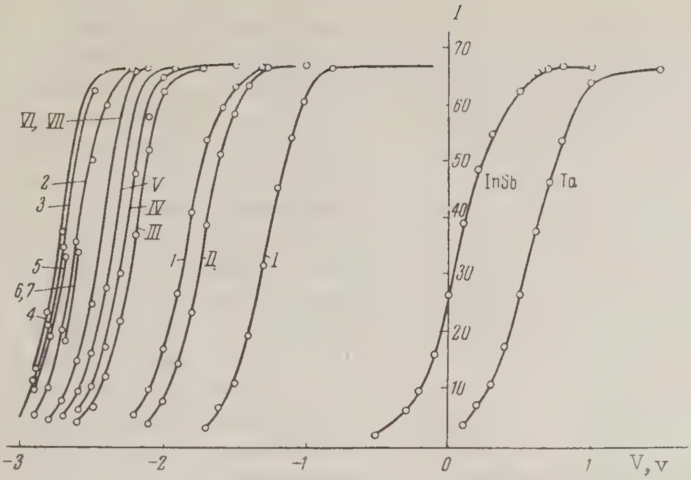

Fig.2. Shift of the current-voltage characteristics of the electron-gun current after application of successive coats of BaO to the investigated surfaces. Roman numerals pertain to InSb; Arabic numerals to Ta.

The behavior of the semiconductor characteristics is somewhat different. In this case there is no reverse shift of the characteristics with thickening of the BaO coating; the characteristic reaches its extreme (left) position with the sixth evaporation of BaO. Hence in this case one cannot say which displacement and, consequently, what change of the work function characterizes the optimum InSb-BaO system. One can obtain some such indication, however, from the results of photoelectric measurements. In some cases, however, there is observed a very small reverse shift of the InSb characteristics. In general the experimental data show that there is only a minor difference between the work functions of InSb-BaO and BaO.

In the case of application of a tapering thickness film of BaO a picture similar to that in Fig.2 is observed, except that in this case, of course, the variation in the position of current-voltage characteristics is a function of the coordinate of the thickness strips rather than of the number of successive coatings.

Comparing the positions of characteristics 1 and I, 2 and II, etc. in Fig.2, we conclude that during the initial stages of evaporation equal concentrations of BaO molecules on the InSb and Ta surfaces lead to an appreciably stronger effect in the case of the metal. But, inasmuch as the successive curves for the semiconductor shift progressively to the extreme position without reverse displacement, we cannot in the given case say for which of the investigated systems the optimum decrease of the work function is attained earlier.

In this case we also cannot show the concentration dependence of the change in work function due to the uncertainty in the amounts of evaporated BaO. For this reason we undertook special experiments, employing special BaO sources yielding a constant molecular flux; the amount of BaO deposited during a given interval was monitored by means of auxiliary targets. In this case the BaO concentration in the investigated surface was directly proportional

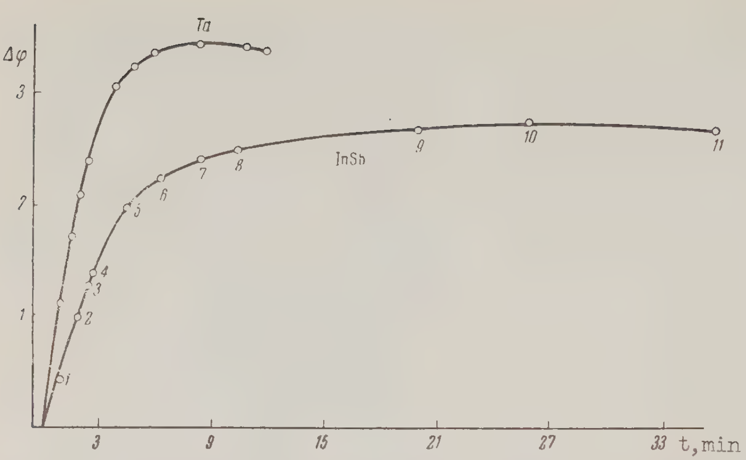

Fig.3. Variation in the change in work function Δφ of tantalum and Ag_2Te with time of evaporated application of BaO.

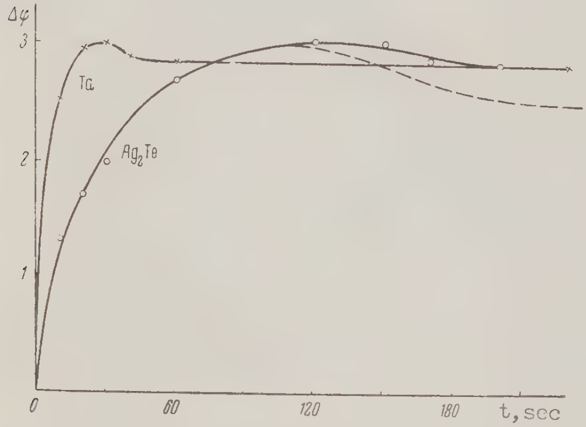

Fig.4. Variation of the change in work function Δφ of tantalum and InSb with the time of application of BaO (the rates of evaporation in the experiments of Figs.3 & 4 were different).

to the evaporating time and hence one could use the time (directly proportional to the concentration) in plotting the concentration dependence. The results of such experiments with InSb and Ta are shown in Fig.3, and with Ag_2Te and Ta in Fig.4. Here we observe small maxima in the curves characterizing the semiconductor samples as well. In one case for Ag_2Te we observed an increase of ~0.5 ev in the work function after the optimum decrease, i.e., the maximum in the curve was more pronounced than usual, as shown schematically by the dash line in Fig.4.

The data of Figs.3 & 4 again indicate the more rapid change in the work function for metallic cathodes and the fact that the optimum coating thickness is attained earlier for such cathodes (as compared with semiconductor cathodes). Photoelectric control experiments led to analogous results. In one of these experiments we applied tapering thickness BaO coatings to a semiconductor (Ag_2Te) and a metallic (Ta) surface from an evaporator positioned symmetrically relative to these surfaces. In scanning the surfaces with the light probe, the maximum of the photocurrent from Ta-BaO was obtained from a section with a thinner coating of BaO than in the case of Ag_2Te-BaO. According to the data of Figs.3 & 4, the optimum concentration of BaO molecules on the investigated semiconductors is 4-5 times greater than on the metal. These data are of interest from the standpoint of theoretical consideration of the interaction of dipole molecules with metallic semiconductor surfaces.

Examination of the characteristics shown in Fig.2 reveals that characteristics for Ta-BaO have begun to shift back to the right after the fourth BaO application and that curves 6 and 7 have merged, indicating that this is the extreme position of the curves corresponding to the contact potential for a very thin film of BaO on a Ta base. This extreme, limiting position in the case of InSb is indicated by the merging of curves VI and VII. Of course, neither position is "extreme" in the rigorous sense. Upon the attainment of sufficiently thick barium oxide coatings the contact potentials for both semiconductor and metal surfaces should become equal. But in the given case the BaO film is still appreciably thinner than Debye depth. It is not surprising, therefore, that being on different bases the BaO films give rise to different values of the work function. Interesting, too, is the fact that the coating on the more electropositive InSb base is characterized by a larger work function than the BaO coating on the more electronegative Ta base. This also indicates that the character of the interaction of BaO with metallic and semiconductor bases is different, which is what leads to the observed inversion of the contact potential difference between thin films of BaO on InSb and on Ta. The jumps in contact potential on the surface of these bases produced by the first layer of BaO persist with further thickening of the barium oxide coating.

With reduction of the work function, the spectral characteristics of the external photoeffect are shifted to the long wavelength side. Comparative data for the InSb and Ta samples characterized by the curves of Fig.2 are shown in Fig.5. Here 0 identifies the initial curve for pure InSb; I, II & III identify the characteristics attained after the 1st, 2nd and 3rd evaporations of BaO. After the fourth application, the photoeffect began to decrease. The decrease of the photoeffect for the metallic cathode (curves 1, 2 & 3) begins to be evident from the third application. Comparing these data with the data of Fig.2, we note the interesting fact that the photoelectronic emission from a metallic photocathode with a BaO coating begins to decrease before the minimum work function is attained. We cannot determine from the curves of Fig. 2 whether this is also true for the semiconductor. On the contrary, we hoped to establish the change in work function corresponding to the optimum BaO coating thickness from the photoeffect. According to the photoeffect indications this change corresponds in Fig.2 to the shift of characteristics between III and IV.

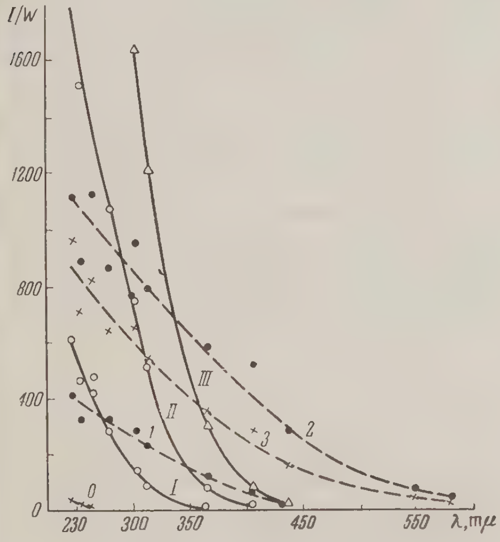

Fig.5. Spectral characteristics of photoelectron emission from Ta-BaO and InSb-BaO for different BaO concentrations on the cathodes.

In view of the results obtained for the metallic cathode, one may ask whether there is not agreement or correlation between the optimum photocurrent and the minimum work function in the case of the investigated semiconductor as well. In cases when the dependence of the type illustrated in Figs.3 & 4 is characterized by a curve with a maximum, the beginning of the decrease of the photocurrent from the semiconductor is observed before attainment of the minimum work function. Thus, for example, for the InSb-BaO sample (Fig.3) it was found that the sensitivity of the photocathode differs very little in the states corresponding to points 7 and 8, while the sensitivity in the state corresponding to point 10 is appreciably lower. Thus the optimum apparently corresponded to some point in the neighborhood of 8. In the case of Ag_2Te this effect was even more pronounced.

It will also be seen from Fig.5 that the spectral characteristics of the semiconductor cathode are appreciably steeper than the characteristics of the metallic one, which is in agreement with the data of other investigators for noncoated cathodes and in qualitative agreement with the generally accepted picture of the energy spectrum of electron states in semiconductors and metals. The same observations apply to the characteristics obtained for Ag_2Te-BaO and Ta-BaO as shown in Fig.6. The shape of the tail of the Ag_2Te-BaO characteristic, plotted to an enlarged scale, indicates the presence of some osrt of auxiliary characteristic (in addition to the fundamental one), probably associated with some mechanical impurity in the cathode, possibly due to partial decomposition of the Ag_2Te during evaporation. No such tail with a maximum was observed for the other cathodes.

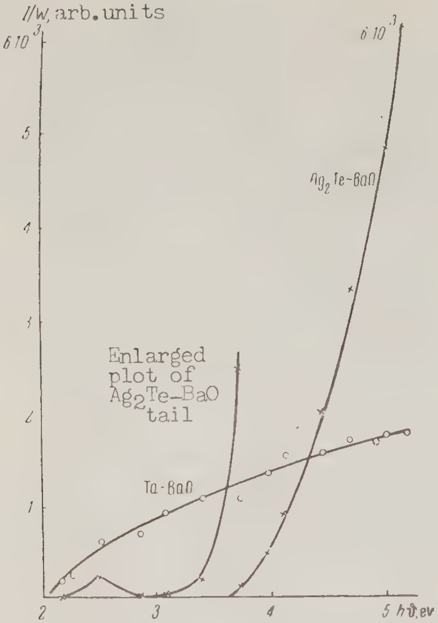

Fig.6. Spectral characteristics of the photoelectron emission from Ta-BaO and Ag_2Te-BaO at approximately optimum thicknesses of the barium oxide coating.

In the case of the Ta-BaO cathode we checked the feasibility of applying Fowler's method of processing the spectral characteristic. The results are shown in Fig.7, where the circles indicate points recorded with a glass optics monochromator and the crosses points recorded with a quartz monochromator. As determined by the Fowler method, the work function φ_0 for this case proved to be 1.7 ev. The value of φ_0 determined in the same manner for the initial state of the cathode was 4.5 ev.

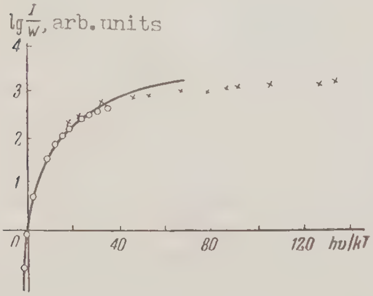

Fig.7. Spectral characteristic of Ta-BaO processed by the Fowler method. Solid curves - Fowler plot; points - experimental values (see text); the experimental points have been shifted for determining the threshold energy $h\nu_0$ = 1.7 ev.

As an extension of Fowler's method for metals to semiconductors, Apker, Taft & Dickey[4] suggested approximating the shape of the spectral quantum efficiency characteristics for the intrinsic photoemission of semiconductor cathodes by an expression of the form

$$I = a(h\nu - h\nu_0)^n,$$

where $h\nu_0 = \varphi_0$ and is the photoelectric threshold energy.

Treatment of the principal part of the Ag_2Te-BaO characteristic shown in Fig.6 by this procedure yields the expression

$$I = a(h\nu - 3.17)^n.$$

The data for InSb given by curve III in Fig.5 as described by $I = a(h\nu - 2.4)^3$. The constant a in these expressions characterizes the emissivity of the photocathode and is numerically equal to the quantum yield for light with $h\nu$ 1 ev greater than the threshold value $h\nu_0$. The value so obtained is small compared with the value for an efficient semiconductor cathode, such as a cesium-antimony cathode. It should be noted in conclusion that the above approximation can be realized only in a limited spectral range.

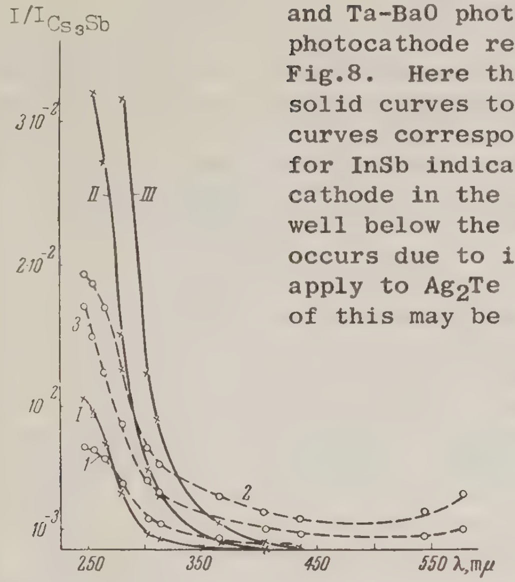

Fig.8. Relative spectral sensitivities of Ta-BaO and InSb-BaO photocathodes referred to the sensitivity of a cesium-antimony photocathode. Curves 1,2 & 3 pertain to Ta-BaO with different barium oxide coating thicknesses; Curves I,II & III pertain to InSb-BaO with different coating thicknesses.

Comparison of the spectral sensitivities of InSb-BaO and Ta-BaO photocathodes with the sensitivity of a Cs_3Sb photocathode resulted in the data shown graphically in Fig.8. Here the dash curves pertain to tantalum; the solid curves to indium antimonide; the numeration of the curves corresponds to the numeration in Fig.5. The data for InSb indicate the relatively low efficiency of this cathode in the investigated region, even at wavelengths well below the red limit, although the photoeffect here occurs due to intrinsic electrons. The same observations apply to Ag_2Te photocathodes. One of the possible causes of this may be strong energy dissipation due to scattering of the photoelectrons by the valence band electrons, inasmuch as in these cases the energy gaps are very narrow.

Turning to the data for Ta-BaO (curve 2), we want to emphasize that as a result of decrease of the work function by about 3 ev, the values obtained here in the spectral range from 400 to 600 mμ are equivalent to the data obtained for pure metals in the ultraviolet region up to $h\nu \approx 6$ ev. The quantum efficiency in this region is of the same order of magnitude as for metals. The shorter wavelength region corresponds to the intermediate region between the ordinary ultraviolet and the far vacuum ultraviolet (λ = 1000-500 Å) in which Wainfan et al[5] recently investigated the photoelectric emission from tantalum. In this region ($h\nu \approx 6$-8 ev) the quantum efficiency of a tantalum cathode increases noticeably (the quantum efficiency of Cs_3Sb photocathodes in the 400-500 mμ region changes little[6]), apparently tending to a value of a few percent, as was found in the $h\nu > 12$ ev region for tantalum without an oxide coating.

Conclusions

The method of reducing the work function by applying evaporated BaO coatings allows of extending the spectral interval of the photoelectric response of photocathodes; in most cases it makes it possible to shift the edge of the spectral characteristic into the visible region.

Comparative investigations of metallic and semiconductor cathodes showed that the concentration of dipole BaO molecules requisite for obtaining the minimum work function of a metal (Ta) is smaller by a factor of 4-5 as compared with the corresponding concentration for a semiconductor (InSb & Ag_2Te).

For both metallic and semiconductor cathodes decrease of the photoelectron emission in the process of deposition of a BaO coating begins somewhat before attainment of the minimum work function.

The spectral characteristics of Me-BaO (barium oxide coating on metal) photocathodes can be treated by Fowler's method, developed for pure metals. The spectral quantum yield characteristics of semiconductor cathodes with a BaO coating are satisfactorily described within a certain spectral interval by the expression

$$I = a(h\nu - h\nu_0)^n,$$

with $n = 4$ for Ag_2Te and $n = 3$ for InSb.

Despite the intrinsic character of the photoeffect, even far from the red limit the sensitivity of InSb and Ag_2Te photocathodes is appreciably inferior to the sensitivity of an efficient Cs_3Sb photocathode. One of the reasons for this may be the energy loss by photoelectrons moving towards the cathode surface as a result of their interaction with valence band electrons, inasmuch as the width of the forbidden band in such semiconductors is small.

Physical Institute,
Academy of Sciences of the Ukrainian SSR

References

1. P.G.Borziak, Trudy (Proceedings) Inst.fiz., Ukrainian Ac. of Sci., No.2, 3 (1952); Trudy (Transactions) Conference on Cathode Electronics, Vol.22, Pub.by Ukrainian SSR Ac. of Sci., 1952.

2. N.D.Morgulis & V.M.Gavriliuk, Zhur.eksp.i teor.fiz., 30, 149 (1956); V.M.Gavriliuk, Trudy (Proceedings) Inst.fiz., Ukrainian Ac. of Sci., No.5, 87 (1954); Usp.fiz.zhur., 1, 73 (1956).

3. P.G.Borziak & O.G.Sarbei, UFZh, 1, 395 (1956); V.M.Gavriliuk, Izv. AN SSSR, Ser.fiz., 20, 1071 (1956). (Trans., Bulletin, Vol.20, No.9, 967.)

4. L.Apker, E.Taft & J.Dickey, Phys.Rev., 74, 1462 (1948).

5. N.Wainfan, W.C.Walker & G.L.Weissler, J.Appl.Phys., 24, 1318 (1953).

6. V.Zworykin & E.G.Ramberg, Photoelectricity and its Applications, p.58.-N.Y., 1949.

DISCUSSION

A.A.Mostovskii: Did you record curves of photocurrent vs wavelength at different temperatures?

P.G.Borziak: No, we did not.

A.I.Piatnitskii: How did you purify the indium antimonide?

P.G.Borziak: The indium antimonide was obtained from the Semiconductor Institute where it had been zone refined.

A.I.Piatnitskii: Was there no danger of dissociation of the semiconductor during evaporation?

P.G.Borziak: Electron diffraction studies showed that there was no decomposition.

Kireiko: What was the coating thickness corresponding to the maximum decrease of the work function?

P.G.Borziak: The layer thickness was not measured.

N.M.Politova: Did you measure the photoconductivity with a view to determining the internal work function?

P.G.Borziak: No.

E.A.Krasovskii: Did you check the invariance with time of the output of the molecular gun?

P.G.Borziak: Yes, we checked this by means of special control targets.

K.B.Tolpygo: There is reason for pessimism as regards attempts to find a method of processing the spectral characteristics of photoemission from semiconductors for the purpose of determining the "red limit", that is, of developing a technique for semiconductors similar to that developed by Fowler for metals.

To what is Fowler's success for metals due? First, it is due to the fact that the same photoeffect mechanism is common to almost all metals. In metals there is a continuous spectrum of levels with an almost constant density in the vicinity of the Fermi brim, the filling of these levels is described by Fermi's statistics. As a result, the spectral distribution of the photoeffect in a narrow frequency interval is described with great accuracy by Fowler's simple and general theory. The standard curve method allows of determining the position of the Fermi level relative to the vacuum and, consequently, of determining the work function, even though there is no clear cut "threshold" of the photoeffect.

In contrast, in semiconductors and dielectrics there is a great diversity of energy schemes and photoeffect mechanisms, so that elaboration of a universally applicable theory becomes impossible. The "threshold" of the photoeffect might be determined as the distance from the upper edge of the filled band to the vacuum; experiment, however, usually does not show an abrupt disappearance of photoemission at frequencies below the "threshold" frequency, and there is little hope of developing a universal photoeffect theory for frequencies close to the "threshold" one. Actually, direct transition from the top of the filled band to the vacuum may prove to be forbidden either because the vacuum level is in the forbidden band or because these levels are characterized by different values of the wave vector K. In this case there may be forbidden transitions with participation of phonons or by virtue of the perturbing effect of lattice defects. Hence the intensity of the fundamental photoeffect will be greatly weakened and will depend on the temperature and the character of the lattice defects. It is possible that the fundamental "photoeffect" will prove to be comparable with the impurity photoeffect. In a number of semiconductors (for example, germanium) impurity levels occupy a wide energy spectrum and extend almost to the space charge region. Finally, the external photoeffect may have an exciton character: initially there is formed an exciton, the energy of which is then transferred to an electron; in this case the photoeffect "threshold" is determined by the intensity of absorption at the edge of the exciton band.

In view of the great diversity of the energy schemes and photoeffect mechanisms, one cannot hope to encompass the wavelength dependence of I by a simple universal formula, containing the limiting wavelength λ_o as a parameter. One should not even attempt to do this. At most one can try to establish some simple typical cases when the photocurrent is determined by some one transition mechanism and then for each case try to find a theoretical or semiempirical equation for $I = f(\lambda)$. We can determine what type of photoeffect we are dealing with in any given case from experiment. In some cases (impurity photoeffect) the limiting wavelength λ_o may be merely an "effective" quantity. As for the method of processing the curves according to Apker et al -$I\sim(\nu-\nu_0)^n$-it must be noted that this method has no physical justification, is not based on any specific theory of the photoeffect. Hence it is doubtful whether one can attribute a physical meaning to ν_0.

I.M.Dykman: In connection with the remarks of K.B.Tolpygo, I would like to note that the red limit for semiconductors, like every concept in physics, must be clearly defined. Only on this condition does it have real meaning. One must clearly distinguish between the photoemission from the host material of the semiconductor and the photoeffect due to the impurity, regardless of whether the latter effect is of an exciton or other character. In the case of the photoeffect from the host material, the red limit is determined by the minimum energy which leads to the appearance of a photocurrent at zero temperature. This definition has clear physical meaning and yields, at least in principle, a clear indication of how the red limit should be determined.

Although there are always impurities in ordinary photoconductors, one can reasonably assume that the photocurrent from the impurities depends on their concentration. Since the number of impurity atoms is always much smaller than the number of host material atoms, one can always recognize the effect due to impurities. Naturally, one can determine a red limit for each kind of impurity, just as one can determine the red limit for the host material.

It follows, therefore, that the red limit for semiconductors is a physical concept and that we need only develop a technique for measuring it, a technique, for example, similar to that of Fowler for metals.

P.G. Borziak also noted that the procedure proposed by Apker & Taft is not well-founded and is not applicable in general. From this, however, one must not conclude that the concept of the red limit as such is valueless.

INVESTIGATION OF PHOTOCATHODES BY THE RADIOACTIVE TRACER TECHNIQUE

- N.A. Soboleva

In the preparation of thin oxygen-cesium photocathodes, even with satisfactory reproducibility of their emission properties, there is commonly observed a considerable scatter of the layer conductivity and the fatigue characteristics. Thus, the spread of the longitudinal resistance values of cathode layers prepared by exactly the same procedure may extend over 6-7 orders of magnitude. In investigating the fatigue of cathodes, according to the data of our plant laboratory, we encounter three distinct groups of cathodes: cathodes which show virtually no fatigue under standard operating conditions, cathodes that show pronounced fatigue and cathodes that exhibit only weak fatigue.

An oxygen-cesium photocathode is a complex conglomerate, wherein structural characteristics of the layer play a decisive role in determining the cathode parameters. Nevertheless, the proportion of components entering into the composition of the cathode may also be important where scatter of the physical values is concerned. In preparing such cathodes the initial amount of silver used (and, consequently, the amount oxidized) is monitored by optical measurements and may be determined even more accurately by weighing the silver batch before and after evaporation. The amount of cesium in the cathode is monitored only indirectly by measuring the thermionic work function, which to an appreciable extent depends on the surface concentration of cesium adsorbed on the cathode and does not yield any direct indication of the total (volume) cesium content in the layer. Yet, as analysis of resistance measurements of the coating carried out on a large number of cathodes in different stages of preparation showed, the maximum scatter as regards conductivity occurs precisely at the stage of activation of the cathode with cesium and is not reduced in the subsequent deposition-of-silver stages.

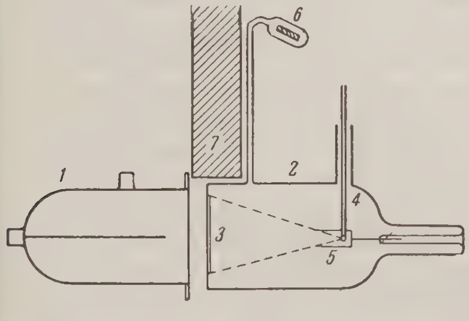

Fig.1. Experimental apparatus and counter: 1) ionization counter with end window, 2) photocell, 3) photocathode on flat end window (glass), 4) retractable evaporator with weighed amount of silver, 5) evaporator shield defining the size of the cathode and serving as the anode, 6) ampoule with cesium, 7) heavy lead plate shielding counter from cesium in ampoule 6.

In the present work we used the technique of radioactive tracers for determining the amount of cesium in cathodes. Radioactive Cs^{134} (half-life 2.3 years) in the form of the chloride was added to the usual cesium chloride; the mixture was then reduced to metallic cesium and used for activating cathodes in the conventional manner. Finally, the radiation intensity from the cathode was measured by means of a 40 mm diameter end-window SI-2B β-counter. We chose this type of end-window β-counter primarily owing to the convenience of coupling it to the flat glass on which the photocathodes were prepared (Fig.1).

The design of the apparatus was such that deposition of cesium on the metallic components (particularly, on the shield 5 surrounding the evaporator) did not introduce an appreciable error into the pulse count from the cathode glass; to this end the shield was positioned far (60 mm) from the cathode glass so that the radiation from it amounted to not over 5-10% of the total activity in the bulb.

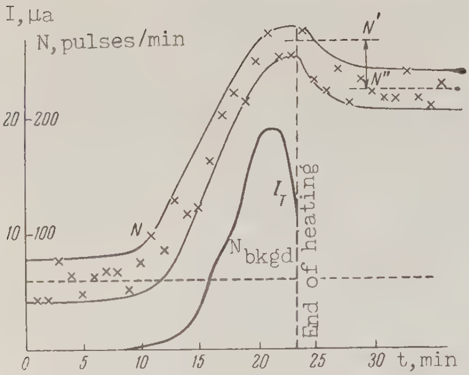

Fig.2. Variation of the thermionic emission and the intensity of radioactive radiation from the cathode in the process of activation.

Placing the assembly in the activation furnace (for cooling, the counter was wrapped in wet asbestos with a stream of air directed on it, which kept the counter temperature down to 80°), we recorded the variation in the pulse count in the process of activation of the cathode. One of the curves obtained in this manner is reproduced in Fig.2.

As will be evident from the figure, the arrival of cesium on the cathode is marked by a rise of the thermionic current. After the thermionic current goes to a maximum, there is observed something like saturation of the cathode with cesium, i.e., a very much slower increase of cesium concentration in the region of over-cesiation. After sealing off of the cesium ampoule, the pulse count from the cathode falls off, apparently, due to evacuation of the cesium vapor from the test bulb. This cesium vapor in the bulb is responsible for a certain pulse-count background. The magnitude of this background (N' - N''), as may be seen from Fig.2, amounts to about 20% relative to the activity of the cathode with the given experimental geometry and pumping conditions.

After repeat evaporation of silver and heating of the cathode, its activity is reduced by a further 10-15%. Control experiments involving heating of clean glass and nonoxidized silver in cesium vapor failed to show any appreciable increase of activity in the test bulb.

On the basis of measurements carried out with six test bulbs (average cathode sensitivity 25 μamp/lumen), it may be concluded that the activation process is independent of the initial amount of cesium, which was always present in an excess amount in the cesium ampoule. Thus measurements with the counter showed that when batches of reduced cesium are loaded into sections of thin walled capillary tubes, the weight of a cesium charge may vary from 1.5 to 8 mg. After activation, in all cases 80 to 95% of the initial cesium remains in the ampoule. Of the expended portion of the cesium only 10 to 25% is condensed in the test bulb, the remainder is evacuated (it condenses on the walls of the vacuum line near the furnace).

In order to determine the distribution of cesium over the sections of a completed tube, a test bulb was cut into narrow rings and the activity of each section was measured with the counter. The average results for such a test are shown in Fig.3. As may be seen the cesium is adsorbed by the glass primarily in the vicinity of the cathode; the cesium concentration drops sharply as we go further from the cathode. Similar results were obtained by Turk[1] for an image orthicon, except that he found relatively greater cesium concentrations on the glass. In the case of our photocell, of the total amount of cesium present in the sealed off bulb, 60-80% was bound in the cathode having an area of 12 cm^2, 12-25% was distributed over the other glass area (area - 180 cm^2) and the remaining 10-15% was deposited on the nickel shield (12 cm^2). In the case of over-cesiation, the cesium concentration on the cathode changes very little, but the fraction of cesium on the glass and metal shield increases appreciably. Thus, for example, a cathode in a bulb of the same size, sealed off 3 min after the thermionic current began to fall off, contained

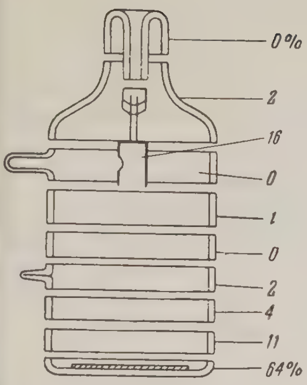

Fig.3. Distribution of cesium over the sections of a photocell tube.

only 35% of the total amount of cesium in the bulb. The deposits on the glass and the metallic shield accounted for 32% each.

We determined the actual amount of cesium in the cathodes by spreading weighed amounts of "tagged" cesium chloride in a water-alcohol suspension over a glass plate having the same dimensions as the cathode and monitoring the activity in the same manner as the cathodes. The cesium chloride we used had a relatively low activity: 0.02 g of the active chloride, the activity of which at the time of measurement was 2.2 millicurie, was mixed with 12 g of ordinary cesium chloride. A 100 μg batch of this mixed salt (equal to 80 μg of pure cesium) when spread over a glass plate 12 cm^2 in area yielded approximately 80 pulses per min.

These measurements showed that cathodes with an initial silver layer thickness of 3-4 μg/cm^2 contained from 6 to 8 μg cesium. If it be assumed that the initial silver layer is wholly oxidized it may be inferred that approximately 70-75% of the cesium enters into chemical combination in the reduction reaction during activation; the remainder (25-30%) is adsorbed on the cathode (in the volume or on the surface) in the free state. It may safely be assumed that all the silver oxide is reduced in the process.

In strongly over-cesiated cathodes the amount of excess free cesium is somewhat higher; in some cases it attains as much as 50% of the total amount present in the cathode. The cesium is adsorbed on the glass in the vicinity of the cathode in the form of a film with a mean density of the order of 0.1 μg/cm^2. Taking the atomic radius of cesium to be 2.55 Å, calculations show that such a film is close to monatomic. However, in view of the fact that the amount of cesium adsorbed on the glass falls off rapidly with increasing distance from the cathode no conduction between edge electrodes was observed.

The accuracy of determination of the amount of cesium from the pulse count for individual sections of the tube depends only on the uniformity of distribution of the radioactive impurity in the initial cesium chlroide powder, i.e., in the percent content of radioactive cesium chloride and the thoroughness of mixing. In our experiments the spread of specific activity values for different batches was ±10%. A more concentrated mixture should assure a greater uniformity of the tagged salt and, consequently, a higher accuracy of measurement. The error in measuring the activity from the number of pulses can be indefinitely reduced by increasing the counting time. The error in determining the amount of condensed silver depends primarily on the accuracy of measuring the distance from the evaporator to the glass surface (in our experiments the uncertainty was evaluated to be 5%).

The uncertainty in determining the amount of cesium on the cathode without cutting open the bulb is further increased by the influence of radiation from the other components of the test tube. Nevertheless, with a constant geometry of the tubes and a sufficiently high accuracy of mounting the components, we can establish a definite relationship between the emission parameters (pulse counts from the cathode) and the actual cesium content in the cathode. Our statistical analysis showed that the scatter as regards amount of cesium in cathodes prepared with the same initial silver coating, as indicated by the transparency, attains approximately ±50% relative to a certain optimum concentration characteristic of most (~75%) of the tested cathodes. This optimum concentration corresponds to the maximum sensitivity and maximum displacement of the spectral characteristics to the long wavelength side.

We were not able in our experiments to establish a relation between the amount of cesium and the resistivity of the layer. Measurements of the number of pulses from the cathode in the process of fatigue (to 100 hours operation) showed so insignificant a decrease of radioactivity that it may be concluded that even in the case of great fatigue the total amount of cesium in the cathode does not decrease significantly. Likewise there is no appreciable decrease in the pulse count when the cathode is heated up to 150°.

The above results are only preliminary data; the experiments were designed primarily to evaluate the potentialities of the described procedure.

Moscow Power Institute

Reference

1. J.Turk, Electronics, 2, 267 (1956).

DISCUSSION

N.D.Galinskii: Did you measure the amount of cesium deposited on the walls of the bulb?

N.A.Soboleva: Yes, we did.

N.D.Morgulis: What was the specific activity?

N.A.Soboleva: 0.2 millicurie per gram CsCl.

N.D.Morgulis: What was the surface concentration of cesium on the glass?

N.A.Soboleva: I cannot give exact figures, but there was no noticeable conductivity over the glass.

N.D.Morgulis: Did you take into account the background activity in the volume of the bulb?

N.A.Soboleva: Yes we did.

N.D.Morgulis declared that one should welcome this application of the radioactive tracer technique to the investigation of photocathodes.

FIELD EMISSION PATTERNS OF TUNGSTEN AND MOLYBDENUM CARBIDE CRYSTALS

- A.P.Komar & Iu.N.Talanin

In our work with the electron projector[1-3] we repeatedly observed[4] images with hexagonal symmetry from tungsten (occasionally) and molybdenum (frequently) points.

This appeared strange inasmuch as tungsten and molybdenum have a body-centered cubic lattice so that theoretically the image should not exhibit elements of hexagonal symmetry. Taking into account the relatively poor vacuum ($\sim 10^{-7}$ mm Hg) and the possible presence of carbon-containing impurities (from the hydrocarbon grease employed in the vacuum line joints), we hypothesized[4,5] that the observed hexagonal images were due to the carbides W_2C and Mo_2C, formon the tungsten and molybdenum single crystals, for, as is known[6], the structure of these carbides is hexagonal. In these early experiments[4] we also established that the (0001) face of the carbide always coincides with the (011) face of the cubic crystal. We explained this as being due to the similarity of the structure of these faces.

Inasmuch as on the basis of the early experimental data it could not be positively affirmed that the observed images were actually due to W_2C and Mo_2C, the experiments were continued. The original photographs as well as additional photographs taken in our laboratory by A.P.Kuritsnya were subject to more careful scrutiny and analysis.

Experimental technique

The experiments were repeated under better vacuum conditions as regards both degree of vacuum and accuracy of regulation. The projector assembly, which is diagrammed in Fig.1, had no joints but had provision for "contaminating" the points with certain carbon-containing substance. With a view to duplicating as closely as possible the conditions that might have obtained in the earlier projectors with joints, we used Di-A vacuum oil, "Ramsay" vacuum lubricant and picein. These substances were placed in a branch tube immersed in a Dewar with liquid nitrogen. The set-up also had provision for admitting benzene into the projector bulb; the admission of benzene was metered by means of a capillary. In addition, oxygen at a pressure of up to $\sim 10^{-5}$ mm Hg could be injected into the projector bulb from a silver tube heated by means of a nichrome element.

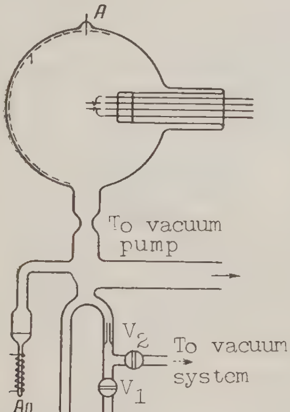

Fig.1. Projector and associated equipment for admission of carbon-containing substances and oxygen.

For the sake of convenience two to four tungsten or molybdenum points were mounted in each projector bulb. One could observe the formation of carbide on each one of them individually; the presence of the other points did not affect the image yielded by each one. The projector was connected to the vacuum system by a coupling tube and could be sealed off if desired.

In addition to the usual monitoring and measuring instruments, the electron projector was coupled to a 4-loop oscillograph. This continuously recorded 1) the current I_H and voltage U_H of the arc heating the point, 2) the emission current I_a and voltage U_a applied to the projector and 3) the instant of photography and the exposure time. For the most part the rate of film advance was 1 mm/sec. The sensitivity of the oscillograph circuit could be varied over a wide range.

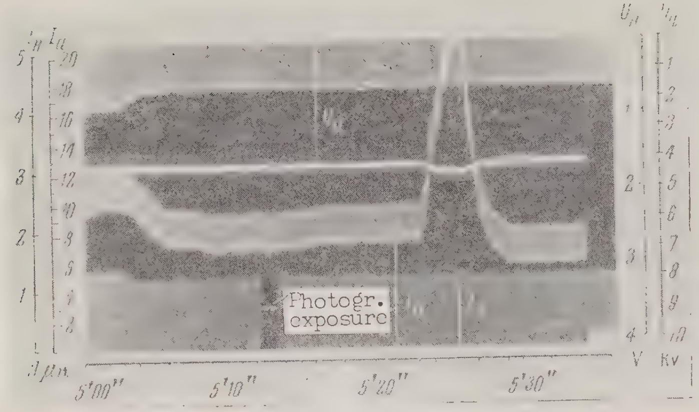

Fig.2. Photographic record of experimental conditions as indicated by the loop oscillograph.

A typical photographic record is shown in Fig. 2. The abscissae and ordinates of the recorded curves were determined by means of a special scaling templet. Although in view of the appreciable width of the lines the reading accuracy was not very high, nevertheless the photographic record provided an indispensable means of monitoring the variations of the experimental parameters, which is particularly important when the image on the screen is being photographed by a motion picture camera.

The angles between the faces and crystal axes were determined from the photographs of the image on the screen by means of a set of co-ordinate grids (Fig.3), plotted taking into account the geometry of the instrument, the position of the point relative to the screen, the curvature of the screen, the convergence of the electron beam, the distance of the camera lens from the convex screen and similar factors.

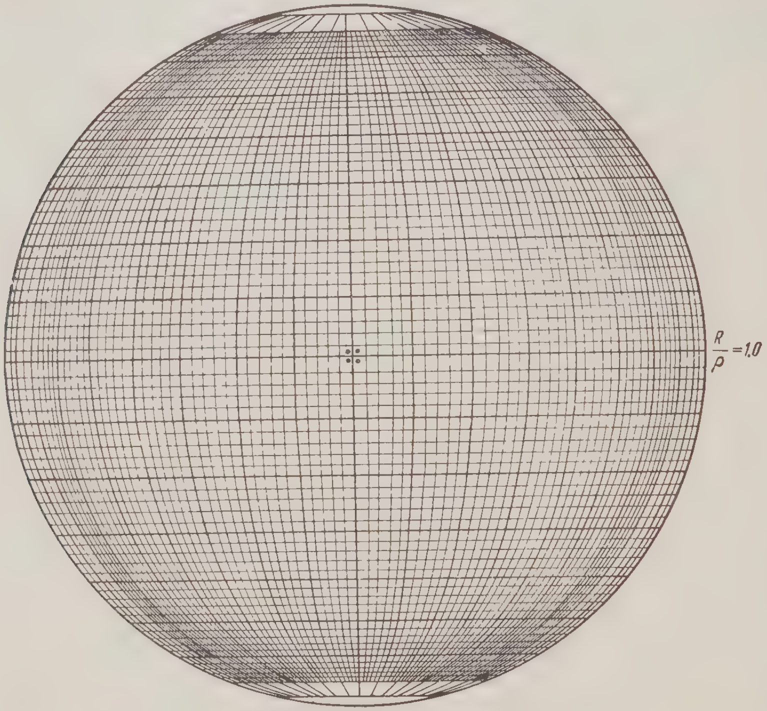

Fig.3,a

Fig.3,a,b & c. Coordinate grids for determining angles between crystal faces and axes, plotted taking into account the experimental geometry for different values of R/ρ, where R is the distance from the point to the screen and ρ is the radius of curvature of the screen.

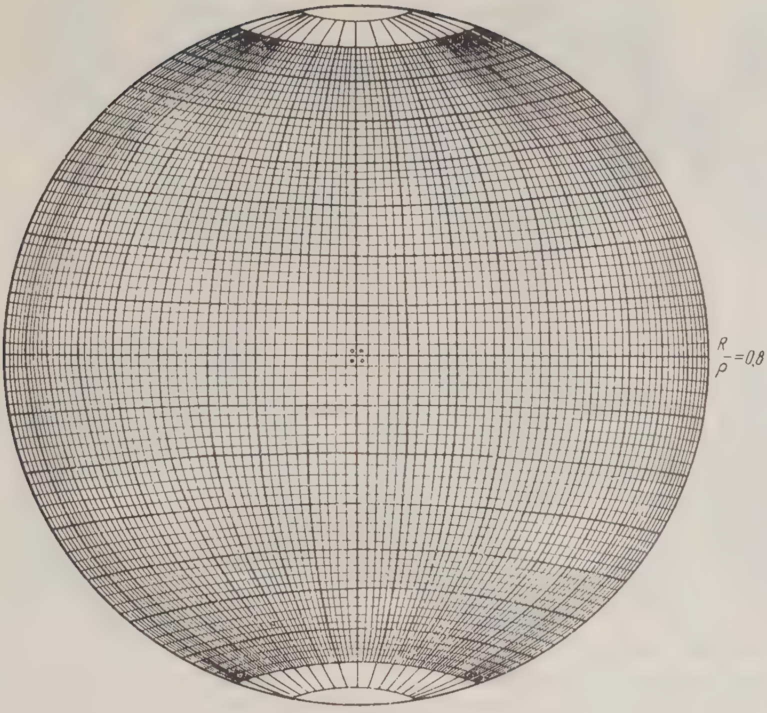

Fig.3,b

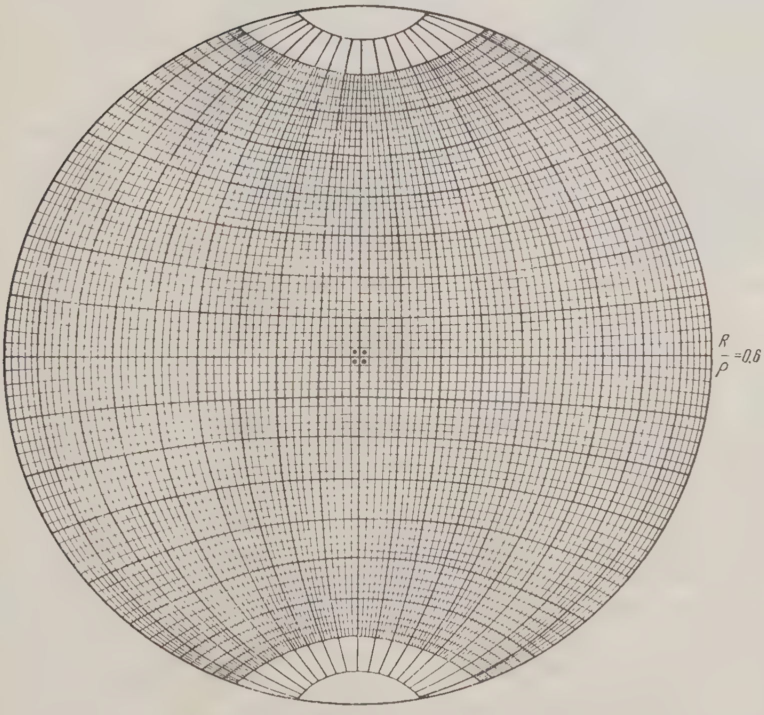

Fig.3,c

Results and discussion

The initial crystal in most cases was a rounded cubic tungsten or molybdenum crystal, yielding an image such as is shown in Fig.4,a. The character of the image and its stability together with the very slow variation of the emission current after heating of the point indicated that we had a high vacuum and a clean crystal surface. According to the indications of the LM-2 ionization pressure gage, the vacuum was better than 10^{-7} mm Hg.

However, even under such nearly ideal vacuum conditions, sometimes (incident to heating of the point for the purpose of degassing) there appeared a "ribbed" structure (Fig.4, b). In a number of cases the appearance of a ribbed crystal was the result of transformation of an already formed rounded crystal. In such cases the ribbed crystals retained the symmetry elements of the initial cubic crystal, i.e., exhibited the same orientation as the rounded crystal.

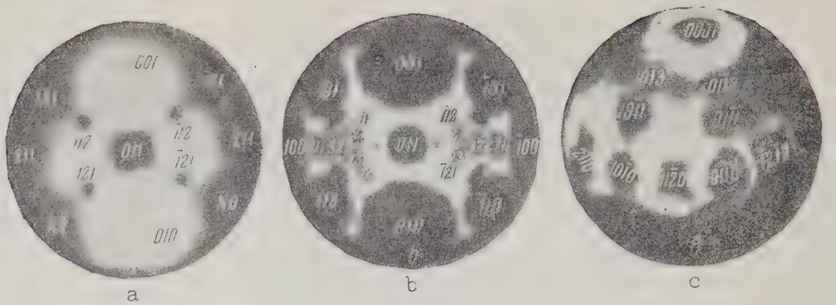

Fig.4. Crystal point images: a) rounded, b) "ribbed" and c) hexagonal.

Investigators in this field are unanimous in assuming that the appearance of a ribbed crystal is connected with the influence of carbon or materials containing carbon on the tungsten or molybdenum crystal. Under our conditions such impurities could undoubtedly be present in the residual gas so that there was nothing surprising about the formation of ribbed crystals.

Of the different carbon-containing substances tested, D1-A vacuum oil proved to be the least conducive to formation of hexagonal crystals (Fig.4,c). Even by intense evaporation of the oil, heated to the boiling point, onto heated points or condensation of the oil on cold points with subsequent heating, we did not succeed in obtaining hexagonal crystals on tungsten, although such hexagonal crystals appeared in most cases on molybdenum under identical conditions. In contrast, introduction of vacuum lubricant, picein and, particularly, benzene almost always led to the formation of a hexagonal crystal on both molybdenum and tungsten. It must be noted, however, that the formation of a hexagonal crystal on molybdenum usually occurred at a lower temperature (800-1000°) than on tungsten (1200-1400°).

We noted no substantial difference in the formation of hexagonal crystals on rounded and ribbed crystals except that often a ribbed crystal proved to be a sort of intermediate stage between a rounded and a hexagonal one and that in the reverse transformation from a hexagonal crystal there always appeared a ribbed cubic crystal.

With continuous pumping of the projector, i.e., under vacuum conditions not excluding the presence of carbon-contaminants, hexagonal crystals are stable as regards high temperature (Fig.5,c). Upon the admission of oxygen at a pressure of 10^{-5} mm Hg and heating of the point to 1200-1300°, there was observed formation of a cubic crystal in the region of the basal face of the hexagonal crystal (Fig.5, f & g). In a sealed off projector with a vaporized getter, wherein the vacuum was about 10^{-8}-10^{-9} mm Hg, a hexagonal crystal after heating to 2400-2500° transformed into a cubic ribbed crystal (Fig.5, h) which underwent no further alteration.

The effect of heating in the case of an hexagonal crystal both in the presence of oxygen and in vacuum could consist only of irreversible removal of carbon from its surface and further from its volume; hence a ribbed cubic crystal forming as a result of heating must contain less carbon than the initial hexagonal crystal.

This is also indicated by the fact that usually a ribbed cubic crystal appeared first and later transformed into a hexagonal one.

Most of the photographs with hexagonal images of tungsten and molybdenum crystals exhibit such clear indications of hexagonal symmetry (hexagonal basal

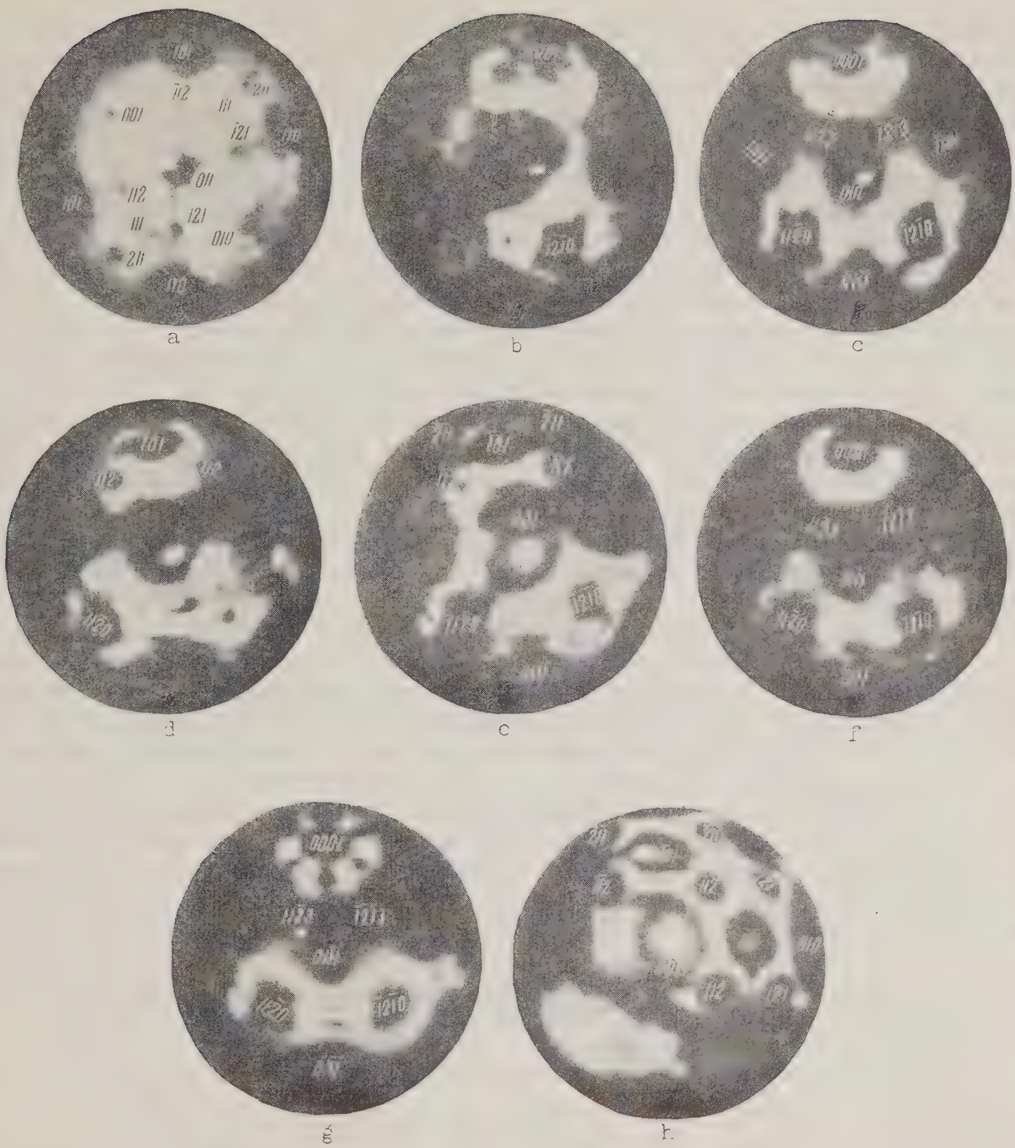

Fig.5. Formation of carbide on tungsten: 1) initial rounded crystal, b) beginning of formation of carbide, T = 1300°, c) formation of hexagonal crystal, d) breakdown of hexagonal crystal in the presence of oxygen, p = 10^{-5} mm Hg, T = 1200-1300°, e) regeneration of hexagonal crystal after elimination of oxygen, f) formation of hexagonal crystal in sealed off projector after heating to T = 1500°, g) same after heating to T = 2200-2300°, h) transformation of hexagonal crystal to a cubic ribbed crystal after heating to 2400-2500°.

plane, zone of prism faces perpendicular to the basal plane and at 30° to each other, etc.) that any suspicion that these images are due to some unique arrangement of extraneous substances on the cubic crystals must be rejected, i.e., there can be no doubt that the crystal yielding the image is actually an hexagonal crystal.

The formation of hexagonal crystals on tungsten and molybdenum under our conditions has much in common with the familiar characteristics of formation of carbides on these metals[7]. The appearance of hexagonal crystals under our conditions and their absence in the case of evaporation of free carbon onto the metal (Klein's experiment[8]) are in agreement with the data of Kreimer, Efros & Voronkova[9] who showed that the formation of tungsten carbide occurs primarily as a result of interaction of the gaseous medium, i.e., that for the formation of the carbide there must be present more active carbon, carbon forming as a result of decomposition of hydrocarbon molecules. There are ample data[7] that carbides can form only with a certain composition of the gaseous medium and in a certain temperature range, so that there is nothing surprising in the fact that hexagonal crystals were not obtained in the electron projector in random experiments when the requisite conditions were not fulfilled.

The frequent appearance of hexagonal crystal on molybdenum and their comparatively rare formation on tungsten may be explained by the fact that the conditions as regards composition of the gaseous medium are more rigorous for tungsten than for molybdenum. This follows from the phase diagrams for the W-C and Mo-C systems (see Ref.7), according to which tungsten carbides have a much narrower homogeneity region (limits of solubility of carbon in the carbides) than molybdenum carbides. The appearance of hexagonal crystals on molybdenum at lower temperatures than on tungsten is explained by the fact that the formation of the carbide is the result of reactive diffusion[10] for which the activation energy in the case of molybdenum is lower than in the case of tungsten[11]. The hexagonal symmetry of the crystals, the fact that they appear in the presence of carbon-containing substances and only under conditions that favor the formation of tungsten and molybdenum carbides, taken together leave no doubt that the hexagonal crystals observed on tungsten and molybdenum points in the electron projector are actually the carbides of these metals. It must be recalled, however, that both tungsten and molybdenum have two carbides each, i.e., W_2C and Mo_2C and WC and MoC; hence we must determine which of these is responsible for the observed hexagonal crystals. The structure and parameters of these carbides as given in the literature[6,7 & 12] are listed in the accompanying table.

Crystallographic parameters of tungsten and molybdenum carbides

Carbide	Lattice	*a*	*c*	*c/a*
W_2C	Close-packed hexagonal	2.986	4.712	1.578
Mo_2C	Same	3.012	4.735	1.572
WC	Simple hexagonal	2.901	2.831	0.976
MoC	Same	2.901	2.768	0.960

The data in the table pertain to the arrangement of the metal atoms and have been fairly accurately determined by x-ray diffraction analysis. We do not show in the table the existence of two modifications of W_2C and Mo_2C, described by Bokii[6] inasmuch as their structure and parameters are similar; nor do we show the fluctuation of some of the parameters as a function of the carbon content in the carbide inasmuch as these are irrelevant to our purpose.

As for the carbon atoms in tungsten and molybdenum carbide, x-ray diffraction analysis does not allow of directly determining their positions, but this can be done from geometric considerations and certain other, indirect data. In the light of present knowledge it can safely be assumed that the structure of carbides and the arrangement of the metal and carbon atoms in

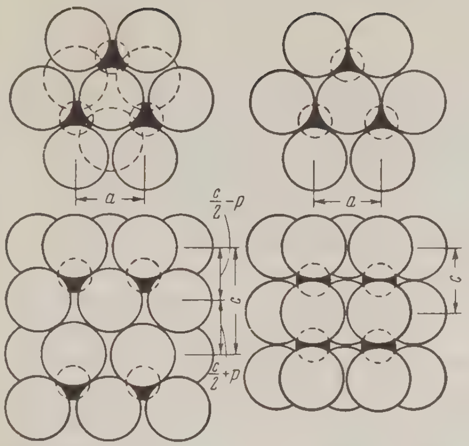
a
c/2 −p
a
c
c/2 +p
c

Fig.6. Structure of tungsten and molybdenum carbides: W_2C, Mo_2C, WC and MoC ($p \approx 0.02$ Å).

them are very much as pictured in Fig.6. In both structures the carbon atoms are arranged along the *c* axis one above the other, forming a simple hexagonal lattice inserted between the metal atoms.

Utilizing the above data on the structure of carbides, we calculated the angles between the *c* axis and the normals to the most probable faces of the two principal zones that could form on hexagonal crystals with $c/a = 1.58$ and $c/a = 0.976$. The results of these calculations are shown in the form of diagrams in Fig.7. The left-hand diagram pertains to one of the zones of the body-centered cubic crystal with which the corresponding zone of a hexagonal crystal should coincide if the principal of orientational correspondence is fulfilled.

The measurement of the angles between the faces (or more accurately speaking, between the normal to the face and the *c* axis) was carried out from the photographs of the hexagonal crystals by means of the above mentioned coordinate grids. The attainable accuracy depended on the extent to which the closest available grid corresponded to the particular projection of the image in the given photograph and on the extent to which the center of the face (which could not always be very precisely determined in the photograph) coincided with the emergence of the normal to the given face. In most cases we were, however, able to attain an accuracy of 3-5° for the absolute values of the angles and a somewhat better accuracy for the difference between close angles. From measurements made in this way on a large number of photographs we obtained values of 0°, 20°, 30°, 60° and 90° for the faces of one zone and 0°, 55° and 90° for the faces of the other.

Comparison of the measured and calculated angular values (see Fig.7)

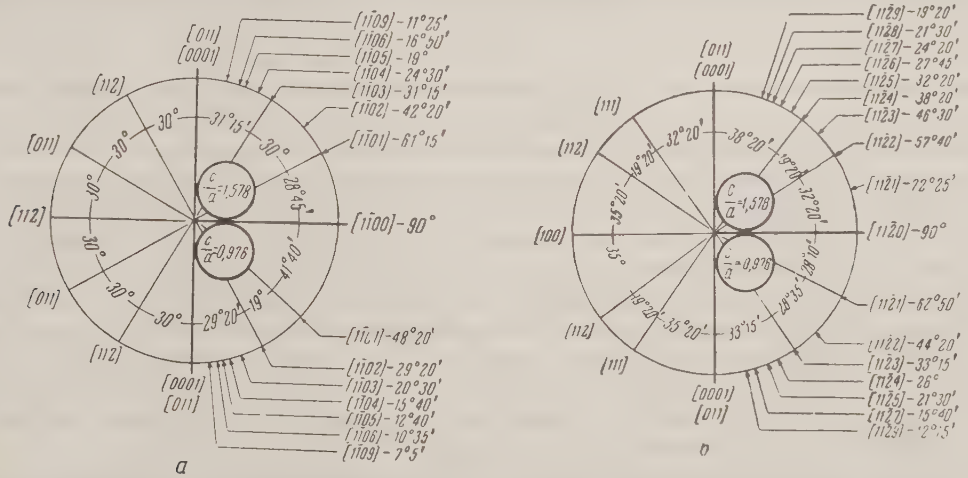
[011]
[0001]
[112]
[011]
[112]
[011]
[112]
[0001]
[011]
[11̄09] - 11°25'
[11̄06] - 16°50'
[11̄05] - 19°
[11̄04] - 24°30'
[11̄03] - 31°15'
[11̄02] - 42°20'
[11̄01] - 61°15'
[11̄00] - 90°
[11̄01] - 48°20'
[11̄02] - 29°20'
[11̄03] - 20°30'
[11̄04] - 15°40'
[11̄05] - 12°40'
[11̄06] - 10°35'
[11̄09] - 7°5'
30°
31°15'
30°
30°
30°
28°45'
30°
41°40'
30°
30°
29°20'
19°
c/a = 1,578
c/a = 0,976
a
[011]
[0001]
[111]
[112]
[100]
[112]
[111]
[0001]
[011]
[112̄9] - 19°20'
[112̄8] - 21°30'
[112̄7] - 24°20'
[112̄6] - 27°45'
[112̄5] - 32°20'
[112̄4] - 38°20'
[112̄3] - 46°30'
[112̄2] - 57°40'
[112̄1] - 72°25'
[112̄0] - 90°
[112̄1] - 62°50'
[112̄2] - 44°20'
[112̄3] - 33°15'
[112̄4] - 26°
[112̄5] - 21°30'
[112̄7] - 15°40'
[112̄9] - 12°15'
32°20'
38°20'
19°20'
19°20'
35°20'
32°20'
35°
28°10'
19°20'
35°20'
33°15'
28°35'
c/a = 1,578
c/a = 0,976
б

Fig.7. Diagrams illustrating arrangement of faces and angles between them for the a) [111] and b) [011] zones of a body-centered cubic crystal and for the a) [1120] and b) [1100] zones of hexagonal crystals with $c/a = 1.587$ and $c/a = 0.976$.

showed that the best agreement obtained for an hexagonal crystal with the ratio $c/a = 1.58$, i.e., indicated that the hexagonal crystals forming on tungsten and molybdenum in the electron projector were crystals of W_2C and Mo_2C.

Substantiation of our deduction that the carbides formed on the tungsten and molybdenum are W_2C and Mo_2C may be found in the work of Pfau & Rix[13] who observed the shape of WC crystals grown from Ni-WC and Co-WC melts. Furthermore, from analysis of the structure of WC, it was established that this carbide crystallizes in the form of ditrigonal dipyramids (trigonohedral antihemihedra) which are very unlikely to yield an hexagonal image.

We deemed it desirable to analyze the earlier[4] observed coincidence of the (0001) face of the hexagonal crystal with the (011) face of the cubic crystal from the standpoint of the principle of orientational correspondence. As is known, this principle was established, checked and substantiated as a result of x-ray diffraction studies[12,14 & 15] and also from direct observation in the electron projector[16-19] for the case of allotropic transformations. According to the orientational correspondence principle, the change in structure in an allotropic transformation must occur so that any given set of mutually parallel closely packed planes and conjunction of mutually parallel closely packed rows in a crystal must preserve their orientation unchanged.

In the case of the transformation accompanied by the transition of a body-centered cubic lattice to an hexagonal one this means that the (0001) face of the hexagonal crystal must coincide with the (011) face of the cubic crystal and the $(11\bar{2}0)$ face of the hexagonal crystal with the (111) face of the cubic crystal.

In conformity with this condition the hexagonal crystal can be oriented in twelve different ways relative to the initial body-centered cubic crystal, while the cubic crystal can be oriented in six different ways relative to the initial hexagonal one (for a more detailed discussion see Ref.20).

In all the observed cases of carbide formation, both on tungsten and molybdenum, the condition of orientational correspondence was realized. As is clearly evident from the numerous photographs and the corresponding polar figures plotted from the photographs with the aid of the above mentioned coordinate grids, in each case the hexagonal carbide crystal was oriented relative to the original cubic one so that the (011) face of the cubic crystal coincided with the (0001) face of the hexagonal crystal and the (111) face of the cubic crystal coincided with the $(11\bar{2}0)$ face of the hexagonal one, regardless of whether the cubic crystal was rounded or ribbed. According to the available data relative to oriented transformations in crystals, realization of these conditions corresponds to reciprocal transformation of body-centered cubic and hexagonal densely packed lattices and hence serves as additional evidence that the carbides formed in our electron projector were W_2C and Mo_2C.

The fact that the orientation of the hexagonal crystal relative to the cubic one was the same regardless of whether the cubic crystal was rounded or ribbed can be taken as evidence of identity of the structure of the rounded and ribbed crystals, i.e., proof that the structure of the ribbed crystals was also of the body-centered cubic type. The identity of the structures is also substantiated by the fact that the orientation of the rounded and ribbed crystals remained the same when one transformed into the other.

The conditions of orientational correspondence were realized even in the case when a cubic crystal (Fig.5,a), having transformed into an hexagonal one (Fig.5,c) and back to a cubic one (Fig.5,d & e) proved to be rotated relative to the initial position: both cubic crystals - the initial and the final - were regularly oriented relative to the intermediate hexagonal crystal in con-

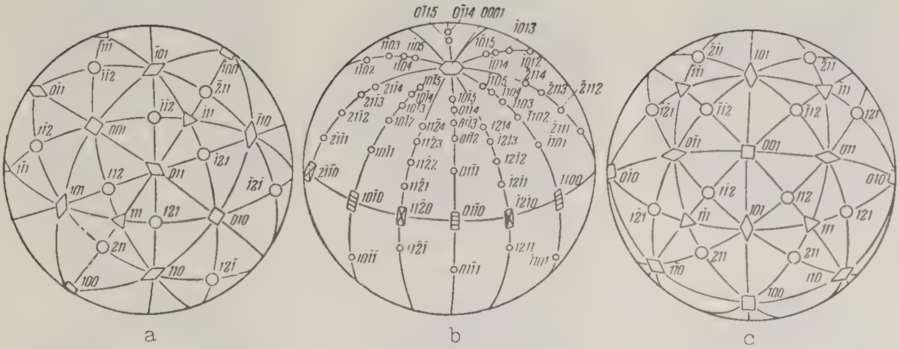

Fig.8. Polar figures corresponding to Fig.5.

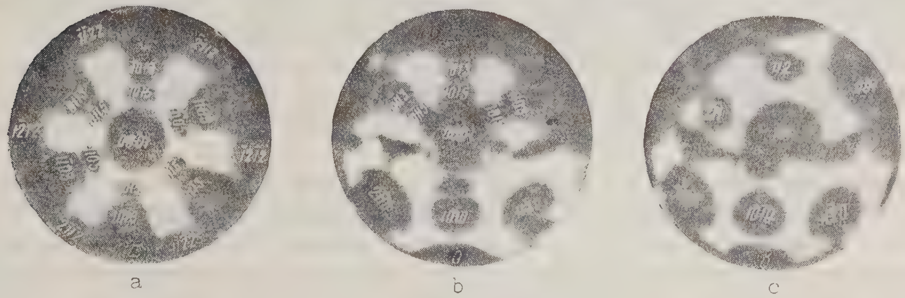

Fig.9. Formation of carbide on molybdenum: a) hexagonal crystal with basal face perpendicular to point electrode axis, b) appearance of band of faces of the prism of a second hexagonal crystal, c) transformation of one of the hexagonal crystals into a cubic ribbed crystal.

formity with the orientational correspondence principle (also see the polar figures in Fig.8).

Further proof is furnished by the case illustrated in Fig.9 where near a hexagonal crystal (a) there formed as a result of high temperature heating under conditions of relatively poor vacuum a set of faces of another hexagonal crystal (b) and both these proved to be regularly oriented relative to the ribbed cubic crystal that appeared as a result of transformation of one of the hexagonal crystals (c); the corresponding polar figures are shown in Fig.10.

In addition to orientation of the succeeding crystal relative to the preceding one, we must also consider the orientation of the crystals relative to the axis of the needle point.

The cubic crystals were usually oriented so that the (011) face was perpendicular to the needle point axis, the other face being at corresponding angles to it. This orientation follows from the texture (fibre orientation) in the tungsten wire used for preparing the point. With this initial orientation of the cubic crystal, the hexagonal crystal forming from it, in conformity with the principle of orientational correspondence, may be oriented in one of the six following ways relative to the point axis: one orientation with the [0001] axis parallel to the point axis, one orientation with [0001] axis perpendicular to the point axis and four orientations with the [$\bar{0}$001] axis at an angle of 60° to the point electrode axis.

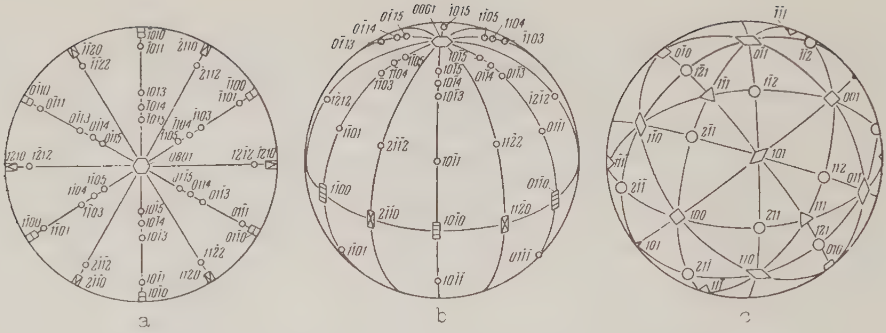

Fig.10. Polar figures corresponding to Fig.9.

In our work with tungsten and molybdenum points we observed all these orientations except the second ([0001] axis perpendicular to the point axis). Only in rare cases (particularly on tungsten) did we observe the orientation of the carbide with the [0001] axis parallel to the point axis (Fig.9,a). In most cases we obtained the various orientations with the [0001] axis inclined at an angle of 60°.

A possible explanation of this is the fact that the probability of each of the first two orientations is 1/6, while the total probability of the last four is 4/6. Possibly if we had had a larger number of cases of formation of carbide crystals we would have also observed the orientation with the [0001] axis perpendicular to the center line of the electrode. No less plausible in our opinion, however, is another explanation, namely, that in the case of orientation of the crystal with the [0001] axis at 60° to the point axis, we have coincidence of the greatest number of faces of the cubic and hexagonal crystals over the entire point (including its base), i.e., a minimal change in faceting and, consequently, in the free surface energy.

In the case of orientational transformation there is always the possibility of simultaneous appearance and subsequent coexistence of several crystals, differently oriented but still fulfilling the conditions of orientational correspondence in view of the possible multiple orientations.

In most cases under our conditions one crystal transformed into only one crystal, for example, one cubic crystal into one hexagonal crystal. There were, however, a number of individual cases where next to an already formed hexagonal crystal there appeared the base prism of another hexagonal crystal (Fig.9,b).

We observed an interesting sequence in the case of a molybdenum point which, to judge from the image (Fig.11,a), had traces of oxygen contamination. After admission of vacuum grease vapor with the point heated to 800-900° near each [111] direction of the cubic crystal there appeared three faces which, from their configuration, can be identified as the $(11\bar{2}0)$ faces of a hexagonal crystal (11,b). These faces are oriented relative to the cubic crystal so that the prism face zone of the hexagonal crystal coincides with the [011] zone of the cubic crystal. Here we have some deviation from rigorous orientational correspondence: although the (011) face closely coincides with the $(1\bar{1}00)$ face, there is some divergence as regards the (111) and $(11\bar{2}0)$ faces. There are no indications of formation of the basal face of the hexagonal crystal.

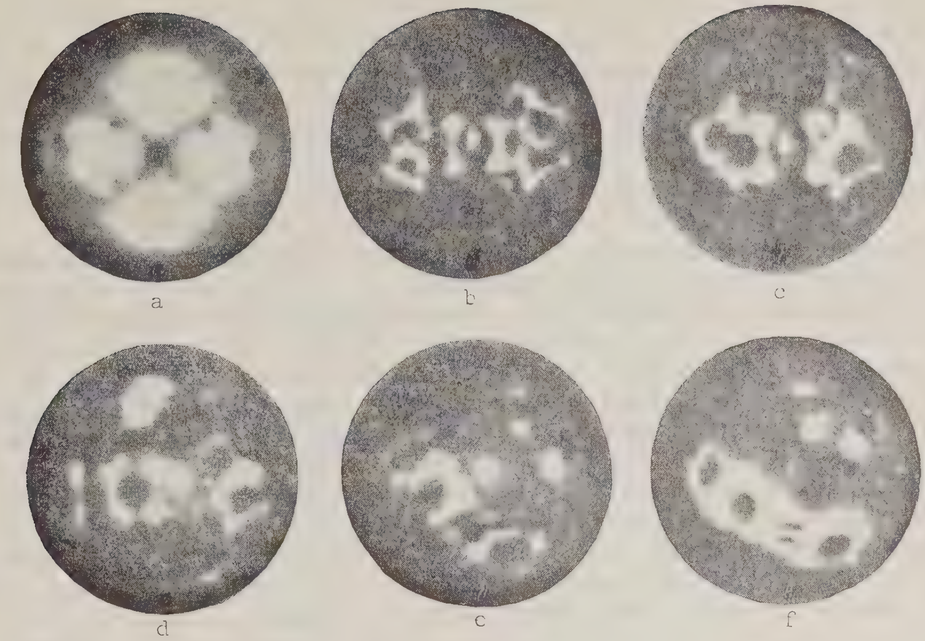

Fig.11. Formation of carbide on molybdenum point.

Subsequent heating to 1200-1300° brought a change in the arrangement in the prism faces and led to the disappearance of some of them (Fig.11,c & d). After several heatings there formed one hexagonal crystal with well developed prism faces and a nascent basal plane (Fig.11,f). The orientation of this crystal is consistent with the conditions of orientational correspondence, namely, the (0001) face coincides with the (011) face and the $(11\bar{2}0)$ face with the (111) face.

Apparently, in such cases the process of carbidization of a molybdenum crystal occurs in the following manner. At first the carbide face forms on the surface of a metallic crystal simultaneously at several points with conservation of structural correspondence at each point. Next the carbidization extends into the depth of the crystal simultaneously with the onset of collective recrystallization. Finally, the carbidization encompasses the entire volume and there is retained and formed one (occasionally two or more) large hexagonal crystal oriented in the regular manner relative to the initial cubic crystal.

We are frankly puzzled by the absence of WC and MoC, for these carbides should presumably form concurrently with W_2C and Mo_2C. We must emphasize, however, that numerous measurements of the angle on hexagonal crystals in the projector never yielded values corresponding to the structure with $c/a = 0.976$.

We are still unclear as regards the nature of the cubic "ribbed" crystals which commonly appear prior to the formation of the hexagonal crystals.

Leningrad Physical-Technical Institute,
Academy of Sciences of the USSR

References

1. B.M.Tsarev, Usp.fiz.nauk., 36, 181 (1948).
2. Elektronnaia mikroskopiia (Electron microscopy), 1954.
3. E.W.Müller, Ergebn. exakt. Naturwiss., 27, 290 (1953).
4. A.P.Komar & Iu.N.Talanin, Izv.AN SSSR, Ser.fiz., 20, 1137 (1956). (Trans., Bulletin, 20, No.10, 1029.)
5. A.P.Komar & Iu.N.Talanin, Sb.Rost.kristallov (Symposium on Crystal Growth), p.110-118, 1957.
6. G.B.Bokii, Vvedenie v kristallokhimiiu (Introduction to Crystal Chemistry), Moscow State University, 1954.
7. G.V.Samsonov & Ia.S.Umanskii, Tverdye soedineniia tugoplavkikh metallov (Solid compounds of high melting point metals), 1957.
8. R.Klein, J.Chem.Phys., 22, 1406 (1954).
9. G.S.Kreimer, L.D.Efros & E.A.Voronkova, Zhur.tekh.fiz., 22, 858 (1952).
10. V.Z.Bugakov, Diffuziia v metallakh i splavakh (Diffusion in metals and alloys), 1949.
11. G.V.Samsonov & V.P.Latysheva, Physics of Metals and Metallurgy, 2, 309 (1956).
12. A.A.Ivensen & G.V.Kurdiumov, Vestnik metallopromyshlennosti (Journal of the Metal Industry), No.9-10. 165 (1930).
13. H.Pfau & W.Rix, Z.Metallkunde, 45, 116 (1954).
14. G.V.Kurdiumov & G.Zaks, Vestnik metallopromyshlennosti (Journal of Metal Industry), No.9-10, 165 (1930).
15. W.G.Burgers, Physika, 7, 561 (1934).
16. A.P.Komar & V.N.Shrednik, Zhur.eksp.i teor.fiz., 32, 184 (1957).
17. H.Schleicher, Z.Naturforsch.a., 7, 471 (1952).
18. E.G.Brock, Phys.Rev., 100, 1619 (1955).
19. O.Buhl & C.Schüler, Z.Metallkunde, 48, 116 (1957).
20. A.P.Komar & V.N.Shrednik, Physics of Metals and Metallurgy, 5, 3 (1957).

DISCUSSION

I.L.Sokol'skaia: Cubic carbide is more stable than the hexagonal form as regards heating in vacuum. The tungsten lattice "swells" incident to the formation of the hexagonal carbide. How then can one explain the formation first of WC and MoC and only then of W_2C and Mo_2C?

Iu.N.Talanin: W_2C and Mo_2C are not formed immediately due to distension of the lattice. Even a greater volumetric change occurs in the formation of WC and MoC. In speaking of the formation of single crystals we do not have in mind the formation of a complete crystal, but only "excrescences" on individual faces of the initial crystal with a corresponding composition. On macroscopic samples the carbidization process is $W \rightarrow WC \rightarrow W_2C$. Apparently this sequence also holds for a single crystal point.

B.G.Smirnov: At what temperature were the W_2C and Mo_2C formed?

Iu.N.Talanin: At 1400 to 1800°K.

N.A.Gorbatyi: Did you carry out experiments involving deposition of carbon onto the point from a carbon filament?

Iu.N.Talanin: No, but apparently for the formation of carbides the carbon must be in the nascent state.

G.N.Shuppe: In the carbidization of a point by the industrial technique in a mixture of benzene and hydrogen we did not succeed in obtaining symmetrical pictures in the projector. Sometimes, however, we accidentally obtained pictures similar to those shown today. We feel that this pattern is due not to a carbide but to "dirty" tungsten. Measurement of angles for the purpose of determining the structure is a risky procedure inasmuch as it is difficult to take into account the coefficient of compression.

A.P.Komar: It is not surprising that the industrial carbidization technique did not yield positive results. At high carbon concentrations there is obtained a polycrystalline formation with dark contours. A necessary condition is a slow rate of carbidization. Not much carbon is necessary for "accidental" formation of carbide. Small amounts of different hydrocarbons may be present on the glass, the mounting components, etc.

In determining the angles, the compression coefficient was determined with fair accuracy from the picture for pure tungsten for which the values of the angles are well known from crystallography. Our overall error in measurement does not exceed 2-3°.

I.L.Sokol'skaia: In connection with attempts to carbidize a tungsten point by the commercial technique in our laboratory we noted an appreciable swelling of the point by observation under an optical microscope. Attempts to obtain carbides by evaporating carbon from a carbon filament onto the tungsten led only to the formation of a "ribbed" point (similar to that reported by Klein). Hexagonal tungsten carbide was obtained only upon the introduction of hydrocarbons into the projector and the following two necessary conditions were fulfilled: 1) low partial pressure of the hydrocarbon vapor and 2) preliminary formation of a tungsten single crystal on the tip of the point by heating in a high vacuum.

When these conditions were not fulfilled there formed very fine, readily detached crystals and the point rapidly disintegrated. Hexagonal patterns were obtained, as a rule, after formation of a "ribbed" crystal.

"Ribbed" crystals also frequently formed accidentally, possibly due to the chance presence of traces of organic materials in the bulb; in particular, "ribbed" crystals were always obtained as a result of heating of the point after evaporative deposition of copper phthalocyamin.

ADSORPTION OF ZIRCONIUM AND BARIUM ON TUNGSTEN AND THE RESULTANT WORK FUNCTION

- V.N. Shrednik

Introduction

The field emission projector technique[1], which was used in the present work, is very convenient for investigating emissive coatings. It has already been used many times for this purpose,[2-6] and always yielded valuable information on the effect occurring on a single crystal surface. By menas of a field emission projector one can observe the course of surface processes with an amplification of the order of 10^5 and a resolution of 40-50 Å. It is not difficult to realize in the projector bulb a vacuum sufficiently high to keep the investigated surface free of adsorbed gases for hours and even days. Finally, the field emission technique allows of obtaining diverse quantitative data and is one of the procedures for determining the work function that does not require heating of the investigated layer.

The Zr-W system has not hitherto been investigated in detail. Dushman and his co-workers[7] showed that a Zr monolayer on tungsten has a work function equal to 3.15 ev (the work function of Zr, according to averaged data[8], is 3.84 ev) and found that the behavior of Zr on W is in many respects similar to the behavior of Th on W. Investigation of Zr coatings on tungsten single crystals is of interest not only from the standpoint of cathode electronics but also from that of the physics of metals (surface diffusion, alteration of the lattice, etc.). Below we shall report only on the part of our investigation of the behavior of Zr on W pertaining to variation of the emissive properties of Zr condensed on W with increasing thickness of the coating.

The behavior of Ba on tungsten single crystals has been repeatedly investigated by means of an electron projector.[2,4,5 & 9] Hence in the present research we carried out only qualitative experiments with Ba on W, primarily for the purpose of comparing the behavior of Ba with that of Zr on a tungsten base.

Experimental Procedure

In determining the work function φ from observation of field emission one must know the field strength (E) at the emitter surface, associated with the specific geometry of the cathode. The last is always difficult to determine precisely. Hence we used the method, originated by Haefer[10], based on the fact that a thin film of substance evaporated onto a tungsten needle point does not significantly alter the geometry of the point so that the factor α in the formula $E = \alpha V$ (V is the applied voltage) remains virtually the same. The work function of pure tungsten being known, the factor α can be determined by means of the Fowler-Nordheim[11] equation:

$$j = 1.55\cdot10^{-6}\,\frac{E^2}{\varphi}\exp\left[-6.83\cdot10^{7}\,\frac{\varphi^{3/2}}{E}\,\vartheta(y)\right], \qquad (1)$$

where j is the current density, $\vartheta(y)$ is the elliptic Nordheim function as corrected by Burgers et al[12], and $y = \frac{3.78\cdot10^{-4}\sqrt{E}}{\varphi}$; j, E and φ are measured in amp/cm^2, v/cm^2 and v, respectively.

In the present investigation we measured the total current I and the voltage V and then plotted log I/V^2 versus $1/V$: these semilogarithmic plots proved to be straight lines down to the minimal measured current densities

(>1 amp/cm^2). Then from the ratio of the slopes (tangents) of the straight-line plots for the investigated layer and for pure tungsten ($\tan \beta_x$ and $\tan \beta_W$, respectively), we could determine the work function of the coating with reference to the work function φ_W of tungsten by means of the formula

$$\varphi_x = \varphi_W \left(\frac{\tan \beta_x}{\tan \beta_W} \right)^{2/3} . \tag{2}$$

The work function of tungsten was assumed to be 4.5 ev. Actually, however, the work function of the initial tungsten surface may have differed somewhat from 4.5 ev inasmuch as the tungsten may have contained some Zr impurity, which is difficult to eliminate wholly. Hence this procedure is not ideal for determining the absolute value of φ. Nevertheless, the relative work function as determined by means of Eq. (2) is a more reliable indication of the true value of φ than, say, the voltage required to obtain a given emission current. This criterion is not infrequently used in work with an electron projector inasmuch as the $\log I/V^2 = f(1/V)$ plots are frequently displaced parallel to themselves.

Eq. (2) was derived without neglecting the Nordheim function $\vartheta(y)$ in (1). The decrease in the potential barrier height due to the Schottky effect, taken into account formally by introducing the $\vartheta(y)$ function, changes the transmissivity of the barrier through which the electrons tunnel, but this barely affects the derivative of this transmissivity with respect to $(1/E)$.[12] Mathematically this means that $\vartheta(y)$ is almost a parabola. The values of E and φ found in measuring the work function of Zr coatings on W yield values of in the interval $0.55 \geqslant y \geqslant 0.35$. In this interval we can make the approximation $\vartheta(y) = 0.965 - 1.1\, y^2$, which deviates from the tabular values by no more than 0.45%, and in this way eliminate all further dependence on E in the exponential of Eq. (1).

The work function found from the total current $I = \int_S j\,dS$ (where S is the area of the emitter), is an average value. In the same way as was done for the thermal emission[13], one can show that the mean field emission work function is given by

$$\overline{\varphi^{3/2}} = \frac{\int_S j \varphi^{3/2}(x, y)\, dS}{\int_S j\, dS} . \tag{3}$$

Since the φ-dependence of the field emission current is even more pronounced than that of the thermal emission current, it may be assumed that the field emission work function will to an even greater extent be the work function of the strongly emitting sections of the cathode, i.e., of the sections where φ is small.

Observation of field emission patterns shows that often there are appreciable differences as regards the brightness of different sections. Let us consider the nature of the experimentally determined mean work function $\bar{\varphi}$ obtained from these strongly emitting sections. Thus, for the i-th section with a work function φ_i, we can write

$$I_i / V^2 = A_i \exp\left(-B \varphi_i^{3/2} \frac{1}{E}\right).$$

Here, in the weighting factors A_i the quantity that differs most strongly from one section of the cathode to another is the section area S_i. If experiment gives a good straight line for log $I/V^2 = f(1/V)$, one can assert that when setting up the sum $I = \sum_i I_i$ for the total current, the arguments of the exponentials do not differ greatly from each other, since in the sum they give approximately an exponential. Obviously, the weaker the field, the greater will be the effect of the differences between sections with different work functions and the more the semilog plots will deviate from straight lines. The upper bound of the spread in φ_i values for a given E, in order that log I/V^2 be sufficiently close to linear in $1/V$ is given by

$$B(\varphi_i^{3/2} - \bar{\varphi}^{3/2}) < E. \tag{4}$$

For fields producing a field emission with a current density $j = 1$ amp/cm^2 (which is a very small value for field emission), requirement (4) gives a maximum allowable spread in φ_i values of ±0.15 ev for $\bar{\varphi} = 4.5$ ev, and ±0.1 ev for $\bar{\varphi} = 3$ ev. When (4) is satisfied, the work function determined from the slope of the field emission curves is defined as the weighted mean

$$\bar{\varphi}^{3/2} = \frac{\sum_{i=1}^{n} A_i \varphi_i^{3/2}}{\sum_{i=1}^{n} A_i}. \tag{5}$$

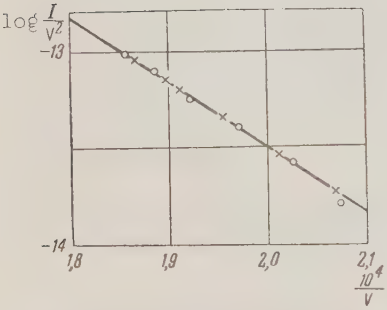

Fig.1. Reproducibility of the log $I/V^2 = f(1/V)$ characteristics for a Zr coating on W of the type characterized in Fig.6,d after exposure in vacuum.

The vacuum in the sealed off projectors used in our work was, presumably, better than 10^{-11} mm Hg where the pressure of the gases influencing the emission is concerned; it was determined from the rate of change of the pattern on the tube screen and of the emission characteristics during exposure in vacuum[14]. The stability of the characteristics is illustrated in Fig.1; the repeat measurement points, as indicated by crosses, were recorded after 16 hours exposure in vacuum of one of the coatings of Zr on W; it will be seen that they fall almost exactly in line with the initial points. The method of obtaining such a vacuum has been described earlier.[15] In actual fact we had more to fear from alteration of the emission characteristics during the period of observation inasmuch as with the high voltage turned on, the rate of contamination or disintegration of the emitter surface due to bombardment by ions coming primarily from the screen was appreciably higher than during "inactive" holding in vacuum. Hence in those cases when heating between recording of successive points was inadmissible the field was applied for the minimal period and we tried to avoid recording the characteristics with heavy currents (>10 microamp). Since, as a rule, the points satisfactorily fitted a straight line, we deemed it sufficient to obtain 6-7 points. The temperature of the emitter and vaporizer was measured by means of an optical pyrometer in the region from 800 to 2000°; it was extrapolated into the region of lower temperatures from a plot of the resistance of the heater filament vs T.

The zirconium was evaporated onto the points from the side from a drop of Zr on a tungsten wire which was always heated to the same temperature

(~1700°). Aside from thorough outgassing, the purity of the deposited zirconium was assured by the fact that the vapor pressure of the various possible compounds of Zr with the residual gases is low compared with the vapor pressure of Zr at the evaporating temperature. The barium was evaporated by a similar procedure from a tantalum cup filled with a mixture of barium carbonate and appropriate reducing metals. In evaporation of Zr and Ba on the approximately hemispherical surface of the point, their concentration over the surface as a function of the angle of incidence is given by the formula:

$$N = N_0 \cos \gamma \qquad (6)$$

where N is the number of Zr or Ba atoms per cm^2 tungsten surface, γ is the angle of incidence and N_0 is the concentration of deposited atoms in the case when the surface is perpendicular to the atomic beam, i.e., when $\gamma = 0$.

Results

A. Adsorption of Zr and Ba on W

We determined the variation of the mean work function $\bar{\varphi}$ with the evaporation time of Zr for a number of tungsten points. In these experiments the points were at room temperature. The Zr was evaporated in successive small batches. It was assumed that in this manner we could observe a minimum of the work function, corresponding to the stage when the largest area of the point electrode is covered with a monolayer; after this $\bar{\varphi}$ should increase as the monolayer area is reduced incident to the continued build up in thickness. Actually, however, all the $\bar{\varphi}$ vs evaporating time curves did not go through a minimum; instead we obtained a gradual transition from the work function for W to a constant low value which decreased no further with deposition of greater amounts of Zr and which, apparently, equalled the work function of Zr. The curves obtained for two tungsten points are shown in Fig.2; the scatter of the values for the horizontal sections of the curves is intrinsic to the experimental procedure.

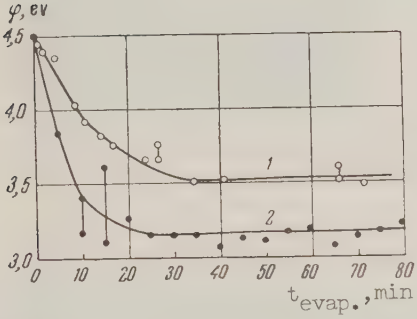

Fig.2. Variation of $\bar{\varphi}$ with the time of evaporation of Zr onto W: 1) point having a radius of 1.2 μ (see Figs.3 & 7), 2) point having a radius of 0.4 μ (see Fig.6).

The photographs of Fig.3,a-d illustrate individual stages of successive deposition. Typical here is the fact that with a short evaporation time (Fig.3,b) the peripheral region of the tungsten crystal on the side of the Zr source is "brought out" in the pattern. This is connected with the fact that decrease of the field from the tip of the point to the periphery is compensated (in the sense of its influence on the current density) by the decrease of the Zr concentration from the periphery to the tip. The darkening of the far lateral regions (Fig.3,c) may therefore be the first indication that the greater part of the point is covered with a thicker than monatomic layer of Zr, characterized by the same work function at all points. If there were a band with $\varphi < \varphi_{Zr}$ extending across the evaporated coating, then from the evaporator side it would be bounded by a sharp dark zone (we shall see this in the case of Ba), inasmuch as here the Zr concentration would be higher

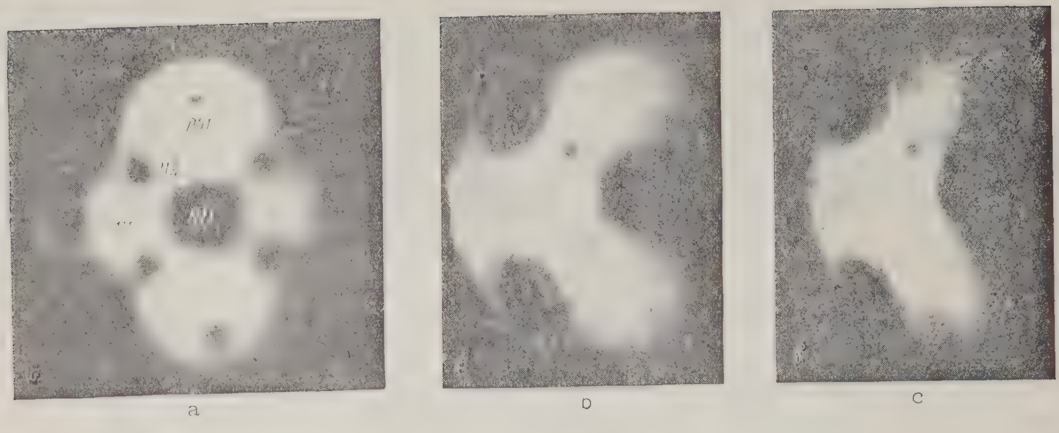

a b c

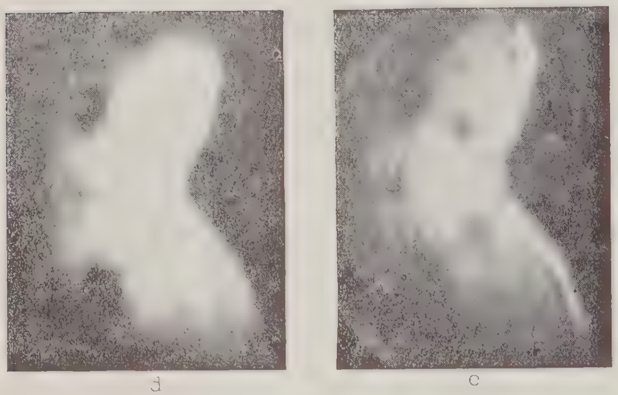

d e

Fig.3. Emission patterns obtained during evaporation of Zr onto a 1.2 μ radius tungsten point: a) clean tungsten, $\varphi = 4.5$ ev, b) 9 min evaporation, $\varphi = 4.0$ ev, c) 35 min evaporation, $\varphi = 3.5$ ev, d) 170 min evaporation; e) after 5 min heating at 530°. The light spot in the center is a crystallite. T = 530°.

and the field weaker. Actually, there is no such band and with all thicknesses of the Zr coating there is observed approximately the same emission over an extensive area of the crystal.

The photographs of Fig.4 show a series of emission patterns obtained with successive evaporation of barium on a tungsten point; in contrast with Zr, Ba yields a definite minimum of the work function at room temperature. This minimum has been observed by two independent groups of investigators[16,17] by the contact potential difference procedure. In these pictures one can clearly see how the strongly emitting band becomes narrower and moves towards the tip of the tungsten point with increasing deposition of barium. The emission contrast between the optimum coatings of Ba and Zr on W with respect to thick Ba and Zr layers should be the same inasmuch as the ratio of the work functions of these layers in both cases is approximately the same (~0.8). Apparently, at room temperature there is not formed a layer of Zr on tungsten with a work function having a lower value than the work function of Zr in the bulk.

A dark band bounding the bright region on the side of the evaporator appears after several minutes heating of a thick layer of Zr on W at ~500° (Figs. 3,e and 5,b). At this temperature slow migration of Zr over the tungsten is observed only on the (011) face (Fig.3,e). It is logical to assume that formation of a layer with a minimum work function in the Zr-W system requires a lower activation energy than that necessary for migration of Zr over the smoothest (110) face of the tungsten crystal.

The evaporation of barium onto tungsten experiment was repeated at a

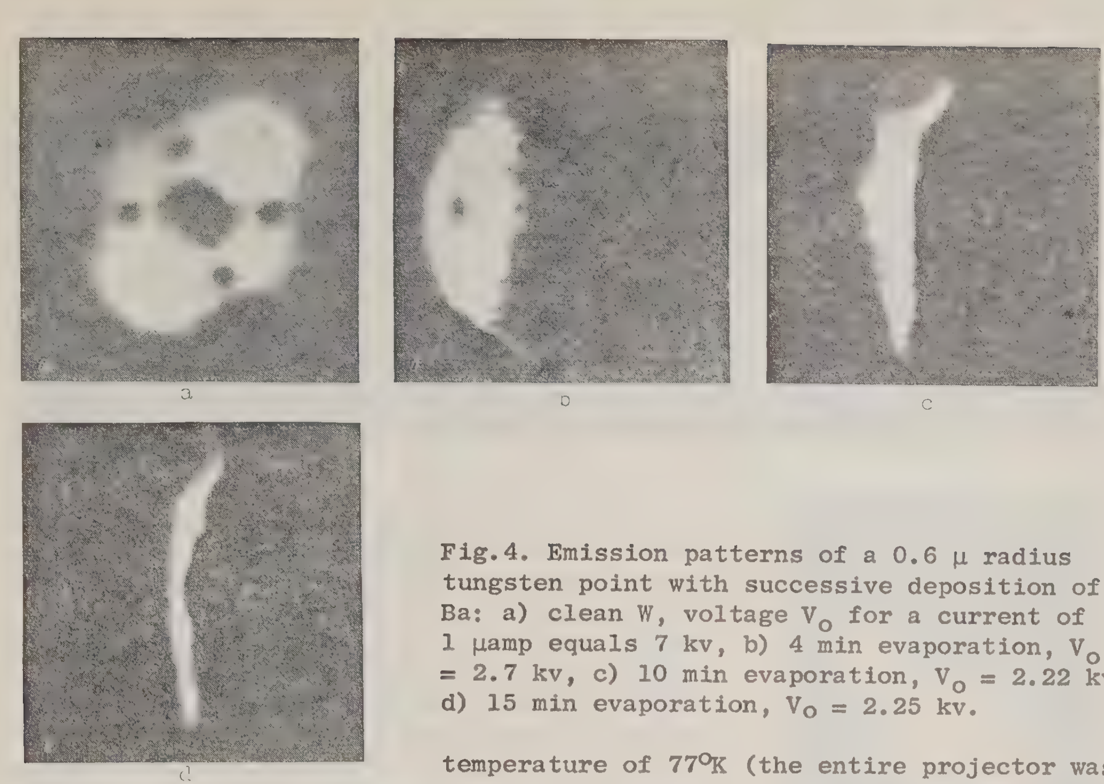

Fig.4. Emission patterns of a 0.6 μ radius tungsten point with successive deposition of Ba: a) clean W, voltage V_o for a current of 1 μamp equals 7 kv, b) 4 min evaporation, $V_o =$ $= 2.7$ kv, c) 10 min evaporation, $V_o = 2.22$ kv, d) 15 min evaporation, $V_o = 2.25$ kv.

temperature of 77°K (the entire projector was immersed in liquid nitrogen); the sharp emission band, similar to that shown in Fig.4,d, formed at this temperature as well.

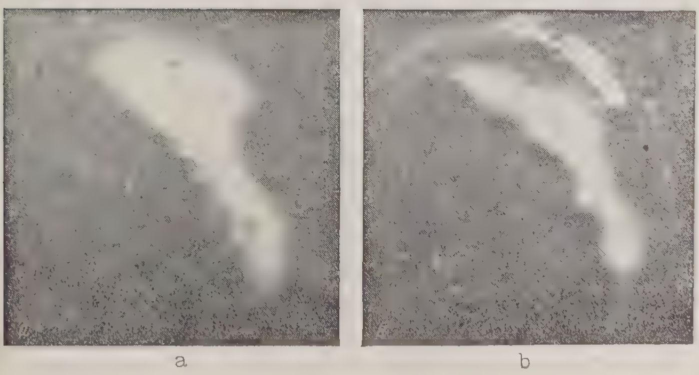

Fig.5. Formation of a dark band on the side of evaporation during heating of a layer of Zr on W: a) layer of Zr on W prior to heating (the thickness of the layer corresponds to the point where the φ vs evaporating time curves level out), b) Zr layer after 2 min heating at 500°. Crystallites are discernible in the region where the amount of Zr is particularly great. T = = 500° (all the other patterns, except 3,d were photographed with the point at room temperature).

B. Adsorption of Zr on a dispersed layer of Zr on W

The work function of a thick unheated layer of Zr condensed on W (i.e., of a Zr layer produced by prolonged evaporation) probably equals the work function of pure Zr. This value as determined from the horizontal section of the curve (Fig.2) is somewhat below "normal" owing to the sensitivity of the field emission procedure to roughness of the layer, leading to local intensification of the field. It is logical to assume that the roughness (we have in mind here unevennesses of atomic dimensions) of a layer evaporated onto a cold substrate is greater

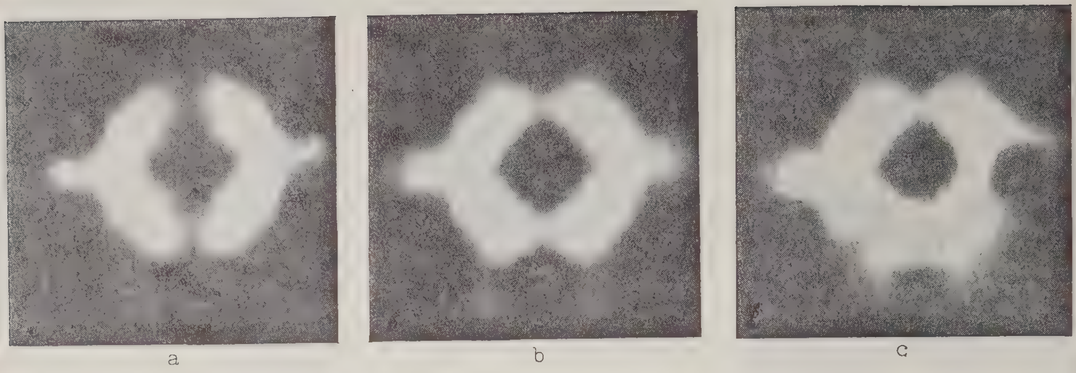

Fig.6. Effect of additional evaporation of Zr onto a dispersed layer of Zr on W (radius of tungsten point - 0.4 μ): a) pattern obtained after evaporation of a thick (more than 10 atomic layers) coating of Zr and subsequent heating at 1300° for 4 hours, φ = 3.1 ev; b) after further 1 hour heating at 1500°, φ = = 3.25 ev, c) after additional evaporation of Zr for 30 minutes onto the layer yielding pattern b, d) "30 minute" layer on clean tungsten.

than that of a dispersed, heated layer. By dispersion of the Zr condensate over the entire surface of the tungsten crystal and some evaporation of the Zr through heating of the point (to a temperature of about 1300° for some hours), one can obtain a Zr surface that is appreciably less rough and at the same time exhibits a lower mean work function (Fig.6,a). With further heating of the point at 1500°, the work function begins to rise, which indicates that there occurs considerable evaporation of the Zr from the point (Fig.6,b). It may be hypothesized that the patterns of Fig.6,a & b correspond either to a layer of Zr on W with a minimum work function or that there have formed macroscopic "ridges" on the (112) faces, i.e., that the shape of the crystal has been modified and that the reduction of φ is only apparent. In order to determine which of these cases actually obtains, we evaporated an additional amount of Zr onto this point at room temperature; the Zr was evaporated for 30 minutes to obtain an added thickness corresponding to that for which curve 1 in Fig.2 straightens out. As may be seen in Fig.6,c the evaporated layer proved to be darker than the substrate. The pattern of Fig.6,d shows the appearance of a "30 minute" layer of Zr on clean tungsten, i.e., the initial pattern for this point. It is noteworthy that the abrupt darkening contour in Fig.6,c is asymmetric and roughly coincides with the boundary of the luminous area in the same region in Fig.6,d. Thus the experiment convincingly shows that a dispersed Zr layer (Fig.6,a & b) is characterized by a lower work function than an unheated condensate, i.e., a lower work function than bulk zirconium. The different darkening of the (111) face areas and the regions surrounding the [100] direction shows that with the same amount of condensed Zr either the decrease of emission differs for different faces or the local field is stronger in the regions surrounding the [100] direction.

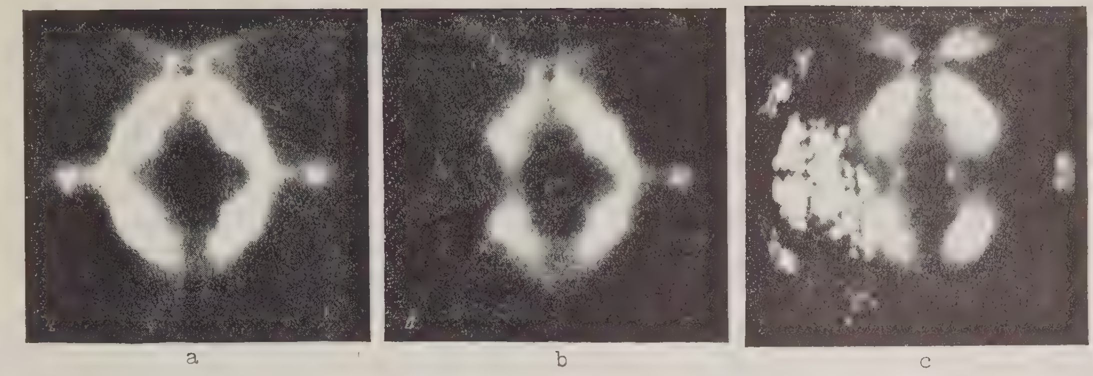

Fig.7. Effect of additional evaporation of Zr onto a dispersed layer of Zr on W (radius of tungsten point - 1.2 μ): a) layer of Zr on W similar to that in Fig.6,a, $\varphi = 3.4$ ev, V = 7.4 kv, I = 4 microamp; b) 10 min evaporation of Zr onto the layer pictured in Fig.7,a, V = = 7.4 kv, I = 2.4 microamp; c) dispersion of the additionally evaporated layer of Zr (total 35 minutes evaporation) for 10 min at 600°.

The experiments were repeated with another thicker ($r = 1.2\mu$) tungsten point. Heating yielded a surface (Fig.7,a) similar to that of the point in Fig.6,a. After 10 min additional evaporation of Zr onto this surface there was obtained the emission pattern shown in Fig.7,b. The pattern obtained with a layer of equal thickness on clean tungsten is shown in Fig.3,b. Thus this experiment substantiates the fact that at least in the vicinity of the (111) face there is obtained a coating with a work function lower than that of pure Zr. On the (112) face sections there are apparently formed "hills" intensifying the local field inasmuch as the emission from these sections was not "quenched" by additional evaporation of Zr onto the point. Upon heating of the layer to 500-600°, the second (111) region also becomes darker presumably due to migration of Zr to the right (in the picture) side of the point (Fig.7,c). On the evaporator side, where the amount of Zr is large (in all, there was condensed a 35 minute layer, i.e., a layer of the same thickness as in Fig.3,c), there form crystallites that sharply intensify the local field. The darkening of the (111) regions in Figs.6,c and 7,b might be explained by the formation of flats; this explanation, however, scarcely holds up in view of the low mobility of Zr atoms on W at room temperature. In general the experiments demonstrate that a Zr layer with a minimum work function in the case of Zr coatings on W is formed only as a result of heating.

Discussion

One can propose two possible explanations for the necessity of an expenditure of a certain activation energy for the formation of a coating with a minimum work function.

1. It is obvious that in the case of adsorption of atoms on a "cold" surface, when surface migration is strongly hindered or impossible, the formation of the second layer begins before the first layer is filled. But even if we assume that the second layer begins to form only after completion of the first layer, we must realize that the first adsorbed layer cannot attain the maximum possible packing without free migration of the adsorbed atoms over the surface if their radius is greater than the minimum distance between

"adsorption spaces" (areas available for adsorption). Langmuir[18] was the first to note this fact and the distinctive features of formation of two surface phases connected therewith.

To clarify the above let us imagine a checker-board grid (the (100) face of tungsten) on which, in view of geometrical considerations, the adsorbed atoms can be located only on every other "space" (square) in each row (in the case of Zr on W this situation will also obtain for other faces, in particular, the (110) face). Obviously, in the case of statistical arrival of atoms on the grid there will form both "black square" phase and "white square" phase islands (Fig.8). At the lines of contact of the islands there will form boundaries with a lower surface density of the adsorbed layer. At higher temperatures, particularly in the presence of individual atoms of the second layer, characterized by a higher mobility than the atoms of the first layer, there will obtain conditions favoring displacement of the boundaries and merging of the islands belonging to the same phase. Then even small successive displacements of individual atoms can lead to appreciable displacements of the interphase boundaries. As a result of this process there can be formed one phase with a degree of covering θ (fraction of monatomic layer) equal to unity. If we assume that the minimal work function corresponds to $\theta = 1$, the described model not only explains the necessity of an activation energy for formation of a layer with a minimal work function but also the fact that this activation energy is lower than the activation energy necessary for migration (surface diffusion) over the "smoothest" face. The difference in activation energies stems from the fact that in the case of migration all the surface atoms move, whereas in the case under consideration we need have only small displacements of individual atoms or movement of atoms in the second layer (in our case, Zr over Zr), which, of course, involves a lower energy. Langmuir[18] showed that with statistical filling of the adsorption "spaces", in the absence of mobility of the adsorbed atoms, the maximum attainable degree of covering is 0.73. With this degree of covering the work function of a layer of Zr on W is approximately equal to the work function of bulk Zr, and if we bear in mind that with further arrival of evaporated Zr there begins filling of the second layer, we see why the emission from an unheated Zr condensate on W remains constant over a wide range of evaporation times. Thus an activation energy (heating) is necessary for formation of a minimum work function layer with $\theta = 1$.

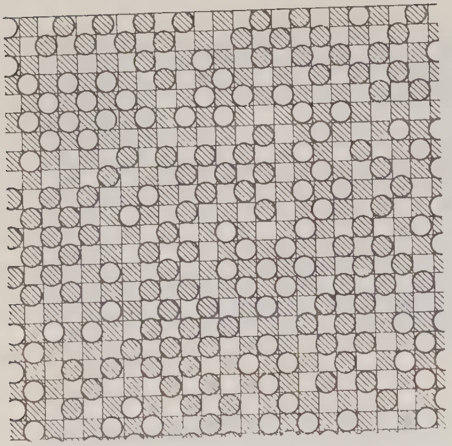

Fig.8. Model of two surface phases after Langmuir.

2. The second possible explanation does not require the assumption that θ must equal unity for the work function to be minimal. According to present-day concepts atoms of electropositive (work function depressing) metals on a tungsten surface must be partially ionized[19,20]. Partial ionization is a purely quantum effect. The degree of ionization will be the greater, the smaller the difference between the work function φ of the substrate and the ionization potential V_i of the adsorbed atoms and the higher the valence of the adsorbed atoms. It may be hypothesized that the zirconium atoms adsorbed on tungsten at room temperature are either not ionized at all or only weakly ionized in view of the large difference between $V_{i_{Zr}}$ and φ_W (2.4 ev). Heating of the layer leads to excitation of the surface Zr atoms (which is equivalent to reduction of the ionization potential) and to increase of the degree of partial

ionization. The state of partial ionization of Zr on W is, apparently, energetically more advantageous than the preceding nonionized state inasmuch as the process of decrease of the work function is irreversible.

It should be noted that in adsorption on a metal characterized by a continuous electron energy spectrum both the ground and excited levels of the adsorbed atoms are "smeared out" into a band with a multitude of levels and different probabilities of the electrons remaining at these levels. An excited adsorbed atom has a large number of possible states, corresponding to unoccupied levels in the metal, which leads to deeper partial ionization of the adsorbed atoms and, consequently, to reduction of the work function.

The fact that the effects observed for Zr on tungsten are absent in the case of Ba on tungsten may be explained by the great difference between the properties of zirconium and barium atoms. In view of the greater polarizability of Ba atoms their lower ionization potential and their greater mobility on W (as compared with Zr atoms) and the pronounced difference between the structure of the outer electron shells of Zr and Ba, it is obviously futile to look for extensive analogies in the behavior of Zr and Ba on tungsten. Apparently, effects similar to those observed for Zr on W may be expected in systems such as Th-W, U-W, etc.

In conclusion the writer desires to thank A.P.Komar for discussion of the results and interest in the work and Iu.N.Talanin for a number of critical observations.

Leningrad Physical-Technical Institute,
Academy of Sciences of the USSR

References

1. E.W.Müller, Ergebn.Exakt.Naturwiss., 27, 290 (1953).
2. M.Benjamin & R.O.Jenkins, Proc.Roy.Soc.A, 180, 225 (1942).
3. I.L.Sokol'skaia, Izv.AN SSSR, Ser.fiz., 15, 472 (1951).
4. J.A.Becker, Bell System Techn.J., 30, 907 (1951).
5. M.Drechsler, Z.Electrochem., 58, 340 (1954).
6. N.A.Gorbatyi & G.N.Shippe, Zhur.tekh.fiz., 25, 1364 (1955).
7. S.Dushman, D.Dennison & W.B.Reynolds, Phys.Rev., 29, 903 (1927).
8. H.B.Michaelson, J.Appl.Phys., 21, 536 (1950).
9. S.T.Martin, Phys.Rev., 56, 947 (1939).
10. R.H.Haefer, Z.Phys., 116, 604 (1940).
11. A.Sommerfeld & H.Bethe, Handb.d.Phys., Bd. 24 - Berlin, 1933.
12. R.E.Burgers, H.Kroemer & J.M.Houston, Phys.Rev., 90, 515 (1953).
13. L.N.Dobretsov, Elektronnaia i ionnaia emissiia (Electron and ion emission), M., 1952.
14. F.Ashworth, Advances in Electronics, 3,I.-1951.
15. A.P.Komar & V.N.Shrednik, Fiz.metallov i metallovedenie, (Physics of metals and metallurgy), 5, No.3 (1957).
16. P.I.Lukirskii, S.A.Vekshinskii, A.N.Sozina & T.V.Tsareva, Zhur.eksp. i teor.fiz., 1, 71 (1931).
17. V.M.Gavriliuk, Trudy (Proceedings) Physical Institute, Ukrainian SSR Acad.of Sci., 5, 87 (1954).
18. I.Langmuir, Uspekhi khim., 10, 570 (1941); J.Chem.Soc., 511 (1940).
19. R.Gurney, Phys.Rev., 47, 479 (1935).
20. V.L.Bonch-Bruevich, Usp.fiz.nauk., 40, 369 (1950).

ON THE POSSIBILITY OF UTILIZING BOMBARDMENT-INDUCED CONDUCTANCE FOR SIGNAL AMPLIFICATION

- A.M.Bonch-Bruevich, E.S.Grishin & U.B.Soltamov

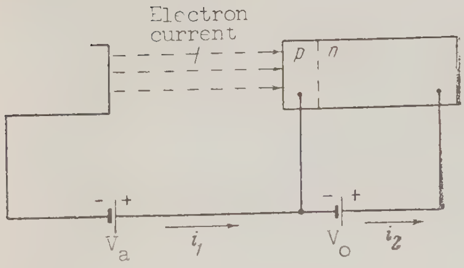

Fig.1. Cathodoamplification in a p-n junction.

When a semiconductor with a p-n junction under reverse voltage near the surface is bombarded with electrons (Fig.1) there is observed an effect that (by anology with cathodoluminescence) may be termed cathodoamplification; specifically, there is induced in the p-n junction circuit a minority carrier current i_2 related to the primary electron current i_1 by a factor α. Under certain conditions $\alpha > 1$.

It has been shown[1] that

1) the current induced in the p-n junction circuit with a reverse voltage V_o exceeding a few tenths of a volt is independent of the reverse voltage;

2) the induced current i_2 varies linearly with i_1 at constant primary electron energy eV_a, i.e., the ratio $\alpha = i_2/i_1$ with eV_a = const. is constant and independent of the electron beam density; this ratio may be called the cathodoamplification factor of the p-n junction;

3) the factor α depends on the specific properties of the semiconductor and the primary electron energy eV_a.

The factor α attains a value of the order of 100 for Ge even at comparatively low values of eV_a (300-400 ev).

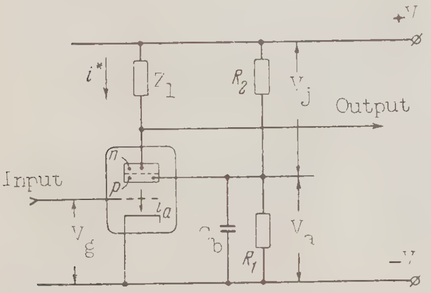

Fig.2. Schematic of amplifier circuit based on an electron-semiconductor tube. C_b - blocking capacitor.

Cathodoamplification in p-n junctions can be used for detecting electron fluxes. In particular, this effect may be employed for increasing the transconductance of vacuum tubes.

In this application the metal plate of the tube should be replaced by a semiconductor one with a p-n junction under reverse voltage close to the surface facing the cathode.

Fig.2 presents the schematic diagram of an amplifier circuit based on such a combined electron-semiconductor tube. The anode voltage V_a and the voltage V_j for supplying the p-n junction are taken from a divider R_1 & R_2. The load impedance Z_1 is connected in the p-n junction circuit, while the magnitude of the anode current i_a is controlled by the grid voltage V_g, as in an ordinary tube. Due to cathodoamplification of the plate current in the p-n junction, the transconductance g_m^* exceeds the transconductance g_m in an ordinary vacuum tube with the same electrode geometry by a factor of α, i.e., $g_m^* = \alpha g_m$.

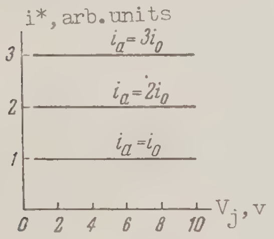

Fig.3. Variation of load current with voltage on the p-n junction in the amplifier circuit.

The general variation of the load current i^* as a function of voltage V_j applied across the p-n junction is shown in Fig.3; the basic parameter here is the magnitude of plate current i_a.

Development of electron-semiconductor tubes will, of course, involve extensive further research on stability, proper temperature conditions, etc.

Reference

1. U.B.Soltamov & E.S.Grushin, Zhur.tekh.fiz., 28, No.7 (1958).

DISCUSSION

M.I.Elinson: What was the magnitude of the beam current?

U.B.Soltamov: The beam current varied between 10^{-8} and 10^{-6} amp.

M.I.Elinson: Over what range of beam current was the relationship between the current induced in the p-n junction circuit and the primary-electron current linear?

U.B.Soltamov: The relationship was linear over the entire beam current range investigated.

M.I.Elinson: At what value of V_o across the junction did saturation of the p-n junction current set in?

U.B.Soltamov: At a few tenths of a volt.

N.L.Iasnopol'skii: What is the maximum permissible temperature for normal operation of the p-n junction?

U.B.Soltamov: This question was not studied.

M.B.Sinel'nikov: What was the minimum current detected by the junction?

U.B.Soltamov: In our experiments the beam current was 10^{-8} to 10^{-6} amp. Obviously, for excessively small currents, the effect will be masked by the junction noise.

OPTICAL PROPERTIES OF ALKALINE EARTH CARBONATE LAYERS

- I.S.Gorban'

In vacuum tube engineering one frequently has to deal with thin layers of different materials which, optically speaking, are turbid media, i.e., a suspension of individual fine particles. Specifically we have in mind here photosensitive layers and oxide paste coatings whose optical and emissive properties are structure dependent. The present work was concerned with the influence of structure on the optical properties of carbonate paste layers.

Recently there appeared a report[1] on attempts to utilize the change in intensity of a light beam passing through an oxide coating for the purpose of measuring its thickness. These experiments are primarily of interest in connection with mass production of oxide-coated cathodes, where the procedure offers the possibility of controlling the layer thickness in the process of application and hence a means of standardization and quality control. It therefore appeared expedient to carry out a detailed investigation of scattering of light passing through carbonate layers of finite thickness, i.e., carbonate layers of the type utilized in fabricating oxide-coated cathodes. Attention was concentrated on evaluating the possibilities of measuring the thickness and density of coatings. The results obtained should be generally applicable to scattering layers of finite thickness.

1. Measurement procedure

The experimental samples were prepared on glass plates measuring from 10 x 10 to 30 x 30 mm onto which uniform paste layers of different thickness and consistency were applied by spraying. The coating thickness was controlled by the spraying time, while the structure was varied by the degree of atomization. The thickness and roughness (the latter characterizes the layer density) were measured by the conventional procedure by means of an MIS-11 microscope. We investigated samples with thicknesses ranging from 10 to 220 μ and roughness values from 4 to 20 μ. Triple, double and fine-grain double carbonate pastes were used. The coating density was determined by weighing.

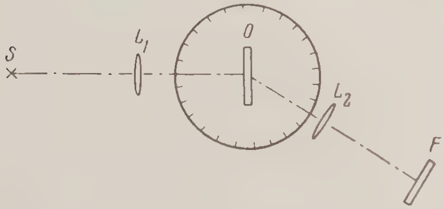

Fig.1. Diagram of measurement set-up.

The light scattering was measured by means of the simple set-up diagrammed in Fig.1. Light from the source S, located at the focus of the lens L_1 was directed onto the sample 0 and then by means of lens L_2 thrown on the FESS photocell F. The entire system L_2F could be rotated relative to the sample, the angle of rotation being read off the goniometer scale. In working with polarized light the system L_2F was replaced by a Cornu polarimeter for measuring the degree of polarization and a polarizer was introduced between lens L_1 and the sample. The set-up was purposely kept simple with a view to facilitating industrial utilization of the procedure provided the experiments yielded positive results. For industrial purposes a "control" glass plate could be placed in each frame or group of frames of cathodes to be coated and sprayed at the same time and in the same way as the cathodes.

2. Attenuation of the light beam passing through a carbonate layer

The weakening of an intense light beam passing through the sample is governed by the law for light scattering in turbid media. For measuring the scattering coefficient one must mount the source, sample and light detector in a straight line. Initially the sample should be replaced by a clear glass plate; the reading of the galvanometer coupled to the photocell will then indicate the intensity of the incident beam (only slightly attenuated by reflection from the plate). The reading of the galvanometer with the sample again in place will characterize the intensity of the beam weakened by the paste layer. The ratio of the two readings, provided they are in the linear range of the photocell, gives the attenuation factor.

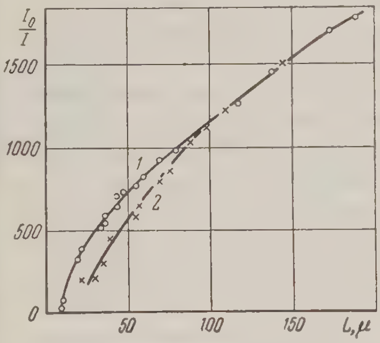

Fig.2. Variation of light weakening with layer thickness for different degrees of roughness: 1) d ≈ 5 μ and 2) d ≈ 12 μ.

Fig.2 shows a system of two curves characterizing the variation of the attenuation coefficient (I_0/I) as a function of the layer thickness L. Curve 1 pertains to samples with a roughness d ≈ 5 μ; curve 2 to samples with a roughness d ≈ 12 μ. The density of the first series of coatings is therefore somewhat greater than that of the second. It will be noted that the curves have two somewhat different sections: in the range of small thicknesses, the degree of attenuation at first increases rapidly with increasing coating thickness; then the rate of increase is slowed. Our investigations showed that the transition from one section to the other (i.e., the change in slope) for layers of different chemical composition but prepared under the same conditions lies within approximately the same thickness range. It may therefore be inferred, in view of the physical similarity of the properties of different carbonates, that with the same geometric structure of the coating the scattering ability and hence the thickness vs attenuation curve will be only weakly dependent on the composition of the paste.

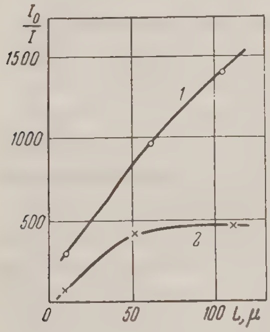

Fig.3. Variation of attenuation as a function of the layer thickness for two different densities: 1) $\gamma \approx 1.3$ g/cm^3 and 2) $\gamma \approx 0.75$ g/cm^3.

Another feature of the experimental results is that the character of the thickness vs attenuation curves depends on the structure of the layers (density or roughness). When the conditions of application are more or less the same, significant differences in the degree of attenuation for samples of different roughness are observed only in the region of small thicknesses. In the region of great thicknesses the curves virtually coincide. The difference between the shape of the curves was particularly great for samples prepared under very different spraying conditions. This can be seen in Fig.3 where curve 1 pertains to samples with a coating density $\gamma \approx 1.3$ g/cm^3, while curve 2 is for samples with $\gamma \approx 0.75$ g/cm^3.

At low scattering-particle concentrations the variation of scattering intensity with layer thickness is exponential. This regularity is familiar from and is extensively used in atmospheric optics. An attempt to represent our experimental data by an exponential curve showed, however, that this law does not apply to our case

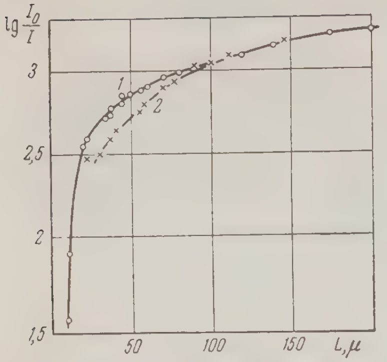

Fig. 4. Attenuation curves plotted in semilogarithmic coordinates.

(Fig. 4). The deviation is particularly great in the region of small thicknesses. The inapplicability of this law to carbonate layers of finite thickness, wherein the concentration of scattering heterogeneities is very great, can be explained as follows. The intensity of light passing through the scattering layer may be represented by the sum

$$I = I_0 + I_1 + I_2 + I_3 + \dots,$$

where I_0 is the intensity of the direct beam not undergoing multiple reflection from the layer heterogeneities, I_1 is the intensity pertaining to first order scattering, I_2 to second order scattering and so on. Shuleikin[2], Ambartsumian[3] and Girinym & Stepanov[4] have published detailed theoretical analyses of the intensities involved in the above formula; these analyses indicate the inapplicability of the exponential law to the present case. It is found that in the region of very small thicknesses, where I_0 is large compared to the other terms, the exponential law does characterize the variation in intensity. In the region of great thicknesses, where I_0 is small compared with the other terms, the exponential law can again be used. However, the constants entering into the analytic expressions in the former and latter cases are substantially different. Between the two thickness regions there is a transition region wherein the exponential law is invalid.

Experiments carried out by Timofeeva[5] have qualitatively substantiated these theoretical deductions. Thus our results indicate that most of our samples belong in the intermediate region where the magnitude of I_0 is comparable to that of the other terms in the sum. Apparently, our smaller thickness samples fall into the theoretically predicted transition region, while the thicker samples belong in the second exponential range.

What has been said above pertains primarily to the case of uniform distribution in depth of the density of the turbid layer. It is known, however, that the density of layers obtained by spraying is not uniform in depth. Obviously, this must lead to even greater deviations from the exponential law. According to the experimental results, the position of the break in the thickness vs attenuation curve depends, other conditions being equal, on the density of the oxide coating. This, in view of the resultant ambiguities involved, greatly hampers development of a procedure for determining the thickness of samples from the transmission. The procedure can, therefore, be used only where an invariable spraying technique and, consequently, a constant coating density are assured. With present-day technology one can standardize the spraying operation fairly well. In this case analysis of the measurement errors shows that the thickness can be measured with an accuracy of several percent. It must be emphasized, however, that the procedure is not "universal" in the sense that a set of calibration curves can be used for determining the thickness of any and all carbonate layers; on the contrary, a given set of curves can be used only in conjunction with layers sprayed on under identical conditions.

3. Spatial distribution of light scattered by carbonate layers

Analysis of the above curves shows that with increase in coating density the character of the attenuation is increasingly affected by higher order scattering. Obviously, with increasing contribution from higher order scattering the probability of deviation of the light rays from the direction of the incident beam will increase. It follows, therefore, that the angular distribution of the scattered light (i.e., the shape of the scattering indicatrix) must depend strongly on the coating density. Hence the next stage of our research was devoted to investigating the shape of the scattering indicatrices.

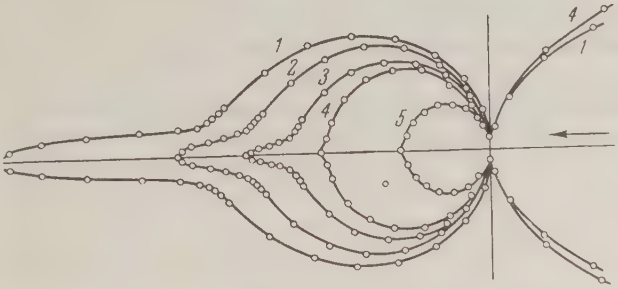

Fig.5. Scattering indicatrices for triple carbonate coatings: 1) L = 28 μ, d = 15 μ, 2) L = = 32 μ, d = 17 μ, 3) L = 40 μ, d = 16 μ, 4) L = = 45 μ, d = 18 μ, 5) L = 100 μ, d = 16 μ.

Fig.5 shows a family of scattering indicatrices for samples with about the same density but characterized by different thicknesses. Noteworthy is the fact that the scattering indicatrices do not have the usual monotonic, more or less oval shape but are distinguished by the presence of a "tail" extending in the direction of the incident beam and decreasing in length with increasing thickness of the layer. This extension or tail is obviously due to the direct beam and lower order scattering, while the intensity of the light scattered through larger angles is due to higher order scattering.

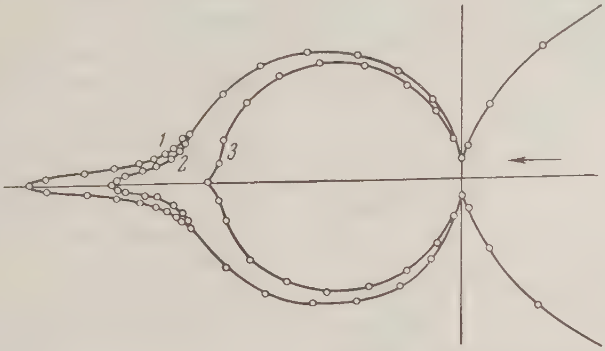

Fig.6. Scattering indicatrices for triple carbonate coatings: 1) L = 40 μ, d = 20 μ, 2) L = = 40 μ, d = 16 μ, 3) L = 43 μ, d = 5 μ.

In the region of small thicknesses the relative contribution from lower order is greater than from the higher order scattering, while in the range of large thicknesses the contribution from higher order scattering predominates. The shape of the indicatrices also depends on the structure of the carbonate layer. By way of illustration in Fig.6 we show a set of curves obtained for layers of the same thickness but different densities as characterized by the degree of roughness. With increasing layer density the contribution from lower orders decreases, that from higher orders of scattering increases. Comparison of these results with the transmission curves given above shows that the thickness interval in which the "tail" disappears approximately coincides with the thickness interval identified by the break in the transmission curves.

4. Discussion

The correlation between the shape of the scattering indicatrices and the thickness and density of the coating can be used for simultaneous determination of these two quantities provided the carbonate grain size distribution in the paste is approximately constant. For such determinations one need measure only two intensities: the intensity of the light transmitted directly forward (the ratio I_0/I_{0°) and the relative intensity at some angle, for example, at 10° (the ratio I_0/I_{10°).

As will be obvious from the above, the ratios I_0/I_{0° and I_{0°/I_{10° will be different functions of the same quantities, namely, the thickness L and the layer density γ, i.e.,

$$\frac{I_0}{I_{0^\circ}} = f(L,\gamma), \text{ and } \frac{I_{0^\circ}}{I_{10^\circ}} = \varphi(L,\gamma).$$

Inasmuch as the analytic expressions for $f(L,\gamma)$ and $\varphi(L,\gamma)$ are unknown, it is necessary to solve these equations graphically. To this end we must first obtain two sets of calibration curves such as those shown in Fig.7.

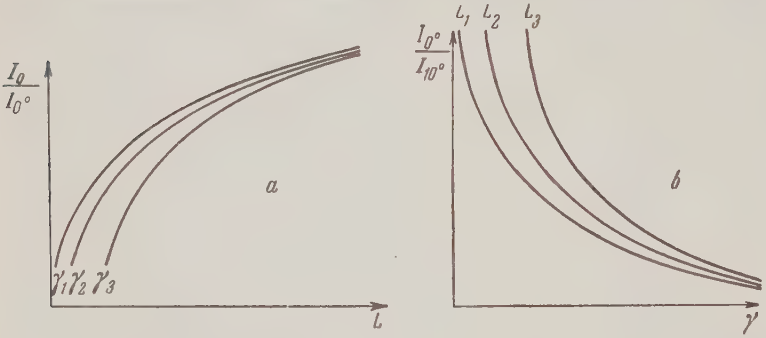

Fig.7. Sets of calibration curves giving the dependence of a) the attenuation as a function of the thickness for different density values, and b) the ratio of scattering intensities forward and at a given angle as a function of the density for different thicknesses.

Each curve in Fig.7,a characterizes the variation of the attenuation of the light beam as a function of the coating thickness for a given layer density. Each curve in Fig.7,b characterizes variation of I_{0°/I_{10° as a function of the density for a given value of L. Let us now assume that for some given sample we have determined

$$\frac{I_0}{I_{0^\circ}} = f \text{ and } \frac{I_{0^\circ}}{I_{10^\circ}} = \varphi.$$

From the a curves we can now obtain a set of values of γ and L that correspond to a common value of I_0/I_{0°. Similarly from the b curves we can obtain another set of values of γ and L, each pair of which yields the same value of I_{0°/I_{10°. If we now plot both sets of γ-L pairs in γ,L coordinates (Fig.8), the point of intersection of the two curves will give us the values of γ and L for the investigated sample.

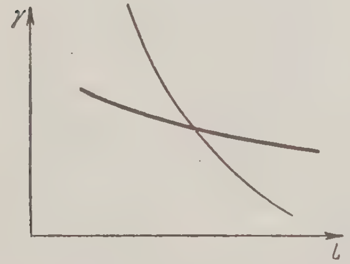

Fig.8. Plot for simultaneous determination of γ and L.

Conclusions

1. It has been shown that the character of light scattering by carbonate layers depends on the density and thickness of the coating.

2. We propose an optical method for simultaneous measurements of the thickness and density of oxide layers of the type employed in preparing oxide-coated cathodes. The procedure can be advantageously used under plant conditions if the gaging operation can be reduced to measurement of the two intensities I_0o and $I_{10}o$, which can readily be done if the density γ and thickness L values can be correlated with certain standard conditions.

3. The results obtained apparently characterize certain general regularities common to turbid media distributed in layers of finite thickness.

In conclusion I desire to express my gratitude to Prof. N.G.Morgulis, corresponding member of the Ukrainian SSR Academy of Sciences, and Assoc. Prof. N.D.Nakhodkin for their attention and for discussion of the results and to A.F.Sribina, graduate student at Kiev State University, who contributed to the present work through her participation in the measurements.

"T.G.Shevchenko" Kiev State University

References

1. Y.Nakamura & S.Odada & Y.Kato, Vide, 51, 1 (1954).
2. V.V.Shuleikin, Fizika moria (Physics of the Sea), 1953.
3. V.A.Ambartsumian, Izv.AN SSSR, Ser.geogr., No.3, (1942).
4. O.P.Girin & B.I.Stepanov, Zhur.eksp.i teor.fiz., 27, No.4 (1954).
5. V.A.Timofeeva, Doklady AN SSSR, 76, 5 & 6 (1951).

COMPACTED POWDER CATHODES OF BARIUM-CALCIUM ALUMINATES AND TUNGSTATES

- A.I.Mel'nikov, A.V.Morozov, B.N.Popov & A.A.Maklakov

Introduction

In view of the need for heavy emission currents (particularly, in superhigh frequency tubes), we now have an imperative need to develop new types of cathodes inasmuch as ordinary oxide-coated cathodes cannot satisfy the high emission current density requirements set by new equipment.

Porous metal cathodes (L-cathodes) allow of drawing a heavy density current and have a number of other positive features, but at the same time they have a number of shortcomings connected primarily with difficulties of fabrication: specifically they require airtight sealing of the cell with the activating agent and prolonged outgassing and activation owing to the appreciable evolution of gas forming as a result of decomposition of barium carbonates.

An obvious means of circumventing this difficulty was to combine the cathode cell in which the activating substance is formed with the metallic sponge by introducing the barium compound into the sponge pores. According to the method of introduction of the active substance into the sponge, we distinguish between impregnated cathodes, first suggested by Levi[1], and compacted or compressed cathodes, proposed by Huber & Freytag[2].

Fig.1 shows one possible compressed cathode design; this consists of a molybdenum cylinder into which the mixture consisting of the activate material, tungsten powder and a reducing agent is compressed. Reaction of the components at the operating temperature of the cathode leads to the formation of free barium and activation of the cathode.

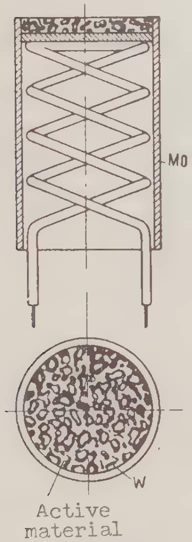

Fig.1. Compressed powder cathode.

Coppola & Hughes[3,4] tried to use barium oxide as the active material. In view of the fact, however, that the rate of reaction of barium oxide with tungsten is high at the operating temperature of the cathode, there occurs intensive evaporation of the barium and as a result the cathode is short-lived. In addition, barium oxide is very unstable in air due to the fact that it absorbs water vapor and carbon dioxide.

The use of barium oxide as the active material also proved inexpedient because in the process of decomposition it liberates carbon dioxide which oxidizes the reducing agent.

Hence there was an obvious need for finding other more suitable barium compounds. There is no detailed information in the literature on the technology of preparation of active materials or on the technology of fabrication of compressed and impregnated cathodes. Consequently, the purpose of our work was to develop the technology of fabrication of compressed cathodes.

We investigated compounds of barium obtained through the reaction of barium and calcium oxide with acids and amphoteric oxides; in addition to preparation of barium aluminates and cathodes thereof, we synthesized barium-calcium tungstate (a material not hitherto described in the literature) and used it to prepare compressed cathodes which had already been partially tested.

Technology of preparation of the active materials

Active materials intended for emitters must meet the following requirements: they must liberate free barium in interacting with a reducing agent, be sufficiently stable in air and must not evolve excessive amounts of gas during formation of the cathode in the tube.

The first stage of our research consisted of preparing the active materials, namely, barium-calcium aluminates and tungstates.

The initial components taken in preparing the aluminates were 5 moles barium carbonate, 3 moles calcium carbonate and 2 moles aluminum oxide. The chemically pure components were thoroughly ground and mixed in special barrels, precluding the entry of any extraneous materials in the process. Most suitable for this purpose proved to be tumbling barrels lined on the inside with sheet molybdenum and molybdenum balls. The mixing and grinding were carried on for 8 hours. The size of the resultant particles did not exceed 5 μ. Then the mixture was compressed into pellets at a pressure of 1 ton/cm^2 and sintered in an atmosphere of nitrogen, hydrogen or in air for 2 hours at 1400°.

The reactions of formation of barium aluminate and barium-calcium aluminate are

$$3BaCO_3 + Al_2O_3 = Ba_3Al_2O_6 + 3CO_2, \tag{1}$$

$$2BaCO_3 + CaCO_3 + Al_2O_3 = Ba_2CaAl_2O_6 + 3CO_2. \tag{2}$$

In subsequent work we used aluminum hydroxide instead of aluminum oxide. Better results were obtained with the hydroxide probably because in heating it transforms into aluminum oxide with a highly developed surface which enhances its reactivity.

As noted above, we also developed a method of preparing barium-calcium-tungstate. The initial mixture in this case consisted of 2.5 moles barium carbonate, 0.5 moles calcium carbonate and 1 mole tungsten trioxide. The technology of preparation was substantially similar to that described above for the aluminate.

The formation reaction is

$$2BaCO_3 + CaCO_3 + WO_3 = Ba_2CaWO_6 + 3CO_2. \tag{3}$$

The rate of formation of the active materials depends primarily on the reaction temperature. At different stages of the process this rate may be limited by different factors. In the initial period, for example, it may be limited by the rate of the chemical reaction itself; at later stages, as the final product begins to form (in interlayers), the limiting factor may be the rate of diffusion of the initial components through the layers of the product.

In the synthesis of barium-calcium tungstate, owing to the considerable vapor pressure of tungsten trioxide and barium oxide, the interaction of the components in the initial stage probably occurs in the vapor phase and depends on the rate of volatilization of the tungsten and barium oxides. In this case the reaction rate, according to Ginstling[5], is a function of the particle radius r:

$$\frac{dG}{d\tau} = f(r)$$

where G is the amount of volatilized material and τ is the time.

In later stages the rate of the process must be limited by the rate of diffusion of the initial components through the tungstate layers forming on the particle boundaries.

Consequently, important factors in the preparation of active materials are the particle size, uniform particle distribution and adequate compacting of the particles to insure the necessary contact between them. The last is particularly important when the interaction between components depends on diffusion.

At present we are perfecting a new method of synthesizing tungstates and aluminates; this is based on joint precipitation of compounds that after sintering form the desired tungstate or aluminate. This procedure allows of obtaining a highly homogeneous mixture of the components, which is very important in preparing active materials.

The quality of the synthesized active materials was checked by testing them in cathodes, determining their stability in air and x-ray diffraction studies.

Inadequate stability of active materials in air makes it difficult to use them in preparing cathodes. The degree of stability can also serve as a qualitative characteristic of the degree to which the synthesis reaction goes to completion.

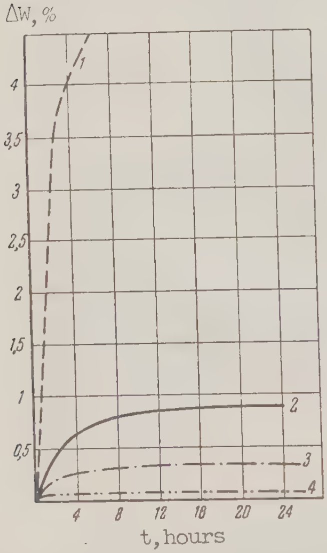

Fig.2. Variation in weight of active materials when exposed to air: 1) barium oxide, 2) barium-calcium aluminate, 3) barium-calcium tungstate, 4) monotungstate.

Water vapor and carbon dioxide absorbed from the air may later be liberated during the forming of the cathode and thereupon oxidize the surface of the reducer grains and hinder activation. The curves in Fig.2 show the variation in weight of the various components with the time of exposure to air and thus characterize the stability of the materials.

X-ray diffraction studies carried out under the supervision of E.P.Ostapchenko showed that our synthesis procedure is characterized by good reproducibility of the final products.

According to approximate measurements, the melting point of the barium-calcium aluminate is 1650°; that of barium-calcium tungstate is 1900°.

Preparation of cathodes

The mixtures used for preparing compressed cathodes consisted of the active material, powdered metal and a reducing agent. By way of reducing agents we tested silicon, titanium, aluminum, tungsten carbide and carbon. The content of these substances in the mixture was varied from 0.1 to 10%.

The mixture used for preparing barium-calcium tungstate cathodes had the following proportions by weight: 9.5% tungstate, 90% powdered tungsten and 0.5% reducing agent. The best results, evaluated as described above, were obtained when aluminum was used as the reducing agent.

No reducing agent was used in preparing aluminate cathodes; in this case the tungsten served as reducer.

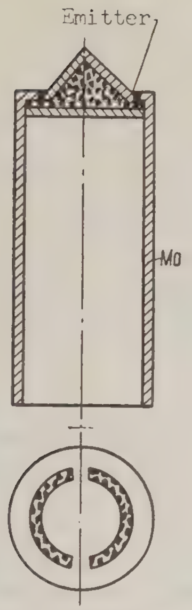

Fig.3. Compressed cathode with ring shaped emitting surface.

The powder particle size did not exceed 5 μ.

The mixture in each case was thoroughly ground and mixed for 8 hours in a molybdenum lined barrel with molybdenum balls and then was pressed into a molybdenum cylinder 2 to 6 mm in diameter at a pressure of 15-20 ton/cm^2.

The compressed mixture cathodes were baked in an atmosphere of hydrogen for 3-5 min at 1750° in the case of the aluminates and at 1900° in the case of the tungstates.

In addition to the usual wafer cathodes, we prepared cathodes with a more complicated emitting surface. To this end a cut-out of appropriate shape was made in the bottom of the molbydenum cup receiving the compressed mixture. In a variant procedure, a cathode plate of the desired shape was cut by electric discharge machining from an annealed cathode wafer; this was then platinum soldered to the molybdenum base. One such cathode with a ring shaped emitting surface is shown in Fig.3.

In the process of sintering, the active material fuses and then in hardening binds the tungsten particles. Inasmuch as the mixtures were compacted at high pressures, shrinkage was negligible and the resultant cathodes firmly adhered to the molybdenum cylinder walls.

During sintering there occurs intense reaction of the active material with the reducing agent. Part of the free barium released in the process is evaporated, part remains in the cathode.

For aluminate cathodes there occurs, first, the dissociation reaction

$$Ba_3Al_2O_6 \rightarrow 2BaO + BaAl_2O_4 \qquad (4)$$

and, second the following reaction between the tungsten and the formed barium oxide:

$$6BaO + W = 3Ba + Ba_3WO_6. \qquad (5)$$

The last reaction favors further dissociation of the aluminate into barium oxide and the monoaluminate.

In the case of tungstate cathodes, the free barium is formed by the reaction[2]

$$2Ba_3WO_6 + 6Al = 3Ba + 3BaAl_2O_4 + 2W. \qquad (6)$$

Actually, however, there occurs a more complex interaction between the reagents inasmuch as aluminum forms intermetallic compounds with tungsten. In addition, it may interact with barium forming Al_4Ba, Al_5Ba, etc.[6]

In the case of barium-calcium tungstate, in its reaction with aluminum there forms free calcium which may also yield compounds with aluminum (Al_2Ca, Al_3Ca, etc.). In the presence of free calcium oxide or barium oxide these compounds will react with them with the formation of the free metal[6], for example,

$$6CaO + Al_2Ca \rightarrow 4\,Ca + Ca_3Al_2O_6. \qquad (7)$$

Similarly to the decomposition of barium aluminate according to Eq.(4), there may occur dissociation of the tungstate (primarily during sintering of the cathodes at 1900°):

$$Ba_3WO_6 \rightleftarrows 2BaO + BaWO_4. \qquad (8)$$

In this case the barium oxide can react with the reducing agent[6]:

$$6BaO + 2Al \rightleftarrows 3Ba + Ba_3Al_2O_6. \qquad (9)$$

The formation of intermetallic compounds and solid solutions of aluminum and tungsten should be regarded as a favorable factor where operation of the cathode is concerned. At a high sintering temperature and in subsequent operation of the cathode, free aluminum may wholly or partially evaporate. As is known, formation of intermetallic compounds leads to negative deviation from Raoult's law (appearance of a minimum in the vapor pressure vs component concentration curve), i.e., the vapor pressure and rate of evaporation in this case are appreciably reduced.

Small amounts of water vapor and carbon dioxide, present in the tungstate, could partially or wholly oxidize the aluminum thus minimizing its usefulness as the reducing agent. The oxidation of aluminum is inhibited when it is present in the form of an intermetallic compound.

As a result of reaction between the compressed particles there are formed, as will be evident from the above formulas, new substances (monoaluminates and monotungstates); hence in the process of operation of the cathode there occurs a slow alteration in the composition of the emitter.

The degree of compacting of the initial mixture is very important where the emission characteristics and the service life of the cathode are concerned. A high compacting pressure, small particle size, uniform distribution of the particles and homogeneous sintering are essential for increasing the area of contact between the active material and the reducing agent. These factors determine the course of the solid phase reaction accompanied by the liberation of barium. On the other hand, migration of barium over the surface of the contacting particles of tungsten and the active material in the compressed mass and the rate of evaporation of barium, which determines the life of the cathode, also depend on the porosity of the compressed mass (although diffusion, probably, is of secondary importance inasmuch as the active material is distributed throughout the entire volume of the cathode).

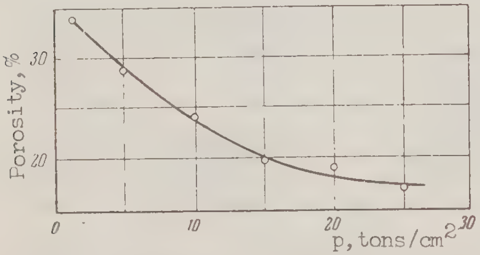

Fig.4. Variation of the porosity of the compressed mass as a function of the compacting pressure.

Fig.4 shows the variation of the porosity of compressed tungstate mixtures as a function of the compacting pressure. Fig.5 shows the variation of the emission characteristics of the resultant cathodes as a function of the compacting pressure. As may be seen from the curves, increasing the compacting pressure above 25 tons/cm² leads to only minor increase of the density and has little effect on the emission properties of the resultant cathodes. Lower compacting pressures lead to a reduction of the emission current and shortening of the service life of the cathode. Control of the density of the compacted mass by varying the sintering time is inexpedient in view of the high rate of the reaction (leading to loss of barium) at high temperatures.

We also carried out experiments in which layers of various substances - tungsten, tungsten carbide, tantalum and carbon - were pressed onto the surface of the compacted cathodes with a view to forming the emitting surface. In the case of pressing on of tungsten, the emission current did not differ

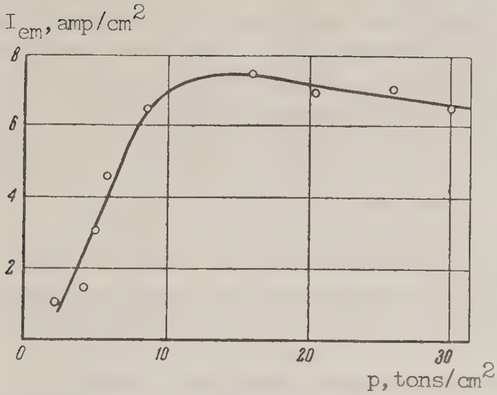

Fig.5. Variation of the emission current density as a function of the compacting pressure.

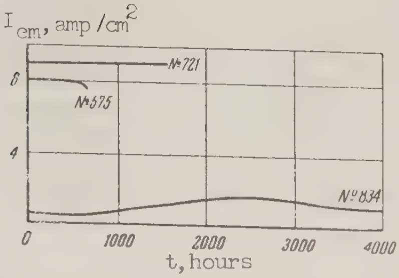

Fig.6. Life (current vs time) curve for barium-calcium and barium tungstate cathodes: Nos.721 & 834 - tungstate cathodes prepared with calcium oxide; No.575 - tungstate cathodes prepared without barium oxide.

from that from ordinary cathodes; the other tested substances reduced the emission current.

We also investigated the influence of the proportions of tungstate and tungsten in the cathode on the emission current. We found that variation of the tungstate content in a rather wide range has no significant effect on the emission current. In preparing tungstate cathodes the calcium oxide content in the active material was varied from 0.5 to 2 mole per mole tungsten trioxide. It was found that variation of the calcium oxide content within this range has no significant influence on the emission current, but does affect the useful life of the cathode (Fig.6).

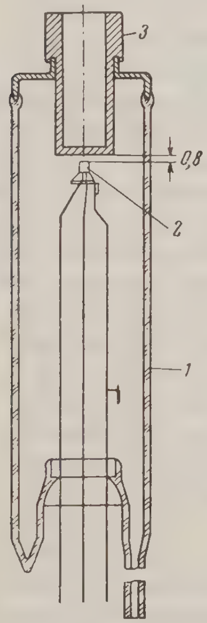

Fig.7. Experimental diode: 1) envelope, 2) cathode, 3) anode.

Testing of cathodes

The cathodes were tested in experimental diodes of the type pictured in Fig.7. The pretest treatment of the cathodes consisted of 5-10 min outgassing and activation at 1200° for 10-15 min with gradual increase of the plate voltage to 300 v.

Inasmuch as the primary purpose of the testing was qualitative evaluation of the different emitter compositions no precise measurements of the saturation emission were made. It proved sufficient for our purposes to determine the current-voltage characteristics at some given temperature (or at several temperatures) under constant conditions. To facilitate comparison the same diode geometry was used in all cases.

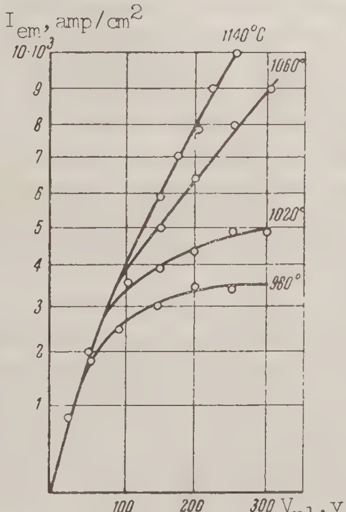

←Fig.8. Current-voltage characteristics of a cathode prepared of barium-calcium tungstate (static conditions).

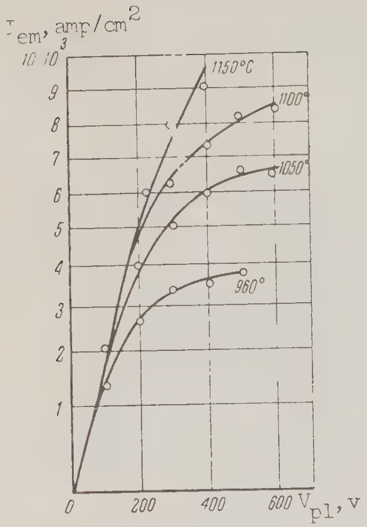

Fig.9. Current-voltage characteristics of a cathode prepared of barium-calcium aluminate (static conditions).

Fig.8 shows the current-voltage characteristics of a barium-calcium tungstate cathode; Fig.9 gives the characteristics of a barium-calcium aluminate cathode.

The useful life of the cathodes was determined in diodes with cooled copper plates. The useful life curves for barium-calcium and barium tungstate cathodes are shown in Fig.6.

Conclusions

Compressed cathodes prepared of barium-calcium tungstates and aluminates allow of drawing emission currents of densities up to 8 amp/cm^2. At this current density the useful life is over 1000 hours; at lower current densities (2-3 amp/cm^2) the useful life exceeds 4000 hours. The cathodes are characterized by good mechanical and electrical stability and are readily reactivated after poisoning.

The cathodes were tested in experimental diodes with water cooled copper anodes (the tests were similar to those on cathodes of a similar type described by Huber & Freytag[2]).

The technology of preparation of the compressed cathodes is simpler than that for L-cathodes.

The emission characteristics and useful life of the cathodes depend on the properties of the active material. In this respect barium-calcium tungstate has certain advantages over aluminates, owing to its greater stability in air. Barium-calcium tungstate is superior to barium tungstate as far as the useful life of the cathodes is concerned.

To a certain extent one can vary and ameliorate the emission characteristics and useful life of compressed cathodes by varying the grain size of the initial powders and the processing conditions (compressing, sintering, etc.).

The presence of calcium oxide in aluminates, as was shown by Brodie & Jenkins[7,8] increases the emission from impregnated cathodes, i.e., the emission current increases with increase of the nonmetallic component containing calcium oxide on the emitting surface (increase of the aluminate content in the mixture). This is explained by the fact that the emission from the sections occupied by the nonmetallic component is higher than from the sections occupied by tungsten. The useful life of cathodes of aluminates is also increased by the addition of calcium oxide; this is apparently connected with the presence of a barium activated calcium oxide film.

The situation is somewhat different in the case of barium-calcium tungstate, which compound was synthesized for the first time in our work. Preliminary experiments showed that variation of the tungstate content in the emitter over a rather wide range has no noticeable influence on the emission current.

It is as yet impossible to give a definitive interpretation of this effect. It may be hypothesized that a) sections occupied by the tungstate have the same emissivity as activated tungsten and b) the entire emitting surface in the course of preparation of the cathode (or in the process of activation) becomes covered with barium-calcium tungstate as a result of reaction with the tungsten of the barium and calcium oxide formed in the process of dissociation. The reactions in question probably are[9]:

$$6BaO + W = Ba_3WO_6 + 3Ba, \qquad (10)$$

$$6CaO + W = Ca_3WO_6 + 3Ca. \qquad (11)$$

The preparation and testing in compressed cathodes of other active materials (barium chromates, thoriates, etc.) is of undoubted interest. Research along these lines is underway.

It would also be of interest to investigate the kinetics of solid phase processes occurring in compressed cathodes, the rate of evaporation of barium and the nature of the emitting surface layer.

References

1. R.Levi, Conven.Rec., IRE, Part 6, p.40, 1953.
2. H.Huber & J.Freytag, Vide, 54, 310 (1954).
3. R.Hughes & P.Coppola, J.Appl.Phys., 23, 1261 (1952).
4. P.Coppola & R.Hughes, Proc.IRE, 44, 351 (1956).
5. A.M.Ginstling, Zhur.prikl.khim. (Journal of Applied Chemistry), 7, 718 (1952).
6. V.A.Pazukhin & A.Ia.Fisher, Vakuum v metallurgii (Vacuum in metallurgy), 1956.
7. D.J.Brodie & R.Jenkins, J.Appl.Phys., 18, 27 (1957).
8. D.J.Brodie & R.Jenkins, J.Electronics, March, 457 (1957).
9. J.R.Hughes, P.Coppola & J.Evans, J.Appl.Phys., 23, 635 (1952).

DISCUSSION

S.D.Uman: What is the approximate service life at 1000°K?

A.I.Mel'nikov: About 4500 hours with a current density of 2-2.5 amp/cm^2.

Z.V.Kukushkina: What is the emission under pulse conditions?

A.I.Mel'nikov: According to preliminary data, 50-100 amp/cm^2.

L.G.Sherstnev: How do you explain the difference between the current-voltage characteristics under static and pulse conditions?

A.I.Mel'nikov: Under static conditions the current is limited by overloading of the plate.

E.P.Ostapchenko: Were reactions (6) and (4) checked? Were these reactions carried out in the solid phase?

A.I.Mel'nikov: The formulas were taken from the literature. The reactions were carried out in the solid phase.

A.A.Gugnin: What was the vacuum in the diode and did the cathodes have getter properties?

A.I.Mel'nikov: The pressure was of the order of 10^{-5}-10^{-6} mm Hg. Obviously, the cathodes had some getter attributes but no special investigation of this was made.

A.I.Figner: Do the tungstates have any advantages over aluminates?

A.I.Mel'nikov: Hughes & Coppola do not give a preparation procedure for aluminates. The aluminates made in our laboratory absorbed carbon dioxide and moisture from the air. The emission data for aluminate cathodes are characterized by poor reproducibility.

A.I.Figner: Is the emission increased by addition of BaO?

A.I.Mel'nikov: In the case of tungstate cathodes the only noticeable result of addition of BaO is increase of the useful life.

A.I.Figner: Did you evaluate the resistance of the tungstate layer?

A.I.Mel'nikov: We made no specific measurements, but some heating incident to passage of current was observed, which was minor inasmuch as the primary role is played by tungsten.

ELECTRIC BREAKDOWN OF THIN LAYERS OF ALUNDUM

- S.N.Koikov & A.N.Tsikin

Thin layers of alundum (aluminum oxide) are used as insulating coatings on vacuum tube heaters to prevent shorting between the heater base and the cathode. Alundum coatings in radio tubes operate under difficult conditions, i.e., at a temperature of 1400-1700°K and in a relatively intense electric field. Factory tests show that an appreciable percentage of rejected tubes fall into this category because of puncture of the alundum coating. Hence investigation of electric breakdown of alundum at high temperatures is of undoubted interest, particularly from the standpoint of production of long-lived radio tubes.

1. Test procedure

Most of the experiments were performed at a pressure of 10^{-4}-10^{-6} mm Hg in the temperature range from 300 to 2000°K on special samples that allowed of obtaining good contact of the electrodes with the alundum and thus accurately evaluating the strength of the electric field in the alundum. The alundum coating was applied to a molybdenum ribbon (base) which served as one of the electrodes. The external contacts were molybdenum discs which were mounted in contact with the alundum surface prior to firing and as a result of firing adhered firmly to the alundum. Another series of experiments was carried out on production heaters mounted in cathodes and on special samples in which the base was a tungsten or molybdenum filament and the external electrodes (probes) did not make good contact with the alundum. The coatings were fired in vacuum at 1900-2000°K. In the test the bases were grounded and a high dc voltage was applied to the external electrode. The temperature was determined from the resistance of the base.

The short term breakdown voltages were determined with the voltage on the sample being raised to the breakdown value within 3-5 sec. In aging tests we determined the time from the beginning of the test to breakdown of the alundum layer (the lifetime) at a given voltage and temperature. At least ten similar tests were run in determining each breakdown voltage and lifetime value.

2. Short-term electric strength

The results obtained for alundum coatings applied on molybdenum ribbon with good contact between the external electrodes and the alundum surface are given in Figs.1 & 2. It will be seen that in the thickness range from 15 to 120 μ the breakdown voltage increases linearly with the alundum coating thickness.* At temperatures above 1700°K the dependence of the breakdown voltage on the layer thickness becomes weak and this indicates that thermal (rather than pure electric) breakdown of alundum occurs at high temperatures.

The breakdown voltage is weakly dependent on the temperature in the range from 300 to 1600°K and falls off sharply at higher temperatures (Fig.2). The plot of log V_{br} as a function of 1/T in the temperature range above 1600°K is a straight line; consequently, the temperature dependence of the breakdown voltage is given by

---

*On the basis of these tests heaters with an increased coating thickness are now being installed in a number of radio tubes produced at the "Svetlana" Plant.

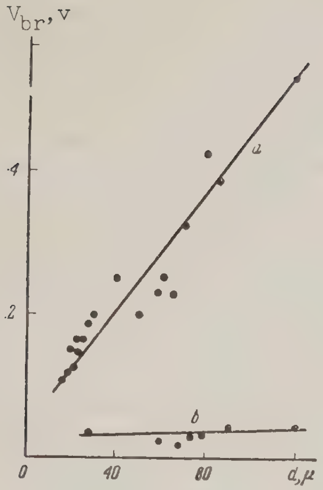

Fig.1. Variation of the short term breakdown voltage on the thickness of the alundum coating: a) at T = = 300°K, b) T = 2000°K.

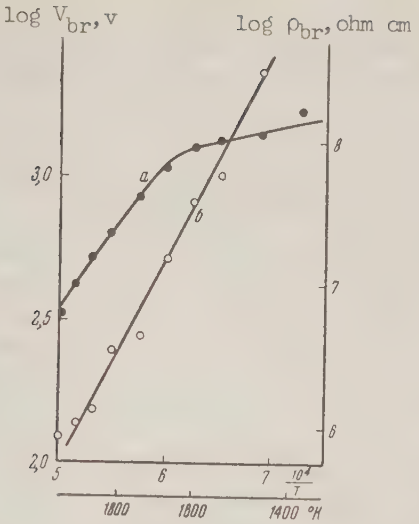

Fig.2. Variation of the breakdown voltage a and resistivity b of alundum with temperature. Coating thickness 50 μ.

$$V_{br} = V_0 e^{\frac{\delta}{kT}}. \tag{1}$$

At voltages close to the breakdown value, the electric conductivity of thin alundum layers is several times greater than in weak fields. In weak fields[1], however, the temperature dependence of the conductivity prior to breakdown is exponential (Fig.2) and is described by

$$\sigma_{br} = \sigma_0 e^{-\frac{\varepsilon\varphi}{kT}}. \tag{2}$$

For all the investigated samples $\delta/\varepsilon\varphi = 0.42-0.56$, which again indicates that the thermal form of breakdown obtains in alundum at high temperatures.[2]

To leave no doubt regarding the form of breakdown occurring at high temperatures, we carried out an approximate calculation of the breakdown voltage of alundum coatings according to the thermal breakdown theories of Koikov.[3] It was found that the breakdown voltage values in a range of high temperatures are given by

$$V_{br} = \sqrt{\frac{2k\rho_k}{a}}, \tag{3}$$

where ρ_k is the resistivity of the alundum layer prior to breakdown, k is the thermal conductivity of alundum and $aT_{\text{к}}$ is the exponent in the equality $\rho_k = \rho_0 e^{-aT_{\text{к}}}$ ($T_{\text{к}}$ is the temperature of the base). The calculated values differ from the experimental ones by a factor not exceeding 1.5-2 which is well within the limits of the experimental error and simplifying assumptions made in the calculations. Thus all the cited results confirmed that the breakdown of alundum at high temperatures is thermal.

3. Pulse electric strength

The results characterizing the variation of the breakdown strength of alundum coatings with the temperature and pulse duration are shown in Fig.3. As in the case of dc breakdown tests, the plot of log V_{br} as a function of 1/T obtained in testing alundum coatings with pulses of 10^{-5}--10^{-2} sec duration are broken straight lines. With decreasing pulse width, the break point is shifted to the side of higher temperatures. In the region of high temperatures log $V_{br} = f(1/T)$ is characterized by parallel straight lines with the same slope as the straight line characterizing this dependence for dc voltages. The breakdown voltage at any given temperature increases with decreasing pulse duration. The variation of the pulse breakdown voltage with coating thickness, like that of the dc breakdown voltage, is linear and the slope of the straight line characterizing the dependence decreases with increasing temperature. All these results show that in the case of pulses of 10^{-5} sec or more duration the breakdown of alundum at high temperatures is thermal.

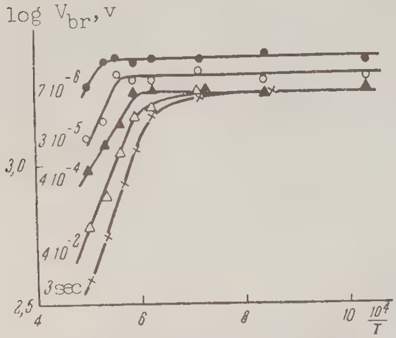

Fig.3. Variation of breakdown voltage with temperature and pulse duration. Coating thickness 60 μ.

In the range of low temperatures the breakdown voltage with pulses, as with dc, is weakly dependent on the temperature and begins to increase with decreasing pulse width only for pulse durations less than 10^{-4} sec.

4. Aging of alundum coatings

As a result of prolonged exposure to the influence of an electric field and high temperature there occur in alundum, as in other dielectrics, changes impairing the dielectric properties and leading finally to breakdown. These processes, which are usually called aging of insulation, determine the useful lifetime of heaters. The results of our investigation of aging of alundum coatings on molybdenum ribbon are shown in Figs.4 & 5. The variation of log V_{br} as a function of log τ at a given temperature (Fig.4) and the variation of log τ as a function of 1/T at a given voltage (Fig.5) are characterized by straight lines; hence there obtain the following empirical relationship:

$$V_{br} = A\tau^{-n}, \qquad (4)$$

$$\tau = \tau_0 e^{\frac{\gamma}{kT}}, \qquad (5)$$

where τ is the lifetime. These results indicate that the aging of alundum coatings under the influence of an electric field and temperature is subject to the regularities obtaining generally for organic dielectrics.

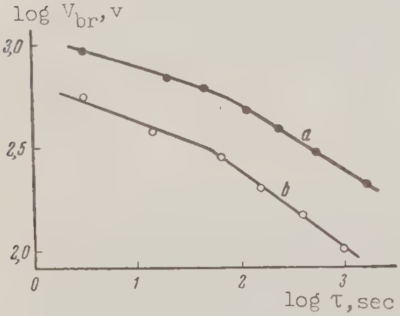

Fig.4. Variation of log V_{br} with time (log τ): a) coating thickness 60 μ, b) coating thickness 30 μ.

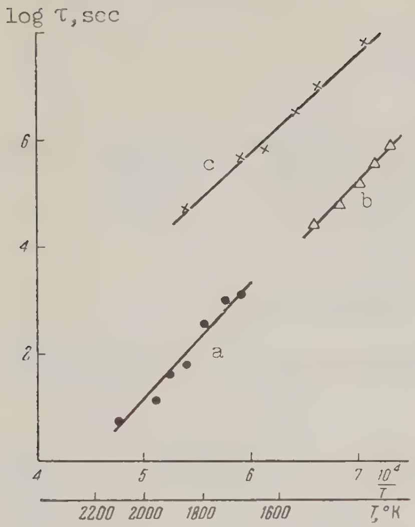

Fig.5. Variation of log τ as a function of 1/T:
a) alundum coatings on molybdenum ribbon at V = 200 v;
b) heaters (according to the data of other authors) at V = 200 v,
c) V = 36 v.

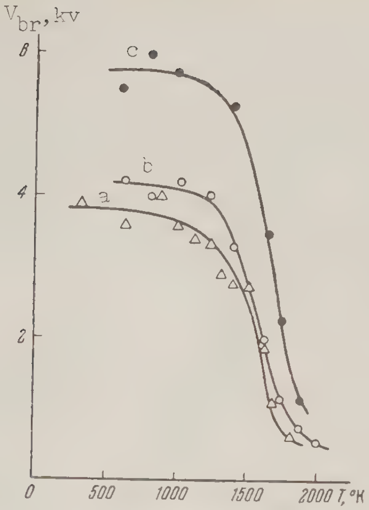

Fig.6. Temperature dependence of the breakdown voltage with good (a) and poor (b,c) contact between the external electrode and the alundum (coating thickness 70-80 μ): a) with both negative and positive potential on the base, b) positive potential on base, c) negative potential on base.

5. Electric strength and aging in the case of loose contact of the external electrodes

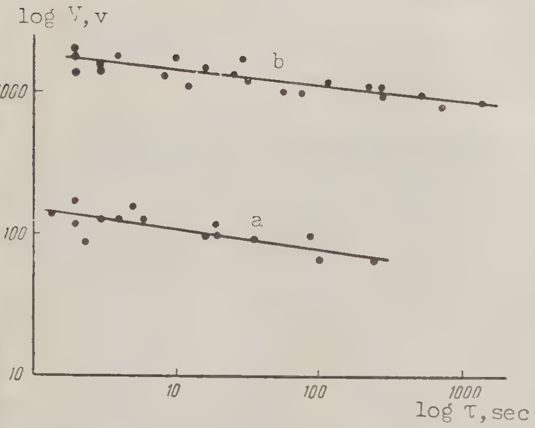

Fig.7. Variation of log V as a function of log τ with a) a positive and b) a negative potential on the base in the case of loose contact. Layer thickness 25 μ.

In the course of tests on heaters off the production line and on experimental samples having loose contact between the external electrode and the alundum, we observed a pronounced dependence of the breakdown voltage and lifetime on the polarity of the electrodes (Figs.6 & 7): in the entire temperature range the breakdown voltage values both for long and short exposure times were several times greater with a negative potential on the base than with a positive one.* This dependence is obviously due to inadequate contact between the external electrode and the alundum inasmuch as it was not observed in the entire test temperature range where intimate contact between the electrode and alundum was provided (Fig.6).

---

*In view of this since 1952 tests at the "Svetlana" Plant are carried out with unfavorable heater-cathode polarity, i.e., with a negative potential on the cathode.

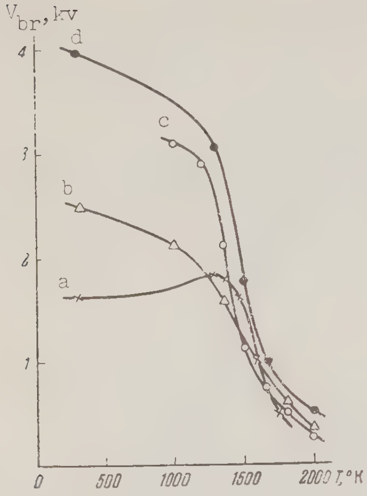

Fig.8. Comparison of temperature dependences of breakdown voltage for alundum coatings on regular heaters (a), molybdenum ribbon (b) and filaments with probe electrodes (c & d). Positive potential on base; coating thickness 50 μ.

Lastly, it will be evident from Fig.8 that the values and temperature dependences of the breakdown voltage with a positive potential on the base are virtually the same in the region of high temperatures with either polarity of the external electrode. Consequently, the regularities established for special samples in this temperature range should be valid for production heaters as well.

Conclusions

1. At temperatures above 1400-1500°K the breakdown of alundum both with dc and pulse voltages is thermal.

2. In the temperature range from 300 to 1400°K the regularities characteristic of thermal breakdown are not observed. Presumably in this temperature range there obtains electric breakdown typical of porous dielectrics.

3. The observed dependence of the breakdown voltage on the polarity of the electrodes is connected with poor (loose) contact of the external electrode with the surface of the alundum coating.

4. The aging of alundum coatings under the influence of electric fields and high temperatures is characterized by the regularities established for the aging of organic dielectrics.

The present work was carried out in collaboration with the quality control department of the "Svetlana" Plant.

"M.I.Kalinin" Leningrad Polytechnic Institute

References

1. A.R.Shul'man, Trudy (Proceedings) NII MRTP, 2-3 (30-31), 3 (1956).
2. A.F.Val'ter (Walther), (Editor) Fizika dielektrikov (Physics of Dielectrics), M., 1932.
3. S.N.Koikov, Nauchno-tekhn.inf.biul. (Scientific-technical information bulletin), Leningrad Polytechnic Institute, No.10, 1957.
4. S.N.Koikov & A.N.Tsikin, Zhur.tekh.fiz., 26, 2248 (1956).

TRANSIENT PROCESSES IN HEATERS

- Iu.K.Shalabutov

Introduction

The principal quantities determining the electric characteristics of cathode heaters in vacuum tubes are the heater-cathode leakage current I_{hc}* and the breakdown voltage of the material forming the coating of the heater.

There have been a number of investigations[1-3] devoted to measurements of I_{hc} and the conductivity of alundum which is the usual heater coating material. There are also a number of reports in the literature[4-6] giving data on the electric strength of aluminum oxide. No one has so far been able to establish any direct correlation between the magnitude of I_{hc} (measured under static conditions) and the useful service life of heaters.

Inasmuch as during extended operation of the heater there apparently occur irreversible processes in its coating, one of the possible ways of establishing a relationship between the service life of the heater and the selective characteristics is investigation of transient processes in the heater coating. The presumed existence of such processes has been mentioned by a number of authors[1,2 & 7], but to the best of our knowledge there has been no systematic investigation of these processes.

In the present report we give the results of investigation of the current flow processes occurring when an alternating voltage V_{hc} is applied between the cathode and heater. The study was carried out by means of a CR curve tracer[8] which was used to record the current-voltage characteristics: $I_{hc} = f(V_{hc})$. The lower bound of the measured current was $6 \cdot 10^{-9}$ amp. The characteristics were usually recorded at a frequency of 50 cps. Some of the measurements were made by means of the pulse set-up designed by M.A.Shepsenvol and M.P.Svin'in; in this case the current sensitivity of the circuit was $6 \cdot 10^{-8}$ amp.

Results of Measurement

1. Shape of the dynamic current-voltage characteristic of I_{hc} and polarization in the heater coating.

For most of the investigated vacuum tubes the dynamic current-voltage characteristic is represented by a curve having a large hysteresis loop in the $V_{hc} < 0$ region and sometimes a small loop in the $V_{hc} > 0$ region (Fig.1). Part of the curve (BCODE) virtually duplicates the static current-voltage characteristic of I_{hc}.

Thus the difference between the dynamic current-voltage characteristic and the static one is that the former has hysteresis loops. The shape of the loop with $V_{hc} < 0$ indicates that there exists a process leading to a rapid increase in current at the instant $V_{hc} = 0$, a process subsequently replaced by smooth decrease of the current with increasing negative V_{hc}.

The shape of the characteristic generally does not depend on the frequency of V_{hc} in the range from 20 cycles to 2 kc. At 5 kc the curve degenerates into an ellipse whose major semi-axis is approximately equal to $(+I_{hc}) + (I_h)$ (Fig.1). Changing the amplitude of V_{hc} from 20 to 200 v leads to an

---

* The polarities of the leakage current I_{hc} and voltage V_{hc} are taken from the heater, i.e., we write $+I_{hc}$ and $+V_{hc}$ when the cathode is positive relative to the heater.

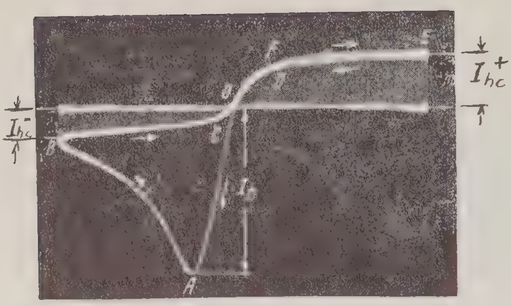

Fig.1. Dynamic current-voltage characteristic of the leakage current I_{hc}. $V_H = 6.3$ v; $V_{hc} = 30$ v. The arrows indicate the direction of the CR beam trace.

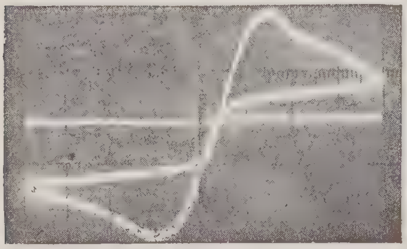

Fig.2. Dynamic characteristic of I_{hc} with overheating: $V_H = 12$ v; $V_{hc} = 30$ v.

increase of the OA section of the characteristic (hereinafter designated by I_h - see Fig.1) and an increase in the slope of the positive branch of the curve in the region of saturation. Increase of the heater temperature from 1300 to 1800° K leads to an increase of I_{hc} (primarily in the positive region) and in the case of tubes that have seen service for a prolonged period to an increase in the area of the hysteresis loop in the $V_{hc} > 0$ region (Fig.2). It is useful to compare these data with the results of investigation of I_{hc} in pulsed operation. A positive rectangular voltage pulse V_{hc} gives rise to a rectangular current pulse I_{hc}, whose trailing edge is accompanied by a large overshoot of current of opposite sign. The negative current pulse is characterized by a decrease of the current during the entire duration of the pulse.

The above facts can be explained by assuming, in accord with Shul'man[3], that there are ions in the heater coating. Then the current I_{hc} may be interpreted as being the superimposition of the conductivity (electronic and ionic) current on the thermionic emission current.

The hysteresis loop and the saturation of the characteristic at $V_{hc} < 0$ (section BO in Fig.1) suggests the occurrence of polarization in the heater coating and the formation of superficial electrode layers. The polarization is probably connected with displacement of ions and the formation of a space charge; the existence of a space charge is indicated by the noncorrespondence of the current values of the static and dynamic conditions and by the change occurring in the shape of the characteristics at a frequency of ~5 kc. It may be noted that back in 1938 Graffunder[2] gave the results of measurement of the variation of I_{hc} with time indicating the presence of polarization effects in the heater coating.

In order to check this hypothesis, we measured the variation in time of I_{hc} (Fig.3) for tubes with a heater coating applied by catophoresis (less dense coatings) and by anaphoresis (more dense coatings). We found that the application of a constant voltage leads to the appearance of a heavy current which then falls off to a certain stationary value. Then the voltage source was disconnected and the cathode-heater section was coupled directly to a galvanometer. First there was a kick of current in the opposite direction, after which the current fell off comparatively slowly with time. This time behavior of the current is characteristic of high voltage polarization.[9]

The dynamic current-voltage characteristics obviously describe the initial sections of the descending part of the curve in Fig.3. The hysteresis loop in the $V_{hc} < 0$ region can be attributed to the ionic current during the period of dissipation of the space charge formed during the interval when $V_{hc} > 0$ and to the formation of a superficial electrode layer[10] (region of "saturation" with $V_{hc} < 0$).

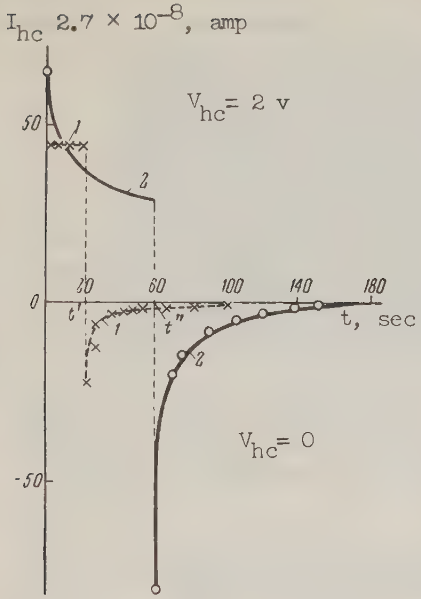

Fig.3. Variation of I_{hc} in time with application and removal of a voltage V_{hc}. Curves: 1) cataphoretic coating, 2) anaphoretic coating. The voltage $V_{hc} = +2v$ was applied from t = 0 to t = t' and t = t'', respectively.

The hysteresis loop in the dynamic current-voltage characteristics and the decrease of the leakage current with time are indicative of accumulation of charge in the heated heater in an applied electric field; it is significant that usually there is a hysteresis loop only in the negative region of the characteristic and that the hysteresis loop in the positive region appears only at high temperatures in the case of tubes that have been operated for a considerable period.

We felt that it would be of interest to evaluate the magnitude of the charge produced in the heater coating and to determine its dependence on the temperature and voltage V_{hc}. To this end the cathode-heater section of the tested tubes was connected to a conventional circuit for measuring charge by means of a ballistic galvanometer (Fig.4,b). Virtually all 30 of the investigated tubes exhibited a similar dependence of the charge Q on the temperature (or the heater voltage V_H) as recorded at constant V_{hc}. A typical curve is shown in Fig.4,a. It will be seen that the character of the variation of the charge with temperature is strongly dependent on the sign of V_{hc}. Whereas with $V_{hc} > 0$ the curve rises monotonically, with $V_{hc} < 0$ there is obtained a curve with a minimum located at about 1550°K ($V_H = 7.5$ v); significantly, this is the temperature at which the sharp rise of the curve for $V_{hc} > 0$ begins. Very similar $Q = f(V_H)$ curves for $V_{hc} > 0$ were obtained for all the tested tubes, both of domestic and foreign manufacture.

It is significant, however, that in a number of tubes the charge corresponding to $V_{hc} < 0$ in Fig.4,a is absent; in the case of these tubes with both polarities of V_{hc}, the $Q = f(V_H)$ curve coincides within the limits of the experimental error with the positive monotonically rising curve shown in Fig.4,a.

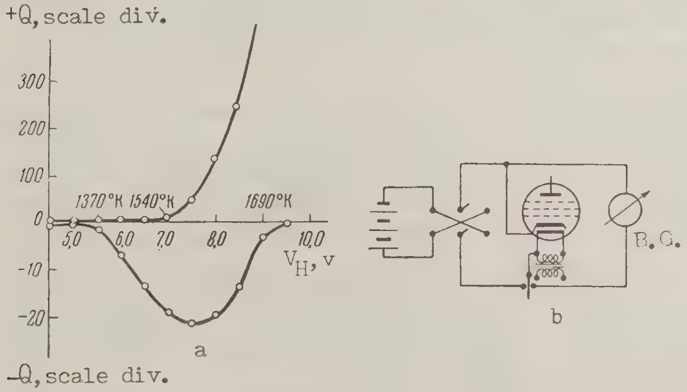

a

b

Fig.4. a) Variation of the charge Q in the heater coating with the temperature for $V_{hc} = 20$; b) circuit used for the ballistic measurement.

Thus there are three temperature regions characterized by different behavior of the charge in the heater coating. From 300 to 1200°K the charge at $V_{hc} > 0$ is small, but increases for $V_{hc} < 0$ (and there obtains a hysteresis loop, increasing in size with temperature, in the negative region of the dynamic characteristic). Next, at $T \approx 1500$°K the charge at $V_{hc} > 0$ begins to increase noticeably, while at the same time the charge for $V_{hc} < 0$ passes through a maximum value and begins to decrease. Finally, at $T \approx 1700^\circ K$ the charge at $V_{hc} < 0$ vanishes, while the charge for $V_{hc} > 0$ continues to increase sharply. At the same time there appears a loop in the $V_{hc} > 0$ region in the dynamic characteristic.

2. Connection between the polarization effect and impurities in the heater coating

It would appear natural to relate the polarization effect in the heater coating with defects in the coating and the presence of various impurities in it. Impurity ions can participate in the conduction through the coating, serve as sources of electrons and also produce a space charge giving rise to polarization effects.

An indirect substantiation of this is that microscopic investigation of the coatings of heaters of most of the tubes showed that they had dark spots, traces of puncture and in some cases vitrified droplets and similar defects. In all these cases the dynamic characteristic had the shape shown in Fig.1 (with a hysteresis loop in the $V_{hc} < 0$ region).

A. Dependence of the shape of the dynamic characteristic on the form of impurity in the coating. Effect of aging of the heater.

We do not have available heaters with coatings containing deliberately introduced impurities. Hence we investigated 60 tubes whose cathode bases contained strontium, calcium and calcium with tungsten. The heaters of these tubes were not subjected to treatment in the presence of an electric field. All the tubes had passed through a prolonged service life test and it could therefore be assumed that there were present at least minor quantities of these elements in the superficial layer of the heater coatings.

In most cases (75-80%) heaters with impurities exhibited different characteristics with different impurities. Thus heaters with strontium impurity showed characteristics of the type shown in Fig.5,a, distinguished by the absence of hysteresis loops. The magnitude of the leakage current was of the order of a microampere. The dynamic characteristics of tube heaters with calcium impurity had the shape shown in Fig.5,b, i.e., intermediate between the shape exhibited by the strontium impurity tubes and tubes with calcium and tungsten present in the heater coating. (The characteristics of the last are similar to that shown in Fig.1). All the tubes whose dynamic characteristics do not fit into this classification had characteristics analogous to that pictured in Fig.1.

Heating of the heaters of all types to $\sim 1800^\circ K$ irreversibly transformed their characteristics to the most common form, that of Fig.1. Characteristics of this type were observed for most of the investigated heaters, particularly those of tubes that had been in service for some time.

As is known, the presence of alkali metal ions in the heater coating results in the appearance of large negative currents in the static and dynamic characteristics. Such a heater in the untreated state has the dynamic characteristics of the rectifier type[11] (similar to that shown in Fig.5,a) with transmission in the cathode-to-heater direction. Subsequent heating in a field, (or without one), leads to increase of the positive current and the appearance of saturation in the negative branch of the curve, often accompanied by a hysteresis loop (shape of curve as in Fig.1). In pre-aging of the cathode, the heater is held at a temperature of up to $1800^\circ K$ without a field. This results in a sharp increase in the leakage current and enlargement of

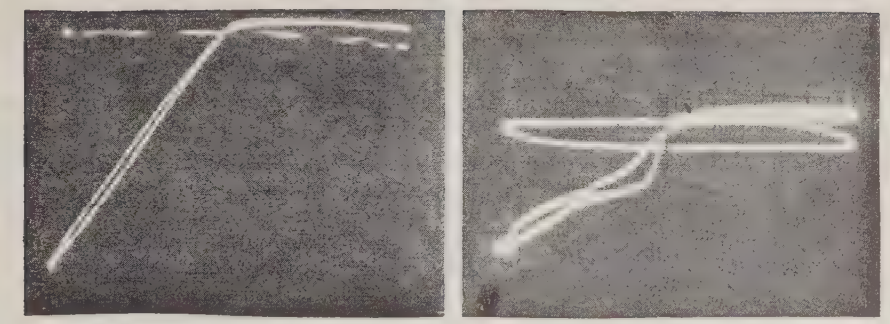

a b

Fig.5. Dependence of the current-voltage characteristics on the alloying material in the heater base: a) strontium, b) calcium.

Aging conditions			I_{hc} after aging, microamp
V_H, v	V_{hc}, v	t, min	
			0.8*
7.5	—200	60	4,0
12,0	0	2.5	16,0
10.0	0	15,0	16,0
7,5	~127	20.0	6,0
7,0	+200	20.0	3,0

Note: The values of the current I_{hc} given in the table are average values for 20 tubes; the measurements in all cases (including those before aging (*)) were carried out under dynamic conditions with V_H = 6 v and V_{hc} = = 30 v.

the hysteresis loop area. Subsequent aging with a field reduces the leakage current but the hysteresis loops persist.

The described variation in the shape of the curve is consistent with the concept regarding the aging mechanism proposed by Shul'man[3] who infers that in the process of aging part of the ions are eliminated by evaporation, while the remaining ions are transferred under the influence of the field to the base of the heater where they remain for a long time in a "frozen" state inasmuch as the operating temperature is lower than the pre-aging temperature. As a result the leakage current is reduced. Ions of the alkaline earth metals have an analogous effect on the shape of the current-voltage characteristics (see above), but with the difference that their removal from the coating proves to be virtually impossible.

This circumstance may be connected with the fact that, as has been shown in his thesis by L.Kh.Ash (advisor M.A.Eremeev), the degree of ionization of impurity atoms in alundum depends on the ionization potential and the temperature. It is possible therefore that in the temperature interval in question alkali metal impurities are almost wholly ionized and eliminated, while alkaline earth metals whose ionization potentials are appreciably higher are ionized only partially, so that an appreciable fraction of the atoms remains in the coating.

The shape of the current-voltage characteristics observed in the case of alkaline earth metals may be explained from two standpoints. Alkaline earth oxides may form on the inner surface of the cathode sleeve and thus give rise to an appreciable thermionic current. The other possibility is the presence of a rectifying effect on the alundum-nickel interface. This mechanism is undoubtedly also important but its relative contribution to the total leakage current has not been established.

As noted above, where tungsten is present in the heater coating, the current-voltage characteristics exhibit pronounced hysteresis loops after heat treatment of the heater. That there is a relation between the polarization effect and tungsten impurity (and in general the base material) is indicated by the appreciable enhancement of polarization effects observed by us in tubes that had been subjected to a prolonged service test at elevated temperatures. The fact that some new unused tubes do not exhibit hysteresis loops substantiates this inference. Since it has been experimentally established (see Ref.3, for example) that tungsten is present in the surface coatings of heaters that have been in operation for a prolonged period, it is natural to associate the hysteresis loops in the $V_{hc} < 0$ region with the presence of tungsten or its compound in the heater coating.

One cannot, however, explain all the observed facts solely on the basis of the assumption of polarization effects associated with the presence of tungsten in the coating. One is forced to infer that there exist in heater coatings at least two different types of impurities, behaving in a different manner and producing different effects.

The first group includes impurities of alkali and alkaline earth metals. Their presence in the coating increases the leakage current due to ionic and additional electronic conductivity. If the operating temperature is lower than the artificial aging temperature, the influence of the alkali metals may be reduced to a minimum, while that of the alkaline earth metals is difficult to diminish. An appreciable leakage current persists in their presence.

It is a fact that the leakage current may either increase or decrease during the service life of a tube. From the above described viewpoint, an increase in the concentration of impurity ions (for example, due to diffusion from the heater base) should lead to an increase of the heater current with time. On the other hand, in the case of removal of impurity atoms with time (for example, by evaporation) we should have a decrease of the leakage current and the appearance of hysteresis loops in the current-voltage characteristics. This effect, which is observed by us for a large number of tubes, indicates, apparently, that the coatings were not sufficiently aged.

Inasmuch as impurities of this group are usually mobile, they may participate in high voltage polarization.

The second group of impurities stems from reactions between the heater base and the alundum. If the heater is operated at temperatures not exceeding $1500^{\circ}K$, the tungsten and tungsten compound impurities produced by these reactions accumulate in the base and impair the electric properties of the alundum layer overlying the heater core. The tungsten impurities can reach the surface of the heater only in the case of very porous coatings. This is evinced by the absence of blackening of anaphoretic coatings whose density is greater than that of other types of coatings. In all cases increasing the temperature of the heater to $\sim 1500^{\circ}K$ leads to diffusion of the tungsten impurity throughout the volume of the coating. Thus prolonged operation of the heater leads to irreversible increase in the surface concentration of impurities of the second group (tungsten and its compounds) and hence to deterioration of the electric properties of the coating.

B. Influence of impurities on the polarity and magnitude of the charge built up in the heater coating under the influence of an electric field

As was noted above, for many tubes the $Q = f(V_H)$ curve has two branches, corresponding to different polarities of V_{hc}. Obviously, there obtain two competing polarization processes, one of which predominates in the region of relatively low temperatures, while the other begins to be important at ~1500°K and predominates over the other at higher temperatures.

We recall that in the temperature interval from 1300 to 1500°K there is a sharp change in the electric conductivity of alundum (at these temperatures there is observed a break in the $\ln\sigma = f(1/T)$ curve[3]), an appreciable decrease of the breakdown or puncture voltage[4] and a break in the curve characterizing the temperature dependence of the diffusion coefficient ($\ln D = f(1/T)$ curve[12]). Approximately at these same temperatures there is observed a sharp increase in the leakage current and transition from characteristics of the type shown in Fig.5,a & b to the type shown in Fig.1.

It follows from diffusion theory that diffusion over the surface of the alundum grains predominates in the temperature interval from 0.03 to 0.52 T_m (where T_m is the melting point in °K), which according to Ref.12 is equivalent to 500 to 1200°K. At higher temperatures ($\gtrsim$1500°K), we have the beginning of volume diffusion which is partially connected with the appearance of new defects (see Refs.12 & 13); in the case of alundum these are probably Frenkel defects.

In view of the above data one may propose the following hypothesis: up to a temperature of 1200-1300°K only movement of impurity ions over cracks, pores and other imperfections is possible in the coating and the total number of migrating impurity ions is small. Positive ions emerging to the surface at $V_{hc} < 0$ are neutralized upon coming into contact with the cathode or are evaporated from the surface of the coating. Hence there is only one hysteresis loop (in the $V_{hc} < 0$ region) in the dynamic characteristics.

At higher temperatures ($\gtrsim$1500°K) volume diffusion begins and impurity atoms are distributed throughout the entire coating and move in both directions (from the surface to the base and vice versa, depending on the polarity of V_{hc}) thus giving rise to the second hysteresis loop at $V_{hc} > 0$ (Fig.2).

Finally, in order to explain the influence of tungsten impurity we must, in addition to high voltage polarization, invoke the mechanism of polarization on the boundaries of inclusions. According to von Hippel[14] for such polarization to occur there must be present two media with different values of dielectric constant and conductivity as well as free current carriers capable of moving between the electrodes (in our case between the heater base and the cathode).

It may be assumed that this polarization mechanism develops on the grain boundaries between the alundum and the tungsten inclusions formed in the process of high temperature aging or during prolonged operation of the heater, i.e., inclusions probably present in all the investigated cases.

At low temperatures the role of current carriers may be played by electrons and impurity ions; at high tempteratures the ions of the Al_2O_3 lattice probably contribute to the conductivity. If we assume that the contribution of the last to the conductivity is greater at high ($\gtrsim$1500°K) temperatures than that of the regular impurity ions, one can understand the universal character of the positive branch in the curve of Fig.4.

Thus there are apparently two polarization mechanisms operating in the coating: the first - high voltage polarization - is significant in the low temperature region, while the second - polarization at interfaces - is important in the high temperature range. The first type of polarization depends on the presence of impurities and on the polarity of V_{hc}, while the second is independent of the polarity of V_{hc}.

Lastly, we must make note of a special mechanism of appearance of polarization effects, developing in the case of "partial" breakdown of the coating.[15]

Apparently in this case, too, there form impurities in the coating. This phenomenon is illustrated in Fig.6.

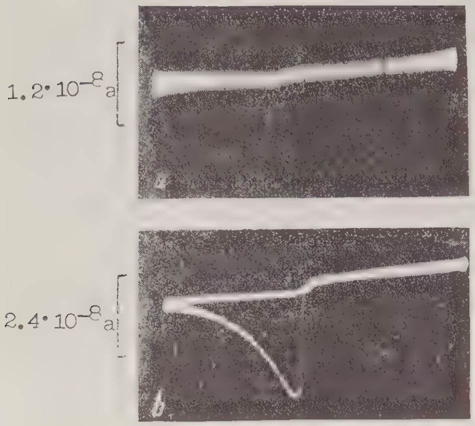

Fig.6. Change in the shape of the dynamic characteristic incident to breakdown: a) prior to breakdown, b) after breakdown at V_H = 20 v; V_{hc} = -400 v; 12SK7(RCA) tube.

C. Dependence of the shape of the current-voltage heater characteristic on V_{hc} at small V_{hc} values. Role of the surface layer.

With a view to clarifying the nature of the currents flowing through the heater we felt it would be of interest to study the behavior of the dynamic characteristics in the region of low voltages, particularly, in view of the reports in the literature[7] that the shape of the characteristics undergoes a pronounced change in going from low to high voltages.

Investigation of the dynamic characteristics at different values of V_{hc} showed that the characteristics do have a different shape in different V_{hc} intervals. In the V_{hc} range from 0 to 10 v, the dynamic characteristic has the shape shown in Fig.5,a, i.e., represents a conjunction of the positive branch of the usual characteristic (Fig.1) and the current I_h. In the interval from 12 to 15 v there appears the familiar hysteresis loop in the $V_{hc} < 0$ region and this increases in size with increasing voltage. At ~20 v the dynamic characteristic assumes its usual shape. As V_{hc} is decreased the hysteresis loop disappears at about 12-15 v.

Let us consider the possible processes evinced by the positive and negative branches of the current-voltage characteristic.

As has been shown by Shul'man[3], the thermionic emission of alundum is not low; therefore one can ascribe part of the current at $V_{hc} > 0$ to it (particularly in the region of saturation). At the same time there can be no doubt regarding the existence of contact through which electronic conductivity is realized between the heater coating and the cathode. Undoubtedly the dynamic characteristics obtained at low voltages reflect these two processes. That is, the low voltage characteristics are due to a combination of the thermionic emission current (positive region) and the electronic conductivity current, which is comparatively large in the negative region and small in the positive one. This last may be due to rectifying contact between the alundum and the nickel.

The electronic character of the negative current at low V_{hc} values is substantiated by the fact that it (like the negative current) is independent of the frequency. Also frequency independent is the value of I_h in the usual characteristics. Consequently, the negative current at low values of V_{hc} and I_h is of electronic origin and due both to the external field and the field associated with the electrode surface of the layer.

We recall that characteristics of the rectifier type at high V_{hc} values are observed in the case of a high concentration of alkali or alkaline earth ions in the coating. It is possible that here there develops a barrier layer, in consequence of which the polarization effects are masked by a large conductivity current.

The appearance of hysteresis loops when the voltage is increased to 10-15 v may be connected with ionic processes. Let us assume that as a result of aging there forms on the coating surface a layer virtually free of impurity ions. The thickness of this layer may be roughly evaluated from the magnitude of the charge Q and the applied voltage. The approximate thickness proves to be 10^{-4} cm. For a hysteresis loop to appear, obviously, the impurity ions must be able to pass through this depleted layer to the cathode during the time of increase of V_{hc}. From the magnitude of the charge one can evaluate the ion concentration, which proves to be of the order of 10^{15}-10^{16} cm^{-3}, and the mobility of these ions (assuming the electric conductivity at operating temperatures to be 10^{-6} mho/cm). The mobility of the ions evaluated in this manner proves to be about 10^{-4} cm^2 v^{-1} sec, i.e., the usual value for ionic conductivity. Ions with this mobility can penetrate an impoverished layer of the indicated thickness during about 1/4 the period of variation of V_{hc} with a voltage of 10-15 between the cathode and the heater.

Thus we have a possible explanation for the observed change in shape of the current-voltage characteristics in going from small to large values of V_{hc} (the assumed penetration by ions of the ion depleted layer on the surface of the heater coating).

The formation of an ion-depleted layer may occur not only under the influence of aging but also when the heater is fired in a hydrogen furnace as is done, for example, in fabricating crystal detectors.[16] In fact, coatings fired at 1800°K have a thicker depleted layer. In this case the hysteresis loop does not appear in the leakage current characteristics even after prolonged operation of the heater. It is possible that here an important role is also played by the high density of the surface layer in that it impedes diffusion of all impurities to the surface.

3. Correlation between polarization effects and the service life of heaters

As noted above it proved impossible to correlate the absolute values of the leakage current measured under static conditions with the useful service life of heaters. Equally fruitless proved to be attempts to correlate the service life with the absolute values of leakage current measured under alternating current or pulse conditions. For a number of tubes there appeared to be some correlation between the service life and the current ratio I^{+}_{hc}/I^{-}_{hc} (I^{+}_{hc} and I^{-}_{hc} as defined in Fig.1). Further investigations, however, failed to substantiate this result. Nevertheless, it may be regarded as established that the value of this ratio does decrease during the period of operation of the heater (Fig.7). A number of measurements have shown that during prolonged operation this ratio tends to unity.

In general the service life of a heater is probably determined by a number of different factors so that any attempt to relate it to any one factor as for example I^{+}_{hc}/I^{-}_{hc} (i.e., the ratio of the thermionic emission current to the conductivity current in the field of the surface layer) could not but prove disappointing. Since the above cited results show that there is a connection between hysteresis loops in the dynamic characteristics and the presence of impurities in the coating, it appeared logical to introduce as correlation parameter some quantity characterizing the hysteresis loop. In the first approximation this can be done by means of the ratio I^{+}_{hc}/I^{-}_{hc} over I_h/I^{-}_{hc}, i.e., by introducing the correlation parameter

$$\mu = \frac{I^{+}_{hc}}{I^{+}_{hc}} \cdot \frac{I^{-}_{hc}}{I_h} .$$

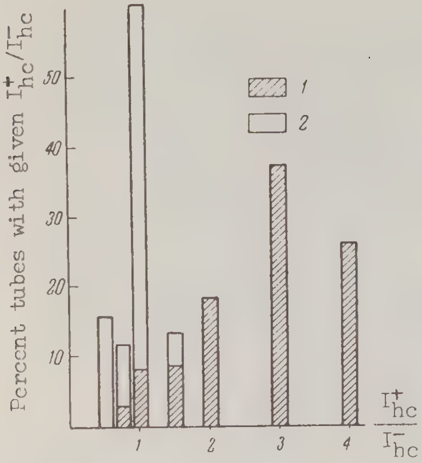

Fig.7. Change in the relative number of tubes with different values of the ratio $I^+_{hc}/$ $/I^-_{hc}$ before and after normal service life tests: 1) before test, 2) after 500 hours operation.

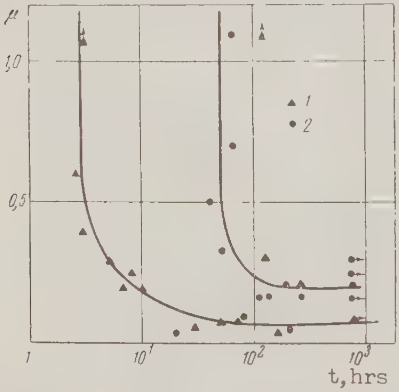

Fig.8. Variation of the parameter μ with the service life of tubes: 1) $V_{hc} = -500$ v, 2) $V_{hc} = -400$ v. $V_H = 7.5$ v.

As may be seen from the curves of Fig.8 there appears to be some correlation between the parameter μ and the service life of heaters.

Apparently, the utilized ratios - I^+_{hc}/I^-_{hc}, characterizing the symmetry of the characteristics and I_h/I^-_{hc}, characterizing the hysteresis effects - are highly significant, but undoubtedly there are other factors affecting the service life that are not taken into account by these ratios. If these could be properly allowed for the correlation would probably be improved. Unfortunately, the actual dependence of the service life on all the different factors affecting it may turn out to be much more complicated than would appear at present.

Summary

1. Systematic investigation of the current-voltage characteristics of the leakage current ($I_{hc} = f(V_{hc})$ by the procedure developed earlier[8] brought to light appreciable differences between the static and dynamic characteristics of the leakage current both as regards the amplitude of the current (lower in static case) and as regards the shape of the curves. The divergences as regards the strength of the current and the hysteresis loops appearing in the dynamic characteristics can be ascribed to the influence of space charge in the surface coating.

2. Comparison of the dynamic characteristics with the variation of I_{hc} in pulsed operation and the character of variation of the current with time indicates the existence of polarization effects in the coating. There appear to be two competing polarization mechanisms: high voltage polarization and polarization on inclusion boundaries.

3. The ionic character of the transient processes in the heater is substantiated by the change in the shape of the dynamic current-voltage characteristic of the leakage current as a result of aging treatment and operation of the heater.

4. Prolonged service life tests lead to a reduction of the ratio I^+_{hc}/I^-_{hc} (measured under dynamic or pulse conditions). Just before breakdown of the heater coating this ratio approaches unity.

5. Impurities appear in the coating not only during fabrication of the tube but also during its operation (regular operation or service life tests) and incident to electric breakdown of the heater coating.

6. Transient processes in heaters appear to be connected with impurities and defects in the coating.

7. Heating a heater to a high temperature (1800°K) by raising the filament current impairs its electric properties. In contrast, heating the coating to the same temperature from the outside (i.e., in a hydrogen atmosphere) appreciably improves its insulation properties.

8. Our work led to derivation of the parameter

$$\mu = \frac{I^{+}_{hc}}{I^{+}_{hc}} \cdot \frac{I^{-}_{hc}}{I_{h}}$$

which appears to show some correlation with the useful life of heaters.

Conclusions

1. Investigations of transient processes in tube heaters showed that ionic and polarization processes in them play a substantial role and may have an appreciable influence on the electric properties of the heater coating.

2. Present data on the static characteristics of the electric properties of tube heaters are in themselves inadequate and must be supplemented by taking into account transient processes.

3. On the basis of our investigation of transient processes in heaters we have been able to deduce a correlation parameter by means of which one can to some extent predict the useful life of individual heaters. There can be no doubt, however, that the correlation parameter relating the dynamic current-voltage characteristic of the leakage current with the probable service life of the heater is in need of modification and revision with a view to taking into account the influence of other factors affecting the useful life of cathode heaters.

The author takes this occasion to express his gratitude to A.R.Shul'man for guidance in the work and to Iu.P.Maslakovets for much valuable advice.

"M.I.Kalinin" Leningrad Polytechnic Institute

References

1. H.Klemperer, Electronic Engng., 55, 981 (1936).
2. W.Graffunder, Die Telefunken Röhre, 12, 57 (1938).
3. A.R.Shul'man, Trudy NII MRTP (Transactions, Scientific Research Institute of the Ministry of the Radio Engineering Industry), No.2-3, 3-45 (1956).
4. S.N.Koikov & A.N.Tsikin, Zhur.tekh.fiz., 26, 2248 (1956).
5. R.Sato & H.Yamamoto, Toshibo Rev., 8, 58 (1953).
6. G.H.Metson, Proc.Inst.Electr.Engrs., B-102, 678 (1955).
7. Electronic Industries & Tele-Tech, 1, 56 (1957).
8. Iu.K.Shalobutov, Nauchno-tekhnicheskii biulleten' OKB (Scientific technical Bulletin OKB), No.6 (1958).
9. A.F.Ioffe, Fizika poluprobodnikiv (Physics of Semiconductors), M.-L, 1957.
10. P.P.Kobeko, Amorfnye veshchestva (Amorphous substances), 1952.
11. H.K.Henisch, Semiconductor rectifiers (Cited in Russ.trans.), 1951.
12. J.N.Gregory & S.Moordath, Trans. Faraday Soc., 47, 844, 1064 b (1951).
13. T.K.Koval'chik & Iu.P.Maslakovets, Zhur.tekh.fiz., 26, 1417 (1956).
14. A.von Hippel, Dielectrics and Waves, N.Y., 1954.
15. S.Whitehead, Dielectric Breakdown of Solids (Cited in Russ.trans.),M., 1957.
16. Kristallicheskie detektory (Crystal detectors), Pub.Sov.radio, 1950.

DISCUSSION

V.F.Kovalenko: Please describe the physical nature of the transient processes in heater coatings.

Iu.K.Shalabutov: Various impurities - primarily positive ions - are present in a coating. During the aging of the heater some of them are transferred into the base, some remain in the surface layer. Moving from one "electrode" to the other these ions form a space charge and give rise to polarization effects. At high temperatures all these effects in heaters undergo a change; apparently, there appear new current carriers.

N.I.Figner: If you associate the hysteresis loops with presence of tungsten, it is not clear to me why these were not detected in the case of a heater in a nickel cathode not alloyed with tungsten; the tungsten should first penetrate from the side of the base which is a higher temperature than the cathode.

Iu.K.Shalabutov: The hysteresis loops are evinced first in tubes that have operated for a prolonged period. In the case of freshly prepared heaters, the initial characteristics often indicate the presence of alkali impurities. Part of these impurities are volatilized during the aging treatment but, on the other hand, tungsten and its oxides penetrate into the coating during heating of the heater at high temperatures. The presence of tungsten impurity in the cathode base leads apparently to reduction of the resistance in the alundum surface layer and to its contamination.

O.Ia.Mlodik: Did you try to separate completely the cathode from the heater?

Iu.K.Shalabutov: Emission characteristics were obtained only for experimental tubes. The current pulses differed little from square ones.

I.I.Pepenova: What effects are observed when the base is of different material?

Iu.K.Shalabutov: The general character of the effect is the same with a base of J-alloy but the current and size of the hysteresis loops are appreciably larger.

O.Ia.Mlodik: To what Iu.K.Shalabutov has said, one must add the hypothesis of Nergaard regarding the drop of emission as a result of "draining away" of donors from the surface. This should supplement the picture of the observed effects.

S.A.Obolenskii: At present intensive research on heaters is being carried out in a number of institutions. The purpose of this research is to increase the dependability and insure a longer service life. The physics of heaters is very complex and as time goes on there appear to be more and more factors that are significant. Not all the problems have as yet been fully examined. The service life criterion or parameter proposed by Iu.K.Shalabutov is too artificial; hence the validity is a priori questionable, particularly, since it has not been tested experimentally to any extent. Further research in this direction is essential.

DESIGN OF A VIBRATION-RESISTANT HEATER WITH AN ENHANCED SERVICE LIFE FOR HIGH-TEMPERATURE CATHODES

- L.A. Timoshin

The effective service life and resistance to vibration of some present-day vacuum tubes employing L-cathodes* are often limited by the unsatisfactory quality of the cathode heater. Such heaters are commonly made of spiral wound tungsten wire 60 to 200 μ thick, covered with alundum either by electrophorensis or spraying followed by firing at 1650-1700° in an atmosphere of hydrogen. Failure of heaters of this type (inserted in an L-cathode) usually occurs after some 400-700 hours of operation.

Examination of defective heaters revealed the following:

a) The alundum coating becomes gray and friable and partially disappears (but no scaling) from some areas of the tungsten filament.

b) The molybdenum sleeve of the L-cathode becomes covered on the inside with a dense black deposit. X-ray analysis shows that this deposit contains aluminum and molybdenum. Similar compounds of aluminum with iron and nickel are known and are extensively used as black coatings for some tube components.

c) The surface of the exposed areas of the tungsten wire appears rough.

d) A tarnish-like deposit appears at the end of the alundum tubes containing the heater leads; this deposit consists of fine needle-like crystals clearly distinguishable with a magnification of 75-100 X. Spectroscopic analysis shows that large amounts of tungsten are present in this deposit.

It must be noted that failures of this type do not occur in the case of oxide-coated cathode heaters. This is due to the fact that the operating temperature of L-cathode heaters is appreciably higher than the temperature of oxide-coated heaters; the operating temperature is usually 1500-1600° and attains as much as 1800° in activating the cathode.

Our specific research problem was to develop a heater for high-temperature cathodes, having high mechanical strength and a useful life of at least 5000 hours.

Judging from the data in the literature the following factors may be involved in the breakdown of alundum coatings:

a) Direct interaction between the tungsten and the alundum.[1-3]

b) Electron bombardment of the tungsten from the cathode base, resulting in the appearance of tungsten ions. According to Metson et al[4], the use of a nonporous heater coating almost wholly eliminates the deleterious effects of electron bombardment.

c) The presence of oxygen adsorbed by the alundum coating; this oxygen is not wholly eliminated during heating of the tubes and gives rise to processes leading to the destruction of the alundum coating.[5]

Without going into a detailed analysis of these views regarding the mechanism of destruction of heater coatings, we note that in our opinion the most effective measure for improving the quality of high-temperature heaters is provision of a nonporous vacuum-tight insulating coating. The vacuum tightness requirement is necessary not because a nonporous coating prevents access of electrons to the tungsten base[4], but because it protects the tungsten from interaction with such gases as carbon dioxide, oxygen and water vapor.

In addition, a vacuum-tight coating inhibits interaction of the tungsten with the alundum (at high temperature), a process which may occur wherever the two materials come into contact. Experiments substantiated the above inferences.

---

*L-cathode = porous metal film cathodes, usually W or Mo "filled" with Ba, Sr, etc.

Thus our principal problem reduced to obtaining a vacuum-tight coating having high insulating properties and good mechanical strength and capable of retaining these attributes for a prolonged period at 1600°.

Taking these requirements and the technological aspects of preparing coatings into account, we rejected the idea of using high-temperature enamels or attempting to fuse the alundum coatings as recommended by Metson et al[4] and turned our attention to investigating the potentialities of mixtures of oxides.

The best results were obtained with a mixture of alundum and beryllium oxide (1:1 molar proportions), fusing at 1850-1900°.

The following procedure was worked out for preparing heaters. A preformed cylinder of alundum ceramic is inserted into the heater alundum-coated in the conventional manner. This assembly is then again coated with alundum and over this is applied a thin layer consisting of a fused and powdered mixture of alundum and beryllium oxide. The coated assembly is fired at 1850-1900° in an atmosphere of hydrogen. At this temperature the alundum-beryllium oxide mixture fuses and impregnates the underlying alundum making it vacuum-tight. The lead ends of the molybdenum heater remain untreated in order to avoid brittleness of the leads.

Heaters prepared in this manner have a high mechanical strength (resistance to vibration) and to date have passed service tests of up to 4200 hours. Tests in actual tubes have also yielded favorable results.

References

1. Wartenberg & Moehl, Z.Phys.Chem., 128, H.5-6, 439 (1927).
2. Wartenberg, Chemie - Ing - Techn., 26, N.8/9, 509 (1954).
3. Sato & Yamamoto, Toshiba Review, 9, N 1, 74-77 (1954).
4. G.H.Metson, E.F.Rickard & F.M.Hewlett, Proc.IEE, Part B, 102, 678 (1955).
5. E.Rysckewitsch, Oxydkeramik, 132-133.-Springer, Berlin, 1948.

DISCUSSION

I.L.Gandel'sman: What is the thickness of the insulating layer?

L.A.Timoshin: 50-60 μ.

G.G.Shamaev: Does the degree of destruction of the alundum coating depend to any extent on the polarity of the heating voltage?

L.A.Timoshin: We did not specifically study this effect, but we noted in running tests with dc that there is some dependence.

O.Ia.Mlodik: What is the cathode firing time?

L.A.Timoshin: One half to one minute.

SOME TECHNOLOGICAL PROCEDURES FOR REDUCING CATHODE-HEATER LEAKAGE CURRENT

- G.Ia.Pivovarov & Iu.A.Semenov

In the production of receiving, amplifying and other vacuum tubes with indirectly heated cathodes a certain percentage of tubes always has to be rejected due to excessive cathode-heater leakage current. There are a number of causes of leakage current of varying relative importance. In our research on the problem particular attention was paid to the following factors: cleanness of the inside surface of the cathodes, the grain composition of the alundum coating, the presence of impurities in the alundum and the pre-aging conditions.

The purpose of the work was purely practical and the research was carried out under regular production conditions on subminiature tubes.

Thus, in the process of organizing production of the 6D6A (6Д6А) tubes (cathode base diameter 0.6 mm) a large percentage of the rejected tubes were rejected for being substandard as regards leakage current. In analyzing the rejects, it was found that about 60% of the heaters had droplets of metal on their surface (Fig.1). In some cases these droplets even resulted in shorts. It was found that these droplets were nickel remaining on the inner surface of the sleeve after cutting and not removed therefrom in the conventional operation. Ultrasonic cleaning of the pieces in trichloroethylene almost wholly eliminated this factor. Introduction of ultrasonic cleaning of the cathodes resulted in the reduction of rejects for excessive leakage current in the case of the 6D6A tube by 40% (percentage of rejects for this reason prior to introduction of ultrasonic cleaning 3.5%; percentage after, 2.1%).

It is known that the grain composition of the alundum has an appreciable influence on the quality of the heaters prepared by the "railroad" procedure.

The alundum powders of domestic manufacture have up to 95% particles of up to 3 μ diameter. At our request the alundum supplier prepared batches of powder with an average grain size of 2-3, 5-7 and 10-14 μ. Heaters prepared using these powders showed different degrees of shrinkage of the insulation layer: 18.2, 15 and 12.5%, respectively.

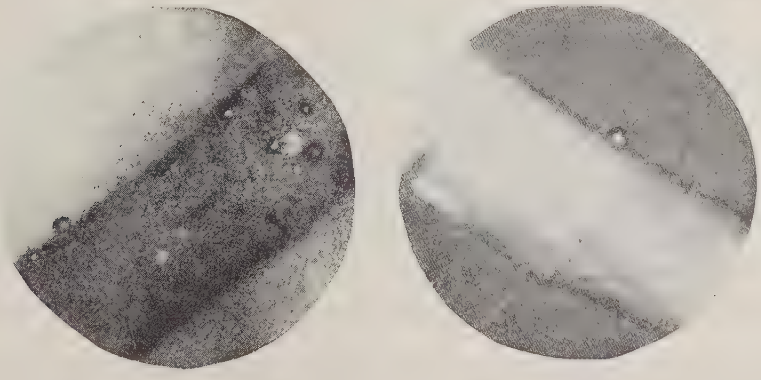

Fig.1. Microphotographs of sections of heaters of tubes rejected for excessive leakage current (Magnification 600 X).

The different nature of the shrinkages was also evinced in the magnitude and number of microcracks in the coating (Fig.2) which, as is known[1], is important where electric breakdown of the heater is concerned (width of the microcracks: 9-15 μ, 5-7 μ and 3-5 μ, respectively).

The results of service life tests on heaters of 6Zh1B (6Ж1Б) tubes prepared using 2-3 and 10-14 μ grain size alundum are shown in Fig.3. In the case of the finer grain alundum the value of the leakage current increases to 19 and 11 microamp, respectively, for positive and negative polarity, while the corresponding values for the coarse grained aluminum oxide are 9 and 1 microamp.

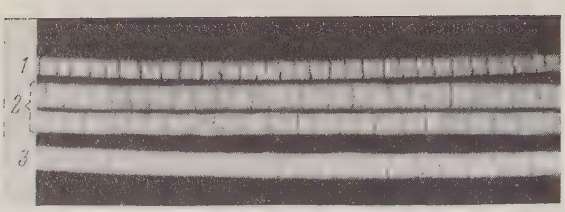

Fig.2. External view of heater prepared with different sizes of alundum grains: 1) 2-3 μ, 2) 5-7 μ and 3) 10-14 μ.

Chemical impurities in the alundum have an effect both on the quality of the alundum suspension used in the cataphoretic method of application and on the leakage current of the cathode-heater assembly. The characteristics of different batches of alundum are listed in the accompanying table. With increasing impurity concentration the electric conductivity of of the alundum suspension in water increases and the efficiency of the suspension decreases.

Table

Characteristics of different batches of alundum

Alundum batch No.	$(NO'_3+Cl'+SO'_4+Na_2O)$, %	Na_2O, %	ρ water suspension, ohm-cm
266	0,0620	0,05	9600
170	0,1215	0,1	8100
173	0,1350	0,1	7700
264	0,1160	0,1	6600
214	0,1325	0,1	5900
181	0,1470	0,1	5000
244	0,1663	0,1	4750
61	0,3540	0,3	3300

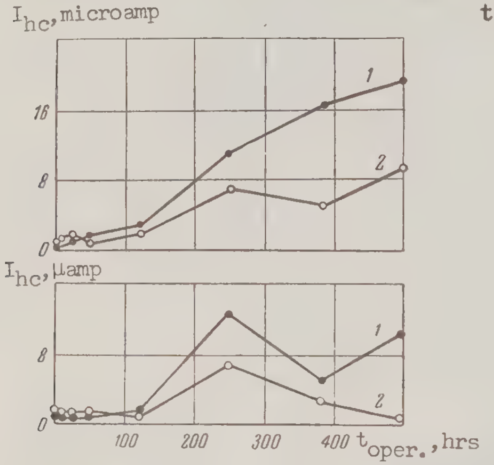

Fig.3. Variation of the cathode-heater leakage current in 6Zh1B tubes during operation. Alundum grain size: 1) 2-3 μ; 2) 10-14 μ.

Suspensions with a large amount of impurities in the alundum also undergo a large change (by a factor of 2-2.5) in electric conductivity in storage, particularly during the first 5 days. To remove impurities from unsatisfactory batches of alundum, the material was treated by boiling twice in distilled water and subsequent heating to 850-900°. This treatment reduced the impurities by a factor of 2-3 and materially lowered the number of rejected tubes (in the case of 6N8S (6H8C) tubes the reduction as regards leakage current rejects amounted to 30%).

The aging procedure is an important factor where the behavior of the cathode-heater assembly is concerned. Important research on this problem has been carried out by A.R.Shul'man. For some types of tubes alternating polarity was used for the aging operation. Aging tests with different polarities showed the following:

Aging current	Percent rejects for excessive leakage current
+ on heater	16.1
- on heater	0.48
± on heater	8.25

Consistent aging with negative polarity on the heater gave an appreciable reduction in rejects; the percentage of rejects was reduced from 6.5 to 3.06% for the 6Zh2B tubes and from 7.3 to 2.18% for the 6S6B tubes.

Increasing the cathode to heater voltage during the aging from 150 to 190 v resulted in the reduction of the percentage of rejects from 4.37 to 1.29% for the 6Zh1B tubes.

The measures outlined above appreciably reduce the percentage of rejects for excessive leakage current and appreciably enhance the quality of receiver tube production.

References

1. G.H.Metson, E.F.Rickard & F.M.Hewlett, Proc.IEE, part B, IX, 102, 678 (1955).

DISCUSSION

K.G.Kondrashova: Please summarize the results obtained in the experiments with different grain size.

G.Ia.Privovarov: With increasing grain size the shrinkage is reduced, the number and size of cracks is decreased and the continuity of the coating is improved.

Frid: Was the same coating thickness used for the different grain sizes?

G.Ia.Pivavarov: Yes, before firing the thickness was the same.

B.I.Vasserman: The leakage current decreases with increasing grain size not as a result of the reduction in the number of cracks but apparently as a result of enhanced purity.

O.Ia.Mlodik: I don't agree with Comrade Vasserman. The cracks form a ready avenue for the migration of atoms from the base. As a result there is observed blackening of the alundum surface. This was remarked on in the report of Shul'man and Chelnokov.

I.I.Pepenova: What specifications must the alundum suppliers meet?

G.Ia.Pivovarov: They must meet the extant official Technical Specifications for this material.

Bulletin of the Academy of Sciences of the USSR - Physical Series
Vol. 22, No. 5 - May 1958

Transactions of the Eighth Conference on Cathode Electronics

TABLE OF CONTENTS

	Page Orig.	Page Trans.
Investigation of discrete energy losses of electrons in Mg, MgO, BeO and Ge - N.B.Gornyi	475	481
Secondary electron emission from alkali halide single crystals at low primary energies - S.A.Fridrikhov & G.N.Goriacheva	486	491
Secondary emission from thorium oxide activated with barium - B.N.Popov & V.F.Koliverdov	496	499
Behavior of composite secondary emitters in extended operation - E.G.Kormakova & V.G.Pavlovskaia	505	509
Some characteristics of new commercial photomultiplier tubes - L.G.Leiteizen, A.G.Berkovskii, B.M.Glukhovskoi, O.S.Korol'kova & E.I.Tarasova	513	516
Secondary emission from composite emitters in the range of high secondary-emission coefficient values - R.M.Aranovich & A.I.Piatnitskii	518	521
Some features of the retarding potential curves of surface activated cathodes. - V.N.Lepeshinskaia & T.M.Sukova	528	531
Secondary emission characteristics of magnesium and beryllium alloy cathodes after short-term activation - V.L.Borisov & V.N.Lepeshinskaia	534	537
Kinetics of charge build-up on a dielectric surface under electron bombardment - I.R.Zakirova & S.A.Fridrikhov	546	547
Energy distribution of secondary electrons from oxide coated metal surfaces - M.L.Kapitsa	557	557
Some properties of multialkali photocathodes - A.A.Mostovskii, O.B.Vorob'eva & K.A.Maiskaia	561	561
Photoelectron emission from some semiconductor and metal cathodes with a reduced work function - P.G.Borziak, V.F.Bibik & O.G.Sarbei	566	565
Investigation of photocathodes by the radioactive tracer technique - N.A.Soboleva	576	575
Field emission patterns of tungsten and molybdenum carbide crystals - A.P.Komar & Iu.N.Talanin	580	579

Adsorption of zirconium and barium on tungsten and the resultant work function - V.N.Shrednik 594 592

On the possibility of utilizing bombardment-induced conductance for signal amplification - A.M.Bonch-Bruevich, E.S.Grishin & U.B.Soltamov 605 602

Optical properties of alkaline earth carbonate layers - I.S.Gorban' 607 604

Compacted powder cathodes of barium-calcium aluminates and tungstates - A.I.Mel'nikov, A.V.Morozov, B.N.Popov & A.A.Maklakov 613 610

Electric breakdown of thin layers of alundum - S.N.Koikov & A.N.Tsikin 622 618

Transient processes in heaters - Iu.K.Shalabutov 628 623

Design of a vibration-resistant heater with an enhanced service life for high-temperature cathodes - L.A.Timoshin 640 635

Some technological procedures for reducing cathode-heater leakage current - G.Ia.Pivovarov & Iu.A.Semenov 642 637

Translated in 1959 by
Columbia Technical Translations
5 Vermont Ave., White Plains, N.Y.

Transactions
# of the
Eleventh All-Union Conference on Theoretical Spectroscopy*

(Moscow, 2-10 December 1957)

- To be continued in Vol.22, Nos. 9 and 11 -

Chairman of the Conference Organizing Committee:
Dr. S.L.Mandel'shtam

Responsible editors of the Spectroscopy Conference Transations:
Dr.V.K.Prokof'ev & Dr.A.R.Striganov

---

*While in the original of the present issue of the Bulletin the conference is designated as the Eleventh All-Union Conference on Atomic Spectroscopy, in Vol.22, Nos. 9 and 11 it is called the Eleventh Conference on Theoretical Spectroscopy. It will be evident from the Opening Address and the nature of the papers that the latter term is more truly descriptive. - Trans. Editor.

OPENING ADDRESS

- S.L.Mandel'shtam

Comrades, our Eleventh All-Union Conference on Spectroscopy is meeting a few days after celebration of the Fortieth Anniversary of the Great October Revolution. Accordingly, the Commission on Spectroscopy at the USSR Academy of Sciences and the organizing committee have decided to dedicate our Conference to this great date in history.

Spectroscopy, like all other branches of science, has scored some very noteworty achievements in our country during these forty years. A number of very important spectroscopic discoveries have been made in the USSR - I have in mind combined scattering of light [the Raman effect] and the Vavilov-Ćerenkov effect - and there have been many important contributions to the progress of the spectroscopy of atoms and molecules - it is enough to mention here the work of D.S.Rozhdestvenskii, S.I.Vavilov, G.S.Landsberg, V.A.Fok, A.N.Terenin, V.N.Kondrat'ev and their numerous colleagues and students. There have been great developments, too, in the field of applied spectroscopy - atomic and molecular spectroscopic analysis has become an invaluable tool in scientific research and industrial quality control. By now several thousand spectroscopists are at work in the scientific institutes, universities and industrial plants of the USSR. We have seen the creation of an instrument-building industry that is capable of supplying us with first-class spectroscopic equipment.

Later we shall hear the special report of S.E.Frish devoted to the achievements of Soviet spectroscopy during the past four decades.

This year Soviet physics and all world science, and particularly, we spectroscopists, have suffered a great and irreparable loss: the death of Academician Grigori Samuilovich Landsberg, outstanding scientist, unchallenged leader of Soviet spectroscopists, organizer and moving spirit of the Commission of Spectroscopy and our conferences.

G.S.Landsberg must be credited with outstanding discoveries and the creation of new fields of spectroscopic research; his name is indissolubly linked with the development in our country of spectroscopic analysis, one of the most important applications of physics.

We shall most acutely feel this great loss during the time of our conference, for everyone will remember the important part our late colleague played in insuring the success of past conferences.

I request everyone to rise in honor of his memory.

* * *

Our Eleventh Conference differs from preceding conferences. The number of participants and reports presented at the last few conferences increased rapidly from year to year. The last conference, held in [illegible], attracted about [illegible] participants and heard 300 reports. In view of this the conference had to be held in sections and this prevented many of those present from hearing reports of special interest to them. Hence the Commission on Spectroscopy decided to try in the future to hold separate conferences devoted to the physical problems of atomic and molecular spectroscopy and conferencesdevoted to the applications of spectroscopy, alternating them at yearly intervals. The present, Eleventh Conference is concerned with physical problems, the next, the Twelfth Conference, will be devoted to applied spectroscopy. It must be noted, however, that the program of the present conference does not comprise all problems of physical spectroscopy but only some of them, namely, theoretical and

experimental determination of atomic constants, plasma spectroscopy, spectroscopy of crystals (including the exciton problem), spectroscopy of transition states (vapor-liquid-solid) and investigation of molecular interactions by spectroscopic methods. At the same time, in contrast to preceding conferences, the program of our conference includes the topic of molecular luminescence. The problems of molecular luminescence are inseparable from those of molecular spectroscopy in general and hence it is natural to include them in our program.

Obviously, the distinction between problems and topic pertaining to physical spectroscopy and those pertaining to applied spectroscopy is in many cases purely arbitrary. It must be borne in mind that it is planned to present at the Twelfth Conference, which will be devoted to applied spectroscopy, reports on research of a physical character, that is, on theoretical investigations that form the basis for practical analytic procedures. In many cases in deciding whether a given report should be presented at the Eleventh or the Twelfth Conference, a clear cut decision was indeed difficult.

In making up the agenda of the conference the organizing committee also departed from the traditional practice of separating reports into molecular and atomic sections. In recent years there has appeared a dangerous split of spectroscopists into "molecular" and "atomic". In order to allow all conferees to hear and discuss reports of interest to them in all branches of spectroscopy, it was decided to make all morning meetings joint sessions. At all these meetings, there will be presented reports on various problems of atomic and molecular spectroscopy that are of more general interest. The evening sessions will comprise two sections that will hear reports of a more special nature, but these sections too will not have a pronounced "atomic" or "molecular" slant.

In examining the agenda of our conference, we can note the welcome fact of an increase in the number of theoretical investigations. As we know, many theoretical physicists in recent years have been diverted to other problems, much to the disadvantage of spectroscopy as a whole. At present the situation is changing - although slowly - for the better. There is an increase - perhaps not as rapid as one could wish - in a number of investigations carried out by means of electronic computers which are often of inestimable aid to our theoreticians.

We shall hear a large number of reports devoted to the exciton problem. Whereas at the Lvov Conference, there were only a few reports on this problem, here we have more than ten theoretical and experimental communications devoted to this interesting topic.

Other topics, such as the spectroscopy of crystals, investigation of molecular interactions and molecular luminescence, are well represented. The agenda is somewhat weaker as regards reports on the spectroscopy of atoms.

As in previous years there are very few investigations in the field of radio-spectroscopy. Unfortunately, this apparently characterizes the situation in this field in the USSR: this important branch of spectroscopic investigation is inadequately developed in our country.

To our deep regret the work of astrophysicists is not represented at the conference.

Although the subject of equipment will be considered primarily at the forthcoming Twelfth Conference, the organizing committee deemed it desirable to include in the present agenda a brief informative report on new spectroscopic instruments. We shall also hear a report on the documentation of infrared spectra. The organization of such documentation in the USSR is one of the urgent problems faced by the Commission on Spectroscopy and it would be desirable to have an exchange of views regarding the most suitable form of such documentation.

Further, in considering our agenda it should be recalled that we are separated from the last conference not by two years, as usual, but only be a little more than one year. Nevertheless, as you see, the agenda of the Conference has a plethora of important and interesting reports. Hence we can speak with justifiable pride of the high level of spectroscopic investigations in our country. At the same time, it will be seen from the conference agenda that there are a number of serious gaps in the spectroscopy research front, that in some fields we seriously lag behind world science. The Presidium of the USSR Academy of Sciences has classified the question of the "Atomic and molecular spectroscopy and its applications in investigation of the structure and composition of matter" as among the most important facing Soviet science. Under the guidance and with the participation of Academician G.S.Landsberg there was elaborated a five year plan for fundamental research in this field, combining the activities of a number of institutes of the USSR Academy of Sciences, the Academies of Sciences of the Union Republics, and various institutions of higher learning and industrial institutes. There has been organized an advisory committee whose function will be to coordinate all these investigations.

No small part of this work of coordination are our conferences, including the present one. We trust that the present conference will make a serious contribution to the further development to spectroscopic research in the USSR.

In recent years Soviet spectroscopists have strengthened their ties with their colleagues abroad. Soviet spectroscopists participated in international and national conferences in England, the German Democratic Republic, the Federal German Republic, Holland, Italy, the United States of America, France, Czechoslovakia and the Federal Republic of Yugoslavia.

With a view to strengthening these bonds, at the invitation of the USSR Academy of Sciences, there is participating in our 11th Conference a large group of foreign scientists: Prof.Badareu (Rumania), Prof.Bartels (Germany), Prof. & Mme.Grillot (France), Prof.Dieke (USA), Prof.LeConte (France), Prof. Lochte-Holtgreven (Germany), Prof.Ritchel (Germany Democratic Republic), Prof. Thompson (England), Prof.Janke (German Democratic Republic), Prof.Hadji (Yugoslavia), Prof.Chou Tun-Tsin (Peoples Republic of China).

Allow me, in the name of all those present, the organizing committee and the Commission on Spectroscopy, to extend a heartfelt welcome to our dear guests.

I wish us all success in our work. I hereby declare the Eleventh Conference on Spectroscopy open.

FORTY YEARS DEVELOPMENT OF SOVIET SPECTROSCOPY

- S.E.Frish

Comrades, less than a month ago we celebrated a historic occasion - the Fortieth Anniversary of the Great October Socialist Revolution. During this period the Soviet Union has made gigantic strides forward in the realm of science. Like other sciences, Soviet spectroscopy too has been greatly advanced.

Now, in retrospect, it may be instructive to trace the development of Soviet optics and to see which specific conditions tended to further this development and which to retard it. We must learn from our mistakes as well as from our achievements, if we want to raise Soviet science to still greater heights.

In examining the development of optics in our country, we must note that immediately after the great Socialist Revolution there were formed, in Moscow and Leningrad, groups of scientists who concerned themselves with the various branches of optics, particularly spectroscopy. The names of three outstanding Soviet physicists - D.S.Rozhdestvenskii, L.I.Mandel'shtam and S.I.Vavilov - at once come to mind in connection with these groups. It is not my intention to give you a detailed account of the evolution of these groups or to relate the entire history of the beginning and subsequent development of Soviet spectroscopy. To tell the story as it deserves to be told would take too long, while a mere recital of facts would be dull and not particularly useful. I shall therefore take the liberty of dwelling mainly on the work of the group headed by D.S.Rozhdestvenskii, partly because I am most familiar with it and partly because it offers an excellent illustration of the specific conditions under which Soviet optics developed.

Rozhdestvenskii grasped at once the tremendous potentialities offered by the Soviet Government for scientific and technological progress. Late in 1918 - hardly more than a year after the October Revolution - he and A.F.Ioffe approached the Commissariat of Education, as it was then known, with a request for establishment of two new physics institutes: an Optical Institute and a Physico-Technical Roentgenological Institute. The Soviet Government welcomed this initiative on the part of the two scientists and despite the difficulties by which it was beset - the Civil War was then at its height - founded both institutes.

Rozhdestvenskii was one of the few pre-revolutionary scientists who did not dwell in the ivory tower of theoretical abstractions but who clearly realized the need for close links between pure and applied science. Moreover, Rozhdestvenskii saw this relation not in terms of occasional practical application of scientific discoveries, but as a close, sustained and forward-looking collaboration. He realized that science must generate new ideas which could be used for technology, while technology, for its part, must give science both new problems to solve and new and powerful tools to solve them with.

In organizing the Optical Institute, Rozhdestvensky had in mind an establishment of an entirely new type unknown in Czarist Russia. As he himself wrote later:"We were all enthusiastic supporters of the same idea: to make the Optical Institute into a new type of institution, one in which scientific and technological functions would be inextricably linked together."

These words serve to emphasize the first basic feature of Soviet science - the deep organic bond that exists between science and technology, a bond whose purpose is not to solve some of the limited, purely technical problems of the day, but to offer wider scope for the development of both science and

technology. So close an interrelationship is possible only in a socialist country, where technological development is not governed by the mercenary interests of capitalist enterprises, and there can be no doubt that it constitutes one of the basic causes of the successes of Soviet science.

The second distinguishing feature of the evolution of Soviet science in general, and Soviet optics in particular, is the planning of research. The planning of future scientific work is a highly complex matter. Before the revolution, the generally accepted notion was that "pure" science was in a special position and that its development could not be planned but must be left to the creative genius of individual scientists.

Those of us who were studying under Rozhdestvenskii in the early years of the Revolution have never forgotten that from the time the Optical Institute was organized Rozhdestvenskii was to be found in the ranks of the scientists who were already beginning to insist that scientific research must be planned. As he himself has written, "This question (scientific planning) is fraught with the new forms and new tempoes of progress of both industry and culture."

Planning has fully justified the hopes that were placed in it; we are now fully aware that neither the conquest of atomic energy, nor the launching of the first man-made satellite (the Sputnik), nor the achievements of Soviet optics and spectroscopy would have been possible if Soviet science had been permitted to develop chaotically, without careful planning. At the same time, I should like to emphasize that broad planning can be closely correlated with individual creative initiative. Indeed, plans for future research can be drawn up only with the enlightened assistance of broad scientific groups. At the Academy of Sciences of the USSR nowadays an increasing role is being played in such planning by the various commissions, which in turn maintain contact with even wider scientific circles. A great deal is being done to prepare monographs on separate scientific problems. In particular, our own Commission on Spectroscopy prepared a monograph on "Atomic and molecular spectroscopy and its applications in investigation of the structure and composition of matter". The Scientific-Technical Council of the Ministry of Higher Education is drawing up scientific research plans on a large scale. Such planning is bound to be successful because many groups of scientists are asked to take part in it.

Another distinguishing characteristic of scientific research in the Soviet Union is the close liaison between the different sciences and the coordination of the work of scientists in different branches. Historically, this brings us back once again to the time when the Optical Institute was organized, and it must be said that Rozhdestvenskii at that early stage raised the question of the close bond between optics and all other sciences, especially chemistry. Aware of the link between physics and chemistry, divining the future use in chemistry of refined and exact spectroscopic methods, he said that contact between the two sciences would give rise to "a practical chemistry, which will understand the processes it studies in minutest detail and which will manipulate the atom as a driver steers his car."

Since then, close contact between allied disciplines has become a characteristic feature of Soviet science and must be counted among the causes of its success.

I realize that I have dwelt at some length on the activities of D.S. Rozhdestvenskii and his school and on their contribution to the founding of Soviet optics and spectroscopy; in doing so I had no intention of minimizing the part played by other scientists and other groups. Our Soviet science is a collective undertaking, developed jointly by groups of scientists represent-

ing many schools and trends of thought. Historically speaking, Rozhdestvenskii was connected with the beginnings of atomic spectroscopy and the early stages of the optical industry. Other outstanding Soviet scientists had a hand in the development of other branches of optics and spectroscopy; for example, L.I. Mandel'shtam was prominently associated with laying the groundwork of molecular spectroscopy and using spectroscopy to study the properties of matter; S.I. Vavilov with furthering work on luminescence and certain other branches of optics; and G.S.Landsberg with developing spectrum analysis and introducing spectroanalytic methods into industry.

As you all know, L.I.Mandel'shtam and G.S.Landsberg, working independently, at the same time as the Indian physicist Raman, discovered the phenomenon of combined light scattering [the Raman effect]. Further development of their work opened a new field of application of optical methods to the investigation of molecular structure and the structure of matter in different physical states. The new [Raman] technique became one of the most widely used procedures for investigating intermolecular forces and there is a tremendous literature on it in all countries. Its use led to particularly good results in ascertaining the structure of complex organic molecules. Indeed, the development of modern molecular physics and modern chemistry, particularly organic chemistry, is unthinkable without it.

In addition to this new method, other methods of molecular spectroscopy, based on light absorption and fluorescence, are being successfully evolved in the Soviet Union. As time will not allow me to describe them all, I will merely mention E.F.Gross's research on absorption spectra, which led to the discovery of the exciton, and A.N.Terenin's investigation of surface layers of solids by optical methods and of the adsorption mechanism and the nature of catalytic processes. Work on molecular spectroscopy accounts for a large portion of all spectroscopic research in the USSR.

S.I.Vavilov's school has been concerned mainly with the luminescence of liquids and solids, but, in speaking of its work, one must also mention a number of investigations into the fundamental classical and quantum properties of light. These include S.I.Vavilov's studies of the radiation of dipole and quadrupole emitters and the fluctuations of the light flux, and the discovery of the Vavilov—Čerenkov effect.

Since the thirties, the Commission on Spectroscopy of the Academy of Sciences of the USSR, headed for many years by G.S.Landsberg, has played an important part in the development of Soviet spectroscopy.

Today spectroscopy has expanded far beyond its original narrow scope. Modern spectroscopy helps physicists to study the structure of matter in all its states - gaseous, liquid and solid. It enables them to ascertain the detailed structure of atoms and molecules and to study the properties of atomic nuclei by means of the so-called hyperfine structure of spectroscopic lines. Spectroscopic methods are of the greatest usefulness in investigating fast processes. New radiospectroscopic methods, closely akin to those of conventional spectroscopy, have been evolved. Important scientific work in all these branches is now in progress in the USSR.

The development of spectroscopic analysis is of tremendous practical value. Although spectroscopic analysis problems are not on the agenda of this Conference, I should like to say a few words about a feature of the development of that analysis peculiar to the Soviet Union. From the very outset, spectroscopic analysis techniques in our country were elaborated by optical physicists, who worked simultaneously in several branches of spectroscopic theory. As a result, the methods of applied spectroscopic analysis were developed on a sound scientific basis. Consequently, correct and original solutions were

found to a number of complex problems of modern spectroscopic analysis and entirely new procedures were evolved, such as evaporation for purity-analysis of high-melting point metals, isotopic equalization for emission analysis of gases in metals, electrodeless high-frequency excitation for quantitative analysis of gas mixtures, etc.

These achievements in the field of spectroscopy would have been impossible without the development of instrument-building technology. In recent years, our industry has initiated production of a large number of completely modern spectroscopic instruments. It gives me particular satisfaction to note that diffraction gratings are now being fabricated in the USSR. F.M.Gerasimov has made a whole series of truly first-class gratings that throw up to 60% of the incident light into the desired order.

In mentioning our achievements with legitimate pride, we nonetheless must not close our eyes to our past and present shortcomings, with a view to remedying them as quickly as possible.

One of these shortcomings, in my opinion, is the as yet inadequate contact between the scientists working in the field of spectroscopy and engineers in the industry turning out spectroscopic instruments. As I have said, one of the founders of our optical industry, D.S.Rozhdestvenskii, advocated the closest possible liaison between the two. Regrettably, at times we tend to forget this wise precept. Similarly, we do not always maintain the necessary contacts with related sciences and the link between experimental workers and theoreticians is not always what it should be. As a result, certain new methods and lines of research have been evolving slowly. For example, the introduction into spectroscopy of modern photoelectronics has not proceeded at a sufficiently rapid pace, radiospectroscopy has not made sufficient progress, not enough use has been made of computers to solve problems of theoretical spectroscopy.

There have been shortcomings in scientific planning as well. The Academy of Sciences of the USSR should maintain better liaison with the Academies of the Union Republics and with the various institutions of higher learning. The general development of science in all the Union Republics, attained by dint of fraternal endeavor, is a prerequisite for the growth of Soviet culture. We should meet each other more often and share our experience.

We should establish closer contacts with scientists in the People's Democracies and with our colleagues in other countries. This Conference differs from the preceding ones in that it is attended by guests from abroad. I trust that our friendly encounters and discussions will be useful to all participants and will help to strengthen the cause of peace.

Spectroscopic conferences have always played an important part in advancing our science. Personal meetings and exchanges of views give a fresh impetus to creative research. We have accomplished much in forty years, but still more remains to be done.

It is my hope that the present Conference, too, will clear the way for further achievements by Soviet science - a science whose objective is the welfare of the Soviet people.

quently, n_{eff} according to Eq.(1), is greater than n for valence electrons by a factor of four.

Even from this it will be evident that separation of electrons into free and bound electrons is highly arbitrary. In a number of cases the inner electrons undoubtedly take part in the plasma oscillations. Under these conditions the object of theory is to consider all the atomic electrons ("inhomogeneous plasma") jointly and thereby determine to what extent the core electrons are involved in the plasmons. At the same time, through this approach one can determine what optical effects may be associated with plasmons. In homogeneous plasma direct interaction of plasmons with light is impossible inasmuch as in such plasma the plasma oscillations are longitudinal. In inhomogeneous plasma, however, longitudinal and transverse waves are not separable from each other.[8] Hence in principle one can have absorption of a photon with excitation of a plasmon and, vice versa, radiative decay of a plasmon. Finally, even in a homogeneous plasma plasmons can be indirectly evinced in optical phenomena inasmuch as in entering into Coulomb interaction with an optically active electron they modulate its state.

These are the problems that will be considered briefly in the present report (for details, see Refs.9 & 10).

2. First we must establish the systematics of plasma levels in an inhomogeneous degenerate electron gas formed by all the electrons of the crystal atoms and the symmetry properties of the functions describing a plasmon, for example, perturbations of the density $n(\mathbf{r},t) = n_0(\mathbf{r}) + n_1(\mathbf{r},\ t)$.

Fundamental to the theory is the fact that plasmons can exist only for long wavelengths, i.e., if the n gradients are sufficiently small. For such plasmons in a homogeneous plasma there have been developed methods that we can utilize in our case.

First, we can proceed from the kinetic equation for electrons (in case of necessity from the quantum equation), utilizing the smallness of the perturbation, linearize the problem, go over to a set of equations for moments of distribution in velocity space and limit our consideration to the first equations of this system[3] (such cut off of the system is possible if the gradients in the plasmon wave are small). This approximation may be termed the "quasi-hydrodynamic" approximation.[3] In the case of inhomogeneous plasma in a lattice, we obtain a linear set of equations with coefficients depending on $n_0(\mathbf{r})$ and hence having the periodicity of the lattice. Hence the solutions of this equation (just as, for example, for the Schrödinger one-electron equation in a crystal) must be of the form

$$n_1(\mathbf{r}, t) = \exp[i(\mathbf{kr} - \omega t)]\, u_{\mathbf{k}}(\mathbf{r}), \tag{3}$$

where k is the quasiwave vector and $u_{\mathbf{k}}(\mathbf{r})$ varies periodically with the lattice period.

To find $u_{\mathbf{k}}$ we must solve equations in which n_0 is replaced by the unperturbed distribution taken, for example, from the Thomas-Fermi method in tabulated form. A number of properties of the equations can be deduced simply from the attributes of the solution (3).[9]

We can, however, have recourse to a somewhat more rough but much more convenient "hydrodynamic approximation".[2,11] Namely, one can treat the fluctuations of the gas density by means of the usual hydrodynamic equations with the equation of state for a Fermi gas. In the case of a homogeneous plasma (which serves for verifying the method), we also obtain the dispersion relation (1); however, in the second term in the right hand side, which, as noted above is small, there appears the incorrect coefficient 5/9. This serves to indicate the inaccuracy of the approximation.

In any case to establish the systematics of the terms, we first use the procedure of dividing the lattice into individual cells[12,13] and then with appropriate boundary conditions at the surface of the cells limit the region under consideration to one cell. Expanding the solution in spherical functions, we obtain the following results.

The frequency spectrum of the plasmons in the crystal consists of bands. The state inside a given band is characterized by the wave vector k. In it are superposed different internal oscillations of the cell characterized by different numbers l and m. Only with k = 0 does there remain one definite internal oscillation. The band itself may therefore be characterized by the indices n_r, l_0 and m_0 of that state of the single cell into which the plasmon transforms in the limit $k \to 0$. Here l and m are the azimuthal and magnetic quantum numbers of the electron density oscillations in the cell and n_r is an analog of the radial quantum number.

The utilized approximation is valid only for sufficiently small density gradients (for "long wavelengths" - see above). Hence it is probable that actually the lowest band is realized. States with higher energies are not realized and go over into individual electron excitations.

3. Thus we obtain the plasma wave in the form of an electron density wave, distributed over the entire crystal and modulated within the bounds of each cell, where, in general, the oscillations may have a dipole character (l = 1), so that direct interaction with light is in general not precluded. However, if we consider the interaction with light from the standpoint of the quasi-classical approach, the result is essentially negative. One can, for example, either simply calculate the emission of light from the given current distribution or develop a more general scheme reminiscent of perturbation theory in quantum mechanics.[9] It is found that the law of conservation of momentum requires for an "optically active plasmon" that k be small (it must be equal to k for light). At the same time, interaction with light can be realized only in the case when, within the limits of the cell, dipole oscillation is represented in the plasmon (l = 1). It is found that these two conditions are incompatible for the lowest band of the plasmon spectrum ($l_0 = 0$). They can obtain only for a higher band with $l_0 = 1$. As already noted, however, it is probable that this band is not realized inasmuch as the corresponding plasmons are too rapidly transformed into individual electron excitations.

If nevertheless we assume that an optically active state is realized, we can calculate its radiation width Γ_r as the probability of disappearance of the plasmon and its transformation into a photon. It is found that this probability is the same as for isolated atoms (taken in an amount equal to the number of atoms in the crystal), but that the dipole moment is proportional to the effective number of electrons per cell participating in the plasmon oscillation. Its value can be determined only through numerical solution of the equations. From the characteristic energy losses we know, however, that in some elements (Cu) this number is substantially greater than the number of valence electrons. From the standpoint of the principle involved, it is interesting to note that in such a radiative transition we would have coherent interaction of many electrons with light. The intensity would be proportional to n^2_{ef}. Even here, however, the radiation width is considerably smaller than the width due to transition to individual electron excitations: in the majority of cases the plasmon disappears in a radiationless transition.

4. Let us now turn to optical processes in which plasmons may be manifested indirectly. The fact that a plasmon is capable of strong interaction with an individual electron (as is evinced by the great width of the plasmons levels) must assure substantial indirect participation of plasmons in optical

transitions of individual electrons. Here there is no need to take into account inhomogeneity of the plasma and we can speak of transverse plasmon waves in a homogeneous plasma. The Coulomb field of such a save perturbs the state of an individual electron, modulating with the plasmon frequency ω. Hence in optical interactions of this electron there may be evinced the plasmon frequency and so on.

We have considered three processes of this type[10]; in each case we have assumed that the initial state of the individual electron participating in the process is the K state with a large effective nuclear charge $Z_{eff} \gg 1$, and that the plasmon energy is much smaller than $E_0 = \frac{1}{2} \cdot \frac{me^4}{\hbar^2} Z_{eff}^2$ and than the energy of the final state of the electron.

A. Excitation of a plasmon with absorption of an x-ray photon and its influence on the fine structure of the x-ray absorption edge. From the standpoint of the perturbation theory this process consists of the following: the x-ray photon is absorbed by an inner shell electron of one of the atoms; as a result the electron is excited to an intermediate state. From this intermediate state the electron goes over into a state in the continuum, exciting a plasmon through Coulomb interaction. The cross section σ for the process is inversely proportional to Z_{eff}^2 (just as the cross section σ_0 for simple absorption of a photon), where Z_{eff} is the effective nuclear charge for the absorbing electron in the initial state. It is particularly great for absorption by the outer electrons: $Z_{eff} \sim 1$. The final equation is

$$\frac{\sigma}{\sigma_0} = \frac{a_0 k_c}{\pi} \cdot \frac{\alpha(E')}{\alpha(E)} \left(\frac{E'}{E}\right) \tag{4}$$

where

$$E = \hbar\omega_0 - E_0; \quad E' = E - \hbar\omega;$$

[illegible]

(here $\alpha(E)$ is the level density for the continuum, ω_0 is the photon frequency, ω is the plasmon frequency, k_c is the maximum plasmon momentum and $a_0 k_c \sim 1$). This equation shows that if in the electron spectrum close to the edge of the absorption band there is a region of enhanced level density $\alpha(E)$, i.e., an absorption maximum, there must also exist additional maxima connected with excitation of plasmons and displaced relative to the normal position by an amount equal to the plasmon energy.

B. Raman scattering with participation of a plasmon. The usual scattering of an x-ray photon by one of the inner electrons may be accompanied by transfer of part of the photon energy to a plasmon, which in this case is excited as a result of Coulomb interaction with the scattering electron. This will lead to the appearance in the scattered radiation spectrum of a line shifted by the magnitude of the plasmon energy. The cross section σ for the process relative to the cross section for simple scattering by the entire electron shell [illegible] will be

$$\frac{\sigma}{\sigma_0} = [illegible] \tag{5}$$

(here $\hbar\omega$ [illegible] $\hbar\omega_0$ [illegible] E_n [illegible] E_n and ζ is the number of electrons in the shell; for the K-shell ζ = 2). Thus here too the cross section has an appreciable magnitude. There is a definite correlation between the scattering intensity and the frequency shift.

C. Light absorption at the plasmon frequency. Regardless of the "optical activity" of the plasmon, a light photon with an energy equal to the plasmon energy may excite a plasmon not directly but by interacting with one of the shell electrons, which then through Coulomb interaction with the other electrons will excite the plasmon. It can be shown that the probability of such absorption is the same as for an atom with the square of the matrix element equal to

$$x_{\mathrm{eff}}^2 = \left(\frac{1}{e}\right)^2\left(\frac{4}{3}\right)^4 \frac{\text{[illegible]}}{V_0}\cdot\frac{\text{[illegible]}}{\hbar^3\omega}\cdot\frac{\text{[illegible]}}{Z_{\mathrm{eff}}^4}$$

(here V_0 is the atomic volume), i.e., is less than usual for an atom by a factor of Z_{eff}^4.

The probability of this process rises with decreasing Z_{eff}. Hence it may be assumed that with participation of the outer atomic electrons, the probability of such excitation of a plasmon is very small. This means that separation of plasmons into optically active and optically inactive is very arbitrary and that excitation of plasmons upon absorption of light of frequency ω must occur with considerable probability.

Other effect in addition to those considered above are possible: for example, emission of an x-ray photon in an $ns \to n's$ transition with simultaneous excitation of a plasmon (without which this process is apparently impossible).

Thus investigation of different optical effects may be useful for establishing the reality of plasmons and determination of their properties. One should exercize due caution, however, in identifying other observed processes with those considered above inasmuch as qualitatively such processes in most cases are also possible, when the role of the plasmon is assumed by a second electron.

"P.N.Lebedev" Physical Institute,
Academy of Sciences of the USSR

References

1. D.Pines, Rev.Mod.Phys., 28, 194 (1956). Russian trans. in Usp.fiz. nauk, 62, 399 (1957)
2. I.I.Goldman, Zhur.eksp.i teor.fiz., 17, 681 (1947).
3. V.P.Silin, Zhur.eksp.i teor.fiz., 23, 641, 649 (1952); Trudy (Proceedings) "P.N.Lebedev" Physical Institute, USSR Acad. of Sci., 6, 201 (1955).
4. D.N.Zubarev, Zhur.eksp.i teor.fiz., 25, 548 (1953).
5. P.A.Wolff, Phys.Rev., 92, 18 (1953).
6. H.Kanazawa, Progr.Theor.Phys., 13, 227 (1955).
7. H.Frohlich & H.Pelzer, Proc.Phys.Soc.A, 68, 525 (1955).
8. A.A.Vlasov, Teoriia mnogikh chastits (Many particle theory), Section 48, M.-L., 1950.
9. E.L.Feinberg, Zhur.eksp.i teor.fiz., 34, No.5, 1125 (1958).
10. I.I.Sobel'man & E.L.Feinberg, Zhur.eksp.i teor.fiz., 34, 494 (1958). (Trans., JETP, 34, 339.).
11. F.Bloch, Z.Phys., 81, 363 (1933).
12. E.Wigner & F.Seitz, Phys.Rev., 43, 804 (1933).
13. J.Slater, Revs.Mod.Phys., 6, 209 (1934).

EXCITATION OF SPECTRAL LINES IN THE NEGATIVE GLOW OF A GAS DISCHARGE

- S.E.Frish & I.P.Bogdanova

It has been shown in a number of investigations that in the vicinity of the cathode there is an excess of fast electrons, as compared with the number of such electrons in the positive column of the gas discharge. This was shown most convincingly by Kagan & Malyshev[1] by means of probe measurements. The presence of such fast electrons is also substantiated by spectroscopic data, namely, by the fact that there are present in the negative glow ionic lines that are normally absent from the positive column spectrum. Fast electrons must obviously have a certain influence on the excitation of neutral atoms. Hence in the negative glow (as compared with the positive column) one may expect a different energy distribution of atoms and, consequently, a different distribution of intensities in the spectrum. We carried out observations of gas spectra emitted in a hollow cathode, for the purpose of detecting these distinctive features of the negative glow.

A hollow cathode was chosen in view of the higher intensity of luminescence inside it as compared with the glow of gases close to a flat electrode; the choice was also dictated by considerations of experimental convenience. The glow of gases in a hollow cathode as regards basic characteristics is a typical negative glow. The experiments were carried out with discharges in neon.

In the measurements of Ref.1, Bogdanova & Chen Ki-T'hek[2] used a discharge tube with a hollow cathode 15 mm in diameter and 130 mm in length; inside the cathode there was a porcelain disc which could be moved by means of a magnet. This allowed of varying the length of the luminous column and thereby regulating the amount of self-absorption of the lines. The values of $N_i f_{ik}$ for the lower levels associated with the observed spectral lines were then calculated from the reabsorption by the procedure described in Ref.3. Finally, the concentration N_i of atoms was determined from the experimental values of $N_i f_{ik}$ and the known values of f_{ik}. The measurements were carried out in the range of discharge currents from 0.7 to 4.4 ma/cm^2 and gas pressures from 0.5 to 1.1 mm Hg. Thus there were determined the concentrations of neon atoms in the $3s^3P_0^0$-, $3s^3P_1^0$-, $3s^3P_2^0$- and $3s^1P_1^0$- states. The results of measurement for different discharge current densities at a pressure of 0.7 mm Hg are shown graphically in Fig.1.

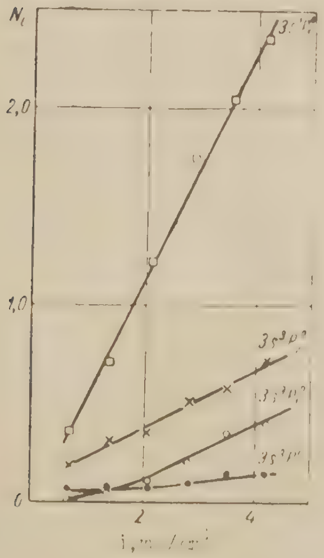

Fig.1. Concentration of neon atoms in the $3s^3P_{0,1,2}^0$- and $3s^1P_1^0$-states in a hollow cathode at p = 0.7 mm Hg.

For the higher energy states, pertaining to the $2p^53p$ electronic configuration of neon, the population of the levels was determined from the absolute line intensities. The absolute intensities were found by comparison of the line intensity with the intensity of emission of a tungsten filament, the temperature of which was measured by means of a pyrometer. Due account was taken of reabsorption. The concentrations of neon atoms in the $3p^1S_0$-, $3p^3P_2$- and $3p^3D_3$-states were determined in this manner. The results are shown in Fig.2.

Similar measurements were carried out for the positive column (Figs.3 & 4) in the same current density and pressure ranges. In addition, for the positive

column the electron temperature T_e was determined and the electron concentration N_e was measured by the probe procedure.

For the positive column the measured populations of the $3s$ and $3p$ levels differ from the values that should ostensibly obtain with a small contribution from collisions, when the emptying of the levels occurs primarily through spontaneous transitions, and from the values that would obtain with statistical equilibrium (large contribution from collisions). In the case of a Boltzmann distribution with $T = T_e$ the concentration of neon atoms in the $3s^3P^0_2$ state under our conditions should presumably be $3.0 \cdot 10^{14}$ cm^{-3}, whereas according to our measurements the concentration is $1.8 \cdot 10^{11}$ cm^{-3}. The ratio of populations of the $3s^3P^0_{2,1,0}$ and $3s^1P^0_1$- states should be 1 : 0.6 : : 0.19 : 0.57, whereas according to the measurements the relative values are 1 : 0.19 : 0.13 : 0.08. Thus the equilibrium population of the $3s^1P^0_1$ level should have been 7 times greater than that actually observed.

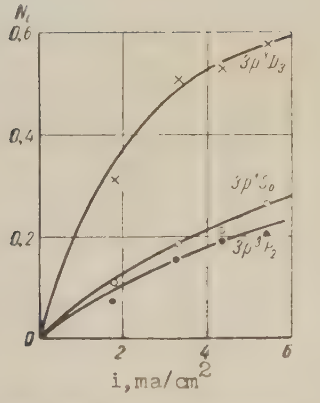

Fig.2. Concentration of neon atoms in the $3p^1S_0$-, $3p^3P_2$- and $3p^3D_3$-states in a hollow cathode at p = 0.7 mm Hg.

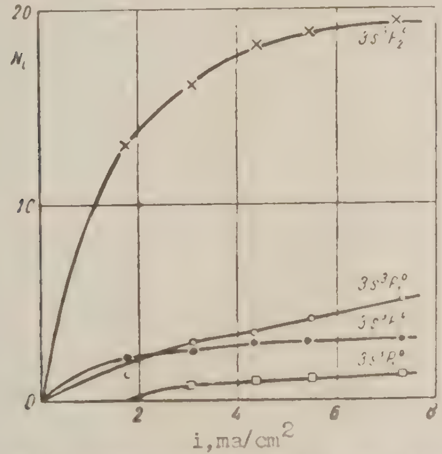

Fig.3. Concentration of neon atoms in the $3s^3P^0_{0,1,2}$ and $3s^1P^0_1$ states in the positive column at p = 0.7 mm Hg.

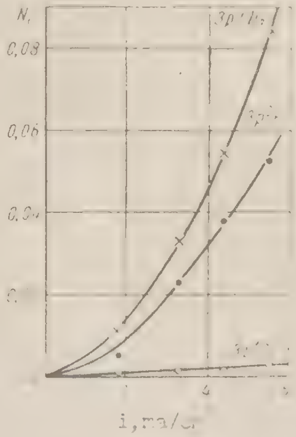

Fig.4. Concentration of neon atoms in the [illegible] and [illegible] states in the positive column at p = 0.7 mm Hg.

The level population in the hollow cathode differs even more from the equilibrium value. The $3s^1P^0_1$ level (the highest of the four [illegible] levels) is most densely populated. In the case of an equilibrium distribution this would not be true at any temperature. The absolute value of the concentration of atoms in $3s$ states in a hollow cathode is somewhat lower than in the positive column at the same discharge current density. On the other hand, the occupation of the $3p$ states in the hollow cathode is approximately an order of magnitude higher than in the positive column. This substantiates the hypothesis that a group of fast electrons is present in the hollow cathode. These fast electrons give rise to an anomolously high population of the high-lying levels pertaining to the $2p^53p$ electron configuration. The character of the increase

of population of the $3p$ levels with increasing discharge current density gives reason to assume that in a hollow cathode the $3p$ levels are excited primarily directly from the $^1S_0$ ground state.

Scientific Research Physical Institute
Leningrad State University

References

1. Iu.M.Kagan & G.M.Malyshev, Zhur.tekh.fiz., 23, 950 (1953).
2. I.P.Bogdanova & Chen Ki-T'hek, Optika i spektroskopiia (Optics and Spectroscopy), 2, 681 (1957).
3. S.E.Frish & I.P.Bogdanova, In sb. "Pamiati S.I.Vavilova" (Symposium dedicated to the memory of S.I.Vavilov), M.-L., 1952.

ADIABATIC APPROXIMATION IN THE QUANTUM THEORY OF ATOMS

- M.G.Veselov and I.B.Bersuker

1. Complete separability of variables is usually assumed when performing quantum mechanical calculations involving many-electron systems; i.e., the wave function of the system is constructed of one-electron functions. The use of one-electron states in complex systems is justified by replacing the potential in which the individual electrons move, a potential which depends on the coordinates of all the electrons, by an effective field averaged in some way over the coordinates of all the electrons other than the one being considered.

Simple physical considerations will show that the errors introduced by this averaging process differ for the inner and outer electron shells. The velocity differences between the optical and core electrons make it reasonable to assume that the electron cloud of the core responds adiabatically and non-inertially to the motion of the relatively slow outer electrons. We therefore propose to break up the quantum mechanical many-electron problem into two stages, in the same way as the motion of the electrons and the nucleus are treated in the theory of molecules. The total wave function ψ of the system is obtained by multiplying the wave function U_n of the core electrons by the wave function φ of the $N-n$ outer electrons. First, we consider the quantum mechanical problem of the core electrons for various space configurations of the outer ones. We have

$$\left[H_{\text{core}} + \sum_{i=1}^{n} \sum_{k=n+1}^{N} V(r_{ik})\right] U(r_1, \ldots, r_n; r_{n+1}, \ldots, r_N) =$$

$$= W(r_{n+1}, \ldots, r_N)\, U(r_1, \ldots, r_n; r_{n+1}, \ldots, r_N). \qquad (1)$$

Here H_{core} is the core-electron Hamiltonian minus the interaction with the outer electrons; the double sum $\Sigma\Sigma V(r_{ik})$ expresses this interaction. Obviously, U contains the coordinates of the outer electrons as parameters, while the energy W of the core is a function of these coordinates and plays the role of a potential energy in the outer-electron wave equation:

$$[H_{\text{out}} + W(r_{n+1}, \ldots, r_N)]\, \varphi(r_{n+1}, \ldots, r_N) = E\varphi(r_{n+1}, \ldots, r_N), \qquad (2)$$

Here H_{out} is the outer-electron Hamiltonian without the interaction with the core electrons, and E is the total energy of the system. In Eq.(2) we drop terms containing derivatives of the function with respect to the outer electron coordinates.

This approach is a sort of incomplete separation of variables and includes the polarization of the core by the outer electrons and the inverse effect of this polarization on them. This polarization effect may be of importance in describing some properties of atoms. For example, when the outer shell contains a single electron (as in a monovalent or an excited atom), neglect of this polarization effect is the principal reason for the remaining disagreement between experimentally obtained optical terms and those calculated by the self-consistent field method with exchange.

2. A calculation to evaluate and illustrate the adiabatic approximation has been undertaken for lithium. The ratio of T_e, the period of the outer electrons, to T_i, the same period for the inner electrons, may be used as a simple criterion for the applicability of our approximation. Using the formulas for hydrogen-like atoms, we have

$$[illegible] \tag{3}$$

where n is the principal quantum number and Z is the nuclear charge. For the $1s$- and $2s$-electrons of lithium, this ratio is about 30 or 40.

For the K shell electrons, we took wave functions of the form

$$U(r; r_e) = A(1 - \gamma\alpha r\cos\theta)\, e^{-\alpha r}, \tag{4}$$

where θ is the polar angle with respect to the axis determined by the $2s$ electron, and the parameters $\gamma(r_e)$ and $\alpha(r_e)$ are obtained variationally (these parameters are functions of the $2s$-electron's position.

The parameter γ, which characterizes the polarization, takes on its maximum value of 0.15 when $r_e = 0.4$ a.u.; α varies monotonically from a value of 1.6875 for $r_e = 0$ to a limit of 2.6875 as r_e increases without bound. Therefore, in contrast to what obtains in the self-consistent field treatment, the core wave function and hence also the field produced by the core depend strongly on the position of the outer electron. In particular, the potential at the origin is 4.375 a.u., rather than the value of 5.375 obtained by the Hartree-Fock method.

We integrated the outer-electron equation numerically for the $2s$, $2p$ and $3p$ states. Although the energies obtained in this way are somewhat better than those given by the Hartree-Fock method, they still differ noticeably from experiment. It would seem that the remaining divergence could be largely eliminated by taking exchange into account.

We note also that the wave functions we obtain for the valence electron differ noticeably from those given by the Hartree-Fock method, especially close to the nucleus. This may be of interest in calculating some nuclear effects.

3. We next applied the adiabatic approximation to a theoretical derivation of the formula describing the influence of the polarization of the core on the optical electron transition probabilities. This formula was previously obtained by one of the authors[1] from simple physical considerations.

In the adiabatic approximation the matrix element for the dipole transition from state A to state B is of the form

$$\left(\sum_{i=1}^{N} r_i\right)_{AB} = \int\cdots\int \varphi_A^* \sum_{i=n+1}^{N} \mathbf{r}_i \varphi_B\, d\tau_{n+1}, \ldots, d\tau_N$$

$$+ \int\cdots\int \varphi_A^* \varphi_B\, d\tau_{n+1}, \ldots, d\tau_N \int\cdots\int U^* \sum_{i=1}^{n} \mathbf{r}_i U\, d\tau_1, \ldots, d\tau_n. \tag{5}$$

Introducing the notation

$$\mathbf{G}(r_{n+1}, \ldots, r_N) = \int\cdots\int U^* \sum_{i=1}^{n} \mathbf{r}_i U\, d\tau_1, \ldots, d\tau_n, \tag{6}$$

we have

$$\left(\sum_{i=1}^{N} \mathbf{r}_i\right)_{AB} = \left(\sum_{i=n+1}^{N} \mathbf{r}_i\right)_{AB} + [\mathbf{G}(r_{n+1}, \ldots, r_N)]_{AB}, \tag{7}$$

and the transition probability formula is of the form

$$P_{AB} = 4\pi^2 \left|\left\{\mathbf{E}(\omega_{AB})\left[\sum_{i=n+1}^{N} \mathbf{r}_i + \mathbf{G}(r_{n+1}, \ldots, r_N)\right]_{AB}\right\}\right|^2. \tag{8}$$

Unlike the usual equation, this one contains not only the dipole moment of the optical electrons, but a correction function G which describes the influence of the core on the optical transitions. As is easily seen from (6),

this function can be thought of as the dipole moment induced in the core by the optical electrons.

If we treat the interaction between the inner and outer electrons as a perturbation in Eq.(1) (in integrating the self-consistent field equations of monovalent atoms, this term is usually neglected), we obtain ordinary separation of variables in the zeroth approximation. The corresponding matrix element of the dipole moment then becomes*

$$\left(\sum_{i=1}^{N}\mathbf{r}_i\right)_{AB}=\int\cdots\int\varphi_A^{*}\sum_{i=n+1}^{N}\mathbf{r}_i\varphi_B d\tau_{n+1},\ldots,d\tau_N. \tag{9}$$

In the first approximation of perturbation theory, we obtain (if we have complete separation of variables for the inner electrons in the zeroth approximation)

$$\mathbf{G}(r_{n+1},\ldots,r_N)=2\sum_{i=1}^{n}\sum_{k=n+1}^{N}\sum_{j}{}'\frac{V_{ji}(r_k)\,\mathbf{r}_{ij}}{E_j-E_i}. \tag{10}$$

where

$$V_{ji}(r)=\int\frac{\psi_j^{*}(r')\psi_i(r')}{|\mathbf{r}-\mathbf{r}'|}d\tau'. \tag{11}$$

These equations are the same as Eqs.(4) and (5) of Ref.1.

Leningrad State University

References

1. I.B.Bersuker, Present issue of the Bulletin.
2. M.G.Veselov, Zhur.exp.i teor.fiz., 19, 959 (1949).

---

* Strictly speaking, (9) is obtained by separation of variables only if we neglect the lack of orthogonality of φ_A and φ_B and the difference between U_A and U_B. When these are included, we get corrections of higher accuracy than our calculations.[2]

TWO-ELECTRON MODEL APPROXIMATION AND THE SO-CALLED ANOMALY IN THE SPECTRA OF CARBON, NITROGEN AND OXYGEN

- A.P.Jucys, Ia.I.Vizbaraite, V.I.Kavetskis & I.V.Batarunas

Introduction

The incomplete separation of variables[1] and the many-configuration approximation[2] provide two means of improving quantum mechanical calculations for atoms. Both methods are based on a partial departure from the approximation based on one-electron states. Both of these refinements, but especially the first, become involved in great mathematical difficulties when applied to many-electron atoms but are feasible for two-electron systems. The present communication is concerned with an approximation based on two-electron states described by improved two-electron wave functions.

The wave function of each electron pair will be constructed by means of a refined calculation, and the wave function of the entire system will be the antisymmetrized product of the wave functions for the different electron pairs. This will be called the two-electron model and our problem resembles that of improving calculations for molecules[3]. Depending on the specific problem, the two-electron model will be applied to the electron pairs for which the one-electron model is found to be inadequate; in the case of all the other electrons the one-electron model will be retained.

We shall construct two-electron wave functions by means of a many-configuration approximation, which is simpler than calculations based on incomplete separation of variables. The two-electron wave function can be written as follows:

$$\Psi = \sum_{k} \alpha_k \Psi_k, \qquad (1)$$

where Ψ_k is the wave function corresponding to that of the k configuration in the one-electron approximation.

Three-electron systems

Let us consider the normal and first excited configurations of lithium type atoms. Following Ref.4, we use five configurations for the two inner electrons, as follows:

$$1s^2 - 2p'^2 - 2s'^2 - 3d'^2 - 3p'^2, \qquad (2)$$

and one-electron states for the outer electron. The antisymmetrized product of the two-electron function for the $1s$ electrons and the valence-electron function nl is represented by

$$(1s^2 - 2p'^2 - 2s'^2 - 3d'^2 - 3p'^2)\,nl. \qquad (3)$$

Calculations for the $1s^2 2s$ and $1s^2 2p$ configurations of lithium using the Fock self-consistent field method with a many-configuration correction based on the two-electron model give energies of -7.472 and -7.404 a.u., respectively, compared with -7.433 and -7.365 a.u. when the conventional Fock self-consistent field method is used. The experimental values are -7.478 and -7.410 a.u., respectively.

On the anomaly in the spectra of carbon, nitrogen and oxygen

The configuration $1s^22s^22p^q$ with $q = 2,3,4$, yields "anomalous" energy differences between the terms. For carbon and oxygen this anomaly lies in the fact that experiment gives 1.13 for the ratio

$$\frac{{}^1S - {}^1D}{{}^1D - {}^3P} \tag{4}$$

whereas the one-electron theoretical model gives 1.5. The experimental value of

$$\frac{{}^2P - {}^2D}{{}^2D - {}^4S} \tag{5}$$

for nitrogen is 0.5, while the theoretical value is 0.67.

The two-configuration approximation $1s^22s^22p^2 - 1s^22p^4$, on the assumption that the $2p$ radial wave function is identical in both configurations, reduced (4) from 1.5 to 0.7-0.8 for doubly-ionized oxygen[5] and neutral carbon[6]. These results were not essentially affected by changing the $2p$ wave function[7,8] or by corrections involving a large number of configurations[9]. We shall use the two-electron model in an attempt to eliminate the anomaly and shall apply it only to the $2p$ electrons which are the electrons responsible for different terms. It is reasonable to assume identical radial wave functions for equivalent electrons. The wave function of a shell of equivalent electrons is then given by Eq.(2.4) of Ref.10.

Calculations by means of the two-electron model resulted in the values 1.1 and 0.5 for (4) and (5), respectively, in good agreement with experiment.

Discussion

In our procedure the wave function of the entire atom contains a number of one-electron wave functions with identical quantum numbers nl but different physical significance. Some of these functions describe electron states (the $1s$ and nl functions in (3)), while others (primed in (3)) improve the wave functions of different electrons (the $1s$ shell in (3)). There is an essential difference between these two groups of wave functions. For helium and beryllium the behavior of the functions is the same in both the common one-configuration approximation ahd the two-electron model, as is evident from the figures in Ref.11. The two-electron model and the ordinary many-configuration models of the $1s^22p$ lithium configuration are essentially different. The accompanying figure shows the following radial wave functions: $1s$ (inner electrons), $2p$ (outer electron) and $2p'$ (improvement of inner electron wave function). We see that the wave function which improves the inner-electron wave function is closer to the $1s$ function than to the outer-electron wave function. In the

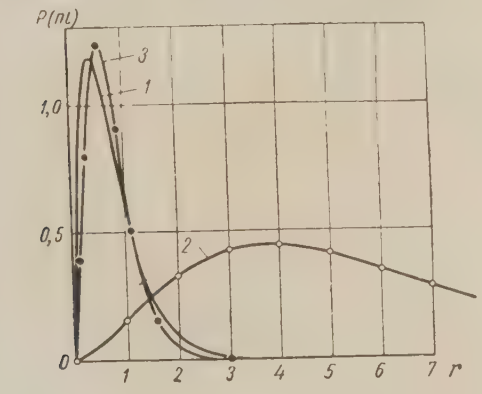

←Comparison of one-electron radial wave functions: $1s$ (curve 1), $2p$ (curve 2) and $2p'$ (curve 3) for the lithium atom in the two-electron many-configuration approximation $(1s^2 - 2p'^2 - \ldots)2p$

ordinary many-configuration approximation these two functions are assumed equal in advance, so that it is practically impossible to obtain any correction.

The fact that the correcting wave functions are very close to the original wave functions has the important consequence that the electron shell structure of atoms is preserved in the many-configuration approximation on which the two-electron model is based. In an earlier stage of development of the many-configuration approximation (using one-electron wave functions determined in a one-configuration approximation), the shell structure lost its meaning and was regarded as an approximation[12]. We thus see that the use of one-electron wave functions determined in a many-configuration approximation based on a two-electron model fully restores the electron shell picture.

Numerical calculations show that the many-configuration approximation based on the two-electron model is an improvement over the conventional many-configuration approximation and can eliminate the appreciable discrepancy between the theoretical and experimental results for the ratios between the energy differences of terms.

Institute of Physics and Mathematics of the
Acadmy of Sciences of the Lithuanian SSR,
Vilna State Pedagogical Institute
and
"V.Kapsukas" Vilna State University

References

1. V.A.Fók, M.G.Veselov & M.I.Petrashen', Zhur.eksp.i teor.fiz., 10, 723 (1940).
2. A.P.Iutsis (Jucys), Zhur.eksp.i teor.fiz., 23, 129 (1952).
3. V.A.Fok, Doklady AN SSSR, 73, 735 (1952).
4. Ia.I.Vizbaraite, V.I.Kavetskis & A.P.Iutsis, Optika i spektroskopiia (Optics & spectroscopy), 1, 282 (1956).
5. D.R.Hartree & B.Swirles, Proc.Cambridge Philos.Soc., 33, 240 (1937).
6. A.Jucys, Proc.Roy.Soc.A, 173, 59 (1939).
7. B.Jeffreys, Proc.Cambridge Philos.Soc., 38, 290 (1942).
8. A.Jucys, J.Phys., 11, 49 (1947).
9. A.P.Iutsis (Jucys), Zhur.eksp.i teor.fiz., 19, 565 (1949).
10. A.P.Iutsis & V.I.Kavetskis, Trudy, Lith.AN, Bl, 9 (1956).
11. A.P.Iutsis, Trudy (Transactions) Tenth Conference on Spectroscopy, Lvov University, 2, 86 (1958).
12. A.Daudel, S.Odiot & H.Brion, J.Phys.et radium, 15, 804 (1954).

ONE-ELECTRON WAVE FUNCTIONS OF Tl^+ IN CERTAIN CRYSTALS

- M. I. Petrashen' and T. L. Gutman

In attempting to calculate the absorption and emission of crystal phosphors one naturally begins with the central-ion model (which is the simplest model), wherein the emission center is an activator ion that replaces a cation of the host material at a lattice site.[1] Here the Born-Oppenheimer approximation can be used, so that in the first stage of the calculation all ions can be regarded as having fixed positions. Activator ions are acted on by the crystal lattice field, so that the positions and intensities of phosphor bands cannot be calculated satisfactorily when free-ion wave functions are used. This accounts for the failure of Knox and Dexter[2] to calculate correctly the ratio of oscillator strengths for the $^1S_0 \to {}^3P_1$ and $^1S_0 \to {}^1P_1$ transitions of Tl^+.

We have developed a more consistent method of obtaining one-electron wave functions for activator ions than that described in Ref. 1. Wave functions obtained in this way for Tl^+ in a KCl-Tl phosphor were used to compute the ratio

$$\frac{f_{^1S_0 - {}^3P_1}}{f_{^1S_0 - {}^1P_1}}$$

1. The one-electron wave functions of a central ion are eigenfunctions of the Hartree-Fock equation

$$-\frac{1}{2}\Delta\psi_k + \left[-\frac{Z}{r} + V(\mathbf{r})\right]\psi_k(\mathbf{r}) - A^{\circ}\psi_k + U(\mathbf{r})\psi_k - A\psi_k = E_k\psi_k. \qquad (1)$$

Here $V(\mathbf{r})$ is the electron screening potential of the central ion, $U(\mathbf{r})$ is the electrostatic potential of the lattice field and A and A^{O} are operators for exchange with the central-ion electrons and lattice electrons, respectively.

All terms in (1), which describe the field, can be expanded in infinite series of lattice harmonics of identical representation of the crystalline symmetry group. We shall confine ourselves to cubic symmetry and use the wave function

$$\psi_k(\mathbf{r}) = \sum_i \frac{1}{r} f_i(r) K_i^{(\alpha)}(\vartheta, \varphi),$$

where K_i^{α} are cubic harmonics of the representation for the given state.

By separating the variables in (1), we obtain an infinite set of integro-differential equations for $f_i(r)$, which can be solved only approximately in different ways, depending on the nature of the assumed physical model.

2. In the present problem the central ion is an impurity ion which retains its identity in the crystal. Therefore in (1) we regard $U(r)$ and A, which take the lattice field into account, as perturbation operators and thus extend the situation obtaining for $r < a$ (where is the lattice constant) over the entire crystal. Then, first, all higher terms of the expansion in cubic harmonics should be regarded as small compared to the first few terms and, second, we can use perturbation theory to obtain the zeroth-approximation eigenvalue E_k of (1).

Our first assumption results in a set of equations for $f_i(r)$, where each equation includes one function more than the preceding equation. The first equation contains only the first function in the expansion, so that its solution is independent of the number of terms used in the expansion. E_k, which appears in all equations, is regarded as a previously determined parameter. This will be called the simplified system. The approximate method of solution of this simplified system, given in Ref. 1, is based on the physical assumption that the field of the lattice forms a barrier of height ΔE for electrons of the

central ion, located at a distance of the order of one lattice constant from the core of the central ion.

3. Representing E_k and the eigenfunction ψ_k in (1) by $E_k = E_k^0 + \Delta E_k$ and $\psi_k = \psi_k^0 + \psi_k'$, where E_k^0 and ψ_k^0 are the eigenvalue and eigenfunction derived from the free-ion equation, we obtain

$$\Delta E_k = \Delta E_k^U + \Delta E_k^A = \int \psi_k^{0^2}(\mathbf{r})\, U(\mathbf{r})\, d\tau + \int \psi_k^0(\mathbf{r})\, A\psi_k^0(\mathbf{r})\, d\tau.$$

In calculating ΔE_k^U it is convenient to separate out a term representing the potential U_0 of a point lattice by setting $U(\mathbf{r}) = U_0(\mathbf{r}) + \Delta U$. In calculating $\int \psi_k^{0^2}(\mathbf{r})\, \Delta U\, d\tau = \Delta E_k''$, it is evidently sufficient to regard only nearest neighbors of the central ion as non-points. $\Delta E_k' = \int U_0 \psi_k^{0^2}(\mathbf{r})\, d\tau$ is calculated in Ref.1. The calculation gives

$$\Delta E_k'(U_0) = \Delta E_k'(a) \quad \text{and} \quad \Delta E_k'' = \Delta E_k''(a, \Delta a),$$

where Δa is the displacement of nearest neighbors of the central ion.

It is evident that determination of the equilibrium configuration for a given state of the system requires calculations of several values of a and Δa.

Calculation of $\Delta E_A = \int \psi_k^0(\mathbf{r})\, A\psi_k^0(\mathbf{r})\, d\tau$ is more complicated; we calculated this quantity using Slater's method to include exchange with electrons of the crystal.

4. Approximate solutions of the simplified equations require knowledge of the one-electron functions for the free Tl⁺ ion; for this purpose the Hartree self-consistent field method was used. Since the wave functions of Tl⁺ in the crystal were intended for use in determining oscillator strengths, we preferred the one-electron functions obtained by a semi-empirical method for divalent atoms[3] over the Hartree functions. This procedure allows of dropping terms for intermediate coupling in Tl⁺ in calculating the oscillator strengths.

The calculation for Tl⁺ in a crystal has thus far been carried to the first approximation. The first few equations, corresponding to the states under consideration, have been solved, also the calculations for the KCl lattice constant have been completed.

In the calculation of ΔE the six Cl⁻ ions closest to the activator ion were taken into consideration by means of Hartree wave functions. A provisional estimate of the ratio of $f_{^1S_0,\,^3P_1}$ to $f_{^1S_0,\,^1P_1}$ suggests that a more accurate calculation will lead to considerably better agreement with experiment than was obtained by the American physicists.

References

1. M.I.Petrashen', A.V.Ivanova & G.Wol'f, Vestnik (Journal), Leningrad State University, 10, 29 (1956).

2. R.S.Knox & D.L.Dexter, Phys.Rev., 104, 1245 (1956).

3. M.I.Petrashen' & I.V.Abarenkov, Trudy (Transactions), Tenth Conference on Spectroscopy, Lvov State University, 2, 1958.

CALCULATION OF ONE-ELECTRON WAVE FUNCTIONS AND OSCILLATOR STRENGTHS BY MEANS OF AN ELECTRONIC COMPUTER

- L.A.Vainshtein

Of paramount importance in the calculation of oscillator strengths and other optical characteristics are the optical electron wave functions, particularly their behavior when the electron is at a relatively great distance from the nucleus. At present, in solving such problems by means of electronic computers, in most cases for purely technical reasons one must use the one-electron approximation or simple corrections thereto. Apparently, most convenient in this case is the semi-empirical method[1-3] which involves solving the Schrödinger equation for an optical electron situated in the central effective field of the atomic core, the experimental value of the ionization energy being used as the eigenvalue.

Previously, the author[4] proposed calculating the field of the atomic core by means of linearly deformed wave functions, selecting the deformation parameter so as to obtain the correct eigenvalue. This method was used for calculating wave functions and oscillator strengths on an electronic computer without taking exchange terms into account. Now a program has been set up and preliminary calculations carried out taking exchange into account. The work was done on a universal "Strela" computer.

The problem reduces[4] to solution of an equation of the form

$$\frac{d^2\Phi}{dx^2} + \left[\frac{2\zeta(x)}{x}\omega - \frac{l(l+1)}{x^2} - \alpha^2\omega^2\right]\Phi = \frac{\omega}{x} G(\Phi|x),$$

where $f(r) = \Phi(r/\omega)$ is the sought radial function of the optical electron, $\zeta(r)$ is the effective charge of the atomic residue (core), $x = r/\omega$, $\alpha^2 = E_{\text{exp}}$, ω is the deformation parameter and G is an exchange operator which is a functional of Φ. The solution procedure is essentially the same as described in Ref.4. Exchange is taken into account by the method of successive approximations; we took G = 0 in the zeroth approximation. The second approximation already proved to be close to the first. The computing program, as that used in Ref.4, is applicable to any state or atom.

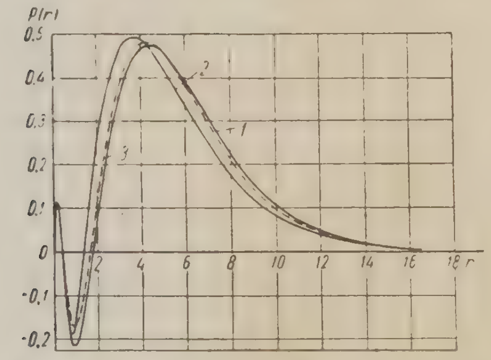

Wave functions of the $4p$ electron of Ca calculated taking exchange into account (fourth approximation - curve 1) and without taking exchange into account (zeroth approximation - curve 2), and wave functions obtained by the Hartree-Fock method (curve 3).

In all cases account was taken of exchange only with the electrons of one shell of the atomic residue, that closest to the optical electron. To determine the dependence of G on the accuracy of defining the wave functions of the atomic residue, we carried out calculations using rough nodefree analytic functions and numerical functions (the last were calculated by the computer by means of the same program). It was found that both the former and the latter lead to virtually the same $f(r)$. A similar result was obtained in Ref.4 with regard to the effective charge $\zeta(r)$. Thus deformation of the atomic core function allows of using nodefree analytic functions for calculating both the ordinary and the exchange potential, which greatly simplifies the computations.

For the same energy parameters, the wave functions calculated in the present work agree with the Hartree-Fock functions

at least in the region of the principal maximum and for large radii. By way of example, the wave functions of a $4p$ electron in the 4^3P state of Ca are shown in the accompanying figure.

The following are the calculated oscillator strengths for the resonance transitions in In and Tl:

Atom	Transition	Without Exchange	With Exchange	Experimental
In	$5^2P_{1/2} - 6^2S$	0.115	0.158	0.20 (Ref.6)
Tl	$6^2P_{1/2} - 7^2S$	0.145	0.191	0.04[*] (Ref.5)

Thus the disagreement with experiment, noted in the work of Ref.4, still remains even when exchange is taken into account. In the case of divalent atoms (for example, Ca), the divergence is still greater. Calculations have been carried out so far only for a small number of transitions and the corresponding experimental results in many cases are not particularly reliable, nevertheless the available data indicate that in a number of cases taking exchange into account does not lead to agreement with experiment. Presumably to obtain more accurate values one must go beyond the framework of the one-electron approximation.

"P.N.Lebedev" Physical Institute,
Academy of Sciences of the USSR

References

1. L.Biermann, Z.Astrophys., 22, 157 (1943).
2. D.Botes & A.Damgaard, Phil.Trans.Roy.Soc., 242, 101 (1949).
3. M.I.Petrashen' & I.V.Abarenkov, Vestn. (Journal) Leningrad University, No.5, 141 (1954).
4. L.A.Vainshtein, Optika i spektroskopiia (Optics and Spectroscopy), 3, 313 (1957).
5. G.S.Kvater, Zhur.eksp.i teor.fiz., 11, 421 (1941).
6. Iu.I.Ostrovskii, N.P.Penkin & L.N.Shabanov, Present issue of the Bulletin.

---

[*] In the course of the discussion following the report, L.V.Gurvich noted that this value is wrong inasmuch as it was obtained on the basis of an incorrect value of thallium vapor concentration. The corrected value is 0.14, which is considerably closer to the calculated one.

DETERMINATION OF MOLECULAR DISSOCIATION ENERGIES FROM FLAME REACTION EQUILIBRIUM STUDIES

- L.V.Gurvich & I.V.Veits

In recent years Sugden et al[1,2], Huldt and Lagerqvist[3,4] and the present authors[5,6] developed procedures for investigating the dissociation energies of metallic compounds by studying the equilibrium of reactions between metals and gaseous products of flame combustion. The most convenient of these methods determines the partial pressure P_M of a metal from its line intensities in a flame spectrum. Assuming that the metal is present in the flame only in the form of atoms M and molecules MX, the partial pressure P_{MX} of the given compound is given by

$$P_{MX} = P_{\Sigma M} - P_M$$

where $P_{\Sigma M}$ is the total pressure of the metallic compounds in the flame.*

When the flame temperature and partial pressure of gas X have been determined or calculated, it is easy to calculate the dissociation energy of MX from

$$D_0(\mathrm{MX}) = T(\Delta\Phi_T^* - R\ln K_p), \qquad (1)$$

where $K_p = \frac{P_M P_X}{P_{MX}}$, R = 1.98726 cal/mole/deg and $\Delta\Phi_T^*$ is the change in the reduced thermodynamic potential. An analysis of the accuracy of this method subject to the conditions that $P_{\Sigma M} : P_M = n \gg 1$ and $P_M + P_{MX} = P_{\Sigma M}$, which denote a low degree of dissociation of MX and the absence of any other metallic compound in the flame, yields the following limit of error in determining $D_o(\mathrm{MX})$:

$$\Delta[D_0(\mathrm{MX})] = \left[\frac{D_0(\mathrm{MX})}{T} + R\left(\frac{C_2 E_m}{T} - 1\right)\right]\Delta T + [\Delta(\Delta\Phi_T^*) + R(0.25 + \delta A_{mn})]T, \qquad (2)$$

where ΔT and $\Delta(\Delta\Phi_T^*)$ are the absolute errors in T and $\Delta\Phi_T^*$; δA_{mn} is the relative error in the probability of the transition and E_m is the corresponding excitation energy in cm^{-1}.

It must be noted, however, that in (2) the term $R\left(\frac{C_2 E_m}{T} - 1\right)$ must be preceded by the coefficient $\frac{n}{n-1}$, which is equal to 1 for $n \gg 1$ and approaches ∞ for $P_M \longrightarrow P_{\Sigma M}$. Moreover, when $P_M \longrightarrow P_{\Sigma M}$, there is a sharp increase in the error of P_{MX} defined as the difference between $P_{\Sigma M}$ and P_M. The accuracy therefore diminishes with the value of the ratio $P_{\Sigma M}/P_M$. Analysis shows that satisfactory accuracy is assured when $P_M \leqslant P_{\Sigma M}/3$. Therefore the dissociation energy of MX can be determined by the given method only when

$$D_0(\mathrm{MX}) \geqslant T(\Delta\Phi_T^* + 1.38 - R\ln PX). \qquad (3)$$

Reduced accuracy also results from the presence of other metallic compounds in the flame, and when $P_{MX} < 0.5\ (P_{\Sigma M} - P_M)$, it becomes impossible to determine $D_o(\mathrm{MX})$. Since most metals form stable compounds with oxygen, this last circumstance usually rules out the given method for determining the dissociation energies of other metallic compounds in oxygenous flames.[8]

---

*It was shown in Refs.5 and 7 that when compounds MY or M_nX_m are formed in a flame, their partial pressures can be calculated from P_{MX} if the equilibrium constants of their dissociation reactions are known.

The method in question was used to investigate the dissociation energies of diatomic oxides of Group III elements (BO, AlO, GaO, InO, TlO), experimental data on which are unreliable or lacking in the literature. $C_2H_2 + O_2$, $H_2 + O_2$ and $CO + O_2$ flames with different proportions of the gases were used. The experimental procedure has been described earlier[5,6]. The metals were introduced into the flames in the form of solutions of their sulfates and chlorides; boron was introduced as $Na_2B_4O_7$. The partial metal pressures were determined by measuring the intensity of the resonance lines associated with the $^2S_{1/2} \to {}^2P_{1/2,3/2}$ transitions. Table 1 gives the transition probabilities used in the calculations.

Table 1

Transition probabilities used in the calculations

Atom	λ, A	f (Refs. in [])	A_{mn}, sec^{-1}
Al	3961,5	0,065 [10]; 0,1 [11]	$5,5 \cdot 10^7$; $8,4 \cdot 10^7$
Ga	4033	0,13 [12]	$5,28 \cdot 10^7$
	4171	0,135 [12]	$1,03 \cdot 10^8$
Ia	4102	0,201 [12]	$7,9 \cdot 10^7$
	4511	0,218 [12]	$1,4 \cdot 10^8$
Tl	5350	0,14 [13]	$6,5 \cdot 10^7$
Li	6708	0,72 [14]	$3,6 \cdot 10^7$
Na	5890	0,33 [15]; 0,4 [16] *	$6,25 \cdot 10^7$; $7,3 \cdot 10^7$
	5896	0,67 [15]; 0,80 [16] *	$6,25 \cdot 10^7$; $7,3 \cdot 10^7$

*Adjusted in accordance with more accurate data on the pressure of saturated sodium vapor.

It proved impossible to determine the partial pressure of boron, since B lines were not excited in the flames used. Equilibrium calculations for reactions between boron and combustion products using the data of Ref.9 on the thermodynamic properties of boric oxides indicated that the absence of boron lines can be accounted for by the high stability of its oxides, resulting in the low value of P_B (below $1 \cdot 10^{-10}$ atm) in the given flames. We measured the partial pressures of aluminum, gallium, indium and thallium in different flames, and after the calculation of $P_{\Sigma M} = \frac{x_{H_2O} C_M}{55.5 \Sigma N_i}$ (see Ref.5), the partial pressures of AlO, GaO and InO were obtained from the relation $P_{MO} = P_{\Sigma M} - P_M$. Equilibrium calculations for reactions between these metals and flame gases indicated that the partial pressures of their other compounds, including Al_2O_3, Al_2O and GaOH, are less than 5% of $P_{\Sigma M}$ and that their presence in flames can thus not affect the determination of the dissociation energies of AlO, GaO and InO. By investigating D_0(TlO), it was found that under the experimental conditions P_{Tl} amounts to 70-90% of $P_{\Sigma Tl}$. The given method could thus be used to determine only the upper bound for the dissociation energy of this molecule.

Table 2 gives our values for the dissociation energies and those found in the literature as well as the upper bounds of the Ga-OH and Tl-OH binding energies obtained through measurements of P_M in flames with different hydroxyl contents.

Since the described procedure cannot be used to investigate the dissociation energies of compounds of metals and other elements in oxygenous flames, we studied the dissociation of LiCl and NaCl molecules in a mixed $H_2 + Cl_2$ flame. Metallic Cl salts and Na_2CO_3 were introduced into the flame in a stream of hydrogen by means of a Lundegarth atomizer. For the 1.00 H_2 + + 0.80 Cl_2 + 0.016 H_2O (liquid) flame that was used, the theoretical tempera-

ture was 2450°K, while the temperature determined from reversal of Na D lines was 2450 ± 100° K[*]. Partial metal pressures were determined from the absolute intensities of the Na 5890 A, Na 5896 A and Li 6708 A lines, the transition probabilities for which are given in Table 1. Thermodynamic calculations showed that in calculating P_{NaCl} and P_{LiCl}, we can neglect the formation of other compounds of these metals in the flame, including M_2Cl_2, MH and MOH. However, an essential part is played by the ionization of Li and especially Na atoms, with the result that in a hydrogen-chlorine flame, P_{Na^+} is equal to over 30% of $P_{\Sigma Na}$. The partial pressures of the compounds in question were therefore determined from the relation

Table 2

Dissociation energies (Kcal/mole)

Molecule	Our data	Data of other authors: Refs. in[]
AlO	137 ±4 *1, *2	138±9 [17]; 21 [18]; 81 [19]; 95 *3
GaO	115,6±3	68 *3
InO	103 ±5	26 [20]
TlO	<90	~ 0 [20]
Ga—OH	<108	—
Tl—OH	<70	—
LiCl	118 ±4	118 [21]; 115 [22]
NaCl	98,5±3,0 *1	97,6±1,3 [21]

*1 With two possible values of A_{mn}.

*2 The calculation of P_{Al} in Ref.7 contains an error.

*3 Calculated by means of the Birge-Sponer extrapolation.

$$P_{MCl} = P_{\Sigma M} - P_M - P_{M^+}$$

where P_{M^+} was obtained by solving the three simultaneous equations

$$P_{M^+} = P_e P_{Cl^-}; \quad \frac{P_{M^+} P_e}{P_M} = K_1 \text{ and } \frac{P_{Cl} P_e}{P_{Cl^-}} = K_2$$

Table 2 gives the values found for the dissociation energies of LiCl and NaCl.

This is the first work in which the equilibrium of flame reactions is used to determine molecular dissociation energies that have already been determined quite accurately by other methods. The good agreement between the two values of D_o(NaCl) demonstrates the possibility of using flame studies for exact determination of molecular dissociation energies. The large discrepancy between the values obtained for D_o(AlO) and D_o(InO) and the data given in Refs.18-20 results from an incorrect interpretation of the spectra of these two molecules. For AlO this is confirmed by recently published data (Ref.23), while for InO we have only one source of information for the spectrum (Ref.24) and further investigation is desirable. However, by comparing the constants of BO, AlO, GaO and InO we can already show that Howell's[20] low value for the dissociation energy of InO is incorrect. We can also infer that D_o (TlO) differs from zero and that, consequently, further attempts to obtain the spectrum of this molecule are indicated.

Institute of Mineral Fuels,
Academy of Sciences of the USSR

---

[*] More detailed information on the flame studies will be found in Ref.3.

References

1. T.M.Sugden, Fifth Symposium on Combustion, p.405, New York,195?,
2. T.M.Sugden, Trans.Faraday Soc., 52, 1469 (1956).
3. L.Huldt & A.Lagergvist, Arkiv.Fysik, 2, 333 (1950).
4, L.Huldt & A.Lagergvist,ibid., 3, 525 (1951).
5. I.V.Veits & L.V.Gurvich, Optika i spektroskopiia, (Optics and Spectroscopy)1, 22 (1956).
6. I.V.Veits & L.V.Gurvich, Zhur.fiz.khim., 31, 2306 (1957).
7. I.V.Veits & L.V.Gurvich, Doklady AN SSSR, 108, 659 (1956).
8. L.V.Gurvich & I.V.Veits, ibid., 116, 811 (1957).
9. V.Huff, S.Gordon & V.Morrell, NACA, Report 1037, 1950.
10. E.I.Nikonova, Dissertation, State Optical Inst., 1956.
11. L.A.Vainshtein, Present issue of the Bulletin, p.668.
12. G.I.Ostrovskii & N.P.Penkin, Optika i spektroskopiia, 4, No.6 (1958).
13. L.V.Gurvich, ibid., 5, No.6 (1958).
14. G.Steppenson, Nature, 167, 156 (1951).
15. S.L.Mandel'shtam, Vvedenie v spektral'nyi analiz. (Introduction to spectral analysis) M.-L, 1946.
16. G.S.Kvater, Izv.AN SSSR, Ser.fiz., 9, 236 (1945).
17. L.Brewer & A.Searcy, J.Amer.Chem.Soc., 73, 5308 (1951).
18. B.Rosen, Physica, 12, 184 (1946).
19. G.Herzberg, Spectra of Diatomic Molecules, 2nd Ed., N.Y., London, 1950.
20. H.G.Howell, Proc.Phys.Soc., 57, 32 (1945).
21. F.D.Rossini et al, NBS USA, Circ.500.
22. A.G.Gaydon, Dissociation Energy and Spectra of Diatomic Molecules, 2nd edition, London, 1953.
23. A.Lagergvist, N.E.Nillson & R.F.Barrow, Proc.Phys.Soc., A 69, 356 (1956).
24. W.W.Watson & A.Shambon, Phys.Rev., 50, 607 (1936).

DEPENDENCE OF THE INTEGRAL INTENSITY OF SPECTRUM LINES ON THE ABSOLUTE CONCENTRATION OF ATOMS IN AN ARC DISCHARGE

- I.V.Dvornikova

The question of the relation between the concentration of an element in the source and the intensity of the spectrum lines is one of the most important in spectrochemical analysis. However, the "growth curves" characterizing this dependence have been thoroughly studied only for uniform light sources[1]; they have not been adequately investigated for arcs, sparks and other sources commonly used in spectroscopic analysis. The principal difficulty in obtaining growth curves for such sources stems from the lack of simple and dependable methods of determining the atomic concentration in the discharge cloud. In view of this, growth curves are frequently plotted on the basis of the element concentration in the electrodes rather than in the discharge cloud itself. Obviously, with this procedure the dependence in question is affected by the complicated process of entry of the material into the interelectrode gap. As a result, the growth curve is distorted and comparison of experimental values with the theoretical data is hampered.

In the present work we attempted to measure the absolute concentration of atoms in the interelectrode gap from self-absorption of the spectrum lines.

It is a familiar fact that with increasing concentration of atoms of a given element in the source, self-absorption of the lines of this element increases and leads to broadening and finally to self-reversal of the lines. In their review article on self-absorption of spectrum lines in nonuniform sources, Cowan & Dieke[2] show that the magnitude of reabsorption of a given spectrum line depends primarily on the absorption in the source, characterized by the parameter p, and on the degree of inhomogeneity of the source, characterized by the parameter n. The absorption parameter p is proportional to the transition probability B for the given spectral line (or the oscillator strength f), the concentration N of atoms at the lower level and the extent or length l of the source. The magnitude of n varies from 1 to ∞, depending on the degree of inhomogeneity of the source; for a uniform source $n = 1$, while for a source in which the emitting and absorbing atoms are spatially separated $n = \infty$. By means of the theory of Cowan & Dieke one can calculate the contour of a self-absorbed line for any values of p and n.

From the mathematical expression describing the contour of the spectrum line, one can readily establish the functional dependence of the line width on the absorption parameter p and the relation between the parameter p and the depth of the "dip" in the self-reversed line contour. The character of both dependences changes somewhat with changes in the degree of inhomogeneity of the source. The curves shown in Fig.1 characterize the variation of δ/δ_0 with p for different values of n; δ_0 is the initial line half-width for an infinitely thin layer; δ is the observed half-width.

The variation of the depth of the dip in a self-reversed line, i.e., $\log I_{max}/I_0$, with p for different values of n is shown in Fig.2; here I_{max} is the intensity at the maximum of the self-reversed line and I_0 is the intensity at the center of the line.

Having measured the half-width of a given self-absorbed line or the depth of the dip in a self-reversed line, one can by means of the curves of Figs.1 & 2 determine the absorption parameter p and, consequently, the absolute concentration of atoms in the discharge plasma (if the absolute value of the oscillator strength for the given line is known). It will be noted, however, that for determining the value of p from the curves of Figs.1 & 2 one must also know

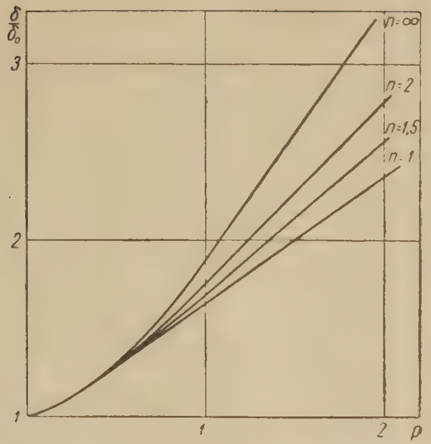

Fig.1. Variation of the relative line half-width with the absorption parameter p and the degree of inhomogeneity n of the source.

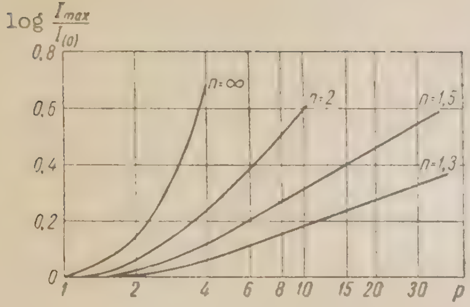

Fig.2. Variation of the depth of the dip in a self-reversed line with the absorption parameter p and the degree of inhomogeneity n of the source.

the degree of inhomogeneity n of the light source. The value of n can be determined from the lines of a self-reversed multiplet for which the oscillator strength ratio is known.[2] Having measured the depth of the dips in the multiplet lines, we determine the values of p for these lines from the curves of Fig.2 and then, inasmuch as p is proportional to f, choose the curve that for the found values of p yields a ratio equal to the ratio of the oscillator strength for the given multiplet lines. This obviously gives us n. It was found from the green triplet of chromium that for an arc freely burning in air $n = 1.5$.

In view of the fact that the Cowan-Dieke theory[2] is based on an assumption (invariance of the line contour for a given source) that does not, strictly speaking, hold for an arc discharge, we felt it would be of interest to compare the method of determining the absolute atomic concentrations from the self-absorption of spectrum lines with some other procedure. To this end we carried out a series of special experiments in which the concentration of atoms was determined simultaneously from the self-absorption and by the Rozhdestvenskii "method of hooks". The experiments showed no substantial systematic divergence between the results obtained by the two methods. These experiments have been described in more detail in our report presented at the Tenth Conference on Spectroscopy.

Usually growth curves are plotted in the form of the variation of the logarithm of the integral intensity I_0 of the spectrum line with the logarithm of the product Nf. Inasmuch as the absorption parameter p is proportional to Nf, we deemed it expedient to plot the growth curve in log I_0 vs log p coordinates. We determined the integral intensities of the lines of the two chromium triplets (4497, 4546 & 4580 Å and 5204, 5206 & 5208 Å). All these lines have a common lower level and the oscillator strength ratios for them are known.[3] The magnitude of p for the 5208 A line was determined experimentally from the line contour, while for the other lines p was calculated on the basis of the oscillator strength ratios.

The experimental set-up is shown schematically in Fig.3. The light from the source 1 passes through the condenser lens 2 and falls on the Fabry-Perot interferometer 3. The lens 4 focuses the interference pattern on the slit 5 of the ISP-51 spectrograph. Lens 6 is mounted on a slide and can be moved into

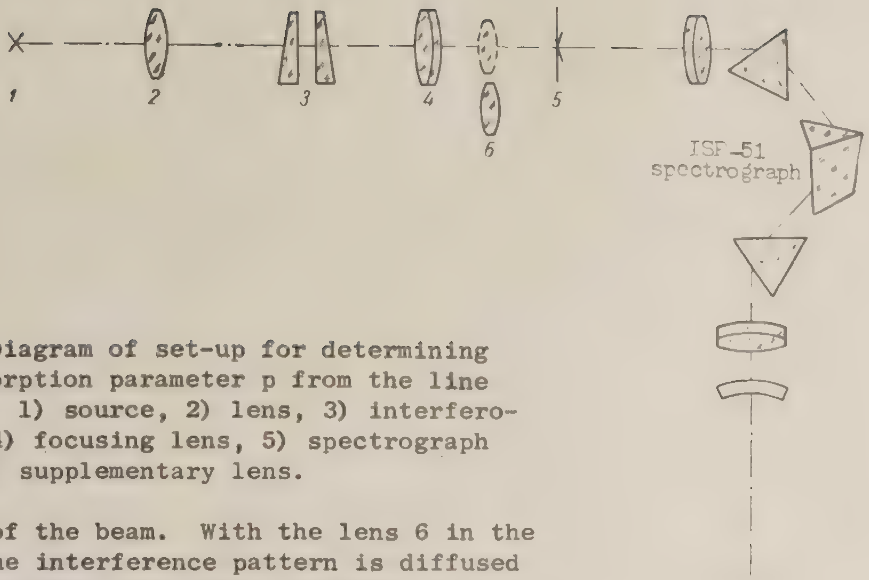

Fig.3. Diagram of set-up for determining the absorption parameter p from the line contour: 1) source, 2) lens, 3) interferometer, 4) focusing lens, 5) spectrograph slit, 6) supplementary lens.

or out of the beam. With the lens 6 in the beam, the interference pattern is diffused with the result that the illumination of the slit becomes uniform.

The order of photographing was the following: first with lens 6 out of the way we photographed the line contour for determining p; the second photograph was made with the lens 6 in the beam and served for determining the integral intensity of the line; finally the interference pattern was photographed again for control purposes.

Usually the values of p obtained from the first and third photographs differed little; whenever the divergence exceeded 20%, the given series of photographs was discarded. By way of electrodes we used samples of Ni-Cr alloy containing 2%, 9.37% or 74% Cr. The auxiliary electrode was a copper rod. All the Ni-Cr alloy samples contained the same amount of iron, consequently the 4384 Å line of iron was chosen as the reference line. The spectra for all four samples were photographed one after the other, then we photographed a step weakener and developed the entire series of photographs simultaneously. The developed films were photometered in the conventional manner. In all we obtained five series of films for somewhat different conditions of burning of the arc. A separate growth curve was plotted on the basis of each series.

The resultant experimental growth curves were compared with the theoretical curve calculated taking into account the degree of inhomogeneity of the source. The integral intensities were evaluated graphically for $n = 1.5$ and a series of values of p in the range from 0.01 to 100. As may be seen from Fig.4 the experimental points satisfactorily fit the theoretical growth curve 1. The scatter of the experimental points is ±10% on the average. Curve 2 in this figure is the growth curve for a homogeneous source. It will be seen that at small values of p the curves fully coincide, while at large values of p they diverge slightly. It will be evident, therefore, that inhomogeneity of the source has relatively little influence on the shape of the growth curve.

The 45° slope obtained for both the experimental and the theoretical growth curves again indicates that in the range of low concentrations of atoms in the source, the relation between the concentration of the element and the intensity of the spectrum lines is linear. The deviations from linearity not infrequently observed may be explained, apparently, either by the influence

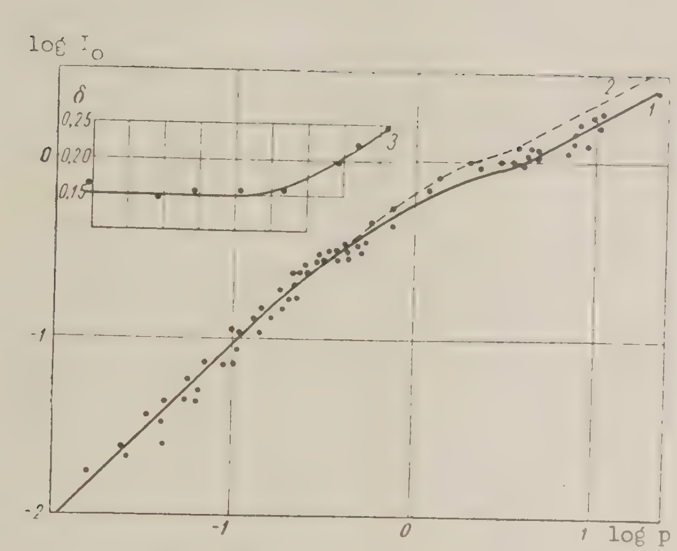

Fig.4. Comparison of the theoretical variation of the logarithm of the integral intensity with the logarithm of the absorption parameter p (growth curve) with the experimental data: 1) theoretical curve, 2) growth curve for a homogeneous source; points - experimental, 3) curve characterizing the increase in the line half-width with increase of p.

of the processes involved in the entry of the material into the discharge cloud or by the fact that the concentration of the material in the arc is not sufficiently low so that the intensity is reduced by self-absorption. It will be evident from the growth curve that self-absorption begins to play a significant role beginning with log p = 0.5, which corresponds to $Nf = 3\cdot10^{11}$. This is approximately one order of magnitude lower than the value reported by V.M.Mel'chenko[4].

Curve 3 in Fig.4 shows the increase of the line width with increase of p. It will readily be noted that the line width begins to increase at approximately the same value of p as the one at which the growth curve begins to bend over. This correlation was also noted in the work of I.M.Nagibina[5].

References

1. A.Unzol'd, Fizika zvezdnykh atmosfer (Physics of stellar atmospheres), M, 1949.

2. R.D.Cowan & G.H.Dieke, Revs.Mod.Phys., 20,418 (1948).

3. Iu.I.Ostrovskii & N.P.Penkin, Optika i spektroskopiia (Optics and Spectroscopy), 3, 193 (1957).

4. V.S.Mel'chenko, Optika i spektroskopiia, 1, 321 (1956).

5. I.M.Nagibina, Dissertation, Leningrad Institute of Precision Mechanics and Optics, 1955.

DETERMINATION OF THE RELATIVE OSCILLATOR STRENGTHS IN AN ARC DISCHARGE FROM THE WIDTH OF THE SPECTRUM LINES

- I.M.Nagibina

We utilized the theory of Cowan & Dieke[1] and the deductions following therefrom for measuring the concentration of atoms or ions in an ac arc discharge and for determining the relative oscillator strengths for some transitions.

The measurements were carried out in the region of the "growth curve" corresponding to the bend in this curve and to concentrations in the discharge at which there obtains broadening of the spectrum lines but still no self-reversal.

We used carbon electrodes and applied a thin layer of an appropriate salt of the investigated element to the end surface of the lower electrode. The degree of inhomogeneity of the discharge cloud was determined beforehand.

Having measured the line width, one can determine the absorption parameter p^*(see Ref.2 - the preceding article) from the theoretical curves characterizing the variation of the line width with the absorption parameter, and then from the value of the absorption parameter one can calculate the concentration N_a of unexcited atoms by means of the formula

$$p = \frac{le^2}{2mc} \cdot \frac{1}{\delta_0} f N_a, \tag{1}$$

where f is the absolute value of the oscillator strength, δ_0 is the line width for an infinitely thin layer and l is the thickness of the source.

In our experiments we determined the linear dependence of the width of certain Fe I, Mg II, Mn II and Ca II lines on the concentration of atoms or ions in the discharge.

From Eq.(1) we have the possibility of determining the relative oscillator strengths for transitions to the common lower level on the basis of the relationship

$$\frac{p_1}{p_2} = \frac{f_1}{f_2} \cdot \frac{\delta_{2,0}}{\delta_{1,0}}, \tag{2}$$

where p_1 and p_2 are the absorption parameters for the investigated transitions under the given experimental conditions in the presence of broadening and $\delta_{1,0}$ and $\delta_{2,0}$ are the corresponding line widths for an infinitely thin layer.

Practical realization of the proposed procedure for determining the relative oscillator strength is relatively simple. If one works in the region of small absorption, there is no necessity for determining the degree of inhomogeneity of the cloud inasmuch as the $\delta/\delta_0 = f(p)$ curves for different degrees of inhomogeneity of the source (see Ref.2), coincide in the region close to the origin of the coordinates. One need only experimentally select a concentration at which there is noticeable broadening of the investigated lines and accurately measure their width δ by means of a high resolution spectrometer.

The results of our measurements for some elements are shown in the accompanying table. The measurements for Mg II were carried out by G.V.Kolliopina.

The suggested method can also be utilized for evaluating the absolute values of the oscillator strengths, but this requires some additional investigation.

Relative oscillator strength values for some Ca II, Fe I, Mn II, and Mg II lines

Element	λ, Å	Transition	Values of f_1/f_2 Our data	 Data of other authors
CaII	3933,66 3968,47	$4^2S_{1/2} - 4^2P_{3/2}$ $4^2S_{1/2} - 4^2P_{1/2}$	2,05	1,96(Ref.3)
FeI	3047,60 2994,43	$a^5D_2 - y^5D^0_3$ $a^5D_3 - y^5D^0_2$	1,34	1,31(Ref.4)
MnII	2949,20 2939,30 2933,05	$a^5S_2 - z^5P^0_3$ $a^5S_2 - z^5P^0_2$ $a^5S_2 - z^5P^0_1$	7,0 : 5,1 : 3,1 ±2.8 %	7,0 : 5,05 : : 3,0 (Ref.5)
MgII	2795,2 2802,7	$1^2S_{1/2} - 2^2P_{3/2}$ $1^2S_{1/2} - 2^2P_{1/2}$	2,09±6,8 %	—
MnII	2576,11 2593,73 2695,10	$a^7S_3 - z^7P^0_4$ $a^7S_3 - z^7P^0_3$ $a^7S_3 - z^7P^0_1$	9 : 6.7 : 5,2 ± 3.0%	9:6.2:4,3 (Ref.5) (calculated)

Leningrad Institute of Precision Mechanics and Optics

References

1. R.D.Cowan & G.H.Dieke, Rev.Mod.Phys., 20, 418 (1948).
2. I.V.Dvornikova, Present issue of the Bulletin, p.674.
3. E.I.Nikonova & V.K.Prokof'ev, Optika i spektroskopiia (Optics and Spectroscopy), 1, 290 (1956).
4. N.P.Penkin & G.F.Parchevskii, Vestnik, Leningrad University, 11, 113, (1954).
5. Seward, Phys.Rev., 37, 344 (1931).

ISOTOPE SHIFT IN THE SPECTRA OF CERIUM AND ZIRCONIUM

- Iu.P.Dontsov & L.A.Korostyleva

We investigated the isotope shifts near the magic numbers 50 and 82. In going from N = 82 to N = 84, Murakawa & Ross[1] and Arroe[2] observed anomalies in the magnitude of the shift; their results, however, are not in agreement. There has been no experimental proof until now of any discontinuity in the progression of the isotope shift in the vicinity of the magic neutron number 50.

For investigating the isotope shift in the spectra of cerium and zirconium we employed the usual technique of excitation and photography of the spectra commonly employed in such studies.[3] In the case of Ce^{136}, Ce^{138} and Ce^{140} this shift is less than the half-width of the spectrum lines. Hence the shift was determined by the graphic procedure on the assumption that the line components of these isotopes are equally spaced in accordance with their mass numbers. The shift between the components was taken such that the half-width of the contour plotted by graphic addition of the contours of the individual components would be equal to the half-width of the spectrum line of the enriched sample. The line contours of the individual isotopes were plotted taking into account the respective percentages present in the sample.

The isotope shift in the zirconium spectrum, as in that of cerium, proved to be less than the half-width of the spectrum lines. Hence in working with zirconium we used four different discharge tubes, each containing one of the enriched isotopes; these were aligned successively with the spectrograph axis and the respective spectra photographed on the same plate. The shift was determined by the displacement of the interference maxima of the investigated lines with reference to a fiducial mark imposed on each spectrogram. Further calculations were carried out as though all the components of the isotope structure were on the same spectrogram. The constancy of the interference pattern relative to the fiducial mark in going from one spectrum to another was checked with reference to the position of the fringes of one of the argon lines. The isotopic composition of the samples was duly taken into account in determining the true magnitude of the isotope shift.

In the case of the isotopes Ce^{136}, Ce^{138}, Ce^{140} and Ce^{142} we investigated the shift of four lines. The mean value of the ratio $\Delta\nu_{140-142}:\Delta\nu_{138-140}$ proved to be 3.85, i.e., the 140-142 shift proved to be almost 4 times greater than the 138-140 shift. In addition the isotope shift in the spectrum of cerium between the 140 and 142 isotopes was measured for 102 lines. These data were utilized for extending the classification of the cerium spectrum.

The isotope shift in the zirconium spectrum was investigated for 46 lines of the neutral atom. The observed shift, except for three cases, is negative and its magnitude generally, as in the case of the volume effect, depends primarily on the configuration of the transition and only weakly on its multiplicity. In the case of some lines the isotope shift is determined by the sum of the volume and mass effects; in the case of other lines, only by the mass effect. This made it possible to evaluate the volume part of the isotope shift in the spectrum of zirconium:

$$\Delta\nu_{vol(90-92)} = -5\cdot 10^{-3}\ cm^{-1} \text{ and } \Delta\nu_{vol(92-94)} = -2\cdot 10^{-3}\ cm^{-1}.$$

Thus the volume effect in the spectrum of zirconium, although considerably smaller than the mass effect, makes an appreciable contribution to the total shift. On the basis of the data obtained we were able to refine the classification of some spectral lines of zirconium.

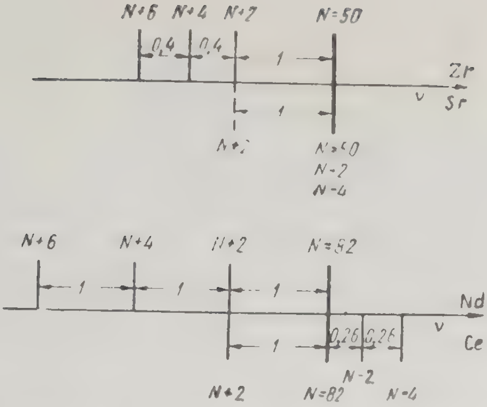

Relative positions of line components of isotopes near the magic numbers 50 and 82 (solid lines - positions of components with experimentally measured shift; dash lines - inferred position of Sr^{90} component).

The results of our measurements show that the shifts of the cerium isotope lines are of the same order of magnitude as in the spectrum of barium. On the other hand, the observed shift of the components of the lines of cerium 140 to 142 agrees with the data of Brix & Frank[4], which indicates that the magnitude of the anomaly in going from N = = 82 to N = 84 was correctly determined.

To detect the discontinuity near N = 50, one must investigate the isotope shift both between isotopes with neutron numbers less than and with neutron numbers greater than the magic number. Zirconium, however, does not have isotopes with less than 50 neutrons. In a recent contribution, Hughes[5] shows that the volume shift of the line components of strontium isotopes with $N < 50$ is nil within the limits of the experimental error. Consequently, the results of our evaluation of the volume effect between zirconium 90 and 92 serve as indirect confirmation of the presence of a similar discontinuity in the isotope shift near N = 50 as in the case of cerium. For direct proof of this one must determine the magnitude of the volume effect between strontium 88 and 90.

Aside from the established similarity in the behavior in the isotope shift near N = 50, 82 and 126, there is also observed a difference in the behavior of the spectrum of zirconium: in the zirconium spectrum $\Delta\nu_{vol}(90-92)$ is larger than $\Delta\nu_{vol}(90-94)$, whereas in the spectra of neodymium and samarium (N = 82) the shift between the corresponding pairs of isotopes is the same (see the accompanying figure which shows the relative position of the line components of isotopes close to the magic numbers 50 and 82).

In the theory of the volume effect developed by Wilets, Hill & Ford[6] all the isotope shift anomalies are explained by variations in the deformation of the nucleus. It is known, however, that nuclei containing a magic number of neutrons are spherically symmetric. An excess or deficiency of a few neutrons cannot lead to deformation of the nucleus: the addition of a new pair of neutrons to the closed shell leads only to a sharp increase of the nuclear radius, which is evinced in the form of discontinuities in the isotope shift in going through a magic number. Filling of different subshells, as the number of neutrons is increased, can also lead to a considerable deviation from the $r = = R_0 \cdot A^{1/3}$ law. In view of this it may be assumed that the difference between the magnitudes of the 90-92 and 90-94 isotope shifts in the spectrum of zirconium is connected with the fact that the 52nd and 54th neutron pairs fill different subshells.

In conclusion the authors desire to thank A.R. Striganov for suggesting the subject and his interest in the work.

References

1. K.Murakawa & J.S.Ross, Phys.Rev., 83, 1272 (1951).
2. H.Arroe, Phys.Rev., 93, 94 (1954).
3. L.A.Korostyleva, A.R.Striganov & N.M.Iashin, Zhur.eksp.i teor.fiz., 28, 471 (1955).
4. P.Brix & H.Frank, Z.Phys., 127, 289 (1950).
5. R.H.Hughes, Phys.Rev., 105, 1260 (1957).
6. L.Wilets, D.L.Hill & K.W.Ford, Phys.Rev., 91, 1488 (1953).

ISOTOPE SHIFT IN THE SPECTRUM OF IONIZED URANIUM

- N.G.Morozova & G.P.Startsev

The isotope effect in the spectrum of uranium was discovered and initially investigated by observing the spectrum lines of singly and doubly ionized uranium isotopes.[1-4] The isotope shift in uranium has been studied most thoroughly and fully by Striganov & Korostyleva[5] in their work aimed at establishing the correlation between shift and the electron configurations and determining the shift in the different terms. The regularities characterizing the isotope shift in the spectrum of uranium were established experimentally from observation of the shifts in the classified lines of U^{238} and U^{235}. All the lines whose terms pertain to configurations with penetrating s^2 and s electrons exhibit the greatest negative shift (the components of the lighter isotope are shifted to the side of higher wave numbers). Lines whose terms pertain to higher electron configurations with non-penetrating f and d electrons exhibit smaller and only positive shifts. The mean shifts in the lines of uranium for each configuration of the lowest term are summarized in Table 1.

Table 1

Line shift in the spectrum of uranium for different isotopes and term configurations

State of atom & configuration of lowest term	[illegible] cm^{-1}	
	Striganov (Ref.5)	McNally (Ref.[illegible])
[illegible]	[illegible]	[illegible]
[illegible]	[illegible]	[illegible]
[illegible]	[illegible]	[illegible]
[illegible]	[illegible]	[illegible]
[illegible]	[illegible]	[illegible]
[illegible]	[illegible]	[illegible]
[illegible]	[illegible]	[illegible]

The present work was devoted to the investigation of the isotope shift in the spectrum of ionized uranium, which we have described in an earlier contribution[6]. At the time, we assumed that this spectrum may be attributed to uranium ions with a higher degree of ionization than U^+. Subsequently, we separated the spectra associated with different degrees of ionization on the basis of investigation of the polar effect; these results further substantiated our assumption. Apparently, the spectrum described in Ref.1 is the spectrum of triply ionized uranium.

The investigation of the isotope shift of the spectrum lines was carried out by means of a 600 line/mm, concave (5.2 meter) diffraction grating in a Paschen-Runge mounting. The source was a low voltage pulse discharge circuit with minimal inductivity; it is diagrammed in Fig.1.

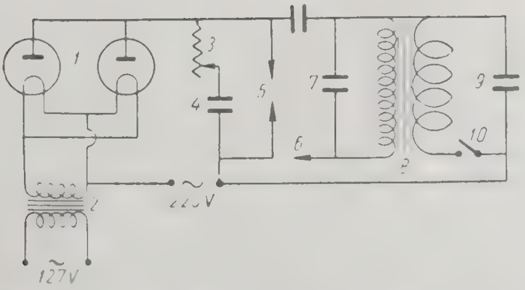

Fig.1. Diagram of low voltage pulse source: 1) VG-236 tubes, 2) heater transformer, 3) rheostat, 4) bank of EF, 4000 μμf, 300 v capacitors, 5) discharge gap, 6) auxiliary gap, 7) 150 μμf, 300 v capacitor, 8) transformer, 9) 20 μf, 300 v capacitor, 10) switch, 11) separation capacitor.

The lower electrode was a briquette compressed of a mixture of the oxide of one of the uranium isotopes with copper powder; the upper electrode was a copper rod. The spectra of the uranium 238, 235 and 233 isotopes were photographed together with the spectrum of iron on Agfa ultraviolet plates in the second and third orders (dispersion 1.6 and 1.05 Å/mm, respectively). About 100 pulse discharges were required for each exposure. For more accurate determination of the unshifted line posi-

tions, we superimposed copper spectra, excited in an ac arc (i = 4 amp, exposure 5 sec) on the isotope spectra.

The shifts of most lines were measured on two or three plates by means of an IZA-2 comparator and the results averaged. The wavelengths of the ionized uranium lines, their intensities, evaluated visually in the 10-point scale, and the magnitudes of the isotope shifts are listed in Table 2.

Of the 200 lines investigated, 175 exhibit a positive shift (the light isotope component is displaced to the side of higher wave numbers) and only 25 lines exhibit a negative shift. It is noteworthy that all the lines with a negative shift are located in the short-wavelength region of the spectrum - approximately to 2700 Å.

Only a few lines have small shifts of the order of 0.1-0.2 cm^{-1}; for most lines the 235-238 shifts fall within the range from 0.3 to 0.7 cm^{-1}, while the 233-238 shifts lie in the range from 0.5 to 0.9 cm^{-1}. The maximum shifts are $\Delta\nu_{235-238} \approx +1.6$ cm^{-1} and $\Delta\nu_{233-238} \approx +2.3$ cm^{-1}.

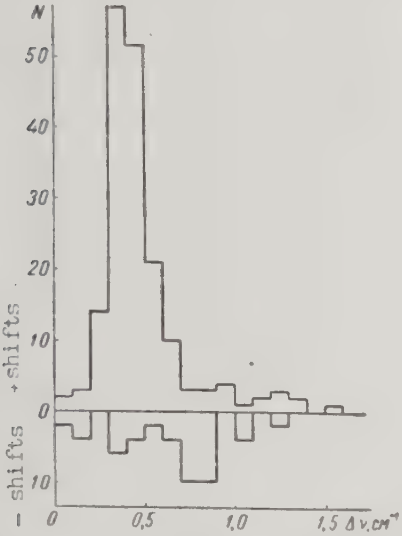

Fig.2. Distribution in magnitude of isotope shifts.

Fig.2 shows a histogram of the distribution in the number of lines with different isotope shifts $\Delta\nu_{238-235}$; the numbers of lines with positive shifts are plotted above the 0-axis; the numbers of lines with negative shifts are plotted downward. The histogram shows a pronounced maximum for positive displacements of 0.3-0.5 cm^{-1} and a small maximum for negative displacements of 0.7-0.9 cm^{-1}. Lower rises are evident in the region of lines with positive shifts > 0.8 cm^{-1}. It must be noted that all such lines are characterized by a relatively low intensity (1-3 in the 10-point scale).

Conclusions

1. The investigated lines in the spectrum of uranium can be divided into three groups, each corresponding to transitions to levels with different electronic configurations. The principal group is composed of lines with positive shifts of the order of 0.3-0.5 cm^{-1}. The second group includes the lines with positive shifts > 0.8 cm^{-1}. The third group comprises lines with negative shifts of 0.7-0.9 cm^{-1}.

2. According to the theory of the volume effect in heavy elements, the energy levels of the lighter isotopes should lie deeper than the levels of the heavier isotopes. Insofar as the isotope shift of lines is connected with displacement of energy levels, obviously in most cases negative shifts will be evident for the lines that correspond to transitions from a nondisplaced or weakly displaced term to a displaced one. And, on the contrary, positive shifts will be observed in lines that correspond to transitions from a displaced term to a nondisplaced one. Thus the lines of the third group with negative shifts are probably associated with $7p \rightarrow 7s$ transitions; lines of the principal group with positive 0.3-0.5 cm^{-1} shifts are associated with $7p \rightarrow 6d$ or $6d \rightarrow 5f$ transitions. The weak lines of the second group with positive > 0.8 cm^{-1} transitions are possibly associated with less intense $7s \rightarrow 5f$ transitions.

Table 2

Wavelengths, intensities and isotope shifts of the lines in the spectrum of ionized uranium*

λ, Å	Intensity (10-point scale)	Isotope shift			
		$\Delta\lambda_{235-238}$, Å	$\Delta\lambda_{233-238}$, Å	$\Delta\nu_{235-238}$, cm^{-1}	$\Delta\nu_{233-238}$, cm^{-1}
2394.124	1	0,075	0,120	1,31	2,10
2457,958	2	0,036	0,053	0,60	0,89
2471,974	4	0,023	0,040	0,38	0,65
2488,815	1	—0,049	—0,089	—0,81	—1,43
2502,752	2	0,020	0,032	0,32	0,51
2503,296	2	0,023	0,036	0,37	0,57
2508,297	5	—0,065	—0,109	—1,03	—1,73
2542,553	4	0,036	0,064	0,56	0,99
2546,439	3	—0,051	—0,089	—0,80	—1,38
2548,166	4	—0,049	—0,079	—0,76	—1,22
2555,918	6	—0,021	—0,035	—0,33	—0,54
2563,206	3	—0,055	—0,096	—0,84	—1,46
2564,902	2	0,074	0,102	1,12	1,55
2572,209	5	—0,053	—0,082	—0,80	—1,24
2575,727	2	—0,006	—0,010	—0,09	—0,15
2576,571	6	—0,067	—0,106	—1,01	—1,60
2585,472	1	0,063	0,090	0,94	1,34
2587,357	2	—0,013	—0,036	—0,19	—0,54
2587,519	2	—0,037	—0,064	—0,55	—0,96
2594,816	2	—0,010	—0,019	—0,15	—0,28
2606,166	1	—0,023	—0,037	—0,34	—0,54
2606,979	5	0,023	0,035	0,34	0,51
2610,405	5	—0,046	—0,072	—0,68	—1,06
2612,817	4	0,025	0,037	0,37	0,55
2624,271	5	—0,052	—0,082	—0,074	—1,19
2625,493	3	—0,024	—0,046	—0,35	—0,67
2627,567	10	0,025	0,039	0,36	0,56
2645,129	1	—0,057	—0,089	—0,81	—1,27
2647,015	3	—0,061	—0,101	—0,88	—1,45
2647,421	3	—0,028	—0,052	—0,41	—0,74
2649,508	2	0,051	0,084	0,73	1,20
2650,585	1	0,037	0,046	0,53	0,65
2651,828	10	0,030	0,038	0,43	0,55
2659,942	4	0,044	0,073	0,62	1,03
2668,938	8	0,053	0,082	0,74	1,15
2673,925	8	0,034	0,055	0,47	0,77
2674,898	3	0,025	0,046	0,35	0,64
2675,598	2	—0,035	—0,065	—0,49	—0,91
2677,325	1	0,031	0,051	0,43	0,71
2680,413	2	—0,052	—0,078	—0,72	—1,08
2682,289	10	0,030	0,046	0,41	0,64
2685,939	4	0,025	0,051	0,35	0,70
2690,005	9	0,030	0,048	0,41	0,66
2693,310	3	0,057	0,101	0,79	1,39
2695,890	3	0,030	0,049	0,41	0,67
2702,822	3	0,101	0,150	1,38	2,05
2703,894	3	0,040	0,062	0,55	0,85
2709,777	2	—0,064	—0,101	—0,87	—1,38
2729,522	3	0,038	0,058	0,52	0,79
2730,805	9	0,033	0,049	0,45	0,66
2738,503	9	0,032	0,047	0,43	0,63
2739,737	9	0,041	0,067	0,55	0,89
2747,146	3	0,039	0,052	0,52	0,69
2748,279	1	0,027	0,042	0,36	0,56
2749,725	2	0,037	0,050	0,49	0,66
2756,280	10	0,032	0,046	0,42	0,60

---

*The lines listed in Table 2 have been attributed to the given spectrum primarily on the basis of the variation in their intensity under different discharge conditions. For a number of lines the classification has been checked on the basis of the variation in line intensity near the electrodes and in a magnetic field.

λ, Å	Intensity	Isotope shift			
		$\Delta\lambda_{235-238}$, Å	$\Delta\lambda_{233-238}$, Å	$\Delta\nu_{235-238}$, cm^{-1}	$\Delta\nu_{233-238}$, cm^{-1}
2762,416	10	0,037	0,053	0,48	0,70
2780,855	4	0,029	0,045	0,37	0,58
2784,361	10	0,024	0,041	0,31	0,53
2785,709	8	0,031	0,050	0,40	0,64
2797,642	1	0,044	0,050	0,57	0,64
2811,481	2	0,042	0,061	0,53	0,77
2818,297	2	0,028	0,042	0,35	0,53
2839,100	3	0,028	0,042	0,35	0,53
2858,761	10	0,027	0,051	0,33	0,62
2863,034	5	0,031	0,047	0,38	0,57
2870,103	3	0,032	0,052	0,39	0,63
2879,116	4	0,033	0,049	0,40	0,59
2879,595	4	0,031	0,049	0,37	0,59
2880,282	4	0,029	0,047	0,35	0,57
2880,802	3	0,103	0,150	1,24	1,80
2894,585	4	0,032	0,048	0,38	0,57
2903,601	4	0,030	0,050	0,35	0,59
2912,897	2	0,077	0,114	0,90	1,34
2916,473	1	0,081	0,128	0,95	1,50
2919,484	1	0,077	0,107	0,90	1,26
2927,160	5	0,031	0,048	0,36	0,56
2933,142	8	0,039	0,054	0,45	0,63
2940,395	6	0,034	0,050	0,39	0,58
2943,370	1	0,027	0,053	0,31	0,61
2945,302	2	0,033	0,049	0,38	0,56
2957,715	8	0,055	0,077	0,63	0,88
2960,263	8	0,037	0,063	0,42	0,72
2982,768	6	0,026	0,046	0,29	0,52
2985,586	1	0,061	0,079	0,68	0,89
2987,311	3	0,038	0,054	0,43	0,60
3005,694	2	0,035	0,052	0,39	0,58
3006,814	2	0,036	0,055	0,40	0,60
3009,273	1	0,033	0,061	0,36	0,67
3013,863	10	0,032	0,048	0,35	0,53
3023,417	1	0,036	0,059	0,39	0,65
3026,773	3	0,049	0,064	0,53	0,70
3032,192	3	0,027	0,047	0,29	0,51
3041,205	2	0,038	0,061	0,41	0,66
3044,849	5	0,046	0,077	[illegible]	0,83
3065,528	5	0,051	0,083	[illegible]	0,88
3068,293	4	0,045	0,077	0,48	0,82
3074,769	9	0,037	0,067	0,39	[illegible]
3086,040	10	0,045	0,083	0,47	0,87
3093,890	7	0,064	0,093	0,67	0,97
3095,188	7	0,040	0,067	0,42	0,70
3103,720	7	0,035	0,067	[illegible]	[illegible]
3122,238	6	0,043	0,078	0,44	0,80
3122,890	3	0,046	0,083	0,47	0,85
3128,360	7	0,062	0,104	[illegible]	1,06
3129,091	3	0,043	0,078	0,44	0,80
3133,661	1	0,051	0,097	0,52	[illegible]
3135,018	2	0,049	0,072	[illegible]	0,73
3137,568	3	0,054	0,081	[illegible]	0,82
3140,007	3	0,096	0,156	[illegible]	[illegible]
3147,457	1	0,054	0,083	[illegible]	0,84
3151,682	1	0,155	0,227	[illegible]	[illegible]
3157,381	1	0,013	0,049	[illegible]	[illegible]**
3159,839	1	0,048	0,078	0,48	0,78
3162,512	5	0,041	0,067	0,41	0,67
3163,791	2	0,067	0,103	0,67	1,03
3174,735	3	0,040	0,075	0,40	0,74
3181,200	9	0,038	0,072	0,38	0,71
3184,463	3	0,043	0,072	0,42	0,71
3189,858	3	0,045	0,078	0,44	0,77
3192,874	1	0,049	0,085	0,48	0,83
3196,743	1	0,128	0,206	1,25	2,01
3199,175	5	0,041	0,077	0,40	0,75
3202,544	2	0,051	0,089	0,50	0,87
3206,279	1	0,110	0,158	1,07	1,54

**Value may include an appreciable error.

λ, Å	Intensity	Isotope shift			
		$\Delta\lambda_{235-238}$, Å	$\Delta\lambda_{233-238}$, Å	$\Delta\nu_{235-238}$, cm^{-1}	$\Delta\nu_{233-238}$, cm^{-1}
3212,435	2	0,048	0,083	0,46	0,80
3217,435	7	0,042	0,075	0,40	0,72
3228,505	3	0,070	0,113	0,67	1,09
3230,206	7	0,046	0,030	0,44	0,77
3250,852	10	0,059	0,100	0,56	0,94
3264,719	5	0,048	0,085	0,45	0,80
3274,505	4	0,056	0,091	0,52	0,85
3277,048	3	0,043	0,078	0,40	0,73
3278,485	3	0,072	0,132	0,67	1,23
3280,626	6	0,046	0,076	0,43	0,70
3285,690	3	0,043	0,073	0,40	0,67
3291,885	3	0,089	0,153	0,82	1,42
3302,325	2	0,041	0,076	0,38	0,70
3309,502	7	0.046	0,078	0,42	0,71
3312,278	2	0,124	0,182	1,13	1,66
3323,561	1	0,051	0,072	0,46	0,65
3327,043	6	0,054	0,081	0,49	0,73
3328,568	6	0,049	0,078	0,44	0,70
3330,423	6	0,045	0,077	0,41	0,69
3338,836	2	0,049	0,078	0,44	0,70
3346,052	10	0,048	0,081	0,43	0,72
3355,028	2	0,056	0,083	0,50	0,73
3360,158	6	0,051	0,089	0,45	0,79
3363,728	6	0,061	0,113	0,54	1,00
3366,914	5	0,054	0,086	0,48	0,76
3375,297	6	0,045	0,089	0,39	0,78
3378,545	6	0,049	0,085	0,43	0,74
3388,465	2	0,029	0,059	0,25	0,51
3390,558	4	0,051	0,083	0,44	0,72
3394,302	4	0,056	0,086	0,48	0,74
3408,979	3	0,054	0,092	0,46	0,79
3417,843	8	0,060	0,095	0,51	0,81
3447,805	3	0,067	0,111	0,56	0,93
3448,440	9	0,048	0,073	0,40	0,61
3468,472	8	0,048	0,073	0,40	0,60
3488,603	1	0,064	0,101	0,52	0,83
3494,453	6	0,048	0,086	0,39	0,70
3521,925	1	0,035	0,051	0,28	0,41
3533,003	1	0,156	0,248	1,25	1,98
3539,933	6	0,044	0,067	0,35	0,53
3548,770	1	0,019	0,029	0,15	0,23
3552,431	3	0,032	0,127	0,25	1,00**
3563,321	6	0,054	0,083	0,42	0,65
3573,458	1	0,054	0,083	0,42	0,65
3600,716	6	0,048	0,073	0,37	0,56
3610,333	7	0,054	0,085	0,41	0,64
3619,398	2	0,038	0,073	0,29	0,56
3646,005	2	0,035	0,051	0,26	0,38
3685,979	4	0,048	0,076	0,35	0,56
3704,338	2	0,064	0,095	0,47	0,69
3719,900	7	0,051	0,089	0,37	0,64
3777,894	4	0,041	0,060	0,29	0,42
3785,854	4	0,051	0,083	0,36	0,58
3833,580	1	0,057	0,070	0,39	0,48
3856,546	4	0,038	0,060	0,25	0,40
3863,389	4	0,038	0,089	0,25	0,60
3865,512	4	0,057	0,095	0,38	0,64
3878,986	3	0,057	0,086	0,38	0,57
3909,500	2	0,060	0,111	0,39	0,73
3999,832	4	0,048	0,092	0,30	0,58
4057,364	1	0,067	0,098	0,41	0,60
4128,966	2	0,048	0,080	0,28	0,47
4158,600	3	0,054	0,102	0,31	0,59
4193,434	2	0,064	0,089	0,36	0,50
4202,825	5	0,054	0,086	0,30	0,49
4204,506	1	0,029	0,083	0,16	0,47**
4362,922	1	0,092	0,144	0,48	0,76
4363,663	1	0,067	0,089	0,35	0,47
4377,026	1	0,077	0,115	0,40	0,60

Striganov & Korostyleva in investigating the lines of uranium observed an odd-even stagger, i.e., additional shifts of the lines of odd isotopes as compared with the lines of even isotopes to the side of displacement of components of isotopes having smaller mass numbers. In the spectrum of ionized uranium, too, for most lines the magnitude of the isotope shift per mass unit is greater between the even isotope U^{238} and the odd isotope U^{235} than between the odd isotopes U^{235} and U^{233}.

The average value of the ratio of these shifts for all the investigated lines is $\Delta\nu_{238-235}/\Delta\nu_{235-233} \approx 1.17$, which is in agreement with the data of other authors.

References

1. O.E.Anderson & H.E.White, Phys.Rev., 71, 911 (1947).
2. L.E.Burkhart, G.Stukenbroeker & S.Adams, Phys.Rev., 75, 83 (1949).
3. J.R.McNally, J.Opt.Soc.America, 39, 271 (1949).
4. D.D.Smith, G.Stukenbroeker & J.R.McNally, Phys.Rev., 84, 383 (1951).
5. A.R.Striganov & L.A.Korostyleva, Zhur.eksp.i teor.fiz., 29 (4), 10, 393 (1955).
6. N.G.Morozova & G.P.Startsev, Optika i spektroskopiia (Optics and Spectroscopy), 2, 382 (1957).

ON THE ACCURACY OF DETERMINATION OF THE HYPERFINE STRUCTURE CONSTANTS FROM OPTICAL MEASUREMENTS

- N.I.Kaliteeveskii, V.I.Perel', and M.P.Chaika

The extensive literature devoted to the determination of nuclear spins by optical measurements includes some papers on the errors that are often encountered when the spins are calculated by quantum mechanical approximation methods. Less attention has been devoted to the accuracy of the intermediate step in which the hyperfine structure (hfs) constants are found from the experimental data. Yet this problem is of primary interest, since if one knows the hfs constants, one can calculate some very important nuclear constants without recourse to quantum mechanics (for example, the ratios of the magnetic or quadrupole moments of two isotopes of a given element).

If one assumes that the noncentral interaction of the nucleus of the electron shells of an atom is due only to the magnetic and quadrupole interactions, it follows, as was shown by Casimir,[1] that each sublevel of the hfs satisfies the formula

$$\nu = \nu_0 + \frac{A}{2} C + BC(C+1), \tag{1}$$

where A and B are the hfs constants used in calculating the magnetic and quadrupole moments of the nucleus and C is the following combination of the quantum numbers:

$$C = F(F+1) - I(I+1) - J(J+1).$$

If the hfs consists of more than three sublevels, the number of levels is greater than the number of unknowns (ν_0, A, and B), and in performing the calculations the mean error may be found by the method of least squares. Then ΔA and ΔB, the errors arising from the experimental uncertainties $\delta(\Delta\nu_i)$ in the determinations of the hfs level spacing, are found in the usual way.

When the spacing is measured, however, in addition to random errors there may occur systematic errors which are difficult to avoid if the line structure is not entirely resolved, if there is some overlap which is insufficiently accounted for, etc. Systematic errors may also arise in the not uncommon situation when the spacing is determined from more than one plate obtained with etalons of different thickness. The occurrence of systematic errors in the measurement of the hfs spacing will lead to incorrect values of A and B and hence will affect the results obtained in calculating of the quadrupole moment of the nucleus. If the outlined procedure is used and the results are reduced statistically, it is difficult to discover any error made in the hfs constants. It is therefore expedient to have another, independent procedure for treating the experimental data. Such a procedure is that recently suggested by Schwartz[2] for finding the higher moments (octupole, etc.) from radiospectroscopic measurements.

It can be shown that if the noncentral interaction of the nucleus and the electron shells is treated as a perturbation and one goes only to the first approximation*, one arrives at the result

$$\Delta\nu_F = \sum_{k=1}^{n} A_k M_{kF}, \tag{2}$$

---

*The second approximation need be used only when the width of the fine structure is of the same order as the hsf splitting.

with no further assumptions. Here n is the number of intervals between the hfs sublevels and A_1 and A_2 are hfs constants related to A and B by the equations

$$A_1 = IJA \quad \text{and} \quad A_2 = \frac{2I(2I-1)J(2J-1)}{3}B.$$

The M_{kI} are numbers depending only on the quantum numbers of the given sublevel, with

$$M_{1F} = \frac{1}{2IJ}C \quad \text{and} \quad M_{2F} = \frac{6}{2I2J(2J-1)(2I-1)}\left[C(C+1) - \frac{4}{3}I(I+1)J(J+1)\right].$$

Further, $\Delta\nu_l$ is calculated from the centroid of the hfs multiplet. The sum in (2) is not taken to infinity, since the M_{kF} vanish for $k > 2I$ or $k > 2J$ (depending on which of these quantum numbers is the smaller); therefore the sum contains as many terms as there are intervals in the hfs multiplet.

The A_k are calculated by the expression

$$A_k = N_k \sum_F (2F+1) M_{kF} \Delta\nu_F, \tag{3}$$

where the N_k are numbers depending on I and J; in this case $\Delta\nu_F$ can be calculated from any hfs component. The uncertainties in the A_k due to experimental errors are given by

$$\delta A_k = N_k \sum_F (2F+1) \,|M_{kF}|\, \delta(\Delta\nu_F).$$

We thus have a simple procedure for calculating the hfs constants. Of course, if there are systematic experimental errors, this procedure may also give incorrect values for A and B, but the fact that (2) contains A_k coefficients which depend on the cube and higher powers of C can sometimes be used to separate out the pure parabolic dependence. Furthermore, agreement between the values of A and B as determined by the two independent methods is a good guarantee that there are no systematic errors.

We shall illustrate these general remarks by two examples showing the application of Schwartz's method to optical spectroscopy.

The first of these is the determination of the hfs constants for U^{233} and U^{235} (Refs.3 & 4). We give below the values of the A_k for the 227_8 term (from the structure of the 6464.97 A line of U^{235}), as well as those for A and B. All the values are in 10^{-3} cm^{-1}.

$A_1 = 103 \pm 1.$
$A_2 = -15.6 \pm 1.$
$A_3 = 0.28 \pm 0.8$
$A_4 = -0.12 \pm 0.4$

$A_5 = -0.05 \pm 0.12$
$A_6 = -0.006 \pm 0.02$
$A_7 = -0.0007 \pm 0.006$

$A = 3.68 \pm 0.04.$
$B = -0.0093 \pm 0.0005.$

The values of A and B obtained in this way are in excellent agreement with those obtained earlier[3] by Casimir's formula, namely

$$A = 3.66 \text{ and } B = 0.0095 \pm 0.002.$$

Similar calculations were performed for the 227_8, 205_8, and 169_7 terms of U^{233}, and these were also found to give quite satisfactory agreement for the values of A and B as obtained by the two independent methods. A consideration of these results shows that in the given case the systematic errors are minor and have no significant effect on the accuracy with which the hfs constants are determined.

The results are quite different in the case of the odd isotopes of copper.[5] In this case one finds a significant difference in the values of B as given by

the two methods. We give below the A_k for the ${}^2D_{5/2}$ term of copper isotopes and the values of A and B as determined by Schwartz's method:

$$\begin{array}{llll} \quad Cu^{63} & \quad Cu^{65} & & \\ A_1 = \;\; 138 \quad \pm 1, & 148 \quad \pm 1, & A_{63} = 61.6 \pm 0.5, & A_{65} = 65.8 \pm 0.5, \\ A_2 = - \; 1.22 \pm 0.3, & -1.09 \pm 0.3, & B_{63} = \; 0.20 \pm 0.05, & B_{65} = \; 0.18 \pm 0.05. \\ A_3 = \quad 0.18 \pm 0.05, & \; 0.097 \pm 0.05, & & \end{array}$$

In a previous work[5] calculation by Casimir's method gave

$$\begin{array}{ll} A_{63} = 61.4, & A_{65} = 65.7, \\ B_{63} = \; 0.30, & B_{65} = \; 0.23. \end{array}$$

We see that the values of B given by these two methods differ by a factor of 1.5, although the values of A are in satisfactory agreement.

The earlier[5] calculations of the quadrupole moments of Cu^{63} and Cu^{65} give much higher values than those obtained by Bleany[6] on the basis of paramagnetic resonance (see table).

Comparison of different methods for finding the hfs constants of copper isotopes

According to	Quadrupole moment in 10^{-24} cm^2		Quadrupole-moment ratio
	Cu^{63}	Cu^{65}	Q_{63}/Q_{65}
Present authors,[5] using the method			
of Casimir	—0.28	—0.22	1.28
of Schwartz	—0.19	—0.17	1.12
Bleany,[6] from paramagnetic resonance	– 0.15	–0.14	
Radiospectroscopic measurements[7]			1.08

The quadrupole-moment ratio Q_{63}/Q_{65} as obtained previously by the present authors[5] is also large compared to Krüger's[7] radiospectroscopic value. The hfs constants obtained by Schwartz's method agree better with the radiospectroscopic values than do those obtained by Casimir's method, as is illustrated in the table. This shows the advantage of using the method we suggest to supplement the usual one for processing the experimental data.

Schwartz's method can be used to calculate moments of higher order. One may ask in this connection whether it is possible to establish the existence of a nuclear octupole moment from optical measurements. Although the values we have presented above for the A_k constants for the ${}^2D_{5/2}$ term of copper show a value of A_3 which is greater than the random error, it would be unwise to assign this value to an octupole interaction. This is because according to Schwartz[2] the octupole moment of any nucleus (in appropriate units) should be of the same order as its quadrupole moment. A rough calculation then shows that one may expect A_3/A_2 to be about equal to 10^{-6}.

Jaccarino et al[8] and Kusch & Eck[9] obtained ratios of this order of magnitude in their determinations of the octupole moments of I^{127} and In^{115}.

One may therefore consider the accuracy of optical measurements to be clearly insufficient for finding the higher moments. Thus the A_3 value mentioned above reflects not an octupole interaction, but some systematic error in the measurement of the hfs sublevels.

Physical Institute
Leningrad State University

References

1. H.Casimir, On the interaction between atomic nuclei and electrons (Teyler's Tweede Genootschap, Haarlem 1936).

2. C.Schwartz, Phys.Rev., 97, 380 (1955).

3. N.I.Kaliteevskii & M.P.Chaika, Optika i spektroskopiia (Optics & spectroscopy), 1, 809 (1956).

4. N.I.Kaliteevskii & M.P.Chaika, Doklady AN SSSR, 103, 49 (1955); Vestnik, Leningrad State University, No.11, 121 (1955).

5. N.I.Kaliteevskii & M.P.Chaika, Optika i spektroskopiia, 1, 606 (1956).

6. B.Bleany, K.Bowers & R.Trenam, Proc.Phys.Soc., A66, 410 (1953).

7. H.Krüger & U.Meyer-Berkhout, Z.Phys., 132, 171 (1952).

8. V.Jaccarino, King, Satten & Stoke, Phys.Rev., 94, 1798 (1954).

9. P.Kusch & T.Eck, Phys.Rev., 94, 1799 (1954).

ON TEMPERATURE DETERMINATION FROM MOLECULAR BAND SPECTRA

- L.V.Leskov & L.P.Vasil'eva

The method of determining the temperature from electronic-vibrational spectra of diatomic molecules, such as CN, C_2 and certain others, in cases when the rotational structure is not resolved was developed in the work of Ornstein, Smit and their co-workers.[1-5] Until recently it was assumed that the accuracy of this method is generally low.[6] The present report is concerned with the accuracy of determining the probability of electronic-vibrational transitions and the accuracy of temperature measurements, the feasibility of utilizing different specific molecules for pyrometric purposes and reabsorption in molecular bands.

We consider the question of the accuracy of theoretical determination of the transition probability with reference to the specific case of the following bands of the violet system of CN: 3883 & 3871 Å (0—0 and 1—1 transitions) and 4216 & 4197 Å (0—1 and 1—2 transitions). The results of experimental and theoretical investigations in which the transition probabilities for these bands were determined are summarized in Table 1.

The accuracy of calculating the transition probability $p(v', v'')$ is determined by

1) the accuracy of the method used in calculating the Franck-Condon factors; the most accurate are the methods based on utilizing the Morse potential function;*

2) the accuracy of the Franck-Condon principle (the pertinent theory is developed in Ref.19-20); it must be noted that the accuracy of determining the dependence of the electronic moment of the transition $R_e(r)$ on the internuclear distance does not exceed 5%; however, inside each sequence (Δv = const) this error is appreciably smaller and for $p(1,1)/p(0,0)$ it amounts to 1%, while for $p(1,2)/p(0,1)$ it is less than 0.2%;

3) the accuracy of defining the molecular constants ω_e, $\omega_e x_e$, and r_e; the values of these for the $B^2\Sigma$ and $X^2\Sigma$ states of CN, as given in different references, are listed in Table 2. Utilizing the data in this table, we obtained the following values for the indicated ratios by means of the formulas given by Manneback[12] (setting $\omega_e' = \omega_e'' = \omega_e$) and Bates[14]:

$$\frac{p(1,1)}{p(0,0)} = 0.88 \pm 0.02, \qquad \frac{p(1,2)}{p(0,1)} = 1.62 \pm 0.02. \tag{1}$$

Somers[5], on the basis of analysis of extensive experimental data, obtained:

$$\frac{p(1,2)}{p(0,1)} = 1.62 \pm 0.02.$$

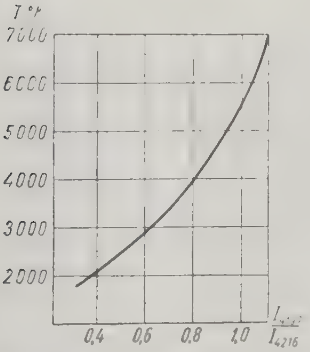

Fig.1. Pyrometric curve for relative intensity of CN 4216 and 4197 A band heads.

Using this value we constructed the pyrometric curve shown in Fig.1 for the ratio of intensities of the 4216 and 4197 Å CN band heads on the basis of the general form of the pyrometric equation.[4]

This method allows of measuring the temperature of a gas in the range from 2000 to 7000°K with an accuracy of 2 to 10% (if the accuracy of measuring the relative intensity $2\Delta I/I$ is at least 4%); the systematic error due to inaccuracy in determining the transition probability equals 0.5 to 2%, respectively.

---

*The accuracy of these methods decreases for large quantum numbers v.

Table 1

Experimental and theoretical values
of transitions probabilities for the CN molecule

A. Experimental values

λ, Å	(v', v'')	According to Refs.				
		[1]	[7]	[8]	[9]	[5]
3883	0,0	1,000	0,842	0,759	1,000	—
3871	1,1	0,870	0,640	0,529	0,813	—
$q = p_2/p_1$	—	0,870	0,760	0,697	0,813	0,870
4216	0,1	0,055	0,132	0,148	0,092	—
4197	1,2	0,095	0,212	0,176	0,133	
$q = p_2/p_1$	—	1,73	1,61	1,19	1,45	1,62

B. Theoretical values determined by different methods

λ, Å	Method of harmonic approximation			Perturbation method		
	[10]	[11]	[12*]	[13]	[13**]	[14**]
3883	—	1,000	1,000	0,910	0,910	0,916
3871	—	0,822	0,826	0,810	0,770	0,771
$q = p_2/p_1$	—	0,822	0,826	0,890	0,846	0,842
4216	—	0,095	0,094	0,030	0,090	0,082
4197	—	0,169	0,176	0,060	0,120	0,146
$q = p_2/p_1$	2,00	1,78	1,87	2,00	1,33	1,78

λ, Å	By means of simplified Morse function				By means of Morse function	Taking R_e into account
	[9]	[15]	[16]	[17**]	[15]	
3883	1,000	0,917	0,920	0,912	0,920	1,000
3871	0,848	0,785	0,788	0,753	0,787	0,880
$q = p_2/p_1$	0,848	0,856	0,857	0,826	0,855	0,880
4216	0,088	0,073	0,075	0,073	0,074	0,058
4197	0,159	0,121	0,122	0,138	0,121	0,094
$q = p_2/p_1$	1,81	1,66	1,63	1,88	1,64	1,62

*Results of our calculations.
**Taking into account the r_e-shift of the wave function.

Inasmuch as our analysis of the accuracy of calculating the transition probability $p(v', v'')$ and the accuracy of measuring the temperature is applicable to other molecules as well, it may be concluded that the accuracy of determining the temperature from the band spectra of such molecules is also determined primarily by the accuracy of measuring the intensity.

Similarly, utilizing the transition probabilities from Ref.15, one can deduce the pyrometric formula for the 4382 and 4365 Å bands of the Swan C_2 system:

$$\frac{2067}{T} = 0.612 + \log\frac{I_1}{I_2} . \qquad (2)$$

By way of another example, let us consider the possibility of measuring the temperature from the bands of the red system of CuO. The rotational-vibrational structure of this system has been analyzed in the work of Mahanti[26],

Table 2

Molecular constants of CN

State	Ref.	Constants				
		ω_e	$\omega_e x_e$	B_e	r_e	α
$A^2\Sigma$	[22]	2069,39	13,95	1,9002		0,0173
	[23]	2068,79	13,176	—	—	—
	[24]	2068,705	13,144	1,8996	1,1718	0,01735
	[25]	2068,705	13,144	1,8991	1,1719	0,01735
	[17]	2068,61	13,144	1,8989	1,1720	0,01722
$B^2\Sigma$	[22]	2164,13	20,25	1,9701	1,1506	0,0222
	[24]	2164,13	20,25	1,9701	1,1506	0,0215
	[25]	2164,13	20,25	1,9701	1,1506	0,0215
	[17]	2163,9	20,2	1,9735	1,1497	0,023

Lejenne & Rosen[27] and Guntsch[28]. We used the recursion formula of Manneback to evaluate the transition probabilities on the basis of the data of Lejenne & Rosen and Mahanti. The results proved to be in conflict with the experimentally observed intensity distribution in the bands of CuO. Using the data of Guntsch, we calculated the transition probabilities for the 6147 and 6162 Å bands by the method of α-averaging the Morse potential function taking into account the r_e-shift[21] and obtained the following pyrometric formula for these bands

$$\frac{201}{T} = 0.107 + \log \frac{I_{6162}}{I_{6147}}. \tag{3}$$

The error in determining the temperature according to this formula with $2\Delta I/I$ = 4% and T = 4000°K amounts to 35%. This means that, in contrast to CN and C_2, the CuO molecule is unsuitable for temperature measurements.

One can propose the following simple criterion for evaluating the suitability of the given molecule for pyrometric purposes:

$$T \lesssim 3\omega_e' \cdot \Delta v, \tag{4}$$

where $\Delta v = |v_1 - v_2|$. Where this condition is not fulfilled, the relative error in determining the temperature will exceed the error in measuring the intensity by more than a factor of two. For example, for CuO at T = 4000°K, $T/\omega_e'\Delta v =$ = 14.

Temperature determination from the molecular bands is impossible if the intensity of these bands is altered by reabsorption. In cases when the rotational structure of the bands remains unresolved, it is difficult to check for the absence of reabsorption. Let us see how one can determine for the 4216 and 3883 Å CN bands, for example, the molecular concentration beginning with which reabsorption at a given temperature and pressure begins to exert a significant influence on the intensity of the bands. According to Sobolev,[29] reabsorption begins to have a substantial effect when the emitter concentration N exceeds a certain limiting or critical value N_{crit}, defined by the following relationship

$$\frac{C}{\sqrt{T}}\, l N_{crit} f \Phi\left(\frac{p}{T}\right) = 0.04. \tag{5}$$

Here C is a constant peculiar to the given emitter, l is the thickness of the emitting layer, $\Phi(x)$ is a monotonically decreasing function and f is the oscillator strength equal to

$$j = f_{cl}\,\frac{p(v',v'')}{\sum\limits_{v',v''} p(v',v'')}\,\frac{S_{J'}}{\sum\limits_{J'} S_{J'}}, \tag{6}$$

where $S_{J'} = J' + 1$ is the strength of the rotational line.

According to Herzberg[24] and White[30],

$$f_{cl} = 0.026,\ f_{peak}(4216) = 1.25\cdot 10^{-6} \quad \text{and} \quad f_{peak}(3883) = 1.8\cdot 10^{-5}. \tag{7}$$

Results obtained by means of the above formula are listed in Table 3.

Table 3

N_{crit} (radicals/cm^3) for CN for two bands and two gas pressures

T°, K	(0,0)		(0,1)	
	1 atmos.	20 atmos	1 atmos.	20 atmos.
2000	$2{,}4\cdot 10^{15}$	$2{,}5\cdot 10^{16}$	$3{,}1\cdot 10^{16}$	$3{,}9\cdot 10^{17}$
4000	$2{,}6\cdot 10^{15}$	$1{,}7\cdot 10^{16}$	$3{,}5\cdot 10^{16}$	$2{,}2\cdot 10^{17}$
6000	$2{,}8\cdot 10^{15}$	$1{,}5\cdot 10^{16}$	$3{,}7\cdot 10^{16}$	$1{,}9\cdot 10^{17}$

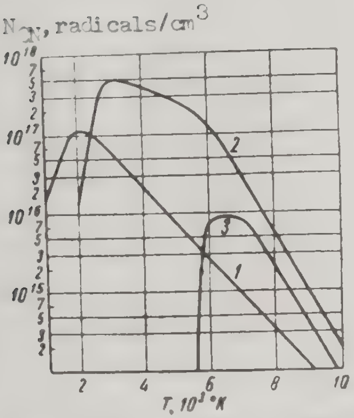

Fig.2. Temperature dependence of the concentration of CN in the arc gas: 1) curve plotted on the basis of the data of Ref.31, 2) according to refined initial data, and 3) for "periarc" gas (gas near but not in the arc).

The curves of Fig.2 characterize the variation of the concentration of CN with the temperature of the arc gas. Curve 1 was plotted on the basis of the data of Ref.31; curve 2 was plotted by us by the same method but using more accurate dissociation potentials[32] and taking into account the formation of dicyan[33]. In both cases it was assumed that the arc gas comprises 30% carbon derivatives[34]. Curve 3 was plotted for a gas containing 10% carbon derivatives (weak-current arc or periarc gas surrounding a heavy-current arc).

Assuming l = 0.3 cm and T = 6000°K, for a weak-current arc, we find from Table 3 that $N_{crit}(0,0) = 0.9\cdot 10^{16}$ and $N_{crit}(0,1) = 5\cdot 10^{16}$ radicals/cm^3. Our theoretical value for N_{CN} lies between $0.7\cdot 10^{16}$ and $1.3\cdot 10^{17}$ radicals/cm^3 (see Fig.2). This means that the CN bands are not reabsorbed in a weak-current arc. Fig.3a shows a microphotogram of the CN band spectrum obtained in the absence of reabsorption; Fig.3b shows a microphotogram of the spectrum with the CN bands distorted by reabsorption (discharge at elevated pressure).

The authors desire to express their deep gratitude to V.K.Prokof'ev for guidance in the work.

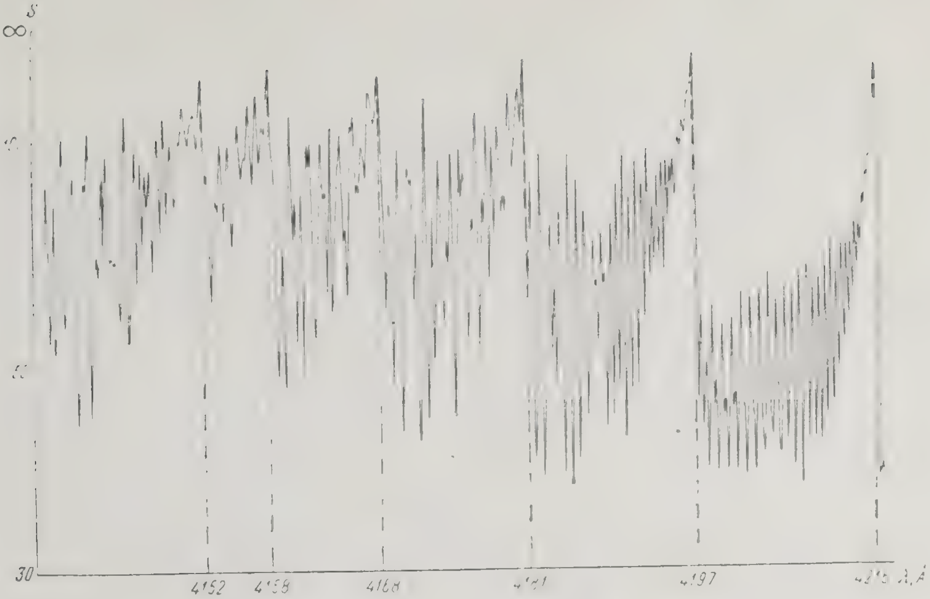

Fig.3a. Microphotogram of CN bands obtained in the absence of reabsorption.

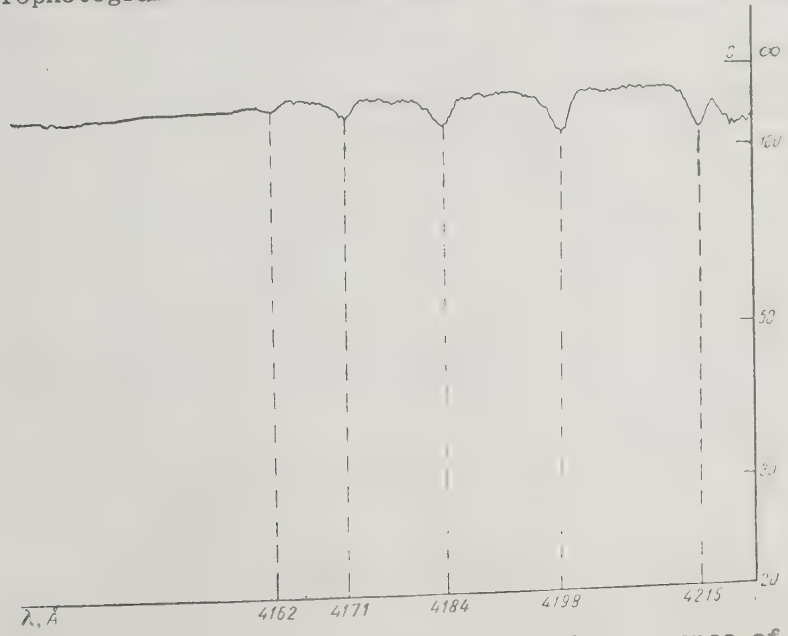

Fig.3b. Microphotogram of CN bands obtained in the presence of strong reabsorption.

References

1. H.Brinkman, Dissertation, Utrecht, 1937.
2. M.Smit-Miessen & J.Spier, Physica, 9, 193, 422 (1942).
3. J.Spier & J.Smit, Physica, 9, 597 (1942).
4. J.Smit, Dissertation, Utrecht, 1950.
5. P.Somers, Dissertation, Utrecht, 1954.
6. A.Gaydon & H.Wolfhard, Flames, their Structure, Radiation and Temperature, 252, 1953.
7. N.Tawde, Proc.Ind.Acad.Sci., 3, 140 (1936).
8. N.Tawde & S.Trivedi, Proc.Phys.Soc.(London), 51, 733 (1939).
9. A.Floyd & R.King, JOSA, 45, 249 (1955).
10. K.Wurm, Z.Astrophys., 5, 260 (1930).
11. A.A.McKellar, Buscombe, Pub.Domin.Astrophys.Observ.Victoria, 23, 1946.
12. C.Manneback, Physica, 17, 1001 (1951).
13. M.Pillow, Proc.Phys.Soc.A., 64, 772 (1951).
14. D.Bates, Monthly Notices, 112, 614 (1952).
15. W.Jarmain, P.Fraser & R.Nicholls, Astrophys.J., 119, 286 (1954).
16. P.Fraser, Proc.Phys.Soc.A., 67, 939 (1954).
17. A.Douglas & P.Routly, Astrophys.J., Suppl.S., 9, 295 (1955).
18. R.Nicholls, Proc.Phys.Soc., A, 69, 741 (1956).
19. P.Fraser, Canad.J.Phys., 32, 515 (1954).
20. R.Nicholls & W.Jarmain, Proc.Phys.Soc.A., 69, 253 (1956).
21. P.Fraser & W.Jarmain, Proc.Phys.Soc.A, 66, 1145, 1153 (1953).
22. W.Jevons, Proc.Roy.Soc.A, 112, 407 (1926).
23. F.Jenkins & K.Roots, Phys.Rev., 39, 16 (1932).
24. G.Herzberg, Molecular Spectra and Molecular Structure, I.Diatomic Molecules, II ed., New York, 1950.
25. Constantes Selectionnes, Donness Spectroscopiques concernant les Molecules Diatomiques, Paris, 1951.
26. P.Mahanti, Nature, 125, 819 (1930).
27. J.Lejenne & B.Rosen, Bull.Soc.Soy.Sci.
28. A.Guntsch, Nature, 157, 662, 1946; Arkiv. Mat., Ast.,Fys., 33, A, 2 (1945).
29. N.N.Sobolev, Trudy (Proceedings), Physical Institute, USSR Academy of Sciences, 7, 161 (1956).
30. J.White, J.Chem.Phys., 8, 79 (1940).
31. R.Wienecke, Z.Physik, 146, 39 (1956).
32. A.Gaydon, Dissociation Energies and Spectra of Diatomic Molecules, II, ed., 1952.
33. E.Rutner, W.McLain & K.Scheller, J.Chem.Phys., 24, 173 (1956).
34. H.Maecker, Z.Physik, 136, 119 (1953).

MOTION OF IONS IN PLASMA

- Iu.M.Kagan

The knowledge of the motion of ions in plasma is fundamental to the solution of a number of problems in gas discharge dynamics. Yet whereas there are a number of theoretical and experimental investigations concerning the velocity distribution of electrons in plasma, there are no data relative to the distribution in velocity of ions. Attempts to obtain such data by the probe technique proved to be fruitless.

Hence there was developed a spectroscopic method$^{1-5}$ which consists of investigating the ionic line contours with observation along and across the discharge tube and investigation of the line shifts in observing along the discharge axis. If the discharge conditions are such that the principal cause of broadening is the Doppler effect (and this is true in discharge plasma at low pressure), then investigation of the line shift yields information on the ion drift velocity and investigation of the shape and half-width of the lines yields information on the distribution in energy of the ions and their "temperature".

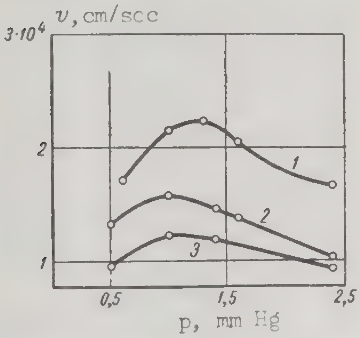

Fig.1. Variation of the ion transport velocity along the axis of a discharge tube with the pressure and current strength: 1) i = 400 milliamp, 2) i = 300 milliamp, 3) i = 200 milliamp.

Such discharge conditions were realized in inert gases at pressures of 0.1 to 3 mm Hg and current densities up to 50 amp/cm^2. Such relatively high current densities were obtained by contracting the central portion of the discharge tube. The ionic lines under these conditions were characterized by appreciable intensity. There were carried out systematic interferometric measurements of the line contours of atoms and ions in argon and measurements of the shifts in argon, neon, krypton and xenon. In view of the smallness of the shifts a special method was employed for measuring them.^{2}

The variation of the ion drift velocity with the pressure for different strengths of the discharge current in argon is shown in Fig.1 and for a discharge current of 400 milliamp in argon, krypton and xenon in Fig.2. It is noteworthy that the drift velocity does not vary monotonically with the pressure but exhibits a maximum at a certain pressure.

Examination of the lines showed that the line contour is a Doppler one, shifted in the direction of the longitudinal field and that the ionic gas, in observation along the axis of the discharge tube, may be characterized by a "temperature" T_p which somewhat exceed the temperature T of the atoms and, like the displacement, varies nonmonotonically with the pressure and has a maximum at a certain pressure. This can be seen in Fig.3. In measurement of the line contour with observation across the tube the "temperature" of the ionic gas T* is appreciably higher than T and increases monotonically with decreasing pressure (Fig.4).

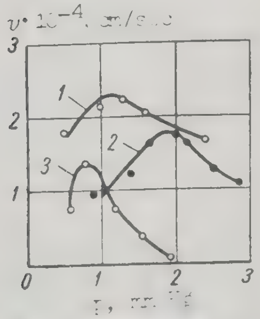

Fig.2. Variation of the ion transport velocity with the gas pressure at a current of 400 milliamp" 1) A, 2) Kr, 3) Xe.

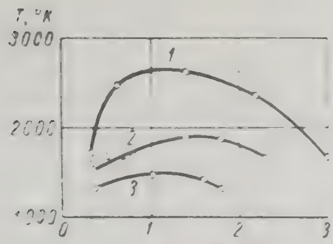

Fig.3

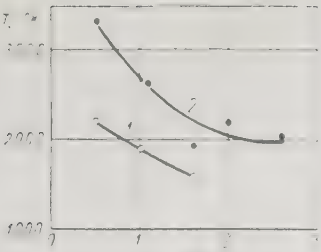

Fig.4

Fig.3. Variation of the "temperature" T_p of the ionic gas with the pressure (observation along the axis of the discharge tube) and the current strength: 1) i = 250 milliam, 2) 120 milliamp and 3) 60 milliamp.

Fig.4. Variation of the temperature T of the atoms (curve 1) and the "temperature" T* (observation across the discharge tube) curve 2) with the pressure.

Further measurements in argon were carried out in a discharge tube whose central part was somewhat widened (to 4 mm diameter). This allowed of sealing in the probes directly in the investigated discharge gap and of measuring, with reference to the ionic parts of the probe characteristics[6,7], the electron concentration N_e and the temperature T_e of the electron gas.[8] As may be seen from Fig.5 N_e and T_e vary nonmonotonically with the discharge current. This may obviously be explained by rarefaction of the gas in the discharge gap with increasing discharge current density - an effect which has been observed by a number of authors.

Measurements of the relative intensities of A II lines with variations in the discharge conditions in conjunction with probe measurements indicated that the excitation of ions by electron collision under the investigated condition is primarily a step process. Only in the case of step formation of excited ions and a short lifetime of the excited state will the contour of the ion lines be determined by the ion velocity distribution function; information on this function can be obtained from spectroscopic observations.

For interpreting the experimentally determined regularities one must first choose an appropriate model for ion-atom interaction. Analysis of the experimental and theoretical material on the interaction of ions with atoms of the parent gas (and this case is the most important in gas discharge physics) shows that the fundamental interaction process is that of resonance charge exchange.

Let us consider the simplest case of the two-dimensional problem, corresponding to experiments on determining the drift velocity of ions in the parent gas in an external homogeneous electric field.[9] The kinetic equation for this case is of the form

$$\frac{eE}{MN}\cdot\frac{\partial f}{\partial v_z}=n(v)\int f(\underline{v}')\,|\underline{v}-\underline{v}'|\,q(|\underline{v}-\underline{v}'|)\,d\underline{v}'-f(\underline{v})\times\int n(\underline{v}')\,|\underline{v}-\underline{v}'|\,q(|\underline{v}-\underline{v}'|)\,d\underline{v}', \quad (1)$$

where $f(\underline{v})$ and $n(v)$ are functions characterizing the velocity distribution of the ions and atoms, N is the concentration of atoms, E is the field strength, $q(|\underline{v}-\underline{v}'|)$ is the effective charge exchange section, e is the charge and M is the mass of an ion.

Assuming the charge exchange cross section q to be independent of the velocity, which is not inconsistent with the experimental data for low energies,

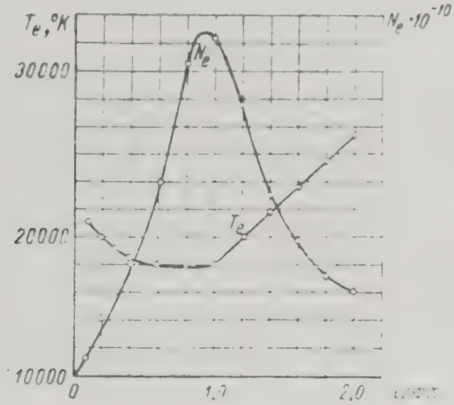

Fig.5. Variation of the electron gas temperature T_e and electron concentration N_e in argon with the discharge current at a pressure p = 1.75 mm Hg.

we can obtain the solution for Eq.(1). For the ion drift velocity $\bar{v}_z$ in the direction of the field we obtain

a) $$\bar{v}_z = \sqrt{\frac{2}{\pi} \cdot \frac{eE}{MqN}}, \quad \text{for strong fields} \quad (2)$$

b) $$\bar{v}_z = 0.5 \frac{eE}{qN\sqrt{3kTM}}, \quad \text{for weak fields} \quad (3)$$

and approximately

c) $$\bar{v}_z = \sqrt{\frac{2}{\pi} \cdot \frac{eE}{MqN}} \cdot F\left(\sqrt{\frac{3qNkT}{2eE}}\right), \quad (4)$$

for any arbitrary field, where F is a known function.

These functional dependences are in agreement with experimental determinations of the drift velocity of ions in inert gases.[10,11] The results of calculations of the drift velocity as a function of the quantity E/p_0 are shown by the solid line curves in Figs.6 & 7.

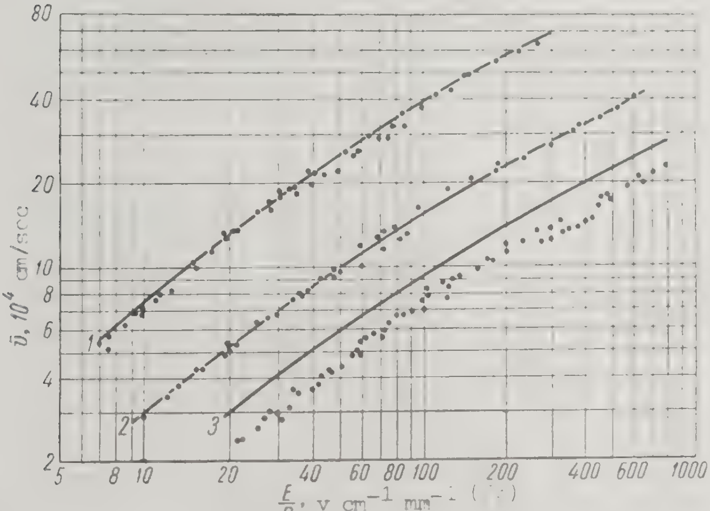

Fig.6. Calculated (curves) and measured (points) drift velocities of ions of 1) helium, 2) neon and 3) argon in the respective parent gases.

The above results are not yet applicable directly to the motion of ions in the positive column of a discharge. In a positive column, in addition to the longitudinal field, there also exist ionization, a transverse field directed towards the walls and escape of ions to the tube walls. The last factor is particularly important at low pressures when the departure of ions to the walls may be the primary factor limiting the motion of ions along the axis of the tube. At sufficiently low pressures one can neglect ion-ion collisions; in this case the kinetic equation for a cylindrical discharge tube becomes[12]

$$Lf = \frac{eE_r(\rho)}{M}\left[\cos\varphi \frac{\partial f}{\partial v_\rho} - \frac{\sin\varphi}{v_\rho} \cdot \frac{\partial f}{\partial\varphi}\right] + v_\rho\left[\cos\varphi \frac{\partial f}{\partial\rho} - \frac{\sin\varphi}{\rho} \cdot \frac{\partial f}{\partial\varphi}\right] + \frac{eE}{M} \cdot \frac{\partial f}{\partial v_z} - zN_e n(v) = 0 \quad (5)$$

with the boundary condition $f = 0$ with $\rho = R$ and $\cos\varphi < 0$, where v_z is the projection of the velocity on the axis of the tube, v_ρ is the projection of the velocity on the plane normal to the tube axis, φ is the angle between the perpendicular to the axis passing through the given point and the velocity

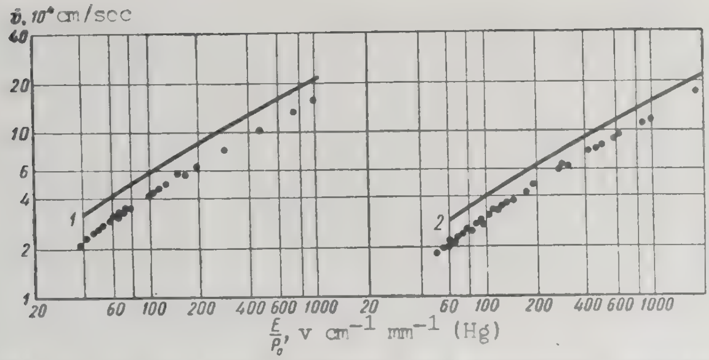

Fig.7. Calculated (curves) and measured (points) drift velocities of ions of 1) krypton and 2) xenon in the respective parent gases.

component perpendicular to the axis, $E_\perp(\rho)$ is the intensity of the transverse field, z is the number of ionizations per electron per sec and N_e is the electron concentration.

Then for the ion drift velocity along the tube axis we obtain

$$\bar{v}_z = 0.69\frac{eE}{Mz}, \tag{6}$$

and for the "temperature" T_p of the ions with observation along the axis

$$T_p = T + 0.82\frac{e^2}{kM}\cdot\frac{E^2}{z^2}. \tag{7}$$

Eqs.(5) and (6) acquire direct physical meaning if we bear in mind that $1/z = \tau$, where τ is the mean time the ion remains in the discharge.

Averaging over the cross section of the discharge tube and utilizing the known variation of the transverse field in the region of low temperatures, we obtain for the transverse temperature of the ions[13]

$$T^* = 0.56\,T + 0.13\,T_e, \tag{8}$$

where T_e is the electron gas temperature. It will be evident that at low pressures T^* may appreciably exceed T. To explain the experimental results one must extend the theory to the case of arbitrary pressures, when the right hand side of Eq.(5) contains a term $(\partial f/\partial t)_{st}$.[14] For approximate solution of the kinetic equation in this case one can use the method in which the ionic velocity distribution function is written in the form

$$f = \left(\frac{M}{2\pi k}\right)^{3/2}\frac{n_p}{\sqrt{T_p T_\psi T_z}}\exp\left[-\frac{M}{2kT_z}(v_z-\bar{v}_z)^2-\frac{M}{2kT_\rho}(v_\rho-\bar{v}_\rho)^2-\frac{M}{2kT_\psi}v_\psi^2\right], \tag{9}$$

where v_z, v_ρ and v_ψ are the projections of the ion velocities on the orthogonal axes of the cylindrical system of coordinates and n_p, T_p, T_ψ, T_ρ, $\bar{v}_z$ and $\bar{v}_\rho$ are parameters that are functions of the distance from the axis and are defined by integral conditions of the form

$$\int\varphi(v_z, v_\rho, v_\psi)\,Lf\,d\underline{v} = \int\varphi(v_z, v_\rho, v_\psi\left(\frac{\partial f}{\partial t}\right)_{st}d\underline{v}. \tag{10}$$

Setting $\varphi(v)$ equal to 1, v_z, v_ρ, v_ρ^2, v_z^2 and v_ψ^2, we obtain six equations for determining the six parameters.

For the ion drift velocity in the vicinity of the axis, we obtain approximately

$$\bar{v}_z = \frac{\frac{eE}{M}}{1.4\cdot z+\frac{16}{3\sqrt{\pi}}\cdot\frac{1}{\lambda}\sqrt{\frac{kT}{M}}}. \tag{11}$$

It will be evident from Eq.(4) that at low pressures $\bar{v}_z$ can increase with pressure due to increase of E and some decrease of z. At high pressures $\bar{v}_z$ must

decrease with pressure due to decrease of the mean free path λ. Thus $\overline{v_z}$ varies nonmonotonically with the pressure, which explains the results of the interferometric measurements.

To obtain a similar general expression for T_p one must carry out a more precise calculation. However, even without this one can show that the "temperature" T_p of the ions corresponding to their movement along the discharge axis varies nonmonotonically with the pressure. In the limiting case of low pressures it increases according to Eq.(7). In the limiting case of high pressures, carrying out the calculation for the plane case (at high pressures this approximation is permissible since the effect of escape of ions to the walls is negligibly small), we obtain

$$T_p = T\left(1 + \frac{3\pi}{256} \cdot \frac{e^2E^2}{k^2T^2}\lambda^2\right). \tag{12}$$

As will be seen, T_p falls off with increasing pressure. Therefore T_p must have a maximum at a certain pressure. To determine the position of this maximum one must carry out the more precise calculation referred to above.

Thus the theory gives a satisfactory qualitative explanation of the data obtained from interferometric measurements. Quantitative comparisons are as yet impossible in view of the influence of rarefaction of the gas under the conditions in which the interferometric measurements were performed and the lack of data relative to the value of ε under these conditions.

References

1. S.E.Frish & Iu.M.Kagan, Zhur.eksp.i teor.fiz., 12, 342 (1942).
2. S.E.Frish & Iu.M.Kagan, ibid., 17, 577 (1947).
3. S.E.Frish & Iu.M.Kagan, ibid., 18, 519 (1948).
4. S.E.Frish & Iu.M.Kagan, Izv.AN SSSR, Ser.fiz., 12, 358 (1948).
5. V.M.Zakharova, Optika i spektroskopiia (Optics & Spectroscopy), 1, 636 (1956).
6. Iu.M.Kagan & V.I.Perel', Doklady AN SSSR, 91, 1321 (1953).
7. Iu.M.Kagan, V.I.Perel' & P.O.Ripatti, Vestnik, Leningrad Univ., 8, 129 (1955).
8. V.M.Zakharova & Iu.M.Kagan, Optika i spektroskopiia, 1, 627 (1956).
9. Iu.M.Kagan & V.I.Perel', Doklady AN SSSR, 98, 575 (1954).
10. J.A.Hornbeck, Phys.Rev., 83, 374 (1951); ibid., 84, 615 (1951).
11. R.N.Varney, Phys.Rev., 88, 362 (1952); ibid., 89, 708 (1953).
12. Iu.M.Kagan & V.I.Perel', Optika i spektroskopiia, 2, 298 (1957).
13. Iu.M.Kagan & V.I.Perel', ibid., 4, 3 (1958).
14. Iu.M.Kagan & V.I.Perel', ibid., 4, 285 (1958).
15. B.N.Kliarfel'd, Trudy (Proceedings), All-Union Electrotechnical Institute, No.41, 165 (1941).

ON THE POSSIBILITY OF UTILIZING SPECTRUM LINES AS WAVELENGTH NORMS AND A LENGTH STANDARD

- N.R.Batarchukova

As long ago as 1829 Jacques Babinet suggested the possibility of adoption of some wavelength of light in vacuum as an invariant and reproducible standard of length. Until now, however, despite the fact that light waves are being used extensively for practical measurements of length, the question of selection of a new standard of length instead of the platinum-iridium meter remains open. In interferometric measurements the reproducible and immutable standard of length is the wavelength of the red line of natural cadmium. Investigations carried out during the past 50 years have shown that in accepting a new definition of the unit of length the wavelength of a light wave must be not only reproducible and invariant, as is the wavelength of the red line of natural cadmium, but it must also have the character of a natural constant. This is why in 1953 at the session of the Advisory Committee on the Definition of the Meter[1], established by the International Committee on Weights and Measures in 1952, it was resolved that "when the time comes the meter must be defined by the wavelength of light radiation propagating in vacuum with both the observer and emitter at rest relative to each other. This radiation must be defined by two spectral terms of an atom whose spectrum should not have hyperfine structure. The spectral terms must not be subjected to external perturbing influences."

This definition of the future standard of length actually endows it with the character of a natural constant. But, on the other hand, it is difficult to imagine how an emitting atom can be fully shielded from all perturbing influences. From theoretical considerations it can be stated that the radiation will be closest to the natural if the gas is excited at a low pressure and one selects a spectral line associated with transitions that comprise terms with not very large values of the principal quantum number. One must also take all measures to minimize all symmetric broadening of the line so as to insure the maximum attainable accuracy in determining the wavelength. It must be emphasized that the physicists and metrologists, concerned with selecting a new standard of length, were guided not only by these theoretical considerations but primarily aimed at obtaining lines without hyperfine structure and hence set themselves the task of investigating all the lines without hyperfine structure. As a first step there were investigated the spectrum lines of four isotopes of mercury, krypton and cadmium.

The green line of Hg^{198}, the yellowish-green line of Kr^{86} and the red line of Cd^{114} were proposed as standards instead of the red line of natural cadmium back in 1953. At that time, however, the Advisory Committee on Definition of the Meter found that the proposals regarding all three of these spectrum lines are inadequately documented, and selection of a new standard of length (primary norm) was put off pending final comparative investigations of all monoisotopic radiations. Hence in the period from 1953 to 1957 all work aimed at selection of a new spectrum line was directed, on the one hand, along the line of detailed investigation of already proposed radiations and improvement of light sources and, on the other hand, the investigation of the radiation of other even-even elements. Aside from the four isotopes of mercury, krypton and cadmium, the even-even nuclides include isotopes of xenon, thorium and lead. The four isotopes of xenon and thorium were investigated in recent years in West Germany.[2]

The purpose of our work was investigation of the visible region of the spectrum of Pb^{206} with a view to evaluating the possibility of choosing its radiation as the new standard of length and wavelength.

The light source in the work was an electrodeless tube of fused quartz filled with 3-4 mg Pb^{206} and pure argon at a pressure of 1-2 mm Hg. The lead spectrum was excited by means of an LC-generator with a frequency of 180-200 Mc.

It proved feasible to observe a large number of relatively bright lines in the spectrum of lead in the electrodeless discharge, provided the light source was heated to 480-500°. Investigation of the radiation consisted of visual evaluation of the visibility of the interference pattern in the lines of Pb^{206} with different path differences in the interferometer.

Primary attention was given to the green line of Pb^{206} with λ = 5005 Å; the wavelength of this line was compared with that of the red line of Cd^{114}. By way of high resolution instruments we used two Fabry-Perot etalons (a tubular etalon of fused quartz with a distance of 100 between the mirrors and a conventional etalon with a spacer of 16.5 mm). Interferometric spectrograms were obtained for two path differences (33 and 200 mm). Measurement of the diamteres of the interference fringes was carried out on a photoelectric comparator.[3] The refined value for the wavelength of the green line of Pb^{206} obtained by the method of coincidence of fractional parts of the interference orders was λ = 5005.4301 Å with an accuracy of within $2 \cdot 10^{-4}$ Å.

As a result of the study, it may be stated that under conditions of an electrodeless discharge with heating of the source to 450-500° the spectrum lines of Pb^{206} as regards width and reproducibility of the wavelength are somewhat inferior to the red line of Cd^{114} and the lines of Kr^{86} and Hg^{198}. This, however, must be regarded as a preliminary conclusion. One can, for example, use lead iodide instead of pure lead. The excitation of the lead spectrum in this compound occurs at a source temperature some 2.5 times lower than for pure lead. This should, of course, allow of appreciably narrowing the lead lines. In addition, it must be noted that the lead which we had available for our investigations had an inadequately high percent of enrichment with the 206 isotope (80%), whereas at present one can obtain lead samples consisting of 100% Pb^{206} (from the decay of polonium). Hence it should be of interest to continue the investigation using the pure 206 isotope in an improved light source. Even if the lines of this lead isotope are not found suitable for a new standard of length, they can undoubtedly be utilized in interferometric practice as auxiliary standards and in spectroscopy as secondary norms. In connection with adoption of a new primary wavelength norm, undoubtedly secondary norms will also be reviewed and in doing so attention should be given to the lines in the spectrum of Pb^{206}.

A report on the present work was presented at the September 1957 session of the Advisory Committee on Definition of the Meter as material on the investigation of the radiation of monoisotopic light sources; after careful consideration of the results of all investigations carried out in the period from 1953 to 1957 in different national metrological laboratories and in the International Bureau, a primary wavelength standard was chosen. Final adoption of the primary as well as of secondary norms is on the agenda of the August 1958 meeting of the General Astronomic International Assembly in Moscow. The decision of the Advisory Committee is only a preliminary recommendation for the General Assembly.

The Advisory Committee on Definition of the Meter recommends "that the meter be defined in terms of the radiation corresponding to the transition between the $2p_{10}$ and $5d_5$ levels of the Kr^{86} atom and taken equal to 1,650,763.73

times the wavelength of this radiation in vacuum." This recommendation was adopted unanimously despite the fact that there were also proposed other radiations which as regards their metrological qualities are possibly no whit inferior to the accepted orange line of Kr^{86}.

Investigation of the accuracy of reproducibility of the meter by means of the platinum-iridium rod showed that the ruled meter can no longer satisfy the requirements of modern metrology and that the adoption of a new definition of the meter in terms of a wavelength is imperative to insure continued progress to the field of measurement of length. Hence debate of the question which particular radiation should be used for defining the meter should no longer be allowed to delay conversion in principle to the new definition of the unit of length. If further investigations of monochromatic light sources lead to the discovery of other better radiations, the line now chosen can readily be replaced by another one.

References

1. Tirage à part. Proc. Verb. C.I.Pds et Mes., XXIV. -M. (1953).

2. E.Engelhard, Proc.Verb.C.I.Pds. et Mes. (1957).

3. A.I.Kartashev, Trudy (Proceedings), VNIIM (All-Union Scientific Research Institute of Metrology), No.26 (86), 30 (1955).

OBSERVATION OF ANOMALOUS DISPERSION IN SHORT-TERM PROCESSES

- A.M.Shukhtin and V.S.Egorov

The use of Rozhdestvenskii's method of "hooks" is based on recording spectrograms by means of a low-transmission interferometer system. The commonly used exposure times (from a few minutes to a few seconds) allow of obtaining excellent spectrograms and are satisfactory for determination of atomic constants (f numbers) or the study of such phenomena as dc conduction in gases. But this procedure cannot, of course, be used to study processes that involve rapid changes in the interference pattern, particularly explosive processes lasting only microseconds as well as all types of rapid transient processes. We undertook to adopt the "hook" method to the study of such processes. Inasmuch as the observed pattern must not change while it is being photographed, the exposure time cannot comprise more than a certain fraction of the duration of the process involved and must be a few orders of magnitude shorter than usual.

This can be achieved by enhancing the sensitivity of the radiation detector, increasing the brightness of the continuous spectrum source and enhancing the transmission factor of the apparatus. In order to reduce the exposure time we used a powerful pulsed source and attempted to obtain a spectrogram from each brief flash appropriately synchronized with the process to be studied. A similar procedure has already been used successfully by other investigators.[1]

Although the effective aperture of our optical system was lower than that of the equipment used by others[1], we were able to obtain spectrograms during single flashes of 20-30 μsec duration. The apparatus has been described elsewhere.[2] Here we shall give only the preliminary results of certain investigations, which have not yet been carried to completion and should therefore be regarded merely as illustrations of the potentialities of the method. In the first experiments a discharge tube of the type shown schematically in Fig.1 was introduced into one of the interferometer light beams. The tube was filled with gas (neon or hydrogen) and a furnace was used to create a cloud of sodium vapor in its middle section. The vapor gradually diffused and formed a metallic mirror surface on the tube walls near the furnace. The pulse discharged through the tube and synchronized with the continuous spectrum flash was approximately rectangular with a duration of ~250 μsec and an amplitude of ~800 amp. We photographed the "hooks" at the yellow sodium doublet lines before the discharge (Fig.2a), during the flat part of the pulse (Fig.2b) and several hundred microseconds after the pulse (Fig.2c). It will be evident from the patterns that while during passage of the current anomalous dispersion disappears entirely, after passage of the current its magnitude is many times greater than the dispersion observed before the pulse. This large growth of dispersion is evidently produced by the stripping of Na atoms from the mirror surface through radiation heating or particle bombardment. The disappearance of dispersion during the flow of current may result from atomic transitions to higher energy states, the transport of matter from the observed region or negative dispersion. The amount of negative dispersion depends on the atomic concentration at the upper level of a given transition.

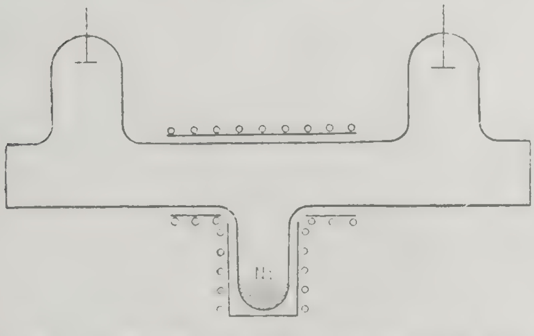

Fig.1. Diagram of discharge tube for studying short-term processes by the method of "hooks".

OBSERVATION OF ANOMALOUS DISPERSION IN SHORT-TERM PROCESSES

- A.M.Shukhtin and V.S.Egorov

The use of Rozhdestvenskii's method of "hooks" is based on recording spectrograms by means of a low-transmission interferometer system. The commonly used exposure times (from a few minutes to a few seconds) allow of obtaining excellent spectrograms and are satisfactory for determination of atomic constants (f numbers) or the study of such phenomena as dc conduction in gases. But this procedure cannot, of course, be used to study processes that involve rapid changes in the interference pattern, particularly explosive processes lasting only microseconds as well as all types of rapid transient processes. We undertook to adopt the "hook" method to the study of such processes. Inasmuch as the observed pattern must not change while it is being photographed, the exposure time cannot comprise more than a certain fraction of the duration of the process involved and must be a few orders of magnitude shorter than usual.

This can be achieved by enhancing the sensitivity of the radiation detector, increasing the brightness of the continuous spectrum source and enhancing the transmission factor of the apparatus. In order to reduce the exposure time we used a powerful pulsed source and attempted to obtain a spectrogram from each brief flash appropriately synchronized with the process to be studied. A similar procedure has already been used successfully by other investigators.[1]

Although the effective aperture of our optical system was lower than that of the equipment used by others[1], we were able to obtain spectrograms during single flashes of 20-30 μsec duration. The apparatus has been described elsewhere.[2] Here we shall give only the preliminary results of certain investigations, which have not yet been carried to completion and should therefore be regarded merely as illustrations of the potentialities of the method. In the first experiments a discharge tube of the type shown schematically in Fig.1 was introduced into one of the interferometer light beams. The tube was filled with gas (neon or hydrogen) and a furnace was used to create a cloud of sodium vapor in its middle section. The vapor gradually diffused and formed a metallic mirror surface on the tube walls near the furnace. The pulse discharged through the tube and synchronized with the continuous spectrum flash was approximately rectangular with a duration of ~250 μsec and an amplitude of ~800 amp. We photographed the "hooks" at the yellow sodium doublet lines before the discharge (Fig.2a), during the flat part of the pulse (Fig.2b) and several hundred microseconds after the pulse (Fig.2c). It will be evident from the patterns that while during passage of the current anomalous dispersion disappears entirely, after passage of the current its magnitude is many times greater than the dispersion observed before the pulse. This large growth of dispersion is evidently produced by the stripping of Na atoms from the mirror surface through radiation heating or particle bombardment. The disappearance of dispersion during the flow of current may result from atomic transitions to higher energy states, the transport of matter from the observed region or negative dispersion. The amount of negative dispersion depends on the atomic concentration at the upper level of a given transition.

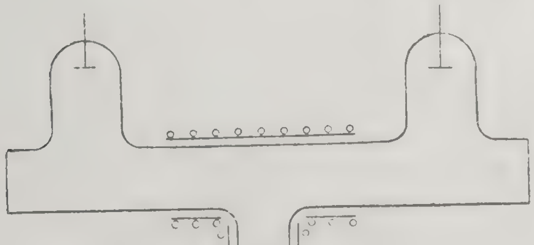

Fig.1. Diagram of discharge tube for studying short-term processes by the method of "hooks".

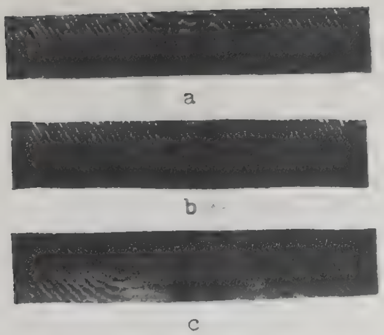

Fig.2. Interference pattern near the sodium yellow doublet: a) before discharge, b) during flat part of pulse, c) a few hundred microseconds after the pulse.

The absence of dispersion near side series lines indicates a low atomic concentration in the first excited state as well as a small negative dispersion term. The flow of current can change the velocity and character of particle motion and result in the transport of matter. In our case such transport in the longitudinal direction cannot affect the amount of dispersion. Dispersion is reduced by transport to the tube walls and by atomic transitions to excited states. Therefore the disappearance of dispersion under the influence of a pulse may be due to atomic excitation and ionization and reduced vapor density in the observed region. By evaluating the role of each of these factors in reducing dispersion, we could determine the degree of excitation and the true density of matter in the discharge gap; this was the principal purpose of our furthur experiments.

Sodium has a low ionization potential so that the lines of Na ions lie in the far ultraviolet, where observation of dispersion is precluded. We considered it advisable to investigate the variation of dispersion with a higher ionization potential, using substances for which it would be possible to determine simultaneously the atomic concentrations in both excited and ionized states.

A tube similar to that of Fig.1, but without Na, was filled with Ne at 0.5-1.5 mm Hg and inserted into the interferometer. Dispersion was observed near the lines in the red-yellow region, whose lower levels correspond to the $2p^5 3s$ electron configuration. Observations showed that a small degree of dispersion appears immediately after passage of the leading edge of the pulse and slowly increases during the period of the pulse; after cut-off of the current there is a sharp rise followed by gradual falling off to zero in 800-1000 µsec.

This behavior of the dispersion agrees with absorption data on the concentration of excited atoms[3] and is interpreted most simply as follows: During passage of the pulse the gas is strongly excited and ionized, with atoms making transitions to high-lying energy levels. The atomic concentration in the first excited state is low and varies somewhat over the flat part of the pulse, which thus represents an unsteady discharge state. After the current is cut off, the atoms make cascade transitions to intermediate levels, corresponding to the $2p^5 3s$ configuration, which gives rise to high concentrations at these levels. However, observations of dispersion in magnesium and mercury vapors cannot be interpreted as easily in this manner. The experimental procedure for these elements was the same as previously. Dispersion was observed near resonance lines whose lower levels corresponded to excited atomic states as well as near the resonance lines of magnesium ions. The dispersion in the vicinity of the atomic resonance lines decreased sharply or disappeared entirely immediately after switching on the current or a little after the leading edge of the current pulse. No dispersion was observed near lines corresponding to excited atomic Hg states, either during or following the pulse. A relatively insignificant amount of dispersion appeared near magnesium ion resonance lines during the passage of current.

Thus with the passage of a pulse through either mercury or magnesium vapor the concentration of normal atoms is sharply reduced, the concentration

of excited atoms is negligibly small and the Mg II concentration is also small. Following passage of the pulse, the concentration of normal atoms is gradually restored but no appreciable concentration of excited atoms builds up. The behavior of Mg and Hg vapors thus differs from that of Ne and suggests that there is considerable transport of material out of the observed region during a pulse. Another possible explanation is that during passage of a pulse, multiple ionization occurs with the ions by-passing the first excited state in returning to the ground state. Further investigation is required to determine which of these explanations is correct.

The authors are greatly indebted to S.E.Frish for his assistance in planning the work.

Physical Institute,
Leningrad State University

References

1. G.G.Dolgov & S.L.Mandel'shtam, Zhur.eksp.i teor.fiz., 24, 691; R.W.Norrisch & G.Porter, Nature, 164, 658 (1948); G.Herzberg & D.Ramsay, J.Chem.Phys., 20, 347 (1952).

2. A.M.Shukhtin & V.S.Egorov, Optika i spektroskopiia, 2, 543 (1957).

3. M.Biondi, Phys.Rev., 90, 730 (1953); B.Blevis, J.Anderson & R.McKay, Canadian Jour.Phys., 35, 941 (1957).

CONTRIBUTION TO THE THEORY OF LINE BROADENING IN PLASMA

- V. I. Kogan

1. In this paper we report briefly on some considerations following from the theory of line broadening due to the Stark effect, taking into account the perturbation of an atom by the electric field produced by a large number of moving charged particles. This is the only rigorous method of comparing the results of statistical and impact broadening calculations. For the Stark effect such studies have thus far always assumed successive collisions between an atom and individual perturbing particles.[1-4] This "binary" model becomes less adequate as the range of interaction between the atom and particles increases, a factor has not been taken into account in the impact theory and its extensions. However, for the linear Stark effect (which has the longest range among the broadening mechanisms) the impact theory gives divergent values of the width and especially of the shift of the Stark components.[1,2] In our opinion this proves that the binary scheme is inapplicable in this case.*

2. In our theory it is assumed that: a) not only the ions but also the electrons can be described classically, b) the positions of charged particles are not correlated, i.e., their spatial distribution is random for a given mean density and their motion is rectilinear, c) the perturbing field is uniform throughout an atom, and d) the field acts adiabatically on the atom. Under these assumptions the Fourier expansion of the wavetrain emitted by a perturbed equivalent oscillator gives the shape of any Stark component in the classical adiabatic approximation.

We introduce the following notation: ω_0 is the unperturbed line frequency, ω is the observed frequency, $\varkappa(t)$ is the instantaneous frequency shift of the equivalent oscillator, $\mathrm{E}\,(t)$ is the field at the center of an atom, generated by the ions and electrons, T is the plasma temperature and N is the density of ions and electrons (it is assumed that for all extreme transitions N = const);

$$v_{0\mathrm{i}} \equiv (2kT/m_\mathrm{i})^{1/2} \text{ and } v_{0\mathrm{e}} \equiv (2kT/m_\mathrm{e})^{1/2},$$

α and β are the linear and quadratic Stark effect constants defined by

$$\varkappa_{\mathrm{lin}} = \alpha e^{-1}|\mathrm{E}| \text{ and } \varkappa_{\mathrm{quad}} = \beta e^{-2}E^2.$$

The general expressions obtained for the Stark component intensity distribution $I(\omega)$ are extremely complicated (see Ref.5). Below we give the results of simplifying them for the range of values of greatest interest.

3. We start with the linear Stark effect. When only ions are taken into account, we obtain for sufficiently large values of the dimensionless parameter $h_\mathrm{i} = N(\alpha/v_{0\mathrm{i}})^3$ or $(\omega-\omega_0)$:

$$I_{h\,\mathrm{i}}(\omega) = (\Delta\omega_0)^{-1}\{H[(\omega-\omega_0)/\Delta\omega_0] + h_\mathrm{i}^{-1/3} S[(\omega-\omega_0)/\Delta\omega_0]\}, \qquad (1)$$

where $\Delta\omega_0 = 2.60\,\alpha N^{2/3}$, H is the Holtsmark function and the function S (given analytically in Ref.5) is characterized in the accompanying table.

The "generalized" statistical approximation (1) contains an additional correction for thermal ion motion. When $h_\mathrm{i} \gg 1$,**the Holtsmark theory holds

---

*We cannot ignore this divergent shift by arguing that the line as a whole is symmetrical[1] since the effective width is determined by the shifts of the components.

**The numerical criterion is given in Sec.7.

x	$S(x)\cdot 10^3$	x	$S(x)\cdot 10^4$
0,0	−3,66	2,0	134
0,1	−3,45	2,4	80,8
0,2	−3,29	2,8	37,9
0,4	−2,66	3,2	13,0
0,6	−1,67	3,4	5,86
0,8	−0,589	3,8	− 1,60
1,0	+0,376	4,2	− 3,95
1,2	1,09	4,6	− 4,23
1,4	1,50	5,0	− 3,71
1,6	1,64	$\rightarrow\infty$	$-447x^{-7/2}$

for $\omega-\omega_0 \gg N^{1/3}v_{0i}$, i.e., over almost the entire contour of the component (the calculation of $I(\omega)$ has not yet been completed for the region $\omega-\omega_0 \lesssim N^{1/3}v_{0i}$). When $h_i \ll 1$ the correction is small only far out on the wings of the line, where (1) is represented by

$$I(\omega) = 2\pi N\alpha^{3/2}(\omega-\omega_0)^{-5/2}\times[1-(5/81)\,v_{0i}^2\alpha^{-1}(\omega-\omega_0)^{-1}], \tag{2}$$

so that the Holtsmark theory holds for $\omega-\omega_0 \gg v_{0i}^2\alpha^{-1}$.

4. For small values of h_i (the "quasi-binary" case), we obtain

$$I_{h_i}(\omega) = \alpha v_{0i}^{-2}F_{h_i}[(\omega-\omega_0-\lambda_1\Delta\omega_0)\,\alpha v_{0i}^{-2}], \tag{3}$$

where λ_1 = 3.41 is the first moment of the Holtsmark distribution and $F_{h_i}(x)$ is a function, the analytic form of which is given in Ref.5. When $(\omega-\omega_0-\lambda_1\Delta\omega_0) \gg v_{0i}^2\alpha^{-1}$, (3) becomes (2); consequently, the quasi-binary and generalized statistical approximations are not entirely alternative. For $\omega-\omega_0-\lambda_1\Delta\omega_0 \lesssim v_{0i}^2\alpha^{-1}$ (the "quasi-impact" part of the component dominant), we have

$$F_{h_i}(x) \approx \pi^{-1}\int_0^\infty \cos[(x+\pi^{7/2}h_i)\,y]\exp[-2\pi^{5/2}h_i y\ln(0.520y)]\,dy \tag{4}$$

and the corresponding $I_{h_i}(\omega)$ from (3). The peak of the curve represented by (3) and (4) is shifted by the amount $\omega-\omega_0 \approx \lambda_1\Delta\omega_0$, while its width is $\sim N\alpha^2 v_{0i}^{-1} \ll \Delta\omega_0$. When $v_{0i}\rightarrow\infty$, we have $I_{h_i}(\omega)\rightarrow\delta(\omega-\omega_0-\lambda_1\Delta\omega_0)$, i.e., a static shift of the component corresponding to the field distribution $E=\lambda_1\cdot 2.60\,eN^{2/3}$ averaged over the Holtsmark distribution.

Thus when $h_i \ll 1$, the influence of the collective moving ions (in the adiabatic model) reduces essentially to "static" Stark splitting by a mean field, accompanied by impact broadening of separate components. The principal effect, which is the splitting, can also be obtained directly - a precise result is obtained by generalizing the rule for calculating the shift given in Refs.1 and 2, and the order of magnitude is obtained if instead of arbitrarily dropping the divergent shift in the impact theory[1,2] we cut off the corresponding integral at the distance $\sim N^{-1/3}$ (which takes into account the mutual compensation at greater distances). The principal qualitative result is that the effective line width as a whole for $h_i \ll 1$ is determined by the same dependence as for $h_i \gg 1$: $\delta\omega \sim \bar{\alpha}N^{2/3}$ ($\bar{\alpha}$ is an effective Stark constant) rather than $\delta\omega \sim N(\alpha)^2 v_{0i}^{-1}$ which is given by the existing impact theory.

5. The results given in Sec.4 above show that the impact theory is wrong in its usual inference that for the linear Stark effect electrons have a smaller broadening effect than ions. Ions and electrons must be taken into

account together. When $h_i \gg h_e \gg 1$ or $h_e \ll h_i \ll 1$ $(h_e \equiv N(\alpha / v_{0e})^3)$, $I(\omega)$ is obtained by substituting 2N for N in the results given in Secs.3 & 4. The most interesting case occurs when $h_i \gg 1$ and $h_e \ll 1$. Since our model is only a rough approximation as regards electrons, we can confine ourselves to the limiting case $v_{0i} = 0$ and $v_{0e} = \infty$. The results for this are given in Ref.5. The final component shape is, roughly speaking, a superposition of two effects - an "electronic" shift and "ionic" broadening - which are of comparable magnitude.

6. For the quadratic Stark effect we can confine ourselves to one kind of perturbing particles. In the limit $v_0 \to 0$ the corresponding Holtsmark formula is obtained. In the most interesting practical "binary" case $g \equiv N\beta / v_0 \ll 1$. the line shape (see Ref.5) agrees with the obtained by applying formally to this case $(\varkappa_j = \beta r_j^{-4})$ the Lenz-Anderson theory[7,3], which is based on the "scalar" addition of perturbations from separate particles: $\varkappa = \varkappa_1 + \varkappa_2 + \ldots + \varkappa_j$. This is reasonable since for $g \ll 1$ the average number of perturbing particles within the Weisskopf radius is small, so that the character of perturbation addition is unimportant. Thus the "scalar" theory[7,3] (which, as its authors fail to mention, is strictly applicable only to the case $\varkappa_j \sim r_j^{-6}$ and not to $\varkappa_j \propto r_j^{-2}$) is equivalent for $\varkappa_j \propto r_j^{-4}$ to the binary approximation of the discussed "vector" theory, which is based on the addition of fields. When $\omega - \omega_0 \gg v_0^{4/3}\beta^{-1/3}$ the binary formula gives a statistical formula for the line wing, and for $\omega - \omega_0 < v_0^{4/3}\beta^{-1/3}$ and farther to the "left" (most of the line) it gives the impact broadening formula. Ref.3 discusses the shape of the "negative" (low intensity) wing.

The analysis shows that even for $g \ll 1$ the binary approximation and, of course, the impact theory, are strictly speaking invalid near the maximum of $I(\omega)$; this part of the line is influenced simultaneously by many particles, but this has little practical effect on the results of the impact theory.

7. We shall now discuss briefly the validity of the assumptions enumerated in Sec.2. All the values refer to hydrogen, n is the principal quantum number of the upper level, N is always expressed in cm^{-3} and T in ev. Assumption (a) holds for $T \gg 13.5\, n^{-1}$ (see Ref.8); assumption (b) holds for $T \gg 2 \cdot 10^{-5} N^{1/3}$, which follows from Ref.9; assumption (c) holds only for the quadratic Stark effect[2]; for the linear effect the most serious limitation of the described theory is assumption (d). An analysis of this limitation[5] leads to the conclusion that the results of Sec.3 (and of Sec.4 for the line wing) are reliable quantitatively and that the results of Sec.4 are valid qualitatively for the quasi-impact region. The result mentioned in Sec.5 is only qualitative, although it must be emphasized that this result takes into account the simultaneous influence $(\sim N^{2/3})$ of many "distant" electrons, whereas the existing theories (including the quantum theory) of impact broadening (reviewed in Ref. 4) are of purely binary character, i.e., they take only nearby electrons into account $(\propto N/v_{0e})$.* It can thus be inferred that these theories do not describe the principal factor $(\propto N^{2/3})$ in electron broadening.

From Secs.3 & 4 we can also derive both the "frequency" and integral criteria for the applicability of the statistical and quasi-impact approximations.

Thus when $h_i > 0.004$, the influence of ions is mainly statistical, while when $h_i < 0.004$, it is mainly of a quasi-impact nature; $h_i = 0.004$ corresponds to

---

*The theory given in Ref.10 is also essentially equivalent to the binary approximation.

$$T \approx 1 \cdot 10^{-11} (\bar{\alpha})^2 N^{2/3};$$

the values of $\bar{\alpha}$ for Balmer lines are given in Ref.1. The half-width in the Holtsmark case (neglecting electrons) is given by

$$\delta\omega\,(\mathrm{sec}^{-1}) \approx 15.6\,\bar{\alpha} N^{2/3};$$

in the quasi-impact case we have

$$\delta\omega \approx 17.7 \bar{\alpha} N^{2/3};$$

when electrons are taken into account, we have $\delta\omega \approx 23 \bar{\alpha} N^{2/3}$.

I am deeply indebted to M.A.Leontovich for valuable suggestions and discussions, to G.I.Biriuk for numerical computations and to V.S.Fursov, I.I. Sobel'man, D.A.Frank-Kamenetskii and S.Iu.Luk'ianov for discussions of the results.

Moscow Engineering-Physical Institute

References

1. A.Unzold, in "Sovermennye problemy astrofiziki i fiziki Solntsa" (Modern problems of astrophysics and physics of the Sun), M. 1951.
2. I.I.Sobel'man, Usp.fiz.nauk, 54, 551 (1954).
3. S.Ch'en & M.Takeo, Revs.Mod.Phys., 29, 20 (1957).
4. R.Breene, Revs.Mod.Phys., 29, 94 (1957).
5. B.I.Kogan, Doklady AN SSSR, 118, 5, 907 (1958).
6. S.Chandrasekhar, Stochastic problems in physics and astronomy. (Cited in Russian trans.M.1947.)
7. W.Lenz, Z.Phys., 80, 423 (1933).
8. H.Margenau & B.Kivel, Phys.Rev., 98, 1822 (1955).
9. G.Ecker, Z.Phys., 148, 593 (1957).
10. I.I.Sobel'man, Optika i spektroskopiia (Optics and spectroscopy), 1, 617 (1956).

BROADENING AND SHIFT OF SPECTRAL LINES IN HIGHLY IONIZED PLASMA

- L.A.Vainshtein, V.K.Koloshnikov, M.A.Mazing, S.L.Mandel'shtam & I.I.Sobel'man

In studies of line broadening usually only the shape and width of the lines are studied. This, however, does not yield complete information on the character of the atomic perturbation inasmuch as the line shape does not depend on the interaction law, while for proper utilization of the line width data one must know the constant C and the concentration of perturbing particles, the values of which are generally not known with adequate reliability.

It would appear feasible, however, to obtain appreciably more information on the processes leading to line broadening if one simultaneously measures the width and shift of the lines.

The principal interaction leading to broadening and shift of spectral lines in highly ionized plasma is interaction with charged particles.

The impact broadening theory gives the following expressions for the width and shift of lines with a quadratic Stark effect:[1]

$$\gamma = 11.4 C_4^{2/3} v^{1/3} N, \tag{1}$$

$$\Delta = 9.8 C_4^{2/3} v^{1/3} N, \tag{2}$$

where C_4 is the quadratic Stark effect constant, v is the velocity and N is the density of the perturbing particles.

As will be evident from Eqs.(1) and (2), the width-to-shift ratio does not depend on C_4, v and N, for obviously we always have $\gamma/\Delta = 1.16$. For interaction of another kind, for example, of the type leading to the rise of van der Waals forces, $\gamma/\Delta = 2.8$. Thus, in the framework of impact broadening theory the width-to-shift ratio may be said to characterize the type of interaction.

In earlier work we used this ratio to determine the relative contributions of the Stark and van der Waals effects to broadening of Ca I lines in the plasma of an arc discharge.[2]

The purpose of the present investigation was to elucidate the character of interaction of the emitting atoms with charged particles and in particular to check the validity of Eq.(1) for lines with a quadratic Stark effect.

We investigated spark discharges, where by virtue of the high degree of ionization and the prevailing temperature one can expect the line shift and broadening to be due to interaction with charged particles, namely, electrons and ions. By way of subject we chose the lines of doubly ionized argon; there are data on the Stark effect available for many A II lines.[3]

The measurements were made by the photographic technique. The accuracy of measurement of the width was 10%; the accuracy as regards the shift ~0.05--0.1 Å. We measured the width and shift of more than 20 A II lines with widely differing values of C_4. The results are characterized by the average values shown in the accompanying table.

C_4, cm^4 sec^{-1}	No. of lines measured	γ, A	Δ, A
$\leqslant 5\cdot 10^{-15}$	18	$0.5 \div 0{,}7$	$\leqslant 0.1$
$5\cdot 10^{-14}$	5	$1 \div 2$	~ 0.3
$5\cdot 10^{-13}$	5	$1.5 \div 2$	~ 0.7

The shape of the investigated lines is symmetrical. Evaluations show that impact broadening theory should be applicable under our conditions. The data listed in the table, however, proved to be in sharp conflict with the predictions of impact theory. Thus a change of C_4 by two orders of magnitude should correspond to a change in width $\gamma \sim C_4^{2/3} \approx 20$, whereas the line width actually changes by a factor of 2-3. As for the ratio γ/Δ, the experimental values lie in the range from 2 to 10, while, as noted above, theory gives 1.16. Finally, while the shift does vary more rapidly than the width, its variation is slower than follows from the $\Delta \sim C_4^{2/3}$ law.

Thus our experimental data are in complete disagreement with theory. This, apparently, is connected with the fact that the initial expression for the frequency shift of an atomic oscillator $\Delta\omega \quad C_4/R^4$, where R is the distance to the perturbing electron, is not applicable to the investigated lines. As is known, the principal role in line broadening is played by electrons passing at the range

$$R \leqslant \rho_4 = 1.16\left(\frac{\pi}{2} \cdot \frac{C_4}{v}\right)^{2/3}$$

where ρ_4 is the Weisskopf radius, which in our case is of the order of a few ångstroms. With such close trajectories the field produced by the electron proves to be so strong that the Stark effect tends to become linear instead of quadratic. Evaluations show that the transition from the quadratic to the linear Stark effect actually does obtain for the investigated lines ($\Delta\omega \sim C_4/\rho^4$) is greater than or equal to the distance to the nearest perturbing term.

In addition, the collision time $\tau \approx \rho_4/v$ with ρ_4 = 4-10 Å and $v \sim 10^8$ cm/sec proves to be of the same order of magnitude as $1/\omega$, where ω is the frequency of the emitted radiation. Thus there is apparently no justification for assuming the field to be a slowly varying, quasistatic one, as is commonly done in present impact broadening theory. The enumerated factors can be taken into account quantitatively; the corresponding calculations are now being carried out.

"P.N.Lebedev" Physical Institute,
Academy of Sciences of the USSR

References

1. I.I.Sobel'man, Usp.fiz.nauk, 54, 551 (1954).
2. M.A.Mazing & S.L.Mandel'shtam, Optika i spektroskopiia (Optics and Spectroscopy), 2, 276 (1957).
3. L.Minnhagen, Ark.Mat., Ast.Fys., 35A, No.16 (1948).

TEMPERATURE MEASUREMENT OF THE GLOWING VAPOR CLOUD IN PULSE DISCHARGES

- A.A.Labuda, E.G.Martinkov & I.G.Nekrashevich

One of the procedures now in use for measuring the temperature of luminous gases and vapors is that of Ornstein, which is predicated on the existence of thermodynamic equilibrium in the discharge cloud. In the case of a luminous cloud forming in a pulse discharge (spark or explosion of a wire), however, thermodynamic equilibrium as a whole is absent, so that indiscriminate application of the Ornstein method in such cases is not justified. It is justifiable to use the Ornstein procedure only if the following conditions are fulfilled:

1) the observed volume of the discharge cloud must be so small and the time of observation must be so short that it may be assumed that within the given volume and time the temperature is constant, and

2) there is established in the observed volume during the short exposure time a local state close to equilibrium.

In cases where these two conditions were not fulfilled, the results of temperature measurements on the same discharge proved to be different, depending on the pair of lines chosen for observation.[1] A theoretical analysis of this phenomenon has been given by Huldt.[2]

One can satisfactorily approach the above conditions by carrying out time-scan measurements of the spectrum from a small volume of the glowing cloud, i.e., obtaining a spectral streak picture.

The purpose of the present work was to clarify the applicability of the Ornstein technique for determining high temperatures in the glowing vapor cloud in a spark discharge or electric explosion of metal wires. It was established that a discharge through a fine metal wire ($d \leqslant 0.05$ mm) does not differ substantially from a spark discharge through an air gap, except at the initial stage. The advantage of the exploding wire technique, however, is that it allows of varying and accurately determining the amount of evaporated material.

The parameters of the discharge circuit were $V_0 = 1$ to 5 kv, $C = 2$ to 22 μf, $R_{aux} = 0$ to 2 ohm, $L = 8$ to 65 μh.

We investigated single discharge pulses in air at atmospheric pressure. In addition to aperiodic pulses we also used square ones.

The "streak" spectra were obtained by means of a rotating mirror synchronized with a double oscillograph for recording current and voltage oscillograms. The set-up, which has been described earlier[3], allowed of obtaining records of the spectrum in the visible region with a resolution in time down to 1 microsec. The spectrograms were processed by the usual methods of photographic photometry, taking into account the continuous background and the sensitivity of the photographic film.

Below we give some of the results obtained.

In the course of investigating the time variation of the relative intensity of the spectrum lines in different parts of the discharge, we found that spectrum lines with different energies of the upper level are excited both in different zones arranged concentrically about the discharge axis and at different instants.

In general the line intensity maxima do not coincide with each other or with maximum current. The higher the energy of the upper level of the spectrum line, the closer to the discharge axis is its intensity maximum and the earlier it occurs in time. This is illustrated by Figs.1 & 2. Fig.1 shows the variation of the relative intensity of spectrum lines with different values of the upper level energy as a function of the distance from the discharge axis; Fig.2 shows the variation of the relative intensities with time. Both figures

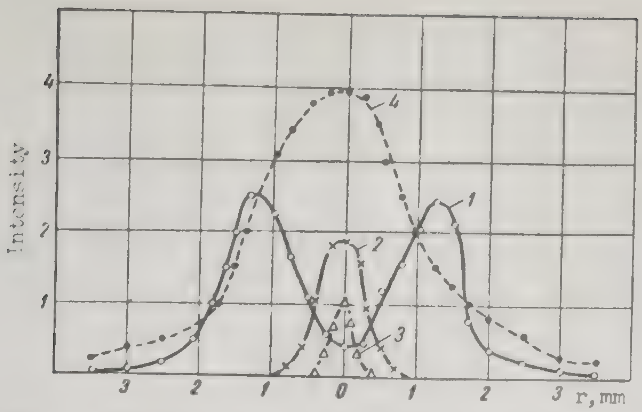

Fig.1. Variation of the relative intensity of spectrum lines with the distance from the discharge axis for a pulse discharge through a fine metallic wire: 1) Fe I, $\lambda = 4222.2$ Å, $E_i = 5.38$ ev; 2) Al II, $\lambda = 4663.05$ Å, $E_i = 19.23$ ev; 3) Al III, $\lambda = 4479.07$ Å, $E_i = 48.35$ Ev; 4) background.

pertain to the case of electric explosion of a wire. Similar results were obtained for spark discharges.

Bearing in mind that lines with higher upper levels attain a maximum intensity value at higher temperatures,[2] one can, from the relative intensity distributions, judge of the distribution and variation of temperature in the discharge. Hence one can assert (Fig.2) that the highest temperature is attained at the center of the discharge in the initial stage, where the lines of air peak (N II line - Fig.2, curve 1). We specifically investigated the applicability of the Ornstein procedure for determining the temperature from the relative intensity of two spectrum lines. We proceeded on the assumption that in a spark discharge in air at atmospheric pressure, as well as in the explosion of a wire in the second stage, sometime after the beginning of the discharge, there is established a local state of the particles close to the equilibrium one. The temperature in this case is a function of the time and distance from the discharge axis. This assumption is substantiated by the data of Mandel'shtam & Sukhodrev[4] and Weizel & Rompe[5], and also by indirect experiments that have been carried out by many investigators and checked by us. In these experiments it was established that

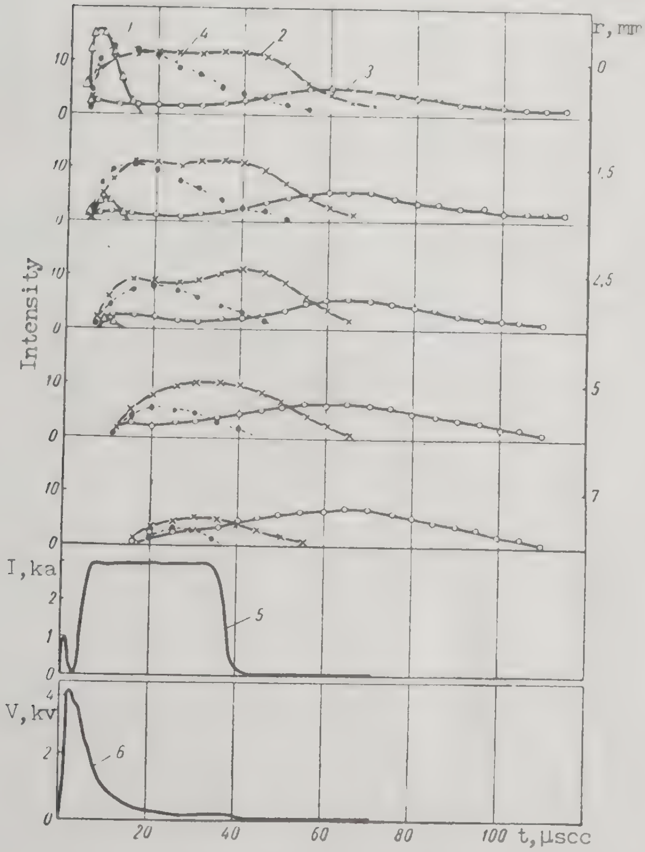

←Fig.2. Variation of the relative intensity of spectrum lines with time from the instant of beginning of the pulse discharge through a fine metallic wire and with the distance from the discharge axis: 1) N II, $\lambda = 4447.04$ Å, $E_i = 37.735$ ev; 2) Ba II, $\lambda = 4934.09$ Å, $E_i = 7.72$ ev; 3) Ba I, $\lambda = 6063.12$ Å, $E_i = 3.18$ ev; 4) background, 5) current, 6) voltage.

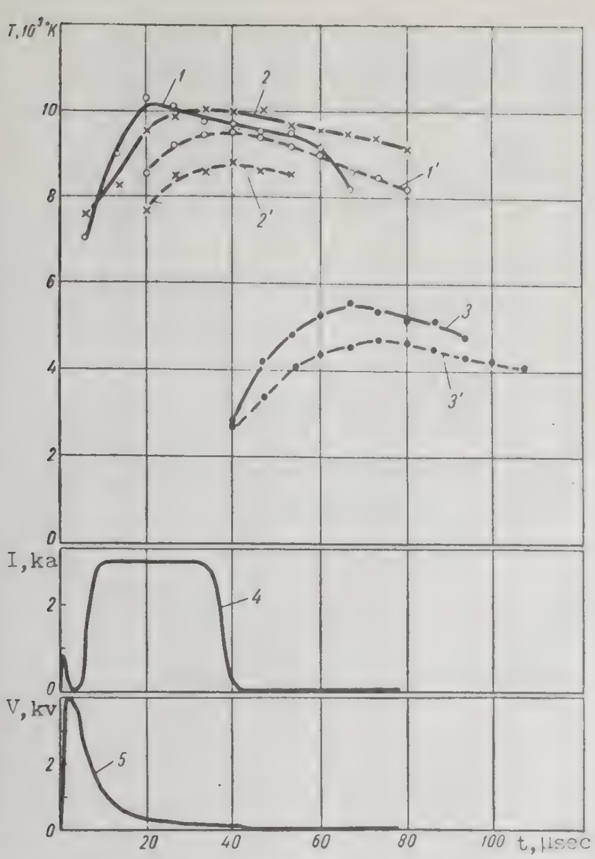

Fig.3. Time variation of temperature: 1) from the Ba II 4934/4524 lines, 2) from the Ba II 4934/4899 lines, 3) from the Ba I 6063/5519 lines (in the direction towards the center of the explosion cloud); 1', 2' & 3') same but with observation of parts of the cloud at a distance of 7 mm from the discharge axis.

a) the variation with time of the relative intensity of spectrum lines with close values of the upper level energy is identical,[6] and

b) the temperature values determined from pairs of spectrum lines within the same narrow excitation energy interval are equal.[7]

As a result of the investigation it was found that the variation with time of the temperature during the half period of the discharge, as determined from the relative intensity of two spectrum lines, is characterized by a curve with one maximum. The higher the energy of the upper level of these lines, the earlier the temperature vs time curve peaks.

This may be seen in Fig.3 which shows the variation with time of the temperature determined from spark and arc lines.

For the zone furthest from the discharge axis, the temperature determined from the relative intensity of two spectrum lines with close upper level energy values is virtually the same for different metals.

It should be noted that differences in temperature obtained from lines with very different upper level energies have been interpreted by some investigators as proof of the absence of thermodynamic equilibrium in discharge plasma.[1]

In applying the Ornstein technique for determining the temperature, it should be borne in mind that the values of the relative transition probabilities usually obtained by theoretical calculations, play the role of a certain parameter which does not, however, take into account the configuration of the source. An illustrative example is the fact that from measurements of the lines of singly ionized Ba with upper level energies $E_i \approx$ 7-10 ev, we obtain overestimated temperature values: $T \approx$ 35,000-40,000°K.

In contrast for an arc (for which the $A_i g_i$ values were determined), these lines yield a reasonable value of the temperature. We therefore recalculated the values of $A_i g_i$ on the basis of theoretical and experimentally determined values of T at which the maximum intensity of these lines occurs. The curves of Fig.3 give the temperature values after recalculation.

Thus the results of our experiments show that the Ornstein procedure can be used for measuring the temperature in a spark discharge or wire explosion

only if one takes into account the zonal distribution and variation with time of the line excitation. In view of this it appears impossible to deduce the temperature by this procedure from the relative intensity of two spectrum lines with appreciably different upper level energies (for example, from a spark and an arc line), inasmuch as they are excited in different discharge zones, where the temperatures are different, and at different instants in time.

"V.I.Lenin" Belorussian State University

References

1. G.C.Williams, J.D.Craggs & W.Hopwood, Proc.Phys.Soc., B, 62, 49 (1949).
2. L.Huldt, Spectrochem.Acta, 7, 264 (1955).
3. A.A.Labuda, E.G.Martinkov, I.G.Nekrashevich & D.A.Taumin, Uch.zap. (Scientific records), Belorussian State University, Phys.Series, 41, 53 (1958).
4. S.L.Mandel'shtam & M.K.Sukhodrev, Zhur.eksp.i teor.fiz., 24, 701 (1953).
5. W.Weizel & R.Rompe, Theorie elektrischen Lichtbogen und Funken, Leipzig, 1949.
6. L.A.Vainshtein, A.M.Leontovich, L.P.Maliavkin & S.L.Mandel'shtam, Zhur.eksp.i teor.fiz., 24, 326 (1953).
7. L.Blitzer, Jour.Opt.Soc.Amer., 41, 440 (1951).

MEASUREMENT OF OSCILLATOR STRENGTHS IN ATOMIC SPECTRA

- Iu.I.Ostrovskii, N.P.Penkin & L.N.Shabanova

1. Results of measurements of the f numbers of spectrum lines of atoms with an unfilled 3d shell

We measured the relative f numbers of the spectrum lines of Sc, Ti, V, Cr, Mn, Fe, Co and Ni by the method of Rozhdestvenskii "hooks" on the interferometric set-up comprising a high temperature vacuum furnace, described earlier.[1-7] Measurements similar to ours have been carried out by King and his co-workers[8-13] by the method of total absorption. These investigators carried out measurements for all the above mentioned atoms except Sc and Mn.

The method of "hooks" is characterized by a lower sensitivity as compared with the method of absorption (about one order of magnitude). In our set-up one cannot photograph the "hooks" near the absorption lines whose departure levels lie more than 1.5 ev above the ground level (an exception are the four lines of scandium for which the energy of the low-lying level is 1.85 ev). Moreover the accuracy obtainable by the method of "hooks" becomes very poor when the difference between the wavelengths of the spectrum lines is less than 0.5 Å. For these reasons we measured the oscillator strengths of appreciably fewer lines of all the enumerated atoms than were determined by the method of total absorption. Our measurements, however, have the advantage that, being carried out by the method of "hooks", they are considerably more reliable. In measurements by the absorption procedure of the relative f numbers of lines differing greatly as regards intensity one must carry out the comparison with reference to a line of intermediate intensity which can, of course, lead to appreciable errors. The method of "hooks", on the other hand, allows of measuring the ratio $\frac{N_1 f_1}{N_2 f_2} \sim 10^5$ with considerable accuracy.

In measurements of weak absorption lines their intensity may be distorted by any of the following factors: 1) continuous radiation from incandescent graphite particles (this may be a significant factor in the case of King's furnace at high temperatures), 2) light scattering in the spectrograph and 3) "ghosts" (when a diffraction grating is used); such distortion naturally leads to incorrect f values.

We may note the following regarding our measurements by the "hook" procedure of the relative f numbers of the spectrum lines of atoms with an unfilled 3d shell:

1) For strong lines originating from the ground level the f numbers are determined with an error not exceeding 5%; for medium and weak lines the error is less than 15%, while for lines from excited levels, the uncertainty may be as great as 25%.

2) For all atoms except chromium, the f numbers of the strongest absorption lines from excited levels are several times greater than the f numbers of lines from the ground level.

3) Comparison of the intramultiplet line intensities calculated by the Kronig-Henley formulas with the intensities obtained from our measurements show that in the case of Fe, Co and Ni atoms there is strong deviation from L-S coupling.

4) For most spectrum lines the f numbers measured by the method of "hooks" differ from the f values obtained by King and his co-workers[8-13] by not more than 30%. For about 20% of the lines, however, the f numbers differ by an appreciable factor. These discrepancies cannot be explained by errors in

measuring the temperature of the furnace or by errors of the method of "hooks". We are inclined to attribute them to uncertainties inherent in the total absorption method.

The method of "hooks" yields reliable information on the f numbers, but it can only be used to measure the oscillator strengths of a relatively small number of spectrum lines. Hence complete information on oscillator strengths can be gained only through use of the "hook" method and the absorption and emission procedures in proper conjunction.

Knowledge of the absolute values of the f numbers of spectrum lines of atoms with a filling 3d shell is important in astrophysics and spectroscopy. For this reason Ostrovskii & Penkin[14] measured the absolute f numbers of the resonance lines of Cr, Mn and Cu. A column of vapor of the investigated metal was obtained in evacuated and sealed off quartz tubes which were mounted in a resistance furnace. The method of "hooks" allows of measuring the product $N_i f_{ik}$. The concentration N_i of absorbing atoms necessary for determining the f_{ik} numbers is calculated by means of formulas characterizing the temperature dependence of the saturated vapor pressure.

2. Absolute f numbers of the spectrum lines of elements of Group III

The f numbers of the spectrum lines of gallium have been measured and calculated quantum mechanically by a number of investigators.[15-18] As far as we know, the absolute values of the f numbers of the other elements of Group III of the periodic table have not been measured. Ostrovskii & Penkin[19] obtained photographs of the "hooks" near the absorption lines of gallium (Fig.1) and indium, departing from the $^2P_{1/2}$ and $^2P_{3/2}$ levels, which allowed of determining the absolute f numbers of these lines. We measured the quantities $N_i f_{ik}$ with an accuracy of within 2-3%. The gallium atom concentration was calculated from the results of Speiser & Johnston[20]; that of indium by means of the formula given by Anderson[21]. In view of the inadequate accuracy of the data obtained in the above mentioned investigators, the absolute f numbers of the lines of indium and gallium comprise an uncertainty of 10-15 and 20-30%, respectively. The results of our measurements are summarized in Table 1.

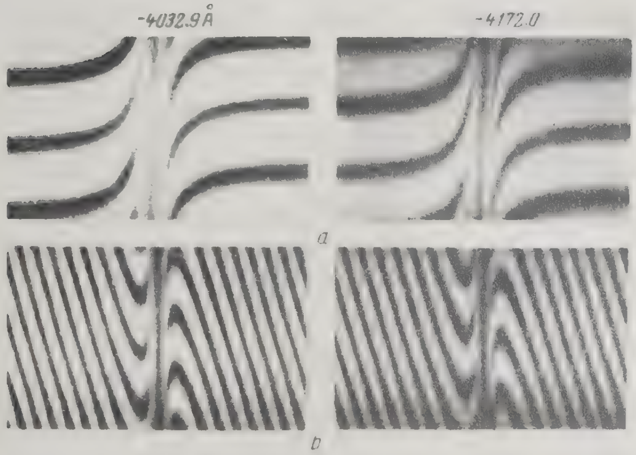

Fig.1. Photographs of dispersion (a) and "hooks" (b) at the lines of the head doublet in the sharp series of gallium (T = 1400°K; d = 12.0 cm).

Calculations of the oscillator strengths of some Ga I and In I lines were carried out by Vainshtein[22]. For the 4032 Å Ga I line the result of his calculation is in satisfactory agreement with our experimental data: $f_{\text{calc}} = 0.097$, $f_{\text{meas}} = 0.129$, while for the 4102 Å In I line the calculated value ($f_{\text{calc}} = 0.114$) is almost half the measured value ($f_{\text{meas}} = 0.201$). In our opinion these divergences are due to the errors inherent in the quantum mechanical computation. Possibly refinement of the calculations, in particular taking into account exchange and polarization effects, may reduce the divergence between the experimental and theo-

Table 1
Absolute values of the f numbers of the spectrum lines of Ga and In

Transitions	GaI		InI	
	λ	f	λ	f
$^2P^\circ_{3/2} - {}^2S_{1/2}$	4172	0,135	4511	0,218
$^2P^\circ_{1/2} - {}^2S_{1/2}$	4032	0,129	4102	0,201
$^2P^\circ_{3/2} - {}^2D_{5/2}$	2943	0,287	3256	0,509
$^2P^\circ_{1/2} - {}^2D_{3/2}$	2874	0,318	3039	0,503
$^2P^\circ_{3/2} - {}^2D_{3/2}$	2944	0,038	3258	0,079

retical data. As for the relative values of the oscillator strengths of the spectrum lines of elements of Group III, in addition to the results obtained in the present work for gallium and indium, there are accurate data available for Al I (Refs.23 & 24) and Tl I (Refs.25 & 26).

3. Absolute values of the f numbers of Mg I, Ca I, Sr I and Ba I resonance lines

We made attempts to measure the absolute values of the oscillator strengths of the resonance lines of Al I, Mg I, Ca I and Ba I. These attempts, however, were not successful due to the strong reaction of these metals in the vapor state with quartz. Hence the usual measurement procedure was modified. Using the "hook" and total absorption procedures simultaneously one can measure the absolute values of the f numbers without realizing a vapor column having a definite length and temperature with a known concentration of absorbing atoms.

As is known the method of "hooks" allows of determining the product $N_i f_{ik}$ if one measures the distance Δ_{ik} between the peaks of the "hooks". The theory of this method[27] leads to the formula

$$N_i f_{ik} = \frac{\pi m c^2 K_{ik}}{e^2 d \lambda_{ik}^3} \Delta_{ik}^2 .$$

where e is the charge and m is the mass of an electron, c is the velocity of light, λ_{ik} is the wavelength of the absorption line, d is the length of the vapor column and K_{ik} is a constant peculiar to the method of "hooks", determined by the thickness and the index of refraction of the planeparallel plate introduced into the interferometer for forming the "hooks".

On the other hand, it is known that if the pressure of the absorbing gas or vapor is so low (10^{-3}-10^{-2} mm Hg) that the Holtsmark broadening can be neglected and $k_\lambda d$ has a value equal to a few thousand, the shape of the absorption line will be determined exclusively by its edges.[28] In this case the equivalent of the width A_λ of the absorption line will be

$$A_\lambda = \frac{\lambda_{ik}^2 e}{m^{1/2} c^{3/2}} \sqrt{N_i f_{ik} \gamma_k d}.$$

Having measured A_λ and Δ_{ik} simultaneously, one can find the attenuation coefficient γ_k from the following expression derived from the above two equations:

$$\gamma_k = \frac{c}{\pi \lambda_{ik} K_{ik}} \left(\frac{A_\lambda}{\Delta_{ik}} \right)^2 .$$

For resonance lines, in the case of absence of high density emission, we have

$$\gamma_k = A_{ki}.$$

Consequently, measuring Δ_{ik} and A_λ under identical conditions, we can find γ_k and from it A_{ki} or f_{ik}. Thus use of the two methods in conjunction allows of measuring the absolute f numbers of absorption lines of a large number of elements, including elements difficult to vaporize. Simultaneous measurement of the total absorption and the dispersion frees us of the necessity of using the equations for saturated vapor pressure. As is known, the

Table 2

Absolute values of the f numbers of the spectrum lines of Mg, Ca, Sr and Ba according to our data and the data of other investigators

Element	Y, Å	f		
		Our data	Data of other authors (Refs.* in [].)	
			Exper.	Theor.
Mg	2852	1,2±0,3	—	1,674 [31]
Ca	4227	1,3±0,2	2,3 [29]	1,458 [32]
Sr	4607	1,5±0,2	—	—
Ba	5535	1,7±0,2	1,8 [30]	—

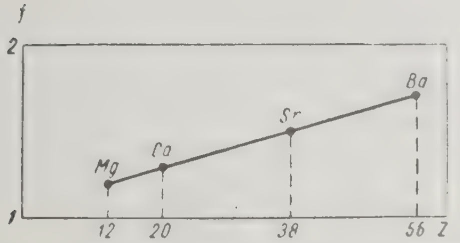

Fig.2. Variation of the f numbers of resonance lines $(^1S_0-^1P_1)$ of the rare earth elements with the atomic number.

low accuracy of these equations is frequently the principal source of error in measurements of absolute f numbers. To check the combined procedure, we measured the f number of the In I $^2P_{1/2}-{}^2S_{1/2}$ (λ = 4102 Å) line; we obtained 0.20, which is in good agreement with results obtained by the method of "hooks".

We used the combined procedure to determine the absolute f numbers of the resonance lines of Mg I, Ca I, Sr I and Ba I. Our results are compared with the data of other investigators in Table 2.

There have been published a number of calculations by approximate quantum mechanical methods of the oscillator strengths of the resonance lines of magnesium and calcium. In Table 2 we give only the results obtained by Trefftz, which in our opinion, are the most accurate. From a comparison of the data in the table it will be evident that 1) for the barium atom our results are in good agreement with the data of Wessel[30] obtained by the method of absorption in an atomic bean and 2) for the resonance line of calcium our f number is in good agreement with the f number calculated by Trefftz and differs greatly from that measured by Steinhäuser[29]. This divergence may be attributed to errors in the work of Steinhäuser in which the results were obtained using an insufficiently accurate method of measuring the depolarization of the resonance fluorescence in the magnetic field.

The accuracy of the f numbers obtained by the procedure of simultaneous measurement of absorption and dispersion is not very high, but it can be enhanced through the use of photoelectric procedures for recording the total absorption.

In Fig.2 we show the variation of the f numbers as measured in our work with the atomic number of the respective elements. It will be seen that the f numbers increase linearly with Z.

Physical Institute,
Leningrad State University

References

1. D.S.Rozhdestvenskii & N.P.Penkin, J.Phys., USSR, 5, 319 (1941).

2. N.P.Penkin, Zhur.eksp.i teor.fiz., 17, 355 (1947).

3. Iu.I.Ostrobskii, G.F.Parchevskii & N.P.Penkin, Optika i spektroskopiia (Optics and Spectroscopy), 1, 821 (1956).

4. N.P.Penkin, Zhur.eksp.i teor.fiz., 17, 1114 (1947).

5. G.F.Parchevskii & P.N.Penkin, Vestnik, Leningrad State University, 11, 113 (1954).

6. Iu.I.Ostrovskii & N.P.Penkin, Optika i spektroskopiia, 3, 391 (1957).
7. Iu.I.Ostrovskii & P.N.Penkin, ibid., 5, No.6 (1958).
8. R.B.King, Astrophys.J., 106, 376 (1947).
9. R.B.King, Astrophys.J., 108, 87 (1948).
10. R.B.King, B.R.Parnes, M.H.Davis & K.H.Olsen, J.Opt.Soc.America, 45, 350 (1955).
11. A.J.Hill & R.B.King, J.Opt.Soc.America, 41 315 (1951).
12. R.B.King & A.S.King, Astrophys.J., 82, 377 (1935).
13. R.B.King & A.S.King, Astrophys.J., 87, 24 (1938).
14. Iu.I.Ostrovskii & P.N.Penkin, Optika i spektroskopiia, 3, 193 (1957).
15. W.Kuhn, Naturwissenschaften, 13, 724 (1925).
16. F.Müller, Helv.phys.acta, 7, 813 (1934).
17. G.S.Kvater, Zhur.eksp.i teor.fiz., 11, 421 (1941).
18. G.Stephenson, Proc.Phys.Soc., A 64, 458 (1951).
19. Iu.I.Ostrovskii & P.N.Penkin Optika i spektroskopiia, 4, No.6 (1958).
20. R.Speiser & H.Johnston, J.Amer.Chem.Soc., 75, 1469 (1953).
21. J.Anderson, J.Chem.Soc. (London), 141 (1943).
22. L.A.Vainshtein, Present issue of the Bulletin, p.668.
23. E.I.Nikonova & V.K.Prokof'ev, Optika i spektroskopiia, 1, 290 (1956).
24. Iu.I.Ostrovskii, ibid., 2, 673 (1957).
25. V.K.Prokof'ev & A.N.Fillipov, Zhur.eksp.i teor.fiz., 4, 31 (1934).
26. G.S.Kvater, Zhur.eksp.i teor.fiz., 5, 426 (1935).
27. D.S.Rozhdestvenskii, Raboty po anomal'noi dispersii v parakh metallov (Work on anomalous dispersion in metal vapors) M.-L., 1951.
28. A.Mitchell & M.Zemansky, Resonance radiation and excited atoms, Chapter III (cited in Russian trans., M., 1937); A.Unzold, Physics of stellar atmospheres, Chapter VIII (cited in Russian trans., M., 1949).
29. A.Steinhäuser, A.Phys., 99, 300 (1936).
30. G.Wessel, Z.Phys., 126, 440 (1949); Z.Phys., 130, 100 (1951).
31. D.Trefftz, Z.Astrophys., 28, 67 (1950).
32. E.Trefftz, Z.Astrophys., 29, 287 (1951).

SPECTROSCOPIC INVESTIGATION OF THE STATE OF A GAS BEHIND A SHOCK WAVE

- N.N.Sobolev, A.V.Potapov, V.F.Kitaeva, F.S.Faizullov,
V.N.Aliamovskii, E.T.Antropov & I.L.Isaev

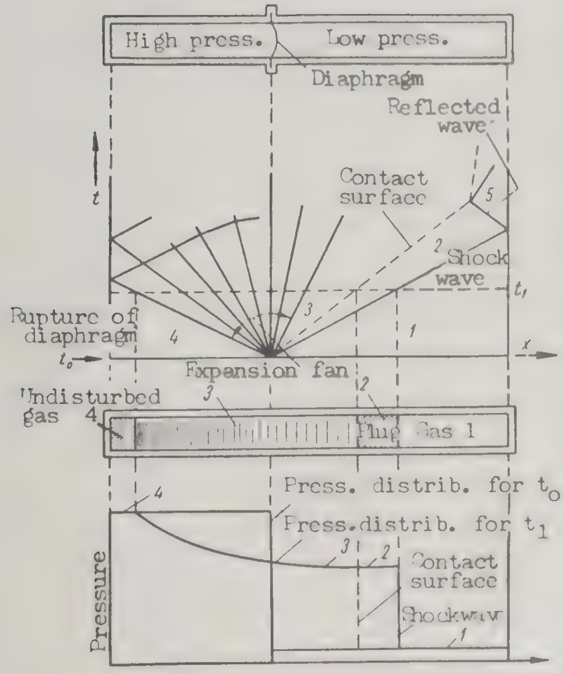
High press.
Low press.
Diaphragm
Reflected wave
t
Contact surface
5
2
Shock wave
t_1
3
Rupture of diaphragm
4
1
x
t_0
Expansion fan
2
Undisturbed gas 4
3
Plug
Gas 1
4
Press. distrib. for t_0
Press.distrib. for t_1
3
2
Contact surface
Shockwave
1
Pressure

Fig.1. Operation of a shock tube.

One of the most convenient procedures for obtaining a high temperature plasma for purposes of laboratory study is the shock tube technique.[1] The procedure is simple in principle and in practice amounts essentially to the following (Fig.1). The shock tube is divided by a diaphragm into two sections: a high pressure and a low pressure chamber. As the pressure in the high pressure chamber is increased, there arrives a time T_0 when the diaphragm ruptures. Owing to the pressure discontinuity at the boundary between the two gases 1 and 4, a shock wave is propagated in gas 1 and a rarefaction wave in gas 4. Between the shock wave front and the contact surface separating the "driving" and "driven" gas there is formed a section 2 of gas 1 heated to a high temperature. Hereinafter for the sake of brevity we shall refer to this section 2 as the "plug". The plug moves with a velocity u_2 that is somewhat lower than the velocity of U_s of the shock wave. The temperature T_2 of the plug will be higher, the lower the molecular weight of the driving gas 4 and the higher the molecular weight of the driven gas 1 (other conditions being equal). Knowing the shock wave velocity, we can by means of the laws of conservation of

mass

$$\rho_1 U_s = \rho_2 (U_s - u_2), \tag{1}$$

momentum

$$p_1 + \rho_1 U_s^2 = p_2 + \rho_2 (U_s - u_2)^2, \tag{2}$$

energy

$$H_1 + \frac{1}{2} U_s^2 = H_2 + \frac{1}{2} (U_s - u_2)^2 \tag{3}$$

and the relations defining the enthalpy

$$H = \frac{5}{2} (1+\alpha) R_0 T + \alpha \frac{q_0}{m_0}, \tag{4}$$

degree of ionization

$$\alpha = \left\{ 2.540 \cdot 10^5 \frac{p}{T^{5/2}} \exp\left(\frac{1.821 \cdot 10^5}{T} \right) + 1 \right\}^{-1/2} \tag{5}$$

state of the gas

$$\frac{p}{\rho} = (1+\alpha) R_0 T, \tag{6}$$

find the six unknown parameters p_2, ρ_2, u_2 H_2, T_2 and α_2 characterizing the state of the monatomic gas in the plug. Here q_0 is the ionization potential of gas 1.

The results of calculation of the data for argon by means of Eqs.(1)-(6) are shown in Fig.2.[1] The temperature, density and degree of ionization of the gas in the plug are shown graphically as functions of the Mach number

$$M_1 = U/a_1.$$

where a_1 is the velocity of sound in gas 1.

Similar calculations can be carried out for air (Fig.3), but they are complicated by the necessity of taking into account dissociation of O_2 and N_2.[2] As will be evident from a comparison of Figs.2 and 3, at the same Mach number the temperature of air is lower than that of argon owing to dissociation and to the fact that the specific heat of air (a diatomic gas) is higher than the specific heat of argon (a monatomic gas). The data on the states of air and argon behind a shock wave, shown in Figs.2 & 3, characterize the potentialities of the shock tube technique.

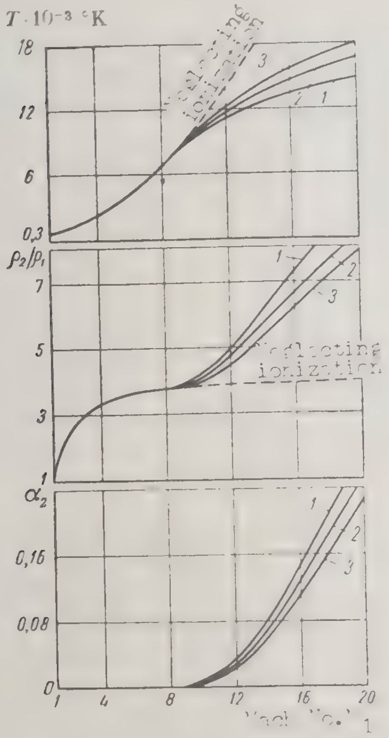

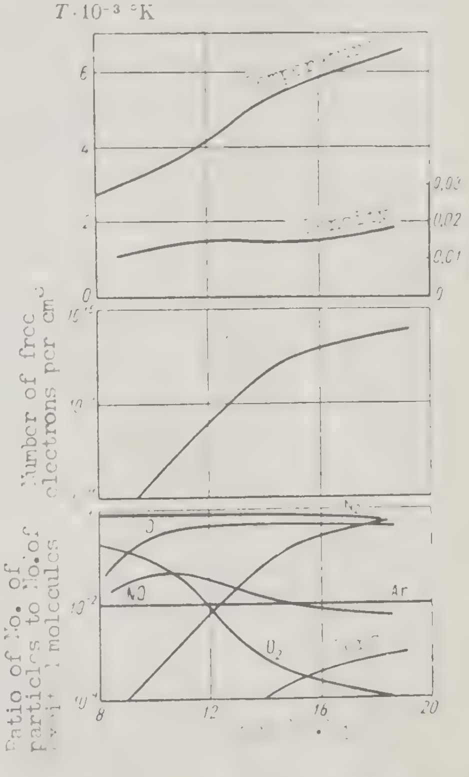

Fig.2. State of argon behind the shock wave: 1) p_1 = 10 mm Hg, 2) 50 mm Hg and 3) 150 mm Hg.

Fig.3. State of air behind shock wave, p_1 = 1 mm Hg. (The density is expressed in terms of the normal pressure and temperature.)

To determine the validity of the predictions of gas dynamics theory we must turn to experiment. The necessity of experimental verification is obvious inasmuch as in carrying out gas dynamics calculations there are commonly made a number of assumptions that are not always fully justified. In particular need of verification is the principal assumption made in such calculations, namely, the assumption of thermodynamic equilibrium in the plug, i.e., in the gas behind the shock wave.

The fundamental parameter characterizing the state of the gas behind the shock wave is the temperature. Hence the importance of comparing the theoretical data on the temperature with the experimental is obvious. No such verifi-

cation has as yet been carried out owing to the lack of a reliable method of measuring the gas temperature behind a shock wave.

The present work was concerned with developing a procedure for measuring the temperature of air behind a shock wave, carrying out systematic measurements of the temperature and comparing the results of experiment with theory.

Description of apparatus

The basic component of the set-up used in the investigation was a steel pipe with an inside diameter of 92 mm (Fig.4). The inside surface of the pipe was smoothly machined and chrome plated. The length of the high pressure chamber I was 0.5 mm; the length of the low pressure chamber III was 4 mm. The two chambers were separated by an aluminum diaphragm. The driving gas was hydrogen which was fed into the high pressure chamber from cylinders. The maximum working pressure in chamber I did not exceed 150 atmospheres. The air filling the low pressure chamber was evacuated by a forepump to the appropriate pressure, the range of pressures used being from 1 to 50 mm Hg. The velocity of the shock wave was measured by means of the ionization gage units G_1 and G_2, the signals from which were recorded by an IV-13 oscilloscope with a spiral sweep. The emission spectrum of the gas behind the shock wave was recorded photographically by means of ISP-51 spectrographs facing viewing windows in the sides of the shock tube. To allow of simultaneous electric recording of two spectrum lines, we constructed a two-channel photo-electric attachment (PEA) for the ISP-51 spectrograph; subsequently, this was replaced by a four-channel attachment, which, in addition to the line intensities, simultaneously recorded the intensity of the background in the vicinity of the lines. The line intensities were recorded by means of a two-gun OK-17 M oscillograph.

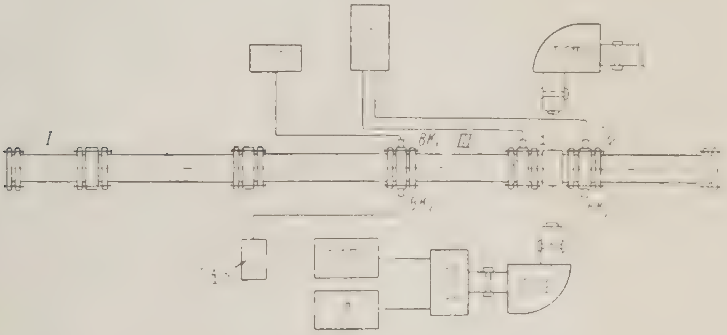

Fig.4. Diagram of experimental set-up. I & III - high and low pressure chambers, V - vacuum gage, BK_1, BK_2 & BK_3 - valves, G_1 & G_2 - ionization gages, TD - timing device, ISP - ISP-51 spectrograph, PEA - photoelectric attachment, HVR - stabilized high voltage rectifier, 0 - oscillograph, Dic - dicyan supply.

Method of relative intensities

Our preliminary experiments showed that upon introduction of lithium or sodium salts into the shock tube there is excited a number of spectrum lines of Li and Na, suitable for measuring the temperature by the method of relative intensities. The intensities were measured both photographically and photoelectrically. The experimental data were reduced both by means of the expression valid in the absence of reabsorption

$$T = -\frac{E_1 - E_2}{k}\left\{\ln\frac{I_1}{I_2} - \ln\frac{A_1 g_1 \lambda_2}{A_2 g_2 \lambda_1}\right\}^{-1}, \tag{7}$$

and by means of the equation applicable in the case of complete reabsorption of the spectral lines[3]:

$$T = -\frac{E_1 - E_2}{k}\left\{\ln\frac{I_1}{I_2} - 2\ln\frac{\lambda_2}{\lambda_1} - \frac{1}{2}\ln\frac{A_1 g_1}{A_2 g_2} - \frac{1}{5}\ln\frac{C_{61}}{C_{62}}\right\}^{-1}. \qquad (8)$$

The transition probabilities for the Li and Na lines were taken from Ref.4 as the averages of the experimental and theoretical values.

Extensive experimentation showed that different pairs of lines give different temperature values with a spread of up to 1000°. The scatter of temperature values determined from the same pair of lines in different experiments far exceeded the limits of the experimental error associated with uncertainty in measurement of the spectrum line intensities. It was obvious that further experimentation was indicated. A check of the degree of reabsorption, realized by measuring the intensities of the components of Na doublets, showed that the intensity of sodium lines attains a measurable value in the gas behind the shock wave at concentrations of Na at which there is noticeable deviation from linear dependence of the intensity on the concentration.

Analysis of high-speed motion picture photographs of the plug near the end of the shock tube led us to conclude that the sodium vapor is concentrated primarily in a boundary layer, 5-7 mm thick, next to the tube walls and that the recorded radiation of the Na line primarily characterizes the state of this layer rather than the state of the gas in the entire plug.

The most conclusive experiments were carried out with the plug being colored by sodium salts from a plate positioned along the diameter of the tube and with the boundary layer cut off or diverted by means of a special device.

In the case of a shock wave velocity of 3.7 km/sec and a calculated (theoretical) temperature of 3900°K, the temperature determined from the sodium lines was 3000°K, the data being reduced by means of Eq.(8) inasmuch as with coloring of the plug with sodium salt from the diametral plate it could be assumed that the lines were fully reabsorbed.

It was concluded that the substantial difference between the theoretical and experimental temperature values was due to changes in the thermodynamic properties of air owing to the admixture of sodium salt. Evaluation of the sodium content in the plug and the degree of reabsorption of the doublet components indicated that the Na concentration was about 1%. Energy losses due to fusion, evaporation and dissociation of NaCl resulted in the experimental temperature being approximately 1000° lower than the calculated air temperature.

Thus one of the fundamental shortcomings of the method of determining the temperature from the relative intensity of the Li and Na lines was coloring of the air by means of salt introduced into the shock tube in the solid state. As a result, the principal radiation of the Li and Na lines came from the boundary layer next to the walls and not from the central portion of the plug. To obviate this shortcoming, it was necessary to color the air from a centrally located plate and to cut off or divert the boundary layer; obviously, both measures could seriously affect the dynamic characteristics of the flow.

Accordingly, we decided it would be expedient to realize the coloring of the air with an appropriate luminous gas. We developed a procedure for introducing dicyan into the shock tube; this dissociated incident to passage of the shock wave and yielded the characteristic emission bands of cyanogen. The temperature was measured from the violet system of the CN vibrational bands by the procedure developed by Smit[5] and Somers[6].

The first experiments on determining the temperature from the CN 4216-4197 Å bands ($\Delta v = -1$) yielded promising results. With a shock wave velocity of 3.6 km/sec and a calculated temperature of 3760°K, we obtained an experimental temperature of 3700+500°K; measurement of the temperature, however, from the CN 3883-3872 Å ($\Delta v = 0$) yielded a value of 6000-7000°K. It was thought that the excessively high temperature value obtained in this case could be explained by reabsorption; reduction of the dicyan concentration from 20 to 0.2%, however, did not change the experimental temperature value obtained from the CN 3883-3872 Å bands. Measurement of the temperature from the relative intensity of the bands of the $\Delta v = -1$ system with a 2% concentration of $(CN)_2$ in nitrogen showed that with a shock wave velocity of 3.7 km/sec and a calculated temperature of 4700°, the temperature values obtained from different band pairs varied over the extensive range from 2700 to 7300°K. Analysis of the data led us to the conclusion that this spread cannot be due exclusively to reabsorption, but is apparently connected with the fact that equilibrium distribution of the CN molecules over the vibrational levels does not have time to be established under the conditions of the experiment.

Generalized method of reversal of spectrum lines

Earlier one of us in collaboration with Sviridov[7] proposed a generalized method of reversal of spectrum lines by means of which one can perform measurements of the temperature of heated gases without observing the instant of reversal. In this procedure the optical system commonly employed in the method of reversal of spectral lines was used and the following measurements are made: the intensity of emission of the gas at the spectral line

$$I_x = aC_1\lambda^{-5}e^{-C_2/\lambda T_x}\delta\lambda, \tag{9}$$

the intensity of emission in the spectral line of the gas transilluminated by a comparison source

$$I_{x+s} = C_1\lambda^{-5}e^{-C_2/\lambda T_s}\Delta\lambda + aC_1\lambda^{-5}e^{-C_2/\lambda T_x}\delta\lambda - aC_1\lambda^{-5}e^{-C_2/\lambda T_s}\delta\lambda, \tag{10}$$

the intensity of the emission of the comparison source

$$I_s = C_1\lambda^{-5}e^{-C_2/\lambda T_s}\Delta\lambda \tag{11}$$

The temperature is then determined by means of the relationship

$$T_x = T_s\left[1 + \frac{\lambda T_s}{C_2}\ln\left(1 - \frac{I_{x+s} - I_s}{I_x}\right)\right]^{-1}. \tag{12}$$

where $\delta\lambda$ is the line width, a is the absorption at the line wavelength, $\Delta\lambda$ is the spectral width of the monochromator slit, T is the true temperature of the gas behind the shock wave and T_s is the brightness temperature of the comparison source (lamp). In our experiments by way of comparison sources we used a heat lamp with a tungsten filament (brightness temperature 2680°K) and a 1000 watt xenon lamp with a maximum brightness temperature of 5000°K at λ = 5890 Å.

The temperature of air and nitrogen in the plug was measured with reference to the D line of Na. The contamination naturally present in the air and nitrogen was sufficient for obtaining the requisite intensity of the Na D line.

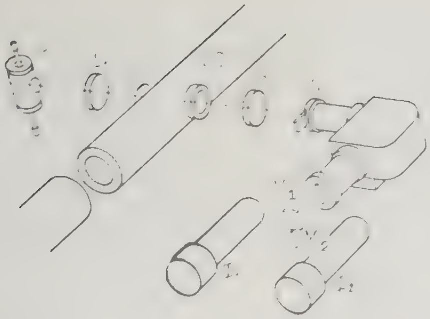

Fig.5. Diagram of set-up for measuring the temperature by the method of reversal of spectrum lines: R - standard (reference) light source, L_1 & L_2 - lenses, ST - shock tube, S_1 & S_2 - entry and exit monochromator slits, M_1 & M_2 - mirrors, Φ_1 & Φ_2 - photomultipliers.

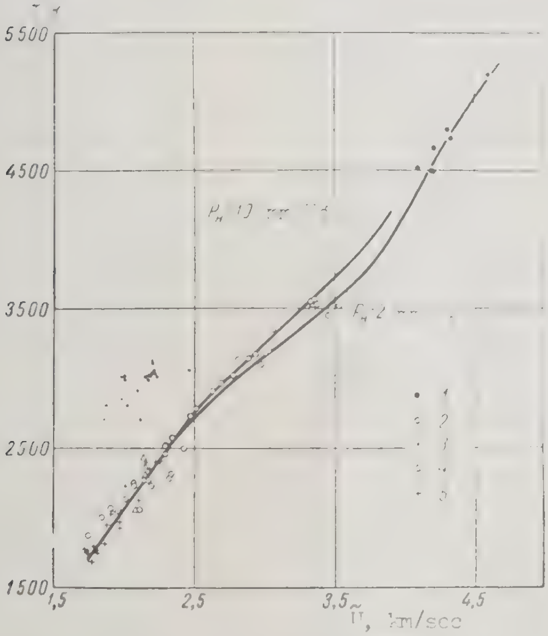

Fig.6. Results of measurement of temperature of nitrogen and air behind the shock wave by the photoelectric method of reversal of spectrum lines: 1) air, p_H = 2 mm Hg, 2) air, p_H = = 10 mm Hg, 3) air, p_H = 50 mm Hg, 4) nitrogen, p_H = 10 mm Hg, 5) nitrogen, p_H = 50 mm Hg; (p_H is the pressure in chamber III in Fig.4).

The optical system of the set-up is shown in Fig.5. The lines were recorded photoelectrically by means of a two-gun OK-17 M oscillograph.

Two neighboring sections of the shock tube were projected on the appropriately divided curved entry slit of the ISP-51 spectrograph. One of the shock tube sections was transilluminated by the reference source. The two intensities I_x and I_{x+s} - - I_s, necessary and sufficient for determining the temperature by means of Eq.(12) were measured simultaneously. The intensity $I_{x+s} - I_s$ was measured directly from the oscillogram inasmuch as the oscillograph amplifier was biased to block out I_s, the constant component due to the comparison source proper. Calibration for the relative sensitivity of the channels was realized by recording the emission from the plug while not illuminated by the auxiliary source.

The results of temperature measurement by means of this procedure are shown in Fig.6. The solid line curves represent values obtained by theoretical calculation. As may be seen from the figure, the experimental points fit the calculated curves satisfactorily. The average scatter does not exceed 100°.

The group of points 3 at some distance from the calculated curve was obtained in measuring the temperature of air with an initial pressure of 50 mm Hg. We assumed that the calibrated temperature values are due to burning at the contact surface. When air was replaced with nitrogen, thus eliminating the process of burning, at the same 50 mm Hg pressure we obtained the experimental points 5 which lie close to the theoretical curves.

The good agreement between theory and experiment, shown in Fig.6, validates the assumption on which the theoretical calculations are based, namely, that the gas behind the shock wave is in thermodynamic equilibrium. Furthermore, the agreement indicates that the energy of dissociation of nitrogen is 9.76 ev, for this was the value used in our calculations.

Fig.6 gives the maximum values of the temperature observed in the plug at the indicated shock-wave velocities. The developed photoelectric method of reversal of spectral lines also enabled us to obtain data on the temperature distribution along the length of the plug; for lack of space, however, we cannot give or discuss these data here.

We believe that the developed method for measuring temperatures can be extensively used for the investigation of stationary and nonstationary high temperature flames. The measurable temperature range can be extended by using pulsed light sources which may have a brightness temperature as high as 20,000-30,000°K.

"P.N.Lebedev" Physical Institute,
Academy of Sciences of the USSR

References

1. E.L.Resler, Chi-Lin Shao & A.Kantrowitz, J.Appl.Phys., 23, 1390 (1952).

2. L.Lamb, Chi-Lin Shao, J.Appl.Phys.28, 754 (1957).

3. N.N.Sobolev, Zhur.eksp.i teor.fiz., 19, 25 (1949); Trudy (Proceedings Physical Institute of the USSR Acad. of Sci., 7, 159 (1956).

4. A.P.Dronov, A.G.Sviridov & N.N.Sobolev, Optika i spektroskopiia (Optics and Spectroscopy), 5, No.4 (1958).

5. J.A.Smit, Het verkrijgen en meten van constante hoge temperaturen. - Utrecht, 1956; J.L.Spier & J.A.Smit, Physica, 9, 597 (1942); M.M.Smit-Meissen & J.L.Spier, Physica, 9, 193 (1942); J.L.Spier & M.M.Smit-Meissen, Physica, 9, 422 (1942).

6. P.J.Womers, Onderzoek van een boogontlading in stikstof bij verhoogde druk. - Nijmegen, 1954.

7. A.G.Sviridov & N.N.Sobolev, Zhur.eksp.i teor.fiz., 24, 93 (1953); N.N.Sobolev, Trudy (Proceedings), Physical Institute of the USSR Acad. of Sci., 7, 195 (1956).

NEW SPECTROSCOPIC INSTRUMENTS IN THE USSR

- V.K.Prokof'ev

A survey of new instruments developed up to 1954 was given in our report presented to the Ninth Conference on Spectroscopy in Tartu (Estonian SSR).[1] During the past three years there has been created several new models of spectroscopic instruments for visual observation, photography and photoelectric recording of spectra.

1. Instruments for Emission Spectrum Analysis and Investigation of Spectra

SL-12 steeloscope. The new model SL-12 steeloscope is equipped with a photometric wedge with a transmission from 3 to 100%; this allows of equalizing the intensity of the analytic lines and thereby enhancing the accuracy of measurement. The steeloscope stand serves as the housing for the excitation power unit which can supply either a 2 to 4 amp ac arc or a low voltage spark.

ISP-28 quartz spectrograph. This instrument is an improved model of the ISP-22 spectrograph in which all the controls are centralized. The time relay controls the burning and exposure times (in a range from 0 to 360 sec) and also advances the cassette 3 mm after each exposure. The air tight housing (ShT-9 or ShT-10) for the electrodes reduces the noise from the spark, minimizes external radio interference and makes it possible to evacuate the source chamber. The spectrum excitation equipment consists of a new model ac arc and low voltage spark generator (DG-2) and a controlled high voltage spark generator (IG-3). The design and installation of the generators insure complete suppression of external radio interference.

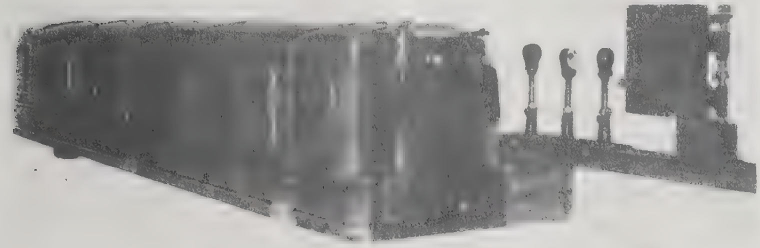

Fig.1. DFS-8 Diffraction spectrograph.

DFS-8 diffraction spectrograph (Fig.1). This instrument is intended for photographing the spectrum in sections of 1000 Å on 13 x 18 plates in the region from 2000 to 10,000 Å with a plate factor of 6 Å/mm in the first order. The spectrograph has a plane 600 line/mm 120 x 60 mm grating. The autocollimation system with a spherical f = 2600 mm mirror is of the vertically symmetric design.

The new model SPP-1 spectroprojector is intended for the examination of spectrograms measuring up to 13 x 24 cm with a magnification of 10 X or 20 X on a 300 mm diameter screen. A demountable 5 power microscope is provided for examining details. This model has provision for making marks on the spectrogram plates where necessary.

FES-1 photoelectric steelometer.[2] This equipment (Fig.2) consists of a constant deviation three-prism glass spectrograph a with a collimator and camera each having a focal distance of 300 mm, an air tight stand for the source electrodes b, an ac arc and low voltage spark generator (GEU-1) c, with electronic control of emission, provision for varying the emission phase and a built in electronic time relay[3] and a indicating-recording unit d. The

radiation is detected by two cesium-antimony SPV-9 photocells with very low dark current ($\sim 10^{-15}$ amp).; one photocell senses the nondispersed light reflected from the first surface of the first prism; the second receives the light energy of the spectrum line centered on the exit slit of the instrument. The line setting is controlled visually with the aid of a microscope. The instrument employs a storage type circuit with a dynamic capacitor and at the output gives the relative intensities of the analytic lines and the nondispersed light as an internal standard.

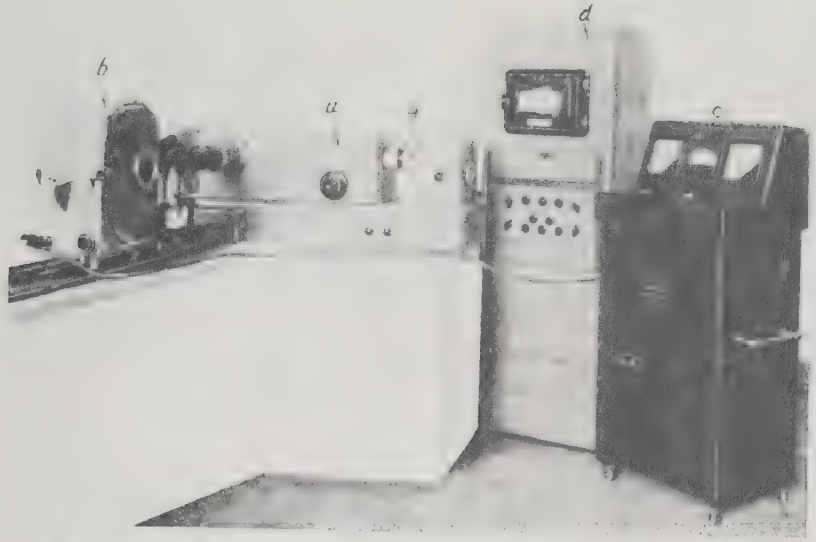

Fig.2. FES-1 photoelectric steelometer: a) main housing with three prisms and the collimating and focusing systems, b) air tight cabinet stand for electrodes (source), c) GEU-1 source generator, d) indicating-recording unit, amplifiers and power supply.

The DFS-10 photoelectric spectrometer with a concave diffraction grating of 2 meter radius is intended for general spectroanalytic use. The instrument covers the range from 2300 to 5400 Å with a plate factor of 4 Å/mm in the first order. The 1200 line/mm 70 x 50 mm diffraction grating is incorporated in a Paschen-Runge mounting. There are 36 slits with cesium-antimony STsV-9 photocells (dark current $\sim 10^{-15}$ amp) arranged along the circumference of the Rowland circle.

The spectrum is excited by the GEU-1 ac arc and low voltage spark generator with electronic control. The indicating-recording system measures the logarithm of the ratio of charges on the storage capacitors, i.e., at the output gives the logarithm of the relative intensities of the analytic line pair (or may be adjusted to read concentrations directly).[4] Up to 12 spectrum lines can be recorded simultaneously. The equipment provides for the possibility of carrying out analyses according to different programs.

2. Instruments for the Vacuum Ultraviolet

The Sp-41 double prism monochromator has lithium fluoride optics and provision for photoelectric recording. The $\sim 67^{\circ}$ prism has a Wadsworth mirror mounted parallel to its base; thus the axes of the collimator and camera are parallel to each other. The main casing (Fig.3), through which the entire system is evacuated, houses the simple monochromator system; to this can be attached an auxiliary tube with the second optical system, thus giving double monochromatization. The sensing element is an FEU-19 photomultiplier with an end photocathode; the outside surface of the end component is coated with fluorescent material. The photocurrent is amplified by a dc amplifier and indicated by a pointer instrument. The lenses are 15 mm in diameter and have

focal lengths of f_{1300} = = 161 mm and f_{2500} = = 212 mm.

The DFS-5 large vacuum diffraction spectrograph is intended for photographic work in the 500 to 2000 Å region. It has a concave (R = = 3 meter) 1200 line/mm 100 x 60 mm diffraction grating in a Paschen-Runge mounting with normal light incidence.

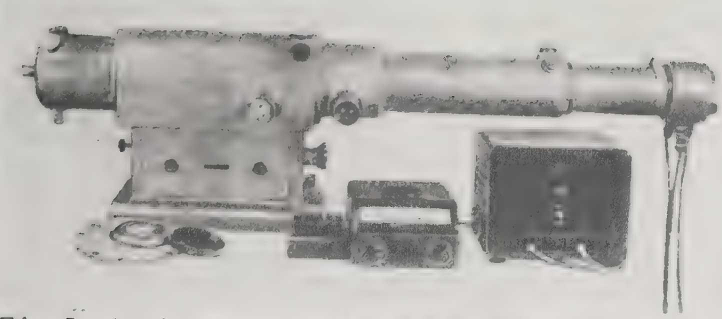

Fig.3. SP-41 double prism monochromator for the vacuum ultraviolet.

3. High Transmission Instruments

Two new instruments for recording of weak emission spectra (luminescence, Raman, etc.) photoelectrically are now available. One of these instruments utilizes the ISP-51 three prism glass optics spectrograph as the dispersing component. The usual photographic camera is replaced by a special exit (focusing) FEP-1 collimator with a focal length of 300 mm (relative aperture 1:5). The exit slit of this collimator is viewed by an FEU-17 photomultiplier with a cesium-antimony cathode. The photocurrent is amplified by a dc amplifier and fed into an EPP-09 automatic recorder.

The DFS-12 recording diffraction-grating spectrograph has double monochromatization to eliminate scattered light.[5] The optical system of the instrument is based on the Ebert-Fasti principle. The plane gratings have 600 line/mm and measure 150 x 140 mm; the focal length of the mirrors is 800 mm. The gratings work in the second order and yield a plate factor of 5.2 Å/mm with double monochromatization. The instrument can also be operated as a simple monochromator; in which case the plate factor is 10.4 Å/mm. The radiation sensing element is an FEU-19 photomultiplier coupled to a dc amplifier. The output is recorded by an EPP-09 recorder. The instrument covers the spectral range from 3600 to 6500 Å; the scanning rate is variable from 0.25 to 25 Å/min.

A group of particularly large aperture spectrographs with plane diffraction gratings (SP-48, 49 & 50) has been developed for the study of the spectra from very weak sources (the night sky, auroras, weak luminescence, etc.); these are described in Ref.6.

The specific problems involved in the investigation of the spectra of short-term emissions (flashes, pulse and spark discharges) call for high transmission spectroscopic instruments with provision for recording the spectra during a very brief interval or during different phases of the emission. In view of the very brief duration of the effect, it is essential to obtain the maximum possible resolution in time. Two high speed photoelectric spectrometers have been developed for this purpose. One of these - the SP-61 high speed photoelectric spectrometer with a 150 x 140 mm 600 line/mm plane diffraction grating - operates on the scanning principle and records the spectrum on 36 mm film; the spectrum in the visible region (4000 to 6500 Å) or in the near infrared (6500 to 11,000 Å) is recorded within a period of 0.002 sec with a plate factor of 26 Å/mm (focal length 300 mm). The spectrum is formed on the surface of a cylinder; coincindent with this surface is a rotating cylinder with 40 slits which are arranged so that when the cylinder is rotated two neighboring slits pass each over half the spectrum during 0.002 sec. Behind each of the two slits is an FEU-19 or FEU-22 photomultiplier. After appropriate amplifi-

cation, the photomultiplier signals are fed into an oscillograph; the vertical deflection of the oscillograph beam is photographed on 36 mm film fed at high speed in the direction perpendicular to the displacement of the beam.

The other instrument is the SP-64 high speed photoelectric four-channel spectrometer with a 600 line/mm, 150 x 140 mm plane diffraction grating; it employs the autocollimation principle and has an f = 600 mm lens. The plate factors are 13.5 and 27 Å/mm, respectively, in the second and first orders for the 3800-6500 Å and 6500-11,000 Å regions. Four exit slits with FEU-19 or FEU-22 photomultipliers, mounted on rigid arms with the center of rotation near the focusing lens, moved along the arc of the Rowland circle. The positions of the slits are fixed on the guide arc by means of detents, the recesses for which are spaced every 10 mm; an adjustment screw provides for intermediate positioning. In addition, focusing is realized with respect to a scale on each arm. A microscope mounted in a special recess near each slit serves for visual control of the position of the exit slit with reference to visible lines in the second order. The slits can be positioned to view very close lines or a given line and the background in its vicinity.

After appropriate amplification, the signals from the photomultipliers are applied to an OK-17 M pulse oscillograph with a two-gun electron tube. The deflection of the beam is recorded by a high speed camera. The instrument is capable of a time resolution of $1 \cdot 10^{-6}$ sec.

4. Instruments for Absorption Spectrum Analysis

SFD-1 spectrophotometer. This instrument has a 600 line/mm, 100 x 90 mm replica diffraction grating; it is designed for spectrophotometry in the ultraviolet, visible and near infrared regions of the spectrum (220 to 1100 mμ). The SFD-1 is a considerably improved and modernized version of the SF-4 spectrophotometer.

Fig.4. IKS-14 two-beam infrared spectrometer: 1) mounting cabinet housing amplifier and recorder, 2) spectrometer, 3) two-beam source, 4) power supply.

The IKS-12 spectrometer for the infrared differs from the familiar IKS-11 in that it is equipped with an automatic EPP-09 recorder.

The IKS-14 spectrometer for the infrared region (Fig.4) employs a two-beam system. The optical system and prism set are similar to those of the IKS-12 spectrometer. The radiation source is a Silit resistor rod; the radiation for the two-beam system is picked up from two close sections on the surface of the rod.

The radiation detector is a semiconductor or metallic bolometer coupled to a vacuum tube amplifier. The spectrum is recorded by a pen recorder. The instrument covers the region from 0.75 to 20 μ. The instrument has provision for automatic control of the slit width to maintain a constant energy level. The spectrum is recorded to a uniform wavelength or wave number scale. The reference points corresponding to 5, 10 or 20 divisions of the wavelength drum are imposed on the recorder chart in the process of recording. The time for covering the working range of the instrument can be varied from 4 to 1420 min.

Fig.4 gives a general view of this instrument. The entire amplifying system and recorder are housed in cabinet 1 which serves as the stand for the spectroscopic instrument 2 and the two-beam illuminating system 3. The sample cells are inserted into the gap between 2 and 3.

Conclusion

We have given a very brief description of the salient characteristics of some of the spectroscopic instruments developed in the USSR during the 1955-1957 period. It will be evident that diffraction gratings - ruled and replicas - are extensively used in the new equipment. It will also be noted that there are now many more spectroscopic instruments with photoelectric recording.

References

1. V.K.Prokof'ev, Izv.AN SSSR, Ser.fiz., 18, 643 (1954). (Trans. Bulletin, 18, No.6, 330.)

2. I.S.Abramson, Zavodsk. laboratoriia (Industrial laboratory), 20, 168 (1954).

3. M.I.Demidov, N.N.Ogurtsova & I.V.Podmoshenskii, Izv.AN SSSR, Ser.fiz., 19, 72 (1955). (Trans. Bulletin, 19, No.1, 82.)

4. I.V.Podmoshenskii & L.D.Kondrasheva, Izv.AN SSSR, Ser.fiz., 19, 36 (1955). (Trans. Bulletin, 19, No.1, 37.)

5. B.A.Kiselev, Optika i spektroskopiia (Optics & Spectroscopy), 1, 597 (1956).

6. N.G.Gerasimova & A.V.Iakovleva, PTE (Instruments and experimental techniques), 1, 83 (1956).

SPECTRUM OF OPTICALLY DENSE PLASMA

- H.Bartels

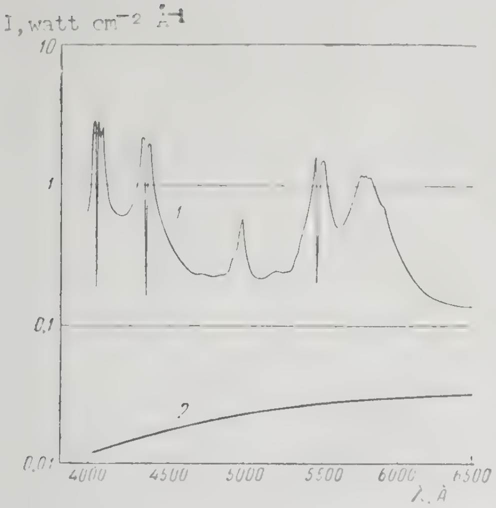

Fig.1. Spectra of a highly loaded high pressure mercury arc and a carbon arc crater.

Typical features of the spectra emitted by high density plasmas are a strong continuous background and exceptionally broad highly self-reversed lines. By way of illustration Fig.1 shows the spectrum of a high-pressure mercury arc operated at maximum load. The curve is plotted in terms of the intensity in watt/cm^2-Å vs the wavelength; for purposes of comparison the spectrum of a carbon arc crater is given in the lower part of the figure (curve 2). The intensity distribution in the spectrum of so dense a plasma does not give a true picture of the emission inasmuch as it is distorted by the strong reabsorption in the plasma. As examination of the self-absorption contours shows, the relationship are particularly complicated by inhomogeneity of the emitting layer. An obvious question is what can we learn regarding the physical relationships in the discharge column from the intensity distribution in such spectra? We are dealing here essentially with a matter of spectroscopic technique. I will first give the underlying fundamental relationships, without formal proof, and then illustrate their application using the example of temperature measurement. In addition, I shall briefly mention the other possibilities this approach offers.

Let us draw a cross section of the discharge column (plasma) as shown in Fig.2. Let B be the ray along which the spectrum is observed. Along this ray, then, we measure the depth t from the front boundary of the plasma; t_o is the thickness of the plasma column along the ray. Expressing the intensity in terms of the emission coefficient ε_λ and the absorption coefficient $\varkappa$, we obtain

$$I_\lambda = \int_0^{t_0} \varepsilon_\lambda(t)\, dt \exp\left\{-\int_0^{t} \varkappa(t')\, dt'\right\}.$$

Let us introduce, as is done in astrophysics, the optical depth

$$\tau = \int_0^{t} \varkappa(t')\, dt'$$

and the notation

$$\frac{\varepsilon}{\varkappa} = J\,,$$

we then obtain

$$I_\lambda = \int J(\tau)\, e^{-\tau} d\tau. \qquad (1)$$

The representation of the intensity in this form, however, is not particularly helpful for the solution of our problem. Hence let us formulate this relationship in a different way. Let us proceed from the power emitted along

the entire ray. This is equal to

$$\int_0^{t_0} \varepsilon_\lambda(t)\,dt = \int_0^{\tau_0} J(\tau)\,d\tau;$$

however, only a fraction Φ of this power emerges from the plasma, so that

$$I_\lambda = \Phi \int_0^{\tau_0} J(\tau)\,d\tau. \tag{2}$$

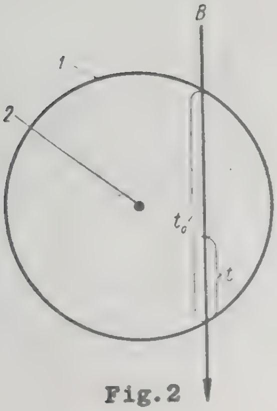

Fig.2

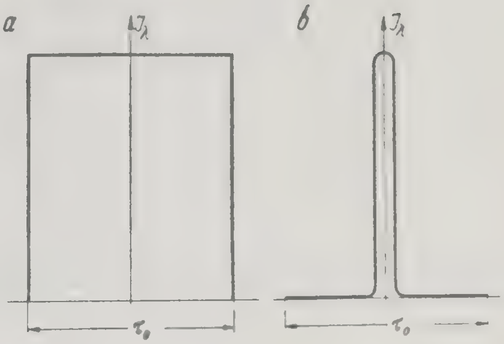

Fig. 3

Fig.2. Diagram for calculation of intensity: 1) boundary of plasma, 2) plasma axis, B - ray along which the spectrum is observed.

Fig.3. Diagram of limiting cases: a) homogeneous layer, b) glowing filament in an only absorbing shell.

Hereinafter we assume that in the plane of ray B all the quantities depend only on the radius and specifically that J_λ monotonically decreases with increasing distance from the center. The extent of decrease of J_λ is not restricted by any assumptions and therefore can lie anywhere between the two limiting cases shown in Fig.3, i.e., the case of a "homogeneous layer" and the case of a "glowing filament inside an only absorbing shell". Under these conditions J_λ falls off along each ray from the maximum value $J_{\lambda\max}$ symmetrically to both sides; averaging over the entire optical depth we will have a mean value $\bar{J}^\tau$. We can then set

$$\int_0^{\tau_0} J_\lambda(\tau)\,d\tau = \tau_0 \bar{J}_\lambda^\tau = \tau_0 M J_{\lambda\max},$$

where M, defined by

$$M = \frac{1}{\tau_0}\int_0^{\tau_0} \frac{J_\lambda(\tau)}{J_{\lambda\max}}\,d\tau.$$

depends only on the character of the function $J_\lambda(\tau)$, is independent of τ_0 and in any case is smaller than 1. Then from (2) we have

$$I_\lambda = J_{\lambda\max} M \tau_0 \Phi(\tau_0) = J_{\lambda\max} M Y(\tau_0); \tag{3}$$

in this expression $Y(\tau_0)$ is the only factor dependent on τ_0. We can readily write the equivalents of $Y(\tau_0)$ for the two limiting cases; these are $1-e^{-\tau_0}$ and $\tau_0 e^{-\frac{\tau_0}{2}}$, respectively. As was shown in Ref.1, one can draw a number of far-reaching deductions from a comparison of Eqs.(3) and (1). The entire

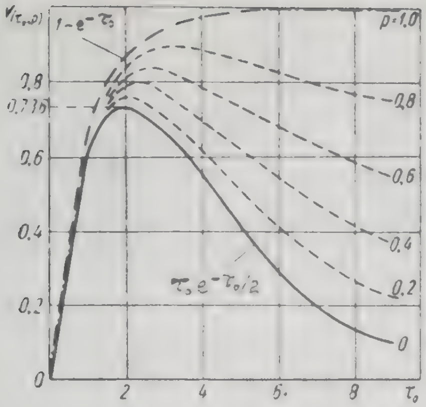

Fig.4. One-parameter family of curves
$\bar{Y}(\tau_0, p) = e^{-\frac{\tau_0}{2}} \cdot \left\{\left[\frac{\tau_0}{2}(1-p) + p \sinh\frac{\tau_0}{2}\right] + \frac{1}{\sqrt{p}} \sinh\frac{\tau_0\sqrt{p}}{2}\right\}$

diversity of $Y(\tau_0)$ functions consistent with symmetry of the plasma column and monotonic decrease of the function $J_\lambda(r)$ lies between the two limiting curves. And even in the case of appreciable layer thicknesses it can with good approximation be represented by a one-parameter family of curves. This parameter depends in a definite manner on the character of the function $J_\lambda(\tau)$. This family of curves is shown in Fig.4.

The representation of the intensity in the form

$$I_\lambda = J_{\lambda_{\max}} M Y(\tau_0, \; p) \qquad (4)$$

acquires particularly characteristic attributes if we introduce the Boltzmann distribution and thereby take into account the spatial distribution of temperature. If in addition we disregard the induced transitions, we can set*

$$J_\lambda = \frac{2hc^2}{\lambda^5} e^{-\frac{hc}{\lambda} \cdot \frac{1}{kT}} . \qquad (5)$$

It was shown in Ref.3 that under these assumptions M and p with decreasing temperature approach the limiting conditions, which nevertheless still give a good approximation for higher temperatures and still depend in a simple manner on the excitation potential V and the frequency ν. Thus, for example, for arc lines (with the exception of resonance lines in arc spectra, to which the above discussion does not apply), we obtain

$$M = \sqrt{\frac{eV_a}{eV_a + h\nu}} ,$$

where V_a is the excitation potential for the lower term. ** Similar expressions can be deduced for the continuum and spark lines. In the framework of this approximation

$$p = \frac{6}{\pi} \operatorname{arc\,tg} \frac{M^2}{\sqrt{1+2M^2}} .$$

Fig.5 shows that in the case of mercury, for example, M and p vary consistently, if only by a small amount, with wavelength.

---

*We shall have more to say regarding Eq.(5) below. As was shown in Ref.2, the influence of forced transitions can also be taken into account; here, however, they do not play any significant role.

**In calculating the limiting values we must also take into account the influence on the ray of the temperature in the vicinity of the maximum. It is assumed that the temperature variation in the vicinity of the maximum may be closely approximated by a second order parabola. The line shape can also influence the limiting value, but in general only in the case when the line width is strongly dependent on the concentration of ions or electrons.

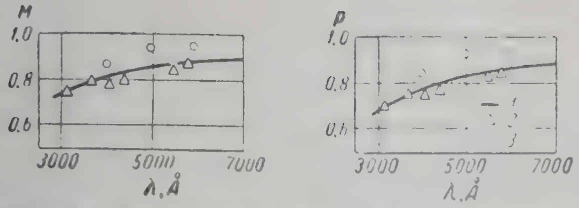

Fig.5. Values of M and p for the mercury spectrum: 1) continuous spectrum of neutral atom, 2) lines of neutral atom, 3) lines of singly charged ion.

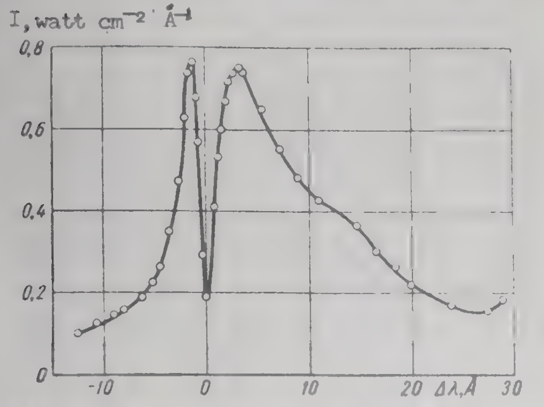

Fig.6. Self-reversal of the Hg 4358 A line.

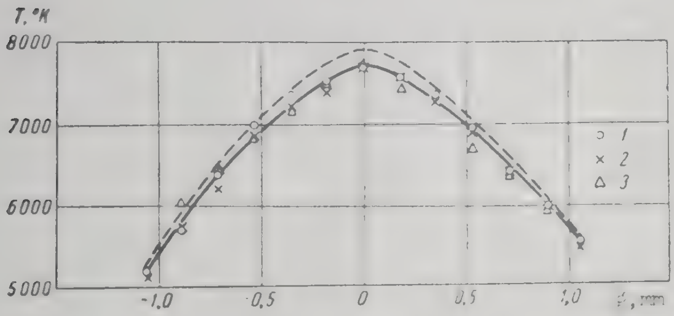

Fig.7. Radial temperature distribution in a high pressure mercury arc as determined from three lines: 1) λ = 4047 A, 2) 4358 A and 3) 5461 A. Dash lines - final refined curve obtained by iteration.

Inasmuch as both M and p are known with good approximation, the only unknowns remaining in equation (4) for the intensity are $J_{\lambda_{\max}}$ and τ.

Let us consider the self-reversal of spectrum lines from the standpoint of the above formulation for the intensity. By way of example let us take the 4358 Å line of mercury (Fig.6). $J_{\lambda_{\max}}$ is virtually constant over the entire line; the same may be said in the first approximation regarding M and p. Then the variation in intensity is determined exclusively by $Y(\tau_0, p)$; τ_0 increases monotonically to the center of the line. Hence the value of Y increases to a maximum and then falls off.* Hence the maxima of the self-reversed contour correspond to maximum values of $Y_{\max}(p)$ that are dependent only on p. The optical layer thickness $\hat{\tau}_0$ at the point of the maximum is also determined by p. Here we have the possibility of a quantitative verification of the theory. For the 5461 Å line we have $p =$ $= 0.82$, whence $\hat{\tau}_0 = 3.5$. Direct measurements by a light shift technique gave, for the optical thickness corresponding to the wavelength of both maxima, values of 3.3 and 3.5, respectively. The deviations lie within the limits of the experimental error.

Further, knowing the intensity of the two maxima we have the possibility of determining the temperature. For the intensity of these maxima we can write

$$I_{\lambda_{\max}} = J_{\lambda_{\max}} M Y_{\max}(p).$$

Here all the quantities are known except $J_{\lambda_{\max}}$. Consequently, from the measured value of the intensity $I_{\lambda_{\max}}$ we can calculate the temperature $T_{\max}$.

---

*On the basis of a somewhat different and less general consideration of the problem Cowan & Dieke[4] arrived at a similar concept of self-reversal. Here, however, we shall discuss only the results that follow from the above formulation.

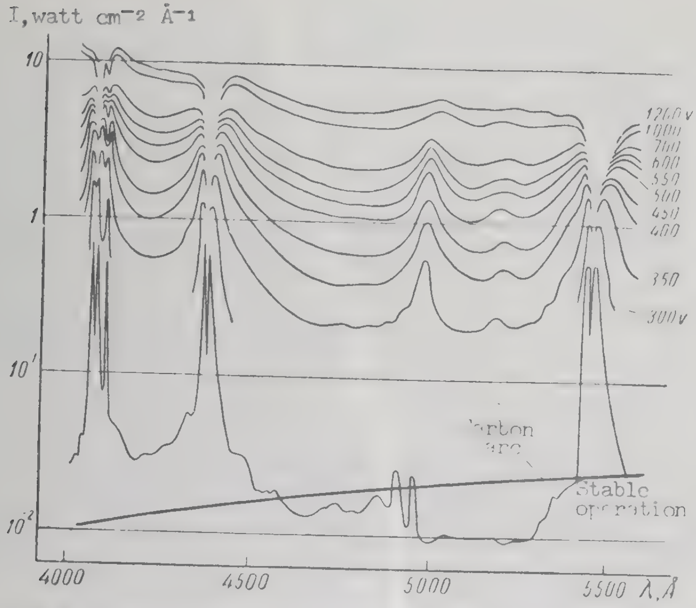

Fig.8. Intensity distribution in a high pressure mercury arc spectrum under pulse discharge conditions as a function of the voltage on the capacitor.

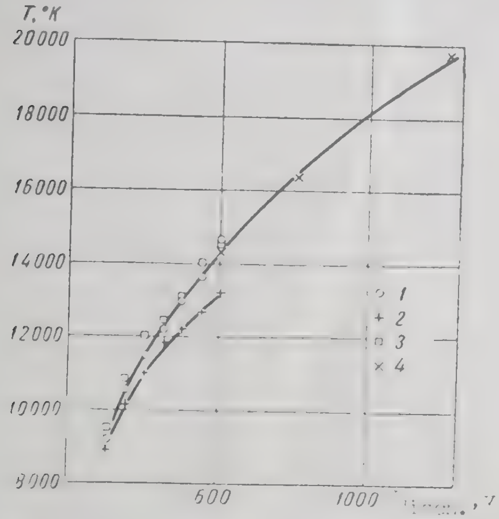

Fig.9. Temperature variation with the discharge voltage as obtained with reference to four lines: 1) λ = 5461 Å, 2) 4358 Å, 3) 4046 Å and 4) 3983 Å.

By virtue of the fact that the observations are made across the plasma column, from such measurements there is obtained the radial temperature variation with an accuracy corresponding to the degree of approximation with which the values of M and p are known. One can, however, utilizing the first approximation for the temperature variation, calculate better values of M and p and then the temperature variation more accurately. The temperature distribution determined in this manner by Gönig[5] in a high-pressure mercury tube is shown in Fig.7. Another example of temperature measurement may be cited. Capacitor discharges were superimposed on the steady operation of a high-pressure mercury tube and the spectrum measured at the instants of strongest emission. Fig.8 shows the results obtained by Meier[6] for the spectrum in the visible region with increasing "impact" voltage. Temperature determinations from the self-reversed contours of arc lines are allowable only to 600 v inasmuch as at higher temperatures the assumptions made above prove to be inadequate. Measurements can, however, be extended with reference to the 3983 Å spark line which only begins to self-reverse at higher temperatures. Measurements with respect to different lines (Fig.9) show that the results for the 5461 and 4046 Å arc lines are in good agreement and match the data obtained from the spark line, whereas the temperature determined from the 4358 Å line diverges increasingly from the others with increasing "impact" voltage. It was hypothesized that the occupation of the terms was somewhat distorted due to strong absorption of the 2536 Å resonance line.*

In closing I would like to say a few words regarding the possibility of determining other quantities from the measured spectral intensity distribution. It follows from Eq.(4) that one can determine with good approximation

---

*See footnote, next page.

the function $Y(\tau, p)$ and thence $\tau(\lambda)$ from the ratio I/I_{max} (I_{max} is the intensity at the self reversed contour closest to I_λ) for any given λ.[7]

Lines with strong self reversal can in a sense be used as plasma probes inasmuch as the center of gravity of the line, which makes a considerable contribution to its emission, is shifted from the axis of the plasma to its edge if we go in the spectrum from the side of the line to its center. Observation of the phase shift of light modulation and the wavelength dependence of the shift inside a line with strong self reversal enabled Swicker to demonstrate the presence of radial heat waves in a current modulated high-pressure tube.[8]

Physikalisches Institut
Technische Hochschule Hannover

References

1. H.Bartels, Z.Phys., 125, 597 (1949).
2. H.Bartels, Z.Phys., 136, 411 (1953).
3. H.Bartels, Z.Phys., 128, 546 (1950).
4. R.D.Cowan & G.H.Dieke, Rev.Mod.Phys., 20, 418 (1948).
5. W.Gönig, Z.Phys., 131, 603 (1952).
6. H.Meier, Z.Phys., 149, 40 (1957).
7. H.Bartels & R.Beuchelt, Z.Phys., 149, 523, 608 (1957); 150, 526 (1958).
8. H.Zwicker, Naturwissenschaften, 44, 439 (1957).

---

*Here we must again emphasize the important role played by Eq.(5) in the entire investigation. Initially one may regard T as the parameter that determines the value of J_λ. Otherwise, one cannot introduce T into the formal calculation. Consequently, the temperature measured with respect to each line purely formally describes the ratio of the populations of both terms. Only in the case when the measurements give the same temperature with respect to all lines does the Boltzmann distribution obtain.

PROBABILITY OF OPTICAL TRANSITIONS IN ATOMS AND MOLECULES WITH A POLARIZING CORE

- I.B.Bersuker

Introduction

We know that in general there is considerable disagreement between the results of calculations of optical transition probabilities in atoms and molecules and the experimental data. Thus the oscillator strength for the resonance transition in monovalent Na as calculated[1] by the Hartree-Fock method is f^{3p}_{3s} = 1.03, while measurements[2] by the dispersion technique yield a value of 1.24. An even greater divergence between experimental and calculated values is obtained for non-resonance transitions, for the sum of oscillator strengths and for atoms of other elements (to say nothing of molecules).

The Hartree-Fock method for atoms gives the most accurate results consistent with complete separation of variables. Hence further refinement of methods of calculating transition probabilities must be predicated on getting away from the limitations imposed by complete separation of variables. One may logically attempt to take into account some of the effects of incomplete separation of variables by means of wave functions derived by the method of complete separation of variables. The most important of these effects in our opinion is the influence of the core on optical electron transitions. The present investigation was devoted to taking this effect into account.

1. Improved expression for the probability of optical transitions in a many-electron system

In the method of separation of the variables associated with the inner and optical electrons, the latter are regarded essentially as moving independently in a certain mean field U produced by the former. Dependence of the transition probability only on the dipole moment of the optical electrons means that in the wave field there is added to the optical electron Hamiltonian only the perturbation

$$W = (\vec{\mathscr{E}} \cdot \sum_{i=1}^{p} \mathbf{r}_i),$$

where p is the number of optical electrons.

This procedure, however, fails to take into account the fact that under the influence of the field of the electromagnetic wave, the core of the system is immediately polarized and this polarization gives rise to an additional, time-dependent oscillation affecting the optical electrons. Formally, one should insert into the expression for the mean field U the wave functions of the inner electrons deformed in the wave field, so that instead of the former U, we will have U' = U + W'. Accordingly, the new Hamiltonian will be of the form

$$H = -\frac{1}{2} \sum \Delta_k + U + W' + W, \qquad (1)$$

and the transition probability will be given by

$$P_{AB} = 4\pi^2 | W_{AB}(\omega_{AB}) + W'_{AB}(\omega_{AB}) |^2. \qquad (2)$$

Using perturbation theory to calculate the deformed wave functions of the core and taking into account the fact that the frequency of the wave is appreciably greater than the transition frequency of each of the inner elec-

trons, we obtain

$$W' = (\vec{\mathscr{E}}, \sum_{i=1}^{p} \mathbf{G}(\mathbf{r}_i)), \tag{3}$$

where

$$\mathbf{G}(\mathbf{r}_i) = 2 \sum_{j=p+1}^{N} \sum_{k}{}' \frac{V_{kj}(\mathbf{r}_i)\, \mathbf{r}_{jk}}{E_k - E_j}, \tag{4}$$

while

$$V_{kj}(\mathbf{r}_i) = \int \frac{\varphi_j^{(0)}(\mathbf{r}')\, \varphi_k^{(0)}(\mathbf{r}')}{|\mathbf{r}' - \mathbf{r}_i|} d\tau'. \tag{5}$$

In these equations N is the total number of electrons in the system and $\varphi_j^{(0)}(\mathbf{r})$ and $\varphi_k^{0}(\mathbf{r})$ are the unperturbed wave functions of the core. The index takes on all possible values including the continuum, except $k = j$.

Substitution of Eq. (3) into (2) yields a new more accurate expression for the transition probability in the many-electron system:

$$P_{AB} = 4\pi^2 \left| \left(\vec{\mathscr{E}}, \left[\sum_{i=1}^{p} \mathbf{r}_i + \mathbf{G}(\mathbf{r}_i) \right]_{AB} \right) \right|^2. \tag{6}$$

This differs from the usual transition probability equation by the presence of the correction function $\mathbf{G}(\mathbf{r}_i)$, taking into account the influence of the core on transitions of the system corresponding to transitions of optical electrons. We may also note that Eq. (6) has been more rigorously substantiated in the so-called adiabatic approximation[3].

2. Oscillator strength for atomic transitions

The more accurate transition probability equation (6) makes it possible to introduce a corresponding correction into the formula for the oscillator strength. For a monovalent atom, for example, the oscillator strength is given by

$$f_{nl}^{n'l'} = Q_{nl}^{n'l'} (E_{n'l'} - E_{nl}) \left[\int_0^{\infty} P(nl\,|\,r)\, P(n'l'\,|\,r)\, (r + G(r))\, dr \right]^2,$$

where $Q_{nl}^{n'l'}$ is the appropriate constant. Precise calculation of the correction function $G(r)$ according to (4) is very difficult. An approximate evaluation of $G(r)$ can, however, be carried out by means of a simplification commonly utilized in calculating polarizabilities. It consists of taking out from under the summation over k in (4) a mean value $\overline{(1/E_k - E_j)} = 1/I_j$, where I_j is taken equal to the corresponding ionization potential. After this simplification (4) can be calculated precisely by means of the known wave functions of the inner electrons.

Calculations of the oscillator strength for the resonance transition in Na yielded f_{3s}^{3p} = 1.22 (the experimental value of this oscillator strength is 1.24). If we recall that the calculated value of f_{3s}^{3p} without taking the correction function into account is 1.03, it becomes clear that taking into account the influence of the core on optical transitions is essential.

One can also propose a somewhat rougher representation of $G(r)$ that allows of even further simplification of the calculation of the correction for the influence of the core. Let us assume that the atomic core is spherically symmetric and polarizes isotropically as a whole. Then the additional perturbation can be taken equal to the energy of an optical electron in the field of a uniformly polarized dielectric sphere and the expression for $G(r)$ becomes

$$\mathbf{G}(\mathbf{r}) = \begin{cases} \alpha \dfrac{\mathbf{r}}{r_0^3} & \text{for } r \leq r_0, \\ \alpha \dfrac{\mathbf{r}}{r^3} & \text{for } r \geq r_0, \end{cases} \tag{7}$$

where α, the polarizability, and r_0, the radius of the core, can be taken from experimental data.

3. Correction to the summation theorem for oscillator strengths

Rigorous formulation of the theorem on summation of oscillator strengths, following from the fundamental principles of quantum mechanics, pertains to all the transitions of the system as a whole. As for its formulation only for optical electrons (i.e., that the sum of the oscillator strengths for all optical transitions from the given state to all possible other states is equal to the number of optical electrons), it is essentially an approximation corresponding to the approximation of the method of complete separation of variables. According to Fock[4], the sum of the oscillator strengths for optical transitions in a monovalent atom must be of the form

$$\sum_{n'l'}' f_{nl}^{n'l'} = 1 + \sum_{n_i l'} \left| f_{nl}^{n_i l'} \right| + g, \tag{8}$$

where the $f_{nl}^{n_i l'}$ denote oscillator strengths for fictitious transitions to inner occupied states of the core and the prime on the summation sign means that these transitions are excluded from the sum.

The results of calculations according to Eq. (8) still diverge appreciably from the experimental data. Thus calculations yield a value of 1.031 for the sum of the oscillator strengths of the principal series of Na, while experiment gives 1.26.

In view of the correction for the influence of the core introduced by us into the expression for the oscillator strengths, one must also introduce a corresponding correction into the equation for the sum of the oscillator strengths. Operations similar to those performed by Fock lead to the following result:

$$\sum_{n'l'}' f_{nl}^{n'l'} = 1 + \sum_{n_i l'} \left| f_{nl}^{n_i l'} \right| + g + D_{nl}, \tag{9}$$

where

$$D_{nl} = \frac{1}{3} \int_0^\infty \left[2 \frac{dG}{dr} + \left(\frac{dG}{dr} \right)^2 \right] P^2(nl, r)\, dr + \frac{2}{3} \int_0^\infty \left[2 \frac{G}{r} + \left(\frac{G}{r} \right)^2 \right] P^2(nl, r)\, dr. \tag{10}$$

Computation by means of these equations using the approximation of Eq. (7) yields a value of $\Sigma f = 1.276$ for the principal series of Na, which is in fairly good agreement with the above cited optical data.

4. Electron transitions in molecules

In cases when the core of the system does not possess spherical symmetry the correction function $\mathbf{G}(\mathbf{r})$ in the equation for the transition probability leads to breach of the usual familiar selection rules for electron transitions. In order to determine the new selection rules, we need only consider the symmetry of the additional perturbation.

We assume that the field of an individual element of the polarizing molecular core is a dipole one. Then the additional perturbation to which an optical electron is subjected by the core element is characterized by

$$W' = \alpha_{\sigma\rho} E_\rho \frac{(\mathbf{r}-\mathbf{R})_\sigma}{|\mathbf{r}-\mathbf{R}|^3}, \quad \sigma, \rho = x, y, z. \tag{11}$$

Here $\mathbf{R}$ is the radius vector and $\alpha_{\sigma\rho}$ is the polarizability tensor of the molecular core element under consideration. Knowing the symmetry properties of the perturbation and the symmetry group to which the given molecule belongs, one can, by the methods of group theory, establish the allowed transitions. Calculations of this kind were carried out for some point groups and it was found that for most groups perturbation symmetry of the type characterized by Eq.(11) allows new types of transitions, forbidden by the usual selection rules. Among these transitions there are, for example, ordinarily forbidden $\Delta - \Sigma$ and $\Sigma^+ - \Sigma^-$ transitions, that have been observed experimentally in oxygen.

5. Infrared spectrum with Raman spectrum frequencies

A more accurate equation for the transition probability can also be derived for vibrational-rotational transitions of nuclei; in this case the correction term will correspond to the influence of immediate polarization of the electron shell. In this case the additional perturbation can be written in the form

$$W' = (\{\alpha_{\sigma\rho}\} \vec{\mathscr{E}}, \mathbf{f}(\mathbf{R})). \tag{12}$$

Here $\{\alpha_{\sigma\rho}\} \vec{\mathscr{E}}$ is the dipole moment of the electron cloud induced by the field of the electromagnetic wave and the function $\mathbf{f}(\mathbf{R})$ is selected so that Eq.(12) describes the energy of interaction of nuclei with inertialess polarization of the elements of the electron shell in the field of the wave. The function $\mathbf{f}(\mathbf{R})$ can be expanded in a series in small deviations of $\mathbf{R}$ from the equilibrium position $\mathbf{R}_0$ and the expansion limited to the zeroth term (bearing in mind that $\alpha_{\sigma\rho}$ is expanded into a similar series). Then the matrix elements of the expression entering into the formula for the probability of vibrational-rotational transitions can be described by integrals of the form

$$\int \psi_A(\mathbf{R})\, \alpha_{\sigma\rho} \psi_B(\mathbf{R})\, d\tau_R. \tag{13}$$

Integral (13) does not differ in any way from the corresponding integral defining the Raman spectrum. It follows therefore that infrared absorption with frequencies of the Raman spectrum is possible.

I wish to thank M.G.Veselov for discussion and valuable advice.

Physical Institute
Leningrad State University

References

1. V.Fock & M.Petrashen, Sow.Phys., 8, 547 (1935).
2. G.S.Kvater, Izv.AN SSSR, Ser.fiz., 9, 236 (1945).
3. M.G.Veselov & I.B.Bersuker, Present issue of the Bulletin, p. [illegible].
4. V.Fock, Z.Phys., 89, 744 (1934).

EMISSION SPECTRUM OF THE DECOMPOSITION PRODUCTS OF ALIPHATIC HYDROCARBONS AND ALCOHOLS IN AN ELECTRODELESS DISCHARGE

- A.A.Koliubin

1. The electrodeless discharge in the experiments was realized in a 30 mm diameter, 300 mm long quartz tube mounted in a solenoid (50 to 150 turns). The high voltage source supplying the solenoid was a push-pull oscillator with a frequency of 6 Mc.

The measurements were carried out on stationary and flowing vapors. In the case of the former, the tube was connected to the vacuum system which had provision for filling the tube with the desired vapor after evacuation.

For investigations of flowing vapor, we used the tube shown in the accompanying figure; the main tube 1 had side branches at either end, connected by ground joints to bulbs 2 and 3. Bulb 2 was filled with the investigated substance, while bulb 3 was immersed in liquid nitrogen and served as a trap for the condensing decomposition products formed after passage of the vapor through the discharge zone. The main tube was connected directly to the three-way cock 4, coupled to the fore vacuum line.

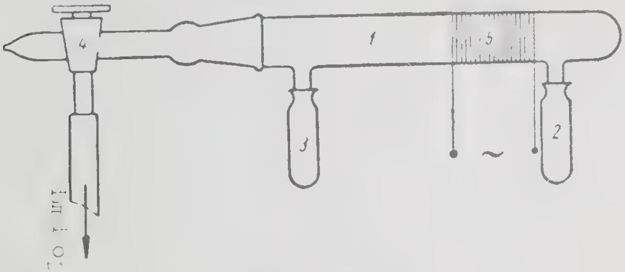

Diagram of electrodeless discharge tube for investigation of flowing vapor: 1) quartz tube, 2) bulb with investigated substance, 3) bulb (trap) for condensation of decomposition products, 4) three-way cock, 5) discharge solenoid.

The discharge tube was first pumped (to remove air) with the investigated substance frozen. After evacuation, but with continued pumping, the substance was allowed to thaw and its vapor entered the discharge zone.

The spectra were observed by means of an ISP-22 spectrograph. The discharge tube was mounted so that its axis was aligned with the optical axis of the spectrograph. The vapor pressure was measured with either a mercury pressure gage or a dibutylphthalate filled manometer.

2. In the emission spectrum of stationary methane we observed the bands and lines of CH (4315 Å and 3890 Å), H_2, H, Hg and the characteristics bands of CO, CN and OH. The relative intensity of the impurity bands decreased with increasing methane pressure.

The character of the spectrum was found to depend on the pressure: with increasing pressure the relative intensity H/CH decreases. If the discharge is realized in methane with a large amount of impurities (for example, in city illuminating gas), the most intense bands are those of CN, CO, CH and OH.

In all the investigated cases, there was observed a pressure effect[1]; this was strongest in the range of low pressures.

3. Discharges in the vapor of methyl alcohol, CH_3OH, yield the spectrum bands and lines of CH, OH, CO, H_2, H, C II, C I and in the case of stationary vapor of CN. The same bands are observed in the spectra of ethyl, butyl and isoamyl alcohol. The character of the alcohol spectra also depends on the pressure.

In the case of flowing vapor, at different rates of pumping (the flow rate was varied by using one or two pumps) there were also observed certain differences in the relative intensities of the spectrum bands and lines

depending on the pressure (Table 2).

In all cases the rotational structure of the OH 3064 Å band of methyl alcohol was strongly developed.

4. The increase in density (blackening in the spectrograms) of the CO bands and the virtually constant value of the density of the OH bands with decrease in the rate of pumping (Table 2) are evidence in favor of the hypothesis that CO is a·product of a secondary reaction, while OH* is a primary reaction product.

Table 1

Pressure dependence of the intensity ratios of the principal bands in the spectrum of CH_3OH for stationary vapor

Spectrogram No.	Vapor pressure mm Hg	Ratio of band & line intensities			
		$\frac{CO_{3303}}{CO_{2975}}$	$\frac{OH_{3064}}{CO_{3303}}$	$\frac{CH_{4315}}{OH_{3064}}$	$\frac{H_{4861}}{CH_{4315}}$
92-III	2	0,54	0,40	13	1,5
92-II	6	0,70	0,32	4,5	0,63
92-I	13	0,70	0,17	2,3	0,45

Table 2

Variation of the intensity ratios of the bands and lines in the spectrum of CH_3OH with the pressure and rate of pumping with flowing vapor

Pressure mm Hg	Pumping rate	Ratio of band intensities			
		$\frac{CO_{3303}}{CO_{2975}}$	$\frac{OH_{3064}}{CO_{3303}}$	$\frac{OH_{4315}}{OH_{3064}}$	$\frac{H_{4340}}{CH_{4315}}$
0,35	2φ	0,62	2,2	2,1	1,2
	φ	0,71	1,4	2,3	1,3
0,45	2φ	0,70	3,1	2,8	0,92
	φ	0,67	1,9	3,1	0,62
0,48	2φ	0,75	2,2	3,5	0,85
	φ	0,72	1,7	3,3	0,95

As was noted above, the gas flow was realized by continuous pumping of the system with one or two pumps (in Table 2 φ indicates one-pump and 2φ two-pump pumping). In the process of pumping the partial pressure of the decomposition products should vary according to the exponential law

$$P = P_0 e^{-\varphi t/v_0},$$

where φ is the pumping rate and v_0 is the volume of the discharge zone; $v_0/\varphi = \tau$ is therefore the mean time the decomposition products remain in the discharge zone. Hence $P = P_0 e^{-t/\tau}$; if we use T to denote the mean time of the process at the given stage of the reaction, we can write

$$P = P_0 e^{-nT/\tau},$$

where $nT = t$ and n is the "number" of the consecutive stage or process. It will be evident that if T is commensurate with τ, the pressure of the decomposition products will fall off rapidly with the "number" of the process.

Since T increases with decreasing pressure, at low pressures the bands associated with primary reaction products will appear most intense. Correlation between spectroscopic density and the pumping rate as well as the order of the reaction (primary or secondary) has been observed in experiments with discharges in water vapor (Table 3).

It is known that in discharges in water vapor, OH* is a product of primary decomposition, while excited H and O are products of secondary processes.[2]

By analogy with the spectrum of water vapor in an electric discharge, it can be shown that the OH radical in our case is also a product of primary decomposition.

Studies by Lyman[3] of the intensity distribution of the rotational lines in the OH 3064 Å band for the Q_1 branch showed that there are two intensity

Table 3

Density of lines and bands in the spectrum of water vapor in an electrodeless discharge

Spectrograph No.	Pumping rate	Pressure, mm Hg	Density of lines in spectrogram			
			H-4861 Å	H-4340 Å	OH-3064 Å	OII-4649 Å
137-I	2φ	0,55	2,46	2,30	1,08	0,38
II	φ	0,55	2,76	2,48	1,09	0,64
138-III	2φ	0,23	2,48	2,30	0,93	0,64
IV	φ	0,23	2,78	2,78	1,04	1,09
137-III	2φ	0,18	1,15	1,30	0,53	0,11
IV	φ	0,18	1,66	1,78	0,61	0,16

maxima. According to the interpretation of Kondrat'ev[2], in discharges in water vapor there occurs the process

$$\vec{e} + H_2O \rightarrow OH^* + H + e.$$

In this process OH* acquires an additional rotational energy corresponding to the intensity maximum with the larger quantum number K. In addition there may also occur direct excitation of OH:

$$\vec{e} + OH \rightarrow OH^* + e.$$

In this process OH cannot acquire a large rotational energy.

As was noted above for methyl alcohol, the rotational structure of the OH 3064 Å band here is also strongly developed. This gives reason to assume that in discharges in CH_3OH vapor there occurs the process

$$\vec{e} + CH_3OH \rightarrow OH^* + CH_3 + e,$$

i.e., that the radical OH* is a primary decomposition product of the alcohol molecule. According to Kondrat'ev interpretation, it may be assumed that direct excitation of OH may also occur.

Qualitatively the spectra of the more complex alcohol in electrodeless discharges are similar to the spectrum of methyl alcohol vapor. Hence by analogy with H_2O and CH_3OH, it may be assumed that in the case of these more complex alcohols the radical OH* is also a primary decomposition product.

Moscow Engineering-Physical Institute

References

1. A.A.Balandin & Ia.T.Eidus, Zhur.fiz.khim., 7, 77 (1936).
2. V.N.Kondrat'ev, Svobodnyi gidroksil (Free hydroxyl), M.-L., 1939.
3. E.R.Lyman, Phys.Ref. 53, 379 (1938).

Measurement of oscillator strengths in atomic spectra - Iu.I.Ostrovskii, N.P.Penkin & L.N.Shabanova 725 720
Spectroscopic investigation of the state of a gas behind a shock wave - N.N.Sobolev, A.V.Potapov, V.F.Kitaeva, F.S.Faizullov, V.N.Aliamovskii, E.T.Antropov & I.L.Isaev 730 725
New spectroscopic instruments in the USSR - V.K.Prokof'ev 737 732
Spectrum of optically dense plasma - H.Bartels 742 737
Probability of optical transitions in atoms and molecules with a polarizing core - I.B.Bersuker 749 743
Emission spectrum of the decomposition products of aliphatic hydrocarbons and alcohols in an electrodeless discharge - A.A.Koliubin 753 747

Translated in 1959 by
Columbia Technical Translations
5 Vermont Ave., White Plains, N.Y.

Bulletin of the Academy of Sciences of the USSR - Physical Series
Vol. 22, No.6
Transactions of the Eleventh All-Union Conference on Theoretical Spectroscopy

TABLE OF CONTENTS

	Page Orig.	Page Trans.
Opening address - S.L.Mandel'shtam	647	645
Forty years development of Soviet spectroscopy - S.E.Frish	650	648
Optical effects of collective electron oscillations in metals - I.I.Sobel'man & E.L.Feinberg	654	652
Excitation of spectral lines in the negative glow of a gas discharge - S.E.Frish & I.P.Bogdanova	659	657
Adiabatic approximation in the quantum theory of atoms - M.G.Veselov & I.B.Bersuker	662	660
Two-electron model approximation and the so-called anomaly in the spectra of carbon, nitrogen and oxygen - A.P.Jucys, Ia.I.Vizbaraite, V.I.Kavetskis & I.V.Batarunas	665	663
One-electron wave functions of Tl^+ in certain crystals - M.I.Petrashen' & T.L.Gutman	668	666
Calculation of one-electron wave functions and oscillator strengths by means of an electronic computer - L.A.Vainshtein	671	668
Determination of molecular dissociation energies from flame reaction equilibrium studies - L.V.Gurvich & I.V.Veits	673	670
Dependence of the integral intensity of spectrum lines on the absolute concentration of atoms in an arc discharge - I.V.Dvornikova	677	674
Determination of the relative oscillator strengths in an arc discharge from the width of the spectrum lines - I.M.Nagibina	681	678
Isotope shift in the spectra of cerium and zirconium - Iu.P.Dontsov & L.A.Korostyleva	683	680
Isotope shift in the spectrum of ionized uranium - N.G.Morozova & G.P.Startsev	686	683
On the accuracy of determination of hyperfine structure constants from optical measurements - N.I.Kaliteevskii, V.I.Perel' & M.P.Chaika	692	689
On temperature determination from molecular band spectra - L.V.Leskov & L.P.Vasil'eva	696	693
Motion of ions in plasma - Iu.M.Kagan	702	699
On the possibility of utilizing spectrum lines as wavelength norms and a length standard - N.R.Batarchukova	708	704
Observation of anomalous dispersion in short-term processes - A.M.Shukhtin & V.S.Egorov	711	707
Contribution to the theory of line broadening in plasma - V.I.Kogan	714	710
Broadening and shift of spectral lines in highly ionized plasma - L.A.Vainshtein, V.G.Koloshnikov, M.A.Mazing, S.L.Mandel'shtam & I.I.Sobel'man	718	714
Temperature measurement of the glowing vapor cloud in pulse discharges - A.A.Labuda, E.G.Martinkov & I.G.Nekrashevich	720	716